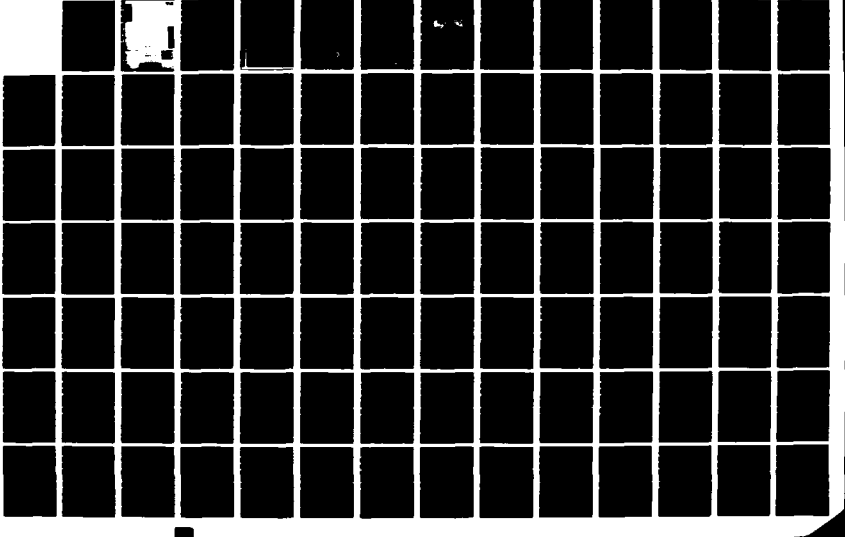
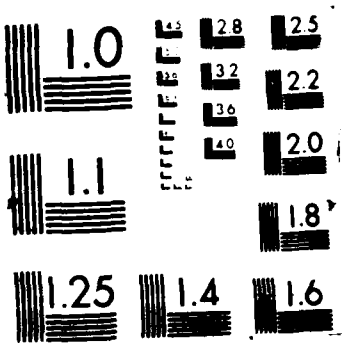
AD-A186 490 UNITED STATES AIR FORCE RESEARCH INITIATION PROGRAM 01/11
1984 RESEARCH REPORTS (U) SOUTHEASTERN CENTER FOR
ELECTRICAL ENGINEERING EDUCATION INC S W D PEELE
UNCLASSIFIED MAY 86 AFOSR-TR-87-1721 F49620-82-C-0035 F/G 15/1 NL




1.0
1.1
1.25
1.4
1.6
1.8
2.0
2.2
2.5
2.8
3.2
3.6
4.0

AD-A186 490

AFOSR SCEEE

# USAF RESEARCH INITIATION PROGRAM

## 1984

# RESEARCH REPORTS

## VOLUME III

CONDUCTED BY
THE SOUTHEASTERN CENTER FOR
ELECTRICAL ENGINEERING EDUCATION

DTIC FILE COPY

PROF. WARREN D. PEELE
PROGRAM DIRECTOR, SCEEE

MAJ. AMOS OTIS
PROGRAM MANAGER, AFOSR

DTIC
ELECTE
NOV 17 1987
S E

This document has been approved for public release and sale; its distribution is unlimited.

UNCLASSIFIED
SECURITY CLASSIFICATION OF THIS PAGE

# REPORT DOCUMENTATION PAGE

Form Approved
OMB No. 0704-0188

1a. REPORT SECURITY CLASSIFICATION
UNCLASSIFIED

1b. RESTRICTIVE MARKINGS

2a. SECURITY CLASSIFICATION AUTHORITY

2b. DECLASSIFICATION / DOWNGRADING SCHEDULE

3. DISTRIBUTION / AVAILABILITY OF REPORT
Approved for public release; distribution unlimited.

4. PERFORMING ORGANIZATION REPORT NUMBER(S)

5. MONITORING ORGANIZATION REPORT NUMBER(S)
AFOSR-TR- 87-1721

6a. NAME OF PERFORMING ORGANIZATION
The Southeastern Center for Electrical Engineering Educatio

6b. OFFICE SYMBOL (If applicable)

7a. NAME OF MONITORING ORGANIZATION
Air Force Office of Scientific Research/XOT

6c. ADDRESS (City, State, and ZIP Code)
11th & Massachusetts Ave.
St. Cloud, Florida 32769

7b. ADDRESS (City, State, and ZIP Code)
Building 410
Bolling AFB, DC 20332

8a. NAME OF FUNDING / SPONSORING ORGANIZATION
AFOSR

8b. OFFICE SYMBOL (If applicable)
XOT

9. PROCUREMENT INSTRUMENT IDENTIFICATION NUMBER
F49620-82-C-0035

8c. ADDRESS (City, State, and ZIP Code)
Building 410
Bolling AFB, DC 20332

10. SOURCE OF FUNDING NUMBERS

| PROGRAM ELEMENT NO. | PROJECT NO. | TASK NO | WORK UNIT ACCESSION NO. |
|---|---|---|---|
| 61102F | 2301 | D5 | |

11. TITLE (Include Security Classification)
USAF Research Initiation Program - Volume 2

12. PERSONAL AUTHOR(S)
Prof. Warren D. Peele

| 13a. TYPE OF REPORT | 13b. TIME COVERED | 14. DATE OF REPORT (Year, Month, Day) | 15. PAGE COUNT |
|---|---|---|---|
| Interim | FROM _____ TO _____ | May 86 | |

16. SUPPLEMENTARY NOTATION

| 17. COSATI CODES | | | 18. SUBJECT TERMS (Continue on reverse if necessary and identify by block number) |
|---|---|---|---|
| FIELD | GROUP | SUB-GROUP | |
| | | | |
| | | | |

19. ABSTRACT (Continue on reverse if necessary and identify by block number)

(SEE REVERSE)

20. DISTRIBUTION / AVAILABILITY OF ABSTRACT
☒ UNCLASSIFIED/UNLIMITED ☐ SAME AS RPT ☐ DTIC USERS

21. ABSTRACT SECURITY CLASSIFICATION
UNCLASSIFIED

| 22a. NAME OF RESPONSIBLE INDIVIDUAL | 22b. TELEPHONE (Include Area Code) | 22c. OFFICE SYMBOL |
|---|---|---|
| Amos Otis, Major, Program Manager | (202) 767-4971 | XOT |

DD Form 1473, JUN 86 Previous editions are obsolete. SECURITY CLASSIFICATION OF THIS PAGE

AFOSR-TR- 87-1721

## INTRODUCTION

### Research Initiation Program - 1984

For several years prior to 1983, AFOSR conducted a special follow-on funding program for Summer Faculty Research Program (SFRP) participants; this was popularly known as the AFOSR Minigrant Program. That program was superceded in 1983 by the Research Initiation Program conducted by SCEEE.

To compete for a 1984 Research Initiation Program award, SFRP participants must submit a complete proposal and proposed budget either during or promptly after their SFRP appointment periods. Awards to the 1984 participants may extend through 15 December 1985.

Each proposal was evaluated for technical excellence, with special emphasis on relevance to continuation of the SFRP effort, as determined by the Air Force laboratory/center. The final selection of awards was the responsibility of AFOSR.

The most effective proposals were those which were closely coordinated with the SFRP Effort Focal Point and which followed the SFRP effort with proposed research having strong prospects for later sustained funding by the Air Force laboratory/center.

The maximum award under the Research Initiation Program is $12,000 plus cost-sharing up to a matching total amount.

The mechanics of applying for a Research Initiation Program award are as follows:

(1) Research Initiation Program proposals of $12,000 plus cost-sharing were to be submitted after August 1, 1984 but no later than November 1, 1984.

(2) Proposals were evaluated and the final award decision was the responsibility of AFOSR after consultation with the Air Force Laboratory/center.

(3) The total available funding limited the number of awards to approximately half the number of 1984 SFRP participants.

(4) Subcontracts were negotiated with the employing institution, designating the SFRP participant as Principal Investigator, with the period of award having a start date no earlier than September 1, 1984 and a completion date no later than December 15, 1985.

Employing institutions were encouraged to cost-share since the program was designed as a research initiation procedure. Budgets included, where applicable, Principal Investigator time, graduate assistant and support effort, equipment and expendable supplies, travel and per diem costs, conference fees, indirect costs, and computer charges.

Volumes I, II, III, and IV of the 1984 Research Initiation Program Report contain copies of reports on the 89 subcontract efforts awarded under this program.

AFOSR-TR- 87-1721

DTIC
ELECTE
NOV 17 1987
S D
E

This document has been approved for public release and sale; its distribution is unlimited.

87

# 1984 USAF/SCEEE RESEARCH INITIATION PROGRAM

Conducted by

Southeastern Center for

Electrical Engineering Education

under

USAF Contract Number F49620-82-C-0035

RESEARCH REPORTS

Volume II of IV

submitted to

Air Force Office of Scientific Research

Bolling Air Force Base

Washington, DC

BY

Southeastern Center for
Electrical Engineering Education

May 1986

Accession For
NTIS GRA&I
DTIC TAB
Unannounced
Justification
By
Distribution/
Availability Codes
Dist | Avail and/or Special
A-1

DTIC COPY INSPECTED

DTIC ELECTE NOV 17 1987

This document has been approved for public release and sale; its distribution is unlimited.



SCEEE
©
1986

# INTRODUCTION

## Research Initiation Program - 1984

For several years prior to 1983, AFOSR conducted a special follow-on funding program for Summer Faculty Research Program (SFRP) participants; this was popularly known as the AFOSR Minigrant Program. That program was superceded in 1983 by the Research Initiation Program conducted by SCEEE.

To compete for a 1984 Research Initiation Program award, SFRP participants must submit a complete proposal and proposed budget either during or promptly after their SFRP appointment periods. Awards to the 1984 participants may extend through 15 December 1985.

Each proposal was evaluated for technical excellence, with special emphasis on relevance to continuation of the SFRP effort, as determined by the Air Force laboratory/center. The final selection of awards was the responsibility of AFOSR.

The most effective proposals were those which were closely coordinated with the SFRP Effort Focal Point and which followed the SFRP effort with proposed research having strong prospects for later sustained funding by the Air Force laboratory/center.

The maximum award under the Research Initiation Program is $12,000 plus cost-sharing up to a matching total amount.

The mechanics of applying for a Research Initiation Program award are as follows:

(1) Research Initiation Program proposals of $12,000 plus cost-sharing were to be submitted after August 1, 1984 but no later than November 1, 1984.

(2) Proposals were evaluated and the final award decision was the responsibility of AFOSR after consultation with the Air Force Laboratory/center.

(3) The total available funding limited the number of awards to approximately half the number of 1984 SFRP participants.

(4) Subcontracts were negotiated with the employing institution, designating the SFRP participant as Principal Investigator, with the period of award having a start date no earlier than September 1, 1984 and a completion date no later than December 15, 1985.

Employing institutions were encouraged to cost-share since the program was designed as a research initiation procedure. Budgets included, where applicable, Principal Investigator time, graduate assistant and support effort, equipment and expendable supplies, travel and per diem costs, conference fees, indirect costs, and computer charges.

Volumes I, II, III, and IV of the 1984 Research Initiation Program Report contain copies of reports on the 89 subcontract efforts awarded under this program.

RESEARCH REPORTS
1984 USAF-SCEEE RESEARCH INITIATION PROGRAM

VOLUME I


| REPORT NO. | TITLE | RESEARCH ASSOCIATE |
|---|---|---|
| 1. | AN ANALYTICAL STUDY OF TWO-STAGE LIGHT GAS GUN PERFORMANCE | Dr. Robert W. Courter |
| 2. | A LOW-COST LOCAL-AREA NETWORK for DESKTOP COMPUTERS | Dr. Myron A. Calhoun |
| 3. | DEVELOPMENT of PREDICTION MODELS for HUMAN TORQUE STRENGTH | Dr. S. Deivanayagam |
| 4. | THE ROLE of ANTIOXIDANT NUTRIENTS in PREVENTING HYPERBARIC OXYGEN DAMAGE to the RETINA | Dr. William L. Stone |
| 5. | THE INFULUENCE of MELTING and REACTANT COMSUMPTION on TEMPERATURE TRANSIENTS in SPHERICAL and CYLINDRICAL CHARGES of EAK | Dr. John W. Sheldon |
| 6. | GEOSTROPHIC ADJUSTMENT in a THREE-DIMENSIONAL MESOSCALE NUMERICAL MODEL of the ATMOSPHERE | Dr. Keith L. Seitter |
| 7. | Report not received on time. Will be provided when available. | Dr. William Czelen |
| 8. | EFFECTS of TEMPERATURE and REACTANT SOLVATION UPON the RATES of GAS-PHASE ION-MOLECULE REACTIONS | Dr. Peter M. Hierl |
| 9. | EFFECTS of NUCLEAR RADIATION on the OPTICAL CHARACTERISTICS of LASER COMPONENTS | Dr. Hermman Donnert |
| 10. | A REVIEW of COMPUTER SIMULATIONS for AIRCRAFT-SURFACE DYNAMICS | Dr. George R. Doyle, Jr. |
| 11. | COMPUTATIN OF TRANSONIC PROJECTILE AERODYNAMICS | Dr. Chen-Chi Hsu |
| 12. | DEVELOPMENT of an ADAPTIVE GRID GENERATION TECHNIQUE for TRANSONIC PROJECTILE BASE FLOW PROBLEMS | Dr. Chris Reed |
| 13. | Report not received on time. Will be provided when available. | Dr. Kendall Nygard |

RESEARCH REPORTS
1984 USAF-SCEEE RESEARCH INITIATION PROGRAM

VOLUME II


| REPORT NO. | TITLE | RESEARCH ASSOCIATE |
|---|---|---|
| 26. | ALTERNATIVE COMPUTATIONAL METHODS for SEPARATED FLOWS about PITCHED FLAT SURFACES | Dr. Larry A. Glasgow |
| 27. | NO TITLE | Dr. Hendrik F. Hameka |
| 28. | FUNCTIONAL ROLE of SEROTONIN in the CEREBELLAR GLOMERULAR SYNAPSE | Dr. Deborah Armstrong |
| 29. | CHOLINE and ETHANOLAMINE PHOSPHOTRANS-FERASE ACTIVITIES in GLOMERULAR PARTICLES ISOLATED FROM BOVINE CEREBELLAR CORTEX | Dr. Robert V. Dorman |
| 30. | DYNAMICS OF LARGE SCALE VORTEX STRUCTURES and QUASI-LARGE SCALE STRUCTURES in the WAKE of a SPLITTER PLATE | Dr. Paul H. Chiu |
| 31. | FLOW PHYSICS THROUGH A PIERCED MEMBRANE | Dr. Louis C. Chow |
| 32. | COMPUTATIONAL STUDIES of RAMJET COMBUSTOR FLOW FIELDS | Dr. K.M. Isaac |
| 33. | FREE STREAM TURBULENCE EFFECTS on TURBULENT HEAT and MOMENTUM TRANSFER | Dr. Paavo Sepri |
| 34. | STUDY of COLD REACTING and COMBUSTING FLOWS AROUND BLUFF-BODY COMBUSTORS | Dr. Richard S. Tankin |
| 35. | NUMERICAL MODELING of MULTIPHASE TURBULENT RECIRCULATING FLOWS in SUDDEN-EXPANSION RAMJET GEOMETRY | Dr. Albert Tong |
| 36. | SiC FIBER REINFORCED GLASS-CERAMIC COMPOSITES in the ZIRCONIA/MAGNESIUM ALUMINOSILICATE SYSTEM | Dr. Charles H. Drummond, III |


Volume III


| | | |
|---|---|---|
| 37. | ARYLOXY SUBSTITUTED PYROMELLITIC DIANHYDRIDES | Dr. William F. Feld |
| 38. | ANGLE RESOLVED ION-SCATTERING STUDY of GaAs SURFACES the EXPERIMENT DESIGN | Dr. Thomas P. Graham |

RESEARCH REPORTS
1984 USAF-SCEEE RESEARCH INITIATION PROGRAM

VOLUME I


| REPORT NO. | TITLE | RESEARCH ASSOCIATE |
|---|---|---|
| 14. | USE of BAYESIAN DECISION THEORY in ASSESSING the POTABILITY of GROUND WATER BASED DRINKING WATER SUPPLIES | Dr. Stephan J. Nix |
| 15. | DESIGN of a DIGITAL EW PASSIVE RECEIVER | Dr. William S. McCormick |
| 16. | DUAL CHANNEL FFT SYSTEM ANALYSIS FACILITY for EVALUATING INTEGRATED COMMUNICATION SYSTEMS | Dr. Paul B. Griesacker |
| 17. | FAR-INFRARED ABSORPTION PROFILES for DISTRIBUTED SHALLOW DONORS in GaAs-GaAlAs HETEROSTRUCTURES | Dr. Ronald L. Greene |
| 18. | EFFECT of POLE PIECES on the AXIAL MAGNETIC FIELD in TRAVELING WAVE TUBES | Dr. James D. Patterson |
| 19. | ENHANCING MPC-DSS to INCLUDE AUTOMATIC RESCHEDULING and ADAPTIVE PERFORMANCE MEASURES | Dr. Philip S. Chong |


Volume II


| | | |
|---|---|---|
| 20. | PARAMETRIC STABILITY in COST ESTIMATING MODELS | Dr. Thomas R. Gulledge, Jr. |
| 21. | ANALYSIS of AIR FORCE VEHICLE CONDITION RATINGS FROM HISTORICAL DATA | Dr. Bruce N. Janson |
| 22. | THE DEVELOPMENT of COMPUTATIONAL EFFICIENCIES in CONTINUUM FINITE ELEMENT CODES USING MATRIX DIFFERENCE EQUATIONS | Dr. Harold C. Sorensen |
| 23. | CENTRIFUGE MODEL STUDY and FINITE ELEMENT ANALYSIS OF BURIED CONCRETE BOX CULVERTS | Dr. Yong S. Kim |
| 24. | EFFECTS of FLUID SHIFTS and HYPOVOLEMIA in INDIVIDUALS with DIFFERENT WORKING CAPACITIES WHILE RESTING at a FIVE DEGREE DECLINATION | Dr. William G. Squires |
| 25. | STRUCTURE OF MOLTEN IMIDAZOLIUM CHLORIDE | Dr. R.D. Murphy |

RESEARCH REPORTS
1984 USAF-SCEEE RESEARCH INITIATION PROGRAM

VOLUME III


| REPORT NO. | TITLE | RESEARCH ASSOCIATE |
|---|---|---|
| 39. | THERMAL DECOMPOSTITION STUDIES of SOME SILAHYDROCARBONS | Dr. Vijay K. Gupta |
| 40. | SILANE-TREATED SILICA FILLERS for USE in FULRORSILICONE ELASTOMERS | Dr. Larry M. Ludwick |
| 41. | RAMAN SPECTROSCOPIC STUDIES in EXTRINSIC P-TYPE SILICON | Dr. James Schneider |
| 42. | GRAIN SIZE CONTROL in META STABLE BETA TITANIUM ALLOYS | Dr. Isaac Weiss |
| 43. | THE IMPACT of EXPERT SYSTEMS on PERFORM-ANCE and COGNITIVE STRATEGIES in DIAGNOSTIC INFERENCE | Dr. Sallie E. Gordon |
| 44. | EFFECTS of ENRICHING a COMPUTER-INSTRUCTED PROCEDURALIZED TASK with EXPLANATORY INFORMATION | Dr. Krystine B. Yaworsky |
| 45. | SPECIFICATION SEARCHES in COVARIANCE STRUCTURE MODELING | Dr. Robert MacCallum |
| 46. | A COMPUTATIONAL MODEL of the HUMAN CARDIOPULMONARY SYSTEM | Dr. David Reynolds |
| 47. | DEVELOPMENT of an OPTIMAL TESTING PROTOCOL for the USAF CRITERION TASK SET (CTS) | Dr. Robert E. Schlegel |
| 48. | CONSTRUCTION of CONCEPT-ATOMS | Dr. Yin-Min Wei |
| 49. | DEVELOPMENT of a HIGH-FREQUENCY LUNG VENTILATION MODEL for TESTING UNDER HYPOBARIC CONDITIONS | Dr. Mukul R. Banerjee |
| 50. | BRILLOUIN SPECTROSCOPY in SYSTEMS of BIOLOGICAL SIGNIFICANCE | Dr. Raj M. Krishnan |
| 51. | STABILIZATION of MODE-LOCKED LASERS | Dr. Odis P. McDuff |
| 52. | RAMAN SPECTROSCOPY of CAROTENOIDS and OTHER MOLECULES in UNSTIMULATED and STIMULATED, CULTURED Y-1 MOUSE ADRENAL TUMOR CELLS | Dr. James J. Mrotek |

RESEARCH REPORTS
1984 USAF-SCEEE RESEARCH INITIATION PROGRAM

VOLUME III

| REPORT NO. | TITLE | RESEARCH ASSOCIATE |
|---|---|---|
| 53. | MILITARY FAMILY STRESS and JOB PERFORMANCE | Dr. Lena Wright Myers |
| 54. | Report not received on time. Will be provided when available | Dr. Walter Salter |
| 55. | Report not received on time. Will be provided when available | Dr. William Thomas |
| 56. | EVALUATION and VALIDATION of ADA PROGRAMMING SUPPORT ENVIRONMENTS | Dr. Mike Burlakoff |
| 57. | KINETICS of HOMOGENEOUS GAS PHASE OXIDATION of HYDRAZINE in AIR | Dr. Datta V. Naik |
| 58. | SOFTWARE CORRECTIONS and EXTENSIONS for an INTEGRATED PARTICLE SIZING SYSTEM | Dr. Arthur M. Sterling |

Volume IV

| | | |
|---|---|---|
| 59. | PREDICTING GASEOUS PHASE ADSORPTION of ORGANIC VAPORS by MICROPOROUS ADSORBENTS | Dr. Martin D. Werner |
| 60. | NO TITLE | Dr. Frank P.Colby, Jr. |
| 61. | SOLAR HARD X-RAY BURSTS and TYPE-II RADIO EMISSIONS | Dr. Gabriel Kojoian |
| 62. | THE PASSIVE MODE LOCKING of an $Nd^{3+}$: YAG LASER WITH a TWO-PHOTON ABSORBER | Dr. Nabil M. Lawandy |
| 63. | PLASMA GENERATION and DIAGNOSTICS for IONOSPHERIC PLASMA SIMULATION | Dr. Bernard McIntyre |
| 64. | STUDY of UNIFIED COMPLEX SUSCEPTIBILITY OVER MILLIMETER and INFRARED REGIONS VIA KRAMERS-KRONIG RELATIONSHIP | Dr. Ken Tomiyama |
| 65. | DETERMINATION of PROFESSIONAL LITERATURE RESOURCES RELATING to USAF FAMILY and LIFE STYLE ATTRIBUTES AND ATTITUDES: SUPPORT for INTERPRETING AFSS DATA | Dr. L.W. Buckalew |

RESEARCH REPORTS
1984 USAF-SCEEE RESEARCH INITIATION PROGRAM

VOLUME IV


| REPORT NO. | TITLE | RESEARCH ASSOCIATE |
|---|---|---|
| 66. | DIFFERENT CAREER STAGES: DIFFERENT DEGREES of COMMITMENT | Dr. Jan Leeman Brooks |
| 67. | A MULTILEVEL EXAMINATION of LEADER-SHIP EFFECTS WITH THE ORGANIZATIONAL ASSESSMENT PACKAGE | Dr. Kevin W. Mossholder |
| 68. | FUSE and SURFACE TRACKING SWITCH MODELS for the SHIVA STAR INDUCTIVE PULSE COMPRESSION SYSTEM | Dr. R. Gerald Colclaser |
| 69. | MODELING the THERMAL LAYER | Dr. Arthur A. Kovitz |
| 70. | DIGITAL INTERPOLATION BASED on FUNCTIONAL ITERATION | Dr. Aldy T. Fam |
| 71. | Report not received on time. Will be provided when available. | Dr. Brian Holmes |
| 72. | NUMERICAL CHARACTERIZATION of MICROSTRIP DISCONTINUITIES on THICK SUBSTRATES | Dr. Robert W. Jackson |
| 73. | A SUBOPTIMUM EXTRAPOLATOR for IMPROVED SPECTRAL ESTIMATION | Dr. Lonnie C. Ludeman |
| 74. | HANDLING FACTS with NON-CONSTANT GROUND TERMS in a KNOWLEDGE-BASED SYSTEM | Dr. John T. Minor |
| 75. | STRUCTURAL MODIFICATION to ENHANCE the ACTIVE VIBRATION CONTROL of LARGE SPACE STRUCTURES | Dr. Franklin E. Eastep |
| 76. | CONSISTENT SHEAR LAG MODELING of DAMAGE in UNIDIRECTONAL COMPOSITE LAMINATES | Dr. Walter F. Jones |
| 77. | NUMERICAL SIMULATION of a SUPERSONIC INLET FLOW | Dr. Meng-Sing Liou |
| 78. | RECONFIGURATION of FLIGHT CONTROL SYSTEM of UNMANNED RESEARCH VEHICLE | Dr. Kuldip S. Rattan |
| 79. | ANALYSIS of ARMOR BRACKETRY | Dr. Hemen Ray |

RESEARCH REPORTS
1984 USAF-SCEEE RESEARCH INITIATION PROGRAM

VOLUME IV


| REPORT NO. | TITLE | RESEARCH ASSOCIATE |
|---|---|---|
| 80. | ESTIMATING SPEED of MENTAL ROTAION THROUGH ITEM PACING | Dr. David F. Lohman |
| 81. | DEVELOPMENT and IMPLEMENTATION of COST-EFFECTIVENESS and UTILITY METHODOLOGIES for the AF PERFORMANCE MEASUREMENT PROJECT | Dr. Robert Vance |
| 82. | A SCANNING ELECTRON MICROSCOPICAL STUDY of PERIOSTEUM from SUBHUMAN PRIMATES | Dr. Gwendolyn B. Howze |
| 83. | AN INVESTIGATION of TEST BIAS on the ARMED SERVICES VOCATIONAL APTITUDE BATTERY (ASVAB) FOR MALES and FEMALES. | Dr. Cynthia A. Ford |
| 84. | MODERNIZATION of AGING HIGH-ALTITUDE ENGINE TEST CELLS | Dr. Doyle E. Hasty |
| 85. | EFFECTS of PYRIDOSTIGMINE in the DIET UPON SIMPLE and COMPLEX BEHAVIORS in the MONGOLIAN GERBIL (MERIONES UNGUICULATUS) | Dr. Arthur Harriman |
| 86. | SYNTHESIS of TRIFLATE and CHLORIDE SALTS of ALKYL N,N BIS (2,2,2-TRIFLUOROETHYL) AMINES | Dr. Gloria L. Anderson |
| 87. | LIQUID ROCKET INSTABILITY MODEL DEVELOPMENT | Dr. Charles E. Mitchell |
| 88. | LAMINARIZATION in HIGHLY ACCELERATED FLOW | Dr. Brian Vick |
| 89. | FUTURE TACTICAL AIR CONTROL SYSTEM DATABASE DESIGN | Dr. William Perrizo |

FINAL REPORT

# PARAMETRIC STABILITY IN COST ESTIMATING MODELS

Prepared For

The Air Force Office of Scientific Research
AFOSR/XOT

and submitted to

The Southeastern Center of Electrical Engineering Education

Contract No. F49620-82-C-0035
Subcontract No. 84 RIP 20

Prepared by: Thomas R. Gulledge, Jr.

Academic Rank: Assistant Professor

Department and University: Department of Quantitative Business Analysis
Louisiana State University

Date: September 10, 1985

FOR OFFICIAL USE ONLY

This document contains data which may be considered contractor sensitive. The data may not be disclosed outside the U.S. Government without prior written permission from McDonnell Aircraft Company.

## ABSTRACT

The purpose of this research was twofold. The first part involved extending a previous cost model for the C141 program to include the F4 program. The second part involved checking parameter stability across programs. If key parameters are stable, then the model can be used to predict across programs using the methodology suggested in [21] and [22]. This research suggests that the key parameters are stable across programs.

## INTRODUCTION

In recent years, there has been an increased interest in researching the made-to-order production situation. Made-to-order production is characterized by a contractual agreement that specifies the number of units to be produced in a fixed time horizon. Many early researchers examined this situation [1,2,3,11,14,15,17,18,19], but they did not present definitive functional forms that were suitable for application. The first truly applicable planning models have only appeared recently [7,8,20,21,22,23,24, 25]. In particular, the model presented by Womer and Gulledge conforms with economic theory, conforms with actual cost behavior on made-to-order programs, and the parameters may be estimated from available cost data. This model was developed under the support of the Air Force Business Research Management Center [22], and is currently available on the COPPER IMPACT computer network. A description of the model is included in Appendix A. The rationale for this type of model is simple. Figure 1 delineates two approaches for estimating the total price of an aircraft in a given program. The usual approach allocates overhead in the plant based on direct labor estimates. Since only a part of overhead costs are fixed, a more realistic allocation scheme involves separating total cost into fixed and variable cost, modeling the variable cost, and then distributing the fixed cost to the production units. This methodology is advocated by Balut [6]. In either case, in the absence of current contractor data, some method is needed to model the direct or variable cost profiles so that DoD planners can analyze many programs simultaneously for various procurement quantities. The model that is analyzed in this research can be used to generate either direct or variable cost profiles.

However, model implementation often involves analyzing programs for which data is scarce, so the question that is addressed in this research

# ESTIMATING APPROACHES

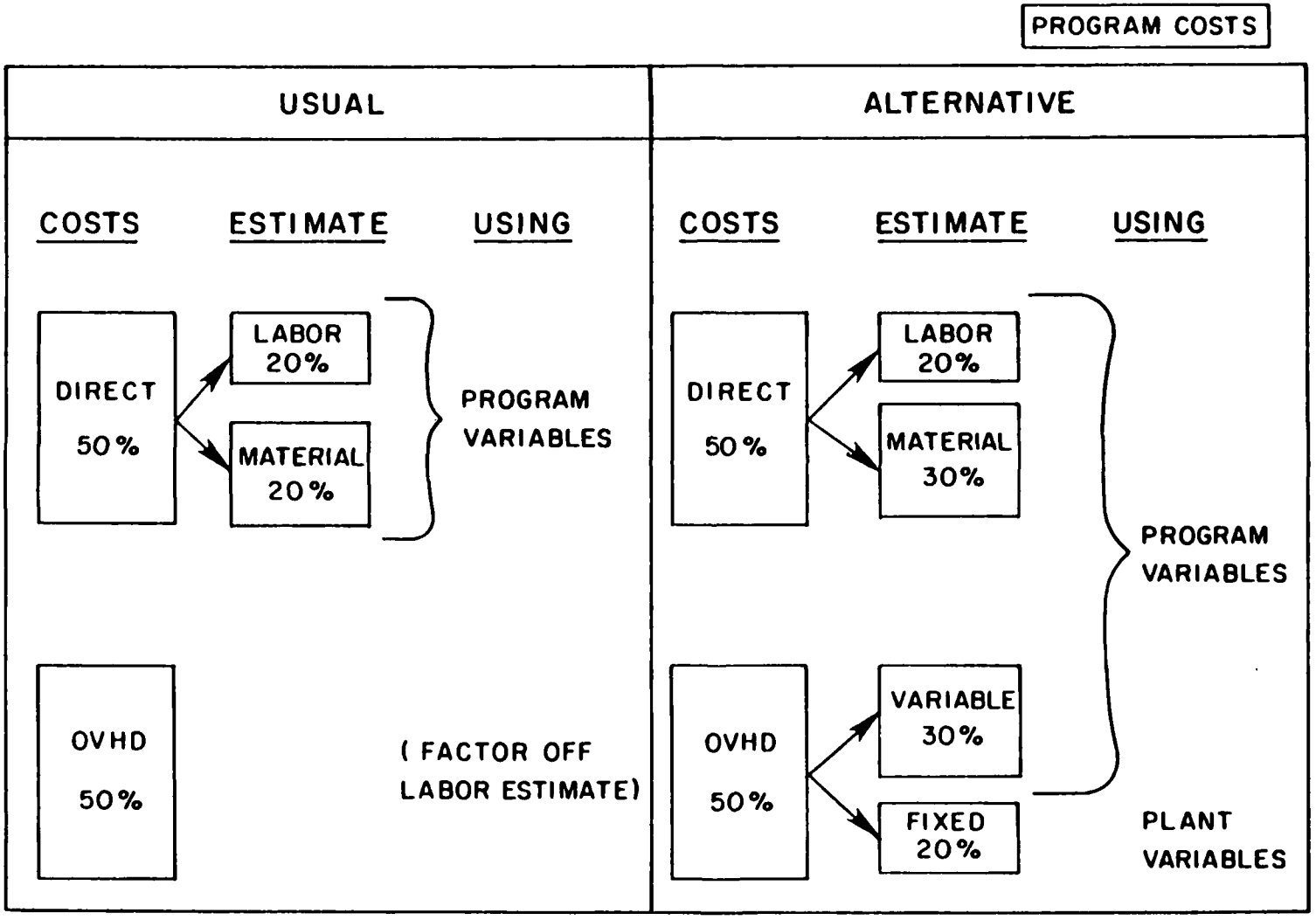



Figure 1. Alternative Estimating Approaches (Source: S.J. Balut).

concerns the application of an existing model to new programs. Of course some quantities are inherently different across programs; e.g., no one expects an F4 aircraft to cost the same as a C141 aircraft. These problems can be handled by rescaling the model as presented in [22]. Learning curve estimates are needed for the model, but these are often also available by analogy with similar programs. The crucial estimate is probably the factor returns parameter. Very little is known about its true value since we have limited experience in estimating this parameter. This research examines, in particular, the stability of this parameter.

During the summer of 1984, Gulledge and Harmon initiated research where the Womer and Gulledge model was applied to the A and B models of the F4 program. The results of this research are promising. It appears that the parameters for the F4 program are surprisingly similar to those for the C141 program. However, because of time limitations the equality hypothesis was not formally tested. This research is documented in Harmon's final report to the Air Force Office of Scientific Research, and it was published as his Masters Thesis at the University of Cincinnati. This work extends that research.

## THE MODEL

The model that is used in the analysis that follows is a modification of the model in Appendix A. It is based on the belief that model specification should be based on economic theory. That is, in lieu of empirical specification, a behavioral assumption is stated, a theoretical model is specified, and an estimable cost function is derived. Consider the following definitions:

$C$ = discounted program cost measured in units of the variable composite resource,

$i$ = the sequence number of an airframe,

$C_i$ = discounted variable cost of a single airframe,

$n$ = the total number of airframes in the production program,

$T_{di}$ = the delivery date for airframe $i$,

$V$ = the average number of airframes in the production process in the facility at time $t$,

$t_{si}$ = the date work begins on airframe $i$; work on all airframes in the same lot is assumed to begin at the lot release date,

$q_i(t)$ = production rate at time $t$ on airframe $i$,

$Q_i(t)$ = cumulative production on airframe $i$ at time $t$,

$x_i(t)$ = rate of resource use at time $t$ on airframe $i$,

$\delta$ = a parameter describing learning prior to airframe $i$,

$\varepsilon$ = a parameter describing learning on airframe $i$,

$\gamma$ = a parameter describing returns to the variable resources,

$\alpha$ = a parameter associated with decreases in labor productivity as an airframe nears completion,

$\nu$ = a parameter describing returns to the length of the production line,

$\rho$ = the discount rate,

$A$ = a constant.

The production function is assumed to be of the following form:

$$q_i(t) = A(i-\tfrac{1}{2})^{\delta} Q_i^{\varepsilon}(t)(t_{di}-t)^{\alpha} x^{1/\gamma}(t) V^{\nu}. \qquad (1)$$

The following parametric assumptions are made:

$$0 \leq \alpha \leq 1, \quad 0 \leq \varepsilon \leq 1, \quad 0 \leq \delta \leq 1, \quad \nu < 0, \quad \gamma > 1.$$

The model is

$$\text{Min } C = \sum_{i=1}^{n} \int_{t_{si}}^{t_{di}} x_i(t) e^{-\rho t} dt$$

$$\text{ST: } q_i(t) = A(i-\tfrac{1}{2})^{\delta} Q_i^{\varepsilon}(t)(t_{di}-t)^{\alpha} x^{1/\gamma}(t) V^{\nu}$$

$$Q_i(t_{di}) = 1 \qquad i = 1, 2, \ldots, n$$

$$Q_i(t_{si}) = 0 \qquad i = 1, 2, \ldots, n.$$

The solution for this model is very similar to that presented in Appendix A. The basic estimable relationship is

$$\sum_{i=k_j}^{n_j} [X_i(T_2) - X_i(T_1)] = \sum_{i=k_j}^{n_j} \beta_0 (i-\tfrac{1}{2})^{-\gamma\delta} \Gamma^{-\gamma} [\rho(t_{di}-t_{si})/(\gamma-1), \beta_1]$$
$$V^{-\gamma\nu}(T_1, T_2)\{\Gamma[\gamma\rho(t_{di}-T_1)/(\gamma-1), \beta_1)]$$
$$-\Gamma[\gamma\rho(t_{di}-T_2)/(\gamma-1), \beta_1]\} \qquad (3)$$

where

$T_1$ = the beginning date of the period of observation,

$T_2$ = the ending date of the period of observation,

$\beta_0$ = a scaling factor,

$\beta_1$ = $\alpha\gamma/(\gamma-1)+1$,

$n_j$ = the last airframe sequence number in the lot,

$k_j$ = the first airframe sequence number in the lot,

and

$\Gamma(,)$ is the incomplete gamma function.

## THE F4 AIRFRAME PROGRAM

The F4 Phantom was developed as a twin-engined two-seat long-range all weather missile fighter for the U.S. Navy. The Phantom operated as a high-performance fighter, attack, and reconnaissance aircraft for the U.S.

Navy, U.S. Air Force, and U.S. Marine Corps. The Phantom was also placed in service with the Royal Navy, Royal Air Force, Royal Australian Air Force, the Imperial Iranian Air Force, the Republic of Korea Air Force, the Israeli Air Force, and the Federal German Luftwaffe. This application examines only the first 10 production job orders of F4A's, F4B's, and F4C's all of which were placed in service by the U.S. armed forces. These aircraft were produced in the late 1950's and the early 1960's. In total, 791 aircraft were analyzed.

The F4 program cost history [13] contains data on primary manufacturing labor hours on blocks of airframes within job orders within contracts. In Harmon's analysis, this data was organized by individual blocks of airframes. The result was 617 observations for estimation. Since some of the data is reported as common hours for airplanes in multiple blocks, it is necessary to assign some hours to the blocks using somewhat arbitrary weighting schemes. For this reason, in this application the data is organized by job order.

The data analysis problems at this stage of the analysis were formidable. Actual delivery schedules were not available, so actual acceptance schedules were used. For all job orders there were small quantities of labor hours that were allocated to the lot after the schedule indicated that all aircraft had been accepted. These were extremely small quantities, but still they were redistributed evenly over all production periods. Also, for the first two job orders there was a 27 month period for which McDonnell Aircraft Company did not report direct manufacturing hours. The model was still initialized at t=0, but the first observation for the estimation does not occur until time period 27.

Job order 720 of contract 62-0383 presented special problems. This job order contained 147 F4-B aircraft. The acceptance schedule separated these aircraft into two groups, 29 and 118 aircraft. The data on labor hours was separated into two groups in the program cost history, but an examination of the data suggested problems associated with the allocation to the 29 aircraft. It appeared that too many hours were allocated to the 29 aircraft, and there was one observation that was an obvious copy and/or accounting error. Therefore the model was estimated using several data configurations.

The model was estimated with the 29 and 118 aircraft reported separately, and with both the outlier included and excluded. The analysis was repeated with the two groups of aircraft combined. By separating the data the number of observations was increased, but the decision was still made to combine the observations and estimate the job order as a complete group of observations. After all data adjustments, the data set contained 236 observations on 791 aircraft. The decision was also made to leave the extreme observation in the data set. This is discussed in a later section of the report.

## ANALYSIS

Since the C141 program was selected as the standard of comparison, it seemed pertinent to reexamine that program. One of the problems noted in that estimation was that the discount rate was apparently not statistically different from zero [22,p.121-122]. After extensive simulations, it was resolved that the nonsignificance was false; i.e., an artifact of the estimation procedure. The problem was caused by a high correlation between the $\rho$ and $\gamma$ estimates. Therefore, $\rho$ was fixed at its estimated value and the parameters were reestimated. The results of this estimation are presented in Table 1.

Table 1

Parameter Estimates and Asymptotic Standard Errors

| Parameter | Estimate | Standard Error |
|---|---|---|
| $\beta_0$ | 1.1460 | .67300 |
| $\beta_1$ | 3.0490 | .4545 |
| $\delta$ | 0.4848 | .06550 |
| $\gamma$ | 1.0016 | .000298 |
| $\nu$ | -0.4408 | .160750 |

These estimates are in close agreement with those presented in [22]. These estimates will be the standard of comparison for the F4 estimates.

The first F4 estimates were made without any consideration of the differences in the three different aircraft models included in the analysis. The results of this estimation are presented in Table 2.

Table 2

Parameter Estimates and Asymptotic Standard Errors

| Parameter | Estimate | Standard Error |
|---|---|---|
| $\beta_0$ | 11.0300 | 1.4100 |
| $\beta_1$ | 4.1730 | 0.5045 |
| $\delta$ | 0.3169 | 0.0432 |
| $\gamma$ | 1.0032 | 0.0004 |
| $\nu$ | 0.2131 | 0.0494 |

These estimates agree with expectations with the exception of the estimate for $\nu$. Our expectations were that our hypothesis about the production cost driver with respect to the average number of units in the plant was probably weak theoretically, and therefore could be difficult to verify empirically. However, a significant positive coefficient was not expected. Our suspicion is that the positive sign follows from not considering the model differences in the 791 aircraft.

To investigate this hypothesis it was necessary to devise a methodology to capture the differences in the models. Intuition suggests that there should be a difference in cost, and this difference should scale the cost function up or down. The first thing that comes to mind is dummy variable regression, but this concept is not clearly defined in nonlinear regression for a model that does not have an additive intervention effect. Since the cost function is shifted in scale by the model changes, the obvious parameter to alter is the scale parameter, $\beta_0$. FORTRAN code was written to incorporate a different scaling factor for each production model of the F4 (The complete code with the data is included in Appendix B). The results of the estimation with the different scaling factors are presented in Table 3.

Table 3

Parameter Estimates and Asymptotic Standard Errors

| Parameter | Estimate | Standard Error |
|---|---|---|
| $\beta_{01}$ | 5.0440 | 0.8795 |
| $\beta_{02}$ | 5.4610 | 1.1850 |
| $\beta_{03}$ | 3.5640 | 0.9835 |
| $\beta_1$ | 4.1470 | 0.4510 |
| $\delta^1$ | 0.3884 | 0.0466 |
| $\gamma$ | 1.0033 | 0.0004 |
| $\nu$ | -0.0003 | 0.0549 |

In this table $\beta_{01}$ is the scaling factor for the F4-A's, $\beta_{02}$ is the scaling factor for the F4-B's, and $\beta_{03}$ is the scaling factor for the F4-C's. These estimates agree with a priori expectations. The estimate for $\nu$ is negative, but not significantly different from zero. We could restrict $\nu$ to be equal to zero, but since the residual variance was computed with 229 degrees of freedom, it would have little impact on the estimates.

One thing worth noting is that the consideration of model differences caused a significant reduction in the error sum of squares. The residual

error variance for the estimation presented in Table 2 was .7773 while that for Table 3 was .6594.

## PREDICTABILITY AND RESIDUAL ANALYSIS

Since the seven parameter model seems more appropriate, all the analysis that follows concerns only that model. A plot of the predicted versus the actual values is presented in Figure 2 (the solid line is the predicted). This plot has several characteristics that should be discussed. First, there is the obvious outlier that was noted earlier in the report. The model was estimated two ways:

1. outlier in the data,
2. outlier corrected.

Surprisingly, the outlier had very little impact on the values of the estimates. Since no real reason could be assigned to the occurrence of the observation, and since the observation had negligible impact, it was left in the data.

The second characteristic concerns the way the model predicts low in the early time periods. The figure is misleading in that it visually assigns equal weight to the early and latter periods. In fact, the early time periods represent a very small number of aircraft relative to the latter time periods. In any case, the model suggested that labor hours be reduced, but McDonnell Aircraft Company correctly chose not to reduce its work force. A shortcoming of this model is that it does not include hiring and firing penalties. This is certainly an area where the research needs to be extended.

The original plan was to analyze the residuals using the methodology presented in [5]; i.e., analyze the projected residuals. For several

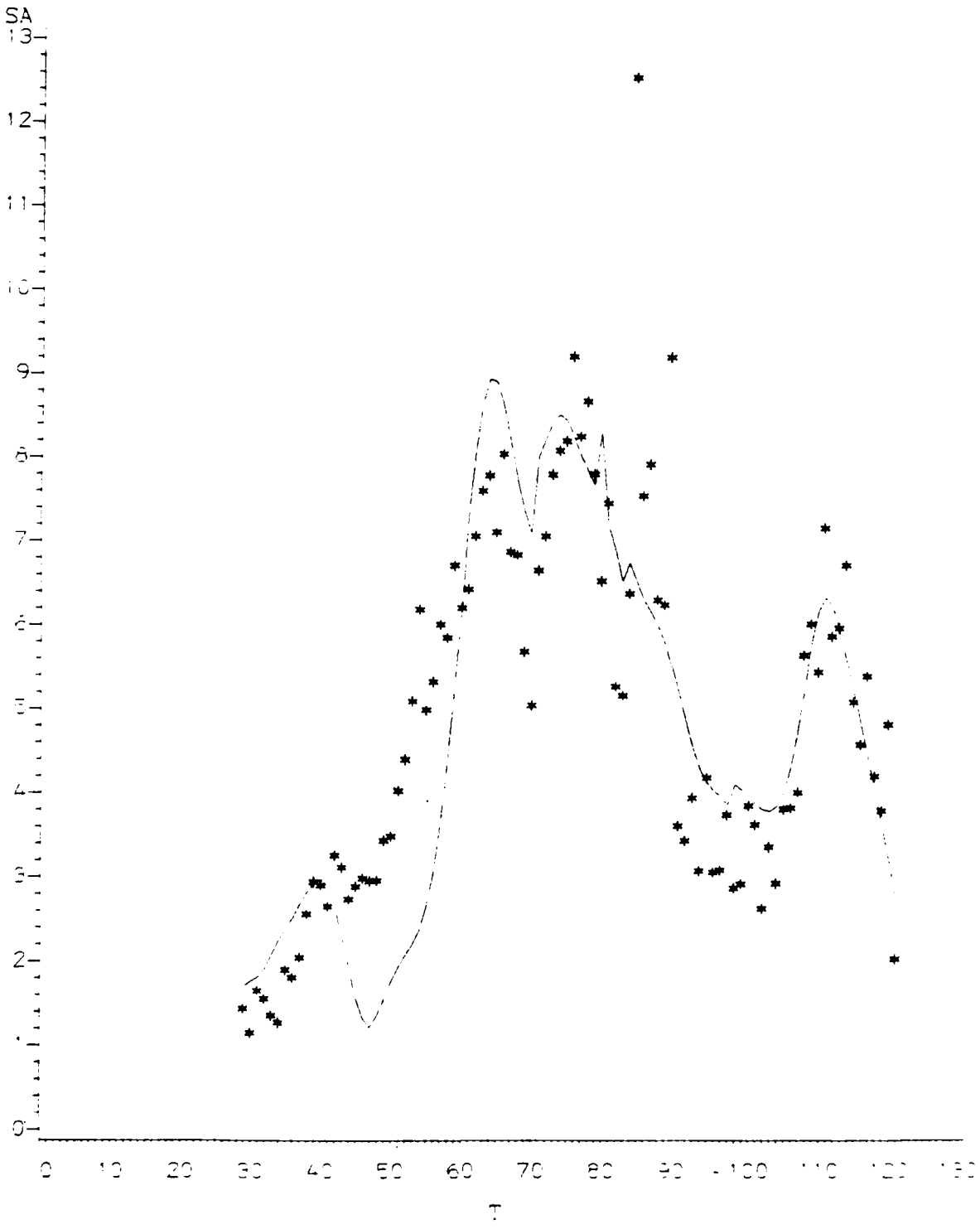

AGGREGATED ACTUALS VERSUS PREDICTE
7 PARAMETER MODEL
SA
13
12
11
10
9
8
7
6
5
4
3
2
1
0
0
10
20
30
40
50
60
70
80
90
100
110
120
130
T

**Figure 2.**

reasons, ordinary residual analysis techniques were used. The first reason is related to an analytical problem, and the second concerns practicality. The analytical problem is that the projected residuals require the second derivative of the sum of squares function. In this case that would be the second derivative of a function that contains incomplete gamma functions. Of course, the derivatives could be obtained numerically, but the programming effort could not be justified in the short research period. The decision to use ordinary residual analysis was reenforced by Cook and Tsai's observation: "further investigation may be needed to determine the best approach in nonlinear regression, but it does appear that the alternative types of residuals will all suffer from the same shortcomings as the ordinary residuals [5, p.9]."

The ordinary residual analysis was straightforward, and the results are predictable from Figure 3. The long string of positive residuals associated with the underprediction is clearly discernible in Figure 3. With the outlier excluded, the latter residuals pass the usual randomness tests, even though there is one short period of time late in the program where the model predicts high. All other things considered, one would have to be satisfied with this model's fit given the nature of the data. That is, this data was not generated within the context of an experimental design; it is actual accounting data.

## COMPARISON WITH THE C141 MODEL

In examining the data in Tables 1 and 2, it is obvious that it makes no sense to compare the scale parameters; $\beta_0$, $\beta_{01}$, $\beta_{02}$, $\beta_{03}$. In fact these parameters are expected a priori to be different. The learning parameter, $\delta$, appears to be different in both models, but the scale parameter, $\gamma$, appears to be very close across models. However, this visual analysis is

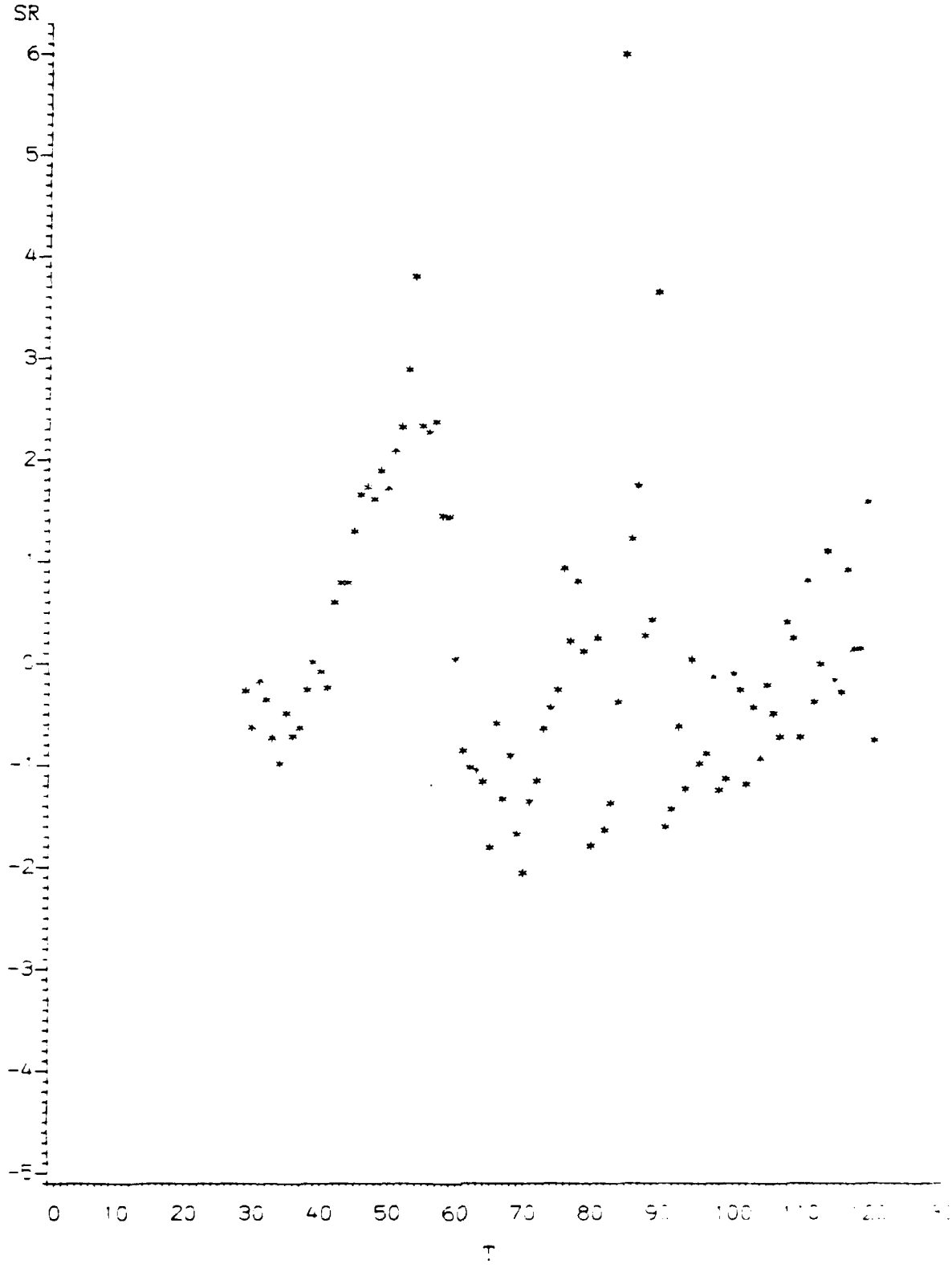

AGGREGATED RESIDUALS
7 PARAMETER MODEL
SR
6
5
4
3
2
1
-1
-2
-3
-4
0
10
20
30
40
50
60
70
80
90
100
T



**Figure 3.**

misleading. If the method of Ratkowsky [16, chapter 7] is used to compare parameters across models, neither the $\gamma$ nor $\delta$ estimates are significantly different. The result with the learning parameter is surprising, but the result with the scale parameter agrees with our earlier research. At this time, no logical reason can be assigned to the statistical equivalence of the learning parameters. This is another area where additional research is desperately needed.

## CONCLUSIONS

The promised deliverables of this research project are summarized below:

1. extend the Womer and Gulledge model to include the F4 airframe program,
2. design a methodology for including model changes within the model,
3. subject the model to extensive diagnostic checking,
4. test for parametric stability across the F4 and C141 programs.

All of the above items have been addressed favorably in the research project. The positiveness of this application reaffirms our commitment to our current research project. Balut, Womer, and Gulledge are currently incorporating this model within a more comprehensive model for repricing aircraft. This model will be used to model variable program costs while other methods will be used to distribute in-plant fixed cost. The proposed model will be a direct competitor with the present multiple regression models that are being used by the Air Force and the Navy.

As a final note, the principal investigator offered to work with Aeronautical Systems Division Personnel in the implementation of this model or a more comprehensive repricing model. That offer is repeated, just for the record.

## REFERENCES


[1] Alchian, A. A. "Costs and Outputs," in the Allocation of Economic Resources edited by M. Abramovitz, Stanford, CA: Stanford University Press, 1959.

[2] Alchian, A. A. "Reliability of Progress Curves in Airframe Production," Econometrica, Vol. 31 (October, 1963), 679-93.

[3] Asher, H. "Cost Quantity Relationships in the Airframe Industry," Rand Report, No. R-291, Santa Monica, CA, 1959.

[4] Assistant Secretary of Defense (Program Analysis and Evaluation) "Acceptance Rates and Tooling Capacity of Selected Military Aircraft" Washington, D.C., 1974.

[5] Cook, R.D. and Chih-Ling Tsai. "Residuals in Nonlinear Regression," To Appear in Biometrika.

[6] Balut, Stephen J. "Redistributing Fixed Overhead Costs," Concepts, Vol. 4 (1981), 63-76.

[7] Gulledge, Thomas R., Jr.; Norman K. Womer; and M. Murat Tarimcilar. "A Discrete Dynamic Optimization Model for Made-to-Order Cost Analysis," Accepted for publication in Decision Sciences, 1984.

[8] Gulledge, Thomas R., Jr.; Norman K. Womer; and James R. Dorroh. Learning and Cost in Airframe Production: A Multiple Output Production Function Approach," Naval Research Logistics Quarterly, Vol. 31 (March, 1984), 67-85.

[9] Gulledge, Thomas R., Jr.; N. K. Womer; and J. D. Camm. "Learning and Production Costs: An Application to A Fighter Airframe Program," Paper Prepared for the DoD/FAI Acquisition Research Symposium, Richmond, Virginia, 1985.

[10] Gulledge, Thomas R., Jr. "Specification and Estimation of Dynamic Cost Functions for Airframe Production Programs," Unpublished Ph.D. thesis. Clemson University, Clemson, South Carolina, 1981.

[11] Hirshleifer, J. "The Firm's Cost Function: A Successful Reconstruction?" Journal of Business, Vol. 35 (July, 1962), 235-255.

[12] Large, J. P., et al. "Production Rate and Production Costs," Rand Report, No. R-1609-PA&E Santa Monica, CA, 1974.

[13] McDonnell Aircraft Company, Department 015. F-4 Cost Data, Report 7290, McDonnell Douglas Corporation, 1972.

[14] Oi, W. Y. "The Neoclassical Foundations of Progress Functions," The Economic Journal, Vol. 77 (September, 1967), 579-594.

[15] Preston, L. E. and E. C. Keachie. "Cost Functions and Progress Functions, "American Economic Review, Vol. 47 (February, 1965), 31-86.

[16] Ratkowsky, D. A. Nonlinear Regression Modeling. New York: Marcel Dekker, 1983.

[17] Rosen, Sherwin. "Learning by Experience as Joint Production," Quarterly Journal of Economics, Vol. 86 (August, 1972), 366-382.

[18] Smith, Larry L. "An Investigation of Changes in Direct Labor Requirements Resulting from Changes in Airframe Production Rate," Unpublished doctoral dissertation, University of Oregon, Eugene, 1976.

[19] Washburn, A. R. "The Effects of Discounting Profits in the Presence of Learning in the Optimization of Production Rates." AIIE Transactions, Vol. 4 (1972), 205-213.

[20] Womer, N. K. and Thomas R. Gulledge, Jr. "A Dynamic Cost Function for an Airframe Production Program," Engineering Costs and Production Economics, Vol. 7 (1983), 213-27.

[21] Womer, N. K. "A Cost Function for Military Airframes," Proceedings of the Ninth Annual DOD/FAI Acquisition Research Symposium, Annapolis, Maryland, 1980.

[22] Womer, N. K. and Thomas R. Gulledge, Jr. Final Report: Cost Functions for Airframe Production Programs. Research project jointly supported by the Air Force Business Research Management Center under Contract F33615-81-K-5116 and the Office of Naval Research under Contract N00014-75-C-0451, 1982.

[23] Womer, N. K. "Estimating Learning Curves from Aggregate Monthly Data," Management Science, Vol. 30 (August, 1984), 982-92.

[24] Womer, N. K. "Learning Curves, Production Rate, and Program Costs," Management Science, Vol. 25 (April, 1979), 312-19.

[25] Womer, N. K. "Some Propositions on Cost Functions," Southern Economic Journal, Vol. 47 (April 1981), 1111-1119.

**Appendix A**

*Engineering Costs and Production Economics* 7 (1983) 213–227
Elsevier Science Publishers B.V., Amsterdam – Printed in The Netherlands



# A DYNAMIC COST FUNCTION FOR AN AIRFRAME PRODUCTION PROGRAM

**Norman K. Womer**

*Clemson University, Clemson, South Caroline, U.S.A.*

**and Thomas R. Gulledge, Jr***

*Louisiana State University, Baton Rouge, Louisiana, U.S.A.*

## ABSTRACT

*This research represents an extension of previous work in the area of estimating military airframe program costs. The effort is unique in that it yields a model of the production process that considers the impact of learning, production rate, and (implicitly) facility size on total program costs. To provide an empirical test of model validity the parameters are estimated for the C141 airframe program. The model's use as a prototype for models of ongoing production programs is illustrated by estimating the cost impact of exogenous changes in the program delivery schedules, e.g. the "crashes" and "stretch-outs" that frequently characterize military airframe production programs.*

## 1. INTRODUCTION

The history of cost estimation in the military airframe industry consists mostly of inaccurate estimates that are insensitive to many production decisions. Congressional concern and the need for better planning capabilities provide the impetus for new research in this area. The approach favored by the Department of Defense is one of estimating parametric cost equations which attempt to model cost as a function of only a few aircraft design and performance characteristics. These models often yield useful planning estimates, but Large and Gillespie [1] show that the models may produce estimates that can be off by as much as 100%. The real limitation of these models is their inability to consider production policy changes which may occur prior to or during the life of a program. To improve upon these techniques, new models must be developed that demonstrate a better understanding of the factors and forces that determine cost.

In contrast to the parametric cost estimating approach, this research involves modeling the production factors that influence cost during an airframe program. In particular, the influences of production rate, learning, and delivery schedules are studied. A modeling effort with this stated purpose requires considerable knowledge of both the planning and production stages in any airflame program.

Before production, a tentative production schedule is developed to help in labor force

*Correspondence to: Thomas R. Gulledge, Jr., Department of Quantitative Business Analysis, 3181 CEBA, Louisiana State University, Baton Rouge, Louisiana 70803, U.S.A.

0167-188X/83/$03.00 © 1983 Elsevier Science Publishers B.V.

planning, tooling, facility needs, ordering of long lead time items, etc. This early period of time is called the planning stage. The tentative production schedule is designed to cover the life of the project, but the formal agreements between the government and the contractor usually cover just one year. The reason is that annual congressional funding, changing national needs, or other exogenous impacts are continually varying throughout the life of the program. This period of changing situations is called the production period. The essence of this research is its ability to capture the relationship between total program cost and both endogenous and exogenous production rate changes during the production period. There is now general agreement that both learning and production rate changes impact total program costs. In the former case, it is usually assumed that production costs fall with cumulative production experience. In the latter, the direction and magnitude of the impact on total cost is less certain. Empirical studies have shown that changes in production rate may be associated with increases, decreases, and no change in total program costs.

## 2. HISTORICAL PERSPECTIVE

Traditional neoclassical economic theory explores the relationship between cost and output rate. With the introduction of Wright's [2] seminal work, a new dimension was added to the empirical study of cost. Wright's paper represents the foundation for many of the progress function studies that are prevalent in the engineering literature. In many instances these early engineering cost studies seemed to contradict neoclassical economic theory. Economic theory purports output rate to be an important determinant of cost, but in most of these engineering studies cost was modeled only as a function of cumulative output. In those studies which considered other variables as determinants of program costs, output rate was often found to be unimportant in predicting cost (see Alchian [3] and Large et al. [4]). There is a remarkable shortage of literature that recognizes the problem or attempts to link the traditional economic approach to the industrial engineering approach. Early researchers such as Asher [5], Alchian [6, 7], Preston and Keachie [8], Oi [9], and Hirshleifer [10] considered the problem in a loose heuristical fashion, and in general their results lacked rigor. Rosen [11] represented the first attempt to solve the problem directly. His work included the theoretical specification of a market structure, the statement of a criterion function, and a straightforward recursive solution to the problem. Although this work is quite noteworthy, it stops short of functional forms sufficiently precise for empirical estimation.

The first real applications oriented integration of the economic and engineering approaches came with the work of Washburn [12] and Womer [13–16]. The present research effort represents the refinement of a more general model [13] for military airframes, so that it may be used to explain the production and cost behavior of a particular airframe project.

## 3. THE C141 PROGRAM

The C141 program produced 284 aircraft during the six-year period from 1962 to 1968. Only one model of the aircraft was produced. Data for this study is drawn from two sources. Orsini [17] reports direct manhours per quarter for each of the 12 lots in the C141 program. He also reports a delivery schedule for the aircraft by month. Orsini attributes these data to the "C141 Financial Management Reports" maintained by the Air Force Plant Representative Office located at the Lockheed – Georgia facility. The schedule of actual aircraft acceptances by month as reported in the OASD (PA&E)

publication "Acceptance Rates and Tooling Capacity for Selected Military Aircraft" [18] was used to check the Orsini delivery data.

These data, like much data on aircraft production, provide labor hours for a period of time (quarterly) and dates and quantities of deliveries. Unfortunately, there is no available information which relates output to the period of time over which labor hours are observed. One approach to this problem, used by Orsini, is to make some assumption about the pace of production on the program and aggregate the quarterly data across lots. In addition to being arbitrary, this appraoch reduces 91 potential observations to 24. Our approach to the data problem is to construct a detailed production model of the aircraft to be delivered in any month. The model is then aggregated to explain the data, rather than the other way around.

Preliminary analysis of the data revealed two additional data problems. First, there were two instances, late in the program, where a small number of labor hours were expended on a production lot after the schedule indicated delivery. This probably is a situation where deliveries were made out of sequence. To remedy this problem the labor hours for the last quarter of lots 9 and 10 were aggregated with those of the previous quarter. This reduced the number of observations by two.

The other problem is that in lots 2 through 8, delivery of the aircraft seems to lag the last expenditure of labor hours by an average of four months. For the other five lots labor hours are expended up to the last month of delivery. To overcome this problem, the deliveries of aircraft in lots 2 through 8 were advanced by four months.

With these adjustments 89 observations on labor hours for 24 quarters for 12 lots were used. These observations, together with the number of aircraft delivered each month, constitute the data for the study.

## 4. PRODUCTION COST DRIVERS

This section discusses four ways in which costs are affected by production decisions. The concept of production cost drivers provides the rationale for the model which follows. That is, the model contains components that attempt to capture the effects of each of the production cost drivers.

The first production cost driver is the concept of learning by doing. The idea is that as the cumulative number of airframes produced becomes larger, the unit costs (or at least labor hours) decrease. This component is the only production cost driver that is sometimes included in parametric cost estimates. It is commonly discussed in both the industrial engineering and the operations research literature, but the learning curve is only rarely mentioned in the production and cost related economics literature.

To introduce the concept of learning and the other production cost drivers the analysis follows Washburn [12] by adopting the concept of a production line as a frame of reference. Learning by doing affects cost by influencing efficiency at each position on the production line. That is, as the number of airframes passing each position on the line increases, yielding more experience, the efficiency at the position increases, thus lowering labor cost. Notice that this process implies that at any point in time the experience on the production line may vary dramatically, e.g. in the C141 program as much as two years elapsed between the lot release date and delivery of an airframe.

The second production cost driver is a different learning effect. Over time learning how to produce more efficiently may take place due to events other than experience at a position on the production line. For example, early in a production program labor hours may be spent to learn how to produce more efficiently. Later in the program this may result in increased efficiency independent

of experience at a point on a line. If this is the case, positions at the end of the line work more efficiently on the same airframe than positions at the beginning of the line. This effect may be related to experience at other locations on the production line. That is, a position late in the production line may benefit from the experience of earlier positions, thus work at later positions proceeds more efficiently than work at early positions on the same airframe.

A third production cost driver is the speed of the production line. Unless there is a learning compensation, increasing the speed of the line is expected to require more labor at each position on the line. Furthermore, due to diminishing returns, the additional labor required is expected to be more than in proportion to the increase in speed. Anyone who has observed the activity around an airframe during production recognizes the likelihood of diminishing returns to labor on that airframe.

The fourth cost driver is the length of the production line. One way to increase delivery rate is to increase the number of positions on the production line, reducing the amount of work to be done at each position, and increasing the total amount of work accomplished per unit of time. If alternative length production lines are planned, this driver may not be a source of variation in unit costs. However, if the length of the line is changed on short notice, unit costs may be affected. For example, increasing the length of the line may result in crowded facilities, overused tools, and inefficient use of other fixed resources. These factors adversely affect the efficiency of production and may result in increased unit costs. This last effect involves an interaction among the airframes that are in the facility at the same point in time. The model of production described in the next section represents an attempt to capture these effects in an estimable analytic model.

## 5. THE MODEL

The model augments a homogeneous production function with a learning hypothesis. The discounted cost of production is minimized subject to a production function constraint, and the optimal time path of resource use is derived. Since factor prices are assumed to be constant over the relevant time period, cost is measured in the units of the variable resoruce. The variables used in the analysis are:

$i$ = an index for a batch of airframes in the same lot ($j$) all of which are to be delivered at time $t_{ij}$,

$n_j$ = the number of batches in lot $j$,

$m$ = the total number of lots in the production program,

$D_{ij}$ = the number of airframes in batch $i$ of lot $j$,

$E_{ij}$ = a measure of experience prior to the midpoint of batch $i$, i.e.,

$$E_{ij} = \sum_{k=1}^{j-1} \sum_{h=1}^{n_j} D_{hk} + \sum_{h=1}^{i-1} D_{hj} + \tfrac{1}{2} D_{ij} ,$$

$V$ = the number of airframes in the production process in the facility at time $t$,

$t_j$ = date work begins for all the batches of lot $j$,

$t_{ij}$ = date work ends for batch $i$ of lot $j$,

$q_{ij}(t)$ = production rate at time $t$ on batch $i$ of lot $j$,

$Q_{ij}(t)$ = cumulative production on batch $i$ of lot $j$ at time $t$, i.e.,

$$\int_{t_j}^{t} q_{ij}(\tau)\, d\tau ,$$

$x_{ij}(t)$ = rate of resource use at time $t$ on batch $i$ of lot $j$,

$\delta$ = a parameter describing learning prior to batch $i$,

$e$ = a parameter describing learning on batch $i$.

$\gamma$ = a parameter describing returns to the variable resources,

$\alpha$ = a parameter associated with decreases in labor productivity as a batch of airplanes nears completion,

$\nu$ = a parameter describing returns to the length of the production line,

$\eta$ = a parameter describing returns to the size of the batch,

$\rho$ = the discount rate,

$C$ = discounted variable program cost,

$C'$ = discounted variable costs for a single batch of airframes.

The production function is assumed to be of the following form:

$$q_{ij}(t) = A V^{\nu} D_{ij}^{\eta} E_{ij}^{\delta} Q_{ij}^{\epsilon}(t)\,(t_{ij} - t)^{\alpha} x_{ij}^{1/\gamma}(t)\,, \qquad (1)$$

where $A$ is a constant. The input $x$ is assumed to be a composite of many inputs whose use rate is variable throughout the production period.

This production function includes the production cost drivers described in the previous section, it conforms to economic production theory, and it also accommodates the fact that the nature of work along the production line changes from position to position. On the other hand, it is still a very simple function, and it can only be expected to describe such a complex production process with some error.

The term $E_{ij}^{\delta}$ describes learning by doing in producing a given batch $i$ in lot $j$. A priori, $\delta$ is expected to be between 0 and 1. The terms $Q_{ij}^{\epsilon}(t)$ and $(t_{ij} - \tau)^{\alpha}$ represent attempts to describe learning that occurs over time during the process of producing batch $i$ of lot $j$. These terms also admit the possibility that the nature of work changes as the airframe moves down the production line. In particular, it is assumed that as the batch delivery date is approached it is more difficult to substitute labor for time in the production process. Both $\epsilon$ and $\alpha$ are expected to be between 0 and 1. Still one more term $t^h$ would have been useful to include in the production function to model this effect. Unfortunately, a solution has not been found for the resulting control problem if time is included in this way. Elsewhere [19], specifications of this type have been dealt with extensively.

The terms $D_{ij}^{\eta}$ and $X_{ij}^{1/\gamma}(t)$ together capture the effect of the speed of the production line. The $D_{ij}^{\eta}$ term represents the number of airframes in the batch (the number of positions on the line occupied by the batch), while $X_{ij}^{1/\gamma}(t)$ captures the effect of applying more labor to any given number of positions. The expectation is for $\eta$ to be between 0 and 1 and $\gamma$ to be greater than 1. Below, it is seen that the effect of learning during the batch and the effect of the number of airframes in a batch cannot be separated with our data.

Finally the term $V^{\nu}$ is intended to capture the effect of assembling alternative numbers of airframes in the same facility. It is assumed that assembling more airframes in the same facility results in a slight decrease in efficiency ($\nu$ is negative and small).

Although the objective of the firm is a function of the wording of the contract, one goal of most contracts is to induce the firm to minimize discounted cost. The problem may be stated as:

$$\text{Min } C = \sum_{j=1}^{m} \sum_{i=1}^{n_j} \int_{t_j}^{t_{ij}} x_{ij}(t) e^{-\rho t}\, dt \qquad (2)$$

subject to

$$q_{ij}(t) = A V^{\nu} D_{ij}^{\eta} E_{ij}^{\delta} Q_{ij}^{\epsilon}(t)\,(t_{ij} - t)^{\alpha} x_{ij}^{1/\gamma}(t)\,,$$

$i = 1, 2, \ldots, n_j$
$j = 1, 2, \ldots, m$

$$Q_{ij}(t_{ij}) = D_{ij}\,, \qquad i = 1, 2, \ldots, n_j$$
$$Q_{ij}(t_j) = 0. \qquad j = 1, 2, \ldots, m$$

Since total cost is monotone nondecreasing and the subproblems are additive, the solution can be obtained by minimizing each of the subproblems. The problem may then be stated as:

$$\text{Min } C' = \int_{t_j}^{t_{ij}} x_{ij}(t)e^{-\rho t}dt \tag{3}$$

subject to

$$q_{ij}(t) = A V^{\nu} D_{ij}^{\eta} E_{ij}^{\delta} Q_{ij}^{\epsilon}(t)\,(t_{ij} - t)^{\alpha} x_{ij}^{1/\gamma}(t)\,,$$
$$Q_{ij}(t_{ij}) = D_{ij}\,,$$
$$Q_{ij}(t_j) = 0.$$

This problem is an optimal control problem which may be solved directly by minimizing the Hamiltonian function. However, the problem can easily be transformed into the problem of Lagrange, which can be solved using classical variational techniques. At this point the redundant $ij$ subscripts are dropped. Solving the constraint for $x(t)$ yields

$$x(t) = q^{\gamma}(t)A^{-\gamma}V^{-\nu\gamma}D^{-\eta\gamma}E^{-\delta\gamma}Q^{-\epsilon\gamma}(t)(t_{ij} - t)^{-\alpha\gamma} \tag{4}$$

A transformation is desired that yields one state variable and one control variable, the control variable being the time rate of change of the state variable. Let

$$Z(t) = A^{-1}V^{-\nu}D^{-\eta}E^{-\delta}Q^{1-\epsilon}(t)/(1 - \epsilon)\,. \tag{5}$$

This implies that

$$z(t) = A^{-1}V^{-\nu}D^{-\eta}E^{-\delta}Q^{-\epsilon}(t)q(t)\,. \tag{6}$$

For the transformed problem $Z(t)$ is the new state variable, and its time derivative, $z(t)$, is the control variable. Formation of the new objective functional requires absorbing the constraint. After using (4) and (6), an expression is obtained for $x(t)$ in terms of the new control variable, i.e.

$$x(t) = z^{\gamma}(t)\,(t_{ij} - t)^{-\gamma\alpha}\,. \tag{7}$$

After substituting into the objective functional and setting the boundary conditions, the following transformed problem is obtained:

$$\text{Min } C' = \int_{t_j}^{t_{ij}} z^{\gamma}(t)(t_{ij} - t)^{-\gamma\alpha}e^{-\rho t}dt = \int_{t_j}^{t_{ij}} I(z,t)dt \tag{8}$$

subject to

$$Z(0) = 0,$$
$$Z(t_{ij}) = A^{-1}V^{-\nu}D^{1-\epsilon-\eta}E^{-\delta}/(1 - \epsilon).$$

Since the intermediate function, $I$, does not depend explicitly on the state variable, the Euler equation is

$$\frac{\partial I}{\partial z} = \gamma z^{\gamma-1}(t)\,(t_{ij} - t)^{-\gamma\alpha}e^{-\rho t} = K_0\,. \tag{9}$$

After solving the Euler equation, the following expression is obtained for optimal $z(t)$:

$$z(t) = K_1(t_{ij} - t)^{\gamma\alpha/(\gamma-1)}e^{\rho t/(\gamma-1)}\,. \tag{10}$$

This also provides a solution for the optimum time path of resource usage, i.e.

$$x(t) = K_1^{\gamma}(t_{ij} - t)^{\alpha\gamma/(\gamma-1)}e^{\gamma\rho t/(\gamma-1)}\,. \tag{11}$$

This optimal solution to the problem is only of transient significance since the value of the constant $K_1$ is unknown. What is needed is an optimal expression for $x(t)$ that is in terms of the variables and parameters of the original problem. To obtain the constant, notice that

$$Z(t) = \int K_1(t_{ij} - \tau)^{\alpha\gamma/(\gamma-1)}e^{\rho\tau/(\gamma-1)}d\tau + K_2\,. \tag{12}$$

Let $\omega = \rho(t_{ij} - \tau)/(\gamma - 1)$, then

$$Z(u) = \int K_1[(\gamma-1)/\rho]^{\alpha\gamma/(\gamma-1)}\omega^{\alpha\gamma/(\gamma-1)} e^{-\omega + \rho t_{ij}/(\gamma-1)}J\,d\omega + K_2 \tag{13}$$

where $J$ is the Jacobian of the transformation. Now, $u(t_j) = \rho(t_{ij} - t)/(\gamma - 1)$ and $u(t_{ij}) = 0$, so choosing 0 and $u$ as the limits of integration the appropriate integral is

$$Z(u) = K_3 \int_0^u \omega^{\alpha\gamma/(\gamma-1)}e^{-\omega}\,d\omega + K_4\,. \tag{14}$$

Integration of this expression yields

$$Z(u) = K_3\,\Gamma[u, \alpha\gamma/(\gamma - 1) + 1] + K_4 \tag{15}$$

where $\Gamma$ is the incomplete gamma function. To satisfy the initial condition that $Z[u(t_j)] = 0$, let

$$Z(u) = -K_3\{\Gamma[\rho(t_{ij} - t_j)/(\gamma - 1), \alpha\gamma/(\gamma - 1)+1] - \Gamma[u, \alpha\gamma/(\gamma - 1)+1]\}. \quad (16)$$

Also let

$$-K_3 = A^{-1}V^{-\nu}E^{-\delta}D^{1-\epsilon-\eta}(1-\epsilon)^{-1}\Gamma^{-1}[\rho(t_{ij} - t_j)/(\gamma - 1), \alpha\gamma/(\gamma - 1)+1], \quad (17)$$

then this implies that $Z$ also satisfies the final condition, $Z[u(t_{ij})] = A^{-1}V^{-\nu}D^{1-\epsilon-\eta}E^{-\delta}/(1-\epsilon)$. Also, note that

$$z(t) = \frac{dZ(u)}{dt} = K_3\,[\rho(t_{ij} - t)/(\gamma - 1)]^{\alpha\gamma/(\gamma - 1)} e^{-\rho(t_{ij} - t)/(\gamma - 1)}\,[-\rho/(\gamma - 1)]. \quad (18)$$

After substituting for $K_3$, the following expression is obtained:

$$z(t) = A^{-1}V^{-\nu}E^{-\delta}D^{1-\epsilon-\eta}(1-\epsilon)^{-1}\Gamma^{-1}\left[\frac{\rho(t_{ij} - t_j)}{(\gamma - 1)}, \frac{\alpha\gamma}{\gamma - 1} + 1\right] \times \left(\frac{\rho(t_{ij} - t)}{(\gamma - 1)}\right)^{\alpha\gamma/(\gamma - 1)} e^{-\rho(t_{ij} - t)/(\gamma - 1)} \left(\frac{\rho}{\gamma - 1}\right). \quad (19)$$

This formulation for optimum $z(t)$ along with (10) provides a direct solution for $K_1$. Substitution for $K_1$ in (11) yields the following optimum time path of resource use:

$$x_{ij}(t) = BV^{-\gamma\nu}E_{ij}^{-\gamma\delta}D_{ij}^{\gamma(1-\epsilon-\eta)}\Gamma^{-\gamma}[\rho(t_{ij} - t)/(\gamma - 1), \alpha\gamma/(\gamma - 1)+1] \times (t_{ij} - t)^{\alpha\gamma/(\gamma - 1)}e^{-\gamma\rho(t_{ij} - t)/(\gamma - 1)}, \quad (20)$$

and $\Gamma[\rho(t_{ij} - t_j)/(\gamma - 1), \alpha\gamma/(\gamma - 1) + 1]$ is the incomplete gamma function. This is the optimal time path for resource use on any batch of airframes.

Since the data presented in the C141 study are quarterly data, the quantity of interest is the total resource use over a quarterly period. If $T_k$ and $T_l$ represent the beginning and ending dates for the quarterly period for some batch $i$, the appropriate expression is:

$$X(T_k) - X(T_l) = \int_{T_l}^{T_k} x(t)\,dt, \quad (21)$$

and using (11) the integral is

$$X(T_k) - X(T_l) = \int_{T_l}^{T_k} K_1^{\gamma}(t_{ij} - t)^{\alpha\gamma/(\gamma - 1)} e^{\gamma\rho t/(\gamma - 1)}\,dt. \quad (22)$$

Let $y = \gamma\rho(t_{ij} - t)/(\gamma - 1)$, then

$$X(T_k) - X(T_l) = -K_1^{\gamma}\int_{\gamma\rho(t_{ij} - T_l)/(\gamma - 1)}^{\gamma\rho(t_{ij} - T_k)/(\gamma - 1)} [(\gamma - 1)/\gamma\rho]^{\alpha\gamma/(\gamma - 1)} \times y^{\alpha\gamma/(\gamma - 1)}e^{-y} e^{\gamma\rho t_{ij}/(\gamma - 1)[-(\gamma - 1)/\gamma\rho]}\,dy. \quad (23)$$

Notice that this is a form of the incomplete gamma function. Integration of (23) yields the following expression for resources used during the interval:

$$X(T_k) - X(T_l) = K_1^{\gamma}\left[\left(\frac{\gamma - 1}{\gamma\rho}\right)^{\alpha\gamma/(\gamma - 1)+1}\right]e^{\gamma\rho t_{ij}/(\gamma - 1)} \times \{\Gamma[\gamma\rho(t_{ij} - T_l)/(\gamma - 1), \alpha\gamma/(\gamma - 1) + 1] - \Gamma[\gamma\rho(t_{ij} - T_k)/(\gamma - 1), \alpha\gamma/(\gamma - 1) + 1]\}. \quad (24)$$

Substituting for $K_1$ and performing the necessary algebra leaves an expression that represents the optimum amount of resource use over an interval of time for an individual batch of airframes, i.e.

$$X_{ij}(T_k) - X_{ij}(T_l) = AV^{-\nu}E_{ij}^{-\delta\gamma}D_{ij}^{\gamma(1-\epsilon-\eta)}(1-\epsilon)^{\gamma} \times \Gamma^{-\gamma}[\rho(t_{ij} - t_j)/(\gamma - 1),$$

$$\alpha\gamma/(\gamma-1)+1]\left(\frac{\rho}{\gamma-1}\right)^{\gamma(\alpha+1)-1}$$

$$\times\ \gamma^{-\alpha\gamma/(\gamma-1)-1}\ \{\Gamma[\gamma\rho(t_{ij}-T_l)/(\gamma-1),$$

$$\alpha\gamma/(\gamma-1)+1]\ -$$

$$\Gamma[\gamma\rho(t_{ij}-T_k)/(\gamma-1),\alpha\gamma/(\gamma-1)+1]\}. \tag{25}$$

Since the data presented by Orsini [17] are quarterly data, the quantity of interest is the total resource use over a quarterly period. If $T_k$ and $T_l$ represent the beginning and ending dates for the quarterly period for some batch $i$, the appropriate expression is:

$$X(T_k)-X(T_l)=\int_{T_l}^{T_k} x(t)\ dt, \tag{26}$$

and using (4) the integral is

$$X_{ij}(T_k)-X_{ij}(T_l)=B'E_{ij}^{-\delta\gamma}D_{ij}^{\gamma(1-\epsilon-\eta)}$$

$$\times\ \Gamma^{-\gamma}[\rho(t_{ij}-t_j)/(\gamma-1),\alpha\gamma/(\gamma-1)+1]\,V^{-\gamma\nu}$$

$$\times\ \{\Gamma[\gamma\rho(t_{ij}-T_l)/(\gamma-1),\alpha\gamma/(\gamma-1)+1]\ -$$

$$\Gamma[\gamma\rho(t_{ij}-T_k)/(\gamma-1),\alpha\gamma/(\gamma-1)+1]\}. \tag{27}$$

Because of the nature of the data it is impossible to observe the quantity on the left side of eqn. (27). What is observable is direct manhours per lot. This means that the observed quantity is

$$\sum_{i=1}^{n_j}\ [X_{ij}(T_k)-X_{ij}(T_l)] \tag{28}$$

where there are $n_j$ batches in lot $j$. For this study, the sum is the observed values of labor hours that are reported in Orsini's data set. This sum and the number of aircraft delivered each month are the variables that are used to test empirically the validity of the model.

## 6. EMPIRICAL RESULTS

To explore the applicability of the theoretical specification, the parameters in (27) are estimated using the C141 data. Let $\beta_0 = \beta'$ and $\beta_1 = \alpha\gamma/(\gamma-1)+1$. Furthermore, since $\epsilon$ and $\eta$ cannot be independently estimated let $\lambda = \epsilon + \eta$. The model may be restated as:

$$\sum_{i=1}^{n_j} X_{ij}(t_k)-X_{ij}(T_l)=\sum_{i=1}^{n_j}\beta_0 E_{ij}^{-\gamma\delta}D_{ij}^{\gamma(1-\lambda)}V^{\nu}$$

$$\times\ \Gamma^{-\gamma}[\rho(t_{ij}-t_j)/(\gamma-1),\beta_1]$$

$$\times\ \{\Gamma[\gamma\rho(t_{ij}-T_l)/(\gamma-1),\beta_1]$$

$$-\Gamma[\gamma\rho(t_{ij}-T_k)/(\gamma-1),\beta_1]\}. \tag{29}$$

Since the monthly delivery dates for each batch within each lot are known, it is possible to estimate the parameters in (29) using nonlinear least squares.

**TABLE 1**

**Parameter estimates and asymptotic standard errors**

| Parameters | Estimates | Standard error |
|---|---|---|
| $\beta_0$ | 1.251 | 0.9 |
| $\beta_1$ | 3.280 | 0.73 |
| $\delta$ | 0.2809 | 0.11 |
| $\lambda$ | 0.2924 | 0.25 |
| $\gamma$ | 1.022 | 0.009 |
| $\nu$ | −0.34 | 0.17 |
| $\rho$ | 0.0289 | 0.008 |

The results of this regression are presented in Table 1. It does not appear that all of the parameters are significantly different from zero, i.e. the asymptotic standard errors for $\beta_0$, $\epsilon$ and $\nu$ seem large, but restricting these parameters to 0 generates large increases in the residual sum of squares. All of the signs of the estimated parameters agree with a priori expectations. In particular, notice that the value of $\gamma$ is significantly greater than 1, indicating that the production function does exhibit decreasing returns to the variable factor. The estimated value of the learning parameter is also consistent with a priori expectations. A $\delta$ value of 0.28 is consistent with an 83% learning curve.

In addition, the estimate for $\beta_1$ has a most

interesting interpretation with respect to the optimal time path of resource use. Notice in (29) that $\beta_1$ is the argument of a gamma function. A gamma function with parameter $\beta_1 = 3.280$ generates a time path for resource use that is consistent with our knowledge of labor productivity patterns for "lots" of airframes. In most cases resource use rises at an increasing rate from time $t_j$ to an inflection point, after which it continues to rise, but at a decreasing rate. Eventually resource usage reaches a maximum and declines thereafter. Simulated time paths of resource use rate and cumulative resource usage for fixed $V$ are presented in Figs 1 and 2. The eventual decline in resource use rate is attributed to a decrease in the marginal product of labor as the delivery date for a batch approaches. That is, before components of the airframe are assembled, adding more labor easily increases the production rate; but after most of the components are assembled, crowding makes it more difficult to increase production rate on a batch by adding more labor. In fact, the rate of labor use on the batch must fall to provide the optimal production rate. In addition, the time-consuming testing procedures that precede delivery may not be compressed by more labor. Therefore, there is a period of time near the end of a project where labor cost is significantly reduced.

As observed this functional form generates a time path of resource use for a batch of airframes that conforms to a better understanding of the production process. However, it is possible to observe the time path of resource use for the entire program. Figure 3 illustrates the predicted time path of resource use for the program and the actual resources used. While the model fits the data well ($R^2 = 0.69$), the model shows more variation with time than exhibited by the data. This is particularly true for the period between quarter 14 and quarter 19 where the model predicts somewhat fewer manhours than used. Perhaps this is because the model included no penalty for hiring or firing costs. Therefore, even though the model predicts that the workforce should decline and then rise again, the company (correctly)

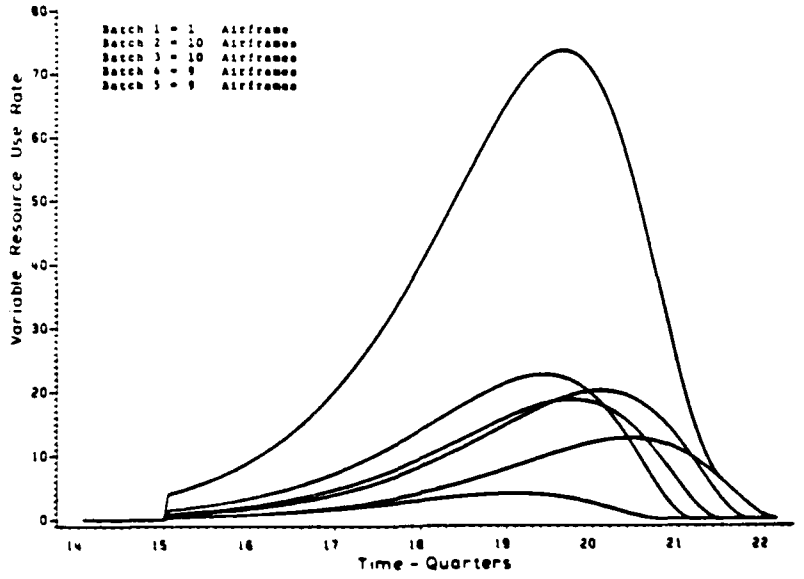



Fig. 1. Simulated optimal time path of resource use rate for a given lot of airframes and the 5 batches within the lot.

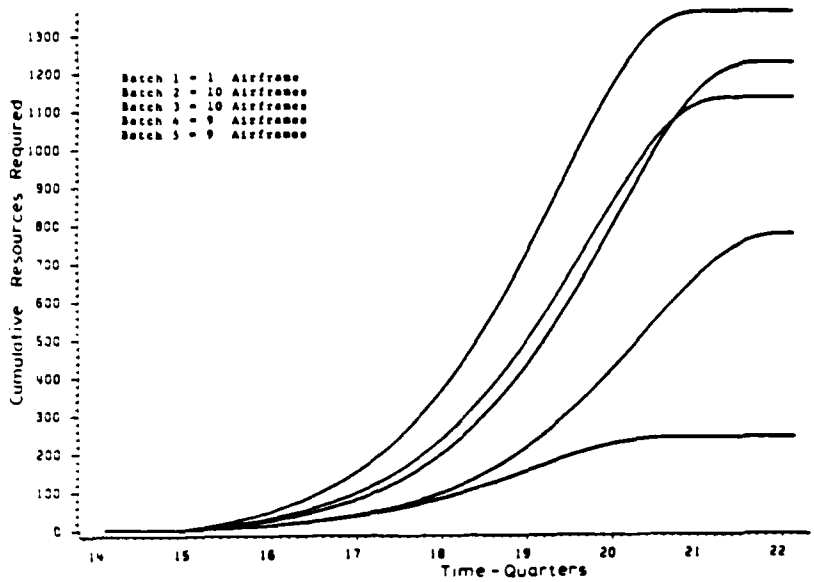



Fig. 2. Simulated optimal time path of cumulative resource usage for a given lot of airframes.

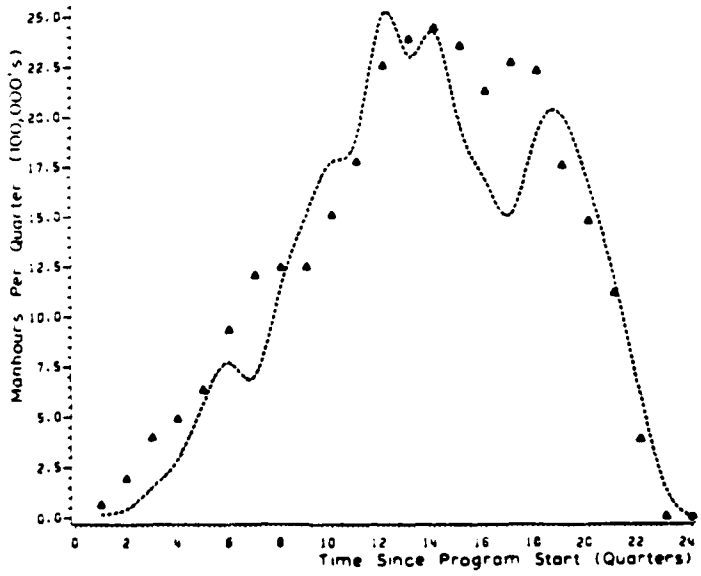



Fig. 3. Predicted time path of resource use for the C141 program and the actual resources used (Δ = actual).

chose to maintain a higher workforce over the relatively brief slump. If this is true, then a more appropriate delivery schedule should have permitted substantial savings on the program. These questions are investigated further in the next section.

## 7. SENSITIVITY ANALYSES

To illustrate further the sensitivity of the model to changes in the delivery schedule the time path of resource use is plotted (eqn. (20) summed over $i$ and $j$) for several hypothetical alternative delivery schedulles. Each of the alternatives represents a small discrete change to the actual delivery schedules.

The first alternative, Fig. 4, has the first airframe in the program delivered one month later. This causes the rate of resource use to be lowered early in the program, but it is increased as the new delivery date is approached. The net effect is a small increase in predicted program cost. This delivery schedule change operates by adding one month to the first batch, increasing $t_{11}$, by increasing $(t_{11} - t_1)$, the time from program start until first delivery; and by increasing $V$ during quarters 5 and 6. The effect of delaying this delivery seems to be to increase the learning applicable to the first unit by providing more time prior to delivery. This effect is offset by the fact that $V$ increases (the number of positions on the line increases). The net effect is a slight rise in program cost and a delay in program costs (and benefits).

The second sensitivity analysis illustrates a shortcoming of combining the airframes into batches. In this instance, the effect of delivering the last airframe one month early is examined. This results in reducing the time to work on the last airframe and the time for learning. It also results in an increase in $V$ during the period when the last airframe was completed. These changes all argue for slightly higher program costs for this alternative. However, if the last airframe is combined with the previous batch of airframes, this also has the effect of reducing the number of batches and increasing the size of the augmented batch. This last effect tends to offset the others, resulting in a very slight

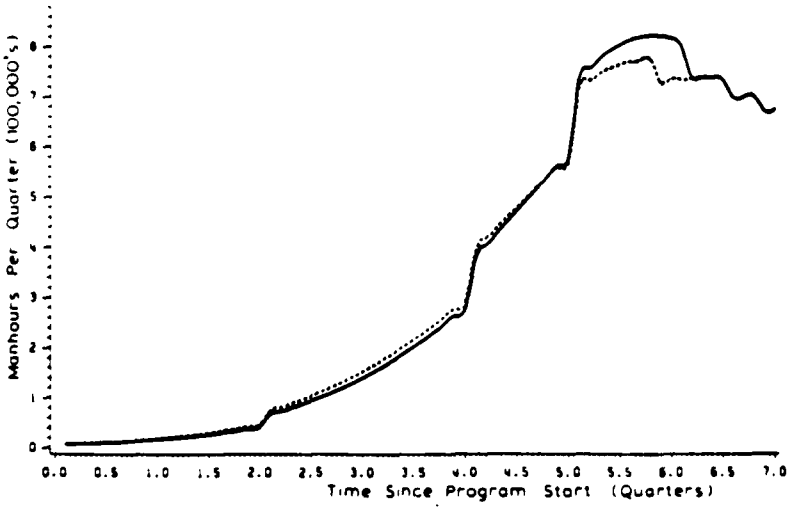



Fig. 4. Predicted time path of resource use when the first airframe is delivered one month late (solid line represents the delayed delivery).




Fig. 5. Predicted time path of resource use when the first airframe is delivered one month early (solid line is altered delivery).

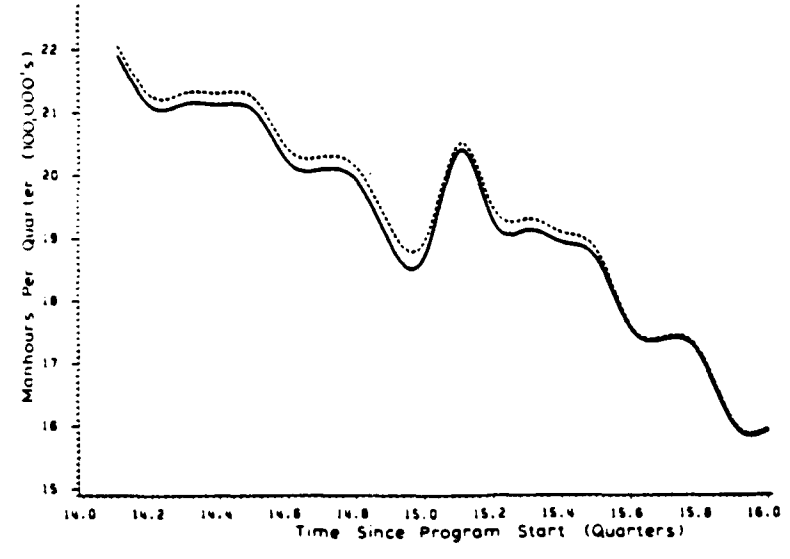



Fig. 6. Predicted time path of resource use when the delivery rate is altered during the program (solid line is altered delivery).

uniform decrease in the time path of resource use. This is illustrated in Fig. 5.

Next, consider the advancement of the delivery of one airframe in the middle of the program. Between the middle of quarter 14 and the middle of quarter 15 deliveries on the C141 program increased from seven per month to nine per month. Only in the first month of quarter 15 were eight air frames delivered. Fig. 6 illustrates the effect of increasing this period where the delivery rate was eight to an entire quarter. Here deliveries are increased by one in the last month of quarter 14 and decreased by one in the second month of quarter 15. This decreases the time available for learning, but it also decreases $V$. The net effect is a uniform decrease in the time path of resource use on the program.

The next simulation considers the effect of changing lot release dates on the program. In Fig. 7 the lot release date for the last lot is delayed until the start of quarter 16. In addition to preventing expenditures on the last lot in quarter 15, $V$ is lower during that quarter, reducing cost for other lots. Also this effectively shifts the work on the last lot to periods of time when $V$ is lower, but these effects are partly offset by the compressed schedule for the last lot. The effect of these changes is a reduction of the time path in quarter 15 coupled with a very small increase in expenditures starting in quarter 16. The net effect of these changes is to reduce program cost.

Finally the effect of an early start on a lot in the middle of the program is considered. In Fig. 8 the release date for lot 7 is moved from the beginning of quarter 11 to the beginning of quarter 10. This increases resource use in quarter 10 by permitting work to take place on lot 7, and resource use is also increased for the other lots because $V$ is higher. Later in the program resource use is decreased due to the lengthening of lot 7. The net effect of these changes is to raise program costs.




Fig. 7. Predicted time path of resource use when the lot release date is altered during the program (solid line is altered time path).

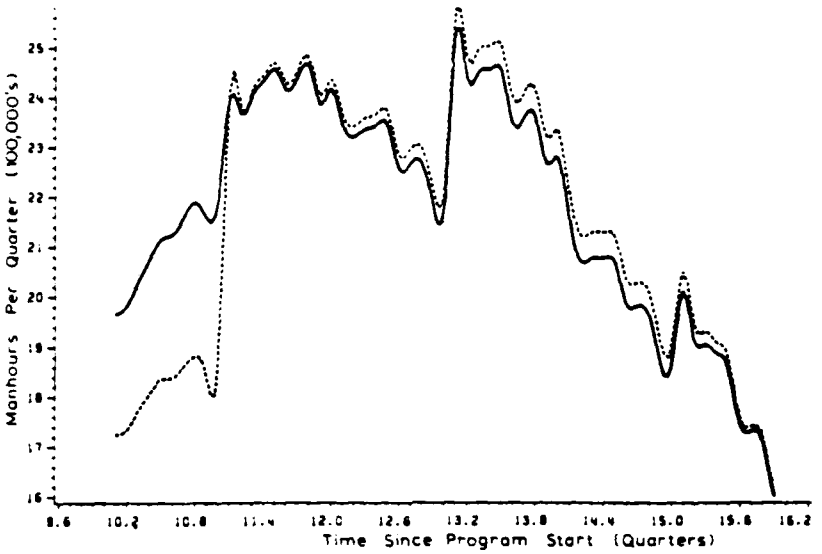



Fig. 8. Predicted time path when a lot in the middle of the program is started early (solid line is altered value).

## 8. SUMMARY

The objective of this study was to provide a model of airframe production that is well grounded in theory, estimated from actual data and sensitive to exogenous delivery schedule effects. In this paper the rationale for such a model is provided, the functional form is derived, the estimation procedure and the parameter estimates are reported, and the sensitivity of the estimated model to delivery schedule changes is examined.

The sensitivity analyses clearly imply that alternative delivery schedules would have resulted in lower costs for the C141 program. In addition, some of these schedules are associated with airframes being delivered to the customer sooner. If so, it is important to ask, "Why were these lower cost and higher benefit schedules not chosen?"

Certainly one possibility is that the decision makers have better insight than the model as to what is best. There are several areas in which flaws in the model may be important. One is the lack of consideration of hiring and firing costs, and a second is the incomplete interaction among the batches that is permitted in the model. To elaborate, the model permits work on a batch neither to start later than the lot release date nor to end sooner than the delivery date. From the point of view of the single batch, neither of these events would ever be optimal; but, if starting late or ending early could affect $V$, then from the point of view of the program, they may be attractive. As it is now, $V$ is completely determined by the lot release dates and delivery schedule. Of course, more and better data might permit more accurate and different estimated parameters.

On the other hand, it is also possible that with a tool which permits decision makers to grasp the program implications of funding cuts, stretchouts, and of altered delivery schedules more optimal decisions will be made. Management science is based on possibilities such as these.

## ACKNOWLEDGEMENTS

This work was supported in part by the Office of Naval Research under Contract N00014-75-C-0451 and by the Air Force Business Research Management Center under Contract F33615-81-K-5116.

## REFERENCES


1 Large, J.P. and Gillespie, K.M.S., 1977. A Critique of Airframe Cost Models, R-2194-AF, The Rand Corporation, Santa Monica, California.

2 Wright, T.P., 1936. Factors affecting the cost of airplanes, Journal of Aeronautical Science, 3: 122–128.

3 Alchian, A.A., 1963. Reliability of progress curves in airframe production, Econometrica, 31: 679–693.

4 Large, J.P., Koffmayer, K. and Kontrovich, F., 1974. Production Rate and Production Costs, R-1609-PA&E, The Rand Corporation, Santa Monica, California.

5 Asher, H., 1956. Cost–Quantity Relationships in the Airframe Industry, R-291, The Rand Corporation, Santa Monica, California.

6 Alchian, A.A., 1959. Costs and outputs, in Abramovitz, M. (ed.), The Allocation of Economic Resources, Stanford University Press, Stanford, California, 23–40.

7 Alchian, A.A. and Allen, W.R., 1964. Exchange and Production Theory in Use, Wadsworth, Belmont, California.

8 Preston, L.E. and Keachie, E.C., 1974. Cost functions and progress functions: an integration, American Economic Review, 54: 100–106.

9 Oi, W.Y., 1967. The neoclassical foundations of progress functions, Economic Journal, 77: 579–594.

10 Hirshleifer, J., 1962. The firm's cost function: a successful reconstruction, Journal of Business, 35: 235–255.

11 Rosen, S., 1972. Learning by experience as joint production, Quarterly Journal of Economics, 86: 366–382.

12 Washburn, A.R., 1972. The effects of discounting profits in the presence of learning in the optimization of production rates, AIIE Transactions, 4: 205–213.

13 Womer, N.K., 1979. Learning curves, production rate, and program costs, Management Science, 25: 312–319.

14 Womer, N.K., 1980. A cost function for military airframes, Occasional Paper Series, Department of Industrial Management, Clemson University, Clemson, South Carolina.

15 Womer, N.K., 1981a. Learning curves and monthly data, Occasional Paper Series, Department of Industrial Management, Clemson University, Clemson, South Carolina.

16 Womer, N.K., 1981b. Some propositions on cost functions, Southern Economic Journal, 47: 1111–1119.

17 Orsini, J.A., 1970. An analysis of theoretical and empirical advances in learning curve concepts since 1966, Master's Thesis, Air Force Institute of Technology, Wright–Patterson AFB, Ohio.

18 Assistant Secretary of Defence (Program and Evaluation), 1974. Acceptance Rates and Tooling Capacity for Selected Military Aircraft, Washington, D.C.

19 Gulledge, T.R., Jr., 1981. Specification and estimation of dynamic cost functions for airframe production programs, Ph.D. Thesis, Clemson University, Clemson, South Carolina.



*(Received October 18, 1982; accepted December 30, 1982)*

Appendix B

```
// EXEC FORTGCLG,TIME=20
//FORT.SYSIN DD *
C
C
C                                *******
C ****************************** MAIN ***************************************
C *                              *******                                      *
C *                                                                           *
C *                                                                           *
C *                                                                           *
C *  NONLINEAR LEAST SQUARES .  THIS PROGRAM CALCULATES NONLINEAR LEAST*
C *  SQUARES ESTIMATES OF THE REVISED MODEL BY HOMER AND GULLEDGE          *
C *  USING MARQUARDTS COMPROMISE.                                         *
C *                                                                           *
C *                                                                           *
C *                                                                           *
C *                                                                           *
C * NOTE..THIS PROGRAM IS SET UP TO TAKE A MAXIMUM OF 500 OBSERVATIONS *
C *   (TIME PERIODS OR LOTS) AND 1000 INDIVIDUAL DELIVERY TIMES (STORED*
C *   IN ARRAY DT).                                                       *
C *   IF MORE THAN THIS IS REQUIRED DIMENSION STATEMENTS MUST BE          *
C *   CHANGED IN BOTH THE MAIN AND SUBROUTINE 'MODEL'                     *
C *                                                                           *
C *                                                                           *
C *    A DESCRIPTION OF THE VARIABLES IS GIVEN IN THE SUBROUTINES.        *
C *                                                                           *
C ***************************************************************************
C
      EXTERNAL MODEL
      COMMON /AREA1/ X(500,6)
      COMMON /AREA2/ DT(1000)
      COMMON /AREA3/ LN(500)
      DIMENSION Y(500),TH(7),DIFF(7),SCRAT(3000),SIGNS(7),DIFZ(7)
      REAL SIGNS/4*1.0,0.0,2*1.0/,DIFF/3*.01,.001,.01,2*.01/,
     &DIFZ/3*.01,.001,.01,2*.01/
      INTEGER START1,QUIT1
      NPROB=1
      NP=7
      ESP1=.00001
      ESP2=.005
      MIT=200.
      FLAM=.01
      FNU=10.
      READ(5,*)NOB,TH(1),TH(2),TH(3),TH(4),TH(5),TH(6),TH(7),NUMLOT
      L1=0
      DO 20 J=1,NUMLOT
      READ(5,*)LTQ
      DO 21 L=1,LTQ
      L1=L1+1
      READ(5,*)Y(L1),X(L1,1),X(L1,2),X(L1,3),X(L1,4),X(L1,5),X(L1,6)
     &,LN(L1)
21    CONTINUE
      START1=X(L1,2)+1
      QUIT1=X(L1,4)
      DO 100 K=START1,QUIT1
      READ(5,*)DT(K)
100   CONTINUE
20    CONTINUE
      CALL UNHAUS(NPROB,MODEL,NOB,Y,NP,TH,DIFF,SIGNS,ESP1,ESP2,MIT,FLAM,
     &FNU,SCRAT)
```

```
      STOP
      END
C
C
C
      SUBROUTINE MODEL(NPROB,TH,F,NOB,NP)
C
C THIS IS A USER SUPPLIED SUBROUTINE THAT EVALUATES A GIVEN FUNCTION
C (F) FOR DIFFERENT VALUES OF THE PARAMETERS (TH).
C
C     NPROB = PROBLEM NUMBER-SCALAR
C     TH    = PARAMETER VALUES-DIMENSIONED AT TH(NP)
C     F     = PREDICTED VALUES FROM REGRESSION EQUATION,
C             DIMENSIONED AT F(NOB)
C     NOB   = SAMPLE SIZE-SCALAR
C     NP    = NUMBER OF UNKNOWN PARAMETERS-SCALAR
C     X     = IND. VARIABLE MATRIX-DIMENSIONED AT X(NOB,NP)
C     X(I,1) = END OF TIME PERIOD (OBSERVATION I)
C     X(I,2) = NO. DELIVERED PRIOR TO THIS LOT
C     X(I,3) = PERIOD WORK BEGAN ON THE LOT
C     X(I,4) = SEQUENCE NUMBER OF THE LAST AIRFRAME IN THE LOT
C     X(I,5) = AVG. NO. IN HOUSE DURING THE PERIOD
C     X(I,6) = START OF THE PERIOD
C      TH(1) = B0.........THE CONSTANT TERM
C      TH(2) = DELTA......THE LEARNING PARAMETER
C      TH(3) = B1.........ALPHA/(GAMMA-1.) +1.
C      TH(4) = GAMMA-1....RETURNS TO SCALE (LESS 1. SO THAT GAMMA >1)
C      TH(5) = RO.........THE DISCOUNT PARAMETER
C      TH(6) = H..........THE PARAMETER ASSOCIATED WITH AVG. IN HOUSE
C              (ALL TH(I) ARE RESTRICTED TO THE SIGN OF INITIALIZATION)
C      NUMLOT = NUMBER OF LOTS
C      LTQ    = NUMBER OF OBSERVATIONS (TIME PERIODS) FOR A LOT
C      LN     = AN ARRAY THAT DEFINES THE LOT NUMBERS
C
      COMMON /AREA1/ X(500,6)
      COMMON /AREA2/ DT(1000)
      COMMON /AREA3/ LN(500)
      DIMENSION F(1),X(1),TH(1)
      INTEGER START,QUIT
      RHO=.001706
      R2=RHO/TH(4)
      IF(R2.LT.0.) PRINT 19
19    FORMAT('ERROR.....B2<0')
      DO 910 I=1,NOB
      IF(LN(I).EQ.10)K=7
      IF(LN(I).EQ.9)K=6
      IF(LN(I).LE.8)K=7
      IF(LN(I).LE.6)K=6
      IF(LN(I).LE.2)K=1
      CT=X(I,1)
      QIN=X(I,2)+.5
      U=0.
      START=X(I,2)+1
      QUIT=X(I,4)
      TO=X(I,3)
      V=X(I,5)
      CT1=X(I,6)
      DO 920 J1=START,QUIT
      TM=DT(J1)
      IF(DT(J1).LE.0.)PRINT 17
```

```
17      FORMAT('ERROR..... A IT IS <=0')
        IF(CT1.GE.TM)GO TO 920
        IF(CT.LE.TM) GO TO 925
        BT=(TM-CT1)*(TH(4)+1.)*B2
        E4=GAMI(TH(3),BT)
        GO TO 930
925     BT=(TM-CT)*(TH(4)+1.)*B2
        BT1=BT+(TH(4)+1.)*B2
        E4=GAMI(TH(3),BT1)-GAMI(TH(3),BT)
930     EQ=Q1N**(-TH(2)*(TH(4)+1.))
        EV=V**(-(TH(4)+1.)*TH(5))
        F2=B2*(TM-T0)
        IF(F2.LT.0.0)PRINT 18
18      FORMAT('ERROR.............F2 <0')
        E=GAMI(TH(3),F2)
        E=E**(-(TH(4)+1.))
        U=U+TH(K)*EQ*E*E4*EV
920     Q1N=Q1N+1.
        F(I)=U
910     CONTINUE
        RETURN
        END
C
C
C
      SUBROUTINE UNHAUS(NPROB,MODEL,NOB,Y,NP,TH,DIFF,SIGNS,EPS1,EPS2,
     @MIT,FLAM,FNU,SCRAT)
C
C                    *************************
C ****************** MARQUARDTS COMPROMISE ******************************
C                    *************************
C
C MARQUARDT, DONALD W.  'AN ALGORITHM FOR LEAST SQUARES ESTIMATION OF
C    NONLINEAR PARAMETERS.' J. SOC. INDUST. APPL. MATH. VOL. XI
C    (JUNE, 1963), 431-34.
C
C        LAMBDA LARGE=STEEPEST DESCENT---SHIFT TO LINEARIZATION
C
C        NPROB   =PROBLEM NUMBER-SCALAR
C        MODEL   =NAME OF SUBROUTINE--MUST DECLARE AS EXTERNAL IN MAIN
C                 LINE-USER SUPPLIED SUBROUTINE TO COMPUTE THE FITTED
C                 VALUES FROM THE REGRESSION EQUATION.
C        NOB     = NUMBER OF OBSERVATIONS-SCALAR
C        Y(I)    =VECTOR OF OBSERVATIONS ON THE DEPENDENT VARIABLE-
C                 DIMENSIONED AT Y(NOB)
C        NP      =NUMBER OF UNKNOWN PARAMETERS-SCALAR
C        TH      =VECTOR OF PARAMETERS-DIMENSIONED AT TH(NP)
C        DIFF    =RELATIVE STEP SIZE IN NUMERICAL DIFFERENTIATION-SAY .01
C                  DIMENSIONED AT DIFF(NP)
C        SIGN    = 0. FOR UNRESTRICTED SEARCH,
C                = 1.  SIGN OF I TH PARAMETER MUST NOT CHANGE-
C                  DIMENSIONED AT SIGN(NP)
C        ESP1    = TERMINATION VALUE OF SUM OF SQUARES S(THETA)-
C                  SAY 10.**-07-SCALAR
C        ESP2    = TERMINATION BASED ON PARAMETERS-SAY 10.**-03
C        MIT     = MAXIMUM NO OF ITERATIONS-SCALAR
C        FLAM    = LAMBDA EQUALS APPROX 0.01-SCALAR
C        FNU     = GAMMA EQUALS APPROX 10.-SCALAR
C        SCRAT   = STORAGE ARRAY.  MAIN LINE DIMENSION GE
C                  5*NP+NP**2+2*NOB+NOB*NP
```

```
C
      DIMENSION SCRAT(1),TH(1),Y(1),DIFF(1),SIGNS(1)
      IA=1
      IB=IA+NP
      IC=IB+NP
      ID=IC+NP
      IE=ID+NP
      IF=IE+NP
      IG=IF+NOB
      IH=IG+NOB
      II=IH+NP*NOB
      IJ=IH
      CALL HAUS59(NPROB,MODEL,NOB,Y,NP,TH,DIFF,SIGNS,EPS1,EPS2,MIT
     @,FLAM,FNU,SCRAT(IA),SCRAT(IB),SCRAT(IC),SCRAT(ID),
     @SCRAT(IE),SCRAT(IF),SCRAT(IG),SCRAT(IH),SCRAT(II),
     @SCRAT(IJ))
      RETURN
      END
C
C
C
      SUBROUTINE HAUS59(NPROB,MODEL,NBO,Y,NQ,TH,DIFZ,SIGNS,EP1S,EP2S,
     @MIT,FLAM,FNU,Q,P,E,PHI,TB,F,R,A,D,DELZ)
C
C     NPROB = VARIABLE INDICATING THE PROBLEM NUMBER
C     MODEL = SUBROUTINE WHICH COMPUTES THE VALUES OF THE MODEL
C     NOB   = NUMBER OF OBSERVATIONS
C     Y     = VECTOR OF OBSERVED FUNCTION VALUES
C     NP    = NUMBER OF UNKNOWN PARAMETERS.
C             NP IS BIGGER THAN 1 AND SMALLER THAN 11 IN THE PROGRAM.
C     TH    = VECTOR OF PARAMETER VALUES
C     DIFF  = VECTOR OF PERTURBATIONS IN TH. IT IS USED TO CACULATE
C             THE NUMERICAL DERIVATIVES OF THE FUNCTION.
C     SIGNS = VECTOR INDICATING THE EXISTENCE OF A PRIORI SIGN
C             RESTRICTIONS.
C     EPS1  = RELATIVE CHANGE OF THE FUNCTION CRITERION
C     EPS2  = PARAMETER CONVERGENCE CRITERION
C     MIT   = MAXIMUM NUMBER OF ITERATIONS
C     FLAM  = STARTING VALUE FOR LAMDA
C     FNU   = VALUE OF NU TO REDUCE LAMDA
C     SCRAT = TEMPORARY STORAGE FOR USE BY UWHAUS
C
C     DIMENSION TH(NQ),DIFZ(NQ),SIGNS(NQ),Y(NBO)
C     DIMENSION Q(NQ),P(NQ),E(NBO),PHI(NQ),TB(NQ)
C     DIMENSION F(NBO),R(NBO)
C     DIMENSION A(NQ,NQ),D(NQ,NQ),DELZ(NBO,NQ)
C
      COMMON /AREA1/X(500,6)
      COMMON /AREA3/LN(500)
      DIMENSION TH(1),DIFZ(1),SIGNS(1),Y(1),Q(1),P(1),E(1)
     @PHI(1),TB(1),F(1),R(1),A(1),D(1),DELZ(1),SUMQ(100),SUMP(100)
      NP=NQ
      NPROB=NPROB
      NOB=NBO
      EPS1=EP1S
      EPS2=EP2S
      NPSQ=NP*NP
      NSCRAC=5*NP+NPSQ+2*NOB+NP*NOB
      PRINT 1000,NPROB,NOB,NP,NSCRAC
      PRINT 1001
```

```
      CALL GASS60(1,NP,TH,TEMP,TEMP)
      PRINT 1002
      CALL GASS60(1,NP,DIFZ,TEMP,TEMP)
      IF(MIN0(NP-1,50-NP,NOB-NP,MIT-1,999-MIT))99,15,15
 15   IF(FNU-1.0)99,99,16
 16   CONTINUE
      DO 19 I=1,NP
      TEMP=ABS(DIFZ(I))
      IF(AMIN1(1.0-TEMP,ABS(TH(I))))99,99,19
19    CONTINUE
      GA=FLAM
      MIT=1
      LAGS=0
      IF(EPS1)5,70,70
5     EPS1=0
70    SSQ=0
      CALL MODEL(NPROB,TH,F,NOB,NP)
C
C ********************     R(I)=Y(I)-F(TH)      **************************
C ******************** INITIAL SUM OF SQUARES **************************
C
      DO 90 I=1,NOB
      R(I)=Y(I)-F(I)
90    SSQ=SSQ+R(I)*R(I)
      PRINT 1003,SSQ
C
C ************************ BEGIN ITERATION *******************************
C
100   GA=GA/FNU
      INTCNT=0
      PRINT 1004,MIT
101   JS=1-NOB
      DO 130 J=1,NP
      TEMP=TH(J)
      P(J)=DIFZ(J)*TH(J)
      TH(J)=TH(J)+P(J)
      Q(J)=0
      JS=JS+NOB
      CALL MODEL(NPROB,TH,DELZ(JS),NOB,NP)
      IJ=JS-1
C
C *********** NUMERICAL EVALUATIONS OF DERIVATIVES ********************
C
      DO 120 I=1,NOB
      IJ=IJ+1
      DELZ(IJ)=DELZ(IJ)-F(I)
120   Q(J)=Q(J)+DELZ(IJ)*R(I)
      Q(J)=Q(J)/P(J)
C
C ********************* Q=XT*R (STEEPEST DESCENT) ***********************
C
130   TH(J)=TEMP
      IF(LAGS)131,131,414
131   DO 150 I=1,NP
      DO 151 J=1,I
      SUM=0.
      KJ=NOB*(J-1)
      KI=NOB*(I-1)
      DO 160 K=1,NOB
      KI=KI+1
```

```
      KJ=KJ+1
160   SUM=SUM+DELZ(KI)*DELZ(KJ)
      TEMP=SUM/(P(I)*P(J))
      JI=J+NP*(I-1)
      D(JI)=TEMP
      IJ=I+NP*(J-1)
151   D(IJ)=TEMP
150   E(I)=SQRT(D(JI))
666   CONTINUE
      DO 153 I=1,NP
      IJ=I-NP
C
C ******* SCALING OF XTRANSPOSE X MATRIX TO D-1/2XTRANS X D-1/2  *******
C *******      SCALING OF XTRANS R  TO D-1/2 XTRANS R           *******
C *******       ADD LAMDA I TO SCALED XTRANS X MATRIX           *******
C
      DO 153 J=1,I
      IJ=IJ+NP
      A(IJ)=D(IJ)/(E(I)*E(J))
      JI=J+NP*(I-1)
153   A(JI)=A(IJ)
C
C ********************** A= SCALED MOMENT MATRIX ************************
C
      II=-NP
      DO 155 I=1,NP
      P(I)=Q(I)/E(I)
      PHI(I)=P(I)
      II=NP+1+II
155   A(II)=A(II)+GA
      I=1
C
C ** CALCULATE THE DETERMINANT AND INVERSE OF D-1/2 XTRANS X D-1/2+LA **
C
       CALL MATIN(A,NP,P,I,DET)
C
C ********************** P/E=CORRECTION VECTOR **************************
C
      STEP=1.0
      SUM1=0.
      SUM2=0.
      SUM3=0.
      DO 231 I=1,NP
      SUM1=P(I)*PHI(I)+SUM1
      SUM2=P(I)*P(I)+SUM2
      SUM3= PHI(I)*PHI(I)+SUM3
231   PHI(I)=P(I)
      TEMP=SUM1/SQRT(SUM2*SUM3)
      TEMP=AMIN1(TEMP,1.0)
      TEMP=57.295*ACOS(TEMP)
      PRINT 1041,DET,TEMP
170   DO 220 I=1,NP
      P(I)=PHI(I)*STEP/E(I)
      TB(I)=TB(I)+P(I)
220   CONTINUE
      PRINT 7000
7000  FORMAT(///' TEST POINT PARAMETER VALUES')
      PRINT 2006,(TB(I),I=1,NP)
      DO 221 I=1,NP
      IF(SIGNS(I)) 221,221,222
```

```
222   IF(SIGN(1.0,TH(I))*SIGN(1.0,TB(I)))663,221,221
221   CONTINUE
      SUMB=0.
      CALL MODEL(NPROB,TB,F,NOB,NP)
      DO 230 I=1,NOB
      R(I)=Y(I)-F(I)
230   SUMB=SUMB+R(I)*R(I)
      PRINT 1043,SUMB
      IF(SUMB-(1.0+EPS1)*SSQ)662,662,663
C
C ******* IF ANGLE LESS THAN 90 DEG THEN DECREASE STEP SIZE ************
C
663   IF(AMIN1(TEMP-90.0,GA)) 665,605,664
665   STEP=STEP/2.0
      INTCNT=INTCNT+1
      IF(INTCNT-36) 170,2700,2700
664   GA=GA*FNU
      INTCNT=INTCNT+1
      IF(INTCNT-36) 666,2700,2700
662   PRINT 1007
      DO 669 I=1,NP
669   TH(I)=TB(I)
      CALL GASS60(1,NP,TH,TEMP,TEMP)
      PRINT 1040,GA,SUMB
      IF(EPS2) 229,229,225
 229  IF(EPS1) 270,270,265
C
C ***************** PARAMETER CONVERGENCE CRITERION *********************
C
225   DO 240 I=1,NP
      IF(ABS(P(I))/(1.E-20+ABS(TH(I)))-EPS2) 240,240,241
241   IF(EPS1) 270,270,265
240   CONTINUE
      PRINT 1009,EPS2
      GO TO 280
C
C *************** SUM OF SQUARES CONVERGENCE CRITERION ****************
C
265   IF(ABS(SUMB-SSQ)-EPS1*SSQ)266,266,270
266   PRINT 1010,EPS1
      GO TO 280
270   SSQ=SUMB
      NIT=NIT+1
      IF(NIT-MIT) 100,100,280
2700  PRINT 2710
2710  FORMAT (// 50H0*** THE SUM OF SQUARES CANNOT BE REDUCED TO THE
     @// 55H SUM SQUARES AT THE END OF THE LAST ITERATION - STOP /     )
C
C  ************************ END ITERATION ******************************
C
C ************** FINAL FUNCTION VALUES AND RESIDUALS ********************
C
280   PRINT 1036
      PRINT 1036
      PRINT 1011
      PRINT 1036
      DO 342 I=1,NOB
342   WRITE(3,*) Y(I),F(I),R(I),X(I,1),LN(I)
      DO 810 JLP=1,100
      SUMC(JLP)=0.0
```

```
810     SUMP(JLP)=0.0
        DO 820 ILP=1,NOB
        JLP=X(ILP,1)
        SUMO(JLP)=SUMO(JLP)+Y(ILP)
820     SUMP(JLP)=SUMP(JLP)+P(ILP)
        DO 845 JLP=1,100
        IF(SUMO(JLP).EQ.0.0) GO TO 850
        PRINT 840,JLP,SUMO(JLP),SUMP(JLP)
840     FORMAT(' ',1X,I4,9X,F12.6,2X,F12.6)
845     CONTINUE
850     CONTINUE
        SSQ=SUMB
        IDF=NOB-NP
        PRINT 1015
        I=0
        CALL MATIN(D,NP,P,I,DET)
        DO 7692 I=1,NP
        II=I+NP*(I-1)
7692    E(I)=SQRT(D(II))
        DO 340 I=1,NP
        JI=I+NP*(I-1)-1
        IJ=I+NP*(I-2)
        DO 340 J=I,NP
        JI=JI+1
        A(JI)=D(JI)/(E(I)*E(J))
        IJ=IJ+NP
340     A(IJ)=A(JI)
        CALL GASS60(3,NP,TEMP,TEMP,A)
        PRINT 1016
        CALL GASS60(1,NP,E,TEMP,TEMP)
        IF(IDF)341,410,341
341     SDEV=SSQ/IDF
        PRINT 1014,SDEV,IDF
        SDEV=SQRT(SDEV)
        DO 391 I=1,NP
        P(I)=TH(I)+2.0*E(I)*SDEV
391     TB(I)=TH(I)-2.0*E(I)*SDEV
        PRINT 1036
        PRINT 1039
        PRINT 1036
        PRINT 1038
        DO 423 I=1,NP
423     PRINT 1037,I,TH(I),TB(I),P(I)
        LACS=1
        GO TO 101
414     DO 415 K=1,NOB
        TEMP=0.
        DO 420 I=1,NP
        DO 420 J=1,NP
        ISUB=K+NOB*(I-1)
        DEBUG1=DELZ(ISUB)
C
C ****************** DEBUG1=DELZ(K+NOB*(I-1)) ****************************
C
        ISUB=K+NOB*(J-1)
        DEBUG2=DELZ(ISUB)
C
C ****************** DEBUG2=DELZ(K+NOB*(J-1)) ****************************
C
        IJ=I+NP*(J-1)
```

```
      DEBUG3=D(IJ)/(DIFZ(I)*TH(I)*DIFZ(J)*TH(J))
420   TEMP=TEMP+DEBUG1*DEBUG2*DEBUG3
      TEMP=2.0*SQRT(TEMP)*SIEV
      B(K)=F(K)+TEMP
415   F(K)=F(K)-TEMP
      PRINT 1008
      IE=0
      DO 425 I=1,NOB,10
      IE=IE+10
      IF(NOB-IE)430,435,435
430   IE=NOB
435   PRINT 2001,(R(J),J=I,IE)
425   PRINT 2006,(F(J),J=I,IE)
410   PRINT 1033, NPROB
      GO TO 9999
 99   PRINT 1034
      GO TO 410
1000  FORMAT(' NONLINEAR ESTIMATION, PROBLEM NUMBER ',I3,//I5,
     @' OBSERVATIONS, ',I5,' PARAMETERS ',I14,' SCRATCH REQUIRED')
1001  FORMAT(//' INITIAL PARAMETER VALUES')
1002  FORMAT(/' PROPORTIONS USED IN CALCULATING DIFFERENCE QUOTIENTS')
1003  FORMAT(/' INITIAL SUM OF SQUARES = ',E12.4)
1004  FORMAT(/////' ************************************************** '
     @,' ITERATION NO. ',I4////)
1007  FORMAT(//' PARAMETER VALUES VIA REGRESSION')
1008  FORMAT(///' APPROXIMATE CONFIDENCE LIMITS FOR EACH FUNCTION VALUE'
     @)
1009  FORMAT(////' ITERATION STOPS - RELATIVE CHANGE IN EACH',
     @' PARAMETER LESS THAN ',E12.4)
1010  FORMAT(////' ITERATION STOPS - RELATIVE CHANGE IN SUM OF',
     @' SQUARES LESS THAN ',E12.4)
1011  FORMAT('** OBSERVED **** FITTED **** RESIDUAL **')
1012  FORMAT(3E12.4)
1014  FORMAT(//' VARIANCE OF RESIDUALS = ',E12.4,1X,I4,
     @' DEGREES OF FREEDOM')
1015  FORMAT(////' CORRELATION MATRIX')
1016  FORMAT(////' NORMALIZING ELEMENTS')
1033  FORMAT(//' END OF PROBLEM NO. ',I3)
1034  FORMAT(/' PARAMETER ERROR')
1036  FORMAT('          ')
1039  FORMAT(/' INDIVIDUAL CONFIDENCE LIMITS FOR EACH PARAMETER ',
     @'(ON LINEAR HYPOTHESIS) ')
1037  FORMAT(I4,3E12.4)
1038  FORMAT('   I     TH(I)       CONFIDENCE  LIMITS    ')
1040  FORMAT (///' LAMBDA = ',E10.3,30X,' SUM OF SQUARES AFTER',
     @' REGRESSION = ',E15.7)
1041  FORMAT(//' DETERMINANT = ',E12.4,6X,' ANGLE IN SCALED COORD. = ',
     @F5.2,' DEGREES')
1043  FORMAT(//' TEST POINT SUM OF SQUARES = ',E12.4)
2001  FORMAT (/5E12.4,//5E12.4)
2006  FORMAT (/5E12.4,//5E12.4)
9999  RETURN
      END
C
C
C
      SUBROUTINE MATIN(A,NVAR,E,NB,DET)
      DIMENSION A(NVAR,1),B(NVAR,1)
      PIVOTM=A(1,1)
      DET=1.0
```

```
      DO 550 ICOL=1,NVAR
      PIVOT=A(ICOL,ICOL)
      PIVOTM=AMIN1(PIVOT,PIVOTM)
      DET=PIVOT*DET
C
C ***************** DIVIDE PIVOT ROW BY PIVOT ELEMENT ******************
C
      A(ICOL,ICOL)=1.0
      PIVOT=AMAX1(PIVOT,1.E-20)
      PIVOT=A(ICOL,ICOL)/PIVOT
      DO 350 L=1,NVAR
350   A(ICOL,L)=A(ICOL,L)*PIVOT
      IF(NB.EQ.0) GO TO 371
      DO 370 L=1,NB
370   B(ICOL,L)=B(ICOL,L)*PIVOT
C
C ******************* REDUCE NON-PIVOT ROWS ****************************
C
371   DO 550 L1=1,NVAR
      IF(L1.EQ.ICOL) GO TO 550
      T=A(L1,ICOL)
      A(L1,ICOL)=0.
      DO 450 L=1,NVAR
450   A(L1,L)=A(L1,L)-A(ICOL,L)*T
      IF(NB.EQ.0) GO TO 550
      DO 500 L=1,NB
500   B(L1,L)=B(L1,L)-B(ICOL,L)*T
550   CONTINUE
      RETURN
      END
C
C
C
      SUBROUTINE GAUSS0(ITYPE,NQ,A,B,C)
C
C THE ONLY FUNCTION OF THIS SUBPROGRAM IS TO CARRY OUT
C VARIOUS PRINTING TASKS.  IT PRINTS THE VALUES OF VARIOUS QUANTITIES
C THAT ARE PASSED IN THE ARGUMENT LIST OVER THE RANGE LOW TO LUP,
C WHERE LUP IS THE NUMBER OF PARAMETERS (VARIABLE UP TO 10).
C
      DIMENSION A(NQ),B(NQ),C(NQ,NQ)
      NP=NQ
      NR=NP/10
      LOW=1
      LUP=10
 10   IF(NR) 15,20,30
 15   RETURN
 20   LUP=NP
      IF(LOW.GT.LUP) RETURN
 30   PRINT 500,(J,J=LOW,LUP)
      GO TO (40,60,80),ITYPE
 40   PRINT 600,(A(J),J=LOW,LUP)
      GO TO 100
 60   PRINT 600,(B(J),J=LOW,LUP)
      GO TO 40
 80   DO 90 I=LOW,LUP
 90   PRINT 720,I,(C(J,I),J=LOW,I)
      LOW2=LUP+1
      IF(LOW2.GT.NP) GO TO 100
      DO 95 I=LOW2,NP
```

```
 95    PRINT 720, I, (C(J,I),J=LOW,LUP)
100    LOW=LOW+10
       LUP=LUP+10
       NB=NB-1
       GO TO 10
500    FORMAT(/5I12,//5I12)
600    FORMAT(/5E12.4,//5E12.4)
720    FORMAT(1H0,I3,1X,5F12.4,/5X,5F12.4)
       RETURN
       END
C
C
C
       FUNCTION GAMI(A,X)
C***REVISION OCTOBER 1, 1980
C***CATEGORY NO.  B5F
C***KEYWORD(S) GAMMA FUNCTION,INCOMPLETE GAMMA FUNCTION,SPECIAL FUNCTION
C***DATE WRITTEN  JULY 1977
C***AUTHOR  FULLERTON W.  (LASL)
C***PURPOSE - COMPUTES THE INCOMPLETE GAMMA FUNCTION
C***DESCRIPTION
C JULY 1977 EDITION.  W. FULLERTON, C3, LOS ALAMOS SCIENTIFIC LAB.
C
C EVALUATE THE INCOMPLETE GAMMA FUNCTION DEFINED BY
C
C GAMI = INTEGRAL FROM T = 0 TO X OF EXP(-T) * T**(A-1.0) .
C
C GAMI IS EVALUATED FOR POSITIVE VALUES OF A AND NON-NEGATIVE VALUES
C OF X.  A SLIGHT DETERIORATION OF 2 OR 3 DIGITS ACCURACY WILL OCCUR
C WHEN GAMI IS VERY LARGE OF VERY SMALL, BECAUSE LOGARITHMIC VARIABLES
C ARE USED.
C
C***ROUTINES CALLED  GAMIT,ALNGAM
       IF(A.LE.0.0) PRINT 970
       IF(X.LT.0.0) PRINT 970
970    FORMAT(' ***** GAMI.....A MUST BE GT 0  AND X GE 0')
       GAMI=0.0
       IF(X.EQ.0.0) RETURN
C
C THE ONLY ERROR POSSIBLE IN THE EXPRESSION BELOW IS A FATAL OVERFLOW.
C
       FACTOR=EXP(ALNGAM(A)+A*ALOG(X))
       GAMI=FACTOR*GAMIT(A,X)
       RETURN
       END
C
C
C
       FUNCTION ALNGAM(X)
C
C***REVISION OCTOBER 1, 1980
C***CATEGORY NO.  B5F,B3
C***KEYWORD(S) LOGARITHM,GAMMA FUNCTION,SPECIAL FUNCTION
C***DATE WRITTEN  JUNE 1977
C***AUTHOR  FULLERTON W.  (LASL)
C***PURPOSE
C COMPUTES THE LOG OF THE ABSOLUTE VALUE OF THE GAMMA FUNCTION.
C***DESCRIPTION
C JUNE 1977 EDITION.   W. FULLERTON, C3, LOS ALAMOS SCIENTIFIC LAB.
C
```

```
C SQ2PIL = ALOG(SQRT(2.*PI)),  SQPI2L = ALOG (SQRT(PI/2.))
C
C***ROUTINES CALLED  R9LGMC,GAMMA,R1MACH
      DATA SQ2PIL / 0.9189385332 0467274E0/
      DATA SQPI2L / 0.2257913526 4472743E0/
      DATA PI     / 3.1415926535 8979324E0/
      DATA XMAX,DXREL /0.,0./
      IF (XMAX.NE.0.)GO TO 10
      XMAX=R1MACH(2)/ALOG(R1MACH(2))
      DXREL=SQRT(R1MACH(4))
10    Y=ABS(X)
      IF(Y.GT.10.0)GO TO 20
C
C ALOG(ABS(GAMMA(X))) FOR  ABS(X).LE.10.0
C
      ALNGAM=ALOG(ABS(GAMMA(X)))
      RETURN
C
C ALOG(ABS(GAMMA(X))) FOR ABS(X).GT.10.0
C
20    IF(Y.GT.XMAX)PRINT 971
971   FORMAT(' ***** ALNGAM  ABS(X) CAUSES OVERFLOW')
      IF(X.GT.0.)ALNGAM=SQ2PIL+(X-0.5)*ALOG(X)-X+R9LGMC(Y)
      IF(X.GT.0.)RETURN
      SINPIY=ABS(SIN(PI*Y))
      IF(SINPIY.EQ.0.)PRINT 972
972   FORMAT(' ***** ALNGAM...  X IS NEGATIVE')
      IF(ABS((X-AINT(X-0.5))/X).LT.DXREL)PRINT 973
973   FORMAT(' ***** ALNGAM...LT HALF PRECISION')
      ALNGAM=SQPI2L+(X-0.5)*ALOG(Y)-X-ALOG(SINPIY)-R9LGMC(Y)
      RETURN
      END
C
C
C
      FUNCTION GAMIT(A, X)
C***REVISION OCTOBER 1, 1980
C***CATEGORY NO.  B5F
C***KEYWORD(S) TRICOMI-S,INCOMPLETE GAMMA FUNCTION,
C  GAMMA FUNCTION,SPECIAL FUNCTION
C***DATE WRITTEN  JULY 1977
C***AUTHOR  FULLERTON W. (LASL)
C***PURPOSE
C COMPUTES TRICOMI-S FORM OF THE INCOMPLETE GAMMA FUNCTION.
C***DESCRIPTION
C JULY 1977 EDITION.  W. FULLERTON, C3, LOS ALAMOS SCIENTIFIC LAB.
C
C EVALUATE TRICOMI-S INCOMPLETE GAMMA FUNCTION DEFINED BY
C
C GAMIT = X**(-A)/GAMMA(A) * INTEGRAL T = 0 TO X OF EXP(-T) * T**(A-1.)
C
C AND ANALYTIC CONTINUATION FOR A .LE. 0.0.  GAMMA(X) IS THE COMPLETE
C GAMMA FUNCTION OF X.  GAMIT IS EVALUATED FOR ARBITRARY REAL VALUES OF
C A AND FOR NON-NEGATIVE VALUES OF X (EVEN THOUGH GAMIT IS DEFINED FOR
C X .LT. 0.0), EXCEPT THAT FOR X = 0 AND A .LE. 0.0, GAMIT IS INFINITE,
C A FATAL ERROR.
C
C      A SLIGHT DETERIORATION OF 2 OR 3 DIGITS ACCURACY WILL OCCUR WHEN
C GAMIT IS VERY LARGE OR VERY SMALL IN ABSOLUTE VALUE, BECAUSE LOG-
C ARITHMIC VARIABLES ARE USED.  ALSO, IF THE PARAMETER A IS VERY CLOSE
```

```
C TO A NEGATIVE INTEGER (BUT NOT A NEGATIVE INTEGER), THERE IS A LOSS
C OF ACCURACY, WHICH IS REPORTED IF THE RESULT IS LESS THAN HALF
C MACHINE PRECISION.
C
C REF. -- W. GAUTSCHI, AN EVALUATION PROCEDURE FOR INCOMPLETE GAMMA
C FUNCTIONS, ACM TRANS. MATH. SOFTWARE.
C
C***ROUTINES CALLED R9LGIC,XERCLR,ALNGAM,R9LGIT,R9GMIT,ALGAMS,GAMI,
C    R1MACH
      DATA ALNEPS,SQEPS,BOT / 3*0.0 /
      IF(ALNEPS.NE.0.0)GO TO 10
      ALNEPS=-ALOG(R1MACH(3))
      SQEPS=SQRT(R1MACH(4))
      BOT=ALOG(R1MACH(1))
10    IF(X.LT.0.0) PRINT 974
974   FORMAT(' ***** GAMIT...X IS NEGATIVE')
      IF(X.NE.0.0) ALX=ALOG(X)
      SGA=1.0
      IF(A.NE.0.0) SGA=SIGN(1.0,A)
      AINTA=AINT(A+0.5*SGA)
      AEPS=A-AINTA
      IF(X.GT.0.0) GO TO 20
      GAMIT=0.0
      IF(AINTA.GT.0.0.OR.AEPS.NE.0.0)GAMIT=GAMR(A+1.0)
      RETURN
20    IF(X.GT.1.0) GO TO 40
      IF(A.GE.(-0.5).OR.AEPS.NE.0.0)CALL ALGAMS(A+1.0,ALGAP1,
     1SGNGAM)
      GAMIT=R9GMIT(A,X,ALGAP1,SGNGAM,ALX)
      RETURN
40    IF(A.LT.X) GO TO 50
      T=R9LGIT(A,X,ALNGAM(A+1.0))
      GAMIT=EXP(T)
      RETURN
50    ALNG=R9LGIC(A,X,ALX)
C
C EVALUATE GAMIT IN TERMS OF EXP(GAMIC(A,X))
C
      H=1.0
      IF(AEPS.EQ.0.0.AND.AINTA.LE.0.0)GO TO 60
      CALL ALGAMS(A+1.0,ALGAP1,SGNGAM)
      T=ALOG(ABS(A))+ALNG-ALGAP1
      IF(T.GT.ALNEPS)GO TO 70
      IF(T.GT.(-ALNEPS))H=1.0-SGA*SGNGAM*EXP(T)
      IF(ABS(H).GT.SQEPS)GO TO 60
      PRINT 975
975   FORMAT(' ***** GAMIT...IT HALF PRECISION')
60    T=-A*ALX+ALOG(ABS(H))
      GAMIT=SIGN(EXP(T),H)
      RETURN
70    T=T-A*ALX
      GAMIT=-SGA*SGNGAM*EXP(T)
      RETURN
      END
C
C
C
      FUNCTION R9LGMC(X)
C
C***REVISION OCTOBER 1, 1980
```

```
C***CATEGORY NO.  B5F
C***KEYWORD(S) CORRECTION FACTOR,LOG GAMMA,SPECIAL FUNCTION
C***DATE WRITTEN  AUGUST 1977
C***AUTHOR  FULLERTON W. (LASL)
C***PURPOSE
C COMPUTES THE LOG GAMMA CORRECTION FACTOR SO THAT
C ALOG(GAMMA(X)) = ALOG(SQRT(2*PI)) + (X-.5)*ALOG(X) - X + R9LGMC(X)
C***DESCRIPTION
C AUGUST 1977 EDITION.  W. FULLERTON, C3, LOS ALAMOS SCIENTIFIC LAB.
C
C COMPUTE THE LOG GAMMA CORRECTION FACTOR FOR X .GE. 10.0 SO THAT
C  ALOG (GAMMA(X)) = ALOG(SQRT(2*PI)) + (X-.5)*ALOG(X) - X + R9LGMC(X)
C
C SERIES FOR ALGM        ON THE INTERVAL  0.TO  1.00000D-02
C WITH WEIGHTED ERROR   3.4CE-16
C LOG WEIGHTED ERROR  15.47
C SIGNIFICANT FIGURES REQUIRED  14.39
C      DECIMAL PLACES REQUIRED  15.86
C
C
C***ROUTINES CALLED  CSEVL,R1MACH,INITS
      DIMENSION ALGMCS(6)
      DATA ALGMCS( 1) /    .1.66389480 45186E0 /
      DATA ALGMCS( 2) /   -.0000138494 817606E0 /
      DATA ALGMCS( 3) /    .0000000098 108256E0 /
      DATA ALGMCS( 4) /   -.0000000000 180912E0 /
      DATA ALGMCS( 5) /    .0000000000 000622E0 /
      DATA ALGMCS( 6) /   -.0000000000 000003E0 /
      DATA NALGM, XBIG, XMAX / 0, 2*0.0 /
      IF(NALGM.NE.0)GO TO 10
      NALGM=INITS(ALGMCS,6,R1MACH(3))
      XBIG=1.0/SQRT(R1MACH(3))
      XMAX=EXP(AMIN1(ALOG(R1MACH(2)/12.0),-ALOG(12.0*R1MACH(1))))
10    IF(X.LT.10.0)PRINT 976
976   FORMAT(' ***** R9LGMC....X MUST BE GE 10')
      IF(X.GE.XMAX)GO TO 20
      R9LGMC=1.0/(12.0*X)
      IF(X.LT.XBIG)R9LGMC=CSEVL(2.0*(10./X)**2-1.,ALGMCS,NALGM)/X
      RETURN
20    R9LGMC=0.0
      PRINT 977
977   FORMAT(' ***** R9LGMC....X TOO BIG, UNDERFLOW')
      RETURN
      END
C
C
C
      FUNCTION GAMR(X)
C***REVISION OCTOBER 1, 1980
C***CATEGORY NO.  B5F
C***KEYWORD(S) RECIPROCAL GAMMA FUNCTION,GAMMA FUNCTION SPECIAL FUNCTION
C***DATE WRITTEN  JULY 1977
C***AUTHOR  FULLERTON W. (LASL)
C***PURPOSE  COMPUTES THE RECIPROCAL OF THE GAMMA FUNCTION.
C***DESCRIPTION
C JULY 1977 EDITION.  W. FULLERTON, C3, LOS ALAMOS SCIENTIFIC LAB.
C THIS ROUTINE, NOT GAMMA(X), SHOULD BE THE FUNDAMENTAL ONE.
C
C***ROUTINES CALLED  ALGAMS,XERCLR,GAMMA,XSETF,XGETF
      GAMR=0.0
```

```
      IF (X.LE.0.0.AND.AINT(X).EQ.X) RETURN
      IF (ABS(X).GT.10.0) GO TO 10
      GAMR=1.0/GAMMA(X)
      RETURN
10    CALL ALGAMS(X,ALNGX,SGNGX)
      GAMR=SGNGX*EXP(-ALNGX)
      RETURN
      END
C
C
C
      SUBROUTINE ALGAMS(X,AIGAM,SGNGAM)
C***REVISION OCTOBER 1, 1980
C***CATEGORY NO.  B5F
C***KEYWORD(S) LOGARITHM,GAMMA FUNCTION,SPECIAL FUNCTION
C***DATE WRITTEN  JULY 1977
C***AUTHOR  FULLERTON W. (LASL)
C***PURPOSE
C COMPUTES LOG(ABS(GAMMA(X))).
C***DESCRIPTION
C JULY 1977 EDITION.  W. FULLERTON, C3, LOS ALAMOS SCIENTIFIC LAB.
C EVALUATE LOG ABS (GAMMA(X)) AND RETURN THE SIGN OF GAMMA(X) IN SGNGAM
C SGNGAM IS EITHER +1.0 OR -1.0.
C***ROUTINES CALLED  ALNGAM
      ALGAM=ALNGAM(X)
      SGNGAM=1.0
      IF (X.GT.0.0) RETURN
      INT=AMOD(-AINT(X),2.0)+0.1
      IF (INT.EQ.0) SGNGAM=-1.0
      RETURN
      END
C
C
C
      FUNCTION R9GMIT(A,X,AIGAP1,SGNGAM,ALX)
C***REVISION OCTOBER 1, 1980
C***CATEGORY NO.  B5F
C***KEYWORD(S) TRICOMI-S,INCOMPLETE GAMMA FUNCTION,GAMMA FUNCTION,
C  SPECIAL FUNCTION,SMALL X
C***DATE WRITTEN  JULY 1977
C***AUTHOR  FULLERTON W. (LASL)
C***PURPOSE
C COMPUTES TRICOMI-S INCOMPLETE GAMMA FUNCTION FOR SMALL X.
C***DESCRIPTION
C JULY 1977 EDITION.  W. FULLERTON, C3, LOS ALAMOS SCIENTIFIC LAB.
C COMPUTE TRICOMI-S INCOMPLETE GAMMA FUNCTION FOR SMALL X.
C***ROUTINES CALLED  ALNGAM,R1MACH
      DATA EPS,BOT /2*0.0/
      IF (EPS.EQ.0.0) EPS=0.5*R1MACH(3)
      IF (BOT.EQ.0.0) BOT=ALOG(R1MACH(1))
      IF (X.LE.0.0) PRINT 978
978   FORMAT(' ***** R9GMIT....X MUST BE GT 0.')
      MA=A+0.5
      IF (A.LT.0.0) MA=A-0.5
      AEPS=A-FLOAT(MA)
      AE=A
      IF (A.LT.(-0.5)) AE=AEPS
      T=1.0
      TE=AE
      S=T
```

```
      DO 20 K=1,200
      FK=K
      TE=-X*TE/FK
      T=TE/(AE+FK)
      S=S+T
      IF(ABS(T).LT.EPS*ABS(S))GO TO 30
20    CONTINUE
      PRINT 979
979   FORMAT(' ***** R9GMIT....NO CONVERGENCE IN 200 TERMS')
30    IF(A.GE.(-0.5))ALGS=-ALGAP1+ALOG(S)
      IF(A.GE.(-0.5))GO TO 60
      ALGS=-ALNGAM(1.0+AEPS)+ALOG(S)
      S=1.0
      M=-MA-1
      IF(M.EQ.0)GO TO 50
      T=1.0
      DO 40 K=1,M
      T=X*T/(AEPS-FLOAT(M+1-K))
      S=S+T
      IF(ABS(T).LT.EPS*ABS(S))GO TO 50
40    CONTINUE
50    R9GMIT=0.0
      ALGS=-FLOAT(MA)*ALOG(X)+ALGS
      IF(S.EQ.0.0.OR.AEPS.EQ.0.0)GO TO 60
      SGNG2=SGNGAM*SIGN(1.0,S)
      ALG2=-X-ALGAP1+ALOG(ABS(S))
      IF(ALG2.GT.BOT) R9GMIT = SGNG2*EXP(ALG2)
      IF(ALGS.GT.BOT) R9GMIT = R9GMIT + EXP(ALGS)
      RETURN
60    R9GMIT=EXP(ALGS)
      RETURN
      END
C
C
C
      FUNCTION R9LGIT(A,X,ALGAP1)
C***REVISION OCTOBER 1, 1980
C***CATEGORY NO.  B5F
C***KEYWORD(S) TRICOMI-S,INCOMPLETE GAMMA FUNCTION,LOGARITHM,
C  PERRON-S CONTINUED FRACTION,SPECIAL FUNCTION
C***DATE WRITTEN  JULY 1977
C***AUTHOR  FULLERTON W.  (LASL)
C***PURPOSE
C COMPUTES THE LOG OF TRICOMI-S INCOMPLETE GAMMA FUNCTION WITH
C PERRON-S CONTINUED FRACTION FOR LARGE X AND FOR A .GE. X.
C***DESCRIPTION
C JULY 1977 EDITION.  W. FULLERTON, C3, LOS ALAMOS SCIENTIFIC LAB.
C
C COMPUTE THE LOG OF TRICOMI-S INCOMPLETE GAMMA FUNCTION WITH PERRON-S
C CONTINUED FRACTION FOR LARGE X AND FOR A .GE. X.
C***ROUTINES CALLED  R1MACH
      DATA EPS, SQEPS / 2*0.0 /
      IF (EPS.EQ.0.0) EPS = 0.5*R1MACH(3)
      IF (SQEPS.EQ.0.0) SQEPS = SQRT(R1MACH(4))
      IF(X.LE.0.0.OR.A.LT.X)PRINT 980
980   FORMAT(' ***** R9LGIT....X MUST BE GT 0. LE A')
      AX=A+X
      A1X=AX+1.0
      R=0.0
      P=1.0
```

```
      S=P
      DO 20 K=1,200
      FK=K
      T=(A+FK)*X*(1.0+R)
      R=T/((AX+FK)*(A1X+FK)-T)
      P=R*P
      S=S+P
      IF(ABS(P).LT.EPS*S)GO TO 30
20    CONTINUE
      PRINT 981
981   FORMAT(' ***** R9LGIT....NO CONVERGENCE IN 200 TERMS')
30    HSTAR=1.0-A*S/A1X
      IF(HSTAR.LT.SQEPS)PRINT 982
982   FORMAT(' ***** R9LGIT.... LT HALF PRECISION')
      R9LGIT=-X-ALGAP1-ALOG(HSTAR)
      RETURN
      END
C
C
C
      FUNCTION R9LGIC(A,X,AIX)
C***REVISION OCTOBER 1, 1980
C***CATEGORY NO.  B5F
C***KEYWORD(S) LOGARITHM,COMPLEMENTARY INCOMPLETE GAMMA FUNCTION,
C  SPECIAL FUNCTION,LARGE X
C***DATE WRITTEN  JULY 1977
C***AUTHOR  FULLERTON W. (LASL)
C***PURPOSE
C COMPUTES THE LOG COMPLEMENTARY INCOMPLETE GAMMA FUNCTION FOR LARGE
C X AND FOR A .LE. X.
C***DESCRIPTION
C JULY 1977 EDITION.  W. FULLERTON, C3, LOS ALAMOS SCIENTIFIC LAB.
C
C COMPUTE THE LOG COMPLEMENTARY INCOMPLETE GAMMA FUNCTION FOR LARGE X
C AND FOR A .LE. X.
C***ROUTINES CALLED R1MACH
      DATA EPS /0.0/
      IF(EPS.EQ.0.0)EPS=0.5*R1MACH(3)
      XPA=X+1.0-A
      XMA=X-1.0-A
      R=0.0
      P=1.0
      S=P
      DO 10 K=1,200
      FK=K
      T=FK*(A-FK)*(1.0+R)
      R=-T/((XMA+2.0*FK)*(XPA+2.0*FK)+T)
      P=R*P
      S=S+P
      IF(ABS(P).LT.EPS*S)GO TO 20
10    CONTINUE
      PRINT 983
983   FORMAT(' ***** R9LGIC....NO CONVERGENCE IN 200 TERMS')
20    R9LGIC=A*ALX-X+ALOG(S/XPA)
      RETURN
      END
C
C
C
      FUNCTION INITS(OS,NOS,ETA)
```

```
C***REVISION OCTOBER 1, 1980
C***CATEGORY NO.  B5R
C***KEYWORD(S) ORTHOGONAL SERIES,INITIALIZE,SPECIAL FUNCTION
C***DATE WRITTEN  APRIL 1977
C***AUTHOR  FULLERTON W. (LASL)
C***PURPOSE
C INITIALIZES AN ORTHOGONAL SERIES SO THAT IT DEFINES THE NUMBER
C OF TERMS TO CARRY IN THE SERIES TO MEET A SPECIFIED ERROR.
C***DESCRIPTION
C APRIL 1977 VERSION.  W. FULLERTON, C3, LOS ALAMOS SCIENTIFIC LAB.
C
C INITIALIZE THE ORTHOGONAL SERIES SO THAT INITS IS THE NUMBER OF TERMS
C NEEDED TO INSURE THE ERROR IS NO LARGER THAN ETA.  ORDINARILY, ETA
C WILL BE CHOSEN TO BE ONE-TENTH MACHINE PRECISION.
C
C   INPUT ARGUMENTS --
C OS      ARRAY OF NOS COEFFICIENTS IN AN ORTHOGONAL SERIES.
C NOS     NUMBER OF COEFFICIENTS IN OS.
C ETA     REQUESTED ACCURACY OF SERIES.
C
      DIMENSION OS(NOS)
      IF(NOS.LT.1) PRINT 984
 984  FORMAT(' ***** INITS.....# OF COEFF LT 1')
      ERR=0.
      DO 10 II=1,NOS
      I=NOS+1-II
      ERR=ERR+ABS(OS(I))
      IF(ERR.GT.ETA)GO TO 20
10    CONTINUE
20    IF(I.EQ.NOS) PRINT 985
985   FORMAT(' ***** INITS.....ETA MAY BE TOO SMALL')
      INITS=I
      RETURN
      END
C
C
C
      FUNCTION CSEVL(X,CS,N)
C***REVISION  OCTOBER 1,1980
C***CATEGORY NO.  B5R
C***KEYWORD(S) CHEBYSHEV,SPECIAL FUNCTION,FNLIB
C***DATE WRITTEN  APRIL,1977
C***AUTHOR  FULLERTON W. (LASL)
C***PURPOSE
C   EVALUATE THE N-TERM CHEBYSHEV SERIES CS AT X.
C***DESCRIPTION
C APRIL 1977 VERSION. W. FULLERTON, C-3, LOS ALAMOS SCIENTIFIC LABORATOR
C INSTALLED ON THE VAX BY DOLORES MONTANO, C-3, 5/80.
C
C EVALUATE THE N-TERM CHEBYSHIV SERIES CS AT X. ADAPTED FROM
C R BROUCKE, ALGORITHM 446, C.A.C.M., 16, 254 (1973). ALSO SEE FOX
C AND PARKER, CHEBYSHEV POLYS IN NUMERICAL ANALYSIS, OXFORD PRESS, P.56.
C
C       INPUT ARGUMENTS --
C X     VALUE AT WHICH THE SERIES IS TO BE EVALUATED.
C CS    ARRAY OF N TERMS OF A CHEBYSHEV SERIES. IN EVAL-
C       UATING CS, ONLY HALF THE FIRST COEF IS SUMMED.
C N     NUMBER OF TERMS IN ARRAY CS.
C
      DIMENSION CS(1)
```

```
      IF(N.LT.1)PRINT 986
986   FORMAT(' ***** CSEVL.....# OF TERMS LE 0.')
      IF(N.GT.1000)PRINT 987
987   FORMAT(' ***** CSEVL.....# OF TERMS GT 1000')
      IF(X.LT.-1.0.OR.X.GT.1.0)PRINT 988
988   FORMAT(' ***** CSEVL.....X OUTSIDE (-1,+1)')
      B1=0.
      B0=0.
      TWOX=2.*X
      DO 10 I=1,N
      B2=B1
      B1=B0
      NI=N+1-I
      B0=TWOX*B1-B2+CS(NI)
10    CONTINUE
      CSEVL=0.5*(B0-B2)
      RETURN
      END
C
C
C
      REAL FUNCTION R1MACH(I)
C
C  SINGLE-PRECISION MACHINE CONSTANTS
C    R1MACH(1) = B**(EMIN-1), THE SMALLEST POSITIVE MAGNITUDE.
C    R1MACH(2) = B**EMAX*(1 - B**(-T)), THE LARGEST MAGNITUDE.
C    R1MACH(3) = B**(-T), THE SMALLEST RELATIVE SPACING.
C    R1MACH(4) = B**(1-T), THE LARGEST RELATIVE SPACING.
C    R1MACH(5) = LOG10(B)
C
      REAL RMACH(5)
C
C     MACHINE CONSTANTS FOR THE IBM 3033 AT CLEMSON UNIVERSITY.
C
      DATA RMACH(1) / Z00100000 /
      DATA RMACH(2) / Z7FFFFFFF /
      DATA RMACH(3) / Z3B100000 /
      DATA RMACH(4) / Z3C100000 /
      DATA RMACH(5) / Z41134413 /
      R1MACH = RMACH(I)
      RETURN
      END
C
C
C
      INTEGER FUNCTION I1MACH(I)
C
C  I/O UNIT NUMBERS.
C    I1MACH( 1) = THE STANDARD INPUT UNIT.
C    I1MACH( 2) = THE STANDARD OUTPUT UNIT.
C    I1MACH( 3) = THE STANDARD PUNCH UNIT.
C    I1MACH( 4) = THE STANDARD ERROR MESSAGE UNIT.
C
C  WORDS.
C    I1MACH( 5) = THE NUMBER OF BITS PER INTEGER STORAGE UNIT.
C    I1MACH( 6) = THE NUMBER OF CHARACTERS PER INTEGER STORAGE UNIT.
C
C  INTEGERS.
C    ASSUME INTEGERS ARE REPRESENTED IN THE S-DIGIT, BASE-A FORM
C               SIGN ( X(S-1)*A**(S-1) + ... + X(1)*A + X(0) )
```

```
C                 WHERE 0 .LE. X(I) .LT. A FOR I=0,...,S-1.
C     I1MACH( 7) = A, THE BASE.
C     I1MACH( 8) = S, THE NUMBER OF BASE-A DIGITS.
C     I1MACH( 9) = A**S - 1, THE LARGEST MAGNITUDE.
C
C   FLOATING-POINT NUMBERS.
C     ASSUME FLOATING-POINT NUMBERS ARE REPRESENTED IN THE T-DIGIT,
C     BASE-B FORM
C                 SIGN (B**E)*( (X(1)/B) + ... + (X(T)/B**T) )
C                 WHERE 0 .LE. X(I) .LT. B FOR I=1,...,T,
C                 0 .LT. X(1), AND EMIN .LE. E .LE. EMAX.
C     I1MACH(10) = B, THE BASE.
C
C   SINGLE-PRECISION
C     I1MACH(11) = T, THE NUMBER OF BASE-B DIGITS.
C     I1MACH(12) = EMIN, THE SMALLEST EXPONENT E.
C     I1MACH(13) = EMAX, THE LARGEST EXPONENT E.
C
C   DOUBLE-PRECISION
C     I1MACH(14) = T, THE NUMBER OF BASE-B DIGITS.
C     I1MACH(15) = EMIN, THE SMALLEST EXPONENT E.
C     I1MACH(16) = EMAX, THE LARGEST EXPONENT E.
C
      INTEGER IMACH(16),OUTPUT
      EQUIVALENCE (IMACH(4),OUTPUT)
C
C     MACHINE CONSTANTS FOR THE IBM 3033 AT CLEMSON UNIVERSITY.
C
      DATA IMACH( 1) /    5 /
      DATA IMACH( 2) /    6 /
      DATA IMACH( 3) /    2 /
      DATA IMACH( 4) /    3 /
      DATA IMACH( 5) /   32 /
      DATA IMACH( 6) /    4 /
      DATA IMACH( 7) /    2 /
      DATA IMACH( 8) /   31 /
      DATA IMACH( 9) / Z7FFFFFFF /
      DATA IMACH(10) /   16 /
      DATA IMACH(11) /    6 /
      DATA IMACH(12) /  -64 /
      DATA IMACH(13) /   63 /
      DATA IMACH(14) /   14 /
      DATA IMACH(15) /  -64 /
      DATA IMACH(16) /   63 /
      IF(I.LT.1.OR.I.GT.16)GO TO 10
      I1MACH=IMACH(I)
      RETURN
 10   WRITE(OUTPUT,9000)
 9000 FORMAT(' ERROR    1 IN I1MACH - I OUT OF BOUNDS')
      RETURN
      END
//GO.FT03F001 DD DSN=QMGUI1.OUTPUT,DISP=SHR
//GO.SYSIN DD *
   236  5.079 -.387 1  4.138    .003315 .002408  5.507  3.602 10
 17
        1.19548   28.       C.      0.       7.      23.000  27. 1
        0.87208   29.       0.      0.       7.      23.000  28. 1
        1.36017   30.       C.      0.       7.      23.000  29. 1
        1.26328   31.       0.      0.       7.      22.500  30. 1
        1.00719   32.       C.      0.       7.      22.000  31. 1
```

```
        0.89211   33.     C.      0.      7.      22.000   32.  1
        1.27575   34.     C.      0.      7.      22.000   33.  1
        1.14815   35.     C.      0.      7.      21.500   34.  1
        1.15231   36.     0.      0.      7.      21.000   35.  1
        1.24936   37.     C.      0.      7.      20.500   36.  1
        1.02576   38.     C.      0.      7.      20.000   37.  1
        0.90939   39.     C.      0.      7.      43.500   38.  1
        0.58287   40.     0.      0.      7.      43.000   39.  1
        0.45301   41.     C.      0.      7.      42.500   41.  1
        0.37731   42.     C.      0.      7.      41.500   42.  1
        0.21011   43.     C.      0.      7.      40.000   43.  1
        0.11133   44.     C.      0.      7.      38.000   44.  1
31.5
35.5
37.5
39.5
41.5
43.5
44.5
 34
        0.23904   28.     7.      0.      23.     23.000   27.  2
        0.26792   29.     7.      0.      23.     23.000   28.  2
        0.28405   30.     7.      0.      23.     23.000   29.  2
        0.28837   31.     7.      0.      23.     22.500   30.  2
        0.33922   32.     7.      0.      23.     22.000   31.  2
        0.37202   33.     7.      0.      23.     22.000   32.  2
        0.61544   34.     7.      0.      23.     22.000   33.  2
        0.64844   35.     7.      0.      23.     21.500   34.  2
        0.88443   36.     7.      0.      23.     21.000   35.  2
        1.30476   37.     7.      0.      23.     20.500   36.  2
        1.90464   38.     7.      0.      23.     20.000   37.  2
        1.96346   39.     7.      0.      23.     43.500   38.  2
        1.94893   40.     7.      0.      23.     43.000   39.  2
        2.37299   41.     7.      0.      23.     42.500   40.  2
        2.21135   42.     7.      0.      23.     41.500   41.  2
        1.90135   43.     7.      0.      23.     40.000   42.  2
        2.00296   44.     7.      0.      23.     38.000   43.  2
        2.02364   45.     7.      0.      23.    108.000   44.  2
        1.89796   46.     7.      0.      23.    105.500   45.  2
        1.76414   47.     7.      0.      23.    102.500   46.  2
        1.82274   48.     7.      0.      23.    101.000   47.  2
        1.58376   49.     7.      0.      23.    101.000   48.  2
        1.49733   50.     7.      0.      23.    101.000   49.  2
        1.39265   51.     7.      0.      23.    101.000   50.  2
        1.36656   52.     7.      0.      23.    101.000   51.  2
        1.29265   53.     7.      0.      23.     99.500   52.  2
        0.75652   54.     7.      0.      23.     98.000   53.  2
        0.36923   55.     7.      0.      23.     97.500   54.  2
        0.11657   56.     7.      0.      23.     95.500   55.  2
        0.09666   57.     7.      0.      23.     94.000   56.  2
        0.06745   58.     7.      0.      23.     94.000   57.  2
        0.03575   59.     7.      0.      23.     93.500   58.  2
        0.04195   60.     7.      0.      23.    165.000   59.  2
        0.02468   61.     7.      0.      23.    164.500   60.  2
42.50
43.50
44.50
45.33
45.67
46.25
```

46.50
46.75
47.25
47.50
47.75
53.25
53.50
53.75
57.50
55.50
30

| | | | | | | |
|---|---|---|---|---|---|---|
| 0.01967 | 39. | 23. | 38. | 47. | 43.500 | 38. 3 |
| 0.10990 | 40. | 23. | 38. | 47. | 43.000 | 39. 3 |
| 0.42763 | 41. | 23. | 38. | 47. | 42.500 | 40. 3 |
| 0.51955 | 42. | 23. | 38. | 47. | 41.500 | 41. 3 |
| 0.61842 | 43. | 23. | 38. | 47. | 40.000 | 42. 3 |
| 0.77169 | 44. | 23. | 38. | 47. | 38.000 | 43. 3 |
| 0.96280 | 45. | 23. | 38. | 47. | 106.000 | 44. 3 |
| 1.05265 | 46. | 23. | 38. | 47. | 105.500 | 45. 3 |
| 1.18733 | 47. | 23. | 38. | 47. | 102.500 | 46. 3 |
| 1.58118 | 48. | 23. | 38. | 47. | 101.000 | 47. 3 |
| 1.80794 | 49. | 23. | 38. | 47. | 101.000 | 48. 3 |
| 2.22878 | 50. | 23. | 38. | 47. | 101.000 | 49. 3 |
| 2.35663 | 51. | 23. | 38. | 47. | 101.000 | 50. 3 |
| 2.71505 | 52. | 23. | 38. | 47. | 101.000 | 51. 3 |
| 3.47529 | 53. | 23. | 38. | 47. | 99.500 | 52. 3 |
| 2.59482 | 54. | 23. | 38. | 47. | 98.000 | 53. 3 |
| 2.91105 | 55. | 23. | 38. | 47. | 97.500 | 54. 3 |
| 2.70636 | 56. | 23. | 38. | 47. | 95.500 | 55. 3 |
| 2.11521 | 57. | 23. | 38. | 47. | 94.000 | 56. 3 |
| 1.90967 | 58. | 23. | 38. | 47. | 94.000 | 57. 3 |
| 1.36859 | 59. | 23. | 38. | 47. | 93.500 | 58. 3 |
| 1.42259 | 60. | 23. | 38. | 47. | 165.000 | 59. 3 |
| 1.45556 | 61. | 23. | 38. | 47. | 164.500 | 60. 3 |
| 1.12204 | 62. | 23. | 38. | 47. | 163.500 | 61. 3 |
| 0.70945 | 63. | 23. | 38. | 47. | 162.500 | 62. 3 |
| 0.23030 | 64. | 23. | 38. | 47. | 161.000 | 63. 3 |
| 0.17782 | 65. | 23. | 38. | 47. | 156.500 | 64. 3 |
| 0.07716 | 66. | 23. | 38. | 47. | 150.500 | 65. 3 |
| 0.03211 | 67. | 23. | 38. | 47. | 142.500 | 66. 3 |
| 0.0000 | 68. | 23. | 38. | 47. | 131.500 | 67. 3 |

56.25
56.50
56.75
61.50
62.50
63.50
64.33
64.67
65.13
65.25
65.38
65.50
65.63
65.75
65.88
66.17
66.33
66.50
66.66

100.33
100.44
100.56
100.67
100.78
100.89
101.11
101.22
101.33
101.44
101.56
101.67
101.78
101.89
102.10
102.20
102.30
102.40
102.50
102.60
102.70
102.80
102.90
103.11
103.22
103.33
103.44
103.56
103.67
103.78
103.89
104.10
104.20
104.30
104.40
104.50
104.60
104.70
104.80
104.90
105.10
105.20
105.30
105.40
105.50
105.60
105.70
105.80
105.90
106.11
106.22
106.33
106.44
106.55
106.67
106.78
106.89
107.11
107.22
107.33

| | | | | | | |
|---|---|---|---|---|---|---|
| 3.05223 | 95. | 341. | 82. | 464. | 534.000 | 94. 9 |
| 3.07767 | 96. | 341. | 82. | 464. | 525.000 | 95. 9 |
| 3.74317 | 97. | 341. | 82. | 464. | 513.500 | 96. 9 |
| 2.72778 | 98. | 341. | 82. | 464. | 962.000 | 97. 9 |
| 2.51151 | 99. | 341. | 82. | 464. | 945.500 | 98. 9 |
| 3.05881 | 100. | 341. | 82. | 464. | 925.000 | 99. 9 |
| 2.11725 | 101. | 341. | 82. | 464. | 901.500 | 100. 9 |
| 1.71578 | 102. | 341. | 82. | 464. | 874.000 | 101. 9 |
| 1.87150 | 103. | 341. | 82. | 464. | 841.000 | 102. 9 |
| 1.34397 | 104. | 341. | 82. | 464. | 806.000 | 103. 9 |
| 1.10247 | 105. | 341. | 82. | 464. | 771.500 | 104. 9 |
| 0.73111 | 106. | 341. | 82. | 464. | 736.000 | 105. 9 |
| 0.45439 | 107. | 341. | 82. | 464. | 828.500 | 106. 9 |
| 0.38147 | 108. | 341. | 82. | 464. | 1170.500 | 107. 9 |
| 0.64337 | 109. | 341. | 82. | 464. | 1143.000 | 108. 9 |
| 0.14513 | 110. | 341. | 82. | 464. | 1109.000 | 109. 9 |

94.17
94.33
94.50
94.67
94.83
95.11
95.22
95.33
95.44
95.56
95.67
95.78
95.89
96.11
96.22
96.33
96.44
96.56
96.67
96.78
96.89
97.11
97.22
97.33
97.44
97.56
97.67
97.78
97.89
98.17
98.33
98.50
98.67
98.83
99.11
99.22
99.33
99.44
99.56
99.67
99.78
99.89
100.11
100.22

93.40
93.47
93.53
93.60
93.67
93.73
93.80
93.87
93.93
94.14
94.29
94.43
94.57
94.71
94.86
 8

| | | | | | | |
|---|---|---|---|---|---|---|
| 0.06254 | 84. | 338. | 83. | 339. | 575.500 | 83. 7 |
| 0.13461 | 85. | 338. | 83. | 339. | 560.500 | 84. 7 |
| 0.09029 | 86. | 338. | 83. | 339. | 547.000 | 85. 7 |
| 0.08536 | 87. | 338. | 83. | 339. | 536.000 | 86. 7 |
| 0.08822 | 88. | 338. | 83. | 339. | 526.500 | 87. 7 |
| 0.09829 | 89. | 338. | 83. | 339. | 516.500 | 88. 7 |
| 0.23207 | 90. | 338. | 83. | 339. | 505.500 | 89. 7 |
| 0.04995 | 91. | 338. | 83. | 339. | 497.000 | 90. 7 |

91.50
 19

| | | | | | | |
|---|---|---|---|---|---|---|
| 0.00135 | 78. | 339. | 77. | 341. | 185.500 | 77. 8 |
| 0.00151 | 79. | 339. | 77. | 341. | 176.500 | 78. 8 |
| 0.00170 | 80. | 339. | 77. | 341. | 164.500 | 79. 8 |
| 0.00107 | 81. | 339. | 77. | 341. | 151.000 | 80. 8 |
| 0.00112 | 82. | 339. | 77. | 341. | 141.500 | 81. 8 |
| 0.02237 | 83. | 339. | 77. | 341. | 255.500 | 82. 8 |
| 0.24645 | 84. | 339. | 77. | 341. | 175.500 | 83. 8 |
| 0.11348 | 85. | 339. | 77. | 341. | 560.500 | 84. 8 |
| 0.14740 | 86. | 339. | 77. | 341. | 547.000 | 85. 8 |
| 0.13638 | 87. | 339. | 77. | 341. | 536.000 | 86. 8 |
| 0.12935 | 88. | 339. | 77. | 341. | 526.500 | 87. 8 |
| 0.19003 | 89. | 339. | 77. | 341. | 516.500 | 88. 8 |
| 0.03224 | 90. | 339. | 77. | 341. | 505.500 | 89. 8 |
| 0.01442 | 91. | 339. | 77. | 341. | 497.000 | 90. 8 |
| 0.02303 | 92. | 339. | 77. | 341. | 482.000 | 91. 8 |
| 0.01145 | 93. | 339. | 77. | 341. | 558.000 | 92. 8 |
| 0.00754 | 94. | 339. | 77. | 341. | 544.500 | 93. 8 |
| 0.00213 | 95. | 339. | 77. | 341. | 534.000 | 94. 8 |
| 0.00255 | 96. | 339. | 77. | 341. | 525.000 | 95. 8 |

94.50
96.50
 28

| | | | | | | |
|---|---|---|---|---|---|---|
| 0.02944 | 83. | 341. | 82. | 464. | 255.500 | 82. 9 |
| 0.80573 | 84. | 341. | 82. | 464. | 575.500 | 83. 9 |
| 1.45618 | 85. | 341. | 82. | 464. | 560.500 | 84. 9 |
| 1.30307 | 86. | 341. | 82. | 464. | 547.000 | 85. 9 |
| 1.14949 | 87. | 341. | 82. | 464. | 536.000 | 86. 9 |
| 1.71016 | 88. | 341. | 82. | 464. | 526.500 | 87. 9 |
| 2.93737 | 89. | 341. | 82. | 464. | 516.500 | 88. 9 |
| 2.13736 | 90. | 341. | 82. | 464. | 505.500 | 89. 9 |
| 2.88715 | 91. | 341. | 82. | 464. | 497.000 | 90. 9 |
| 3.91784 | 92. | 341. | 82. | 464. | 482.000 | 91. 9 |
| 2.66468 | 93. | 341. | 82. | 464. | 558.000 | 92. 9 |
| 3.80929 | 94. | 341. | 82. | 464. | 544.500 | 93. 9 |

87.91
88.10
88.20
88.30
88.40
88.50
88.60
88.70
88.80
88.90
89.08
89.17
89.25
89.33
89.42
89.50
89.58
89.67
89.75
89.83
89.92
90.08
90.17
90.25
90.33
90.42
90.50
90.58
90.67
90.75
90.83
90.92
91.08
91.17
91.25
91.33
91.42
91.50
91.58
91.67
91.75
91.83
91.92
92.08
92.15
92.23
92.31
92.38
92.46
92.54
92.62
92.69
92.77
92.85
92.92
93.07
93.13
93.20
93.27
93.33

83.10
83.20
83.30
83.40
83.50
83.60
83.70
83.80
83.90
84.06
84.13
84.19
84.25
84.31
84.38
84.44
84.50
84.56
84.63
84.69
84.75
84.82
84.88
84.94
85.06
85.13
85.19
85.25
85.31
85.38
85.44
85.50
85.56
85.63
85.69
85.75
85.82
85.88
85.94
86.08
86.15
86.23
86.31
86.39
86.46
86.54
86.62
86.69
86.77
86.85
86.92
87.09
87.18
87.27
87.36
87.45
87.55
87.64
87.73
87.82

80.18
80.24
80.29
80.35
80.41
80.47
80.53
80.59
80.65
80.71
80.76
80.82
80.88
80.94
81.11
81.22
81.33
81.44
81.55
81.67
81.78
81.89
25

| | | | | | | |
|---|---|---|---|---|---|---|
| 0.03193 | 70. | 191. | 69. | 338. | 229.000 | 69. 6 |
| 0.34971 | 71. | 191. | 69. | 338. | 219.000 | 70. 6 |
| 0.90940 | 72. | 191. | 69. | 338. | 211.000 | 71. 6 |
| 1.76691 | 73. | 191. | 69. | 338. | 205.000 | 72. 6 |
| 2.72632 | 74. | 191. | 69. | 338. | 199.000 | 73. 6 |
| 3.85894 | 75. | 191. | 69. | 338. | 191.500 | 74. 6 |
| 5.12589 | 76. | 191. | 69. | 338. | 180.500 | 75. 6 |
| 6.94414 | 77. | 191. | 69. | 338. | 167.000 | 76. 6 |
| 6.85761 | 78. | 191. | 69. | 338. | 185.500 | 77. 6 |
| 6.11974 | 79. | 111. | 69. | 338. | 176.500 | 78. 6 |
| 7.26889 | 80. | 191. | 69. | 338. | 164.500 | 79. 6 |
| 5.21449 | 81. | 191. | 69. | 338. | 151.000 | 80. 6 |
| 5.15660 | 82. | 191. | 69. | 338. | 141.500 | 81. 6 |
| 6.32066 | 83. | 191. | 69. | 338. | 255.500 | 82. 6 |
| 11.42129 | 84. | 191. | 69. | 338. | 275.500 | 83. 6 |
| 5.83803 | 85. | 191. | 69. | 338. | 560.500 | 84. 6 |
| 6.37578 | 86. | 191. | 69. | 338. | 547.000 | 85. 6 |
| 4.92702 | 87. | 191. | 69. | 338. | 536.000 | 86. 6 |
| 4.31611 | 88. | 191. | 69. | 338. | 526.500 | 87. 6 |
| 5.97020 | 89. | 191. | 69. | 338. | 516.500 | 88. 6 |
| 1.20556 | 90. | 191. | 69. | 338. | 505.500 | 89. 6 |
| 0.48470 | 91. | 191. | 69. | 338. | 497.000 | 90. 6 |
| 0 00000 | 92. | 191. | 69. | 338. | 482.000 | 91. 6 |
| 0.39775 | 93. | 191. | 69. | 338. | 558.000 | 92. 6 |
| 0.36704 | 94. | 191. | 69. | 338. | 544.500 | 93. 6 |

80.50
81.33
81.67
82.10
82.20
82.30
82.40
82.50
82.60
82.70
82.80
82.90

| | | | | | | | |
|---|---|---|---|---|---|---|---|
| | 6.07048 | 72. | 119. | 59. | 191. | 211.000 | 71. 5 |
| | 5.99359 | 73. | 119. | 59. | 191. | 205.000 | 72. 5 |
| | 5.38045 | 74. | 119. | 59. | 191. | 199.000 | 73. 5 |
| | 5.28531 | 75. | 119. | 59. | 191. | 191.500 | 74. 5 |
| | 3.12728 | 76. | 119. | 59. | 191. | 180.500 | 75. 5 |
| | 1.72110 | 77. | 119. | 60. | 191. | 167.000 | 76. 5 |
| | 0.94430 | 78. | 119. | 61. | 191. | 185.500 | 77. 5 |
| | 0.39982 | 79. | 119. | 62. | 191. | 176.500 | 78. 5 |
| | 0.17868 | 80. | 119. | 63. | 191. | 164.500 | 79. 5 |
| | 0.04702 | 81. | 119. | 64. | 191. | 151.000 | 80. 5 |

75.25
75.50
75.75
76.07
76.14
76.21
76.29
76.36
76.43
76.50
76.57
76.64
76.71
76.79
76.86
76.93
77.07
77.13
77.20
77.27
77.33
77.40
77.47
77.53
77.60
77.67
77.73
77.80
77.87
77.93
78.08
78.17
78.25
78.33
78.42
78.50
78.58
78.67
78.75
78.83
78.92
79.12
79.25
79.37
79.50
79.62
79.75
79.87
80.06
80.12

69.73
69.82
69.91
70.09
70.18
70.27
70.36
70.45
70.55
70.64
70.73
70.82
70.91
71.09
71.18
71.27
71.36
71.45
71.55
71.64
71.73
71.82
71.91
72.14
72.29
72.43
72.57
72.71
72.86
73.14
73.29
73.43
73.57
73.71
73.86
74.14
74.29
74.43
74.57
74.71
74.86
75.14
75.29
75.43
75.57
75.71
75.86
22

| | | | | | | |
|---|---|---|---|---|---|---|
| 0.09440 | 60. | 119. | 59. | 191. | 165.000 | 59. 5 |
| 0.21798 | 61. | 119. | 59. | 191. | 164.500 | 60. 5 |
| 0.50545 | 62. | 119. | 59. | 191. | 163.500 | 61. 5 |
| 0.72456 | 63. | 119. | 59. | 191. | 162.500 | 62. 5 |
| 1.01639 | 64. | 119. | 59. | 191. | 161.000 | 63. 5 |
| 1.61539 | 65. | 119. | 59. | 191. | 156.500 | 64. 5 |
| 1.86886 | 66. | 119. | 59. | 191. | 150.500 | 65. 5 |
| 2.41520 | 67. | 119. | 59. | 191. | 142.500 | 66. 5 |
| 2.61123 | 68. | 119. | 59. | 191. | 131.500 | 67. 5 |
| 2.96616 | 69. | 119. | 59. | 191. | 121.000 | 68. 5 |
| 4.75018 | 70. | 119. | 59. | 191. | 229.000 | 69. 5 |
| 5.71782 | 71. | 119. | 59. | 191. | 219.000 | 70. 5 |

66.83
67.25
67.50
67.75
68.50
29

| | | | | | | |
|---|---|---|---|---|---|---|
| 0.00996 | 47. | 47. | 46. | 119. | 102.500 | 46. 4 |
| 0.02965 | 48. | 47. | 46. | 119. | 101.000 | 47. 4 |
| 0.08944 | 49. | 47. | 46. | 119. | 101.000 | 48. 4 |
| 0.30266 | 50. | 47. | 46. | 119. | 101.000 | 49. 4 |
| 0.63845 | 51. | 47. | 46. | 119. | 101.000 | 50. 4 |
| 1.00236 | 52. | 47. | 46. | 119. | 101.000 | 51. 4 |
| 1.40825 | 53. | 47. | 46. | 119. | 99.500 | 52. 4 |
| 1.62892 | 54. | 47. | 46. | 119. | 98.000 | 53. 4 |
| 2.03716 | 55. | 47. | 46. | 119. | 97.500 | 54. 4 |
| 3.17816 | 56. | 47. | 46. | 119. | 95.500 | 55. 4 |
| 3.62862 | 57. | 47. | 46. | 119. | 94.000 | 56. 4 |
| 4.72402 | 58. | 47. | 46. | 119. | 94.000 | 57. 4 |
| 4.78499 | 59. | 47. | 46. | 119. | 93.500 | 58. 4 |
| 4.86147 | 60. | 47. | 46. | 119. | 165.500 | 59. 4 |
| 5.34870 | 61. | 47. | 46. | 119. | 164.500 | 60. 4 |
| 5.96560 | 62. | 47. | 46. | 119. | 163.500 | 61. 4 |
| 6.34085 | 63. | 47. | 46. | 119. | 162.500 | 62. 4 |
| 5.85055 | 64. | 47. | 46. | 119. | 161.500 | 63. 4 |
| 6.24051 | 65. | 47. | 46. | 119. | 156.500 | 64. 4 |
| 4.91988 | 66. | 47. | 46. | 119. | 150.500 | 65. 4 |
| 4.38904 | 67. | 47. | 46. | 119. | 142.500 | 66. 4 |
| 3.07483 | 68. | 47. | 46. | 119. | 131.500 | 67. 4 |
| 2.07644 | 69. | 47. | 46. | 119. | 121.000 | 68. 4 |
| 1.87063 | 70. | 47. | 46. | 119. | 229.000 | 69. 4 |
| 0.99034 | 71. | 47. | 46. | 119. | 219.000 | 70. 4 |
| 0.80919 | 72. | 47. | 46. | 119. | 211.000 | 71. 4 |
| 0.31633 | 73. | 47. | 46. | 119. | 205.000 | 72. 4 |
| 0.08406 | 74. | 47. | 46. | 119. | 199.000 | 73. 4 |
| 0.05670 | 75. | 47. | 46. | 119. | 191.500 | 74. 4 |

67.11
67.22
67.33
67.44
67.56
67.67
67.78
67.89
68.09
68.18
68.27
68.36
68.45
68.55
68.64
68.73
68.82
68.91
69.09
69.18
69.27
69.36
69.45
69.55
69.64

107.44
107.56
107.67
107.78
107.89
108.11
108.22
108.33
108.44
108.56
108.67
108.78
108.89
109.17
109.33
109.50
109.67
109.83
110.50
32

| | | | | | | |
|---|---|---|---|---|---|---|
| 0.13513 | 98. | 464. | 97. | 791. | 962.000 | 97. 10 |
| 0.40428 | 99. | 464. | 97. | 791. | 945.500 | 98. 10 |
| 0.79447 | 100. | 464. | 97. | 791. | 925.000 | 99. 10 |
| 1.50403 | 101. | 464. | 97. | 791. | 901.500 | 100. 10 |
| 0.90982 | 102. | 464. | 97. | 791. | 874.000 | 101. 10 |
| 1.48901 | 103. | 464. | 97. | 791. | 841.000 | 102. 10 |
| 1.57734 | 104. | 464. | 97. | 791. | 806.000 | 103. 10 |
| 2.70526 | 105. | 464. | 97. | 791. | 771.500 | 104. 10 |
| 3.09044 | 106. | 464. | 97. | 791. | 736.000 | 105. 10 |
| 3.55258 | 107. | 464. | 97. | 791. | 828.500 | 106. 10 |
| 5.25950 | 108. | 464. | 97. | 791. | 1170.500 | 107. 10 |
| 5.37162 | 109. | 464. | 97. | 791. | 1143.000 | 108. 10 |
| 5.29467 | 110. | 464. | 97. | 791. | 1109.000 | 109. 10 |
| 7.15675 | 111. | 464. | 97. | 791. | 1074.500 | 110. 10 |
| 5.86912 | 112. | 464. | 97. | 791. | 1033.500 | 111. 10 |
| 5.96496 | 113. | 464. | 97. | 791. | 990.500 | 112. 10 |
| 6.71579 | 114. | 464. | 97. | 791. | 951.500 | 113. 10 |
| 5.08034 | 115. | 464. | 97. | 791. | 908.500 | 114. 10 |
| 4.57877 | 116. | 464. | 97. | 791. | 926.000 | 115. 10 |
| 5.39298 | 117. | 464. | 97. | 791. | 827.500 | 116. 10 |
| 4.19785 | 118. | 464. | 97. | 791. | 785.500 | 117. 10 |
| 3.79263 | 119. | 464. | 97. | 791. | 741.000 | 118. 10 |
| 4.82061 | 120. | 464. | 97. | 791. | 697.000 | 119. 10 |
| 2.02787 | 121. | 464. | 97. | 791. | 660.500 | 120. 10 |
| 3.42786 | 122. | 464. | 97. | 791. | 627.500 | 121. 10 |
| 3.26986 | 123. | 464. | 97. | 791. | 1502.500 | 122. 10 |
| 1.90001 | 124. | 464. | 97. | 791. | 1464.500 | 123. 10 |
| 0.83112 | 125. | 464. | 97. | 791. | 1423.000 | 124. 10 |
| 0.81505 | 126. | 464. | 97. | 791. | 1376.500 | 125. 10 |
| 0.43529 | 127. | 464. | 97. | 791. | 1329.500 | 126. 10 |
| 0.15642 | 128. | 464. | 97. | 791. | 1278.000 | 127. 10 |
| 0.05032 | 129. | 464. | 97. | 791. | 1226.500 | 128. 10 |

112.13
112.25
112.38
112.50
112.63
112.75
112.88
113.05

113.11
113.16
113.21
113.26
113.32
113.37
113.42
113.47
113.53
113.58
113.63
113.68
113.74
113.79
113.84
113.89
113.95
114.04
114.07
114.11
114.14
114.18
114.21
114.25
114.29
114.32
114.36
114.39
114.43
114.46
114.50
114.54
114.57
114.61
114.64
114.68
114.71
114.75
114.79
114.82
114.86
114.89
114.93
114.96
115.04
115.08
115.12
115.15
115.19
115.23
115.27
115.31
115.35
115.38
115.42
115.46
115.50
115.54
115.58
115.62

115.65
115.69
115.73
115.77
115.81
115.85
115.88
115.92
115.96
116.04
116.08
116.12
116.16
116.20
116.24
116.28
116.32
116.36
116.40
116.44
116.48
116.52
116.56
116.60
116.64
116.68
116.72
116.76
116.80
116.84
116.88
116.92
116.96
117.04
117.09
117.13
117.17
117.22
117.26
117.30
117.35
117.39
117.43
117.48
117.52
117.57
117.61
117.65
117.70
117.74
117.78
117.83
117.87
117.91
117.96
118.04
118.08
118.12
118.16
118.20

118.24
118.28
118.32
118.36
118.40
118.44
118.48
118.52
118.56
118.60
118.64
118.68
118.72
118.76
118.80
118.84
118.88
118.92
118.96
119.04
119.08
119.13
119.17
119.21
119.25
119.29
119.33
119.38
119.42
119.46
119.50
119.54
119.58
119.63
119.67
119.71
119.75
119.79
119.83
119.88
119.92
119.96
120.04
120.08
120.13
120.17
120.21
120.25
120.29
120.33
120.38
120.42
120.46
120.50
120.54
120.58
120.63
120.67
120.71
120.75

120.79
120.83
120.88
120.92
120.96
121.06
121.12
121.18
121.24
121.29
121.35
121.41
121.47
121.53
121.59
121.65
121.71
121.76
121.82
121.88
121.94
122.05
122.11
122.16
122.21
122.26
122.32
122.37
122.42
122.47
122.53
122.58
122.63
122.68
122.74
122.79
122.84
122.89
122.95
123.05
123.11
123.16
123.21
123.26
123.32
123.37
123.42
123.47
123.53
123.58
123.63
123.68
123.74
123.79
123.84
123.89
123.95
124.06
124.13
124.19

124.25
124.31
124.38
124.44
124.50
124.56
124.63
124.69
124.75
124.81
124.88
124.94
125.05
125.09
125.14
125.18
125.33
125.27
125.32
125.36
125.41
125.45
125.50
125.55
125.59
125.64
125.68
125.73
125.77
125.82
125.86
125.91
125.95
126.05
126.11
126.16
126.21
126.26
126.31
126.36
126.42
126.47
126.53
126.58
126.63
126.68
126.74
126.79
126.84
126.89
126.95
127.06
127.11
127.17
127.22
127.28
127.33
127.39
127.44
127.50

```
127.56
127.61
127.67
127.72
127.78
127.83
127.88
127.94
128.09
128.18
128.27
128.36
128.45
128.54
128.64
128.73
128.82
128.91
129.50
//
```

1984-85 Research Initiation Program

Sponsored by the

AIR FORCE OFFICE OF SCIENTIFIC RESEARCH

Conducted by the

SOUTHEASTERN CENTER FOR ELECTRICAL ENGINEERING EDUCATION

Final Report

# ANALYSIS OF AIR FORCE VEHICLE CONDITION RATINGS FROM HISTORICAL DATA


| | |
|---|---|
| Prepared by: | Bruce N. Janson |
| Academic Rank: | Assistant Professor |
| Address: | Department of Civil Engineering<br>Carnegie-Mellon University<br>Pittsburgh, PA 15213 |
| USAF Research: | Capt. James R. Van Scotter, USAF |
| Date: | July 25, 1985 |

## ANALYSIS OF AIR FORCE VEHICLE CONDITION RATINGS FROM HISTORICAL DATA


### ABSTRACT

The method used by the U.S. Air Force to record historical information on the use, maintenance and repair needs of their vehicles is the Vehicle Information Management System (VIMS). A large number of data elements are recorded daily and compiled monthly for most every vehicle at each Air Force base around the world. One factor that is assigned monthly to each vehicle on the basis of current information is the vehicle's condition rating known as the Replacement Code. Its primary determinants are age, accumulated use, and the cost of a one-time repair if it is needed. As a vehicle's age, use and repair needs indicate a decline in its operational reliability, the condition rating of the vehicle is successively downgraded through a sequence of alphabetic replacement codes, the specifics of which will be further described in later sections.

The replacement code is the primary indicator to a vehicle fleet manager and base-level command of the need for new vehicle procurements. As such, the use of this rating as a guideline for vehicle buy allocations has a direct impact on both the cost and functional capability of base fleets. Considering that the Air Force owns and operates over 100,000 vehicles of roughly 330 different types at both major and minor installations around the world, it is important that the replacement code be a valid measure of a vehicle's condition and anticipated performance. The purpose of this research was to assess the economic validity of the replacement code as a repair or replace indicator, and to evaluate the sensitivity of repair or replace decisions to possible changes in its calculation.

# ANALYSIS OF AIR FORCE VEHICLE CONDITION RATINGS FROM HISTORICAL DATA

## 1 Introduction

Effective vehicle monitoring systems are necessary to track the use, maintenance and condition of a vehicle fleet. These systems can also be used to assist vehicle fleet managers in forecasting inventory needs for new vehicles and parts. The reliability of such forecasts will have significant impacts on vehicle buy decisions and the accuracy of capability assessments. Since the condition of a vehicle is often a prime determinant in how it is used, maintained and repaired, and when it is scheduled to be replaced, the useful life of a vehicle, from procurement to salvage, is affected by both its actual and rated conditions. Examples of equipment maintenance and replacement research are [2,5,12,13,14].

The method used by the U.S. Air Force to record historical information on the use, maintenance and repair needs of their vehicles is the Vehicle Information Management System (VIMS). A large number of data elements are recorded daily and compiled monthly for most every vehicle at each Air Force base around the world. One factor that is assigned monthly to each vehicle on the basis of current information is the vehicle's condition rating known as the Replacement Code. Its primary determinants are age, accumulated use, and the cost of a one-time repair if it is needed. As a vehicle's age, use and repair needs indicate a decline in its operational reliability, the condition rating of the vehicle is successively downgraded through a sequence of alphabetic replacement codes, the specifics of which will be further described in later sections.

The replacement code is the primary indicator to a vehicle fleet manager and base-level command of the need for new vehicle procurements. As such, the use of this rating as a guideline for vehicle buy allocations has a direct impact on both the cost and functional capability of base fleets. Considering that the Air Force owns and operates over 100,000 vehicles of roughly 330 different types at both major and minor installations around the world, it is important that the replacement code be a valid measure of a vehicle's condition and anticipated performance.

From May through July of 1984, this researcher worked with the USAF at the Logistics Management Center at Gunter AFS. The objective of that research was to develop a prototype vehicle fleet analysis system for the Zenith Z-100 microcomputer that could retrieve and utilize VIMS data. During that 10-week research engagement, we identified several potential difficulties with the replacement code as a single measure of a vehicle's condition, reliability, expected future performance and economic value. Several needs for further research to evaluate and recommend improvements to the design and/or use of the vehicle replacement code were identified.

The purpose of this research was to assess the economic validity of the replacement code as a repair or replace indicator, and to evaluate the sensitivity of repair or replace decisions to possible changes in its calculation. Since the replacement code is meant to be a reliable measure of a vehicle's present condition, this indicator should react to significant changes in a vehicle's current performance, but not to incidental repair needs or small variations in other operational costs. An explanation of the replacement code is given first that clarifies the successive ordering of these alphabetic ratings. Then, a description and analysis of the one-time repair limit — a key factor in the determination of a vehicle's replacement code — compares it to the calculated salvage value of a vehicle based upon engineering economic principles.

The importance of accounting for price changes in a one-time repair limit is discussed, and it is shown that price changes are accounted for in VIMS by adjustments to a vehicle's standard price. However, the analysis of VIMS data in this study revealed that these adjustments to standard prices appear to be very inconsistent. Hence, a specific recommendation of this study is to examine whether changes in suppliers' prices are being properly updated and utilized within VIMS for calculating one-time repair limits. Section 6 explains how data was retrieved from a VIMS historical record file for a particular base and organized into a usable dataset. Section 7 then examines the impact that small price adjustments to the one-time repair limit might have on the number of vehicles exceeding this limit. Section 8 concludes this report with a summary and recommendations.

## 2 Review of the Air Force Vehicle Replacement Code

The Replacement Code (RC) is updated and recorded monthly for each vehicle of a base fleet in the monthly historical record file of the Vehicle Information Management System (VIMS). These records are usually maintained on a current VIMS tape for the most recent 12 months. A large number of data items are recorded to this database, but only a select few pertain to the determination of the replacement code. A necessary task in the data analysis portion of this research was to retrieve the following selected data elements from the VIMS tape for a given base and place these into a manageable database.

1. Vehicle Registration Number (VRN)
2. Management Code (MC)
3. Vehicle Equivalents (VEQ)
4. Acceptance Date (AD)
5. Standard Price (SP)
6. Replacement Code (RC)
7. Life Expectancy (LE)
8. One-Time Repair Cost Limit (OTL)
9. One-Time Repair Cost Exceeded (OTX)
10. One-Time Repair Cost Price (OTP)
11. Use Code (UC)
12. Average Daily Use (ADU)
13. Cummulative Use (CU)
14. Direct Labor Cost for Repairs (DLC)
15. Total Parts Cost for Repairs (TPC)

Details pertaining to the retrieval of this data from the VIMS data file are discussed in a later section.

The vehicle replacement code is primarily a function of upon three basic criteria -- age, use and one-time repair. The age of a vehicle can be calculated from its Acceptance Date (AD), which is the date at which the vehicle was actually

delivered to a base by its supplier. Both month and year are recorded in the acceptance date. The year of the acceptance date usually agrees with a vehicle's model year, which is the first two digits of its Vehicle Registration Number (VRN).

A vehicle's AD year can easily be one year later than the model year in cases where a late year purchase carries the acceptance date into the following year. In a few instances, however, the AD year can be very different from the MY if a vehicle has been depot repaired or reassigned to a completely different base. An analysis of VIMS data showed that the one-time repair limit, which will be explained later, is always computed on the basis of the acceptance date, even when it differs from the model year substantially.

The use of a vehicle can be recorded in terms of four different units — miles (M), hours (H), units (U) and kilometers (K). A vehicle's Use Code (UC) indicates the particular units in which the Cummulated Use (CU) and the Average Daily Use (ADU) of that vehicle were recorded. A vehicle's use is always measured in units that are consistent with the Average Annual Standard specified in the Air Force 77-310 Motor Vehicle Management Manual [6], or Technical Order 36A-1-1301 [8], if one is available for that particular vehicle type.

In assigning a replacement code to a particular vehicle, both the age and use of the vehicle are compared against their expected lifetime values. The Life Expectancy (LE) of a vehicle is given in years as one of the data elements in the VIMS historical record file. The lifetime expected use (LEU) of a vehicle equals the life expectancy of the vehicle times its average Annual Use Standard (AUS), where LEU = LE * AUS. Unfortunately, the annual use standard for each vehicle is not recorded as a data element in the VIMS historical record file. This omission makes it very awkward to associate the correct AUS values in AFM 77-310 with the vehicles found in a VIMS historical record file.

Section V of Technical Order 00-25-249 [7] on Vehicle Replacement Codes contains descriptions of the replacement codes as listed in Table 1. Some wording changes, particularly the replacement of Miles/Kilometers with Use, have been made for consistency. It is unclear in TO 00-25-249 whether the Use criterion is ever used to determine the replacement codes of vehicles fo which

## Table 1: Vehicle Replacement Codes

The following descriptions are found in Section V of TO 00-25-249. See TO 36A-1-1301 for vehicle life expectancies and lifetime expected use standards, and AFM 77-310 for additional information.

Abbreviations used are: LE = life expectancy (in years); LEU = lifetime expected use (in M/H/U/K); OTL = one-time repair limit (in dollars).

1. **A - Age, Use and One-Time Repair.** Vehicle has exceeded both its LE and LEU; also requires repairs that would exceed its OTL, and the vehicle repair authority has decided that only minimum essential repairs will be made.

2. **B - Age and One-Time Repair.** Vehicle has exceeded its LE, also requires repairs that would exceed its OTL, and it has been decided that only minimum essential repairs will be made.

3. **C - Use and One-Time Repair.** Vehicle has exceeded its LEU, also requires repairs that would exceed its OTL, and it has been decided that only minimum essential repairs will be made.

4. **D - One-Time Repair.** Vehicle requires repairs that would exceed its OTL, and it has been decided that only minimum essential repairs will be made.

5. **F - Obsolete.** Vehicle has been declared obsolete. Vehicle maintenance will manually enter this code into VIMS upon notification.

6. **G - Age and Use.** Both LE and LEU have been exceeded.

7. **H - Age.** Life expectancy has been exceeded.

8. **J - Use.** Lifetime expected use has been exceeded.

9. **K - Age and Use, 1 Year.** Both LE and LEU will be exceeded within 1 year.

10. **L - Age, 1 Year.** Life expectancy will be exceeded within one year.

11. **M - Use, 1 Year.** Lifetime expected use will be exceeded within one year.

12. **N - Age and Use, 2 Years.** Both LE and LEU will be exceeded within 2 years.

13. **P - Age, 2 Years.** Life expectancy will be exceeded within two years.

14. **Q - Use, 2 Years.** Lifetime expected use will be exceeded within two years.

15. **R - Age, Mid-Life.** Vehicle's age has exceeded one-half of its LE.

16. **S - Depot Repaired Vehicles.** Vehicle was depot repaired less than 3 years ago, see paragraph 5-22 for further instructions.

17. **T - Other.** Assign to vehicles whenever codes A-S or U do not apply.

18. **U - Warranty.** Assign to vehicles under new or remanufacture warranty; does not apply to depot repaired vehicles.

Table 2: Replacement Code Criteria

| | Code | Basic Criteria | | | Time Variables | | | | | Special Catagories | | |
|---|---|---|---|---|---|---|---|---|---|---|---|---|
| # | RC | AGE | USE | OTL | ZL | 1Y | 2Y | HL | WRN | DR | OBS | OTHER |
| 1 | A | X | X | X | X | | | | | | | |
| 2 | B | X | | X | X | | | | | | | |
| 3 | C | | X | X | X | | | | | | | |
| 4 | D | | | X | X | | | | | | | |
| 5 | F | | | | | | | | | | X | |
| 6 | G | X | X | | X | | | | | | | |
| 7 | H | X | | | X | | | | | | | |
| 8 | J | | X | | X | | | | | | | |
| 9 | K | X | X | | | X | | | | | | |
| 10 | L | X | | | | X | | | | | | |
| 11 | M | | X | | | X | | | | | | |
| 12 | N | X | X | | | | X | | | | | |
| 13 | P | X | | | | | X | | | | | |
| 14 | Q | | X | | | | X | | | | | |
| 15 | R | X | | | | | | X | | | | |
| 16 | S | | | | | | | | | X | | |
| 17 | T | | | | | | | | | | | X |
| 18 | U | | | | | | | | X | | | |

Key: RC = replacement code
AGE = age of vehicle (in years).
USE = cummulated use (in M/H/U/K).
OTL = one-time repair limit (in dollars).

ZL = zero life expectancy or lifetime expected use remaining.
1Y = 1 yr life " " " " " "
2Y = 2 yr life " " " " " "
HL = half life expectancy or lifetime expected use remaining.
WRN = vehicle under warranty (essentialy full life remaining).

DR = vehicle depot repaired less than 3 years ago.
OBS = vehicle declared obsolete.
Other = whenever codes A-S or U do not apply.

use is measured in hours. Nevertheless, it is easier to comprehend the successive nature of these replacement codes by observing their common criteria as shown Table 2, where an 'X' indicates that the criterion in a given column applies to the replacement code in a given row.

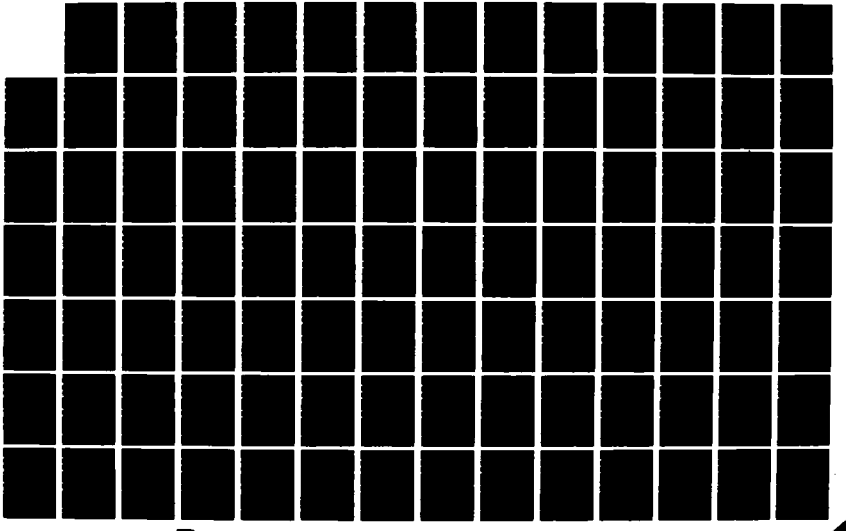
The replacement codes listed in Tables 1 and 2 are mutually exclusive, since all criteria for any one replacement code must be met simultaneously. It is also explained in TO 00-25-249 that sending a vehicle to Depot Repair will revert its replacement code from a letter below L, back up to the letter S, and then down to P. For this reason, all vehicles with replacement codes F, S and T must be treated as special cases. Obsolete and Other are two additional catagories used for vehicles with special circumstances that nullify the standard criteria.

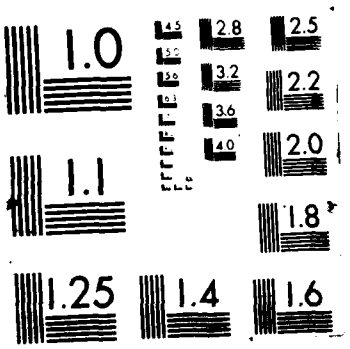
The time variables ZL, 1Y, 2Y, and HL shown in Table 2 can apply to either the life expectancy or the lifetime expected use of a vehicle, as is suggested by the assignment rules for the replacement codes. In terms of life expectancy, ZL (or zero life remaining) implies that the age of the vehicle as measured from its acceptance date has exceeded the life expectancy of the vehicle. In comparison, ZL in terms of LEU implies that the cummulated use of the vehicle has exceeded its lifetime expected use. Life expectancies (in years) and lifetime expected use standards are specified in TO 36A-1-1301 and AFM 77-310 as mentioned above.

Times at which a vehicle has less than one year, two years or half of its life expectancy remaining are directly apparent from the vehicle's age and LE values. It is also clear as to when a vehicle's current CU has exceeded half of its LEU. However, it is unclear as to when a vehicle is said to have less than one [illegible] years of its LEU remaining, since this could be based either on the [illegible] annual use standard (AUS) or upon its own average annual use record [illegible] accurate to classify a vehicle as being within one year of its LE[illegible] difference between its LEU and CU values is less than its own [illegible] as compared to simply being within one AUS of its LEU.

Within the time variable columns of Table 2, a vehicle [illegible] and upward as it gets older. Its transition [illegible] depends, however, upon how intensely it is [illegible]

AD-A186 490 UNITED STATES AIR FORCE RESEARCH INITIATION PROGRAM 02/11
1984 RESEARCH REPORTS (U) SOUTHEASTERN CENTER FOR
ELECTRICAL ENGINEERING EDUCATION INC S W D PEELE
UNCLASSIFIED MAY 86 AFOSR-TR-87-1721 F49620-82-C-0035 F/G 15/1 NL




1.0
1.1
1.25
1.4
1.6
1.8
2.0
2.2
2.5
2.8
3.2
3.6
4.0

less than its AGE times its AUS, then it will be assigned codes R, P, L, H, B and possibly A throughout its lifetime. If a vehicle's use is continually greater than its AGE times its AUS, then it will be assigned codes Q, M, J, C and possibly A throughout its lifetime. A vehicle whose use follows the prescribed AUS fairly closely year after year will probably be assigned codes R, N, K, G and possibly A during its lifetime.

The procedure by which a vehicle's average annual use standard is estimated is not investigated in this research. This value depends upon the fleet size needed at an Air Force base in order to cover all assigned functions, and the intensity of use that a vehicle receives on these assignments. The determination of an optimal fleet size involves many factors including the charcteristics of daily demands for those vehicles, their reliabilibity, and their critical need in the event of an emergency response. As a rule, it is more costly to operate a fleet size in excess of the number of vehicles required to cover all functions with adequate allowance for out-of-commission vehicles.

It is assumed in this research that the annual use standards estimated by the Air Force for its vehicles correctly reflect the trade-offs between fleet size cost and preparedness in that organization. However, the tremendous variety of Air Force base locations and operating conditions does introduce some doubt as to whether a single use standard is appropriate for the same vehicle type at all installations. It is recognized here that a strong need for policy standardization within the Air Force does require that certain simplifying assumptions be made that lead to uniform management directives. Moreover, an analysis of how operating conditions, maintenance procedures and usage intensity affect the useful life of Air Force vehicles is beyond the scope of this research.

The life expectancy of a vehicle and its lifetime expected use are both dependent upon the average annual use of the vehicle and its economical time of replacement. Given that the average annual use of a vehicle is taken to be known and fixed, as opposed to being determined simultaneously with the vehicle's optimal replacement age, the optimal replacement time of a vehicle can be determined theoretically on the basis of its expected operations and maintenance costs. Unfortunately, there is insufficient data in one 12-month VIMS dataset with

which to estimate the optimal replacment age, or useful life expectancy, of any given vehicle type.

Alternatively, the One-Time Repair Limit (OTL) that is updated monthly in the VIMS records can be examined on the basis of available data, and it's calculation can be modified to better reflect the current economic value of a vehicle. In the next section of this report is explained the current procedure used by the Air Force to calculate a vehicle's one-time repair limit. Section 4 shows that the current formula is similar to, but consistently higher than, an alternative calculation of OTL based upon engineering economic calculations of a vehicle's salvage value.

## 3 Explanation of the One-Time Vehicle Repair Limit

Currently, the One-Time Repair Limit (OTL) is primarily an indicator of age and use. It does not reflect the expected operation and maintenance expenses of that particular vehicle type in future years. TO 00-25-249 specifies that OTL for a given vehicle should be calculated on the basis of two different but related ratios. One formula uses AGE/LE ratio, while the other formula uses the CU/LEU ratio. Otherwise, both formulas, as shown by equations (1) and (2), are identical.

$$\begin{aligned} OTL_1 &= SP*(1 - 0.9*AGE/LE) \quad \text{for AGE} <= LE \\ OTL_1 &= SP*(0.1) \quad \text{for AGE} > LE \end{aligned} \tag{1}$$

$$\begin{aligned} OTL_2 &= SP*(1 - 0.9*CU/LEU) \quad \text{for CU} <= LEU \\ OTL_2 &= SP*(0.1) \quad \text{for CU} > LEU \end{aligned} \tag{2}$$

$$OTL = \text{Min}\,[OTL_1, OTL_2] \tag{3}$$

where, SP = Standard Price (of a new vehicle, in dollars)

AGE = Current Date - Acceptance Date (in months)

LE = Life Expectancy (in months)

CU = Cummulated Use (in M/H/U/K units)

LEU = Lifetime Expected Use (in M/H/U/K units)

In the above formulas, LE is multiplied by 12 to convert it to months, and LEU equals LE (in years) times the annual use standard. After calculating both $OTL_1$ and $OTL_2$, the lower of the two is taken as the OTL for that vehicle in that month as given by equation (3).

Figure 1 shows the OTL values for a hypothetical vehicle with a standard has a standard price of $10,000 and a life expectancy of 10 years. It is very straightforward to calculate $OTL_1$ for any vehicle on the basis of its life expectancy and its age calculated from VIMS records. On a graph such as Figure 1, $OTL_1$ can be drawn as a line connecting the standard price at time 0 to 10% of the SP at time LE. For vehicle ages beyond LE, $OTL_1$ is set to 10% of the standard price, as given by equation (1) and shown by the values for $OTL_1$ in Table 3.

By comparison, $OTL_2$ is a function of a vehicle's use, and it will not be straight line unless the vehicle receives the identical amount of use in every month. Moreover, it is not possible to calculate $OTL_2$ directly from VIMS data because the annual use standard for each vehicle type is not included in the VIMS dataset. The graph of $OTL_2$ shown in Figure 1 is based on hypothetical use data for this example vehicle shown in Table 3. Note that in Figure 1, $OTL_2$ is always greater than or equal to $OTL_1$. Only at times when the total cummulated use of a vehicle exceeds its age times its annual use standard will $OTL_2$ will be lower than $OTL_1$. Otherwise, $OTL_1$ will always be lower, which was found to be the case for all vehicle records examined in this study for one particular base.

As explained in the next section, the reasoning behind a one-time repair limit is that it reflects the salvage value of a vehicle at that time. One implication of using the above formulas to determine the one-time repair limit is that the salvage value of a vehicle, no matter how old, is assumed to be atleast 10% of its standard price, which is a common rule for equipment depreciation accounting [4]. A maintenance related reason for the 10% minimum is, however, that it insures the allowance of minimal repairs to vehicles that are needed and are still operational past their expected lifetimes. Otherwise, a very usable vehicle could be left out-of-commission because of needing relatively inexpensive repairs.

## 4 Alternative Calculation of the One-Time Repair Limit

The purpose of setting one-time repair limits on vehicles is to potentially avoid uneconomical repair expenditures on a vehicle beyond its salvage value. The calculation of salvage value for a given vehicle in a given year requires that the

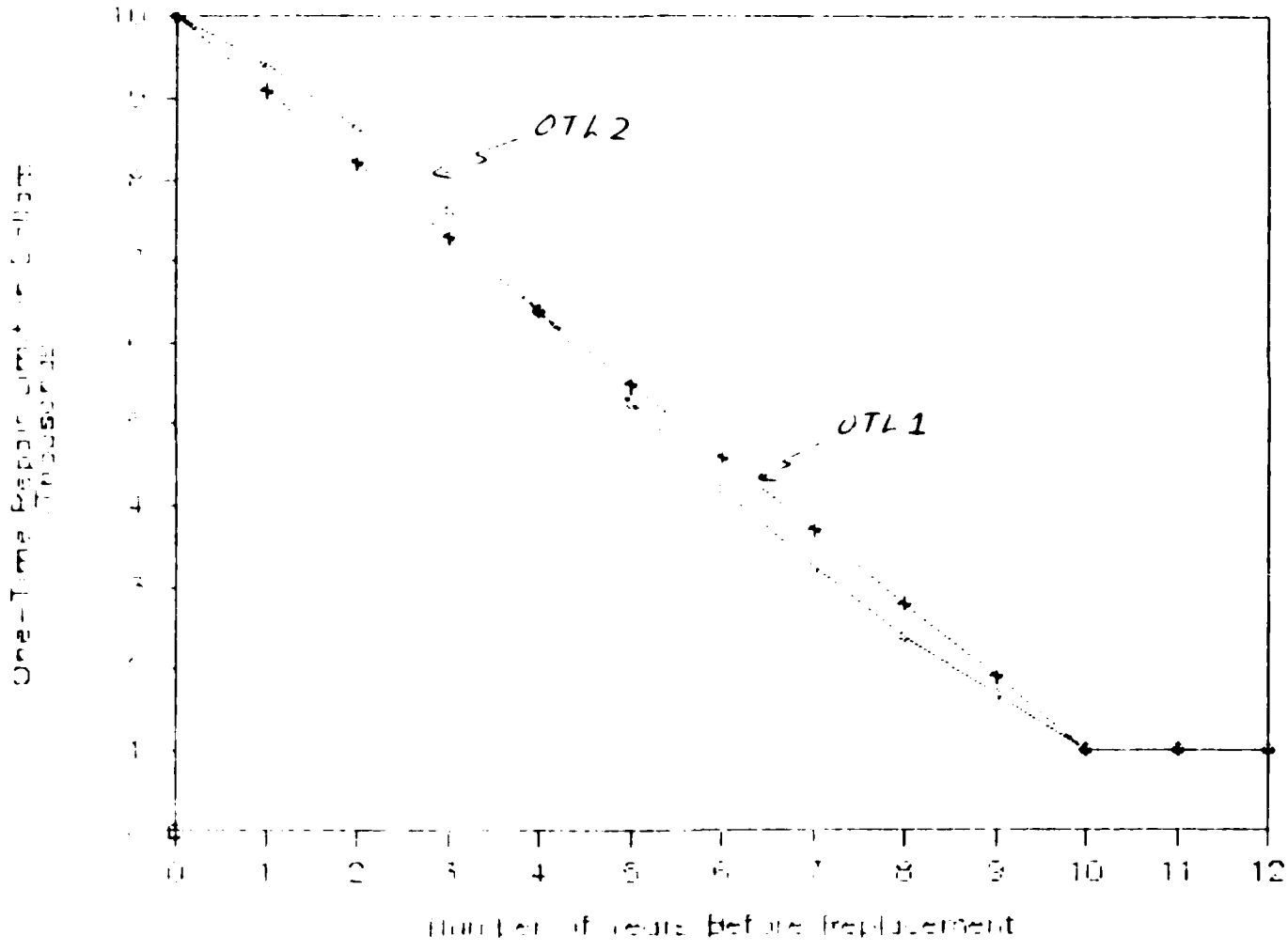
## Table 3: Calculations of $OTL_1$ and $OTL_2$

Listed below are values of annual and cummulated use for a hypothetical vehicle with a standard price of $10000.

| Year | Annual Miles | Total Miles | OTL2 Dollars | OTL1 Dollars | OTL Dollars |
|---|---|---|---|---|---|
| 1 | 5000 | 5000 | 9437.5 | 9100.0 | 9100.0 |
| 2 | 7000 | 12000 | 8650.0 | 8200.0 | 8200.0 |
| 3 | 9000 | 21000 | 7637.5 | 7300.0 | 7300.0 |
| 4 | 11000 | 32000 | 6400.0 | 6400.0 | 6400.0 |
| 5 | 10000 | 42000 | 5275.0 | 5500.0 | 5275.0 |
| 6 | 9500 | 51500 | 4206.3 | 4600.0 | 4206.3 |
| 7 | 8500 | 60000 | 3250.0 | 3700.0 | 3250.0 |
| 8 | 7500 | 67500 | 2406.3 | 2800.0 | 2406.3 |
| 9 | 6500 | 74000 | 1675.0 | 1900.0 | 1675.0 |
| 10 | 6000 | 80000 | 1000.0 | 1000.0 | 1000.0 |
| 11 | 0 | 80000 | 1000.0 | 1000.0 | 1000.0 |
| 12 | 0 | 80000 | 1000.0 | 1000.0 | 1000.0 |

Note: For vehicle in this example, AUS = 8000 mi/yr and LE = 10 yrs.

# Figure 1: Comparison of OTL1 and OTL2



principles of life cycle costing be applied correctly. Textbooks such as [3] and [11] explain the engineering economic principles that are the basis for present value and uniform annual value calculations used in life cycle costing and replacement scheduling of transit equipment [1,9,10].

The calculation of a one-time repair limit based upon engineering economics is equivalent to determining the salvage value of the vehicle in any period. Data required to make this calculation are the vehicle's original purchase price or standard price, its expected operation and maintenance cost in each period, and an appropriate discount rate or oppurtunity cost of capital for the equipment owning organization. If inflation is accounted for within the analysis, then the cash flows in this stream can be expressed in current dollars at time 0 or in "then-current" dollars for each of the time periods. Accounting for inflation requires that a suitable equipment cost price index be available for the analysis period.

The final key assumptions to the calculation of a vehicle's salvage value based upon engineering economics are that:

1. This vehicle can be replaced by an equivalent vehicle at the time that the salvage value of this vehicle equals zero, and that this replacement process can continue forever.

2. The standard price of the replacement vehicle (expressed in time 0 discounted dollars) will equal the time 0 price of the current vehicle.

3. The operation and maintenance costs of the replacement vehicle (expressed in time 0 discounted dollars) will equal the time 0 costs of the current vehicle.

Given that these assumptions are valid, the key to determining a vehicle's economically efficient replacement time is to evaluate the equivalent uniform annual cost (EUAC) of expenditures on this vehicle for alternative replacement times over a realistic planning horizon . In terms of economic efficiency, the optimal replacement time is the one that results in the lowest EUAC.

In order to calculate EUAC values for the $20,000 hypothetical vehicle represented in Figure 1, an assumed set of operations and maintenance costs for this vehicle in each year are listed in Table 4. These annual costs were chosen to represent a typical vehicle expenditure history in which there is a uniform base amount, a slowly increasing gradient of minor repair costs after the first year, and

a more sharply increasing gradient of repair costs after the mid-life of the vehicle. The optimal time to replace this vehicle so as to operate at the minimum EUAC point is 14 years. These EUAC values are listed in Table 4 and shown as a graph in Figure 2.

An explanation of the formula used to calculate the EUAC values for this vehicle is given in Appendix A. One assumption made in calculating these EUAC values is that the expected salvage value of a vehicle at its optimal replacement time will be zero, which is basically true of a rational salvage market if we accept the premise that Brealey and Myers prescribe as the Fundamental Financial Concept of Efficient Capital Markets: [4, pg. 265]

> "If capital markets are efficient, then the purchase or sale of any security at the prevailing market price is a zero-NPV transaction."

Given the salvage market to be efficient, then the one-time repair limit that should be placed upon a vehicle at any time preceeding its replacement date should be equal to the vehicle's salvage value at that time. Salvage values for the example vehicle are also listed in Table 4, where it is shown to equal zero at the end of year 10. The formula used to calculate these salvage values is also explained in Appendix A.

The justification for performing a one-time vehicle repair is that this one-time repair will return the vehicle to the average operating condition of similar vehicles of common age and use. This vehicle is then expected to perform as well as any similar vehicle that could have been purchased at the salvage value. Given that the one-time repair being considered will return a vehicle to average working condition for its remaining lifetime, then the one-time repair limit should equal the salvage value of an average working vehicle of similar type at that point in time. The alternative would be to salvage the vehicle and purchase a different new or used one. However, if the salvage market is working properly, then the value of the unrepaired vehicle should exactly equal the salvage value of a similar working vehicle minus the cost of repairs. The Air Force can validly operate within these principles since they effectively control the salvage values of their own vehicles by setting their own vehicle lifetimes and one-time repair limits.

## Table 4: Calculations of Equivalent Uniform Annual Costs and Economic Salvage Values

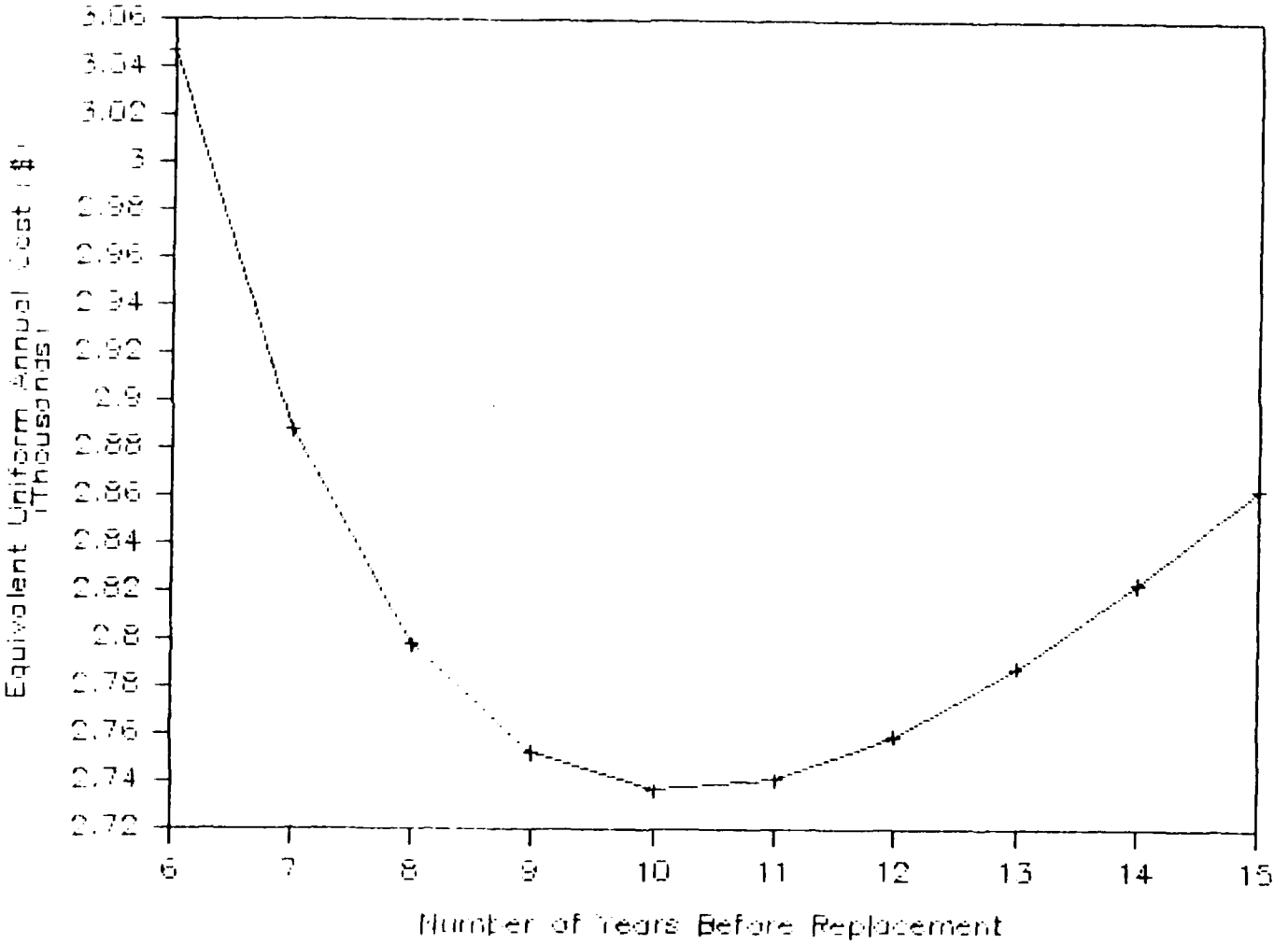
Listed below are hypothetical cash flows for this example vehicle.

| | |
|---|---|
| SP = Standard Price at Time 0 = | 10000 |
| UB = Annual Base O & M Cost = | 500 |
| G1 = Annual O & M Cost Grad = | 100 |
| Y1 = Year in which G1 begins = | 2 |
| G2 = Annual O & M Cost Grad = | 220 |
| Y2 = Year in which G2 begins = | 6 |
| i = Annual Discount Rate = | 0.10 |
| t = Time of Replacement = | 10 |
| UACt = UAC if held to time t = | 2736.82 |
| CPVt = CPV if held to time t = | 16816.59 |

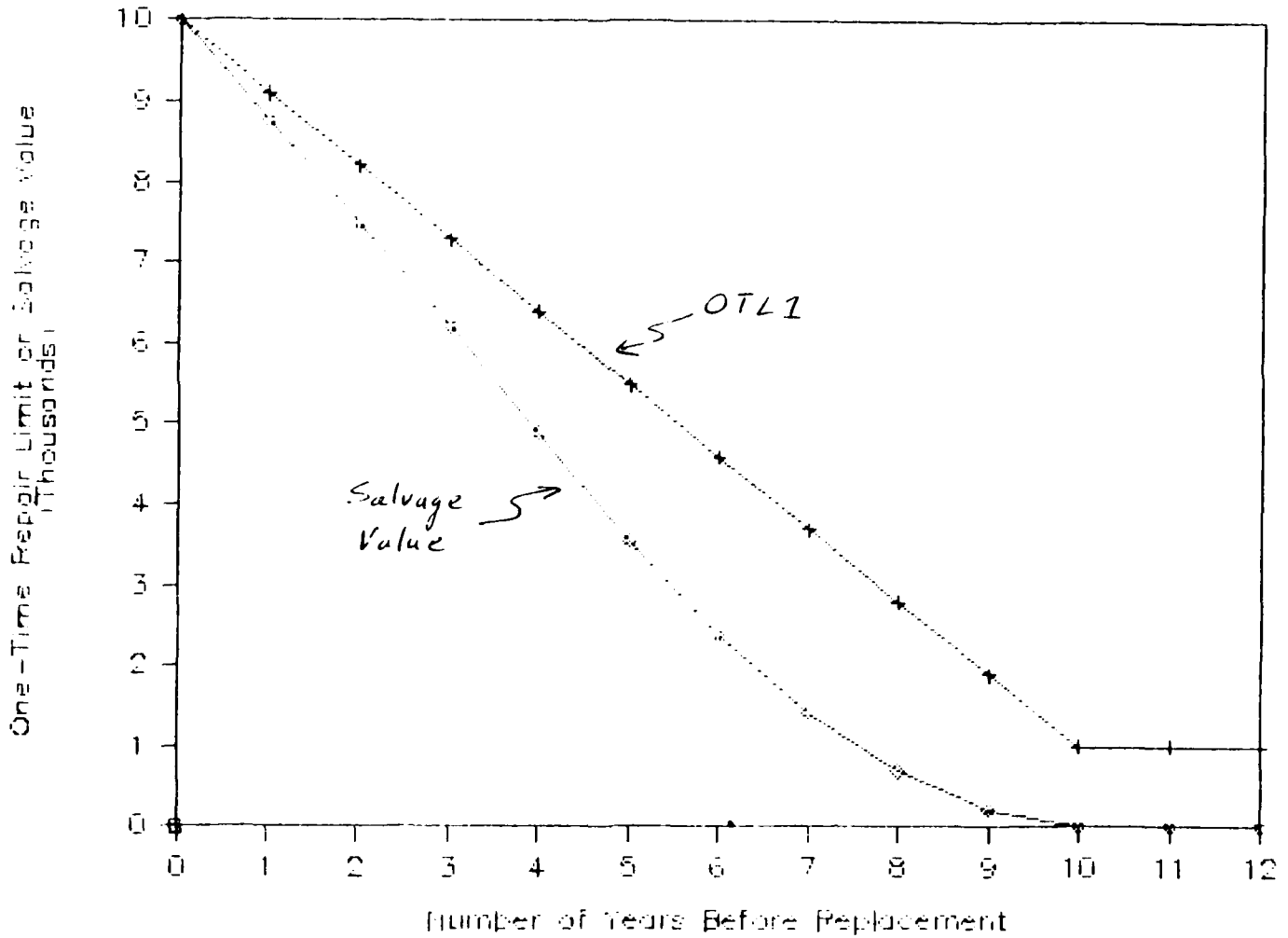
| Replace Time | Cash Flow | CPV | EUAC | Salvage Value |
|---|---|---|---|---|
| 0 | 10000.0 | 10000.0 | 10000.0 | 10000.0 |
| 1 | 500.0 | 10454.5 | 11500.0 | 8763.2 |
| 2 | 600.0 | 10950.4 | 6309.5 | 7502.7 |
| 3 | 700.0 | 11476.3 | 4614.8 | 6216.1 |
| 4 | 800.0 | 12022.7 | 3792.8 | 4900.9 |
| 5 | 900.0 | 12581.6 | 3319.0 | 3554.2 |
| 6 | 1220.0 | 13270.2 | 3046.9 | 2392.8 |
| 7 | 1540.0 | 14060.5 | 2888.1 | 1435.2 |
| 8 | 1860.0 | 14928.2 | 2798.2 | 701.9 |
| 9 | 2180.0 | 15852.7 | 2752.7 | 215.3 |
| 10 | 2500.0 | 16816.6 | 2736.8 | 0.0 |
| 11 | 2820.0 | 17805.0 | 2741.3 | 0.0 |
| 12 | 3140.0 | 18805.5 | 2760.0 | 0.0 |
| 13 | 3460.0 | 19807.7 | 2788.5 | 0.0 |
| 14 | 3780.0 | 20803.1 | 2823.9 | 0.0 |
| 15 | 4100.0 | 21784.6 | 2864.1 | 0.0 |

Note: All cash flow, EUAC and salvage values are expressed in undiscounted dollars for each year. Each cost present value (CPV) amount equals the sum of discounted cash flows up to the end of the year shown.

# Figure 2: Uniform Annual Cost (EUAC)



# Figure 3: OTL1 versus Salvage Value



Theoretically, EUAC curves and salvage values could be estimated for each Air Force vehicle type based upon historical records of operations and maintenance expenditures for similar vehicles. If this were done, the life expectancy of a vehicle, as specified in TO 36A1-1-1301, should agree approximately with the year corresponding to the lowest point of its EUAC curve. Although there does not exist enough data currently available with which to estimate EUAC values for an actual Air Force vehicle type, we can compare the salvage values listed in Table 4 with the values for $OTL_1$ given in Table 1 as shown by the graph in Figure 3. The $OTL_1$ values are consistently higher than salvage values for corresponding years, but we can see by this comparison that $OTL_1$ is a reasonable approximation to economically efficient salvage values. The major reason for any difference is that $OTL_1$ is drawn to 10% of a vehicle's standard price at the time of replacement rather than zero.

Having shown some economic validity to the straightforward calculation of $OTL_1$ given by equation (1), attention must now be given to the fact that both sets of values shown in Figure 3 fail to include the proper treatment of price changes in both repair and replacement costs of a given vehicle. Equipment price changes can occur for a variety of reasons such as technological differences between older vehicles and their replacements, or changes in contract agreements between the Air Force and its suppliers. General inflation or selective input price changes to the vehicle manufacturing industry can also have an impact. Whatever the reason for price changes, it is important to calculate the one-time repair limit in "then-current" dollars for the period in which a repair is being considered. Unless one-time repair limits are adjusted for price changes, a vehicle could be denied an economically justified repair for exceeding a limit based on non-current prices.

The Statistical Abstract of the United States contains producers price indexes for many industrial sectors of the U.S. economy. Price index values for the Transportation Equipment sector for the years 1970-1980 are listed below.

**Producer Price Index Values for Transportation Equipment**

| Year | 1970 | 1973 | 1974 | 1975 | 1976 | 1977 | 1978 | 1979 | 1980 |
|---|---|---|---|---|---|---|---|---|---|
| Index | 100.0 | 110.0 | 120.0 | 135.3 | 144.5 | 154.2 | 165.9 | 179.8 | 197.9 |

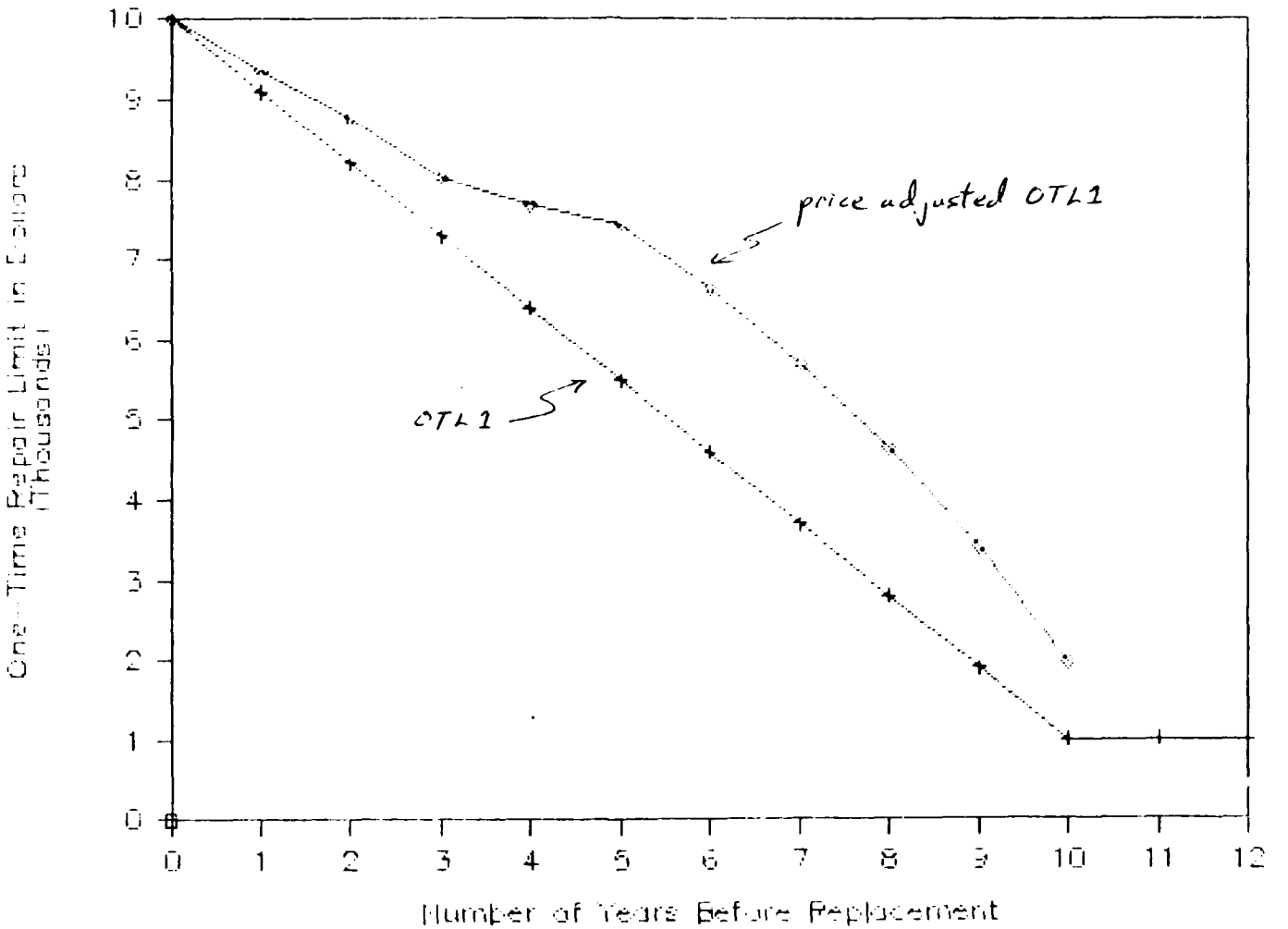
Source: Statistical Abstract of United States (1982-83). The values have been adjusted proportionately so that 1970 equals 100.

Since the above index equals 100 for 1970, each value shown represents the equivalent cost in that year of a comparable equipment expenditure valued at $100 in 1970. In Figure 3 above, if time 0 corresponds to the end of 1970, then time 10 equals the end of 1980. Figure 4 shows both the straightline $OTL_1$ values from Figure 1 and their inflated values after multiplication by the above index values. Note that by the end of year 10 (or 1980), the inflated one-time repair limit is almost twice the value of the uninflated limit.

The same graph of inflated one-time repair limits shown in Figure 4 can be obtained by multiplying the standard price of the vehicle by the index value for each year and drawing the $OTL_1$ line for that year based upon this amount. This method of annually updating the standard price of a replacement vehicle so that OTL values are adjusted proportionately is used by VIMS. Hence, the Standard Price that appears in each monthly vehicle record of the VIMS database can be referred to more appropriately as a Replacement Price.

A caution is provided here concerning economically valid changes in a vehicle's OTL value whenever a change in its standard price reflects technological differences in the replacement vehicle. The effects of general inflation on price levels can often be disregarded from standard engineering economic calculations since, if inflation affects all cash flows in an alternatives analysis to the same degree, then proper analyses with and without adjustments for inflation will result in the same preferred alternative. For example, the optimal replacement time of a vehicle is not affected by general price inflation. Similarly, if a replacement vehicle is technologically and functionally equivalent to the current vehicle, then a supplier's price increase must be responded to by an increase in the one-time repair limit of the current vehicle. However, if a replacement vehicle has been selected that is technologically superior to the current vehicle, and its higher price is acceptable based upon the benefits to be derived from its enhanced capabilities, then the current vehicle might be considered obsolete and thus warrant an even lower one-time repair limit, or an earlier replacement time, than would otherwise be assigned.

# Figure 4: OTL1 and Price Ajusted OTL1



Currently, an obsolete designation can be assigned to the replacement code of a vehicle, which effectively reduces its OTL to zero, since no significant repair work can be authorized. Ideally, the optimal replacement time for the current vehicle should be altered in response to the greater benefits of its technologically superior replacement. However, significant modifications to the current VIMS database and OTL calculations would be required to isolate the effects of these benefit and quality factors on replacement vehicle prices. Hence, the current method of updating the Standard Price based upon the most recently acquired price for a replacement vehicle is a practical alternative.

The primary conclusions of this section are that:

1. Setting one-time repair limits for equipment is a valid method of preventing repair expenditures beyond the current economic value of a vehicle.

2. The economic value of a vehicle, as reflected in its salvage value, can theoretically be determined from the life cycle costs of similar vehicles.

3. The current OTL formula used by the Air Force is similar to, but somewhat higher than, the salvage value of a vehicle based upon engineering economic calculations. Hence, OTL appears to be a generous estimation of a vehicle's true economic value.

4. Since the OTL formula used by the Air Force is based upon a vehicle's standard price, one-time repair limits are affected by any changes to a vehicle's standard price because of general inflation, selective price changes to specific equipment, or technological differences in replacement vehicles. Whatever the reason for price changes, each vehicle's standard price must be adjusted appropriately so that its one-time repair limit is a value comparable to "then-current" dollars at any given time.

The impact of price adjustments to the one-time repair limit on recent repair or replace decisions at a given Air Force base will be examined next by searching a VIMS historical record file for instances in which vehicles had approached or exceeded their OTL's over the last year. The purpose of this analysis is to assess the sensitivity of repair or replace decisions to the one-time repair limit. In short, if a improved method of treating price and technological changes in vehicles were added to the VIMS calculation of OTL values, how much of an impact might this have had on recent repair or replace decisions.

## 5 Retrieval of Data from the VIMS Historical Record File

Initially, all 6507 monthly vehicle assignment, maintenance and use records on tape ARAD6T in file ARADOF were copied to a hard disk file using a tape copy utility on the mainframe computer. Since each record has length 700 (i.e. contains 700 characters), a very large temporary storage allocation was required on the hard disk to store this entire dataset. However, since only a select number of data fields would be required to perform the investigations of this research, a subset of required data elements listed in Table 5 were extracted from this large file and written to a smaller file by program ARADO1 as discussed next.

Listings of all computer programs used in this study to breakout, examine, process, summarize and display the data are included in Appendix B. Each of these programs was written in standard FORTRAN. Initially, ARADO1 is used to produce smaller files of required data elements, but no changes whatsoever were made to the data in this reduction process. Hence, ARADO1 preserves all data entries exactly as they were copied from the ARAD6T tape in this first step of the conversion process.

In scaning through the files produced from ARADO1, it was observed that the consistency of the records was dramatically different for vehicle classes other than D, E and L. There were roughly 20 'K' vehicles preceeding 'L' vehicles in the file, and then some more vehicles with 'K' in their VRN's but not in their mangement codes. There were also many 'X' and 'P' class vehicles in the end of the file with missing management codes or LE values. Hence, the records for vehicle classes other than D, E and L were deleted from the files. This left a total of slightly less than 4000 vehicle records in the dataset to be used in the analysis. The records for these vehicles were then divided into three separate files containing:

1530 records for 135 D vehicles
1048 records for 95 E vehicles
1264 records for 117 L vehicles.

**Table 5: Data Retrieved from the ARADOF File of the ARADGT Tape of Monthly Air Force VIMS Vehicle Records**

| Item# | Field 2X | #Chars | Units | Field Name | Abbrev |
|---|---|---|---|---|---|
| 1 | 3-10 0X | 8 | Alphanumeric | Vehicle Registration Number | VRN |
| 2 | 11-14 33X | 4 | Alphanumeric | Management Code | MC |
| 3 | 48-50 30X | 3 | Whole Vehicles | Vehicle Equivalents | VEQ |
| 4 | 81-84 9X | 4 | Year/Month | Acceptance Date | AD |
| 5 | 94-99 0X | 6 | Whole Dollars | Standard Price | SP |
| 6 | 100 9X | 1 | Alpha | Replacement Code | RC |
| 7 | 110-111 6X | 2 | Whole Years | Life Expectancy | LE |
| 8 | 118-123 0X | 6 | Whole Dollars | One-Time Repair Cost Limit | OTL |
| 9 | 124 0X | 1 | " "=no;"-"=yes | One-Time Repair Cost Exceeded | OTX |
| 10 | 125-131 165X | 7 | Whole Cents | One-Time Repair Cost Price (current estimate if applies) | OTP |
| 11 | 297 0X | 1 | M/H/U/K | Use Code | UC |
| 12 | 298-300 0X | 3 | M/H/U/K | Average Daily Use | ADU |
| 13 | 301-306 98X | 6 | M/H/U/K | Cummulative Use | CU |
| 14 | 395-400 18X | 6 | Whole Cents | Direct Labor Cost for Repairs (excluding accidents) | DLC |
| 15 | 419-425 | 7 | Whole Cents | Total Parts Cost for Repairs (excluding accidents) | TPC |

Note: All of the above values that can change on a monthly basis are shown as "this month" values. These include RC, OTL, OTX, OTP, DLC and TPC. CU accumulates continuously, and ADU is computed on the basis of CU. ADU is not month specific.

### 5.1 Reformating the Records

Program ARADO2 is used as a second step in the conversion process reduce the files from ARADO1 to an essential number of records. The first and last records for each vehicle were always retained, and among the others, only records in which a significant data element changed were written.

1. The following data elements never vary:
   - Vehicle Registration Number (VRN).
   - Management Code (MC).
   - Life Expectancy (LE).
   - Use Code (UC).
2. The following data elements are expected to change monthly, and a change in any of them would not cause the record to be written.
   - Average Daily Use (ADU).
   - Cummulative Use (CU).
   - One-Time Repair Cost Limit (OTL).
   - One-Time Repair Cost Exceeded (OTX).
3. The following data elements can change monthly, and if so, the record was written.
   - Acceptance Date (AD).
   - Standard Price (SP).
   - Replacement Code (RC).
4. The record was written whenever the One-Time Repair Price (OTP) exceeded the One-Time Repair Limit.
5. The Total Parts Cost for Repairs (TPC) and the Direct Labor Cost for Repairs (DLC) do change monthly, and these were accumulated as running totals and simply printed each time a record was otherwise written.

Whenever a record is written, it's first item is the number of the record for this vehicle in the ARADO1 file (e.g. 1 = first monthly record, and 12 = 12th monthly record). Each vehicle should have 12 records for each of 12 months in a year, except for new or salvaged vehicles during the year.

Other adjustments to the data by ARADO2 include deleting the first character of the Total Parts Cost, since it was always found to be a zero or a bracket. The One-Time Repair Price (OTP), the Direct Labor Cost (DLC) and the Total Parts Cost (TPC) were converted from whole cents into whole dollars. In addition, all numeric data elements were written in integer form, and thus all leading zeros were striped away. The output files from ARADO2 were thus of a better form for both visual scanning to numerical analyses.

Note that the Standard Price is included in the set of values that can change monthly. It was anticipated that the standard price of a vehicle would probably show one or two changes in each 12-month period so as to reflect price adjustments in the designated replacement vehicle. However, the adjustments to standard prices found on this VIMS tape revealed many inconsistencies. Changes to standard prices occurred most often in the last monthly records for some but not all vehicles. Instances of both price increases and decreases were found, and sometimes in records other than the last. Furthermore, amomg vehicles of the same type and model year with the same standard price in the first record, some did not receive any change while others received a range of changes. For example, listed below are the standard prices found in the first and last monthly records of ten D541 vehicles in this dataset.

**Standard Prices from Monthly Records of Ten D541 Vehicles**

| Vehicle's Model Year | First Record's Standard Price | Last Record's Standard Price |
|---|---|---|
| 1967 | $7143 | $2857 |
| 1972 | $7143 | $4669 |
| 1972 | $4237 | $4237 |
| 1973 | $4237 | $4676 |
| 1974 | $4237 | $4676 |
| 1975 | $4237 | $4676 |
| 1976 | $7143 | $7143 |
| 1977 | $7143 | $6877 |
| 1977 | $7143 | $5572 |
| 1979 | $4237 | $4676 |

Note that the price given in the first record for each vehicle is either $4237 or $7143, which logically indicates two different D541 vehicle models. By comparison, prices that appear in the last monthly records for these same vehicles

show a great variety of changes. Without examining the records for the following year, it is unclear as to whether these last record prices become the first record prices of the following year's data, or whether these last record prices can be ignored. Nevertheless, the fact that such widely varied price changes are frequently observed in the VIMS data suggests that reasons for these changes need to be investigated. These changes certainly reflect price adjustments for reasons other than general inflation, suppliers' prices changes or technological differences in replacement vehicles.

### 6 Analysis of Vehicles Exceeding Their One-Time Repair Limits

In previous sections was discussed the method by which the one-time repair limit is calculated in VIMS and how adjustments are made to a vehicle's standard price that cause proportional changes in the OTL values for these vehicles. Inconsistencies were noted in the standard price changes observed in the last monthly records for these vehicles, as can be seen by paging through the records shown in Appendix C. However, it was found that OTL values in the vehicle records did most always agree with whatever standard price was given as explained next.

Before compiling statistics for vehicles that had exceeded their one-time repair limits, the OTL values found in the data were compared to equations (1-3). It was found in the data for D, E and L vehicles that OTL was always computed on the basis of a vehicle's age from its acceptance date, and never upon its use. This indicates that either (1) vehicles are not being used anywhere close to their annual use standards, or (2) the VIMS computation of OTL is not computing $OTL_2$ properly before selecting $OTL_1$ as the lower of the two. Not one case was found in 3842 records for 347 vehicles where the value of OTL selected had been calculated on the basis of vehicle use.

The fact that $OTL_1$ is lower than $OTL_2$ for most all vehicles during their lifetimes is not unexpected. The vehicle shown in Figure 1 has an annual use standard of 8000 miles per year. However, in the first year, it was only used 5000 miles. Even if this vehicle were used 9000 miles in each of the following 3 years, $OTL_1$ would still have been lower than $OTL_2$. Hence, we see that if the use of a

vehicle falls behind its standard or expected use up to that point in time, which is very probable for most vehicles at some age, then $OTL_1$ is likely to remain lower than $OTL_2$ for the remainder of that vehicle's life.

A few cases were found among roughly 10 vehicles in which OTL was different from $OTL_1$, but not because it was computed on the basis of vehicle use. These cases simply indicated a very inconsistent calculation of OTL, such as changing the age of the vehicle midstream. Moreover, the acceptance date remained the basis for OTL values, even when the model year of the vehicle and its acceptance date differed substantially, e.g. by as much as ten years. This use of the acceptance date may be the intended policy for cases in which a vehicle is returned from depot repair.

In order to examine just how sensitive repair or replace decisions might be to the one-time repair limit, program ARADO2 extracted a vehicle's record whenever its One-Time Repair Price (OTP) exceeded its one-time repair limit. Vehicles that had exceeded their one-time repair limits in a previous year would not be identified in this analysis. Listed in Table 6 are the numbers of D, E and L vehicles that had a OTP value greater than OTL recorded. The vehicles were grouped according to the percentage range by which their OTP exceeded their OTL. Within this one 12-month period, 10% of the D, E and L vehicles at this base had been estimated to require repairs that exceeded their one-time repair limits. More importantly, the total standard price of replacement vehicles for cases in which OTP was within 25% of its OTL summed to $146,000.

Previous discussions showed how dramatically the effects of inflation can change a vehicle's replacement price, and how varied the standard prices assigned to seemingly identical model vehicles can be. Given the margin for error that exists in properly adjusting standard prices for inflation and technological change, the $146,000 worth of vehicles found above to have had exceeded their one-time repair limits by less than 25% might well have fallen within slightly inflated or otherwise adjusted limits. This indicates that the dollar amount involved in decisions to deny repair of Air Force vehicles because of the one-time repair limit is sensitive to the proper treatment of standard price changes.

**Table 6: Analysis of Vehicles That Exceeded Their One-Time Repair Limits Within the Last Year**

*** TOTAL NUMBER OF VEHICLES IN CLASS D = 135
*** NUMBER OF D VEHICLES EXCEEDING OTL = 18

| RANGE | No. of Vehicles | Total SP | Total OTL | Total OTP |
|---|---|---|---|---|
| 0- 5% | 0 | 0 | 0 | 0 |
| 5- 10% | 0 | 0 | 0 | 0 |
| 10- 15% | 0 | 0 | 0 | 0 |
| 15- 20% | 2 | 76446 | 7645 | 8882 |
| 20- 25% | 0 | 0 | 0 | 0 |
| 25- 50% | 6 | 137423 | 14934 | 19592 |
| 50-100% | 5 | 57713 | 6937 | 12207 |
| 100-500% | 3 | 17208 | 3952 | 9994 |

*** TOTAL NUMBER OF VEHICLES IN CLASS E = 95
*** NUMBER OF E VEHICLES EXCEEDING OTL = 13

| RANGE | No. of Vehicles | Total SP | Total OTL | Total OTP |
|---|---|---|---|---|
| 0- 5% | 4 | 38926 | 3894 | 4001 |
| 5- 10% | 1 | 10196 | 1020 | 1093 |
| 10- 15% | 1 | 10196 | 1020 | 1123 |
| 15- 20% | 1 | 10196 | 1020 | 1194 |
| 20- 25% | 0 | 0 | 0 | 0 |
| 25- 50% | 2 | 18534 | 1854 | 2364 |
| 50-100% | 2 | 16676 | 1668 | 2921 |
| 100-500% | 2 | 16676 | 1668 | 4044 |

*** TOTAL NUMBER OF VEHICLES IN CLASS L = 117
*** NUMBER OF L VEHICLES EXCEEDING OTL = 4

| RANGE | No. of Vehicles | Total SP | Total OTL | Total OTP |
|---|---|---|---|---|
| 0- 5% | 0 | 0 | 0 | 0 |
| 5- 10% | 0 | 0 | 0 | 0 |
| 10- 15% | 0 | 0 | 0 | 0 |
| 15- 20% | 0 | 0 | 0 | 0 |
| 20- 25% | 1 | 25927 | 2593 | 3162 |
| 25- 50% | 2 | 33147 | 3315 | 4304 |
| 50-100% | 0 | 0 | 0 | 0 |
| 100-500% | 1 | 7220 | 722 | 1921 |

Note: RANGE = (OTP-OTL)*100/OTL = percent y which OTL was found to exceed OTP. All other columns show totals for vehicles within these ranges.

It is also interesting to note by scanning through the output from ARADO2 that, for many vehicles, the one year accumulation of direct labor and total parts costs over the last 12 months of records shown, exceeded a vehicle's one-time repair limit while the repairs in any one month did not. It may have been preferable to retire those problem vehicles rather than continue with repairs. Both of these difficulties with the current use of the one-time repair limit require further analysis in order to determine their impact on the efficient allocation of vehicle buy expenditures.

## 7 Summary and Recommendations

Improved forecasts of vehicle repair and replacement needs could assist vehicle fleet managers and base commanders in preparing for future needs rather than having to react to sudden shortfalls in vehicle availability. This study recommends that the current procedure used to adjust the standard price of vehicles, which in turn affects their one-time repair limits be examined more thoroughly for its economic validity. While it is correct to adjust standard prices to reflect the price differences of replacement vehicles, the data indicates that current adjustments to the standard prices are very inconsistent and of such a magnitude as to have a significant impact on the dollar amount of the repair or replace decisions that they are affecting. The analysis showed that vehicles had exceeded their one-time repair limits by less than 25% in a significant number of cases. As a result, those vehicles were potentially denied repair and retired from service at times when repair may have been the preferred alternative.

Several aspects of the vehicle replacement code were also identified in this report as assumptions or rules that may not be universally appropriate to the wide range of daily vehicle uses, operating conditions, and mission support requirements of all Air Force installations. For example, a different weight or critical priority associated with the economic cost of vehicle downtime can greatly affect the best timing of replacement for that vehicle. The critical nature of some vehicles at certain bases may warrant special treatment, but any variance from standard replacement policies must be balanced against demands for uniform treatment within the vehicle buy program.

In many organizations, standardized procedures that lead to uniform management directives are often developed as cost effective responses to the need for efficiency, often at some compromise to special needs and circumstances. The Air Force vehicle buy program is a case in which the advantages of policy standardization are quite apparent. However, while the replacement code can provide for a consistent classification of vehicle conditions, it also overlooks the performance records and special requirements of individual vehicles. Hence, the implications of using a standardized replacement code on the cost and frequency of vehicle replacements in the vehicle buy program should also be examined.

While it is important to recognize the inherent difficulties with using a catagorical vehicle condition rating for all vehicles as opposed to treating individual vehicles on a case-by-case basis, the approach of this research was to accept the need for a standardized index and thus look for ways in which the validity of this index could be improved. It appears that adjustments to standard prices currently maintained in VIMS may not be accounting for supplier's price changes in the correct manner, and that improvements in this regard are very possible after reasons for inconsistencies in theprice adjustments are explained. Another concern mentioned in this report is the method by which vehicle life expectancies are estimated, since this depends upon engineering economic principles as explained.

The ultimate objective of improvements sought to current procedures is to increase the cost effectiveness of expenditures on vehicles and vehicle fleet management costs throughout the Air Force. To this end, repair or replace indicators such as the replacement code that are of direct consequence to the vehicle buy program should be designed to best reflect both the true economic value of a vehicle and its importance to emergency preparedness that the Air Force must consider in its vehicle fleet management directives.

**Acknowledgements**

The author would like to thank Major Dan King and Capt. James Van Scotter of the Air Force Logistics Management Center at Gunter AFS for their help in obtaining and explaining the Air Force documents and data used in this research.

## REFERENCES


1. Armour R.F. (1980) An Economic Analysis of Transit Bus Replacement. *Transit Journal*, Winter 1980.

2. Aronson J.E. and Aronofsky J.S. (1984) A Decision Support System for the Optimization of Equipment Replacement Models. Technical Report 83-OR-7. Department of Operations Research and Engineering Management, Southern Methodist University, Dallas, Texas.

3. Au T. and Au T.P. (1983) *Engineering Economics for Capital Investment Analysis*. Allyn and Bacon, Inc.

4. Brealey R.A. and Myers S.C. (1984) *Principles of Corporate Finance*. McGraw-Hill Book Company, New York.

5. Chand S. and Sethi S. (1979) Planning Horizon Procedures for Machine Replacement Models with Several Possible Replacement Alternatives. *Naval Research Logistics Quarterly* 29(3), pp. 483-493.

6. Department of the Air Force (1983) Air Force Manual 77-310 (Volume I): Acquisition, Management and Use of Motor Vehicles. Washington, D.C.

7. Department of the Air Force (1979) Air Force Technical Order 00-25-049: Maximum Repair Allowances, Repair Codes, and Priority Buy Program for USAF Vehicles. Washington, D.C.

8. Department of the Air Force (1979) Air Force Technical Order 36A-1-1301: Vehicle Management Index File. Washington, D.C.

9. Foerster, J., Miller F., Kosinski M. and Rueda A. (1983) Management Tools for Bus Maintenance — Current Practices and New Methods. Urban Transportation Center, University of Illinois at Chicago Circle, Final Report to the Urban Mass Transportation Administration.

10. Kliem B. and Goeddel D. (1983) Management Tools for Improving Maintenance Performance. *Bus Maintenance Improvement*. Transportation Research Board Special Report #198, Washington D.C.

11. Newnan D.G. (1983) *Engineering Economic Analysis*, (Second Edition). Engineering Press, San Jose, CA.

12. Pierskala W.P. and Voelker J.A. (1976) A Survey of Maintenance Models: The Control and Surveillance of Deteriorating Systems. *Naval Research Logistics Quarterly* 23(3), pp. 353-388.

13. Rapp B. (1974) *Models for Optimal Investment and Maintenance Decisions*. Halsted Press, Stockholm, Sweden.

14. Sethi S. and Chand S. (1979) Planning Horizon Procedures for Machine Replacement Models. *Management Science* 25(2), pp. 140-151.

## Appendix A: Engineering Economic Calculations

Calculations of equivalent uniform annual cost and vehicle salvage values discussed earlier in this report were performed with the following formulas.

Given the cost in each period $C_t$ for t=0 to N periods, the cost present value (CPV) of these expenditure amounts at time 0 equals:

$$CPV = \sum_{t=0}^{N} C_t*[P|F,i,t] = \sum_{t=0}^{N} C_t/(1+i)^t$$

Having found CPV at time 0, EUAC is easily calculated as:

$$EUAC = CPV*[U|P,i,N] = CPV*i(1+i)^N/(1+i)^N-1$$

The time for which EUAC has its minimum value is the optimal replacement time of a vehicle. In an efficient capital market, all activities can supposedly take *place at minimum* cost. *Hence,* the salvage value of a vehicle at any time prior to its replacement time is the difference in the present value at time t of its remaining operation and maintenance costs and the present value at time t of the minimum EUAC times the remaining number of years. For example, if the optimal replacement time of a vehicle were at the end of year 10, the the economic salvage value of this vehicle at the end of year 7 (given that it has performed and is likely to perform as expected and currently has no unusual repair needs) can be calculated as:

$$SV_t = \sum_{t=8}^{10} EUAC^*/(1+i)^{t-7} - \sum_{t=8}^{10} C_t/(1+i)^{t-7}$$

Special formulas can be used to simplify the above calculations for *uniformly increasing gradients of expenditures.* Additional explanation can be found in Au and Au [3].

## Appendix B: Programs Used to Retrieve and Tabulate Vehicle Data from the VIMS Tape

The following pages contain listings of four programs used to retrieve the data from tape used in this study and perform various calculations. The general purpose and use of these programs were explained in the report.

A sample of roughly 40 records output by ARADO1 are shown following its listing. Records for different vehicles can be distinquished by changes in the last four digits of the VRN. Since there were 12 records for most every vehicle, and not every record was needed, program ARADO2 was used to identify and write out only the required records as also explained in the report. The output from ARADO2 for D, E and L vehicles is in Appendix C.

Program ARADO3 was used to identify and group vehicles that exceeded their one-time repair limits within the past year. Program ARADO4 was used to check whether the one-time repair limit for any vehicle was ever calculated on the basis of use instead of age.

```
C * PROGRAM ARAD01 TO RETRIEVE DATA FIELDS FROM THE ARAD6T TAPE *
C   B. JANSON, CARNEGIE-MELLON UNIVERSITY, PITTSBURGH, PA 15213
C
      IMPLICIT INTEGER (A-Z)
      DOUBLE PRECISION IFILE4,IFILE7,VR(20)
C
C         UNIT 4 = DISK INPUT
C         UNIT 5 = TERMINAL INPUT
C         UNIT 6 = TERMINAL OUTPUT
C         UNIT 7 = DISK OUTPUT
C
C   Listed below are the data elements stored in the VRN vector.
C
C   Field# #Chars    Units            Data Element Name          Abbrev.
C     1      8    Alphanumeric     Vehicle Registration Number    VRN
C     2      4    Alphanumeric     Management Code                MC
C     3      3    Whole Vehicles   Vehicle Equivalents            VEQ
C     4      4    Year/Month       Acceptance Date                AD
C     5      6    Whole Dollars    Standard Price                 SP
C     6      1    Alpha            Replacement Code               RC
C     7      2    Whole Years      Life Expectancy                LE
C     8      6    Whole Dollars    One-Time Repair Cost Limit     OTL
C     9      1    " "=no;"-"=yes   One-Time Repair Cost Exceeded  OTX
C    10      7    Whole Cents      One-Time Repair Cost Price     OTP
C    11      1    M/H/U/K          Use Code                       UC
C    12      3    M/H/U/K          Average Daily Use              ADU
C    13      6    M/H/U/K          Cummulative Use                CU
C    14      6    Whole Cents      Direct Labor Cost for Repairs  DLC
C    15      7    Whole Cents      Total Parts Cost for Repairs   TPC
C
      OPEN(UNIT=6,DEVICE='TTY')
      WRITE(6,401)
  401 FORMAT(/1X,'*** AIR FORCE VEHICLE CONDITION RESEARCH *** ')
      WRITE(6,503)
  503 FORMAT(/1X,'TYPE INPUT FILENAME AND PRESS RETURN'/)
      READ (6,400) IFILE4
      WRITE(6,504)
  504 FORMAT(/1X,'TYPE OUTPUT FILENAME AND PRESS RETURN'/)
      READ (6,400) IFILE7
      WRITE(6,505)
  505 FORMAT(/1X,'HOW MANY RECORDS TO SKIP FROM THE INPUT FILE?'/)
      READ (6,*) M
      WRITE(6,506)
  506 FORMAT(/1X,'HOW MANY RECORDS TO READ FROM THE INPUT FILE?'/)
      READ (6,*) N
  400 FORMAT(A10)
C
      OPEN(UNIT=4,DEVICE='DSK',FILE=IFILE4)
      OPEN(UNIT=7,DEVICE='DSK',FILE=IFILE7)
C
      IF(M.EQ.0) GO TO 1
      DO  5 I=1,M
    5 READ (4,100) (VR(J),J=1,15)
C
    1 DO 10 I=1,N
      READ (4,100) (VR(J),J=1,15)
  100 FORMAT(2X,A8,A4,33X,A3,30X,A4,9X,A6,A1,9X,A2,6X,
     >       A6,A1,A7,165X,A1,A3,A6,88X,A6,18X,A7)
      WRITE(7,110) (VR(J),J=1,15)
  110 FORMAT(A8,1X,A4,1X,A3,1X,A4,1X,A6,1X,A1,1X,A2,1X,
```

```
     >       A6,1X,A1,1X,A7,1X,A1,1X,A3,1X,A6,1X,A6,1X,A7)
   10 CONTINUE
C
  999 STOP
      END
```

*** Output from ARADO1 ***

| VRN | MC | VEQ | AD | SP | RC | LE | OTL | OTX | OTP | UC | ADU | CU | DLC | TPC |
|---|---|---|---|---|---|---|---|---|---|---|---|---|---|---|
| 72D00924 | D522 | 055 | 7202 | 082527 | D | 17 | 030098 | - | 0000000 | H | 000 | 000700 | 000000 | 0000000 |
| 72D00924 | D522 | 055 | 7202 | 082527 | D | 17 | 029734 | - | 0000000 | H | 000 | 000700 | 000000 | 0000000 |
| 72D00924 | D522 | 055 | 7202 | 082527 | D | 17 | 029370 | - | 0000000 | H | 000 | 000700 | 000000 | 0000000 |
| 72D00924 | D522 | 055 | 7202 | 082527 | D | 17 | 029006 | - | 0000000 | H | 000 | 000700 | 000000 | 0000000 |
| 72D00924 | D522 | 055 | 7202 | 038804 | D | 17 | 013467 | - | 0000000 | H | 000 | 000700 | 000000 | 0000000 |
| 67D00471 | D541 | 016 | 1167 | 007143 | B | 12 | 000714 | - | 0000000 | H | 001 | 003244 | 000000 | {022794 |
| 67D00471 | D541 | 016 | 1167 | 007143 | B | 12 | 000714 | - | 0154495 | H | 001 | 003251 | 066564 | {008893 |
| 67D00471 | D541 | 016 | 1167 | 007143 | B | 12 | 000714 | - | 0000000 | H | 001 | 003269 | 000000 | 0000000 |
| 67D00471 | D541 | 016 | 1167 | 007143 | B | 12 | 000714 | - | 0000000 | H | 001 | 003289 | 000000 | 0000000 |
| 67D00471 | D541 | 016 | 1167 | 007143 | B | 12 | 000714 | - | 0000000 | H | 001 | 003281 | 000000 | 0000000 |
| 67D00471 | D541 | 016 | 1167 | 007143 | B | 12 | 000714 | - | 0000000 | H | 001 | 003270 | 000000 | {004212 |
| 67D00471 | D541 | 016 | 1167 | 007143 | B | 12 | 000714 | - | 0000000 | H | 000 | 003270 | 033763 | {008670 |
| 67D00471 | D541 | 016 | 1167 | 007143 | B | 12 | 000714 | - | 0000000 | H | 000 | 003292 | 000000 | 0000000 |
| 67D00471 | D541 | 016 | 1167 | 007143 | B | 12 | 000714 | - | 0000000 | H | 001 | 003291 | 019798 | {008894 |
| 67D00471 | D541 | 016 | 1167 | 007143 | B | 12 | 000714 | - | 0000000 | H | 001 | 003296 | 000000 | 0000000 |
| 67D00471 | D541 | 016 | 1167 | 007143 | B | 12 | 000714 | - | 0000000 | H | 000 | 003310 | 004292 | 0000000 |
| 67D00471 | D541 | 016 | 1167 | 002857 | B | 12 | 000286 | - | 0000000 | H | 000 | 003338 | 000000 | 0000000 |
| 72D00390 | D541 | 016 | 7209 | 007143 | D | 12 | 001339 | - | 0000000 | H | 001 | 002526 | 000000 | 0000000 |
| 72D00390 | D541 | 016 | 7209 | 007143 | D | 12 | 001295 | - | 0000000 | H | 001 | 002527 | 002064 | 0000000 |
| 72D00390 | D541 | 016 | 7209 | 007143 | D | 12 | 001250 | - | 0000000 | H | 001 | 002533 | 000000 | 0000000 |
| 72D00390 | D541 | 016 | 7209 | 007143 | D | 12 | 001205 | - | 0000000 | H | 000 | 002533 | 000000 | {004052 |
| 72D00390 | D541 | 016 | 7209 | 007143 | D | 12 | 001161 | - | 0000000 | H | 000 | 002541 | 072511 | {003458 |
| 72D00390 | D541 | 016 | 7209 | 007143 | D | 12 | 001116 | - | 0000000 | H | 000 | 002548 | 004180 | 0000000 |
| 72D00390 | D541 | 016 | 7209 | 007143 | D | 12 | 001071 | - | 0000000 | H | 000 | 002560 | 014772 | 0000000 |
| 72D00390 | D541 | 016 | 7209 | 007143 | D | 12 | 001027 | - | 0000000 | H | 016 | 002562 | 033138 | 0000000 |
| 72D00390 | D541 | 016 | 7209 | 007143 | D | 12 | 000982 | - | 0000000 | H | 013 | 002568 | 018766 | {034896 |
| 72D00390 | D541 | 016 | 7209 | 007143 | D | 12 | 000938 | - | 0000000 | H | 010 | 002570 | 017816 | {022732 |
| 72D00390 | D541 | 016 | 7209 | 007143 | D | 12 | 000893 | - | 0000000 | H | 007 | 002578 | 036483 | {008132 |
| 72D00390 | D541 | 016 | 7209 | 004669 | D | 12 | 000554 | - | 0000000 | H | 005 | 002578 | 002653 | 0000000 |
| 72D00432 | D541 | 016 | 7210 | 004237 | D | 12 | 000821 | - | 0000000 | H | 000 | 002387 | 007740 | 0000000 |
| 72D00432 | D541 | 016 | 7210 | 004237 | D | 12 | 000794 | - | 0000000 | H | 001 | 002416 | 000000 | 0000000 |
| 72D00432 | D541 | 016 | 7210 | 004237 | D | 12 | 000768 | - | 0000000 | H | 001 | 002450 | 008216 | 0000000 |
| 72D00432 | D541 | 016 | 7210 | 004237 | D | 12 | 000741 | - | 0000000 | H | 001 | 002444 | 009834 | {039302 |
| 72D00432 | D541 | 016 | 7210 | 004237 | D | 12 | 000715 | - | 0000000 | H | 001 | 002464 | 000000 | 0000000 |
| 72D00432 | D541 | 016 | 7210 | 004237 | D | 12 | 000689 | - | 0000000 | H | 001 | 002474 | 000000 | 0000000 |
| 72D00432 | D541 | 016 | 7210 | 004237 | D | 12 | 000662 | - | 0000000 | H | 001 | 002460 | 014243 | {004212 |
| 72D00432 | D541 | 016 | 7210 | 004237 | D | 12 | 000636 | - | 0000000 | H | 001 | 002461 | 031578 | {009108 |
| 72D00432 | D541 | 016 | 7210 | 004237 | D | 12 | 000609 | - | 0000000 | H | 000 | 002470 | 000000 | 0000000 |
| 72D00432 | D541 | 016 | 7210 | 004237 | D | 12 | 000583 | - | 0000000 | H | 000 | 002475 | 000000 | 0000000 |
| 72D00432 | D541 | 016 | 7210 | 004237 | D | 12 | 000556 | - | 0000000 | H | 000 | 002517 | 000000 | 0000000 |
| 72D00432 | D541 | 016 | 7210 | 004237 | D | 12 | 000530 | - | 0000000 | H | 001 | 002589 | 009551 | 0000000 |
| 73D00698 | D541 | 016 | 7404 | 004237 | D | 12 | 001298 | - | 0000000 | H | 001 | 050809 | 035604 | 0000000 |
| 73D00698 | D541 | 016 | 7404 | 004237 | D | 12 | 001271 | - | 0000000 | H | 405 | 050809 | 000000 | 0000000 |
| 73D00698 | D541 | 016 | 7404 | 004237 | D | 12 | 001245 | - | 0000000 | H | 378 | 008769 | 015677 | {005104 |
| 73D00698 | D541 | 016 | 7404 | 004237 | D | 12 | 001218 | - | 0000000 | H | 305 | 008781 | 000000 | 0000000 |
| 73D00698 | D541 | 016 | 7404 | 004237 | D | 12 | 001192 | - | 0000000 | H | 230 | 008866 | 000000 | 0000000 |
| 73D00698 | D541 | 016 | 7404 | 004237 | D | 12 | 001165 | - | 0000000 | H | 157 | 009015 | 021947 | 0000000 |
| 73D00698 | D541 | 016 | 7404 | 004237 | D | 12 | 001139 | - | 0000000 | H | 083 | 009051 | 020047 | {009750 |
| 73D00698 | D541 | 016 | 7404 | 004237 | D | 12 | 001112 | - | 0000000 | H | 009 | 009051 | 018465 | 0000000 |

```
C * PROGRAM ARAD02 TO REFORMAT DATA FIELDS FROM THE ARAD6T TAPE *
C   B. JANSON, CARNEGIE-MELLON UNIVERSITY, PITTSBURGH, PA 15213
C
      IMPLICIT INTEGER (A-Z)
      DOUBLE PRECISION IFILE4,IFILE7
C
C         UNIT 4 = DISK INPUT
C         UNIT 5 = TERMINAL INPUT
C         UNIT 6 = TERMINAL OUTPUT
C         UNIT 7 = DISK OUTPUT
C
C   Listed below are the variable names used in this program.
C     #Chars    Units            Variable Name              Abbrev.
C       4    Alphanumeric     Veh. Reg. Number (1st half)     VRN1
C       4    Alphanumeric     Veh. Reg. Number (2nd half)     VRN2
C       4    Alphanumeric     Management Code                 MC
C       3    Whole Vehicles   Vehicle Equivalents             VEQ
C       4    Year/Month       Acceptance Date                 AD
C       6    Whole Dollars    Standard Price                  SP
C       1    Alpha            Replacement Code                RC
C       2    Whole Years      Life Expectancy                 LE
C       6    Whole Dollars    One-Time Repair Cost Limit      OTL
C       1    " "=no;"-"=yes   One-Time Repair Cost Exceeded   OTX
C       7    Whole Cents      One-Time Repair Cost Price      OTP
C       1    M/H/U/K          Use Code                        UC
C       3    M/H/U/K          Average Daily Use               ADU
C       6    M/H/U/K          Cummulative Use                 CU
C       6    Whole Cents      Direct Labor Cost for Repairs   DLC
C       6    Whole Cents      Total Parts Cost for Repairs    TPC
C
C  Notes: OTP, DLC and TPC are converted to whole dollars in this program.
C   Both DLC and TPC are input for individual months, but are summed over
C   preceeding months and output that way.  Other than the first and last
C   records, which are output for every vehicle, only records in which a
C   vehicle's acceptance data, standard price, or replacement code changed,
C   or in which a one-time repair price was recorded, are written to the
C   output file.  Vehicle Equivalents are not written to the output file.
C
      OPEN(UNIT=6,DEVICE='TTY')
      WRITE(6,401)
  401 FORMAT(/1X,'*** AIR FORCE VEHICLE CONDITION RESEARCH *** ')
      WRITE(6,503)
  503 FORMAT(/1X,'TYPE INPUT FILENAME AND PRESS RETURN'/)
      READ (6,400) IFILE4
      WRITE(6,504)
  504 FORMAT(/1X,'TYPE OUTPUT FILENAME AND PRESS RETURN'/)
      READ (6,400) IFILE7
      WRITE(6,506)
  506 FORMAT(/1X,'HOW MANY RECORDS TO READ FROM THE INPUT FILE?'/)
      READ (6,*) N
  400 FORMAT(A10)
C
      OPEN(UNIT=4,DEVICE='DSK',FILE=IFILE4)
      OPEN(UNIT=7,DEVICE='DSK',FILE=IFILE7)
C
      NV=0
      REC=1
      VREC=1
      READ (4,100) VRN11,VRN21,MC1,VEQ1,AD1,SP1,RC1,LE1,OTL1,OTX1,OTP1,
     >             UC1,ADU1,CU1,DLC1,TPC1
```

```
      OTP1=OTP1/100
      DLC1=DLC1/100
      TPC1=TPC1/100
      WRITE(7,110) VREC,VRN11,VRN21,MC1,AD1,SP1,RC1,LE1,OTL1,OTX1,OTP1,
     >             UC1,ADU1,CU1,DLC1,TPC1
  111 REC=REC+1
      IF(REC.GT.N) GO TO 999
      READ (4,100) VRN12,VRN22,MC2,VEQ2,AD2,SP2,RC2,LE2,OTL2,OTX2,OTP2,
     >             UC2,ADU2,CU2,DLC2,TPC2
      OTP2=OTP2/100
      DLC2=DLC2/100
      TPC2=TPC2/100
      IF(VRN22.EQ.VRN21) GO TO 210
      IF(PRNT.NE.1)
     > WRITE(7,110) VREC,VRN11,VRN21,MC1,AD1,SP1,RC1,LE1,OTL1,OTX1,OTP1,
     >             UC1,ADU1,CU1,DLCT,TPCT
      WRITE(7,*)
      PRNT=0
      VREC=1
      DLCT=DLC2
      TPCT=TPC2
      WRITE(7,110) VREC,VRN12,VRN22,MC2,AD2,SP2,RC2,LE2,OTL2,OTX2,OTP2,
     >             UC2,ADU2,CU2,DLCT,TPCT
      GO TO 222
C
  210 PRNT=0
      VREC=VREC+1
      DLCT=DLCT+DLC2
      TPCT=TPCT+TPC2
      IF(AD2.EQ.AD1.AND.SP2.EQ.SP1.AND.RC2.EQ.RC1.AND.OTP2.LT..8*OTL2)
     > GO TO 222
      PRNT=1
      WRITE(7,110) VREC,VRN12,VRN22,MC2,AD2,SP2,RC2,LE2,OTL2,OTX2,OTP2,
     >             UC2,ADU2,CU2,DLCT,TPCT
C
  222 VRN11=VRN12
      VRN21=VRN22
      MC1=MC2
      AD1=AD2
      SP1=SP2
      RC1=RC2
      LE1=LE2
      OTL1=OTL2
      OTX1=OTX2
      OTP1=OTP2
      UC1=UC2
      ADU1=ADU2
      CU1=CU2
      DLC1=DLC2
      TPC1=TPC2
      GO TO 111
C
  100 FORMAT(A4,A4,1X,A4,1X,I3,1X,I4,1X,I6,1X,A1,1X,I2,1X,
     >       I6,1X,A1,1X,I7,1X,A1,1X,I3,1X,I6,1X,I6,2X,I6)
  110 FORMAT(3X,I3,1X,A4,A4,1X,A4,1X,I4,1X,I6,1X,A1,1X,I2,1X,
     >       I6,1X,A1,1X,I5,1X,A1,1X,I3,1X,I6,1X,I5,2X,I5)
C
  999 STOP
      END
```

```
C • PROGRAM ARADC3 TO EXAMINE VEHICLES THAT HAVE EXCEEDED THEIR •
C • ONE-TIME REPAIR LIMITS WITHIN THE PAST 12 MONTHS OF RECORDS •
C   B. JANSON, CARNEGIE-MELLON UNIVERSITY, PITTSBURGH, PA 15213
C
      IMPLICIT INTEGER (A-Z)
      DOUBLE PRECISION IFILE4,IFILE7,RANGE(8)
      DIMENSION NUMVEH(8),TSP(8),TOTL(8),TOTP(8)
C
C         UNIT 4 = DISK INPUT
C         UNIT 5 = TERMINAL INPUT
C         UNIT 6 = TERMINAL OUTPUT
C         UNIT 7 = DISK OUTPUT
C
C   Listed below are the variable names used in this program.
C     #Chars     Units              Variable Name                Abbrev.
C       4     Alphanumeric     Ven. Reg. Number (1st half)       VRN
C       4     Alphanumeric     Ven. Reg. Number (2nd half)       VRN
C       4     Alphanumeric     Management Code                   MC
C       4     Year/Month       Acceptance Date                   AD
C       6     Whole Dollars    Standard Price                    SP
C       1     Alpha            Replacement Code                  RC
C       2     Whole Years      Life Expectancy                   LE
C       6     Whole Dollars    One-Time Repair Cost Limit        OTL
C       1     " "=no;"-"=yes   One-Time Repair Cost Exceeded     OTX
C       7     Whole Cents      One-Time Repair Cost Price        OTP
C       1     M/H/U/K          Use Code                          UC
C       3     M/H/U/K          Average Daily Use                 ADU
C       6     M/H/U/K          Cummulative Use                   CU
C       6     Whole Cents      Direct Labor Cost for Repairs     DLC
C       6     Whole Cents      Total Parts Cost for Repairs      TPC
C
C  Note: OTP, DLC and TPC are converted to whole dollars in this program.
C  Both DLC and TPC are now cummulative over preceeding months as summed
C    in program ARADC2.
C
      OPEN(UNIT=6,DEVICE='TTY')
      WRITE(6,401)
  401 FORMAT(/1X,'*** AIR FORCE VEHICLE CONDITION RESEARCH ***
      WRITE(6,803)
  803 FORMAT(/1X,'TYPE INPUT FILENAME AND PRESS RETURN')
      READ (6,400) IFILE4
      WRITE(6,804)
C
  804 FORMAT(/1X,'TYPE OUTPUT FILENAME AND PRESS RETURN')
      READ (6,400) IFILE7
      WRITE(6,806)
  806 FORMAT(/1X,'HOW MANY RECORDS TO READ FROM THE INPUT FILE?')
      READ (6,*) N
  400 FORMAT(A10)
C
      OPEN(UNIT=4,DEVICE='DSK',FILE=IFILE4)
      OPEN(UNIT=7,DEVICE='DSK',FILE=IFILE7)
C
      DO 10 I=1,7
      NUMVEH(I)=0
      TSP(I)=0
      TOTL(I)=0
   10 TOTP(I)=0
C
      RANGE(1)='  0-  5%'
```

```
      RANGE(2)='  5- 10%'
      RANGE(3)=' 10- 15%'
      RANGE(4)=' 15- 20%'
      RANGE(5)=' 20- 25%'
      RANGE(6)=' 25- 50%'
      RANGE(7)=' 50-100%'
      RANGE(8)='100-500%'
C
      REC=0
      NVEHS=1
  111 REC=REC+1
      IF(REC.GT.N) GO TO 999
      READ(4,100) VREC,VRN1,VRN2,MC,AD,SP,RC,LE,OTL,OTX,OTP,
     >              UC,ADU,CU,DLC,TPC
      IF(VRN1.EQ.'     ') NVEHS=NVEHS+1
      IF(VRN1.EQ.'     ') GO TO 111
      IF(OTL.LT.10)  GO TO 111
      IF(OTP.GT.0.AND.OTP.LT.OTL) WRITE(6,601)
  601 FORMAT(/1X,'*** OTP FOUND THAT IS LESS THAN OTL. ***'/)
      IF(OTP.LT.OTL) GO TO 111
      IF(OTP.GE.OTL*2.00) ORANGE=8
      IF(OTP.LT.OTL*2.00.AND.OTP.GE.OTL*1.50) ORANGE=7
      IF(OTP.LT.OTL*1.50.AND.OTP.GE.OTL*1.25) ORANGE=6
      IF(OTP.LT.OTL*1.25.AND.OTP.GE.OTL*1.20) ORANGE=5
      IF(OTP.LT.OTL*1.20.AND.OTP.GE.OTL*1.15) ORANGE=4
      IF(OTP.LT.OTL*1.15.AND.OTP.GE.OTL*1.10) ORANGE=3
      IF(OTP.LT.OTL*1.10.AND.OTP.GE.OTL*1.05) ORANGE=2
      IF(OTP.LT.OTL*1.05.AND.OTP.GE.OTL*1.00) ORANGE=1
      NUMVEH(ORANGE)=NUMVEH(ORANGE)+1
      TSP(ORANGE)=TSP(ORANGE)+SP
      TOTL(ORANGE)=TOTL(ORANGE)+OTL
      TOTP(ORANGE)=TOTP(ORANGE)+OTP
      GO TO 111
C
  100 FORMAT(1X,I3,1X,A4,A4,1X,A4,1X,I4,1X,I6,1X,A1,1X,I2,1X,
     >       I6,1X,A1,1X,I5,1X,A1,1X,I3,1X,I6,1X,I5,2X,I5)
C
  999 NVEHS=NVEHS-1
      WRITE(7,109) NVEHS
  109 FORMAT(/1X,'TOTAL NUMBER OF VEHICLES = ',I3//
     >    '  RANGE    NUMVEH    TSP     TOTL     TOTP'/)
      WRITE(7,110)  RANGE(I),NUMVEH(I),TSP(I),TOTL(I),TOTP(I),I=1,8)
  110 FORMAT(A8,2X,I5,I8,I7,I7)
      STOP
      END
```

```
C * PROGRAM ARADO$ TO COUNT THE NUMBER OF VEHICLE RECORDS THAT *
C * ONE-TIME REPAIR LIMIT IS A FUNCTION OF USE RATHER THAN AGE *
C   B. JANSON, CARNEGIE-MELLON UNIVERSITY, PITTSBURGH, PA 15213
C
      IMPLICIT INTEGER (A-Z)
      DOUBLE PRECISION IFILE4,IFILE7
      REAL AGE,LE,OTLX
C
C         UNIT 4 = DISK INPUT
C         UNIT 5 = TERMINAL INPUT
C         UNIT 6 = TERMINAL OUTPUT
C         UNIT 7 = DISK OUTPUT
C
C   Listed below are the variable names used in this program.
C     #Chars    Units            Variable Name              Abbrev.
C       2     Year             VRN Model Year   (Chars 1-2)    MY
C       2     Alphanumeric     Veh. Reg. Number (Chars 3-4)    VRN1
C       4     Alphanumeric     Veh. Reg. Number (Chars 5-8)    VRN2
C       4     Alphanumeric     Management Code                 MC
C       3     Whole Vehicles   Vehicle Equivalents             VEQ
C       4     Year             Acceptance Date                 ADY
C       4     Month (1-12)     Acceptance Date                 ADM
C       6     Whole Dollars    Standard Price                  SP
C       1     Alpha            Replacement Code                RC
C       2     Whole Years      Life Expectancy                 LE
C       6     Whole Dollars    One-Time Repair Cost Limit      OTL
C       1     " "=no;"-"=yes   One-Time Repair Cost Exceeded   OTX
C       7     Whole Cents      One-Time Repair Cost Price      OTP
C       1     M/H/U/K          Use Code                        UC
C       3     M/H/U/K          Average Daily Use               ADU
C       6     M/H/U/K          Cummulative Use                 CU
C       6     Whole Cents      Direct Labor Cost for Repairs   DLC
C       6     Whole Cents      Total Parts Cost for Repairs    TPC
C
       PEN(UNIT=6,DEVICE='TTY')
      WRITE(6,401)
  401 FORMAT(/1X,'*** AIR FORCE VEHICLE CONDITION RESEARCH *** ')
      WRITE(6,503)
  503 FORMAT(/1X,'TYPE INPUT FILENAME AND PRESS RETURN'/)
      READ (6,400) IFILE4
      WRITE(6,504)
  504 FORMAT(/1X,'TYPE OUTPUT FILENAME AND PRESS RETURN'/)
      READ (6,400) IFILE7
      WRITE(6,506)
  506 FORMAT(/1X,'HOW MANY RECORDS TO READ FROM THE INPUT FILE?'/)
      READ (6,*) N
  400 FORMAT(A10)
C
      OPEN(UNIT=4,DEVICE='DSK',FILE=IFILE4)
      OPEN(UNIT=7,DEVICE='DSK',FILE=IFILE7)
C
      REC=1
      VREC=1
      TIME=1
      READ (4,100) MY1,VRN11,VRN21,MC1,VEQ1,ADY1,ADM1,SP1,RC1,LE1,
     >             OTL1,OTX1,OTP1,UC1,ADU1,CU1,DLC1,TPC1
  100 FORMAT(I2,A2,A4,1X,A4,1X,I3,1X,I2,I2,1X,I6,1X,A1,1X,I2,1X,
     >       I6,1X,A1,1X,I7,1X,A1,1X,I3,1X,I6,1X,I6,2X,I6)
C
      IF(ADY1.LT.60) GO TO 111
```

```
      IF(ABS(MY1-ADY1).LE.1) GO TO 205
      WRITE(7,109) VRN21,MY1,ADY1
  109 FORMAT(/1X,'>>> MY NOT EQUAL TO ADY: VRN21 =',A4,2X,4HMY =,I3,
     > 2X,5HADY =,I3)
C     ADY1=MY1
C     ADM1=7
C
  205 AGE=(83-ADY1)*12 +(6+TIME-ADM1)
      LE=LE1*12
      IF(AGE.LE.LE) OTLX=SP1*(1.0-0.9*AGE/LE)
      IF(AGE.GT.LE) OTLX=0.1*SP1
      IF(ABS(OTLX-OTL1).GT.SP1/LE)
     >                    WRITE(7,110) VRN21,SP1,OTL1,OTLX,AGE,LE
  110 FORMAT(/1X,'*** OTL1 NOT EQUAL TO OTL:',3X,5HVRN = ,A4/5X,4HSP =,
     >I6,2X,5HOTL =,I6,2X,6HOTL1 =,F7.0,2X,5HAGE =,F5.0,2X,4HLE =,F5.0)
C
  111 REC=REC+1
      IF(REC.GT.N) GO TO 999
      READ (4,100) MY2,VRN12,VRN22,MC2,VEQ2,ADY2,ADM2,SP2,RC2,LE2,
     >             OTL2,OTX2,OTP2,UC2,ADU2,CU2,DLC2,TPC2
      IF(VRN22.EQ.VRN21) GO TO 210
      VREC=0
      TIME=0
C
  210 VREC=VREC+1
      TIME=TIME+1
      IF(ADY2.LT.60) GO TO 111
      IF(ABS(MY2-ADY2).LE.1) GO TO 215
      WRITE(7,109) VRN22,MY2,ADY2
C     ADY2=MY2
C     ADM2=7
C
  215 AGE=(83-ADY2)*12 +(6+TIME-ADM2)
      LE=LE2*12
      IF(AGE.LE.LE) OTLX=SP2*(1.0-0.9*AGE/LE)
      IF(AGE.GT.LE) OTLX=0.1*SP2
      IF(ABS(OTLX-OTL2).GT.SP2/LE)
     >                    WRITE(7,110) VRN22,SP2,OTL2,OTLX,AGE,LE
C
      MY1=MY2
      VRN11=VRN12
      VRN21=VRN22
      MC1=MC2
      ADY1=ADY2
      ADM1=ADM2
      SP1=SP2
      RC1=RC2
      LE1=LE2
      OTL1=OTL2
      OTX1=OTX2
      OTP1=OTP2
      UC1=UC2
      ADU1=ADU2
      CU1=CU2
      DLC1=DLC2
      TPC1=TPC2
      GO TO 111
C
  999 STOP
      END
```

## Appendix C Listing of Output from Program ARADO2

The following pages contain the output files from program ARADO2. The records shown for D, E and L class vehicles are all records in which a significant data element to this study changed within the 12-month period of data shown by this tape for a particular base.

The columns contain from the left to right the following data items.

| | Units | Variable Name | Abbrev. |
|---|---|---|---|
| 1. | Integer | Monthly Record Number (1-12) | |
| 2. | Alphanumeric | Vehicle Registration Number | VRN2 |
| 3. | Alphanumeric | Management Code | MC |
| 4. | Year/Month | Acceptance Date | AD |
| 5. | Whole Dollars | Standard Price | SP |
| 6. | Alpha | Replacement Code | RC |
| 7. | Whole Years | Life Expectancy | LE |
| 8. | Whole Dollars | One-Time Repair Cost Limit | OTL |
| 9. | " "=no;"-"=yes | One-Time Repair Cost Exceeded | OTX |
| 10. | Whole Cents | One-Time Repair Cost Price | OTP |
| 11. | M/H/U/F | Use Code | UC |
| 12. | M/H/U/F | Average Daily Use | ADU |
| 13. | M/H/U/F | Cummulative Use | CU |
| 14. | Whole Cents | Direct Labor Cost for Repairs | DLC |
| 15. | Whole Cents | Total Parts Cost for Repairs | TPC |

Data items OTP, DLC and TPC are converted from whole cents, as they are recorded to the VAMS tape, to whole dollars in this output. Both DLC and TPC are input for individual months, but are summed over preceeding months and output that way. Other than the first and last records, which are output for every vehicle, only records in which a vehicle's acceptance date, standard price, or replacement code changed, or in which a one-time repair price was recorded, are written to the output file. Vehicle equivalents, a data item originally retrieved by ARADO1 from the VAMS tape, is not written to the ARADO2 output files since it was not needed for this study.

| | | | | | | | | | | | | | |
|---|---|---|---|---|---|---|---|---|---|---|---|---|---|
| 1 | 72D00924 | D522 | 7202 | 82527 | D | 17 | 30098 | - | 0 | H | 0 | 700 | 0 | 0 |
| 5 | 72D00924 | D522 | 7202 | 38804 | D | 17 | 13467 | - | 0 | H | 0 | 700 | 0 | 0 |
| 1 | 67D00471 | D541 | 1167 | 7143 | B | 12 | 714 | - | 0 | H | 1 | 3244 | 0 | 227 |
| 3 | 67D00471 | D541 | 1167 | 7143 | B | 12 | 714 | - | 1544 | H | 1 | 3251 | 665 | 315 |
| 12 | 67D00471 | D541 | 1167 | 0857 | B | 12 | 286 | - | 0 | H | 0 | 3338 | 1241 | 531 |
| 1 | 72D00390 | D541 | 7209 | 7143 | D | 12 | 1339 | - | 0 | H | 1 | 2526 | 0 | 0 |
| 12 | 72D00390 | D541 | 7209 | 4669 | D | 12 | 554 | - | 0 | H | 5 | 2578 | 2019 | 730 |
| 1 | 72D00432 | D541 | 7210 | 4237 | D | 12 | 821 | - | 0 | H | 0 | 2387 | 77 | 0 |
| 12 | 72D00432 | D541 | 7210 | 4237 | D | 12 | 530 | - | 0 | H | 1 | 2589 | 809 | 526 |
| 1 | 73D00698 | D541 | 7404 | 4237 | D | 12 | 1298 | - | 0 | H | 1 | 50809 | 356 | 0 |
| 12 | 73D00698 | D541 | 7404 | 4676 | D | 12 | 1111 | - | 0 | H | 517 | 9500 | 1647 | 433 |
| 1 | 73D00901 | D541 | 7301 | 4237 | D | 12 | 900 | - | 0 | H | 1 | 841 | 0 | 0 |
| 12 | 73D00901 | D541 | 7301 | 4676 | D | 12 | 672 | - | 0 | H | 1 | 971 | 268 | 78 |
| 1 | 75D00361 | D541 | 7506 | 4237 | R | 12 | 1668 | | 0 | H | 0 | 1981 | 0 | 0 |
| 12 | 75D00361 | D541 | 7506 | 4676 | R | 12 | 1520 | | 0 | H | 1 | 2128 | 1694 | 612 |
| 1 | 75D00378 | D541 | 7506 | 4237 | R | 12 | 1668 | | 0 | H | 2 | 2870 | 0 | 0 |
| 12 | 75D00378 | D541 | 7506 | 4676 | R | 12 | 1520 | | 0 | H | 4 | 3478 | 1953 | 932 |
| 1 | 75D00400 | D541 | 7506 | 4237 | R | 12 | 1668 | | 0 | H | 2 | 14037 | 41 | 0 |
| 4 | 75D00400 | D541 | 7506 | 4237 | R | 12 | 1589 | | 2431 | H | 2 | 14141 | 745 | 1194 |
| 12 | 75D00400 | D541 | 7506 | 4676 | R | 12 | 1520 | | 0 | H | 2 | 14499 | 1606 | 1591 |
| 1 | 75D00417 | D541 | 7506 | 4237 | R | 12 | 1668 | | 0 | H | 359 | 19020 | 0 | 0 |
| 12 | 75D00417 | D541 | 7506 | 4676 | R | 12 | 1520 | | 0 | H | 1 | 1390 | 1866 | 733 |
| 1 | 75D00423 | D541 | 7506 | 4237 | R | 12 | 1668 | | 0 | H | 3 | 12779 | 526 | 130 |
| 3 | 75D00423 | D541 | 7506 | 4237 | R | 12 | 1615 | | 2350 | H | 2 | 12807 | 1804 | 782 |
| 12 | 75D00423 | D541 | 7506 | 4676 | R | 12 | 1520 | | 0 | H | 2 | 15152 | 2459 | 985 |
| 1 | 76D00246 | D541 | 7608 | 7143 | R | 12 | 3438 | | 0 | H | 4 | 865 | 0 | 0 |
| 12 | 76D00246 | D541 | 7608 | 7143 | R | 12 | 2946 | | 0 | H | 0 | 697 | 234 | 41 |
| 1 | 76D00247 | D541 | 7608 | 7143 | R | 12 | 3438 | | 0 | H | 1 | 993 | 0 | 0 |
| 12 | 76D00247 | D541 | 7608 | 7143 | R | 12 | 2946 | | 0 | H | 1 | 1505 | 635 | 479 |
| 1 | 76D00248 | D541 | 7608 | 7143 | R | 12 | 3438 | | 0 | H | 4 | 1104 | 0 | 0 |
| 12 | 76D00248 | D541 | 7608 | 7143 | R | 12 | 2946 | | 7738 | H | 29 | 1249 | 3392 | 3662 |
| 1 | 76D00292 | D541 | 7609 | 7143 | R | 12 | 3482 | D | 0 | H | 8 | 2559 | 0 | 0 |
| 12 | 76D00292 | D541 | 7609 | 7143 | R | 12 | 2991 | D | 0 | H | 3 | 1848 | 1286 | 222 |
| 1 | 77D00045 | D541 | 7708 | 7143 | T | 12 | 3973 | D | 0 | H | 1 | 3940 | 443 | 391 |
| 2 | 77D00045 | D541 | 7708 | 7143 | R | 12 | 3929 | D | 0 | H | 1 | 3978 | 509 | 391 |
| 12 | 77D00045 | D541 | 7708 | 6877 | R | 12 | 3353 | D | 0 | H | 0 | 4200 | 1662 | 961 |
| 1 | 77D00046 | D541 | 7708 | 7143 | T | 12 | 3973 | D | 0 | H | 1 | 3381 | 0 | 0 |
| 2 | 77D00046 | D541 | 7708 | 7143 | R | 12 | 3929 | D | 0 | H | 1 | 3389 | 123 | 2 |
| 12 | 77D00046 | D541 | 7708 | 6877 | R | 12 | 3353 | D | 0 | H | 1 | 3495 | 1208 | 994 |
| 1 | 77D00106 | D541 | 7710 | 7143 | T | 12 | 4063 | D | 0 | H | 4 | 4704 | 314 | 510 |
| 4 | 77D00106 | D541 | 7710 | 7143 | R | 12 | 3929 | D | 0 | H | 6 | 5095 | 788 | 708 |
| 12 | 77D00106 | D541 | 7710 | 6877 | R | 12 | 3438 | D | 0 | H | 2 | 5597 | 2152 | 1215 |

| | | | | | | | | | | | | | | |
|---|---|---|---|---|---|---|---|---|---|---|---|---|---|---|
| 1 | 77D00108 | D541 | 7710 | 7143 | T | 12 | 4063 | 0 | 0 | H | 0 | 4410 | 0 | 500 |
| 4 | 77D00108 | D541 | 7710 | 7143 | R | 12 | 3929 | 0 | 0 | H | 209 | 11706 | 498 | 523 |
| 12 | 77D00108 | D541 | 7710 | 6877 | R | 12 | 3438 | 0 | 0 | H | 46 | 5632 | 1944 | 1069 |
| 1 | 77D00134 | D541 | 7709 | 7143 | T | 12 | 4018 | 0 | 0 | H | 1 | 2048 | 41 | 0 |
| 3 | 77D00134 | D541 | 7709 | 7143 | R | 12 | 3929 | 0 | 0 | H | 2 | 2139 | 41 | 0 |
| 12 | 77D00134 | D541 | 7709 | 5572 | R | 12 | 2751 | 0 | 0 | H | 1 | 2208 | 664 | 433 |
| 1 | 77D00135 | D541 | 7709 | 7143 | T | 12 | 4018 | 0 | 0 | H | 10 | 3179 | 0 | 0 |
| 3 | 77D00135 | D541 | 7709 | 7143 | R | 12 | 3929 | 0 | 0 | H | 2 | 3299 | 41 | 229 |
| 12 | 77D00135 | D541 | 7709 | 5572 | R | 12 | 2751 | 0 | 0 | H | 0 | 3288 | 776 | 297 |
| 1 | 78D00367 | D541 | 7904 | 4237 | T | 12 | 2886 | 0 | 0 | H | 43 | 3319 | 564 | 188 |
| 12 | 78D00367 | D541 | 7904 | 4676 | T | 12 | 2864 | 0 | 0 | H | 1 | 1216 | 2054 | 776 |
| 1 | 78D00368 | D541 | 7904 | 4237 | T | 12 | 2886 | 0 | 0 | H | 4 | 5791 | 211 | 50 |
| 12 | 78D00368 | D541 | 7904 | 4676 | T | 12 | 2864 | 0 | 0 | H | 73 | 6347 | 2493 | 1242 |
| 1 | 78D00369 | D541 | 7904 | 4237 | T | 12 | 2886 | 0 | 0 | H | 3 | 2429 | 46 | 41 |
| 12 | 78D00369 | D541 | 7904 | 4676 | T | 12 | 2864 | 0 | 0 | H | 3 | 1688 | 2218 | 962 |
| 1 | 72D00150 | D547 | 7202 | 13369 | L | 12 | 1922 | 0 | 0 | H | 73 | 3072 | 351 | 6 |
| 7 | 72D00150 | D547 | 7202 | 13369 | L | 12 | 1420 | 0 | 0 | H | 1 | 3257 | 1122 | 415 |
| 1 | 70D00350 | D548 | 7001 | 13369 | B | 9 | 1337 | - | 0 | H | 1 | 3598 | 0 | 0 |
| 12 | 70D00350 | D548 | 7001 | 3298 | B | 9 | 330 | - | 0 | H | 0 | 3638 | 346 | 18 |
| 1 | 70D00353 | D548 | 7005 | 13369 | B | 9 | 1337 | - | 0 | H | 0 | 3213 | 0 | 0 |
| 12 | 70D00353 | D548 | 7005 | 3298 | B | 9 | 330 | - | 0 | H | 1 | 3325 | 186 | 0 |
| 1 | 70D00639 | D548 | 7005 | 13369 | B | 9 | 1337 | - | 0 | H | 0 | 1001 | 0 | 0 |
| 12 | 70D00639 | D548 | 7005 | 2831 | B | 9 | 283 | - | 0 | H | 16 | 3137 | 392 | 14 |
| 1 | 70D00640 | D548 | 7004 | 13369 | B | 9 | 1337 | - | 0 | H | 8 | 3304 | 681 | 37 |
| 12 | 70D00640 | D548 | 7004 | 2831 | B | 9 | 283 | - | 0 | H | 20 | 308 | 1691 | 875 |
| 1 | 72D00150 | D548 | 7202 | 13369 | H | 9 | 1337 | 0 | 0 | H | 1 | 3289 | 105 | 30 |
| 4 | 72D00150 | D548 | 7202 | 13369 | H | 9 | 1337 | 0 | 1866 | H | 1 | 3335 | 619 | 1024 |
| 5 | 72D00150 | D548 | 7202 | 2977 | H | 9 | 298 | 0 | 0 | H | 1 | 3350 | 661 | 1024 |
| 1 | 72D00158 | D548 | 7202 | 13369 | B | 9 | 1337 | - | 0 | H | 17 | 2153 | 0 | 0 |
| 12 | 72D00158 | D548 | 7202 | 2977 | B | 9 | 298 | - | 0 | H | 1 | 273 | 609 | 134 |
| 1 | 72D00232 | D548 | 7201 | 13369 | D | 12 | 1838 | - | 0 | H | 0 | 308 | 92 | 0 |
| 8 | 72D00232 | D548 | 7201 | 13369 | B | 9 | 1337 | - | 0 | H | 6 | 372 | 589 | 636 |
| 12 | 72D00232 | D548 | 7201 | 2977 | B | 9 | 298 | - | 0 | H | 1 | 388 | 1287 | 682 |
| 1 | 72D00240 | D548 | 7204 | 13369 | B | 9 | 1337 | - | 0 | H | 0 | 1230 | 567 | 0 |
| 6 | 72D00240 | D548 | 7204 | 13369 | B | 9 | 1337 | - | 2029 | H | 0 | 1235 | 1538 | 245 |
| 12 | 72D00240 | D548 | 7204 | 2977 | B | 9 | 298 | - | 0 | H | 1 | 1265 | 1585 | 245 |
| 1 | 78D00189 | D548 | 7807 | 13369 | R | 9 | 6684 | 0 | 0 | H | 7 | 1358 | 0 | 0 |
| 12 | 78D00189 | D548 | 7807 | 2831 | R | 9 | 1156 | 0 | 0 | H | 4 | 1601 | 887 | 745 |
| 1 | 78D00190 | D548 | 7807 | 13369 | R | 9 | 6684 | 0 | 0 | H | 2 | 3053 | 0 | 0 |
| 12 | 78D00190 | D548 | 7807 | 2831 | R | 9 | 1156 | 0 | 0 | H | 3 | 3737 | 396 | 303 |
| 1 | 78D00191 | D548 | 7807 | 13369 | R | 9 | 6684 | 0 | 0 | H | 6 | 3890 | 0 | 0 |
| 12 | 78D00191 | D548 | 7807 | 2831 | R | 9 | 1156 | 0 | 0 | H | 2 | 4582 | 1340 | 1061 |

| | | | | | | | | | | | | | | |
|---|---|---|---|---|---|---|---|---|---|---|---|---|---|---|
| 1 | 79D00168 | D548 | 7904 | 13369 | T | 9 | 7687 | 0 | 0 | H | 2 | 1007 | 0 | 0 |
| 4 | 79D00168 | D548 | 7904 | 13369 | R | 9 | 7353 | 0 | 0 | H | 3 | 870 | 133 | 18 |
| 12 | 79D00168 | D548 | 7904 | 11397 | R | 9 | 5509 | 0 | 0 | H | 0 | 817 | 326 | 44 |
| 1 | 79D00590 | D548 | 7910 | 13369 | T | 12 | 9609 | 0 | 0 | H | 0 | 336 | 41 | 0 |
| 10 | 79D00590 | D548 | 7910 | 13369 | R | 9 | 7353 | 0 | 0 | H | 0 | 378 | 226 | 0 |
| 12 | 79D00590 | D548 | 7910 | 2831 | R | 9 | 1510 | 0 | 0 | H | 1 | 407 | 242 | 0 |
| 1 | 71D00512 | D560 | 7109 | 13369 | B | 9 | 1337 | - | 0 | H | 3 | 1866 | 0 | 0 |
| 12 | 71D00512 | D560 | 7109 | 2922 | B | 9 | 292 | - | 0 | H | 0 | 2130 | 501 | 948 |
| 1 | 71D00520 | D560 | 7109 | 13369 | B | 9 | 1337 | - | 0 | H | 7 | 2540 | 0 | 0 |
| 12 | 71D00520 | D560 | 7109 | 2922 | B | 9 | 292 | - | 0 | H | 0 | 4287 | 218 | 111 |
| 1 | 71D00570 | D560 | 7110 | 13369 | D | 12 | 1588 | - | 0 | H | 0 | 3480 | 0 | 0 |
| 5 | 71D00570 | D560 | 7110 | 13369 | B | 12 | 1337 | - | 0 | H | 93 | 3486 | 20 | 3 |
| 7 | 71D00570 | D560 | 7110 | 13369 | B | 12 | 1337 | - | 2565 | H | 99 | 4120 | 542 | 1600 |
| 12 | 71D00570 | D560 | 7110 | 2922 | B | 9 | 292 | - | 0 | H | 35 | 4693 | 667 | 1615 |
| 1 | 71D00672 | D560 | 8306 | 13369 | D | 12 | 13285 | - | 0 | H | 0 | 1110 | 123 | 17 |
| 12 | 71D00672 | D560 | 8306 | 2922 | D | 9 | 2630 | - | 0 | H | 3 | 1350 | 1002 | 1045 |
| 1 | 71D00685 | D560 | 7111 | 13369 | B | 9 | 1337 | - | 0 | H | 1 | 3235 | 0 | 0 |
| 4 | 71D00685 | D560 | 7111 | 13369 | B | 9 | 1337 | - | 1781 | H | 1 | 3243 | 1154 | 608 |
| 12 | 71D00685 | D560 | 7111 | 2922 | B | 9 | 292 | - | 0 | H | 1 | 3331 | 1986 | 1263 |
| 1 | 73D00157 | D560 | 7306 | 13369 | B | 9 | 1337 | - | 0 | H | 0 | 2699 | 134 | 0 |
| 12 | 73D00157 | D560 | 7306 | 2922 | B | 9 | 292 | - | 0 | H | 0 | 2788 | 886 | 457 |
| 1 | 73D00418 | D560 | 7305 | 13369 | B | 9 | 1337 | - | 0 | H | 1 | 4057 | 0 | 0 |
| 3 | 73D00418 | D560 | 7305 | 13369 | B | 9 | 1337 | - | 2577 | H | 2 | 4151 | 250 | 2124 |
| 12 | 73D00418 | D560 | 7305 | 2922 | B | 9 | 292 | - | 712 | H | 0 | 4223 | 634 | 2777 |
| 1 | 73D00419 | D560 | 7305 | 13369 | B | 9 | 1337 | - | 0 | H | 0 | 4275 | 196 | 0 |
| 6 | 73D00419 | D560 | 7305 | 13369 | B | 9 | 1337 | - | 2605 | H | 1 | 4020 | 943 | 1381 |
| 12 | 73D00419 | D560 | 7305 | 2922 | B | 9 | 292 | - | 0 | H | 6 | 4752 | 1147 | 1768 |
| 1 | 74D00137 | D560 | 7412 | 13369 | D | 9 | 1894 | - | 0 | H | 2 | 2548 | 92 | 28 |
| 7 | 74D00137 | D560 | 7412 | 13369 | B | 9 | 1337 | - | 0 | H | 9 | 2939 | 768 | 149 |
| 12 | 74D00137 | D560 | 7412 | 2922 | B | 9 | 292 | - | 0 | H | 2 | 1579 | 1174 | 689 |
| 1 | 74D00156 | D560 | 7412 | 13369 | D | 9 | 1894 | - | 0 | H | 23 | 3166 | 0 | 0 |
| 7 | 74D00156 | D560 | 7412 | 13369 | B | 9 | 1337 | - | 0 | H | 1 | 3255 | 40 | 0 |
| 10 | 74D00156 | D560 | 7412 | 13369 | B | 9 | 1337 | - | 1556 | H | 1 | 3255 | 321 | 1007 |
| 12 | 74D00156 | D560 | 7412 | 2922 | B | 9 | 292 | - | 0 | H | 1 | 3278 | 321 | 1007 |
| 1 | 74D00185 | D560 | 7409 | 13369 | D | 9 | 1560 | - | 0 | H | 2 | 1730 | 51 | 0 |
| 4 | 74D00185 | D560 | 7409 | 13369 | B | 9 | 1337 | - | 0 | H | 2 | 1871 | 61 | 0 |
| 5 | 74D00185 | D560 | 7409 | 13369 | B | 9 | 1337 | - | 1758 | H | 2 | 1871 | 621 | 838 |
| 12 | 74D00185 | D560 | 7409 | 2922 | B | 9 | 292 | - | 0 | H | 2 | 1937 | 621 | 1574 |
| 1 | 74D00186 | D560 | 7412 | 13369 | D | 9 | 1894 | - | 0 | H | 21 | 1820 | 0 | 0 |
| 7 | 74D00186 | D560 | 7412 | 13369 | B | 9 | 1337 | - | 0 | H | 2 | 2018 | 124 | 183 |
| 12 | 74D00186 | D560 | 7412 | 2922 | B | 9 | 292 | - | 0 | H | 0 | 1967 | 459 | 195 |
| 1 | 75D00013 | D560 | 7510 | 13369 | P | 9 | 3008 | | 0 | H | 0 | 2847 | 0 | 0 |
| 5 | 75D00013 | D560 | 7510 | 13369 | L | 9 | 2562 | | 0 | H | 14 | 4033 | 1202 | 159 |
| 12 | 75D00013 | D560 | 7510 | 2922 | L | 9 | 390 | | 0 | H | 0 | 4047 | 1400 | 172 |
| 1 | 75D00014 | D560 | 7510 | 13369 | P | 9 | 3008 | | 0 | H | 1 | 3842 | 0 | 0 |

| | | | | | | | | | | | | | | |
|---|---|---|---|---|---|---|---|---|---|---|---|---|---|---|
| 5 | 75D00014 | D560 | 7510 | 13369 | L | 9 | 2562 | | 0 | H | 1 | 3987 | 863 | 133 |
| 12 | 75D00014 | D560 | 7510 | 2922 | L | 9 | 390 | | 0 | H | 1 | 4053 | 1118 | 1424 |
| 1 | 75D00015 | D560 | 7510 | 13369 | P | 9 | 3008 | | 0 | H | 1 | 5571 | 93 | 0 |
| 5 | 75D00015 | D560 | 7510 | 13369 | L | 9 | 2562 | | 0 | H | 2 | 5666 | 846 | 30 |
| 12 | 75D00015 | D560 | 7510 | 2922 | L | 9 | 390 | | 0 | H | 3 | 5829 | 1003 | 411 |
| 1 | 75D00016 | D560 | 7510 | 13369 | P | 9 | 3008 | | 0 | H | 3 | 3825 | 176 | 0 |
| 5 | 75D00016 | D560 | 7510 | 13369 | L | 9 | 2562 | | 0 | H | 1 | 3870 | 176 | 0 |
| 12 | 75D00016 | D560 | 7510 | 2922 | L | 9 | 390 | | 0 | H | 1 | 3959 | 350 | 30 |
| 1 | 75D00017 | D560 | 7510 | 13369 | P | 9 | 3008 | | 0 | H | 1 | 3478 | 0 | 0 |
| 5 | 75D00017 | D560 | 7510 | 13369 | L | 9 | 2562 | | 0 | H | 2 | 3567 | 195 | 39 |
| 12 | 75D00017 | D560 | 7510 | 2922 | L | 9 | 390 | | 0 | H | 1 | 3851 | 1146 | 872 |
| 1 | 76D00098 | D560 | 7612 | 13369 | R | 9 | 4568 | 0 | 0 | H | 1 | 1490 | 0 | 0 |
| 7 | 76D00098 | D560 | 7612 | 13369 | P | 9 | 3899 | 0 | 0 | H | 2 | 1800 | 336 | 1301 |
| 12 | 76D00098 | D560 | 7612 | 11397 | P | 9 | 2849 | 0 | 0 | H | 1 | 1860 | 1565 | 2092 |
| 1 | 76D00100 | D560 | 7612 | 13369 | R | 9 | 4568 | 0 | 0 | H | 2 | 2069 | 0 | 0 |
| 7 | 76D00100 | D560 | 7612 | 13369 | P | 9 | 3899 | 0 | 0 | H | 1 | 2176 | 233 | 10 |
| 12 | 76D00100 | D560 | 7612 | 11397 | P | 9 | 2849 | 0 | 0 | H | 1 | 2168 | 338 | 10 |
| 1 | 76D00159 | D560 | 7701 | 13369 | R | 9 | 4679 | 0 | 0 | H | 0 | 1167 | 603 | 20 |
| 8 | 76D00159 | D560 | 7701 | 13369 | P | 9 | 3899 | 0 | 0 | H | 1 | 1260 | 2207 | 60 |
| 12 | 76D00159 | D560 | 7701 | 11397 | P | 9 | 2944 | 0 | 0 | H | 1 | 1299 | 3146 | 1364 |
| 1 | 79D00158 | D560 | 7906 | 13369 | T | 9 | 7910 | 0 | 0 | H | 10 | 1995 | 103 | 0 |
| 6 | 79D00158 | D560 | 7906 | 13369 | R | 9 | 7353 | 0 | 0 | H | 3 | 2256 | 298 | 600 |
| 12 | 79D00158 | D560 | 7906 | 11397 | R | 9 | 5698 | 0 | 0 | H | 1 | 2364 | 1148 | 706 |
| 1 | 79D00159 | D560 | 7906 | 13369 | T | 9 | 7910 | 0 | 0 | H | 29 | 1545 | 0 | 0 |
| 6 | 79D00159 | D560 | 7906 | 13369 | R | 9 | 7353 | 0 | 0 | H | 1 | 1593 | 1354 | 3321 |
| 12 | 79D00159 | D560 | 7906 | 11397 | R | 9 | 5698 | 0 | 0 | H | 2 | 1799 | 2562 | 5076 |
| 1 | 79D00160 | D560 | 7906 | 13369 | T | 9 | 7910 | 0 | 0 | H | 2 | 1834 | 0 | 0 |
| 6 | 79D00160 | D560 | 7906 | 13369 | R | 9 | 7353 | 0 | 0 | H | 2 | 2066 | 198 | 13 |
| 12 | 79D00160 | D560 | 7906 | 11397 | R | 9 | 5698 | 0 | 0 | H | 2 | 2230 | 1402 | 787 |
| 1 | 83D00129 | D560 | 8212 | 13369 | U | 9 | 12589 | 0 | 0 | H | 4 | 215 | 0 | 283 |
| 6 | 83D00129 | D560 | 8212 | 13369 | T | 9 | 12032 | 0 | 0 | H | 6 | 645 | 154 | 283 |
| 12 | 83D00129 | D560 | 8212 | 13369 | T | 9 | 11364 | 0 | 0 | H | 2 | 1185 | 332 | 382 |
| 1 | 83D00130 | D560 | 8212 | 13369 | U | 9 | 12589 | 0 | 0 | H | 9 | 335 | 15 | 0 |
| 6 | 83D00130 | D560 | 8212 | 13369 | T | 9 | 12032 | 0 | 0 | H | 6 | 764 | 285 | 14 |
| 12 | 83D00130 | D560 | 8212 | 13369 | T | 9 | 11364 | 0 | 0 | H | 2 | 1078 | 332 | 14 |
| 1 | 62D02108 | D569 | 6201 | 67986 | B | 21 | 6799 | - | 0 | H | 1 | 2200 | 0 | 0 |
| 12 | 62D02108 | D569 | 6201 | 12260 | B | 10 | 1226 | - | 0 | H | 3 | 2285 | 0 | 0 |
| 1 | 62D02117 | D569 | 6212 | 67986 | B | 18 | 6799 | - | 0 | H | 4 | 1540 | 0 | 0 |
| 12 | 62D02117 | D569 | 6212 | 12260 | B | 10 | 1226 | - | 0 | H | 7 | 1027 | 2398 | 2758 |
| 1 | 62D02122 | D569 | 6212 | 67986 | B | 18 | 6799 | - | 0 | H | 1 | 1314 | 185 | 0 |
| 12 | 62D02122 | D569 | 6212 | 12260 | B | 10 | 1226 | - | 0 | H | 1 | 1545 | 2812 | 2264 |
| 1 | 67D00758 | D569 | 6708 | 67986 | B | 10 | 6799 | - | 0 | H | 1 | 3483 | 340 | 0 |
| 12 | 67D00758 | D569 | 6708 | 23941 | B | 10 | 2394 | - | 0 | H | 0 | 3533 | 1357 | 3387 |
| 1 | 80D01155 | D569 | 8103 | 67986 | T | 10 | 53709 | 0 | 0 | H | 1 | 616 | 20 | 0 |

| | | | | | | | | | | | | | | |
|---|---|---|---|---|---|---|---|---|---|---|---|---|---|---|
| 12 | 80D01155 | D569 | 8103 | 67986 | T | 10 | 48100 | 0 | 0 | H | 2 | 921 | 1254 | 1381 |
| 1 | 82D00103 | D569 | 8111 | 67986 | T | 10 | 57788 | 0 | 0 | H | 3 | 479 | 0 | 0 |
| 12 | 82D00103 | D569 | 8111 | 67141 | T | 10 | 51531 | 0 | 0 | H | 6 | 854 | 448 | 141 |
| 1 | 82D00104 | D569 | 8111 | 67986 | T | 10 | 57788 | 0 | 0 | H | 1 | 410 | 0 | 0 |
| 12 | 82D00104 | D569 | 8111 | 67141 | T | 10 | 51531 | 0 | 0 | H | 1 | 637 | 666 | 375 |
| 1 | 82D00105 | D569 | 8111 | 67986 | T | 10 | 57788 | 0 | 0 | H | 2 | 619 | 0 | 0 |
| 12 | 82D00105 | D569 | 8111 | 67141 | T | 10 | 51531 | 0 | 0 | H | 20 | 986 | 752 | 404 |
| 1 | 66D01373 | D570 | 6601 | 114646 | B | 10 | 11465 | - | 0 | H | 0 | 1430 | 0 | 0 |
| 12 | 66D01373 | D570 | 6601 | 41591 | B | 10 | 4159 | - | 0 | H | 1 | 1548 | 2523 | 2226 |
| 1 | 66D01385 | D570 | 6601 | 114646 | B | 10 | 11465 | - | 0 | H | 1 | 1147 | 0 | 0 |
| 12 | 66D01385 | D570 | 6601 | 41591 | B | 10 | 4159 | - | 0 | H | 1 | 1147 | 0 | 0 |
| 1 | 84D00600 | D570 | 8401 | 32812 | | 10 | 0 | 0 | 0 | H | 0 | 3 | 0 | 0 |
| 2 | 84D00600 | D570 | 8401 | 70789 | T | 10 | 70258 | 0 | 0 | H | 0 | 3 | 0 | 0 |
| 6 | 84D00600 | D570 | 8401 | 70789 | T | 10 | 68134 | 0 | 0 | H | 35 | 180 | 416 | 145 |
| 1 | 80D00123 | D572 | 8003 | 29355 | T | 10 | 20548 | 0 | 0 | H | 2 | 272 | 30 | 0 |
| 12 | 80D00123 | D572 | 8003 | 28668 | T | 10 | 17702 | 0 | 0 | H | 1 | 1048 | 1356 | 784 |
| 1 | 80D00124 | D572 | 8003 | 29355 | T | 10 | 20548 | 0 | 0 | H | 4 | 845 | 20 | 0 |
| 12 | 80D00124 | D572 | 8003 | 28668 | T | 10 | 17702 | 0 | 0 | H | 1 | 1010 | 856 | 189 |
| 1 | 80D00977 | D572 | 8007 | 29355 | U | 10 | 21429 | | 0 | H | 1 | 636 | 185 | 0 |
| 12 | 80D00977 | D572 | 8007 | 28668 | U | 10 | 18563 | | 0 | H | 1 | 765 | 556 | 294 |
| 1 | 80D00978 | D572 | 8007 | 29355 | T | 12 | 22750 | | 0 | H | 1 | 630 | 98 | 360 |
| 12 | 80D00978 | D572 | 8007 | 28668 | T | 10 | 18563 | | 0 | H | 1 | 731 | 1320 | 1275 |
| 1 | 80D01025 | D592 | 8012 | 54971 | T | 12 | 41915 | 0 | 0 | H | 2 | 1664 | 168 | 76 |
| 5 | 80D01025 | D592 | 8012 | 54971 | T | 12 | 40541 | 0 | 0 | H | 184 | 1811 | 1643 | 390 |
| 1 | 80D00287 | D594 | 8004 | 54398 | T | 12 | 41138 | 0 | 0 | H | 104 | 1087 | 0 | 586 |
| 12 | 80D00287 | D594 | 8004 | 51640 | T | 12 | 35502 | 0 | 0 | H | 0 | 1173 | 2990 | 1856 |
| 1 | 80D01025 | D594 | 8012 | 54971 | T | 12 | 44320 | 0 | 0 | H | 1 | 1376 | 159 | 0 |
| 7 | 80D01025 | D594 | 8012 | 54971 | T | 12 | 42259 | 0 | 0 | H | 3 | 1605 | 1286 | 213 |
| 1 | 83D00242 | D594 | 8307 | 56941 | U | 12 | 0 | 0 | 0 | H | 0 | 21 | 41 | 0 |
| 9 | 83D00242 | D594 | 8307 | 54398 | U | 12 | 51338 | 0 | 0 | H | 2 | 397 | 800 | 514 |
| 11 | 83D00242 | D594 | 8307 | 56941 | T | 12 | 53026 | 0 | 0 | H | 2 | 458 | 1142 | 572 |
| 1 | 70D01080 | D595 | 7007 | 30738 | B | 12 | 3074 | - | 0 | H | 1 | 2550 | 154 | 14 |
| 7 | 70D01080 | D595 | 7007 | 30738 | B | 12 | 3074 | - | 4038 | H | 398 | 2601 | 2163 | 1413 |
| 10 | 70D01080 | D595 | 7007 | 19457 | B | 12 | 1946 | - | 0 | H | 1 | 2659 | 2950 | 1497 |
| 12 | 70D01080 | D595 | 7007 | 19457 | B | 12 | 1946 | - | 0 | H | 1 | 2700 | 3086 | 1497 |
| 1 | 70D01084 | D595 | 7007 | 30738 | B | 12 | 3074 | - | 0 | H | 28 | 5137 | 165 | 0 |
| 10 | 70D01084 | D595 | 7007 | 19457 | B | 12 | 1946 | - | 0 | H | 0 | 2882 | 1322 | 463 |
| 12 | 70D01084 | D595 | 7007 | 19457 | B | 12 | 1946 | - | 0 | H | 0 | 52300 | 2593 | 793 |
| 1 | 75D00521 | D598 | 7501 | 12128 | P | 10 | 2850 | 0 | 0 | H | 1 | 28 | 0 | 0 |
| 8 | 75D00521 | D598 | 7501 | 12128 | L | 10 | 2213 | 0 | 0 | H | 13 | 1010 | 273 | 0 |
| 12 | 75D00521 | D598 | 7501 | 8750 | L | 10 | 1334 | 0 | 0 | H | 1 | 42 | 273 | 0 |
| 1 | 67D01748 | D604 | 6701 | 10213 | B | 12 | 1021 | - | 0 | H | 0 | 558 | 0 | 0 |

| | | | | | | | | | | | | | | |
|---|---|---|---|---|---|---|---|---|---|---|---|---|---|---|
| 12 | 67D01748 | D604 | 6701 | 10213 | B | 12 | 1021 | - | 0 | H | 0 | 599 | 329 | 0 |
| 1 | 72D01168 | D606 | 7211 | 5431 | D | 12 | 1086 | - | 0 | U | 0 | 0 | 41 | 0 |
| 12 | 72D01168 | D606 | 7211 | 1680 | D | 12 | 220 | - | 0 | U | 0 | 0 | 140 | 35 |
| 1 | 75D00462 | D606 | 7510 | 5431 | R | 12 | 2274 | | 0 | U | 1 | 0 | 0 | 0 |
| 12 | 75D00462 | D606 | 7510 | 5431 | R | 12 | 1901 | | 0 | U | 1 | 0 | 433 | 129 |
| 1 | 80D00212 | D606 | 8005 | 5431 | T | 12 | 4141 | | 0 | U | 0 | 0 | 10 | 34 |
| 12 | 80D00212 | D606 | 8005 | 4851 | T | 12 | 3365 | | 0 | U | 0 | 0 | 259 | 39 |
| 1 | 72D00572 | D620 | 7301 | 12257 | B | 10 | 1226 | - | 0 | U | 0 | 0 | 0 | 0 |
| 12 | 72D00572 | D620 | 7301 | 17960 | B | 10 | 1796 | - | 0 | U | 0 | 0 | 326 | 377 |
| 1 | 77D00425 | D620 | 7706 | 12257 | R | 10 | 5546 | 0 | 0 | U | 0 | 0 | 0 | 0 |
| 12 | 77D00425 | D620 | 7706 | 17960 | R | 10 | 6645 | 0 | 0 | U | 0 | 0 | 263 | 0 |
| 1 | 77D00428 | D620 | 7707 | 12257 | R | 10 | 5638 | 0 | 0 | U | 14 | 0 | 0 | 0 |
| 12 | 77D00428 | D620 | 7707 | 17960 | R | 10 | 6780 | 0 | 0 | U | 14 | 0 | 134 | 7 |
| 1 | 79D00214 | D626 | 7907 | 37839 | T | 12 | 24832 | 0 | 0 | H | 2 | 1311 | 315 | 0 |
| 5 | 79D00214 | D626 | 7907 | 29252 | T | 12 | 18465 | 0 | 0 | H | 1 | 1394 | 1823 | 2236 |
| 1 | 79D00215 | D626 | 7907 | 37839 | T | 12 | 24832 | 0 | 0 | H | 1 | 1197 | 316 | 327 |
| 5 | 79D00215 | D626 | 7907 | 29252 | T | 12 | 18465 | 0 | 0 | H | 1 | 1365 | 802 | 656 |
| 1 | 72D00533 | D631 | 7209 | 40247 | B | 10 | 4025 | - | 0 | H | 1 | 1889 | 258 | 732 |
| 12 | 72D00533 | D631 | 7209 | 14911 | B | 10 | 1491 | - | 0 | H | 0 | 1994 | 2523 | 2080 |
| 1 | 72D01194 | D631 | 7205 | 40247 | B | 10 | 4025 | - | 0 | H | 8 | 3432 | 0 | 0 |
| 12 | 72D01194 | D631 | 7205 | 14352 | B | 10 | 1435 | - | 0 | H | 0 | 3618 | 2121 | 2230 |
| 1 | 72D01197 | D631 | 7201 | 40247 | B | 10 | 4025 | - | 0 | H | 9 | 6690 | 103 | 0 |
| 8 | 72D01197 | D631 | 7201 | 40247 | B | 10 | 4025 | - | 0 | H | 2 | 6808 | 731 | 610 |
| 1 | 82D00200 | D631 | 8210 | 40247 | U | 10 | 37530 | 0 | 0 | H | 1 | 191 | 0 | 0 |
| 12 | 82D00200 | D631 | 8210 | 44477 | U | 10 | 37805 | 0 | 0 | H | 2 | 629 | 735 | 877 |
| 1 | 69D01332 | D632 | 6910 | 63077 | B | 10 | 6308 | - | 0 | H | 1 | 4570 | 0 | 0 |
| 3 | 69D01332 | D632 | 6910 | 63077 | B | 10 | 6308 | - | 7326 | H | 1 | 4745 | 2164 | 3485 |
| 7 | 69D01332 | D632 | 6910 | 63077 | B | 10 | 6308 | - | 0 | H | 7 | 4795 | 3126 | 3492 |
| 1 | 69D01333 | D632 | 6910 | 63077 | B | 10 | 6308 | - | 0 | H | 1 | 6074 | 206 | 0 |
| 12 | 69D01333 | D632 | 6910 | 20469 | B | 10 | 2047 | - | 0 | H | 0 | 6239 | 3013 | 2957 |
| 1 | 79D00214 | D632 | 7907 | 37839 | T | 12 | 26487 | 0 | 0 | H | 1 | 1105 | 0 | 0 |
| 7 | 79D00214 | D632 | 7907 | 37839 | T | 12 | 25068 | 0 | 0 | H | 3 | 1287 | 1037 | 315 |
| 1 | 79D00215 | D632 | 7907 | 37839 | T | 12 | 26487 | 0 | 0 | H | 2 | 1046 | 237 | 10 |
| 7 | 79D00215 | D632 | 7907 | 37839 | T | 12 | 25068 | 0 | 0 | H | 1 | 1194 | 878 | 78 |
| 1 | 71D00178 | D640 | 7101 | 83514 | B | 10 | 8351 | - | 0 | H | 19 | 3810 | 0 | 0 |
| 12 | 71D00178 | D640 | 7101 | 30024 | B | 10 | 3002 | - | 0 | H | 54 | 3591 | 4151 | 2250 |
| 1 | 80D01098 | D653 | 8008 | 49864 | T | 12 | 38956 | 0 | 0 | H | 6 | 1601 | 0 | 0 |
| 12 | 80D01098 | D653 | 8008 | 55937 | T | 12 | 39855 | 0 | 0 | H | 3 | 1607 | 1494 | 561 |
| 1 | 80D01099 | D653 | 8008 | 49864 | T | 12 | 38956 | 0 | 0 | H | 112 | 1466 | 454 | 122 |
| 12 | 80D01099 | D653 | 8008 | 55937 | T | 12 | 39855 | 0 | 0 | H | 4 | 1930 | 2269 | 1310 |

| | | | | | | | | | | | | | |
|---|---|---|---|---|---|---|---|---|---|---|---|---|---|
| 1 | 66D00192 | D655 | 6604 | 62341 | B | 12 | 6234 | - | 0 | H | 2 | 593 | 87 | 0 |
| 8 | 66D00192 | D655 | 6604 | 62341 | B | 12 | 6234 | - | 7799 | H | 10 | 717 | 2571 | 4466 |
| 12 | 66D00192 | D655 | 6604 | 13562 | B | 12 | 1356 | - | 0 | H | 2 | 942 | 4115 | 4503 |
| 1 | 66D01294 | D655 | 6605 | 62341 | B | 15 | 6234 | - | 0 | H | 2 | 7203 | 41 | 96 |
| 12 | 66D01294 | D655 | 6605 | 12570 | B | 12 | 1257 | - | 0 | H | 2 | 7475 | 2394 | 2466 |
| 1 | 75D00290 | D655 | 7501 | 62341 | R | 12 | 22599 | 0 | 0 | H | 1 | 1582 | 2654 | 543 |
| 12 | 75D00290 | D655 | 7501 | 27613 | R | 12 | 8111 | 0 | 0 | H | 1 | 1785 | 6211 | 5814 |
| 1 | 66D01241 | D660 | 6611 | 29653 | D | 20 | 7413 | - | 0 | U | 0 | 0 | 0 | 0 |
| 1 | 66D01241 | D660 | 6611 | 29653 | D | 20 | 7413 | - | 0 | U | 0 | 0 | 0 | 0 |
| 1 | 79D00564 | D667 | 7911 | 87344 | T | 12 | 63324 | | 0 | H | 1 | 1123 | 681 | 49 |
| 12 | 79D00564 | D667 | 7911 | 892 | T | 12 | 585 | | 0 | H | 0 | 1210 | 4378 | 2025 |
| 1 | 63D00801 | D676 | 6310 | 19600 | B | 17 | 1960 | - | 0 | H | 0 | 3357 | 0 | 0 |
| 10 | 63D00801 | D676 | 6310 | 19394 | B | 17 | 1939 | - | 0 | H | 0 | 3421 | 861 | 146 |
| 12 | 63D00801 | D676 | 6310 | 4836 | B | 17 | 484 | - | 0 | H | 0 | 3421 | 861 | 923 |
| 1 | 81D00224 | D676 | 8403 | 19600 | T | 17 | 19600 | 0 | 0 | H | 0 | 144 | 42 | 0 |
| 2 | 81D00224 | D676 | 8403 | 19394 | T | 17 | 19308 | 0 | 0 | H | 0 | 149 | 42 | 0 |
| 4 | 81D00224 | D676 | 8403 | 16936 | T | 17 | 16712 | 0 | 0 | H | 0 | 149 | 42 | 0 |
| 1 | 70D00991 | D680 | 7010 | 17113 | D | 15 | 4022 | - | 0 | H | 0 | 1012 | 0 | 0 |
| 10 | 70D00991 | D680 | 7010 | 24674 | D | 15 | 4688 | - | 0 | H | 3 | 1032 | 748 | 43 |
| 11 | 70D00991 | D680 | 7010 | 17113 | D | 15 | 3166 | - | 0 | H | 1 | 829 | 1295 | 608 |
| 12 | 70D00991 | D680 | 7010 | 9055 | D | 15 | 1630 | - | 0 | H | 1 | 829 | 1295 | 608 |
| 1 | 69D00235 | D682 | 6901 | 4808 | D | 25 | 2298 | - | 0 | U | 0 | 0 | 0 | 0 |
| 8 | 69D00235 | D682 | 6901 | 2263 | D | 25 | 1034 | - | 0 | U | 0 | 0 | 36 | 0 |
| 12 | 69D00235 | D682 | 6901 | 2263 | D | 25 | 1007 | - | 0 | U | 0 | 0 | 36 | 0 |
| 1 | 69D01501 | D684 | 8012 | 3428 | D | 25 | 3109 | - | 0 | U | 0 | 0 | 0 | 0 |
| 6 | 69D01501 | D684 | 8012 | 8667 | D | 25 | 7731 | - | 0 | U | 0 | 0 | 0 | 0 |
| 12 | 69D01501 | D684 | 8012 | 2667 | D | 25 | 2331 | - | 0 | U | 0 | 0 | 0 | 0 |
| 1 | 70D01924 | D701 | 7001 | 101379 | B | 12 | 10138 | - | 0 | U | 0 | 0 | 0 | 0 |
| 10 | 70D01924 | D701 | 7001 | 117664 | B | 12 | 11766 | - | 0 | U | 0 | 0 | 1344 | 266 |
| 11 | 70D01924 | D701 | 7001 | 101379 | B | 12 | 10138 | - | 0 | U | 0 | 0 | 1344 | 266 |
| 12 | 70D01924 | D701 | 7001 | 24250 | B | 12 | 2425 | - | 0 | U | 0 | 0 | 1344 | 266 |
| 1 | 66D02755 | D705 | 6601 | 48267 | B | 10 | 4827 | - | 0 | H | 1 | 2698 | 134 | 0 |
| 5 | 66D02755 | D705 | 6601 | 67247 | B | 10 | 6725 | - | 0 | H | 0 | 2676 | 134 | 0 |
| 12 | 66D02755 | D705 | 6601 | 23500 | B | 10 | 2350 | - | 0 | H | 1 | 2684 | 607 | 66 |
| 1 | 67D00933 | D707 | 6704 | 88667 | B | 10 | 8867 | - | 0 | U | 0 | 0 | 0 | 0 |
| 10 | 67D00933 | D707 | 6704 | 300491 | B | 10 | 30049 | - | 0 | U | 0 | 0 | 134 | 1493 |
| 11 | 67D00933 | D707 | 6704 | 88667 | B | 10 | 8867 | - | 0 | U | 0 | 0 | 134 | 1493 |
| 12 | 67D00933 | D707 | 6704 | 86064 | B | 10 | 8606 | - | 0 | U | 0 | 0 | 182 | 1673 |
| 1 | 70D01966 | D715 | 7012 | 14941 | D | 15 | 3661 | - | 0 | U | 0 | 0 | 0 | 0 |
| 10 | 70D01966 | D715 | 7012 | 17794 | D | 15 | 3559 | - | 0 | U | 0 | 0 | 0 | 0 |
| 11 | 70D01966 | D715 | 7012 | 14941 | D | 15 | 2913 | - | 0 | U | 0 | 0 | 0 | 0 |
| 12 | 70D01966 | D715 | 7012 | 6360 | D | 15 | 1208 | - | 0 | U | 0 | 0 | 0 | 0 |
| 1 | 76D00466 | D717 | 7601 | 10039 | R | 15 | 5521 | 0 | 0 | U | 0 | 0 | 0 | 0 |
| 12 | 76D00466 | D717 | 7601 | 2163 | R | 15 | 1071 | 0 | 0 | U | 0 | 0 | 93 | 0 |
| 1 | 71D00167 | D718 | 7101 | 9019 | D | 15 | 2255 | - | 0 | U | 0 | 0 | 41 | 0 |

| | | | | | | | | | | | | | |
|---|---|---|---|---|---|---|---|---|---|---|---|---|---|
| 10 | 71D00167 | D718 | 7101 | 9798 | D | 15 | 2009 | - | 0 | U | 0 | 0 | 326 | 751 |
| 11 | 71D00167 | D718 | 7101 | 9019 | D | 15 | 1804 | - | 0 | U | 0 | 0 | 326 | 751 |
| 12 | 71D00167 | D718 | 7101 | 2300 | D | 15 | 448 | - | 0 | U | 0 | 0 | 326 | 751 |
| 1 | 79D00547 | D718 | 8003 | 9019 | T | 15 | 7215 | | 0 | U | 0 | 0 | 0 | 0 |
| 10 | 79D00547 | D718 | 8003 | 9798 | T | 15 | 7397 | | 0 | U | 0 | 0 | 67 | 0 |
| 11 | 79D00547 | D718 | 8003 | 9019 | T | 15 | 6764 | | 0 | U | 0 | 0 | 67 | 0 |
| 12 | 79D00547 | D718 | 8003 | 7210 | T | 15 | 5371 | | 0 | U | 0 | 0 | 67 | 0 |
| 1 | 66D00397 | D720 | 6612 | 39889 | B | 15 | 3989 | - | 0 | M | 7 | 19386 | 0 | 0 |
| 10 | 66D00397 | D720 | 6612 | 46803 | B | 15 | 4680 | - | 0 | M | 8 | 20640 | 1508 | 552 |
| 11 | 66D00397 | D720 | 6612 | 39889 | B | 15 | 3989 | - | 0 | M | 7 | 20743 | 1679 | 558 |
| 12 | 66D00397 | D720 | 6612 | 12566 | B | 15 | 1257 | - | 0 | M | 6 | 20743 | 1679 | 558 |
| 1 | 64D00062 | D731 | 6408 | 37869 | B | 17 | 3787 | - | 0 | M | 28 | 45556 | 412 | 277 |
| 12 | 64D00062 | D731 | 6408 | 7407 | B | 17 | 741 | - | 0 | M | 8 | 46063 | 2554 | 1498 |
| 1 | 66D00835 | D731 | 6612 | 37869 | D | 17 | 4622 | - | 0 | M | 9 | 45487 | 114 | 11 |
| 7 | 66D00835 | D731 | 6612 | 37869 | B | 17 | 3787 | - | 0 | M | 9 | 46818 | 1243 | 169 |
| 12 | 66D00835 | D731 | 6612 | 10826 | B | 17 | 1083 | - | 0 | M | 3 | 47631 | 2016 | 648 |
| 1 | 70D00830 | D731 | 7005 | 37869 | D | 17 | 11472 | - | 0 | M | 19 | 57809 | 0 | 0 |
| 12 | 70D00830 | D731 | 7005 | 15359 | D | 17 | 3908 | - | 0 | M | 8 | 60147 | 2626 | 1679 |
| 1 | 71D00500 | D731 | 7107 | 37869 | D | 17 | 13811 | - | 0 | M | 10 | 44800 | 0 | 0 |
| 12 | 71D00500 | D731 | 7107 | 28954 | D | 17 | 9155 | - | 0 | M | 4 | 46173 | 2878 | 973 |
| 1 | 72D00309 | D731 | 7203 | 37869 | R | 17 | 15148 | 0 | 0 | M | 82 | 47914 | 0 | 0 |
| 12 | 72D00309 | D731 | 7203 | 28954 | R | 17 | 10176 | 0 | 0 | M | 11 | 51514 | 3400 | 1660 |
| 1 | 72D00596 | D731 | 7209 | 37869 | D | 17 | 16150 | - | 0 | M | 37 | 46347 | 0 | 0 |
| 12 | 72D00596 | D731 | 7209 | 37869 | D | 17 | 14312 | - | 0 | M | 9 | 48583 | 3998 | 1015 |
| 1 | 80D00162 | D765 | 8101 | 20855 | T | 15 | 17727 | 0 | 0 | U | 0 | 0 | 41 | 0 |
| 12 | 80D00162 | D765 | 8101 | 19948 | T | 15 | 15859 | 0 | 0 | U | 0 | 0 | 114 | 0 |
| 1 | 79D00519 | D766 | 1079 | 45927 | G | 12 | 4593 | | 0 | H | 10 | 327 | 41 | 0 |
| 12 | 79D00519 | D766 | 1079 | 38821 | G | 12 | 3882 | | 0 | H | 4 | 150 | 341 | 0 |
| 1 | 79D00381 | D768 | 7902 | 7780 | T | 10 | 4687 | 0 | 0 | H | 2 | 519 | 0 | 0 |
| 8 | 79D00381 | D768 | 7902 | 7780 | R | 10 | 4279 | 0 | 0 | H | 0 | 521 | 161 | 3 |
| 12 | 79D00381 | D768 | 7902 | 13374 | R | 10 | 6954 | 0 | 0 | H | 6 | 612 | 421 | 12 |
| 1 | 79D00553 | D768 | 8005 | 7780 | T | 10 | 5563 | | 0 | H | 0 | 88 | 0 | 0 |
| 12 | 79D00553 | D768 | 8005 | 6425 | T | 10 | 4064 | | 0 | H | 0 | 110 | 945 | 524 |
| 1 | 78D00811 | D772 | 7812 | 29068 | R | 8 | 14080 | 0 | 0 | H | 2 | 638 | 25 | 0 |
| 12 | 78D00811 | D772 | 7812 | 18257 | R | 8 | 6960 | 0 | 0 | H | 0 | 739 | 763 | 303 |

| | | | | | | | | | | | | | |
|---|---|---|---|---|---|---|---|---|---|---|---|---|---|
| 1 | 69E00645 | E801 | 6911 | 8446 | B | 11 | 845 | - | 0 | H | 15 | 3127 | 0 | 0 |
| 2 | 69E00645 | E801 | 6911 | 10196 | B | 11 | 1020 | - | 0 | H | 16 | 2709 | 87 | 0 |
| 5 | 69E00645 | E801 | 6911 | 10196 | B | 11 | 1020 | - | 0 | H | 16 | 2709 | 87 | 0 |
| 1 | 69E00748 | E801 | 6912 | 8446 | B | 11 | 845 | - | 0 | H | 1 | 1338 | 10 | 0 |
| 2 | 69E00748 | E801 | 6912 | 10196 | B | 11 | 1020 | - | 0 | H | 1 | 1423 | 122 | 9 |
| 4 | 69E00748 | E801 | 6912 | 10196 | B | 11 | 1020 | - | 1038 | H | 2 | 1482 | 628 | 231 |
| 6 | 69E00748 | E801 | 6912 | 10196 | B | 11 | 1020 | - | 1123 | H | 1 | 1484 | 1226 | 718 |
| 12 | 69E00748 | E801 | 6912 | 5417 | B | 11 | 542 | - | 0 | H | 1 | 83 | 2058 | 974 |
| 1 | 70E00069 | E801 | 7008 | 8446 | B | 11 | 845 | - | 0 | H | 2 | 3834 | 0 | 0 |
| 2 | 70E00069 | E801 | 7008 | 10196 | B | 11 | 1020 | - | 0 | H | 2 | 3884 | 20 | 0 |
| 12 | 70E00069 | E801 | 7008 | 5417 | B | 11 | 542 | - | 0 | H | 1 | 4154 | 921 | 241 |
| 1 | 70E00070 | E801 | 7008 | 8446 | B | 11 | 845 | - | 0 | H | 1 | 3869 | 0 | 0 |
| 2 | 70E00070 | E801 | 7008 | 10196 | B | 11 | 1020 | - | 0 | H | 1 | 3839 | 169 | 4 |
| 12 | 70E00070 | E801 | 7008 | 5417 | B | 11 | 542 | - | 0 | H | 1 | 3719 | 862 | 380 |
| 1 | 70E00127 | E801 | 7008 | 8446 | B | 11 | 845 | - | 0 | H | 0 | 26 | 254 | 0 |
| 2 | 70E00127 | E801 | 7008 | 10196 | B | 11 | 1020 | - | 0 | H | 0 | 414 | 428 | 4 |
| 5 | 70E00127 | E801 | 7008 | 10196 | B | 11 | 1020 | - | 1040 | H | 4 | 84 | 955 | 35 |
| 12 | 70E00127 | E801 | 7008 | 5417 | B | 11 | 542 | - | 0 | H | 1 | 234 | 1385 | 89 |
| 1 | 70E00128 | E801 | 7008 | 8446 | B | 11 | 845 | - | 0 | H | 2 | 6540 | 10 | 0 |
| 2 | 70E00128 | E801 | 7008 | 10196 | B | 11 | 1020 | - | 0 | H | 1 | 6555 | 10 | 0 |
| 12 | 70E00128 | E801 | 7008 | 5417 | B | 11 | 542 | - | 0 | H | 0 | 6653 | 477 | 286 |
| 1 | 70E00167 | E801 | 7008 | 8446 | B | 11 | 845 | - | 0 | H | 1 | 3354 | 0 | 0 |
| 2 | 70E00167 | E801 | 7008 | 10196 | B | 11 | 1020 | - | 0 | H | 2 | 3302 | 82 | 0 |
| 4 | 70E00167 | E801 | 7008 | 10196 | A | 11 | 1020 | - | 0 | H | 1 | 17365 | 102 | 42 |
| 6 | 70E00167 | E801 | 7008 | 10196 | B | 11 | 1020 | - | 0 | H | 214 | 4400 | 102 | 126 |
| 12 | 70E00167 | E801 | 7008 | 5417 | B | 11 | 542 | - | 0 | H | 0 | 3407 | 696 | 682 |
| 1 | 70E00170 | E801 | 7008 | 8446 | B | 11 | 845 | - | 0 | H | 0 | 5580 | 0 | 412 |
| 2 | 70E00170 | E801 | 7008 | 10196 | B | 11 | 1020 | - | 1194 | H | 0 | 5600 | 534 | 552 |
| 12 | 70E00170 | E801 | 7008 | 5417 | B | 11 | 542 | - | 0 | H | 1 | 5833 | 1010 | 728 |
| 1 | 70E00172 | E801 | 7008 | 8446 | B | 11 | 845 | - | 0 | H | 2 | 5640 | 77 | 0 |
| 2 | 70E00172 | E801 | 7008 | 10196 | B | 11 | 1020 | - | 0 | H | 1 | 5686 | 77 | 0 |
| 12 | 70E00172 | E801 | 7008 | 5417 | B | 11 | 542 | - | 0 | H | 1 | 5930 | 784 | 218 |
| 1 | 70E00178 | E801 | 7008 | 8446 | B | 11 | 845 | - | 0 | H | 1 | 1919 | 0 | 0 |
| 2 | 70E00178 | E801 | 7008 | 10196 | B | 11 | 1020 | - | 0 | H | 1 | 2000 | 46 | 0 |
| 12 | 70E00178 | E801 | 7008 | 5417 | B | 11 | 542 | - | 0 | H | 1 | 1828 | 796 | 203 |
| 1 | 70E00220 | E801 | 7009 | 8446 | B | 11 | 845 | - | 0 | H | 2 | 4670 | 51 | 131 |
| 2 | 70E00220 | E801 | 7009 | 10196 | B | 11 | 1020 | - | 0 | H | 3 | 4728 | 302 | 161 |
| 12 | 70E00220 | E801 | 7009 | 5417 | B | 11 | 542 | - | 0 | H | 2 | 5296 | 1071 | 538 |
| 1 | 72E00271 | E801 | 7209 | 8446 | L | 11 | 960 | 0 | 0 | H | 1 | 1910 | 0 | 0 |
| 2 | 72E00271 | E801 | 7209 | 10196 | L | 11 | 1089 | 0 | 0 | H | 1 | 1949 | 0 | 0 |
| 4 | 72E00271 | E801 | 7209 | 10196 | H | 11 | 1020 | 0 | 0 | H | 1 | 2021 | 108 | 6 |
| 12 | 72E00271 | E801 | 7209 | 5417 | H | 11 | 542 | 0 | 0 | H | 1 | 2253 | 369 | 160 |
| 1 | 72E00684 | E801 | 7208 | 8446 | L | 11 | 902 | 0 | 0 | H | 2 | 1418 | 15 | 240 |
| 2 | 72E00684 | E801 | 7208 | 10196 | L | 11 | 1020 | 0 | 1055 | H | 2 | 1425 | 302 | 760 |
| 3 | 72E00684 | E801 | 7208 | 10196 | H | 11 | 1020 | 0 | 0 | H | 2 | 1452 | 714 | 801 |
| 12 | 72E00684 | E801 | 7208 | 5417 | H | 11 | 542 | 0 | 0 | H | 4 | 2067 | 1283 | 976 |
| 1 | 72E00685 | E801 | 7208 | 8446 | L | 11 | 902 | 0 | 0 | H | 1 | 3202 | 0 | 0 |

| | | | | | | | | | | | | | | |
|---|---|---|---|---|---|---|---|---|---|---|---|---|---|---|
| 2 | 72E00685 | E801 | 7208 | 10196 | L | 11 | 1020 | 0 | 0 | H | 1 | 3210 | 0 | 0 |
| 3 | 72E00685 | E801 | 7208 | 10196 | H | 11 | 1020 | 0 | 0 | H | 1 | 3257 | 0 | 0 |
| 11 | 72E00685 | E801 | 7208 | 10196 | H | 11 | 1020 | 0 | 1093 | H | 1 | 3316 | 1148 | 446 |
| 12 | 72E00685 | E801 | 7208 | 5417 | H | 11 | 542 | 0 | 0 | H | 1 | 3340 | 1211 | 449 |
| 1 | 72E00686 | E801 | 7208 | 8446 | L | 11 | 902 | 0 | 0 | H | 0 | 4020 | 0 | 0 |
| 2 | 72E00686 | E801 | 7208 | 10196 | L | 11 | 1020 | 0 | 0 | H | 2 | 4114 | 0 | 0 |
| 3 | 72E00686 | E801 | 7208 | 10196 | H | 11 | 1020 | 0 | 0 | H | 3 | 4064 | 0 | 0 |
| 12 | 72E00686 | E801 | 7208 | 5417 | H | 11 | 542 | 0 | 0 | H | 1 | 4346 | 538 | 288 |
| 1 | 72E00687 | E801 | 7208 | 8446 | L | 11 | 902 | 0 | 0 | H | 8 | 3568 | 0 | 0 |
| 2 | 72E00687 | E801 | 7208 | 10196 | L | 11 | 1020 | 0 | 0 | H | 4 | 3456 | 46 | 417 |
| 3 | 72E00687 | E801 | 7208 | 10196 | H | 11 | 1020 | 0 | 1093 | H | 4 | 3543 | 415 | 419 |
| 12 | 72E00687 | E801 | 7208 | 5417 | H | 11 | 542 | 0 | 0 | H | 0 | 3499 | 956 | 739 |
| 1 | 72E00688 | E801 | 7208 | 8446 | B | 11 | 902 | - | 0 | H | 1 | 3087 | 244 | 0 |
| 2 | 72E00688 | E801 | 7208 | 10196 | B | 11 | 1020 | - | 0 | H | 1 | 3087 | 244 | 0 |
| 3 | 72E00688 | E801 | 7208 | 10196 | B | 11 | 1020 | - | 0 | H | 1 | 3177 | 254 | 70 |
| 10 | 72E00688 | E801 | 7208 | 10196 | H | 11 | 1020 | | 0 | H | 2 | 3446 | 830 | 120 |
| 12 | 72E00688 | E801 | 7208 | 5417 | H | 11 | 542 | | 0 | H | 1 | 3507 | 872 | 130 |
| 1 | 72E00689 | E801 | 7208 | 8446 | L | 11 | 902 | 0 | 0 | H | 1 | 2588 | 0 | 97 |
| 2 | 72E00689 | E801 | 7208 | 10196 | L | 11 | 1020 | 0 | 0 | H | 1 | 2550 | 287 | 190 |
| 3 | 72E00689 | E801 | 7208 | 10196 | H | 11 | 1020 | 0 | 0 | H | 1 | 2577 | 287 | 190 |
| 12 | 72E00689 | E801 | 7208 | 5417 | H | 11 | 542 | 0 | 0 | H | 1 | 2688 | 488 | 551 |
| 1 | 72E00711 | E801 | 7310 | 8446 | P | 11 | 1708 | 0 | 0 | H | 1 | 4243 | 0 | 0 |
| 2 | 72E00711 | E801 | 7310 | 10196 | P | 11 | 1993 | 0 | 0 | H | 1 | 4243 | 0 | 0 |
| 5 | 72E00711 | E801 | 7310 | 10196 | L | 11 | 1784 | 0 | 0 | H | 1 | 2959 | 421 | 79 |
| 10 | 72E00711 | E801 | 7310 | 10196 | H | 11 | 1437 | | 0 | H | 2 | 3189 | 905 | 394 |
| 11 | 72E00711 | E801 | 7310 | 10196 | L | 11 | 1367 | | 0 | H | 2 | 3189 | 905 | 394 |
| 12 | 72E00711 | E801 | 7310 | 5417 | L | 11 | 689 | | 0 | H | 2 | 3257 | 1058 | 476 |
| 1 | 78E00214 | E801 | 7801 | 8446 | R | 11 | 4645 | 0 | 0 | H | 0 | 817 | 51 | 75 |
| 2 | 78E00214 | E801 | 7801 | 10196 | R | 11 | 5538 | 0 | 0 | H | 0 | 823 | 51 | 75 |
| 12 | 78E00214 | E801 | 7801 | 5717 | R | 11 | 2716 | 0 | 0 | H | 1 | 867 | 352 | 223 |
| 1 | 78E00215 | E801 | 7801 | 8446 | R | 11 | 4645 | 0 | 0 | H | 2 | 1326 | 10 | 0 |
| 2 | 78E00215 | E801 | 7801 | 10196 | R | 11 | 5538 | 0 | 0 | H | 2 | 1376 | 10 | 0 |
| 12 | 78E00215 | E801 | 7801 | 5717 | R | 11 | 2716 | 0 | 0 | H | 1 | 1579 | 300 | 202 |
| 1 | 82E00277 | E801 | 8202 | 8446 | T | 11 | 7467 | 0 | 0 | H | 4 | 854 | 0 | 0 |
| 2 | 82E00277 | E801 | 8202 | 10196 | T | 11 | 8945 | 0 | 0 | H | 3 | 948 | 0 | 0 |
| 12 | 82E00277 | E801 | 8202 | 8755 | T | 11 | 7084 | 0 | 0 | H | 2 | 1532 | 820 | 1020 |
| 1 | 81E00230 | E816 | 8105 | 17440 | T | 8 | 13189 | 0 | 0 | H | 1 | 1118 | 0 | 0 |
| 2 | 81E00230 | E816 | 8105 | 13629 | T | 8 | 10179 | 0 | 0 | H | 2 | 1159 | 15 | 13 |
| 12 | 81E00230 | E816 | 8105 | 14453 | T | 8 | 9440 | 0 | 0 | H | 2 | 1637 | 564 | 815 |
| 1 | 81E00231 | E816 | 8105 | 17440 | T | 8 | 13189 | 0 | 0 | H | 3 | 596 | 0 | 0 |
| 2 | 81E00231 | E816 | 8105 | 13629 | T | 8 | 10179 | 0 | 0 | H | 3 | 620 | 164 | 120 |
| 12 | 81E00231 | E816 | 8105 | 14453 | T | 8 | 9440 | 0 | 0 | H | 1 | 830 | 438 | 193 |
| 1 | 81E00232 | E816 | 8105 | 17440 | T | 8 | 13189 | 0 | 0 | H | 1 | 594 | 103 | 0 |
| 2 | 81E00232 | E816 | 8105 | 13629 | T | 8 | 10179 | 0 | 0 | H | 1 | 630 | 118 | 0 |
| 12 | 81E00232 | E816 | 8105 | 14453 | T | 8 | 9440 | 0 | 0 | H | 3 | 987 | 347 | 203 |
| 1 | 81E00233 | E816 | 8105 | 17440 | T | 8 | 13189 | 0 | 0 | H | 2 | 661 | 0 | 12 |
| 2 | 81E00233 | E816 | 8105 | 13629 | T | 8 | 10179 | 0 | 0 | H | 3 | 989 | 67 | 12 |
| 12 | 81E00233 | E816 | 8105 | 14453 | T | 8 | 9440 | 0 | 0 | H | 2 | 1078 | 518 | 178 |

| | | | | | | | | | | | | | | |
|---|---|---|---|---|---|---|---|---|---|---|---|---|---|---|
| 1 | 81E00234 | E816 | 8005 | 17440 | T | 8 | 11227 | 0 | | 0 | H | 1 | 888 | 0 | 0 |
| 2 | 81E00234 | E816 | 8005 | 13629 | T | 8 | 8646 | 0 | | 0 | H | 1 | 963 | 30 | 0 |
| 11 | 81E00234 | E816 | 8005 | 13629 | R | 8 | 7496 | 0 | | 0 | H | 3 | 1374 | 449 | 318 |
| 12 | 81E00234 | E816 | 8005 | 14453 | R | 8 | 7814 | 0 | | 0 | H | 2 | 1800 | 475 | 313 |
| 1 | 70E00285 | E820 | 7011 | 50340 | B | 8 | 6034 | - | | 0 | H | 0 | 600 | 0 | 0 |
| 2 | 70E00285 | E820 | 7011 | 64057 | B | 8 | 6406 | - | | 0 | H | 0 | 600 | 0 | 0 |
| 12 | 70E00285 | E820 | 7011 | 19551 | B | 8 | 1965 | - | | 0 | H | 9 | 1634 | 1985 | 1388 |
| 1 | 82E00001 | E822 | 8205 | 23449 | T | 10 | 20987 | 0 | | 0 | H | 0 | 5 | 0 | 0 |
| 11 | 82E00001 | E822 | 8205 | 30737 | T | 10 | 26204 | 0 | | 0 | H | 6 | 25 | 338 | 295 |
| 12 | 82E00001 | E822 | 8205 | 30737 | T | 10 | 24974 | 0 | | 0 | H | 6 | 25 | 338 | 295 |
| 1 | 82E00017 | E822 | 8111 | 23449 | T | 10 | 18733 | 0 | | 0 | H | 7 | 2011 | 0 | 0 |
| 2 | 82E00017 | E822 | 8111 | 30737 | T | 10 | 23572 | 0 | | 0 | H | 6 | 2331 | 133 | 145 |
| 12 | 82E00017 | E822 | 8111 | 23449 | T | 10 | 17083 | 0 | | 0 | H | 1 | 2715 | 616 | 523 |
| 1 | 82E00082 | E822 | 8202 | 23449 | T | 10 | 20459 | 0 | | 0 | H | 12 | 549 | 0 | 0 |
| 2 | 82E00082 | E822 | 8202 | 30737 | T | 10 | 26588 | 0 | | 0 | H | 9 | 455 | 77 | 0 |
| 12 | 82E00082 | E822 | 8202 | 23449 | T | 10 | 18525 | 0 | | 0 | H | 10 | 1243 | 1194 | 904 |
| 1 | 83E00401 | E823 | 8212 | 19322 | U | 10 | 18308 | 0 | | 0 | H | 2 | 195 | 0 | 0 |
| 6 | 83E00401 | E823 | 8212 | 19322 | T | 10 | 17583 | 0 | | 0 | H | 1 | 364 | 703 | 38 |
| 12 | 83E00401 | E823 | 8212 | 19322 | T | 10 | 16714 | 0 | | 0 | H | 1 | 571 | 976 | 55 |
| 1 | 83E00423 | E824 | 8306 | 30611 | U | 10 | 30381 | 0 | | 0 | H | 0 | 114 | 0 | 0 |
| 2 | 83E00423 | E824 | 8306 | 34264 | U | 10 | 33750 | 0 | | 0 | H | 4 | 454 | 0 | 0 |
| 12 | 83E00423 | E824 | 8306 | 36820 | T | 10 | 33506 | 0 | | 0 | H | 2 | 189 | 213 | 149 |
| 1 | 70E00546 | E830 | 7009 | 8338 | B | 11 | 834 | - | | 0 | H | 1 | 7468 | 0 | 455 |
| 2 | 70E00546 | E830 | 7009 | 8338 | B | 11 | 834 | - | 1668 | H | 1 | 7480 | 677 | 536 |
| 12 | 70E00546 | E830 | 7009 | 8338 | B | 11 | 834 | - | 0 | H | 1 | 6016 | 1522 | 866 |
| 1 | 70E00549 | E830 | 7009 | 8338 | A | 11 | 834 | - | 0 | H | 1 | 9428 | 0 | 0 |
| 3 | 70E00549 | E830 | 7009 | 8338 | A | 11 | 834 | - | 868 | H | 1 | 9496 | 480 | 0 |
| 6 | 70E00549 | E830 | 7009 | 8338 | B | 11 | 834 | - | 0 | H | 2 | 81 | 806 | 80 |
| 7 | 70E00549 | E830 | 7009 | 8338 | A | 11 | 834 | - | 0 | H | 3 | 9674 | 1006 | 268 |
| 12 | 70E00549 | E830 | 7009 | 8338 | A | 11 | 834 | - | 0 | H | 109 | 9726 | 1316 | 413 |
| 1 | 70E00550 | E830 | 7009 | 8338 | B | 11 | 834 | - | 0 | H | 0 | 1766 | 93 | 14 |
| 12 | 70E00550 | E830 | 7009 | 8338 | B | 11 | 834 | - | 0 | H | 1 | 1989 | 1103 | 479 |
| 1 | 70E00571 | E830 | 7009 | 8338 | B | 11 | 834 | - | 0 | H | 4 | 243 | 108 | 33 |
| 12 | 70E00571 | E830 | 7009 | 8338 | B | 11 | 834 | - | 0 | H | 1 | 749 | 1078 | 673 |
| 1 | 72E00850 | E830 | 7203 | 8338 | H | 11 | 834 | 0 | 0 | H | 1 | 6197 | 77 | 0 |
| 12 | 72E00850 | E830 | 7203 | 8338 | H | 11 | 834 | 0 | 0 | H | 2 | 6643 | 260 | 4 |
| 1 | 72E00851 | E830 | 7203 | 8338 | H | 11 | 834 | 0 | 0 | H | 2 | 250 | 0 | 0 |
| 6 | 72E00851 | E830 | 7203 | 8338 | H | 11 | 834 | 0 | 1349 | H | 3 | 481 | 716 | 172 |
| 12 | 72E00851 | E830 | 7203 | 8338 | H | 11 | 834 | 0 | 0 | H | 78 | 8817 | 1093 | 357 |
| 1 | 72E00852 | E830 | 7203 | 8338 | H | 11 | 834 | 0 | 0 | H | 1 | 3837 | 0 | 0 |
| 12 | 72E00852 | E830 | 7203 | 8338 | H | 11 | 834 | 0 | 0 | H | 1 | 4138 | 731 | 1328 |
| 1 | 72E00853 | E830 | 7203 | 8338 | H | 11 | 834 | 0 | 0 | H | 11 | 8066 | 0 | 0 |
| 6 | 72E00853 | E830 | 7203 | 8338 | H | 11 | 834 | 0 | 1071 | H | 3 | 7064 | 882 | 872 |
| 9 | 72E00853 | E830 | 7203 | 8338 | B | 11 | 834 | - | 0 | H | 2 | 7169 | 1177 | 1489 |
| 10 | 72E00853 | E830 | 7203 | 8338 | B | 11 | 834 | - | 2376 | H | 2 | 7200 | 2167 | 1582 |

| | | | | | | | | | | | | | | |
|---|---|---|---|---|---|---|---|---|---|---|---|---|---|---|
| 12 | 72E00853 | E830 | 7203 | 8338 | B | 11 | 834 | - | 0 | H | 1 | 7314 | 2416 | 1654 |
| 1 | 72E00854 | E830 | 7203 | 8338 | G | 11 | 834 | 0 | 0 | H | 1 | 9469 | 72 | 0 |
| 2 | 72E00854 | E830 | 7203 | 8338 | H | 11 | 834 | 0 | 0 | H | 2 | 8930 | 72 | 161 |
| 6 | 72E00854 | E830 | 7203 | 8338 | G | 11 | 834 | 0 | 0 | H | 1 | 9028 | 266 | 161 |
| 8 | 72E00854 | E830 | 7203 | 8338 | G | 11 | 834 | 0 | 0 | H | 2 | 9053 | 307 | 161 |
| 1 | 72E00855 | E830 | 7203 | 8338 | H | 11 | 834 | 0 | 0 | H | 18 | 5018 | 0 | 0 |
| 12 | 72E00855 | E830 | 7203 | 8338 | H | 11 | 834 | 0 | 0 | H | 1 | 4974 | 634 | 232 |
| 1 | 72E00856 | E830 | 7203 | 8338 | H | 11 | 834 | 0 | 0 | H | 1 | 2883 | 0 | 0 |
| 6 | 72E00856 | E830 | 7203 | 8338 | H | 11 | 834 | 0 | 1572 | H | 1 | 3017 | 724 | 568 |
| 12 | 72E00856 | E830 | 7203 | 8338 | H | 11 | 834 | 0 | 0 | H | 1 | 3067 | 1194 | 725 |
| 1 | 76E00188 | E830 | 7603 | 8338 | R | 11 | 3335 | | 0 | H | 4 | 3109 | 20 | 10 |
| 12 | 76E00188 | E830 | 7603 | 8337 | R | 11 | 2710 | | 0 | H | 2 | 1551 | 1351 | 724 |
| 1 | 78E00646 | E830 | 7909 | 17440 | T | 11 | 11970 | 0 | 0 | H | 2 | 2486 | 0 | 0 |
| 2 | 78E00646 | E830 | 7909 | 13629 | T | 11 | 9262 | 0 | 0 | H | 2 | 2899 | 148 | 364 |
| 8 | 78E00646 | E830 | 7909 | 13629 | R | 8 | 6857 | 0 | 0 | H | 3 | 2931 | 430 | 483 |
| 12 | 78E00646 | E830 | 7909 | 12638 | R | 8 | 5885 | 0 | 0 | H | 1 | 2934 | 1840 | 2830 |
| 1 | 78E00648 | E830 | 7909 | 17440 | T | 11 | 11970 | 0 | 0 | H | 1 | 1333 | 0 | 0 |
| 2 | 78E00648 | E830 | 7909 | 13629 | T | 11 | 9262 | 0 | 0 | H | 1 | 1491 | 118 | 121 |
| 8 | 78E00648 | E830 | 7909 | 13629 | R | 8 | 6857 | 0 | 0 | H | 3 | 2138 | 428 | 516 |
| 12 | 78E00648 | E830 | 7909 | 12638 | R | 8 | 5885 | 0 | 0 | H | 3 | 2515 | 721 | 584 |
| 1 | 78E00476 | E831 | 7811 | 17440 | R | 8 | 8284 | 0 | 0 | H | 0 | 2338 | 0 | 0 |
| 2 | 78E00476 | E831 | 7811 | 13629 | R | 8 | 6346 | 0 | 0 | H | 0 | 2346 | 0 | 0 |
| 12 | 78E00476 | E831 | 7811 | 12638 | R | 8 | 4700 | 0 | 0 | H | 0 | 2419 | 444 | 48 |
| 1 | 78E00478 | E831 | 7811 | 17440 | R | 8 | 8284 | 0 | 0 | H | 1 | 2223 | 0 | 0 |
| 2 | 78E00478 | E831 | 7811 | 13629 | R | 8 | 6346 | 0 | 0 | H | 1 | 2272 | 0 | 0 |
| 12 | 78E00478 | E831 | 7811 | 12638 | R | 8 | 4700 | 0 | 0 | H | 1 | 2244 | 376 | 253 |
| 1 | 78E00488 | E831 | 7811 | 17440 | R | 8 | 8284 | 0 | 0 | H | 3 | 2434 | 0 | 0 |
| 2 | 78E00488 | E831 | 7811 | 13629 | R | 8 | 6346 | 0 | 0 | H | 3 | 2434 | 0 | 0 |
| 12 | 78E00488 | E831 | 7811 | 12638 | R | 8 | 4700 | 0 | 0 | H | 1 | 2671 | 1035 | 621 |
| 1 | 69E01156 | E832 | 6902 | 23449 | B | 10 | 2345 | - | 0 | H | 0 | 2285 | 0 | 0 |
| 2 | 69E01156 | E832 | 6902 | 30737 | B | 10 | 3074 | - | 0 | H | 0 | 2285 | 487 | 1355 |
| 12 | 69E01156 | E832 | 6902 | 9697 | B | 10 | 970 | - | 0 | H | 1 | 1434 | 2099 | 2069 |
| 1 | 70E00484 | E832 | 7101 | 23449 | B | 10 | 2345 | - | 0 | H | 1 | 241 | 36 | 0 |
| 2 | 70E00484 | E832 | 7101 | 30737 | B | 10 | 3074 | - | 0 | H | 1 | 251 | 36 | 0 |
| 5 | 70E00484 | E832 | 7101 | 30737 | B | 10 | 3074 | - | 0 | H | 1 | 251 | 36 | 0 |
| 1 | 70E00485 | E832 | 7101 | 23449 | B | 10 | 2345 | - | 0 | H | 0 | 3176 | 0 | 2 |
| 2 | 70E00485 | E832 | 7101 | 30737 | B | 10 | 3074 | - | 0 | H | 0 | 3188 | 77 | 2 |
| 12 | 70E00485 | E832 | 7101 | 9697 | B | 10 | 970 | - | 0 | H | 0 | 3281 | 554 | 107 |
| 1 | 70E00979 | E832 | 7005 | 23449 | B | 10 | 2345 | - | 0 | H | 14 | 2866 | 443 | 149 |
| 2 | 70E00979 | E832 | 7005 | 30737 | B | 10 | 3074 | - | 0 | H | 9 | 2886 | 720 | 161 |
| 12 | 70E00979 | E832 | 7005 | 9697 | B | 10 | 970 | - | 0 | H | 24 | 2924 | 1402 | 487 |
| 1 | 70E00980 | E832 | 7005 | 23449 | B | 10 | 2345 | - | 0 | H | 1 | 4414 | 15 | 0 |
| 2 | 70E00980 | E832 | 7005 | 30737 | B | 10 | 3074 | - | 0 | H | 1 | 4414 | 15 | 0 |
| 12 | 70E00980 | E832 | 7005 | 9697 | B | 10 | 970 | - | 0 | H | 18 | 6648 | 337 | 18 |
| 1 | 73E00702 | E832 | 7303 | 23449 | H | 10 | 2345 | 0 | 0 | H | 1 | 2629 | 0 | 0 |

| | | | | | | | | | | | | | | |
|---|---|---|---|---|---|---|---|---|---|---|---|---|---|---|
| 2 | 73E00702 | E832 | 7303 | 30737 | H | 10 | 3074 | 0 | 0 | H | 1 | 2642 | 5 | 0 |
| 12 | 73E00702 | E832 | 7303 | 9697 | H | 10 | 970 | 0 | 0 | H | 1 | 1497 | 753 | 3103 |
| 1 | 75E00183 | E832 | 7507 | 23449 | R | 10 | 6566 | | 0 | H | 1 | 1876 | 0 | 0 |
| 2 | 75E00183 | E832 | 7507 | 30737 | P | 10 | 8376 | | 0 | H | 1 | 1876 | 0 | 93 |
| 12 | 75E00183 | E832 | 7507 | 9697 | P | 10 | 1916 | | 0 | H | 0 | 1956 | 2472 | 8382 |
| 1 | 75E00189 | E832 | 7507 | 23449 | R | 10 | 6566 | | 0 | H | 1 | 1296 | 0 | 0 |
| 2 | 75E00189 | E832 | 7507 | 30737 | P | 10 | 8376 | | 0 | H | 1 | 1302 | 0 | 0 |
| 12 | 75E00189 | E832 | 7507 | 9697 | P | 10 | 1916 | | 0 | H | 1 | 1483 | 811 | 362 |
| 1 | 75E00202 | E832 | 7508 | 23449 | R | 10 | 6742 | | 0 | H | 1 | 388 | 0 | 0 |
| 2 | 75E00202 | E832 | 7508 | 30737 | R | 10 | 8606 | | 0 | H | 2 | 187 | 0 | 7 |
| 3 | 75E00202 | E832 | 7508 | 30737 | P | 10 | 8376 | | 0 | H | 3 | 187 | 0 | 7 |
| 12 | 75E00202 | E832 | 7508 | 9697 | P | 10 | 1988 | | 0 | H | 17 | 1177 | 1746 | 3223 |
| 1 | 75E00205 | E832 | 7508 | 23449 | R | 10 | 6742 | | 0 | H | 1 | 4833 | 0 | 0 |
| 2 | 75E00205 | E832 | 7508 | 30737 | R | 10 | 8606 | | 0 | H | 1 | 4863 | 138 | 0 |
| 3 | 75E00205 | E832 | 7508 | 30737 | P | 10 | 8376 | | 0 | H | 1 | 4874 | 226 | 101 |
| 12 | 75E00205 | E832 | 7508 | 9697 | P | 10 | 1988 | | 0 | H | 1 | 5014 | 789 | 470 |
| 1 | 75E00220 | E832 | 7508 | 23449 | R | 10 | 6742 | | 0 | H | 1 | 955 | 30 | 0 |
| 2 | 75E00220 | E832 | 7508 | 30737 | R | 10 | 8606 | | 0 | H | 1 | 966 | 40 | 0 |
| 3 | 75E00220 | E832 | 7508 | 30737 | P | 10 | 8376 | | 0 | H | 1 | 998 | 40 | 0 |
| 12 | 75E00220 | E832 | 7508 | 9697 | P | 10 | 1988 | | 0 | H | 2 | 1216 | 914 | 401 |
| 1 | 77E00164 | E832 | 7711 | 23449 | R | 10 | 11490 | 0 | 0 | H | 1 | 1531 | 46 | 269 |
| 2 | 77E00164 | E832 | 7711 | 30737 | R | 10 | 14831 | 0 | 0 | H | 1 | 1531 | 46 | 269 |
| 12 | 77E00164 | E832 | 7711 | 12501 | R | 10 | 5094 | 0 | 0 | H | 1 | 1803 | 854 | 817 |
| 1 | 77E00169 | E832 | 7711 | 23449 | R | 10 | 11490 | 0 | 0 | H | 1 | 713 | 0 | 0 |
| 2 | 77E00169 | E832 | 7711 | 30737 | R | 10 | 14831 | 0 | 0 | H | 1 | 713 | 0 | 0 |
| 12 | 77E00169 | E832 | 7711 | 12501 | R | 10 | 5094 | 0 | 0 | H | 1 | 958 | 1699 | 1285 |
| 1 | 77E00170 | E832 | 7711 | 23449 | R | 10 | 11490 | 0 | 0 | H | 3 | 1381 | 25 | 0 |
| 2 | 77E00170 | E832 | 7711 | 30737 | R | 10 | 14831 | 0 | 0 | H | 1 | 1396 | 66 | 23 |
| 12 | 77E00170 | E832 | 7711 | 12501 | R | 10 | 5094 | 0 | 0 | H | 8 | 1439 | 738 | 1269 |
| 1 | 77E00174 | E832 | 7711 | 23449 | R | 10 | 11490 | 0 | 0 | H | 70 | 1940 | 0 | 0 |
| 2 | 77E00174 | E832 | 7711 | 30737 | R | 10 | 14831 | 0 | 0 | H | 33 | 1976 | 92 | 254 |
| 12 | 77E00174 | E832 | 7711 | 12501 | R | 10 | 5094 | 0 | 0 | H | 1 | 0 | 1396 | 3052 |
| 1 | 77E00186 | E832 | 7711 | 23449 | R | 10 | 11490 | 0 | 0 | H | 1 | 971 | 0 | 0 |
| 2 | 77E00186 | E832 | 7711 | 30737 | R | 10 | 14831 | 0 | 0 | H | 1 | 1031 | 0 | 0 |
| 12 | 77E00186 | E832 | 7711 | 12501 | R | 10 | 5094 | 0 | 0 | H | 1 | 1113 | 354 | 314 |
| 1 | 77E00193 | E832 | 7711 | 23449 | R | 10 | 11490 | 0 | 0 | H | 1 | 1456 | 108 | 32 |
| 2 | 77E00193 | E832 | 7711 | 30737 | R | 10 | 14831 | 0 | 0 | H | 1 | 1481 | 180 | 64 |
| 12 | 77E00193 | E832 | 7711 | 12501 | R | 10 | 5094 | 0 | 0 | H | 1 | 1631 | 1135 | 780 |
| 1 | 71E00217 | E834 | 7201 | 30611 | B | 10 | 3061 | - | 0 | H | 1 | 3184 | 0 | 106 |
| 2 | 71E00217 | E834 | 7201 | 34264 | B | 10 | 3426 | - | 0 | H | 1 | 3184 | 82 | 142 |
| 3 | 71E00217 | E834 | 7201 | 34264 | B | 10 | 3426 | - | 0 | H | 1 | 3184 | 82 | 142 |
| 1 | 71E00227 | E834 | 7201 | 30611 | B | 10 | 3061 | - | 0 | H | 1 | 4375 | 0 | 0 |
| 2 | 71E00227 | E834 | 7201 | 34264 | B | 10 | 3426 | - | 0 | H | 1 | 4375 | 0 | 0 |
| 7 | 71E00227 | E834 | 7201 | 34264 | B | 10 | 3426 | - | 0 | H | 31 | 4569 | 855 | 132 |
| 1 | 71E00261 | E834 | 7202 | 30611 | B | 10 | 3061 | - | 0 | H | 0 | 1996 | 103 | 0 |
| 2 | 71E00261 | E834 | 7202 | 34264 | B | 10 | 3426 | - | 0 | H | 0 | 2000 | 144 | 13 |

| | | | | | | | | | | | | | | |
|---|---|---|---|---|---|---|---|---|---|---|---|---|---|---|
| 6 | 71E00261 | E834 | 7202 | 34264 | B | 10 | 3426 | - | 0 | H | 0 | 2046 | 221 | 13 |
| 1 | 72E00118 | E834 | 7207 | 30611 | H | 10 | 3061 | 0 | 0 | H | 2 | 2225 | 0 | 42 |
| 2 | 72E00118 | E834 | 7207 | 34264 | H | 10 | 3426 | 0 | 0 | H | 2 | 2244 | 20 | 42 |
| 7 | 72E00118 | E834 | 7207 | 34264 | H | 10 | 3426 | 0 | 0 | H | 1 | 156 | 253 | 48 |
| 1 | 71E00227 | E835 | 7201 | 34264 | B | 10 | 3426 | - | 0 | H | 21 | 4586 | 278 | 0 |
| 8 | 71E00227 | E835 | 7201 | 23321 | B | 10 | 2332 | - | 0 | H | 2 | 4647 | 745 | 822 |
| 1 | 72E00118 | E835 | 7207 | 34264 | H | 10 | 3426 | 0 | 0 | H | 1 | 156 | 136 | 16 |
| 8 | 72E00118 | E835 | 7207 | 23321 | H | 10 | 2332 | 0 | 0 | H | 28 | 2549 | 307 | 125 |
| 1 | 62E02558 | E841 | 6203 | 9892 | B | 15 | 989 | - | 0 | H | 0 | 0 | 41 | 0 |
| 12 | 62E02558 | E841 | 6203 | 9892 | B | 15 | 989 | - | 0 | H | 0 | 0 | 232 | 27 |
| 1 | 83E00782 | E841 | 8310 | 15592 | U | 15 | 15514 | 0 | 0 | H | 0 | 1 | 0 | 0 |
| 2 | 83E00782 | E841 | 8310 | 17806 | U | 15 | 17628 | 0 | 0 | H | 0 | 1 | 0 | 0 |
| 8 | 83E00782 | E841 | 8310 | 15592 | U | 15 | 14968 | 0 | 0 | H | 0 | 15 | 310 | 0 |
| 1 | 67E01196 | E842 | 6703 | 22222 | B | 15 | 2222 | - | 0 | H | 0 | 795 | 0 | 0 |
| 11 | 67E01196 | E842 | 6703 | 21792 | B | 15 | 2179 | - | 0 | H | 0 | 805 | 97 | 0 |
| 12 | 67E01196 | E842 | 6703 | 21792 | B | 15 | 2179 | - | 0 | H | 0 | 805 | 97 | 0 |
| 1 | 82E00083 | E853 | 8202 | 23449 | T | 10 | 20459 | 0 | 0 | H | 4 | 1855 | 0 | 17 |
| 2 | 82E00083 | E853 | 8202 | 30737 | T | 10 | 26588 | 0 | 0 | H | 4 | 1855 | 282 | 73 |
| 10 | 82E00083 | E853 | 8202 | 23449 | T | 10 | 17296 | 0 | 0 | H | 3 | 2624 | 914 | 266 |
| 1 | 72E00942 | E902 | 7206 | 30671 | R | 17 | 12674 | 0 | 0 | H | 1 | 1983 | 154 | 0 |
| 12 | 72E00942 | E902 | 7206 | 16461 | R | 17 | 6000 | 0 | 0 | H | 24 | 2149 | 1410 | 814 |
| 1 | 65E00407 | E935 | 6501 | 144423 | H | 10 | 14442 | | 0 | H | 0 | 214 | 0 | 0 |
| 2 | 65E00407 | E935 | 6501 | 160427 | H | 10 | 16043 | | 0 | H | 0 | 214 | 0 | 0 |
| 11 | 65E00407 | E935 | 6501 | 160427 | H | 10 | 16043 | | 0 | H | 0 | 214 | 0 | 0 |
| 1 | 66E01106 | E935 | 6608 | 144423 | H | 10 | 14442 | 0 | 0 | H | 5 | 397 | 464 | 398 |
| 2 | 66E01106 | E935 | 6608 | 160427 | H | 10 | 16043 | 0 | 0 | H | 4 | 464 | 464 | 398 |
| 3 | 66E01106 | E935 | 6608 | 160427 | B | 10 | 16043 | 0 | 0 | H | 3 | 33791 | 464 | 442 |
| 5 | 66E01106 | E935 | 6608 | 160427 | H | 10 | 16043 | 0 | 0 | H | 295 | 825 | 923 | 549 |
| 10 | 66E01106 | E935 | 6608 | 38751 | H | 10 | 3875 | 0 | 0 | H | 22 | 1438 | 2212 | 972 |
| 1 | 67E01166 | E935 | 6701 | 144423 | B | 10 | 14442 | - | 0 | H | 4 | 767 | 10 | 0 |
| 2 | 67E01166 | E935 | 6701 | 160427 | B | 10 | 16043 | - | 0 | H | 3 | 815 | 10 | 0 |
| 10 | 67E01166 | E935 | 6701 | 160427 | H | 10 | 16043 | | 0 | H | 5 | 824 | 1633 | 492 |
| 12 | 67E01166 | E935 | 6701 | 38751 | H | 10 | 3875 | | 0 | H | 15 | 1042 | 1706 | 492 |
| 1 | 84E00150 | E935 | 8405 | 160427 | U | 10 | 0 | 0 | 0 | H | 0 | 8 | 0 | 0 |
| 2 | 84E00150 | E935 | 8405 | 123600 | U | 10 | 122673 | 0 | 0 | H | 0 | 8 | 0 | 0 |
| 1 | 66E00792 | E952 | 6607 | 9339 | B | 8 | 934 | - | 0 | H | 1 | 3664 | 93 | 0 |
| 12 | 66E00792 | E952 | 6607 | 9339 | B | 8 | 934 | - | 0 | H | 1 | 3826 | 1219 | 562 |
| 1 | 66E00795 | E952 | 6608 | 9339 | B | 8 | 934 | - | 0 | H | 249 | 3498 | 0 | 0 |
| 10 | 66E00795 | E952 | 6608 | 9339 | B | 8 | 934 | - | 0 | H | 16 | 3592 | 348 | 10 |
| 1 | 70E01341 | E954 | 7009 | 12210 | B | 10 | 1221 | - | 0 | H | 0 | 625 | 149 | 1 |
| 6 | 70E01341 | E954 | 7009 | 12210 | B | 10 | 1221 | - | 0 | H | 1 | 680 | 324 | 75 |
| 1 | 69E00413 | E956 | 6909 | 47421 | B | 12 | 4742 | - | 0 | H | 3 | 4211 | 77 | 0 |
| 2 | 69E00413 | E956 | 6909 | 45700 | B | 12 | 4570 | - | 0 | H | 2 | 4293 | 77 | 0 |
| 10 | 69E00413 | E956 | 6909 | 45700 | B | 12 | 4570 | - | 0 | H | 1 | 4385 | 1404 | 1273 |

| | | | | | | | | | | | | | | |
|---|---|---|---|---|---|---|---|---|---|---|---|---|---|---|
| 1 | 75E00556 | E956 | 7501 | 47421 | R | 12 | 17190 | | 0 | H | 1 | 3030 | 0 | 0 |
| 2 | 75E00556 | E956 | 7501 | 45700 | R | 12 | 16281 | | 0 | H | 1 | 3052 | 0 | 0 |
| 12 | 75E00556 | E956 | 7501 | 18034 | R | 12 | 5097 | | 0 | H | 0 | 3185 | 2311 | 4195 |
| 1 | 74E00524 | E957 | 7403 | 47421 | R | 12 | 14226 | 0 | 0 | H | 0 | 1968 | 20 | 0 |
| 2 | 74E00524 | E957 | 7403 | 45700 | R | 12 | 13424 | 0 | 0 | H | 1 | 1993 | 20 | 126 |
| 10 | 74E00524 | E957 | 7403 | 45700 | P | 12 | 11139 | 0 | 0 | H | 0 | 2011 | 843 | 429 |
| 12 | 74E00524 | E957 | 7403 | 25670 | P | 12 | 5936 | 0 | 0 | H | 0 | 2034 | 843 | 429 |
| 1 | 74E00546 | E957 | 7409 | 47421 | R | 12 | 16005 | 0 | 0 | H | 1 | 2473 | 93 | 9 |
| 2 | 74E00546 | E957 | 7409 | 45700 | R | 12 | 15138 | 0 | 0 | H | 1 | 2508 | 108 | 9 |
| 12 | 74E00546 | E957 | 7409 | 25670 | R | 12 | 6899 | 0 | 0 | H | 11 | 2720 | 1174 | 1508 |
| 1 | 76E00037 | E957 | 7609 | 47421 | R | 12 | 23118 | 0 | 0 | H | 1 | 166 | 0 | 0 |
| 2 | 76E00037 | E957 | 7609 | 45700 | R | 12 | 21993 | 0 | 0 | H | 1 | 189 | 128 | 81 |
| 12 | 76E00037 | E957 | 7609 | 25670 | R | 12 | 10749 | 0 | 0 | H | 14 | 1731 | 1871 | 4140 |
| 1 | 76E00038 | E957 | 7609 | 47421 | R | 12 | 23118 | | 0 | H | 1 | 1266 | 0 | 43 |
| 2 | 76E00038 | E957 | 7609 | 45700 | R | 12 | 21993 | | 0 | H | 1 | 13 | 226 | 341 |
| 12 | 76E00038 | E957 | 7609 | 25670 | R | 12 | 10749 | | 0 | H | 13 | 1530 | 1357 | 838 |
| 1 | 82E00707 | E957 | 8205 | 47421 | T | 12 | 43272 | 0 | 0 | H | 4 | 179 | 25 | 0 |
| 2 | 82E00707 | E957 | 8205 | 45700 | T | 12 | 41416 | 0 | 0 | H | 5 | 288 | 107 | 0 |
| 12 | 82E00707 | E957 | 8205 | 39893 | T | 12 | 33660 | 0 | 0 | H | 5 | 458 | 920 | 3359 |
| 1 | 83E00050 | E957 | 8206 | 47421 | T | 12 | 43868 | 0 | 0 | H | 8 | 888 | 0 | 0 |
| 2 | 83E00050 | E957 | 8206 | 45700 | T | 12 | 41701 | 0 | 0 | H | 7 | 888 | 15 | 0 |
| 12 | 83E00050 | E957 | 8206 | 39893 | T | 12 | 33909 | 0 | 0 | H | 9 | 288 | 1231 | 790 |
| 1 | 83E00052 | E957 | 8207 | 47421 | T | 12 | 43864 | 0 | 0 | H | 3 | 182 | 134 | 68 |
| 2 | 83E00052 | E957 | 8207 | 45700 | T | 12 | 41987 | 0 | 0 | H | 3 | 192 | 213 | 83 |
| 12 | 83E00052 | E957 | 8207 | 39893 | T | 12 | 34158 | 0 | 0 | H | 30 | 454 | 620 | 506 |

| | | | | | | | | | | | | | | | |
|---|---|---|---|---|---|---|---|---|---|---|---|---|---|---|---|
| 1 | 77L00280 | L113 | 7701 | 112434 | T | 15 | 68585 | 0 | 0 | M | 27 | 48061 | 0 | 0 |
| 5 | 77L00280 | L113 | 7701 | 152934 | T | 15 | 90231 | 0 | 0 | M | 41 | 18460 | 760 | 2181 |
| 7 | 77L00280 | L113 | 7701 | 152934 | T | 15 | 88702 | 0 | 0 | M | 483 | 51348 | 1332 | 2351 |
| 1 | 77L00292 | L113 | 7701 | 112434 | T | 15 | 68585 | 0 | 0 | M | 22 | 58632 | 87 | 147 |
| 5 | 77L00292 | L113 | 7701 | 152934 | T | 15 | 90231 | 0 | 0 | M | 31 | 61039 | 940 | 201 |
| 7 | 77L00292 | L113 | 7701 | 152934 | T | 15 | 88702 | 0 | 0 | M | 21 | 61884 | 2251 | 995 |
| 1 | 77L00280 | L114 | 7701 | 152934 | T | 15 | 87937 | 0 | 0 | M | 557 | 51348 | 310 | 232 |
| 5 | 77L00280 | L114 | 7701 | 152934 | T | 15 | 84878 | 0 | 0 | M | 92 | 53475 | 873 | 318 |
| 1 | 77L00292 | L114 | 7701 | 152934 | T | 15 | 87937 | 0 | 0 | M | 21 | 62104 | 31 | 0 |
| 5 | 77L00292 | L114 | 7701 | 152934 | T | 15 | 84878 | 0 | 0 | M | 18 | 63690 | 803 | 25 |
| 1 | 65L00671 | L125 | 6500 | 15000 | H | 16 | 1500 | 0 | 0 | H | 0 | 1786 | 0 | 0 |
| 2 | 65L00671 | L125 | 6500 | 113935 | H | 16 | 11394 | 0 | 0 | H | 0 | 1794 | 0 | 0 |
| 11 | 65L00671 | L125 | 6500 | 15000 | H | 16 | 1500 | 0 | 0 | H | 2 | 1907 | 747 | 151 |
| 1 | 70L00696 | L130 | 7011 | 106644 | R | 16 | 30660 | | 0 | H | 1 | 2201 | 469 | 44 |
| 2 | 70L00696 | L130 | 7011 | 113935 | R | 16 | 32222 | | 0 | H | 2 | 2247 | 643 | 44 |
| 12 | 70L00696 | L130 | 7011 | 38274 | R | 16 | 9030 | | 0 | H | 1 | 2504 | 1843 | 442 |
| 1 | 70L00698 | L130 | 7011 | 106644 | R | 16 | 30660 | | 0 | H | 5 | 1459 | 0 | 0 |
| 2 | 70L00698 | L130 | 7011 | 113935 | R | 16 | 32222 | | 0 | H | 5 | 1459 | 0 | 0 |
| 12 | 70L00698 | L130 | 7011 | 38274 | R | 16 | 9030 | | 0 | H | 0 | 1474 | 0 | 0 |
| 1 | 71L00007 | L130 | 7101 | 106644 | R | 16 | 31660 | | 0 | H | 1 | 4004 | 207 | 0 |
| 2 | 71L00007 | L130 | 7101 | 113935 | R | 16 | 33290 | | 0 | H | 1 | 4033 | 207 | 140 |
| 12 | 71L00007 | L130 | 7101 | 38274 | R | 16 | 9389 | | 0 | H | 1 | 4173 | 1905 | 2838 |
| 1 | 71L00065 | L130 | 7110 | 106644 | R | 16 | 36159 | | 0 | H | 1 | 3178 | 0 | 0 |
| 2 | 71L00065 | L130 | 7110 | 113935 | R | 16 | 38097 | | 0 | H | 1 | 3194 | 0 | 0 |
| 12 | 71L00065 | L130 | 7110 | 38274 | R | 16 | 11004 | | 0 | H | 1 | 3361 | 1193 | 377 |
| 1 | 72L00721 | L130 | 7212 | 106644 | S | 16 | 43157 | | 0 | H | 87 | 2620 | 165 | 78 |
| 2 | 72L00721 | L130 | 7212 | 113935 | S | 16 | 45574 | | 0 | H | 97 | 2634 | 288 | 97 |
| 12 | 72L00721 | L130 | 7212 | 38274 | S | 16 | 13516 | | 0 | H | 1 | 2898 | 1423 | 353 |
| 1 | 73L01243 | L130 | 7303 | 106644 | R | 16 | 44657 | | 0 | H | 2 | 258 | 941 | 173 |
| 2 | 73L01243 | L130 | 7303 | 113935 | R | 16 | 47176 | | 0 | H | 2 | 283 | 1955 | 342 |
| 4 | 73L01243 | L130 | 7303 | 113935 | S | 16 | 46108 | | 0 | H | 2 | 417 | 2877 | 776 |
| 12 | 73L01243 | L130 | 7303 | 38274 | S | 16 | 14054 | | 0 | H | 2 | 866 | 5476 | 5158 |
| 1 | 73L01437 | L133 | 7310 | 91779 | R | 15 | 38088 | | 0 | H | 2 | 3969 | 258 | 15 |
| 2 | 73L01437 | L133 | 7310 | 99305 | R | 15 | 40715 | | 0 | H | 2 | 5038 | 947 | 82 |
| 12 | 73L01437 | L133 | 7310 | 22225 | R | 15 | 8001 | | 0 | H | 7 | 4222 | 3316 | 1286 |
| 1 | 79L00123 | L133 | 7905 | 91779 | T | 15 | 68834 | 0 | 0 | H | 2 | 1837 | 278 | 417 |
| 2 | 79L00123 | L133 | 7905 | 99305 | T | 15 | 73982 | 0 | 0 | | 0 | 0 | 278 | 417 |
| 12 | 79L00123 | L133 | 7905 | 55364 | T | 15 | 38478 | 0 | 0 | H | 2 | 2366 | 2869 | 1213 |
| 1 | 79L00124 | L133 | 7905 | 91779 | T | 15 | 68834 | 0 | 0 | H | 1 | 1433 | 0 | 0 |
| 2 | 79L00124 | L133 | 7905 | 99305 | T | 15 | 73982 | 0 | 0 | H | 1 | 1492 | 0 | 0 |
| 12 | 79L00124 | L133 | 7905 | 55364 | T | 15 | 38478 | 0 | 0 | H | 2 | 1769 | 4602 | 3621 |
| 1 | 64L00022 | L143 | 6407 | 381768 | L | 19 | 38177 | | 0 | H | 1 | 2670 | 249 | 0 |
| 2 | 64L00022 | L143 | 6407 | 426582 | H | 19 | 42658 | | 0 | H | 1 | 2670 | 249 | 329 |
| 10 | 64L00022 | L143 | 6407 | 426582 | S | 12 | 42658 | | 0 | H | 10 | 2960 | 1332 | 407 |
| 11 | 64L00022 | L143 | 6407 | 426582 | H | 12 | 42658 | | 0 | H | 10 | 2960 | 1332 | 407 |

| | | | | | | | | | | | | | | |
|---|---|---|---|---|---|---|---|---|---|---|---|---|---|---|
| 1 | 79L00031 | L143 | 7908 | 381768 | T | 12 | 269624 | 0 | 0 | H | 1 | 1453 | 2442 | 0 |
| 2 | 79L00031 | L143 | 7908 | 426582 | T | 12 | 298607 | 0 | 0 | H | 1 | 1468 | 2442 | 1 |
| 12 | 79L00031 | L143 | 7908 | 151894 | T | 12 | 96832 | 0 | 0 | H | 0 | 1528 | 12312 | 20164 |
| 1 | 80L00383 | L143 | 8101 | 381768 | T | 12 | 310186 | 0 | 0 | H | 0 | 550 | 1152 | 0 |
| 2 | 80L00383 | L143 | 8101 | 426582 | T | 12 | 343932 | 0 | 0 | H | 0 | 597 | 1721 | 0 |
| 12 | 80L00383 | L143 | 8101 | 151894 | T | 12 | 112971 | 0 | 0 | H | 9 | 763 | 7036 | 9704 |
| 1 | 84L00094 | L143 | 8404 | 426582 | U | 12 | 423916 | 0 | 0 | H | 0 | 13 | 633 | 295 |
| 2 | 84L00094 | L143 | 8404 | 151894 | U | 12 | 149995 | 0 | 0 | H | 0 | 31 | 770 | 1312 |
| 1 | 84L00096 | L143 | 8405 | 247000 | U | 12 | 245456 | 0 | 0 | H | 0 | 4 | 0 | 0 |
| 1 | 84L00096 | L143 | 8405 | 247000 | U | 12 | 245456 | 0 | 0 | H | 0 | 4 | 0 | 0 |
| 1 | 74L00343 | L145 | 7405 | 223486 | S | 12 | 69839 | | 0 | H | 37 | 3192 | 227 | 0 |
| 2 | 74L00343 | L145 | 7405 | 172171 | S | 12 | 52727 | | 0 | H | 28 | 3287 | 2005 | 150 |
| 12 | 74L00343 | L145 | 7405 | 146039 | S | 12 | 35597 | | 0 | H | 1 | 3446 | 7856 | 17461 |
| 1 | 74L00344 | L145 | 7405 | 223486 | R | 12 | 69839 | | 0 | H | 1 | 2974 | 855 | 54 |
| 2 | 74L00344 | L145 | 7405 | 172171 | R | 12 | 52727 | | 0 | H | 1 | 3016 | 1843 | 171 |
| 12 | 74L00344 | L145 | 7405 | 146039 | P | 12 | 35597 | | 0 | H | 0 | 3142 | 7832 | 15455 |
| 1 | 74L00345 | L145 | 7405 | 223486 | S | 12 | 69839 | | 0 | H | 1 | 2806 | 368 | 0 |
| 2 | 74L00345 | L145 | 7405 | 172171 | S | 12 | 52727 | | 0 | H | 2 | 2859 | 974 | 168 |
| 12 | 74L00345 | L145 | 7405 | 146039 | S | 12 | 35597 | | 0 | H | 0 | 8829 | 11390 | 22283 |
| 1 | 74L00351 | L145 | 7406 | 223486 | S | 12 | 71236 | | 0 | H | 1 | 3114 | 206 | 840 |
| 2 | 74L00351 | L145 | 7406 | 172171 | S | 12 | 53803 | | 0 | H | 1 | 3321 | 647 | 840 |
| 12 | 74L00351 | L145 | 7406 | 146039 | S | 12 | 36510 | | 0 | H | 1 | 2756 | 5296 | 3567 |
| 1 | 75L00393 | L145 | 7506 | 223486 | S | 12 | 87998 | | 0 | H | 4 | 3461 | 165 | 219 |
| 2 | 75L00393 | L145 | 7506 | 172171 | S | 12 | 66716 | | 0 | H | 2 | 3582 | 1068 | 964 |
| 12 | 75L00393 | L145 | 7506 | 1 6039 | S | 12 | 47463 | | 0 | H | 9 | 4371 | 6259 | 5834 |
| 1 | 75L00394 | L145 | 7506 | 223486 | R | 12 | 87998 | | 0 | H | 2 | 2846 | 0 | 0 |
| 2 | 75L00394 | L145 | 7506 | 172171 | R | 12 | 66716 | | 0 | H | 2 | 2926 | 821 | 254 |
| 12 | 75L00394 | L145 | 7506 | 146039 | R | 12 | 47463 | | 0 | H | 2 | 3507 | 7097 | 3889 |
| 1 | 75L00395 | L145 | 7506 | 223486 | R | 12 | 87998 | | 0 | H | 3 | 5312 | 242 | 0 |
| 2 | 75L00395 | L145 | 7506 | 172171 | R | 12 | 66716 | | 0 | H | 3 | 5312 | 1392 | 1746 |
| 12 | 75L00395 | L145 | 7506 | 146039 | R | 12 | 47463 | | 0 | H | 6 | 5887 | 9755 | 9824 |
| 1 | 75L00565 | L145 | 7509 | 223486 | R | 12 | 92188 | 0 | 0 | H | 1 | 1350 | 0 | 0 |
| 2 | 75L00565 | L145 | 7509 | 172171 | R | 12 | 69944 | 0 | 0 | H | 1 | 1350 | 0 | 0 |
| 12 | 75L00565 | L145 | 7509 | 146039 | R | 12 | 50201 | 0 | 0 | H | 4 | 2579 | 9763 | 7260 |
| 1 | 75L00566 | L145 | 7510 | 223486 | R | 12 | 93585 | | 0 | H | 2 | 3703 | 0 | 0 |
| 2 | 75L00566 | L145 | 7510 | 172171 | R | 12 | 71021 | | 0 | H | 2 | 3703 | 0 | 0 |
| 8 | 75L00566 | L145 | 7510 | 172171 | R | 12 | 64564 | | 0 | H | 2 | 3703 | 0 | 0 |
| 1 | 75L00567 | L145 | 7509 | 223486 | R | 12 | 92188 | | 0 | H | 2 | 1782 | 486 | 197 |
| 2 | 75L00567 | L145 | 7509 | 172171 | R | 12 | 69944 | | 0 | H | 2 | 1819 | 711 | 244 |
| 12 | 75L00567 | L145 | 7509 | 146039 | R | 12 | 50201 | | 0 | H | 2 | 2363 | 4522 | 1762 |
| 1 | 75L00568 | L145 | 7509 | 223486 | R | 12 | 92188 | | 0 | H | 0 | 3547 | 0 | 0 |
| 2 | 75L00568 | L145 | 7509 | 172171 | R | 12 | 69944 | | 0 | H | 0 | 3547 | 0 | 0 |
| 8 | 75L00568 | L145 | 7509 | 172171 | R | 12 | 63488 | | 0 | H | 0 | 3547 | 0 | 0 |
| 1 | 74L00203 | L149 | 7403 | 45268 | R | 12 | 13580 | | 0 | M | 66 | 55872 | 181 | 835 |
| 2 | 74L00203 | L149 | 7403 | 28281 | R | 12 | 8308 | | 0 | M | 51 | 55897 | 1305 | 972 |

| | | | | | | | | | | | | | | | |
|---|---|---|---|---|---|---|---|---|---|---|---|---|---|---|---|
| 8 | 74L00203 | L149 | 7403 | 28281 | L | 10 | 3040 | | 0 | M | 9 | 57393 | 1700 | 2291 |
| 9 | 74L00203 | L149 | 7403 | 28281 | D | 10 | 2828 | - | 0 | M | 9 | 57393 | 2418 | 2611 |
| 10 | 74L00203 | L149 | 7403 | 28281 | B | 10 | 2828 | - | 0 | M | 8 | 57618 | 2952 | 2739 |
| 12 | 74L00203 | L149 | 7403 | 12350 | B | 10 | 1235 | - | 0 | M | 7 | 58321 | 3426 | 2995 |
| 1 | 74L00230 | L149 | 7407 | 45268 | R | 12 | 14712 | | 0 | M | 212 | 45828 | 453 | 257 |
| 2 | 74L00230 | L149 | 7407 | 28281 | R | 12 | 9015 | | 0 | M | 147 | 46743 | 607 | 265 |
| 8 | 74L00230 | L149 | 7407 | 28281 | L | 10 | 3889 | | 0 | M | 70 | 51294 | 2237 | 2867 |
| 12 | 74L00230 | L149 | 7407 | 12350 | L | 10 | 1328 | | 0 | M | 37 | 54991 | 2710 | 3388 |
| 1 | 74L00113 | L151 | 7404 | 28054 | L | 10 | 4699 | 0 | 0 | M | 20 | 6540 | 46 | 234 |
| 2 | 74L00113 | L151 | 7404 | 29534 | L | 10 | 4725 | 0 | 0 | M | 11 | 6549 | 1578 | 235 |
| 11 | 74L00113 | L151 | 7404 | 29534 | H | 10 | 2953 | 0 | 0 | M | 43 | 14562 | 3113 | 1408 |
| 12 | 74L00113 | L151 | 7404 | 12511 | H | 10 | 1251 | 0 | 0 | M | 51 | 15774 | 3198 | 1538 |
| 1 | 74L00120 | L151 | 7412 | 28054 | H | 8 | 2805 | | 0 | M | 35 | 56815 | 206 | 22 |
| 2 | 74L00120 | L151 | 7412 | 29534 | H | 8 | 2953 | | 0 | M | 26 | 57030 | 349 | 133 |
| 8 | 74L00120 | L151 | 7412 | 29534 | L | 10 | 5168 | | 0 | M | 5 | 57882 | 1557 | 1568 |
| 12 | 74L00120 | L151 | 7412 | 16342 | L | 10 | 2370 | | 0 | M | 5 | 58598 | 2137 | 2304 |
| 1 | 76L00496 | L151 | 7607 | 28054 | P | 8 | 5961 | | 0 | M | 23 | 66008 | 0 | 0 |
| 2 | 76L00496 | L151 | 7607 | 29534 | L | 8 | 5999 | | 0 | M | 19 | 67664 | 51 | 0 |
| 8 | 76L00496 | L151 | 7607 | 29534 | R | 10 | 9377 | | 0 | M | 34 | 72596 | 490 | 299 |
| 12 | 76L00496 | L151 | 7607 | 12511 | R | 10 | 3597 | | 0 | M | 36 | 76807 | 758 | 513 |
| 1 | 67L00561 | L273 | 6709 | 91442 | H | 10 | 9144 | | 0 | H | 25 | 4116 | 187 | 0 |
| 2 | 67L00561 | L273 | 6709 | 103212 | H | 10 | 10321 | | 0 | H | 19 | 4101 | 412 | 19 |
| 12 | 67L00561 | L273 | 6709 | 34802 | H | 10 | 3480 | | 0 | H | 0 | 905 | 2056 | 1987 |
| 1 | 67L00566 | L273 | 6709 | 91442 | B | 10 | 9144 | - | 0 | H | 70 | 2876 | 0 | 0 |
| 1 | 67L00566 | L273 | 6709 | 91442 | B | 10 | 9144 | - | 0 | H | 70 | 2876 | 0 | 0 |
| 1 | 67L00651 | L273 | 6710 | 91442 | B | 10 | 9144 | - | 0 | H | 4 | 2879 | 0 | 0 |
| 2 | 67L00651 | L273 | 6710 | 103212 | B | 10 | 10321 | - | 0 | H | 1 | 2898 | 154 | 0 |
| 12 | 67L00651 | L273 | 6710 | 34802 | B | 10 | 3480 | - | 0 | H | 1 | 3034 | 1966 | 1278 |
| 1 | 67L01377 | L273 | 6703 | 91442 | S | 10 | 9144 | | 0 | H | 1 | 5481 | 123 | 0 |
| 2 | 67L01377 | L273 | 6703 | 103212 | S | 10 | 10321 | | 0 | H | 24 | 5517 | 123 | 0 |
| 12 | 67L01377 | L273 | 6703 | 34802 | S | 10 | 3480 | | 0 | H | 1 | 3470 | 2019 | 1545 |
| 1 | 72L00986 | L275 | 7210 | 91442 | H | 10 | 9144 | 0 | 0 | H | 53 | 3273 | 0 | 0 |
| 2 | 72L00986 | L275 | 7210 | 103212 | H | 10 | 10321 | 0 | 0 | H | 40 | 3277 | 0 | 0 |
| 12 | 72L00986 | L275 | 7210 | 34802 | H | 10 | 3480 | 0 | 0 | H | 10 | 3749 | 3689 | 4540 |
| 1 | 72L01025 | L275 | 7201 | 91442 | H | 10 | 9144 | 0 | 0 | H | 1 | 4458 | 124 | 3036 |
| 2 | 72L01025 | L275 | 7201 | 103212 | H | 10 | 10321 | 0 | 0 | H | 1 | 4520 | 308 | 3036 |
| 12 | 72L01025 | L275 | 7201 | 34802 | H | 10 | 3480 | 0 | 0 | H | 4 | 4899 | 4041 | 5457 |
| 1 | 72L01027 | L275 | 7210 | 91442 | H | 10 | 9144 | 0 | 0 | H | 1 | 4075 | 0 | 0 |
| 2 | 72L01027 | L275 | 7210 | 103212 | H | 10 | 10321 | 0 | 0 | H | 1 | 4075 | 0 | 0 |
| 6 | 72L01027 | L275 | 7210 | 103212 | S | 10 | 10321 | | 0 | H | 0 | 9 | 313 | 0 |
| 7 | 72L01027 | L275 | 7210 | 103212 | H | 10 | 10321 | | 0 | H | 0 | 51 | 460 | 1120 |
| 12 | 72L01027 | L275 | 7210 | 34802 | H | 10 | 3480 | | 0 | H | 2 | 409 | 1295 | 2055 |
| 1 | 72L01028 | L275 | 7210 | 91442 | H | 10 | 9144 | 0 | 0 | H | 1 | 3294 | 0 | 22 |
| 2 | 72L01028 | L275 | 7210 | 103212 | H | 10 | 10321 | 0 | 0 | H | 1 | 3294 | 277 | 93 |
| 12 | 72L01028 | L275 | 7210 | 34802 | H | 10 | 3480 | 0 | 0 | H | 2 | 0 | 1386 | 1574 |
| 1 | 72L01029 | L275 | 7210 | 91442 | H | 10 | 9144 | 0 | 0 | H | 14 | 3569 | 439 | 0 |
| 2 | 72L01029 | L275 | 7210 | 103212 | H | 10 | 10321 | 0 | 0 | H | 9 | 3632 | 439 | 0 |

| | | | | | | | | | | | | | | |
|---|---|---|---|---|---|---|---|---|---|---|---|---|---|---|
| 12 | 72L01029 | L275 | 7210 | 34802 | H | 10 | 3480 | 0 | 0 | H | 1 | 3849 | 2558 | 1256 |
| 1 | 72L01030 | L275 | 7210 | 91442 | H | 10 | 9144 | 0 | 0 | H | 1 | 3817 | 643 | 95 |
| 2 | 72L01030 | L275 | 7210 | 103212 | H | 10 | 10321 | 0 | 0 | H | 1 | 3822 | 920 | 958 |
| 12 | 72L01030 | L275 | 7210 | 34802 | H | 10 | 3480 | 0 | 0 | H | 4 | 4099 | 2912 | 3116 |
| 1 | 72L01031 | L275 | 7210 | 91442 | H | 10 | 9144 | 0 | 0 | H | 1 | 3858 | 0 | 0 |
| 2 | 72L01031 | L275 | 7210 | 103212 | H | 10 | 10321 | 0 | 0 | H | 1 | 3892 | 0 | 0 |
| 12 | 72L01031 | L275 | 7210 | 34802 | H | 10 | 3480 | 0 | 0 | H | 1 | 4177 | 1744 | 1948 |
| 1 | 73L01154 | L275 | 7301 | 91442 | H | 10 | 9144 | 0 | 0 | H | 1 | 2776 | 124 | 0 |
| 2 | 73L01154 | L275 | 7301 | 103212 | H | 10 | 10321 | 0 | 0 | H | 2 | 28037 | 575 | 19 |
| 12 | 73L01154 | L275 | 7301 | 34802 | H | 10 | 3480 | 0 | 0 | H | 1 | 3164 | 3676 | 8339 |
| 1 | 73L01155 | L275 | 7303 | 91442 | H | 10 | 9144 | 0 | 0 | H | 2 | 411 | 0 | 0 |
| 2 | 73L01155 | L275 | 7303 | 103212 | H | 10 | 10321 | 0 | 0 | H | 1 | 465 | 236 | 0 |
| 12 | 73L01155 | L275 | 7303 | 34802 | H | 10 | 3480 | 0 | 0 | H | 31 | 3433 | 2026 | 4285 |
| 1 | 73L01180 | L275 | 7303 | 91442 | H | 10 | 9144 | 0 | 0 | H | 1 | 2651 | 0 | 0 |
| 2 | 73L01180 | L275 | 7303 | 103212 | H | 10 | 10321 | 0 | 0 | H | 1 | 2684 | 1134 | 26 |
| 12 | 73L01180 | L275 | 7303 | 34802 | H | 10 | 3480 | 0 | 0 | H | 1 | 3178 | 2927 | 1505 |
| 1 | 73L01181 | L275 | 7304 | 91442 | H | 10 | 9144 | 0 | 0 | H | 1 | 3582 | 82 | 0 |
| 2 | 73L01181 | L275 | 7304 | 103212 | H | 10 | 10321 | 0 | 0 | H | 4 | 3600 | 291 | 0 |
| 12 | 73L01181 | L275 | 7304 | 34802 | H | 10 | 3480 | 0 | 0 | H | 1 | 3665 | 1087 | 665 |
| 1 | 73L01182 | L275 | 7304 | 91442 | H | 10 | 9144 | 0 | 0 | H | 1 | 3987 | 0 | 134 |
| 2 | 73L01182 | L275 | 7304 | 103212 | H | 10 | 10321 | 0 | 0 | H | 1 | 3993 | 955 | 313 |
| 12 | 73L01182 | L275 | 7304 | 34802 | H | 10 | 3480 | 0 | 0 | H | 1 | 4394 | 3197 | 1829 |
| 1 | 73L01183 | L275 | 7304 | 91442 | S | 10 | 9144 | | 0 | H | 0 | 56 | 258 | 9 |
| 2 | 73L01183 | L275 | 7304 | 103212 | S | 10 | 10321 | | 0 | H | 1 | 80 | 535 | 21 |
| 12 | 73L01183 | L275 | 7304 | 34802 | S | 10 | 3480 | | 0 | H | 1 | 415 | 2560 | 1791 |
| 1 | 73L01210 | L275 | 7504 | 91442 | P | 10 | 23546 | 0 | 0 | H | 5 | 3409 | 497 | 275 |
| 2 | 73L01210 | L275 | 7504 | 103212 | P | 10 | 25803 | 0 | 0 | H | 4 | 3425 | 517 | 275 |
| 11 | 73L01210 | L275 | 7504 | 103212 | L | 10 | 18836 | 0 | 0 | H | 2 | 3857 | 2797 | 4386 |
| 12 | 73L01210 | L275 | 7504 | 34802 | L | 10 | 6090 | 0 | 0 | H | 2 | 3895 | 2977 | 4431 |
| 1 | 75L00080 | L275 | 7506 | 91442 | P | 10 | 24918 | | 0 | H | 1 | 2878 | 247 | 22 |
| 2 | 75L00080 | L275 | 7506 | 103212 | P | 10 | 27351 | | 0 | H | 2 | 2902 | 596 | 22 |
| 12 | 75L00080 | L275 | 7506 | 45882 | P | 10 | 8718 | | 0 | H | 2 | 3222 | 2276 | 1773 |
| 1 | 75L00082 | L275 | 7506 | 91442 | P | 10 | 24918 | | 0 | H | 2 | 4332 | 0 | 0 |
| 2 | 75L00082 | L275 | 7506 | 103212 | P | 10 | 27351 | | 0 | H | 2 | 2484 | 97 | 107 |
| 12 | 75L00082 | L275 | 7506 | 45882 | P | 10 | 8718 | | 0 | H | 6 | 4838 | 1182 | 516 |
| 1 | 75L00674 | L275 | 7512 | 91442 | R | 10 | 29033 | | 0 | H | 2 | 3456 | 0 | 0 |
| 2 | 75L00674 | L275 | 7512 | 103212 | R | 10 | 31996 | | 0 | H | 1 | 3478 | 164 | 227 |
| 7 | 75L00674 | L275 | 7512 | 103212 | P | 10 | 28125 | | 0 | H | 1 | 3646 | 524 | 2240 |
| 12 | 75L00674 | L275 | 7512 | 45882 | P | 10 | 10782 | | 0 | H | 1 | 3793 | 1345 | 3029 |
| 1 | 75L00691 | L275 | 7512 | 91442 | R | 10 | 29033 | | 0 | H | 1 | 1845 | 0 | 0 |
| 2 | 75L00691 | L275 | 7512 | 103212 | R | 10 | 31996 | | 0 | H | 1 | 1847 | 0 | 0 |
| 7 | 75L00691 | L275 | 7512 | 103212 | P | 10 | 28125 | | 0 | H | 1 | 1958 | 391 | 25 |
| 12 | 75L00691 | L275 | 7512 | 45882 | P | 10 | 10782 | | 0 | H | 1 | 27432 | 809 | 536 |
| 1 | 75L00693 | L275 | 7512 | 91442 | R | 10 | 29033 | | 0 | H | 1 | 3837 | 154 | 0 |
| 2 | 75L00693 | L275 | 7512 | 103212 | R | 10 | 31996 | | 0 | H | 2 | 3906 | 154 | 0 |
| 7 | 75L00693 | L275 | 7512 | 103212 | P | 10 | 28125 | | 0 | H | 2 | 4072 | 1370 | 197 |

| | | | | | | | | | | | | | | |
|---|---|---|---|---|---|---|---|---|---|---|---|---|---|---|
| 12 | 75L00693 | L275 | 7512 | 45882 | P | 10 | 10782 | | 0 | H | 1 | 4189 | 1617 | 1124 |
| 1 | 75L00698 | L275 | 7512 | 91442 | R | 10 | 29033 | | 0 | H | 1 | 4341 | 185 | 1000 |
| 2 | 75L00698 | L275 | 7512 | 103212 | R | 10 | 31996 | | 0 | H | 4 | 4189 | 328 | 1000 |
| 7 | 75L00698 | L275 | 7512 | 103212 | P | 10 | 28125 | | 0 | H | 2 | 4451 | 1625 | 1736 |
| 12 | 75L00698 | L275 | 7512 | 45882 | P | 10 | 10782 | | 0 | H | 2 | 4607 | 2387 | 1826 |
| 1 | 75L00700 | L275 | 7512 | 91442 | R | 10 | 29033 | | 0 | H | 3 | 3754 | 0 | 0 |
| 2 | 75L00700 | L275 | 7512 | 103212 | R | 10 | 31996 | | 0 | H | 3 | 3840 | 400 | 324 |
| 7 | 75L00700 | L275 | 7512 | 103212 | P | 10 | 28125 | | 0 | H | 1 | 3897 | 855 | 905 |
| 12 | 75L00700 | L275 | 7512 | 45882 | P | 10 | 10782 | | 0 | H | 1 | 4033 | 2252 | 1448 |
| 1 | 75L00701 | L275 | 7511 | 91442 | R | 10 | 28347 | | 0 | H | 0 | 1751 | 0 | 0 |
| 2 | 75L00701 | L275 | 7511 | 103212 | R | 10 | 31222 | | 0 | H | 0 | 1751 | 0 | 0 |
| 6 | 75L00701 | L275 | 7511 | 103212 | P | 10 | 28125 | | 0 | H | 0 | 1751 | 0 | 0 |
| 9 | 75L00701 | L275 | 7511 | 103212 | P | 10 | 25803 | | 0 | H | 0 | 1751 | 0 | 0 |
| 1 | 82L00590 | L275 | 8211 | 91442 | U | 10 | 85955 | 0 | 0 | H | 3 | 696 | 20 | 0 |
| 2 | 82L00590 | L275 | 8211 | 103212 | U | 10 | 96245 | 0 | 0 | H | 3 | 818 | 30 | 0 |
| 5 | 82L00590 | L275 | 8211 | 103212 | T | 10 | 93923 | 0 | 0 | H | 3 | 1088 | 500 | 192 |
| 12 | 82L00590 | L275 | 8211 | 81084 | T | 10 | 69530 | 0 | 0 | H | 4 | 1667 | 1228 | 1689 |
| 1 | 82L00591 | L275 | 8211 | 91442 | U | 10 | 85955 | 0 | 0 | H | 4 | 704 | 237 | 0 |
| 2 | 82L00591 | L275 | 8211 | 103212 | U | 10 | 96245 | 0 | 0 | H | 3 | 788 | 648 | 0 |
| 5 | 82L00591 | L275 | 8211 | 103212 | T | 10 | 93923 | 0 | 0 | H | 3 | 1020 | 1031 | 532 |
| 12 | 82L00591 | L275 | 8211 | 81084 | T | 10 | 69530 | 0 | 0 | H | 3 | 1574 | 2097 | 1015 |
| 1 | 82L00592 | L275 | 8211 | 91442 | U | 10 | 85955 | 0 | 0 | H | 0 | 107 | 521 | 0 |
| 2 | 82L00592 | L275 | 8211 | 103212 | U | 10 | 96245 | 0 | 0 | H | 1 | 153 | 705 | 33 |
| 5 | 82L00592 | L275 | 8211 | 103212 | T | 10 | 93923 | 0 | 0 | H | 1 | 357 | 1057 | 33 |
| 12 | 82L00592 | L275 | 8211 | 81084 | T | 10 | 69530 | 0 | 0 | H | 29 | 746 | 2478 | 1367 |
| 1 | 82L00593 | L275 | 8211 | 91442 | U | 10 | 85955 | 0 | 0 | H | 8 | 1019 | 0 | 0 |
| 2 | 82L00593 | L275 | 8211 | 103212 | U | 10 | 96245 | 0 | 0 | H | 8 | 1242 | 0 | 0 |
| 5 | 82L00593 | L275 | 8211 | 103212 | T | 10 | 93923 | 0 | 0 | H | 4 | 1077 | 810 | 2724 |
| 12 | 82L00593 | L275 | 8211 | 81084 | T | 10 | 69530 | 0 | 0 | H | 9 | 1750 | 2001 | 3926 |
| 1 | 82L00597 | L275 | 8211 | 91442 | U | 10 | 85955 | 0 | 0 | H | 3 | 570 | 134 | 0 |
| 2 | 82L00597 | L275 | 8211 | 103212 | U | 10 | 96245 | 0 | 0 | H | 3 | 680 | 503 | 0 |
| 5 | 82L00597 | L275 | 8211 | 103212 | T | 10 | 93923 | 0 | 0 | H | 2 | 692 | 767 | 246 |
| 12 | 82L00597 | L275 | 8211 | 81084 | T | 10 | 69530 | 0 | 0 | H | 2 | 1266 | 3150 | 1011 |
| 1 | 83L00849 | L275 | 8403 | 80402 | U | 10 | 80402 | 0 | 0 | H | 0 | 33 | 83 | 0 |
| 2 | 83L00849 | L275 | 8403 | 103212 | U | 10 | 102438 | 0 | 0 | H | 1 | 89 | 83 | 0 |
| 4 | 83L00849 | L275 | 8403 | 81084 | U | 10 | 79260 | 0 | 0 | H | 1 | 3310 | 83 | 0 |
| 1 | 83L00866 | L275 | 8403 | 80402 | U | 10 | 80402 | 0 | 0 | H | 0 | 16 | 0 | 0 |
| 2 | 83L00866 | L275 | 8403 | 103212 | U | 10 | 102438 | 0 | 0 | H | 0 | 75 | 0 | 0 |
| 4 | 83L00866 | L275 | 8403 | 81084 | U | 10 | 79260 | 0 | 0 | H | 2 | 215 | 96 | 0 |
| 1 | 83L00873 | L275 | 8403 | 80402 | U | 10 | 80402 | 0 | 0 | H | 0 | 21 | 0 | 0 |
| 2 | 83L00873 | L275 | 8403 | 103212 | U | 10 | 102438 | 0 | 0 | H | 0 | 91 | 83 | 0 |
| 4 | 83L00873 | L275 | 8403 | 81084 | U | 10 | 79260 | 0 | 0 | H | 3 | 204 | 199 | 0 |
| 1 | 83L00874 | L275 | 8403 | 80402 | U | 10 | 80402 | 0 | 0 | H | 0 | 19 | 0 | 0 |
| 2 | 83L00874 | L275 | 8403 | 103212 | U | 10 | 102438 | 0 | 0 | H | 0 | 90 | 146 | 0 |
| 4 | 83L00874 | L275 | 8403 | 81084 | U | 10 | 79260 | 0 | 0 | H | 3 | 238 | 178 | 0 |
| 1 | 67L00075 | L276 | 6701 | 100836 | B | 11 | 10084 | - | 0 | H | 0 | 1925 | 0 | 0 |
| 2 | 67L00075 | L276 | 6701 | 100814 | B | 11 | 10081 | - | 0 | H | 0 | 1930 | 92 | 7 |

| | | | | | | | | | | | | | | | |
|---|---|---|---|---|---|---|---|---|---|---|---|---|---|---|---|
| 12 | 67L00075 | L276 | 6701 | 25392 | B | 11 | 2539 | - | 0 | H | 0 | 1960 | 1719 | 1033 |
| 1 | 84L00049 | L276 | 8406 | 93610 | U | 11 | 93610 | 0 | 0 | H | 0 | 502 | 0 | 0 |
| 1 | 84L00049 | L276 | 8406 | 93610 | U | 11 | 93610 | 0 | 0 | H | 0 | 502 | 0 | 0 |
| 1 | 74L00609 | L278 | 7408 | 29704 | R | 12 | 9846 | | 0 | H | 0 | 3565 | 0 | 0 |
| 2 | 74L00609 | L278 | 7408 | 31102 | R | 12 | 10108 | | 0 | H | 1 | 28395 | 308 | 691 |
| 12 | 74L00609 | L278 | 7408 | 18356 | R | 12 | 4818 | | 0 | H | 0 | 2864 | 308 | 2045 |
| 1 | 82L00435 | L305 | 8210 | 86472 | U | 14 | 53749 | 0 | 0 | M | 48 | 230 | 0 | 0 |
| 4 | 82L00435 | L305 | 8210 | 86472 | T | 14 | 52842 | 0 | 0 | M | 49 | 230 | 272 | 28 |
| 5 | 82L00435 | L305 | 8210 | 86472 | T | 14 | 52539 | 0 | 0 | M | 60 | 230 | 272 | 28 |
| 1 | 61L00753 | L350 | 6110 | 71453 | B | 19 | 7145 | - | 0 | H | 0 | 1442 | 0 | 0 |
| 3 | 61L00753 | L350 | 6110 | 104380 | B | 19 | 10438 | - | 0 | H | 0 | 1610 | 71 | 25 |
| 12 | 61L00753 | L350 | 6110 | 19866 | B | 16 | 2987 | - | 0 | H | 2 | 1592 | 1511 | 924 |
| 1 | 68L00909 | L350 | 6806 | 71453 | L | 16 | 10830 | | 0 | H | 48 | 5777 | 0 | 0 |
| 3 | 68L00909 | L350 | 6806 | 104380 | L | 16 | 15331 | | 0 | H | 28 | 3010 | 0 | 0 |
| 12 | 68L00909 | L350 | 6806 | 19400 | L | 16 | 2940 | | 0 | H | 103 | 5352 | 1051 | 270 |
| 1 | 63L00171 | L351 | 363 | 25927 | H | 16 | 2593 | 0 | 0 | M | 16 | 18874 | 145 | 316 |
| 12 | 63L00171 | L351 | 363 | 7220 | H | 16 | 722 | 0 | 0 | M | 51 | 21601 | 2851 | 1987 |
| 1 | 64L00714 | L351 | 6403 | 25927 | L | 20 | 3371 | | 0 | M | 12 | 48069 | 10 | 0 |
| 8 | 64L00714 | L351 | 6403 | 25927 | H | 16 | 2593 | | 0 | M | 20 | 51296 | 1080 | 1179 |
| 12 | 64L00714 | L351 | 6403 | 7220 | H | 16 | 722 | | 0 | M | 181 | 52691 | 2158 | 1248 |
| 1 | 65L00736 | L351 | 6507 | 25927 | B | 16 | 2593 | - | 0 | M | 5 | 119306 | 0 | 0 |
| 6 | 65L00736 | L351 | 6507 | 25927 | B | 16 | 2593 | - | 3334 | M | 8 | 120266 | 665 | 2600 |
| 12 | 65L00736 | L351 | 6507 | 7220 | B | 16 | 722 | - | 0 | M | 6 | 121177 | 999 | 2750 |
| 1 | 65L00763 | L351 | 6501 | 25927 | B | 16 | 2593 | - | 0 | M | 10 | 117091 | 62 | 0 |
| 12 | 65L00763 | L351 | 6501 | 7220 | B | 16 | 722 | - | 970 | M | 8 | 120916 | 1942 | 2053 |
| 1 | 65L00774 | L351 | 6507 | 25927 | B | 16 | 2593 | - | 0 | M | 6 | 29536 | 0 | 0 |
| 10 | 65L00774 | L351 | 6507 | 25927 | H | 16 | 2593 | | 0 | M | 2 | 30435 | 766 | 1281 |
| 12 | 65L00774 | L351 | 6507 | 7220 | H | 16 | 722 | | 0 | M | 3 | 30699 | 1286 | 2622 |
| 1 | 65L00837 | L351 | 6507 | 25927 | B | 16 | 2593 | - | 0 | M | 11 | 44799 | 149 | 0 |
| 10 | 65L00837 | L351 | 6507 | 25927 | H | 16 | 2593 | | 0 | M | 12 | 46686 | 1418 | 371 |
| 12 | 65L00837 | L351 | 6507 | 7220 | H | 16 | 722 | | 0 | M | 8 | 46865 | 1517 | 420 |
| 1 | 65L00892 | L351 | 6511 | 25927 | B | 16 | 2593 | - | 0 | M | 11 | 55279 | 17 | 0 |
| 10 | 65L00892 | L351 | 6511 | 25927 | H | 16 | 2593 | | 0 | M | 7 | 57518 | 2127 | 2430 |
| 12 | 65L00892 | L351 | 6511 | 7220 | H | 16 | 722 | | 1921 | M | 8 | 58055 | 2877 | 3533 |
| 1 | 65L01112 | L351 | 6511 | 25927 | H | 16 | 2593 | | 0 | M | 9 | 40450 | 180 | 168 |
| 9 | 65L01112 | L351 | 6511 | 25927 | H | 16 | 2593 | | 3162 | M | 10 | 42632 | 1250 | 2627 |
| 12 | 65L01112 | L351 | 6511 | 7220 | H | 16 | 722 | | 0 | M | 6 | 43697 | 1276 | 2627 |
| 1 | 65L01113 | L351 | 6511 | 25927 | B | 16 | 2593 | - | 0 | M | 5 | 61258 | 154 | 316 |
| 10 | 65L01113 | L351 | 6511 | 25927 | H | 16 | 2593 | | 0 | M | 18 | 62610 | 1162 | 955 |
| 12 | 65L01113 | L351 | 6511 | 7220 | H | 16 | 722 | | 0 | M | 6 | 45825 | 1289 | 1045 |
| 1 | 68L00543 | L351 | 1068 | 25927 | B | 16 | 2593 | - | 0 | M | 7 | 18233 | 278 | 503 |
| 12 | 68L00543 | L351 | 1068 | 7600 | B | 16 | 2593 | - | 0 | M | 3 | 19594 | 760 | 780 |
| 1 | 68L00570 | L351 | 6811 | 25927 | P | 16 | 4537 | | 0 | M | 17 | 55445 | 340 | 181 |
| 6 | 68L00570 | L351 | 6811 | 25927 | L | 16 | 3930 | | 0 | M | 7 | 56617 | 1845 | 1193 |

| | | | | | | | | | | | | | |
|---|---|---|---|---|---|---|---|---|---|---|---|---|---|
| 12 | 68L00570 | L351 | 6811 | 7600 | L | 16 | 938 | | 0 | M | 84 | 58441 | 3274 | 2086 |
| 1 | 68L00572 | L351 | 6811 | 25927 | P | 16 | 4537 | 0 | 0 | M | 10 | 33070 | 0 | 0 |
| 6 | 68L00572 | L351 | 6811 | 25927 | L | 16 | 3930 | 0 | 0 | M | 8 | 1217 | 1230 | 933 |
| 12 | 68L00572 | L351 | 6811 | 7600 | L | 16 | 938 | 0 | 0 | M | 6 | 2890 | 2394 | 2034 |
| 1 | 70L00550 | L351 | 7003 | 25927 | R | 16 | 6482 | 0 | 0 | M | 4 | 51962 | 72 | 0 |
| 10 | 70L00550 | L351 | 7003 | 25927 | P | 16 | 5388 | 0 | 0 | M | 4 | 52761 | 1409 | 2217 |
| 12 | 70L00550 | L351 | 7003 | 7600 | P | 16 | 1508 | 0 | 0 | M | 4 | 52923 | 1510 | 2225 |
| 1 | 70L00554 | L351 | 7003 | 25927 | R | 16 | 6482 | 0 | 0 | M | 15 | 39740 | 0 | 0 |
| 10 | 70L00554 | L351 | 7003 | 25927 | P | 16 | 5388 | 0 | 0 | M | 18 | 43216 | 1776 | 3103 |
| 12 | 70L00554 | L351 | 7003 | 7600 | P | 16 | 1508 | 0 | 0 | M | 15 | 44411 | 2043 | 3424 |
| 1 | 70L00555 | L351 | 7003 | 25927 | R | 16 | 6482 | 0 | 0 | M | 7 | 39720 | 536 | 374 |
| 10 | 70L00555 | L351 | 7003 | 25927 | P | 16 | 5388 | 0 | 0 | M | 6 | 41434 | 1673 | 6544 |
| 12 | 70L00555 | L351 | 7003 | 7600 | P | 16 | 1508 | 0 | 0 | M | 30 | 43894 | 2273 | 7202 |
| 1 | 70L00556 | L351 | 7003 | 25927 | R | 16 | 6482 | 0 | 0 | M | 5 | 46364 | 441 | 18 |
| 10 | 70L00556 | L351 | 7003 | 25927 | P | 16 | 5388 | 0 | 0 | M | 14 | 49927 | 2661 | 3983 |
| 12 | 70L00556 | L351 | 7003 | 7600 | P | 16 | 1508 | 0 | 0 | M | 11 | 50997 | 3058 | 4027 |
| 1 | 70L00558 | L351 | 7003 | 25927 | R | 16 | 6482 | 0 | 0 | M | 18 | 22545 | 129 | 0 |
| 10 | 70L00558 | L351 | 7003 | 25927 | P | 16 | 5388 | 0 | 0 | M | 20 | 26422 | 1790 | 2152 |
| 12 | 70L00558 | L351 | 7003 | 7600 | P | 16 | 1508 | 0 | 0 | M | 15 | 27355 | 1795 | 2152 |
| 1 | 70L00561 | L351 | 7003 | 25927 | R | 16 | 5631 | 0 | 0 | M | 0 | 9101 | 0 | 0 |
| 3 | 70L00561 | L351 | 7003 | 25927 | P | 16 | 5388 | 0 | 0 | M | 5 | 9929 | 328 | 138 |
| 5 | 70L00561 | L351 | 7003 | 7600 | P | 16 | 1508 | 0 | 0 | M | 11 | 10474 | 521 | 323 |
| 1 | 70L00589 | L351 | 7004 | 25927 | R | 16 | 6603 | 0 | 0 | M | 9 | 38552 | 0 | 0 |
| 11 | 70L00589 | L351 | 7004 | 25927 | P | 16 | 5388 | 0 | 0 | M | 8 | 41248 | 1198 | 1513 |
| 12 | 70L00589 | L351 | 7004 | 7600 | P | 16 | 5266 | 0 | 0 | M | 6 | 41248 | 1358 | 1513 |
| 1 | 70L00591 | L351 | 7004 | 25927 | R | 16 | 6603 | 0 | 0 | M | 10 | 38919 | 0 | 0 |
| 11 | 70L00591 | L351 | 7004 | 25927 | P | 16 | 5388 | 0 | 0 | M | 14 | 42422 | 1351 | 2561 |
| 12 | 70L00591 | L351 | 7004 | 7600 | P | 16 | 1544 | 0 | 0 | M | 11 | 42568 | 1409 | 2707 |
| 1 | 70L00592 | L351 | 7004 | 25927 | R | 16 | 6603 | 0 | 0 | M | 14 | 53953 | 72 | 0 |
| 11 | 70L00592 | L351 | 7004 | 25927 | P | 16 | 5388 | 0 | 0 | M | 7 | 55621 | 893 | 337 |
| 12 | 70L00592 | L351 | 7004 | 7600 | P | 16 | 1544 | 0 | 0 | M | 8 | 55722 | 956 | 338 |
| 1 | 75L00230 | L351 | 7505 | 25927 | R | 16 | 14017 | | 0 | M | 179 | 30350 | 0 | 0 |
| 12 | 75L00230 | L351 | 7505 | 11165 | R | 16 | 5460 | | 0 | M | 10 | 32682 | 2002 | 1804 |
| 1 | 75L00251 | L351 | 7506 | 25927 | R | 16 | 14138 | | 0 | M | 3 | 7450 | 0 | 0 |
| 12 | 75L00251 | L351 | 7506 | 11165 | R | 16 | 5513 | | 0 | M | 3 | 7928 | 550 | 692 |
| 1 | 76L00020 | L351 | 7607 | 25927 | T | 16 | 15718 | | 0 | M | 3 | 13731 | 0 | 0 |
| 12 | 76L00020 | L351 | 7607 | 15126 | T | 16 | 8390 | | 0 | M | 4 | 15073 | 125 | 45 |
| 1 | 76L00060 | L351 | 7603 | 25927 | T | 16 | 15232 | | 0 | M | 14 | 23922 | 154 | 274 |
| 5 | 76L00060 | L351 | 7603 | 25927 | T | 16 | 14746 | | 0 | M | 14 | 25301 | 1070 | 507 |
| 1 | 76L00061 | L351 | 7603 | 25927 | T | 16 | 15232 | | 0 | M | 11 | 27335 | 0 | 0 |
| 9 | 76L00061 | L351 | 7603 | 25927 | R | 16 | 14260 | | 0 | M | 15 | 30572 | 960 | 557 |
| 12 | 76L00061 | L351 | 7603 | 15126 | R | 16 | 8107 | | 0 | M | 17 | 31857 | 1382 | 687 |
| 1 | 80L00070 | L351 | 8002 | 25927 | T | 16 | 20944 | 0 | 0 | M | 7 | 11207 | 0 | 0 |
| 12 | 80L00070 | L351 | 8002 | 32102 | T | 16 | 24277 | 0 | 0 | M | 12 | 15117 | 1089 | 263 |

| | | | | | | | | | | | | | |
|---|---|---|---|---|---|---|---|---|---|---|---|---|---|
| 1 | 63L00028 | L363 | 6402 | 23981 | L | 20 | 3028 | 0 | 0 | U | 0 | 0 | 10 | 0 |
| 9 | 63L00028 | L363 | 6402 | 23981 | H | 20 | 2398 | 0 | 0 | U | 0 | 0 | 259 | 316 |
| 12 | 63L00028 | L363 | 6402 | 6983 | H | 20 | 698 | 0 | 0 | U | 0 | 0 | 342 | 316 |
| 1 | 59L01114 | L389 | 5908 | 112870 | D | 25 | 15689 | - | 0 | U | 0 | 0 | 0 | 0 |
| 10 | 59L01114 | L389 | 5908 | 112870 | L | 25 | 12641 | | 0 | U | 0 | 0 | 40 | 0 |
| 12 | 59L01114 | L389 | 5908 | 35000 | L | 25 | 3710 | | 0 | U | 0 | 0 | 40 | 0 |
| 1 | 63L00577 | L461 | 8306 | 9760 | T | 25 | 9672 | 0 | 0 | U | 0 | 0 | 376 | 114 |
| 8 | 63L00577 | L461 | 8306 | 9760 | T | 25 | 9467 | | 0 | U | 0 | 0 | 376 | 114 |
| 1 | 65L00943 | L461 | 6506 | 9760 | R | 25 | 3406 | 0 | 0 | U | 0 | 0 | 0 | 0 |
| 12 | 65L00943 | L461 | 6506 | 2673 | R | 25 | 845 | 0 | 0 | U | 0 | 0 | 121 | 0 |
| 1 | 68L00678 | L461 | 6805 | 9760 | R | 25 | 4431 | 0 | 0 | U | 0 | 0 | 0 | 0 |
| 12 | 68L00678 | L461 | 6805 | 2673 | R | 25 | 1125 | 0 | 0 | U | 0 | 0 | 1011 | 1752 |
| 1 | 68L00691 | L461 | 6806 | 9760 | R | 25 | 4460 | | 0 | U | 0 | 0 | 0 | 0 |
| 12 | 68L00691 | L461 | 6806 | 2673 | R | 25 | 1133 | | 0 | U | 0 | 0 | 257 | 6 |
| 1 | 69L00442 | L461 | 6903 | 9760 | R | 25 | 4724 | | 0 | U | 0 | 0 | 0 | 0 |
| 12 | 69L00442 | L461 | 6903 | 2730 | R | 25 | 1231 | | 0 | U | 0 | 0 | 539 | 0 |
| 1 | 69L00516 | L461 | 6903 | 9760 | R | 25 | 4724 | | 0 | U | 0 | 0 | 0 | 0 |
| 12 | 69L00516 | L461 | 6903 | 2730 | R | 25 | 1231 | | 0 | U | 0 | 0 | 102 | 5 |
| 1 | 80L00300 | L461 | 8006 | 9760 | T | 25 | 8677 | 0 | 0 | U | 0 | 0 | 185 | 0 |
| 12 | 80L00300 | L461 | 8006 | 9064 | T | 25 | 7759 | 0 | 0 | U | 0 | 0 | 417 | 0 |
| 1 | 68L00420 | L486 | 6902 | 4003 | R | 25 | 1925 | | 0 | U | 0 | 0 | 0 | 0 |
| 2 | 68L00420 | L486 | 6902 | 4113 | R | 25 | 1966 | | 0 | U | 0 | 0 | 0 | 0 |
| 12 | 68L00420 | L486 | 6902 | 3575 | R | 25 | 1602 | | 0 | U | 0 | 0 | 98 | 0 |
| 1 | 68L00421 | L486 | 6902 | 4003 | R | 25 | 1925 | | 0 | U | 0 | 0 | 0 | 0 |
| 2 | 68L00421 | L486 | 6902 | 4113 | R | 25 | 1966 | | 0 | U | 0 | 0 | 0 | 0 |
| 12 | 68L00421 | L486 | 6902 | 3575 | R | 25 | 1602 | | 0 | U | 0 | 0 | 117 | 0 |
| 1 | 68L00422 | L486 | 6902 | 4003 | R | 25 | 1925 | | 0 | U | 0 | 0 | 0 | 0 |
| 2 | 68L00422 | L486 | 6902 | 4113 | R | 25 | 1966 | | 0 | U | 0 | 0 | 20 | 0 |
| 12 | 68L00422 | L486 | 6902 | 3575 | R | 25 | 1602 | | 0 | U | 0 | 0 | 93 | 0 |
| 1 | 63L00780 | L504 | 8310 | 86000 | | 10 | 0 | 0 | 0 | H | 0 | 55 | 0 | 0 |
| 2 | 63L00780 | L504 | 8310 | 77714 | T | 10 | 77131 | 0 | 0 | H | 0 | 55 | 0 | 0 |
| 7 | 63L00780 | L504 | 8310 | 77714 | H | 10 | 74217 | | 0 | H | 5 | 219 | 709 | 1056 |
| 8 | 63L00780 | L504 | 8310 | 77714 | T | 10 | 73634 | | 0 | H | 5 | 226 | 709 | 1056 |
| 9 | 63L00780 | L504 | 8310 | 77714 | T | 10 | 73051 | | 0 | H | 2 | 389 | 746 | 1056 |

1984 USAF-SCEEE RESEARCH INITIATION PROGRAM

Sponsored by the

AIR FORCE OFFICE OF SCIENTIFIC RESEARCH

Conducted by

SOUTHEASTERN CENTER FOR ELECTRICAL ENGINEERING EDUCATION

# FINAL TECHNICAL REPORT

# THE DEVELOPMENT OF COMPUTATIONAL EFFICIENCIES IN CONTINUUM FINITE ELEMENT CODES USING MATRIX DIFFERENCE EQUATIONS


| | |
|---|---|
| Prepared By: | Dr. Harold C. Sorensen |
| Academic Rank: | Associate Professor |
| Department and University: | Civil and Environmental Engineering<br>Washington State University |
| Research Location: | Civil and Environmental Engineering<br>Washington State University |
| USAF Research Focal Point: | Dr. Timothy J. Ross |



| | |
|---|---|
| Date Submitted: | November 25, 1985 |
| Contract No.: | F49620-82-C-0035 |
| Subcontract No.: | 84 RIP 22 |
| Subcontract Term: | 11/16/84-11/15/85 (12 months) |
| Amount Granted: | $12,000 |

# THE DEVELOPMENT OF COMPUTATIONAL EFFICIENCIES IN CONTINUUM FINITE ELEMENT CODES USING MATRIX DIFFERENCE EQUATIONS

by

Harold C. Sorensen

## ABSTRACT

The feasibility of using the Matrix Difference Equation (MDE) theory to effect computational efficiencies in continuum finite element codes has been investigated in this research. The study was centered around the SAMSON2 code, which is a state-of-the-art 2-D code for use in dynamic structural analyses of plane and axisymmetric solids undergoing development within AFWL/NTE.

The SAMSON2 code uses explicit time integration and is particularly suited to the analysis of large displacement, large strain problems involving nonlinear material behavior and structure-media interface (SMI) problems.

The MDE method is applicable only to longitudinally periodic structures within simply supported or guided ends. The use of the MDE method is limited to linear elastic structures (small-displacement theory) for which the principle of superposition is valid. Equilibrium is not satisfied by the method. An approximate solution to the system of equations developed in any problem solution is obtained by a least squares technique. The method involves a Guyan matrix reduction which introduces errors. The eigensolutions obtained by the method are unreliable for the high half of the range of frequencies and should be discarded.

Because of the errors and approximations in the MDE method, the restrictions on geometric and material linearities, and its applicability only to

longitudinal periodic structures, it is concluded that the MDE method has a low potential for improving the computational efficiency of the SAMSON2 code.

Further study of the MDE method with regard to large displacement, large strain type finite element computer codes is not recommended. However, the MDE method could be further studied for usefulness in linear finite element solutions.

## ACKNOWLEDGMENTS

Grateful appreciation is hereby expressed to the Air Force Systems Command, Air Force Office of Scientific Research and the Southeastern Center for Electrical Engineering Education for providing the financial support for this project.

Thanks go to the Air Force Weapons Laboratory, Kirtland, AFB for the opportunity to begin this study during a summer faculty research appointment for the P.I.

Special thanks go to Dr. Arthur Guenther (AFWL) for his support of this project and to Dr. Timothy J. Ross (AFWL/NTE) for originating the idea for this study and for his continued encouragement and support during the research period.

## I. INTRODUCTION

The proposed research project was initiated during the summer 1984 when the P.I. (Dr. Harold C. Sorensen) spent eight weeks at AFWL/NTE, KAFB, NM as a participant in the AFOSR/SCEEE summer faculty research program. Two graduate students (S. S. Miller and R. L. Bigelis) accompanied the P.I. and worked for ten weeks toward the accomplishment of the objective of this research.

During the summer period, the P.I. became familiar with the principles and concepts of the MDE method and with the theory and operation of the SAMSON2 code. One graduate student (S. S. Miller) became very familiar with the logic of the finite element portion of the SAMSON2 code in a programming sense. He is capable of changing the code as it becomes necessary to do so. The other graduate student (R. L. Bigelis) became very familiar with the slideline concept and theory. He is capable of working with the code in this area.

The Matrix Difference Equation (MDE) method has been developed by P. H. Denke, et al. (Ref. 1) at the Douglas Aircraft Corporation and has been shown by them to reduce computational costs associated with elastic analyses of spatially periodic structures. The term "periodic structure" means a structure modeled as a linear array of identical substructures. There must also be a plane of symmetry in each substructure which is one of the key factors in the development of the method.

In the MDE method, the finite element method is applied to one of the identical substructures to obtain a mechanical impedance matrix. A matrix difference equation is derived from the impedance matrix, based on conditions of equilibrium and compatibility at the substructure boundaries. The order of the difference equation is reduced by eliminating the force variables and introducing substructure displacement modes. The solution is found by

calculating the eigenvalues and eigenvectors of a related characteristic equation. The result is a closed form expression in the longitudinal coordinate. The method is considered to be general and applicable to complex structures because of the finite element basis.

A brief summary of the MDE method is as follows.

The finite element model is given in Figure 1.

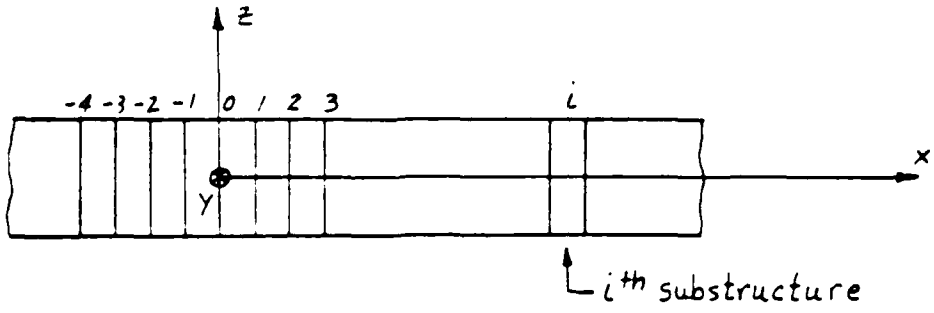



Figure 1. The structure idealized as a linear array of identical substructures.

The linear equation of motion for one substructure in harmonic motion can be written in the following form.

$$\underset{\sim}{A}\,\underset{\sim}{\Delta} = \underset{\sim}{P}_u \tag{1}$$

where $\underset{\sim}{A}$ is the mechanical impedance matrix, $\underset{\sim}{\Delta}$ is a column matrix of complex displacement amplitudes and $\underset{\sim}{P}_u$ is a column matrix of complex external load amplitudes in the unconstrained degrees of freedom.

The impedance matrix is given by

$$\underset{\sim}{A} = \underset{\sim}{K} - \omega^2 \underset{\sim}{M} + i\omega \underset{\sim}{C} \tag{2}$$

wnere $\omega$ = frequency, $i = \sqrt{-1}$ and $\underset{\sim}{K}$, $\underset{\sim}{M}$ and $\underset{\sim}{C}$ = square symmetric stiffness, mass and damping matrices for the substructure derived by standard finite element procedures.

By eliminating the interior degrees of freedom of the substructure, Eq. 1 may be written as

$$\underset{\sim}{A}_B \underset{\sim}{\Delta}_B = \underset{\sim}{P}_{u_B} \tag{3}$$

where

$$\underset{\sim}{A}_B = \underset{\sim}{K}_B - \omega^2 \underset{\sim}{M}_B + i\omega \underset{\sim}{C}_B \tag{4}$$

In Eq. 3 and Eq. 4, the subscript $B$ refers to equivalent boundary matrices associated with the boundary degrees of freedom.

Through an appropriate modal transformation Eq. 3 can be written as

$$\hat{\underset{\sim}{A}}_B \hat{\underset{\sim}{\Delta}}_B = \hat{\underset{\sim}{P}}_{u_B} \tag{5}$$

Equation 5 can be partitioned as follows

$$\left[\begin{array}{c|c} \hat{\underset{\sim}{A}}_{Bll} & \hat{\underset{\sim}{A}}_{Blr} \\ \hline \hat{\underset{\sim}{A}}_{Brl} & \hat{\underset{\sim}{A}}_{Brr} \end{array}\right] \left\{\begin{array}{c} \hat{\underset{\sim}{\Delta}}_{Bl} \\ \hat{\underset{\sim}{\Delta}}_{Br} \end{array}\right\} = \left\{\begin{array}{c} \hat{\underset{\sim}{P}}_{u_{Bl}} \\ \hat{\underset{\sim}{P}}_{u_{Br}} \end{array}\right\} \tag{6}$$

where the subscripts $l$ and $r$ refer to the left and right boundaries of the substructure, respectively.

By expanding Eq. 6 and retaining the force variables, $\hat{\underset{\sim}{P}}_{u_B}$, the following matrix difference can be obtained.

$$\hat{\underset{\sim}{Y}}^{(i+1)} - \hat{\underset{\sim}{N}}\,\hat{\underset{\sim}{Y}}^{(i)} = \underset{\sim}{0} \tag{7}$$

where

$$\hat{\underset{\sim}{N}} = \left[\begin{array}{c|c} -\hat{\underset{\sim}{A}}_{Brr}\hat{\underset{\sim}{A}}_{Blr} & \hat{\underset{\sim}{A}}_{Brl} - \hat{\underset{\sim}{A}}_{Brr}\hat{\underset{\sim}{A}}^{-1}_{Blr}\hat{\underset{\sim}{A}}_{Bll} \\ \hline -\hat{\underset{\sim}{A}}^{-1}_{Blr} & -\hat{\underset{\sim}{A}}^{-1}_{Blr}\hat{\underset{\sim}{A}}_{Bll} \end{array}\right] \quad \& \quad \hat{\underset{\sim}{Y}}^{(i)} = \left\{\begin{array}{c} \hat{P}^{(i)}_{u_{Br}} \\ \hat{\Delta}^{(i)}_{Br} \end{array}\right\} \tag{8}$$

A solution to Eq. 7 is

$$\hat{\underset{\sim}{Y}}^{(i)}_{k} = \hat{\underset{\sim}{G}}_{k}\,\hat{\lambda}^{(i)}_{k} \tag{9}$$

where $\hat{\underset{\sim}{G}}_{k}$ is a column matrix and $\hat{\lambda}^{(i)}_{k}$ is a scalar.

Substituting Eq. 9 into Eq. 7 gives

$$\left(\hat{\underset{\sim}{N}} - \hat{\lambda}_k \underset{\sim}{I}\right) \hat{\underset{\sim}{G}}_k = \underset{\sim}{0} \tag{10}$$

Equation 10 is a characteristic equation which can be solved for the eigenvalues $\hat{\lambda}_k$ and the eigenvectors $\hat{\underset{\sim}{G}}_k$.

The above formulation with force variables retained is useful for solving small problems involving limited numbers of degrees of freedom.

If Eq. 6 is again expanded, but this time with the force variables, $\hat{\underset{\sim}{P}}_{u_B}$, eliminated, the following difference equation can be obtained.

$$\hat{\underset{\sim}{A}}_{Brl} \hat{\underset{\sim}{\Delta}}_{Br}^{(i)} + \left(\hat{\underset{\sim}{A}}_{Bll} + \hat{\underset{\sim}{A}}_{Brr}\right) \hat{\underset{\sim}{\Delta}}_{Br}^{(i+1)} + \hat{\underset{\sim}{A}}_{Blr} \hat{\underset{\sim}{\Delta}}_{Br}^{(i+2)} = \underset{\sim}{0} \tag{11}$$

Equation 11 is solved by the substitution of

$$\hat{\underset{\sim}{\Delta}}_{Br_k} = \hat{\underset{\sim}{G}}_{\Delta_k} \hat{\lambda}_k^{(i)} \tag{12}$$

where $\hat{\underset{\sim}{G}}_{\Delta_k}$ is a column matrix of displacement eigenvectors. This substitution gives the following equation.

$$\left[\hat{\underset{\sim}{A}}_{Blr} \hat{\lambda}_k^2 + \left(\hat{\underset{\sim}{A}}_{Bll} + \hat{\underset{\sim}{A}}_{Brr}\right) \hat{\lambda}_k + \hat{\underset{\sim}{A}}_{Brl}\right] \hat{\underset{\sim}{G}}_{\Delta_k} = \underset{\sim}{0} \tag{13}$$

Equation 13 is a characteristic equation in which the matrices are only half as large as those in Eq. 10, and is, therefore, worth solving even though it is quadratic in $\hat{\lambda}$ .

In the solution for the natural frequencies and the mode shapes for the total structure, a boundary stiffness matrix, $\underset{\sim}{K}_B$ , and a boundary mass matrix, $\underset{\sim}{M}_B$ , are developed for one substructure. These two matrices have the following form.

$$\underset{\sim}{K}_B = \left[\begin{array}{cc|cc} P_{aa} & P_{ab} & q_{aa} & q_{ab} \\ P_{ab}^T & P_{bb} & -q_{ab}^T & q_{bb} \\ \hline q_{aa} & -q_{ab} & P_{aa} & -P_{ab} \\ q_{ab}^T & q_{bb} & -P_{ab}^T & P_{bb} \end{array}\right] \tag{14}$$

$$\underset{\sim}{M}_B = \left[\begin{array}{cc|cc} m_{aa} & m_{ab} & n_{aa} & n_{ab} \\ m_{ab}^T & m_{bb} & -n_{ab}^T & n_{bb} \\ \hline n_{aa} & -n_{ab} & m_{aa} & -m_{ab} \\ n_{ab}^T & n_{bb} & -m_{ab}^T & m_{bb} \end{array}\right] \tag{15}$$

Then two matrices are defined as follows

$$\underset{\sim}{k}_{\nu} = \left[\begin{array}{c|c} p_{aa} + q_{aa}\cos\theta_{\nu} & q_{ab}\sin\theta_{\nu} \\ \hline q_{ab}^{T}\sin\theta_{\nu} & p_{bb} + q_{bb}\cos\theta_{\nu} \end{array}\right] \tag{16}$$

$$\underset{\sim}{m}_{\nu} = \left[\begin{array}{c|c} m_{aa} + n_{aa}\cos\theta_{\nu} & n_{ab}\sin\theta_{\nu} \\ \hline n_{ab}^{T}\sin\theta_{\nu} & m_{bb} + n_{bb}\cos\theta_{\nu} \end{array}\right] \tag{17}$$

where

$$\theta_{\nu} = \frac{\pi\nu}{S} \qquad \nu = 0, 1, 2, \cdots S \tag{18}$$

and where $S$ is the number of substructures in the structure. Thus one $\underset{\sim}{k}_{\nu}$ matrix and one $\underset{\sim}{m}_{\nu}$ matrix are defined for each value of the integer $\nu$.

The following characteristic equation is used in the solution of a structure with simply supported or guided ends.

$$\left(\underset{\sim}{k}_{\nu} - \tilde{\omega}^{2}_{k\nu}\,\underset{\sim}{m}_{\nu}\right)\underset{\sim}{\tilde{G}}_{\Delta k\nu} = \underset{\sim}{0} \tag{19}$$

The matrices $\underset{\sim}{k}_{\nu}$ and $\underset{\sim}{m}_{\nu}$ are square of order $n$, where $n$ is the number of boundary degrees of freedom on one substructure boundary. Therefore, Eq. 19

produces $n$ values of the eigenvalue $\tilde{\omega}_{k\nu}$ and of the eigenvector $\tilde{\underset{\sim}{\zeta}}_{\Delta k\nu}$ for each choice of the integer $\nu$. The eigenvalues which are obtained from Eq. 19 for each value of the integer $\nu$ are coupled in that they range from low values to high values in a definite pattern. The complete solution to the problem is obtained by evaluating Eq. 19 over the entire range of the integer $\nu$.

During the summer period, after studying the theory of the MDE method, the P.I. applied the technique in the solution of a simply supported beam. A beam type finite element was used in the solution. While working through the solution of this simple linear, elastic symmetric problem, many questions arose as to why the method worked in predicting natural frequencies and mode shapes of the simple beam. These questions concerned: (1) the definitions of $\theta_\nu$ and the matrices $\underset{\sim}{k}_\nu$ and $\underset{\sim}{m}_\nu$ ; (2) the basis of the associated characteristic equation; (3) why the natural frequencies occur in patterns of high-low pairs; (4) how the method could be revised to account for unsymmetrical elements; (5) how to incorporate nonlinear effects into the method; etc. Hence, it was concluded that additional study of the MDE method should be undertaken to ascertain the answers to these and related questions. However, this initial study of the MDE method provided enough background on the method to conclude that, if it can be extended to the nonlinear region and incorporated into computer codes like SAMSON2, extremely efficient computations could result.

The MDE method is based on a harmonic modal solution for which the damping matrix is defined as a linear function of the mass and the stiffness (proportional damping). The linear elastic solution process involves an explicit force balance technique. Hence, the following question needs to be

answered. Can the explicit force balance technique in MDE be extended to the nonlinear case?

The SAMSON2 code, developed by T. Belytschko and R. R. Robinson (Ref. 2) of the IIT Research Institute, uses an explicit time integration technique incorporating central finite difference equations to determine nodal accelerations, velocities and displacements resulting from the application of external loads. Strains, stresses and internal forces are determined from these nodal parameters through the use of constitutive equations and material properties. This finite difference technique can exhibit stability problems if the integration time step is too large. In many problems, many small elements are used to obtain the desired calculational accuracy and small time steps are used to guarantee the stability of the finite difference solution. This combination of many elements and many small time steps over the desired time interval results in a major computational task. Hence, there is a need to determine and implement more efficient techniques to reduce the computational effort required in solving these types of problems.

Implicit analysis schemes require matrix operations on a structure stiffness matrix in order to obtain the eigensolutions to any given problem. These implicit schemes do not exhibit computational stability problems in the solution process but they require operations, such as matrix inversion, on relatively large matrices. Explicit time integration techniques are subject to stability problems but do not require the use of matrix operations. The optimum solution technique, therefore, would be one which would use the best part of each type of solution, i.e., an implicit solution scheme with operations on a stiffness matrix of relatively low order. The MDE method has the potential of becoming the optimum solution technique.

During the summer 1984, it was learned that the higher order elements which presently exist in the SAMSON2 code do not work properly. It was also learned that, if these elements could be used in the solutions of problems, the computational process would be more efficient. Hence, it was concluded that, by studying the finite element theory for the higher order elements and comparing this theory to the higher order element definitions in the code and then correcting any errors existing in the code, the code would be more efficient. This study would also provide the necessary background in the finite element logic of the code in order to know where and how to incorporate the MDE approach into the code as MDE is developed

While at AFWL, it also was learned that the slideline model in the SAMSON2 code does not work as well as it was originally intended. Hence, it was concluded that a study should be initiated (1) to investigate the slideline model in order to change it to be more compatible with real world problems and (2) to begin the development of a finite element to replace the slideline model. This study would also provide the necessary background in the structure-media interface (SMI) concept in order to develop an SMI element which will be compatible with the MDE approach and the numerical integration schemes of the SAMSON2 code.

The slideline in the SAMSON2 code has no stiffness. Therefore, it has no harmonic solution, and the following question concerning the slideline concept needs to be answered. How is the slideline to be incorporated into the MDE method which involves a harmonic solution?

## II. OBJECTIVE

Finite element computer codes which are used to solve problems containing a large number of elements are expensive to run. The objective of this research is to effect computational efficiencies in numerical algorithms of continuum finite element codes using the matrix difference equation (MDE) approach. The research will center around the SAMSON2 code, but the general theory should be adaptable to other continuum finite element codes. The SAMSON2 code is a state-of-the-art research tool undergoing development within AFWL/NTE and is a two-dimensional code used for the dynamic analyses of plane and axisymmetric solids. The SAMSON2 code uses explicit time integration and is particularly suited for the analysis of large displacement, large strain problems involving nonlinear material behavior and structure-media interface (SMI) conditions.

During this study, material published by Dr. P. H. Denke and others at the McDonnell Douglas Corporation will be reviewed to determine the applicability of the MDE method to the solution of problems important to the AFWL. Much of what follows are amplifications and physical explanations of the original work.

## III. SCOPE

The scope of the work in this report deals with the study of the MDE theory to obtain the answers to the following questions.

1. What is the basis for the definition of $\theta_\nu$ ?
2. From where are the matrices $\underset{\sim}{k}_\nu$ and $\underset{\sim}{m}_\nu$ derived, and why do they work as defined?
3. Why do high-low frequency pairs occur for the different values of $\nu$ ?

## IV. RESEARCH FINDINGS

The purpose of this section is to provide the results obtained by performing work associated with the scope of this report.

Question 1. What is the basis for the definition of $\theta_\nu$ ?

The definition for $\theta_\nu$ (see p. 11) can be obtained by solving for the free lateral vibrations of a prismatic bar. This solution can be found in any textbook on vibrations (Ref. 3). Only enough of the development is presented here to show how $\theta_\nu$ is defined.

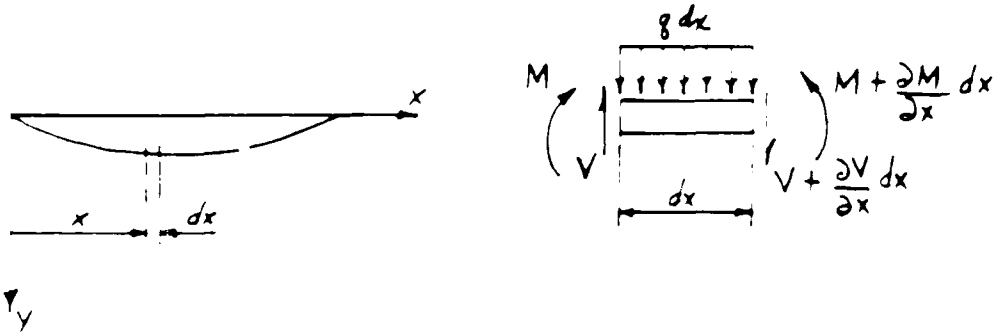



Fig. 3. Laterally Loaded Prismatic Beam

The motion of a vibrating beam is described by the partial differential equation (free vibrations, EI = constant)

$$a^2 \frac{\partial^4 y}{\partial x^4} = - \frac{\partial^2 y}{\partial t^2} \qquad (1)$$

where $a^2 = \frac{EI}{\gamma}$ EI = beam flexural stiffness

$\gamma$ = mass per unit length of the beam

and in which shear and rotary inertia have been neglected. The general solution to this equation is

$$y(x,t) = (C_1 \cosh kx + C_2 \sinh kx + C_3 \cos kx + C_4 \sin kx) A' \cos(\omega t - \phi) \quad (21)$$

where $$\omega = a k^2 \quad (22)$$

For a simply supported beam, the boundary conditions are

1) $y(0,t) = 0$ 2) $y(\ell,t) = 0$ 3) $\frac{\partial^2 y}{\partial x^2}(0,t) = -\frac{M}{EI} = 0$ 4) $\frac{\partial^2 y}{\partial x^2}(\ell,t) = -\frac{M}{EI} = 0$

From BC1 and BC3, $C_1 = C_3 = 0$.

From BC2 and BC4,

$$0 = C_2 \sinh k\ell + C_4 \sin k\ell \quad (23)$$

$$0 = C_2 \sinh k\ell - C_4 \sin k\ell \quad (24)$$

For a nontrivial solution, the determinant of the coefficients in Equations 23 and 24 must be zero. Hence,

$$\sinh k\ell \sin k\ell = 0 \quad (25)$$

Equation 25 can be satisfied provided $\sin k\ell = 0$.

Therefore, $$k\ell = n\pi \qquad n = 1, 2, 3, \ldots \qquad (26)$$

and $$k^2 = \frac{n^2\pi^2}{\ell^2} \qquad (27)$$

We now see from Equations 22 and 27 that a simply supported beam has an infinite number of natural frequencies and modes of vibration.

Note that in Equation 26, n is the number of half sine waves in the simply supported beam associated with each of the various natural modes. This equivalency for n can be verified by the following procedure.

Substitution of Equation 26 into either of Equations 23 or 24 gives $C_2 = 0$. Hence the general solution, Equation 21, reduces to

$$y(x,t) = C_n \sin \frac{n\pi x}{\ell} \cos (\omega_n t - \phi) \qquad (28)$$

Note that the term $\sin \frac{n\pi x}{\ell}$ is a shape function for which only the amplitude varies with time. Plots of $y = \sin \frac{n\pi x}{\ell}$ for n = 1, 2, 3 are as follows:

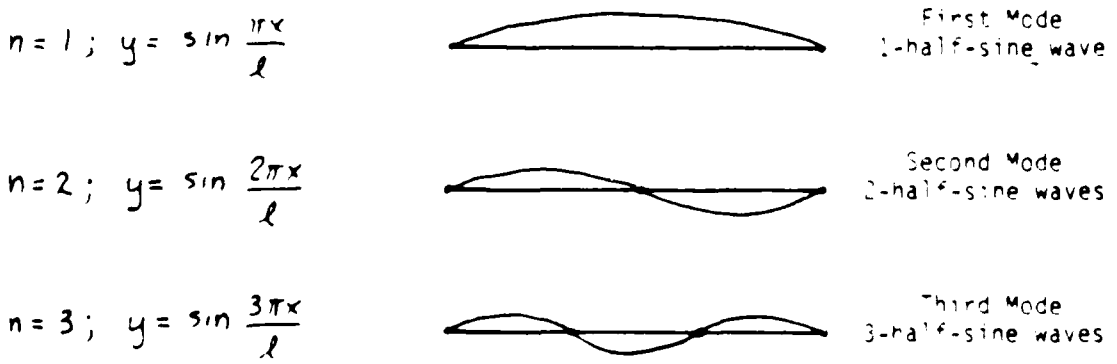



Fig. 3. Mode Shape Patterns

Mode shape patterns similar to those in Fig. 3 can be obtained for a finite number of the mode shapes for a simply supported beam if the length, $\ell$,

of the beam is represented by a finite number of equal length segments, s, where s is associated with the number of modes shapes desired. Then x in the sine term of Equation 28 is represented by a number, i, of the segments within the range of values of s.

For example, if the number of mode shapes desired is 3, then s = 3 and the length of each segment is $\ell/3$, and the beam is represented as shown in Fig. 4. We can write

$$kx = \frac{n\pi x}{\ell} = n\pi\left(\frac{x}{\ell}\right) \equiv \nu\pi\left(\frac{i}{s}\right) = \theta_\nu i \qquad (29)$$

where $kx \equiv \theta_\nu i$, $n \equiv \nu$ and $\frac{x}{\ell} \equiv \frac{i}{s}$ where i is the number of particular segments which locate a particular point along the beam. Hence $y = \sin\frac{\nu\pi i}{s} \equiv \sin\frac{n\pi x}{\ell}$ and the first three mode shape patterns are as shown. It is concluded from Equation 29, that

$$\theta_\nu = \frac{\nu\pi}{s} \qquad \nu = 0, 1, 2 \ldots s \qquad (30)$$

which is the symbolism used in the MDE theory.

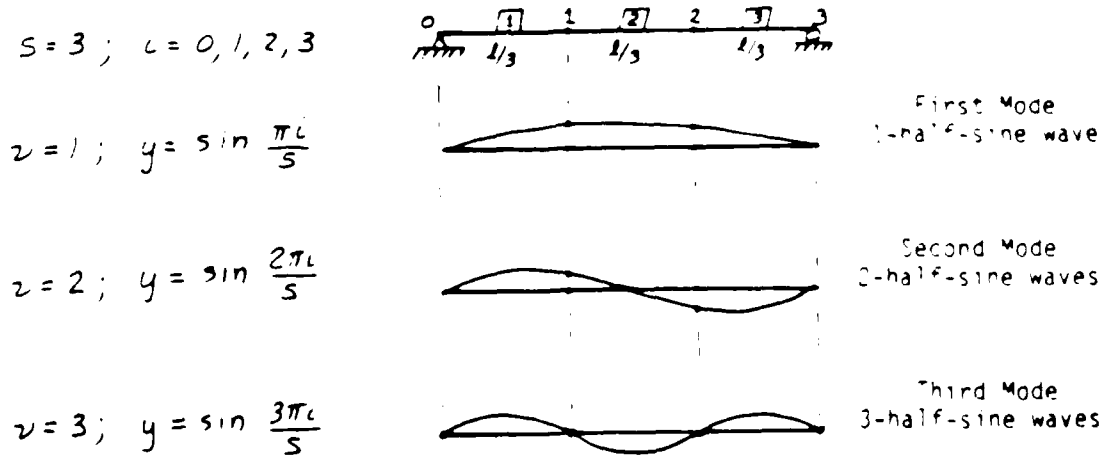



Fig. 4. Mode Shape Patterns

Question 2. From where are the matrices $\underline{k}_\nu$ and $\underline{m}_\nu$ derived, and why do they work as defined?

The matrices $\underline{k}_\nu$ and $\underline{m}_\nu$ (see p. 11) are derived from the substructure stiffness matrix $\underline{K}_B$ and the substructure mass matrix $\underline{M}_B$, respectively, by a transformation of the form

$$\underline{k}_\nu = \underline{T}_s^T \underline{K}_B \underline{T}_s \quad \text{and} \quad \underline{m}_\nu = \underline{T}_s^T \underline{M}_B \underline{T}_s$$

The coordinate transformation matrix, $\underline{T}_s$, is defined as

$$\underline{T}_s = \begin{bmatrix} \underline{I}_a a & 0 \\ 0 & \underline{I}_b b \\ \underline{I}_a b & 0 \\ 0 & \underline{I}_b a \end{bmatrix}$$

where $\underline{I}_a$ and $\underline{I}_b$ are unit matrices have $n_a$ (the number of a-type displacements and $n_b$ (the number of b-type displacements) rows, respectively, and where the scalars a and b are defined as

$$a = \cos\left(\frac{\pi}{4} - \frac{\theta_\nu}{2}\right)$$

$$b = \sin\left(\frac{\pi}{4} - \frac{\theta_\nu}{2}\right)$$

$$\theta_\nu = \frac{\pi \nu}{s} \qquad \nu = 0, 1, 2 \cdots s$$

The two different substructure displacement types are illustrated in Fig. 5. The transverse plane midway between the substructure boundaries is designated as the median cross-section. Type a displacements (vectors) are symmetric about the median cross-section and type b displacements are antisymmetric.

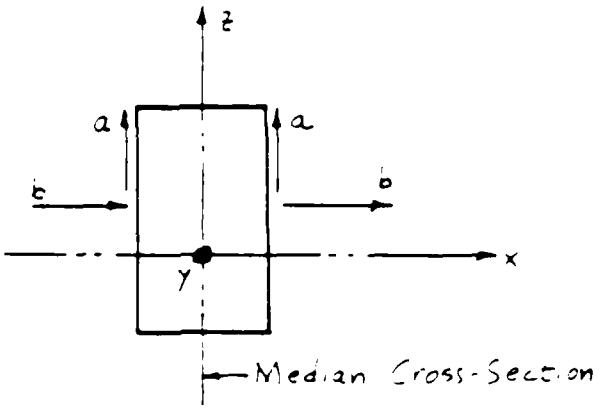



Fig. 5. Substructure Displacement Classification

The transformation, $\underline{T}_s$, has more rows than columns and, therefore, reduces the size of the problem. The forms of the scalars, a and b, have been chosen to preserve the symmetry and the antisymmetry properties of the a-type and b-type displacements through the transformation. The zeros in the transformation are also required in order to preserve the displacements in the proper order, i.e., a-type transform to a-type and b-type transform to b-type. In order for $\underline{b}_\nu$ and $\underline{m}_\nu$ to work as defined, they must be associated with the original substructure. A summary of the transformation procedure required to show this association is as follows.

$$\underline{\Delta}_B^{(c)} = \underline{T}_s \, \underline{\bar{\Delta}}_B^{(c)} \tag{31}$$

where $\underline{\Delta}_B^{(c)}$ is the matrix of the substructure boundary displacements (global sense) and $\underline{\bar{\Delta}}_B^{(c)}$ is the matrix of the transformed substructure boundary displacements (local sense).

Upon substitution

$$\begin{Bmatrix} \underline{\Delta}_{Bla}^{(c)} \\ \underline{\Delta}_{Blb}^{(c)} \\ \underline{\Delta}_{Bra}^{(c)} \\ \underline{\Delta}_{Brb}^{(c)} \end{Bmatrix} = \begin{bmatrix} \underline{I}_a & 0 \\ 0 & \underline{I}_b \\ \underline{I}_a & 0 \\ 0 & \underline{I}_b \end{bmatrix} \begin{Bmatrix} \underline{\bar{\Delta}}_{Ba}^{(c)} \\ \underline{\bar{\Delta}}_{Bb}^{(c)} \end{Bmatrix} \tag{32}$$

In Equation 32, $\underset{\sim}{\Delta}_{B}^{(i)}$ is partitioned according to a and b type displacements on the left and right sides of the substructure. The matrix $\underset{\sim}{\bar{\Delta}}_{B}^{(i)}$ has two partitions to correspond to the partitioning of $\underset{\sim}{r}_s$. The matrices $\underset{\sim}{\bar{\Delta}}_{Ba}^{(i)}$ and $\underset{\sim}{\bar{\Delta}}_{Bb}^{(i)}$ have $n_a$ rows and $n_b$ rows in order to be conformable with $\underset{\sim}{r}_a$ and $\underset{\sim}{r}_b$.

Expanding Equation 32 gives

$$\underset{\sim}{\Delta}_{Bla}^{(i)} = \underset{\sim}{\bar{\Delta}}_{Ba}^{(i)} \cos\left(\frac{\pi}{4} - \frac{\theta_\nu}{2}\right) \tag{33}$$

$$\underset{\sim}{\Delta}_{Blb}^{(i)} = \underset{\sim}{\bar{\Delta}}_{Bb}^{(i)} \sin\left(\frac{\pi}{4} - \frac{\theta_\nu}{2}\right) \tag{34}$$

$$\underset{\sim}{\Delta}_{Bra}^{(i)} = \underset{\sim}{\bar{\Delta}}_{Ba}^{(i)} \sin\left(\frac{\pi}{4} - \frac{\theta_\nu}{2}\right) \tag{35}$$

$$\underset{\sim}{\Delta}_{Brb}^{(i)} = \underset{\sim}{\bar{\Delta}}_{Bb}^{(i)} \cos\left(\frac{\pi}{4} - \frac{\theta_\nu}{2}\right) \tag{36}$$

Combining Equation 33 with 35 and Equation 34 with 36 gives

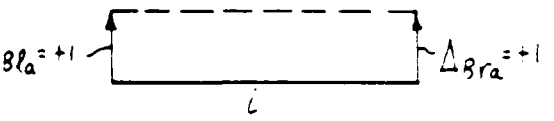
$$\frac{\Delta_{Bra_j}^{(i)}}{\Delta_{Bla_j}^{(i)}} = \frac{\sin\frac{\pi}{4}\left(1 - \frac{2\nu}{5}\right)}{\cos\frac{\pi}{4}\left(1 - \frac{2\nu}{5}\right)} \tag{37}$$

$$\frac{\Delta_{Brb_j}^{(i)}}{\Delta_{Blb_j}^{(i)}} = \frac{\cos\frac{\pi}{4}\left(1 - \frac{2\nu}{5}\right)}{\sin\frac{\pi}{4}\left(1 - \frac{2\nu}{5}\right)} \tag{38}$$

where, for example, $\Delta^{(i)}_{Bra_j}$ means the jth a-type displacement on the right hand boundary of the ith substructure and $\theta_\nu = \frac{\nu\pi}{s}$.

Equation 37 shows that the substructure is constrained so that the ratio of an a-type displacement on the right hand boundary to the corresponding displacement on the left hand boundary has a constant value for all degrees of freedom. This ratio depends on the integer $\nu$. The b-type displacements are similarly restrained. The constraints implied by the transformation, $T_s$, are shown for three values of $\nu$ in Figures 6, 7 and 8.

$$\frac{\Delta^{(i)}_{Bra_j}}{\Delta^{(i)}_{Bla_j}} = \frac{\sin\frac{\pi}{4}}{\cos\frac{\pi}{4}} = \tan\frac{\pi}{4} = \frac{1}{1}$$




$$\frac{\Delta^{(i)}_{Brb_j}}{\Delta^{(i)}_{Blb_j}} = \frac{\cos\frac{\pi}{4}}{\sin\frac{\pi}{4}} = \cot\frac{\pi}{4} = \frac{1}{1}$$

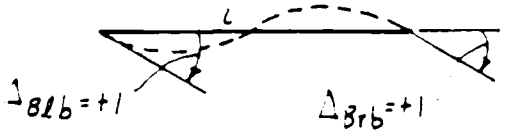
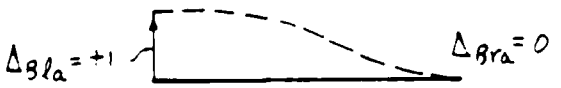



Fig. 6. Substructure Constraints for $\nu = 0$

$$\frac{\Delta^{(i)}_{Bra_j}}{\Delta^{(i)}_{Bla_j}} = \frac{\sin 0}{\cos 0} = \frac{0}{1}$$




$$\frac{\Delta^{(i)}_{Brb_j}}{\Delta^{(i)}_{Blb_j}} = \frac{\cos 0}{\sin 0} = \frac{1}{0}$$

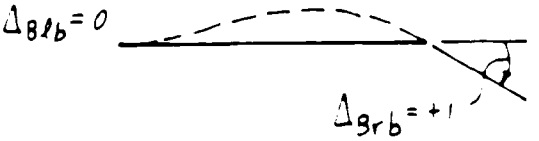



Fig. 7. Substructure Constraints for $\nu = \frac{s}{2}$

$$\frac{\Delta^{(i)}_{Brq_j}}{\Delta^{(i)}_{Blq_j}} = \frac{\sin\frac{-\pi}{4}}{\cos\frac{-\pi}{4}} = \tan\frac{-\pi}{4} = -\frac{1}{1}$$

$$\frac{\Delta^{(i)}_{Brb_j}}{\Delta^{(i)}_{Blb_j}} = \frac{\cos\frac{-\pi}{4}}{\sin\frac{-\pi}{4}} = \cot\frac{-\pi}{4} = -\frac{1}{1}$$

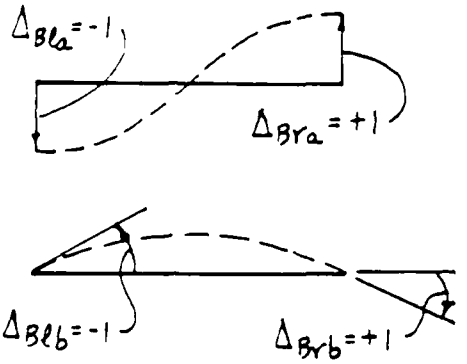



Fig. 8. Substructure Constraints for $\nu = s$

These constraints can be realized physically by mechanical linkages that require the ratios to have the values shown. In particular from Fig. 7 for $\nu = \frac{s}{2}$, all a-type displacements on the right hand boundary and b-type displacements on the left hand boundary are constrained to be zero as shown. Similarly from Fig. 6, the a-type and b-type displacements have equal magnitudes with the same sign and from Fig. 8, the displacements have the same magnitudes but opposite signs. Therefore, the constrained structure is a real structure, and its stiffness and mass matrices are positive definite, for all values of $\nu$.

Upon substitution of $\underset{\sim}{K}_B$ and $\underset{\sim}{T}_s$, the matrix $\underset{\sim}{k}_\nu$ becomes

$$\underset{\sim}{k}_\nu = \left[\begin{array}{c|c} p_{aa}(a^2+b^2) + q_{aa} * 2ab & q_{ab}(a^2-b^2) \\ \hline q_{ab}^T(a^2-b^2) & p_{bb}(a^2+b^2) + q_{bb} * 2ab \end{array}\right] \tag{39}$$

Noting that $a^2+b^2=1$ ; $a^2-b^2=\sin\theta_\nu$ ; $2ab=\cos\theta_\nu$

$$\underset{\sim}{k}_\nu = \left[\begin{array}{c|c} p_{aa}+q_{aa}\cos\theta_\nu & q_{ab}\sin\theta_\nu \\ \hline q_{ab}^T\sin\theta_\nu & p_{bb}+q_{bb}\cos\theta_\nu \end{array}\right] \tag{40}$$

Similarly

$$\underset{\sim}{m}_\nu = \left[\begin{array}{c|c} m_{aa}+n_{aa}\cos\theta_\nu & n_{ab}\sin\theta_\nu \\ \hline n_{ab}^T\sin\theta_\nu & m_{bb}+n_{bb}\cos\theta_\nu \end{array}\right] \tag{41}$$

Thus $\underset{\sim}{k}_\nu$ and $\underset{\sim}{m}_\nu$ are stiffness and mass matrices of the original substructure modified by the constraints implied by the transformations. These constraints can be physically realized. Therefore, $\underset{\sim}{k}_\nu$ and $\underset{\sim}{m}_\nu$ are stiffness and mass matrices of a real structure. They are therefore positive definite, and the eigenvalues $\tilde{\omega}^2_{k\nu}$ of the frequency equation

$$\left[\underset{\sim}{k}_\nu - \tilde{\omega}^2_{k\nu}\,\underset{\sim}{m}_\nu\right]\underset{\sim}{G}_{\Delta k\nu} = \underset{\sim}{0} \tag{42}$$

are real and positive. The corresponding eigenvectors $\underset{\sim}{G}_{\Delta k\nu}$ are real.

Question 3. Why do high-low frequency pairs occur for the different values of $\nu$ ?

The answer to this question is found by examining the solution to Equation 13, which is rewritten here for continuity.

$$\left[ \underset{\sim}{A}_{Blr} \hat{\lambda}_k^2 + (\underset{\sim}{\hat{A}}_{Bll} + \underset{\sim}{\hat{A}}_{Brr}) \hat{\lambda}_k + \underset{\sim}{\hat{A}}_{Brl} \right] \underset{\sim}{\hat{G}}_{\Delta k} = \underset{\sim}{0} \qquad (13)$$

The $\underset{\sim}{A}$ matrices in this equation are of order $\hat{n}$ and the characteristic equation has $2\hat{n}$ eigensolutions, since it is quadratic.

By dividing the $\hat{\lambda}_k$ and rearranging the terms in Equation 13, the characteristic equation can be written in the following form

$$\left( \underset{\sim}{\hat{A}}_{Brl} \frac{1}{\hat{\lambda}_k} + \underset{\sim}{\hat{A}}_{Bll} + \underset{\sim}{\hat{A}}_{Brr} + \underset{\sim}{A}_{Brl} \hat{\lambda}_k \right) \underset{\sim}{\hat{G}}_{\Delta k} = \underset{\sim}{0} \qquad (43)$$

For a nontrivial solution of the characteristic equation to exist, the determinant of the coefficient matrix must be zero, i.e.,

$$\left| \underset{\sim}{\hat{A}}_{Brl} \frac{1}{\hat{\lambda}_k} + \underset{\sim}{\hat{A}}_{Bll} + \underset{\sim}{\hat{A}}_{Brr} + \underset{\sim}{\hat{A}}_{Blr} \hat{\lambda}_k \right| = 0 \qquad (44)$$

The rows and the columns in a determinant may be interchanged without changing its value.

Therefore,

$$\left| \underset{\sim}{\hat{A}}^T_{Brl} \frac{1}{\hat{\lambda}_k} + \underset{\sim}{\hat{A}}^T_{Bll} + \underset{\sim}{\hat{A}}^T_{Brr} + \underset{\sim}{\hat{A}}^T_{Blr} \hat{\lambda}_k \right| = 0 \qquad (45)$$

The boundary impedance matrix can be written in partitioned form as

$$\hat{\underset{\sim}{A}}_B = \left[\begin{array}{c|c} \hat{\underset{\sim}{A}}_{Bll} & \hat{\underset{\sim}{A}}_{Blr} \\ \hat{\underset{\sim}{A}}_{Brl} & \hat{\underset{\sim}{A}}_{Brr} \end{array}\right] \tag{46}$$

This impedance matrix is symmetric, therefore

$$\hat{\underset{\sim}{A}}_{Blr} = \hat{\underset{\sim}{A}}_{Brl}$$

$$\hat{\underset{\sim}{A}}^T_{Bll} = \hat{\underset{\sim}{A}}_{Bll}$$

$$\hat{\underset{\sim}{A}}^T_{Blr} = \hat{\underset{\sim}{A}}_{Blr}$$

$$\hat{\underset{\sim}{A}}^T_{Brr} = \hat{\underset{\sim}{A}}_{Brr}$$

Hence, if $\hat{\lambda}_k$ in Equation 45 is replaced by $1/\hat{\lambda}_k$, the characteristic equation is still satisfied. Therefore, if $\hat{\lambda}_k$ is an eigenvalue, then its reciprocal, $1/\hat{\lambda}_k$, is also an eigenvalue.

Let $\hat{\lambda}_k \equiv \hat{\lambda}_{l_k}$ be an eigenvalue of the characteristic equation, and let $\hat{\lambda}_{g_k} \equiv 1/\hat{\lambda}_{l_k} \equiv 1/\hat{\lambda}_k$ for which $\hat{\lambda}_{g_k}$ must also be an eigenvalue. Hence

$$\hat{\lambda}_{l_k} * \hat{\lambda}_{g_k} = 1 \tag{47}$$

The conclusion is that the eigenvalues occur in reciprocal pairs, such that, one of the values is associated with a low(er) frequency and one with a

great(er) frequency. The subscripts $\ell$ and $g$ refer to "lower" and "greater" as implied in the definitions.

A study of the SAMSON2 code was conducted concurrently with the study of the MDE method. The study concerning the SAMSON2 code has not been completed at this writing and is currently supported by funding provided by the Air Force Weapons Laboratory. However, the SAMSON2 study has progressed far enough to form the conclusion that the results of the SAMSON2 study will not change the findings pertinent to the MDE method as stated in this report. The intermediate results available at this time from the SAMSON2 study will not be reported here but will be discussed in detail in a final report to the AFWL in 1986.

## V. DISCUSSION

The SAMSON2 code is a two-dimensional code to be used for dynamic structural analysis of plane and axisymmetric solids. The program uses explicit time integration and is particularly suited to the analysis of large displacement, large strain problems involving nonlinear material behavior and structure-media (SMI) problems.

In contrast, the Matrix Difference Equation (MDE) method is a hybrid approach that can be expected to increase the efficiency of the finite element analysis only for a particular class of structures. The MDE method is applicable only to periodic structures and is based on the following assumptions.

1. The structure is represented by a finite element model.
2. The model is longitudinally periodic which requires the axis of a linear array of identical substructures to be a straight line.
3. Strains are linear functions of displacements, stresses are linear functions of strains and loads are linear functions of stresses (i.e., geometric and material linearity).
4. Forcing functions are sinusoidal functions of time of a single frequency. Forcing functions include external loads, support displacements and element unassembled deformations. Each forcing function can have its own amplitude and phase angle. Responses to forcing functions of different frequencies can be separately calculated and superimposed in the time domain because of the assumed linearity.
5. The substructure is symmetric about a median plane normal to the longitudinal axis (i.e., longitudinal symmetry).
6. The ends of the structure are simply supported or guided according to generalized definitions.

7. The assembled substructure damping matrix is a linear combination of the assembled mass and stiffness matrices (i.e., proportional damping.

An advantage of the MDE method compared to conventional finite-element analysis is that the responses in the MDE method, such as displacements, are given in closed-form exponential and sinusoidal functions of the longitudinal coordinate. As a result, a significant cost savings in computing should be realized compared to the conventional approach. For example, all of the natural modes and frequencies of a periodic structure of a particular type can be found by calculating the eigensolutions of characteristic equations equal in order to the number of degrees of freedom on one substructure boundary.

An advantage of the MDE approach compared to differential equation analysis employing ordinary or partial differential equations with constant coefficients is that while the structure must be longitudinally periodic, it need not be uniform in any direction, and any boundary conditions can exist along the edges.

However, the SAMSON2 code does not fall into either the category of conventional finite element analysis or that of linear ordinary or partial differential equations with constant coefficients. Therefore, the advantages previously mentioned are not applicable to the SAMSON2 code. In fact, it is the opinion of the writer that the MDE method cannot be incorporated successfully into the SAMSON2 code because the MDE method is too restrictive in its development and use. A list of disadvantages of the MDE method pertinent to the SAMSON2 code is as follows:

1. The structure must be longitudinally periodic. (The SAMSON2 code is used frequently for the solutions of axisymmetric problems.)

2. The structure must have pinned or guided ends. (Too restrictive for SAMSON2.) The solutions to problems with other end conditions by the MDE method are very complicated.

3. The MDE method is founded on linearity. (In direct conflict with the nonlinear capability in SAMSON2.)

4. The substructures must be symmetrical about a median line. (This would eliminate the use of some elements in SAMSON2, e.g., all forms of the triangular element.)

5. Only sinusoidal forcing functions may be used with the MDE method. (It would be difficult to model the high amplitude pressure wave used in the SAMSON2 code as a sine wave.)

6. The MDE method requires the use of a stiffness matrix. (SAMSON2 is based on explicit time integration for which there is no requirement to compute a stiffness matrix.)

7. Weighting factors are needed to obtain solutions by the MDE method for end conditions other than pinned ends or guided ends. These weighting factors have not been derived.

8. The equilibrium condition used in the MDE method results in untransformed forces that only approximately satisfy equilibrium at a loaded boundary. (Dynamic equilibrium is satisfied in the SAMSON2 code through the use of the equation of motion.)

9. The MDE method requires the use of the principle of superposition. Hence, only small displacements are allowed. (Large displacements must be allowed in the code because of the extremely high magnitudes of loads in AFWL problems.) It is the opinion of the writer that the extension of the MDE method to incorporate nonlinear capabilities would be an enormous task.

10. In conventional finite element procedures, a set of equations is solved based on one independent equation per degree of freedom, i.e., per unknown displacement in the problem. In the MDE method, a coordinate transformation is performed to reduce the number of unknowns (displacements) in the problem in order to reduce the computational time required in the solution (refer to the discussion on p. 20).

In MDE, the number of end conditions is equal to twice the number of degrees of freedom on one substructure boundary. Hence, the actual number of scalar equations available for the solution is 2n, where n = the number of degrees of freedom per substructure boundary. After the transformation is applied, the number of unknowns is $2\hat{n}$, where $\hat{n}$ = the number of transformed degrees of freedom per substructure boundary.

Thus, in the MDE method, there exist 2n scalar equations and $2\hat{n}$ unknowns with the number of equations greater than the number of unknowns. Consequently, no solution exists that exactly satisfies all of the equations. However, an approximate solution is obtained based on the method of least squares, which is applicable when a set of real equations has more equations than unknowns. The least squares method gives a solution for which the sum of the squares of the residuals (errors) of the equations being solved is a minimum.

11. The eigenvalues obtained in the MDE method occur in reciprocal related pairs; one low frequency value and one high frequency value. The higher frequency values and the corresponding mode shapes produced by the MDE method tend to be inaccurate and unreliable (the error is greater than 25% even in relatively small problems) and should be discarded. (In many problems of interest to the Air Force the higher frequencies of vibration can contribute significantly to the solution.) The errors result from

several approximations inherent in the MDE method. A discussion of several approximations is given briefly in the following paragraphs.

Errors are attributed to the substructure mass matrix, which is approximate. This mass matrix approximation is associated with the Guyan transformation used in the MDE method as discussed in the following paragraphs.

A Guyan transformation (Ref. 4) is used in the MDE method to reduce the size of the problem. Just as it is necessary to reduce the size of the stiffness matrix for the static structural analysis, the simultaneous reduction of the nondiagonal mass matrix for natural mode analysis is also required.

The general static structural equations

$$\underset{\sim}{F} = \underset{\sim}{K}\,\underset{\sim}{X} \qquad \text{(Force = stiffness * displacement)}$$

can be arranged, so that after partitioning, the following form exists.

$$\begin{bmatrix} \underset{\sim}{F}_B \\ \underset{\sim}{F}_I \end{bmatrix} = \begin{bmatrix} \underset{\sim}{K}_{BB} & \underset{\sim}{K}_{BI} \\ \underset{\sim}{K}_{IB} & \underset{\sim}{K}_{II} \end{bmatrix} \begin{bmatrix} \underset{\sim}{X}_B \\ \underset{\sim}{X}_I \end{bmatrix} \qquad \begin{matrix} B = \text{boundary} \\ I = \text{interior} \end{matrix} \tag{48}$$

Upon expansion, the two resulting equations are

$$\underset{\sim}{F}_B = \underset{\sim}{K}_{BB}\underset{\sim}{X}_B + \underset{\sim}{K}_{BI}\underset{\sim}{X}_I \tag{49}$$

$$\underset{\sim}{F}_I = \underset{\sim}{K}_{IB}\underset{\sim}{X}_B + \underset{\sim}{K}_{II}\underset{\sim}{X}_I \tag{50}$$

From Equation 50

$$\underset{\sim}{X}_I = \underset{\sim}{K}_{II}^{-1}\left(\underset{\sim}{F}_I - \underset{\sim}{K}_{IB}\underset{\sim}{X}_B\right) \tag{51}$$

Substituting Equation 51 into Equation 49 gives

$$\underset{\sim}{F}_B^E = \underset{\sim}{K}_B \underset{\sim}{X}_B \tag{52}$$

where $$\underset{\sim}{K}_B = \underset{\sim}{K}_{BB} - \underset{\sim}{K}_{BI} \underset{\sim}{K}_{II}^{-1} \underset{\sim}{K}_{IB} \tag{53}$$

and $$\underset{\sim}{F}_B^E = \underset{\sim}{F}_B - \underset{\sim}{K}_{BI} \underset{\sim}{K}_{II}^{-1} \underset{\sim}{F}_I \tag{54}$$

Note in Equation 54 that $\underset{\sim}{F}_B$ is a matrix of actual loads applied to the boundary, while $\underset{\sim}{F}_B^E$ is a matrix of equivalent boundary loads.

In a Guyan reduction the internal forces, $\underset{\sim}{F}_I$, are eliminated, i.e., $\underset{\sim}{F}_I = \underset{\sim}{0}$. Hence, with $\underset{\sim}{F}_I = \underset{\sim}{0}$, Equations 51 through 54 give

$$\underset{\sim}{X}_I = - \underset{\sim}{K}_{II}^{-1} \underset{\sim}{K}_{IB} \underset{\sim}{X}_B \tag{55}$$

$$\underset{\sim}{F}_B^E = \underset{\sim}{F}_B = \underset{\sim}{K}_B \underset{\sim}{X}_B \tag{56}$$

and $$\underset{\sim}{K}_B = \underset{\sim}{K}_{BB} - \underset{\sim}{K}_{BI} \underset{\sim}{K}_{II}^{-1} \underset{\sim}{K}_{IB} \tag{57}$$

By comparing Equations 51 and 55, one can see that an error exists in calculating interior displacements, because the effects of the interior loads are not included in a Guyan transformation, i.e., $\underset{\sim}{F}_I = \underset{\sim}{0}$.

The Guyan transformation, $\underline{T}_G$, which produces Equation 55 is

$$\underline{T}_G = \begin{bmatrix} \underline{I} \\ -\underline{K}_{II}^{-1} \underline{K}_{IB} \end{bmatrix} \tag{58}$$

or in equation form, $\underline{X} = \underline{T}_G \underline{X}_B$ , or

$$\begin{bmatrix} \underline{X}_B \\ \underline{X}_I \end{bmatrix} = \begin{bmatrix} \underline{I} \\ -\underline{K}_{II}^{-1} \underline{K}_{IB} \end{bmatrix} \begin{bmatrix} \underline{X}_B \end{bmatrix} \tag{59}$$

If the structure energies are written $T = \frac{1}{2} \dot{\underline{X}}^T \underline{M} \dot{\underline{X}}$ (kinetic energy) and $V = \frac{1}{2} \underline{X}^T \underline{K} \underline{X}$ (potential energy) and the Guyan transformation, $\underline{T}_G$, is used, the result is (Ref. 5)

$$T = \frac{1}{2} \dot{\underline{X}}_B^T \left( \underline{T}_G^T \underline{M} \underline{T}_G \right) \dot{\underline{X}}_B = \frac{1}{2} \dot{\underline{X}}_B^T \underline{M}_R \dot{\underline{X}}_B \tag{60}$$

$$V = \frac{1}{2} \underline{X}_B^T \left( \underline{T}_G^T \underline{K} \underline{T}_G \right) \underline{X}_B = \frac{1}{2} \underline{X}_B^T \underline{K}_R \underline{X}_B \tag{61}$$

from which the reduced stiffness is seen to be

$$\underline{K}_R = \underline{T}_G^T \underline{K} \underline{T}_G \tag{62}$$

and the reduced mass matrix is seen to be

$$\underset{\sim}{M}_R = \underset{\sim}{T}_G^T \underset{\sim}{M} \underset{\sim}{T}_G \tag{63}$$

Evaluation of Equation 62 gives

$$\underset{\sim}{K}_R = \underset{\sim}{K}_{BB} - \underset{\sim}{K}_{BI} \underset{\sim}{K}_{II}^{-1} \underset{\sim}{K}_{IB} \equiv \underset{\sim}{K}_B \tag{64}$$

which is identical to Equation 57.

If the nondiagonal mass matrix is taken as

$$\underset{\sim}{M} = \begin{bmatrix} \underset{\sim}{M}_{BB} & \underset{\sim}{M}_{BI} \\ \underset{\sim}{M}_{IB} & \underset{\sim}{M}_{II} \end{bmatrix} \tag{65}$$

the reduced mass matrix resulting from Equation 63 is

$$\underset{\sim}{M}_R = \underset{\sim}{M}_{BB} - \underset{\sim}{M}_{BI} \underset{\sim}{K}_{II}^{-1} \underset{\sim}{K}_{IB} - \left(\underset{\sim}{K}_{II}^{-1} \underset{\sim}{K}_{IB}\right)\left(\underset{\sim}{M}_{IB} - \underset{\sim}{M}_{II} \underset{\sim}{K}_{II}^{-1} \underset{\sim}{K}_{IB}\right) \tag{66}$$

From Equation 64 it can be seen that in the case of the reduced stiffness matrix, none of the structural complexity is lost by the Guyan transformation, since all elements of the original stiffness matrix contribute. However, in the reduced mass matrix, combinations of stiffnesses and mass elements appear. The result is that the eigensolution problem is not exactly preserved.

Applying the Guyan reduction in the MDE method to the dynamic problem results in another approximation, which is associated with inertia loads. As previously discussed, the Guyan reduction is based on the assumption that interior displacements result from imposed boundary displacements and not from interior loads which are assumed to be zero. Hence, in the dynamic case, large interior inertia loads can be acting even if no external loads are applied to interior nodes.

## VI. CONCLUSIONS

Based on the previous discussion, it is concluded that the potential for the Matrix Difference Equation method to effect any significant computational efficiencies in the SAMSON2 finite element code being developed at AFWL/NTE is very low.

## VII. RECOMMENDATIONS

It is hereby recommended that financial support by the Air Force for future research on the MDE method for possible incorporation into large displacement, large strain type finite element codes be discontinued.

Future work to determine the feasibility of the MDE method for incorporation into more conventional linear elastic finite element codes, because of the reduction in the order matrices used in the MDE method, could be supported.

## VIII. REFERENCES


1. P. H. Denke, G. R. Eide and J. Pickard, "Matrix Difference Equation Analysis of Vibrating Periodic Structures," AIAA Journal, Vol. 13, No. 2, 1975, pp. 160-166.

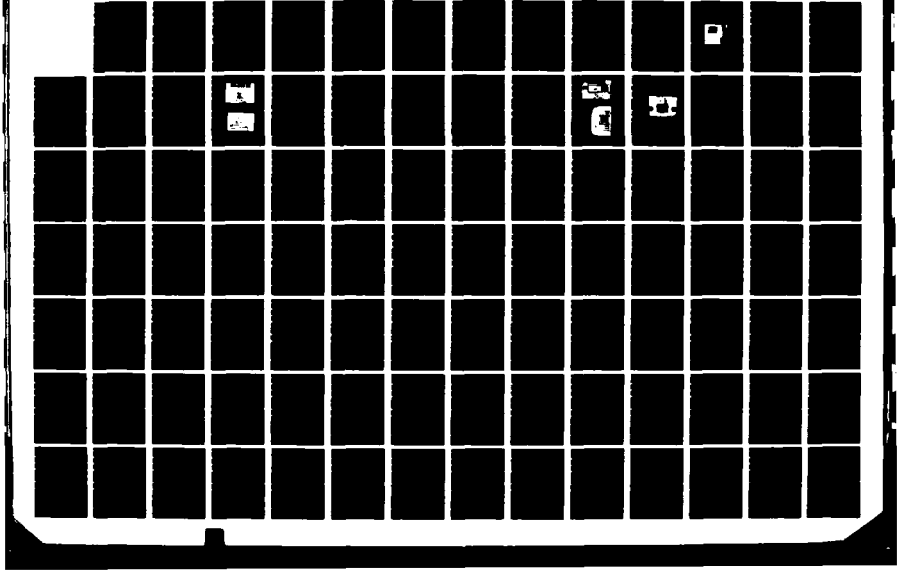
2. T. Belytschko and R. R. Robinson, "SAMSON2: A Nonlinear Two-Dimensional Structure/Media Interaction Computer Code," AFWL Final Report, No. AFWL-TR-81-109, January 1982.

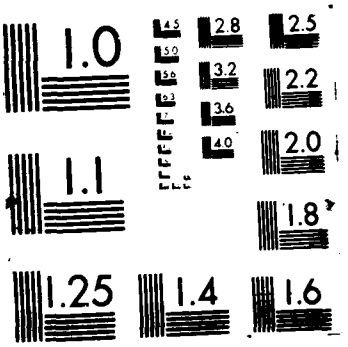
3. G. L. Downey and G. M. Smith, Advanced Dynamics, International Textbook Company, 1960.

4. R. J. Guyan, "Reduction of Stiffness and Mass Matrices," AIAA Journal, Vol. 3, No. 2, p. 380, 1965.

5. R. W. Clough and J. Penzien, Dynamics of Structures, McGraw-Hill Book Company, 1975.

AD-A186 490 UNITED STATES AIR FORCE RESEARCH INITIATION PROGRAM 03/11
1984 RESEARCH REPORTS (U) SOUTHEASTERN CENTER FOR
ELECTRICAL ENGINEERING EDUCATION INC S W D PEELE
UNCLASSIFIED MAY 86 AFOSR-TR-87-1721 F49620-82-C-0035 F/G 15/1 NL




1.0
1.1
1.25
1.4
1.6
2.8
3.2
3.6
4.0
2.5
2.2
2.0
1.8

## IX. BIBLIOGRAPHY


1. C. S. Desai and J. F. Abel, Introduction to the Finite Element Method, Van Nostrand Reinhold Company, 1972.

2. O. C. Zienkiewicz, The Finite Element Method in Engineering Science, McGraw-Hill Book Company, London, 1971.

3. G. Sengupta, "Vibration of Periodic Structures," The Shock and Vibration Digest, Vol. 12, No. 3, March 1980.

4. T. J. R. Hughes and T. Belytschko, "A Précis of Developments in Computational Methods of Transient Analysis," Journal of Applied Mechanics, Vol. 50, December 1983, pp. 1033-1041.

5. D. E. Newland, Random Vibrations and Spectral Analysis, Longman, 1975.

6. D. G. Fertig, Dynamics and Vibration of Structures, John Wiley and Sons, Inc., 1973.

7. J. E. Bowles, Foundation Analysis and Design, Third Edition, McGraw-Hill Book Company, 1982.

8. W. F. Chen, Plasticity in Reinforced Concrete, McGraw-Hill Book Company, 1982.

9. R. L. Burden, D. J. Faires and A. C. Reynolds, Numerical Analysis, Second Edition, Prindle, Weber and Schmidt Publishers, Boston, 1978.

10. S. H. Crandall, Engineering Analysis -- A Survey of Numerical Procedures, McGraw-Hill Book Company, 1956.

11. R. R. Craig, Jr., Structural Dynamics, John Wiley and Sons, Inc., 1981.

12. C. P. Johnson, R. R. Craig, Jr. and A. Yarigicoglu, "Quadratic Reduction for the Eigenproblem," International Journal for Numerical Methods in Engineering, Vol. 15, 1980, pp. 911-923.

13. K-J Bathe, Finite Element Procedures in Engineering Analysis, Prentice-Hall, Inc., 1982.

14. S. Timoshenko and D. H. Young, Vibration Problems in Engineering, Third Edition, D. Van Nostrand Co., Inc., 1955.

1985 USAF-SCEEE RESEARCH INITIATION PROGRAM

Sponsored by the

AIR FORCE OFFICE OF SCIENTIFIC RESEARCH

Conducted by the

SOUTHEASTERN CENTER FOR ELECTRICAL ENGINEERING EDUCATION

FINAL REPORT

# CENTRIFUGE MODEL STUDY AND FINITE ELEMENT ANALYSIS OF BURIED CONCRETE BOX CULVERTS


| | |
|---|---|
| Prepared by: | Dr. Yong S. Kim |
| Academic Rank: | Assistant Professor |
| Department and University: | Department of Civil and Mechanical Engineering<br>McNeese State University |



| | |
|---|---|
| Research Period: | January 1, 1985 - November 30, 1985 |
| Contract No.: | F49620-82-C-0035 |

## ABSTRACT

The centrifuge model technique is used to evaluate the behavior of a of 5-in. X 5-in. concrete box culvert under a 4-in. backfill soil.

Two different types of soil installations are studied: embankment and trench. Results of the centrifuge model study for both installations are compared with each other, and with predictions of a finite element code, CANDE (Culvert ANalysis and DEsign).

Furthermore, the influence of soil stiffness for backfill is studied using finite element analyses. The results of CANDE analyses including nonlinear constitutive models for characterizing culvert and soil, incremental construction and free vertical movement with a symmetric mesh are reported.

# SECTION I

# INTRODUCTION

## A. Purpose

During the past decade, research on soil-structure interaction of circular culverts under embankments was performed by numerous research groups. Empirical data on soil pressure distributions and structural stresses and deflections has been collected for shallow to moderate depth installations. As a result, the soil-structure interaction problems of circular culverts embedded in embankments are better understood, and new design and analysis procedures are being proposed. However, research on box culverts has been limited, and the behavior of box culverts is not well understood. Due to an increased number of box culvert projects (i.e., protective structures), a better understanding of soil-structure interaction and more accurate calculation of soil pressure distributions and concrete section behavior are required. The purpose of this research is, therefore, to study the behavior of buried box culverts under embankments using centrifuge modeling technique and numerical simulations.

## B. Objective

The primary objective of this study is to investigate the soil-structure interaction problems of concrete box culverts under backfills. More specifically, the objectives of this study are to:

1. Develop an experimental technique to simulate the behavior of a prototype box culvert in a centrifuge.

2. Conduct a preliminary series of centrifuge model experiments on a small capacity centrifuge in order to determine the influence of installation types (embankment and trench) on the behavior of the box culvert.

3. Predict the behavior of the box culvert using finite element analysis.

4. Gain experience necessary for model studies in a large capacity centrifuge.

C. Scope

With these objectives in mind, the research is reported in the following sections. They contain a description of the centrifuge facilty used for model study; design and fabrication of an accompanying testing apparatus; investigation of the influence of installation types using a centrifuge model technique and finite element analysis; and investigation of the influence of soil types using finite element analysis. Finally, some potential topics for future research in this area are mentioned.

## SECTION II

## CENTRIFUGE MODEL STUDY

### A. Fundamentals of Centrifuge Modeling

One of the most ideal approaches for obtaining information on the behavior of protype structures is full-scale model testing. A full scale model with the necessary insrumentation (i.e. soil stress meters, pore water pressure transducers, settlement gages and strain gages, etc.) could give the best results for estimating prototype behavior.

Unfortunately, full-scale model testing has serious major drawbacks: mainly, cost and time of construction and operation. Because of these reasons, small scale model testing is becoming a favorite testing method in geotechnical engineering.

However, use of small scale model tests in the laboratory is severely limited when the gravity body force of the structure itself is the principal load on the system, such as in dams and embankments. This limitation is due to two major factors. One is that soil characteristics are nonlinear and overburden dependent, and the other involves stress magnitudes. The stresses in a small scale model due to its own weight are much smaller in magnitude than those in the corresponding prototype system. To eliminate these deficiences, the centrifuge modeling technique has been used since 1931. The increase in unit weight is achieved by placing a model in a centrifuge and spinning it to produce an acceleration field that is equivalent to an artificial gravitational field. In this way the state of stress at every point in the model under an artificial gravitational field is

equal to that at the homologous point in the prototype. This technique has been applied to a variety of geotechnical problems (slope stability, reinforced earth, foundation design, offshore gravity platforms, rockfill dams, tunnels, and burried circular pipes) reported elsewhere (References 1,2,3,4 and 5). Table 2.1 summarizes the scaling rules that have been developed for relating the behavior of the centrifuge model and an equivalent full scale geotechnical structure.

## B. The Centrifuge and Monitoring Systems

### 1. The Centrifuge

The University of California, Davis' geotechnical centrifuge (Schaevitz Type B-8-D rotary accelerator) was used for the present model study. It was designed to apply controlled centrifugal accelerations up to 175 g's or 10,000 g-lbs at a nominal radius of 39 inches. It is capable of reaching a maximum speed of 390 RPM.

The centrifuge includes a welded steel framework to prevent vibration. Sub-assembles including the drive motor, the timing belt drive, the RPM pick-up, the rotating arm assembly, and the terminal box for control and test connections are supported within this framework.

There are two types of buckets available to carry the model; the Schaevitz stationary type and the swing-up type. In this study the swing-up bucket was used. This bucket is held by two arms attached to the spokes by two pivots. This permits the soil surface to remain perpendicular to the vector sum of centrifuge acceleration and the acceleration due to gravity.

Table 2.1 Scaling Relations (Reference 6)

| Quantity | Full Scale (Prototype) | Centrifugal Model at n g's |
|---|---|---|
| Linear Dimension | 1 | $1/n$ |
| Area | 1 | $1/n^2$ |
| Volume | 1 | $1/n^3$ |
| Time | | |
| In Dynamic Terms | 1 | $1/n$ |
| In Diffusion Cases | 1 | $1/n^2$ |
| In Viscous Flow Cases | 1 | 1 |
| Velocity (Distance/Time) | 1 | 1 |
| Acceleration (Distance/Time ) | 1 | n |
| Mass | 1 | $1/n^3$ |
| Force | 1 | $1/n^2$ |
| Energy | 1 | $1/n^3$ |
| Stress (Force/Area) | 1 | 1 |
| Strain (Displacement/Unit Length) | 1 | 1 |
| Density | 1 | 1 |
| Energy Density | 1 | 1 |
| Frequency | | |
| In Dynamic Terms | 1 | n |

Hydraulic and electrical services are available to the model in flight. The hydraulic lines may be used to conduct compressed air or fluids from the outside control area to the model. Eighteen electrical channels are available for sending power to and receive signals from transducers which monitor behavior of the model. Electrical signals are transmitted to the centrifuge rotor and then to the model in flight through a stack of slip rings. Hydraulic services are transmitted through four rotary journals. A general view of the centrifuge and control panel is shown in Figure 2.1.

2. Photographic and Video Recording Systems

A still photographic system is available to permanently record selected moments of the centrifuge model tests. A camera is mounted near the hub of the centrifuge. Thus, still photographs can be taken with an on-board camera-flash unit by remote control during the tests. The photographs may be used later for analyses. In this study a photograpic system was not used. However, a Sony television camera and video recording device were used as the monitoring system. This video camera was mounted near the hub of the centrifuge. It provided not only a continuous and instantaneous monitor of the test while in progress but also a permanent, replayable record of the model tests.

C. Model Box, Concrete Box Culvert and Strain Gages

A centrifuge model box which had been used in a prior investigation at The University of California, Davis was used to contain the soil model. The model box was made of 1/4 inch thick



Figure 2.1 A View of the Centrifuge

aluminum alloy, and was designed to operate under a maximum centrifugal loading of 100 g. The dimensions of the model box were 15 inches long by 15 inches wide by 10 inches high.

The model box culvert was made of Quikrete, a commercial ready-to-use sand (topping) mix, with water-cement ratio of 0.15 (by weight). The model box culvert consisted of a roof, floor, and two side walls and the exterior dimension of the culvert were 9 inches (length) by 5 inches (width) by 5 inches (height). The thickness of these slabs was 0.4 inch.

A commercial strain gage (Gage Type CEA-13-125UW-120) made by Measurements Group, Inc. was used to measure the strains on the surfaces of the culvert. The strain gages were placed at the mid-section of the culvert. Figures 2.2 and 2.3 show the dimensions of the model box culvert and location of the strain gages, respectively. Symmetry was assumed.

D. Microcomputer Based Data Acquisition System

At least fourteen strain gages (seven exterior and seven interior gages) were required to measure the strains for the model study. However, these instruments faced two very difficult problems: 1) a limited number of slip rings were available for data transmission and, 2) brush noise caused by dynamic vibration occurred in the area in which the brush is in contact with the slip ring. To overcome these problems, a microcomputer-based time division data acquisition system (which works as a synchronized channel selector as shown in Figure 2.4) was designed by Li (Reference 7) and installed by Ju (Reference 8) for

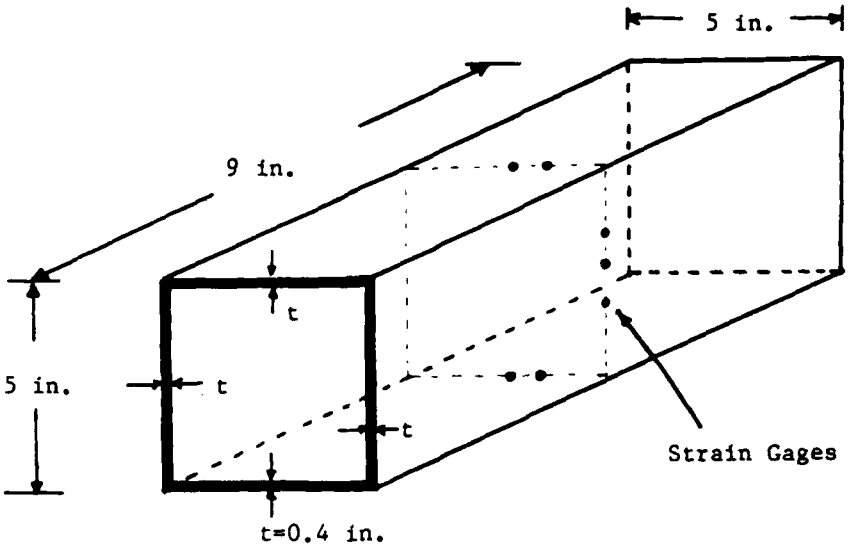



Figure 2.2 Dimensions of the Model Box Culvert

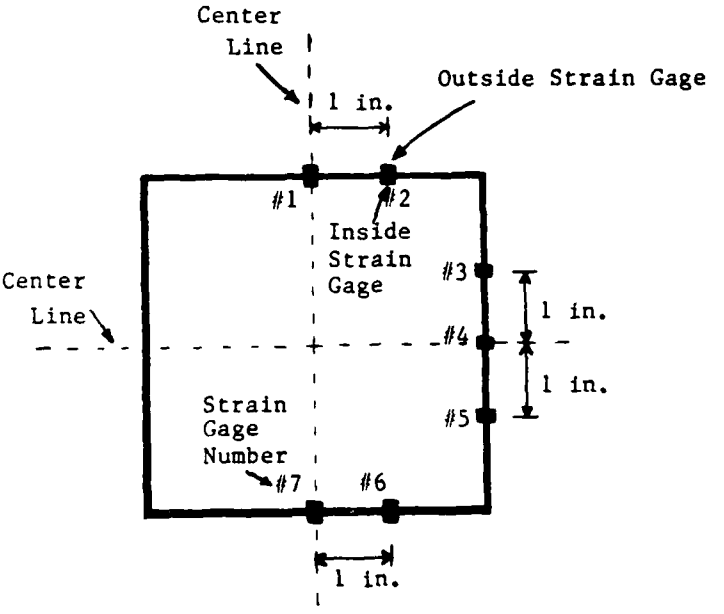



Figure 2.3 Locations of the Strain Gages

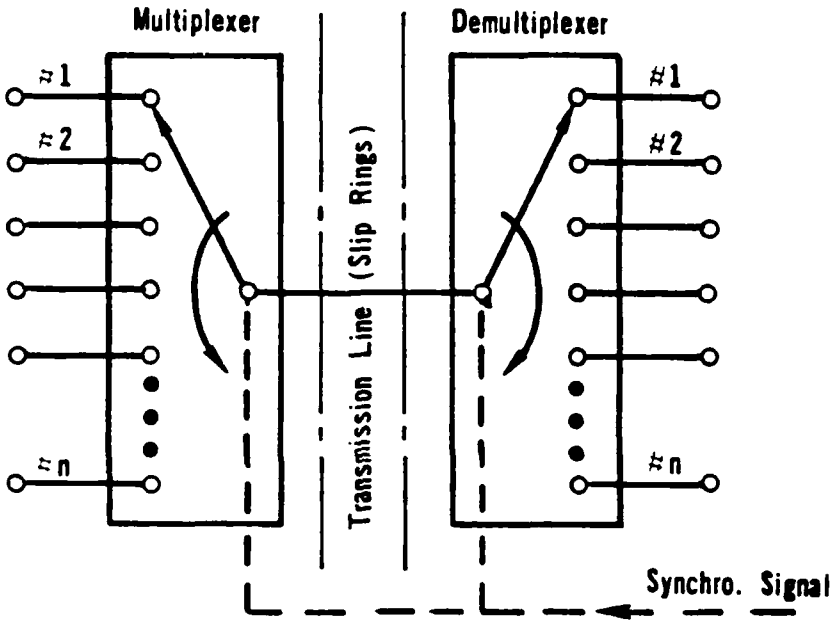



Figure 2.4 A Time Division Multiplexer - Demultiplexer Unit (Reference 9)

the model study. Details of the system are described in Reference 9, and a brief description of the system is illustrated below.

Referring to Figure 2.5, the transducers are connected to the corresponding signal conditioning. Conditioned signals are picked up in a sequential order by the 16-channel multiplexer and then fed through the voltage follower which is linked to a pair of slip rings. Signals transmitted through the slip rings are received by the A-D converter which is connected to a microcomputer. The synchronization signal comes from a pulse generator (output from a channel of the D-A converter). Each pulse causes the shifting of one channel of the multiplexer. At any given instant only one channel of the 16-channel multiplexer is connected to A-D converter. For this system, the synchronization and the demultiplexing functions are executed by software programming. Note that channel 0 of the multiplexer is connected to a fixed voltage, and serves as a reference mark for the computer to identify the position of all channels. Under a specified sampling rate, the computer automatically acquires data from all the channels and converts signal voltages to actual physical quantities to be stored, processed or tabulated by the printer. Figures 2.6 and 2.7 show the multiplexer and data acquisition system utilizing a Radio Shack TRS-80 Model I microcomputer and a printer, respectively.

E. Soil Properties

The soil used in this study is Monterey No.0 sand which is classified as SP in the Unified Soil Classification System. The sand has a specific gravity of 2.65 and a mean grain diameter of about 0.45

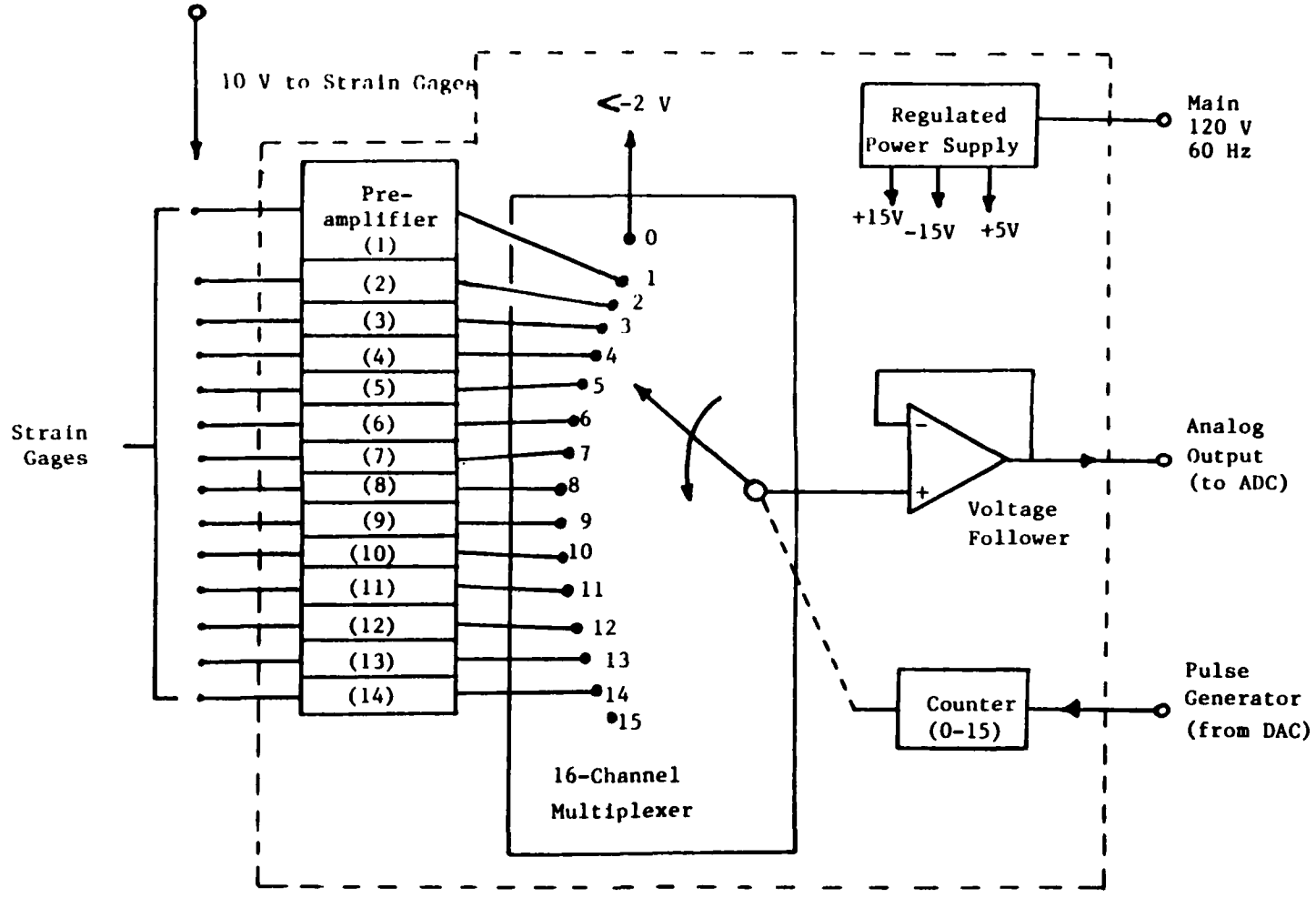



Figure 2.5 A Schematic of a Microcomputer Based Data Acquisition System

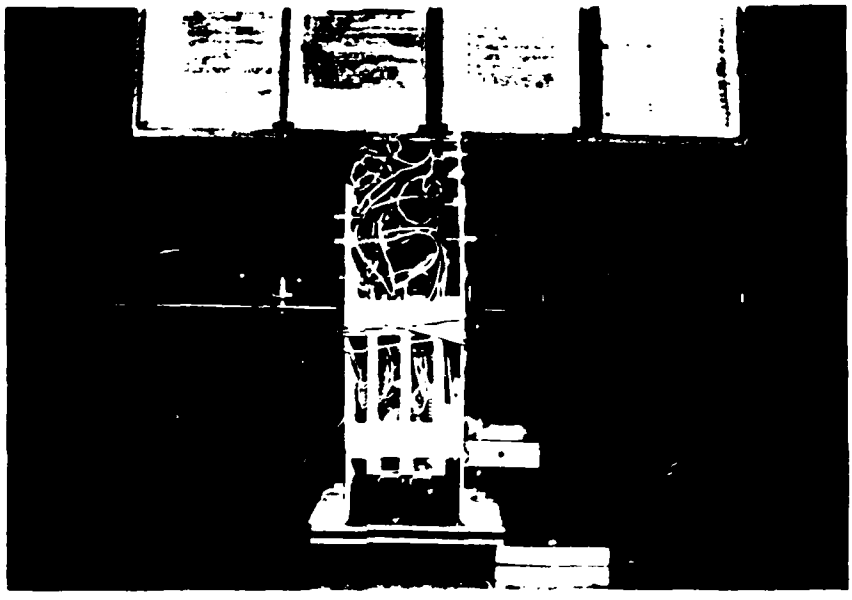


Figure 2.6 A View of Multiplexer

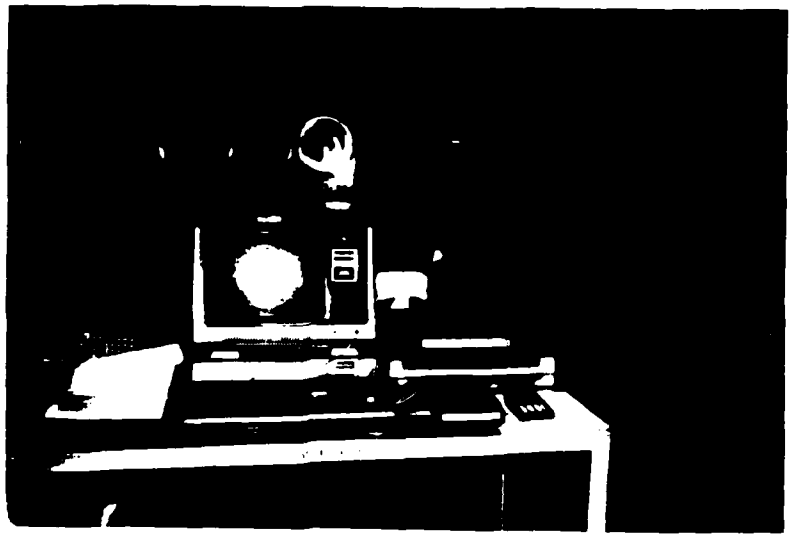


Figure 2.7 A View of a Microcomputer Based Data Acquisition System

mm. Figure 2.8 shows the grain size distribution and Figures 2.9 and 2.10 show the data obtained from the triaxial compression tests for Monterey No.0 sand. The laboratory tests were performed by Yang (Reference 10).

F. Model Preparation

The following steps are involved in preparing a model:

1) The concrete model box culvert was instrumented, and was then placed in the selected installation type (embankment or trench) as shown in Figures 2.11, 2.12 and 2.13.

2) Monterey No.0 sand was pluviated in the direction normal to the axis of the culvert (see Figure 2.14).

3) The completed sample was then transferred to the centrifuge and placed in one of the two swing-up buckets.

4) Instrumentation (T.V. monitor and multiplexer) was securely fastened, and both static and dynamic balancing of the rotating arm were performed prior to testing, thus completing preparation of the model system for centrifuge testing (see Figure 2. 15).

After a model was placed in the swing-up bucket and all required insrumentation was securely mounted in the centrifuge, the model package was slowly brought up to a rotating speed of 195 rpm, equivalent to 60 gravitational pulls.

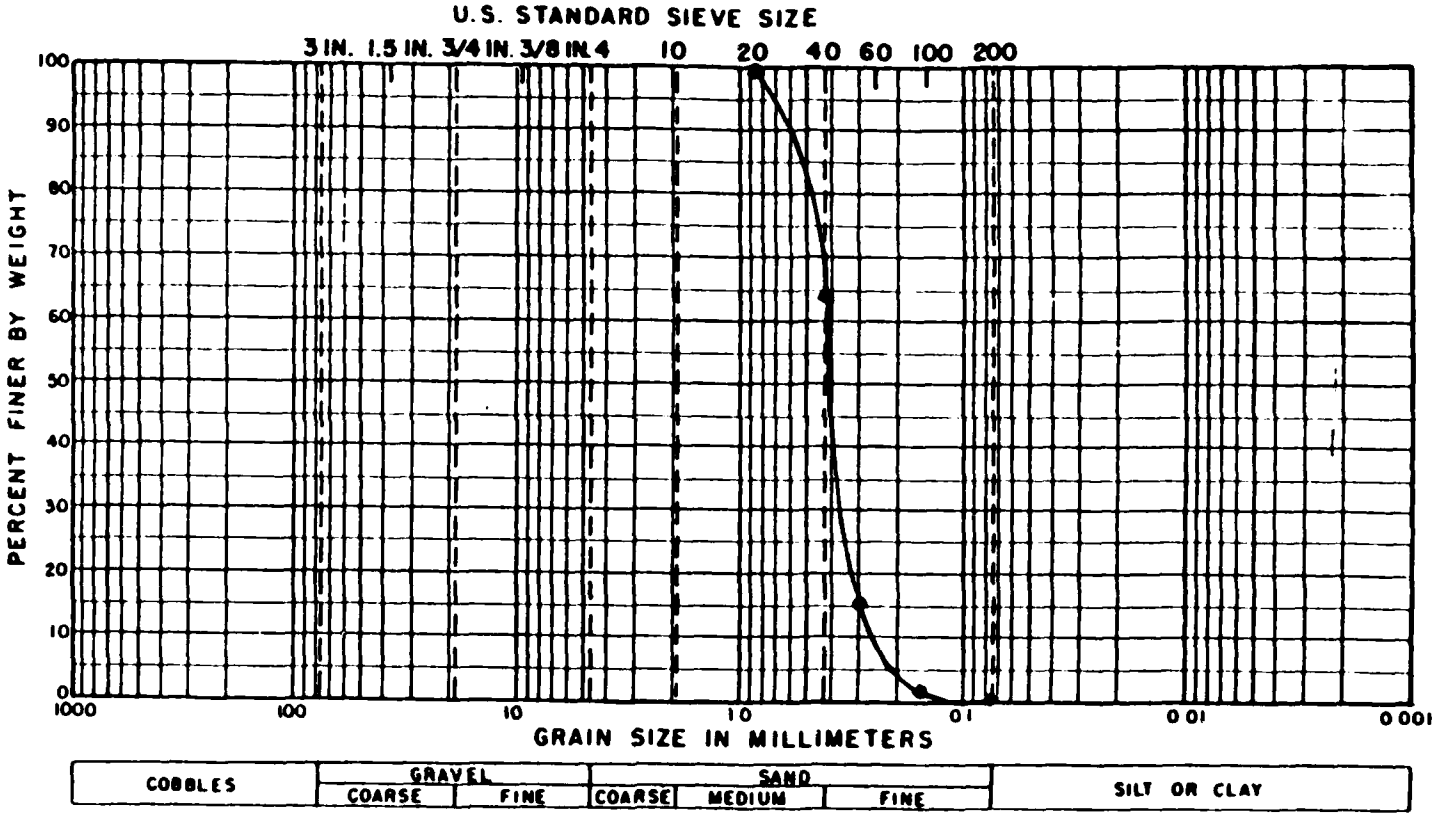



Figure 2.8 Particle Size Distribution for Monterey No.0 Sand (Reference 15)

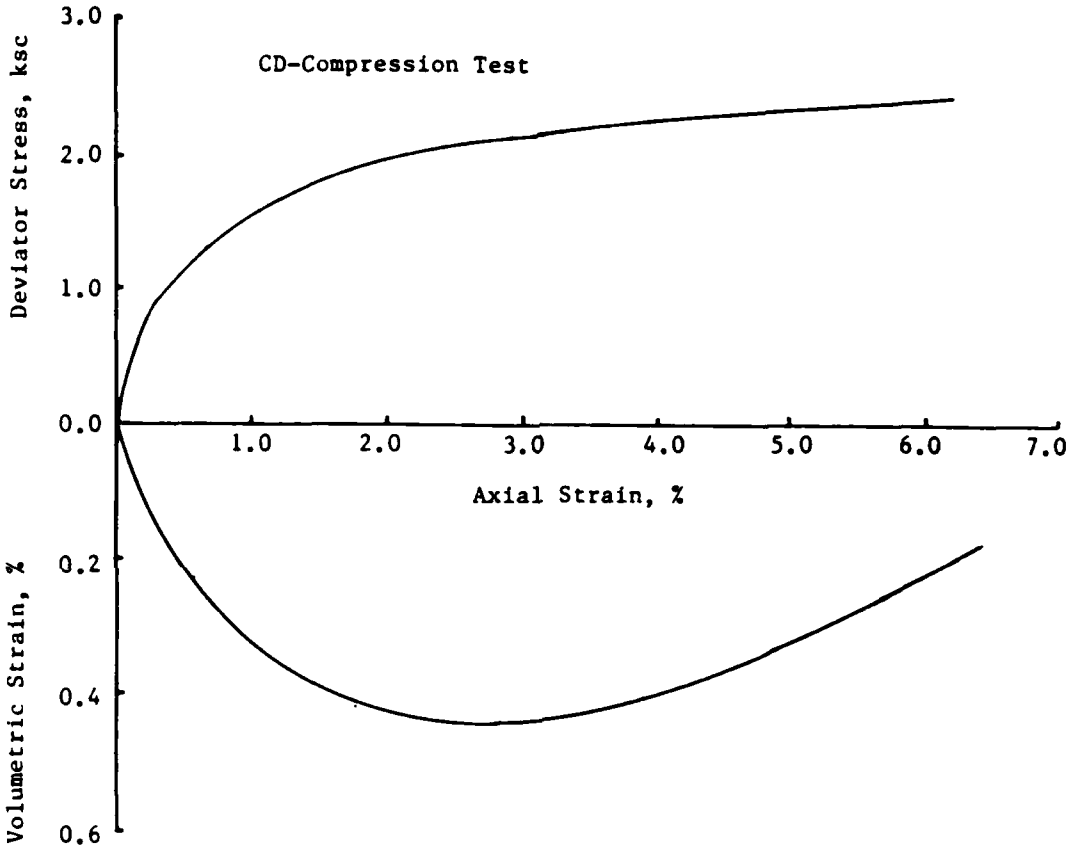



Figure 2.9 Stress-Strain and Volume-Change Curves from CD Triaxial Tests on Monterey No.0 Sand (Reference 15)

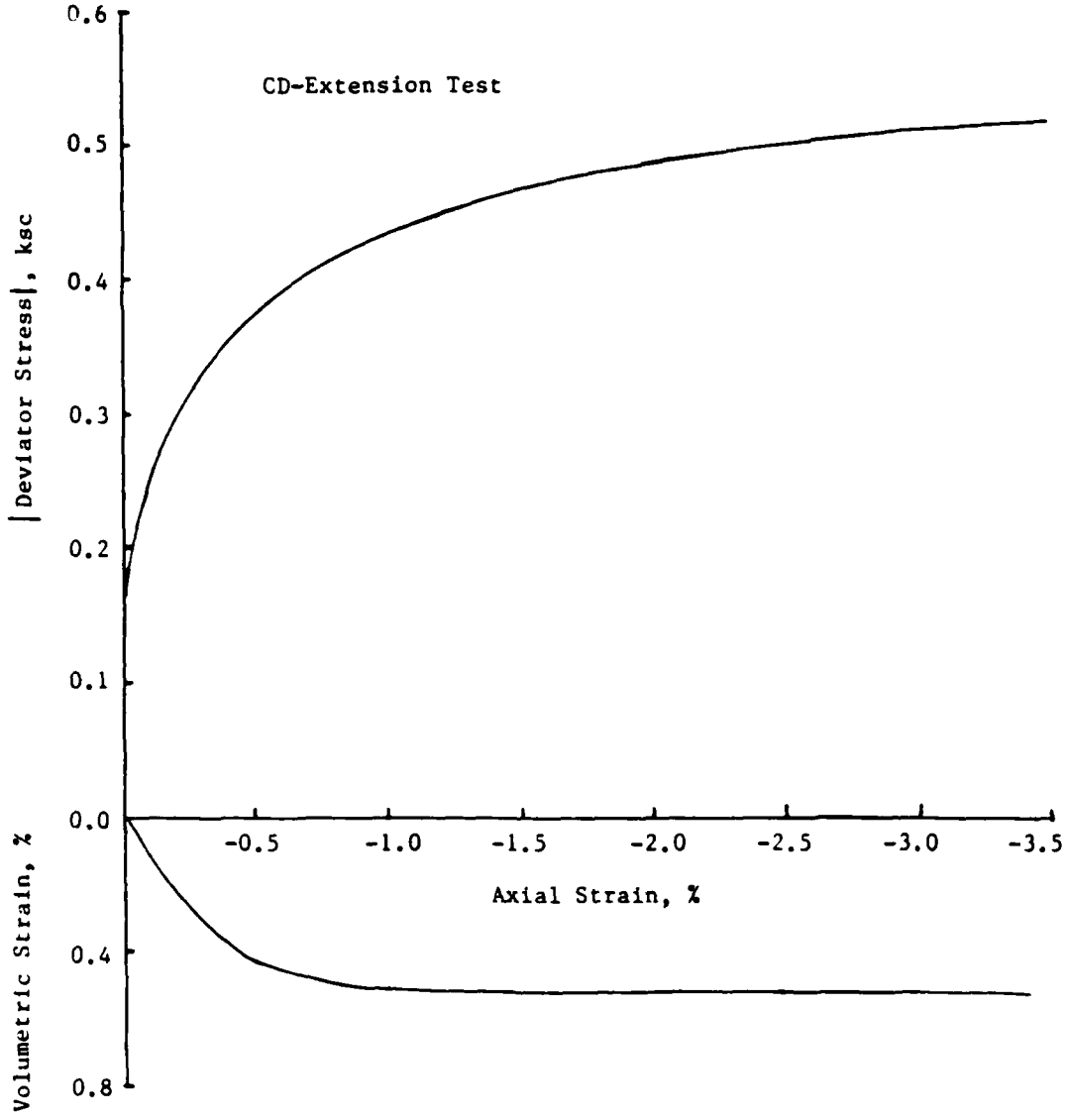



Figure 2.10 Stress-Strain and Volume-Change Curves from CD Triaxial Tests on Monterey No.0 Sand (Reference 15)

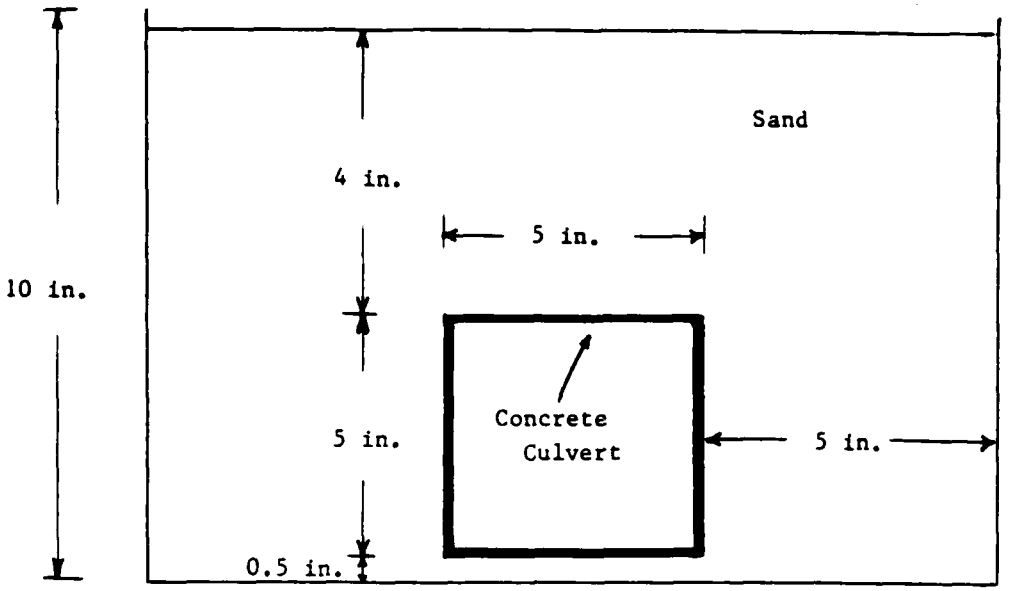



Figure 2.11 Dimensions of Model Package: Embankment Condition

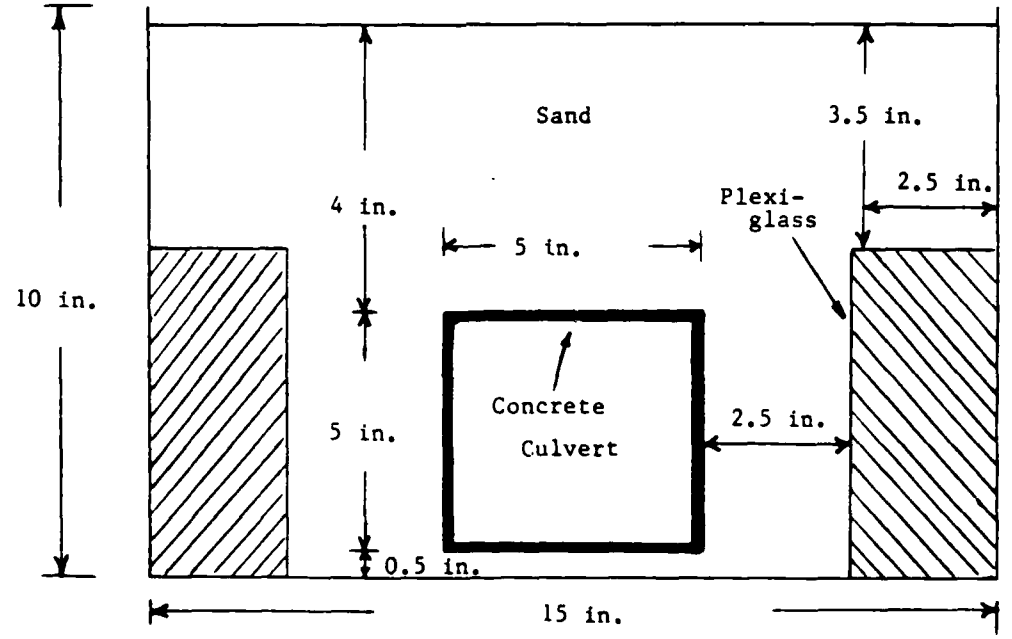



Figure 2.12 Dimensions of Model Package: Trench Condition

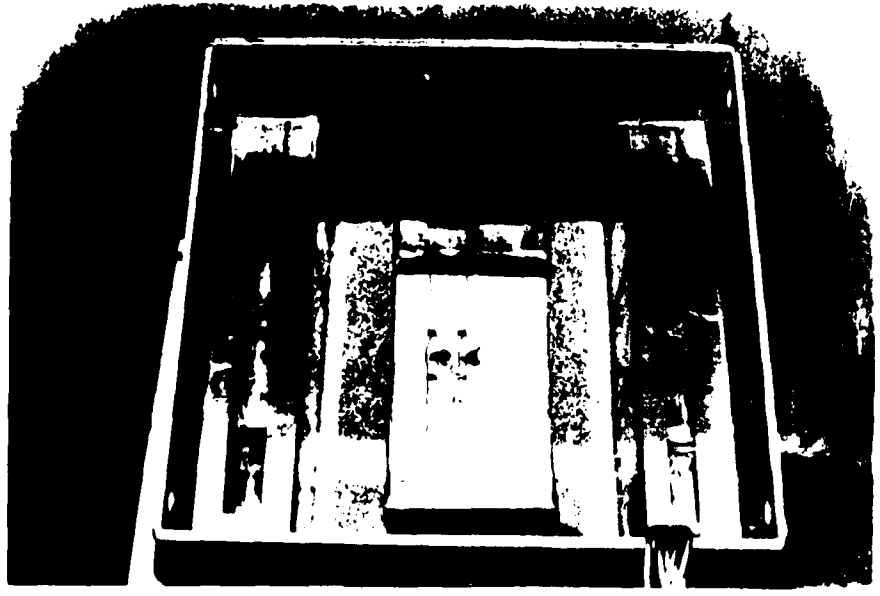


Figure 2.13 A View of Instrumented Concrete Box Culvert in the Model Box



Figure 2.14 A View of Model Preparation

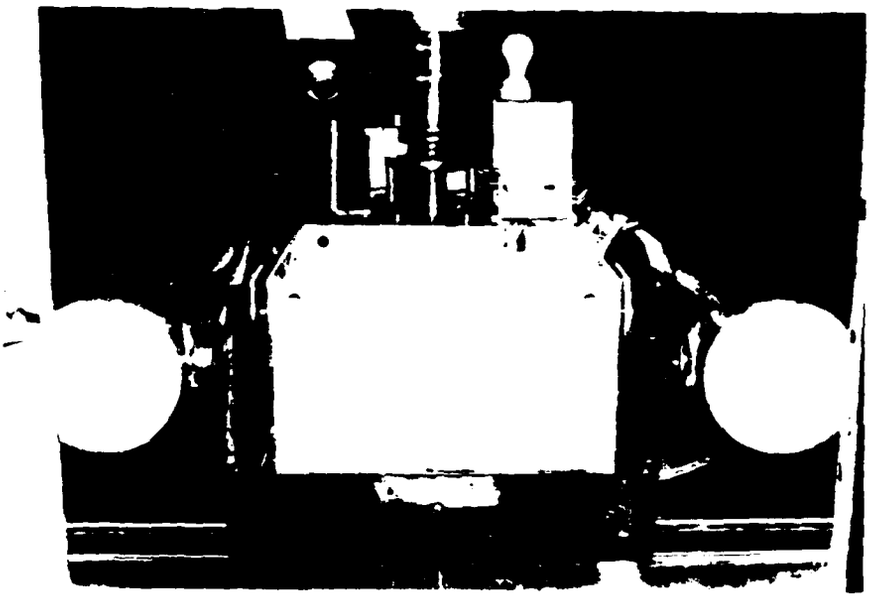


Figure 2.15 A View of Model Package in the Swing-Bucket

## SECTION III

## FINITE ELEMENT ANALYSIS

### A. Description of the Computer Code

The computer code, CANDE (Culvert ANalysis and DEsign), used in this study was developed by Katona et al. (References 11 and 12). The basic assumptions of the program are: plane strain geometry and loading, small displacement theory, and quasistatic response. The following description summarizes salient features of CANDE used in the analysis.

#### 1. Modeling of Culvert

The box culvert was modeled as a series of straight line segments with a one-dimensional beam-column bending element comprising each segment. This bending element employs a plane-strain formulation which neglects shearing deformations. Two nodes with three degrees of freedom per node (horizontal and vertical displacement and a rotation) define each element. At each node, cubic and linear displacement approximations were used in calculations of displacements in the transverse and axial directions, respectively. Figure 3.1 shows the coordinate system of the beam element.

#### 2. Modeling of Soil

Nonconforming quadrilateral and triangular elements were used to represent the soil (see Figure 3.2). The quadrilateral, defined by four nodes with two degrees of freedom (horizontal and vertical

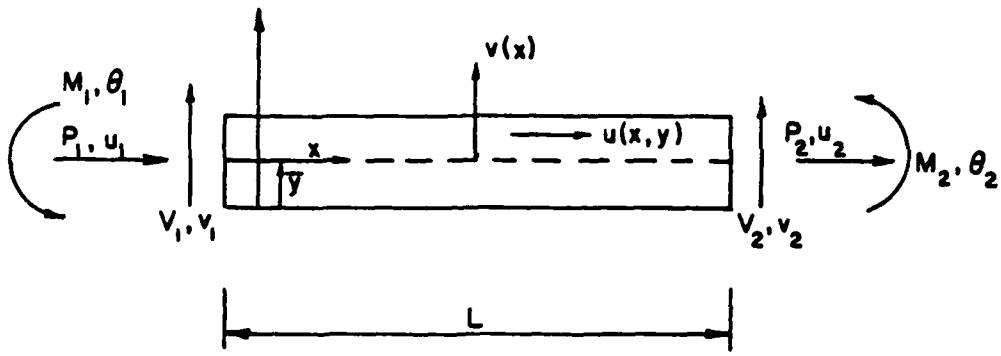



Figure 3.1 Coordinate System for Beam Element in CANDE

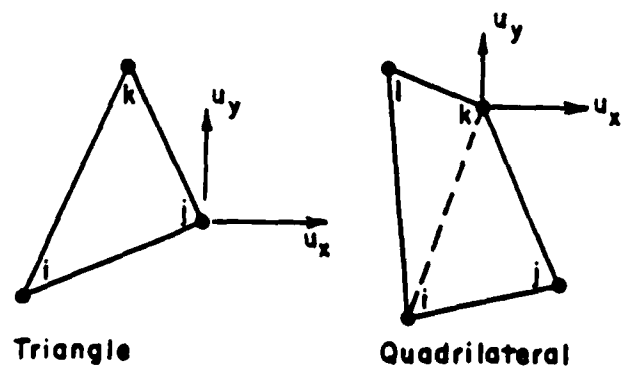



Figure 3.2 Element Types Used for Soil Model in CANDE

displacements) per node comprise two triangles with complete, quadratic, interpolation functions specified within each triangle. Application of appropriate constraints and static condensation procedures result in a four-node quadrilateral element (Reference 11).

There are four material characterizations available for the soil properties: linear elastic; incremental elastic (overburden dependennt); extended-Hardin; and Duncan's hyperbolic stress-strain relationship, which employs tangent Young's modulus and tangent bulk modulus formulations (References 12,13 and 14).

3. Modeling of Slip

A constrained finite element formulation, which is based on a generalized principle of virtual work, was used to model the relative movement of the soil with respect to the pipe at the soil-culvert interface, and relative movement of the soil with respect to the soil-soil interface (i.e., trench). An interface element is defined by a set of paired nodes joining two elements as shown in Figure 3.3. The paired nodes, which have two degree of freedom per node (vertical and horizontal displacement), initially take the same position in space before any loading, but are assigned to separate elements. Therefore, each node responds individually under any applied loading. In addition, a third node, which is assigned between the paired nodes, provides normal and shear forces existing between the paired nodes. It should be observed that these interface forces arise only from the adjoining element interacton and applied forces at the paired nodes.

4. Modeling of Incremental Construction

CANDE uses incremental iterative solution techniques to represent the placing of the culvert and embankment in a series of soil layers as shown in Figure 3.4. The basis of the techniques is superposition of solutions from successive soil layers and a newly added layer. At each increment, iterative calculations determine soil and culvert moduli until equilibrium is approximated within an allowable error.

B. Finite Element Parameters

1. Finite Element Mesh and Boundary Conditions

The finite element grid with boundary conditions used in this study is shown in Figure 3.5. Since the model and its loading is symmetric, only half of the model was analyzed. Boundary conditions on the culvert used in the analysis are shown in the figure: a fixed movement condition in the horizontal direction and free movement condition in the vertical direction. The culvert was represented by 20 beam-column elements, and the soil by 110 quadrillateral elements.

2. Soil-Culvert Interface and Incremental Solution Procedure

A fixed condition was used at the soil-culvert interface. Although it is possible to represent the slip betwen the continuum and beam elements, a current study has demonstated that the influence of slip conditions for this particular geometrical configuration are insignificant (Reference 15). Due to large amounts of CPU (Central Processing Unit) time, and substantial computational costs when slip

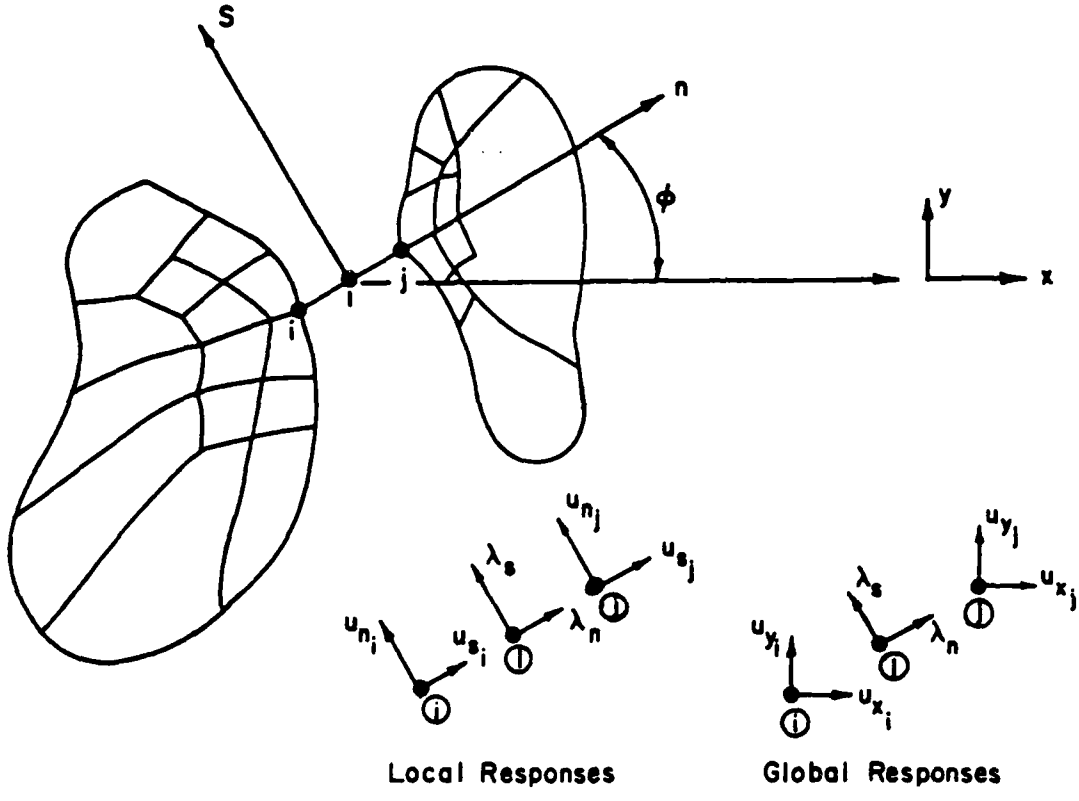



Figure 3.3 Nodes for Constraint Interface Element in CANDE

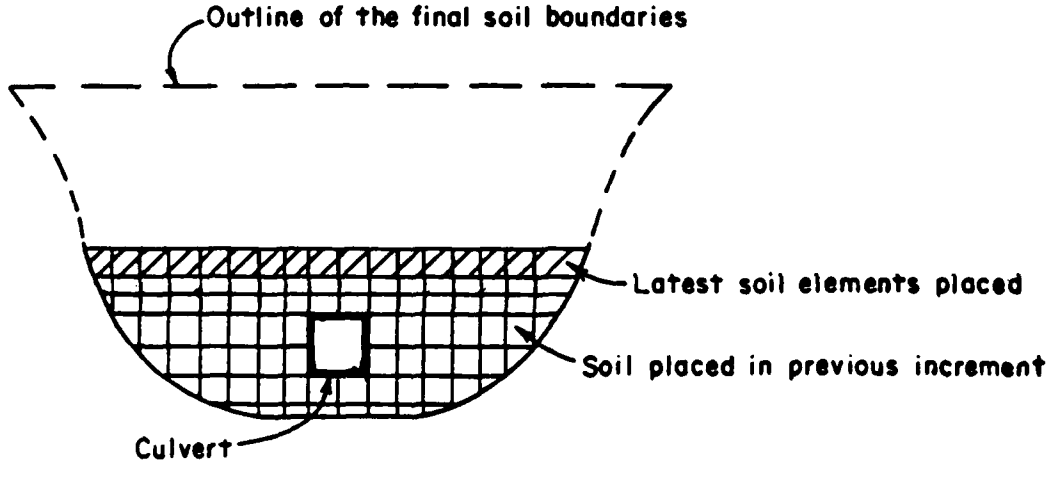



Figure 3.4 Incremental Construction

Number of Nodes: 142

Number of Beam Elements: 20

Number of Quadrilateral Elements: 110

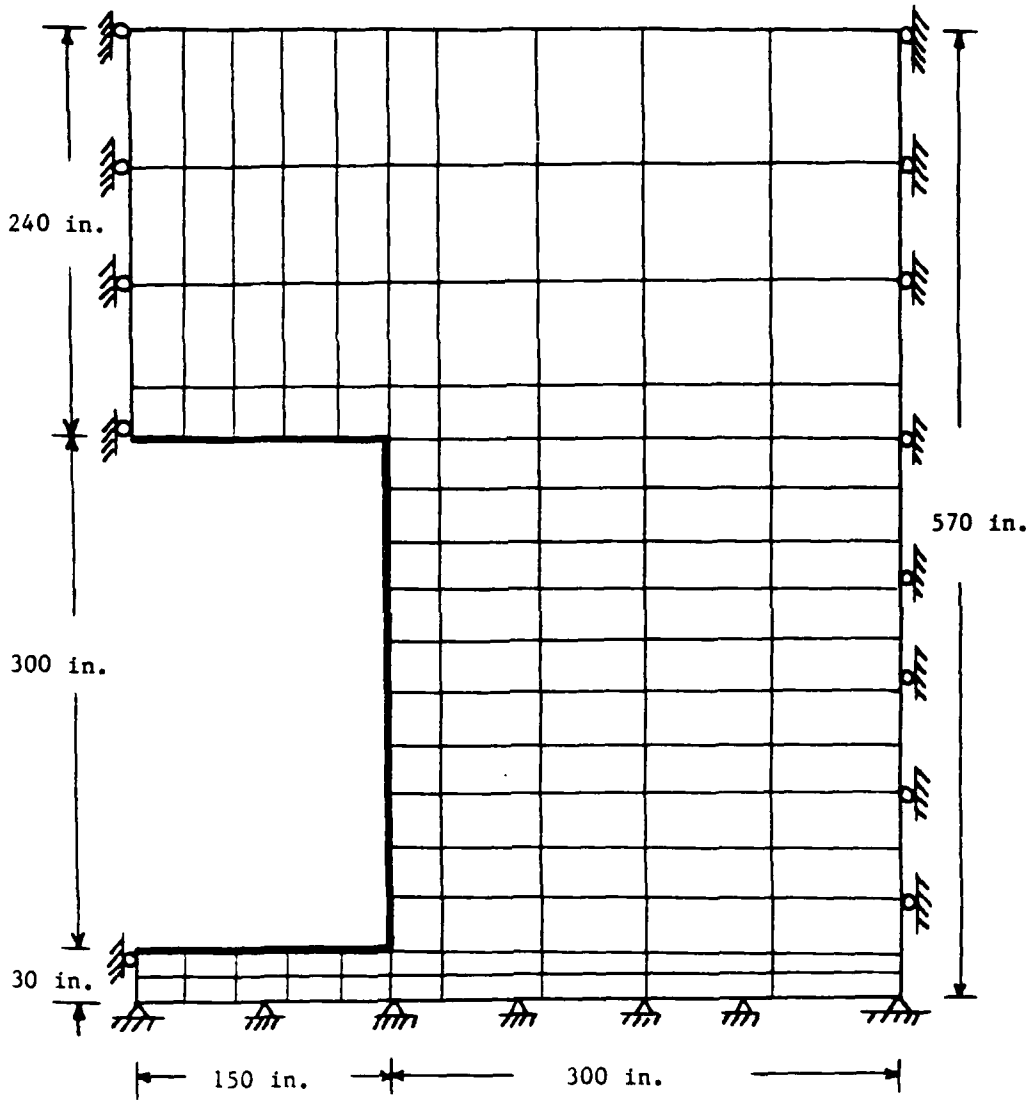



Figure 3.5 Symmetric Mesh

was allowed, the fixed condition was used for the analysis.

The incremental solution procedure for embankment and trench simulated the actual installation process of placing soil layers in a series of lifts. Figures 3.6 and 3.7 show the construction increment numbers of element groups entering sequentially into the system. The first construction increment included placing all bedding pad, in situ soil, and the box culvert elements. Subsequent increments, numbers 2 through 10, were gravity loaded elements of fill soil.

3. Material Properties

The soil model employed in the study is a characterization proposed by Duncan et al. (References 13 and 14) which has had a substantial history of development and application over the last decade. This soil model characterizes soil behavior with a variable tangent Young's modlus and tangent bulk modulus. Eight parameters are needed to define a part :ular soil in loading: K, n, $R_f$, c, Ø, and $\Delta$Ø for the tangent Young's modulus; and $K_b$ and m for the tangent bulk modulus. These parameters can be determined from data obtained by conventional triaxial tests. Table 3.1 shows the parameters used for Monterey No.0 sand in the analysis. These parameters were determined by Duncan (Reference 13).

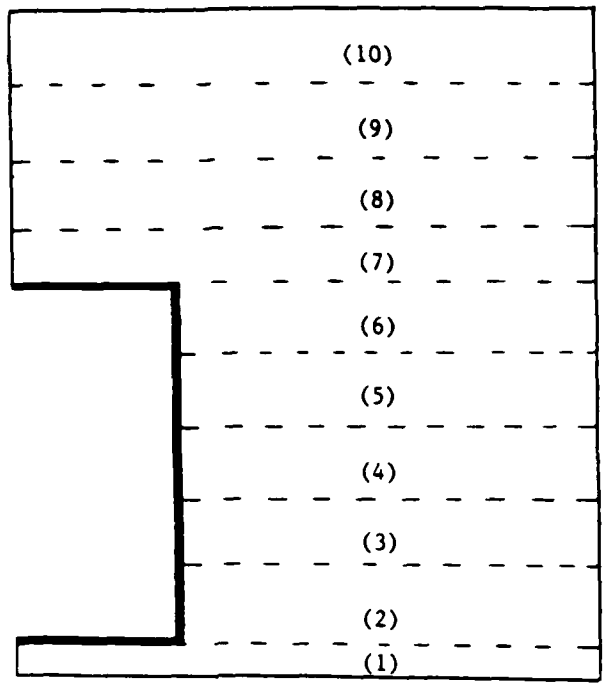



Figure 3.6 Soil Layers and Construction Increments for Embankment Soil Installation

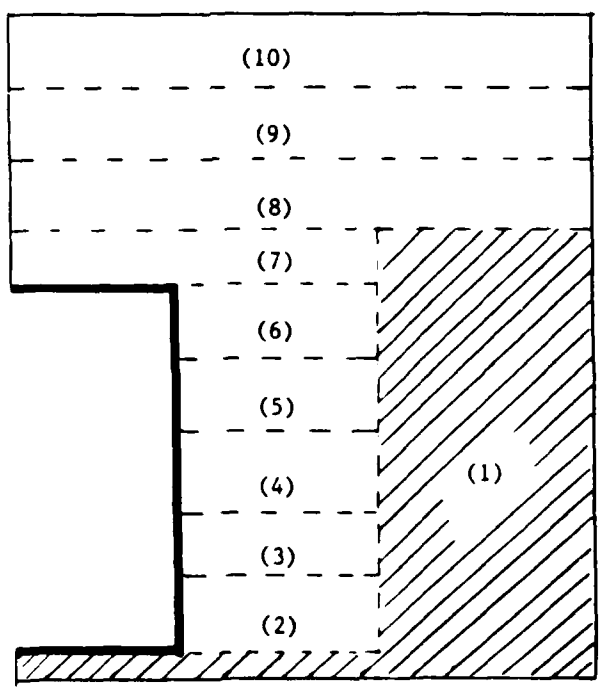



Figure 3.7 Soil Layers and Construction Increments for Trench Soil Installation

Table 3.1 Duncan's Soil Parameters for Monterey No.0 Sand (Reference 13)

| | |
|---|---|
| Cohesion, c | 0.0 |
| Friction Angle, Ø | 35.0° |
| Modulus Number, K | 920.0 |
| Modulus Exponent, n | 0.79 |
| Failure Ratio, $R_f$ | 0.96 |

## SECTION IV

## RESULTS AND DISCUSSION

This section presents results from the numerical analysis and centrifuge model study whose purpose was to investigate the influence of installation types (embankment and trench) and soil types on the structural behavior of a typical box culvert. The input parameters for the centrifuge model study are same as those in the Section II. The numerical results obtained from CANDE in Section IV.B are based on the input parameters discussed in the Section III.B.3 and the input parameters used for the study of soil type influence are described in Section IV.C.

### A. The Influence of Installation Type

#### 1. Bending Moment Distribution

The bending moments developed in the concrete culvert were determined from the results of centrifuge model study and predictions of numerical analyses. Figures 4.1 to 4.9 visually report the variation of moments with depth of fill for nine locations. Figure 4.10 shows the bending moments around the culvert under a simulated fill height of 20 feet.

Figure 4.1 shows the moments for the midspan of the top slab. The moments are initially negligible, and subsequently increase almost linearly with the backfilling process. All the moments are positive throughout the incremental constructions due to the vertical soil pressure which induced inward deflection of the top slab. No negative

moments were detected during the first six construction increments at which the fill height reached the same elevation of the top span of the culvert. This indicates that the box culvert was rigid enough to resist the inward forces on the sides of the culvert under lateral soil pressure.

The largest moment is developed at the upper corner of the culvert as shown in Figure 4.3. As expected, the moments are negative throughout the backfill process.

Figures 4.7 and 4.9 show the moments developed at the corner and midspan of the bottom slab of the culvert, respectively. The results are interesting since the magnitude of those moments are much smaller than the moments at the corner and midspan of the top slab of the culvert. This confirms that the soil pressure exerted on the bottom slab is a function of bedding parameters which are important for culvert design.

The comparison between the results of centrifuge model study and numerical predictions is made on the figures. Typically, Figure 4.10 shows the compared moments around the culvert under fill height of 20 feet. Although agreement between these two results are not excellent in magnitude, centrifuge model and finite element results are in moderately good agreement for shape.

No major difference in structural behavior was observed under two different installation types, embankment and trench. This result may indicate that the influence of the installation type to overall behavior of the box culvert is minimal although the installation type is one of the more important parameters to be considered for circular culverts. However, it should be pointed out that the embankment

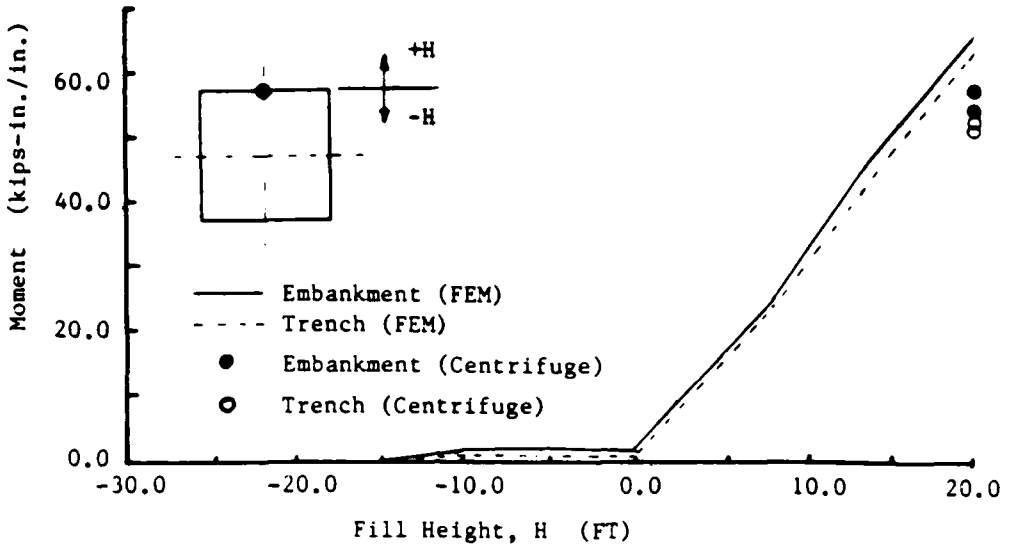



Figure 4.1 Culvert Bending Moments at Strain Gage #1

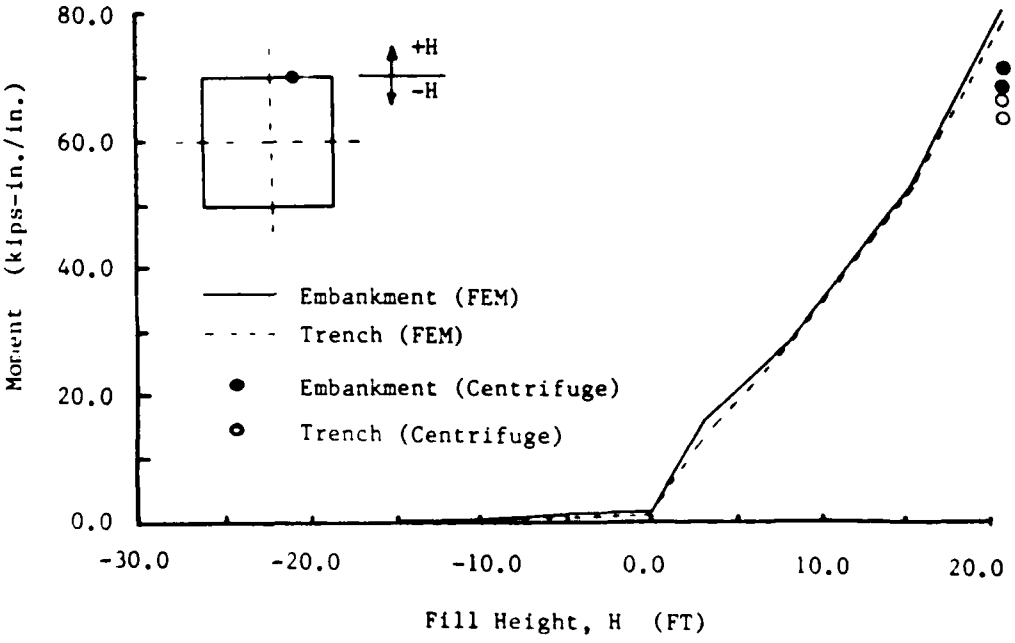



Figure 4.2 Culvert Bending Moments at Strain Gage #2

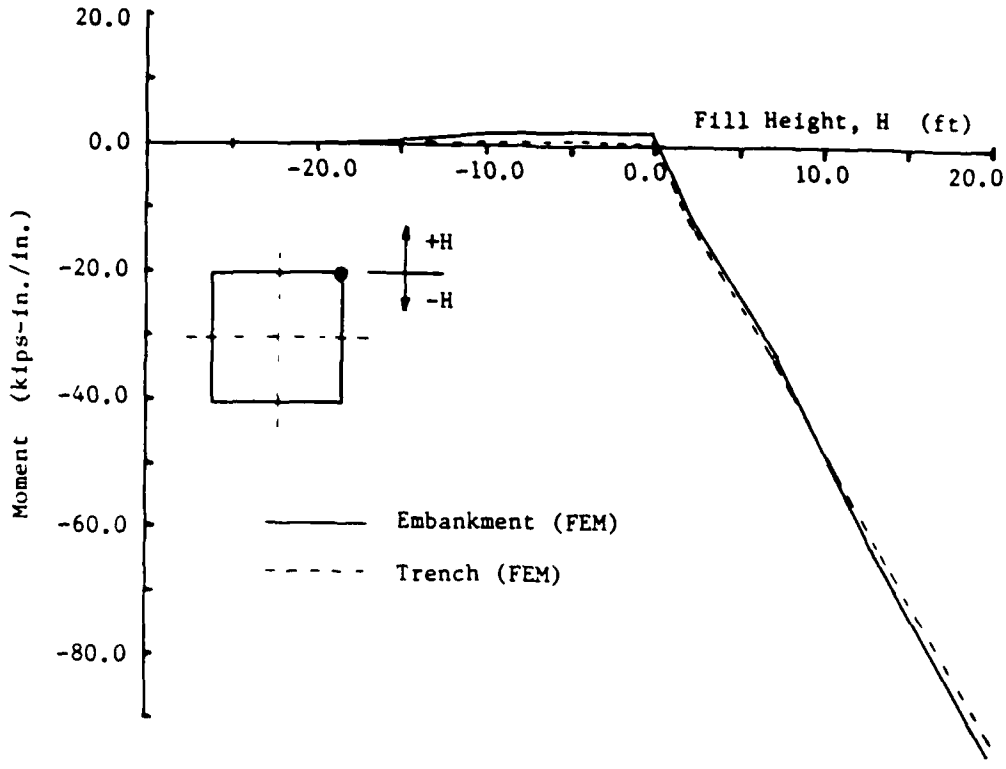



Figure 4.3 Culvert Bending Moments at the Upper Corner

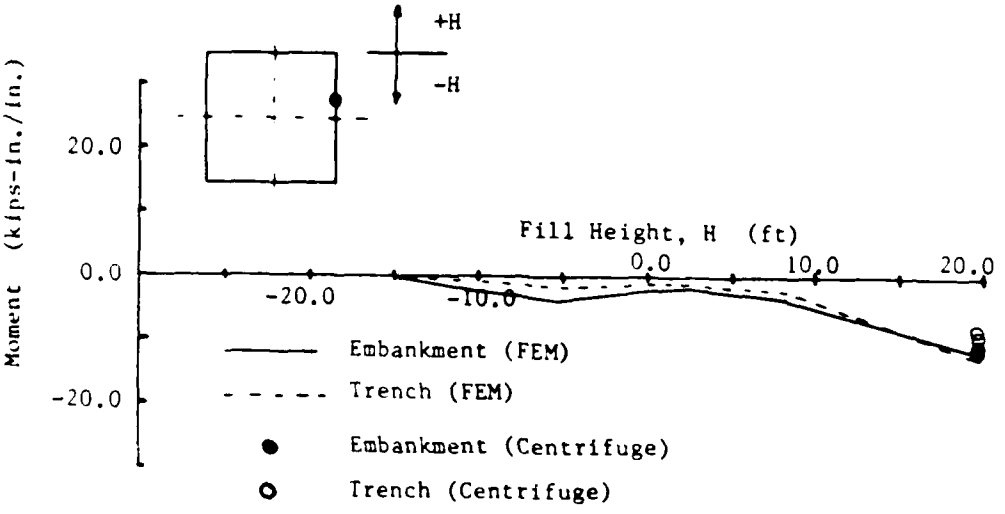



Figure 4.4 Culvert Bending Moments at Strain Gage #3

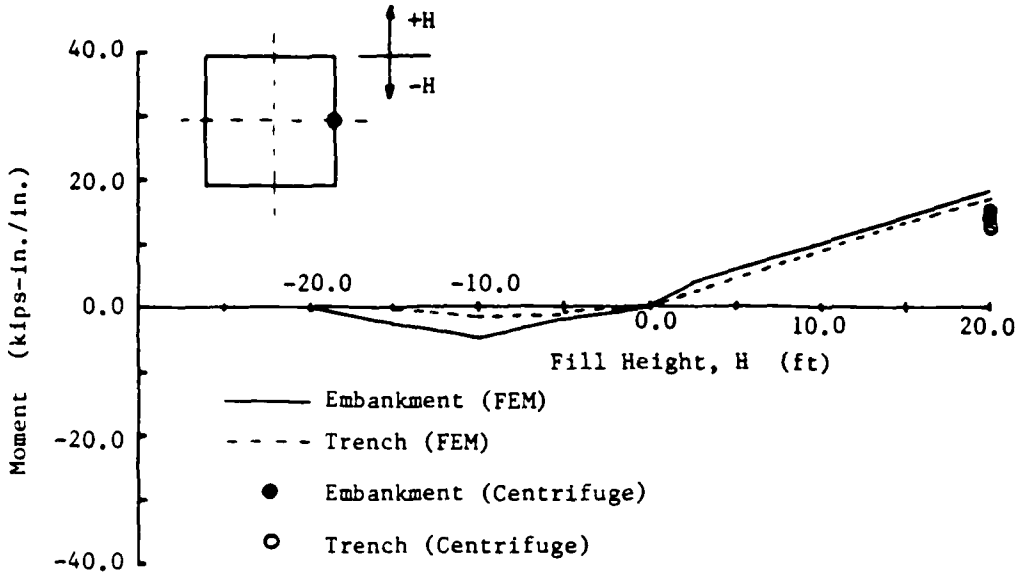
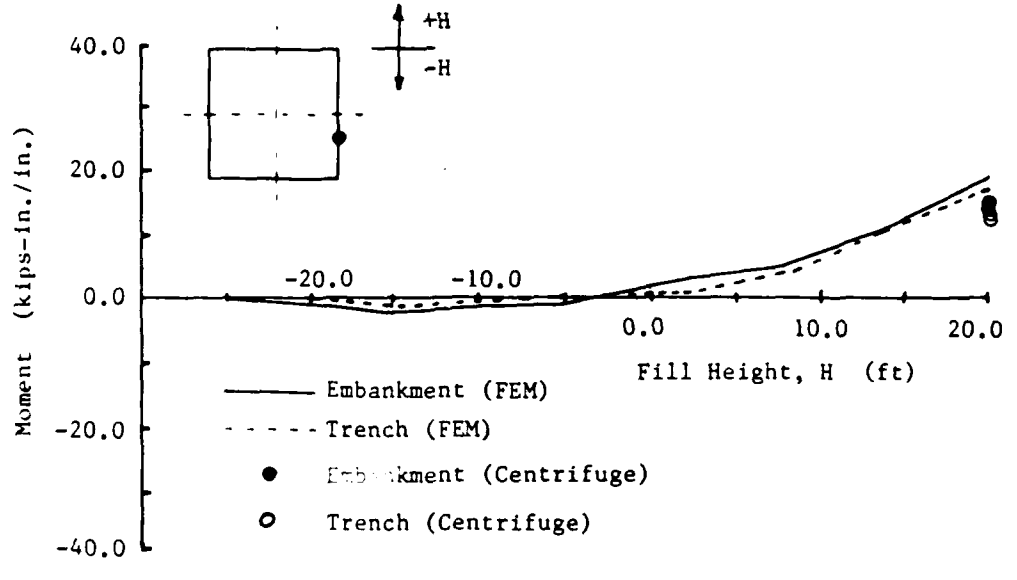



Figure 4.5 Culvert Bending Moments at Strain Gage #4




Ffigure 4.6 Culvert Bending Moments at Strain Gage #5

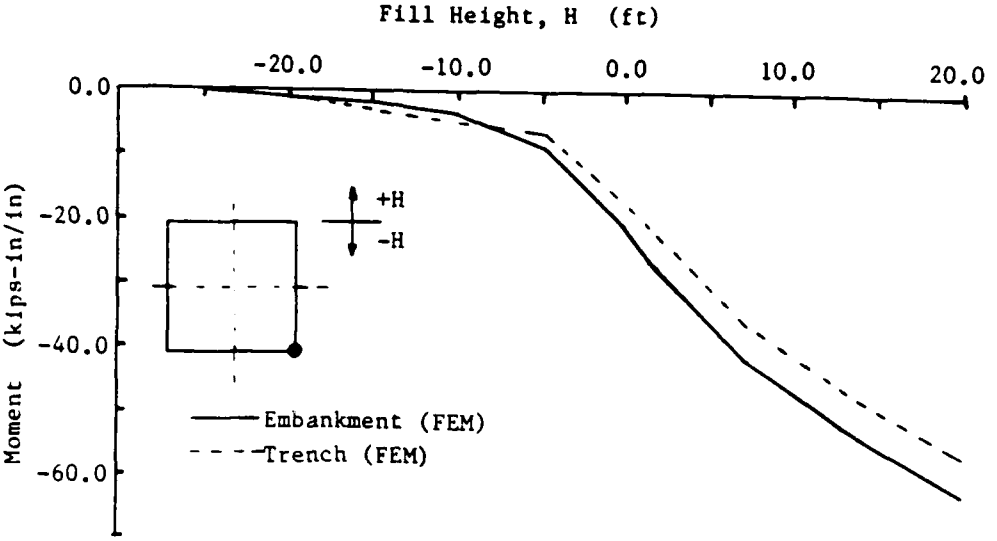



Figure 4.7 Culvert Bending Moments at Bottom Corner

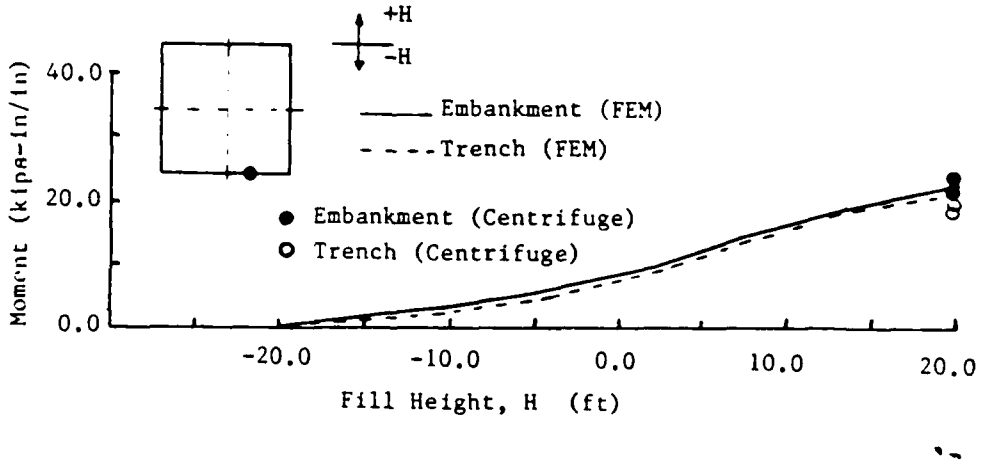



Figure 4.8 Culvert Bending Moments at Strain Gage #6

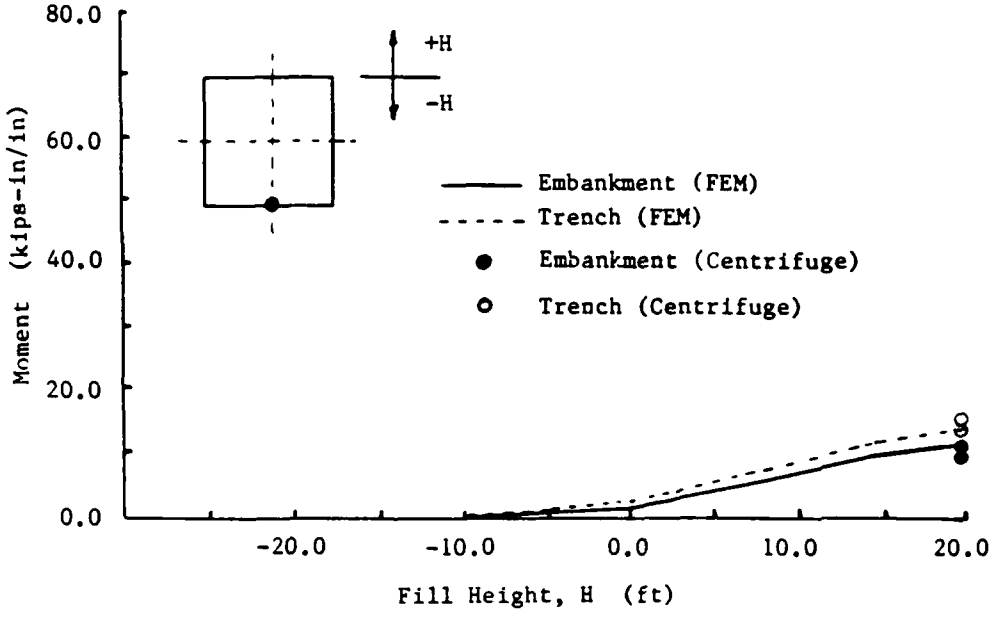



Figure 4.9 Culvert Bending Moments at Strain Gage #7

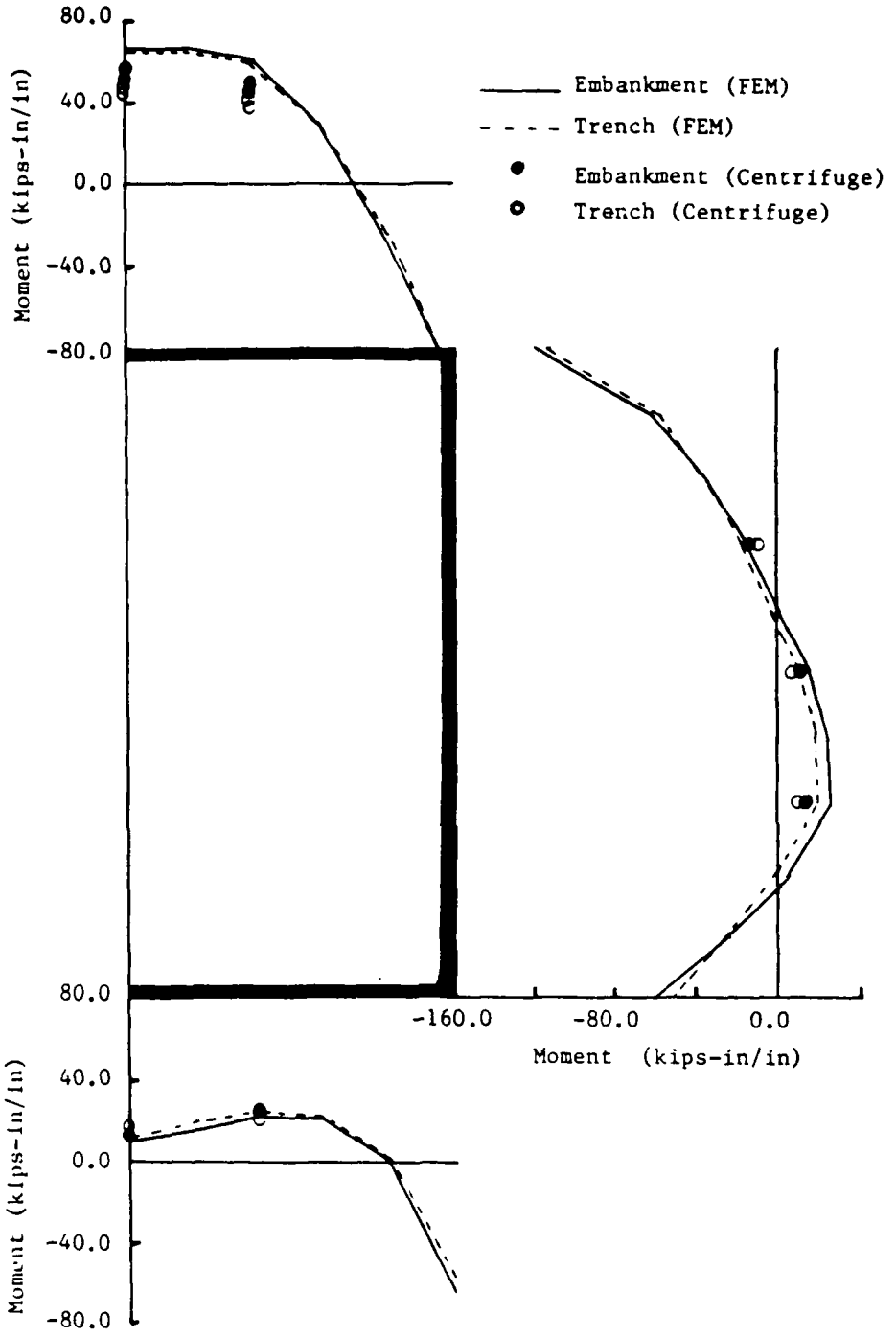



Figure 4.10 Bending Moments around the Culvert at Fill Height = 20 ft

condition produces slightly greater loading conditions.

2. Thrust Distribution

The thrusts developed in the concrete box culvert were determined from the results of the centrifuge model study and predictions of numerical analyses. Figures 4.11 to 4.15 report the variation of thrusts with depth of fill for five locations, while Figure 4.16 shows the thrusts around culvert under fill height of 20 feet.

Figures 4.11 and 4.12 show the thrusts at the midspan and corner of the top slab of the box culvert. The thrusts begin with compressive (positive) forces, but once the depth of fill height exceeds the crown height of the culvert, the thrusts become tensile (negative) forces.

A larger thrust was observed at midspan of the vertical wall as shown in Figure 4.13. No compressive (positive) forces were detected during the early incremental constructions. A drastic increase of tensile (negative) forces may be observed as further backfill is placed over the box culvert.

The thrust distribution around the culvert for fill heights under 20 feet is shown in Figure 4.16. All thrusts are tensile (negative) forces and the largest tensile force occured at approximately one-third of the vertical wall height from the bottom.

The results of centrifuge model study are plotted on the figures. They are similar to those in Section IV.A.1: moderately good agreement in shape, but not excellent agreement in magnitude.

Again, no measure difference in structural behavior is observed between embankment and trench installations except that the embankment

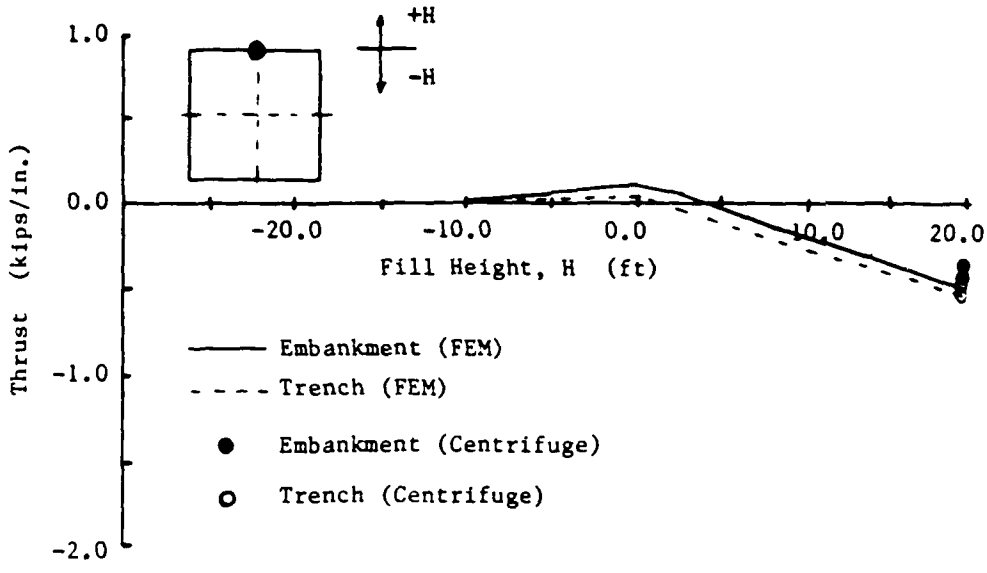



Figure 4.11 Culvert Thrusts at Strain Gage #1

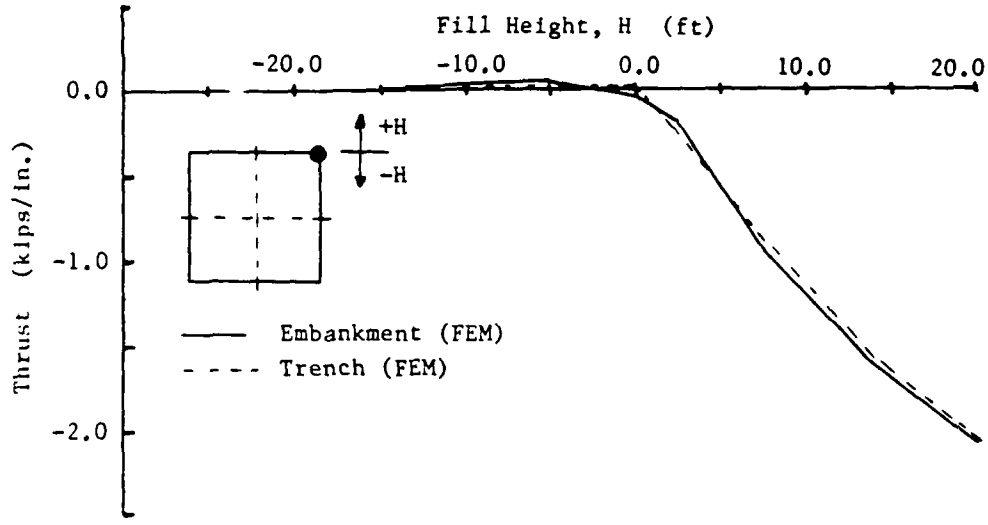



Figure 4.12 Culvert Thrusts at Upper Corner

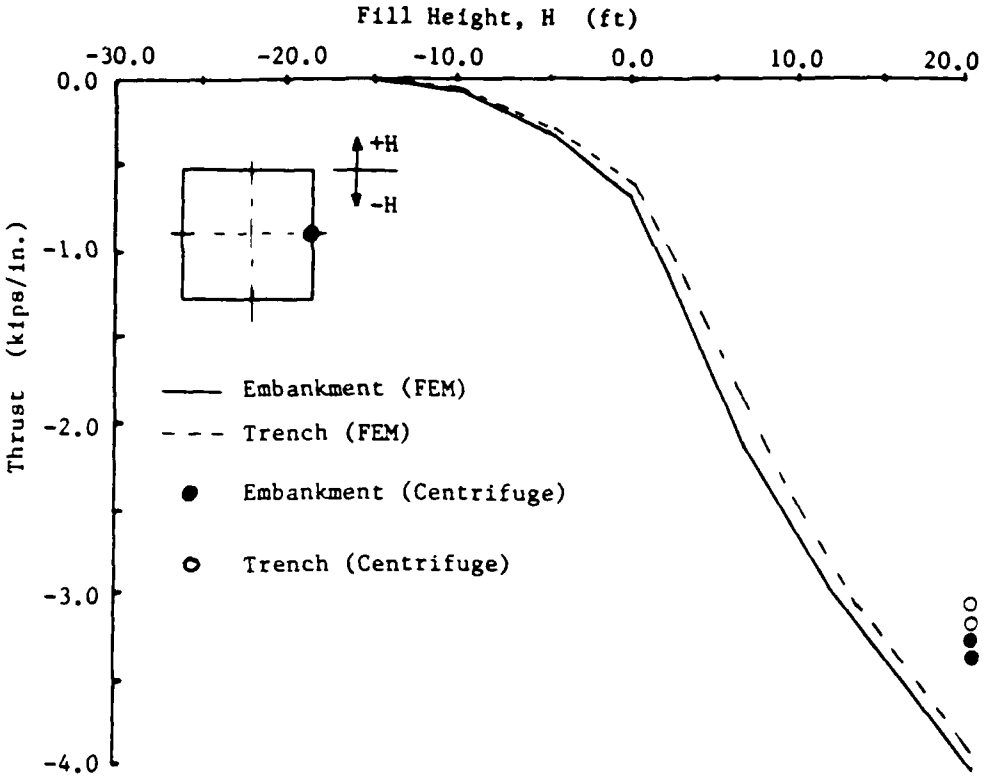



Figure 4.13 Culvert Thrusts at Strain Gage #4

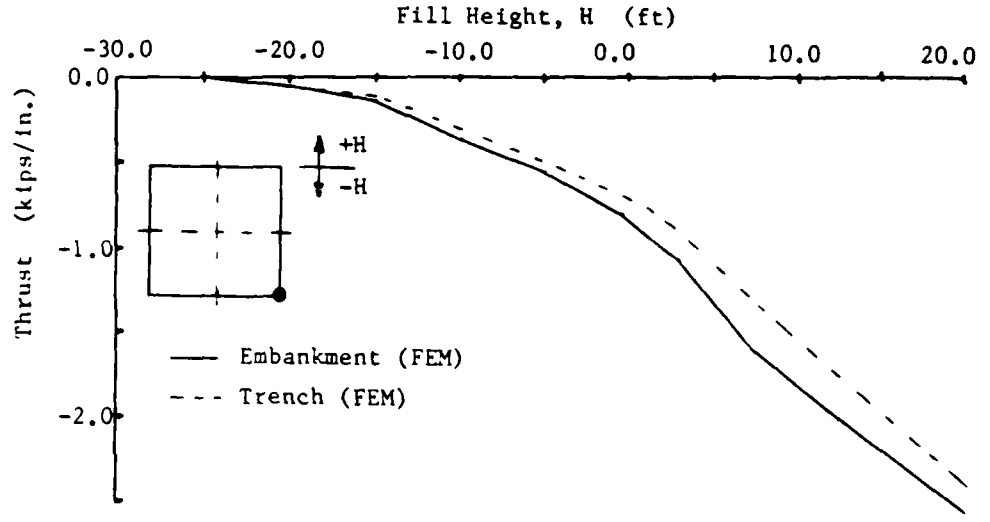



Figure 4.14 Culvert Thrusts at Bottom Corner

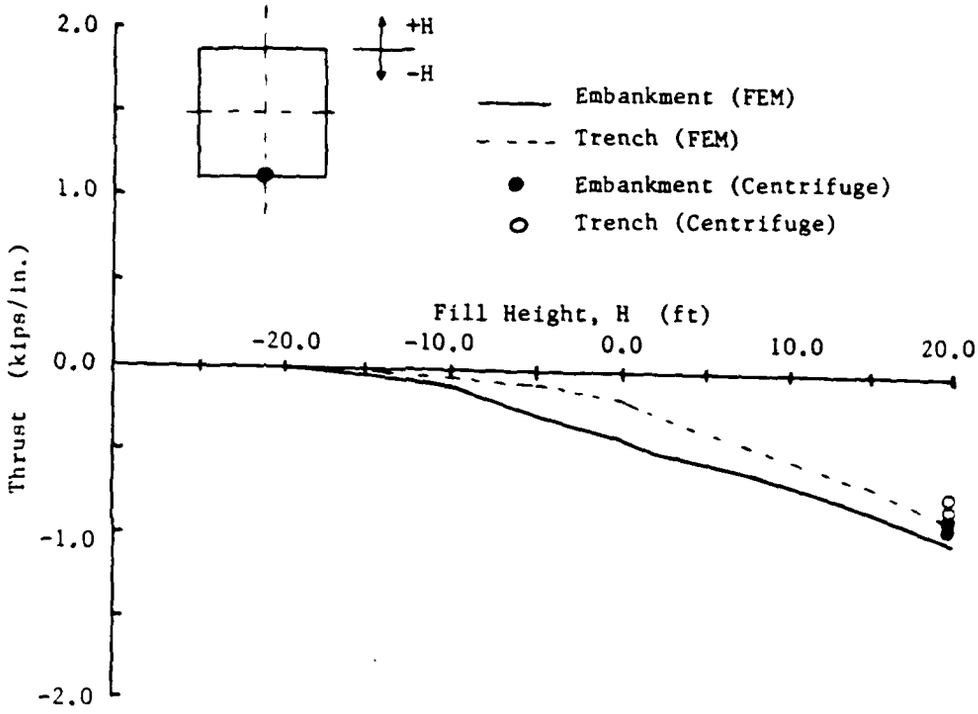



Figure 4.15 Culvert Thrusts at Strain Gage #7

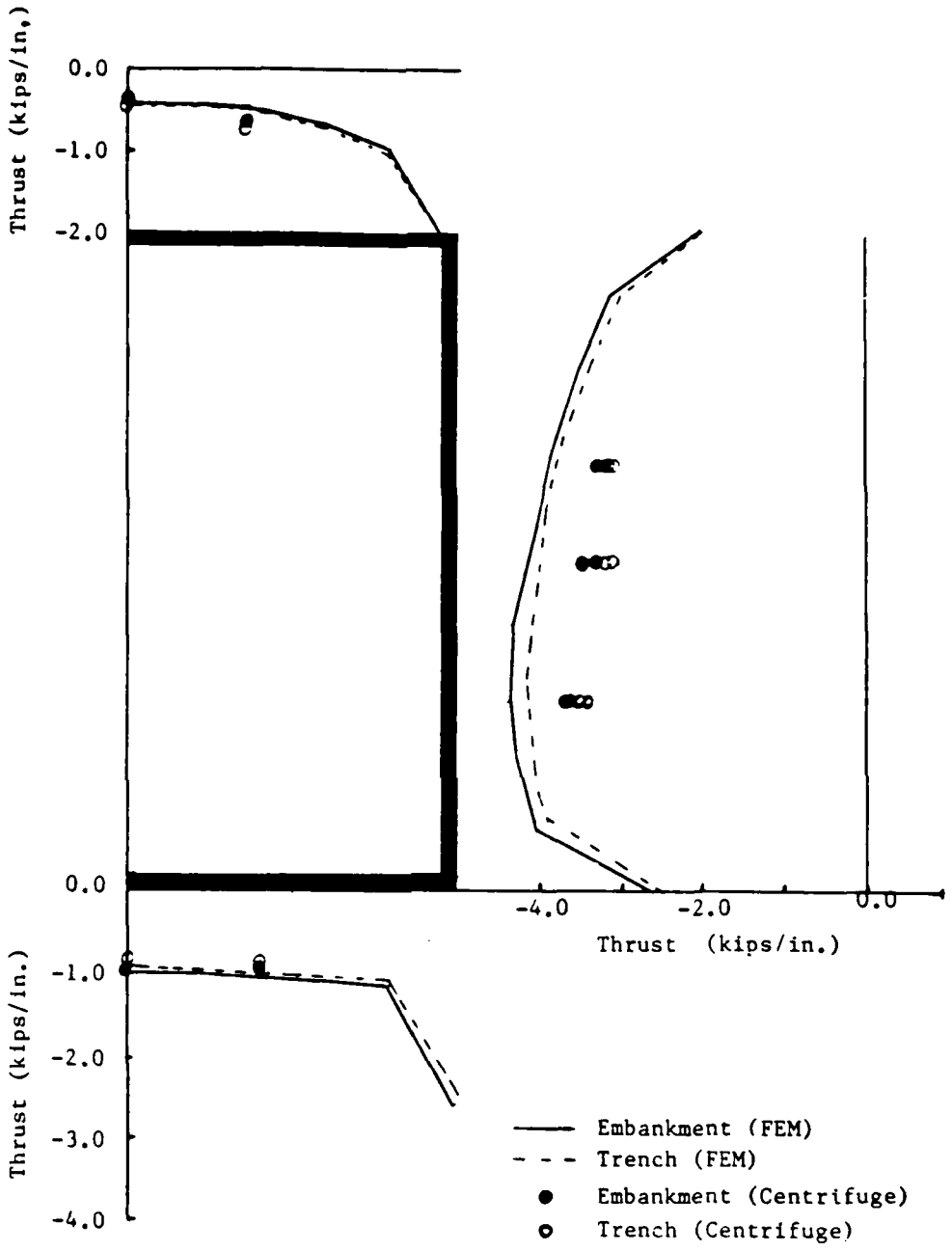



Figure 4.16 Thrusts around the Culvert at Fill Height = 20 ft

condition produces slightly larger magnitudes.

B. The Influence of Soil Type

This subsection presents the predictions of numerical analyses which investigatd the influence of soil type on the behavior of the box culvert. Since no major difference in structural behavior was found between embankment and trench soil installation, only embankment condition was considered for the remainder of the investigation. Two soil types were considered: coarse aggregate (GW type soil) and silty sand (SM type soil). The input parameters for the soil model in CANDE were chosen from standard Duncan's soil parameters in Reference 13. Table 4.1 shows Duncan's hyperbolic parameters used in the analysis.

1. Soil Pressure Distribution

The variation of normal soil pressure at the midspan of the top slab with depth of fill is plottted in Figure 4.17. As can be seen from the figure, GW soil type (coarse aggregate) exhibits lower values of normal soil pressure until the fill height reaches approximately 7 feet. Beyond this it starts to show high values of soil pressure. At a fill height of 20 feet, the soil pressure of GW soil type is almost twice as large as the soil pressure of SM type soil (silty sand). More deformation of the culvert would be expected from higher soil pressure as will be seen later.

The normal soil pressure distribution around the culvert under a fill height of 20 feet is shown in Figure 4.18. This figure reveals an interesting observation. Much higher soil pressure is developed around

Table 4.1 Representative Parameter Values of the Modified Duncan Model (References 12 and 13)

| | GW Soil | SM Soil |
|---|---|---|
| Cohesion, c | 0.0 | 0.0 |
| Friction Angle, Ø | 33.0° | 32.0° |
| Modulus Number, K | 200.0 | 300.0 |
| Modulus Exponent, n | 0.4 | 0.25 |
| Failure Ratio, $R_f$ | 0.7 | 0.7 |
| Bulk Modulus Number, $K_b$ | 50.0 | 250.0 |
| Bulk Modulus Number, m | 0.2 | 0.0 |

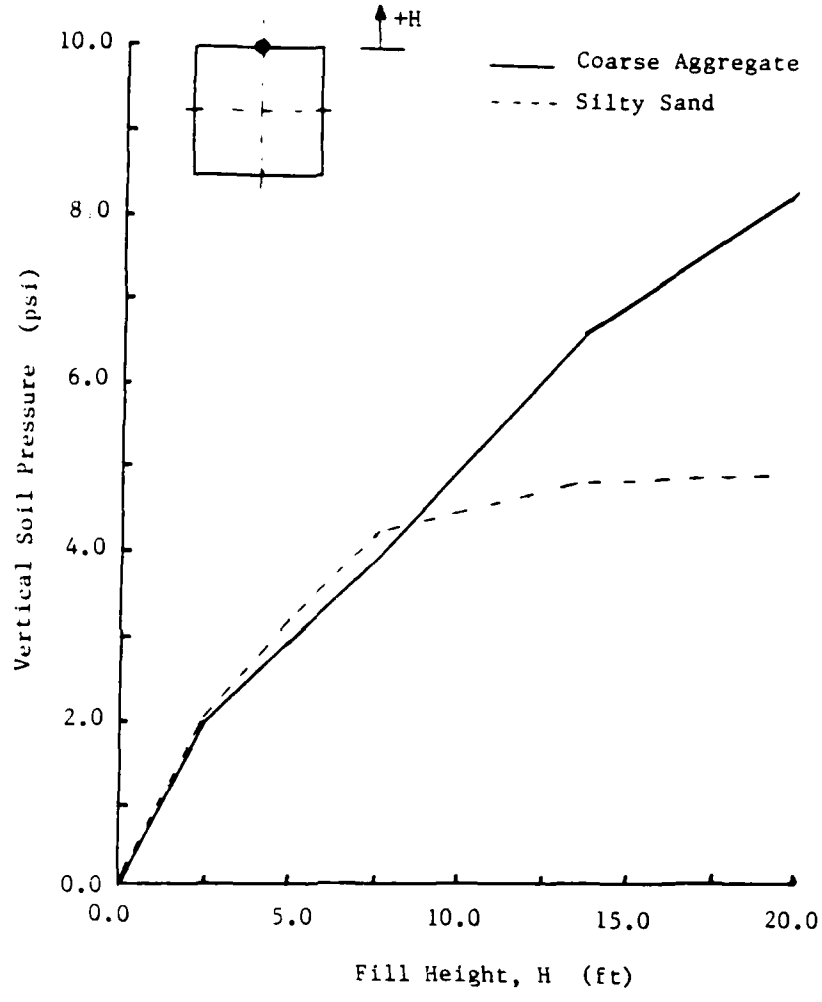



Figure 4.17 Vertical Soil Pressure at Crown

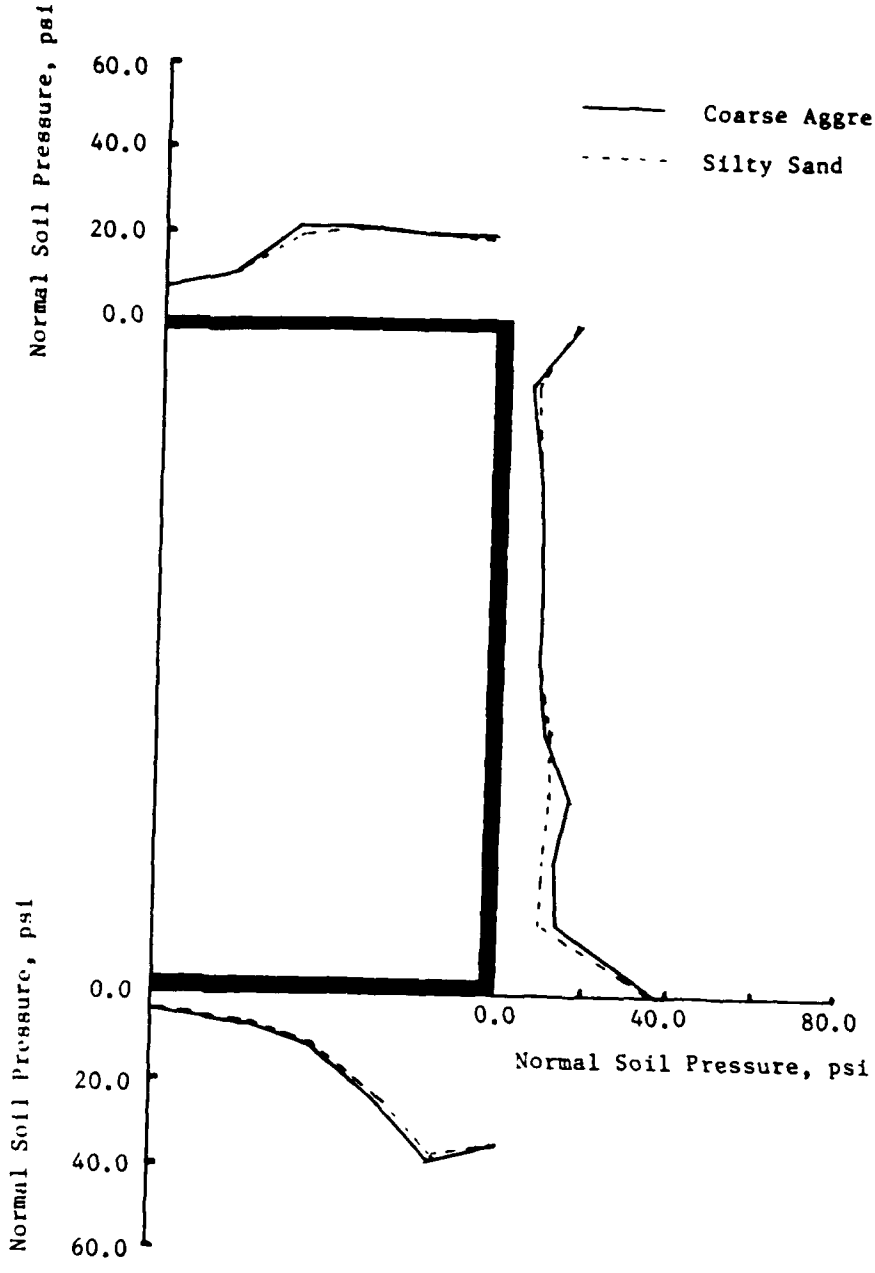



Figure 4.18 Soil Pressure Distribution around the Culvert at Fill Height = 20 ft

the bottom of the culvert. One possible explanation is that since the culvert deforms downward, it is more likely to mobilize passive pressures in the soil adjacent to the bottom corner, with a resultant higher coefficient of soil pressure than is characteristic of the active state.

2. Shape of the Deformed Culvert

Figure 4.19 shows crown deformation versus the depth of fill. SM soil type (silty sand) shows a rising crown deflection until the fill height reaches the crown level of the culvert, followed by a downward linear deformation due to the vertical soil pressure of backfill. By comparison, GW soil type (coarse aggregate) shows no rising crown deflection. The deflection of GW soil type at 20 feet of fill height is about two times larger than the deflection of SM soil type. With the soil pressure previously observed, this confirms that greater deflection of the culvert would be developed from the higher soil pressure.

Figure 4.20 shows the final shape of deformed culvert under the fill height of 20 feet. From this comparison study it is evident that the type of soil is one of major factors governing the behavior of a box culvert, and is an important factor for analysis and design of a box culvert.

3. Bending Moment and Thrust Distribution

Figures 4.21 to 4.25 report the bending moments versus the depth of fill at five locations, and Figure 4.26 shows the bending moment

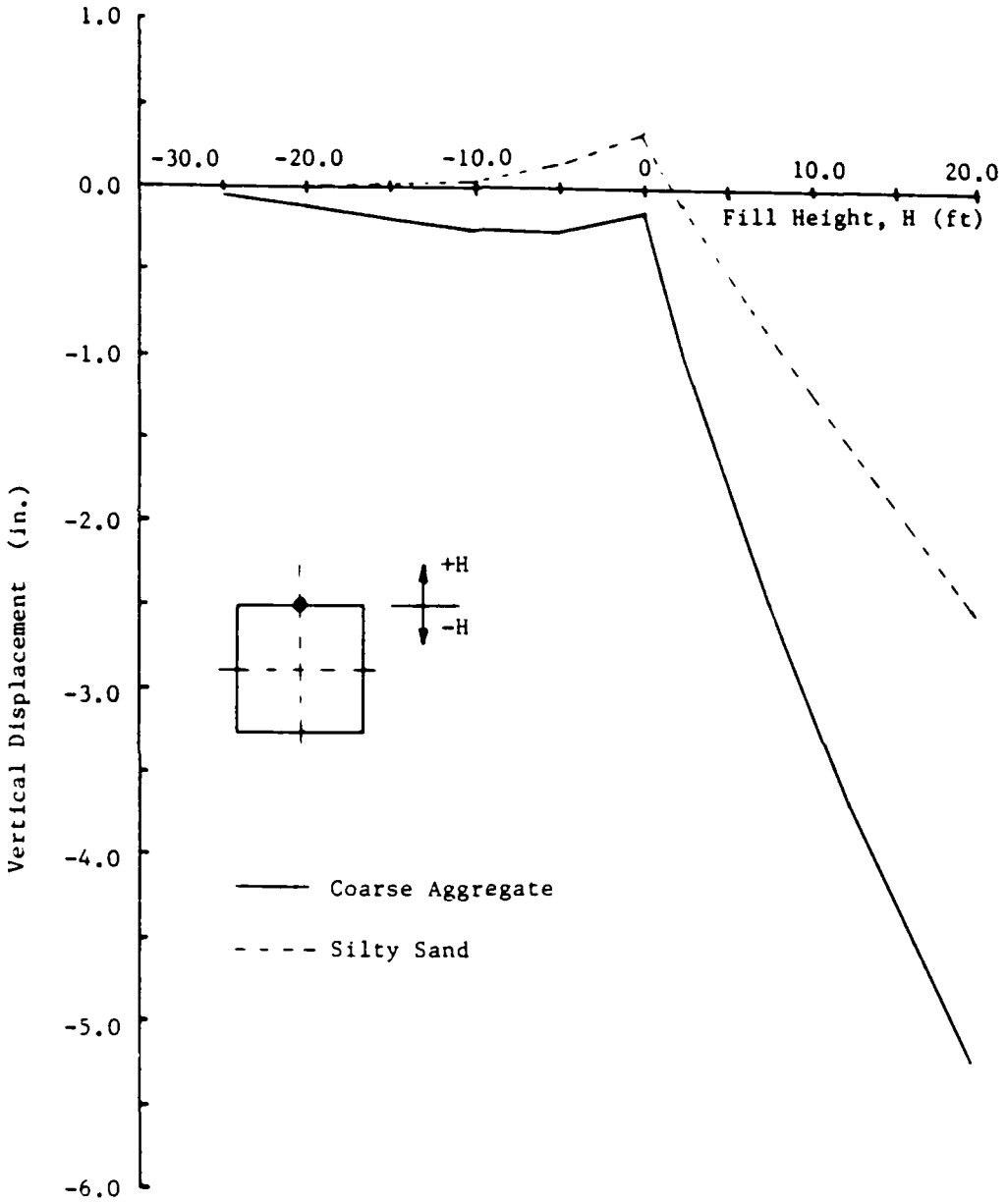



Figure 4.19 Crown Deflection vs. Fill Height

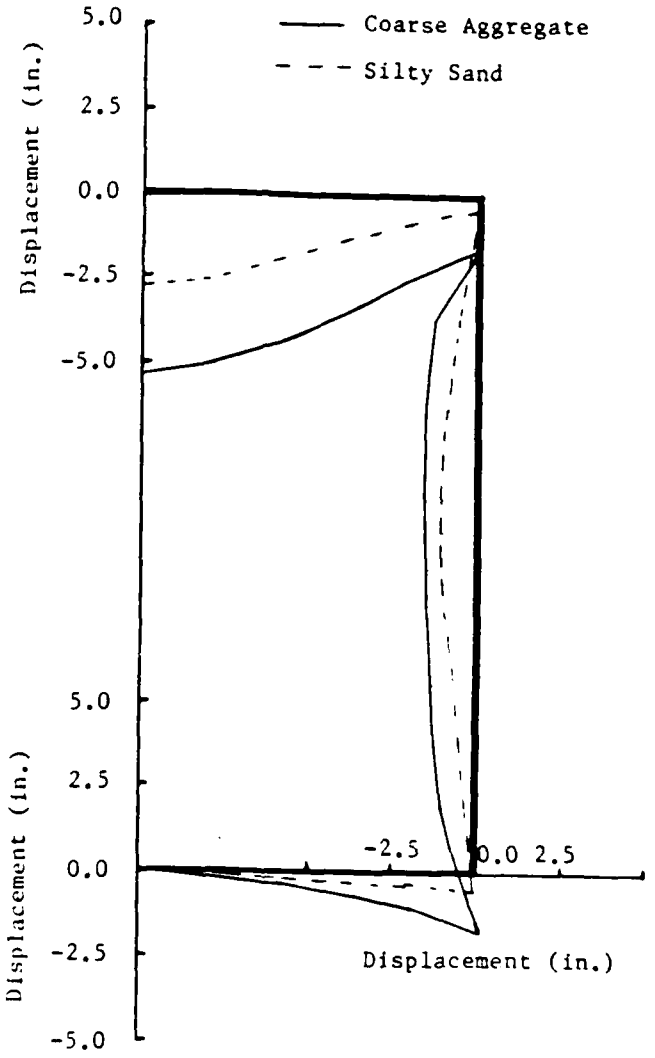



Figure 4.20 Deformed Box Culvert under Fill Height = 20 ft

distribution around culvert under a fill height of 20 feet. Also Figures 4.27 to 4.31 report thrust variations with the depth of fill at five locations. Figure 4.32 shows the thrust distribution around the culvert under fill height of 20 feet.

As expected, the results are similar in shape to those moments and thrusts shown in the previous section. At the end of the last construction increment, positive moments are observed at the midspans of the top slab, vertical wall and bottom slab. Also, negative moments are observed at the top and bottom corners. Finally, the top corner proves to be the most critical section.

Again, all thrusts are tensile (negative) forces under the fill height of 20 feet, and the most critical section is observed to occur one-third of vertical wall height from the bottom.

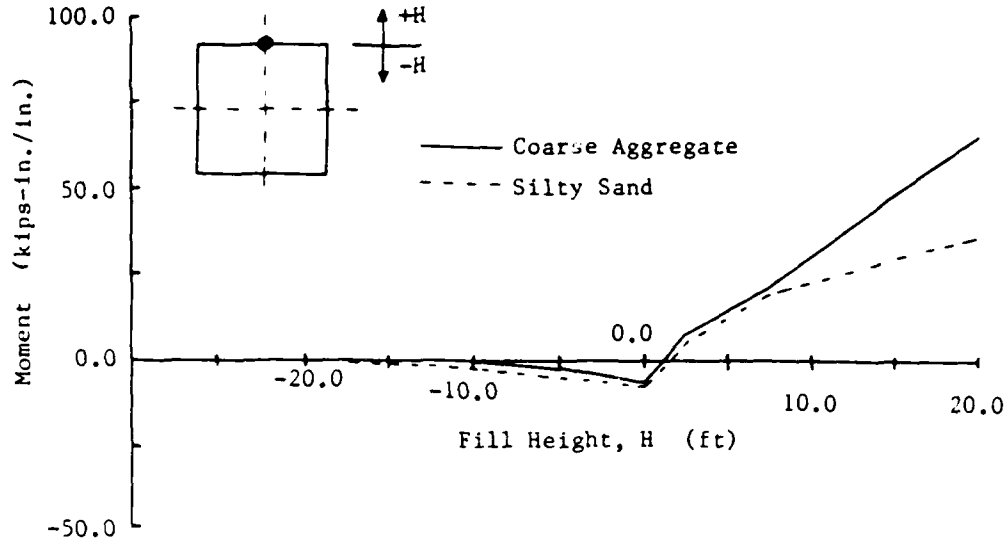



Figure 4.21 Culvert Bending Moments at Strain Gage #1

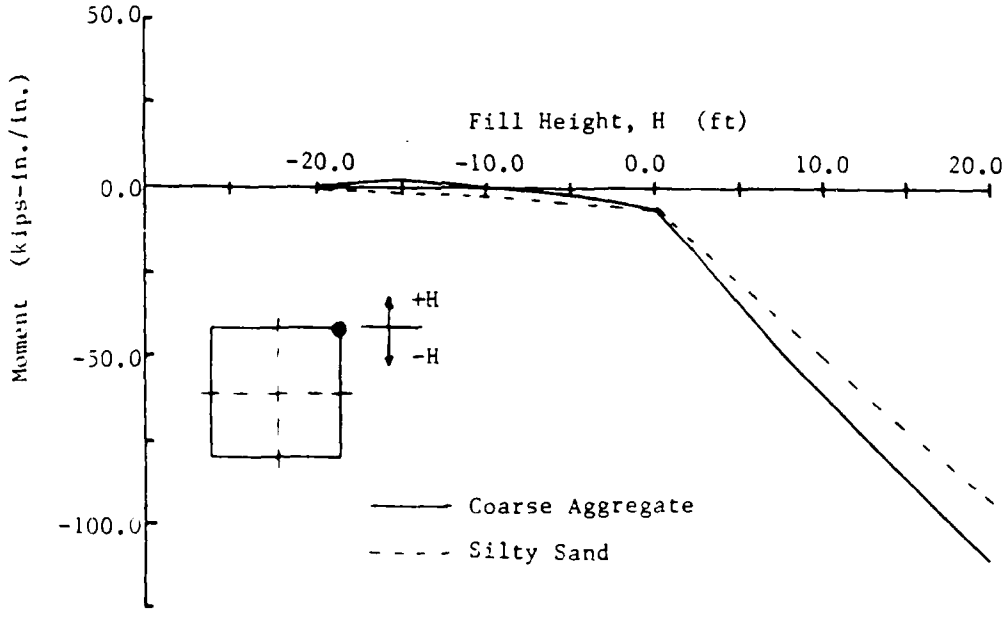



Figure 4.22 Culvert Bending Moments at the Upper Corner

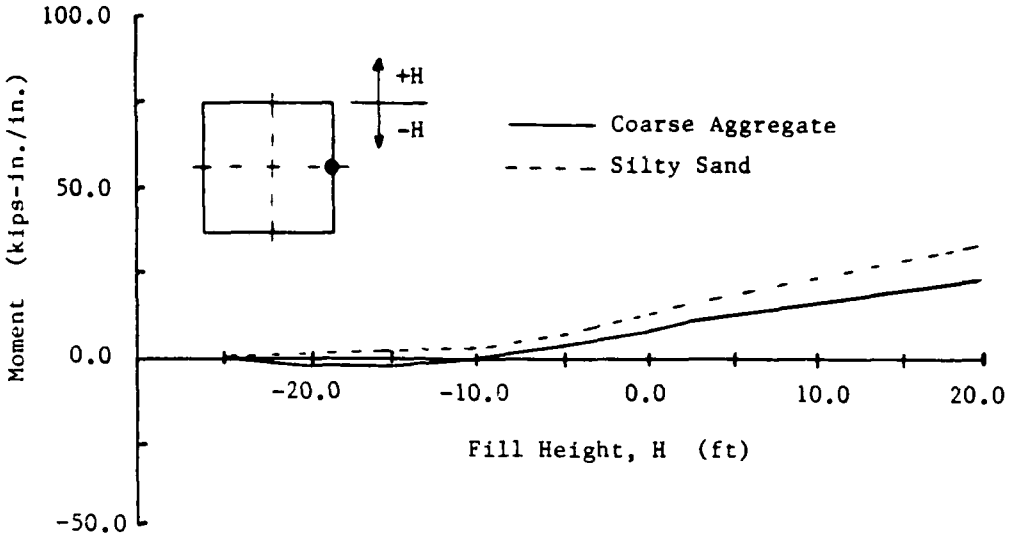



Figure 4.23 Culvert Bending Moments at Strain Gage #4

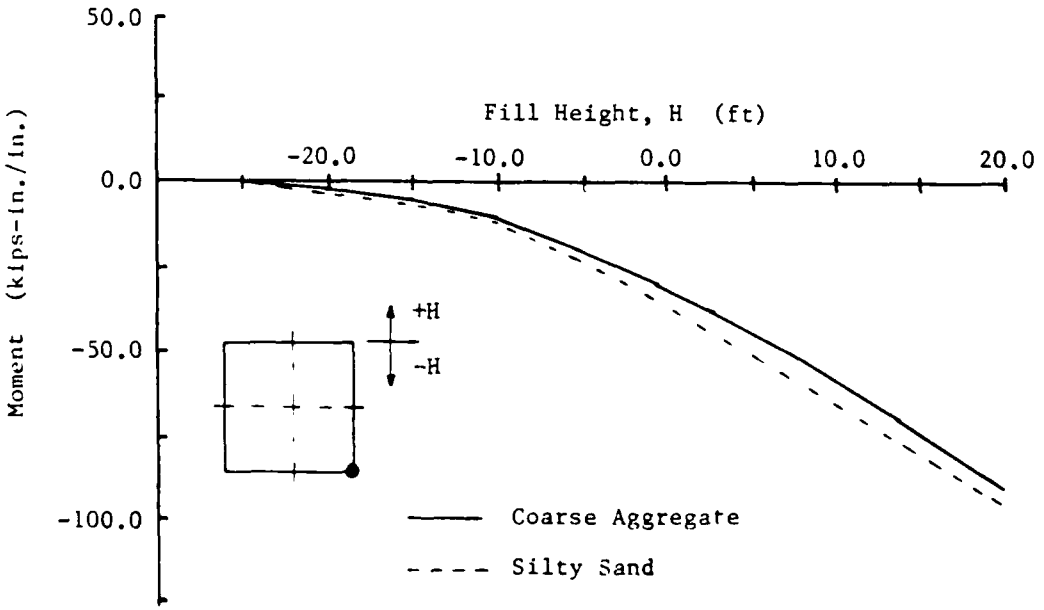



Figure 4.24 Culvert Bending Moments at Bottom Corner

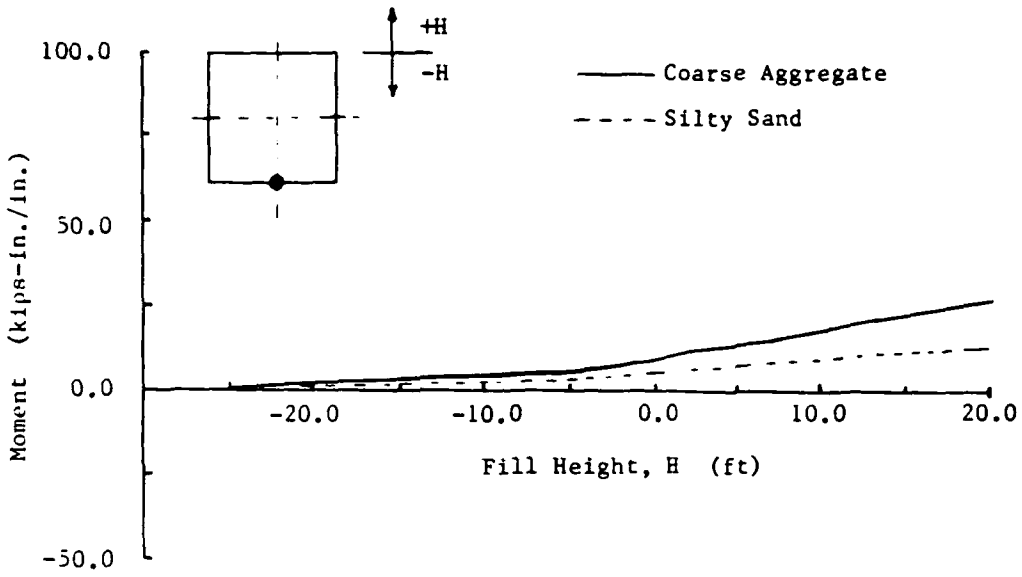



Figure 4.25 Culvert Bending Moments at Strain Gage #7

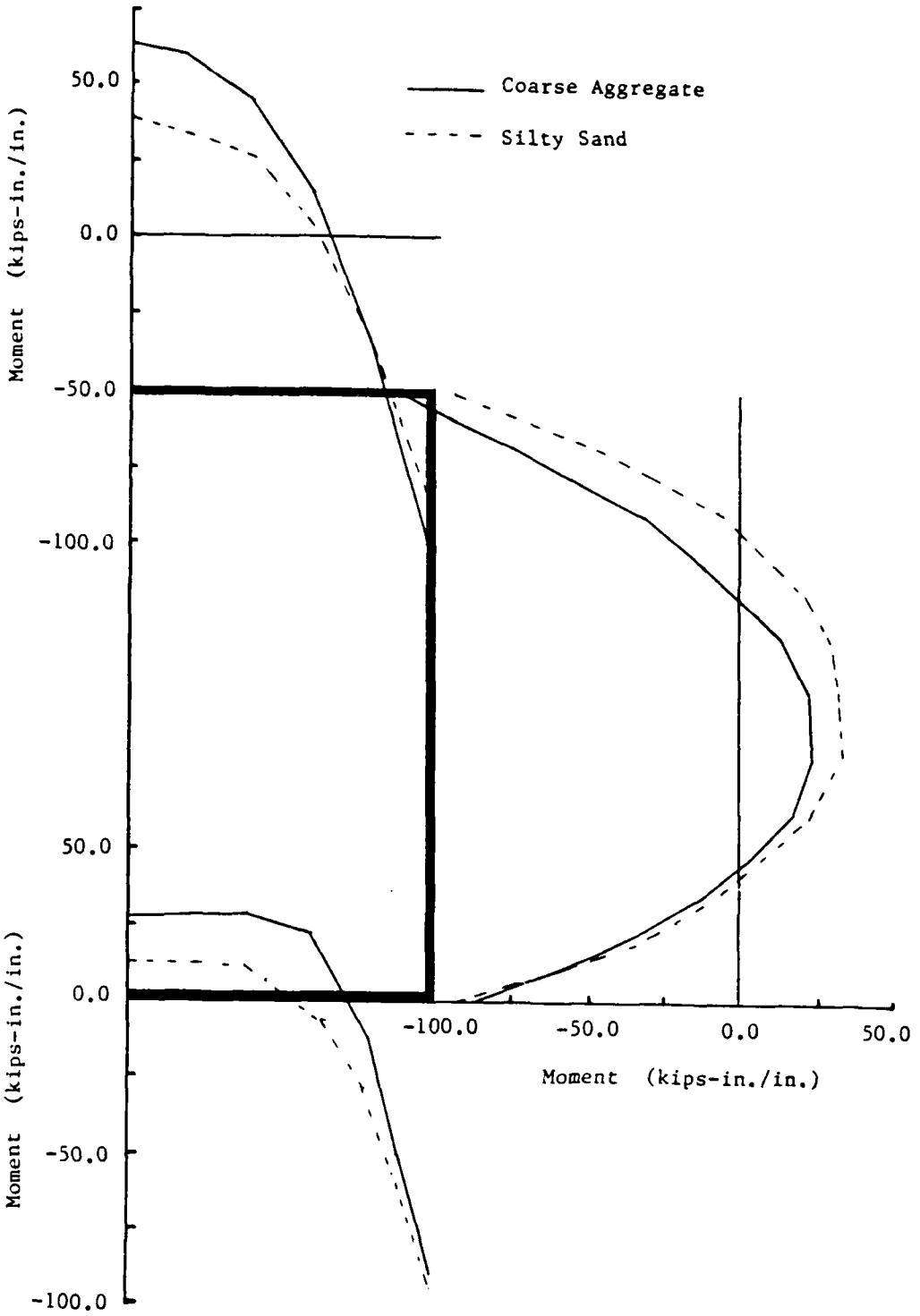



Figure 4.26 Bending Moments around the Culvert at Fill Height = 20 ft

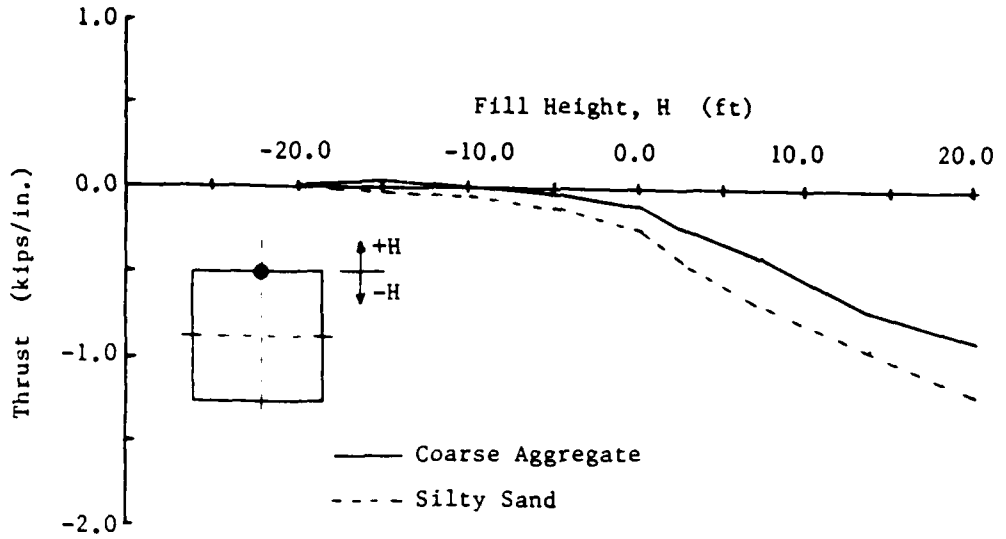



Figure 4.27 Culvert Thrusts at Strain Gage #1

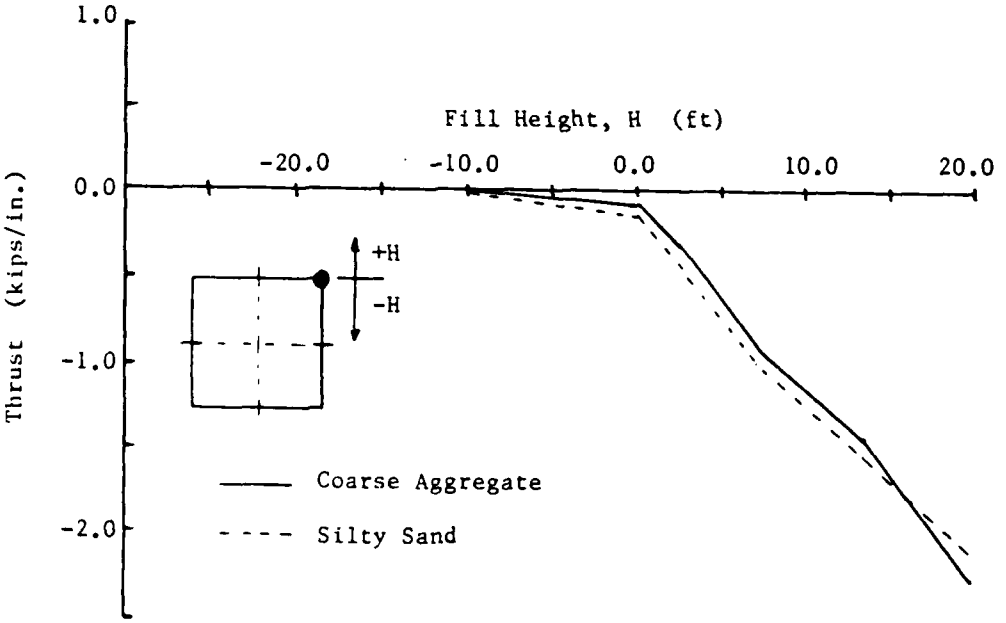



Figure 4.28 Culvert Thrusts at Upper Corner

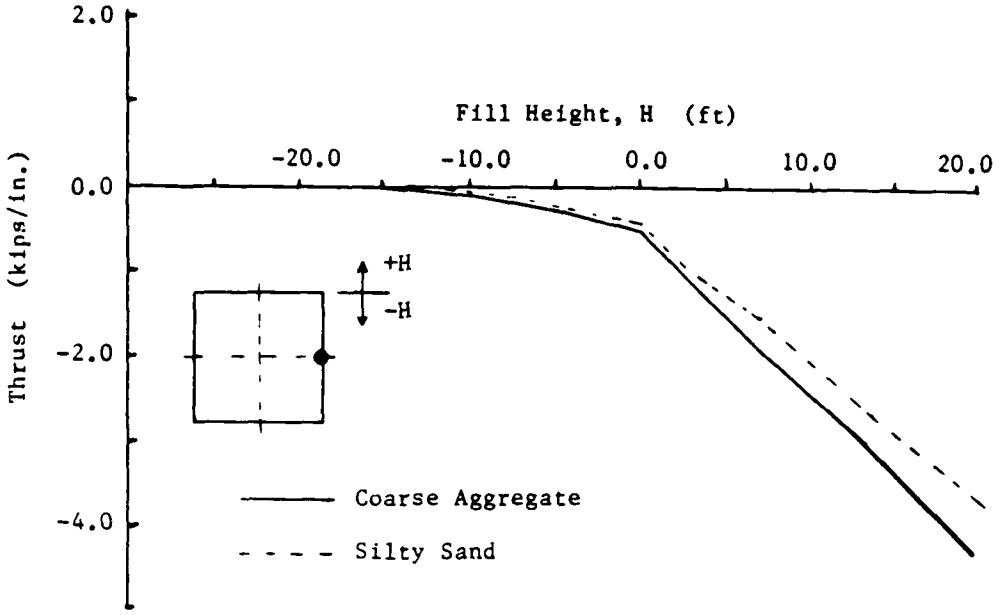



Figure 4.29 Culvert Thrusts at Strain Gage #4

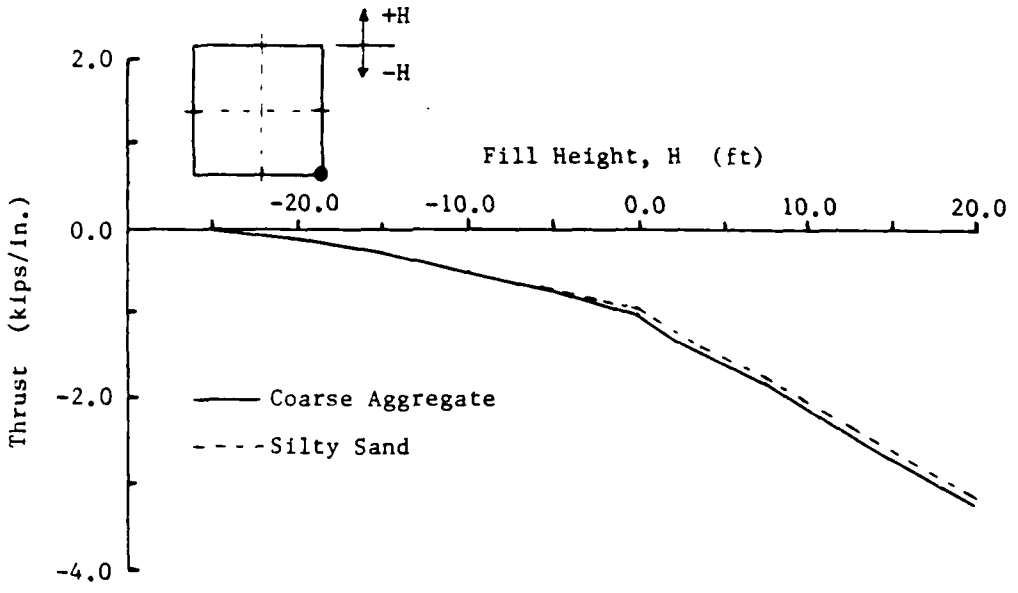



Figure 4.30 Culvert Thrusts at Bottom Corner

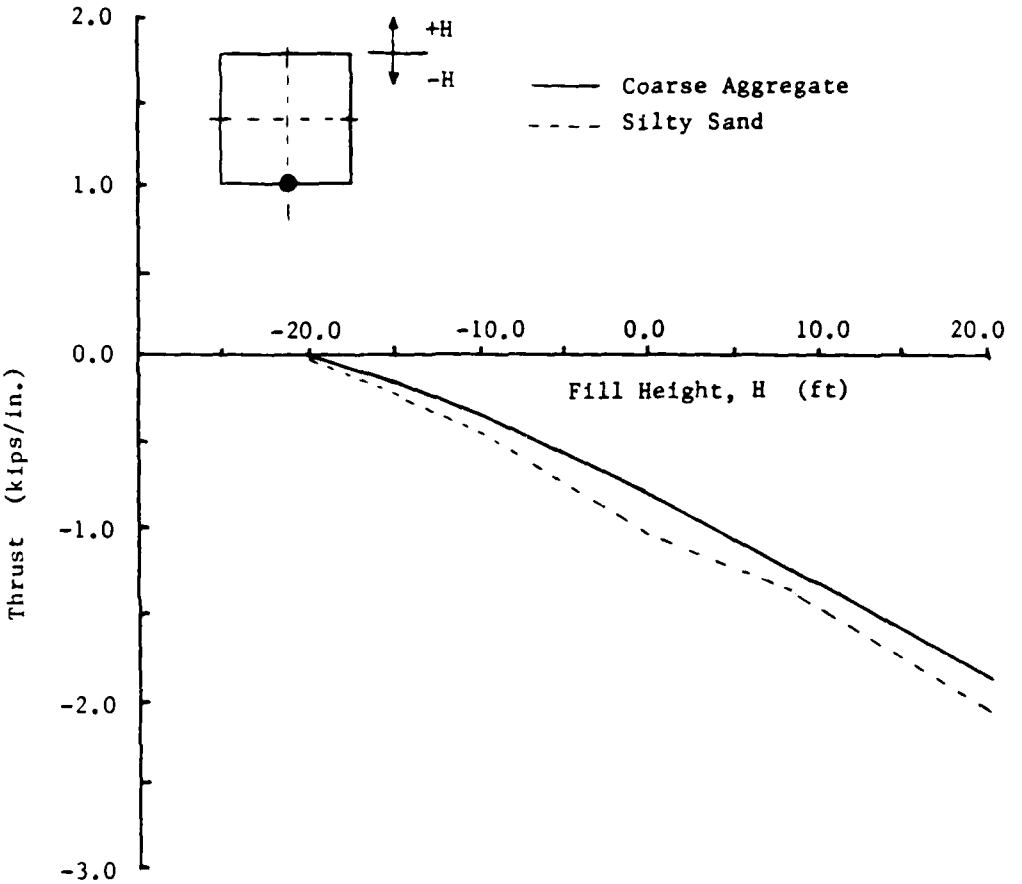



Figure 4.31 Culvert Thrusts at Strain Gage #7

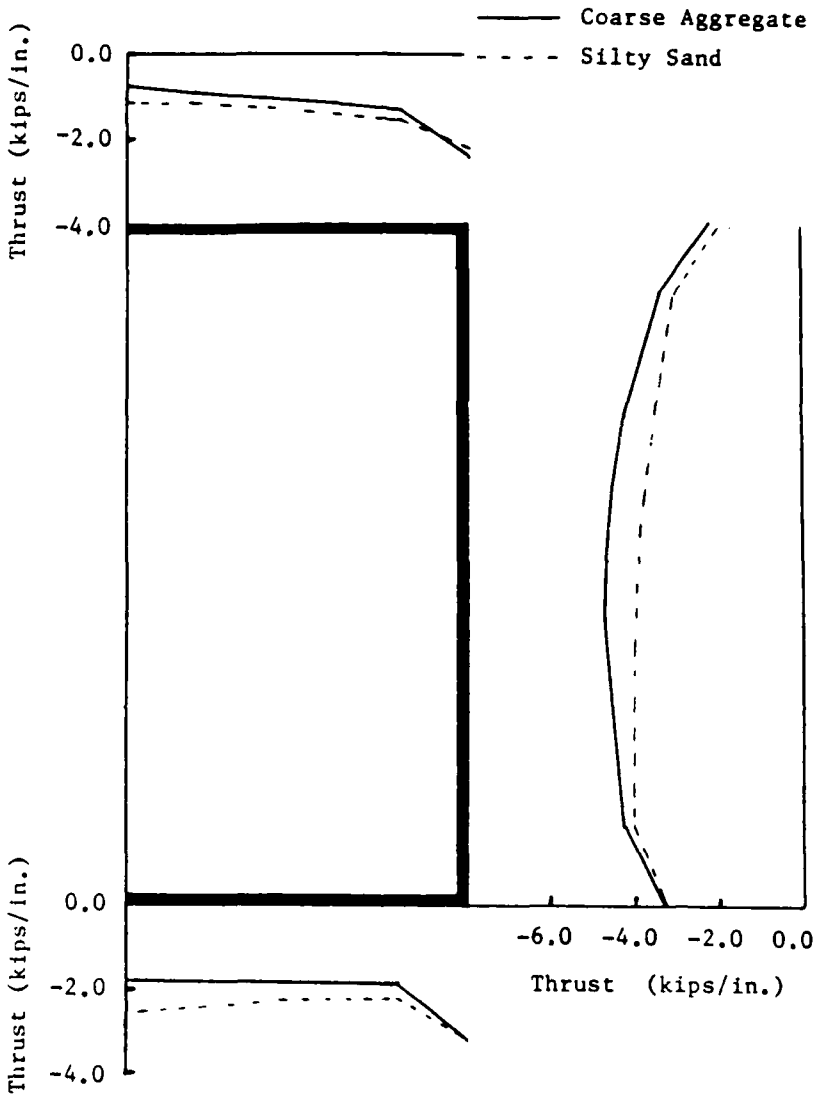



Figure 4.32 Thrusts around the Culvert at Fill Height = 20 ft

## SECTION V

## SUMMARY, CONCLUSIONS AND RECOMMENDATIONS

### A. Summary and Conclusion

This report presents an investigation of the behavior of a concrete box culvert under backfill loads. A centrifuge model technique is used to simulate a prototype structural box culvert, and the measured structural responses are compared with predictions of finite element analyses. Findings and conclusions from this investigation are as follows:

1. The results of the centrifuge model study agree moderately well in shape, but some differences in magnitude are observed when they are compared with the results of finite element analyses.

2. No major difference in structural behavior is observed between trench and embankment soil installation from both the centrifuge model study and numerical analyses except that embankment soil installation produces slightly higher loadings.

3. Maximum bending moment is observed at the upper corner of the culvert as expected.

4. Centrifuge model study and numerical analyses show that all thrusts around the culvert below a fill height of 20 feet are negative (tensile) forces due to deflection of the slab members by soil pressures.

5. Significantly different shapes of the deformed culverts are observed from the finite element analyses when different soil stiffness is used in CANDE. This indicates that soil type is one of important

parameters to be considered in the analysis and design of a culvert.

B. Recommendations

Recommendations for further research based on this study are as follows:

1. The results of centrifuge model study presented in this report are based on the preliminary investigation for the feasibility study of a box culvert in a centrifuge. More comprehensive (extensive) research including culverts of other sizes and geometries, reinforcement, and different soil types and compaction for backfills and bedding parameters is required in order to gain a better understanding of the behavior of a box culvert.

2. In order to achieve accurate model details mentioned in (1) above, a much larger centrifuge is preferable.

3. Once reasonable information is obtained from the comprehensive centrifuge model study and numerical analyses, a field study is necessary to verify the results of centrifuge model study and predictions of finite element analyses.

## REFERENCES


1. Coles, C.K., "Centrifuge Models of a Spile-Reinforced Tunnel," M.S. Thesis, University of California, Davis, June, 1982.

2. Kim, M.M. and Ko, H.Y., "Centrifugal Testing of Soil Slope Models," Transportation Research Record 872, pp. 7-15, 1982.

3. Rowe, P.W. and Craig, W.H., "Application of Models to the Prediction of Offshore Gravity Platform Foundation Performance," International Conference on Offshore Site Investigation, pp. 269-281, Graham and Trotman, London, 1980

4. Shen, C.K., Kim, Y.S., Bang, S. and Mitchell, J., "Centrifuge Modeling of a Lateral Earth Support," Proceedings of the ASCE, Journal of the Geotechnical Engineering Division, Vol. 108, No. GT9, pp. 1150-1164, September, 1982.

5. James, R.G., and Larsen, H., "Centrifugal Model Tests of Buried Rigid Pipes," Proceedings of the Ninth International Conference on Soil Mechanics and Foundation Engineering, Tokyo, Japan, 1977.

6. Scott, R.F., and Morgan, N.R., "Feasibility and Desirability of Constructing a Very Large Centrifuge for Geotechnical Studies," Report 760-170 NSF, California Institute of Technology and JPL, March, 1977.

7. Li, X.S., Personnal communication, Department of Civil Engineering, University of California, Davis, California, 1985.

8. Ju, Personnal communication, Department of Civil Engineering, University of California, Davis, California, 1985.

9. Shen, C.K., Li, X.S. and Kim, Y.S., "Microcomputer Based Data Acquisition Systems for Centrifuge Modeling," Proceedings of the ASTM, Geotechnical Testing Journal, Volume 7, Number 4, pp. 200-204, December, 1984.

10. Yang, F., Personnal communication, Department of Civil Engineering, University of California, Davis, California, 1985.

11. Katona, M.G., Smith, J.M., Odello, R.J., and Allgood, J.R., "CANDE - A Modern Approach for the Structural Design and Analysis of Buried Culverts," Report No. FHWA/RD-77/5, Federal Highway Administration, Washington, D.C., October, 1976.

12. Katona, M.G., Vittes, P.D., Lee, C.H., and Ho. H.T., "CANDE-1980: Box Culverts and Soil Models," Report No. FHWA/RD-80/172, Federal Highway Administration, Washington, D.C., May, 1981.

13. Duncan, J.M., et al., "Strength, Stress-Strain and Bulk Modulus Parameters for Finite Element Analyses of Stresses and Movements in Soil Masses," Report No. UCB/GT/78-02, National Science Foundation, April, 1978.

14. Wong, K.S. and Duncan, J.M., "Hyperbolic Stress-Strain Parameters for Nonlinear Finite Element Analysis of Stresses and Movements in Soil Masses," Report No. TE-74-3, University of California, Berkeley, July, 1974.

15. Gardner, M.P. and Jeyapalan, K., "Preliminary Analysis of the Behavior of Reinforced Concrete Box Culverts," Report No. FHWA/TX-82/50+326-1, September, 1982.

1984 USAF-SCEEE FACULTY SUMMER SUPPORT PROGRAM

Sponsored by the

AIR FORCE OFFICE OF SCIENTIFIC RESEARCH

Conducted by the

SOUTHEASTERN CENTER FOR ELECTRICAL ENGINEERING EDUCATION

FINAL REPORT

# EFFECTS OF FLUID SHIFTS AND HYPOVOLEMIA IN INDIVIDUALS WITH DIFFERENT WORKING CAPACITIES WHILE RESTING AT A FIVE DEGREE DECLINATION


| | |
|---|---|
| Prepared by: | William G. Squires, Ph.D. |
| Academic Department: | Biology |
| University: | Texas Lutheran College |
| Research Location: | Aerospace Physiology Laboratory,<br>Biomedical Division,<br>Crew Technology Branch |
| USAF Research Contact: | Sarah Nunneley, Ph.D. |
| Date: | 1985 |
| Contract No.: | 84 RIP 24<br>F49620-82-C-0035 |

# EFFECTS OF FLUID SHIFTS AND HYPOVOLEMIA IN INDIVIDUALS WITH DIFFERENT WORKING CAPACITIES WHILE RESTING AT A FIVE DEGREE DECLINATION

by

William G. Squires

## ABSTRACT

Data from actual space flight studies have demonstrated functional abnormalities and changes of the cardiovascular system immediately post-flight. Interest lies in what occurs to the body during exposure to zero gravity that could account for these post-flight alterations in cardiovascular functions. During zero gravity or head-down rest, the hydrostatic intra- and extravascular pressure gradients that are normally present in the upright position are abolished or minimized. This causes a headward shift of body fluids from the lower portions of the body cavity. This massive fluid shift induces adaptive changes in other body systems, such that re-exposure to normal gravitational forces produces signs of orthostatic intolerance. These adaptive changes include the following: inhibition of the renin-angiotensin and ADH systems, diuresis, decreased blood volume, weight loss associated with diuresis and decreased blood volume, inhibition of sympathetic activity due to decreased levels of circulating catecholamines and increased activity of the carotid sinus nerve, decreased stroke volume, no change (or slight increase) in arterial pressure, cardiac output, or the contractile state of the heart, compensatory

bradycardia, increased right and left atrial filling pressures and central venous pressure, increased left ventricular end-diastolic volume and left ventricular ejection fraction, decreased leg volumes and increased forearm volumes. Preliminary studies were done on a dog and the expected changes in the cardiovascular parameters were found. Contractility of the heart increased, left ventricular pressure increased, left ventricular end-diastolic pressure increased, heart rate decreased, renal blood flow and carotid blood flow increased, and systemic arterial pressure increased after the dog was tilted five degrees head-down for one hour.

## I. INTRODUCTION:

The major focus of the experiment was to compare responses to zero gravity and orthostatic tolerance post-tilt between individuals with different fitness levels. Understanding the mechanisms involved required elucidation of changes in plasma renin-angiotensin levels, plasma catecholamine levels, body fluid shifts, and segmental volume changes. As a result, further significance could be drawn from this study regarding the use of the head-down tilt method as a means of pre-flight preparation for the pilot.

With the advent of manned space flight new questions have arisen as to the effects of zero gravity on human cardiovascular function. The adaptive responses of man to this new type of environment involve many interrelated and complex organ systems. Data from actual space flight studies have shown no signs of severe cardiovascular impairment but functional abnormalities and changes of the cardiovascular system have been demonstrated immediately post-flight.[6,9,24,30,31,32] Interest lies in what occurs to the body during exposure to zero gravity that could account for these post-flight alterations in cardiovascular function.

Because of time, method, and other limitations during actual space flight studies, it is necessary to develop ground-based simulations of weightlessness. Bed rest and water immersion both produce the same human responses as those seen with prolonged exposure to zero gravity. However, recent

Russian and American studies have demonstrated that a slightly head-down position (from -4° to -6°) produces effects qualitatively similar to those of bed rest except that the adaptation is accelerated. During short-term experiments head-down tilt produces a greater degree of cardiovascular deconditioning then horizontal bed rest of equal duration. Water immersion has also been used to simulate zero gravity, though there are problems inherent in this technique. Prolonged immersion is logistically difficult because of skin lesions due to maceration and presence of hydrostatic pressures alters respiratory mechanisms. The temperature of the bath is also critical. Thermoregulatory mechanisms disturb the hydrostatic effects if the bath is not theroneutral, i.e., kept at 33-35° C. In general, the comparisons of the effects of space flight and head-down tilt support the use of tilt as a simulation method for cardiovascular studies since it, rather than bed rest and water immersion, most closely resembles conditions during weightlessness.

During normal erect posture most blood volume is usually maintained below the level of the heart. Under zero gravity or head-down rest there is a headward shift of body fluids from the lower portions of the body.[5,6,10,18,40,44] Therefore, blood tends to pool in the thoracic cavity. This massive fluid shift induces adaptive changes in other body systems. These changes are referred to in Figure 1.

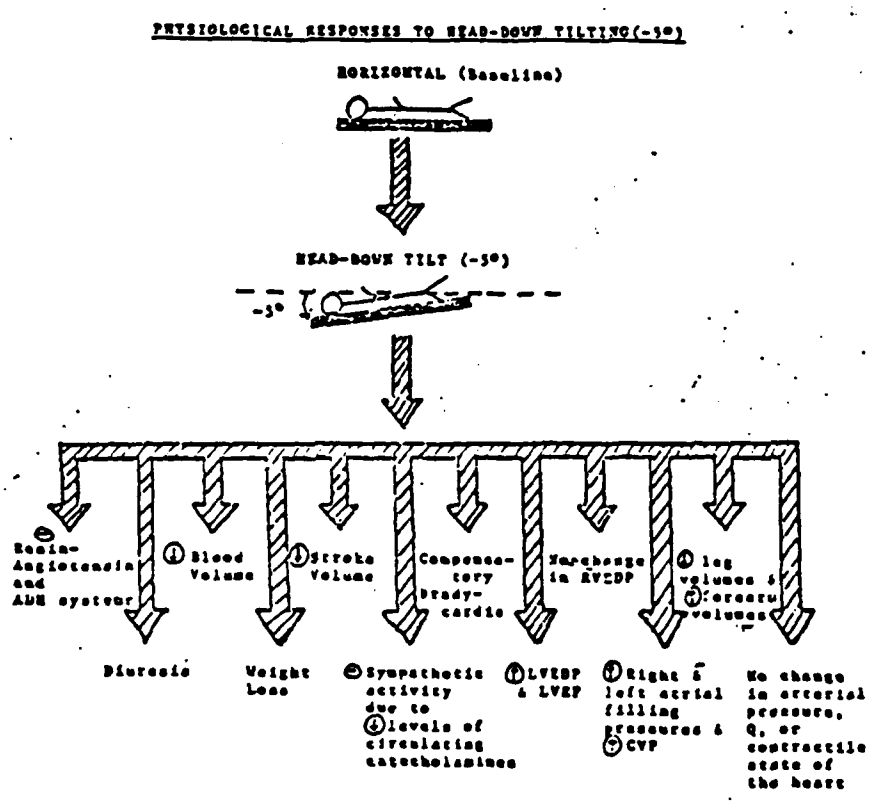



FIGURE 1

Due to the ambitious nature of this project, time limitations and necessary approval of this protocol from the Human Use Committee, this study was not carried out last summer but was done this summer under the same USAF-SCEEE Summer Support Program sponsored by the Air Force Office of Scientific Research. What follows is the protocol for this experiment.

However, a preliminary study involving dog models was undertaken last summer and results showed the expected relative changes in the cardiovascular system of the dog when it was

tilted 5° head-down.

A study similar to the one outlined here using trained and untrained dogs instead of human subjects as the experimental models was also completed in the summer of 1985.

II. OBJECTIVES:

The objects of this experiment are to determine if individuals of different working capacities respond differently to head-down tilting and to elucidate the time course of volume changes in the right and left heart, so that a correlation between these changes with other biochemical and physiological changes may be made. In this way a clearer understanding of the mechanisms involved with volume regulation might be brought forth. Basically, this study was a continuaton of last year's work.

III. PROCEDURES:

A. Human Study: The experiment will use a 2 D echo cardiovascular imaging technique that will measure volume changes in the left heart. Individuals undertaking this protocol will undergo a baseline stress test and 2 D echocardiogram. One week prior to the actual declination study the subject will perform a maximal exercise stress test on the bicycle ergometer so that aerobic capacity can be determined.

The subject will be asked to report to the bedrest facility at 0800 hours on a pre-selected day. He will spend approximately 28 hours in the facility and will be released by approximately 1200 hours the following day. Upon entering the

bedrest facility the subject will recline in a horizontal position on a tilt-table. He will be instrumented with a standard twelve lead ECG, blood pressure cuff and strain gauges to measure anthropomorphic changes. The subject will then be tilted 5° head-down and data collection will take place every 15 minutes for the first hour, every 30 minutes for the next two hours, and once every hour until 1700 hours. No data will be collected during the night. The following morning at 0800 hours there will be another collection of data. At 0900 hours the subject will return to the horizontal position upon which data will also be collected. A post- maximal exercise stress test on the bicycle ergo meter will be conducted and left heart functioning will be studied.

TIMELINE

| ONE WEEK PRIOR: | (Pre) Max Exercise Stress Test (Bicycle ergometer)<br>1st pass $^{201}$Thallium injection (individual attenuations)<br>MUGA — $^{99m}$Technetium injection<br>Max $VO_2$ measurement with radionuclide imaging |
|---|---|
| TIME | ACTIVITY |
| 0800-0900 | Briefing and preparation of the subject<br>$^{99m}$Isotope (technetium) injection |
| 0900 | Horizontal - baseline measurements<br>TILT |
| 0915<br>0930<br>0945<br>1000 | Data collection; radionuclide imaging and blood samples |
| 1030<br>1100 | Data collection; radionuclide imaging and blood samples |
| 1200 | Data collection; radionuclide imaging and blood samples |
| 1200-1300 | Lunch |
| 1300-1700 (hourly) | Data collection; radionuclide imaging and blood sample every Hour |
| 1700-1800 | Dinner |
| 1800-0800 (next day) | Rest in tilt position; no data collection during the night |
| 0900-1000 | $^{99m}$Isotope (technetium) injection<br>RETURN TO HORIZONTAL<br>Data collection; radionuclide imaging and blood sample |
| 1000-1100 | (Post) Max Exercise Stress Test (Bicycle ergometer)<br>Max $VO_2$ measurement with radionuclide imaging |
| 1200 | Dismissal |

FIGURE 2

The approach taken in this protocol will allow elucidation of the time course of volume changes left heart and possible correlation between these changes with other biochemical and physiological changes.

B. Dog Study: A healthy mongrel dog (17.6 kg) was used as an experimental animal. The animal was anesthesized with thiamyl sodium (10 mg/kg i.v.) and ventilated under positive pressure through a cuffed endotracheal tube with a standard volume animal respirator (Harvard Apparatus, Waltham, MA). The animal was positioned on the right side and an incision was made on the left hind leg to expose the saphenous vein into which a catheter was inserted. The catheter was connected to a two-way stopcock so that additional thiamyl sodium could be added to effect. The dog was then placed on its side and a small neck incision was made. The right common carotid was exposed and a pulsed Doppler flow probe tied into place. Careful attention was paid to assure normal carotid artery flow velocity with no constriction. The pulsed Doppler flow probe was calibrated in terms of Doppler frequency shift. A baseline zero can be established and a linear relationship between flow and frequency shift has been established in vivo.[17] A Doppler flow probe was also placed on the right femoral artery under direct vision. Precaution was taken to prevent arterial constriction. The dog was again positioned on the right side and a left flank incision made through which the left renal

artery was identified and encircled with a pulsed Doppler flow probe. As with the other flow probes, careful attention was taken to avoid constriction of the artery. A catheter was inserted into the dog's urinary bladder so that urine output could be measured. Next, a catheter was inserted into the left femoral artery and threaded up into the aorta for measurement of the systemic arterial pressure (Stratham p23Db pressure transducer). Electrocardiographic (ECG) lead AVF was established through a needle lead in all four limbs. A left thoracotomy was performed through the fifth intercostal space and the heart was suspended in a pericardial cradle. With the aid of a purse string suture, a solid state pressure transducer (Koingsberg P-7, Pasadena, CA) was inserted through a stab wound into the left ventricular apex.

The instrumentation allowed for measurement of left ventricular pressure (LVP), left ventricular and diastolic pressure (LVEDP), systemic arterial, systolic and diastolic pressures (SP and DP), heart rate (HR), renal, carotid and femoral artery blood flow (RF,CF,FF), urine output and calculation of the first derivative of left ventricular pressure (LVdP/dt). Recordings were made on an eight channel recorder (Gould brush mark 200).

Following instrumentation, control baseline measurements were made for five minutes of LVP, LVEDP, SP, DP, HR, CF, RF, and FF with the dog in the horizontal position. The dog was then tilted 5° head-down. Measurements were taken every five

minutes for one hour. After one hour head-down the dog was then brought back up to the horizontal position and measurements were taken at five and seven minutes post-tilt. After the last measurements were made, the dog was euthanized with a saturated solution of potassium chloride.

## IV. RESULTS:

The results obtained from this experiment show the expected changes in the cardiovascular parameters. The contractility of the heart increased, left ventricular pressure increased, left ventricular end diastolic pressure increased, heart rate increased, RF and CF increased, and SP and DP increased after the dog was tilted 5° for one hour. Most of the changes occurred during the first 30 minutes head-down and then leveled out for the rest of the hour. When the dog was brought back up to the horizontal position, no change in the readings were evident within five and seven minutes.

## V. RECOMMENDATIONS:

Despite the many studies on man's adaptation to simulated zero gravity, no conclusive evidence exists as to the effect of physical fitness on this response to zero gravity. Although objective comparisons of athletes and non-athletes give variable results, it has been suggested that the more physically fit person (high $VO_2$) is less tolerant to orthostatic stress when volume depleted as a result of diuresis during head-down rest. This loss of blood volume is analogous to heat-releated volume loss.[6,18,19,33]

The investigators in this study would eventually like to find out if, in fact, there are relative physiological and biochemical changes between trained and untrained subjects, dog and human, and if so, to what degree these parameters vary when the subjects go from the horizontal position to a 5° head-down position. Understanding the mechanisms involved requires elucidation of changes in plasma renin-angiotensin levels, plasma catecholamine levels and body fluid shifts. As a result, further significance could be drawn from this study regarding the use of the head-down tilt method as a means of pre-flight preparation for the pilot.

Studies have shown that increased activity of the carotid sinus nerve due to hypervolemia[23,35] or manual stimulation with electrodes[42] results in a reflex decrease in the force of atrial systole by a decrease in sympathetic activity to the heart and an increase in efferent vagal activity to the heart. A suggestion for follow-up research would be to isolate the carotid sinus nerve in an animal model. A small neck incision could be made to expose the left internal carotid artery at its origin where there is a bulbous enlargement, the carotid sinus, which is about 3 mm in diameter and 4 mm in length.[25] It contains an afferent fiber called either the carotid sinus nerve or the Hering nerve which is a branch of the glossopharyngeal nerve (IX). A microelectrode could then be placed on the carotid sinus nerve to measure its electrical activity. Then one could determine if it was stimulation of

the carotid sinus nerve or the reduction in circulating catecholamines that decreases sympathetic activity to the heart resulting in an attenuation of the force of atrial systole.

## Acknowledgement

The author would like to thank the Air Force Office of Scientific Research and the Southeastern Center for Electrical Engineering Education for the opportunity to work on an exciting and mind-stimulating project for the summer. I am grateful for the many things I learned and the interesting experiences I had at Brooks AFB/SAM while honing my research skills. In particular, I would like to acknowledge the Aerospace Physiology Division of the Crew Technology Branch for its hospitality, guidance, patience and excellent working conditions.

Finally, I would like to thank Dr. Carter Alexander for suggesting this area of research, and I would like to acknowledge the collaboration and excellent guidance of Dr. Russell Burton and Dr. Sarah Nunneley.

## REFERENCES


1. Abel, F.L., J.H. Pierce, and W.G. Guntheroth, "Baroreceptors influence on postural changes in blood pressure and carotid blood flow." Am. J. Physiol. Vol. 205(2), pp. 360-364, 1963.

2. Abel, F.L. and J.A. Waldhausen, "Influence of posture and passive tilting on venous return and cardiac output." Am. J. Physiol. Vol. 215(5), pp. 1058-1066, 1968.

3. Auger, R.G., J.E. Zehr, R.G. Siekert, and W.E. Segar. "Position effect on antidiuretic hormone: blood levels in bedrest patients." Arch. Neurol. Vol 23, pp. 513-517, 1970.

4. Bevegard, S., J. Castendors, and L. Lindblad. "Effect of changes in blood volume distribution on circulatory variables and plasma renin activity in man." Acta Physiol. Scand. Vol. 99, pp. 237-245, 1977.

5. Blomqvist, C.G., J.V. Nixon, R.L. Johnson, J.H. Mitchell. "Early cardiovascular adaptation to zero gravity simulated by head-down tilt." Acta Astronautica Vol. 7, pp. 543-553, 1980.

6. Blomqvist, C.G. and H.L. Stone. "Cardiovascular adjustments to gravitational stress." Handbook of Physiology--The Cardiovascular System IV, in publication.

7. Bonde-Peterson, F., Y. Suzki, and T. Sadamoto. "Cardiovascular responses to isometric exercise during simulated zero gravity." The Physiologist pp. 37-38.

8. Brennan, L.A., R.L. Malvin, K.E. Jochim, and D.E. Roberts. "Influence of right and left atrial receptors on plasma concentrations of ADH and renin." Am. J. Physiol. Vol. 221(1), pp. 273-278, 1971.

9. Buderer, M.C., J.A. Rummel, E.L. Michel, D.G. Mauldin, and C.F. Sawin. "Exercise cardiac output following Skylab mission." Aviat. Space Environ. Vol. 47(4), pp. 365-372, 1976.

10. Epstein, M. "Cardiovascular and renal effects of head-out water immersion in man." Circ. Res. Vol. 39(5), pp. 619-628, 1976.

11. Gazenko. O.G., et al. "Effects of various countermeasures against the adverse effects of weightlessness on central circulation in the healthy man." Aviat. Space Environ. Med. Vol. 53(6), pp. 523-530, 1982.

12. Gomez-Sanchez, C., D.C. Kim, N.M. Kaplan. "A radioimmunoassay for plasma aldosterone by immunologic purification." J. Clin. Endocrin. Metab. Vol. 36, pp. 795-798, 1973.

13. Goodall, McC., M. McCally, and J.D. Graveline. "Urinary adrenaline and noradrenaline response to simulated weightless state." Am. J. Physiol. Vol. 206(2), pp. 431-436, 1964.

14. Graveline, D.E. and M. McCally. "Body fluid distribution: implications for zero gravity." Aerosp. Med. Vol. 33 (11), pp. 1281-1290, 1962.

15. Greenleaf, J.E., D. Sciaraffa, E. Schwartz, L.C. Kiel, and P.J. Brock. "Exercise training hypotension: implications for plasma volume, renin, and vasopressin." J. Appl. Physiol.: Respirat. Environ., Exercise Physiol. Vol. 51(2), pp 298-305, 1981.

16. Haber, E., T. Koerner, L.B. Page, B. Klenian, and A. Purnode. "Application of a radioimmunoassay for angiotensin I to the physiological measurements of plasma renin activity in normal human subjects." J. Clin. Endocrinol. Metab. Vol. 29, pp. 1349-1355, 1969.

17. Hartley, C.J., H.G. Hanley, R.M. Lewis, and F.S. Cole. "Synchronized pulsed Doppler blood flow and ultrasonic dimension measurement in conscious dogs." Ultrasound in Med. and Biol. pp. 99-110, 1978.

18. Katkov, V.E., V.V. Chestukkin, R.I. Lapteva, V.A. Yakovleva, V.M. Mikhailov, O. Kh. Zybin, and V.N. Utkin. "Central and cerebral hemodynamics and metabolism of the healthy man during head-down tilting." Aviat. Space Environ. Med. Vol. 50(2), pp. 147-153, 1979

19. Klein, K.E., H.M. Wegmann, and P. Kuklinski. "Athletic endurance training - advantage." Aviat. Space Environ. Med. Vol. 48(3), pp. 215-222, 1977.

20. Klein, K.E., H.M. Wegmann, H. Bruner, and L. Voght. "Physical fitness and tolerance to environmental extremes." Aerosp. Med. Vol. 40(9), pp. 998-1001. 1969.

21. Lamb, L.E., R.L. Johnson, P.M. Stevens, and B.E. Welch. "Cardiovascular deconditioning from space cabin simulator confinement." Aerosp. Med. Vol 35, pp. 420-428, 1964.

22. Liu, C.T., H.E. Hoff, and R.A. Huggins. "Circulatory and respiratory responses to platural changes in the hemorrahagic dog." J. Appl. Physiol. Vol 27(4), pp. 460-464, 1969.

23. Mancia, G., J.T. Shepherd, and D.E. Donald. "Interplay among carotid sinus, cardiopulmonary, and carotid body reflexes in dogs." Am. J. Physiol. Vol. 230(1), pp. 19-24, 1976.

24. Michel, E.L., J.A. Rummel, and C.F. Sawin. "Skylab experiment M-171 'metabolic activity' - results of the first manned mission." In Biomedcal Results from Skylab. (Edited by R.S. Johnston and L.F. Dietlein), pp. 284-312, NASA, Washington, D.C.

25. Miller, M.E. "The head." In Guide to the Dissection of the Dog, p. 289, Ithaca, New York.

26. Miller, P.B., R.L. Johnson, and L.E. Lamb. "Effects of four weeks of absolute bed rest on circulatory functions in man." Aerosp. Med. Vol. 42, pp. 1194-1200, 1964.

27. Myhre, L.G., D.K. Brown, F.G. Hall, and D.B. Dill. "The use of carbon monoxide and T-1824 for determining blood volume." Clin. Chem. Vol. 14, pp. 1197-1205, 1969.

28. Nickel, J.F., L. Levine, and J.A. Gagnon. "Effects of acute passive tiltng on arterial pressure, renal hemodynamics, and urinary electrolyte excretion in the dog." J. Appl. Physiol. Vol. 9, pp. 176-184, 1956.

29. Nixon, J.V., R. Gordon Murray, C. Bryant, R.L. Johnson, J.H. Mitchell, O. Bryan Holland, C. Gomez-Sanchez, P. Vergne-Marini, and C.G. Blomqvist. "Early cardiovascular adaptation to simulated zero gravity." J. Appl. Physiol. Respirat. Environ. Exercise Physiol. Vol. 46(3), pp. 541-548, 1979.

30. Rummel, J.A., E.L. Michel, and C.A. Berry. "Physiological response to exercise after space flight - Apollo 7 to Apolo 11." Aerosp. Med. Vol. 44(3), pp. 235-238, 1973.

31. Rummel, J.A., C.F. Sawin, M.C. Buderer, D.G. Mauldin, and E.L. Michel. "Physiological response to exercise after space flight - Apollo 14 through Apollo 17." Aviat. Space Environ. Med. Vol. 46(5), pp. 679-683, 1975.

32. Rummel, J.A., E.L. Michel, C.F. Sawin, and M.C. Buderer. "Medical experiment M-171: results from the second manned Skylab mission." Aviat. Space Environ. Med. Vol. 47(10), pp. 1056-1060, 1976.

33. Saiki, H., N. Masayuki, M. Sudoh, M. Abe, Y. Taketomi, and M. Naruse. "Effect of athletic training on physical fitness under hypodynamics." The Physiologist, pp. 39-40.

34. Saltin, B., G. Blomqvist, J.H. Mitchell, R.L. Johnson, Jr., K. Wildenthal, and C.B. Chapman. "Response to exercise after bed rest and after training: a longitudinal study of adaptive changes in oxygen transport and body composition." Circ. Suppl. Vol. 7, pp. 1-78, 1968.

35. Sarnoff, S.J., J.P. Gilmore, S.K. Brockman, J.H. Mitchell, R.J. Linden. "Regulatiion of ventricular contraction by the carotid sinus: its effect on atrial and ventricular dynamics." Circ. Res. Vol. 8, pp. 1123-1136, 1960.

36. Siggers, D.C., C. Salter, and P.A. Toseland. "A double isotope dilution method for differential determination of adrenaline and noradrenaline in plasma." Clinica Chemica Acta. Vol. 30, pp. 373-376, 1970.

37. Stegemann, J., U. Meier, W. Skipka, W. Hartleif, B. Hemmer, and U. Tibes. "Effects of a multi-hour immersion with intermittent exercise on urinary excretion and tilt-table tolerance in athletes and nonathletes." Aviat. Space Environ. Med. Vol. 46(1), pp. 26-29, 1975.

38. Stone, H.L. "Cardiac function and exercise training in conscious dogs." J. Appl. Physiol.: Respirat. Environ. Exercise Physiol. Vol. 42(6), pp. 824-832, 1977.

39. Tipton, C.M., R.A. Carey, W.C. Eastim, and H.H. Erickson. "A submaximal test for dogs: evaluation of effects of training, detraining, and cage confinement." J. Appl. Physiol. Vol. 37(2), pp. 271-275, 1974.

40. Tipton, C.M., A.R. Hargens, P.D. Gollnick, S.J. Mubarad, M.R. Gonsalves, and B.J. Tucker. "Influence of head-down tilt on muscle function and Starling forces." Med. Sci. Sports Exercise, Vol. 13(2), p. 102, 1981.

41. Torphy, D.E. "Effects of short-term bed rest and water immersion on plasma volume and catecholamine response to tilting." Aerosp. Med. Vol. 37, pp. 383-387, 1966.

42. Vatner, S.F., D. Franklin, and E. Braunwald. "Effects of anesthesia and sleep on circulatory response to carotid sinus nerve stimulation." Am. J. Physiol. Vol. 230(1), pp. 19-24, 1976.

43. Vogt, F.B. and P.C. Johnson. "Study of effect of water immersion on healthy adult male subjects: plasma volume and fluid-electrolyte changes." Aerosp. Med. Vol. 38, pp. 447-452, 1965.

44. Wilkens, R.W., S.E. Bradley, and C.K. Friedland. "The acute circulatory effects of the head-down position (negative G) in normal man, with a note on some measures designed to relieve cranial congestion in this position." J. Clin. Invest. Vol. 29, pp. 940-949, 1950.

45. Williams, J.A. and J. Fine. "Measurement of blood volume with a mass apparatus." N. Eng. J. Med. Vol. 264, pp. 842-848, 1961.

# STRUCTURE OF MOLTEN IMIDAZOLIUM CHLORIDE

Final Technical Report Submitted to the

SOUTHEASTERN CENTER FOR ELECTRICAL ENGINEERING EDUCATION

Under the Research Initiation Program

Sponsored by the

AIR FORCE OFFICE OF SCIENTIFIC RESEARCH


| | |
|---|---|
| Subcontract Number: | 84 RIP 25 |
| Principal Investigator: | R. D. Murphy |
| Academic Rank: | Professor |
| Department and University: | Department of Physics<br>University of Missouri-Kansas City |
| Starting Date: | November 1, 1984 |
| Report Date: | January 15, 1986 |

## I. INTRODUCTION

This is the final technical report for Subcontract Number 84 RIP 25 under the Research Initiation Program. The research discussed here is an outgrowth of the author's 1984 work[1] as a Summer Faculty Research Participant in the Chemical Sciences Directorate of the Frank J. Seiler Research Laboratory. Research at the Seiler Laboratory has identified a very interesting class of room-temperature molten salts which appear to have a number of most promising applications. The salts which have been studied[2] are mixtures of aluminum chloride and methylethylimidazolium chloride (MEIC), which at least in some concentration ranges are liquid at temperatures well below room temperature.

The substantial promise shown by these liquids has prompted a great deal of effort to determine and understand their chemical and physical properties. Careful measurements of their phase diagram, conductivity, viscosity[3], nuclear magnetic resonance[4] properties, and transport numbers[5] have recently been published. The NMR studies have provided information about the structure of the melts, and a systematic analysis of the concentration dependence of the chemical shifts has strongly suggested the existence in the melts of structure, i.e. a tendency of the ions in solution to form clusters. Specifically, Fannin et al.[4] have proposed that the anions and cations tend to form "chains" of ions of alternating sign. The Monte Carlo calculations of the author[1] lent

considerable support to this picture of the structure of the fluid. In addition, a simple but physically reasonable explanation for the occurrence of this structure in terms of the known behavior of other molten salts[6,7] was proposed.[1]

Although these preliminary results are physically quite plausible and most encouraging, what has been lacking is a direct comparison with experiment. In particular, although the Monte Carlo code produces a quite specific prediction of the liquid structure factor of the current model of MEIC, there have been no experimental studies of the structure of this substance. In general, theoretical work is essential to understanding the X-ray (or neutron) scattering studies of the structure of liquids. For these reasons, the author proposed under the Research Initiation Program a coordinated theoretical and experimental program to study the structure of one of the simplest of the molten salts of interest, namely pure molten MEIC.

## II. PROGRESS MADE UNDER CONTRACT

The experimental portion of the work was done, primarily by Dr. Fred Ross, at the University of Missouri Research Reactor. Liquid X-ray scattering is very different from the X-ray diffraction patterns produced by a crystalline solid. In particular, the intensity is very much less, the Bragg lines are missing, and the "signal" from the liquid is comparable in magnitude to the "noise" from the glass X ray capillary

tubes used to hold the sample; this "noise" must of course be measured and subtracted out. For these reasons, a conventional GE XRD-6 X ray diffractometer was modified as follows: first, a heating stage was constructed to keep the sample molten during the measurements; second, a new detector mounting to bring the detector to a near position for higher intensities was constructed; third, the tubes containing the samples were mounted in contact with temperature sensors to monitor heating; fourth, the scanning in scattering angle and the data collection were automated and computerized to permit the long run times needed to acquire satisfactory statistics.

Problems and frustrating delays were encountered with the equipment, particularly the electronic instrumentation, and with the MEIC (which is notoriously difficult to handle because of its air sensitivity). Nonethless, the following three major, concrete experimental results, the third of which was not proposed because it was thought to be too difficult, were accomplished. First, X-ray scattering data from molten MEIC just above its melting temperature were obtained. Second, Bragg diffraction lines from <u>crystalline</u> MEIC were observed in the same runs when the temperature was lowered to just below melting. Third, <u>crystals</u> of MEIC were grown; pictures taken with a precession camera showed the spots characteristic of crystalline (but not single-crystal) material. Some samples are apparently good enough to permit crystal structure determination.

Due to the aforementioned delays, the experimental data were obtained only very near the end of the contract period. There were delays, too, in acquiring the "theoretical equipment" (an IBM PC and software) needed for the purposes noted in the proposal, namely: contact with the experimental setup and the capability to transfer files of experimental data; storage, plotting, curve-fitting, and analysis of experimental data; and communication with and file transfer to and from the computer facilities at the Seiler Laboratory. Although these problems have now been overcome, time has not yet permitted the detailed analysis of the experimental MEIC data which is required. But substantial computational work on the extension and refinement of the model[1] of a molten salt has continued. The results, which are even more striking than was previously realized, will be presented at the March 1986 meeting of the American Physical Society.[8]

## III. FUTURE WORK

The work which needs to be done most immediately is: first, the X-ray crystallography of crystalline MEIC; secondly, obtaining better statistics for the liquid phase and analyzing the data theoretically. It is the author's firm belief that structure studies will be of increased importance in the study of the molten salts under investigation as possible battery electrolytes at the Seiler Laboratory. There are a number of worthwhile extensions of this work, which, like the work here discussed, are coordinated theoretical and

experimental efforts. The most immediately and obviously important are:

1. It would be highly desirable to do neutron diffraction studies of the crystalline phase of MEIC and neutron scattering studies of its molten phase, since neutron techniques yield information complementary to that obtained by X-ray diffraction. This experimental work could quite well be done at the University of Missouri Research Reactor: this facility has the highest neutron flux of all reactors in American universities and was recently identified by the National Science Foundation as a major materials research center. The author could perform the theoretical work necessary to interpret the neutron data.

2. Because of the intended application of these molten salts as electrolytes in batteries, the question of their transport properties, e.g. their viscosity, electrical conductivity, and mobility, is crucial. As soon as reasonably accurate intermolecular potentials are determined, the molecular dynamics method should be applied to study these transport properties.

3. Finally, of course, it must be noted that the actual melts of greatest interest are more complex: they include aluminum chloride in varying proportions. All of the above steps (computer studies of the structure accompanied by X-ray and if possible neutron diffraction experiments and calculation of the transport properties) should be taken in the case of these melts. Although this is a rather large task, it is

feasible. The initial steps we have taken under the current contract represent a necessary first step and a very good start on this project and the author feels that the preliminary results discussed here strongly justify extension of the present effort.

## IV. SUMMARY AND CONCLUSIONS

Under this Research Initiation Program contract, we have obtained experimental data on the molten phase of MEIC and, although it was not expected, on its crystalline phase. The author has continued, refined, and extended Monte Carlo calculations on clustering phenomena in molten salts. Experimental equipment has been modified to study X-ray scattering from liquids, and "theoretical equipment" has been acquired to make possible close coordination between theoretical and experimental efforts at the University of Missouri and interaction, particularly computational, with the Seiler Laboratory. The major goal of the Research Initiation Program has been fully achieved: within the budget permitted by the RIP (and with some contributions from the University of Missouri), we have laid the foundation for further work, and we feel that the results we have achieved justify extension of this work. We are most grateful to the Air Force Office of Scientific Research for this program; to SCEEE for its most efficient management of it; and to the Seiler Laboratory, especially Dr. John Wilkes, for their hospitality and interest in and support of this project.

## REFERENCES


1. J. S. Wilkes, J. A. Levisky, R. A. Wilson, and C. L. Hussey, Inorg. Chem. 21, 1263 (1982).

2. A. A. Fannin, Jr., D. A. Floreani, L. A. King, J. S. Landers, B. J. Piersma, D. J. Stech, R. L. Vaughn, J. S. Wilkes, and J. L. Williams, J. Phys. Chem. 88, 2614 (1984).

3. A. A. Fannin, Jr., L. A. King, J. A. Levisky, and J. S. Wilkes, J. Phys. Chem. 88, 2609 (1984).

4. R. O. Watts and I. J. McGee, Liquid State Chemical Physics, (John Wiley and Sons, New York, 1976), pp. 80-87.

5. C. J. Dymek and L. A. King, J. Electrochem. Soc. 132, 1375 (1985).

6. J. P. Hansen and I. R. McDonald, Phys. Rev. A 11, 2111 (1975).

7. M. L. Sabougni, A. Rahman and M. Blander, J. Chem. Phys. 80, 2141 (1984).

8. R. D. Murphy, Bull. Am. Phys. Soc. (to appear).

1984-85 RESEARCH INITIATION PROGRAM

Sponsored by the

AIR FORCE OFFICE OF SCIENTIFIC RESEARCH

Conducted by the

SOUTHEASTERN CENTER FOR ELECTRICAL ENGINEERING EDUCATION

FINAL TECHNICAL REPORT

Project 84 RIP 26

# ALTERNATIVE COMPUTATIONAL METHODS FOR SEPARATED FLOWS ABOUT PITCHED FLAT SURFACES


Prepared by: Larry A. Glasgow

Academic Rank: Associate Professor

Department and University: Department of Chemical Engineering, Kansas State University

USAF Contact: Major John M. Walker, FJSRL, USAF Academy, Colorado Springs, CO 80840


Date: October 17, 1985

## INTRODUCTION

The calculation of incompressible flows over airfoils is of immense practical importance to designers concerned with improved aerodynamic efficiency at maneuvering speeds. The most frequently used approach to this problem at present utilizes the two-dimensional Reynolds equation for the mean velocity field in conjunction with a suitable assumption for the Reynolds "stress", i.e., the turbulent inertia tensor. In this method of attack upon the problem, the Navier-Stokes and continuity equations are written

$$\frac{\partial u_i}{\partial t} + u_j \frac{\partial u_i}{\partial x_j} = \frac{1}{\rho} \frac{\partial \sigma_{ij}}{\partial x_j} \tag{1}$$

and

$$\frac{\partial u_i}{\partial x_i} = 0 \tag{2}$$

where $u_i$ is the instantaneous velocity and $\sigma_{ij} = -p\delta_{ij} + 2\mu s_{ij}$ ($\delta_{ij}$ is the Kronecker delta). The Reynolds decomposition is performed in the usual fashion by letting $u = U + u'$; the equations resulting from these substitutions are time-averaged and simplified by noting that the linear terms in the fluctuating quantities are zero for a statistically stationary process. It is important to note that the Reynolds-averaging procedure must be long compared to the characteristic time scales of the turbulence, yet short when compared to the characteristic times of transient phenomena of interest. In some unsteady flow applications, these requirements will be mutually incompatible. Nevertheless, the result of the procedure described above is the Reynolds momentum equation:

$$\frac{\partial U_i}{\partial t} + U_j \frac{\partial U_i}{\partial x_j} = \frac{1}{\rho} \frac{\partial}{\partial x_j} \left(-p\delta_{ij} + 2\mu S_{ij} - \rho u_i u_j\right) \tag{3}$$

It is, of course, the introduction of the $-\rho u_i u_j$ terms that defines the closure problem of turbulence and constitutes the major difficulty confronting any analyst wishing to employ this method of attack upon the problem. In order for the Reynolds equation to be used for the calculation of airfoil flows of interest it is necessary to introduce some kind of approximation for $\tau_{ij} = -\rho u_i u_j$. The simplest possibilities are descendents of Boussinesq's eddy viscosity model or Prandtl's mixing length model. In the former, turbulent momentum transport is modeled by analogy with Newton's law of viscosity--it is assumed that the required components of the turbulent inertia tensor can be represented by transverse gradients of the mean velocity field, multiplied by a turbulent or eddy viscosity. Of course this type of model is seriously deficient since turbulence is a characteristic of the flow and not of the fluid. It has been noted by many fluid dynamicists, including Tennekes and Lumley [1972], that gradient transport models are not appropriate for turbulent flow with multiple length or velocity scales. Prandtl's mixing length model is of the same general nature, except that it was formulated by analogy with the kinetic theory of gases instead of Newton's law of viscosity. Although it depends upon the mean flow gradient in nonlinear fashion, it could hardly be considered a major improvement since fluid particles in turbulence exchange momentum in continuous fashion and not intermittently as is the case with colliding gas molecules. Except under Knudsen flow conditions, the smallest length scales in turbulence (of the order of the Kolmogorov microscale) are many times larger that the molecular mean free path. Despite these obvious and debilitating fundamental deficiencies such models are widely used; Hegna [1981], for example, chose to let

$$\rho u_i u_j = 2\epsilon_m S_{ij} = \epsilon_m \left(\frac{\partial U_i}{\partial x_j} + \frac{\partial U_j}{\partial x_i}\right) \qquad (4)$$

with $\epsilon_m$ represented by

$$\epsilon_i = \mu(k_1 y D_L)^2 \left(\frac{\partial U^2}{\partial y} + \frac{\partial V^2}{\partial x}\right)^{1/2} Re$$

$$\epsilon_o = \mu k_2 u_e \delta^* Re\gamma \qquad (5)$$

with

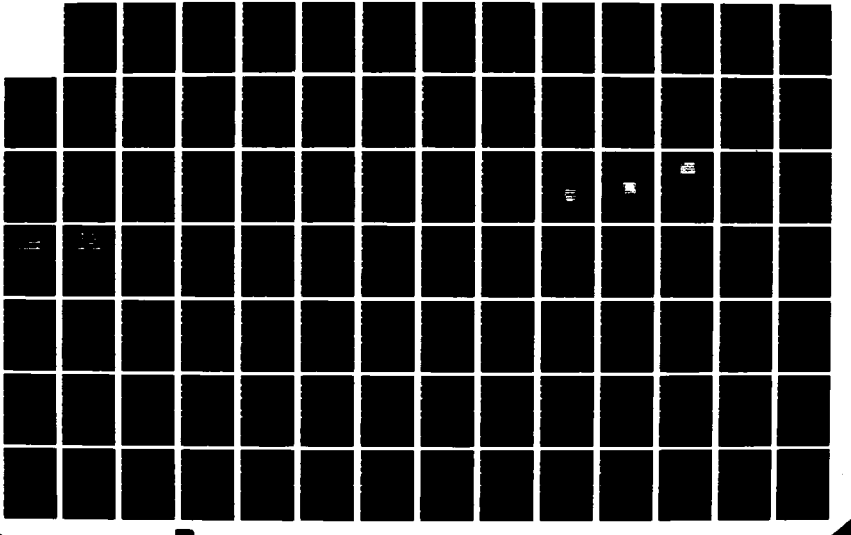
$$D_L = 1-\exp\left(-\frac{y}{A^+}\left|\frac{\partial U}{\partial y}\right|_{y=0} Re\right)^{1/2}$$

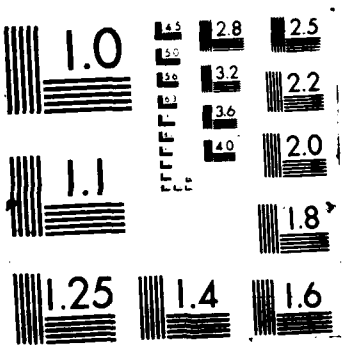
$$\gamma = (1+5.5(y/\delta)^6)^{-1}$$

$$\delta^* = \int_0^\delta (1-U/U_e)dy \qquad (6)$$

The switch from inner to outer models is made when $\epsilon_i$ first exceeds $\epsilon_o$. The gross deficiencies of such a model are obvious and need not be recited here. It is important to remember, however, that this approach is essentially empirical curve-fitting since as Lumley [1980] has pointed out, what is being calculated is the behavior of a fluid with a "different constitutive relation." Indeed, Jobe and Hankey [1980] obtained constants for the above eddy viscosity model for attached flows with constant adverse pressure gradient by adjusting $k_1$, $k_2$, and $A^+$ until calculated and experimental drag coefficients and velocity profiles matched. Thus the results of this type of modeling may produce nearly the correct drag and mean velocity under certain defined or standard conditions, but extrapolation can be dangerous, particularly in situations where there are multiple length and/or velocity scales or additional driving forces such as buoyancy. Despite the well known problems there is currently a huge effort underway in this exact area; the review paper by Kline et al. [1981] gives some indication of the [illegible] of investigators working with the Reynolds equation and turbulence [illegible]. There are many legitimate questions that should be asked about the [illegible] of further work in this area--H. W. Liepmann [1979] [illegible], these efforts "will be of passing interest only

AD-A186 490 UNITED STATES AIR FORCE RESEARCH INITIATION PROGRAM 84/11
1984 RESEARCH REPORTS (U) SOUTHEASTERN CENTER FOR
ELECTRICAL ENGINEERING EDUCATION INC S W D PEELE
UNCLASSIFIED MAY 86 AFOSR-TR-87-1721 F49620-82-C-0035 F/G 15/1 NL




1.0
1.1
1.25
1.4
1.6
1.8
2.0
2.2
2.5
2.8
3.2
3.6
4.0

how gradient transport models used in conjunction with the Reynolds equation will contribute either to our understanding of turbulence or our ability to model the important phenomena.

Assuming that a suitable closure has been achieved, the analyst is still confronted with the task of solving an intractable partial differential equation. Finite difference methods used for problems of this type can be explicit, implicit, or hybrid. Explicit methods are generally easier to program although they are subject to the Courant stability condition which restricts the time increment to

$$\Delta t < \Delta x/(U+a) \tag{7}$$

U + a is the sum of the convection velocity in the x-direction and the speed of sound; a similar restriction exists in the y-direction. Deiwert and Bailey [1984] suggest that explicit methods are a good choice if the time increment constraints are compatible with flow frequency--$\Delta t$ as given by (7) cannot be of the same order as $f^{-1}$. Generally speaking, the thin shear layers found at high Re result in a prohibitive Courant condition and implicit or hybrid methods must be used. Beam and Warming [1978] have devised an ADI sequence for treating the compressible Navier-Stokes equations in conservation-law form; although the alternating-direction implicit or Peaceman-Rachford [1955] method is readily implemented for linear parabolic PDE's such as the heat conduction equation, the nonlinear character of the Navier-Stokes equations is a serious obstacle. Beam and Warming used a truncated Taylor series expansion to achieve linearization but they also caution that the cross-spatial derivatives (e.g., $\partial u_1/\partial x_2$) complicate construction of an efficient algorithm. They employ an explicit representation for these terms without adversely affecting numerical stability.

An alternative hybrid method developed by MacCormack [1978] and used by Hegna [1981], Shang [1978], and others, utilizes equation splitting--an explicit formulation is used for regions dominated by convection and the shear layer is treated implicitly. Deiwert and Bailey [1984] note that it is difficult to efficiently implement this procedure on modern array processors. They also note that finite difference methods in general suffer from aliasing of high frequency energy to larger-scale motions since the grid or mesh with N nodal points can at most support N/2 harmonics of the form $e^{ikx}$.

There are alternatives to the Reynolds equation-turbulence modeling approach; these include sub-grid scale closure models, direct numerical simulation of the Navier-Stokes equations, and the spectral method. Deardorff [1970] has been the principal proponent of sub-grid scale closure--in this method, the large scale motions are explicitly obtained from the Navier-Stokes equations. The very small scale motions are treated statistically and in this manner the Reynolds number limitations of a total numerical simulation are avoided. Orszag [1977], among others, speaks in favor of this approach, noting that the dissipative eddies are less than satisfactory. For purposes of illustration we now consider Deardorff's treatment of planar Poiseuille flow. First, the dependent variables are averaged spatially over the grid spacing:

$$\bar{u}(x,y,x,t) = (1/\Delta x\Delta y\Delta z) \iiint_{x_i - \frac{1}{2}\Delta x_i}^{x_i + \frac{1}{2}\Delta x_i} u(x,y,z,t)\,dx\,dy\,dz \qquad (8)$$

The Navier-Stokes equations can then be written:

$$\frac{\partial u_i}{\partial t} = -\frac{\partial}{\partial x_j}(u_i u_j + u_i' u_j' - \frac{1}{3}\delta_{ij} u_i' u_i') - \frac{\partial}{\partial x_i}(p/\rho_o u^{*2} + \frac{1}{3} u_i' u_i') \qquad (9)$$

In (9), the terms $u'_i u'_j$ represent deviations from the grid-volume means, i.e., the sub-grid scale turbulent inertia tensor; its components are modeled as

$$u'_i u'_j - (1/3)\delta_{ij} u'_l u'_i = -K\left(\frac{\partial u_i}{\partial x_j} + \frac{\partial u_j}{\partial x_i}\right) \tag{10}$$

where K is the sub-grid scale eddy coefficient. It is assumed that

$$K(x,y,z,t) = (c\Delta)^2 \left(\frac{\partial u_i}{\partial x_j}\left(\frac{\partial u_i}{\partial x_j} + \frac{\partial u_j}{\partial x_i}\right)\right)^{1/2} \tag{11}$$

Certainly in this respect, the SGS model is not that much superior to first-order turbulence modeling used in conjunction with the Reynolds momentum equation. Deardorff found that a value of c=0.10 provided realistic results in the integration; larger values were found to produce excessive energy in the sub-grid scale motions. It is essential to remember that this method has been applied to channel flows and atmospheric phenomena--its application to thin shear flows such as turbulent boundary layers will be considerably more difficult.

One would anticipate great difficulty in the direct simulation of the Navier-Stokes equations, since in the past 150 years, only about 75 analytic solutions to the equations have been found--a tribute to the intractability of simultaneous nonlinear partial differential equations. The pursuit of numerical solutions to the full set of equations is hindered by the rapid increase in degrees of freedom (nodal points in finite difference methods) with Reynolds number. Schumann et al. [1980], Liepmann [1979], and Orszag [1977] have all noted that the required degrees of freedom scales with $Re^{9/4}$. If it were possible to deal with a flow where Re=100 with 1000 interior mesh points, the scaling law suggests that $Re=10^4$ would require about $3 \times 10^7$ mesh points. In fact, Orszag notes that an order of magnitude increase in computational power will permit an increase in Re of only 2.15

times and Schumann et al. note that a brute-force simulation on a 10 MIPS machine for $Re=10^4$ would require about 3 years computing time. There are grounds for optimism, however, for free flows and flows in decay, where either the Re is small or the large scale motions can be treated independently of the dissipative structure. There is less reason to be optimistic about success in direct simulation of flows about objects; for turbulent boundary layers or laminar boundary layers undergoing transition, the rapid changes in the streamwise direction cause difficulties in resolution. Furthermore, the downstream or outflow boundary conditions would appear to require complete specification in the wake region--with the concommitant danger that the flow will be over-specified and the results of the direct simulation set in advance.

It appears that for the present purposes, the probability of "success" with either direct simulation or sub-grid scale closure methods is very small. And although the Reynolds equation with turbulence modeling has been and is being widely employed, it too suffers from some serious problems which can be summarized as follows:

1) Correct parameters for the eddy viscosity model(s) will have to be determined for any flow that differs in pressure gradient from those previously treated.

2) There is reason to question implementation of down stream boundary conditions due to the danger of over-specification and the possible upstream propagation of artificial velocity constraints.

3) The averaging process used to obtain the Reynolds equation from Navier-Stokes automatically entails loss of information and it is not at all clear how pervasive this will be with respect to the integral-scale motions.

It is clear, however that the governing PDE will be wrong the instant any first-order closure scheme is incorporated for the turbulent inertia tensor.

4) Deiwert and Bailey [1984], among others, have noted that the application of the Reynolds equation has been limited to two-dimensional flows without freestream turbulence or other perturbation. This type of simulation has resulted in cyclic unsteadiness with a single dominant frequency. More complicated flows will necessitate removal of the Reynolds-averaging restriction.

5) Discrepancies at higher angles of attack in Reynolds equation modeling have been noted by Cebeci et al. [1984] and Shang [1984].

## REVIEW OF LITERATURE

For the above reasons the decision was made to explore the spectral methods described in the monograph of Gottlieb and Orszag [1977] and the review of Gottlieb et al [1984]. Spectral methods have become increasingly popular in recent years resulting in studies of transitional fluid flows [20,32,39], incompressible fluid flow simulations [14,22,25,34,35,36,38,53,54], and most recently for complicated compressible flow fields which include shock waves [12,13,18,45,46]. Interest in spectral methods is due in part to the increased accuracy available for a given number of independent degrees of freedom (i.e. the number of mesh nodes for a finite difference method) in comparison to finite difference techniques; for example see Haidvogel et al. [1980] or Dennis and Quartapelle [1982] for comparisons of accuracy. The spectral methods are often referred to as being infinite-order accurate, that is, if after N terms the error decreases more rapidly than any power of 1/N. Orszag [1971] states that it is possible to decrease the computational time and storage by an order of magnitude. The advent of

the fast Fourier transform in the mid 60's allowed the development of spectral methods, since rapid evaluation of trignometric polynomial coefficients became possible. Much of the work done with respect to fluid dynamics in the area of interest has involved the use of the pseudo-spectral techniques also known as "collocation" or the "method of selected points" (Lanczos [1956]).

Spectral methods represent the solution to the problem as a truncated series of eigenfunctions for the independent varible. The type of series expansion used is based upon the type of boundary condition that is to be satisfied, for example, a periodic boundary condition would suggest the use of a Fourier series representation for the solution. Gottlieb and Orszag [1977] and Orszag [1977] suggest the following series representations:

| Boundary Conditions | Series Representation |
|---|---|
| periodic | exp(inx) |
| inviscid | sin(nx) or cos(nx) |
| no-slip | Chebyshev (Tn(x)) or Legendre (Pn(x)) |

Pseudospectral techniques are deemed the most likely to be appropriate for the problem under consideration; that of computation of separated flow on a pitched airfoil. The principal concept behind pseudospectral calculations as stated by Orszag [1980] is to simply transform freely between physical ($x_j$) and spectral ($a_n$) representations, evaluating each term in whatever representation that term is most accurately, and simply evaluated. Pseudospectral computations have several advantages over spectral algorithms: 1) For complex geometry the solution of the spectral (Galerkin) method requires at least twice the number of fast Fourier transforms than that of the pseudospectral method (collocation); 2) Pseudospectral techniques have significant advantages over spectral techniques when considering

nonlinear partial differential equations since spectral methods can be very computationally expensive in the evaluation of nonlinear partial differential equations.

In order to demonstrate the spectral method consider the one dimensional transient equation:

$$\frac{\partial u}{\partial t} = \frac{\partial^2 u}{\partial x^2} \tag{12}$$

with the boundary and initial conditions

$$u(0,t) = u(\pi,t)=0$$

$$u(x,0) = f(x) \tag{13}$$

the analytic solution to this problem can be shown to be

$$u(x,t) = \sum_{n=1}^{\infty} \left\{ \frac{2}{\pi} \int_0^{\pi} f(x)\sin(nx)dx \right\} \sin(nx)\exp(-n^2 t) \tag{14}$$

Therefore, let $u_N$ be the spectral approximation to u, so that the solution can be approximated as

$$u_N(x,t) = \sum_{n=1}^{N} a_n(t)\sin(nx) \tag{15}$$

Substituting back into equation (12) results in

$$\frac{da_n(t)}{dt} = -n^2 a_n(t) \tag{16}$$

and this set of ordinary differential equations are solved with respect to the initial conditions $a_n(0) = 2/\pi \int_0^{\pi} f(x)\sin(nx)dx$ $(n=1,\ldots,N)$. Gottlieb and Orszag [1977] have shown for this example that $u(x,t)-u_N(x,t)$ goes to zero more rapidly than $\exp(-N^2 t)$ for any $t>0$ and $N\rightarrow\infty$. It can be seen that the spectral approximation of $u(x,t)$ that results is a truncation of the exact solution to N terms. In contrast to this exceedingly good approximation it is possible to construct a spectral method that will arrive at extremely poor results; therefore care must be exercised in the construction of a spectral approximation.

The pseudospectral method is typically chosen over the spectral methods when considering a nonlinear equation. For example consider

$$\frac{\partial u}{\partial t} = \exp(xu)\frac{\partial u}{\partial x} + \frac{\partial^2 u}{\partial x^2} \tag{17}$$

let the approximation $u_N(x,t)$ to $u(x,t)$ be

$$u_N(x,t) = \sum_{n=1}^{N} a_n(t)\psi_n(x) \tag{18}$$

where $\psi_n(x)$ is an orthonormal function. Then the spectral approximation will be

$$\frac{da_n(t)}{dt} = \int \psi_m\left\{\exp[x\Sigma a_n\psi_n]\Sigma a_n\psi_n' + \Sigma a_n\psi_n''\right\} dx \tag{19}$$

It is seen that these equations for $a_n(t)$ are computationally complex due to the resulting integro-differential equation for $a_n(t)$. Therefore, consider the pseudospectral method. First, N collocation points $(x_1, x_2 \ldots, x_N)$ lying within the computational domain are introduced. The approximation (18) is forced to satisfy the governing partial differential equation (17). For example, the following steps would be followed; 1) Determine N coefficients $a_n(t)$ such that

$$u_N(x_j,0) = \sum_{n=1}^{N} a_n(0)\psi_n(x_j) \tag{20}$$

2) Evaluate each term of the governing partial differential equation in either physical or spectral space, whichever gives the most accurate and easily obtainable approximation. For example, $\exp(x_j u_N(x_j,t))$ is evaluated in physical space since the value for $u_N(x_j,t)$ is known and the partial derivatives are evaluated in spectral space since this results in the most accurate representation. 3) Integrate in time with respect to $u_N(x_j,t)$ using the "leap-frog" method or another suitable choice. 4) Repeat steps

1)-3) until the time integration is completed. From this example pseudo-spectral methods are seen to be much easi r to apply to nonlinear equations than corresponding spectral techniques.

The application of boundary conditions in a spectral method can determine the solution's stability. Gottlieb et al. [1981] state that incorrect boundary treatments may give strong instabilities in contrast to finite-difference methods in which this would appear as relatively weak oscillations. Moin and Kim [1980] note that fully explicit pseudospectral solution of the incompressible Navier-Stokes equation have an inherent numerical problem for viscous flows involving solid boundaries, due to enforcing no-slip conditions at the walls. Rudy and Stridwerda [1981] presented a study of inflow and outflow boundary conditions for compressible Navier-Stokes equations of flow past a flat plate. This study, conducted for finite-difference methods of solution, indicates that errors in the data specified at the inflow boundary condition can significantly affect the solution obtained. Gottlieb and Orszag [1977] note spectral methods are extremely sensitive to the formulation of boundary conditions, for example, when improper boundary conditions are imposed, the solution is likely to be "explosively" unstable.

Convergence of the spectral (Galerkin) method has been demonstrated for a Fourier representation with periodic boundary conditions by Hald [1981]. Maday and Quarteroni [1982] have provided stability results and "optimal" convergence rates for Galerkin and pseudospectral approximations (using trigonometric polynomials) for the stationary Navier-Stokes equation with periodic boundary conditions. Canuto [1984] analyzed explicit and implicit methods of imposing boundary conditions for Chebyshev and Legendre approximations of elliptic problems ensuring stability and convergence for these methods. Canuto and Quarteroni [1984] give stability and "optimal"

convergence rates for Chebyshev collocation approximations of variable coefficient elliptic problems with Dirichlet or Neumann-type boundary conditions. Pasciak [1980] investigated spectral and pseudospectral representations of advection equations with the intention of introducing a framework in which finite elements analysis can be applied to spectral methods. In addition error estimates are given for fully discrete explicit pseudospectral as well as semidiscrete spectral and pseudospectral methods.

Some additional considerations are necessary. In the case of a discontinuity, the rate of convergence in the region of the discontinuity is seriously degraded, but spectral approximations are still normally more accurate than corresponding finite difference representations [10]. Additionally, the error is localized better by the spectral method such that less local dissipation is required to smooth the discontinuities. If dissipation or a filtering technique is not used Gibb's phenomena is seen in the region of the discontinuity, and, the resulting error from the lack of smoothing pollutes the solution globally [40]. Majda et al. [1978] have shown for general linear hyperbolic Cauchy problems with nonsmooth initial data that the appropriate smoothing techniques applied to the equation results in stability and that this smoothing combined with smoothing of the initial data gives rise to infinite order accuracy away from the discontinuities of the exact solution. The most prominent examples of discontinuities that have been examined by spectral methods are treatments of shock waves [12,13,18,33,45,46,50,55]. A variety of filters and dissipation functions have been used to damp the oscillations occurring in the solution due to the discontinuity. For example, one sided Schumann filter [12,33], von Hann window filter [18,46], second and fourth-order artificial viscosity [45,50], artificial density [50] as well as the method of

Boris and Book [1976], orginally developed for the construction of finite difference algorithms involving strong shocks [55], have been able to produce an accurate smooth solution for this type of problem. In addition, Gottlieb et al. [1981] used a low-pass spectral filter to remove the high frequency waves that lead to instability and a "cosmetic" filter (a one-sided Schumann filter) to find a nonoscillatory numerical solution.

The spectral and pseudospectral methods have been used successfully to model wakes [33], internally separated flows [22], flow past flat plates [36,53,54] and transonic flows past airfoils [13,50]. The areas of concern to the present work are: representation of two dimensional flow past a pitched plate, problems encountered due to imposition of boundary conditions, and separation that is certain to occur [27].

Both Plotkin [1982] and Kumar and Yajnik [1980] considered separated flow based on the stream function equation

$$\psi_y\psi_{yyx} - \psi_x\psi_{yyy} = Re^{-1}\psi_{yyyy} \tag{21}$$

One of the problems that Kumar and Yajnik note about this problem is the presence of reverse flow--the equation is said to be of mixed-parabolic type. The theory of such equations is not sufficiently developed to indicate boundary conditions that permit solution. Furthermore, the steady-state equation considered by both Plotkin and Kumar and Yajnik must be replaced by a more general representation:

$$(\psi_y \frac{\partial}{\partial x} - \psi_x \frac{\partial}{\partial y})\nabla\psi = Re^{-1}\nabla^2\psi \tag{22}$$

This stream function equation was used by Mei and Plotkin [1984] in determining confined laminar wakes.

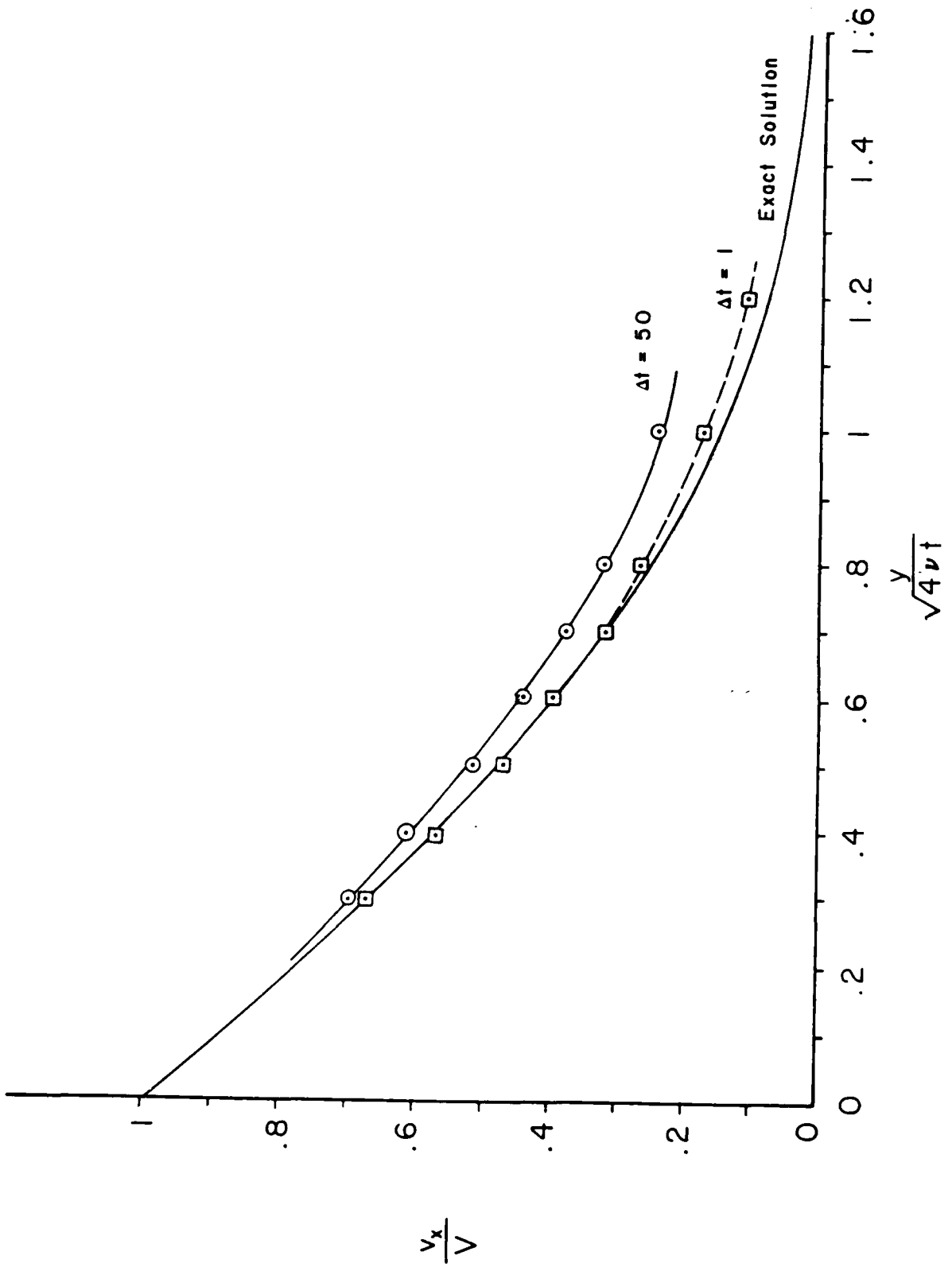
Symmetric flow past a flat plate has been treated by Orszag [1971] and Taylor and Murdock [1980],[1981]. Planar flow has been investigated by Moin and Kim [1980], Orszag and Kells [1980] and Kleiser [1982]. Taylor and

Murdock studied the flow over a flat plate in a range of $1.2x10^5<Re<3.8x10^5$, which is well within the turbulent flow regime. The velocity profile was solved as perturbation about the Blasius velocity profile. Taylor and Murdock used a mesh of 17x17 to solve for the velocity profile, while Orszag used nine collocation points to approximate a one dimensional boundary layer, both studies resulted in accurate approximations.

The treatments of transonic flow by Gottlieb et al. [1984b] and Streett et al. [1985] are interesting in that spectral methods (Chebyshev collocation) are being used. The treatment of transonic flow over an airfoil can be viewed as state-of-the-art in the use of spectral methods because of the difficulty posed by the sharp shock gradients and the computational competition with finite difference methods. Again, it is seen that separation causes difficulty as Streett et al. note that the potential equation which is being solved becomes a mixed elliptic-hyperbolic type and admits weak solutions with discontinuities. Streett et al. use artificial viscosity with a directional bias introduced in the potential equation in the supersonic region to suppress the appearance of compression and expansion shocks due to the presence of a supersonic bubble. It is apparent that the use of multigrid techniques has made spectral methods for steady compressible flow competitive with finite difference methods for problems of aerodynamic interest.

## SOME ILLUSTRATIVE NUMERICAL EXAMPLES

Successful application of spectral method is still something of an art--experience in the selection of appropriate series expansions is a virtual necessity. To illustrate this point and the method in general, a number of


Exact Solution
Δt = 1
Δt = 50
0
.2
.4
.6
.8
1
1.2
1.4
1.6
$\frac{v_x}{V}$
$\frac{y}{\sqrt{4\nu t}}$

$$\phi = \frac{v_z}{(p_o - p_L)R^2/4\mu L} \quad ; \quad \xi = \frac{r}{R} \quad ; \quad \tau = \frac{\mu t}{\rho R^2}$$

at $\tau=0$ a pressure gradient $(p_o - p_L)/L$ is impressed upon the system. This is a more interesting problem because of the variable coefficient $1/\xi$. The analytic solution for this problem is

$$\phi = (1-\xi^2) - 8 \sum_{n=1}^{\infty} \frac{J_o(\alpha_n \xi)}{\alpha_n^3 J_1(\alpha_n)} e^{-\alpha_n^2 \tau} \tag{27}$$

The pseudospectral approximation, $\phi_n$, to the solution, $\phi$, was represented by a Chebyshev polymonial expansion with the coefficients being determined at each time step. Nine terms were included in the series and a time increment of 0.001 was used for integration of equation (26) with an Euler predictor

$$\bar{\phi}(t_2,\xi) - \phi(t_1,\xi) = \int_{t_1}^{t_2} (4 + \frac{1}{\xi}\frac{\partial}{\partial \xi}(\xi \frac{\partial \phi}{\partial \xi}))dt \tag{28}$$

Table 1 illustrates the results obtained for this problem integrated with $\tau=0.05$. It should be noted that a fairly accurate solution was obtained even though few terms were used in the series approximation of the solution. Though this problem may be more demanding than Stokes first problem due to the presence of a varible coefficient it also cannot be regarded as a demanding test.

The classical Gratez thermal entrance length problem was selected as the final example--primarily because the exact solution is known. However, this is a more strenuous test of the method because of the initial discontinuity (producing an infinite Nusselt number). The governing equation after insertion of the parabolic velocity distribution is

$$RePr[1-r^{*2}]\frac{\partial \theta}{dz^*} = \frac{1}{r^*}\frac{\partial}{\partial r^*}(r^* \frac{\partial \theta}{\partial r^*}) \tag{29}$$

| $\xi$ | $\phi(0.05,\xi)$ | $\phi_N(0.05,\xi)$ | % Error |
|---|---|---|---|
| 1 | 0 | 0 | 0 |
| 0.9239 | 0.1054 | 0.07848 | 25.5 |
| 0.7071 | 0.2056 | 0.1796 | 12.6 |
| 0.3827 | 0.1941 | 0.1998 | 3.0 |
| 0 | 0.2000 | 0.2032 | 1.6 |

Table 1: Comparison of Pseudospectral prediction of unsteady laminar flow to the analytical solution with 4 terms of the series being retained. (Eq. (27)).

The difficulty arising at the wall where r=R is apparent. It was also thought likely that the Euler predictor used previously would prove inadequate, so the fourth-order Adams-Bashforth method was used in its place, although the Euler expression was used to get started. Some oscillatory behavior was detected originally in the approximate solution and this was dealt with by incorporation of limited digital filtering. The predictor formulation is again

$$\theta(r^*, z^*_2) \quad \theta(r^*, z^*_1) = \int_{z^*_1}^{z^*_2} \frac{1}{RePr(r^* r^{*3})} \frac{\partial}{\partial r^*} \left(r^* \frac{\partial \theta}{\partial r^*}\right) dz^* \qquad (30)$$

where

$$\theta = \Sigma a_n(z^*) F_n(r^*)$$

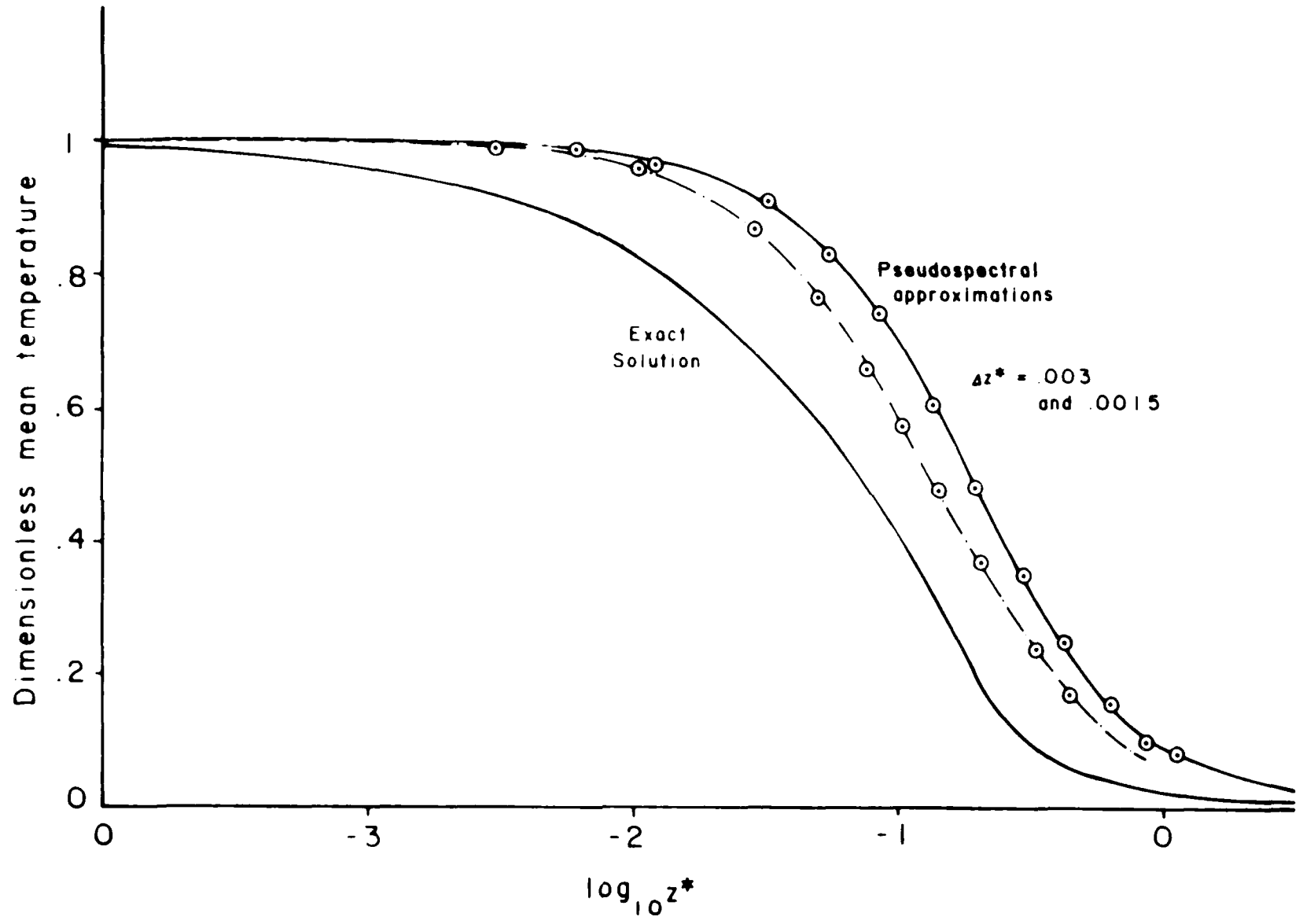
Figure 2 illustrates the results obtained using a dimensionless axial ($z^*$) increment of 0.003; the abcissa is dimensionless axial distance and the ordinate is dimensionless mean temperature. The approximate solution is qualitatively good, but quantitatively disappointing. Clearly a reduced step-size would be necessary in order to produce an acceptable approximation.

## EXTERNAL SEPARATED FLOWS

Consider the two dimensional incompressible Navier Stokes equation for flow past a pitched flat plate expressed in terms of the stream function

$$\frac{\partial}{\partial t}\nabla\psi = (\psi_y \frac{\partial}{\partial x} \quad \psi_x \frac{\partial}{\partial y})\nabla\psi \quad \nu\nabla^2\psi \qquad (31)$$

The transient response of the flow to a periodic forcing function is the ultimate goal, but the first step is to consider the steady state solution. A Fourier spectral solution for the steady state form of equation (31) was presented by Mei and Plotkin [1984] for confined laminar wakes. The use of the Fourier spectral method by Mei and Plotkin was made possible due to


Dimensionless mean temperature
1
.8
.6
.4
.2
0
0
-3
-2
-1
0
$\log_{10} z^*$
Pseudospectral approximations
Exact Solution
$\Delta z^* = .003$ and .0015

periodic boundary conditions. In the present study a pseudospectral approximation will be used based on orthogonal Chebyshev or Legendre polynomials. Relating the collocation points to the structure of Chebyshev or Legendre polynomials results in good approximations. It should be noted that it is possible to use equally-spaced Chebyshev collocation, but as the number of data points increase beyond 10 Chebyshev interpolation rapidly decreases in accuracy [52]. This decrease in accuracy is not a problem when considering a Legendre expansion.

The problem with equally spaced points for the Chebyshev collocation can be avoided if interpolation points on the interval (-1,1) are chosen to be

$$x_j = \cos(\frac{\pi j}{N}); \quad (j=0,1,\quad ,N) \tag{32}$$

for a Nth order Chebyshev polynomial approximation. A Chebyshev polynomial of degree n is defined as

$$T_n(x) = \cos(n \arccos(x)) \tag{33}$$

it follows that

$$T_n(x_j) = \cos(\frac{\pi jn}{N}), \quad (j=0,1,\quad ,N)$$

The Chebyshev polynomials lend themselves to the use of the Fourier transform to determine interpolation coefficients. The Legendre polynomials do not lend themselves to the Fourier transform, but, Taylor et al [1984] have shown that in general the fast Fourier transform and Crout reduction with partial pivoting require approximately the same amount of computational time if the defining matrix for the Crout reduction is not changed. Therefore it should be possible to use either Chebyshev polynomials with a fast Fourier transform or Legendre polynomials with Crout reduction and partial pivoting.

The question then arises which of these polynomial approximations would be most appropriate under the conditions being considered. The Chebyshev

polynomials have the advantage of concentrating the collocation points in the regions of x=-1 and x=1. While the Legendre can be defined at any point in the system, but are typically equally spaced. Pseudospectral Chebyshev methods are commonly seen used in the literature this is in part due to the availability of fast Fourier transforms (FFT's) and a general belief that direct matrix inversion is not as fast as the FFT. It was decided to use Chebyshev polynomials on the basis of the availability of the FFT. The use of Chebyshev collocation will ensure that a large number of interpolation points are near the plate in the region of the greatest gradient. Finlayson [1980] notes that collocation may not be satisfactory when the solution domain contains steep gradients, which is the situation that is expected with thin shear layers.

The Falkner Skan equation was used as a tool to estimate the accuracy of the pseudospectral approximation for separated flow present on the back side of an inclined plate. Based on a fourth order Runge-Kutta solution of the Falkner Skan equation ($\beta$ = 0.125)

$$f''' + ff'' + \beta(1 - f'^2) = 0 \tag{35}$$

with boundary conditions

$$f = f' = 0, \ \eta = 0$$

$$f' = 1, \ \eta = \infty \tag{36}$$

a Chebyshev interpolation function was evaluated for N=10, 20 and 40. The evaluation was based on a comparison of the first and second derivatives found using a pseudospectral evaluation and those obtained by the Runge-Kutta method. The coefficients for the pseudospectral approximation are obtained by a Fourier transform. Three separate observations were made from these evaluations. 1) In one trial the data used for the value of $f(\eta)$ at each collocation point was rounded to three significant figures with N=20.

This resulted in large oscillations of the first derivative as suggested by Osher [1984] and Majda et al [1978] 2) Increasing the number of collocation points from 10 to 20 to 40 did not significantly affect the accuracy of the resulting approximations. 3) The accuracy of a derivative decreased approximately one order of magnitude for each increase in the order of differentation. A compilation of these results is presented in Tables 2 and 3.

Based upon the above, it was decided to use a steady state stream function vorticity representation for the flow

$$\frac{\partial \omega}{\partial x}\frac{\partial \psi}{\partial y} - \frac{\partial \omega}{\partial y}\frac{\partial \psi}{\partial x} = \frac{1}{Re}\left(\frac{\partial^2 \omega}{\partial x^2} + \frac{\partial^2 \omega}{\partial y^2}\right) \tag{37}$$

$$\omega = -\frac{1}{2}\left(\frac{\partial^2 \psi}{\partial x^2} + \frac{\partial^2 \psi}{\partial y^2}\right) \tag{38}$$

with the boundary conditions

$$\psi(x,0) = \psi_x(x,0) = \psi_y(x,0) = 0 \qquad 1 \le x \le a \tag{39}$$

$$\psi(x,\infty) = \psi(\infty, y) = \psi_{free\ stream} \tag{40}$$

$$\omega(\infty,y) = \omega(x,\infty) = 0 \tag{41}$$

$$\omega(x,0) = -\frac{1}{2}\frac{\partial^2 \psi}{\partial y^2} \qquad 1 \le x \le a \tag{42}$$

Then the stream function and vorticity can be approximated by

$$\psi(x_i, y_j) = \sum_{n=0}^{N} a_n(x_i) f_n(y_j)$$

$$\omega(x_i, y_j) = \sum_{n=0}^{N} \alpha_n(x_i) f_n(y_j) \tag{43}$$

This representation was chosen to make use of the increased accuracy of pseudospectral approximations along the axis in which the greatest amount of change will occur. Gottlieb et al [1984a] note that a finite difference representation is typically used along the vertical axis and a pseudo spectral representation along the horizontal axis. The solution is split

| $\eta$ | $f''(\eta)$ | RK | N=10 | N=20 | N=20 (3 significant figures) | N=40 |
|---|---|---|---|---|---|---|
| 0.1958 | | 0.025576 | 0.024552 | 0.024773 | 0.023739 | 0.023847 |
| 0.7639 | | 0.072826 | 0.074226 | 0.072494 | 0.084111 | 0.073005 |
| 1.649 | | 0.067062 | 0.065499 | 0.066957 | 0.079243 | 0.067009 |
| 2.764 | | 0.088610 | 0.086654 | 0.088983 | 0.071295 | 0.088778 |
| 4.000 | | 0.45786 | 0.45962 | 0.45794 | 0.45309 | 0.45790 |
| 5.236 | | 0.84314 | 0.84205 | 0.84291 | 0.85391 | 0.84302 |
| 6.351 | | 0.98166 | 0.98236 | 0.98171 | 0.94579 | 0.98163 |
| 7.236 | | 0.99963 | 0.99931 | 0.99964 | 1.05521 | 0.99965 |
| 7.804 | | 1.00106 | 1.00118 | 1.00105 | 1.07258 | 1.00111 |
| 8.000 | | 1.00116 | 1.00101 | 1.00119 | 0.95798 | 1.00130 |

Table 2 Comparisons of the first derivative of the Falkner Skan equation for a 4th order Runge Kutta method and Chebyshev collocation where N represents the number of terms retained in the series expansion

| $\eta$ | $f''(\eta)$ | RK | N=10 | N=20 | N=20<br>3 significant figures | N=40 |
|---|---|---|---|---|---|---|
| 0.1958 | | 0.11855 | 0.11514 | 0.13321 | 0.14046 | 0.13404 |
| 0.7639 | | 0.04837 | -0.04922 | 0.04922 | -0.02698 | -0.04577 |
| 1.649 | | 0.06256 | 0.06346 | 0.06193 | 0.07137 | 0.05968 |
| 2.764 | | 0.22016 | 0.21912 | 0.21990 | 0.18439 | 0.22008 |
| 4.000 | | 0.35247 | 0.35299 | 0.35490 | 0.31807 | 0.35865 |
| 5.236 | | 0.22321 | 0.22364 | 0.22300 | 0.17815 | 0.22307 |
| 6.351 | | 0.04637 | 0.04527 | 0.04592 | 0.09232 | 0.04413 |
| 7.236 | | 0.00537 | 0.00632 | 0.00530 | 0.14462 | 0.00500 |
| 7.804 | | $8\times10^{-4}$ | $1.1\times10^{-4}$ | $7.5\times10^{-4}$ | 0.68487 | $6.5\times10^{-4}$ |
| 8.000 | | $3.5\times10^{-4}$ | 0.00103 | 0.00121 | -2.82886 | 0.00721 |

Table 3: Comparisons of the second derivative of the Falkner-Skan Equation for a 4th order Runge-Kutta method and Chebyshev collocation where N represents the number of terms retained in the series expansion.

into an upper and lower region for above and below the plate and having the numerical boundary conditions

$$\omega^u(x,0) = \omega^\ell(x,0) \qquad a < x < -a$$
$$\psi^u(x,0) = \psi^\ell(x,0) \qquad a < x < -a \tag{44}$$

where the superscripts u and $\ell$ refer to he upper and lower regions respectively.

The following computational scheme was then used to evaluate the flow. The mesh nodes for the stream function were initialize using an equation given in Lamb [1945] that has been corrected for the angle of attack and transformed to Cartesian coordinates (Appendix A). The vorticity was initialized as zero everywhere except on the plate where a first order finite difference evaluation was performed based on methods found in Roache [1972]

$$\omega(x,0) = \frac{2(\psi_{\omega+1} \; \psi_\omega)}{\Delta n^2} + 0(\Delta n) \tag{45}$$

where $\Delta n$ is the distance from the wall (w) to the mesh node normal to the wall (w+1). The following steps were then followed in obtaining a solution:

1) Determine the pseudospectral coefficients to the Chebyshev polynomials at each $(x,y_j)$ combination.

2) Starting at the leading edge of the flow field evaluate the derivatives with respect to y for that column.

3) Equation (37) is solved with respect to $\omega$ for a finite difference representation of the x derivative.

4) Equation (38) is solved with respect to $\psi$ for a finite difference representation of the x derivative.

5) Steps 3) and 4) are repeated for each value of $\omega$ and $\psi$ in the column.

6) Move to the next column and repeat steps 2) through 5).

7) Repeat for the second region.

8) Satisfy the numerical boundary conditions.

9) Continue steps 1) through 8) until convergence is achieved.

In order to estimate the accuracy of the above algorithm a central finite difference algorithm for the stream function representation (22) was developed. The successive under relaxation algorithm was based on the same boundary conditions as given by equations (39)-(40).

Both the finite difference and pseudospectral algorithms were explosively unstable. The fact that both algorithms were unstable suggests that improper boundary conditions are being applied.

LITERATURE CITED


[1] Beam, R. M., R. F. Warming. AIAA J. 16:393 (1978).

[2] Boris, J. P., and D. L. Book. J. Comp. Phys. 20:397 (1976)

[3] Canuto, C., Computing Methods in Applied Sciences and Engineering VI, pp. 335-351, Elsevier Science Pub. (N. Holland) (1984).

[4] Canuto, C. and A. Quarteroni. Spectral Methods for Partial Differential Equations, pp. 55-78, SIAM Philadelphia (1984).

[5] Cebeci, T., K. Stewartson and J. H. Whitelaw, Numerical and Physical Aspects of Aerodynamic Flows II, pp. 1-40, Springer-Verlag, New York (1984).

[6] Deardorff, J. W. J. Fluid Mech., 41:453 (1970).

[7] Derivent, G. S. and H. E. Bailey. Numerical and Physical Aspects of Aerodynamic Flows II, pp. 63-78, Springer-Verlag, New York (1984).

[8] Dennis, S. C. R. and L. Quartapelle. J. Comp. Phys. 52:448 (1983).

[9] Finlayson, B. Nonlinear Analysis in Chemical Engineering, McGraw-Hill, New York (1980).

[10] Gottlieb, D. and S. A. Orszag. Numerical Analysis of Spectral Methods: Theory and Applications, SIAM, Philadelphia (1977).

[11] Gottlieb, D., M. Y. Hussaini and S. A. Orszag. Spectral Methods for Partial Differential Equations, pp. 1-54, SIAM, Philadelphia (1984a).

[12] Gottlieb, D., L. Lustman and S. A. Orszag, SIAM, J. Sci. Stat. Comput. 2:296 (1981).

[13] Gottlieb, D., L. Lustman and C. Streett. Spectral Methods for Partial Differential Equations, pp. 79-95, SIAM, Philadelphia (1984b).

[14] Haidvogel, D. B., A. R. Robinson and E. E. Schulman. J. Comp. Phys. 34:1 (1980).

[15] Hald, O. H. J. Comp. Phys. 40:305 (1981).

[16] Hegna, H. A., AFWAL-TR-81-3053 (October 1981).

[17] Hegna, H. A., AIAA 82-0092 (January 1982).

[18] Hussaini, M. Y. and T. A. Zang. Spectral Methods for Partial Differential Equations, pp. 119-140, SIAM, Philadelphia (1984).

[19] Jobe, C. E. and W. L. Hankey. AIAA J. 18:1394 (1980).

[20] Kleiser, L. Lecture Notes in Physics Vol. 170, pp. 280-285, Springer-Verlag, New York (1982).

[21] Kline, S. J., R. L. Wooley. J. Fluids Engr. 100:180 (1978).

[22] Kumar, A. and K. S. Yajnik. J. Fluid Mech. 97:27 (1980).

[23] Lamb, H. Hydrodynamics, Dover, New York (1945).

[24] Lanczos, C. Applied Analysis, Prentics Hall Inc. Englewood Cliffs, N.J. (1956).

[25] Leonard, A. and A. Wrey. Lecture Notes in Physics Vol. 170, pp. 335-342, Springer-Verlag, New York (1982).

[26] Liepmann, H. W. Amer. Scientist, 67:221 (1979).

[27] Lugt, H. J. and H. J. Haussling. J. Fluid Mech. 65:711 (1974).

[28] Lumley, J. L. Prediction Methods for Turbulent Flows, pp. 1-32, Hemisphere, Washington (1980).

[29] MacCormack, R. W. An Efficient Numerical Method for Solving the Time-Dependent Compressible Navier-Stokes Equations at High Reynolds Numbers, NASA TM 73129.

[30] Maday, Y. and A. Quarteroni. SIAM J. Numer. Anal. 19:761 (1982).

[31] Majda, A., J. McDonough and S. Osher. Math. Comp. 32:1041 (1978).

[32] Marcus, P. S., S. A. Orszag and A. T. Patera. Lecture Notes in Physics Vol. 170, pp. 371-376, Springer-Verlag (1982).

[33] Mei, R. W. and A. Plotkin. AIAA 84-1616 (June 1984).

[34] Moin, P. Lecture Notes in Physics Vol. 170 pp. 55-76, Springer-Verlag, New York (1982).

[35] Moin, P. and J. Kim. J. Comp. Phys. 35:381 (1980).

[36] Orszag, S. A. Stud. Appl. Math. 50:293 (1971).

[37] Orszag, S. A. Handbook of Turbulence, pp. 281-314, Plenum, New York (1977).

[38] Orszag, S. A. J. Comp. Phys. 37:70 (1980).

[39] Orszag, S. A. and L. C. Kells. J. Fluid Mech. 96:159 (1980).

[40] Osher, S. Spectral Methods for Partial Differential Equations, pp. 209-216, SIAM, Philadelphia (1984).

[41] Pasciak, J.E. Math. Comp. 35:1081 (1980).

[42] Peaceman, D. W., H. H. Rachford. J. Soc. Indust. Appl. Math. 3:28 (1955).

[43] Roache, P. J. Computational Fluid Dynamics, Hermosa Pub., Albuquerque (1982).

[44] Rudy, D. H. and J. C. Strikwerda. Comp. and Fluids, 9:327 (1981).

[45] Sakell, L. AIAA J., 22:929 (1984).

[46] Salas, M. D., T.A. Zang and M. Y. Hussaini. Lecture Notes in Physisc Vol. 170, pp. 461-467, Springer-Verlag, New York (1982).

[47] Schumann, U., Grotzbach, G., and L. Kleiser. Prediction Methods for Turbulent Flows, pp. 123-258, Hemisphere, Washington (1980).

[48] Shang, J. S. AIAA J., 16:496 (1978).

[49] Shang, J. S. AIAA 84-1549 (June 1984).

[50] Streett, C. L., T. A. Zang and M. Y. Hussaini. J. Comp. Phys. 57:43 (1985).

[51] Taylor, T. D. Spectral Methods for Partial Differential Equations, pp. 257-267, SIAM, Philadelphia, (1984).

[52] Taylor, T. D., R. S. Hirsh and M. M. Nadworny. Comp. and F. ids, 12:1 (1984).

[53] Taylor, T. D. and J. W. Murdock. Lecture Notes in Mathematics Vol. 771, pp. 519-537, Springer-Verlag, New York, (1980).

[54] Taylor, T. D. and J. W. Murdock. Comp. & Fluids 9:255 (1981).

[55] Taylor, T. D., R. B. Myers and J. H. Albert. Comp. & Fluids, 9:469 (1981).

[56] Tennekes, H. and J. L. Lumley. A First Course in Turbulence, MIT, Cambridge (1972).

## Appendix A

Lamb [1945] gives the following representation for the stream function for flow past a flat plate pitched at angle of 45°

$$\psi = -\frac{cq_\infty}{\sqrt{2}} \sinh\xi(\cos\eta - \sin\eta) \tag{A1}$$

whose edges are located at $x = \pm c$ and where $q_\infty$ is the free stream velocity. This equation was derived from the relation describing fluid motion relative to an elliptic cylinder

$$\psi = -c\left\{ v \sinh\xi\cos\eta - u \sinh\xi\sin\xi\right\} \tag{A2}$$

where $u$ and $v$ are the x and y components of velocity with respect to the plate. Then $\psi$ can be represented as

$$\psi = -c\, q_\infty\cos\theta\sinh\xi\left\{\tan\theta\cos\eta-\sin\eta\right\} \tag{A3}$$

where $\theta$ is the angle of attack for the plate. Cartesian coordinates and elliptic coordinates are related in the following fashion

$$x = c\cosh(\xi)\cos(\eta) \tag{A4}$$

$$y = c\sinh(\xi)\sin(\eta) \tag{A5}$$

The following relation

$$\frac{x^2}{c^2\cos^2\eta} - \frac{y^2}{c^2\sin^2\eta} = 1 \tag{A6}$$

along with the definition of a point on a hyperbola and the relation of sinh to cosh define the following relations for the stream function in Cartesian coordinates

$$\psi = -q_\infty\cos\theta\left\{ \tan\theta\sqrt{x^2 - \frac{1}{4}\left(\sqrt{(c+x)^2+y^2} - \sqrt{(c-x)^2+y^2}\right)^2} - y \right\} \tag{A7}$$

for $x>0$, and

$$\psi = q_\infty\cos\theta\left\{ \tan\theta\sqrt{x^2 - \frac{1}{4}\left(\sqrt{(c+x)^2+y^2} - \sqrt{(c-x)^2+y^2}\right)^2} - y \right\} \tag{A8}$$

for $x<0$.

SCEEE

Final report on subcontract 84 RIP 27 by
H.P. Hameka, Department of Chemistry,
University of Pennsylvania

During a stay at the Frank J. Seiler Research Laboratory in the summer of 1984 I completed a calculation of ESR coupling constants for a series of small organic radicals, namely methyl, allyl, ethyl and vinyl. My research efforts supported by subconstract 84 RIP 27 involved the extension of these calculations to larger systems, varying from the phenyl radical to mono-, di- and tri-nitro phenyl and benzyl radicals.

During the past year we have accumulated an extensive amount of theoretical data on the radicals mentioned above, varying from phenyl to trinitro-benzyl. Unfortunately we found that the procedure that gave us satisfactory theoretical results for the smaller radicals did not lead to good agreement with the experimental data for the larger radicals.

In order to improve the accuracy of our calculations we first developed a method for removing higher-order spin contaminations from the UHF results. This led to some improvements but we did not judge these improvements as sufficient. We concluded that the discrepancies are due to the small non-orthorgonality between the unpaired orbital and the orbitals of the other spins. We are now engaged in calculations where these non-orthogonality effects are determined so that they can be eliminated.

We hope that the latter calculations will lead to improved agreement between theory and experiment so that we can feel confident about publishing our results. However, we have not yet reached that stage.

We plan to continue work on this problem and we hope to obtain satisfactory results within the next year.

1985 USAF-SCEEE RESEARCH INITIATION PROGRAM

Sponsored by the

AIR FORCE OFFICE OF SCIENTIFIC RESEARCH

Conducted by the

SOUTHEASTERN CENTER FOR ELECTRICAL ENGINEERING EDUCATION

FINAL REPORT

# FUNCTIONAL ROLE OF SEROTONIN IN THE CEREBELLAR GLOMERULAR SYNAPSE


| | |
|---|---|
| Prepared by: | Dr. Deborah Armstrong |
| Academic Rank: | Assistant Professor |
| Department and University: | Division of Life Sciences<br>University of Texas at San Antonio |



| | |
|---|---|
| Date: | APRIL 12, 1986 |
| Contract No: | 84 RIP 28 |

# FUNCTIONAL ROLE OF SEROTONIN IN THE CEREBELLAR GLOMERULAR SYNAPSE

by

Deborah L. Armstrong, Ph.D

## ABSTRACT

Stimulation of the dorsal raphe resulted in modulation of granule cell spontaneous activity. This provides support for the proposal that serotonin functions as a transmitter in the granular layer of the cerebellar cortex, however, the diversity of the observed responses does not permit a precise determination of the nature of the activated synapses. Of the eleven cells that responded consistently, six displayed decreased spontaneous activity, three were excited by the stimulation, and four cells displayed a biphasic response of initial excitation followed by inhibition. The iontophoretic application of serotonin decreased the spontaneous activity of the majority of cells tested and this effect could not be blocked by methysergide. Several cells were excited by serotonin application and this effect could be blocked by methysergide.

## I. INTRODUCTION

Based on evidence from anatomical, physiological, and biochemical studies serotonergic efferents of the brain stem raphe nuclei contribute to the mossy fiber system innervation of the cerebellar glomeruli. The anatomical mapping includes fluorescent histochemistry (4,13) and autoradiography following intracisternal injection of $^{3}$H-serotonin (7). In both cases labeling was identified within structures resembling the large mossy fiber rosette terminal (25). Additional orthograde transport studies (6,8,12) ,use of retrogradely transported horseradish peroxidase (8,21) and immunocytochemistry (5) have verified the existance of 5-HT fibers within the cerebellum, however, the innervation is complex. Chan-Palay (8) describes three distinct systems: mossy fibers, fine axons that ascend to the molecular layer and bifurcate in manner resembling parallel fibers, and finally, a diffuse axonal system that innervates both the deep cerebellar nuclei and the cerebellar cortex.

Physiolgical studies to determine the functional significance of these serotonergic fibers are scarce and concentrate on Purkinje cell responses to raphe stimulation or iontophoresis of serotonergic agents (7,21-24). However, they do demonstrate that serotonergic mechanisms probably play a role in modulating cerebellar cortical activity. Obviously, a more thorough investigation of serotonergic transmission in the granular layer is needed.

The results of recent uptake studies utilizing an

isolated glomerular preparation have shown that a high affinity uptake system for serotonin does exist in this region (26). These studies are part of an ongoing project to identify cerebellar glomeruli neurotransmitter systems and their interactions with one another. The positive results of these experiments have provided a solid base on which to begin an investigation of the physiological responses of cerebellar granule cells to serotonergic stimulation.

## II. OBJECTIVES

The primary objective of this research initation project was to determine the response of granule cells to raphe stimulation. Since the dorsal raphe is such a well defined cluster of serotonergic cells in the rat we elected to begin with this particular nucleus. It is also one of four raphe nuclei that anatomical studies have shown to project to the cerebellar cortex. An initial sampling of recording electrode placements in the lateral hemisphere foli was planned to determine whether or not specific regions were more likely to contain responsive cells. To strengthen the proposal that responses were indeed mediated via activation of serotonergic synapses a second group of experiments was planned in which recordings made with multibarrel electrodes would enable the iontophoretic application of serotonergic receptor antagonists during stimulation evoked responses. These experiments would aid in determining the functional role of serotonin in information processing at the level of the cerebellar glomerular synapse.

## III. GRANULE CELL RESPONSE TO DORSAL RAPHE STIMULATION

The majority of experiments examining serotonin's influence on cerebellar activity have dealt with Purkinje or subcortical cell responses to raphe stimulation. Utilizing extracellular recording techniques, Strahlendorf et al (22) have reported that stimulation of the raphe centralis superior or inferior produces initial bursting of fastigial and Purkinje cells followed by reduced spontaneous activity lasting up to 1600 msec. When stimulation of the sensorimotor cortex or radial nerve was applied during this period of raphe conditioning evoked spike activity was suppressed to an even greater extent than spontaneous activity, leading to the suggestion that serotonin modulates the ratio of spontaneous activity (noise) to evoked activity (specific responses to afferent signals) (24). Since very little information is known about the possible role of serotonin in the modulation of granule cell activity our initial experiments were planned to simply investigate the direct affect of raphe stimulation on granule cells.

### METHODS

Adult Sprague-Dawley rats from Holztman suppliers were used. Animals were anesthetized with urethane (1.5 mg/kg body weight) injected intraperitoneally and supplemented as needed. Rectal temperature was continuously monitored and body temperature maintained at 37-0.5 C by means of a heating pad equipped with a negative feedback circuit. After placement in

a stereotaxic headholder and exposure of the skull surface the occipital bone was removed to expose the lateral aspects of the vermis and the cerebellar hemisphere. After removal of the overlying dura matter a 1% solution of agar in physiological saline was placed on the cortical surface to prevent drying and reduce surface noise. An additional hole was made in the skull for positioning of the stimulating electrode, coordinates: A -6.5, L +1.0, V 6.5-7.0, into the dorsal raphe (14). Extracellular recordings were made with glass capillary electrodes drawn and bicken to a tip diameter of 5-10 um (1 to 5 Megohm impedances), filled with 3 M NaCl saturated with fast green for later verification of electrode tip placement. Unit activity and field potentials were amplified by a high input impedance preamplifier and audio amplifier, displayed on a Tektronix storage oscilloscope for photography, and then fed into a window discriminator (20) for signal sorting. Data was stored on magnetic tape for further analysis or relayed to a chart recorder for on line observations. The recording electrode microdrives were tilted to fascilitate electrode penetration into the crowns of the cerebellar folia. Concentric bipolar stimulating electrodes (Rhodes Medical Instrumets, Inc.) were used to apply single rectangular pulses(60 Hz), 0.5 msec in duration and ranging from 0-500 mA intensity, using a WPI Programmable stimulator.

RESULTS

The response to dorsal raphe stimulation was not as robust as we had anticipated. Out of the 87 cells sampled in

the granule layer only 11 responded consistantly to stimulation. Six of these cells displayed decreased spontaneous activity, three were excited by the stimulation and four cells displayed a biphasic response of initial excitation followed by a long period of suppressed activity. The location of these cells in the intermediate to far lateral anterior lateral hemisphere corresponded to areas expected to have significant innervation by serotonergic fibers (5) although they were not concentrated in any one folia or defined region.

Figure 1 illustrates the response of a cell whose spontaneous activity was suppressed by raphe stimulation. The high frequency, low amplitude action potentials of this cell found at a depth of 560 um below the surface suggest that it is indeed a granule cell(9). With increasing stimulus intensities the degree of supression increases to a maximum duration of 230 msec.

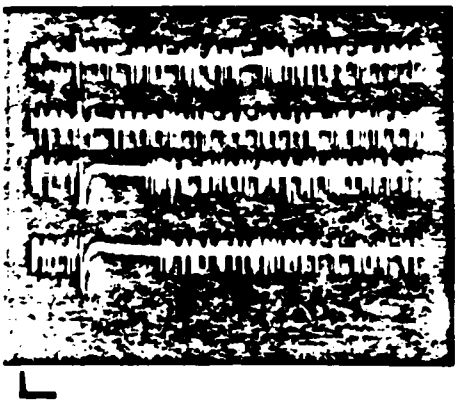


Fig. 1. Response of granule cell to single pulse stimulation of the dorsal raphe. Each trace formed by three beam sweeps. Stimulus indicated by artifact to the left of each trace. From top to bottom traces indicate: control baseline, 20, 30, and 50uA stimulus intensity. Scale markers denote 100msec and 1mv.

Figure 2 illustrates the biphasic type response that was observed in four cells. This type of response resembles that of Purkije cells as described by Strahlendorf et al (22). The average latency for onset of the stimulatory phase was 25 msec. followed by a longer (200-250 msec) inhibition. The pure excitatory response that was observed in three cells had a much shorter latency (10-15 msec) as illustrated in Figure 3. It is interesting to note that this effect was apparent in granular layer regions displaying lower spontaneous activity. It is possible that this response was masked at other sites by ongoing background stimulation.

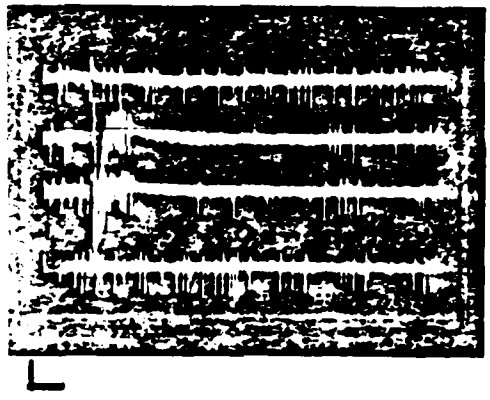


Fig 2. Example of granule cell responding to dorsal raphe stimulation with initial bursting activity followed by a long period of suppressed activity. Top and bottom traces are control baseline sweeps. Second and third middle traces display response to 20 and 30 uA stimulus intensity. Scale markers denote 50 msec and 1mV.

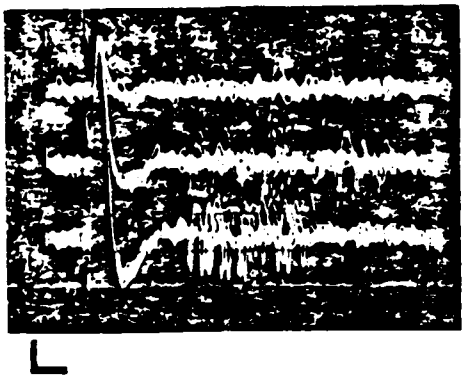


Figure 3. Example of granule layer cell activated by dorsal raphe stimulation. Each trace formed by five beam sweeps. From top to bottom the traces indicate: control baseline, 30, 40, and 60 uA stimulus intensity. Scale markers denote 5msec and 1mV.

The small number of cells encountered in the granular layer that responded to our stimulation was disappointing. However, the highest number of responsive cells were identified during the latter part of the research period following some procedural modifications. We now believe that our original stimulating arrangement may have been causing some damage to the raphe neurons, thus lessening the probability of producing normal stimulus responses. Because of time limitations we proceeded with the iontophoretic studies alone rather than combined with stimulation effects.

## IV. IONTOPHORESIS OF SEROTONERGIC AGENTS

At best one could say that the literature on neuronal responses to local application of serotonergic compounds is

varied and, in some cases, actually contradictory and confusing. Part of the problem can be atributed to the existance of more than one class of serotonin receptor (18,19). An attempt has been made to categorize these classes, 5-$HT_1$ and 5-$HT_2$, into inhibitory and excitatory receptors, respectively (1) and this does aid in organizing the literature, however, it is the more rigorous use of intracellular recording techniques that show the most promise for determining serotonin's synaptic functions. One clear picture that is emerging is the important role of K+ conductance in the mediation of serotonin's effects (15-17).

To begin our investigation of the effects of local application of serotonin in the granular layer, we wanted to replicate the findings reported by Bloom et al (7) who described increased activity of granule cells in response 5-HT iontophoresis. *This would be expected if the transmitter were* stimulating postsynaptic receptors of mossy fiber synapses within the glomeruli. A multibarrel recording arrangement was emloyed to test for the effects of serotonergic receptor antagonists during transmitter application.

METHODS

Seven barrel glass capillary pipette electrodes (Frederick Haer) were drawn and broken to a tip diameter of 6-10 um. Two of the outer barrels were filled with 1.0 monosodium glutamate and 0.15 M NaCl. The NaCl barrel was used for current balancing and control ejections. The other barrels contained combinations of 5-hydroxy-tryptamine creatinine sulfate (0.5

M) and receptor antagonists including cyproheptadine HCl (14.6 mM), methysergide maleate (0.01 M) M). The pH of all chemicals used were adjusted as needed and each solution was filtered (Millipore Corp., 0.22 um). The chemicals were electrophoretically applied to neurons by calibrated DC currents using a Neurophore BH-2 microiontophoresis system (Medical Systems Corp.). Control procedures for assessing microiontophoretic effects were carried out. A retaining current of 5 nA was utilized to prevent the spontaneous diffusion of active ions from the capillary barrels. To study the interaction between chemicals one was applied continuously while the other was applied at regular intervals.

RESULTS

A total of 33 cells were tested with serotonergic agents and glutamate. Five of these cells did not display a reliable response to glutamate and are excluded from this discussion. Of the remaining 28, the majority, nineteen, were inhibited by 5-HT. An example of this response is illustrated in Figure 4. The reduction in activity is significant and endures beyond the pericd of drug application. At higher doses ( > 50 nAmps) several cells oscillated in activity before returning to a normal baseline. Application of methysergide using current levels that did not directly affect cell activity had no or very little affect on this supression of activity. There are several reports in the literature of 5-HT receptor antagonists having minimal affect on serotonin induced inhibition (1,15,16).

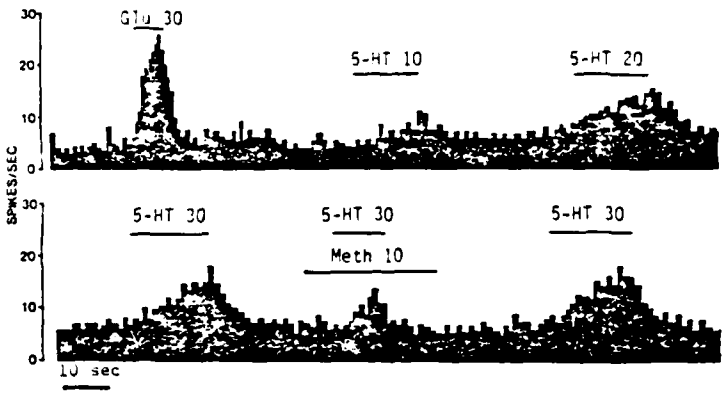



Figure 5. Example of increased activity of granule cell in response to serotonin application. This effect could be partially blocked by ejection of methysergide (Meth).

RECOMMENDATIONS

Despite the limited number of cells that responded to stimulation the results are very exciting in terms of providing a frame work for deliniating distinct serotonergic pathways based on the type of response illicited in granule cells. The prolonged inhibitory response indicates a type of humoral modulation that could be mediated by the fine serotonergic fibers that do not appear to make definite synaptic contacts with target cells within the granular and molecular layers. The fact that some granule cells did respond with short latency bursts supports the idea of serotonergic mossy fiber innervation. At the present time we are concentrating on integrating the stimulation and iontophoretic techniques as we had originally planned.

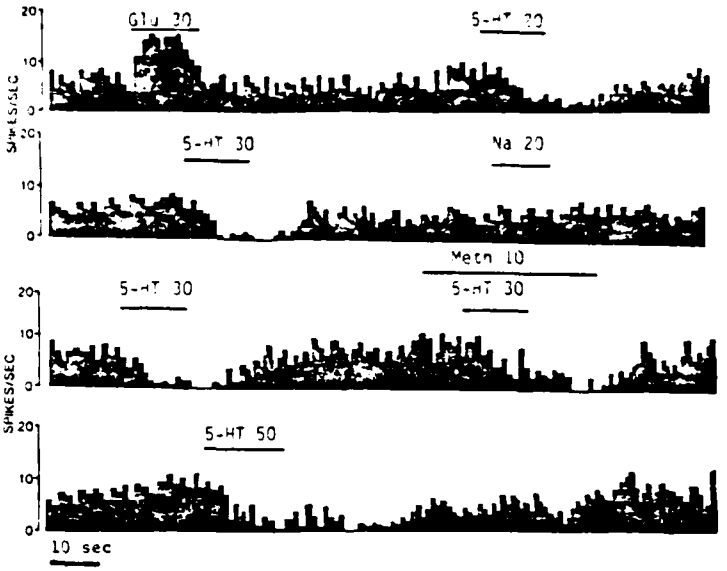



Figure 4. Reduction of granule cell activity in response to pulses of serotonin (5-HT). Rows are from continuous strip chart record of activity (spikes/sec) of single cell. Bars indicate duration and intensity (nAmps) of current application. Application of 5-HT receptor antagonist methysergide (Meth) did not block inhibitory effect. Glu indicates glutamate.

Of the nine cells that were not inhibited by 5-HT, seven displayed increased activity and two were not affected by any level of 5-HT ejection current. Figure 5 illustrates this excitatory response and as can be seen the effect could be blocked by methysergide. The excitatory response differed from that produced by glutamate in that it was not as immediate in onset and offset, however, the excitation never display the long duration that characterized the inhibitory responses.

## REFERENCES


1. Aghjanian, G. K. and R. Y. Wang. Physiology and Pharmacology of central serotonergic neurons. In: Psychopharmacology: A Generation of Progress. M. A. Lipton, A. DiMascio and K. F. Killam (eds.) Raven Press, New York, 1978.

2. Aghajanian, G.K. and C.P. Vandermaelen. Intracellular recordings from serotonergic dorsal raphe neurons: pacemaker potentials and the effect of LSD. Brain Res. 238: 463-469,1982.

3. Aghajanian, G.K. and J.M. Lakoski. Hyperpolrization of serotonergic neurons by serotonin and LSD: studies in brain slices showing increased K+ conductance. Brain Res. 305: 181-185, 1984.

4. Anden, N. E., K. Fuxe and U. Ungerstedt. Monoamine pathways to the cerebellum and cerebral cortex. Experientia 23: 838-839, 1967.

5. Bishop, G. A., R. H. Ho and J. S. King. Localization of serotonin immunoreactivity in the deep cerebellar nuclei of the opossum. Neurosci. Abstr. 10: 750, 1984.

6. Bobillier, P., S.Seguin, F. Petitjean, D. Salvert, M. Touret and M. Jouvet. The raphe nuclei of the cat brainstem: A topographical atlas of their efferent projections as revealed by autoradiography. Brain Res. 113: 449-486, 1976.

7. Bloom, F. E., B. J. Hoffer, G. R. Siggins, J. L. Barker and R. A. Nicoll. Effects of serotonin on central neurons: microiontophoretic application. Fed. Proc. 31: 97-106,1976.

8. Chan-Palay, V. Cerebellar Dentate Nucleus: Organization, Cytology and Transmitters. Berlin: Springer-Verlag, 1977.

9. Eccles, J. C., M. Ito and J. Szentagothai. The Cerebellum as a Neuronal Machine. Springer-Verlag, New york, 1967.

10. Eccles, J. C., K. Sasaki, and P. Strata. The potential fields generated in the cerebellar cortex by a mossy fiber volly. Exp. Brain Res. 3: 58-80, 1967.

11. Eccles, J. C., K. Sasaki and P. Strata. A comparison of the inhibitory actions of Golgi cells and of basket cells. Exp. Brain Res. 3; 81-94, 1967.

12. Halaris, A. E., B. E. Jones and R. Moore. Axonal transport in serotonin neurons of the midbrain raphe. Brain Res. 66: 555-574, 1976.

13. Hokfelt, T. and K. Fuxe. Cerebellar monoamine nerve terminals, a new type of afferent fibers to the cortex cerebelli. Exp. Brain Res. 9: 63-73, 1969.

14. Konig, J. R. F. and R. A. Klippel. The Rat Brain: A Stereotaxic Atlas of the Forebrain and Lower Parts of the Brain Stem. Baltimore: Williams and Wilkins, 1963.

15. McCall, R. B. and G. K. Aghajanian. Serotonergic facilitation of facial motoneuron excitation. Brain Res. 169: 11-27, 1967.

16. McCall, R.B. Serotonergic excitation of sympathetic preganglionic neurons: a microiontophoretic study. Brain Res. 289: 121-127, 1983.

17. Park, M.R., J.A. Gonzales-Vegas and S.K. Kitai. Serotonergic excitation from dorsal raphe stimulation recorded intracellularly from rat caudate-putamen. Brain Research 243: 49-58, 1982.

18. Peroutka, S. J., R. M. Lebovitz and S. H. Snyder. Two distinct central serotonin receptors with different physiological functions. Science 212: 827-829,1981.

19. Peroutka, S. J. and S. H. Snyder. Multiple serotonin receptors: differential binding of ($^3$H)5-hydroxytryptamine, ($^3$H)Lysergic Acid Diethylamide and ($^3$H)Spiroperidol. Mol. Pharmacol 16: 687-699, 1979.

20. Peterson, R. C., A. D. Simpson, M. J. Wayner and H. Yagi. A window discriminator for sorting electrical signals. Physiol. Behav. 4: 865-867, 1969.

21. Shinnar, S., R. J. Maciewicz and R. J. Shofer. A raphe projection to cat cerebellar cortex. Brain Res. 97: 139-143, 1973.

22. Strahlendorf, J. C., H. K. Srahlendorf and C. D. Barnes. Modulation of cerebellar neuronal activity by raphe stimulation. Brain Res. 169: 565-569, 1979.

23. Strahlendorf, J. C. and G. D. Hubbard. Serotonergic interactions with rat cerebellar purkinje cells. Brain Res. Bull. 11: 265-269, 1983.

24. Strahlendorf J. C., H. K. Strahlendorf and C. D. Barnes. Comparative aspects of raphe-induced modulation of evoked and spontaneous cerebellar unit activity. In: The Role of Peptides and Amino Acids as Neurotransmitters, pgs. 217-225. Alan Liss, New York, 1981.

25. Szentagothai, J. Glomerular synapses, complex synaptic arrangements, and their operational significance. The Neurosciences. 427-443, 1970.

26. Terrian, D.M., W.I. Butcher, P.H. Wu and D.L. Armstrong. Isolation of glomeruli from areas of bovine cerebellum and comparison of $^{3}$ serotonin uptake. Brain Res. Bull. 14: 469, 1985.

## Acknowledgement

The author would like to thank the USAF School of Aerospace Medicine, the Southeastern Center for Electrical Engineering Education and Air Force Office of Scientific Research for providing the support needed to carry out and complete this research project. A special thank you goes to Dr. David Terrian for his helpful ideas and support throughout the past two years.

# CHOLINE AND ETHANOLAMINE PHOSPHOTRANSFERASE ACTIVITIES IN GLOMERULAR PARTICLES ISOLATED FROM BOVINE CEREBELLAR CORTEX

Robert V. Dorman*, Scott B. Bischoff** and David M. Terrian**

*Dept. Biological Sciences, Kent State University, Kent, OH 44242

**USAF School of Aerospace Medicine, Clinical Sciences Division, Brooks AFB, TX 78235

Correspondence to: Dr. Robert V. Dorman
Dept. Biological Sciences
Kent State University
Kent, OH 44242

Running Title: Lipid Metabolism in Cerebellar Glomeruli

ABSTRACT

Isolated cerebellar glomeruli provide a relatively homogenous subcellular fraction, which can be used to study the biochemical events related to chemical transmission within a well-characterized central synapse. Choline and ethanolamine phosphotransferase activities were identified and partially characterized in this nerve ending preparation. Choline phosphotransferase associated with the glomerular particles required $Mg^{2+}$, while ethanolamine phosphotransferase required $Mn^{2+}$ for optimal activities. Both enzymes were inhibited by exogenous $Ca^{2+}$. The apparent Vmax values were 35.9 and 10.0 nmol/hr/mg protein for the choline and ethanolamine phosphotransferases, respectively. The apparent Km value for the CDPcholine substrate was 28.6 μM, and the Km for CDPethanolamine was 8.6 μM. Neither enzyme responded to the various adenine nucleotides, neurotransmitters or neurotransmitter agonists tested. However, exposure of the glomerular particles to cytidine nucleotides inhibited ethanolamine phosphotransferase activity and stimulated choline phosphotransferase activity.

## INTRODUCTION

The cerebellar glomerulus consist of the large terminals of the mossy fibers, granule cell dendrites, Golgi cell terminals and dendrites and a protective glial sheath (1-3). The synaptic connections in this complex have been described (4). Methods have been reported for the isolation of intact and functional glomerular particles (5-7). The enriched glomerular fraction provides a useful model for the investigation of synaptic events, since the isolated glomeruli retain their morphological and functional integrity. The mossy fiber terminals retain many of their synaptic connections and are filled with synaptic vesicles (5,6,8). The glomerular particles respire, actively transport neurotransmitters and amino acids and they contain the enzymes involved in mitochondrial function and neurotransmitter synthesis (6-9). Terrian et al.(8) have recently described an improved method for the purification of cerebellar glomeruli.

Choline and ethanolamine phosphotransferases were identified and partially characterized in the purified glomerular fraction in order to further assess the metabolic capabilities of this unique nerve ending preparation. Choline phosphotransferase (CDPcholine: 1,2-diradylglycerol choline phosphotransferase; EC 2.7.8.2) and ethanolamine phosphotransferase (CDPethanolamine: 1,2-diradylglycerol ethanolamine phosphotransferase; EC 2.7.8.1) catalyze the final steps in the synthesis of the choline and

ethanolamine glycerophospholipids, respectively. The enzymes catalyze the transfer of either phosphocholine or phosphoethanolamine from the cytidine nucleotide carrier to a diglyceride acceptor (10). These enzymes have been identified in other CNS membrane preparations. They are most active in cerebral microsomes (11-13) and they have been assayed in isolated neurons and glia (14). They have also been identified in purified CNS myelin (15,16), microsomes prepared from the hypomyelinated brains of jimpy and quaking mutant mice (17,18), and cerebral synaptosomes (19,20). It has been suggested that the phosphotransferases associated with synaptosomes may be involved in the membrane events related to neurotransmission, since they are influenced by neurotransmitters and cAMP (20).

The isolated cerebellar glomeruli were used to show the presence of choline and ethanolamine phosphotransferases in cerebellum, since they have not yet been identified in cerebellar membrane preparations. Also, the phosphotransferases were partially characterized prior to assessing their potential involvement in synaptic events in this nerve ending preparation. Phosphotransferase activities were measured in the presence of neurotransmitters thought to be endogenous to cerebellar glomeruli, their agonists and nucleotides implicated in either stimulus-secretion coupling, or phospholipid synthesis.

## EXPERIMENTAL PROCEDURES

### MATERIALS

The [methyl-14C]-cytidine diphosphocholine and the Aquasol II were obtained from New England Nuclear, while the [ethanolamine-1,2-14C]-cytidine diphosphoethanolamine was purchased from ICN. The radioactive cytidine nucleotides were diluted with unlabeled CDPcholine and CDPethanolamine (Sigma Chemical Co.). The neurotransmitters, neurotransmitter agonists, adenine and cytidine nucleotides, 1,2-diolein and Ficoll 400 were purchased from Sigma Chemical Co.

### ISOLATION OF CEREBELLAR GLOMERULI

A purified glomeruli fraction (PGF) was prepared from bovine cerebellar cortex. Cerebella were obtained at a slaughterhouse within 15 minutes of sacrifice. They were placed in ice for transport and the vermal cortices were removed by dissection. This tissue was rinsed in ice-cold saline and minced with scissors prior to manual homogenization in 9 volumes of 0.3 M sucrose, using a modified Dounce homogenizer, according to the method of Hajos et al.(5). Magnesium ions (1 mM $MgSO_4$) were included in all solutions used in the preparation of the PGF. The procedures used to isolate the enriched glomeruli fraction have

:cently been described by Terrian et al.(8). A number of sub-fractions were obtained during the preparation of the PGF, including the crude nuclear and crude mitochondrial fractions. These fractions contain the microsomal elements. Medullated fibers were separated from the crude glomeruli fraction in order to obtain the purified glomeruli fraction. Each of these sub-fractions was assayed for choline and ethanolamine phosphotransferase activities. Aliquots of each PGF preparation were taken for determination of protein concentration (21). The remainder was diluted with 9 volumes of 10 mM Tris-HCl buffer, pH 7.45, prior to estimation of choline and ethanolamine phosphotransferase activities.

PHOSPHOTRANSFERASE ASSAYS

Choline and ethanolamine phosphotransferase assays were performed for 30 minutes at 37°C in a total volume of 1.0 ml. Typical incubations contained 1-2 mg PGF protein and 20 to 80 µM [14C]CDPcholine or [14C]CDPethanolamine (each at 2 nCi/nmol) in 10 mM Tris-HCl buffer, pH 7.45. Choline phosphotransferase assays normally contained 100 mM $MgCl_2$, while ethanolamine phosphotransferase assays included 10 mM $MnCl_2$. The neurotransmitters, neurotransmitter agonists, cytidine and adenine nucleotides were present at 1 mM concentrations. The 1,2-diolein was suspended by high speed vortexing for five minutes in 10 mM

Tris-HCl (pH 7.45), in the presence of 0.022% Triton X-100. The 1,2-diolein concentrations ranged from 0.5 to 10 mM, in order to determine Km values for the diglyceride substrate. Triton X-100 was found to provide for greater phosphotransferase activities than either Brij 35 or Tween 80 and had a final concentration of 0.02% in the incubations which included 1,2-diolein. Some of the glomerular preparations were exposed to 5 mM Tris buffer for 60 min at 4°C for lysis of the vesicles according to Lai and Clark (22). All reactions were stopped by the addition of 5 ml of chloroform: methanol (2:1, v:v) and the total lipids were extracted and washed according to Folch et al.(23).

The radioactivity in the total lipid extract was used as the measure of phosphotransferase activities after thin layer chromatography (24) was used to show that the [14C]CDPcholine labeled only the choline glycerophospholipids and the [14C]CDPethanolamine labeled only the ethanolamine glycerophospholipids. The incorporation of radiolabeled substrates was determined by liquid scintillation counting in a Beckman LS-230 counter, with Aquasol II as the cocktail. F-tests were performed to show significant differences in phosphotransferase activities due to exposure of the PGF to neurotransmitters, transmitter agonists or nucleotides. Student's t-test was then used to determine which treatment groups were significantly different from untreated controls.

## RESULTS

### Characterization of Phosphotransferase Activities in the PGF

Choline and ethanolamine phosphotransferase activities were detected in all membrane fractions isolated from bovine cerebellar cortex, including the purified glomeruli fraction. The phosphotransferases were partially characterized in the PGF. The incorporation of radiolabled precursors into their respective phospholipids were enzymic, since both activities were abolished by exposure to 100°C for ten minutes. Also, the rates of isotope incorporation were linear over 30 minutes of incubation, and the activities were dependent on protein concentrations, between 0.2 and 3.0 mg glomerular protein (data not shown). Both phosphotransferase enzymes exhibited a pH optimum near 8.0 (Figure 1). Routine assays were then carried out at 37°C, for 30 minutes, at pH 7.45, in the presence of 1-2 mg glomerular protein.

The cation requirements of the phosphotransferases were determined. Choline phosphotransferase was most active in the presence of 100 mM $MgCl_2$, while ethanolamine phosphotransferase activity was optimal in the presence of 10 mM $MnCl_2$. Both phosphotransferases were inhibited by $Ca^{2+}$ in the presence of optimal concentrations of either $Mg^{2+}$ or $Mn^{2+}$ (Table I).

Distribution of Phosphotransferases in Subcellular Fractions

Choline and ethananolamine phosphotranserase activities were identified in all particulate fractions isolated during the preparation of the PGF (Table II). The phosphotransferase activities in the crude nuclear and crude mitochondrial fractions were almost twice that of the homogenate. The supernatant recovered following sedimentation of the crude glomeruli fraction contained phosphotransferase activities that were about 10% of those found in the homogenate (data not shown). When the crude glomeruli fraction was further purified by sedimentation through 1.2 M sucrose, the medullated fiber fraction exhibited a decline in phosphotransferase activities when compared to the crude glomeruli fraction, while the activities in the purified glomeruli fraction were about doubled compared to the crude preparation. The purified glomeruli fraction had phosphotransferase activities which were comparable to those in the homogenate. Also, hypontonic lysis of the PGF particles by the method of Lai and Clark (22) did not significantly alter the activity of either enzyme.

Kinetic Parameters and Treatment Effects

Estimates of Km and Vmax values were made for both enzymes

in the PGF. Vmax values were determined in the presence of 10 mM 1,2-diolein and either 100 μM CDPcholine or CDPethanolamine. The Km values were determined using various concentrations of diglyceride and nucleotide substrates. The results are shown in Table III. The apparent Vmax value for the choline phosphotransferase was 3.5 times greater than the value for the ethanolamine phosphotransferase. The apparent Km values for the choline phosphotransferase were 2.9 mM for the diglyceride substrate and 28.6 μM for the CDPcholine. Ethanolamine phosphotransferase exhibited similar Km values for the 1,2-diolein and the cytidine nucleotide.

Isolated glomeruli were exposed to exogenous neurotransmitters, neurotransmitter agonists and nucleotides which have been implicated in transmission processes and the effects of the treatments on phosphotransferase activities were determined (Figure 2). Exogenous diglycerides were not added to the incubations and CDPcholine and CDPethanolamine concentrations were 20 μM. ATP and cAMP (1 mM) had no effect on the activity of either enzyme, when compared to untreated controls. Equimolar concentrations (1 mM) of the neurotransmitters norepinephrine (NE), 5-hydroxytryptamine (5-HT) and gamma-aminobutyric acid (GABA), and the transmitter agonists muscimol, quisqualic acid and carbamylcholine, also had no effect on the activity of either phosphotransferase. However, cytidine nucleotides induced significant and opposite effects on the enzyme activities. Choline

phosphotransferase activity was increased 37% by CTP ($p < 0.01$), 45% by CDP ($p < 0.01$) and 44% by CMP ($p < 0.001$) when compared to untreated controls. Conversely, ethanolamine phosphotransferase activity was inhibited 20% by CTP ($p < 0.01$), 15% by CDP ($p < 0.01$) and 35% by CMP ($p < 0.001$) when compared to controls.

## DISCUSSION

The ability to isolate cerebellar glomeruli as a relatively homogenous subcellular fraction has enabled investigators to study the biochemical events underlying synaptic transmission within a central synapse that has been extensively characterized. Choline and ethanolamine phosphotransferase enzyme activities were identified in isolated glomerular particles as part of continuing studies of the biochemical events related to synaptic activities in this nerve ending preparation. The enzymes were partially characterized, in order to determine their general requirements, prior to assessing their involvement in glomerular functions by testing the effects of neurotransmitters and nucleotides believed to be endogenous to cerebellar glomeruli. Also, there are no known reports on phosphotransferase activities in the cerebellum.

Most of the requirements of the PGF enzymes were similar to those for phosphotransferases from other regions and subcellular fractions of the CNS. Enzyme activities were dependent on protein concentrations, were linear over 30 minutes of incubation and were abolished by exposure to 100°C for ten minutes. Both enzymes had a pH optimum near 8.0, which is consistent with reported values (14, 15). Ethanolamine phosphotransferase required 10 mM $Mn^{2+}$ for optimal activity, which is similar to values reported for brain microsomes (25), purified CNS myelin

(16) and synaptosomes isolated from cerebral cortex (20). However, choline phosphotransferase required 100 mM $Mg^{2+}$, which is 2 to 10 times greater than values reported for other CNS membrane preparations (11, 20, 26). Both enzymes were inhibited by $Ca^{2+}$, as has been shown in rat brain microsomes (11), isolated neurons and glia (14) and cerebral synaptosomes (20).

Phosphotransferase activities were measured in all particulate fractions isolated during the preparation of the PGF, in order to determine the subcellular distribution of the enzymes in cerebellar cortex. Both enzymes were present in all fractions and the distributions were similar to those reported for other CNS regions. The crude nuclear and crude mitochondrial fractions were the most active and this is consistent with results from other brain regions, since these fractions contain the microsomal elements of the cerebellar cortex (5) and the microsomal fraction is the most enriched source of phosphotransferase activities in nerve tissues (11, 13, 16). However, nuclear envelopes and mitochondrial fractions also contain these enzymes (12, 19, 26) and these membrane bounded organelles are also found in the crude nuclear and mitochondrial fractions. Sedimentation of the crude glomeruli fraction through 1.2 M sucrose separates the medullated fibers from the purified glomeruli and resulted in a moderate enrichment of the activities in the PGF, since the medullated fibers contained lower activities than the purified glomeruli.

Although there was no enrichment of enzyme activities in the PGF when compared to homogenate, there were substantial activities in the PGF. Further work is required to determine which of the PGF membranes contain the phosphotransferases, since the PGF includes neuronal and glial constituents and subcellular membrane components, such as mitochondria and endoplasmic reticulum. Regardless of the relative contributions of the various membrane components, it is clear that the purified glomeruli fraction isolated from cerebellar cortex is able to synthesize choline and ethanolamine glycerophospholipids.

The kinetic parameters for the enzymes were similar to those reported for other nerve ending preparations. The apparent Vmax value for the choline phosphotransferase in the PGF was 3.5 times greater than the Vmax for the ethanolamine phosphotransferase. The greater activity of the choline phosphotransferase is consistent with the previously observed differences in the relative distribution of these enzymes in other CNS membrane preparations (11-14) and reflects the uneven distribution of the choline and ethanolamine glycerophospholipids in cerebellar cortex (27). The activities of these enzymes in the PGF were less than the activities in brain microsomes (28), but they were similar to those reported for cerebral synaptosomes (20). Both enzymes had comparable affinities for the diglyceride and cytidine nucleotide substrates and these apparent Km values were similar to those

described in cerebral synaptosomes (20).

Even though the observed characteristics of the PGF enzymes were similar to those reported for other nerve ending preparations, the mechanisms involved in control of their activities may be different. The phosphotransferases in the PGF were unaffected by 1 mM ATP and cAMP, in the presence of subsaturating concentrations of diglycerides and CDPcholine and CDP-ethanolamine. However, adenine nucleotides have been shown to affect phosphotransferase activities in other membrane preparations. Both phosphotransferases are inhibited by ATP in rat liver microsomes (29-31), but only ethanolamine phosphotransferase activity is inhibited in chicken brain microsomes (32). Also, 1 mM ATP stimulates choline phosphotransferase activity, but not ethanolamine phosphotransferase activity in cerebral synaptosomes and the same effect is observed in the presence of 1 μM cAMP (20). These effects may be related to chemical transmission processes observed in cerebral synaptosomes. However, such influences were not expressed in the isolated glomeruli, since ATP and cAMP had no effect on the activity of either enzyme under the present experimental conditions.

The neurotransmitters NE, 5-HT and GABA, and the transmitter agonists muscimol, quisqualic acid and carbamylcholine, also had no effect on the activity of either phosphotransferase enzyme in isolated cerebellar glomeruli. These chemicals were chosen because they have been implicated in nervous system

function in general and glomerular function in particular (33,34). Subsaturating concentrations of diglycerides and CDPcholine and CDPethanolamine were used in all the treatment experiments, because the enzymes are unlikely to be saturated in vivo, and subsaturating substrate concentrations should allow for the observance of either competitive or noncompetitive treatment effects. Treatment concentrations of 1 mM were chosen because such concentrations have been shown to be effective in other membrane preparations (20,32). Therefore, the lack of transmitter effects on the activities of these enzymes is interpreted to indicate that neither enzyme is involved in receptor mediated processes in this nerve ending preparation. However, more extensive screening must be done in order to eliminate the possibility that the phosphotransferases are involved in the transmission processes related to a particular neurotransmitter.

Although neither phosphotransferase responded to neurotransmitters or agonists, they were both affected by exogneous cytidine nucleotides. The presence of 1 mM CTP, CDP or CMP stimulated choline phosphotransferase activity and inhibited ethanolamine phosphotransferase activity in the PGF. Although there is no known role for the cytidine compounds in neurotransmission, they appear to be involved in the regulation of choline and ethanolamine glycerophospholipid synthesis in cerebellar glomeruli. This regulation may be directly expressed at the

level of the enzymes, or it may involve control of endogenous substrate levels. For example, cytidine nucleotides have been shown to alter the rate of phosphatidic acid formation in rat brain homogenates (35), which may affect the availability of endogenous diglycerides. Also, we found that CTP, CDP and CMP stimulated the incorporation of [14C]acetate into cerebral diglycerides in vitro and in vivo (unpublished results). The cytidine nucleotides may also affect the endogenous levels of CDPcholine or CDPethanolamine, as has been shown in virus infected HeLa cells (36). Further work must be done to clarify the effects of the cytidine nuleotides, since these compounds appear to be involved in the control mechanisms for the synthesis of the major phospholipid constituents of the associated membranes.

Acknowledgements: We would like to thank Mary Beth Hofstetter for her excellent technical help. This work was supported in part by the U.S. Air Force: AFOSR/AFSC, F49620-82-C-0035 (RVD) and a grant from AFOSR #2312W3 (DMT).

## FIGURE LEGENDS

Figure 1. The effects of pH on the activities of choline and ethanolamine phosphotransferase enzymes in the purified glomeruli fraction. The assays were performed as described in the Experimental Procedures, while the buffer pH was varied from 6.0 to 9.0. Choline phosphotransferase assays included 100 mM $MgCl_2$, while ethanolamine phosphotransferase assays included 10 mM $MnCl_2$. The results are given as the mean values of at least three separate determinations.

Figure 2. The effects of nucleotides, neurotransmitters and neurotransmitter agonists on choline and ethanolamine phosphotransferase activities in the purified glomeruli fraction. The assays included 20 uM [14C]CDPcholine or [14C]CDPethanolamine. The neurotransmitters, transmitter agonists and nucleotides were included at 1 mM concentrations. Diglycerides were not added to the incubations and the assays were performed as previously described. The results were obtained from at least six separate determinations. (NE)norepinephrine, GABA(gamma-aminobutyric acid, 5-HT(5-hydroxytryptamine); (*$p < 0.01$; **$p < 0.001$ compared to untreated controls; Student's t-test).

## REFERENCES


1. Hamori, J. 1965. Identification in cerebellar isles of Golgi II axon endings by aid of experimental degeneration, pages 291-292, in Titlebalch, M.(ed.), Proc. of the Third European Regional Conference of Electron Microscopy, Pub. House of the Czechoslovak Acad. of Sci., Prague.

2. Hamori, J. and Szentagothai, J. 1966. Participation of Golgi neuron processes in the cerebellar glomeruli: an electron microscope study. Exp. Brain Res. 2:35-48.

3. Fox, C. A., Hillman, D. E., Siegesmund, K. A. and Dutta, C. R. 1967. The primate cerebellar cortex: a Golgi and electron microscope study. Prog. Brain Res. 25:174-225.

4. Szentogothai, J. 1970. Glomerular synapses, complex synaptic arrangements, and their operational significance, pages 427-443, in Schmitt, F.O.(ed.), The Neurosciences: Second Study Program, Rockefeller Univ. Press, New York.

5. Hajos, F., Tapia, R., Wilkin, G., Johnson, A.L. and Balazs, R. 1974. Subcellular fractionation of rat cerebellum: an electron microscopic and biochemical investigation. I. Preservation of large fragments of the cerebellar glomeruli. Brain Res. 70:261-279.

6. Tapia, R., Hajos, F., Wilkin, G., Johnson, A. and Balazs, R. 1974. Subcellular fractionation of rat cerebellum: an electron microscopic and biochemical investigation. Brain Res. 70:285-299.

7. Hamberger, A., Hansson, H.-A., Lazarewicz, J. W., Lundh, T. and Sellstrom, A. 1975. The cerebellar glomerulus: isolation and metabolic properties of a purified fraction. J. Neurochem. 27:267-272.

8. Terrian, D. M., Butcher, W. I., Wu, P. H. and Armstrong, D. L. 1985. Isolation of glomeruli from areas of bovine cerebellum and comparison of [3H]serotonin uptake. Brain Res. Bull. 14:469-475.

9. Wilson, J. E., Wilkin, G. P. and Balazs, R. 1976. Metabolic properties of a purified preparation of large fragments of the cerebellar glomeruli: glucose metabolism and amino acid uptake. J. Neurochem. 26:957-965.

10. Van den Bosch, H. 1974. Phosphoglyceride metabolism. Ann. Rev. Biochem. 43:243-277.

11. McCaman, R. E. and Cook, K. 1966. Intermediary metabolism of phospholipids in brain tissue. III. Phosphocholine-glyceride transferase. J. Biol. Chem. 241:3390-3394.

12. Ansell, G. B. and Metcalfe, R. F. 1968. Labelling of brain phosphatidylethanolamine and ethanolamine plasmalogen from cytidine diphosphate ethanolamine in vitro. Biochem. J. 109:29.

13. Goracci, G., Horrocks, L. A., and Porcellati, G. 1978. Studies of rat brain choline and ethanolamine phosphotransferases using labeled alkylacylglycerol as substrate with evidence for reversibility of the reaction. Adv. Exp. Med. Biol. 101:269-278.

14. Freysz, L. and Mandel, P. 1974. Etude comparative de la biosynthese des phosphatidylcholines dans les neurons et les

cellules gliales de cerveau de poulet. Febs. Lett. 40:110-113.

15. Toews, A. D., Horrocks, L. A. and King, J. S. 1976. Simultaneous isolation of purified microsomal and myelin fractions from rat spinal cord. J. Neurochem. 27:25-31.

16. Wu, P.-S. and Ledeen, R. W. 1980. Evidence for the presence of CDP-ethanolamine: 1,2-diacyl-sn-glycerol ethanolaminephosphotransferase in rat central nervous system myelin. J. Neurochem. 35:659-666.

17. Dorman, R. V., Freysz, L. and Horrocks, L. A. 1977. Synthesis of ethanolamine phosphoglycerides by microsomes from the brains of jimpy and quaking mice. J. Neurochem. 29:231-233.

18. Schneider, W. J. and Vance, D. E. 1978. Activities of choline kinase, cholinephosphate cytydyltransferase and CDP-choline: 1,2-diacylglycerol cholinephosphtransferase in brain from normal and quaking mice. J. Neurochem. 30:1599-1601.

19. Possmayer, F., Kleine, L., Duwe, G., Stewart-DeHaan, J., Wong, T., MacPherson, C. F. C. and Harding, P. G. R. 1979. Differences in the subcellular and subsynaptosomal distribution of the putative endoplasmic reticulum markers NADPH-cytochrome c reductase, estrone sulfate sulfohydrolase and CDP-choline-diacylglycerol cholinephosphotransferase in rat brain. J. Neurochem. 32:889-906.

20. Strosznajder, J., Radominska-Pyrek, A. and Horrocks, L. A. 1979. Choline and ethanolamine glycerophospholipid synthesis in isolated synaptosomes of rat brain. Biochim. Biophys. Acta 574:48-56.

21. Lowry, O.H., Rosebrough, N. J., Farr, A. L. and Randall, R. J.

1951. Protein measurement with the Folin phenol reagent. J. Biol. Chem. 193:265-275.

22. Lai, J. C. K. and Clark, J. B. 1976. Preparation and properties of mitochondria derived from synaptososmes. Biochem. J. 154:423-432.

23. Folch, J., Lees, M. and Sloane-Stanley, G. H. 1957. A simple method for the isolation and purification of total lipids from animal tissues. J. Biol. Chem. 226:497-509.

24. Horrocks, L. A. and Sun, G. Y. 1972. Ethanolamine plasmalogens, pages 223-231, in Rodnight, R. and Marks, N. (eds.), Research Methods in Neurochemistry, Plenum Press, New York.

25. Roberti, R., Binaglia, L., Francescangeli, E., Goracci, G. and Porcellati, G. 1975. Enzymic synthesis of 1-alkyl-2-acyl-sn-glycero-3-phosphorylethanolamine through ethanolaminephosphotransferase activity in neuronal and glial cells of rabbit in vitro. Lipids 3:121-127.

26. Baker, R. R. and Chang, H.-I. 1982. Cholinephosphotransferase activities in microsomes and neuronal nuclei isolated from immature rabbit cerebral cortex: the use of endogenously generated diacylglycerols as substrate. Can. J. Biochem. 60:724-733.

27. Geison, R. L., Flangas, A. L. and Kornguth, S. E. 1974. Total glycerophospholipid fatty acid and phospholipid class composition of nerve ending and related fractions from fetal and adult pig cerebellum and adult pig whole brain cortex. Lipids 9:756-764

28. Radominska-Pyrek, A., Strosznajder, J., Dabrowiecki, Z., Chojnacki,

T. and Horrocks, L. A. 1976. Effects of free fatty acids on the enzymic synthesis of diacyl and ether types of choline and ethanolamine phosphoglycerides. J. Lipid Res. 17:657-662.

29. De Kruyff, B., Van Golde, L. M. G. and Van Deenen, L. L. M. 1970. Utilization of diacylglycerol species by cholinephosphotransferase, ethanolaminephosphotransferase and diacylglycerol acyltransferase in rat liver microsomes. Biochim. Biophys. Acta 210:425-435.

30. Sribney, M., Knowles, C. L. and Lyman, E. M. 1976. Regulation of phosphatidlycholine synthesis in rat liver endoplasmic reticulum. Biochem. J. 156:507-514.

31. Litepio, R. G. and Sribney, M. 1977. Inhibition of rat liver CDPethanolamine: 1,2-diacylglycerol ethanolaminephosphotransferase activity by ATP and pantothenic acid derivitives. Can. J. Biochem. 55:1049-1056.

32. Freysz, L., Horrocks, L. A. and Mandel, P. 1978. Ethanolamine and choline phosphotransferases of chicken brain, pages 252-268, in Gatt, S., Freysz, L. and Mandel, P. (eds.), Enzymes of Lipid Metabolism, Plenum Press, New York.

33. Levi, G. 1984. Release of putative transmitter amino acids, pages 463-509, in Lajtha, A. (ed.), Handbook of Neurochemistry, Vol. 6, Plenum Press, New York.

34. Chan-Palay, V. 1977. The indoleamine afferent axons to the cerebellum, pages 330-453, in Cerebellar Dentate Nucleus: Organization, Cytology and Transmitters, Springer-Verlag, New York.

35. Possmayer, F. and Mudd, J. B. 1971. The regulation of sn-glycerol-3-phosphate acylation by cytidine nucleotides in rat brain cerebral hemispheres. Biochim. Biophys. Acta 239:217-233.

36. Choy, P. C., Paddon, H. B. and Vance, D. E. 1980. An increase in cytoplasmic CTP accelerates the reaction catalyzed by CTP:phosphocholine cytidylyltransferase in poliovirus-infected HeLa cells. J. Biol. Chem. 255:1070-1073.

37. Eisenthal, R. and Cornish-Bowden, A. 1974. The direct linear plot. A new graphical procedure for estimating enzyme kinetic parameters. Biochem. J. 139:715-720.

TABLE I

CATION DEPENDENCE OF CHOLINE AND ETHANOLAMINE PHOSPHOTRANSFERASE ENZYMES IN THE PURIFIED GLOMERULI FRACTION

nmol/hr/mg protein ± S.D

| ADDITION (mM) | | CHOLINE PHOSPHOTRANSFERASE | ETHANOLAMINE PHOSPHOTRANSFERASE |
|---|---|---|---|
| none | | 0.07 ± 0.03 | 0.11 ± 0.01 |
| $MgCl_2$ | 1.0 | 0.18 ± 0.04 | 0.86 ± 0.17 |
| | 10.0 | 2.06 ± 0.36 | 0.84 ± 0.12 |
| | 20.0 | 3.10 ± 0.53 | 0.[illegible] ± 0.[illegible] |
| | 100.0 | 4.34 ± 0.48 | 0.[illegible] ± 0.03 |
| | 200.0 | 4.30 ± 0.07 | [illegible] |
| $MnCl_2$ | 0.1 | 1.54 ± 0.03 | [illegible] |
| | 1.0 | 2.38 ± 0.16 | 1.26 ± 0.[illegible] |
| | 10.0 | 2.37 ± 0.18 | 1.28 ± 0.[illegible] |
| | 20.0 | 2.06 ± 0.16 | 1.14 ± 0.22 |
| | 50.0 | nd | 0.71 ± 0.04 |
| $CaCl_2$ | 50.0 | nd | 0.35 ± 0.01 |
| | 200.0 | 0.04 ±0.01 | nd |

Incubations were performed at 37°C for 30 minutes in 10 mM Tris-HCl buffer (pH 7.45), containing 1-2 mg PGF protein and 40 µM [14C]CDPcholine or 20 µM [14C]CDPethanolamine (each at 2 nCi/nmol). The incubations containing $CaCl_2$ also contained optimal concentrations of either $MnCl_2$ or $MgCl_2$. The total lipids were extracted and counted as described in Experimental Procedures. The results are expressed as nmol of isotope incorporated/hour/mg glomerular protein. nd = not determined.

TABLE II

CHOLINE AND ETHANOLAMINE PHOSPHOTRANSFERASE ACTIVITIES IN SUBCELLULAR FRACTIONS ISOLATED FROM CEREBELLAR CORTEX

nmol/hr/mg protein ± S.D.

| FRACTIONS | CHOLINE PHOSPHOTRANSFERASE | ETHANOLAMINE PHOSPHOTRANSFERASE |
|---|---|---|
| HOMOGENATE | 3.42 ± 0.85 | 1.76 ± 0.66 |
| NUCLEAR FRACTION | 6.45 ± 0.58 | 3.18 ± 0.57 |
| MITOCHONDRIAL FRAC. | 5.64 ± 0.92 | 2.45 ± 0.29 |
| CRUDE GLOMERULI | 1.81 ± 0.15 | 1.19 ± 0.21 |
| MEDULLATED FIBERS | 1.07 ± 0.24 | 0.87 ± 0.18 |
| PURIFIED GLOMERULI | 3.56 ± 0.36 | 1.89 ± 0.40 |

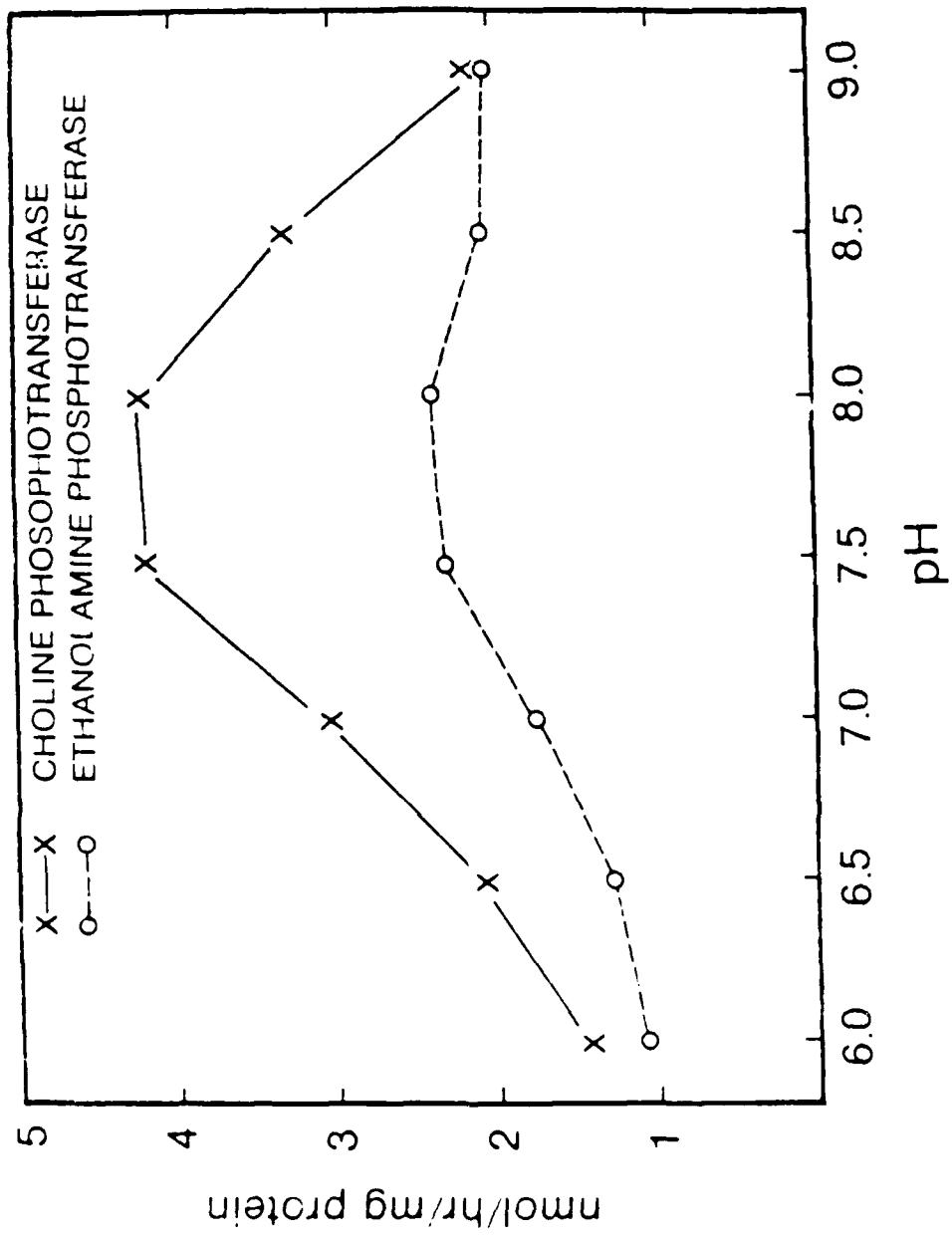
Assays were performed as described in Experimental Procedures. Each subfraction was isolated during the preparation of the PGF and all were suspended in 10 mM Tris-HCl (pH 7.15) and immediately assayed. The results represent the activities determined in at least three separate subfraction preparations.

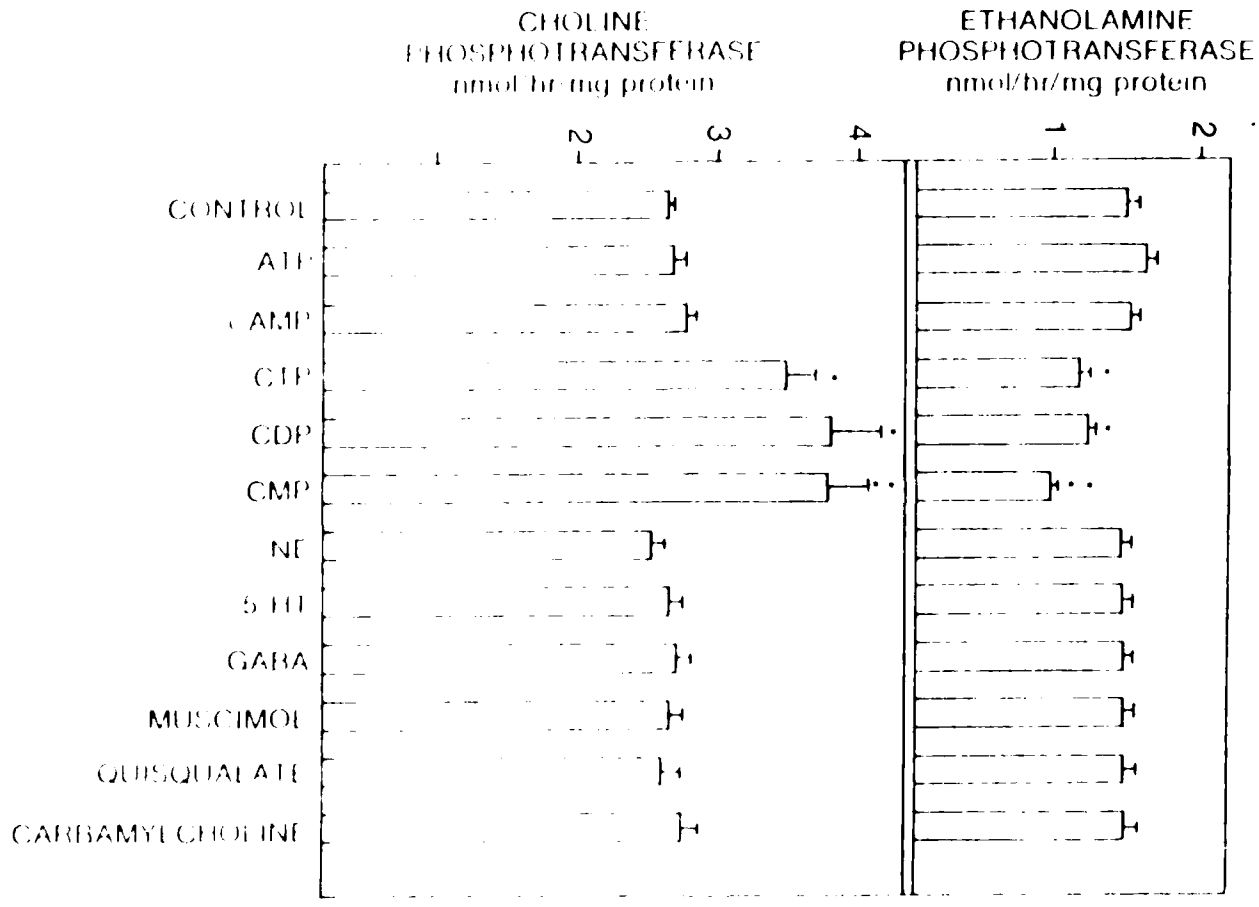
TABLE III

ESTIMATES OF Km AND Vmax VALUES FOR CHOLINE AND ETHANOLAMINE PHOSPHOTRANSFERASE ENZYMES IN THE PURIFIED GLOMERULI FRACTION

| | CHOLINE PHOSPHOTRANSFERASE | ETHANOLAMINE PHOSPHOTRANSFERASE |
|---|---|---|
| Vmax | | |
| nmol/hr/mg prot. | 45.9 | 10.0 |
| Km | | |
| 1,2-diolein (mM) | 2.9 | 2.1 |
| CDPcholine (μM) | 28.6 | --- |
| CDPethanolamine (μM) | --- | 6.5 |

Assays were performed as described in Experimental Procedures, except exogenous diglycerides (1,2-diolein) were included at concentrations from 0.5 to 10.0 mM, and [14C]CDPcholine and [14C]CDPethanolamine concentrations were varied from 5 to 100 μM. The apparent Km and Vmax values were estimated from the results of four separate experiments, according to Eisenthal and Cornish-Bowden (37).


CHOLINE PHOSOPHOTRANSFERASE
ETHANOLAMINE PHOSPHOTRANSFERASE
nmol/hr/mg protein
pH
5
4
3
2
1
6.0
6.5
7.0
7.5
8.0
8.5
9.0


CHOLINE
PHOSPHOTRANSFERASE
nmol/hr/mg protein
ETHANOLAMINE
PHOSPHOTRANSFERASE
nmol/hr/mg protein
CONTROL
ATP
cAMP
CTP
CDP
CMP
NE
5-HT
GABA
MUSCIMOL
QUISQUALATE
CARBAMYLCHOLINE

# Dynamics of Large Scale Vortex Structures And Quasi-Large Scale Structures in the Wake of a Splitter Plate

## Part I - Structure of Steady Base Flow

by

Steven A. Lottes and Paul H.H. Chiu

Department of Mechanical Engineering
The University of Illinois at Chicago
Chicago Illinois

May 1, 1986

## ABSTRACT

This study is an integral part of the research on vortex shedding from a splitter plate that separates a low speed hot flow and a high speed cold. This paper extends Goldstein, Cheng, Kovitz, and Chiu's wake solutions to the flow configuration involving the asymmetric mixing of two streams of different velocity with prescribed temperature and velocity ratio at the trailing edge of the plate. The predicted wake structure in the proximity of the trailing edge reveals momentum transport from faster to slower stream which shifts the point of zero shear from the center of the wake into the slower hot stream. Effects of coupling between energy and momentum due to property variation in the presence of steep temperature gradients are also found to be significant. A two sided mixing layer structure of the trailing wake and it probable effects on vortex shedding is described and research in progress for Part II is discussed.

## INTRODUCTION

The physical mechanisms and conditions for the generation of large scale dynamic structures and subsequent growth or damping within the wake of bluff bodies has become an important area basic research with application to the engineering of combustors. Fuel efficiency, noise generation, including rumble which may lead to mechanical damage or shortened component life, and the ability of the bluff body to stabilize the flame may all be greatly affected by the generation and subsequent shedding of large scale structures from the wakes of bluff bodies.

Many experimental researchers have reported that combustion suppresses vortex shedding from the wakes of bluff bodies [1-4]. However, experimental studies at Wright Aeronautical Propulsion Laboratory by Roquemore et al. [5-8] with bluff body stabilized combustion in a long cylindrical tunnel produced much evidence of vortex shedding. Sturgess and Syed [9] proposed that the vortex shedding was the result of acoustic interaction with the natural frequencies of the long combustion tunnel. Experiments by Roquemore et al. [10] using a unique laser sheet-lighting technique showed the formation and rolling up process of vortices on the wake interface of an unducted bluff body combustor operated in a cold flow mode. When operated with combustion disturbances grew and propagated along the interface to the tip of the wake, but the characteristic rolling up observed in the cold flow was absent in the hot flow cases. These experiments are providing much information about

the types of large scale dynamic structures that occur in bluff body wakes and the conditions under which they occur in the flow field.

Theoretical work, based on knowledge gained in experiments, is needed to identify the physical mechanisms which lead to the formation of the various large scale structures in bluff body wakes and to determine the parameters which control the growth rates of these structures. Efforts at analysis or direct numerical simulation of these flows are hampered by their complexity including their fundamental 3-dimensional nature as revealed in the films of Roquemore et al. [10]. Even 2-dimensional unsteady computations use large amounts of computing resources; 3-dimensional unsteady computations with enough nodes to avoid grid sensitivity are prohibitively expensive on current large computers. Under these circumstances theoretical studies which deal with a simplified geometry and concentrate on a few of the characteristics of the flow considered most important, such as the present of shear layer with a large temperature gradient across the layer.

In an initial analytical effort in the study of disturbance formation and growth, Chiu [11] simplified the geometry by considering the interaction of two semi-infinite streams. Additional simplifying assumptions were the absence of body or viscous forces with the shear layer idealized as a vortex sheet in the presence of an initial step temperature difference across the streams. Results of the analysis yielded stability conditions, and disturbance growth rates and propagation velocities

for the idealized flow. In particular, in the absence of mass injection, the flow is always unstable, even in the presence of a temperature difference across the streams. However, as the temperature ratio approaches infinity, the rate of disturbance growth approaches zero. If effects of viscous damping were taken into account another point of neutral stability at some finite temperature ratio would be expected.

The work reported here seeks to relax three of the major simplifying assumptions of Chiu's initial study. These include the assumption of an infinitely thin vortex sheet, the assumption of semi-infinite streams, and the assumption of an inviscid fluid model. The geometry is kept simple by considering the flow in the wake of a splitter plate (figure 1). The free-stream velocities of the upper and lower streams are different producing a shear layer in the downstream of the plate. The temperatures of the two streams are also different. For definiteness, the upper stream is taken to be fast and cold compared to the lower stream. The gravity vector is assumed not to have a component in the computational plane, and therefore, this choice of free-stream velocities and temperatures has no implications in regards to the effects of buoyancy on the stability or other characteristics of the flow. The choice is meant to correspond in some important aspects to an incoming stream of cold air interacting with a hot slower moving stream in the recirculation zone behind a bluff body in a bluff body combustor.

The planned basis for this work was the work of Goldstein [12], and later that of Kovitz [13], and Chiu [14]. These

researchers developed solutions in the form of universal functions for the flow in the near wake of a flat plate which matched Blasius profiles at the trailing edge of the plate. The near wake is considered to be a prime candidate breeding ground for vortices or other large scale structures which grow and propagate into the downstream, therefore use of these earlier methods along with judicious use of modern computational methods appears to offer the opportunity to make substantial progress on the problems of interest in this study. Unfortunately the solutions generated in this earlier work could not be used as the steady state basis of the current study, because that work assumed the flowfield to be symmetric about the centerline (the free-stream velocities of the streams were assumed to be equal), and certain property variations were assumed small, in particular the density-viscosity product, to allow decoupling of the momentum and energy equations. In fact as the temperature of air at atmospheric pressure varies from 300K to 1200K, property variations can be quite significant; the density-viscosity product varies, for example, by 56 percent. With the availability of computers and modern computational techniques, decoupling of the momentum and energy equations is not required to obtain a solution.

The effects of shear and of property variation due to large temperature gradients in the flowfield are considered to be of central importance in the study of the growth of disturbances at the interface between the two streams. Therefore, this study has been divided into two parts. The first part pro-

vides a steady flow generalization of earlier work which allows for streams of different velocities, and takes better account of property variation within the flowfield. The second part encompasses the unsteady stability analysis of the generalized splitter plate wake flow.

The remainder of this paper will deal with Part I. The formulation of the steady flow problem with its generalizations are presented, followed by a discussion of applicable numerical techniques. The formulation leads to a sequence of systems of ordinary differential equations. A computer program which solves the zero order system is included in the appendix. Solutions of the zero order system are presented and discussed.

## OBJECTIVES

The objectives of this part of the research effort are to produce a solution procedure in the form of a computer program for a generalized steady state near plate wake flow problem. The results will provide new near wake flow solutions for steady flow as well as a basis for stability analysis of the near plate wake region. The generalization will relax the assumptions of Kovitz [13] that the freestream velocities of the two streams are equal, and that the density-viscosity product is constant.

## MATHEMATICAL FORMULATION

### Problem Definition and Method of Analysis

The near wake region of a splitter plate is considered as shown is figure 1. The subscript 1 refers to the upper half plane, while 2 refers to the lower half plane. $U_1$ and $U_2$ are the free-stream velocities. Blasius profiles are assumed at the coordinate origin at the trailing edge of the plate. The temperature profiles are taken to be uniform at the origin. For definiteness $U_1$ is taken to be greater than or equal to $U_2$ and $T_2$ is taken to be greater than or equal to $T_1$. The methods of analysis of Goldstein [12] and subsequently Kovitz [13] are applied to the governing equations. In this approach a Howarth transformation is applied to the governing equations which yields an incompressible form of the continuity equation. The additional assumption of constant density-viscosity product, not applied here, yields an incompressible momentum equation and decouples momentum and energy equations. This study does not make this constant property assumption and consequently leaves the momentum and energy equations coupled. The equations are nondimensionalized in the same way as Kovitz [13] so that the base solution can be compared with his to partially verify the computer program. Although the flow is not self similar, a similarity type transformation is preformed to reduce the dependence of the y-profiles on the streamwise position and to put the equations in a form that can be easily matched to Blasius profiles at the origin. A series solution in terms of

streamwise coordinate and functions of the cross-stream coordinate is then assumed. Substitution into the governing equations yields a sequence of systems of ordinary differential equations, each of which is relatively simple to solve numerically from solutions of the systems of lower order.

Assumptions

The assumptions are similar to those of Kovitz [13], with the exception of those already noted and the condition of no chemical reaction. These assumptions are also consistent with those frequently used in stability analysis of similar types of flows [15].

a. The flow is assumed to be 2-dimensional, initially laminar, and governed by boundary layer type equations.
b. There are no external or body forces.
c. The mean pressure is constant.
d. There is no chemical reaction.
e. Stoke's hypothesis holds: bulk viscosity = $-2\mu/3$
f. The fluid is a perfect gas.

Governing Equations

For convenience the flowfield is divided into an upper and a lower half plane, and governing equations are formulated for each half plane. To economize on notation and presentation of equations, only equations for the upper half plane are given since those for the lower half plane are exactly the same if the y-coordinate for the lower half plane is taken to be poin-

ting downward. Other notation includes a ^ appearing over variables to denote a physical plane variable, a ~ to denote a Howarth transformed variable, and no over symbol to denote a nondimensionalized transformed variable. A coordinate subscript denotes differentiation with respect to that coordinate, and a prime denotes differentiation with respect to $\eta$.

Under the assumptions given, the governing equations are:

$$(\hat{\rho}\hat{u})_{\hat{x}} + (\hat{\rho}\hat{v})_{\hat{y}} = 0$$

$$\hat{\rho}\hat{u}\hat{u}_{\hat{x}} + \hat{\rho}\hat{v}\hat{u}_{\hat{y}} = (\hat{\mu}\hat{u}_{\hat{y}})_{\hat{y}}$$

$$\hat{\rho}\hat{c}_p(\hat{u}\hat{T}_{\hat{x}} + \hat{v}\hat{T}_{\hat{y}}) - (\hat{\lambda}\hat{T}_{\hat{y}})_{\hat{y}} = 0$$

$$\hat{P} = \hat{\rho}R\hat{T}$$

The Howarth Transform is:

$$\tilde{x} = \hat{x}, \qquad \tilde{y} = \int_0^{\hat{y}} \hat{\rho}(\hat{x},y)/\rho_1 \, dy$$

$$\hat{u} = \tilde{u}, \qquad \hat{v} = \rho_1/\tilde{\rho}(\tilde{v} - \tilde{u}\,\partial\tilde{y}/\partial\hat{x})$$

Applying the transform yields:

$$\tilde{u}_{\tilde{x}} + \tilde{v}_{\tilde{y}} = 0$$

$$\tilde{u}\tilde{u}_{\tilde{x}} + \tilde{v}\tilde{u}_{\tilde{y}} = -(\tilde{\rho}\tilde{\mu}/\rho_1^2\ \tilde{u}_{\tilde{y}})_{\tilde{y}}$$

$$\tilde{u}\tilde{T}_{\tilde{x}} + \tilde{v}\tilde{T}_{\tilde{y}} = 1/(\rho_1\tilde{c}_p)\ (\tilde{\rho}\tilde{\lambda}/\rho_1\ \tilde{T}_{\tilde{y}})_{\tilde{y}}$$

$$\tilde{P} = \tilde{\rho}R\tilde{T}$$

Nondimensionalization

The following nondimensional variables are defined:

$$x = \tilde{x}/(4L), \qquad y = \sqrt{R}\,\tilde{y}/(4L)$$

$$u = \tilde{u}/U_1, \qquad v = \sqrt{R}\,\tilde{v}/U_1$$

$$\theta = \tilde{T}/T_\infty, \qquad R = 4\rho_1 U_1 L/\mu_1$$

$$\rho = \tilde{\rho}/\rho_1, \qquad \tilde{\mu} = \tilde{\mu}/\mu_1$$

$$\lambda = \tilde{\lambda}/\lambda_1 \qquad c_p = \tilde{c}_p/c_{p1}$$

Substituting these definitions into the Howarth transformed equations yields:

$$u_x + v_y = 0$$

$$uu_x + vu_y = (\rho\mu\, u_y)_y$$

$$u\theta_x + v\theta_y = 1/(c_p P_r)\ (\rho\lambda\ \theta_y)_y$$

$$\rho = R_T/\theta, \quad \text{where } R_T = T_1/T_2$$

Now consider the stream function defined by:

$$\psi_y = u, \quad \text{and} \quad -\psi_x = v$$

Assume that this stream function can be written in the form:

$$\psi = \epsilon^{m-1} f(\epsilon, \eta) \quad \text{then} \quad u = \epsilon f'/3$$

where

$$\epsilon = x^{1/m}, \quad \text{and} \quad \eta = yx^{-1/m}/m$$

Matching Blasius profiles at the origin requires that m=3. Transforming to $(\eta,\epsilon)$ coordinates and substituting the stream function into the governing equations satisfies the continuity equation identically and yields the following momentum and energy equations:

$$(\rho\mu f'')' + 2ff'' - f'^2 = \epsilon(f'\partial f'/\partial\epsilon - f''\partial f/\partial\epsilon)$$

$$(\rho\lambda\theta')' + 2f\theta' = (1/P_r c_p)\epsilon(f'\partial\theta/\partial\epsilon - \theta'\partial f/\partial\epsilon)$$

For large $\epsilon$, these equations could be solved numerically using free-stream values of the upper and lower streams as boundary conditions and continuity of variables and their gradients at the centerline as junction conditions. However, a solution for small $\epsilon$ is sought here which requires matching the Blasius velocity profiles as $\epsilon \to 0$ and $\eta \to \infty$ for small constant y. To find a small $\epsilon$ solution, expand the dependent variables in series about $\epsilon = 0$:

$$f(\eta,\epsilon) = \Sigma\, \epsilon^j f_j(\eta), \qquad \theta(\eta,\epsilon) = \Sigma\, \epsilon^j \theta_j(\eta)$$

To handle property variation, approximate data for $\rho\mu$ and $\rho\lambda$ as third degree polynomials:

$$\rho\mu = \sum_{j=0}^{3} a_j \theta^j, \qquad \rho\lambda = \sum_{j=0}^{3} e_j \theta^j$$

Using the expansion of $\theta$, write:

$$\theta^2 = \Sigma C_j \epsilon^j, \quad \text{where} \quad \begin{aligned} C_0 &= \theta_0^2, \\ C_1 &= 2\theta_0\theta_1, \\ C_2 &= 2\theta_0\theta_2 + \theta_1^2, \\ C_3 &= 2\theta_0\theta_3 + \theta_1\theta_2, \ \ldots \end{aligned}$$

$$\theta^3 = \Sigma D_j \epsilon^j, \quad \text{where} \quad \begin{aligned} D_0 &= \theta_0^3, \\ D_1 &= 3\theta_0^2\theta_1, \\ D_2 &= 3\theta_0^2\theta_2 + 3\theta_0\theta_1^2, \\ D_3 &= 3\theta_0^2\theta_3 + 6\theta_0\theta_1\theta_2 + \theta_1^3, \ \ldots \end{aligned}$$

Substitution of these series into the polynomial approximations for $\rho\mu$ and $\rho\lambda$ yields:

$$\rho\mu = \Sigma\, E_j \epsilon^j, \qquad \rho\lambda = \Sigma\, F_j \epsilon^j$$

where:

$$\begin{aligned} E_0 &= a_0 + a_1\theta_0 + a_2 C_0 + a_3 D_0 \\ E_j &= a_1\theta_j + a_2 C_j + a_3 D_j \qquad \text{for } j > 0 \end{aligned}$$

$$\begin{aligned} F_0 &= e_0 + e_1\theta_0 + e_2 C_0 + e_3 D_0 \\ F_j &= e_1\theta_j + e_2 C_j + e_3 D_j \qquad \text{for } j > 0 \end{aligned}$$

Since $c_p$ variation is small compared to other parameters and does not affect the zero order system, $c_p$ is taken to be constant and equal to its mean value over the temperature interval. Normalized by the free-stream value of the upper stream, this value is slightly greater than one. To simplify the equations of higher order, the product $P_r c_p$, which is close to one for air in the range 300-1200K, is taken to be one. Substitution of the series into the momentum and energy equations yields equations of the form:

$$\Sigma G_j \epsilon^j = 0, \qquad \Sigma H_j \epsilon^j = 0,$$

Since $\epsilon$ is arbitrary, $G_j = 0$ and $H_j = 0$ for all $j$, which yields the following sets of equations (nonhomogeneous terms have been moved to the right hand side):

Order $j$ Momentum Equations: $G_j = 0$

$$0: \quad E_0 f_0''' + (2f_0 + E_0') f_0'' - (f_0')^2 = 0$$

$$1: \quad E_0 f_1''' + (2f_0 + E_0') f_1'' - 3f_0' f_1 + 3f_0'' f_1 = -E_1 f_0''' - E_1' f_0''$$

$$2: \quad E_0 f_2''' + (2f_0 + E_0') f_2'' - 4f_0' f_2' + 4f_0'' f_2 = -E_1 f_1''' - E_1' f_1'' - E_2 f_0''' - E_2' f_0'' - 3f_1 f_1'' + (f_1')^2$$

$$3: \quad E_0 f_3''' + (2f_0 + E_0') f_3'' - 5f_0' f_3' + 5f_0'' f_3 = -E_1 f_2''' - E_1' f_2'' - E_2 f_1''' - E_2' f_1'' - E_3 f_0''' - E_3' f_0'' - 3f_1 f_2'' - 4f_2 f_1'' + 5f_1' f_2'$$

Order $j$ Energy Equations: $H_j = 0$

$$0: \quad F_0 \theta_0'' + (2f_0 + F_0') \theta_0' = 0$$

$$1: \quad F_0 \theta_1'' + (2f_0 + F_0') \theta_1' - f_0' \theta_1 = -F_1 \theta_0'' - (F_1' + 3f_1) \theta_0'$$

$$2: \quad F_0 \theta_2'' + (2f_0 + F_0') \theta_2' - 2f_0' \theta_2 = -F_1 \theta_1'' - (F_1' + 3f_1) \theta_1' + f_1' \theta_1 - F_2 \theta_0'' - (F_2' + 4f_2) \theta_0'$$

$$3: \quad F_0 \theta_3'' + (2f_0 + F_0') \theta_3' - 3f_0' \theta_3 = -F_1 \theta_2'' - (F_1' + 3f_1) \theta_2' + 2f_1' \theta_2 - F_2 \theta_1'' - (F_2' + 4f_2) \theta_1' + f_2' \theta_1 - F_3 \theta_0'' - (F_3' + 5f_3) \theta_0'$$

With proper boundary and junction conditions, these coupled pairs of ordinary differential equations can be solved numerically for each order in succession beginning with order zero.

## Boundary and Junction Conditions

To discus junction conditions, upper and lower stream variables must be distinguished even though the equations are

the same. Therefore lower stream variables will be identified with an overbar in the discussion to follow. A primary objective of this part of the research is to find steady state solutions to be used as a basis for analyzing the stability of the interface between the two streams in Part II. Because the interface occurs at y=0, solutions for small y are sought, which match the Blasius velocity profiles at trailing edge of the plate as x approaches zero.

Boundary Conditions to Match Blasius Velocity Profiles at x=0

The Blasius velocity profile at x=0 is given by [12]:

$$u_o = a_1 y + a_4 y^4 + a_7 y^7 + \ldots$$

where

$$a_1 = \alpha/2,\quad a_4 = -0.5\alpha^4/4!,\quad a_7 = 5.5\alpha^7/7!,\quad \ldots$$

and $\alpha = 1.32824$

The limiting process to match the Blasius velocity profile allows $x=\epsilon^3$ to approach zero while holding $y=3\epsilon\eta$ constant at some small value. With $u=\epsilon f'/3=\Sigma\epsilon^{j+1}f^j/3$, the limit $u\to u_o$ as $x\to 0$ and y=constant is equivalent to:

$$\lim_{\substack{\eta\to\infty \\ \epsilon\eta=\text{const.}}} \Sigma\epsilon^j f_{j-i} = \Sigma\epsilon^j a_j 3^{j+1}\eta^j, \qquad j=1,2,\ldots$$

Matching powers of $\epsilon$ in the limit requires that:

$$\lim_{\eta\to\infty} f_{j-i}/\eta^j = 3^{j+1}a_j$$

in particular as $\eta\to\infty$ :

$$f_0/\eta \to 5.97708, \quad f_1/\eta^2 \to 0$$

$$f_2/\eta \to 0, \quad f_3/\eta^2 \to -8.93136$$

The upper and lower stream velocity profiles at x=0 are related

by:

$$u_o(|y|)/U_1 = \bar{u}_o(|y|)/U_2 \quad \text{or} \quad \bar{u}_o = u_o/\lambda$$

where: $\lambda = U_1/U_2$

Consequently, the boundary conditions for the lower stream become:

$$\lim_{\eta \to \infty} \bar{f}_{j-1}/\eta^j = 3^{j-1}a_j/\lambda$$

in particular as $\eta \to \infty$ :

$$\bar{f}_0/\eta \to 5.97708/\lambda, \quad \bar{f}_1/\eta^2 \to 0$$

$$\bar{f}_2/\eta \to 0, \quad \bar{f}_3/\eta^2 \to -8.93136/\lambda$$

Because the inlet temperature is taken to be uniform in each stream in this study, the boundary conditions for $\theta_j$ and $\bar{\theta}_j$ are simply:

$$\theta_0 \to \lambda_T, \quad \bar{\theta}_0 \to 1, \quad \text{as } \eta \to \infty$$

$$\theta_j \to 0, \quad \bar{\theta}_j \to 0, \quad \text{as } \eta \to \infty$$

Junction Conditions at the Interface Between the Streams

The junction conditions are derived from the continuity of streamlines, velocity, shear stress, temperature, and temperature gradient at the interface between the two streams.

Without loss of generality, take $f(0,0)=0$, assigning the dividing streamline the value 0. Continuity of streamlines requires that $f_j(0)=\bar{f}_j(0)$, and therefore:

$$f(0,0) = f_0(0) = \bar{f}_0(0) = 0$$

To obtain sufficient conditions to solve the systems of order $j>0$, assume that the deviation of the zero streamline from the $\epsilon$-axis is negligibly small for small $\epsilon$. According to Crane [16], relaxing this assumption requires taking into consider-

ation terms in the Navier Stokes equations which were neglected under the boundary layer flow assumption. This small deviation assumption is adequate for stability analysis and to determine initial growth rate of disturbances, but would not be adequate to follow long term evolution of disturbances into large rolled up vortices in the downstream of the flow. Using this assumption yields:

$$f_j(0) = \bar{f}_j(0) = 0, \qquad \text{for} \quad j > 1$$

Continuity of velocity, $u=\bar{u}$ at $\eta=0$, yields:

$$f'(\xi,0) = \bar{f}'(\xi,0)$$

and so $f_j(0) = \bar{f}_j(0)$ for all $j$

The choice of lower stream $\eta$ coordinate as positive downward requires that gradients match in magnitude but have opposite sign at $\eta=0$. Continuity of shear stress yields therefore:

$$\bar{f}''(\xi,0) = -f''(\xi,0)$$

and so $\bar{f}_j'(0) = -f_j'(0)$ for all $j$

Similarly, continuity of temperature and temperature gradient at $\eta=0$ yields:

$$\bar{\theta}_j(0) = \theta_j(0)$$

$$\bar{\theta}_j(0) = -\theta_j(0) \qquad \text{for all } j$$

## NUMERICAL METHOD

In the previous section, the problem was formulated as a sequence of systems of ordinary differential equations, each system containing four equations. Because these systems are not initial value problems, straight forward numerical integration to obtain a solution is not possible, and iterative techniques must be used. Two such techniques, the Shooting Method, and the Integral Method were considered, and a hybrid combination of the two was implemented for solution of the zero order system. The shooting method is discussed in most textbooks on numerical analysis; it generally converges rapidly once the guessed parameters at the initial point are sufficiently close to the solution. In this problem the obvious candidate for the initial point is the interface between the two streams with the guessed parameters being the junction values of the variables. The presence of four unknown parameters ($f_o, f_o', \theta_o, \theta_o$) at the initial point ($\eta=0$) makes successful implementation of a shooting method a very difficult task. The integral method has been successfully used by Minkowicz to obtain solutions to a variety of boundary layer problems where application of other methods would have been very difficult, see for example [17]. The integral method converts the system of differential equations into integral equations and proceeds by iteratively improving guesses of the unknown functions over the problem interval through successive numerical evaluation of the integrals. When under-relaxation is used, this method is not nearly as sensitive to the initial guess as the shooting method. Eval-

uation uation of junction parameters for the momentum equations proved to be a problem with the integral method because differences of large nearly equal numbers were involved, which resulted in unacceptable loss of computational significance. As a result of these difficulties, a hybrid algorithm using the shooting method to solve the momentum equations and the integral method to solve the energy equations was developed.

Shooting Algorithm for Momentum Equations

The momentum equations are coupled to the energy equations via the functions $E_1$, $\bar{E}_1$, and their derivatives appearing in the coefficients of the momentum equations. During one overall iteration, these functions are computed from the latest tentative solution of the energy equations and held constant during solution of the momentum equations.

For computational convenience in the solution of the zero order system, $f_o''(0)$ is taken as given instead of the parameter $\Omega_\nu$. This approach further reduces the shooting method to one with only one unknown quantity at the initial point. The value of $\Omega_\nu$ is then computed from the converged solution. This method will not work for solution of the higher order systems, however, because the value of $\Omega_\nu$ is fixed by the solution of the zero order system. The higher order systems require the use of a two parameter shooting method.

The shooting method uses a Runge Kutta algorithm to compute the functions $f_o$, $f\acute{o}$, and $f\acute{o}'$ over the interval $(0,\infty)$, starting at $\eta=0$, using the differential equation, the known

values $f_o(0)$, $f_o'(0)$, and the guessed value $f_o'(0)$. In practice, computation stops at some finite $\eta=\eta_\infty$ which is sufficiently large so that functions have reached their asymptotic behavior to within a desired tolerance. $\eta_\infty = 4$ was found to be sufficiently large in this study. The known boundary value at the end of the interval, $\eta=\infty$, is then compared with the computed result and used to compute an improved guess of $f_o'(0)$ as follows:

Let $s$ = current guess of $f_o'(0)$

$s^-$ = value of $s$ from previous iteration

$s^+$ = improved $s$ computed from current iteration results

Treat $f_o'(\infty)$ as a function of $s$, then:

$$f_o'(\infty,s^+) = f_o'(\infty,s) + \partial f_o'/\partial s(s^+-s) = a$$

where $a = 5.97708$

Estimate the partial derivative as:

$$b = [f_o'(\infty,s)-f_o'(\infty,s^-)]/[s-s^-] = \partial f_o'/\partial s$$

Solve the Taylor expansion for $s^+$ giving:

$$s^+ = s - [f_o'(\infty,s)-a]/b$$

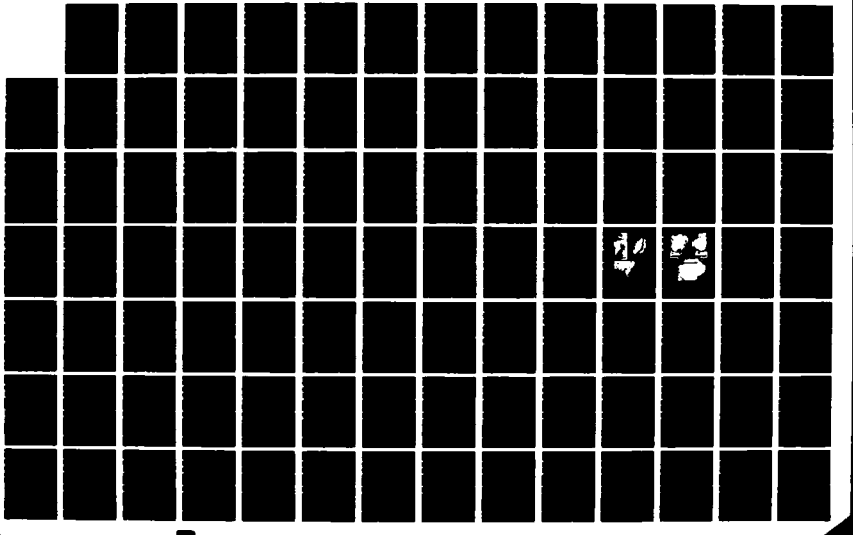
Using the iteration formula above, iteration continues until:

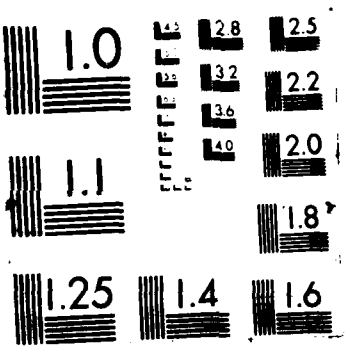
$$(s^+-s)/s < 10^{-n}$$

Upon convergence profiles for the upper stream are known along with the values at $\eta=0$, therefore, the Runge Kutta algorithm can be used to compute the profiles over the lower stream. The results of the lower stream computation are then used to compute $\Omega_\cup$ according to:

$$\Omega_\cup = a/f_o'(\infty)$$

AD-A186 490 UNITED STATES AIR FORCE RESEARCH INITIATION PROGRAM 05/11
1984 RESEARCH REPORTS (U) SOUTHEASTERN CENTER FOR
ELECTRICAL ENGINEERING EDUCATION INC S W D PEELE
UNCLASSIFIED MAY 86 AFOSR-TR-87-1721 F49620-82-C-0035 F/G 15/1 NL




1.0
1.1
1.25
1.4
1.6
1.8
2.0
2.2
2.5
2.8
3.2
3.6
4.0

## Integral Method for Energy Equations

This section will present the integral equations for the zero order energy equations. Derivation of the method for higher orders is similar.

To simplify notation, define:

$$\bar{R}_e = (2\bar{f}_o + \bar{F}_o')/\bar{F}_o, \qquad R_e = (2f_o + F_o')/F_o$$

$$\beta(\eta) = \exp\left[-\int_{\phi 0}^{\phi\eta} R_e(s)\,ds\right], \qquad \bar{\beta}(\eta) = \exp\left[-\int_{\phi 0}^{\phi\eta} R_e(s)\,ds\right]$$

$$I(\eta) = \int_{\phi 0}^{\phi\eta} \beta(t)\,dt, \qquad \bar{I}(\eta) = \int_{\phi 0}^{\phi\eta} \bar{\beta}(t)\,dt$$

The zero order energy equations can be converted into the following integral equations:

$$\theta_o'(\eta) = \theta_o'(0)\beta(\eta)$$

$$\bar{\theta}_o'(\eta) = -\bar{\theta}_o'(0)\bar{\beta}(\eta)$$

$$\theta_o(\eta) = \theta_o(0) + \theta_o'(0)I(\eta)$$

$$\bar{\theta}_o(\eta) = \theta_o(0) - \bar{\theta}_o'(0)\bar{I}(\eta)$$

Application of boundary and junction conditions leads to:

$$\theta_o'(0) = [\Omega_T - 1]/[I(\infty) + \bar{I}(\infty)]$$

$$\theta_o(0) = [I(\infty) + \Omega_T\bar{I}(\infty)]/[I(\infty) + \bar{I}(\infty)]$$

The integral method computation proceeds as follows:

1. Guess $\theta_o$, $\bar{\theta}_o$, $\theta_o'$, and $\bar{\theta}_o'$ for $\eta = 1$ to $\infty$.
2. Use current guesses of $\theta_o$, $\bar{\theta}_o$, $\theta_o'$, and $\bar{\theta}_o'$ to compute $F_o$, $F_o'$, $\bar{F}_o$, and $\bar{F}_o'$ over the interval.
3. Use results of step 2 and current tentative solution of momentum equations to compute $R_e$ and $\bar{R}_e$.
4. Using numerical integration by trapezoidal rule compute $\beta$, $\bar{\beta}$, $I$, and $\bar{I}$.

5. From the values of I and $\overline{I}$ at the end of the interval compute $\theta_o(0)$ and $\theta_o'(0)$.
6. Use results of step 4 and 5 to compute new profiles of $\theta_o(\eta)$, $\theta_o'(\eta)$, $\overline{\theta_o}(\eta)$, and $\overline{\theta_o'}(\eta)$ over the domain.
7. If iteration has not converged, go to step 2.

Hybrid Algorithm for Zero Order System

The hybrid algorithm uses the shooting method to solve the momentum equations and the integral method to solve the energy equations in succession, repeating the process until convergence of the entire coupled system is obtained. A Fortran program implementing this algorithm is listed in the appendix. The results of a computation can be saved on disk for later input as known coefficient functions in a program which solves the equations which arise in stability analysis of the flow.

The program is written in Microsoft Fortran for an IBM PC or compatible computer. The universality of Fortran however allows uploading to a mainframe computer with minor modifications in print and disk storage routines.

## RESULTS AND DISCUSSION

A central issue in this research is whether or not property variation within the flowfield has a significant effect on flow dynamics which might also affect the stability of the flow. If the $\rho\mu$ constant assumption is valid for flows with a large temperature gradient, then the momentum equation can be decoupled from the energy equation, and temperature variations within the flow would have negligible effects on the dynamics of the flow. This proposition would mean that a flow with combustion would be dynamically equivalent to some isothermal flow. Figure 12 shows the normalized density viscosity product versus normalized temperature for air at atmospheric pressure in the range 300K to 1200K. Assuming $\rho\mu$ constant approximates these curves as a constant one. From the degree of variation shown in figure 12, a property variation effect on the flow would appear to be expected. Such an effect would mean that a flow with combustion fed with a cold air stream is fundamentally different from any isothermal flow no matter how inlet velocities, etc. are adjusted to achieve Reynolds number similarity between the cold and combusting flows. The computer program developed here solves only the zero order system of equations for the flowfield variables. The solution does, however, give the leading term in the series expansion of these variables, and is sufficient to investigate the main effects of property variation in a steady flow.

The zero order system of equations was solved for a variety of flow conditions using the program listed in the appen-

dix. Runs for isothermal flow ($T_1/T_2 = 1$) with a symmetric wake ($U_1/U_2 = 1$) were made and compared with the results of Goldstein [12], which were re-computed to more significant figures and tabulated by Kovitz [13], verifying the programs capability to solve the momentum equations against a known solution.

Runs were subsequently made for temperature ratios, $T_1/T_2$, of 1, .5, and .25. For computational convenience these runs were made holding $f_0'(0)$ constant at 2. $f_0'(0)$ is proportional to the leading term of the shear stress along the centerline, and therefore, these runs represent flows with an approximately constant centerline shear stress. Results are shown plotted in figures 2-6. These plots show profiles for the leading term of the stream function, u velocity, u velocity gradient in $\eta$ direction, temperature, and temperature gradient over both the upper and lower streams. For clarity, the lower stream variables are plotted in terms of the upper stream independent variable $\eta=-\bar{\eta}$.

If property variation had negligible effect on flow dynamics, figures 2-4 would show no variation as the temperature ratio decreased. However, these figures do show significant changes in the steady flow of the hot stream as the temperature of the hot fluid is doubled (green lines) and then quadrupled (red lines) as compared to the free stream value of the upper stream. As the temperature of the lower stream increases, the velocity profiles become steeper, which means that the stress in the hot stream increases in magnitude. Since both streams are transporting momentum into the wake toward the

velocity minimum, there is a layer across which the stress reverses sign (figure 4). As temperature increases in the lower stream, this layer becomes thinner and the stress difference across it increases. Whether these differences would have a stabilizing or unstabilizing on the flow is not known.

Temperature profiles are shown in figure 5. These profiles show a smooth transition from the free-stream value of the upper stream to that of the lower stream as expected. They converge to one as $\eta \rightarrow (-\infty)$ because the temperatures are normalized by the free-stream value of the hot lower stream. Figure 6 shows temperature gradient profiles. These are always negative because the lower stream was chosen to be the hot stream, and so temperature decreases as $\eta$ increases. These plots also show that as the temperature difference across the streams increases, the profiles steepen, while the thickness of the thermal layer across which the change occurs remains the same. This behavior is due to the step nature of the inlet temperature profiles.

Numerous computer runs were also made for isothermal but asymmetric plate wake flows with varying velocity ratios. The purpose of these runs was to study the steady state effects of having streams of unequal velocities interact across the near plate wake. The results of 300 such runs were collected and are shown plotted in figures 7 to 10.

Figure 7 shows $f\delta'(0)$, which is proportional to the leading term of the shear stress, versus the velocity ratio. As expected, the shear increases as the velocity ratio increases.

The point of minimum u velocity at the rear edge of the plate must move from the centerline out to the free-stream of the slower stream as the two streams adjust to each other in the downstream of the wake. Because the lower stream was chosen as the slower stream, the point of minimum velocity therefore occurs in the lower stream. The position of this point in terms of (x,y) in the near wake region is actually governed by the need to match the Blasius profiles of the incoming streams which determined the definition of $\eta$:

$$\eta = y/(3x^{1/3})$$

The point of u velocity minimum is determined by:

$$f_0''(\eta_{min}) = 0$$

This point, in terms of the $\eta$ coordinate, is fixed for a given velocity ratio $U_1/U_2$, and represents the depth of penetration of the kinematic effects of the faster upper stream into the slower lower stream by transport of momentum through shear forces. From the equation relating $\eta$, x, and y:

$$y_{min} = 3\eta_{min} x^{1/3}$$

In terms (x,y) coordinates, $\eta_{min}$ gives the rate at which the point of zero shear moves into the hot stream as x is increased from zero at the trailing edge of the plate.

Figure 8 shows the relation between $\eta_{min}$ and velocity ratio. As velocity ratio increases, $\eta_{min}$ also increases, meaning that at fixed x, the point of zero shear moves deeper and deeper into the hot stream. This shift could have a significant effect on the stability of the flow, and might account for some of the stabilizing effect of the hot stream.

Figures 9 and 10 show the effect of velocity ratio on the leading term of u velocity at the point of velocity minimum and on the centerline. As the velocity of the lower stream relative to the upper stream decreases, the u velocity at the velocity minimum also decreases as expected. This effect is less apparent at the centerline where transfer of momentum from the upper stream maintains a higher velocity.

## CONCLUSION

Goldstein, Cheng, Kovitz, and Chiu's wake solutions were extended to the asymmetric mixing of two streams of different velocity with prescribed temperature and velocity ratio at the trailing edge of the plate. The predicted wake structure in the proximity of the trailing edge revealed momentum transport from faster to slower stream which shifts the point of minimum velocity from the center of the wake into the slower hot stream.

Remarkably, the flow configuration near the trailing edge has a slow speed region sandwiched between the upper and lower regions which both have velocities higher than the central slow speed region. As a result, flow in this region is expected to have a propensity to double sided vortex shedding. However, this dynamic configuration starts at the trailing edge and terminates at the point when the minimum velocity in the wake approaches the free stream velocity of the slower stream. This dynamic configuration is a unique characteristic of the trailing edge wake. This structure is distinctly different from a conventional shear layer without a minimum velocity point in the layer. This two sided mixing region structure is conjectured to have vortex shedding characteristics which are significantly different from a conventional single sided mixing layer. These and other aspects will be studied in Part II of the present research program.

Effects of coupling between energy and momentum due to property variation in the presence of steep temperature gradients were also found to be significant.

The problem formulation, based on the methods of the previous researchers, lead to a sequence of systems of ordinary differential equations which allowed such frugal use of computer resources that solution on an IBM PC with math co-processor chip is feasible. While solution of the stability problem in Part II of this research, which will use the program developed here as its base, may require uploading to a mainframe computer, the initial development of this program on a PC was much more efficient than working on a mainframe shared by a large user community.

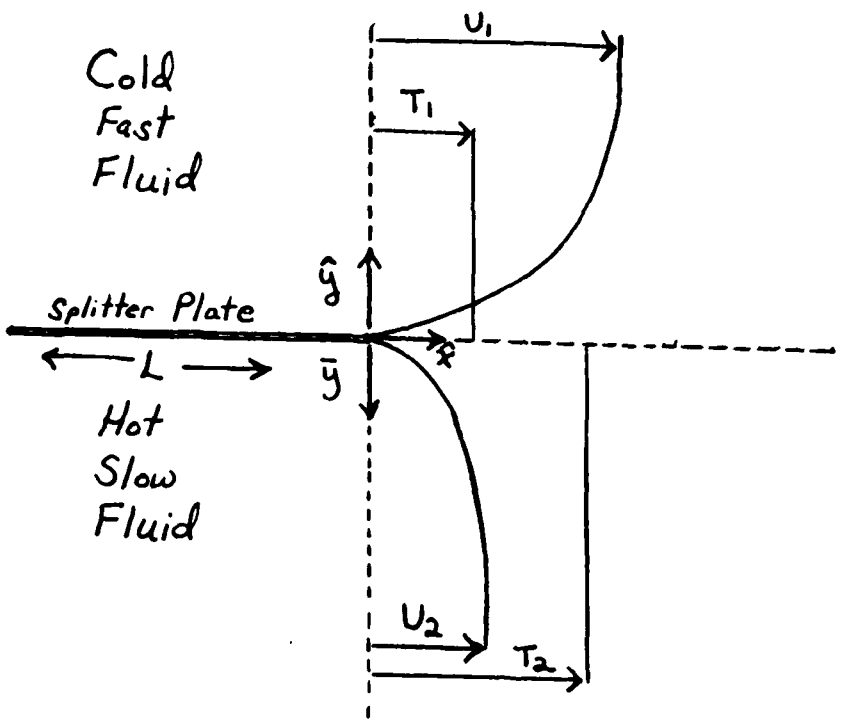



Fig. 1 - Inlet Velocity and Temperature Profiles

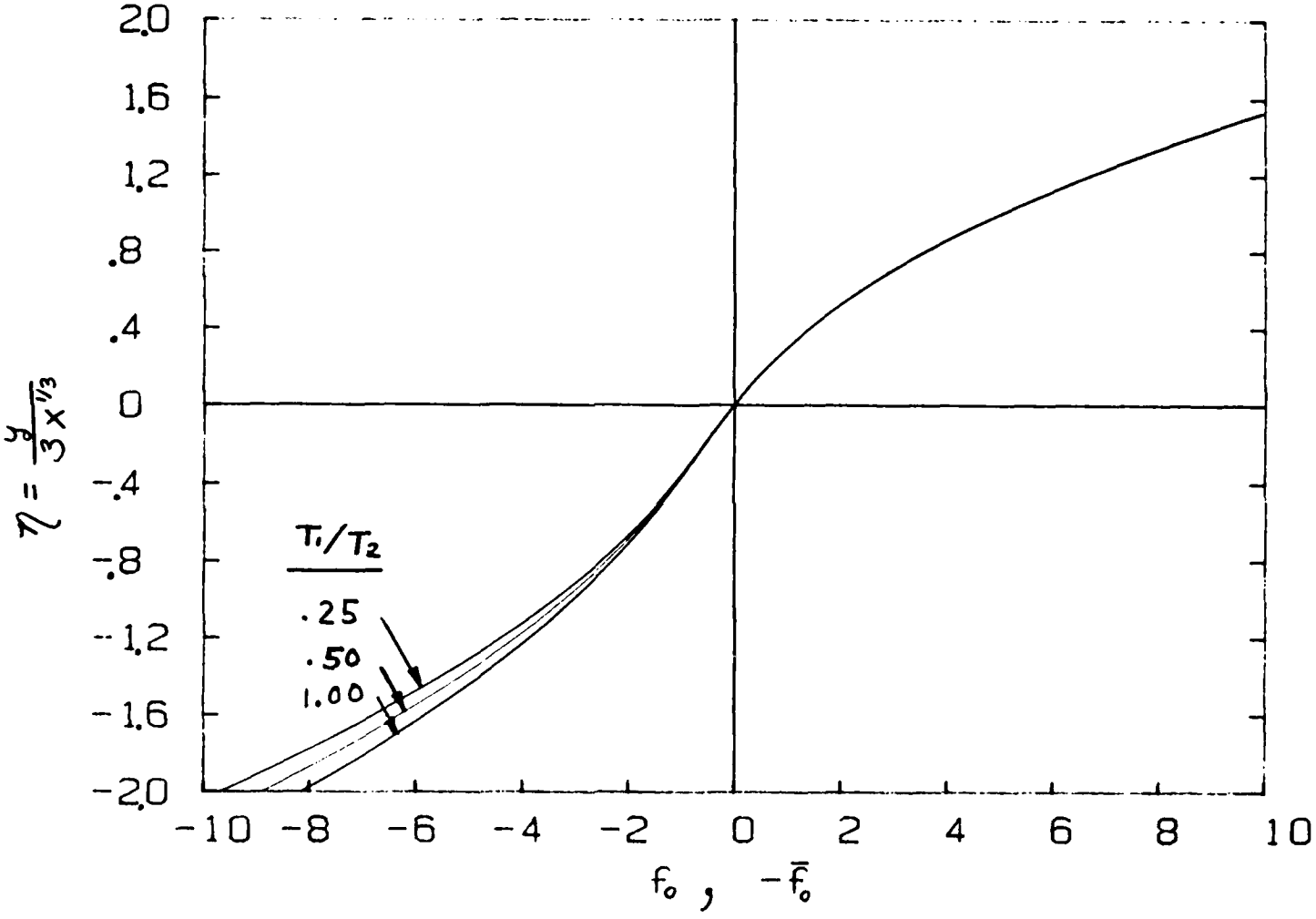



Fig. 2: Stream Function Profiles

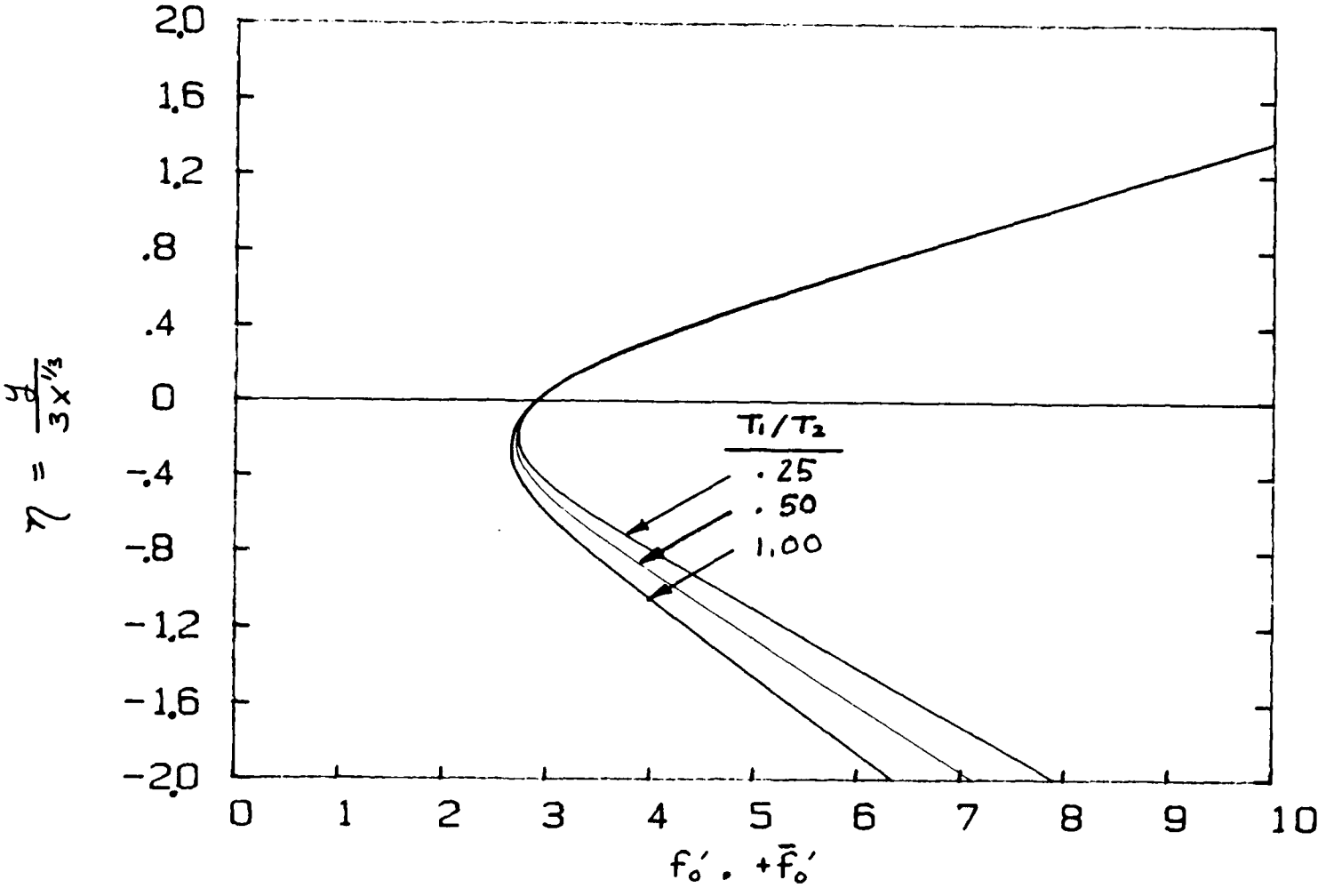



Fig. 3: Zero Order Velocity Profiles

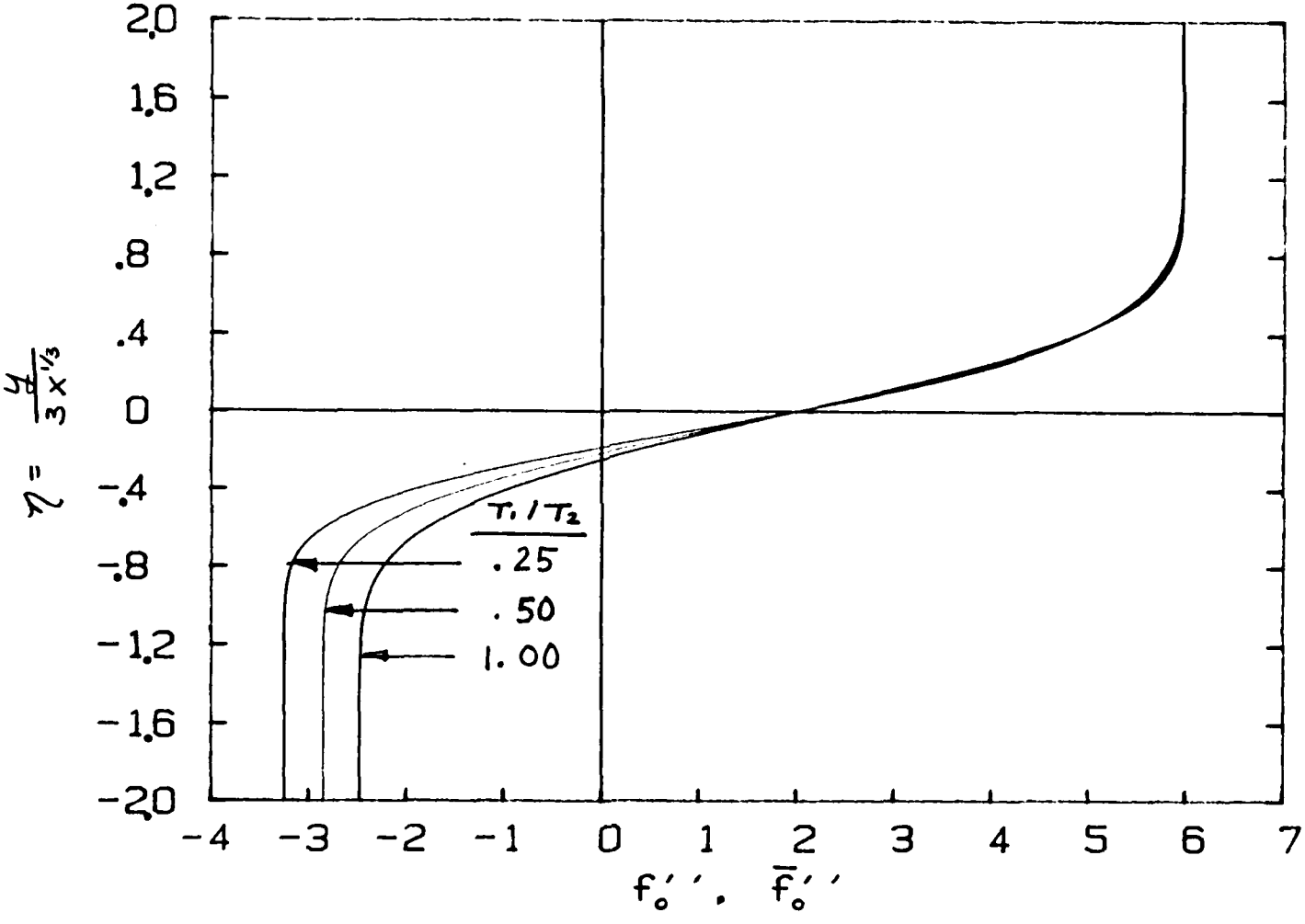



Fig. 4: Zero Order Vel. Grad. Profiles

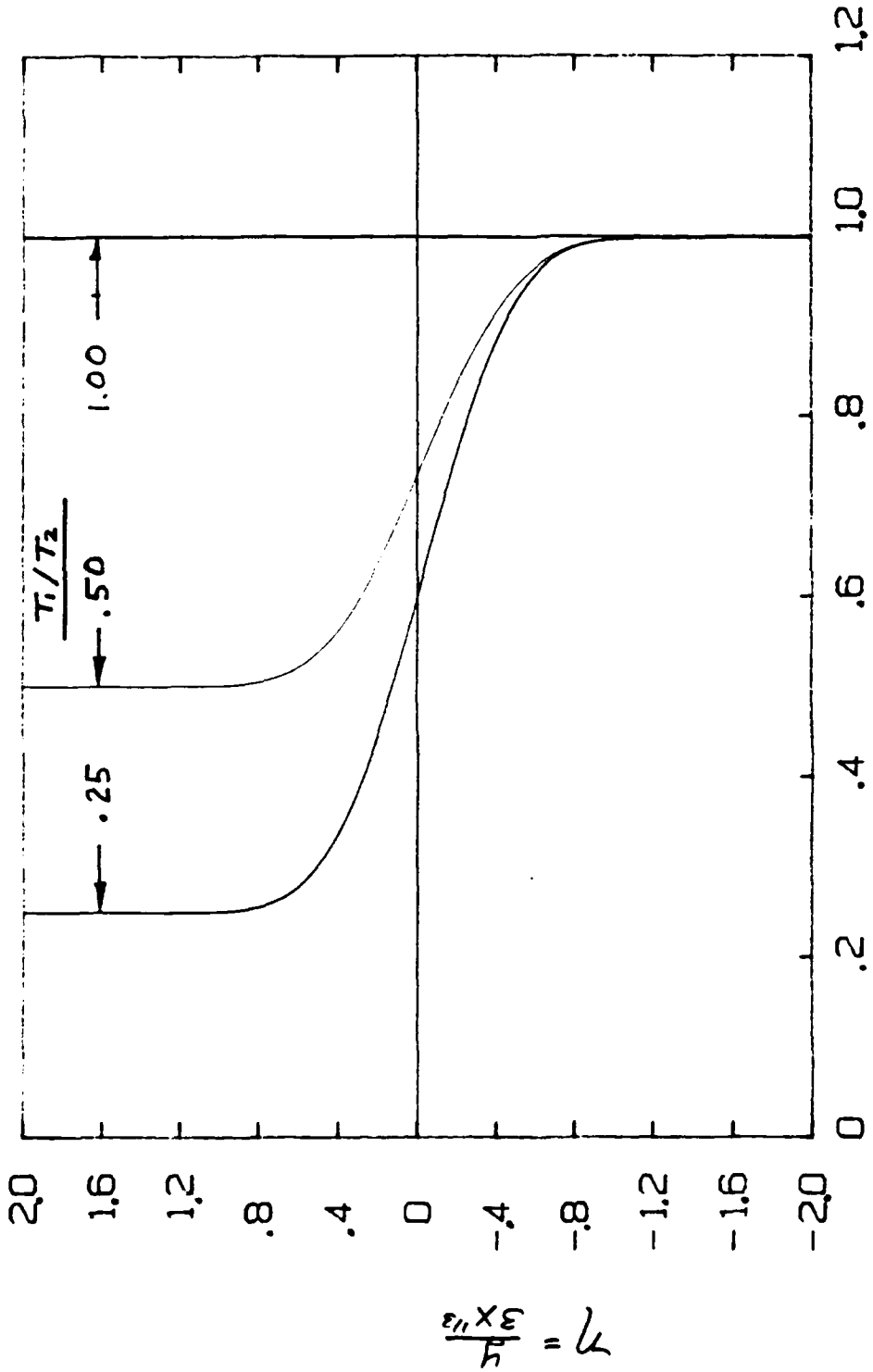



Fig. 5 : Temperature Profiles

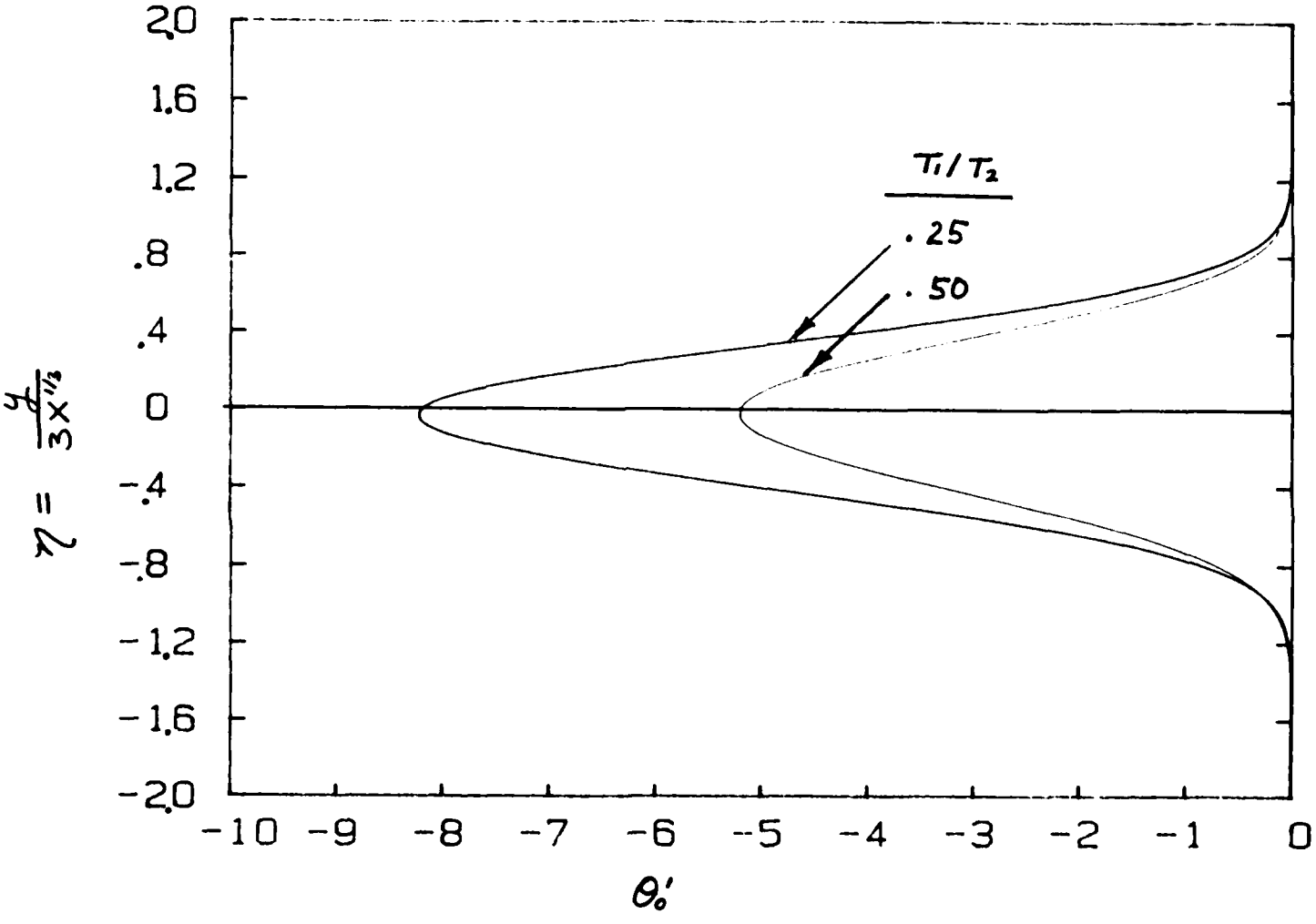



Fig. 6 : Temperature Gradient Profiles

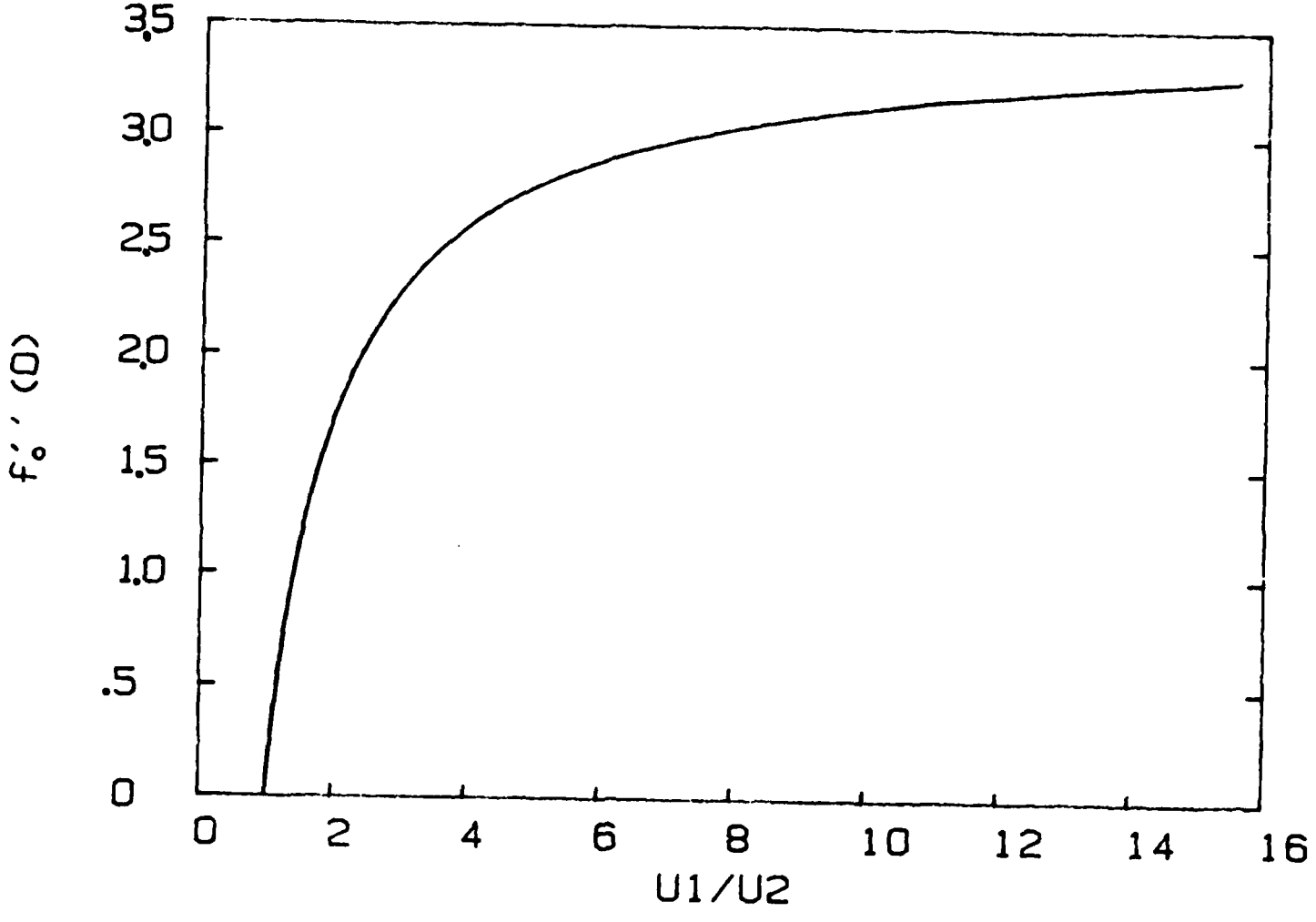



Fig. 7 : $f_0''(0)$ vs. Velocity Ratio

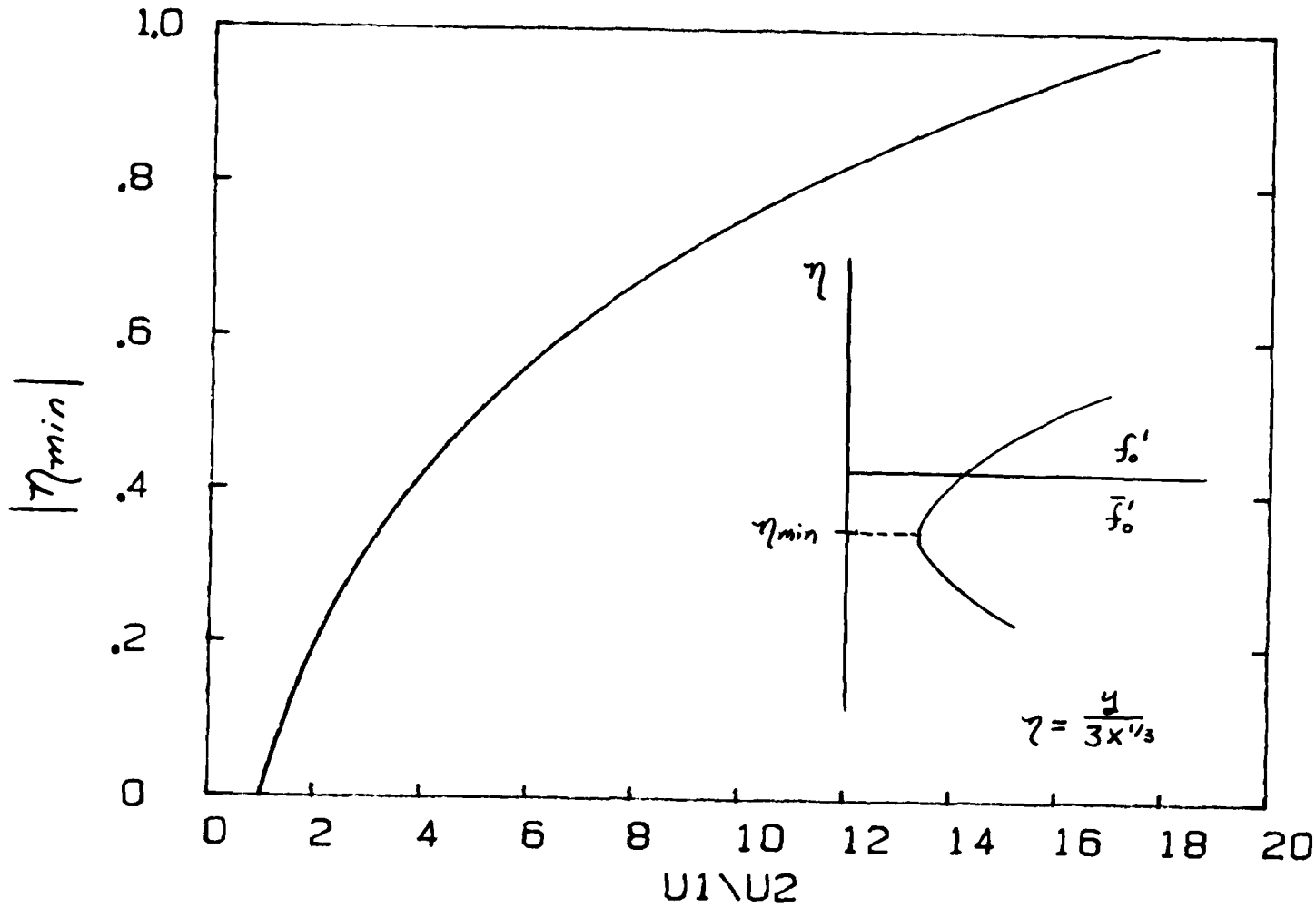



Fig. 8 : Velocity Ratio vs. $\eta_{min}$

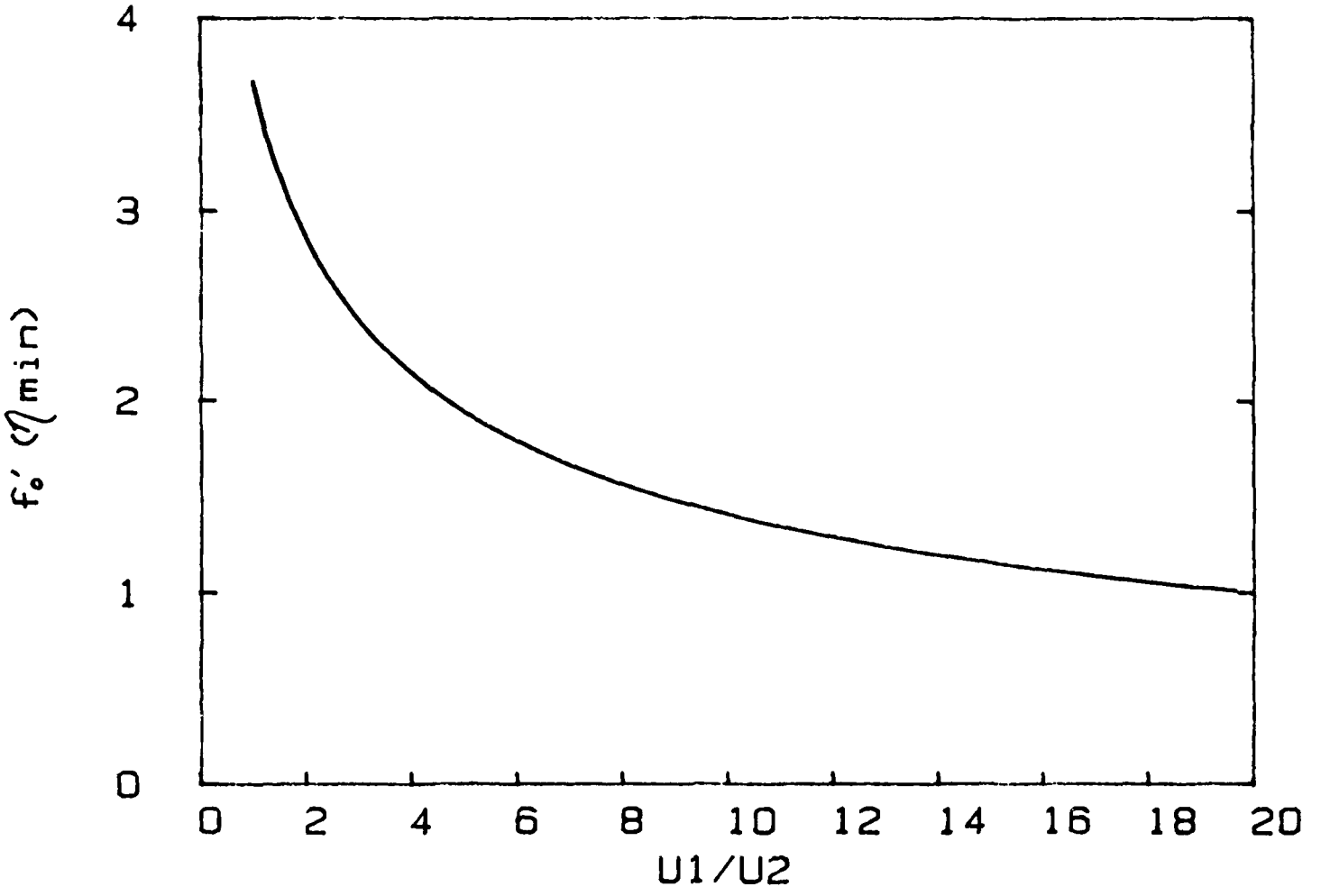



Fig. 9 : Min. $f_o'$ vs. Velocity Ratio

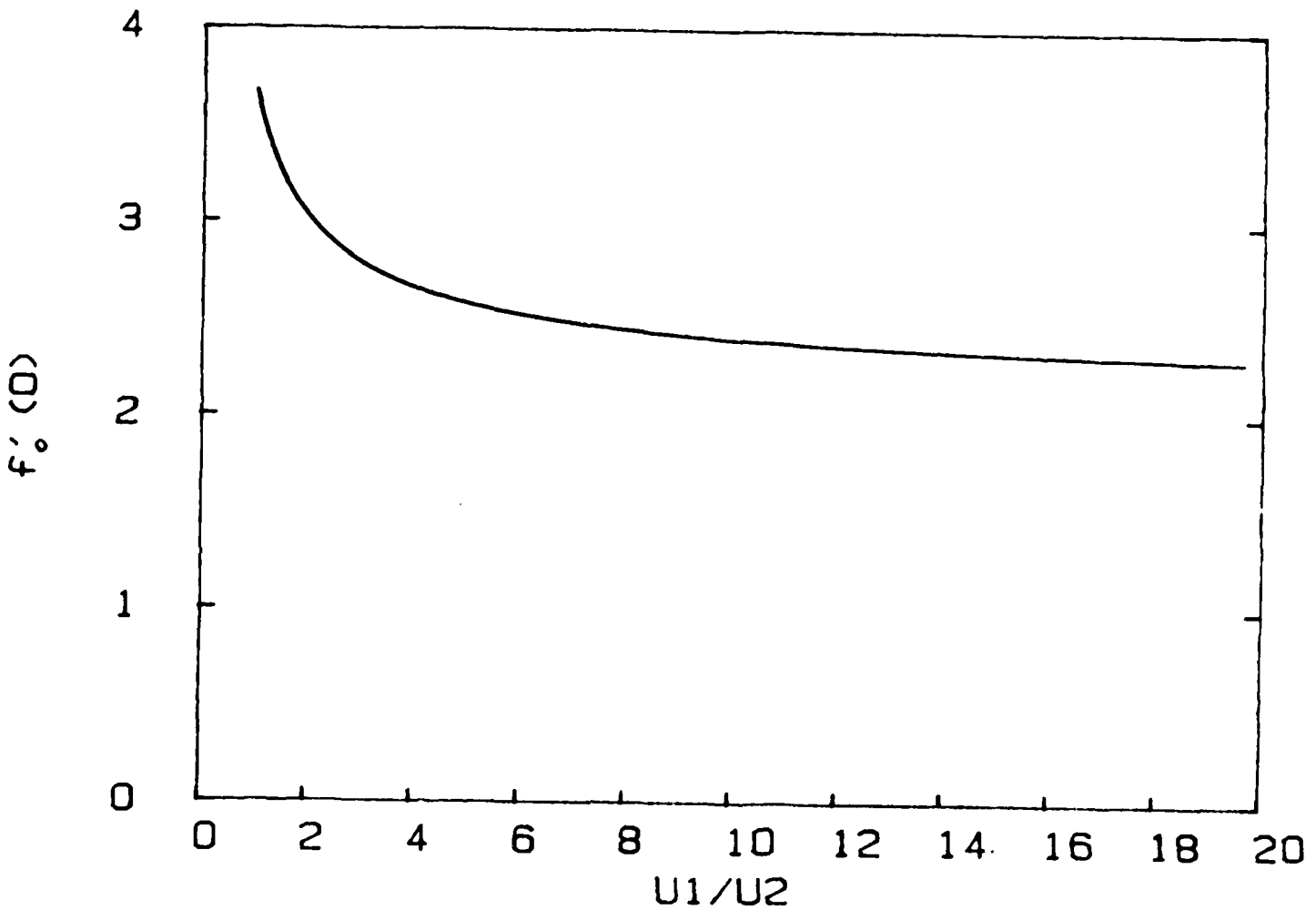



Fig. 10 : f′(0) vs. Velocity Ratio

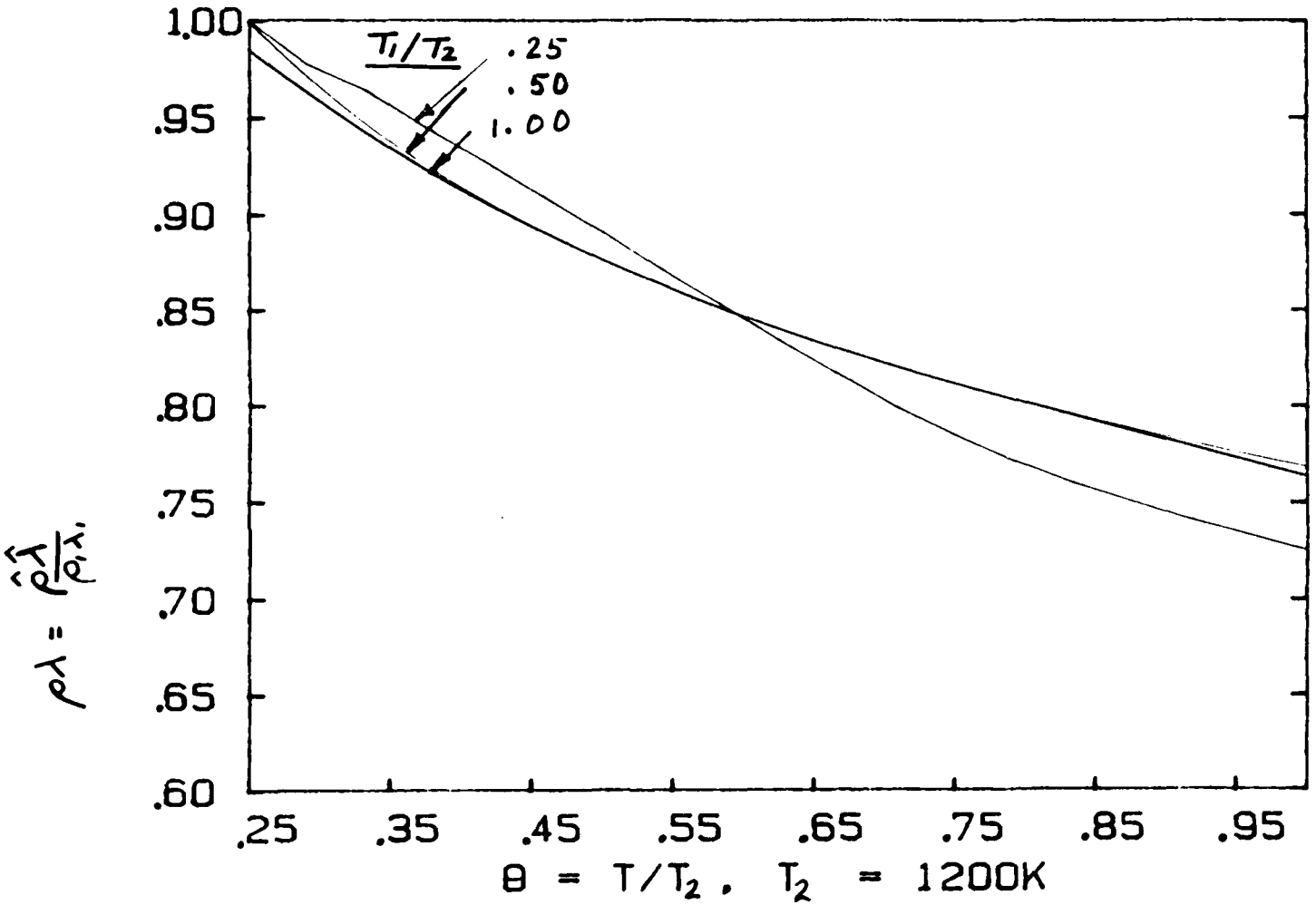



Fig. 11 : Density * Conductivity for Air

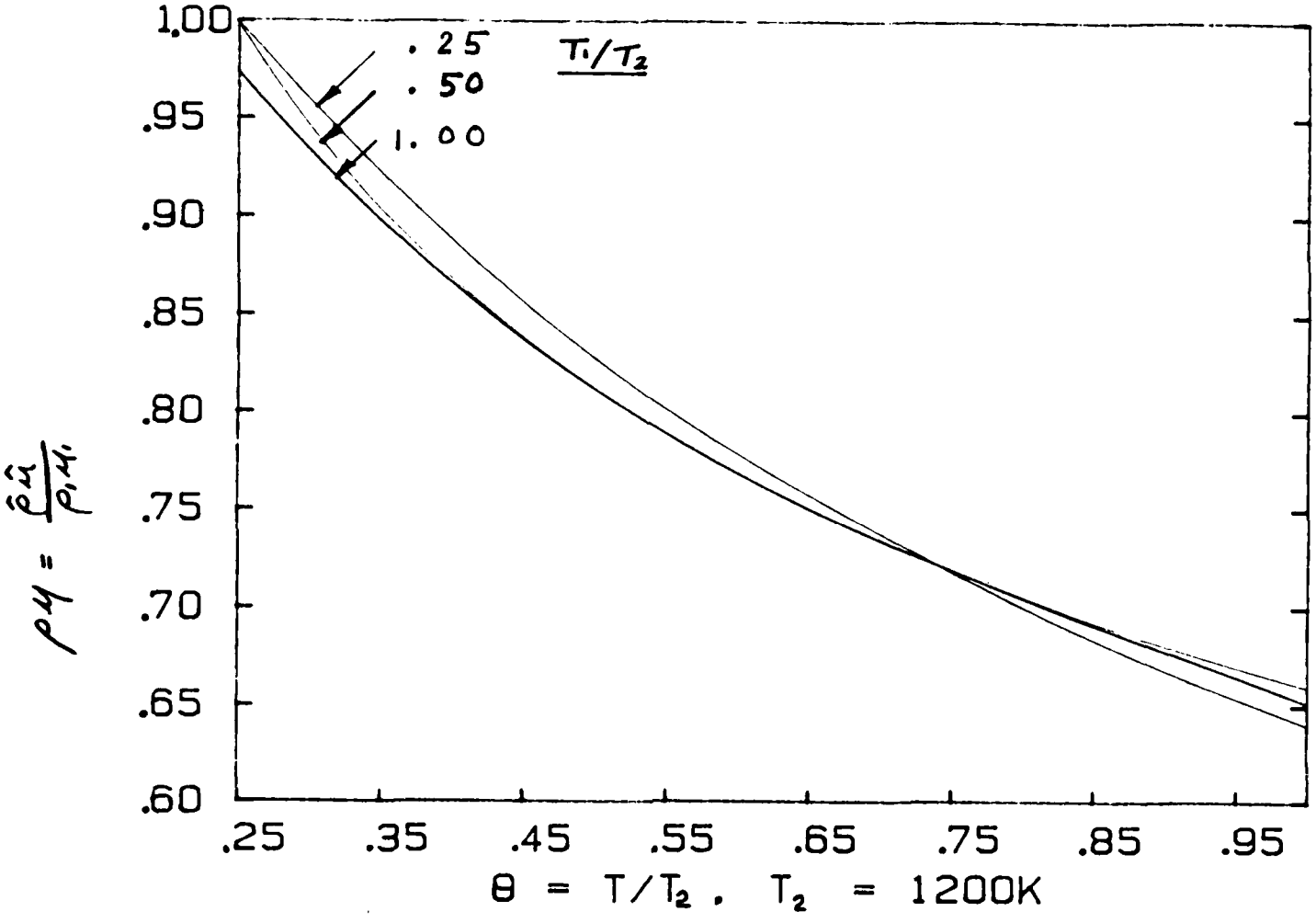



Fig. 12 : Density * Viscosity for Air

## REFERENCES


1. Fujii, S., and K. Eguchi, "A Comparison of Cold and Reacting Flows Around a Bluff-Body Flame Stabilizer," J. Fluids Eng., Vol. 103, p. 328, June 1981.

2. Masri, A.R., and R.W. Bilger, "Turbulent Diffusion Flames of Hydrocarbon Fuel Stabilized as a Bluff-Body," Presented at the 21st Combustion Symposium (International), Ann Arbor, Michigan, August 1984.

3. Williams, C.G., H.C. Hottel, and A.C. Scurlock, "Flame Stabilization and Propagation in High Velocity Gas Streams," Third Symposium on Combustion and Flame and Explosion Phenomena, 1949, p. 21.

4. Kaskan, W.E., and A.E. Noreen, "High Frequency Oscillations of a Flame Held by a Bluff-Body," Trans. Am. Soc. Mech. Engrs., August 1955, p. 885.

5. Roquemore, W.M., et. al., "Utilization of Laser Diagnostics to Evaluate Combustor Models," AGARD No. 353, Combustion Problems in Turbine Engines, Sept. 1981, Vol. 19, pp. 1151-1157.

6. Roquemore, W.M., et. al., "Influence of the Vortex Shedding Process of a Bluff-Body Diffusion Flame," AIAA-83-0335, January 1983.

7. Roquemore, W.M., and R.L. Britton, "Investigation of the Dynamic Behavior of a Bluff-Body Diffusion Flame Using Flame Emission," AIAA-82-0178, January 1982.

8. Roquemore, W.M., R.P. Bradley, J.S. Stutrud, C.M. Reeves, and L. Krishnamurthy, "Preliminary Evaluation of a Combustor for Use in Modeling and Diagnostics Development," ASME 80-GT-93.

9. Sturgess, G.J., and S.A. Syed, "Dynamic Behavior of Turbulent Flow in a Widely-Spaced Co-Axial Jet Diffusion Flame Combustor," AIAA-83-0575, January, 1983.

10. Roquemore, W.M., R.S. Tankin, H.H. Chiu, and S.A. Lottes, "The Role of Vortex Shedding in a Bluff-Body Combustor, paper presented at the ASME 105th Winter Annual Meeting, Symposium on Experimental Measurements and Techniques in Turbulent Reactive Flows.

11. Chiu, H.H., Dynamics of Vortex Shedding and Quasi-large Scale Structures in a Bluff-Body Combustor, Final Report 1984 USAF SCEEE Summer Faculty Research Program, October 1984.

12. Goldstein, S., "Concerning Some Solutions of the Boundary Layer Equations in Hydrodynamics," Proc. Cambridge Phil. Soc., Vol. 26, 1930, pp. 1-30.

13. Kovitz, A.A., "Ignition in the Laminar Wake of a Flat Plate," PhD Thesis, Princeton University, 1956.

14. Cheng, S.I., and H.H. Chiu, "Mixing and Chemical Reaction in an Initially Non-Uniform Temperature Field," Int. J. Heat Mass Transfer, Vol. 1, pp. 280-293.

15. Lin, C.C., Theory of Hydrodynamic Stability, Cambridge University Press, 1955.

16. Crane, L.J., "The Laminar and Turbulent Mixing of Jets of Compressible Fluid. Part II The Mixing of Two Semi-infinite Streams, J. Fluid Mech., 1957.

17. Minkowycz, W.J., and P. Cheng, "Free Convection About a Vertical Cylinder Embedded in a Porous Medium," Int. J. Heat Mass Transfer, Vol. 19, pp. 805-813, 1976.

```
C  Splitter Plate Wake
C  with Large Temperature Gradient
C  Solution of Zeroth Order Functions
C
C     Author: S.A. Lottes,                              Nov. 15, 1985
C
C     This routine solves the zero order system of differential
C     equations for a nonsymmetric plate wake using the shooting
C     method with a Runge-Kutta routine for the momentum equations
C     and the integral method for the energy equations.
C
C              E f''' + (2f+E')f'' - f' = 0
C
C              Ē f̄''' + (2f̄+Ē')f̄'' - f̄' = 0
C
C              F θ +(2f + F')θ' = 0
C
C              F̄ θ̄ +(2f̄ + F̄')θ̄' = 0
C
C     B.C.s:  f(0) = 0,     f''(∞) = 5.97708
C
C             f̄(0) = 0,     f̄''(∞) = 5.97708/(U1/U2)
C
C             f'(0)=f̄'(0), f''(0)= -f̄''(0)
C
C             θ(∞)=T1/T2,   θ̄(∞)=1
C
C             θ(0)=θ̄(0),    θ'(0)= -θ̄'(0)
C
C     Main Variable Assignments:
C
C         f  -  F0,   f̄  -  F0B,  f'  -  F0P,  f̄'  -  F0PB,
C
C         f''-  F0PP, f̄'' - F0PPB
C
C         θ  -  T0,   θ̄  -  T0B,  θ'  -  T0P,  θ̄'  -  T0PB,
C
C         E  -  EV,   Ē  -  EVB,  E'  -  EVP,  Ē'  -  EVPB,
C
C         F  -  ET,   F̄  -  ETB,  F'  -  ETP,  F̄'  -  ETPB,
C
C         T1/T2 - T1DT2
C         U1/U2 - U1DU2
C
C     Inputs: User is prompted for the inputs, which are entered as
C             integers or floating point numbers with decimal point
C             separated by commas.
C
C             1) f''(0)
C
C             2) Guess for f'(0).
C
C             3) Length of interval.
C
C             4) Step size and print step size.
C
```

```
C              5) Temperature ratio T1/T2
C
C      Outputs: The program prints function values
C               and slopes over the interval.
C
C               U1\U2
C-----------------------------------------------------------------------
C                                                                      |
C      Initialization and collection of inputs                         |
C______________________________________________________________________|
C
$NOFLOATCALLS
$LARGE
$DEBUG
       IMPLICIT REAL*8 (A-H,O-Z)
       CHARACTER*64 FNAME
       CHARACTER*18 UPPER,LOWER
       CHARACTER*10 NAME
C
       DIMENSION Y(3),F(3)
       COMMON/VECTF/F0(801),F0B(801),F0P(801),F0PB(801),
      1           F0PP(801),F0PPB(801),FB(801),FBB(802),X(801)
       COMMON/VECTT/T0(801),T0B(801),T0P(801),T0PB(801),
      1             TB(801),TBB(801)
       COMMON/EV/EV(1601),EVB(1601),EVP(1601),EVPB(1601)
       COMMON/ET/ET(801),ETB(801),ETP(801),ETPB(801)
       COMMON/PROP/AV0,AV1,AV2,AV3,AK0,AK1,AK2,AK3
       COMMON/PARM/DX,IXE,IXE2,IPB,ITMAX,RF,T1DT2,T00,XL,IFP,
      1            UPPER,LOWER,U1DU2,U1DU2B
       COMMON/PARMS/Y0,YPPL,YP00,YP01,YPP0
C      Read initial values, guesses, and parameters.
C
       WRITE(*,1)
1      FORMAT(10X,'Zero Order Plate Wake'//)
       WRITE(*,3)
3      FORMAT(1X,'Enter T1DT2: '\)
       READ(*,60)T1DT2
       WRITE(*,5)
5      FORMAT(10X,'Enter DDf(0): '\)
       READ(*,60)YPP0
       WRITE(*,7)
7      FORMAT(10X,'Enter guesses for Df(0): '\)
       READ(*,60)YP00,YP01
       WRITE(*,9)
9      FORMAT(10X,'Enter xl: '\)
       READ(*,60) XL
       WRITE(*,11)
11     FORMAT(/10X,'Enter no.of points and points/print: '\)
       READ(*,40) IXE,IPB
       WRITE(*,13)
13     FORMAT(10X,'For full print enter 1, abbreviated print enter 0:' \)
       READ(*,40)IFP
40     FORMAT(5I9)
60     FORMAT(4F14.9)
C
C      Set constants
```

```
C
      UPPER='Upper Half Plane'
      LOWER='Lower Half Plane'
      IXE2=2*IXE-1
      Y0=0.
      YPPL=5.97708
      ITMAX=1000
      DX=XL/(IXE-1)
      DO 52 I=1,IXE
52    X(I)=(I-1)*DX
C     RF = Relaxation factor used in temperature field computation
      RF=.3
C
C     Set Initial Guess for Temperature Dependent Coefficients
C
      DO 70 I=1,IXE
      ET(I)=1.
      ETP(I)=0.
      ETB(I)=1.
      ETPB(I)=0.
70    CONTINUE
      DO 72 I=1,IXE2
      EV(I)=1.
      EVP(I)=0.
      EVB(I)=1.
      EVPB(I)=0.
72    CONTINUE
C
C     Initial Guess of Centerline Temp Fn
C
      T00=(T1DT2+1)/2
C
C     Initialize Coefficients for Property Computation
C
C     Taylor Series for Nonealized Density*Viscosity
C
      TVP=T1DT2**.3
      TM=(T1DT2+1)/2
      BV0=TVP/TM**.3
      BV1=-.3*TVP/TM**1.3
      BV2=.195*TVP/TM**2.3
      BV3=-.897*TVP/TM**3.3/6
      AV0=BV0-TM*(BV1-TM*(BV2-TM*BV3))
      AV1=BV1-TM*(2*BV2-3*BV3*TM)
      AV2=BV2-3*BV3*TM
      AV3=BV3
C
C     Taylor Series for Density*Conductivity
C
      TKP=T1DT2**.19
      BK0=TKP/TM**.19
      BK1=-.19*TKP/TM**1.19
      BK2= .11305*TKP/TM**2.19
      BK3=-.0825265*TKP/TM**3.19
      AK0=BK0-TM*(BK1-TM*(BK2-TM*BK3))
      AK1=BK1-TM*(2*BK2-3*BK3*TM)
```

```
      AK2=BK2-3*BK3*TM
      AK3=BK3
C
      CALL VELOCITY
      CALL TEMP
C
      DO 80 I=1,IXE
      FS(I)=F0(I)
      FSB(I)=F0B(I)
      TS(I)=T0(I)
      TSB(I)=T0B(I)
80    CONTINUE
      U1DU2S=U1DU2
C-----------------------------------------------------------------
C
C     Main Iteration Loop
C
C     The program alternately computes the velocity and temperature
C     fields beginning with the velocity field. The velocity and
C     temperature fields are computed iteratatively in subroutines.
C
C     Because f''(0) is specified for convenience in the computation,
C     the velocity ratio U1DU2 is computed from the results.
C
C     Overall convergence is checked by verifying that the maximum
C     stream function change and change in U1DU2 is below a preset
C     tolerance level after an interveening temperature computation,
C     and that the maximum change in temperature is below a preset
C     tolerance after an interveening velocity computation.
C-----------------------------------------------------------------
      DO 200 IT=1,ITMAX

      CALL VELOCITY
      CALL TEMP

      CHGMX=DABS(U1DU2-U1DU2S)/U1DU2
      DO 110 I=2,IXE
      D1=DABS(F0(I)-FS(I))/F0(I)
      D2=DABS(T0(I)-TS(I))/T0(I)
      D3=DABS(F0B(I)-FSB(I))/F0B(I)
      D4=DABS(T0B(I)-TSB(I))/T0B(I)
      CHGMX=DMAX1(D1,D2,D3,D4,CHGMX)
      FS(I)=F0(I)
      TS(I)=T0(I)
      FSB(I)=F0B(I)
      TSB(I)=T0B(I)
110   CONTINUE
      U1DU2S=U1DU2
      WRITE(*,120)CHGMX
120   FORMAT(/10X,' *************  CHGMX=',G16.4,' **************'/)
      IF(CHGMX.LE.1D-7)GO TO 300
200   CONTINUE
C-----------------------------------------------------------------
C
C     Check and print results
C-----------------------------------------------------------------
```

```
C
300   CALL VPRINT(F0,1,IXE,'F0         ')
      CALL VPRINT(F0B,1,IXE,'F0B        ')
      CALL VPRINT(F0P,1,IXE,'F0P        ')
      CALL VPRINT(F0PB,1,IXE,'F0PB       ')
      CALL VPRINT(F0PP,1,IXE,'F0PP       ')
      CALL VPRINT(F0PPB,1,IXE,'F0PPB      ')
      CALL VPRINT(T0,1,IXE,'T0         ')
      CALL VPRINT(T0B,1,IXE,'T0B        ')
      CALL VPRINT(T0P,1,IXE,'T0P        ')
      CALL VPRINT(T0PB,1,IXE,'T0PB       ')
      WRITE(*,305)U1DU2
305   FORMAT(/1X,'--------- U1DU2 = ',816.8,' ----------'/)
C-----------------------------------------------------------------
C
C     Write Results on Disk
C-----------------------------------------------------------------
C
2999  WRITE(*,3000)
3000  FORMAT(1X,'Enter 1 to save results on disk: '\)
      READ(*,3001)ISAVE
3001  FORMAT(I5)
      IF(ISAVE.NE.0)THEN
                    FNAME='D:N.0'
                    CALL WDISK(X,FNAME,IXE)
                    FNAME='D:F0.X'
                    CALL WDISK(F0,FNAME,IXE)
                    FNAME='D:F0P.X'
                    CALL WDISK(F0P,FNAME,IXE)
                    FNAME='D:F0PP.X'
                    CALL WDISK(F0PP,FNAME,IXE)
                    FNAME='D:F0B.X'
                    CALL WDISK(F0B,FNAME,IXE)
                    FNAME='D:F0PB.X'
                    CALL WDISK(F0PB,FNAME,IXE)
                    FNAME='D:F0PPB.X'
                    CALL WDISK(F0PPB,FNAME,IXE)
                    FNAME='D:T0.X'
                    CALL WDISK(T0,FNAME,IXE)
                    FNAME='D:T0B.X'
                    CALL WDISK(T0B,FNAME,IXE)
                    FNAME='D:T0P.X'
                    CALL WDISK(T0P,FNAME,IXE)
                    FNAME='D:T0PB.X'
                    CALL WDISK(T0PB,FNAME,IXE)
            ENDIF
      STOP
      END
C-----------------------------------------------------------------
C
C     Velocity Distribution Computation
C-----------------------------------------------------------------
C
      SUBROUTINE VELOCITY

      IMPLICIT REAL*8 (A-H,O-Z)
```

```
      CHARACTER*64 FNAME
      CHARACTER*18 UPPER,LOWER
      CHARACTER*10 NAME
      DIMENSION Y(3),F(3)
      COMMON/VECTF/F0(801),F0B(801),F0P(801),F0PB(801),
     1          F0PP(801),F0PPB(801),FB(801),FBB(802),X(801)
      COMMON/EV/EV(1601),EVB(1601),EVP(1601),EVPB(1601)
      COMMON/PROP/AV0,AV1,AV2,AV3,AK0,AK1,AK2,AK3
      COMMON/PARM/DX,IXE,IXE2,IPS,ITMAX,RF,T1DT2,T00,XL,IFP,
     1            UPPER,LOWER,U1DU2,U1DU2S
      COMMON/PARM8/Y0,YPPL,YP00,YP01,YPP0
C
      JX=1
      Y(1)=YPP0
      Y(2)=YP00
      Y(3)=Y0
      CALL RUNGE0(Y,JX,IXE,DX,X,F0,F0P,F0PP,EV,EVP,0)
      YPPL0=Y(1)
      WRITE(*,81)
81    FORMAT(/1X,'Velocity Computation Iteration'/)
      I=0
      WRITE(*,90)I,YP00,YPPL0
90    FORMAT(1X,I4,' FP0=',G18.12,' FPPL=',G18.12)
C
      DO 300 I=1,ITMAX
      JX=1
      Y(1)=YPP0
      Y(2)=YP01
      Y(3)=Y0
      CALL RUNGE0(Y,JX,IXE,DX,X,F0,F0P,F0PP,EV,EVP,0)
      YPPL1=Y(1)
      A=(YPPL1-YPPL0)/(YP01-YP00)
      YPPL0=YPPL1
      YP00=YP01
      YP01=YP00-(YPPL1-YPPL)/A
      ERR=DABS((YPPL-YPPL1)/YPPL)
      WRITE(*,100)I,YP00,YPPL0,ERR
100   FORMAT(1X,I4,' FP0=',G18.12,' FPPL=',G18.12,' ERR=',G12.4)
      IF(ERR.LT.1D-8)GO TO 1000
300   CONTINUE
1000  F0(1)=Y0
      F0P(1)=YP01
      F0PP(1)=YPP0
      JX=1
      Y(1)=YPP0
      Y(2)=YP01
      Y(3)=Y0
      CALL RUNGE0(Y,JX,IXE,DX,X,F0,F0P,F0PP,EV,EVP,1)
      IF(IFP.EQ.1)CALL PRINT(X,F0,F0P,F0PP,IXE,IPS,UPPER)
C
      F0B(1)=Y0
      F0PB(1)=YP01
      F0PPB(1)= -YPP0
      JX=1
      Y(1)= -YPP0
      Y(2)=YP01
```

```
      Y(3)=YO
      CALL RUNGEO(Y,JX,IXE,DX,X,FOB,FOPB,FOPPB,EVB,EVPB,1)
      IF(IFP.EQ.1)CALL PRINT(X,FOB,FOPB,FOPPB,IXE,IPS,LOWER)
      YPPLB=Y(1)
      U1DU2=YPPL/YPPLB
      WRITE(*,1300)U1DU2
1300  FORMAT(/1X,'U1DU2= ',E16.8/)
      RETURN
      END
C-------------------------------------------------------------
C                                                             |
C     Temperature Distribution Computation                    |
C-------------------------------------------------------------|
C
      SUBROUTINE TEMP

      IMPLICIT REAL*8 (A-H,O-Z)
      CHARACTER*64 FNAME
      CHARACTER*16 UPPER,LOWER
      CHARACTER*10 NAME

      DIMENSION A(801),AB(801)
      DIMENSION RT(801),RTB(801)
      DIMENSION SESRT(801),SESRTB(801)
      DIMENSION SRT(801),SRTB(801)

      COMMON/VECTT/TO(801),TOB(801),TOP(801),TOPB(801),
     1             TS(801),TSB(801)
      COMMON/VECTF/FO(801),FOB(801),FOP(801),FOPB(801),
     1          FOPP(801),FOPPB(801),FS(801),FSB(802),X(801)
      COMMON/PARM/DX,IXE,IXE2,IPS,ITMAX,RF,T1DT2,TOO,XL,IFP,
     1            UPPER,LOWER,U1DU2,U1DU2S
      COMMON/EV/EV(1601),EVB(1601),EVP(1601),EVPB(1601)
      COMMON/ET/ET(801),ETB(801),ETP(801),ETPB(801)
      COMMON/PROP/AV0,AV1,AV2,AV3,AK0,AK1,AK2,AK3
      WRITE(*,401)
401   FORMAT(/1X,'Temperature Field Computation Iteration'/)
C
      DO 500 ITERT=1,ITMAX
      DO 420 I=1,IXE
      RT(I)=(2*FO(I)+ETP(I))/ET(I)
      RTB(I)=(2*FOB(I)+ETPB(I))/ETB(I)
420   CONTINUE
C
      IF(IFP.EQ.1)THEN
         CALL VPRINT(RT,1,IXE,'RT        ')
         CALL VPRINT(RTB,1,IXE,'RTB       ')
      ENDIF
C
      CALL TRPINT(RT,SRT,IXE,1)
      CAL' TRPINT(RTB,SRTB,IXE,1)
C
C
C     Compute SRT = ∫(0 to XE) RT dX , SRTB = ∫(0 to XE) RTB dX
C
C
```

```
      DO 450 I=1,IXE
      A(I)=DEXP(-SRT(I))
      AB(I)=DEXP(-SRTB(I))
450   CONTINUE
      CALL TRPINT(A,SESRT,IXE,1)
      CALL TRPINT(AB,SESRTB,IXE,1)
C
C     Compute new centerline temperature.
C
      TOONEW=(SESRT(IXE)+T1DT2*SESRTB(IXE))/(SESRT(IXE)+SESRTB(IXE))
      RDT00=DABS((TOONEW-T00)/T00)
      T00=T00 + RF*(TOONEW-T00)
      TOP0=(T1DT2-1)/(SESRT(IXE)+SESRTB(IXE))
C
C     Compute new temperature and temperature gradient profiles.
C
      DO 470 I=1,IXE
      T0(I)=TOP0*SESRT(I)+T00
      TOB(I)=-TOP0*SESRTB(I)+T00
      TOP(I)=TOP0*A(I)
      TOPB(I)=-TOP0*AB(I)
470   CONTINUE
C
      IF(IFP.EQ.1)THEN
                  CALL VPRINT(T0,1,IXE,'T0 NEW     ')
                  CALL VPRINT(TOB,1,IXE,'TOB NEW    ')
                  CALL VPRINT(TOP,1,IXE,'TOP NEW    ')
                  CALL VPRINT(TOPB,1,IXE,'TOPB NEW   ')
      ENDIF
C
C     Recompute property dependent part of coefficient RT.
C
      DO 472 I=1,IXE
      ET(I)=AK0+T0(I)*(AK1+T0(I)*(AK2+T0(I)*AK3))
      ETB(I)=AK0+TOB(I)*(AK1+TOB(I)*(AK2+TOB(I)*AK3))
      ETP(I)=TOP(I)*(AK1+T0(I)*(2*AK2+T0(I)*3*AK3))
      ETPB(I)=TOPB(I)*(AK1+TOB(I)*(2*AK2+TOB(I)*3*AK3))
472   CONTINUE
C
      IF(IFP.EQ.1)THEN
                  CALL VPRINT(ET,1,IXE,'ET NEW     ')
                  CALL VPRINT(ETB,1,IXE,'ETB NEW    ')
                  CALL VPRINT(ETP,1,IXE,'ETP NEW    ')
                  CALL VPRINT(ETPB,1,IXE,'ETPB NEW   ')
      ENDIF
C
      WRITE(*,480)ITERT,TOONEW,RDT00
480   FORMAT(5X,I4,' TOONEW=',E18.9,' RDT00=',E12.3)
      IF(RDT00.LE.1D-8)GO TO 600
500   CONTINUE
C
C     Get ready to return to momentum iteration
C
C     Recompute property dependent part of coefficients
C     for momentum equations
C
```

```
600   DO 610 I=1,IXE
      J=2*I-1
      EV(J)=AV0+T0(I)*(AV1+T0(I)*(AV2+T0(I)*AV3))
      EVB(J)=AV0+TOB(I)*(AV1+TOB(I)*(AV2+TOB(I)*AV3))
      EVP(J)=TOP(I)*(AV1+T0(I)*(2*AV2+T0(I)*3*AV3))
      EVPB(J)=TOPB(I)*(AV1+TOB(I)*(2*AV2+TOB(I)*3*AV3))
610   CONTINUE
      DO 620 I=2,IXE2-1,2
      EV(I)=(EV(I-1)+EV(I+1))/2
      EVB(I)=(EVB(I-1)+EVB(I+1))/2
      EVP(I)=(EVP(I-1)+EVP(I+1))/2
      EVPB(I)=(EVPB(I-1)+EVPB(I+1))/2
620   CONTINUE
C
      IF(IFP.EQ.1)THEN
                  CALL VPRINT(EV,1,IXE,'EV NEW     ')
                  CALL VPRINT(EVB,1,IXE,'EVB NEW    ')
                  CALL VPRINT(EVP,1,IXE,'EVP NEW    ')
                  CALL VPRINT(EVPB,1,IXE,'EVPB NEW  ')
      ENDIF
C
      RETURN
      END
C
C-----------------------------------------------------------------
C
C     Runge Kutta Routine to Compute f0, f0b and derivatives
C-----------------------------------------------------------------
C
      SUBROUTINE RUNGE0(Y,JX,IXE,DX,X,Y0,Y0P,Y0PP,EV,EVP,IS)
      IMPLICIT REAL*8 (A-H,O-Z)
      DIMENSION Y(6),F(6),X(801),Y0(801),Y0P(801),Y0PP(801)
      DIMENSION EV(1601),EVP(1601)
      N=3
      DO 30 I=2,IXE
         DO 10 M=1,4
            CALL RUNGE(N,Y,F,JX,DX,M)
            F(1)=(-(2*Y(3)+EVP(JX))*Y(1)+Y(2)*Y(2))/EV(JX)
            F(2)=Y(1)
            F(3)=Y(2)
10       CONTINUE
         CALL RUNGE(N,Y,F,JX,DX,5)
         IF(IS.EQ.1)THEN
            Y0(I)=Y(3)
            Y0P(I)=Y(2)
            Y0PP(I)=Y(1)
         ENDIF
30    CONTINUE
      RETURN
      END
C-----------------------------------------------------------------
C
C     Runge Kutta Half Step Routine
C-----------------------------------------------------------------
C
      SUBROUTINE RUNGE(N,Y,F,JX,DX,M)
```

```
      IMPLICIT REAL*8 (A-H,O-Z)
      DIMENSION Y(3),F(3),Q(3)
      GO TO (1,4,5,3,7),M
1     DO 2 I=1,N
2        Q(I) = 0.
      A = .5
      RETURN
3     A = 1.7071067811865475244
4     JX = JX + 1
5     DO 6 I=1,N
         Y(I) = Y(I) + A*(F(I)*DX - Q(I))
6        Q(I) = 2.*A*DX*F(I) + (1.-3.*A)*Q(I)
      A = .2928932188134524756
      RETURN
7     DO 8 I = 1,N
8        Y(I) = Y(I) + DX*F(I)/6. - Q(I)/3.
      RETURN
      END
C-----------------------------------------------------------------
C
C     Subroutine for local integral of a function
C     using the trapazoidal rule.
C-----------------------------------------------------------------
C
C     F -  Vector containing input function
C     SF - Vector containing output local integral
C          SF(I)= integral from LLIM to IX.
C     NP - Number of points, including end points in
C          the interval for integration.
C     DX - Step size: X distance between points.
C     LLIM - F index for lower limit for integration
C
      SUBROUTINE TRPINT(F,SF,NP,LLIM)
C
      IMPLICIT REAL*8 (A-H,O-Z)
      CHARACTER*18 UPPER,LOWER
      COMMON/PARM/DX,IXE,IXE2,IPS,ITMAX,RF,TIDT2,TOO,XL,IFP,
     1            UPPER,LOWER,U1DU2,U1DU2S
      DIMENSION F(801),SF(801)
      SF(LLIM)=0.
      DO 100 I=LLIM+1,LLIM+NP-1
100      SF(I)=SF(I-1) + DX* (F(I-1) + F(I))/2.
      RETURN
      END
C-----------------------------------------------------------------
C
C     Save a Vector on Disk
C-----------------------------------------------------------------
C
      SUBROUTINE WDISK(V,FILE,IMAX)
      IMPLICIT REAL*8 (A-H,O-Z)
      CHARACTER*64 FILE
      DIMENSION V(801)
      OPEN (6,FILE=FILE,STATUS='NEW',ACCESS='SEQUENTIAL')
      WRITE(6,10)(V(I),I=1,IMAX)
10    FORMAT(1X,F18.12)
```

```
      CLOSE(6)
      RETURN
      END
C-----------------------------------------------------------------
C
C     Subroutine to do table output to printer
C
C-----------------------------------------------------------------
C
      SUBROUTINE PRINT(X,G,GP,GPP,IXE,IPS,REGION)
      IMPLICIT REAL*8 (A-H,O-Z)
      DIMENSION X(801),G(801),GP(801),GPP(801)
      CHARACTER*18 REGION
      WRITE(*,1)
1     FORMAT(1X,/26X,'Table of Function Values')
      WRITE(*,3)REGION
3     FORMAT(28X,A18,
     1//6X,'x',20x,'DDf',17X,'Df',15X,'f'/)
      WRITE(*,1200)(X(I),GPP(I),GP(I),G(I),I=1,IXE-1,IPS)
      WRITE(*,1200)X(IXE),GPP(IXE),GP(IXE),G(IXE)
      RETURN
1200  FORMAT(1X,G15.7,2X,G19.12,2X,G19.12,2X,G19.12)
      END
C-----------------------------------------------------------------
C
C     Subroutine to do vector output to printer
C
C-----------------------------------------------------------------
C
      SUBROUTINE VPRINT(V,IO,LP,NAME)
      IMPLICIT REAL*8 (A-H,O-Z)
      CHARACTER*18 UPPER,LOWER
      COMMON/PARM/DX,IXE,IXE2,IPS,ITMAX,RF,T1DT2,T00,XL,IFP,
     1            UPPER,LOWER,U1DU2,U1DU2S
      DIMENSION V(801)
      CHARACTER*10 NAME
      WRITE(*,5)NAME
5     FORMAT(/5X,'VARIABLE: ',A12/)
      IX=IO
      IF(IX.GT.IXE)RETURN
      WRITE(*,90)(I,DX*(I-1),NAME,V(I),I=IX,LP-1,IPS)
      IF(LP.EQ.IXE)GO TO 60
50    WRITE(*,90)LP,DX*(LP-1),NAME,V(LP)
      RETURN
60    WRITE(*,98)IXE,DX*(IXE-1),NAME,V(IXE)
      RETURN
90    FORMAT(4X,'I= ',I3,6X,'X= ',G12.4,6X,A10,'=',1X,G22.14)
98    FORMAT(4X,'IE ',I3,6X,'E= ',G12.4,6X,A10,'=',1X,G22.14)
      END
```

# Flow Physics Through a Pierced Membrane

Final Report

to

Southeastern Center for Electrical Engineering Education

by

L.C. Chow (Principal Investigator)

D.E. Tilton (Graduate Student)

Washington State University
Pullman, WA 99164-2920

December 31, 1985

AF Contract F49620-82-C-0035
Subcontract 84 RIP 31

ABSTRACT:

The objective of this research was to further investigate the feasibility of a flexible radiator for rejecting large quantities of waste heat in space. An experiment designed to assess the potential damages caused by micrometeroids was carried out. This involved piercing different membrane materials with various needles and computing corresponding mass loss rates for two cases. In one case a layer of condensate covered the membrane. In the other case, the test section was filled with superheated steam only. From the data obtained it is concluded that mass loss for the condensate case is high, but not critical. It is believed that gravity may account for a large percentage of this high mass loss rate. For the superheated steam case, mass loss is very low and would not significantly effect radiator performance. Considering the radiator's intended operation, total mass loss rates would probably not be significant. Therefore the flexible radiator concept is sound and should be further developed.

INTRODUCTION:

Advancing space technology, especially defense applications indicates a need to develop new space radiators capable of rejecting large quantities of waste heat. One suggested radiator for this purpose is to be constructed in the shape of a large cylinder, from a lightweight flexible material.[1] Hot components will be sprayed with water. This water would flash vaporize and fill the cylinder causing it to extend into space. As the vapor cooled it would condense on the cylinder wall where it could be pumped out of the radiator. A constant retraction force would be applied to pull the radiator back inside the spacecraft as the volume decreased due to condensation. This force would also be used to keep the two phase mixture inside at constant saturation pressure and temperature.

Unlike radiators with rigid structures this radiator is only exposed to the harmful space environment when it is in operation. Even though this is a relatively short period of time, the radiators susceptibility to damage from micrometeoriods must be evaluated. These particles travel through space at approximately 20 km/s. Since the radiator is lightweight and flexible, it is probable that punctures will occur. No previous research has been done to determine what will happen to the internal fluid and vapor under these circumstances. The experiment conducted was designed to simulate this situation. In this manner, the extent of potential damage and its effects on radiator performance could be determined.

## EXPERIMENTAL APPARATUS & PROCEDURES

The experimental apparatus is represented by the schematic diagram in Figure 1. The test section, located in the bell jar of the Veeco Ve-400 vacuum machine, is a double walled stainless steel vessel. It has an aluminum membrane holder on the bottom. An electrically controlled 15 watt solenoid, bolted to a cross-member in the test section, is used to pierce the membrane using a needle attachment threaded into the plunger. Constant temperature water is pumped from the Neslab EX-100 Exacal constant temperature bath through the outer wall of the vessel to keep the internal contents at constant conditions. This water is also circulated through the copper coils in the steam generation vessel for the same purpose. The temperature is monitored in both vessels using type T thermocouples and an Omega 21764 digital thermometer. The two Celesco E1PD pressure transducers, located on the top of each vessel are linked to a Hewlett Packard 7100 B strip chart recorder using Celesco CDIO carrier demodulators.

After a new membrane has been installed, the entire system is evacuated. The bell jar is pumped down to 0.1 mm Hg using a Duo Seal model 1397 mechanical vacuum pump. The steam generation vessel and test section are evacuated using a Duo Seal model 1402 auxiliary mechanical pump to approximately the same pressure. Then a given amount of water is added using a calibrated syringe. The location of water addition for each case is indicated in Figure 1. Either superheated steam or saturated steam with a condensate layer covering one side of the membrane will

occupy the test section. The other side of the membrane will be exposed to the vacuum environment in the bell jar. For both cases, the valve between the test section and the steam generation vessel is closed at the time of the test. When the desired conditions in the test section are obtained, the solenoid is activated to puncture the membrane. For the condensate case, there is no pressure or temperature drop as condensate is expelled from the test section. Therefore, the mass loss rate is calculated by estimating the time it takes for the entire condensate layer to leak out. Sample data collected for this case is given in Table 1, where $T_{sat}$ is the saturation temperature, $V_{add}$ is the volume of liquid added, and t is the time required to expell the entire layer of condensate. For the steam case the pressure loss versus time is recorded by the strip chart recorder. The temperature and pressure, $T_1$ and $P_1$ are noted just prior to puncture. As vapor escapes from the test section the pressure in the bell jar increases. This pressure rise is monitored by the pressure thermocouple gage in the vacuum test machine. As soon as this pressure rises above 1.0 mm Hg, the mass loss rate begins to decrease. Therefore the test is ended and the new temperature and pressure in the test section, $T_2$ and $P_2$ are recorded. The time is read from the strip chart recorder plot. Sample data collected for this case is given in Table 2.

## RESULTS AND DISCUSSION

In the case where a condensate layer was covering the membrane, it was predicted that the hole might seal itself by the following process. At the instant of puncture, a small percentage of liquid would flash vaporize when suddenly exposed to a vacuum. It would absorb its latent heat of vaporization from the remaining water in the vicinity of the hole, causing it to freeze and plug up the hole.

This process was not observed even when using the smallest needle available, which punctured a hole of 0.029 mm$^2$. Apparently, the water was expelled from the hole faster than the sealing process could take place. The water did freeze when it landed on the viewing mirror below the test section. Mass loss rates for this case were determined by the method shown in sample calculation #1, Appendix 1. A summary of results is given in Table 3, and graphically in Figure 2. A hole of .029 mm$^2$ gave a mass loss rate of approximately 2.73 kg/hr. For a 25 MW Radiator[1], we can assume an operating time of one hour, a total working fluid mass of 500 kg, and a radiator size of 3 m in diameter by 100 m long. Using a probability model [2,3] as shown in sample calculation #2, a radiator this size can expect a 0.2% chance of being struck by a micrometeoroid large enough to puncture the hole discussed. Under these circumstances, the total reduction in mass is less than 0.6% of the total working fluid. This indicates that the mass loss associated with this case may not be significant. However, as meteoroid size decreases, the chance of puncture increases. Therefore it is possible that many smaller holes will be present. The possibility of sealing in these

smaller holes has not been ruled out. As hole size decreases, the surface tension and viscosity of the water play an increasing role in slowing down the flow rate of water. This may result in freezing before expulsion causing the hole to seal itself as discussed earlier.

The mass loss rates predicted by this experiment may be much higher than would occur in space. This is due to the fact that the pressure difference caused the membrane to curve and the puncture was located in the bottom as seen in Figure 3. On earth gravity was responsible for delivering more condensate to the vicinity of the hole. In space, the lack of a body force may greatly diminish the mass loss rates. A small amount of condensate would leak out and leave the hole exposed to steam only as seen in Figure 4. This would cause continued leakage to occur according to the steam only case.

In the steam only case, mass loss was seen to be so low that it is insignificant and will not effect radiator performance. The results for this case, obtained according to sample calculation #3, are summarized in Table 4. The experimentally determined mass loss rates versus puncture area can be seen graphically in Figure 5. The slope of this plot is the average mass flux. This value compared nicely to the theoretical[4] prediction from choked flow, as seen in sample calculations 4 & 5.

The experimental mass flux was 0.1250 kg/hr $mm^2$ and the theoretical value was 0.1216 kg/hr $mm^2$. This is less than a 20% difference including the experimental uncertainty which is given in Appendix 2.

Assuming the same puncture conditions and radiator dimensions, the mass loss is only 0.00363 kg/hr or a $7.25 \times 10^{-4}$% decrease in total mass.

This experiment is not truly representative of actual operation in that superheated steam near 70°C and 20 kPa was used experimentally. In reality, saturated steam at 70°C and 31.19 kPa would occupy the radiator. Therefore, the actual mass loss rate for this case would be higher but still insignificant.

For each of the two cases previously discussed, two different membrane materials were tested. One was a clear plastic laminate 0.152 mm thick. The other was a plastic - aluminum film laminate 0.137 mm thick. Table 5 lists material type, actual hole area, A, needle cross-sectional area, An, and the ratio An/A for each run. Due to the wide variation in the area ratio, no correlation can be made between needle size and hole size for the two materials tested. Examples of the different punctures are shown in Figures 6 and 7. The clear plastic stretched more readily and then puncture was fairly clean and round. The aluminum - plastic material ripped when the needle was forced through. Due to the irregular hole shapes area calculation was difficult. Pictures of the punctures were taken at high magnification. A grid was used to estimate the area in the photograph. This value was then reduced by the magnification factor to determine the actual puncture area. The error associated with this calculation is probably not more than 10%.

## CONCLUSIONS & RECOMMENDATIONS

From the experimental results obtained, it is concluded that damage due to micrometeoroics will not significantly effect radiator performance. The total mass loss over the entire operating period probably would not exceed two percent in the worst case. However considering the results of the condensate case it is highly desirable to minimize the thickness of the condensate layer as much as possible. This will reduce mass loss, as well as, thermal resistance to heat transfer. Also, when considering a design for liquid return, care should be taken in avoiding the delivery of condensate to the vicinity of a hole.

To more accurately determine the extent of damage in space, the condensate case should be redone in a zero-gravity environment. The effects of gravity on mass loss may be great for this case. Without gravity, the flow rate through the hole will decrease . For this reason, it is entirely possible that the sealing process discussed will occur more readily. If not, the lack of a mechanism to deliver more condensate to the vicinity of the hole, may still diminish mass loss significantly.

In any case the mass loss estimates provided here are the maximum that could possibly occur. Since these are acceptable, micrometeoroid damage will not be a problem, and the flexible radiator concept should be further researched and developed.

REFERENCES

1) L.C. Chow, E.T. Mahefkey and J.E. Yokajty, "Low Temperature Expandable Megawatt Pulse Power Radiator," AIAA 20th Thermophysics Conference, 1985, AIAA Paper 85-1076.

2) Meteoroid Environment Model - 1969, NASA SP-8013, 1969.

3) Meteoroid Damage Assessment, NASA SP-8042, 1970.

4) K. Oswatitsch and G. Kuerti, Gas Dynamics, Academic Press Inc., 1956, p. 51.

5) J.P. Holman, Thermodynamics, third edition, McGraw Hill, 1980, Steam Tables.

| RUN | $T_{sat}$ ± 0.2°C | $V_{add}$ ± 0.2cm³ | t ± 1.0 sec |
|---|---|---|---|
| 1 | 70.2 | 5.1 | 5.6 |
| 2 | 67.. | 5.1 | 5.4 |
| 3 | 68.6 | 6.3 | 6.0 |
| 4 | 66.8 | 7.0 | 6.0 |

TABLE 1: Raw Data: Condensate Case

| RUN sec | $T_1$ ± 0.2°C | $P_1$ ± 0.2kPa | $T_2$ ± 0.2°C | $P_2$ ± 0.2 kPa | t ± 0.3 |
|---|---|---|---|---|---|
| 5 | 70.2 | 21.67 | 68.6 | 20.99 | 62.0 |
| 6 | 68.2 | 19.98 | 67.4 | 19.19 | 20.5 |
| 7 | 71.0 | 18.29 | 70.2 | 16.94 | 26.0 |
| 8 | 70.8 | 19.9[illegible] | 69.6 | 19.03 | 8.5 |
| 9 | 70.4 | 22.23 | 69.4 | 20.54 | 7.3 |
| 6 | 70.2 | 20.54 | 68.6 | 17.73 | 7.5 |
| 7 | 70.2 | 21.10 | 69.4 | 19.42 | 3.0 |

TABLE 2: Raw Data: Steam Case

| RUN | $\dot{M}$ ± 10% kg/hr | A ± 10% mm² | Mflux ± 20% kg/hr mm² |
|---|---|---|---|
| 1 | 2.73 | 0.029 | 94.14 |
| 2 | 2.87 | 0.036 | 79.72 |
| 3 | 3.27 | 0.046 | 71.09 |
| 4 | 3.71 | 0.050 | 74.20 |

TABLE 3: Results: Condensate Case

| RUN | $\dot{M}$ ± 20% kg/hr | A ± 10% mm² |
|---|---|---|
| 5 | 0.00081 | 0.008 |
| 6 | 0.00316 | 0.026 |
| 7 | 0.00435 | 0.039 |
| 8 | 0.00898 | 0.080 |
| 9 | 0.0193 | 0.172 |
| 10 | 0.0314 | 0.221 |
| 11 | 0.0470 | 0.370 |

MASS FLUX = 0.1250 kg/hr mm²

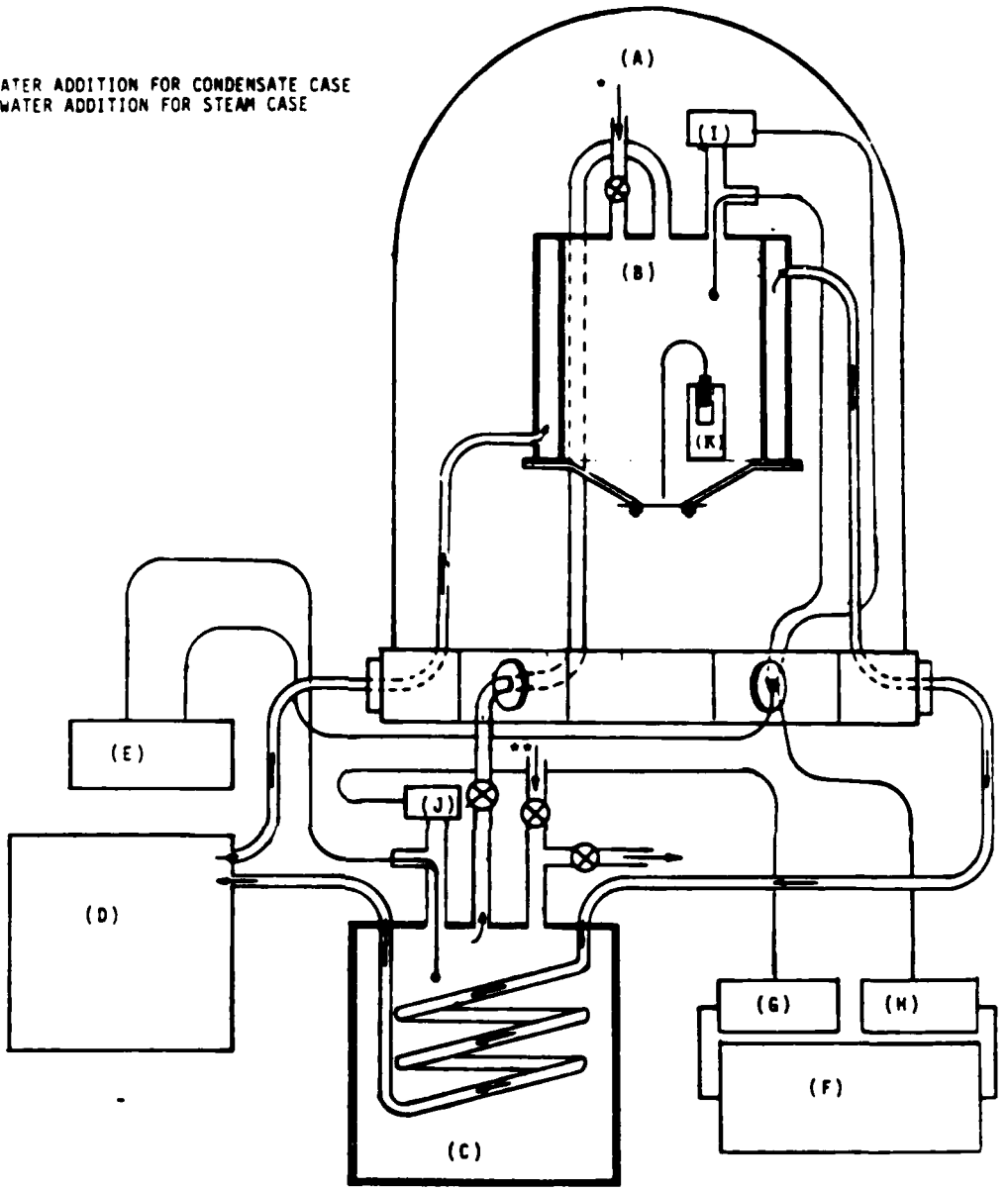
TABLE 4: Results: Steam Case

| RUN | MATERIAL | A($mm^2$) | An($mm^2$) | An/A |
|---|---|---|---|---|
| 1 | C | 0.11- | 0.029 | 3.93 |
| 2 | C | 0.257 | 0.036 | 7.14 |
| 3 | C | 0.114 | 0.046 | 2.48 |
| 4 | A | 0.257 | 0.050 | 5.14 |
| 5 | C | 0.114 | 0.008 | 14.25 |
| 6 | A | 0.257 | 0.026 | 9.88 |
| 7 | A | 0.621 | 0.039 | 15.92 |
| 8 | A | 0.456 | 0.080 | 5.70 |
| 9 | C | 0.811 | 0.172 | 4.72 |
| 10 | A | 1.267 | 0.221 | 5.73 |
| 11 | A | 2.011 | 0.370 | 5.43 |

Clear Plastic Average An/A = 6.50

Aluminum-Plastic Average An/A = 7.97

TABLE 5: PUNCTURE AREA AND NEEDLE AREA DATA.




(A)-BELL JAR, VEECO VE-400 VACUUM TEST MACHINE (V=100000cc)
(B)-STAINLESS STEEL DOUBLE WALL TEST SECTION (V=3800cc)
(C)-STEAM GENERATION VESSEL (V=22500cc)
(D)-NESLAB EX-100 EXACAL CIRCULATING CONSTANT TEMPERATURE BATH
(E)-OMEGA 21764 DIGITAL THERMOMETER
(F)-HEWLETT PACKARD 7100B STRIP CHART RECORDER
(G)&(H)-CELESCO CD10 CARRIER DEMODULATORS
(I)&(J)-CELESCO E1PD PRESSURE TRANSDUCERS
(K)-SOLENOID-NEEDLE PUNCTURE ASSEMBLY

**FIGURE 1:** APPARATUS SCHEMATIC

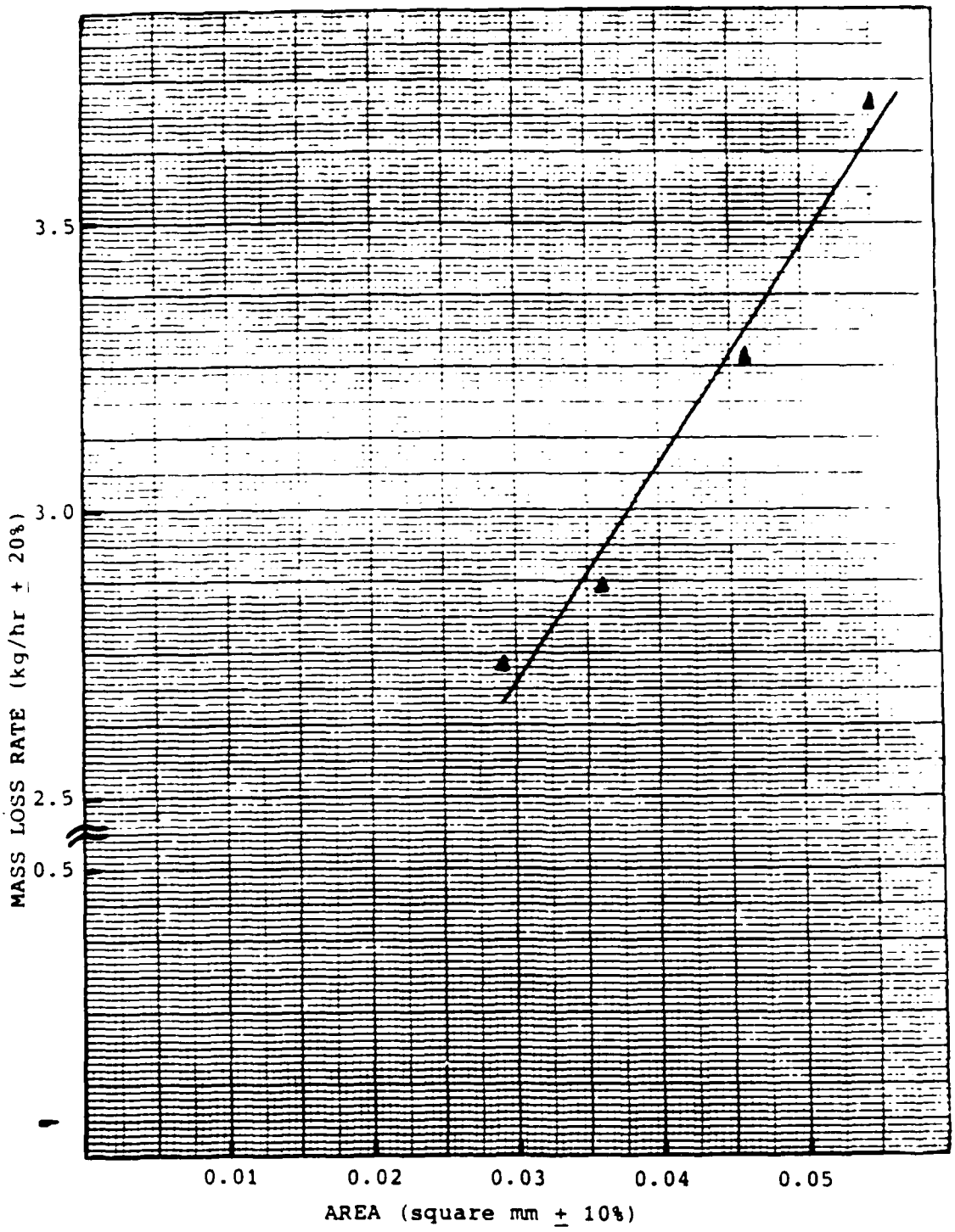



**FIGURE 2:** MASS LOSS RATE vs. PUNCTURE AREA (CONDENSATE CASE)

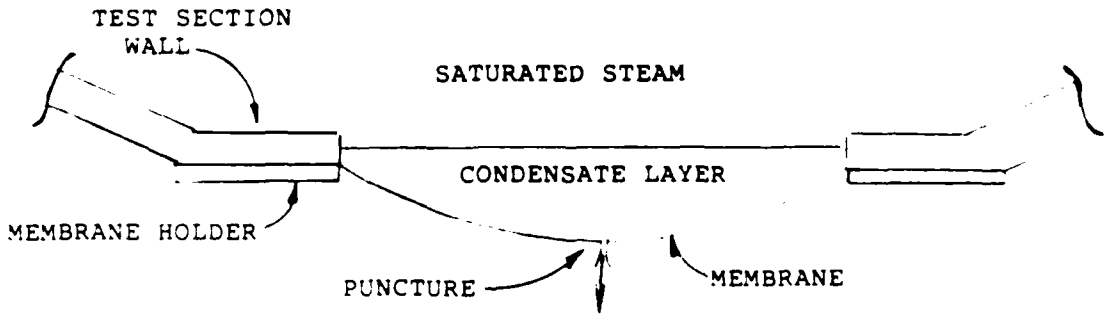



**FIGURE 3:** GRAVITATIONAL DELIVERY OF CONDENSATE TO PUNCTURE

---

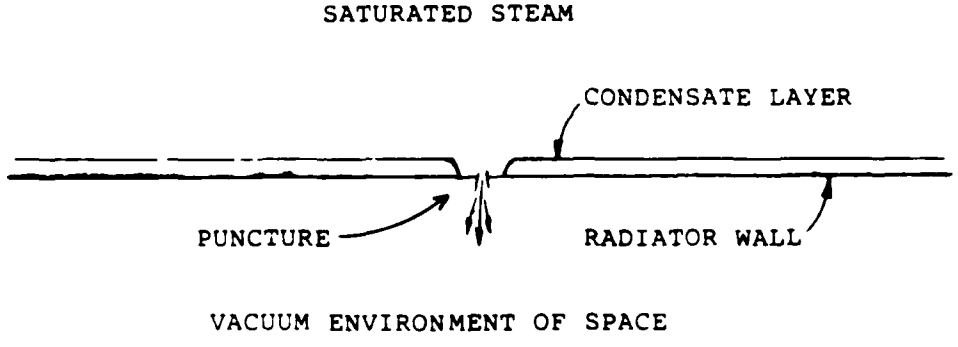



**FIGURE 4:** ZERO-G, NO CONDENSATE DELIVERY TO PUNCTURE

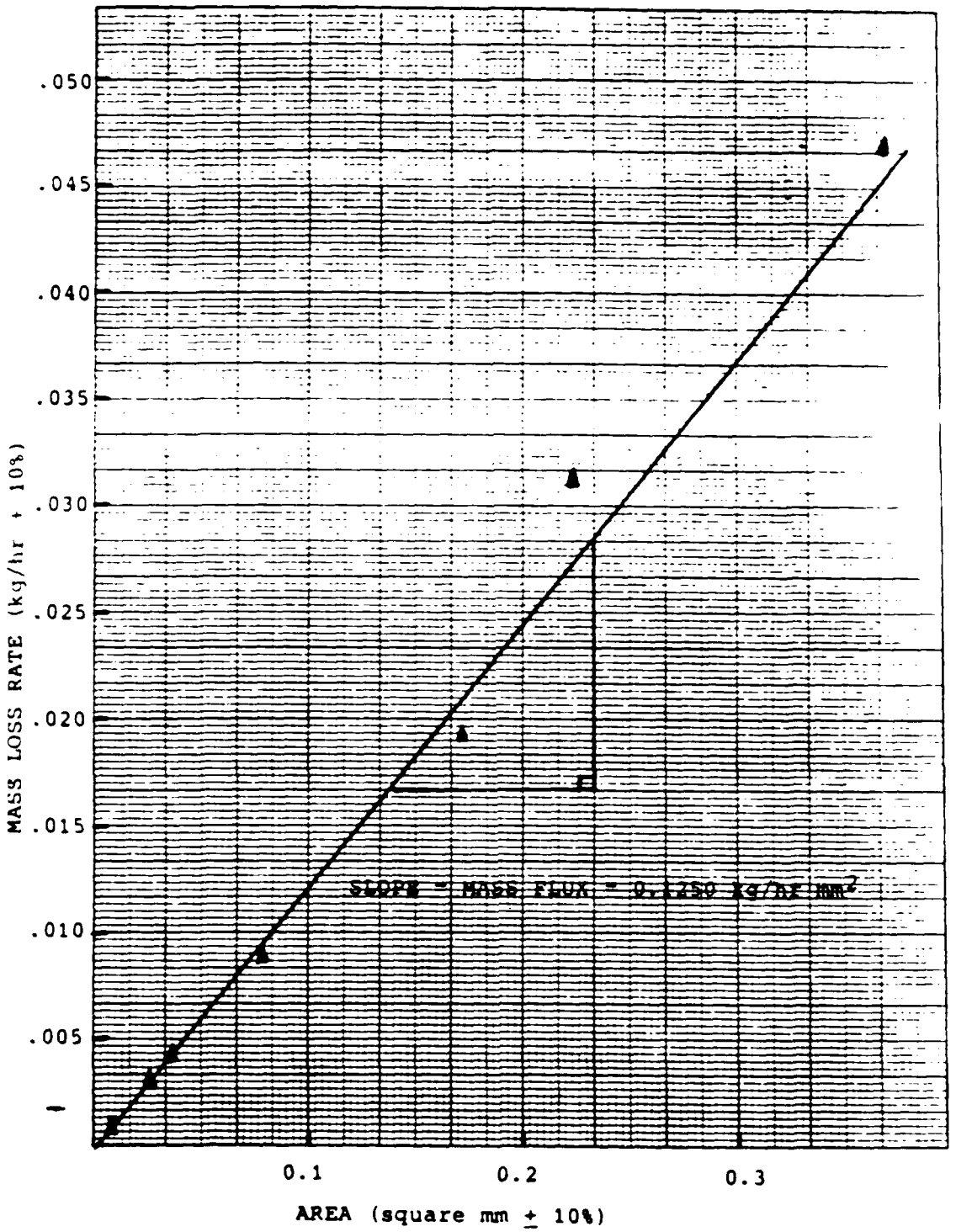



**FIGURE 5:** MASS LOSS RATE vs. AREA (STEAM CASE)

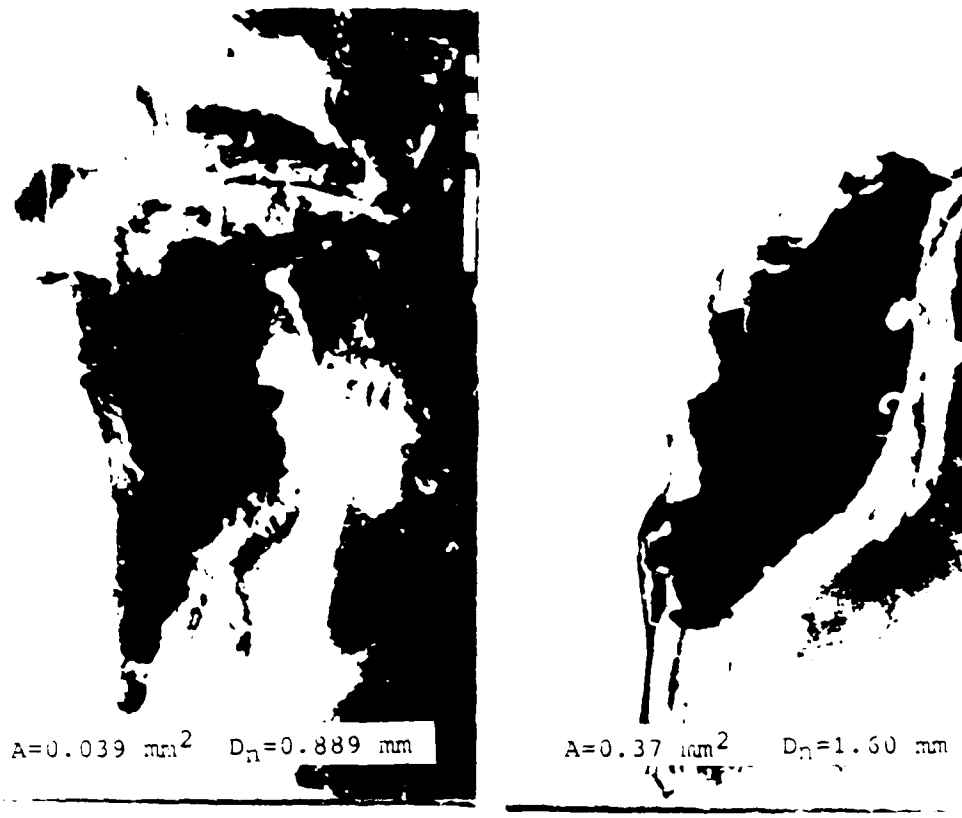



**FIGURE 6:** EXAMPLE PUNCTURES, ALUMINUM-PLASTIC LAMINATE

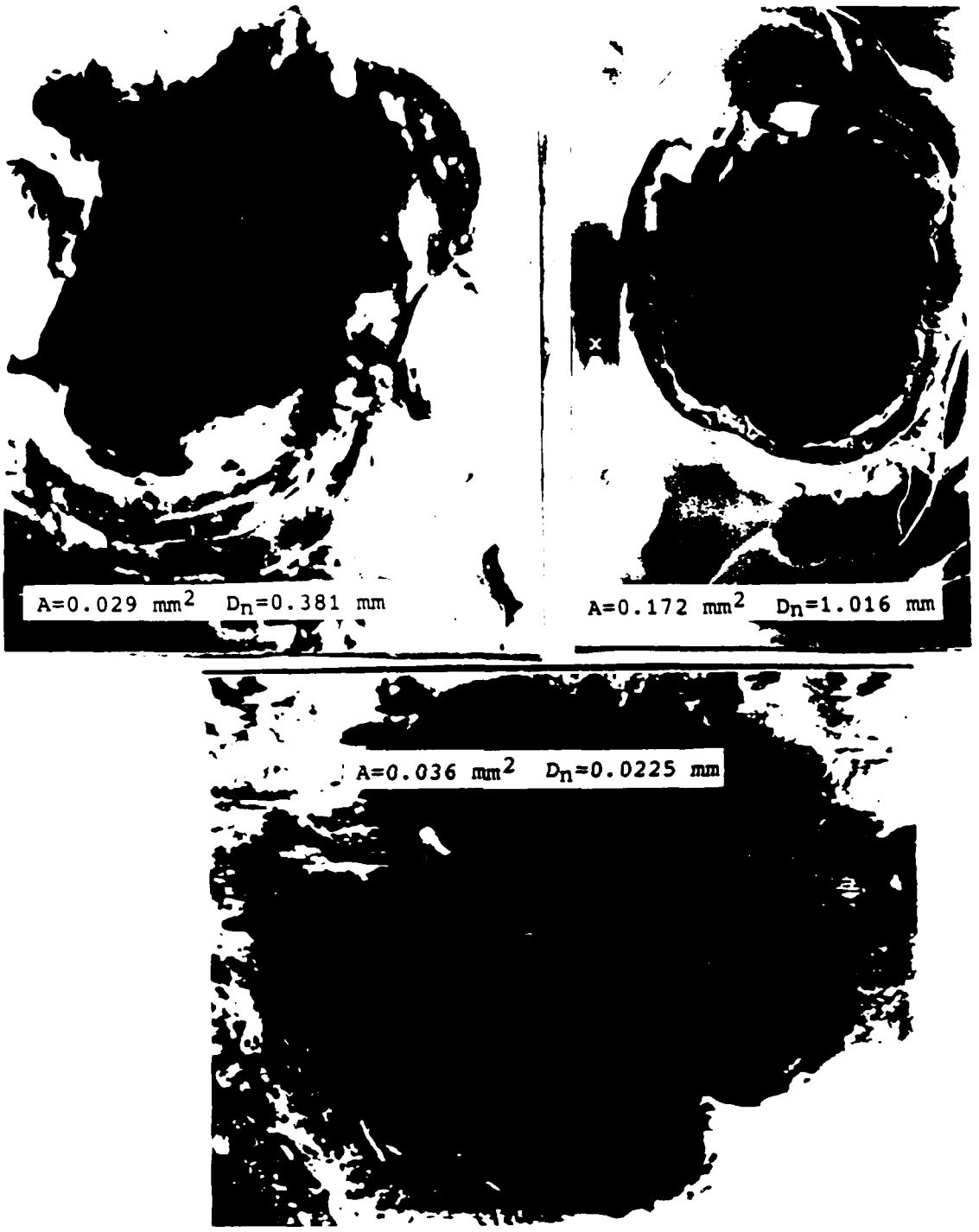



FIGURE 7: EXAMPLE PUNCTURES, CLEAR PLASTIC LAMINATE

# APPENDIX 1

## SAMPLE CALCULATIONS

SAMPLE CALCULATIONS #1 (Condensate Case)

Raw Data:

$T = 70.2°C$

$V_{added} = 5.1\ cm^3$ at 70°C $\quad M_{add} = 4.99g$

$V_{test\ sect} = 3800\ cm^3$

$v_{tot} = 3800\ cm^3/4.99g = 761.5\ cm^3/g$

From (8) J.P. Holman, Thermodynamics

$v_f = 1.0228\ cm^3/g$

$v_g = 5042\ cm^3/g$

$v_{tot} = v_f + x(v_g - v_f)$

$761.5 = 1.0228 + x(5042 - 1.0228)$

$x = 0.151$

$(1 - x) = 0.849$

grams of condensate layer = (0.849)(4.99) = 4.24 g

$\dot{m} = 4.24\ g/5.6\ sec = 0.757\ g/s$

$\dot{M} = 2.73\ kg/hr$

$M_{flux} = \dot{M}/A$

$M_{flux} = 94.14\ kg/hr\ mm^2$

==========

SAMPLE CALCULATION #2

Puncture Probability

From References (2) and (3) for a meteoroid of mass $10^{-6}$ grams or less

$$\log_{10} N_t = -14.37 - 1.213 \log_{10} M$$

where $N_t$ = Number of particles of mass, m or greater per square meter of space per second.

M = Meteoroid mass in grams.

Assume a meteoroid mass density of 0.5 grams/cm³ for all meteoroids.

For hole area = 0.029 mm²

Assuming the micrometeroid has the same cross-sectional area as the hole volume of meteoroid, V = 0.030 mm³ = $3.0 \times 10^{-5}$ cm³

$$m = 1/(5 \times 10^{-5}) \text{ grams.}$$

$$\log_{10} N_t = -14.37 - 1.213 \log_{10} 1.5 \times 10^{-5}$$

$$N_t = 3.0 \times 10^{-9} \text{ particles/m}^2\text{s}$$

ASSUME: Average radiator cross sectional area = 150m²

Operating time of 1 hour = 3600 seconds

Number of punctures = $N_t \times A \times t$

$$= 0.00164$$

∴ There is less than a 0.2% chance that a puncture this size or greater will occur.

SAMPLE CALCULATION #3 (Steam only)

Raw Data: $T_1 = 70.4°C$ $T_2 = 69.4°C$

$P_1 = 22.23$ kPa $P_2 = 20.54$ kPa

$t = 7.3$ sec

Since $Z \approx 1.0$; Use Ideal Gas Law

$$v = \frac{RT}{P}$$

$v_1 = 7119.3 \text{ cm}^3/\text{g}$

$v_2 = 7682.6 \text{ cm}^3/\text{g}$

Volume of Test Section: $V = 3800 \text{ cm}^3$

$m_1 = 3800 \text{ cm}^3/7119.3 \text{ cm}^3/\text{g} = 0.5338\text{g}$

$m_2 = 3800 \text{ cm}^3/7682.6 \text{ cm}^3/\text{g} = 0.4946\text{g}$

$$\dot{m} = \frac{m_1 - m_2}{t} = \frac{0.5338 - 0.4946}{7.3}$$

$\dot{m} = 0.00536$ g/s

$\dot{m} = 0.0193$ g/hr

From slope of $\dot{m}$ vs a steam case plot

$M_{flux} = 0.1250$ kg/hr mm²

SAMPLE CALCULATIONS #4 Steam Case (theoretical)

From (4) Oswatitsch/Kuerti, Gas Dynamics, 1956

The mass flux of a vapor leaking from a vessel into a vacuum through an orifice is given by the choked flow equation:

$$M_{flux} = \left(\frac{2}{\gamma + 1}\right)^{\frac{\gamma + 1}{2(\gamma - 1)}} C_o \rho_o$$

where $C_c$ = speed of sound at internal conditions

$\rho_o$ = vapor density at internal conditions

$\gamma$ = ratio of specific heats

For $H_2O$ vapor at 70°C, 20 kPa

$\gamma = 1.33$

$R = 460.6$ J/kg K

$T_c = 342.2$K

$C_o = (\gamma RT_o)^{\frac{1}{2}} = 457.85$ m/s

From Ideal Gas Law, Z=1.0

$$\rho_o = \frac{P_o}{RT_o} = 0.1265 \text{ Kg/m}^3$$

$M_{flux} = 33.78$ kg/sm²

$M_{flux} = 0.1216$ Kg/hr-mm²

SAMPLE CALCULATION #5

Experimental and theoretical comparison (Steam case)

From slope of $\dot{m}$ vs A plot

experimental $M_{flux}$ - 0.1250 kg/hr mm$^2$

From sample calculation #2

theoretical $M_{flux}$ = 0.1216 kg/hr mm$^2$

% error = $\frac{0.1250 - 0.1216}{0.1250} \times 100 = 2.27\%$

% error = 2.27%

including Uncertainity Calculation in Appendix 2

% error = < 20%

# APPENDIX 2

# UNCERTAINTY ANALYSIS

UNCERTAINTY ANALYSIS:

All uncertainty calculations were performed in the standard way, such that the uncertainty in any value F, $\omega_F$, is given by:

$$\frac{\omega_F}{F} = \left( \left( \frac{\partial F}{\partial v_1} \omega_{v_1} \right)^2 + \left( \frac{\partial F}{\partial v_2} \omega_{v_2} \right)^2 + \cdots \left( \frac{\partial F}{\partial v_n} \omega_{v_n} \right)^2 \right)^{\frac{1}{2}}$$

Where: $F = F(v_1, v_2, \ldots v_n)$

CONDENSATE CASE:

mass flow rate; $\frac{\omega_m}{m} = 20\%$

mass flux; $\frac{\omega_{M_{flux}}}{M_{flux}} = 25\%$

STEAM CASE:

mass flow rate; $\frac{\omega_m}{m} = 10\%$

mass flux; $\frac{\omega_{M_{flux}}}{M_{flux}} = 15\%$

PUNCTURE AREA:

area; $\frac{\omega_A}{A} = 10\%$

Technical Memorandum MAE-TM-18

# Computational Studies of Ramjet Combustor Flowfields

K. M. Isaac

Department of Mechanical and Aerospace Engineering

University of Missouri-Rolla

January 1986

## ABSTRACT

Computation of combustion chamber flowfields has been of interest in recent years because of the enormous benefits to be reaped from the improvements in ramjet/turbojet engine performance. An investigation was undertaken to evaluate proposed modifications to the turbulence model to account for low turbulence Reynolds number effect and streamline curvature effect. The vehicle for this computational study was a computer program which was used to solve the fully-elliptic Navier-Stokes equations based on the methodology of Gosman et al. The program is currently capable of calculating compressible, recirculating, axisymmetric or two-dimensional, internal flows. This report describes new studies conducted on the recirculating combustor flowfield by using modified forms of the k-e turbulence model. Details of the methodology adopted for calculating compressible flow are also discussed in this report.

## NOMENCLATURE

| | | |
|---|---|---|
| D | - | chamber diameter |
| d | - | inlet diameter |
| f | - | constant in turbulence model |
| G | - | generation term in turbulence model |
| H | - | total enthalpy |
| K | - | constant in turbulence model |
| k | - | turbulent kinetic energy, thermal conductivity |
| l | - | macro length scale |
| S | - | source term |
| s | - | coordinate tangential to streamlines |
| n | - | coordinate normal to streamlines |
| u | - | velocity component in the axial direction |
| v | - | velocity component in the radial direction |
| P | - | rate of generation of turbulence energy |
| p | - | time-mean pressure |
| T | - | static tempe ature |
| R | - | gas constant |
| Re | - | Reynolds number |
| r | - | radial coordinate |
| x | - | axial coordinate |
| y | - | distance normal to the wall |
| $\alpha$ | - | constant in turbulence model |
| $\beta$ | - | constant in turbulence model |
| $\delta$ | - | shear layer thickness |
| $\Gamma$ | - | exchange coefficient |
| $\mu$ | - | dynamic viscosity |

$\nu$ - kinematic viscosity

$\epsilon$ - turbulent energy dissipation rate

$\rho$ - density

$\sigma$ - Prandtl-Schmidt number

$\tau$ - shear stress

$\Phi$ - variable representing various flow parameters

Subscripts

in - inlet

ref - reference

t - turbulent parameters

## INTRODUCTION

Combustion chamber designs for turbojet and ramjet engines that have been developed over the last few decades have resulted in improved designs having much higher levels of performance. The designers, however, are faced with trial and error procedures because of the uncertainties in predictive capability. The reasons for this are many. The interplay of several physical phenomena, such as turbulence, multiphase flow, and chemical reaction, makes the flowfield very complex and, therefore, difficult to analyze. Very often the flowfield is three-dimensional in nature, and this imposes severe limitations on the computations in terms of storage and computation time. When a computer code is successfully developed, it is often found that there are few experimental data available to prescribe the boundary conditions meaningfully or to compare with the predictions.

Some encouraging developments have taken place in recent years that address some of the problems discussed above. Good progress has been made in the numerical modeling of the (Navier-Stokes) equations governing recirculating flowfields typical of a ramjet/turbojet combustion chamber. Turbulence models capable of predicting the flowfields in a wide range of physical situations, such as free shear flows (jets and wakes), wall-bounded flows (boundary-layers), and confined jets, have been developed. Chemical reaction models of varying degrees of sophistication are currently being used for combusting flows. These models range from a reactants-and-products equilibrium chemistry model to finite-rate chemistry models with multi-step reactions involving several chemical species. Recent developments in nonintrusive experimental techniques have made it possible to make accurate measurements of mean velocity and turbulence even in highly turbulent,

recirculating flow regions. Therefore, it is now possible to accurately specify the boundary conditions for the solution of the equations; one is also able to make meaningful comparisons between experiments and predictions without unduly worrying about experimental uncertainties.

Some combustor configurations that are currently being investigated are the dump combustor and the center bluff body combustor (Figures 1 and 2). The dump combustor appears to be particularly attractive because of its ability to decelerate the flow and create recirculating zones for flame holding and flame stabilization without a significant amount of pressure loss.

## BACKGROUND

The numerical solution of the time-averaged, fully elliptic Navier-Stokes equations poses several difficulties because of the coupled, nonlinear nature of the equations. The solution becomes particularly cumbersome when the flowfield considered is multidimensional, turbulent, compressible, and chemically reacting. Turbulence introduces additional complexities because of what is known as the 'closure' problem, which makes it necessary to resort to turbulence modeling[1-16]. In compressible flows, an additional equation (the energy equation) must be solved, and the fluid density becomes a variable and must be calculated from an equation of state. Chemical reaction introduces additional equations for the transport of various chemical species.

The first aspect of the problem that was dealt with in the present study was the numerical algorithm for solving the set of nonlinear, coupled, partial differential equations governing the flowfield. Solutions of the two-dimensional flow problems have been obtained in the past with vorticity and stream function as the dependent variables. A more widely used approach was developed by Patankar and Spalding[13] who employed the SIMPLE (Semi -

Implicit - Pressure - Linked - Equations) algorithm for solving the equations in primitive variables. Their method has several features in common with the earlier work of Harlow and Welch[16]. Some of the deficiencies of these methods have been widely recognized, and recently some alternative methods have been proposed[13-17] to overcome these deficiencies. Some of these methods are still in the development stage, and, therefore, their applicability is yet to be tested. The SIMPLE algorithm has been widely used for the solution of the Navier - Stokes equations governing parabolic as well as elliptic (recirculating) flows. Despite its shortcomings, the method has successfully predicted a wide range of flowfields. Several investigators have used the method to predict the flowfield in combustion chambers of different geometries[17-22].

The problems of turbulence modeling are still intriguing investigators in the field. One approach, which has gained wide popularity, is the $k-\epsilon$ model[1] in which k and $\epsilon$ represent respectively the turbulent kinetic energy and its dissipation rate. The $k-\epsilon$ model treats trubulence by means of transport equations for these two variables. Several versions of the $k-\epsilon$ model are in use; however, none of them gives uniformly good results for vastly varying flow conditions. Other approaches, such as Reynolds stress models and pdf models, can be found in the literature. It appears that the $k-\epsilon$ model offers more satisfactory results over a wide range of flow conditions in comparison to the other turbulence models, which give good predictions in some cases and perform poorly in others. Recent use by the principal investigator of a computer code for calculating compressible, recirculating flow in internal geometries has brought to the surface some deficiencies of the predictive efforts that have been expended in this area[23]. It was felt that predictions could be improved by using a turbulence model which takes into account the

characteristics of recirculating flows. Regions of the flowfield where the streamlines have large curvature are known to yield unrealistic predictions when the standard $k-\epsilon$ model of turbulence is used. Furthermore, the effects of turbulence Reynolds number on the flowfield are also largely unknown. The present study was directed towards addressing these two problems.

## THE TURBULENCE MODEL

The turbulence model that is most widely used in the prediction of flowfields in internal geometries is the $k-\epsilon$ model in which $k$ and $\epsilon$ are, respectively the turbulent kinetic energy and its dissipation rate. The model prescribes these quantities in terms of the transport equations for these variables. The equations of continuity, momenta, energy, and the two transport equations for $k$ and $\epsilon$ are given in the appendix. The reason for representing all the equations in one general form is the ease of numerical implementation. The transport equations for $k$ and $\epsilon$ are reproduced below for clarity.

$$\frac{\partial}{\partial x}(\rho u k) + \frac{1}{r}\frac{\partial}{\partial r}(\rho v r k) = \frac{\partial}{\partial x}\left[\left(\mu + \frac{\mu_t}{\sigma_k}\right)\frac{\partial k}{\partial x}\right] + \frac{1}{r}\frac{\partial}{\partial r}\left[r\left(\mu + \frac{\mu_t}{\sigma_k}\right)\frac{\partial k}{\partial r}\right] + G - \rho\epsilon \qquad (1)$$

$$\frac{\partial}{\partial x}(\rho u \epsilon) + \frac{1}{r}\frac{\partial}{\partial r}(\rho v r \epsilon) = \frac{\partial}{\partial x}\left[\left(\mu + \frac{\mu_t}{\sigma_\epsilon}\right)\frac{\partial \epsilon}{\partial x}\right] + \frac{1}{r}\frac{\partial}{\partial r}\left[r\left(\mu + \frac{\mu_t}{\sigma_\epsilon}\right)\frac{\partial \epsilon}{\partial r}\right] + C_1\frac{\epsilon}{k}G - C_2\frac{\rho\epsilon^2}{k} \qquad (2)$$

In addition, the auxiliary relation for turbulent viscosity is given by

$$\mu_t = C_\mu \rho \frac{k^2}{\epsilon} \qquad (3)$$

The terms $\sigma_k$, $\sigma_\epsilon$, $C_1$, $C_2$ and $C_\mu$ which appear in the equations for $k$, $\epsilon$ and $\mu_t$ equations, are empirical constants, which must be determined by adjusting their values to fit experimental data. The above equations apply in

regions of high turbulence Reynolds number where the molecular viscosity is negligible. The expression for the turbulent Reynolds number is

$$Re_t = u'l/\nu \qquad (4)$$

in which u' is the fluctuating velocity, and l the macro length scale.(This is of the order of the transverse dimensions of the geometry)

Several investigators[7,11,13] previously concluded that for low turbulent Reynolds number flows, the viscous dissipation is important, and, therefore, its effects must be accounted for in the turbulence model. Jones and Launder and Chien proposed modifications to account for low turbulence Reynolds number. The essentials features of the two models are the same; however, a few differences may be noticed in their detailed implementation. A brief review of the two models is given below.

1.Jones and Launder Model

This model is closely related to the Harlow and Nakayama[8] model which also contains proposals for the way in which molecular viscosity exerts direct influence on the turbulence when the turbulence Reynolds number is low. The Jones and Launder model has been widely tested for a range of flow conditions. Their model was able to predict the observed behavior of the wall Stanton number in flows in which laminarization was present. They enlarged the model in the following three ways.

i) Viscous diffusion of k and $\epsilon$ was included.

ii) The empirical constants in the transport equations were made functions of the turbulent Reynolds number.

iii) Terms were added to account for the fact that dissipation processes are not isotropic.

The k and the $\epsilon$ equations for this model are as follows.

turbulent kinetic energy:

(5)

Energy dissipation rate:

$$\frac{\partial}{\partial x}(\rho u \epsilon) + \frac{1}{r}\frac{\partial}{\partial r}(\rho v r \epsilon) = \frac{\partial}{\partial x}\left[\left(\mu + \frac{\mu_t}{\sigma\epsilon}\right)\frac{\partial \epsilon}{\partial x}\right] + \frac{1}{r}\frac{\partial}{\partial r}\left[r\left(\mu + \frac{\mu_t}{\sigma\epsilon}\right)\frac{\partial \epsilon}{\partial r}\right]$$

$$+ C_1' \frac{\epsilon}{k} G - C_2' \rho \frac{\epsilon^2}{k} + 2\mu\mu_t \frac{\partial^2 u}{\partial y^2} \qquad (6)$$

Eddy viscosity:

$$\mu_t = C_\mu' \rho \frac{k^2}{\epsilon} \qquad (7)$$

Turbulent thermal conductivity:

$$k_t = C_p \mu_t / \sigma_h \qquad (8)$$

In the above equation set the C's and the $\sigma$'s retain the values assigned to them in the standard k- $\epsilon$ model. (Table 1) The influence of the Reynolds number is introduced by way of the f's which are assigned the following forms.

$$f_1 = 1 \qquad (9)$$

$$f_2 = 1 - 3 \exp\left(-Re_t\right) \qquad (10)$$

$$f_\mu = \exp\left[-2.5 / (1 + Re_t/50)\right] \qquad (11)$$

where $Re_t = \rho k^2/\mu\epsilon$ may be interpreted as the Reynolds number of turbulence. These authors made $\epsilon$ as the isotropic part of dissipation and made it go to zero at the wall because they could achieve decisive

computational advantages. They showed that the total dissipation at the wall becomes equal to the last term on the right hand side of the energy equation. In addition they used another term $2\mu\mu_t \frac{\delta^2 u}{\delta y^2}$ in the dissipation equation in order to obtain better agreement with experimental data. They did not offer any explanation for the presence of this term except for the fact that the inclusion of this term provided better agreement with experimental data. They chose $f_2$ so that the model, when applied to the calculation of the decay of grid tu. oulence, accorded with experiment for both high and low turbulence intensities. The form of the function $f_\mu$ was determined by focusing on the prediction of constant stress couette flow wherein the turbulent viscosity formula given above was not used to calculate turbulent viscosity. Instead, $\mu_t$ was obtained by way of the Van Driest form of the mixing length formula. This practice enabled attention to be focused on the $\epsilon$ equation which was then adjusted to produce a reasonable turbulence energy distribution in the viscous sublayer region.

2.Hanjelic and Launder Model

Hanjelic and Launder[10] discussed the specific effects of viscosity on the various transport processes. They presented numerical solutions for turbulent channel flows at low Reynolds number as well as a case of severely accelerated boundary-layer in which the turbulent shear stress becomes negligible compared with viscous stresses.

The equation for dissipative transport has been used in the following form by Hanjelic and Launder.

$$\frac{D\varepsilon}{Dt} = C_{\varepsilon 1} \frac{\varepsilon}{k} P - C_{\varepsilon 2} \frac{\varepsilon^2}{k} - C_\varepsilon \frac{\partial}{\partial x_k} \left\{ \frac{k}{\varepsilon} \overline{U_k U_\ell} \frac{\partial \varepsilon}{\partial x_\ell} \right\} \qquad (12)$$

where P is the rate of generation of turbulence energy by the mean strain

rate. Tennekes and Lumley[48] omitted the first term in Eq. 12 on the grounds that the term containing the mean field variables were of a smaller order. However, Hanjelic and Launder argued that a positive source term must be present in the equation so as to avoid physically unacceptable form of modeling. Lumley and Khajeh Nouri[49] preferred to have the term $(u_i u_j/k - 2/3\delta_{ij})^2 \epsilon$ instead of P in Eq. 12. Hanjelic and Launder preferred to use P rather follow the argument of Lumley and Khajeh Nouri. Extensive numerical testing conducted using P has been put forth as a reason for their choice of the term P in their model. In a homogeneous decaying turbulent flow Eq. 12 becomes

$$\frac{D\varepsilon}{Dt} = - C_{\varepsilon 2} \frac{\varepsilon^2}{k} \tag{13}$$

A consequence of this equation is that the turbulent kinetic energy decays at a rate of $x^{-n}$ where x is the distance downstream of the grid which generates the turbulence and n is an index whose value is given by

$$n = \frac{1}{(C_{\varepsilon 2} - 1)} \tag{14}$$

The variation of n behind the grid is between 1.8 and 2.5 as observed from experiments. Hanjelic and Launder assumed that this variation was entirely due to the diminution of the turbulence Reynolds number $Re_\lambda$. Therefore, they argued that $C_{\varepsilon 2}$ should be a function of $Re_\lambda$. The particular form of the dependence was based on the experiments of Batchelor and Townsend. Thus,

$$\frac{D\varepsilon}{Dt} = - C_{\varepsilon 2} f_\varepsilon \varepsilon^2/k \tag{15}$$

$$f_\varepsilon = 1 - \frac{0.4}{1.8} \exp \left[ - \left(\frac{Re_\lambda}{6}\right)^2 \right] \tag{16}$$

3.Chien's model

Chien[7] added kinematic viscosity $\nu$ to account for molecular diffusion of k and $\epsilon$. The dissipation term in the $\epsilon$ equation was modified to fit the data of decaying grid turbulence at high as well as low turbulent Reynolds numbers. Chien's handling of the effect of the presence of the solid wall is different from that of previous authors. He uses Taylor series expansion of the fluctuating velocity components near the wall. He showed, by the use of the continuity equation and the no slip condition at the wall, that

$$k \sim y^a$$

$$\nu_t \quad y^a$$

It can be shown by Taylor series expansion near the wall that isotropic dissipation is

$$\epsilon \sim y^N$$

Chien showed that the true rate of energy dissipation is given by

$$D = 2\nu k/y^a \tag{17}$$

in which $\nu$ is the kinematic viscosity, k the turbulent kinetic energy and y the distance from the wall. Therefore, the low turbulent form of the k equation can be written as

$$\frac{Dk}{Dt} = \frac{\partial}{\partial y}\left[(\nu + \nu_t)\frac{\partial k}{\partial y}\right] + \nu_t\left(\frac{\partial u}{\partial y}\right)^2 - \varepsilon - \frac{2\nu k}{y^2} \tag{18}$$

This equation differs from the standard form of the k-$\epsilon$ model because of the presence of the last term on the right hand side. The $\epsilon$ equation gets modified in Chien's model as

$$\frac{D\epsilon}{Dt} = \frac{\partial}{\partial y}\left[(\nu + \frac{\nu_t}{\sigma_\epsilon})\frac{\partial \epsilon}{\partial y}\right] + C_1 \frac{\epsilon}{k} \nu_t \left(\frac{\partial u}{\partial y}\right)^2 - \frac{\epsilon}{k}\left[C_2 f_\varepsilon \varepsilon + \frac{2\nu k}{y^2} \exp\left(-C_4 u^* y/\nu\right)\right] \tag{19}$$

in which $f_\epsilon$ is given by Eq. 16 and $u^*$ denotes the friction velocity. Chien used $C_\infty = 0.5$ in the above equation.

4.Present Modifications of the above Models

Modified forms of the Jones and Launder model and the Chien model were used for the present study. The modifications were implemented because of the realization that wall bounded flows are different from the flow in the inviscid core of a confined jet. It is reasonable to assume that the flow is isotropic in the inviscid core region; therefore, the presently proposed model differs from those cited above in that the nonisotropy terms are absent. Moreover, the present calculations did not use terms to account for wall damping effects. Eqs. 5 and 6 were modified to reflect these changes. The term $2\mu\left(\frac{\partial k^{1/2}}{\partial y}\right)^2$ was dropped from Eq. 5 and indicated earlier the term $2\mu\mu_t \frac{\partial^2 u}{\partial y^2}$ was also dropped from Eq. 6. Jones and Launder introduced the last term in Eq. 6 purely on the basis of obtaining better agreement with experimental data of wall bounded flows; it is felt that this is not a sufficient reason to introduce this term in the present calculations.

In order to investigate the usefulness of the two models in flow regimes characterized by a sudden axisymmetric expansion, a different and complete set of calculations were performed using the modified form of Chien's model. All the additional terms to account for low turbulent Reynolds number effects in Chien's model were carefully examined. It was concluded that for the present study only the term $C_2 f_\epsilon \frac{\epsilon^2}{k}$ in Eq. 19 needs to be retained. The basis for this conclusion is the fact that in the inviscid core the other effects discussed in Chien's paper are not important.

## 5. Streamline Curvature Effects

Another aspect of the turbulence model that was investigated is the effect of streamline curvature. This is particularly important in the recirculation region where one comes across large curvature of the streamlines. Bradshaw[24] reviewed the experimental studies to determine the effects of streamline curvature on turbulent flows and concluded that the standard turbulence models (mixing length and k-$\epsilon$ models) do not reflect the sensitivity of turbulence to streamline curvature. Modifications of the k-$\epsilon$ model to account for streamline curvature were reported by Leschziner and Rodi[11]. These modifications are based on Gibson's algebraic stress model[8]. The algebraic stress equation is written in general form as

$$P_{ij} = \alpha \frac{\epsilon}{k}\left(\overline{u_i u_j} - \frac{2}{3}\delta_{ij}\, k\right) + \beta\left(P_{ij} - \frac{2}{3}\delta_{ij}\, P_k\right) + \frac{2}{3}\delta_{ij}\,\epsilon \qquad (20)$$

In which $P_{ij}$ is the production of turbulent stress $\overline{u_i u_j}$, and $\alpha$ and $\beta$ are constants, which assume the values of 1.5 and 0.6 respectively as given Leschziner and Rodi.[11] The term $P_k$ stands for the production of turbulent kinetic energy, and $\delta_{ij}$ is the Kronecker delta. Gibson's algebraic stress model assumes local equilibrium -- total energy supply is equal to the total energy dissipation. Under this assumption one can write $P_k = \epsilon$, and the above equation reduces to

$$\frac{\overline{u_i u_j}}{k} = \frac{1-\beta}{\alpha\epsilon} P_{ij} - \frac{2}{3}\,\frac{\delta_{ij}}{\alpha}(1 - \alpha - \beta). \qquad (21)$$

In order to see the effect of streamline curvature, this equation can be written in the streamline coordinates $(s,n)$, in which $s$ is the streamwise coordinate, and $n$ the normal coordinate.

$$P_{ss} = -2\,\overline{u_s^2}\,\frac{\partial U_s}{\partial s} - 2\,\overline{u_s u_n}\,\left(\frac{\partial U_s}{\partial n} + \frac{U_s}{R_c}\right) \tag{22}$$

$$P_{nn} = -2\,\overline{u_n^2}\,\frac{\partial U_n}{\partial n} + 4\,\overline{u_n u_s}\,\frac{U_s}{R_c} \tag{23}$$

$$P_{ns} = -\,\overline{u_s^2}\,\frac{\partial U_s}{\partial n} + (2\,\overline{u_s^2} - \overline{u_n^2})\,\frac{U_s}{R_c} + \overline{u_n u_s}\,\frac{U_r}{r} \tag{24}$$

In the above equations, $R_c$ is the radius of curvature of the streamline, and $U_r$ the mean velocity in the radial direction. Further simplifications are achieved by Leschziner and Rodi[11] by stipulating that

$$\frac{U_r}{r} = \frac{\partial U_s}{\partial s} = \frac{\partial U_n}{\partial n} = 0 \tag{25}$$

Although it appears reasonable to assume that $\partial U_s/\partial s = \partial U_n/\partial n = 0$, the additional assumption that $U_r/r = 0$ does not seem to be a particularly sound one. This may be easily seen from Figure 3. The ratio $U_r/r$ does have appreciable values in places where the streamlines have large inclinations with reference to the axis (plane) of symmetry. Therefore, $U_r/r$ was retained in the present calculations. The modified form of the shear stress equation was obtained from Eqs. 22-24.

$$-\,\overline{u_s u_n} = \frac{-\,K_1 K_2}{\left[1 + 8\,K_1^2\,\frac{k^2}{\epsilon}\left(\frac{\partial U_s}{\partial n} + \frac{U_s}{R_c} - K_1\,\frac{k}{\epsilon}\,\frac{U_r}{r}\right)\right]}\,\frac{k^2}{\epsilon}\,\left(\frac{\partial U_s}{\partial n} - \frac{U_s}{R_c}\right) \tag{26}$$

in which

$$K_1 = (1 - \beta)/\alpha \text{ , and}$$

$$K_2 = 2\,(1 - \alpha - \beta)/(3\alpha)$$

By comparing Eq.26 to the expression for eddy viscosity,

it can be easily seen that

$$C'_\mu = \frac{K_1 K_2}{\left[1 + 8 K_1^2 \frac{k^2}{\varepsilon}\left(\frac{\partial U_s}{\partial n} + \frac{U_s}{R_c} - K_1 \frac{k}{\varepsilon}\frac{U_r}{r}\right]\right.} \cdot \qquad (27)$$

Except for the retention of the term $K_1 k \frac{U_r}{r}$, the expression for $C_\mu$ is the same as that given by Leschziner and Rodi[11]. The value of 0.09 was used for $K_1 K_e$ following the argument given by these authors.

## GOVERNING EQUATIONS AND NUMERICAL MODELING

The equations governing the compressible, axisymmetric, turbulent flow of a perfect gas can be written in a convenient form as

$$\frac{1}{r}\left[\frac{\partial}{\partial x}(\rho u r \phi) + \frac{\partial}{\partial r}(\rho v r \phi) - \frac{\partial}{\partial x}\left(r\Gamma_\phi \frac{\partial \phi}{\partial x}\right) - \frac{\partial}{\partial r}\left(r\Gamma_\phi \frac{\partial \phi}{\partial x}\right)\right] = S_\phi \qquad (28)$$

In the above equation the variables $\Phi$ and $\Gamma_\Phi$ assume different meanings for the equations of continuity, momentum, energy, turbulent kinetic energy and its dissipation rate. The general form of the equations given by Eq. 28 is particularly useful for their numerical solution.

For compressible flows density is also a variable and it is calculated using the equation of state for a perfect gas. For chemically reacting flows there will be additional equations for species continuity and chemical reaction rates.

The partial differential equations of continuity, momentum, energy and the turbulent quantities represented by the general form given by Eq. 28 are solved by the SIMPLE algorithm of Ref. 13. Details of the solution procedure may be found in several other references also[14-23]. The discretization equations are obtained by integrating the partial differential equations over the cell control volumes formed about the grid lines in the solution domain. A

lucid explanation of its advantages over other differencing methods is given by Patankar[27]. Suffice to state that the procedure ensures conservation of quantities such as mass, momentum and energy over any group of control volumes and therefore, over the whole computational domain. The pressure field is initially guessed and it is corrected at each iteration stage by means of a pressure correction equation. A staggered grid approach and a central/upwind differencing scheme are used in applying the equations; the advantages of these can be found in Ref. 27. A line-relaxation procedure is used for the solution of the equations. Convergence is improved by reliance on under-relaxation factors which control the variation of dependent variables from iteration to iteration. A mesh size of 21x35 was used for the present calculations. The mesh is nonuniformly arranged in order to provide better resolution in regions of high gradients of the flow variables.

The energy equation warrants particular mention. The compressible form of the energy equation was used for the present calculations and therefore, density was treated as a variable. It was calculated from the perfect gas equation of state

$$p = \rho RT$$

This method of calculating density is a departure from the previous methods in which the density is calculated using density correction equations. The present procedure makes the calculation of density more elegant and straight forward. Variations of the dynamic viscosity $\mu$ and the thermal conductivity $\kappa$ with temperature are calculated using Sutherland's formulas for viscosity and thermal conductivity. They are given below.

$$\frac{\mu}{\mu_{ref}} = \left(\frac{T}{T_{ref}}\right)^{3/2} \frac{T_{ref} + 110}{T + 110}$$

$$\frac{k}{k_{ref}} = \left(\frac{T_{ref}}{T}\right)^{3/2} \frac{T_{ref} + 195}{T + 195} \qquad (30)$$

Two methods were used for the numerical implementation of the procedure for obtaining compressible flow solutions.

The steps involved in the first method is illustrated by means of the flow diagram given in Figure 4 and may be summarized as follows:

1. Obtain a converged solution for an incompressible flow case (Mach number less than 0.2).

2. Store the solution variables on restart files in non-dimensional form.

3. Increase the inlet velocity by a small increment and repeat the solution procedure using variables stored in the non-dimensional form from the previous solution as the initial guesses; this will give a new set of non-dimensional variables to be stored on restart files.

4. Repeat steps 2 and 3 till the inlet velocity reaches the desired value in the subsonic compressible regime.

It should be noted that the non-dimensional form of the variables is particularly useful for their usage as starting values in the solution procedure. Since the solution proceeds in steps of small increments of the flow variables, faster convergence is achieved. The reason for the faster convergence may be due to the fact that the initial guesses for the flow variables are close to the true solution. Thus, special formulations for the density and pressure correction equations are avoided.

The second method was based on the use of the perfect gas equation of state in the differential form. The perfect gas equation of state may be differentiated to obtain an expression for the density change in terms of pressure and temperature. The resulting expression is

$$d\rho = \frac{dp}{RT} - \frac{\rho dT}{T} \tag{31}$$

The above form was used to calculate the change in density at every iteration stage. The new density was then calculated by adding this incremental change to the old value of the density. The advantage in using this method can be seen from the fact that the expression for density change involves the pressure change dp. Therefore, round-off errors may be smaller if this expression is used. It is also possible to control the change in density from iteration to iteration by means of an under-relaxation factor for density. The use of an under-relaxation factor for density was seen to improve convergence.

## BOUNDARY CONDITIONS

In the SIMPLE procedure the boundary conditions are applied by modifying the discretization equations for the boundary cell control volumes. The no slip condition is applied for the velocities at the solid walls; at the axis of symmetry the normal derivatives of the flow variables except the radial velcity are set equal to zero. The radial velocity itself must be set equal to zero at the axis of symmetry in order to avoid multiple values of the variable there. The present code (ECFLOW) has options for three types of boundary conditions for the energy equation. The Dirichlet boundary condition is used for cases where the wall temperature is specified; the Neumann boundary condition is used for adiabatic wall cases and the Robbin boundary condition is used for cases with prescribed wall heat flux. The boundary conditions for the k and the $\varepsilon$ equations are applied by means of wall functions which are used to avoid the use of extremely fine computational mesh near the wall. The rationale for the use of the wall functions is given by Chieng and Launder*.

## RESULTS AND DISCUSSION

### Turbulence Models

An exhaustive study of turbulence models applicable to low turbulence Reynolds number regions and recirculating flow regions have been conducted. Models proposed by other investigators as well as modifications appropriate to the present problem have been tried. The influence of the various terms in the turbulence models were investigated from the point of view of their physical realism and their ability to improve predictions of the flow regimes encountered in combustion chambers.

The present study was conducted with the primary goal of predicting recirculating flowfields which are present in many internal flows associated with propulsion systems. The need for reexamining the turbulence models for this type of flowfield arises from the fact that the turbulence models rely heavily on empiricism. One severe drawback of the existing turbulence models is that they have been tested only against simple flows such as free jets and boundary-layers for which experimental data existed at the time these models were developed. The difficulty in obtaining turbulence and mean flow data in recirculating flowfields is well recognized. Hence the built-in bias in the models towards satisfying free-jet flow and boundary-layer flow phenomena.

Reliable and accurate experimental data for flowfields with high levels of turbulence are beginning to appear in literature[28]. The advances in non-intrusive optical flow diagnostics techniques are the major reason for this development. The present study is an attempt to use the recently available experimental data to evaluate the turbulence models that are currently being used. modifications are suggested, where appropriate, to improve the predictions.

The inviscid core that is present at the entrance of a sudden pipe

expansion is a region of low turbulent Reynolds number. However, no turbulence model exists to adequately treat this region. Hanjelic and Launder have specifically stated that their low turbulence Reynolds number model is not suitable for free-shear flows. Attempt was made in the present study to obtain a suitable form for the low turbulence Reynolds number model that can be used in the inviscid core region. Hanjelic and Launder used the term $f_\epsilon$ given by Eq. 16 in their calculations. However, calculations performed with the sign changed in the expression (so that $F_\epsilon$ becomes greater than 1) showed better agreement with the data for the turbulence energy decay along the center-line. This difference in the decay rate of the turbulence energy, as compared to the decay of grid turbulence may be explained on the grounds that a region of high turbulence surrounds the inviscid core and it is likely to exert significant influence on the evolution of turbulence within the inviscid core. The effect of the influence of the outer region on the flow within the inviscid core may be illustrated with the help of the sketches given in Figure 5. In all the three cases the incoming flow is assumed to be uniform (top-hat shape) with low levels of turbulence. Case (a) is a free jet in a quiscent medium. Case (b) is the flow from a hole-in-a-disk arrangement. Case (c) is the flow in a sudden pipe expansion.

The turbulence models that can be found in the literature do not take due account of the influence of the boundary conditions on the evolving flow. For example, will the decay of turbulence in the inviscid core region be the same in all the three cases illustrated in Figure 5? The present study indicates that the presence of the boundaries must be taken into consideration, not just as a local influence, but in a more global manner.

The streamline curvature modifications of Leschziner and Rodi did not improve the predictions in the recirculating flow region. The reason for this

behavior may lie in the fact that many sweeping assumptions were made in formulating this model. Omitting the term $U_r/r$ without sound justification is one example where the assumptions are not based on valid argument. However, when this term was included in the calculations, it was seen that the solution did not converge.

The present study is inconclusive as far as the modifications to the turbulence models are concerned. Even though it has been established that the existing models are not adequate to treat turbulence in recirculating flows, certain general directions towards improving these models can be suggested based on the present study. A definite form for the improved model with the values of the empirical constants requires much further study. More experimental data on highly turbulent recirculating flows are immediately needed to correlate the models with experiments.

Compressible Flow Calculations

Some results from a compressible flow case with a nominal (inlet) velocity of 150 m/s are presented in Figures 6-8. The static temperature of the air at the inlet for this case was 300 °K. The temperature boundary conditions used for this case are insulated side (East) wall and constant temperature top (North) wall. Therefore, the temperature contours in this case resulted solely from compressibility effects. Contour plots of vorticity, temperature and turbulent kinetic energy are shown in these figures. All the plots are given in the non-dimensional form by using appropriate non-dimensionalizing parameters.

The vorticity contours in Figure 6 are clustered near the entrance around the step where the diameter changes from the smaller to the larger. Physically this region represents the boundary region between the inviscid core and the recirculation region. It is interesting to note that the recirculation region

is one of low vorticity; therefore, this region behaves like a free vortex.

The temperature contours are shown in Figure 7. The high temperature region lies downstream of the recirculation region and it can be seen that the rise in temperature in this region is caused by the deceleration of the flow because of the expansion and the resulting rise in static temperature. There exists a large region close to sudden expansion plane where the temperature is more or less uniform. This rapid attainment of uniformity in temperature is encouraging because it is one of the qualities that one looks for in a combustor. However, it should be cautioned that the temperature distribution in a reacting flow will depend also on the fuel-air distribution, and therefore, on the location and configuration of the fuel injectors. Another factor that will become important while considering temperature distribution in reacting flows is the wall boundary condition. As the heat transfer to the wall increases, it is expected that the region of uniform temperature seen in Figure 7 will shrink in size and move towards the center of the chamber.

The contours of turbulent kinetic energy are shown in Figure 8. Its maximum is seen to be at a downstream distance of about one diameter. Radially, the maximum occurs at the same distance as the smaller diameter of the inlet. Approximately this is the region where the expanding forward flow region and the recirculation region meet. Therefore, this constitutes the shear layer and it is natural to expect the highest levels of turbulence to occur in this region. The usefulness of the contour plots of the flow parameters to a designer can be easily seen from this figure. For the fuel air to mix to the maximum extent the fuel must enter the chamber from the periphery of the inlet.

## CONCLUSIONS

The present study has resulted in a computer code capable of predicting recirculating compressible flow in axisymmetric ducts. Some of the deficiencies of the existing turbulence models are identified in the present study and modifications are suggested. Very useful information from the compressible flow solution that could be of direct use to the designer is obtained from the present study.

In addition to improving the fluid dynamic model, several coding improvements were implemented, some of which are discussed below.

The computer code was extensively modified to make input and output more efficient. Presently all the data are input using a separate input file rather than specifying them within the program by means of source statements. This has made it possible to reduce the number of compilations necessary while conducting parametric study to see the influence of the various parameters in the governing equations. Another significant modification that was incorporated into the program is the provision for temporary storage and retrieval. This feature is very useful when the compressible flow equations are being solved.

While the program was being tested it was noticed that it took several iterations for some of the residual source sums to attain values below the ones specified as convergence criteria. As a remedy the use of double precision arithmetic was tried and this resulted in convergence with less number of iterations. All the calculations in the program presently use double precision arithmetic. It is felt that as the complexity of the calculations increase as a result of additional equations that must be solved while solving more complex flowfields, double precision arithmetic will become essential in order to preserve accuracy.

All the modifications to the program has been profusely documented

internally with the help of comment statements in order to aid other users in getting easily acquainted with the program. Other users can now run the program with a minimum investment of their time. The extensive internal documentation also facilitates future changes with little effort. Thus, calculations with a different chemical species arising, for example, from the use of fuel-air mixture, is straight forward and easy to implement. Or, as another example, a different turbulence model may be attempted by incorporating it as another option.

## REFERENCES


1. Launder, B. E. and D. B. Spalding, Mathematical Models of Turbulence, Academic Press, London, 1972.
2. Bradshaw, P., Ferriss, D. H. and Atwell, N. P., "Calculation of Boundary Layer Development Using the Turbulent Energy Equation," J. Fluid Mech., vol.28, 1967, pp. 593-616.
3. Harlow, F. H. and Nakayama, P. I., "Transport of Turbulence Energy Decay Rate," Los Alamos Sci. Lab. Rep. LA 3854, 1968.
4. Lumley, J. L., and Khajeh Nouri, B. J., "Computational Modeling of Turbulent Transport," Adv. Geophys. Vol. 18A, 1974, pp. 169-192.
5. Wilcox, D. C. and Rubesin, M. W., "Progress in Turbulence Modeling for Complex Flow Fields including the effect of Compressibility," NASA TP 1517, 1980.
6. Gibson, M. M. and Rodi, W.,"A Reynolds Stress Closure Model for Turbulence Applied to the Calculation of a Highly Curved Mixing Layer," J. Fluid Mechanics, Vol. 103, 1981.
7. Chien, K. Y., "Predictions of Channel Boundary-Layer Flows with a Low-Reynolds-Number Turbulence Model," AIAA J., Vol. 20, 1982, pp. 33-38.
8. Bywater, R. J., "Velocity Space Description of Certain Turbulent Free Shear Flow Characteristics," AIAA J., Vol. 20, No. 6, June 1982.
9. Chieng, C. C. and Launder, B. E., "On the Calculation of Turbulent Heat Transport Downstream from an Abrupt Pipe Expansion," Numerical Heat Transfer, 3, pp. 189-207, 1980.
10. Hanjelic, K. and Launder, B. E., "Contribution towards a Reynolds-stress Closure for Low Reynolds-number Turbulence," J. Fluid Mech., vol. 74, 1976, pp. 593-610.
11. Leschziner, M. A. and Rodi, W., "Calculation of Annular and Twin Parallel

Jets Using Various Discretization Schemes and Turbulence-Model Variations," J. Fluids Engng., 103, A352, 1981.

12. Jones, W. P. and Launder, B. E., "The Prediction of Laminarization with Two-Equation Model of Turbulence," Intl. J. Heat and Mass Transfer, Vol. 15, 1972, pp. 301-304.

13. Patankar, S. V. and Spalding, D. B., "A Calculation Procedure for Heat, Mass and Momentum Transfer in Three-Dimensional Parabolic Flows," Int. J. Heat Mass Transfer, vol. 15, 1972, pp. 1787-1806.

14. Harlow, F. H. and Welch, J. E., "Numerical Calculation of Time-dependent Viscous Incompressible Flow," Phys. Fluids, Vol. 8, 1965, pp. 2182-2189.

15. Raithby, G. D., "Skew Upstream Differencing Schemes for Problems involving Fluid Flow," Computer Methods in Applied Mechanics and Engineering Vol. 9, 1976, pp. 153-164.

16. Leonard, B. P., "Stable and Accurate Convective Modeling Procedure Based on Quadratic Upstream Interpolation," Computer Methods in Applied Mechanics and Engineering, Vol. 19, 1979, pp. 59-98.

17. Krishnamurthy, L. and Park, S. O. "Streamline Curvature Effects in Confined Isothermal Recirculating Flowfields Behind an Axisymmetric Bluff Body: Numerical Calculations with the k- Turbulence Model," Fourth Symposium on Turbulent Shear Flows, Karlsruhe, F. R. Germany, September 1983.

18. Gosman, A. D. and Ideraih, F. J. K., "TEACH-2E: A General Computer Program for Two-Dimensional Turbulent Recirculating Flows," Report, Dept. of Mech. Eng., Imperial College, 1976.

19. Lilley, D. G. and Rhode, D. L. "A Computer Code for Swirling Turbulent Axisymmetric Recirculating Flows in Practical Isothermal Combustor Geometries," NASA-CR-3442, 1982.

20. Boray, R. S. and Chang, C., "Flow Studies of Dump Combustors," Fifth International Symposium on Airbreathing Engines," Bangalore, India, February 1981.

21. Sindir, M. M. and Harsha, P. T., "Assessment of Turbulence Models for Scramjet Flowfields," SAI Rept. No. 82-038-CHA, 1982.

22. Harsh, W. H., "Numerical Modeling of Ramjet Combustors," Air Force Aero Propulsion Lab. Report AFWAL-TR-82-2113, Wright Patterson Air Force Base, 1983.

23. Isaac, K. M., "Computational Study of Ramjet Combustor Flowfields," AFOSR/SCEEE Summer Faculty Research Program Report, 1984.

24. Tennekes, H. and Lumley, J. L., A First Course in Turbulence, The MIT Press, 1972.

25. Batchelor, G. K. and Townsend, A. A., "Decay of Isotropic Turbulence in the Final Period," Proc. Roy. Soc. A 194, 1948.

26. Bradshaw, P., "Effects of Streamwise Curvature on Turbulent Flows," AGARDograph No. 196, 1973.

27. Patankar, S. V., Numerical Heat Transfer and Fluid Flow, Hemisphere, Washington, DC, 1980.

28. Craig, R. R., Nejad, A. S., Hahn, E. Y., and Schwertzkopf, K. G., "A General Approach for Obtaining Unbiased LDV Data in Highly Turbulent Non-reacting and Reacting Flows," AIAA-84-0366, AIAA 22nd Aerospace Sciences Meeting, 1984.

## APPENDIX

The governing equations for the conservation of mass, momentum, energy, the turbulent kinetic engery and the energy dissipation rate can be cast in the general form:

$$\frac{1}{r}\left[\frac{\partial}{\partial x}(\rho u r\phi) + \frac{\partial}{\partial r}(\rho v r\phi) - \frac{\partial}{\partial x}\left(r\Gamma_\phi \frac{\partial \phi}{\partial x}\right) - \frac{\partial}{\partial r}\left(r\Gamma_\phi \frac{\partial \phi}{\partial r}\right)\right] = S_\phi \qquad (1)$$

where $\phi$ stands for the variables shown in the table. The forms for the source term $S_\phi$ are also given in the table.

Table 1. The Form of the Source Term in the General Equation for $\phi$ (Eq. (1))

| $\phi$ | $S_\phi$ |
|---|---|
| u | $-\frac{\partial p}{\partial x} + S^u$ |
| v | $-\frac{\partial p}{\partial r} + \frac{\rho w^2}{r} - \frac{2\mu v}{r^2} + S^v$ |
| w | $-\frac{\rho v w}{r} - \frac{w}{r^2}\frac{\partial}{\partial r}(r\mu)$ |
| h | 0 |
| k | $G - C_D \rho \varepsilon$ |
| $\varepsilon$ | $(C_1 \varepsilon G - C_2 \rho \varepsilon^2)/k$ |

The quantities $S^u$, $S^v$ and G appearing in the source terms have the following meaning.

$$S^u = \frac{\partial}{\partial x}\left(\mu \frac{\partial u}{\partial x}\right) + \frac{1}{r}\frac{\partial}{\partial r}\left(r\mu \frac{\partial v}{\partial x}\right) \qquad (2)$$

$$S^v = \frac{\partial}{\partial x}\left(\mu \frac{\partial u}{\partial r}\right) + \frac{1}{r}\frac{\partial}{\partial r}\left(r\mu \frac{\partial v}{\partial r}\right) \qquad (3)$$

$$G = \mu\left[2\left\{\left(\frac{\partial u}{\partial x}\right)^2 + \left(\frac{\partial v}{\partial r}\right)^2 + \left(\frac{v}{r}\right)^2\right\} + \left(\frac{\partial u}{\partial r} + \frac{\partial v}{\partial x}\right)^2 + \left\{r\frac{\partial}{\partial r}(w/r)\right\}^2 + \left(\frac{\partial w}{\partial x}\right)^2\right] \qquad (4)$$

| $C_\mu$ | $C_1$ | $C_2$ | $C_D$ | $\sigma_k$ | $\sigma_\varepsilon$ |
|---|---|---|---|---|---|
| 0.09 | 1.44 | 1.92 | 0.96 | 1.0 | 1.2174 |

Table 1. Constants used in the k - ε Turbulence Model

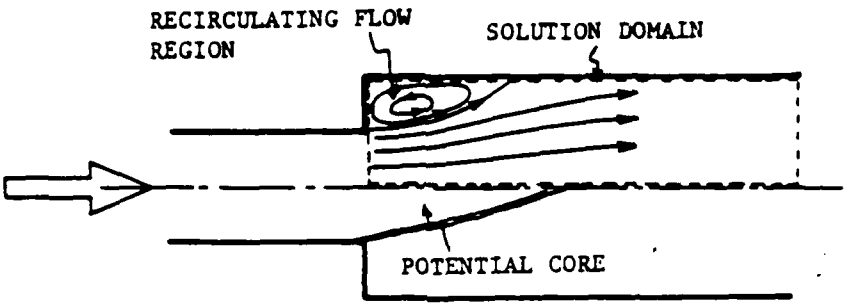



Figure 1. Schematic of Dump Combustor

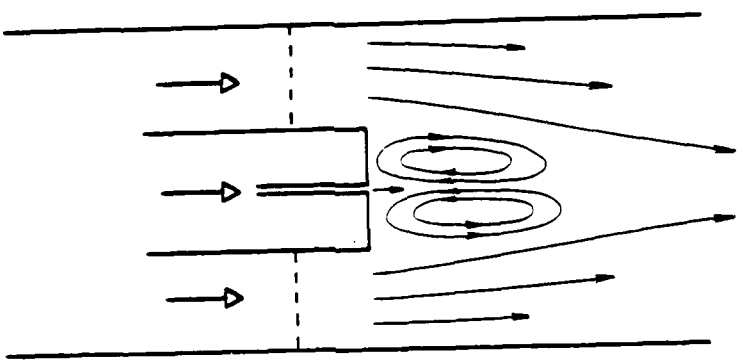


Figure 2. Schematic of Center Bluff Body Combustor

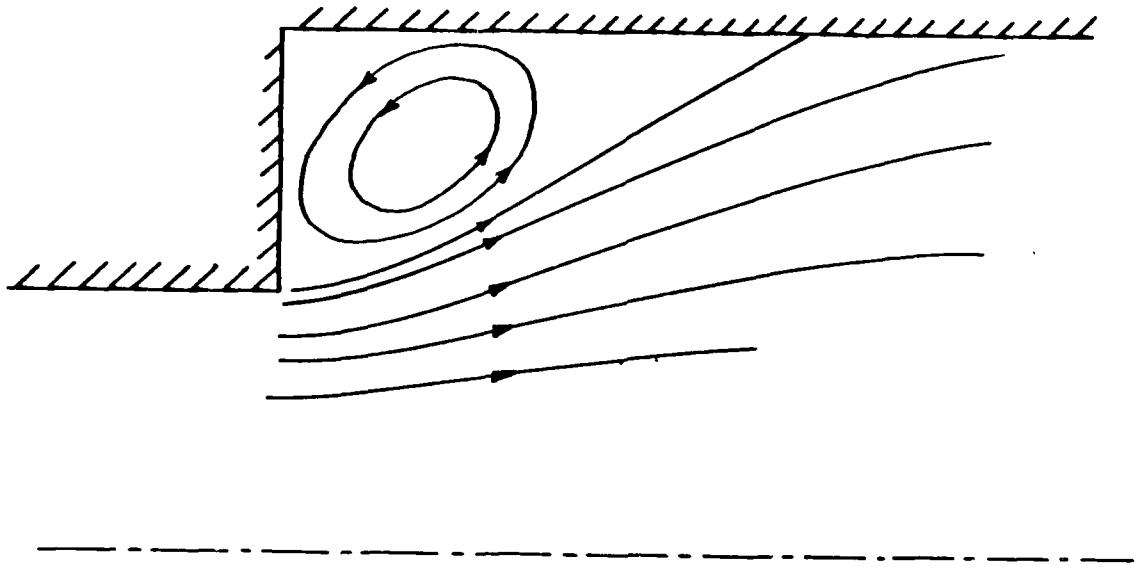


Figure 3. SCHEMATIC OF THE DUMP COMBUSTOR SHOWING THE RECIRCULATION REGION WHERE $U_r/r$ MAY NOT BE NEGLIGIBLE

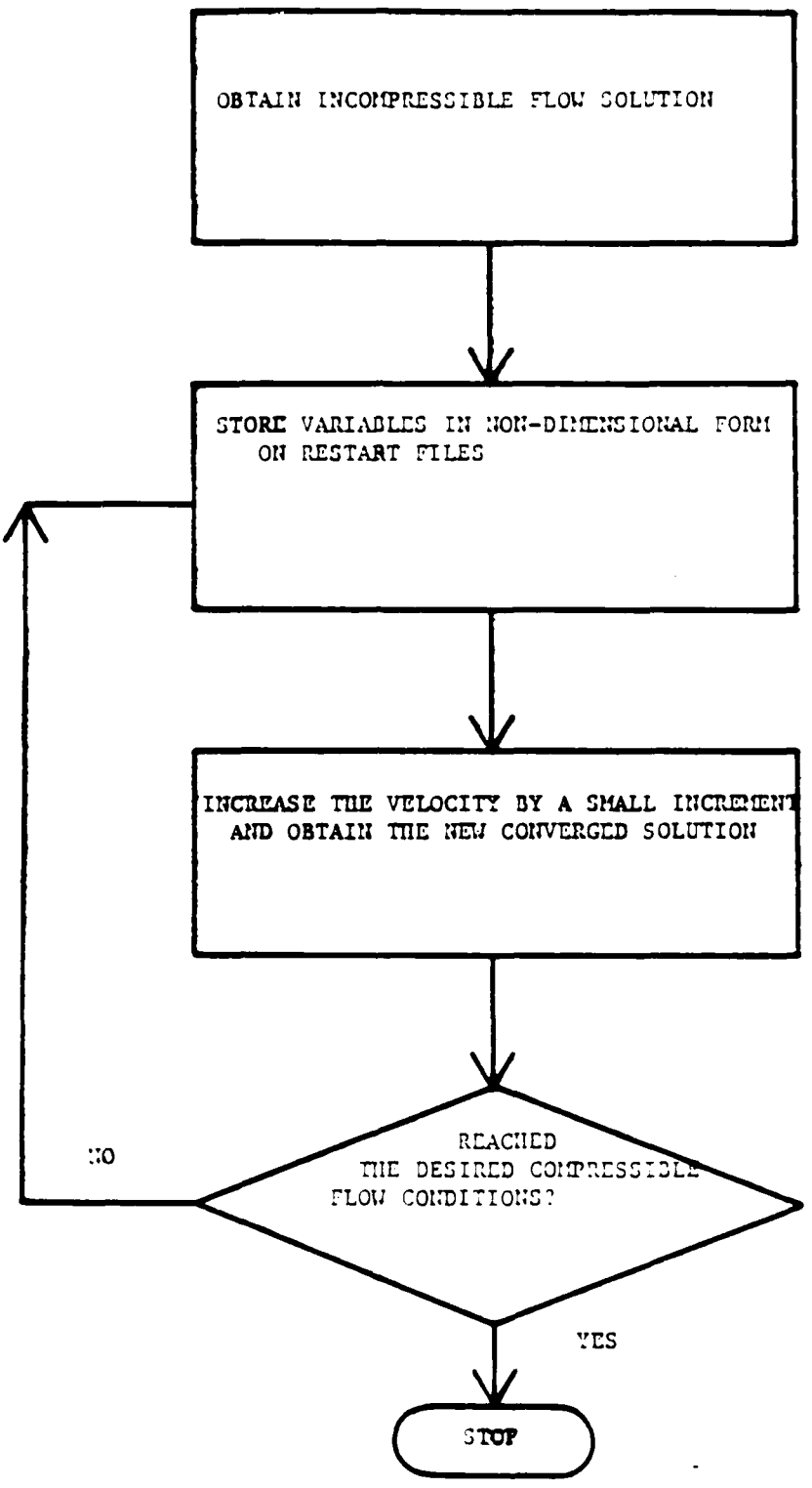



FIGURE 4 . SOLUTION PROCEDURE FOR COMPRESSIBLE NAVIER-STOKES EQUATIONS.

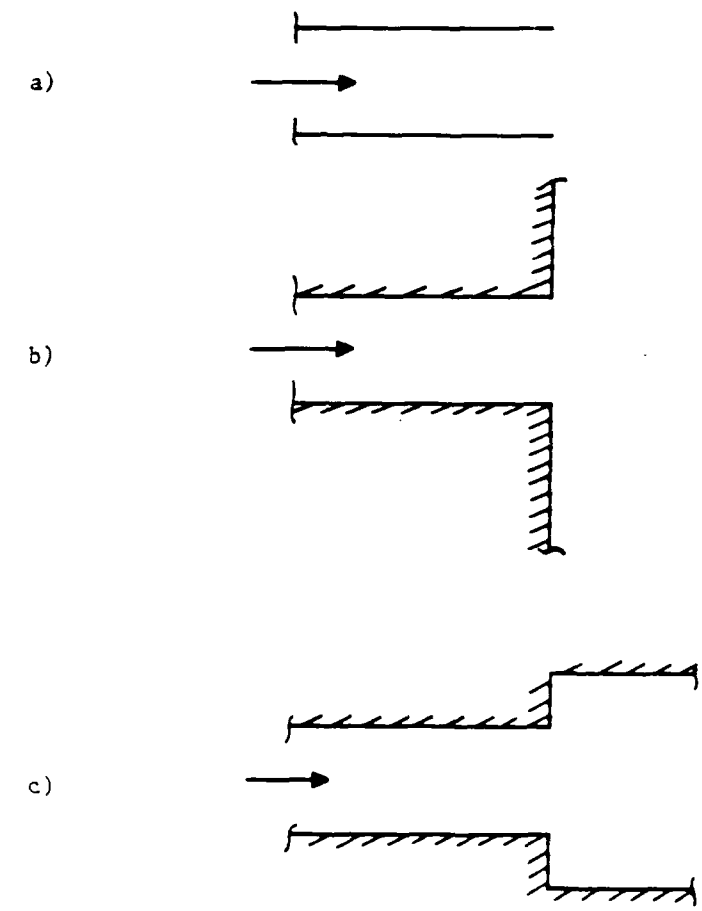
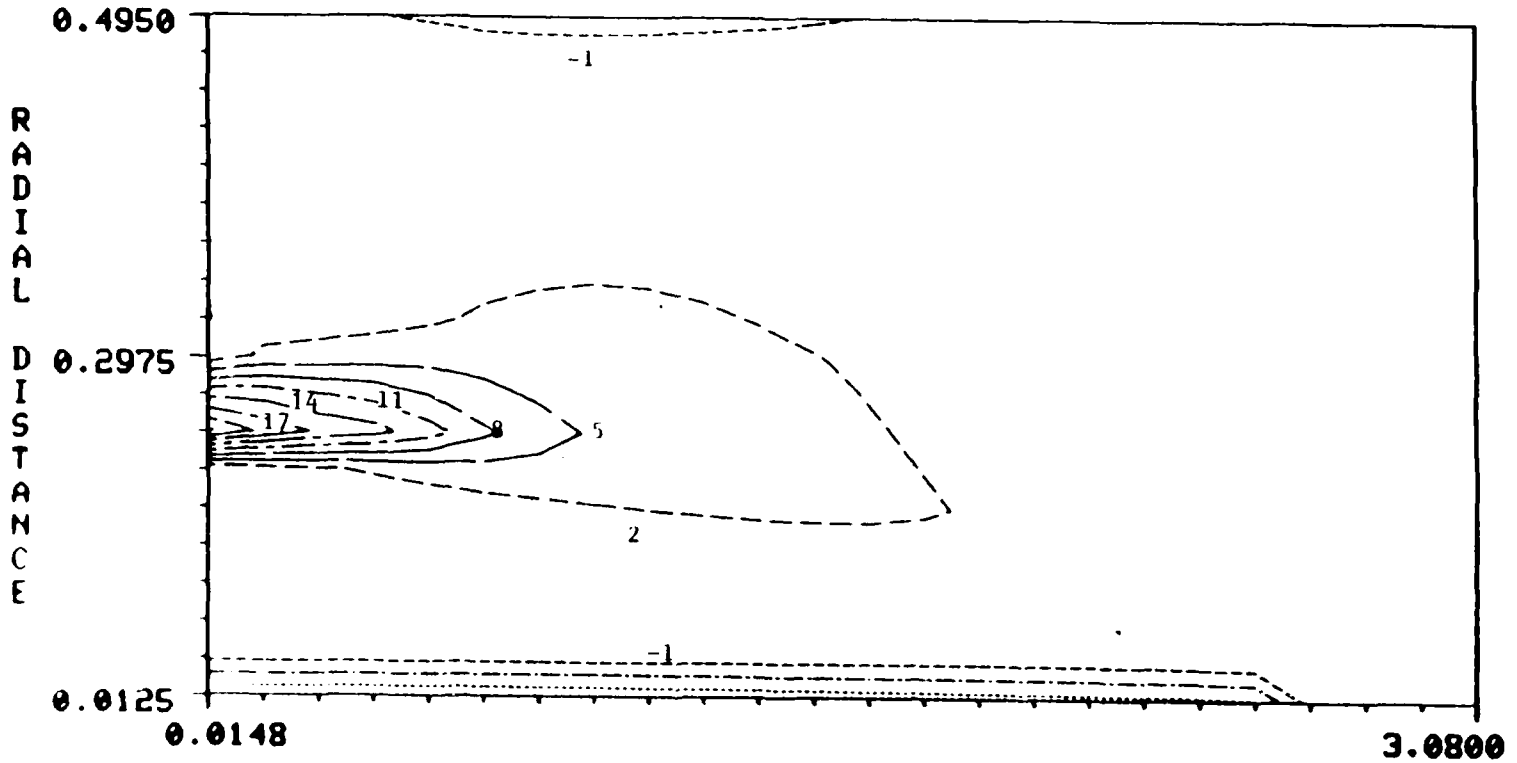



Figure 5. Different Jet Exit Conditions

a) Free Jet in Quiscent Medium

b) Hole-in-a-disk arrangement

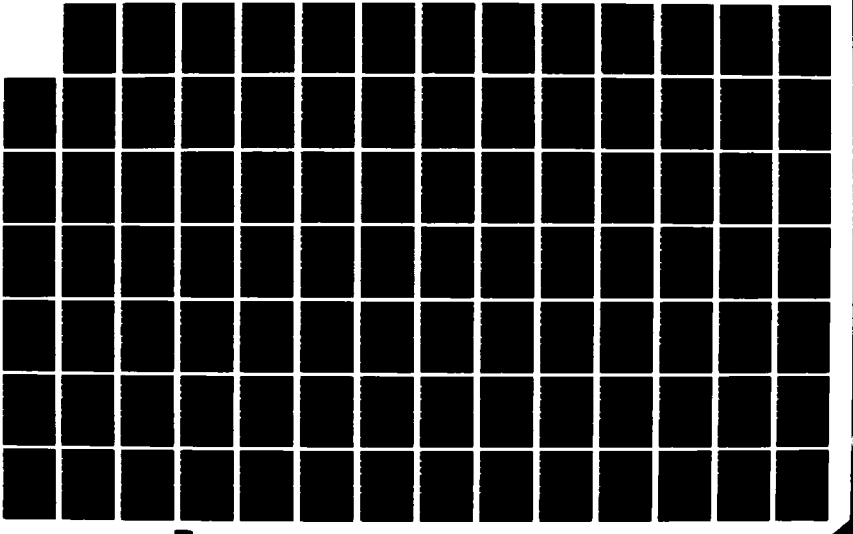
c) Confined Jet

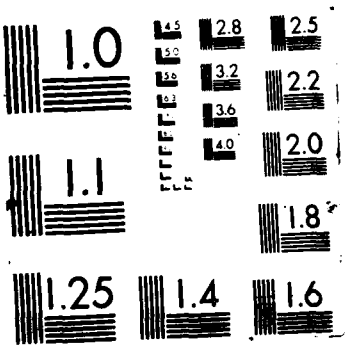


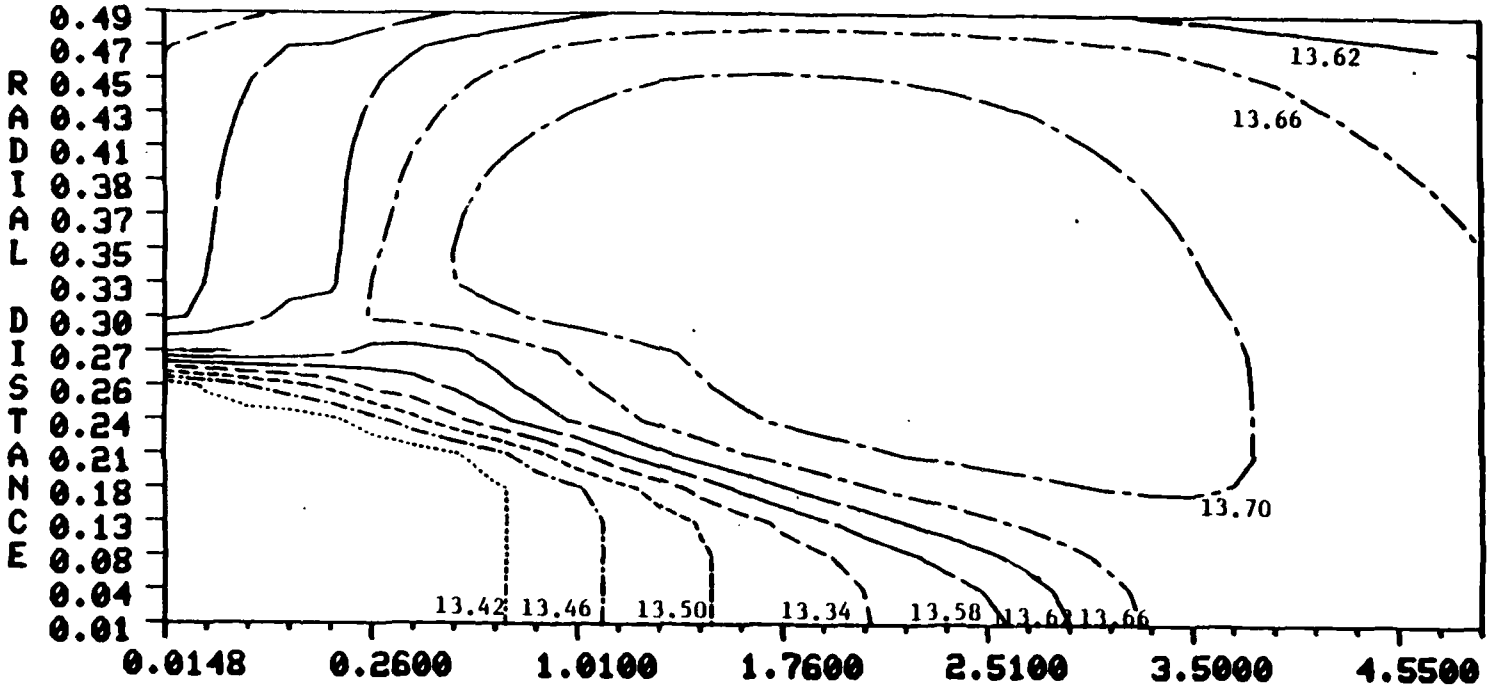

Axial Distance (Diameter)

Figure 6. Non-dimensional Vorticity Contours

AD-A186 490 UNITED STATES AIR FORCE RESEARCH INITIATION PROGRAM 06/11
1984 RESEARCH REPORTS (U) SOUTHEASTERN CENTER FOR
ELECTRICAL ENGINEERING EDUCATION INC S W D PEELE
UNCLASSIFIED MAY 86 AFOSR-TR-87-1721 F49620-82-C-0035 F/G 15/1 NL




1.0
1.1
1.25
1.4
1.6
1.8
2.0
2.2
2.5
2.8
3.2
3.6
4.0




Axial Distance (Diameters)

Figure 7. Non-dimensional Temperature Contours

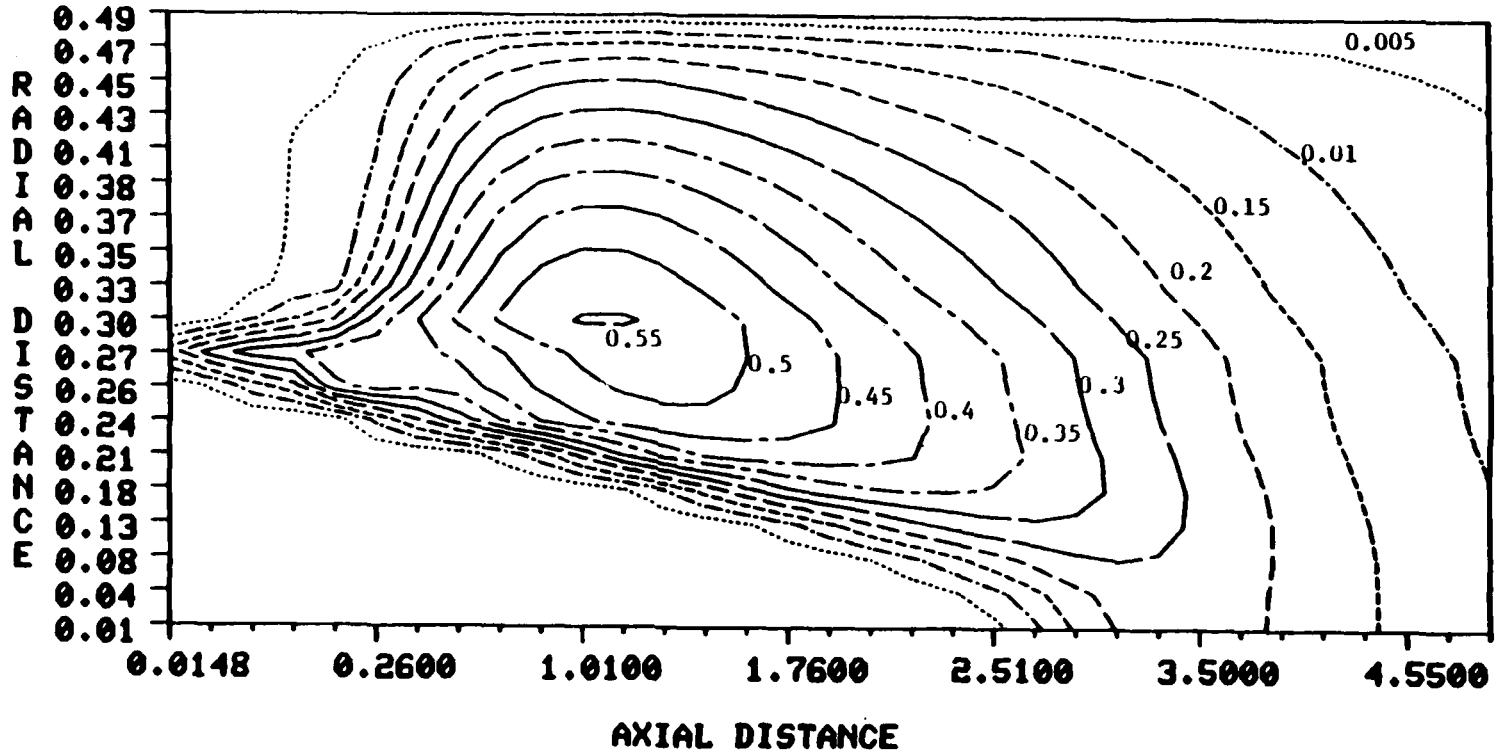



Figure 8. Non-Dimensional Turbulent Energy Contours

1985 RESEARCH INITIATION IN SCIENCE AND ENGINEERING PROGRAM

Sponsored by the

AIR FORCE OFFICE OF SCIENTIFIC RESEARCH

Conducted by the

SOUTHEASTERN CENTER FOR ELECTRICAL ENGINEERING EDUCATION

FINAL REPORT

# FREE STREAM TURBULENCE EFFECTS ON TURBULENT HEAT AND MOMENTUM TRANSFER


| | |
|---|---|
| Prepared by: | Dr. Paavo Sepri<br>and Mr. Baek Youn |
| Academic ranks: | Associate Professor<br>and Graduate Assistant |
| Department and University: | School of A.M.N.E.<br>University of Oklahoma |
| USAF Laboratory Location: | Air Force Wright Aeronautical Laboratories<br>Aero-Propulsion Laboratory<br>Turbine Engine Division<br>Components Branch |
| USAF Research Contacts: | Dr. Richard Rivir<br>and Mr. Charles D. MacArthur |
| Date: | August 31, 1985 |
| Contract No.: | F49620-82-C-0035 |

# FREE STREAM TURBULENCE EFFECTS ON TURBULENT HEAT AND MOMENTUM TRANSFER

By

Paavo Sepri and Baek Youn

## ABSTRACT

Attention is focused on the computational predictability of turbulent boundary layers influenced by free stream turbulence (FST). One practical application lies in the area of improving turbine blade performance and enhancing the attendant lifespan. The approach herein has consisted of further scrutiny of recently published data, improved modeling of turbulent fluxes, and computations with the code STANCOOL. Four novel results have been achieved which are presented for the first time in this report. First, an analytical representation is proposed which is shown to approximate well the mean profiles of velocity and temperature throughout a turbulent boundary layer. A triple-deck exponential function is demonstrated to approximate laminar as well as turbulent profiles by appropriate changes of the parameters. FST effects are incorporated into the model by explicit variations in the coefficients. Second, through observations and fitting of data, the turbulent boundary layer is shown to be composed of three layers, for which length scales are proposed in a preliminary fashion. Third, by use of the observed triple exponential, a novel integro-differential model is proposed for the Reynolds stress and turbulent heat flux terms. Fourth, a remarkable analytical solution is found to describe a turbulent boundary layer for the case of a particular form for the Reynolds stress. Analytical expressions are derived for the turbulent Prandtl number profile for two limiting cases. Modifications of and computations with the code, STANCOOL, demonstrate improved agreement with available data for the case of a flat plate.

## ACKNOWLEDGEMENTS

The authors gratefully acknowledge the opportunity and financial support extended to them by the Air Force Systems Command, the Air Force Office of Scientific Research, and the Southeastern Center for Electrical Engineering Education. This investigation was conducted under Contract F49620-82-C-0035. The Graduate College of the University of Oklahoma has also contributed to this investigation through cost-sharing of the expenses. Finally, the authors wish to thank Ms. Lynn Crussel for expeditious typing of the manuscript.

# 1.0 INTRODUCTION

## 1.1 Background

The transport of mass, momentum, and energy across turbulent boundary layers is a subject that is rich in practical application, and consequently it has received considerable attention in several disciplines of science and engineering. The present investigation has been motivated primarily by the continuing need for improvements in computational tools used for predicting heat transfer in the complicated aerothermal environment of turbine engines. Improvements in state-of-the-art engine design and efficiency will rely increasingly on computer codes which can predict alterations in performance and turbine blade cooling requirements under adverse thermal conditions. One goal is to increase the lifespan of turbine blades while minimizing the auxiliary power needed to cool the components effectively. For this purpose it is necessary to have accurate knowledge of heating distributions on the blade surfaces under varying operating conditions.

The present investigation is in continuation of the work initiated in 1984 by P. Sepri under the USAF-SCEEE Summer Faculty Research Program, which was conducted at the Aero-Propulsion Laboratory at Wright-Patterson Air Force Base. The final report [1] for that research, and the ensuing proposal [2] for the present study, may serve as additional background references. The particular issue under investigation concerns the increase in heat transfer that is observed to occur in turbulent boundary layers which are subjected to elevated levels of free stream turbulence (FST). Clearly, the gaseous flow around turbine blades contains a high degree of FST owing to the high mass flux which is forced through confined spaces obstructed by a sequence of engine components. The actual flow in the engine is further complicated by several factors, among which are: three dimensional mean flow, rotational

effects, non-equilibrium turbulence, transonic flow effects, corner flow interactions, strong acoustic coupling, and possibly incomplete combustion which influences fluid transport properties as well as temperature distributions. Despite the best of attempts, it is currently not possible to claim a computational capability which addresses all of these factors simultaneously and accurately.

Recent descriptions of FST effects on the structure of heated turbulent boundary layers have been reported by Simonich and Bradshaw [3], Bayley and Priddy [4], and Pedisius, et al. [5]. Additional background material may be obtained from References [6-14]. In the present report considerable reference is made to the excellent experimental data published in the past few years by Blair [15-21]. His measurements include extensive turbulence statistics and profiles in the boundary layer adjacent to a heated flat plate, for which the FST is varied parametrically. One of the objectives of Blair's experimentation has been to produce a detailed and reliable characterization of FST effects on boundary layers of a fundamental type which may help in understanding the actual turbine flow environment.

With the availability of Blair's data, it has been of interest to compare his results with predictions from computer codes. Among the many codes developed in the industry for the purpose of calculating turbulent boundary layers [22], the one utilized for this investigation is STANCOOL, which is a modified version of STAN5 [23,24] developed by Crawford and Kays. This code, as well as many others, introduces a turbulent Prandtl number profile throughout the boundary layer, through which turbulent heat transport is likened to the relatively more studied momentum transport in the manner of the Reynolds analogy. The deviation in the Reynolds analogy is often described at a solid surface by the local ratio of Stanton number to half of the skin

friction coefficient, $2S_t/C_f$, which is termed the Reynolds analogy factor, with unity denoting a perfect analogy. Earlier investigations [10-14] have conflicted in their reports of the dependence of turbulent heating on the level of FST, some even claiming no effect. More recent data [3-5,18] indicate that the Reynolds analogy factor increases with increasing FST intensity.

Upon the availability of Blair's data, MacArthur [25] undertook a preliminary evaluation of the predictive capability of two options in STANCOOL. These options are comprised of a standard mixing length model and a model incorporating the turbulence kinetic energy equation [23]. Although the comparisons yielded favorable results in some cases, significant departures were noted in other cases in two respects; namely, the onset and duration of transition and the level of heating with increasing FST. Unexpectedly, MacArthur's comparisons revealed that occasionally the two computational options agreed with each other better than either did with the data. While the mixing length model does not provide for a mechanism for FST effects, it was anticipated that the kinetic energy option would introduce these effects through the external boundary condition. MacArthur's observations are also supported by the work of Winstanley, et al. [26].

Sepri and Ebert [1] continued MacArthur's initiative with the objective of seeking a turbulence model that reflects an improved prediction of FST influence on turbulent transport through the boundary layer. A preliminary turbulence model based on the work of Miyazaki and Sparrow [27] was utilized with the result of improved comparison with Blair's data. During the course of investigation, novel observations were made concerning an exponential wake structure in the turbulent boundary layer, which appeared only at the higher levels of FST.

Although the results reported by Sepri and Ebert were promising, the

preliminary model was clearly an oversimplification of a complicated phenomenon. With only one adjustable parameter in the Reynolds stress, it was not possible to obtain simultaneously a good match of the mean velocity profile as well as the skin friction variation along the wall. It became clear that the FST influenced both the wake region and the wall region in separate ways. These results and observations have lead to the present investigation, in which further improvements are sought.

## 1.2 Objectives

With the observation that FST influences the wall region as well as the wake region, it has been proposed [2] to extend the preliminary model to account for effects which were initially excluded. The study was to include five objectives, which have been addressed in phases.

First, reconsideration of the FST model used in 1984 has suggested a refinement based on the observation that inclusion of the transverse velocity at the edge of the boundary layer, $v_e$, would alter slightly two of the coefficients previously utilized in the model. Furthermore, a third coefficient would be introduced which would alter the Reynolds stress model in the wall region, as desired. The first objective has been to analyze this extended version of the mixing length model.

The second objective has consisted of further analysis of the exponential wake decay which was first observed in the 1984 investigation. It was evident from Blair's data [18] that the trigonometric wake function proposed by Coles [28] ceases to be an adequate representation of a turbulent boundary layer which is subjected to high levels of FST. However, the exponential function [1] serves very well under these conditions. It has been proposed [2] to analyze the turbulent boundary layer as being a composite structure consisting

of the exponential wake and a wall region, for which the functional description would be studied from Blair's data. In fact, it was suggested [2] that the turbulent boundary layer might consist of three layers, of which the outermost would comprise the decay into the free stream. In the present investigation it has emerged that the turbulent boundary layer indeed exhibits three layers, in which different physical mechanisms dominate.

The third objective has been to consider a simpler limiting case of the turbulent boundary layer with the hope of understanding better the mechanisms of transfer and to simplify the modeling of turbulent transport. The case of a uniform suction turbulent boundary layer has been suggested [2] for this purpose, in which all spatial dependences would occur in the transverse dimension (y) only. In this case all of the describing equations may be integrated once with no additional approximations required. The resulting equations describe flux relations explicitly, among which are the Reynolds stress and turbulent heat transfer terms. This objective has been met herein as a special case of a more general formulation.

The fourth objective has been to consider the energy equation in parallel with the momentum equation, with the intention of modeling the turbulent Prandtl number profile in the boundary layer. In this connection it was observed in Blair's data that his values for $P_{rt}$ declined rapidly at the boundary layer edge. An explanation was offered by Sepri and Ebert [1] in terms of channel flow contamination of the measurements. Another goal of the present investigation has been to search the literature for other evidence (or lack thereof) of such a decline in $P_{rt}$. Along with this task, it has been an objective to propose a model for the $P_{rt}$ profile which accounts for variations in FST.

The fifth objective has comprised of comparisons between updated mixing

length models in the code STANCOOL and Blair's data. Here, the hope has been that the effects of FST could be incorporated into an accurate, yet simple, model for the purpose of predicting the evolution of skin friction, heat transfer, and mean profiles in a turbulent boundary layer over a flat plate. Such a model has emerged from this investigation, and the comparison with the data is favorable.

## 1.3 Content

In order to meet the objectives, the investigation has proceeded in several phases. As an end result, three conclusions and descriptions have emerged which are in addition to the original objectives. These are: an analytical description which approximates the profiles of mean velocity and mean temperature throughout the turbulent boundary layer, an analytical solution to the turbulent boundary layer for a special Reynolds stress distribution, and a general formulation of Reynolds stress and turbulent heat transfer in terms of mean profiles. This last formulation does require additional closure assumptions, which are suggested for the present problem.

The first phase of investigation has consisted of further scrutiny of Blair's data with the objective of characterization of the wall layer so that the two layer modeling could commence. The details will be described later, but in essence Blair's data have revealed the existence of further exponential layers within the boundary layer, including the approach to the wall itself. These observations have been modeled in an analytical functional representation. The character of the exponential layers is seen to change explicitly with the variation of FST. The whole layer formula for the turbulent boundary layer is presented for the first time herein, and it is believed to be the most accurate representation of this kind yet achieved.

The exponential characterization of the mean profiles provides a direct means for modeling the Reynolds stress and turbulent heat transfer terms. Formal integrations of the momentum and energy equations yield formulas for these turbulent fluxes, as detailed in the subsequent section. Additional independent closure relations are required to complete the modeling, but these are directly observable from Blair's data.

After having achieved a formal relationship between the turbulent fluxes and the mean profiles, it has become apparent that a particular analytical solution may be obtained among the variables. This solution exists provided the Reynolds stress and the turbulent Prandtl number take on specific shapes, which incidentally, are not unreasonable. There are two primary benefits obtained from this analytical solution. First, it serves as an excellent check for any code such as STANCOOL. By altering only a few statements in subroutine AUX, the code may be run and checked against the analytical solution for the purpose of code verification. Second, the analytical solution displays explicitly the interrelationships among the various physical mechanisms at work in the turbulent boundary layer. In this sense, this analytical test solution serves a better function than does the originally proposed suction boundary layer. Here, the boundary layer grows in the downstream direction, and no artificial suction boundary condition is required. In addition, it is noted that no analytical solution is available for either the laminar boundary layer as described by the Blasius Equation or for the actual turbulent boundary layer. However, the analytical test case forms a remarkable middle ground between the two real flows.

Through analysis of the energy equation in parallel with the momentum equation, a formulation of $P_{rt}$ has been achieved which may be used for more general applications. By considering limiting forms of this formulation, a

model is proposed for comparison with Blair's data. It is clear from the relationships that $P_{rt}$ modeling in general can not be as simple as is often assumed in local gradient models. The results of $P_{rt}$ discussions in several references are summarized.

The last part of the present investigation involves comparisons of the latest STANCOOL computations with Blair's data for the case of vanishing pressure gradient. Recommendations are presented for further investigation.

## 2.0 FORMULATION

### 2.1 Describing Equations

The basic equations utilized for the computation of a turbulent boundary layer will be listed here as a beginning point for the discussion. The initial equations will be of sufficient generality to describe many boundary layer flows, while it is not considered appropriate to begin with complete generality. The equations listed here correspond to the ones utilized in STANCOOL, and the notation is standard although it differs somewhat from that which is used by Crawford and Kays in regard to enthalpy. In dealing with gaseous boundary layers which involve significant heat transfer it is important to account for density variations throughout the boundary layer, and secondly to recognize that molecular transport coefficients depend on the local temperature. For turbulent boundary layers, the possibility of significant density fluctuations raises the unfortunate complexity of additional correlations involving this density. There are two accepted ways to treat the density variations; one is explicit, and the other is to use a mass averaged velocity decomposition, as has been introduced by Favre [29]. In accordance with the assumptions listed in the next section, the conservation of mass equation may be expressed as follows in the explicit method:

$$\frac{\partial}{\partial x_k} (\rho u_k + \langle \rho' u'_k \rangle) = 0 \qquad (1)$$

Here, the subscript, k, denotes the Einstein summation convention, and the angled brackets denote the averaging process resulting in correlations between the density fluctuations and the velocity fluctuations. The other variables, without the brackets, are understood to represent mean profiles. Since the

explicit averaging process introduces additional unknown density correlations (although they may in fact be negligible in some cases), the Favre type averaging results in less cumbersome expressions. Here, we define two new variables as follows:

$$m(t,x) = \rho u(t,x) \tag{2}$$

$$n(t,x) = \rho v(t,x) \tag{3}$$

The averaging process applied to the product form yields an alternative expression for the conservation of mass equation:

$$\frac{\partial}{\partial x}(m) + \frac{\partial}{\partial y}(n) = 0 \tag{4}$$

Here, the fluctuation averages vanish by construction:

$$\langle m' \rangle = 0 = \langle n' \rangle \tag{5}$$

Of course, the formalism still must retain the identities:

$$m = \rho u + \langle \rho' u' \rangle \tag{6}$$

$$n = \rho v + \langle \rho' v' \rangle \tag{7}$$

By utilization of mass averaging, the streamwise momentum equation in the boundary layer is:

$$\frac{\partial}{\partial x}(mu) + \frac{\partial}{\partial y}(nu) + \frac{\partial}{\partial x}(p) = \frac{\partial}{\partial y}\{\mu(\frac{\partial u}{\partial y}) - \langle n'u' \rangle\} \tag{8}$$

Here, additional assumptions have been made as listed in the next section. The mass averaged Reynolds stress term is $\langle n'u' \rangle$. In this boundary layer formulation, the momentum equation transverse to the plane of the wall reduces to the statement that the mean pressure varies only in the streamwise direction, and is prescribed by the flow external to the boundary layer. The equation for total energy, written in terms of stagnation enthalpy, H, is expressed in the boundary layer as:

$$\frac{\partial}{\partial x}(mH) + \frac{\partial}{\partial y}(nH) = \frac{\partial}{\partial y}\{\frac{\mu}{P_r}\frac{\partial}{\partial y}(H) - \langle n'H' \rangle + G\} \tag{9}$$

where: $P_r = \frac{\mu C_p}{k}$ (molecular Prandtl number)

$$H = h + \frac{1}{2}(u)^2$$

$$\langle n'H' \rangle = C_p \langle n'T' \rangle + u \langle n'u' \rangle$$

$$G = \left(1 - \frac{1}{P_r}\right) \frac{\partial}{\partial y} \left\{\frac{1}{2}(u)^2\right\}$$

It is also appropriate to record the thermal energy equation which is obtained by subtraction of the kinetic energy from the total energy equation. There results:

$$\frac{\partial}{\partial x}(mC_pT) + \frac{\partial}{\partial y}(nC_pT) = \frac{\partial}{\partial y}\left\{k \frac{\partial}{\partial y}(T) - C_p \langle n'T' \rangle + \Phi\right\} \qquad (10)$$

where: $\Phi$ denotes the viscous dissipation.

Finally, the equation of state for the gaseous flow is assumed to apply:

$$p = \rho RT \qquad (11)$$

## 2.2 Assumptions

For the sake of completeness, the major assumptions inherent in the above formulation will be recorded here.

(1) The turbulence is in steady state so that its statistics are stationary.

(2) The flow is statistically two dimensional so that there are no variations in the spanwise (z) direction. Furthermore, there is no mean flow in the spanwise direction.

(3) The standard boundary layer assumptions are invoked so that second derivatives in the x direction are neglected in comparison to those in the y direction.

(4) All terms in the y momentum equation are neglegible so that the pressure varies only in the x direction, to this order of approximation.

(5) The turbulent boundary layer is sufficiently near an equilibrium condition so that variations in turbulence structure in the x direction are negligible compared to those in the y direction.

(6) The velocity field is approximately solenoidal so that terms involving the second coefficient of viscosity in the momentum equation are negligible.

(7) Gravitational effects are negligible.

Later in the present investigation, the following additional assumptions will be employed:

(8) Density variations produce effects of secondary importance in the momentum equation.

(9) Thermal energy terms dominate the energy equation for the cases of interest. The flows under consideration here are low Mach number flows with relatively moderate heat transfer. In approximation, the contributions of turbulence kinetic energy, mean kinetic energy, and viscous dissipation are small in comparison to the thermal component. This is not to say that these energies are negligible in other equations of the hierarchy. For the sake of concreteness, the following typical magnitudes are noted:

$$\frac{C_p(T_w - T_e)}{\frac{1}{2}(u)^2} \approx (6000\ \frac{ft^2}{s^2 °R})\ \frac{(30°R)}{\frac{1}{2}(100\ \frac{ft}{s})^2} = 36$$

(9) Although $T'$ and $\rho'$ are significant in this problem their contributions to the averaged ideal gas equation are negligible:

$$p = \rho RT \qquad \text{where} \qquad \frac{\rho' T'}{\rho T} \approx o(10^{-4})$$

(10) The boundary layer in this investigation will be over a flat plate so that the pressure gradient vanishes.

## 2.3 Derivations

The equations listed previously suffer from the usual closure problem well known in the study of turbulence. Although there is an infinity of correlations that might be considered, the ones of immediate concern are the lowest order ones appearing in the momentum and energy equations; namely, $\langle n'u' \rangle$ and $\langle n'T' \rangle$. The momentum equation may be viewed as determining the evolution of the mean velocity field, provided the mean pressure, density and the Reynolds stress are supplied from other independent relations. Of course, proper boundary conditions also must be included in the solution procedure. Parallel statements may be made for the temperature field and the energy equation. The approach taken here will be to integrate Eqs. (8) and (9) formally to obtain explicit relations for the turbulent fluxes in terms of integrals and derivatives of the mean variables. This procedure does not constitute a closure scheme by itself, but it does provide a description of the unknown fluxes whenever the mean profiles can be accurately obtained from experiments, say. The method can be extended into a closure scheme, as discussed later, if appropriate additional information is inserted into the integrals of the mean profiles. It is believed that this closure method is introduced for the first time herein, although basic integral relations have appeared earlier [39].

Before embarking on the new approach, it is useful to mention the method used in the traditional mixing length hypothesis, which is also the first option provided in STANCOOL. Closure of the basic equations is effected by the following additional model:

$$\langle u'v' \rangle = \epsilon_m \frac{\partial u}{\partial y} \tag{12}$$

$$\langle v'T' \rangle = \epsilon_H \frac{\partial T}{\partial y} \tag{13}$$

where:
$$\epsilon_m = \ell^2 \left|\frac{\partial u}{\partial y}\right| \tag{14}$$

The turbulent Prandtl number is introduced as the ratio:

$$P_{rt} = \frac{\epsilon_m}{\epsilon_H} \tag{15}$$

With these relations the system of equations becomes closed, provided the mixing length, $\ell$, and $P_{rt}$ are specified throughout the boundary layer. Of course, the closure problem has simply been shifted to the specification of these alternative unknown functions. However, several heuristic arguments may be introduced which describe these variations in approximate ways. The objective of the present investigation is to seek formulations of $\epsilon_m$ and $P_{rt}$ which take into account the effects of FST.

The first step in the present method consists of a formal integration of the momentum (Eq. (8) and Eq. (4)) from the wall to an arbitrary location in the boundary layer. There results:

$$\langle n'u' \rangle = uu_y - \tau_w - u\left(n_w - \int_0^y m_x d\xi\right) - \int_0^y (mu)_x d\xi - p_x y \tag{16}$$

In this equation the subscripts x,y refer to partial differentiation in these directions respectively, and the subscript w refers to evaluation at the wall. Here, $\tau_w$ is the local shear stress at the wall, and $n_w$ is the local transpiration rate at the wall, which vanishes for an impermeable surface. Furthermore, $p_x$ denotes the imposed pressure gradient, which vanishes for the case of a flat plate in the absence of external influences. For the present investigation, the case of the flat plate will be assumed henceforth, and the plate will also be taken to be impermeable, although these restrictions pose

no difficulty if generalization is desired. The physical interpretation of Eq. (16) is worth mentioning: the various terms represent the several mechanisms for momentum flux. The constant of integration, $\tau_w$, obtained from evaluation at the wall, may be viewed as the net effect of momentum transfer resulting from the other terms. The equation may also be interpreted as a limiting form of the control volume approach, in which the change in streamwise momentum flux is evaluated across two transverse surfaces that are infinitesimally separated in x. The term involving $n_w$ describes the change in momentum by vertical convection through the top surface and also the wall in cases of nonvanishing transpiration. The Reynolds stress term and the molecular viscosity term represent the transfer of momentum through shearing action via turbulent and molecular motions respectively. Lastly, boundary layers with impressed pressure gradients will undergo a change in momentum flux as a result of the streamwise variation of pressure applied to the transverse control surfaces. It is important to note the satisfaction of the two limits of Eq. (16); namely, at the wall and at the boundary layer edge:

$$\mu\left(\frac{\partial u}{\partial y}\right)_{y=0} = \tau_w \tag{17}$$

Here, the Reynolds stress vanishes according to its limiting form near the solid surface. At the boundary layer edge:

$$\tau_w = u_e \int_0^\infty m_x dy - \int_0^\infty (mu)_x dy \tag{18}$$

The last equation is a particular form of the usual von Karman momentum integral equation. Here, at the boundary layer edge, it is assumed that the Reynolds stress vanishes along with the gradient of the mean velocity. If the mean velocity profile is specified in some manner, then Eq. (18) provides a means of determining the local wall shear. Alternatively, Eq. (18) provides a

constraint on parameters that are used in analytical approximations of the velocity field. It is interesting to note that a second integral constraint may be obtained by one further integration of Eq. (16), as follows (flat plate, impermeable wall):

$$uu = y\tau_w + \int_0^y \langle n'u' \rangle d\xi + \int_0^y \left[ \int_0^\xi (mu)_x d\zeta - u \int_0^\xi (m)_x d\zeta \right] d\xi \qquad (19)$$

In the limit as y exceeds the boundary layer edge, the left hand side becomes $uu_e$, which is prescribed by the external flow, and the right hand side approaches a finite form achieved through integration by parts and utilization of Eq. (18) for an expression for $\tau_w$. Thus, Eq. (19) constitutes an additional constraint that must be satisfied by the Reynolds stress and mean velocity profiles.

The energy equation may be integrated in a parallel fashion to provide an expression for the turbulent heat transfer term. The result is as follows:

$$\langle n'H' \rangle = q_w + \frac{\mu}{P_r} \frac{\partial H}{\partial y} + \left(1 - \frac{1}{P_r}\right) u \frac{\partial u}{\partial y} + H \int_0^y m_x d\xi - \int_0^y (mH)_x d\xi \qquad (20)$$

The physical interpretation of this equation is similar to that of the momentum equation, except that Eq. (20) describes the various mechanisms of heat and kinetic energy fluxes. If the mean velocity and mean temperature profiles were known, say by experimental means, then Eq. (20) could be used to calculate the turbulent heat flux. With turbulent heat and momentum fluxes thus determined, the turbulent Prandtl number, $P_{rt}$, may be directly calculated by an appropriate ratio obtained from the two.

Since no additional information has been introduced into the above discussion, it now remains to formulate a closure scheme based on these integral equations. This scheme relies on observations obtained from Blair's data, which will be presented in the next section. It turns out to be

possible to formulate rather general expressions for $\epsilon_m$ and $P_{rt}$. According to experimental observations, we define the following function, $\phi$, to describe the mean velocity field:

$$\frac{u}{u_e} = 1 - \exp(-\phi[x,y]) \tag{21}$$

According to the no slip condition, $\phi$ must vanish at the wall, and in order to satisfy the external boundary condition, $\phi$ must become unbounded beyond the boundary layer edge. It is emphasized that at this point no additional assumptions have been imposed, and that Eq. (21) merely serves as a definition. The exponential form yields the following expressions upon differentiation:

$$u_x = u_e \phi_x \exp(-\phi) \tag{22}$$

$$u_y = u_e \phi_y \exp(-\phi) \tag{23}$$

Therefore, x and y derivatives of the mean velocity field are related by the following expression:

$$u_x = \frac{u_y \phi_x}{\phi_y} \tag{24}$$

From the experimental evidence presented later, it will be apparent that $\phi$ has a benign behavior such that the ratio of its derivatives can be easily modeled. As a limiting case, and for the sake of convenience of presentation, the incompressible approximation will be discussed below. For cases of moderate heating, as in Blair's experiment, it can be shown that the variations in mean density influence the velocity field only as a small perturbation. Substitution of Eq. (24) into Eq. (16) yields the following representation for the Reynolds stress:

$$-\langle u'v' \rangle = u_\tau^2 - \nu u_y - u \int_0^y u_y \left(\frac{\phi_x}{\phi_y}\right) d\xi + 2 \int_0^y u u_y \left(\frac{\phi_x}{\phi_y}\right) d\xi \tag{25}$$

Here, $u_\tau$ represents the friction velocity which is defined as $(\frac{\tau_w}{\rho_w})^{1/2}$. It now becomes evident how the Reynolds stress might be calculated in terms of the mean velocity. If the $\phi$ function can be effectively modeled (including FST effects), then Eq. (25) may be directly utilized for the calculation of $\langle u'v' \rangle$. The x variation does not appear explicitly in the mean velocity profile, so that a simple integration routine may be executed at each streamwise location of the marching procedure. This method is similar to the mixing length method in that the unknown behavior of the Reynolds stress has been shifted to another unknown function. The method will be advantageous only if $\phi$ will admit a simple and accurate modeling. This turns out to be the case. A further correspondence may be made between the original mixing length hypothesis given in Eqs. (12-14) and the modeling proposed in Eq. (25). Utilization of Eq. (18) and factorization of the velocity derivative yields the following expression:

$$-\langle u'v' \rangle = \varepsilon_m \left(\frac{\partial u}{\partial y}\right) \tag{26}$$

where: $$\varepsilon_m = -\nu + \frac{1}{\phi_y} \int_0^\infty U_y F \, d\xi + \frac{U_e}{U_y} \int_y^\infty U_y F \, d\xi - \frac{2}{U_y} \int_y^\infty U U_y \, F d\xi \tag{27}$$

and: $$F \equiv \phi_x / \phi_y$$

Therefore, with a specification of $\phi$, the eddy viscosity is directly calculable. It is further interesting to note that the unknown functions u, v, and $\langle u'v' \rangle$ may all be directly calculated from the single unknown $\phi$. A similar analysis leads to a general formulation for the turbulent heat flux, which then may be used to model the turbulent Prandtl number. However, these equations will be deferred to the next section in which specific models will be discussed.

# 3.0 COMPUTATIONAL MODELS

## 3.1 Observation of Three Layers

The first phase of the investigation has involved further scrutiny of Blair's data with the objective of extending the exponential wake model observed in 1984 to include the wall layer also. The effect of FST in the wake region was clearly displayed by a marked decrease in curvature of the exponential function as the FST was increased [1]. The pursuit of this approach has lead to a remarkable analytical approximation which describes the entire turbulent boundary layer. In Fig. 1 is displayed a comparison of Blair's data for mean velocity at x=84 in. with grid configuration 4 (highest FST [18]) and a straight line least squares fit for the outer portion of the boundary layer. It is clear that the wake region follows a linear exponential decay for the velocity deficit there. In attempting to characterize the wall region, Blair's data have been subtracted from the extension of the straight line to the wall. It appeared that this difference also followed an exponential behavior. In order to highlight the behavior, the difference has been plotted in a magnified semilogarithmic format as shown in Fig. 2. It is astonishing that the previous form seems to have repeated itself on a scale which is approximately one order to magnitude smaller. A straight line curve fit is also displayed in Fig. 2 through the outer portion of this smaller region. The residue between the data closest to the wall and the second straight line has been plotted in a third semilogarithmic format, and the results are displayed in Fig. 3. Here, the characteristic length scale is approximately one order of magnitude smaller than that of the intermediate region. It is further astonishing that these data also fall on a straight line to good approximation. The scatter in the data becomes magnified in

these successive refinements. The composite function has the following analytical representation:

$$\frac{u}{u_e} = 1 - \exp(-A_1 - B_1\eta + \exp[-A_2 - B_2\eta + \exp\{-A_3 - B_3\eta\}]) \qquad (28)$$

where: $\eta = \frac{y}{\delta}$ and $\delta$ represents the local boundary layer thickness. A constraint is imposed on the coefficients in the exponentials by the no slip condition:

$$A_1 = \exp[-A_2 + \exp\{-A_3\}] \qquad (29)$$

Figures 4-6 display comparisons between the above analytical function (with coefficients matched to Blair's data) and the data profiles themselves. Fig. 4 accentuates the wake region, Fig. 5 shows the usual linear comparison, and Fig. 6 (the most interesting) accentuates the wall region in a format similar to the Clauser type plot, except that the variables have not been scaled with the friction velocity. All three figures exhibit a very satisfactory agreement. The innermost comparison may be improved by another choice of $A_3$, $B_3$ above. To the authors' awareness, the above analytical expression is the first whole layer formula to describe a turbulent boundary layer to such accuracy. In Fig. 6 the influence of each of the three exponentials is also displayed. These curves indicate the sizes and locations of the three sublayers.

After the presentation of the curve fit, several questions arise which ought to be addressed. First, is the functional form adequate for describing the evolution of the boundary layer? Subsequent figures will show that all the profiles generated by Blair can be well fit by extensions of the above form. Second, how does the functional form change with varying levels of FST? Blair's data demonstrate that the outer layer coefficients depend strongly on the level of FST. Third, if there are truly three layers of

different sizes, what physical mechanisms dominate in these regions, and how do these scales evolve in the boundary layer? Possible explanations for these scales will be presented later. Fourth, what connection do these scales have to the classical notions of 'wake' and 'wall' regions? This is related to the third issue. Fifth, is the triple exponential with several adjustable coefficients simply an artifact of curve fitting, or does it contain an inherent representation of the physics of the problem? Perhaps other functions sufficiently rich in coefficients could do equally well at the fitting. A definitive answer is not presented herein, although two points are offered: (1) For the cases of high FST the linear exponentials fit very well over substantial ranges of the boundary layer. It is unlikely that any other simple function provides a better characterization. (2) Even if the triple exponential were not to comprise a fundamental representation, it nevertheless follows the data to such good accuracy that it may be used beneficially for engineering calculations. Last, how might the exponential representation be exploited for purposes of mixing length modeling which also accounts for the effects of FST? The method here will consist of utilization of Blair's data to model the $\nu$ function described in the previous section.

## 3.2 Effect of FST

With the appearance of a special case of the triple deck exponential, it is now of interest to seek a characterization of the coefficients as a function of x location, and also to observe the variation of the function as the level of FST is varied parametrically. In 1984 [2] it was observed that the wake portion of the boundary layer could be described by a linear exponential for the higher levels of FST only. In Fig. 7 the wake is shown for the lowest level of FST (grid 0) at $x = 84$ in. Since it can be shown that the outer portion of a laminar boundary layer decays exponentially with a quadratic

argument into the free stream, the previous linear curve fit is now extended to a quadratic one in this figure. Qualitatively it is clear that the quadratic fit is good if the free stream turbulence is at a low level, and that a linear fit is good if the FST level is high.

It is of interest to consider the extent of agreement of the previous function with the velocity profile of a laminar boundary layer. First, upstream of transition the flow is laminar, and second, a quadratic wake fit seems to be appropriate for cases of low FST. In Fig. 8 is shown the comparison between a quadratic wake fit and a numerical solution of the Blasius Equation. The agreement is excellent for the outer 80% of the laminar boundary layer. Since it can be shown that the first two terms of the inner layers are linear and quartic in y, a quartic inner exponential is assumed to describe the wall region. The results of the composite function are displayed in Figs. 9-11. The agreement is remarkably good, and could be improved by further refinement of the parameters in the wall region.

With the above observations in mind, Blair's data have been fit with least squares quadratics for various x locations and three levels of FST (grids 0, 2, and 4) in order to observe these influences on the coefficients of the exponentials. The procedure has been the same for all cases: (1) Fit the wake region first, excluding approximately the inner 25% of the boundary layer, (2) Subtract the inner data from the outer fit, (3) Fit the intermediate region to a quadratic curve, (4) Subtract the remaining data closest to the wall from the composite curve, (5) Fit a third quadratic to the innermost layer. Admittedly, this procedure introduces many coefficients, and the results are not entirely free of personal and somewhat arbitrary judgment. However, the results have been quite satisfactory. In Figures 12-15 are shown progressions of mean velocity profiles for grid 4 at x locations 12, 36, 52,

and 84 inches respectively. The analytical curves fit through the data are seen to describe the boundary layer profiles quite well, and now these functions may be used to advantage in the computational scheme. Three features are noteworthy. First, the wake region of the boundary layer scales very well with the local boundary layer thickness. This may be seen by the superposition of the curves (and data) at the various x locations, especially in the semilogarithmic wake format. Second, the inner two scales grow at a rate which is slower than the growth of $\delta$. This may be observed by the significant lengthening of the curves as x increases. These two observations are well known in the study of turbulent boundary layers. Third, although the intermediate portions of these curves [Figs. 12-15] are almost approximated by straight lines, it is clear from the data that there is always some amount of curvature there. The classical notion of the logarithmic layer may be regained in approximation from the analytical curve fit by an expansion in this intermediate region. However, the linear logarithmic term is only the first in the expansion, and clearly, the figures display a point of inflection.

The effects of FST are shown to be incorporated into the analytical fits in the sequence of Figures 16-23, which correspond to Blair's grid 2 and grid 0 cases. At the various x locations it may be seen from the semilogarithmic wake plots (not shown) that the boundary layer is strongly influenced by FST as the curvature term in the quadratic decreases markedly as the FST increases. The coefficients utilized in these exponentials are listed in Table 1.

As with most experiments involving turbulent boundary layers, Blair's data shown in the above plots suffer from the inability to approach close enough to the wall (into the laminar sublayer). This is caused primarily by the small

size of his apparatus. It is clear from Figs. 12-23 that the wall shear is determined predominantly by the character of the innermost wall layer. In fact, in the curve fitting, it is possible to alter the coefficients of the third layer so that $C_f$ changes by 100% while the outer two layers appear to be unaffected in the figures. In an effort to characterize the third layer, the data of Coantic [30] and Kline, et al. [31] have been fit to the exponential representation in Figs. 24-27. These data are among those which approach farthest into the sublayer (Coantic's data even lie within unity y+). Since tabulations of these data were not available to the authors, there is an additional error in the plots owing to subjective reading from published graphs. Nevertheless, the curve fits appear to be very satisfactory. It may be shown that the analytical representation approaches the correct wall behavior (i.e. $u^+ \to y^+$ as $y^+ \to 0$). The most effective method of determining wall shear involves a full log-log plot of the velocity profile, as shown in Figs. 28 and 29 for the data of Coantic and Kline, et al. The shift in the linear portion provides $\tau_w$ directly. However, most experimental data (including Blair's) do not extend into the linear region.

In the attempt to characterize turbulent heat transfer, it is important to fit the mean temperature profiles in parallel with those of the mean velocity. Figures 30-41 demonstrate that the previous exponential is also a good representation of the mean temperature distributions. In Table 2 are listed the corresponding coefficients for these functions. Although there are slight differences, it is apparent that on the whole the velocity and temperature profiles are very similar.

After having achieved a characterization of the mean profiles, the next phase of the investigation involves making use of this information to model the unknown Reynolds stress and turbulent heat flux terms. In this process,

the aim is to simplify the dependences of the coefficients appearing in the exponentials to account for two major effects; namely, the variations with x and with FST.

### 3.3 Turbulent Fluxes

The scrutiny of Blair's data has revealed that the mean velocity and mean temperature distributions in a turbulent boundary layer may be described well by the functional form:

$$\frac{u}{u_e} = 1 - \exp(-\phi_1 + \exp[-\phi_2 + \exp\{-\phi_3\}]) \qquad (30)$$

where:

$$\phi_1 = a_1 + b_1\eta + c_1\eta^2 \quad ; \quad \eta = \frac{y}{\delta}$$

$$\phi_2 = a_2 + b_2\xi + c_2\xi^2 \quad ; \quad \xi = \frac{y}{\varepsilon}$$

$$\phi_3 = a_3 + b_3\zeta + c_3\zeta^2 \quad ; \quad \zeta = \frac{y}{\lambda}$$

or equivalently:

$$\phi_1 = A_1 + B_1\eta + C_1\eta^2$$

$$\phi_2 = A_2 + B_2\eta + C_2\eta^2$$

$$\phi_3 = A_3 + B_3\eta + C_3\eta^2$$

Here, $\delta$, $\varepsilon$, and $\lambda$ represent the characteristic length scales corresponding to the three regions observed in the analytic fits of Blair's data. It remains to determine what their dependences are and how best to characterize the coefficients. It is assumed that the coefficients a, b, c are independent of x, and that the boundary layer evolution is scaled into the characteristic lengths, whereas the coefficients A, B, C cannot be independent of x. A similar expression may be written for the temperature field. In the wake region, the numbers appearing in Tables 1 and 2 indicate that the following

model is appropriate for the coefficients:

$$a_1 = 1.45 - 0.09I_e$$

$$b_1 = -1.0 + I_e \qquad (31)$$

$$c_1 = \begin{cases} 5.0 - I_e & \text{for} \quad 0 < I_e < 5.0 \\ 0 & \text{for} \quad I_e > 5.0 \end{cases}$$

where:

$$I_e = (100)\left(\frac{k_e}{u_e}\right)$$

$$k_e = \langle (u')^2 + (v')^2 + (w')^2 \rangle^{1/2}|_{y>\delta}$$

Although there is some scatter in the values obtained by curve fitting, the tables do indicate that these coefficients do not vary with x to first approximation. This statement is in accord with the notion that the wake region scales with the boundary layer thickness, $\delta$. A similar model is made for the outer layer of the mean temperature field. In this manner, the above model introduces FST explicitly into the description of the turbulent fluxes.

The behavior of the two inner layers is somewhat more difficult to describe. The traditional characterization of a turbulent boundary layer is in terms of the 'wake' and 'wall' regions only, and no mention is usually made of three distinct layers which scale with three different lengths. The terms laminar sublayer, buffer layer, and logarithmic wall layer are intended to apply within the wall layer, and all of these are assumed to be characterized by the single length scale, $\nu/u_\tau$. Recent investigations [32-34] have called into question the classical notion of the logarithmic wall region on the grounds that an overlap region may not exist between the wake and wall functions. In these investigations a third merging layer is discussed, but the arguments have not been widely accepted yet, and the topic is one of ongoing research. The triple exponential observed herein may have a

connection to these proposals. For the present, we make the following observations. As the solid wall is approached, the mean velocity and mean temperature fields must satisfy several constraints imposed by their Taylor series expansions about y=0. For velocity, one obtains:

$$u(x,y) = \tau_w \frac{y}{\mu} + p_x \frac{y^2}{2\mu} + (0)y^3 + o(y^4) + \ldots \tag{32}$$

In fact, a more comprehensive argument results in a nonvanishing coefficient for the $y^3$ term owing to an effect attributable to the y momentum equation. However, this effect is small, and will be neglected here. For an incompressible flow one may show that the effect of Reynolds stress is introduced into the expansion explicitly only in the $y^4$ term, although the turbulence is also implicit in an increased value for $\tau_w$. From the Taylor series expansion, and from observation of experimental data, it is customary to utilize the friction velocity, $u_\tau$, in scaling both the mean velocity and the y coordinate in the wall region. Since Blair's data have thus far been presented in terms of the dimensionless ratio, $\frac{u}{u_e}$, we may seek to express the Taylor series expansion in that form. By such a procedure, it becomes apparent that two length scales are possible; namely:

$$\begin{aligned} \ell_1 &= \frac{\nu}{u_\tau} \\ \ell_2 &= u_e \frac{\mu}{\tau_w} \end{aligned} \tag{33}$$

The first length scale is the usual one defined by the friction velocity, whereas the second one is larger by the factor, $\frac{u_e}{u_\tau}$, which typically represents an increase of an order of magnitude or more. It is interesting to note that $\ell_1$ is independent of the free stream explicitly, whereas $\ell_2$ contains an intermediate dependence on both $u_e$ and $u_\tau$. At present, it is not clear from the analytical fits of Blair's data whether or not the two inner length scales

should be identified with $\ell_1$ and $\ell_2$. However, expansion of $\frac{u}{u_\tau}$ naturally involves use of $\ell_1$, whereas expansion of $\frac{u}{u_e}$ involves $\ell_2$. These expansions are identical through their first order terms. Higher order terms in the respective expansions begin to differ in the nature of their coefficients. However, in the triple exponential, the dominant term in each layer near the wall is the linear one. Since the form used here is $\frac{u}{u_e}$, both inner layers will be assumed to scale with $\ell_2$, which is in accord with the usual 'law of the wall' to first order.

In view of the exponential form and the limiting behavior imposed by the Taylor series expansion, there are now three additional constraints that must be satisfied among the coefficients of the triple exponential. By evaluation of the first derivative of velocity at the wall, one obtains the relation:

$$\frac{\tau_w}{\mu u_e} = \frac{b_1}{\delta} + a_1\left(\frac{b_2}{\epsilon} + \frac{b_3 \exp(-a_3)}{\lambda}\right) \tag{34}$$

This equation indicates that the shear stress depends on all three length scales. However, since the innermost length scale is by far the smallest, one expects that the third term dominates the expression. This is also in accord the observation that the shear stress is determined by the velocity derivative evaluated at the wall. Therefore, Eqs. (33) and (34) also support the notion that $\lambda$ ought to be identified with $\ell_2$ to first order. Thus, for convenience of the present modeling, we choose:

$$\lambda = \mu \frac{u_e}{\tau_w} \tag{35}$$

The second and third terms in the Taylor series expansion provide two further constraints on the coefficients. For a flat plate the second and third derivatives of mean velocity vanish at the wall. From these conditions, we choose to determine the curvature coefficients $C_2$ and $C_3$, which are the most difficult to ascertain from curve fitting of the data as well. There results:

$$C_3 = \frac{2h_1^3 + 3g_1(h_1^2 - 2C_1) + 2A_1g_1^3 + B_3^3 A_1 \exp(-A_3)}{6A_1(2g_1 + B_3)\exp(-A_3)} \tag{36}$$

$$C_2 = \frac{1}{2}\left[g_1^2 + (B_3^2 - 2C_3)\exp(-A_3) + (h_1^2 - 2C_1)/A_1\right] \tag{37}$$

where:

$$g_1 = -B_2 - B_3 \exp(-A_3)$$

$$h_1 = -B_1 + A_1 g_1$$

In order to complete the specification of the coefficients in this model, we note the following dependences observed from curve fitting of Blair's data:

$$A_2 = 0.2 + 0.2I_e$$

$$B_2 = 2.0 + 4.0I_e \tag{38}$$

$$B_3 = b_3\left(\frac{\delta\tau_w}{\mu u_e}\right) \quad \text{where: } b_3 = 1.3$$

It appears from Blair's data that the intermediate layer is influenced by the degree of FST quite strongly but that the coefficients $A_2$, $B_2$ do not depend on x appreciably. The innermost coefficients $B_3$, $C_3$ are seen to vary strongly with x as given above. Therefore, Blair's data suggest that $\lambda$ and $\epsilon$ are not identical.

With the mean velocity field specified as above, it now remains to formulate the model for the Reynolds stress, and similarly for $P_{rt}$. In order

$$\tau_w = \rho_e u_e^2 A \frac{d\delta}{dx} \tag{44}$$

A comparison of the two limits of the Reynolds stress relation (Eq. (25)) now reveals a connection between the inner and outer scales of a turbulent boundary layer and the mechanism by which FST influences the wall shear. In the wake region, FST clearly influences the rate of boundary layer growth and the character of the $\phi$ function. The evolution of this wake region is connected with a change in the streamwise momentum deficit that is created by the wall shear as given by Eq. (44). Finally, the inner scale, $\lambda$, is dependent upon the local value of $\tau_w$ as described by Eq. (35) (or perhaps Eq. (33)).

Values for the proportionate increases of the scales may be approximated from the observations that:

$$\begin{aligned} \delta &\sim x^{4/5} \\ \tau_w &\sim x^{-1/5} \end{aligned} \tag{45}$$

These usually accepted dependences are in accord with Eq. (44) above. Then it follows that:

$$\frac{\delta_x}{\delta} = \frac{4}{5}\left(\frac{1}{x}\right) \tag{46}$$

For the length scales $\ell_1$ and $\ell_2$ it follows that:

$$\frac{\ell 1_x}{\ell_1} = \frac{1}{10}\left(\frac{1}{x}\right) \qquad \text{and} \qquad \frac{\ell 2_x}{\ell_2} = \frac{1}{5}\left(\frac{1}{x}\right) \tag{47}$$

more generally, for any power law dependence,

$$\ell \sim x^m$$

it follows that

$$\frac{\ell_x}{\ell} = \frac{m}{x} \tag{48}$$

The important and fortuitous property of all these dependences is that $\left(\frac{1}{x}\right)$ is

to utilize the general formula given in Eq. (25), the x and y derivatives of the specific $\phi$ function are required, and for the present case these are:

$$-\phi_x = \eta\left(\frac{\delta_x}{\delta}\right)(b_1 + 2c_1\eta) + E\{\xi\left(\frac{\epsilon_x}{\epsilon}\right)(b_2 + 2c_2\xi) + e^{-\phi 3}\zeta\left(\frac{\lambda_x}{\lambda}\right)(b_3 + 2c_3\zeta)\} \quad (39)$$

$$\phi_y = \frac{(b_1 + 2c_1\eta)}{\delta} + E\left\{\frac{b_2 + 2c_2\xi}{\epsilon} + e^{-\phi 3}\,\frac{(b_3 + 2c_3\zeta)}{\lambda}\right\} \quad (40)$$

$$\text{where } E = \exp(-\phi_2 + \exp[-\phi_3])$$

The ratio of these two functions appears in the general Reynolds stress model given in Eq. (25). While this ratio is a complicated expression, it is interesting to observe that in each of the three successive layers the ratio is well approximated by the simpler forms:

$$y\left(\frac{\lambda_x}{\lambda}\right) \quad ; \quad y\left(\frac{\epsilon_x}{\epsilon}\right) \quad ; \quad y\left(\frac{\delta_x}{\delta}\right) \quad (41)$$

Therefore, the Reynolds stress is essentially determined by the proportionate variation of the three length scales. Since the boundary layer thickness is a quantity which is calculated at each streamwise step in STANCOOL, the ratio $\frac{\delta_x}{\delta}$ may be directly obtained in the process. Similarly, since $\epsilon$ and $\lambda$ depend on $\tau_w$, which is also calculated, these streamwise variations may also be obtained. For present expository purposes, we proceed to an even simpler model. The von Karman momentum integral equation (Eq. (18)) may be rewritten in the more familiar form:

$$\tau_w = \rho_e u_e^2 \frac{d\theta}{dx} \qquad \text{where} \qquad \theta \triangleq \int_0^\infty \frac{u}{u_e}\left(1 - \frac{u}{u_e}\right)dy \quad (42)$$

Although the mean velocity profile depends on three length scales, it is clear that the momentum thickness, $\theta$, is predominently determined by $\delta$. Therefore:

$$\theta = A\delta \qquad \text{where} \qquad A \equiv \text{constant} \quad (43)$$

Equation (42) becomes:

to utilize the general formula given in Eq. (25), the x and y derivatives of the specific $\phi$ function are required, and for the present case these are:

$$-\phi_x = \eta\left(\frac{\delta_x}{\delta}\right)(b_1 + 2c_1\eta) + E\{\xi\left(\frac{\epsilon_x}{\epsilon}\right)(b_2 + 2c_2\xi) + e^{-\phi_3}\zeta\left(\frac{\lambda_x}{\lambda}\right)(b_3 + 2c_3\zeta)\} \quad (39)$$

$$\phi_y = \frac{(b_1 + 2c_1\eta)}{\delta} + E\{\frac{b_2 + 2c_2\xi}{\epsilon} + e^{-\phi_3}\frac{(b_3 + 2c_3\zeta)}{\lambda}\} \quad (40)$$

$$\text{where } E = \exp(-\phi_2 + \exp[-\phi_3])$$

The ratio of these two functions appears in the general Reynolds stress model given in Eq. (25). While this ratio is a complicated expression, it is interesting to observe that in each of the three successive layers the ratio is well approximated by the simpler forms:

$$y\left(\frac{\lambda_x}{\lambda}\right) \quad ; \quad y\left(\frac{\epsilon_x}{\epsilon}\right) \quad ; \quad y\left(\frac{\delta_x}{\delta}\right) \quad (41)$$

Therefore, the Reynolds stress is essentially determined by the proportionate variation of the three length scales. Since the boundary layer thickness is a quantity which is calculated at each streamwise step in STANCOOL, the ratio $\frac{\delta_x}{\delta}$ may be directly obtained in the process. Similarly, since $\epsilon$ and $\lambda$ depend on $\tau_w$, which is also calculated, these streamwise variations may also be obtained. For present expository purposes, we proceed to an even simpler model. The von Karman momentum integral equation (Eq. (18)) may be rewritten in the more familiar form:

$$\tau_w = \rho_e u_e^2 \frac{d\theta}{dx} \qquad \text{where} \qquad \theta \triangleq \int_0^\infty \frac{u}{u_e}\left(1 - \frac{u}{u_e}\right)dy \quad (42)$$

Although the mean velocity profile depends on three length scales, it is clear that the momentum thickness, $\theta$, is predominently determined by $\delta$. Therefore:

$$\theta = A\delta \qquad \text{where} \qquad A \equiv \text{constant} \quad (43)$$

Equation (42) becomes:

$$\tau_w \equiv \rho_e u_e^2 A \frac{d\delta}{dx} \tag{44}$$

A comparison of the two limits of the Reynolds stress relation (Eq. (25)) now reveals a connection between the inner and outer scales of a turbulent boundary layer and the mechanism by which FST influences the wall shear. In the wake region, FST clearly influences the rate of boundary layer growth and the character of the $\phi$ function. The evolution of this wake region is connected with a change in the streamwise momentum deficit that is created by the wall shear as given by Eq. (44). Finally, the inner scale, $\lambda$, is dependent upon the local value of $\tau_w$ as described by Eq. (35) (or perhaps Eq. (33)).

Values for the proportionate increases of the scales may be approximated from the observations that:

$$\begin{aligned} \delta &\sim x^{4/5} \\ \tau_w &\sim x^{-1/5} \end{aligned} \tag{45}$$

These usually accepted dependences are in accord with Eq. (44) above. Then it follows that:

$$\frac{\delta_x}{\delta} = \frac{4}{5}\left(\frac{1}{x}\right) \tag{46}$$

For the length scales $\ell_1$ and $\ell_2$ it follows that:

$$\frac{\ell_{1x}}{\ell_1} = \frac{1}{10}\left(\frac{1}{x}\right) \qquad \text{and} \qquad \frac{\ell_{2x}}{\ell_2} = \frac{1}{5}\left(\frac{1}{x}\right) \tag{47}$$

more generally, for any power law dependence,

$$\ell \sim x^m$$

it follows that

$$\frac{\ell_x}{\ell} = \frac{m}{x} \tag{48}$$

The important and fortuitous property of all these dependences is that $\left(\frac{1}{x}\right)$ is

a common factor of any power law variation in the scales, and that this factor cancels in the Reynolds stress modeling to yield from Eq. (27) the result:

$$\frac{-\langle u'v' \rangle}{U_\tau^2} = -\frac{U_y}{U_y|_\bullet} + \frac{\frac{U_y}{\phi_y}\int_0^y U_y\, F d\xi + U_e\int_y^\infty U_y\, F d\xi - 2\int_y^\infty UU_y\, F d\xi}{U_e\int_y^\infty U_y\, F d\xi - 2\int_0^\infty UU_y\, F d\xi} \qquad (49)$$

where:

$$F = \frac{myF_1 + (nyF_2 + lyF_3)\exp(-\phi_2 + \exp[-\phi_3])}{F_1 + (F_2 + F_3)\exp(-\phi_2 + \exp[-\phi_3])}$$

and $F_1 = b_1 + 2\,c_1\,n$ ; $m = 4/5$

$F_2 = b_2 + 2\,c_2\,n$ ; $n = 1/5$

$F_3 = (b_3 + 2\,c_3\,n)e^{-\phi 3}$ ; $l = 1/10$

In this model, the x derivatives have cancelled, and the Reynolds stress is computable at every streamwise station explicitly. A parallel argument holds for the energy equation, from which an explicit equation may then be obtained for the $P_{rt}$ profile throughout the boundary layer. The next section provides a more compact illustration of the procedure.

### 3.4 Particular Analytical Solution

The general procedure described above admits a particular solution which is extremely interesting for two reasons: (1) The solution thus obtained provides a means for checking the accuracy and consistency of any turbulent boundary layer code such as STANCOOL. (2) The analytical solution provides insights into the physical mechanisms at work in a turbulent boundary layer. It is emphasized, however, that this particular solution of the equations does not correspond to a realistic turbulent boundary layer because the turbulent

fluxes are artificially constructed. The solution has originated from two points of view. First, it has been observed that in the wake region at high FST, the exponential function, $\phi$, is linear in y. Second, one attempts to seek the simplest case for description which falls within the general realm of the problem. These points lead to consideration of the following mean velocity profile:

$$\frac{u}{u_e} = 1 - e^{-By} \qquad \text{where} \qquad B = B(x) \tag{50}$$

From the definition of the displacement thickness, one obtains:

$$B = \frac{1}{\delta^*} \tag{51}$$

From the conservation of mass equation, one obtains:

$$\frac{v}{u_e} = \delta_x^*[1 - (1 + \hat{\eta})e^{-\hat{\eta}}] \qquad \text{where} \qquad \hat{\eta} \triangleq y/\delta^* \tag{52}$$

From the momentum equation (Eq. (25)), one obtains:

$$\frac{-\langle u'v' \rangle}{U_e^2} = \delta_x^*[\hat{\eta} + \frac{1}{2}(e^{-\hat{\eta}} - 1)]e^{-\hat{\eta}} \tag{53}$$

Satisfaction of the two limits of the momentum equation results in the condition:

$$\delta_x^* = \frac{2\nu}{U_e \delta^*} \tag{54}$$

integration of which yields the growth rate:

$$\frac{\delta^*(x)}{\delta^*(0)} = \{1 + \frac{4\nu x}{U_e(\delta_0^*)^2}\}^{1/2} \tag{55}$$

In the turbulence kinetic energy equation and in the related Reynolds stress equation appear two terms of physical significance (among others); namely, the viscous dissipation, and turbulence production. Here, it is of interest to compute these terms for the particular analytical solution.

Although the viscous dissipation due to the turbulent fluctuations generally dominates that due to the mean velocity, the latter profile is given here explicitly since the turbulence kinetic energy has not yet been addressed in the modeling.

$$D \triangleq \mu u_y^2 = \frac{\rho u_\tau^4}{\nu} e^{-2\hat{n}} \tag{56}$$

The turbulence production term is:

$$P \triangleq -u_y \langle u'v' \rangle = \frac{2\rho u_\tau^4}{\nu} e^{-2\hat{n}} \left[\hat{n} + \frac{1}{2}\left(e^{-\hat{n}} - 1\right)\right] \tag{57}$$

From these various profiles, one may define several weighted "characteristic" lengths, with the hope of identification with those observed from Blair's data.

dissipation scale:
$$\ell_D \triangleq \frac{\int_0^\infty y D\, dy}{\int_0^\infty D\, dy} = \frac{\delta^*}{2} \tag{58}$$

production scale:
$$\ell_P \triangleq \frac{\int_0^\infty y P\, dy}{\int_0^\infty P\, dy} = \frac{13\delta^*}{12} \tag{59}$$

Reynolds stress scale:
$$\ell_R \triangleq \frac{\int_0^\infty y \langle u'v' \rangle dy}{\int_0^\infty \langle u'v' \rangle dy} = \frac{13\delta^*}{6} \tag{60}$$

Before proceeding with the energy equation, a few comments of interpretation are appropriate. First, the above mathematical curiosity falls in a middle ground between laminar and turbulent flows. The square root growth rate of the boundary layer thickness ($\delta \cong 5.3\delta^*$) along with similarity with respect to only one length scale( i.e. $\delta^*$) are properties reminiscent of

laminar boundary layers. However, in order for such a simple profile to maintain itself, a psuedo-Reynolds stress is required to transmit a shear stress to the wall which exceeds that of the laminar case. Although this Reynolds stress (Eq. (53)) exhibits well behaved properties throughout the boundary layer, it does decrease towards the wall in proportion to $\hat{n}$, which is slower than the $\hat{n}^3$ expected for an actual turbulent boundary layer. However, for illustrative purposes, none of these qualities present serious drawbacks. The view taken for zeroth order closure of the turbulent boundary layer is that the mean profiles are determined in a continuous manner by specification of the turbulent flux profiles. If the turbulent fluxes were to vanish identically, the solution would be the laminar one. As the turbulent fluxes are increased parametrically to their fully turbulent values, then the mean profiles are likewise altered continuously to their final shapes. The interpretation of the above solution is that if the Reynolds stress were to take on the form given by Eq. (53), then the mean profiles which would satisfy the equations of motion would assume the corresponding functions given above.

In order to appreciate the connection to the turbulent Prandtl number, the analytical solution will now be extended to include the energy equation as well. We explore the consequences resulting from the following mean temperature profile:

$$\frac{T - T_e}{T_w - T_e} = e^{-\beta y/\delta^*} \tag{61}$$

where $\beta$ is a factor which permits the thermal boundary layer to grow at a rate differing from that of the momentum layer.

By utilization of the assumptions listed in Section 2.2, the energy equation may be integrated directly to give the result:

$$-\langle v'T' \rangle = \varepsilon_H T_y \tag{62}$$

where

$$\epsilon_H = \left[ -\frac{2\nu}{\beta^2(1+\beta)} + \frac{2\nu}{\beta}\frac{1-\beta}{(\beta+\hat{n})} + \frac{2\nu u}{\tau_w(\beta+1)} U_y \right]$$

In order to achieve this result, it has been necessary to make the additional assumption that $\beta$ is constant. It may be shown that $\beta$ is related to the molecular Prandtl number as follows:

$$\beta^2(1+\beta) = 2P_r \tag{63}$$

One concludes an analytical profile for $P_{rt}$:

$$P_{rt} = \frac{[e^{-\hat{n}} - 1 + 2\hat{n}]}{\left[\frac{2}{(\beta+1)}(e^{-\hat{n}} - 1) + \frac{2}{\beta}\hat{n}\right]} \tag{64}$$

The turbulent Prandtl number is smoothly bounded by:

$$\frac{\beta(\beta+1)}{2} \geq P_{rt} \geq \beta \tag{65}$$

for which the limits depend upon the choice of the molecular Prandtl number.

The analytical solution presented here will be further discussed and compared with STANCOOL calculations in Section 4.

### 3.5 Limiting Forms

Equations have now been presented for the turbulent fluxes in a sequence beginning with the general form, continuing with specific observations obtained from Blair's data, and ending with an instructive but artificial particular analytical solution. Since it does not appear possible to obtain a representation of the Reynolds stress throughout the boundary layer by analytical integration of Eq. (25), it is of interest to seek asymptotic characterizations in the two limits: near the wall and in the wake. These may

be of use in computational procedures.

The wall region is of importance owing to its immediate connection to the wall shear and heat flux, which are of practical concern. Unfortunately, it is experimentally very difficult to obtain direct measurements of Reynolds stress into the buffer layer since this region is so minute. Furthermore, the presence of the wall contaminates such measurements. From the analytical point of view, the usual argument proceeds from Taylor series expansions about $y = 0$. If the flow is assumed to be incompressible, and by invoking the no slip condition, the conservation of mass equation yields for the vertical velocity component:

$$v(t,\underline{x}) = \frac{\partial^2 v}{\partial y^2}\Big|_o \frac{y^2}{2} + o(y^3) \tag{66}$$

Since the streamwise velocity component is linear in y to first order, one concludes for the Reynolds stress:

$$\langle u'v' \rangle = c(x)y^3 + o(y^4) \tag{67}$$

One cautionary remark involves the assumption of incompressibility. If the flow were to contain significant variations of $\frac{\partial \rho'}{\partial t}$, then the leading term above would be proportional to $y^2$. A second remark is that it is possible (although unlikely) that the fluctuations leading to the coefficient, $c(x)$, are uncorrelated so that the leading nonvanishing term actually becomes of order $y^4$. Here, the correct representation is assumed to be given by Eq. (67). It should be noted that the commonly accepted van Driest damping factor [35], which is also utilized in STANCOOL, results in the $y^4$ limiting behavior.

Next, it will be shown that the general form proposed for the Reynolds stress Eq. (25) is in agreement with the limit given in Eq. (67) above. The Taylor series expansion for $\phi$ near the wall is:

$$\phi = \phi^{(0)}(x) + \phi^{(1)}(x)\, y + \phi^{(2)}(x)\, \frac{y^2}{2} + \ldots \qquad (68)$$

then: $$\phi_y = \phi^{(1)}(x) + \phi^{(2)} y + \phi^{(3)}\, \frac{y^2}{2} + \ldots$$

$$\phi_x = \phi^{(0)}_x + \phi^{(1)}_x\, y + \phi^{(2)}_x\, \frac{y^2}{2} + \ldots$$

Substitution of the above, together with Eq. (32), into Eq. (25) yields for the Reynolds stress:

$$-\langle u'v' \rangle = \frac{\tau_w}{\rho} - \nu[u^{(1)}_o + u^{(4)}_o\, \frac{y^3}{6} + ..] - [u^{(1)}_o y + u^{(4)}_o\, \frac{y^4}{24}] \int_0^y [u^{(1)}_o + o(y^3)]\cdot$$

$$[\frac{\phi^{(0)}_x + \phi^{(1)}_x y + \ldots}{\phi^{(1)} + \phi^{(2)} y + ..}]dy + 2\int_0^y [u^{(1)}_o y + o(y^4)]\, [\frac{\phi^{(0)}_x + \phi^{(1)}_x y + \ldots}{\phi^{(1)} + \phi^{(2)} y + ..}]dy \qquad (69)$$

Upon integration, one obtains after some cancelation of terms:

$$-\langle u'v' \rangle = [-\nu u^{(4)}_o + (u^{(1)}_o)^2 (\frac{\phi^{(1)}_x}{\phi^{(1)}} + \frac{\phi^{(0)}_x\, \phi^{(2)}}{(\phi^{(1)})^2})]\, \frac{y^3}{6} + O(y^4) \qquad (70)$$

Therefore, it is verified that the use of Eq. (25) in further modeling of the Reynolds stress leads to a behavior at the wall which has the correct limiting form in regard to y dependence. However, the magnitude of the coefficient of $y^3$ remains to be specified through the model, and this depends on the coefficients appearing in the triple deck exponential.

In the wake region, Eq. (25) leads to a directly integrable form upon noting that the inner exponentials become negligible there. In this case:

$$\frac{u}{u_e} \to 1 - e^{-\phi 1} \qquad \text{for} \qquad y >> \varepsilon \qquad (71)$$

where $$\phi_1 = A_1 + B_1\, y/\delta + C_1 (y/\delta)^2$$

and $$\frac{\phi_x}{\phi_y} \to -y\, (\frac{\delta_x}{\delta}) \qquad \text{for} \qquad y >> \varepsilon \qquad (72)$$

Eq. (25) may be re-written as:

$$-\langle u'v'\rangle = -\nu u_y + (u_e-u)\int_0^{\infty} u_y\left(\frac{\phi x}{\phi y}\right)dy' + u\int_y^{\infty} u_y\left(\frac{\phi x}{\phi y}\right)dy' - 2\int_y^{\infty} u u_y\left(\frac{\phi x}{\phi y}\right)dy'$$

The terms require the following integrations:

$$\int_y^{\infty} e^{-\phi 1}\left[B_1 + 2C_1\,\frac{y}{\delta}\right]\left[-y\,\frac{\delta x}{\delta^2}\right]dy' \tag{73}$$

and

$$\int_y^{\infty} e^{-\phi 1}\left[1-e^{-\phi 1}\right]\left[B_1 + 2C_1\,\frac{y}{\delta}\right]\left[-y\,\frac{\delta x}{\delta^2}\right]dy' \tag{74}$$

These integrals may be rendered in terms of the error function and exponentials. For present purposes, however, only the case of high FST will be considered, for which: $C_1 = 0$. Then the above integrals are:

$$-\int_y^{\infty} e^{-A_1-B_1 y/\delta} B_1 y\,\frac{\delta x}{\delta^2}\,dy' = -\frac{\delta x}{B_1}\,e^{-A_1-B_1 y/\delta}\left[\frac{B_1 y}{\delta}+1\right] \tag{75}$$

$$-\int_y^{\infty} e^{-2A_1-2B_1 y/\delta} B_1 y\,\frac{\delta x}{\delta^2}\,dy' = -\frac{\delta x}{4B_1}\,e^{-2A_1-2B_1 y/\delta}\left[\frac{2B_1 y}{\delta}+1\right] \tag{76}$$

Under these conditions the Reynolds stress has the expression:

$$-\langle u'v'\rangle = U_y\left\{-\nu - \frac{V_{e(x)}}{B_1} + \frac{U_e\delta x}{B_1^2}\left(1+\frac{B_1 y}{\delta}\right) + \frac{1}{2}\,\frac{\delta x}{B_1^3}\,Uy\right\} \tag{77}$$

Where the coefficient, $B_1$, depends on the degree of FST. From the momentum integral equation it is also evident that $\delta_x$ is proportional to $U_\tau^2$.

Eq. (77) is in agreement with the 1984 investigation [1], in which the eddy viscosity is seen to increase linearly with y in the wake region. This earlier observation has now been shown to be a special case of the more general formulation expressed by Eq. (25).

## 3.6 The Suction Boundary Layer

The suction boundary layer was originally proposed for investigation [2] for the purpose of providing a simple limiting case of the actual boundary layer. Although this is still an interesting pursuit, and it will be described in this section, the recently obtained analytical solution presented earlier serves in this capacity even more admirably. The advantage posed by the suction boundary layer is that, by appropriate control, the flow statistics are independent of the x dimension, thereby permitting one exact integration of all the describing equations in the hierarchy. An approximation of this hypothetical flow condition could be achieved in reality through careful tailoring of upstream, downstream, and suction influences on the boundary layer. Theoretically, we envisage an infinite porous flat plate over which flows a uniform gas at a temperature differing from that of the wall. The viscous layer is maintained at a uniform and constant thickness through the agency of steady suction control. The "free stream" could be laminar or even uniformly turbulent, provided an energy mechanism maintains the turbulence. As the flow passes through the shear layer adjacent to the wall, the turbulence production terms will generate a non-vanishing Reynolds stress distribution. The thermal structure may be maintained at steady state by heat transfer mechanisms within the wall. Previous investigations concerning the suction boundary layer are mentioned by Schlichting [36] and recently by Gol'dshtik, et al. [37].

The suction boundary layer comprises a special case of the earlier equations, such that all x derivatives are taken to vanish identically. However, the wall boundary conditions now must include a non-vanishing velocity component perpendicular to the plane of the wall. The integrated form of the x momentum equation (Eq. (16)) becomes:

$$\langle n'u' \rangle = \mu u_y - \tau_w - u n_w \tag{78}$$

The conservation of mass equation yields (Eqs. (4) and (7)):

$$n = \rho v + \langle \rho' v' \rangle \equiv n_w \equiv \text{constant} \tag{79}$$

The Reynolds stress is assumed to vanish as y approaches infinity, along with the mean velocity gradient. Eq. (78) then provides an exact and explicit result for the wall shear:

$$\tau_w = -u_\infty n_\omega > 0 \quad \text{since} \quad n_\omega < 0$$

$$\text{or:} \qquad \tau_w = -\rho_\infty u_\infty v_\infty \tag{80}$$

The interesting observation here is that, regardless of turbulence intensity, the wall shear is generated solely from the conversion of the mean x momentum in the free stream to the vanishing x momentum condition at the wall. Eq. (78) provides a connection between the velocity profile and the Reynolds stress distribution. If $\frac{u}{u_\infty} = 1 - e^{-\phi}$, then Eq. (78) becomes:

$$\langle n'u' \rangle = [\mu \phi_y + n_w] u_\infty e^{-\phi} \tag{81}$$

$$\text{where} \qquad \phi(0) = 0 \quad \text{and} \quad \phi_y|_0 = -\frac{n_w}{\mu}$$

Here, $\phi$ is expected to have a form similar to the one observed in Blair's data.

An alternative interpretation of Eq. (78) leads to an explicit solution for the velocity field in terms of the Reynolds stress. By integration, one obtains:

$$\frac{U}{U_\infty} = 1 - e^{\xi} - \frac{e^{\xi}}{\tau_w} \int_0^{\xi} \langle n'u' \rangle e^{-\zeta} \, d\zeta \tag{82}$$

$$\text{where} \qquad \xi \triangleq \int_0^y \frac{n_w}{\mu} \, dy \equiv \frac{n_w y}{\mu} = \frac{\rho_\infty v_\infty y}{\mu} < 0$$

The laminar solution is the exponential one with vanishing Reynolds stress above. For the turbulent case, the mean velocity depends continuously on the shape of the Reynolds stress.

For varying levels of FST, the coefficients implicit in the $\phi$ function are expected to vary in a manner similar to those observed in Blair's data. In this case, the wake region of Eq. (81) reduces to the form:

$$\langle n'u' \rangle = \rho u \left( \frac{B_1 + 2C_1(y/\delta)}{\delta} \right) + n_w \rho u_\infty e^{-A_1 - B_1(y/\delta) - C_1(y/\delta)^2} \qquad (83)$$

Here, $A_1$, $B_1$, $C_1$, are assumed to depend on FST as described by Eq. (31). It is clear that length scales which characterize the FST would influence these coefficients as well as the intensity level of FST. It is further clear that such a dependence is not likely to be of a simple one dimensional kind, but that each dominant wave number in the power spectral density would exert its own influence. However, an averaged effect might be achieved by considering the longitudinal integral length scale:

$$\Lambda_f \triangleq \int_0^\infty f(y,r)\,dr \qquad (84)$$

where $$f \triangleq \langle u'(y,x)u'(y,x+r) \rangle$$

Although some previous investigators [3,5,38] have claimed that turbulence transport in the boundary layer is most sensitive to integral scales of the size of $\delta$, it is considered here to be a topic of further research.

In parallel with the momentum equation, the energy equation (9) may also be directly integrated once to give:

$$\langle n'H' \rangle = \frac{\mu}{P_r} H_y - n_w(H - H_w) - q_w + u\left(1 - \frac{1}{P_r}\right) u\, u_y \qquad (85)$$

By evaluation at the wall and in the free stream, one obtains:

$$q_w = - n_w(H_\infty - H_w) = KT_y|_w \qquad (86)$$

The physical interpretation of this flow situation is that the flux of total energy in the y direction remains invariant with y, whereas specific transport mechanisms may dominate in different regions. At the wall, the net energy flux is composed of a combination of thermal conduction and heat convection through the porous wall. In the momentum equation, the corresponding invariant is a combination of local shear stress and streamwise momentum flux in the y direction.

In order to arrive at an expression for $P_{rt}$, the following decomposition is noted:

$$\langle n'H' \rangle = C_p\langle n'T' \rangle + u\langle n'u' \rangle + v\langle n'v' \rangle + \langle n'k'^2 \rangle \qquad (87)$$

For cases of dominant thermal energy content, the last two terms may be neglected to obtain from Eqs. (85) and (87):

$$C_p\langle n'T' \rangle = KT_y - n_w C_p(T-T_\infty) + \frac{n_w}{2}(U_\infty - U)^2 \qquad (88)$$

The turbulent Prandtl number is then:

$$P_{rt} = \frac{\varepsilon_M}{\varepsilon_H} = \frac{\langle n'u' \rangle T_y}{\langle n'T' \rangle U_y} = \frac{[\mu U_y + n_w(U_\infty - U)]T_y}{[KT_y + n_w C_p(T_\infty - T) + \frac{n_w}{2}(U_\infty - U)^2]U_y} \qquad (89)$$

This equation expresses the turbulent Prandtl number directly in terms of the mean velocity and temperature fields. The expression becomes indeterminate at both the wall and in the free stream.

The above analysis provides valuable physical insight into several of the processes at work in a turbulent boundary layer. The major difference in the

usual flat plate boundary layer is the growth of the boundary layer thickness with x, whereas this thickness is constant for the uniform suction layer. Also in the boundary layer, both the fluxes of energy and momentum are not quite invariant with respect to y as they are here, owing to the growing streamwise integral deficits.

# 4.0 RESULTS

## 4.1 STANCHEK - Analytical Comparison

The initial effort with the code STANCOOL consisted of slight alterations in format so that it would be compatible with the IBM 3081 system at the University of Oklahoma. After several weeks, the code was producing results that duplicated the computations obtained in 1984 at AFWAL/POTC by Sepri and Ebert [1]. The next phase consisted of modifications to the turbulent flux models as described in the proposal [2] for the 1985 investigation. These modifications occur primarily in the subroutine AUX. The version of STANCOOL now at OU contains five separate options in the broader category of mixing length models in the code. These are: (1) the original MLH, (2) the MLH as modified by Sepri and Ebert (denoted FST1), (3) the extended MLH as described in [2] (denoted FST2), (4) the version designed to calculate the case corresponding to the analytical solution (denoted STANCHEK), and (5) the latest turbulent flux model based on the integral relations presented earlier (denoted FST3). In this section the results of STANCHEK are discussed.

The lowest order turbulence closure rests on the notion that if the Reynolds stress distribution is presented along with the $P_{rt}$ profile, then a boundary layer code, such as STANCOOL, may be used to calculate the mean velocity and mean temperature profiles, along with the $C_f$ and $S_t$ distributions on the wall. In STANCHEK, $\langle u'v' \rangle$ and $P_{rt}$ are modified in AUX to agree with the analytical profiles given by Eq. (53) and Eq. (64) respectively. STANCOOL is then run as usual to produce the flow field solution. Here, we compare these calculated results with the analytical solution presented in Section 3.4. This check procedure is considered to be quite useful since the number of alterations of STANCOOL consists of only approximately ten lines.

In order to set the stage, the behavior of the analytical solution will be described first. In Fig. 42 is presented a scaled schematic of the particular analytical boundary layer. The configuration of the flat plate corresponds to Blair's experiment. Shown in the figure are computer plots of $\delta^*(x)$, $\delta(x)$ and two mean velocity profiles located at the initial and final stations used by Blair for measurement. The square root boundary layer singularity is evident at the leading edge of the plate. The Reynolds number variation is also indicated along the abscissa. The profiles consist of the exponential given by Eq. (50). Fig. 43 displays both the Reynolds stress profile (Eq. (53)) and the mean normal velocity profile (Eq. (52)) in the boundary layer. These curves are qualitatively similar to those expected for an actual turbulent boundary layer.

The profiles of viscous dissipation (mean velocity only), turbulence production, and Reynolds stress are shown in Fig. 44. Also indicated are the various profile averaged length scales describing these mechanisms. It is clear that a turbulent boundary layer may be described by several length scales beginning with the dissipation scale, continuing with the production scale, and finally ending with the boundary layer thickness itself. For the actual turbulent boundary layer, these characteristic inner scales lie closer to the wall itself. It is suggested here that the three characteristic scales observed in the triple exponential might correspond to those of viscous dissipation, Reynolds stress, and $\delta$, in increasing order. However, this identification has not been firmly established herein, and it remains a subject for further investigation.

In Fig. 45 are displayed the relative growths and profiles of the mean temperature and velocity fields. The molecular Prandtl number is taken to be 0.71, so that this calculation corresponds to the case of an air flow over a heated (or cooled plate). The thermal boundary layer is seen to be

approximately 15% thicker than the viscous layer. The variation of $P_{rt}$ in the boundary layer is shown in Fig. 46 as given by Eq. (64). The three curves correspond to molecular Prandtl numbers of 0.112, 0.71 and 3.328. For these particular cases of the analytical solution, $P_{rt}$ approaches constant levels in the wake region of the boundary layer and beyond. However, it is important to note that such smooth $P_{rt}$ profiles would not result if the wall temperature along the plate were not constant (e.g. a step change in temperature).

Given the analytical solution described above, it is of interest to ascertain how well STANCOOL calculates this solution. In Fig. 47 is shown a comparison of the analytical solution (symbols) with the STANCOOL result (curve) for the velocity profile at x = 84 in. "Transition" is forced at the leading edge of the plate. Both profiles are presented scaled with respect to their own boundary layer displacement thicknesses. The agreement appears to be excellent in this representation. However, there are two discrepancies to be noted which are not evident in this figure. The first is shown in Fig. 48 which magnifies the wake region of the boundary layer. It is clear that STANCOOL has reproduced the exponential character of this particular solution remarkably well except at the boundary edge, near which numerical errors cause a departure of the calculation from the true nature of the decay. In Fig. 47 this departure is not apparent at all because the error magnitude is less than 1% of the free stream velocity. One might expect such a small error not to be significant; however, in fact, the calculation of the boundary layer thickness is extremely sensitive to the nature of the decay rate at the edge. This leads directly to the second discrepancy; namely, the growth rate of the boundary layer thickness as calculated by STANCOOL is approximately 6% less than that of the analytical solution. The velocity profiles in Fig. 47 are replotted in Fig. 49 with the abscissa scaled with respect to an internally calculated ~. A measurable

mismatch is exhibited, which is solely due to an error in the $\delta$ calculation in STANCOOL. This, in fact, also provides a partial explanation for some of the profile mismatches described in the earlier work of 1984 [1]. The $\delta$ calculated by STANCOOL does not always match the actual $\delta$ measured by Blair. A more suitable abscissa is comprised of $y/\delta^*$, since this is not as sensitive to small discrepancies at the boundary layer edge.

Fig. 50 further demonstrates the above discrepancy. The analytical and calculated "Reynolds stresses" in STANCHEK are in fact forced to be identical with respect to $y/\delta$. After computation these profiles are rescaled with respect to $\delta^*$ and the resulting mismatch is displayed in Fig. 50. Last, Fig. 51 displays the comparison of mean temperatures obtained by using the $P_{rt}$ profile given by Eq. (64). The discrepancy shown here is attributed to a similar difference in growth rates of the respective thermal boundary layer thicknesses. A resolution of this problem in the calculation of $\delta$ in STANCOOL has not yet emerged, and this topic remains for further investigation. In summary, however, it is gratifying that such a simple alteration of the STANCOOL mixing length hypothesis has yielded excellent profiles except for the scaling of the boundary layer thickness.

## 4.2 Comparison with Boundary Layer Data

Another benefit of the analytical solution is that it alerts the user of STANCOOL to another possible discrepancy in calculations of real boundary layers, although upon reflection, this possibility is obvious. Much of the profile mismatch shown in Reference [1] might be attributable to a disparity between calculated and measured boundary layer thicknesses, which is a comparison that must be considered here as well. The results presented in this section correspond to utilization of the model described by Eq. (49), and this

option in STANCOOL is the one denoted by FST3. Although this model permits the calculation of an eddy viscosity, $\varepsilon_m$, based on mean velocity profiles, an identification with the mixing length hypothesis is not quite appropriate. First, a mixing length is not introduced in the model, and second, the resulting eddy viscosity is not entirely proportional to $U_y$, as it is in the MLH.

The mixing length extension described in the proposal for this investigation [2] is denoted FST2 in STANCOOL, and it has also been executed with partial success. A parametric variation of FST influence on the inner layer (denoted by C[2]) has indeed demonstrated that wall and wake regions may be separately controlled and calculated by variations of the parameters of A, B, and C. However, a rational intrinsic modeling for C has not become apparent from the study of Blair's data, whereas the formulation given by Eq. (49) has such an advantage. Since FST3 is considered superior to FST2 at this juncture, only the former results will be displayed here.

In Figs. 52 and 53 are shown Reynolds stress comparisons between Blair's data at x = 84 in. and the calculated profiles utilizing FST3. In these calculations the coefficients in the exponentials are taken to have representative constant values, and no attempt has been made to match the curve fits of Blair's data at every x location. It is clear that the streamwise evolutions of these Reynolds stress profiles agree well with those measured at x = 84 in. for both the bounding cases of low FST (0.25%) and high FST (5%), except for a slight mismatch of boundary layer thicknesses which was shown earlier to be attributable to STANCOOL.

Corresponding plots for mean velocity profiles are shown in Figs. 54 and 55. Here also, the calculated and measured profiles display a good agreement in the particulars of their shapes, although slight shifts in the $\delta$'s are observable. The mean temperature comparisons are shown in Figs. 56 and

57 with qualitatively similar results, except that the mismatch is more pronounced. This mismatch may be attributable to two causes. First, the $P_{rt}$ profile is assumed to be unity throughout the boundary layer, because of lack of time for including the improved modeling. Second, it is not evident to what extent the discrepancy between the calculated and measured thermal thicknesses causes the observed mismatch.

These figures demonstrate that the modeling procedure has excellent promise, although there has not yet been sufficient time to bring the work to completion. Several avenues connected with the exponential structure require further investigation, and these will be discussed in Section 5.

## 4.3 Turbulent Prandtl Number

The turbulent Prandtl number has been introduced into the study of boundary layers primarily for two reasons: (1) to highlight the strong similarity that may occur between the momentum and energy equations, and (2) to provide a convenient numerical method for obtaining solutions which involve a coupling of the velocity and temperature fields. Originally, the Reynolds analogy was meant to be applicable under the restriction of unity Prandtl number (either molecular or turbulent). Recently, computational schemes have employed $P_{rt}$ profiles which vary significantly from unity throughout the boundary layer. It seems clear that the postulation of a $P_{rt}$ profile can be artificial under some circumstances (as may be that of the Prandtl mixing length), and these are the cases in which the viscous and thermal boundary layers bear little similarity to each other. Even with a close resemblance, the subtle variations in $P_{rt}$ may be difficult to model.

One example for which the viscous and thermal layers are markedly different is the case of a step increase in wall temperature in a boundary layer that

already has a developed viscous region. One might argue that in the neighborhood of the thermal jump the thermal boundary layer hypothesis is invalidated, and also that the developing thermal layer requires a certain distance in which to equilibrate. However, even substantially downstream of the jump, there will be a mismatch in thermal and viscous thicknesses. In such a circumstance, it is of interest to question the validity of the Reynolds analogy and also the significance of the turbulent Prandtl number. Even in this case, it is not obvious that the assumption of constant $P_{rt}$ is a poor one. Recall the definition:

$$P_{rt} = \frac{\epsilon_m}{\epsilon_H} = \frac{\langle u'v' \rangle T_y}{\langle v'T' \rangle U_y} \qquad (90)$$

Beyond the thermal layer the mean temperature gradient vanishes while $\langle u'v' \rangle$ and $U_y$ do not vanish in the larger viscous layer. However, one would also expect $\langle v'T' \rangle$ to vanish beyond the thermal layer. Therefore, depending on the respective rates of decline, it is possible for $P_{rt}$ to remain constant or be mildly varying. Similarly, it is possible for $P_{rt}$ to remain constant whenever any of the four factors becomes either large or small, provided the effect is compensated appropriately by the other factors. In fact, the gross trends do compensate in just such a manner. However, we are now in a position to discuss two examples for which the gross trends do not compensate adequately, and these bring into question the general suitability of calculating heat transfer via $P_{rt}$ modeling.

The first example has been provided during the 1984 investigation [1], in which an explanation was offered for the large decline of $P_{rt}$ in several of the wake regions observed by Blair. Owing to asymmetries in the experiment, $\langle u'v' \rangle$ appears to have a zero crossing external to the boundary layer before such a crossing is achieved by $U_y$. By the experimental arrangement, $\langle v'T' \rangle$ and $T_y$

never have zero crossings in this case. Consequently, $P_{rt}$ also has a zero crossing, and the wake region $P_{rt}$ profile declines in a sensitive manner, which is extremely difficult to model. All four factors in Eq. (90) tend to zero at differing rates. In this case, the $P_{rt}$ behavior is not dominated at all by a similarity of $\langle v'T' \rangle$ to $\langle u'v' \rangle$ or of $T_y$ to $U_y$. Another related observation of Blair's data has been given for the case of high FST, for which the wake decay of the mean temperature profile is exponential, whereas the decline of $\langle v'T' \rangle$ is exponential at <u>half</u> that rate [1]. In reconsidering the thermal jump problem in which a smaller thermal layer is embedded within a larger viscous layer, it becomes highly questionable whether the declines of $T_y$ and $\langle v'T' \rangle$ are similar enough to maintain a constant $P_{rt}$. Clearly, the dissimilarity between momentum and energy cannot be compensated to result in a constant $P_{rt}$.

The second example is provided by the exact particular solution described in Section 3.4. An extension of the analysis to include variable $\beta(x)$ leads to the explicit formula:

$$P_{rt} = \frac{\left[\frac{2y}{\delta^*} - 1\right] + \frac{\nu}{u_\tau^2} u_y}{-\frac{1}{Pr} + \frac{2}{\beta}\left\{-1 + \frac{1}{\beta} + \frac{y}{\delta^*}\right\} + \frac{2}{\beta}\frac{\nu}{u_\tau^2} u_y \left\{1 - \frac{1}{\beta + 1}\right\} + \text{TERM}} \qquad (91)$$

$$\text{where TERM} = \frac{\beta_x}{\delta^*_x}\left\{-\frac{2\delta^*}{\beta^3}\left(1 + \frac{\beta y}{\delta^*}\right) + \frac{2\nu}{u_\tau^2} u_y \frac{\delta^*}{\beta(\beta+1)^2}\left(1 + \frac{y[\beta + 1]}{\delta^*}\right)\right\}$$

Although Fig. 46 exhibits mildly varying profiles of $P_{rt}$, these cases are chosen such that the origins for the thermal and viscous layers coincide. Even here there is a variation of $P_{rt}$ throughout the boundary layer. For the more severe comparison of a step change in wall temperature, it is clear from Eq. (91) that the $P_{rt}$ profile becomes more strongly varying in the y direction. Furthermore, if either $q_w$ or $T_w$ varies with x (as in most real cases), then the $P_{rt}$ profile

also becomes x dependent. Although in Blair's experiments $q_w$ was held constant, the wall temperature varied significantly with x. One may view a continuous thermal change with x to consist of a superposition of many infinitesimal jumps in wall temperature. Each such change propagates into the boundary layer in a manner similar to the embedded thermal layer described above. Therefore, the thermal boundary layer is a subtle composite of a history of upstream variations that is quite distinct from the development of the momentum layer. Although every reasonable model for $P_{rt}$ will give results for heat transfer that may appear to be correct qualitatively, the quantitative degree of accuracy and predictability would appear to be difficult to ascertain.

In view of the foregoing two examples, it is tentatively concluded that $P_{rt}$ modeling is an inadequate approach for turbine blade heat transfer calculations. However, the more general and novel formulations for $\langle u'v' \rangle$ and $\langle v'T' \rangle$ given in Eqs. (25) and (20) provide an intriguing alternative which does not suffer from the problems mentioned for $P_{rt}$ modeling. The factors, $\epsilon_m$ and $\epsilon_H$, are directly calculable in terms of modeled mean profiles (or calculated mean profiles in a marching scheme). There is no need to form a ratio of quantities which vanish at different rates; thus, the difficulty of a sensitive indeterminacy is avoided. Furthermore, wall temperature history effects may be directly incorporated into the integral scheme in which $\langle v'T' \rangle$ is calculated via successive mean temperature (and velocity) profiles. In parallel, a modeling is not required for the Prandtl mixing length if Eq. (25) is utilized to calculate the Reynolds stress. It has become clear from study of the wake region at high FST that the eddy viscosity is not adequately represented by $\ell^2 \frac{\partial u}{\partial y}$ there, but rather by a term proportional to y itself. The formulation given by Eq. (27) provides a direct means of calculating the eddy viscosity throughout the

boundary layer. These directions are proposed for further research.

In order to close the discussion of $P_{rt}$, a summary will be given here of several earlier works on the subject. The search for investigations dealing with $P_{rt}$ has yielded References [37,39-71], and these may be classified into three categories: wall boundary layers, wakes and jets, and pipes and channels. A graphical summary of the relevant boundary layer trends is presented in Fig. 58. The work by Rotta [39] is often referred to as a good description of the decline of $P_{rt}$ in the outer boundary layer. In fact, he proposed his simple function through observations of pipe data taken by Ludwieg [40]. Similarly, it should be noted that the commonly accepted method for calculating $\tau_w$ in a [illegible] boundary layer utilizing the logarithmic fit with the von Karman constant, K, has originated from experimental work in pipe flow [36], in which the wall shear is more readily measured than in the boundary layer. In Fig. 58 are summarized the recent works by Simpson, et al. [41], Senda, et al. [42], Subramanian and Antonia [43], and Snijders, et al. [44]. These were directed towards measurements of $P_{rt}$ profiles in heated turbulent boundary layers. It is seen that there are significant shifts of $P_{rt}$ level from one experiment to another. Also, all but one of the $P_{rt}$ profiles tend to exhibit marked declines in the wake region, except that the error band is large in both the near wall and far wake regions owing to wall interference and vanishing signals respectively. All of these measurements have been made in tunnels for which channel flow effects are presumably negligible, and they bear similarity to Blair's results. In marked contrast are the $P_{rt}$ profiles exhibited for wakes and jets in free ambients as shown in Fig. 59. In these cases the values for $P_{rt}$ actually tend to increase beyond the viscous layer edge. It is clear that the external behavior is strongly influenced by the relative rates at which the turbulent fluxes and mean gradients vanish. These observations further support the

conclusion promoted herein that the turbulent Prandtl number is a difficult and unreliable parameter to model, and such a methodology ought to be avoided if possible.

## 5.0 CONCLUSIONS AND RECOMMENDATIONS

The direction and content of the present investigation have been guided by the general objective of successfully calculating the evolution and characteristics of turbulent boundary layers involving heat transfer. Although many computational schemes are currently being employed, it is clear that a reliable and fundamental approach has not yet emerged in the technical community [72], and even calculations of the simplest flat plate cases are not completely satisfactory. This state of affairs points out the need for continued fundamental investigations. The specific objective herein has been to study the effects of free stream turbulence (FST) through utilization of Blair's excellent data and through computations and modifications of the code, STANCOOL.

In addition to the tasks mentioned in the proposal for this investigation [2], several other major accomplishments have come to fruition during the course of this eight month effort. First, in the search for a wall layer characterization to match the earlier exponential wake observation, an analytical approximation has been achieved which describes the complete boundary layer profiles of mean velocity and temperature. This analytical description is surprisingly comprehensive and flexible, since it is shown to match laminar as well as turbulent profiles with appropriate changes in the parameters. The effect of FST is explicitly displayed in the coefficients of the triple deck exponential. The function matches the data presented by Coantic [30] and Kline, et al. [31], as well as those of Blair [18]. It is curious that three distinct layers are observed, apparently for the first time herein.

The second accomplishment has been the expression of the Reynolds stress and turbulent heat flux profiles directly in terms of the mean velocity and temperature profiles of the boundary layer through an integro-differential relationship. Scrutiny of Blair's data has permitted a tractable formulation of

this relationship, and the model has been implemented, although this novel work has not yet come to completion. Sample results are exhibited. FST is seen to influence the wake region of the boundary layer explicitly, and the wall region implicitly.

Third, the more general formulation has lead to a remarkable particular analytical solution to the equations describing a turbulent boundary layer. This solution applies to the case of a special form of the Reynold stress distribution, which is not entirely realistic, but the solution is informative. The analytical solution may be used to check the correctness of any turbulent boundary layer code, and it also provides guidance for the interpretation of the physical mechanisms at work in a turbulent boundary layer. The solution is extended to the energy equation, and analytical profiles for $P_{rt}$ are provided for this special case.

Fourth, the study of the suction boundary layer initially proposed is shown to be a special case of the more general formulation presented herein. This case is described, and an explicit formula is presented for the turbulent Prandtl number profile.

Fifth, STANCOOL has been made operational on the IBM 3081 system at the University of Oklahoma, and three recent modifications in turbulence modeling have been incorporated. These consist of (1) STANCHEK, which calculates the analytical test case; (2) FST2, which utilizes a separate variation of wake and wall FST effects in the boundary layer; and (3) FST3, which incorporates the more general and novel integral approach to the turbulent fluxes. These options have been run and compared with data with favorable results. However, the comparisons are not yet complete, and a question has also arisen concerning the rate of boundary layer growth as calculated by STANCOOL. These issues remain for further investigation.

Sixth, a discussion is presented concerning the modeling and calculation of $P_{rt}$ profiles. Several formulas are given for its specification, among which are two explicit analytical ones and one general calculation procedure. A survey of the literature has revealed a disparity in reported $P_{rt}$ profiles. The proposed calculation procedure obviates the need for introducing the $P_{rt}$ profile altogether.

Based on the findings of this investigation, several avenues for continued study are recommended. With the novel observation of a whole layer formula, it is of great interest to perform experimental work that focuses on establishing the validity and accuracy of the triple deck exponential description. The behavior of the three associated length scales is a related topic of further research. It remains to be seen whether a set of universal coefficients in the exponential function may be obtained and how the length scales depend on the evolution of wall shear. Further calculations are recommended with the new integro-differential model for the turbulent fluxes. Although the present calculations demonstrate a good fit in quality, a better match is to be sought in regard to the boundary layer growth rate. The investigation should also be extended to include the cases of boundary layers with non-vanishing pressure gradients, since these are of practical concern. Lastly, there has not been sufficient time to explore fully the general formulation of the $P_{rt}$ profile presented here, and if and its use is to be pursued, then its calculation in STANCOOL requires further work.

## 6.0 REFERENCES


1. Sepri, P. and Ebert, J. L., "Calculation of Enhanced Heating in Turbulent Boundary Layers Influenced by Free Stream Turbulence", 1984 USAF-SCEEE Summer Faculty Research Program, Contract No.: F49620-82-C-0035, Final Report, 27 August 1984.

2. Sepri, P., "Free Stream Turbulence Effects on Turbulent Heat Transfer", Research Proposal submitted to the AFOSR RISE Program, Subcontract No: 84RIP33, start date: 1 January 1985.

3. Simonich, J. C., and Bradshaw, P., "Effect of Free-Stream Turbulence on Heat Transfer through a Turbulent Boundary Layer", ASME Journal of Heat Transfer, Vol. 100, November 1978, pp. 671-677.

4. Bayley, F. J. and Priddy, W. J., "Effects of Free-Stream Turbulence Intensity and Frequency on Heat Transfer to Turbine Blading", ASME Journal of Engineering for Power, Vol. 103, January 1981, pp. 60-64.

5. Pedisius, A. A., Kazimekas, P.-V.A., and Slanciauskas, A. A., "Heat Transfer from a Plate to a High-Turbulence Air Flow", Heat Transfer-Soviet Research, Vol. 11, No. 5, Sept.-Oct. 1979, pp. 125-134.

6. McDonald, H. and Kreskovsky, J. P., "Effect of Free Stream Turbulence on the Boundary Layer", Int. J. Heat Mass Transfer, Vol. 17, 1974, pp. 705-716.

7. Hall, J. D., and Gibbings, J. C., "Influence of Stream Turbulence and Pressure Gradient upon Boundary Layer Transition", Journal of Mechanical Engineering Science, Vol. 14, No. 2, 1972, pp. 134-146.

8. Meier, H. U., and Kreplin, H. -P., "Influence of Freestream Turbulence on Boundary-Layer Development", AIAA Journal, Vol. 18, No. 1, January 1980, pp. 11-15.

9. Krishnamoorthy, V., "Effect of Turbulence on the Heat Transfer in a Laminar and Turbulent Boundary Layer over a Gas Turbine Blade", ASME Paper 82-GT-146, 1982, pp. 1-9.

10. Junkhan, G. H., and Serovy, G. K., "Effects of Free-Stream Turbulence and Pressure Gradient on Flat-Plate Boundary-Layer Velocity Profiles and on Heat Transfer," ASME Journal of Heat Transfer, Vol. 89, May 1967, pp. 169-176.

11. Kestin, J., "The Effect of Free-Stream Turbulence on Heat Transfer Rates", Advances in Heat Transfer, Vol. 3, ed. by T. F. Irvine, Jr., and J. P. Hartnett, Academic Press, London, 1966.

12. Sugawara, S., Sato, T., Hirosyasa, K., and Osaka, H., "The Effect of Free-Stream Turbulence on Heat Transfer from a Flat Plate", NACA Tech. Memo 1441, 1958.

13. Feiler, C. E., and Yaeger, E. B., "Effect of Large-Amplitude Oscillations on Heat Transfer", NASA Tech. Report R-142, 1962.

14. Edwards, A., and Furber, B. N., "The Influence of Free-Stream Turbulence on Heat Transfer by Convection from an Isolated Region on a Plane Surface in Parallel Air Flow", Proc.-Inst. Mech. Engrs. London, Vol. 1970, 1956, p. 941.

15. Blair, M. F., "Influence of Free-Stream Turbulence on Turbulent Boundary Layer Heat Transfer and Mean Profile Development, Parts I & II", ASME Journal of Heat Transfer, Vol. 105, February 1983, pp. 33-47.

16. Blair, M. F., "Influence of Free-Stream Turbulence on Boundary Layer Transition in Favorable Pressure Gradients", ASME Journal of Engineering for Power, Vol. 104, October, 1982, pp. 743-750.

17. Blair, M. F., "The Effect of Free-Stream Turbulence on the Turbulence Structure and Heat Transfer in Zero Pressure Gradient Boundary Layers", United Technologies Research Center Report: R82-915634-2, East Hartford, Conn., November, 1982.

18. Blair, M. F., "Final Data Report-Vol. I-Velocity and Temperature Profile Data for Zero Pressure Gradient, Fully Turbulent Boundary Layers", UTRC Report R81-914388-15, E. Hartford, Conn., January, 1981.

19. Blair, M. F., "Final Data Report-Vol. II-Velocity and Temperature Profile Data for Accelerating, Transitional Boundary Layers", UTRC Report R81-914388-16, E. Hartford, Conn., January 1981.

20. Blair, M. F., "Combined Influence of Free-Stream Turbulence and Favorable Pressure Gradients on Boundary Layer Transition and Heat Transfer, UTRC Report R81-914388-17, E. Hartford, Conn., March 1981.

21. Blair, M. F., "The Influence of Free-Stream Turbulence on the Zero Pressure Gradient Fully Turbulent Boundary Layer", UTRC Report R80-914388-12, E. Hartford, Conn., September 1980.

22. Daniels, L. D., and Browne, W. B., "Calculation of Heat Transfer Rates to Gas Turbine Blades", Int. J. Heat Mass Transfer, Vol. 24, No. 5, 1981, pp. 871-879.

23. Crawford, M. E., and Kays, W. M., "STAN5 - A Program for Numerical Computation of Two-Dimensional Internal and External Boundary Layer Flows", NASA CR-2742, November, 1976.

24. Gaugler, R. E., "Some Modifications to, and Operational Experiences with, the Two-Dimensional, Finite Difference, Boundary-Layer Code, STAN5", ASME Paper 81-GT-89, 1981, pp. 1-5.

25. MacArthur, C. D., "Prediction of Free-Stream Turbulence Effects on Boundary Layer Heat Transfer - An Evaluation of the Heat Transfer Code STAN5", 1983 USAF-SCEEE Graduate Student Summer Support Program, Contact No. F49620-82-0035, 16 September 1983.

26. Winstanley, D.K., Booth, T.C., and Dunn, M.G., "The Predictability of Turbine Vane Convection Heat Transfer", AIAA Paper No. 81-1435, July 27-29, 1981.

27. Miyazaki, H. and Sparrow, E. M., "Analysis of Effects of Free-Stream Turbulence on Heat Transfer and Skin Friction", ASME Journal of Heat Transfer, Vol. 99, November 1977, pp. 614-619.

28. Coles, D., "The Law of the Wake in the Turbulent Boundary Layer," Journal of Fluid Mechanics, Vol. 1, 1956, pp. 191-226.

29. Favre, A., "Statistical Equations of Turbulent Gases", In: "Problems of Hydrodynamics and Continuum Mechanics", SIAM, 1969, pp. 231-266.

30. Coantic, M., "Evolution, en fonction du nombre de Reynolds, de la distribution des vitesses moyennes et turbulentes dans une conduite", Comptes Rendus de Acad. des Sc., Paris, Vol. 264, Serie A, 17 mai 1967, pp. 849-852.

31. Kline, S.J., Reynolds, W.C., Schraub, F.A., and Runstadler, P.W., "The Structure of Turbulent Boundary Layers", Journal of Fluid Mechanics, vol. 30, part 4, 1967, pp. 741-773.

32. Long. R.R., and Chen, T.C., "Experimental Evidence for the Existence of the 'Mesolayer' in Turbulent Systems", Journal of Fluid Mechanics, vol. 105, 1981, pp. 19-59.

33. Afzal, N., "Mesolayer Theory for Turbulent Flows", AIAA Journal, vol. 22, No. 3, March 1984, pp. 437-439.

34. Malkus, W.V.R., "Turbulent Velocity Profiles from Stability Criteria", Journal of Fluid Mechanics, vol. 90, part 3, 1979, pp. 401-414.

35. Van Driest, E.R., "On Turbulent Flow near a Wall", Journal of the Aeronautical Sciences, Vol. 23, 1956, pp. 1007-1011.

36. Schlichting, H., Boundary Layer Theory, McGraw-Hill Book Co., 7th Ed., 1979.

37. Gol'dshtik, M.A., Kutateladze, S.S., and Lifshits, A.M., "Determination of the Turbulent Prandtl Number in an Asymptotic Boundary Layer with Suction", Izvestiya Akademii Nauk. SSSR, Mekhanika Zhidkosti i Gaza, No. 1, Jan.-Feb. 1981, pp. 74-79.

38. Meier, H.U., and Kreplin, H.P., "Influence of Freestream Turbulence on Boundary Layer Development", AIAA Journal, Vol. 18, No. 1, January 1980, pp. 11-15.

39. Rotta, J.C., "Temperaturverteilungen in der Turbulenten Grenzschicht an der Ebenen Platte", Int. J. Heat Mass Transfer, Vol. 7, 1964, pp. 215-228.

40. Ludwieg, H., "Bestimmung des Verhaltnisses der Austauschköffizienten für Warme und Impuls bei turbulenten Grenzschichten", Zeit. Flugwiss., Vol. 4, 1956, pp. 73-81.

41. Simpson, R.L., Whitten, D.G., and Moffat, R.J., "An Experimental Study of the Turbulent Prandtl Number of Air with Injection and Suction", Int. Journal of Heat and Mass Transfer, Vol. 13, 1970, pp. 125-143.

42. Senda, M., Suzuki, K., and Sato, T., "Turbulence Structure Related to the Heat Transfer in a Turbulent Boundary Layer with Injection", Turbulent Shear Flows, Vol. 2, Springer-Verlag, 1980, pp. 143-157.

43. Subramanian, C.S., and Antonia, R.A., "Effects of Reynolds Number on a Slightly Heated Turbulent Boundary Layer", Int. J. Heat Mass Transfer, Vol. 24, No. 11, 1981, pp. 1833-1846.

44. Snijders, A.L., Koppius, A.M., Nieuwvelt, C., "An Experimental Determination of the Turbulent Prandtl Number in the Inner Boundary Layer for Air Flow over a Flat Plate", Int. J. Heat Mass Transfer, Vol. 26, No. 3, 1983, pp. 425-431.

45. Chen, C.P., "Determination Experimentale du Nombre de Prandtl Turbulent pres d'une Paroi Lisse", Int. J. Heat Mass Transfer, Vol. 16, 1973, pp. 1849-1862.

46. Sreenivasan, K.R., Antonia, R.A., and Chambers, A.J., "On the Variation of the Turbulent Prandtl Number in Shear Flows", Int. Comm. Heat Mass Transfer, Vol. 11, 1984, pp. 497-501.

47. Antonia, R.A., "Behaviour of the Turbulent Prandtl Number Near the Wall", Int. J. Heat Mass Transfer, Vol. 23, 1980, pp. 906-908.

48. Browne, L.W.B., and Antonia, R.A., "Measurements of Turbulent Prandtl Number in a Plane Jet", Journal of Heat Transfer, Vol. 105, August 1983, pp. 663-665.

49. Dorfman, A.Sh., "Influence of Turbulent Prandtl Number on Heat Transfer of a Flat Plate", Zhurnal Prikladnoi Mekhaniki i Tekhnicheskoi Fiziki, No. 4, July-Aug. 1984, pp. 81-85.

50. Nakayama, A., Koyama, H., and Ohsawa, S., "Momentum/Heat-Transfer Analogy for Turbulent Boundary Layers in Mild Pressure Gradients", AIAA Journal, Vol. 22, No. 6, 1984, pp. 841-844.

51. Cebeci, T., "A Model for Eddy Conductivity and Turbulent Prandtl Number", Journal of Heat Transfer, May 1973, pp. 227-234.

52. Meier, H.U. and Rotta, J.C., "Experimental and Theoretical Investigations of Temperature Distributions in Supersonic Boundary Layers", AIAA Paper No. 70-744, 1970.

53. Johnson, D.S., "Velocity and Temperature Fluctuation Measurements in a Turbulent Boundary Layer Downstream of a Stepwise Discontinuity in Wall Temperature", Journal of Applied Mechanics, Vol. 26, Trans. ASME, Series E, Vol. 81, No. 3, Sept. 1959, pp. 325-336.

54. Chan, Y.Y., "A Note on the Effect of Turbulent Prandtl Number Distribution on Compressible Turbulent Boundary Layers", C.A.S.I. Transactions, Vol. 6, No. 2, Sept. 1973, pp. 102-104.

55. Rotta, J.C., "Recent Developments in Calculation Methods for Turbulent Boundary Layers with Pressure Gradients and Heat Transfer", J. of Applied Mech., Vol. 33, June 1966, p. 429.

56. Chuang, H., and Renda, R.B., "Turbulent Prandtl Number in Thermally Stratified Shear Flows of Air", Int. J. Heat Mass Transfer, Vol. 12, 1969, pp. 1585-1594.

57. Geshev, P.I., "Influence of Heat conduction of the Wall on the Turbulent Prandtl Number in the Viscous Sublayer", Inzhenerno-Fizicheskii Zhurnal, Vol. 35, No. 2, August 1978, pp. 292-296.

58. Ginzburg, I.P., and Korneva, I.V., "Influence of Turbulent Pr Number on Friction and Heat Transfer at a Plate Immersed in a Turbulent Gas Stream", Inzhenerno-Fizicheskii Zhurnal, Vol. 9, No. 2, 1965, pp. 155-162.

59. Jischa, M., and Rieke, H.B., "About the Prediction of Turbulent Prandtl and Schmidt Numbers from Modeled Transport Equations", Int. J. Heat Mass Transfer, Vol. 22, 1979, pp. 1547-1555.

60. McEligot, D.M., Pickett, P.E., and Taylor, M.F., "Measurement of Wall Region Turbulent Prandtl Numbers in Small Tubes", Int. J. Heat Mass Transfer, Vol. 19, 1976, pp. 799-803.

61. Reynolds, A.J., "The Prediction of Turbulent Prandtl and Schmidt Numbers", Int. J. Heat Mass Transfer, Vol. 18, 1975, pp. 1055-1069.

62. Reynolds, A.J., "The Variation of Turbulent Prandtl and Schmidt Numbers in Wakes and Jets", Int. J. Heat Mass Transfer, Vol. 19, 1976, pp. 757-764.

63. Spalding, D.B., "Contribution to the Theory of Heat Transfer Across a Turbulent Boundary Layer", Int. J. Heat Mass Transfer, Vol. 7, 1964, pp. 743-761.

64. Kestin, J., and Richardson, P.D., "Heat Transfer Across Turbulent, Incompressible Boundary Layers", Int. J. Heat Mass Transfer, Vol. 6, 1963, pp. 147-189.

65. Wassel, A.T., and Catton, I., "Calculation of Turbulent Boundary Layers over Flat Plates with Different Phenomenological Theories of Turbulence and Variable Turbulent Prandtl Number", Int. J. Heat Mass Transfer, Vol. 16, 1973, pp. 1547-1563.

66. Blom, J., "An Experimental Determination of the Turbulent Prandtl Number in a Developing Temperature Boundary Layer", Fourth Int. Heat Transfer Conference, Versailles, Paris, France, August 1970.

67. Snegova, N.P., "Heat Transfer at High Prandtl Numbers in Fully Developed Turburlent Flow", Heat Transfer - Soviet Research, Vol. 3, No. 3, May-June 1971, pp. 129-133.

68. Thomas, L.C., and Ibrahim, M.B., "A Model of the Turbulent Burst Phenomenon: Predictions for Turbulent Prandtl Number", Letters in Heat and Mass Transfer, Vol. 8, 1981, pp. 357-369.

69. Anderson, P.S., Kays, W.M., and Moffat, R.J., "Experimental Results for the Transpired Turbulent Boundary Layer in an Adverse Pressure Gradient", Journal of Fluid Mechanics, Vol. 69, Part 2, 1975, pp. 353-375.

70. Pabst, O., "Die Ausbreitung heisser Gasstrahlen in bewegter Luft", F.W. Flugzeugbau, U.M. No. 8004, 8007, 1944. See: Szablewski, W., "The Diffusion of a hot air jet in air in motion", Tech. Memo. 1288, U.S. Nat. Adv. Comm. Aero., 1950.

71. Reichardt, H., "Impuls-und Warmeaustausch in freier Turbulenz", Zeit. Angew. Math. Mech., No. 24, 1944, pp. 268-272.

72. Patel, V.C., Rodi, W., and Scheurer, G., "Turbulence Models for Near-Wall and Low Reynolds Number Flows: A Review", AIAA Journal, Vol 23, No. 9, Sept. 1985, pp. 1308-1319.

TABLE 1

COEFFICIENTS OF TRIPLE-DECK EXPONENTIAL FUNCTION

FIT BY LEAST SQUARES ERROR TO BLAIR'S DATA [18].

MEAN VELOCITY FIELD

$$\frac{\bar{u}}{u_e} = 1 - \exp[-\phi_1 + \exp\{-\phi_2 + \exp(-\phi_3)\}]$$

where: $\phi_1 = A_1 + B_1 \left(\frac{y}{\delta}\right) + C_1 \left(\frac{y}{\delta}\right)^2$

$$\phi_2 = A_2 + B_2 \left(\frac{y}{\delta}\right) + C_2 \left(\frac{y}{\delta}\right)^2$$

$$\phi_3 = A_3 + B_3 \left(\frac{y}{\delta}\right) + C_3 \left(\frac{y}{\delta}\right)^2$$

CASE

| Grid Config. | X[in] | $A_1$ | $B_1$ | $C_1$ | $A_2$ | $B_2$ | $C_2$ | $A_3$ | $B_3$ | $C_3$ |
|---|---|---|---|---|---|---|---|---|---|---|
| 0 | 12 | 0.449 | -0.537 | 6.067 | 1.801 | 1.513 | 34.70 | 0.0 | 0.0 | 0.0 |
| 0 | 36 | 1.596 | -1.570 | 5.213 | 0.274 | 4.034 | 22.17 | 0.300 | 49.64 | 379.0 |
| 0 | 52 | 1.391 | -0.672 | 4.080 | 0.474 | 5.835 | 22.13 | 0.218 | 76.39 | 251.9 |
| 0 | 84 | 1.347 | -0.465 | 3.861 | 0.481 | 7.958 | 20.97 | 0.250 | 105.8 | 0.0 |
| 2 | 12 | 1.294 | 0.527 | 3.155 | 0.575 | 11.28 | 0.0 | 0.183 | 0.064 | 918.3 |
| 2 | 36 | 1.352 | -0.012 | 3.783 | 0.505 | 7.295 | 12.70 | 0.214 | 74.84 | 431.5 |
| 2 | 52 | 1.299 | 0.306 | 3.604 | 0.545 | 9.926 | 11.25 | 0.214 | 114.5 | 319.1 |
| 2 | 84 | 1.220 | 0.822 | 2.922 | 0.753 | 10.31 | 33.13 | 0.049 | 122.6 | 0.0 |
| 4 | 12 | 1.064 | 2.662 | 1.451 | 1.404 | 19.86 | 0.0 | -0.383 | -9.39 | 1392. |
| 4 | 36 | 1.038 | 3.818 | 0.391 | 1.204 | 19.02 | 117.1 | -0.216 | 67.71 | 4158. |
| 4 | 52 | 1.105 | 3.931 | 0.230 | 0.911 | 24.60 | 41.69 | -0.011 | 86.78 | 14022. |
| 4 | 84 | 1.105 | 4.474 | -0.198 | 1.082 | 18.77 | 186.7 | -0.167 | 192.4 | 1294. |

TABLE 2

COEFFICIENTS OF TRIPLE-DECK EXPONENTIAL FUNCTION

FIT BY LEAST SQUARES ERROR TO BLAIR'S DATA [18].

MEAN TEMPERATURE FIELD

$$\frac{\bar{u}}{u_e} = 1 - \exp[-\phi_1 + \exp\{-\phi_2 + \exp(-\phi_3)\}]$$

where: $\phi_1 = A_1' + B_1' \left(\frac{y}{\delta}\right) + C_1' \left(\frac{y}{\delta}\right)^2$

$\phi_2 = A_2' + B_2' \left(\frac{y}{\delta}\right) + C_2' \left(\frac{y}{\delta}\right)^2$

$\phi_3 = A_3' + B_3' \left(\frac{y}{\delta}\right) + C_3' \left(\frac{y}{\delta}\right)^2$

CASE

| Grid Config. | X[in] | $A_1'$ | $B_1'$ | $C_1'$ | $A_2'$ | $B_2'$ | $C_2'$ | $A_3'$ | $B_3'$ | $C_3'$ |
|---|---|---|---|---|---|---|---|---|---|---|
| 0 | 12 | 0.184 | 1.050 | 4.686 | 2.693 | 3.686 | 10.68 | 0.0 | 0.0 | 0.0 |
| 0 | 36 | 1.096 | -0.037 | 2.980 | 0.598 | 9.818 | 28.23 | 0.371 | 35.61 | 1524.0 |
| 0 | 52 | 1.041 | 0.525 | 2.369 | 0.840 | 11.57 | 23.01 | 0.128 | 56.19 | 431.9 |
| 0 | 84 | 1.140 | 0.511 | 2.443 | 0.890 | 6.857 | 52.71 | -0.0208 | 77.17 | 149.1 |
| 2 | 12 | 0.935 | 1.324 | 1.656 | 1.066 | 24.87 | 0.0 | 0.0 | 0.0 | 0.0 |
| 2 | 36 | 1.036 | 1.506 | 1.626 | 0.850 | 14.93 | 12.87 | 0.122 | 64.94 | 0.0 |
| 2 | 52 | 1.204 | 0.778 | 2.692 | 0.651 | 13.62 | 0.0 | 0.178 | 69.30 | 634.4 |
| 2 | 84 | 1.156 | 1.414 | 1.787 | 0.782 | 14.23 | 0.0 | 0.0758 | 100.5 | 0.0 |
| 4 | 12 | 1.009 | 1.924 | 0.836 | 0.575 | 19.73 | 30.30 | 0.538 | -7.384 | 2979.0 |
| 4 | 36 | 1.147 | 3.355 | 0.799 | 0.927 | 6.954 | 176.9 | -0.0620 | 91.62 | 195.0 |
| 4 | 52 | 1.204 | 3.189 | 0.449 | 1.095 | 8.082 | 43.76 | -0.248 | 90.46 | 0.0 |
| 4 | 84 | 1.200 | 3.901 | 0.0 | 0.672 | 22.87 | 0.0 | 0.158 | 185.1 | 0.0 |

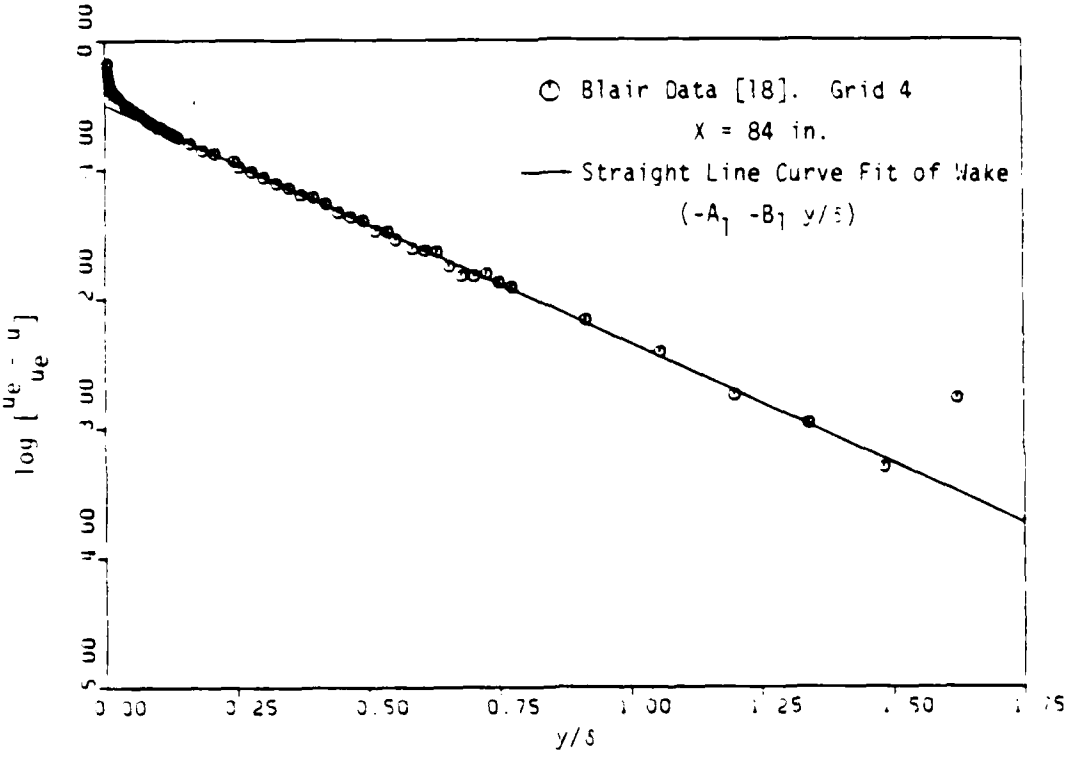



Figure 1: Semilogarithmic profile of mean velocity defect. High FST.

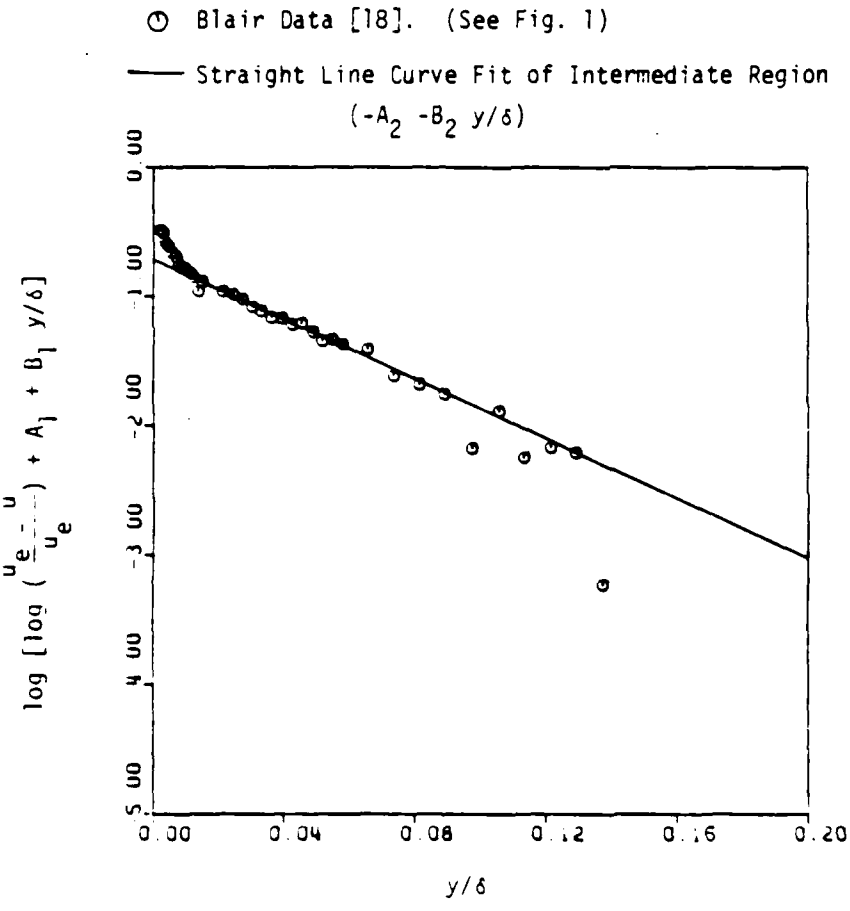



Figure 2: Semilogarithmic profile of mean velocity residue with respect to linear curve fit (see Fig. 1). High FST.

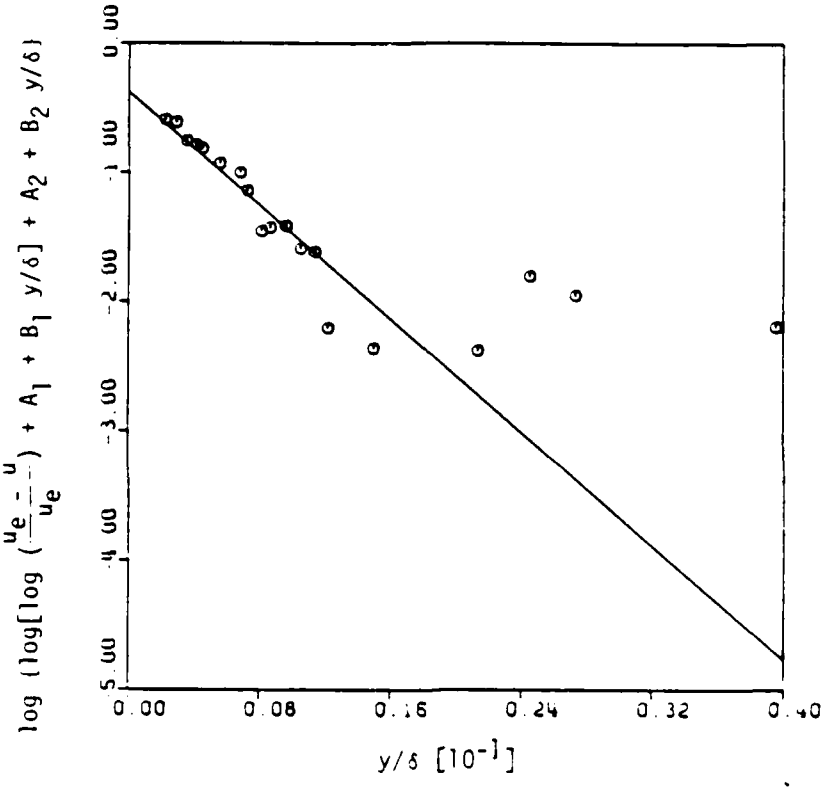



Figure 3: Semilogarithmic profile of innermost velocity region. (See Figs. 1 and 2). High FST.

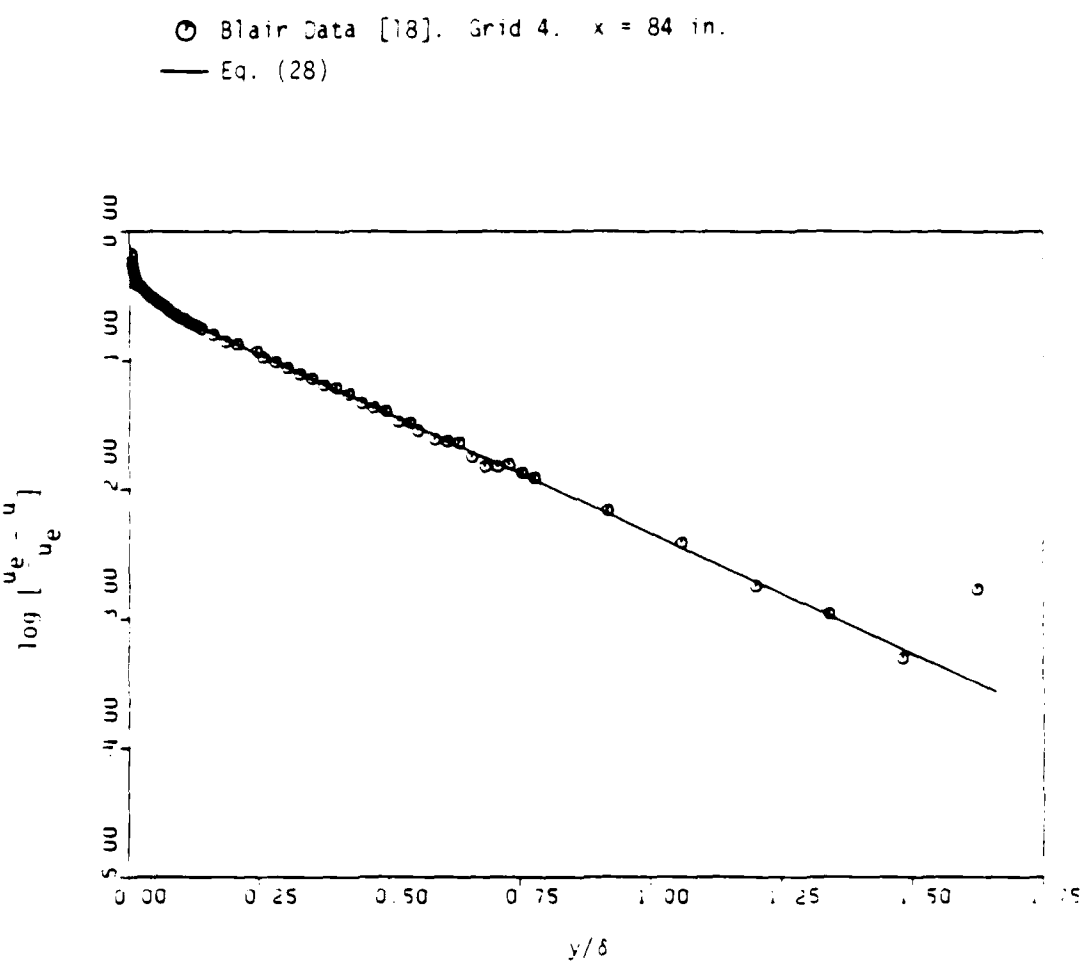



Figure 4: Wake comparison of Blair's data with Eq. (28). High FST.

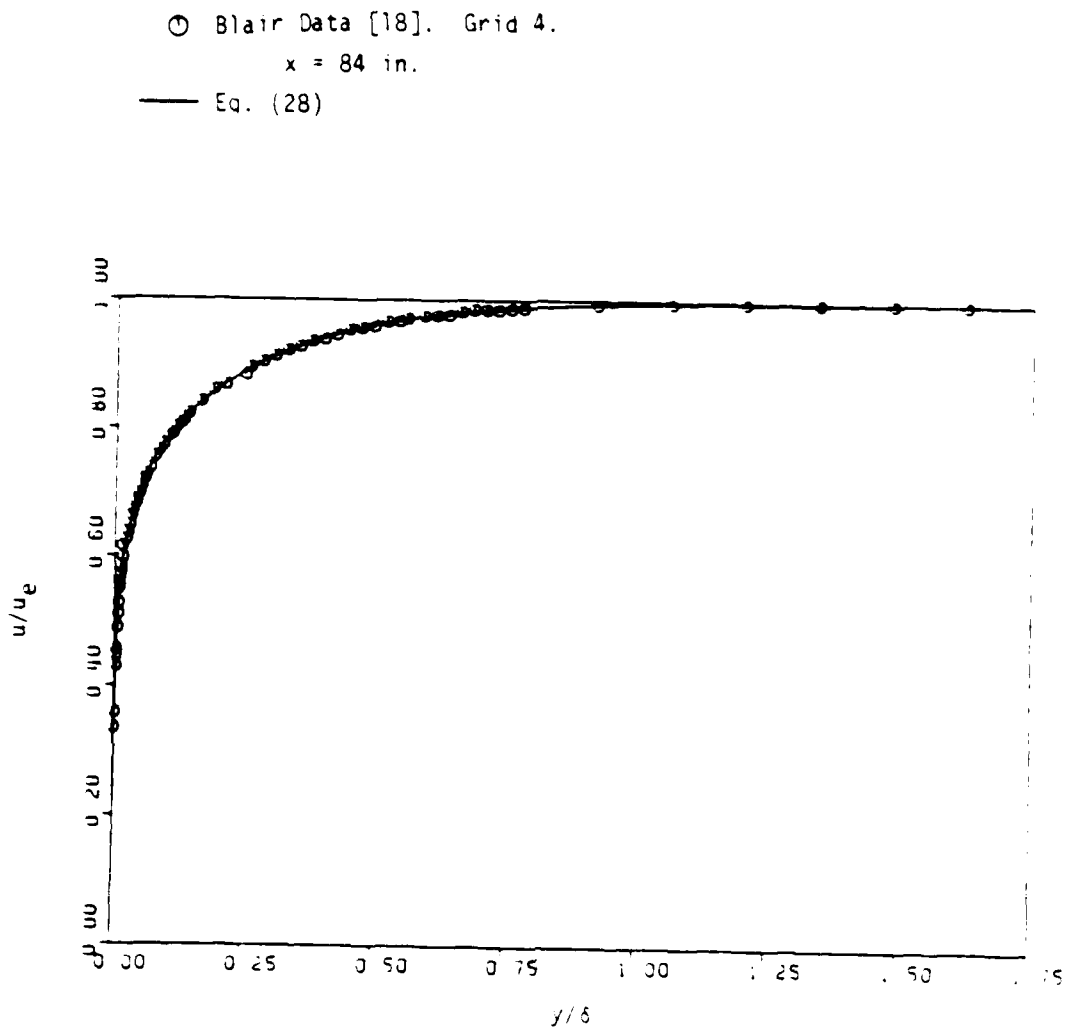



Figure 5. Linear comparison of Blair's data with Eq. (28). High FST.

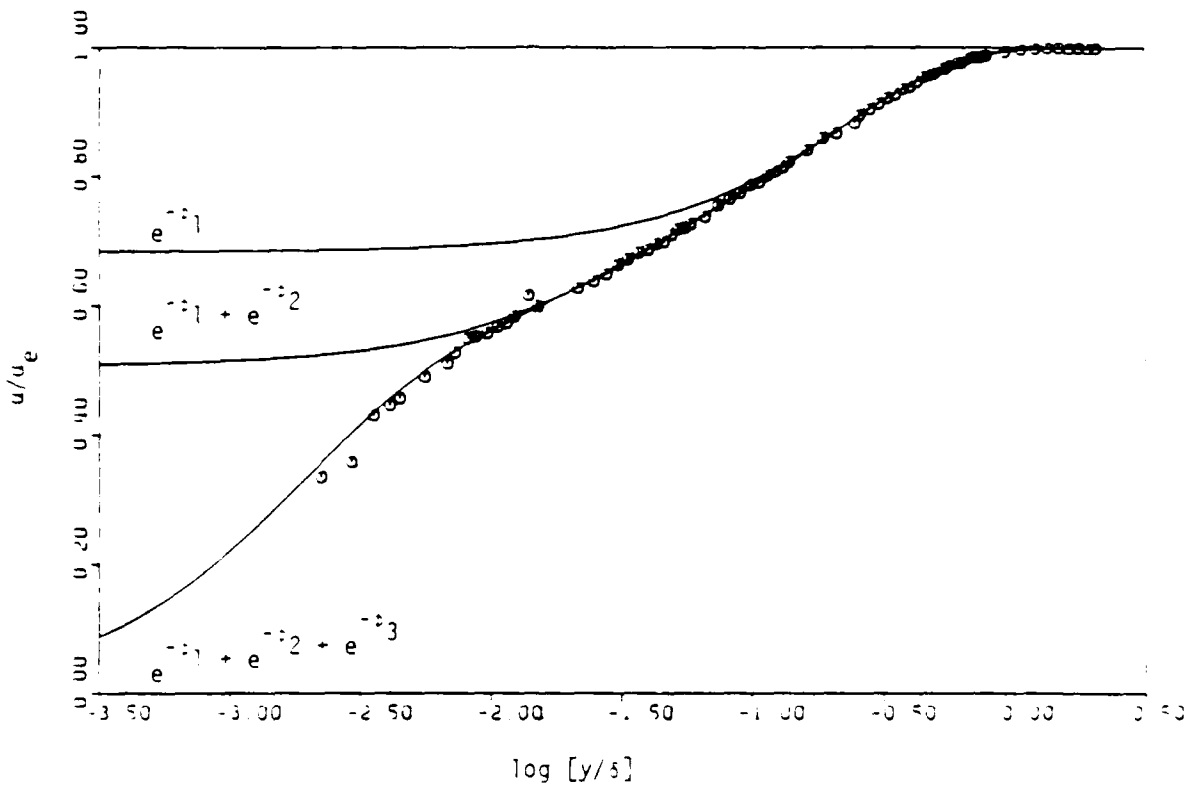



Figure 6: Semilogarithmic comparison of Blair's data with Eq. (28). High FST.

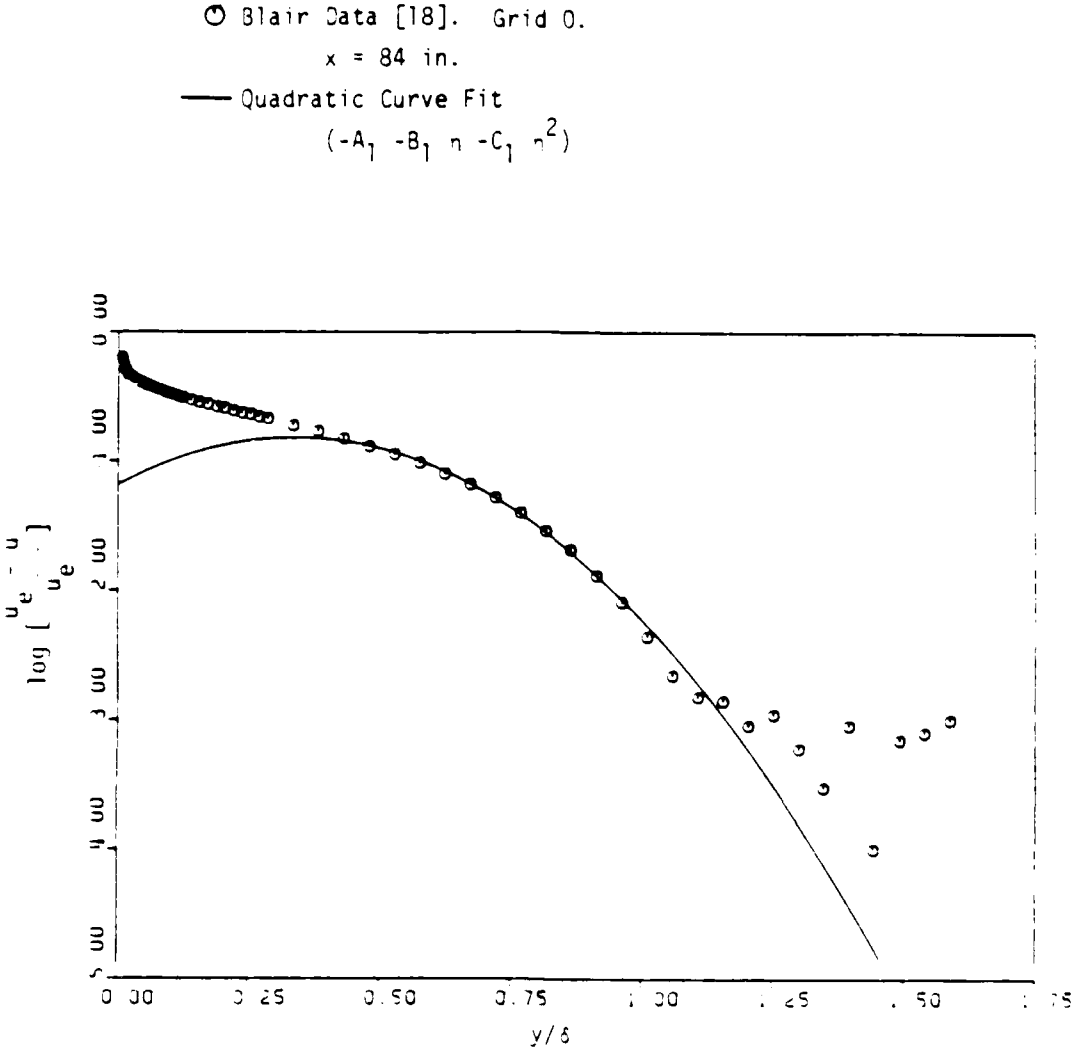



Figure 7: Quadratic fit of mean velocity wake deficit for low FST.

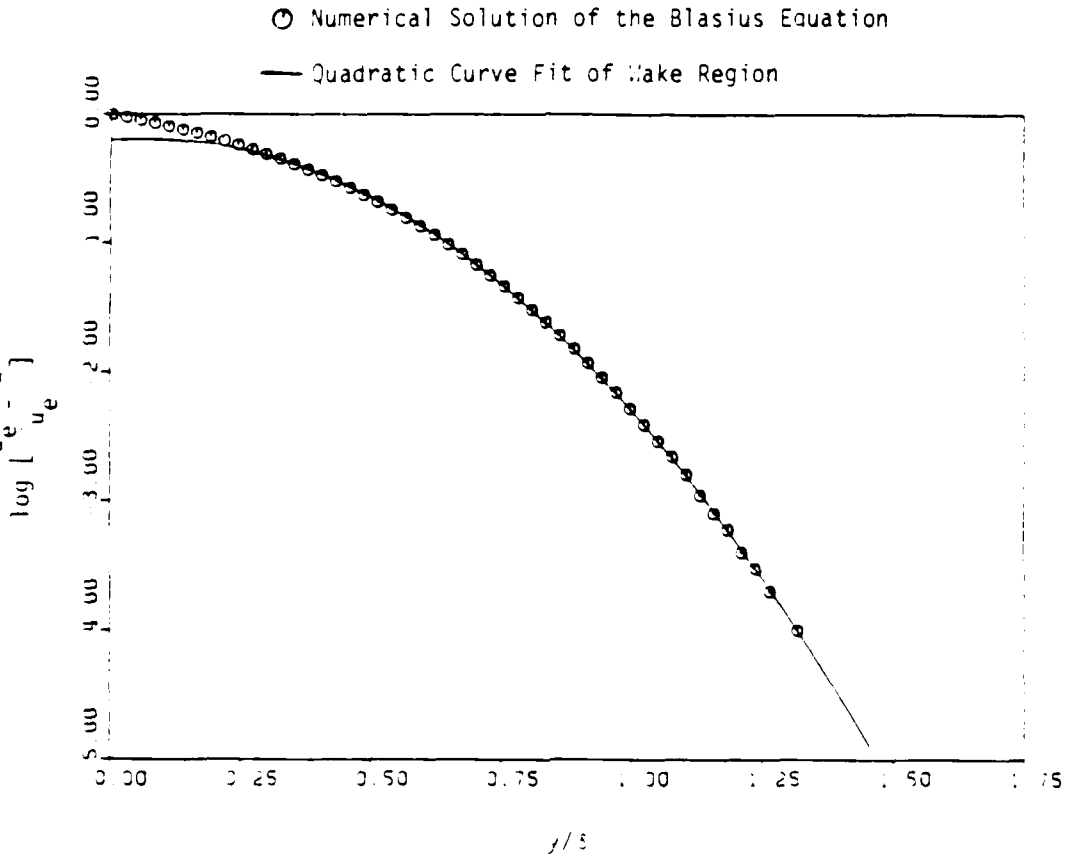



Figure 3: Laminar boundary layer fit by a quadratic wake function.

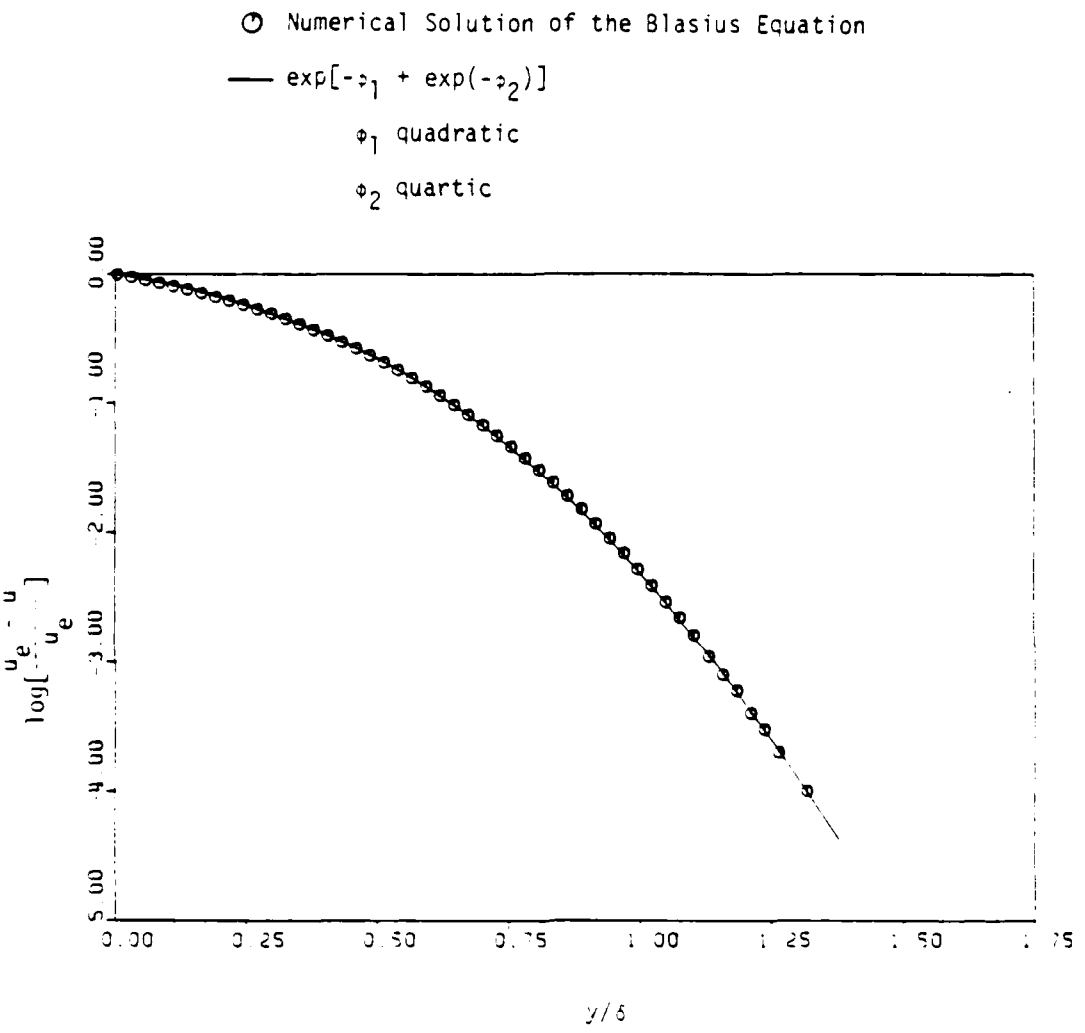



Figure 9: Blasius Solution compared with composite exponential curve fit.

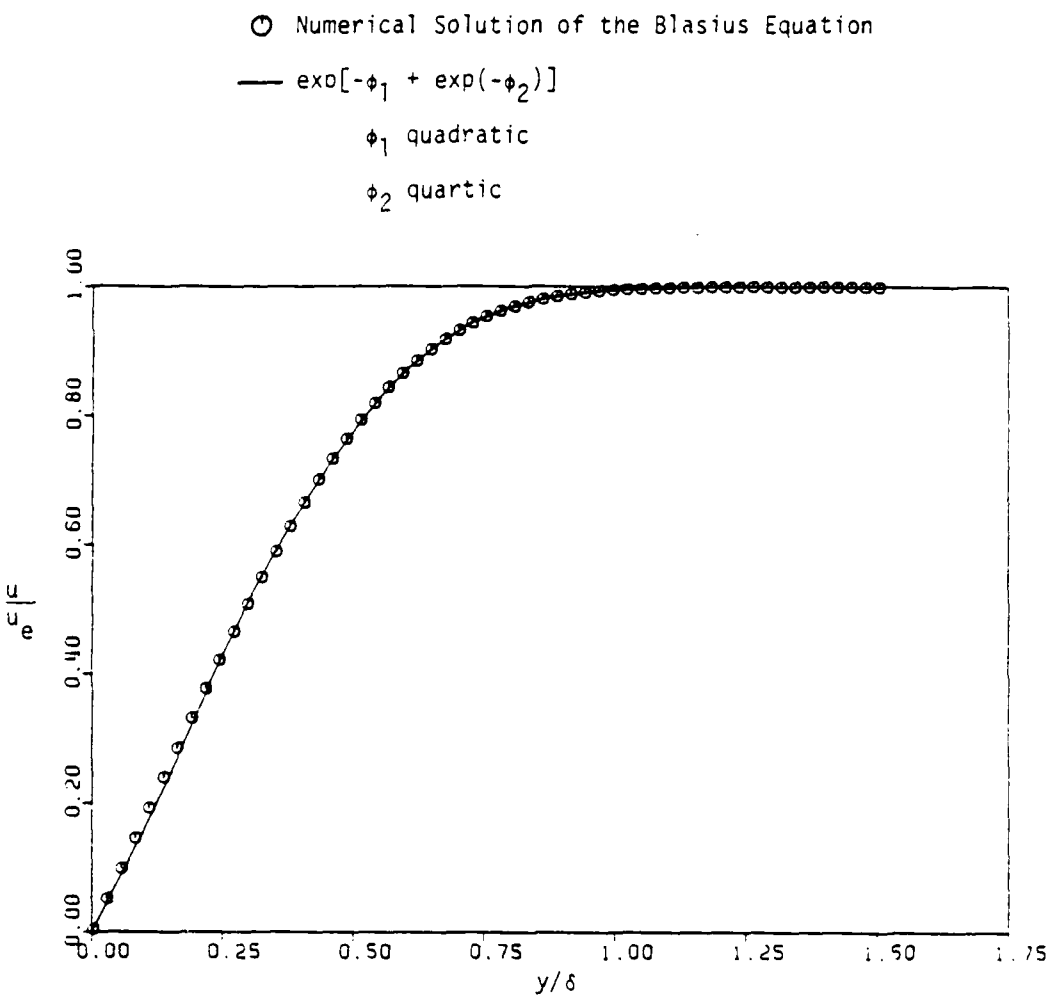



Figure 10: Blasius Solution compared with composite exponential function (linear comparison).

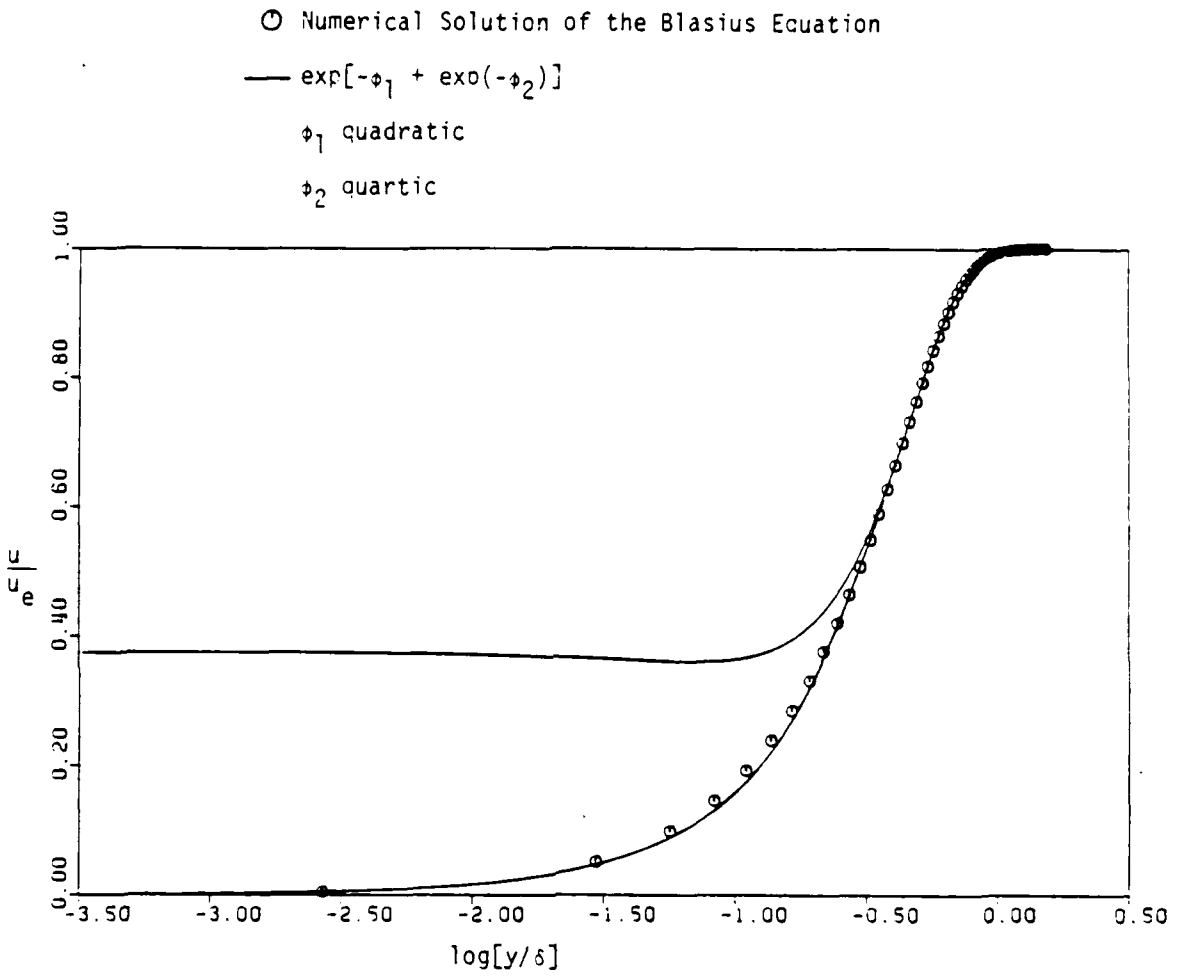



Figure 11: Blasius Solution compared semilogarithmically with composite exponential function.

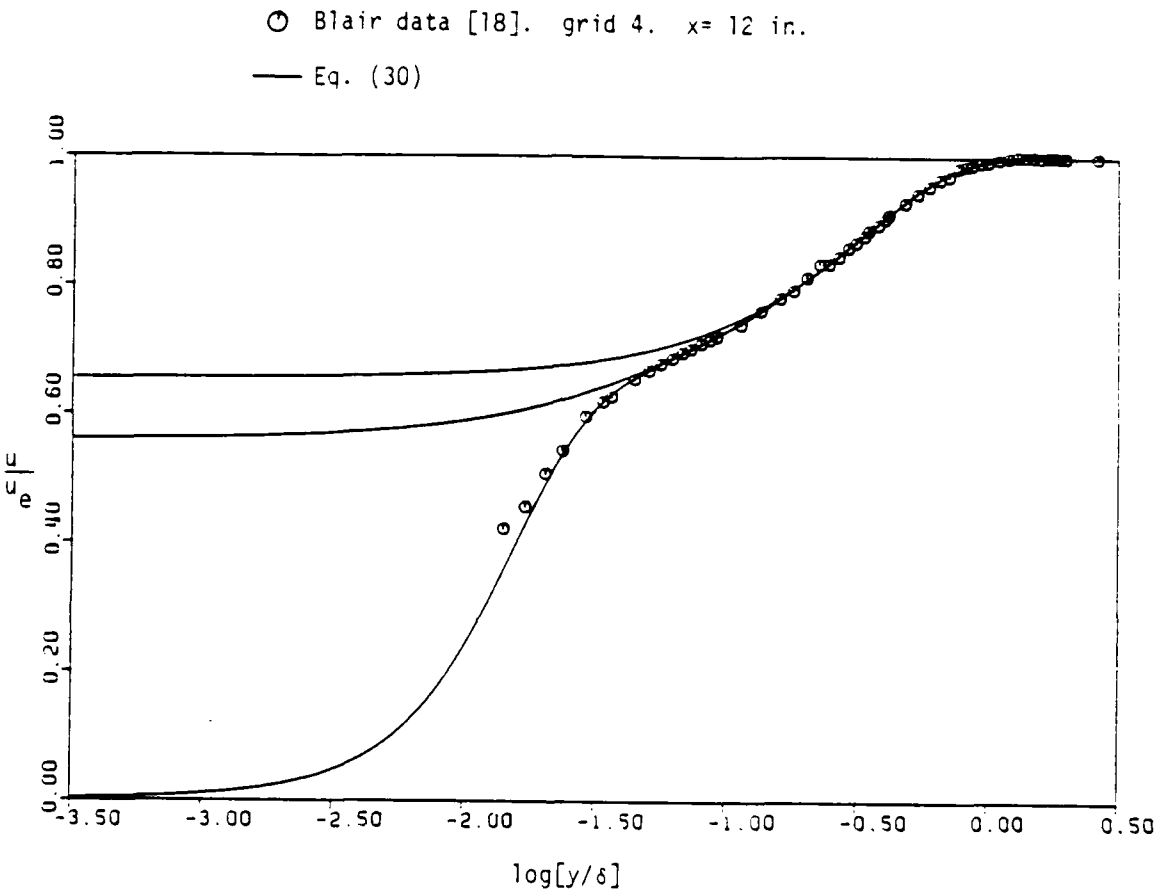



Figure 12: Velocity profile at x = 12 in. Grid 4.

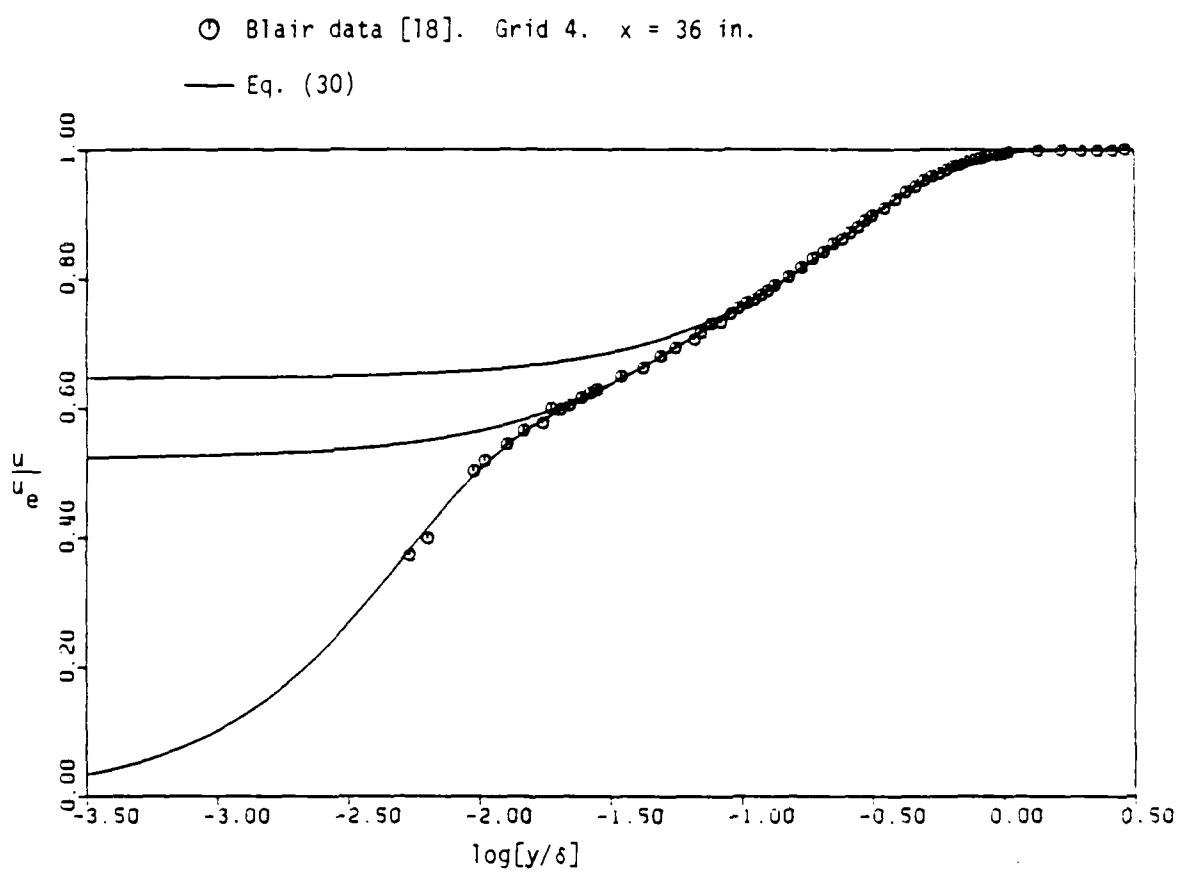



Figure 13: Velocity profile at x = 36 in. Grid 4.

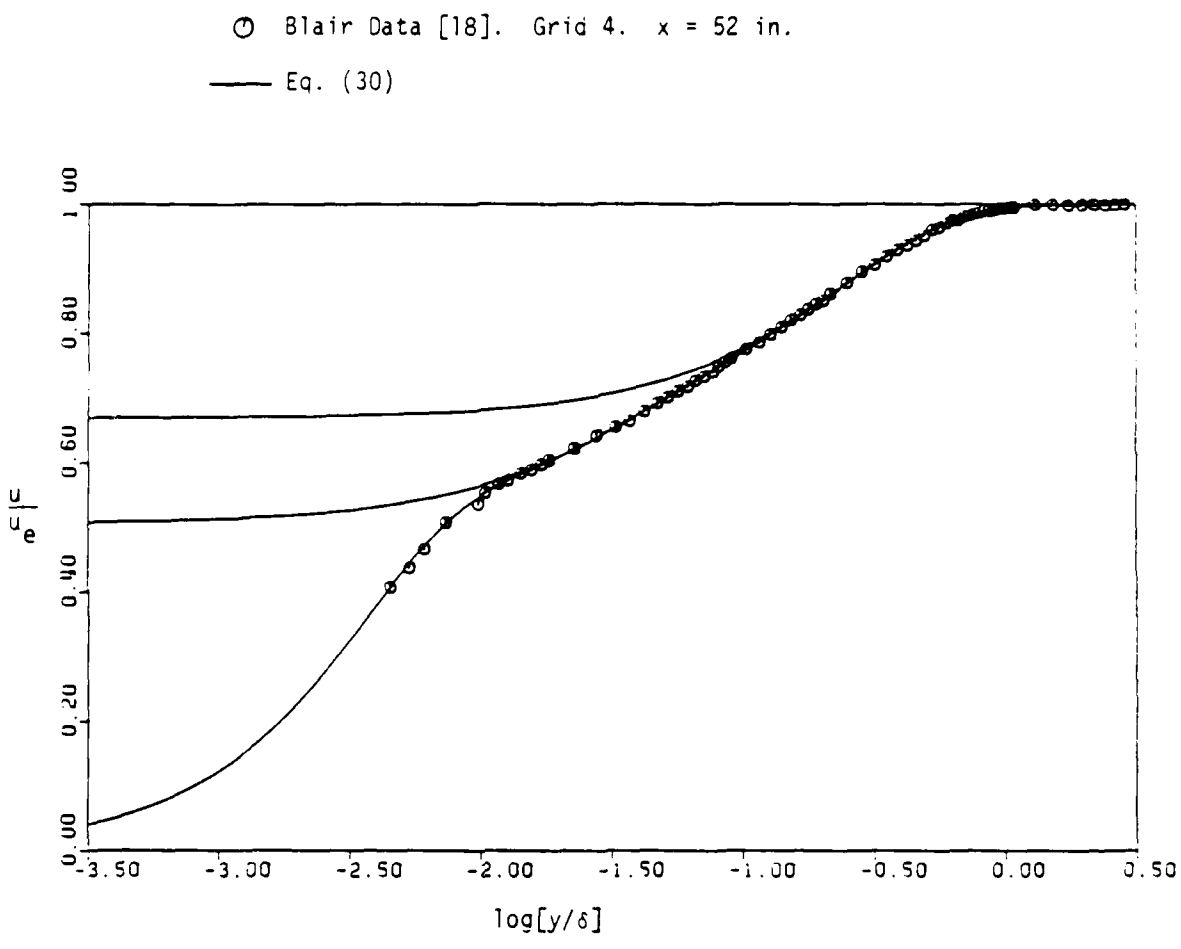



Figure 14: Velocity profile at x = 52 in. Grid 4.

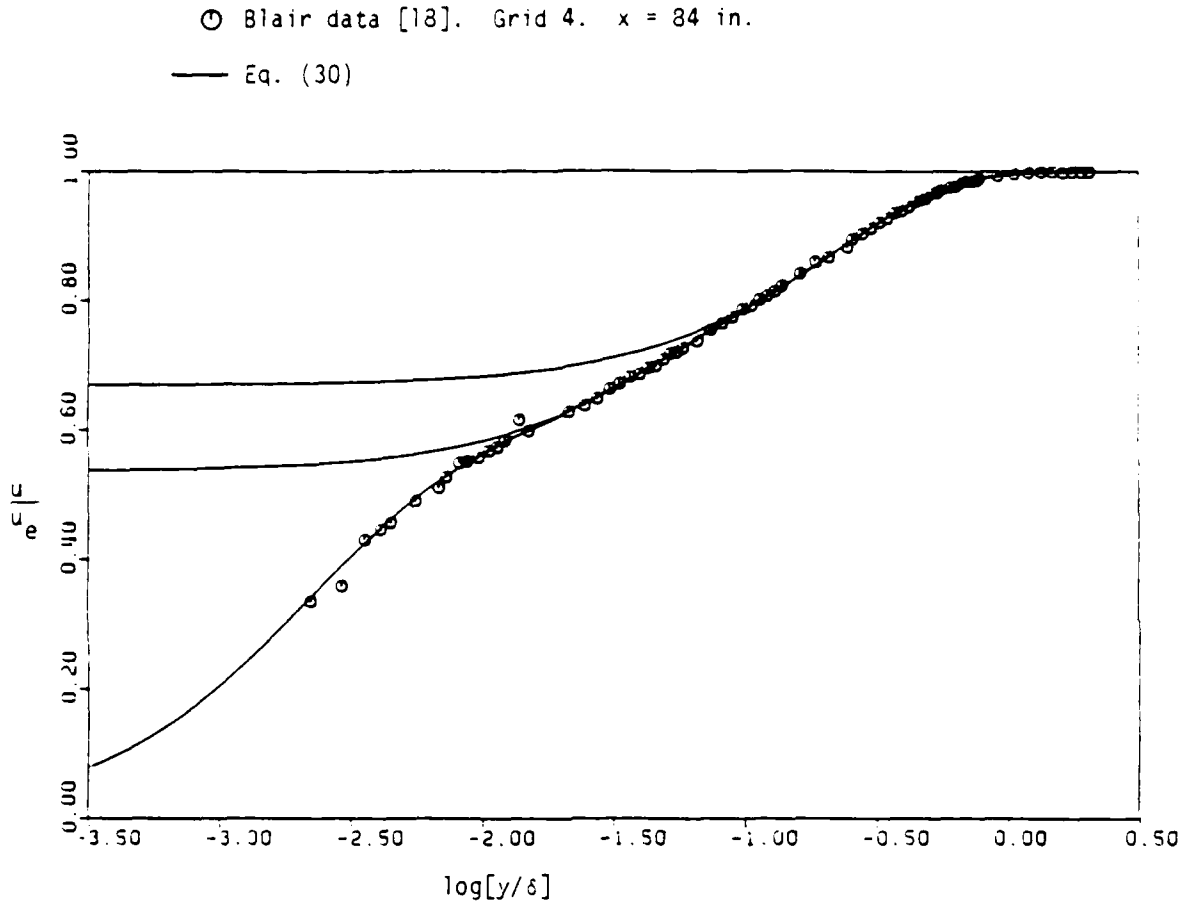



Figure 15: Velocity profile at x = 84 in. Grid 4.

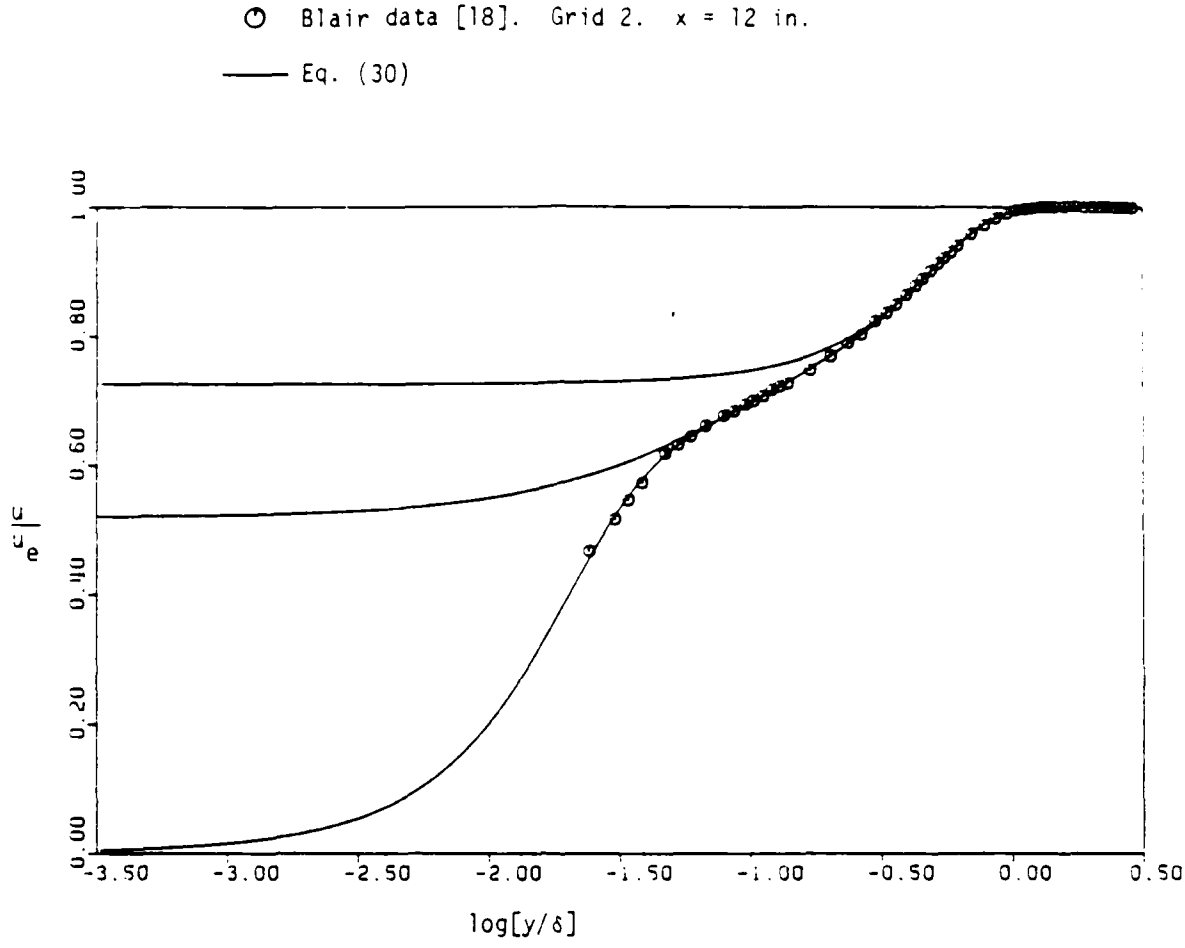



Figure 16: Velocity profile at x = 12 in. Grid 2.

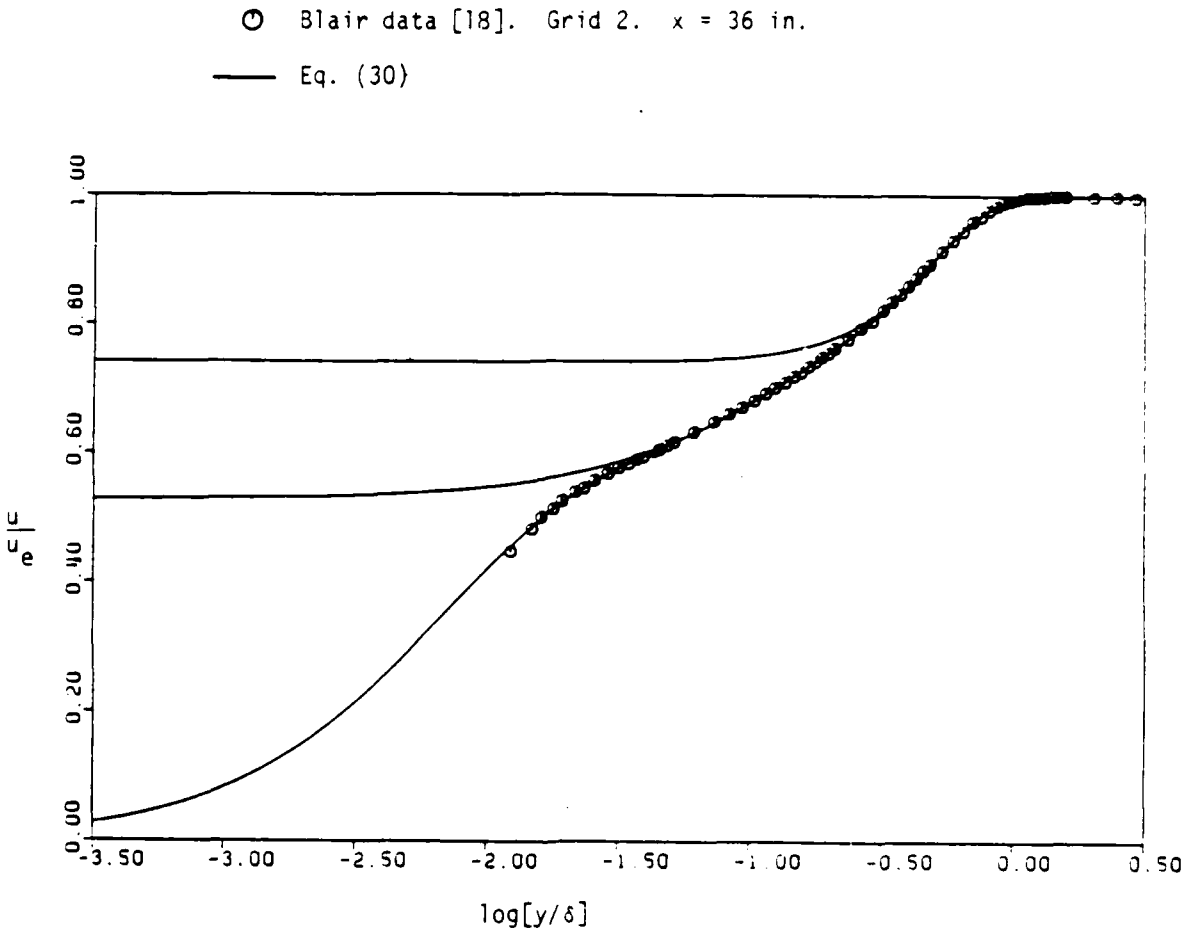



Figure 17: Velocity profile at x = 36 in. Grid 2.

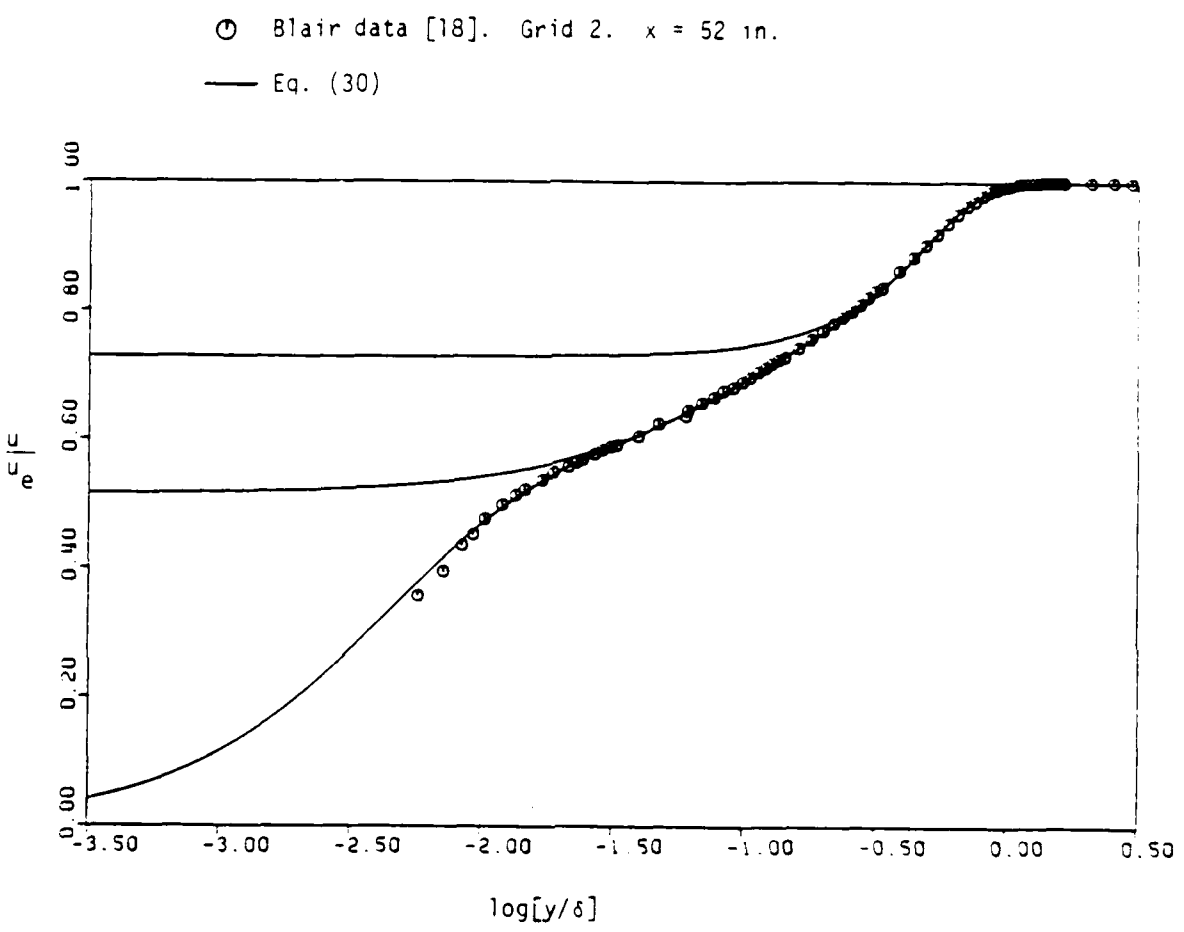



Figure 18: Velocity profile at x = 52 in. Grid 2.

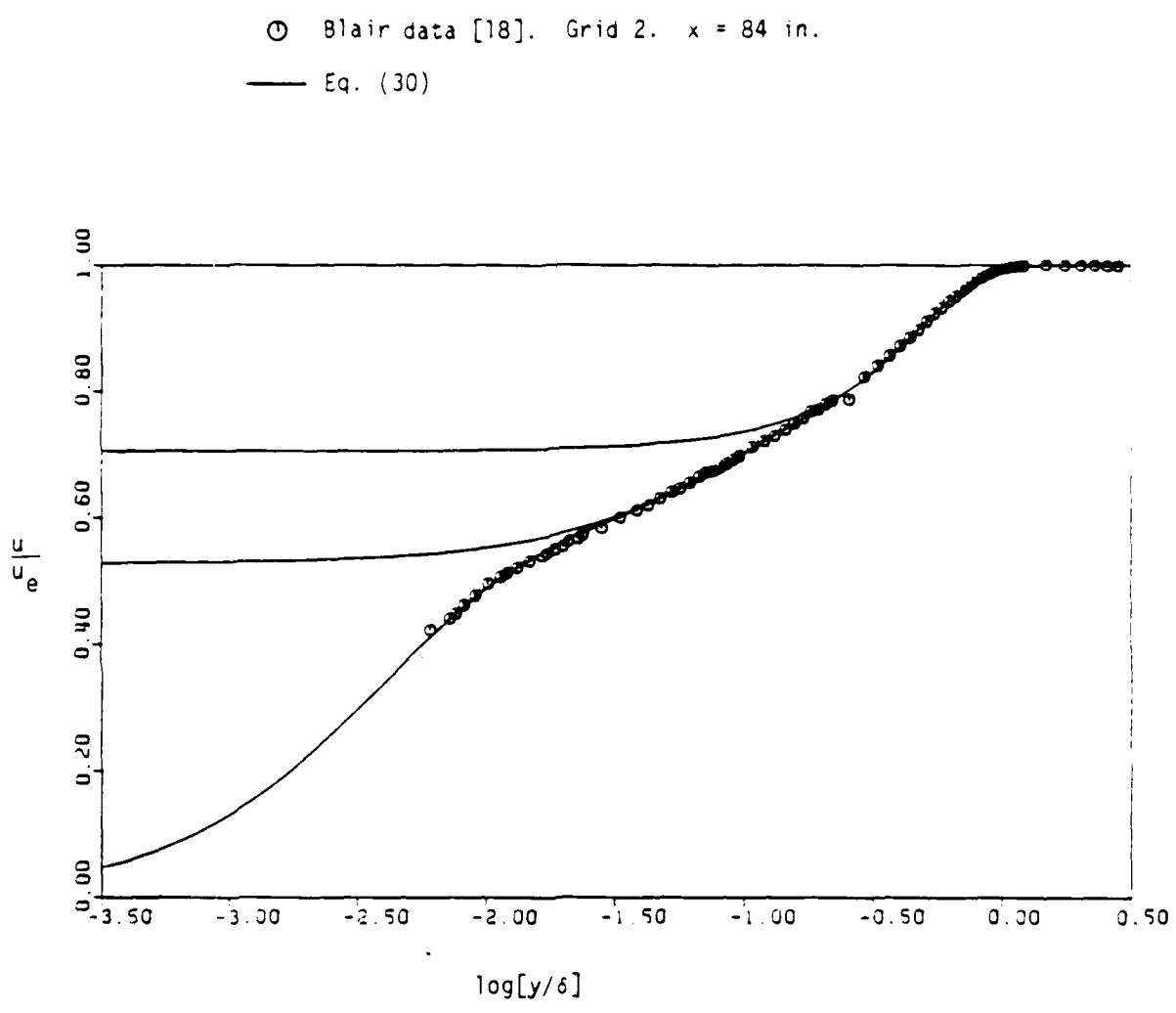



Figure 19: Velocity profile at x = 84 in. Grid 2.

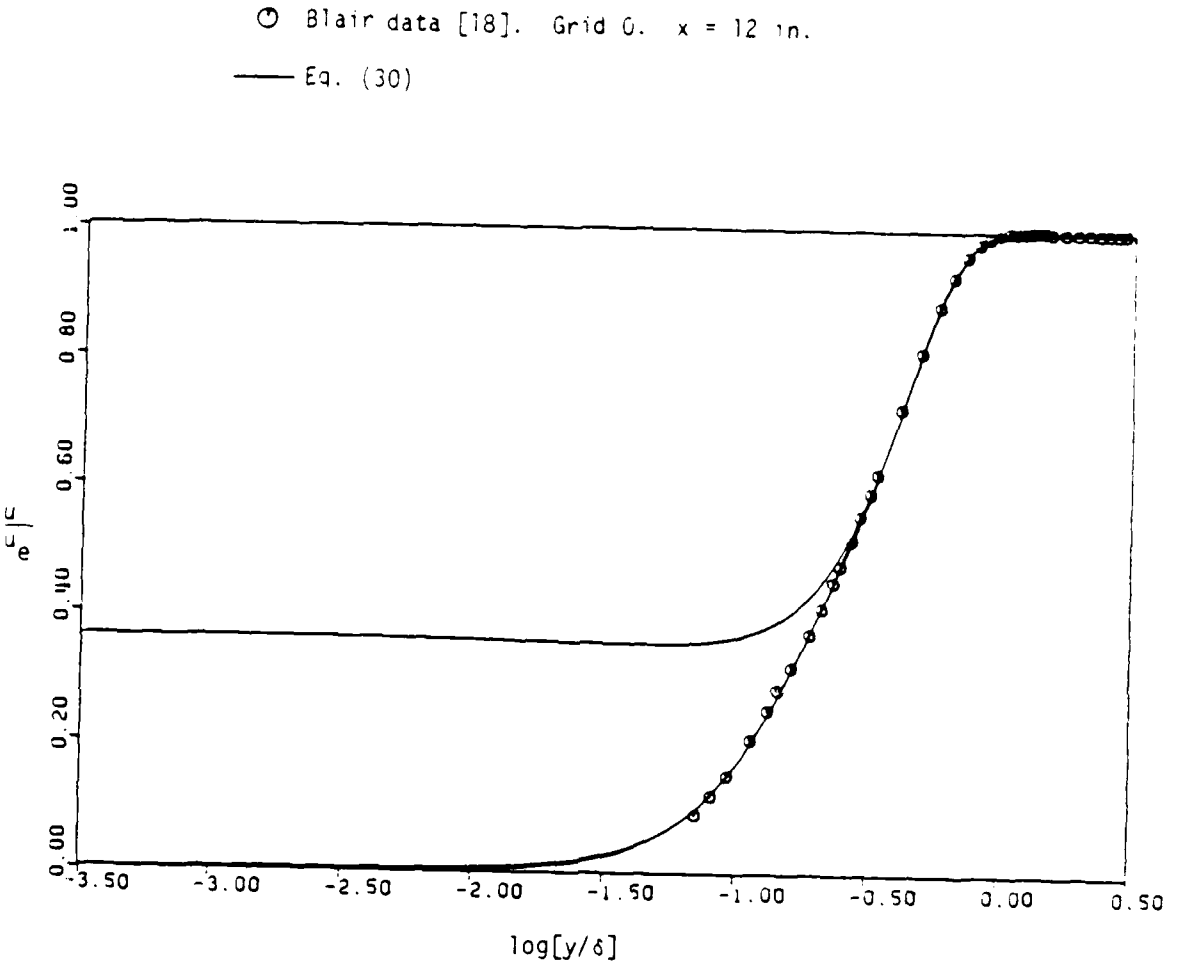



Figure 20: Velocity profile at x = 12 in. Grid 0.

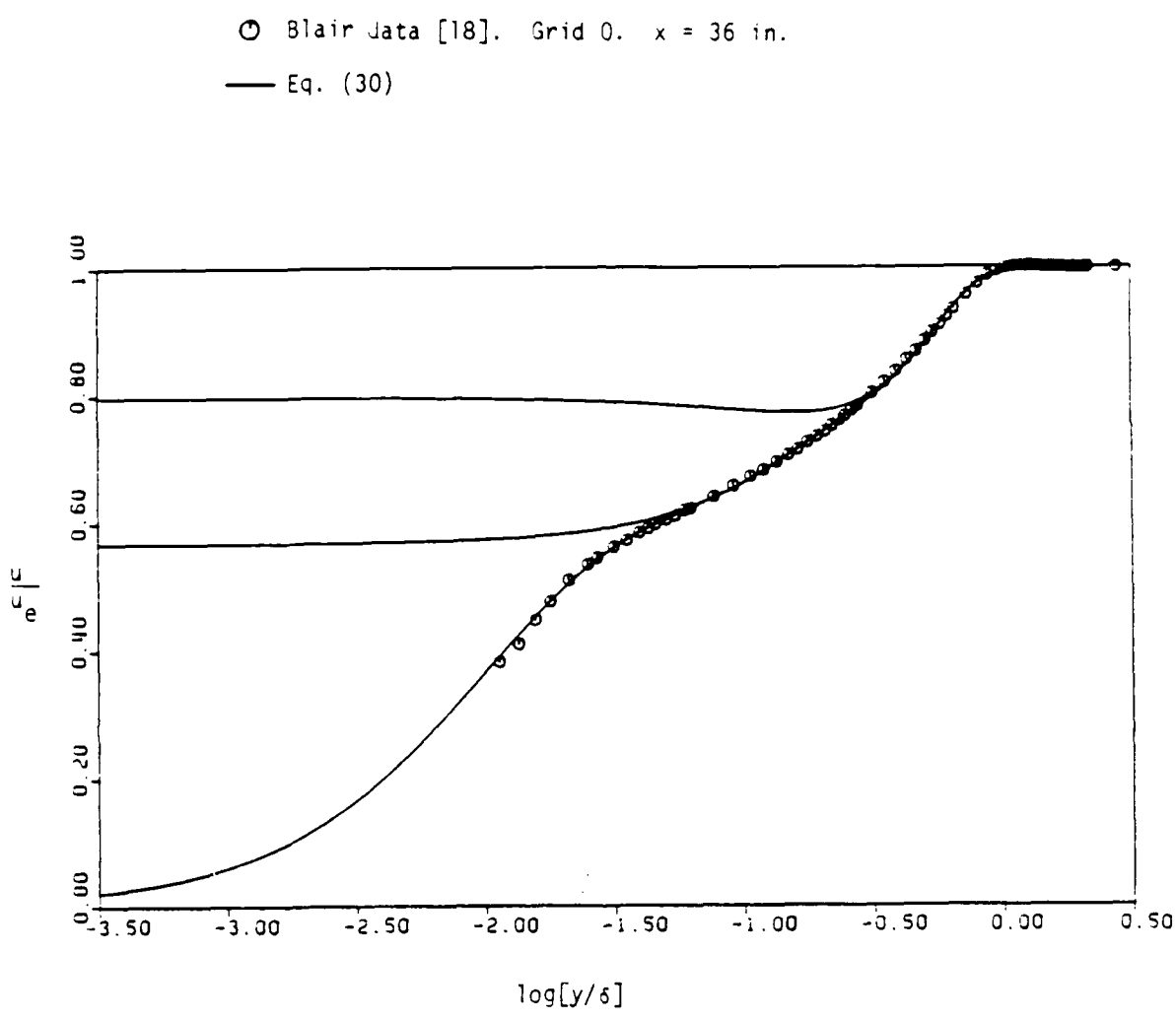



Figure 21: Velocity profile at x = 36 in. Grid 0.

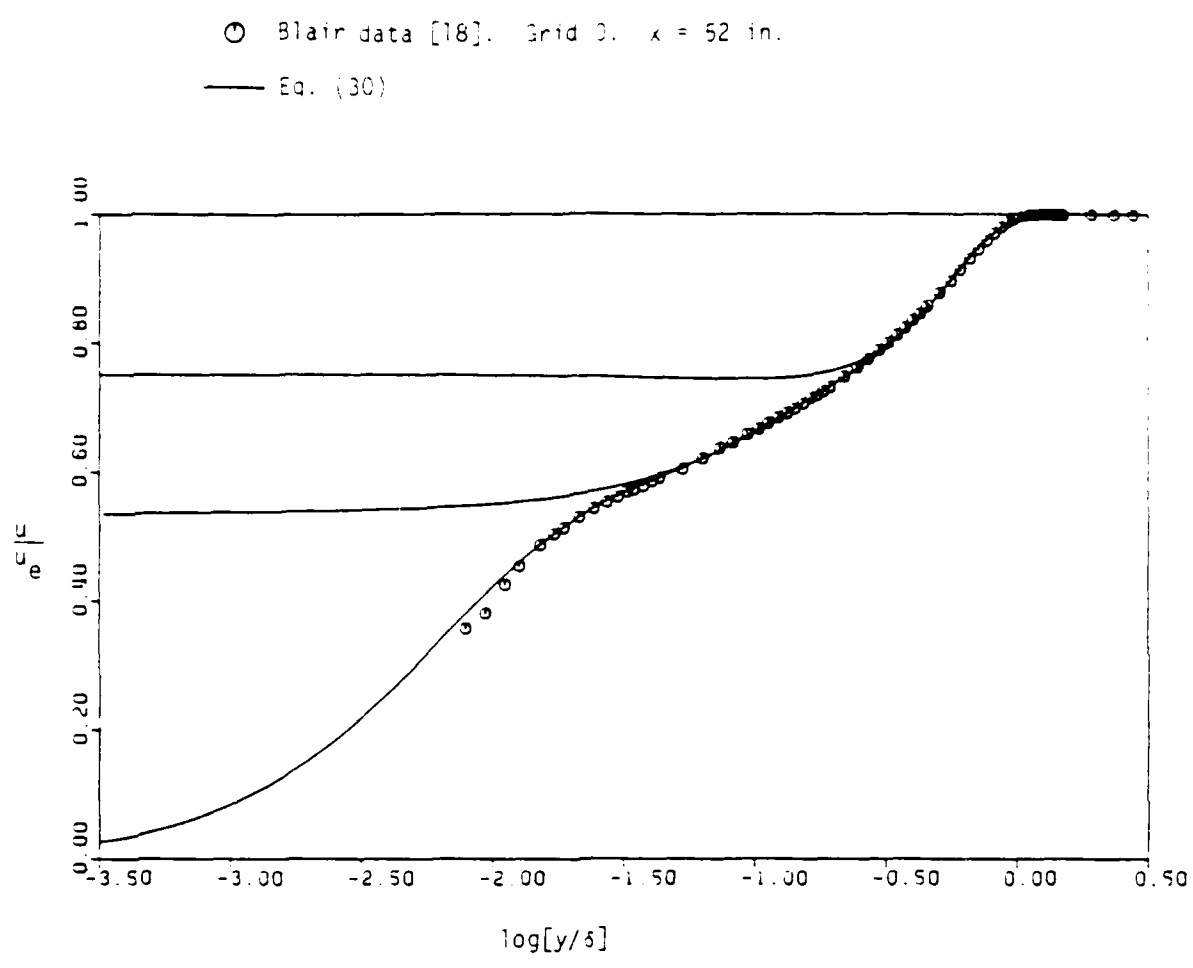



Figure 22: Velocity profile at x = 52 in. Grid 0.

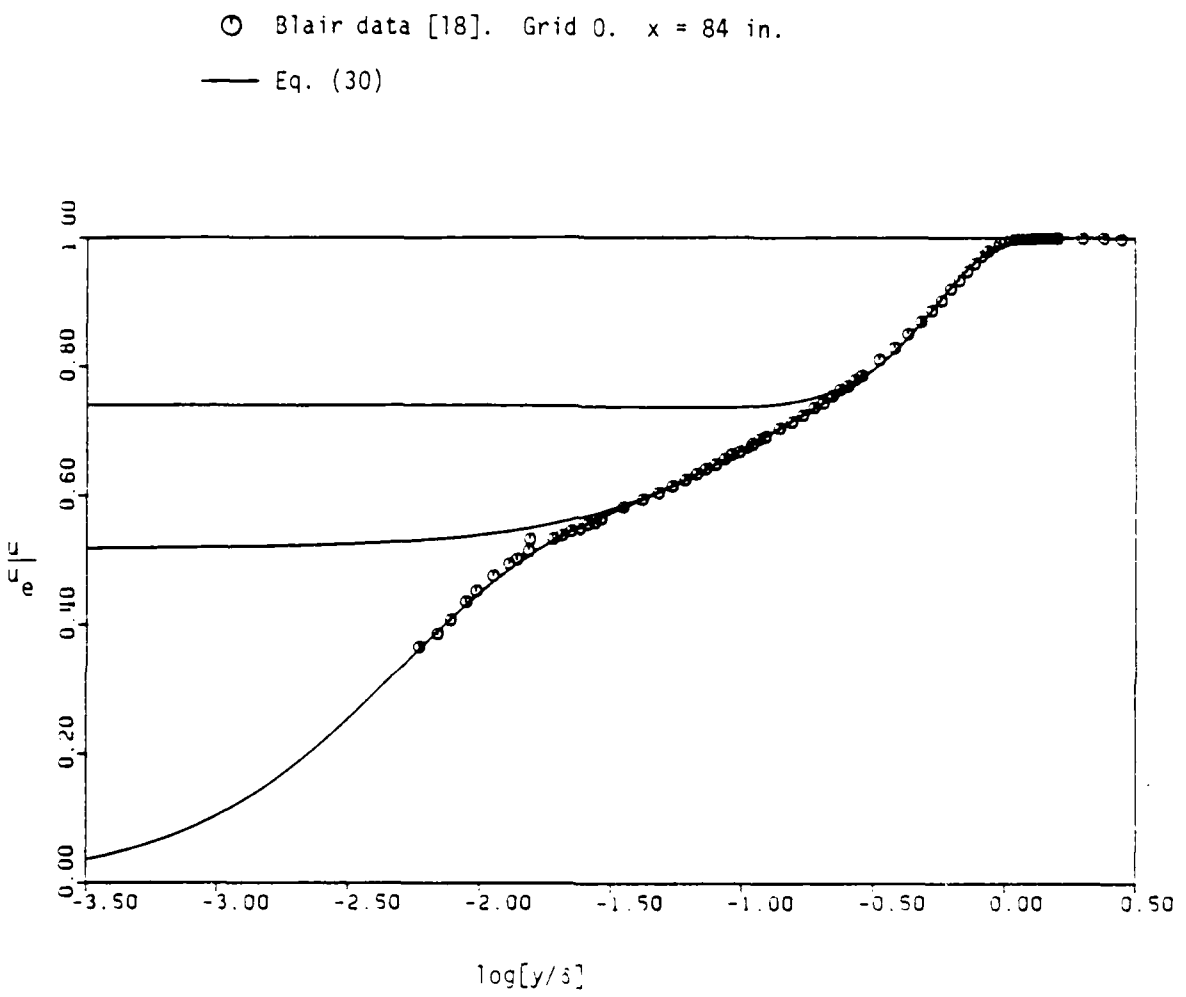
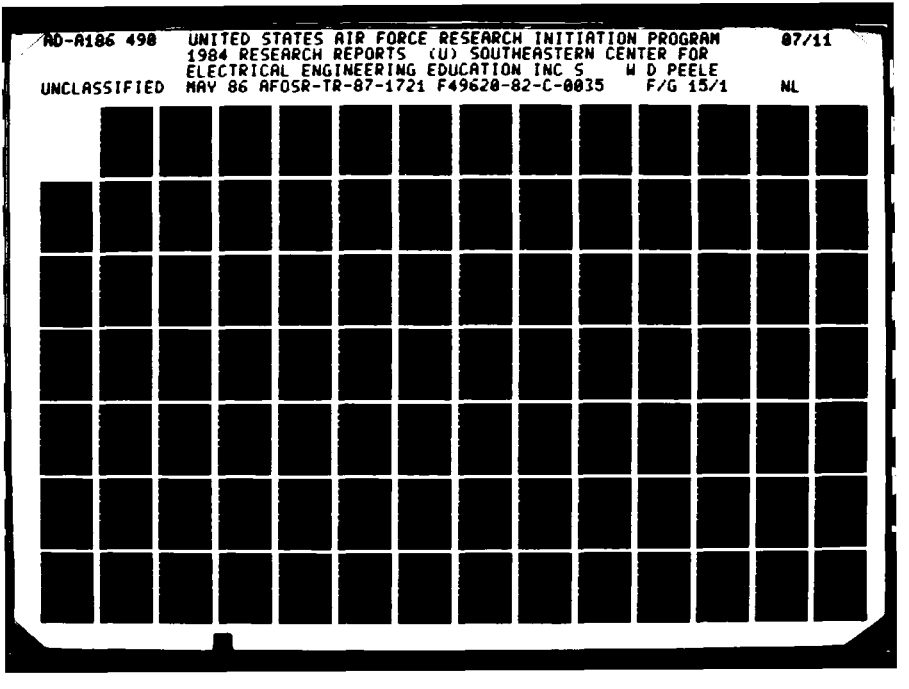
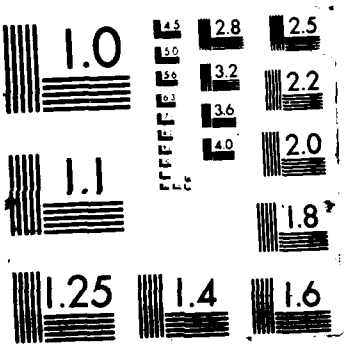



Figure 23: Velocity profile at x = 84 in. Grid 0.


AD-A186 498 UNITED STATES AIR FORCE RESEARCH INITIATION PROGRAM 07/11
1984 RESEARCH REPORTS (U) SOUTHEASTERN CENTER FOR
ELECTRICAL ENGINEERING EDUCATION INC S W D PEELE
UNCLASSIFIED MAY 86 AFOSR-TR-87-1721 F49620-82-C-0035 F/G 15/1 NL


1.0
1.1
1.25
1.4
1.6
1.8
2.0
2.2
2.5
2.8
3.2
3.6
4.0
4.5
5.0
5.6
6.3

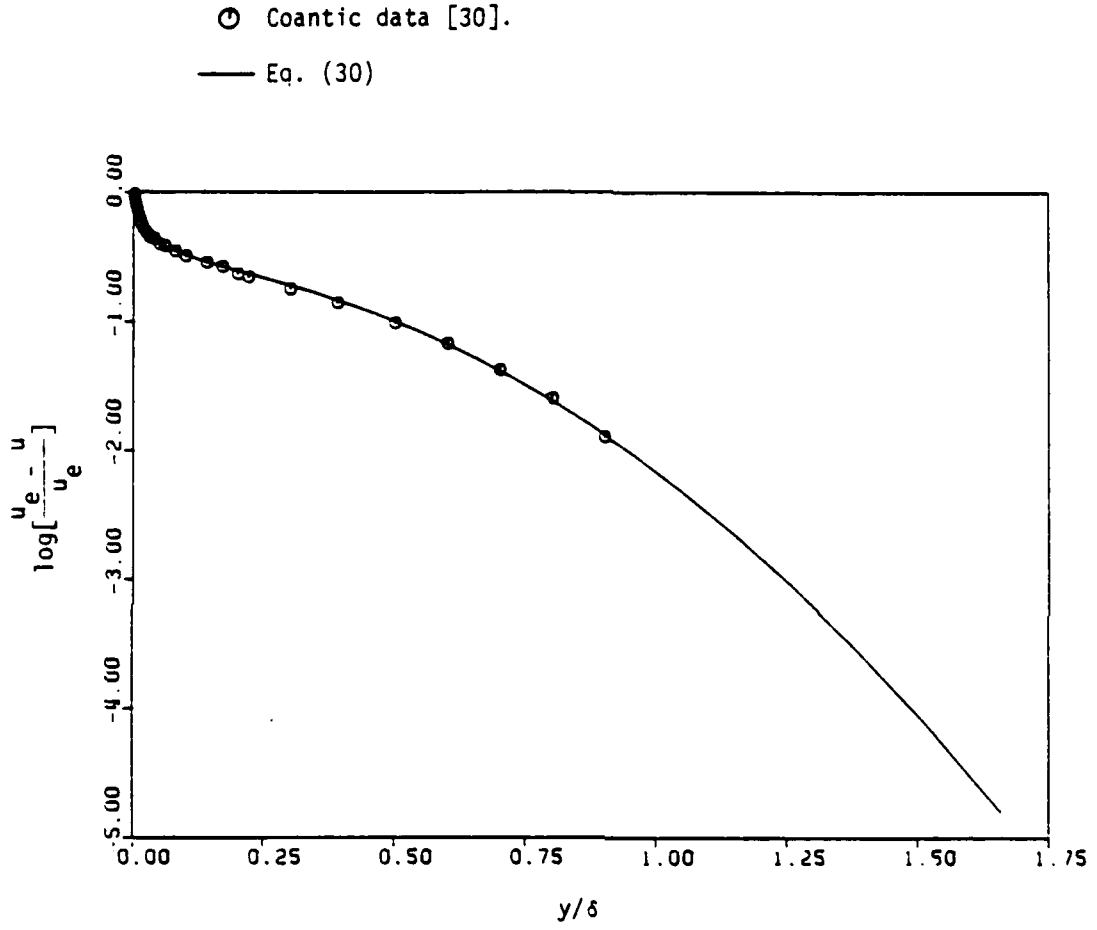



Figure 24: Wake region comparison of velocity defect with Eq. (30). Coantic data.

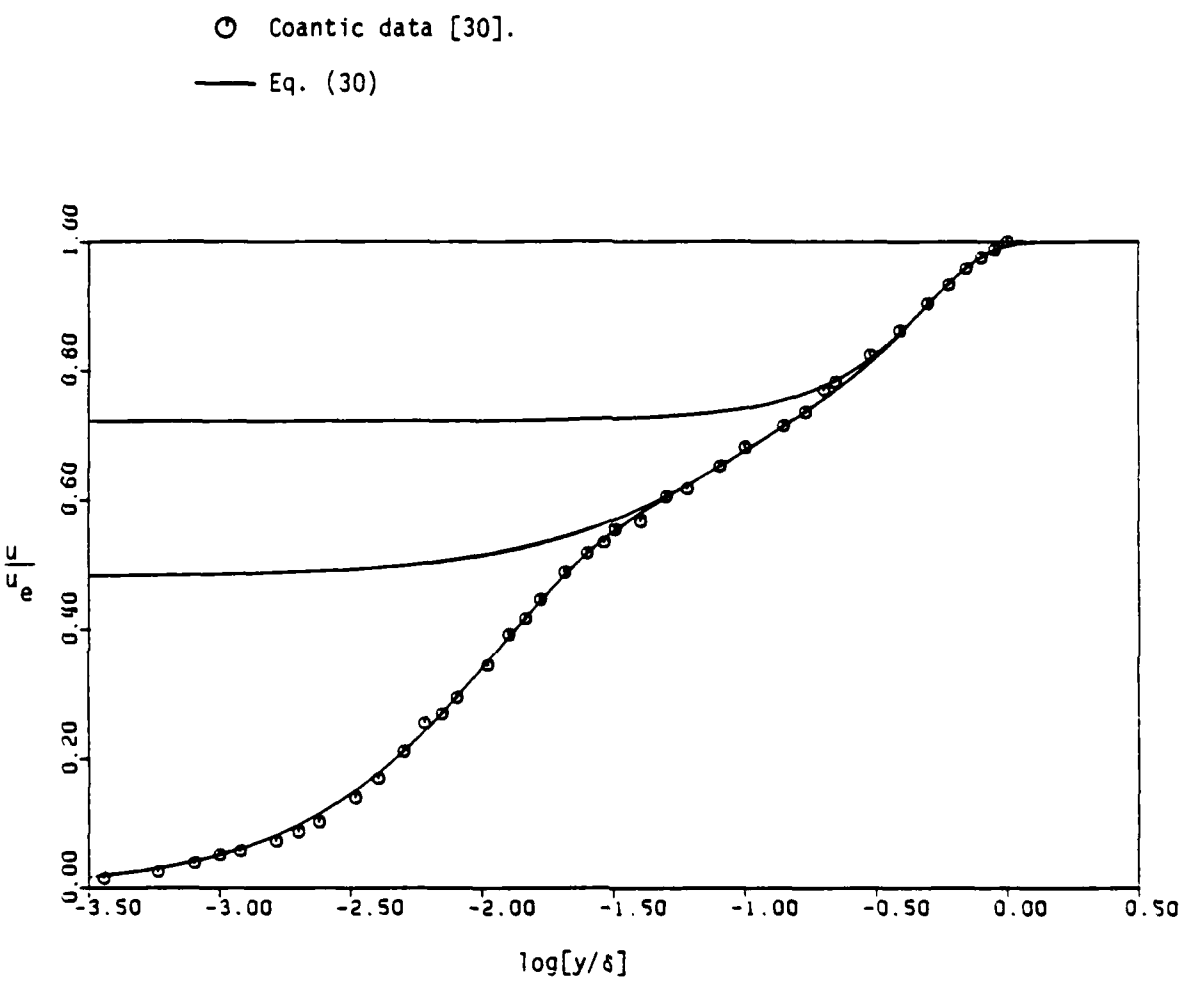



Figure 25: Wall region comparison of Coantic data with Eq. (30).

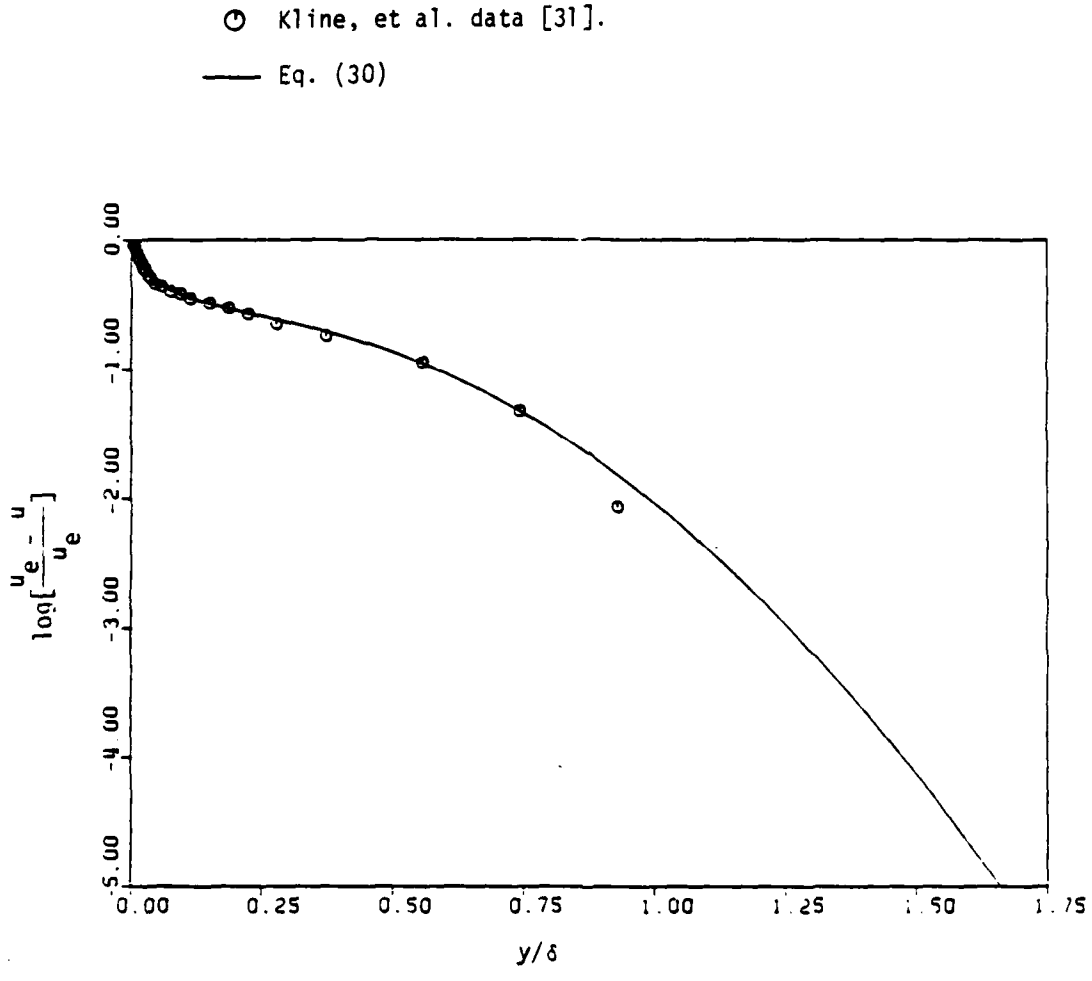



Figure 26: Wake region comparison of velocity defect with Eq. (30). Kline, et al. data.

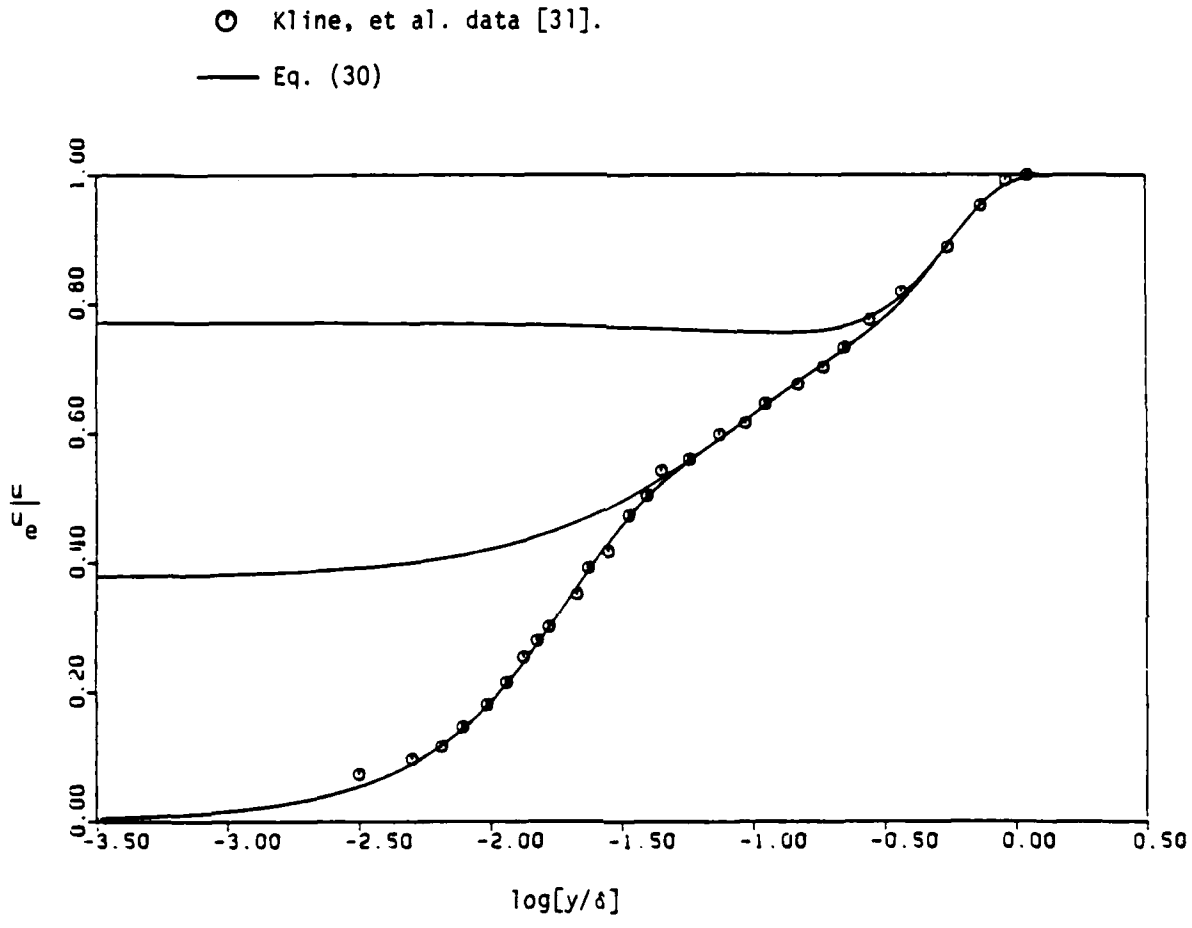



Figure 27: Wall region comparison of Kline, et al data with Eo. (30)

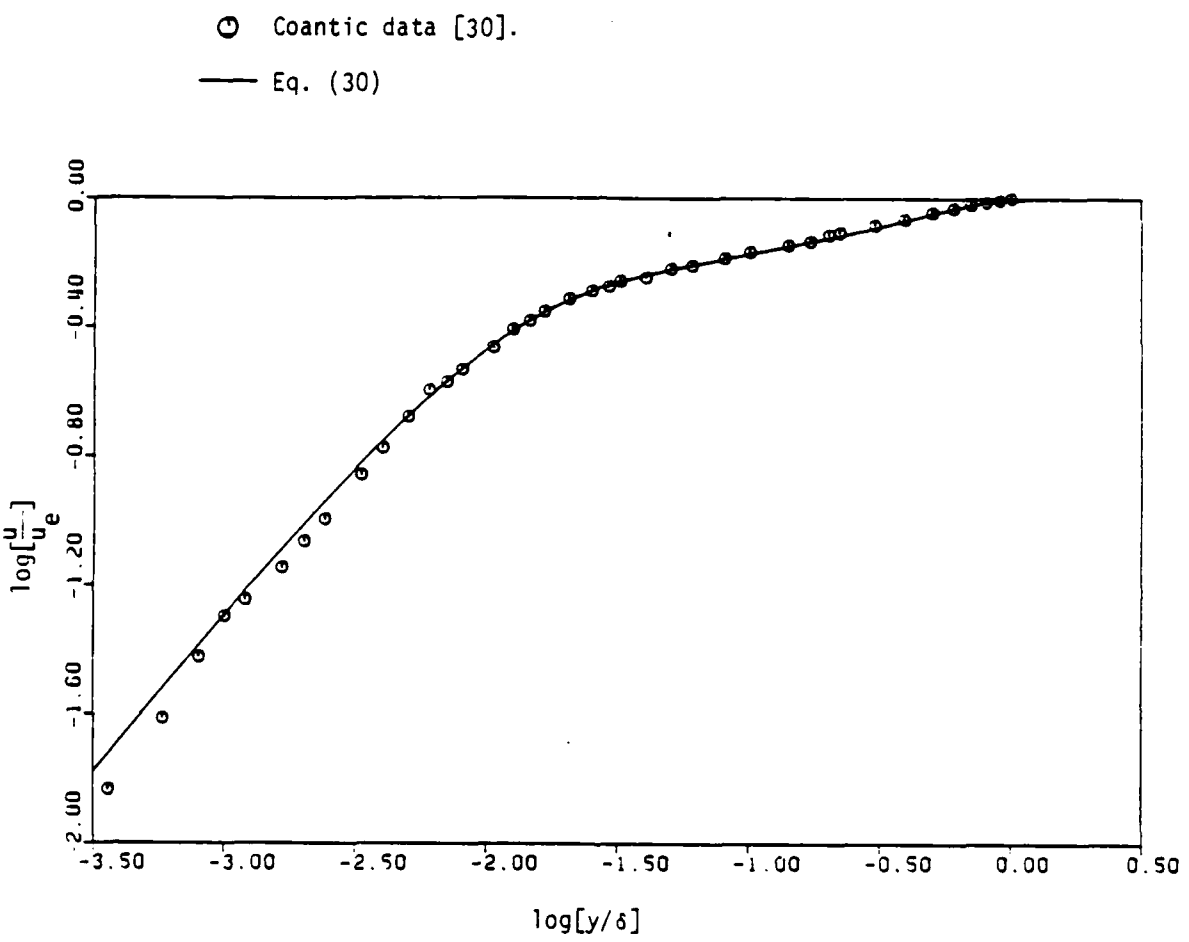



Figure 28: Logarithmic comparison of Coantic data with Eq. (30).

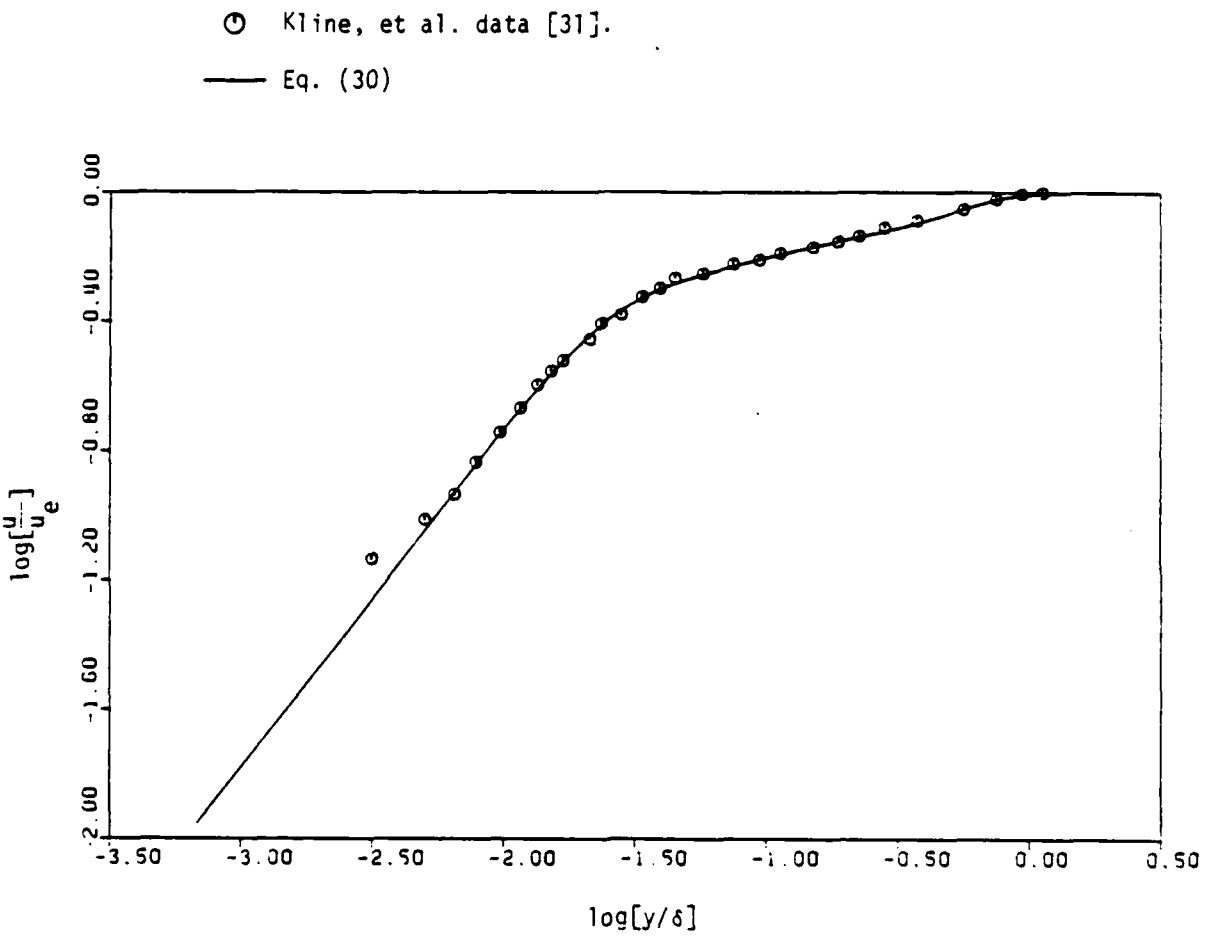



Figure 29: Logarithmic comparison of Kline, et al. data with Eq. (30).

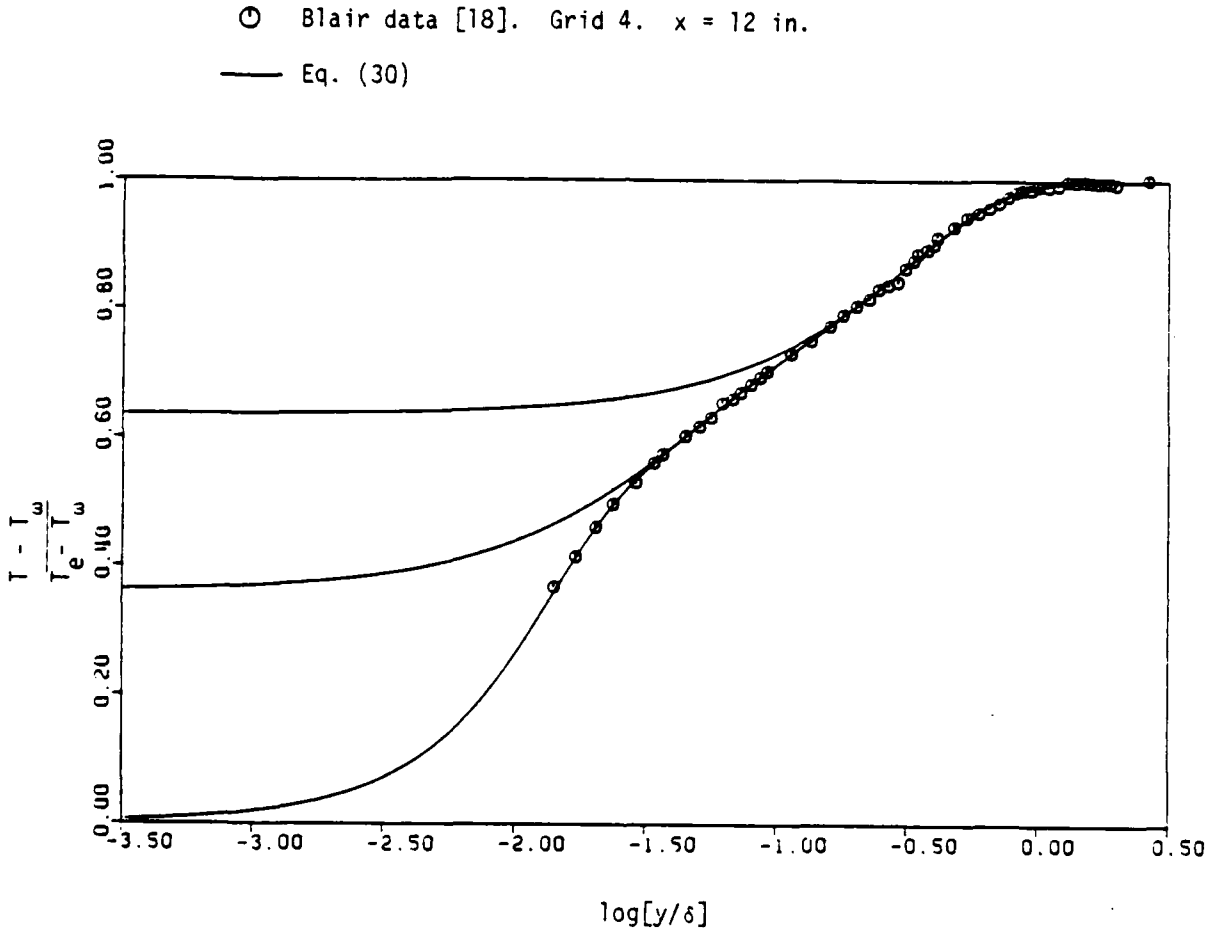



Figure 30: Temperature orofile at x = 12 in. Grid 4.

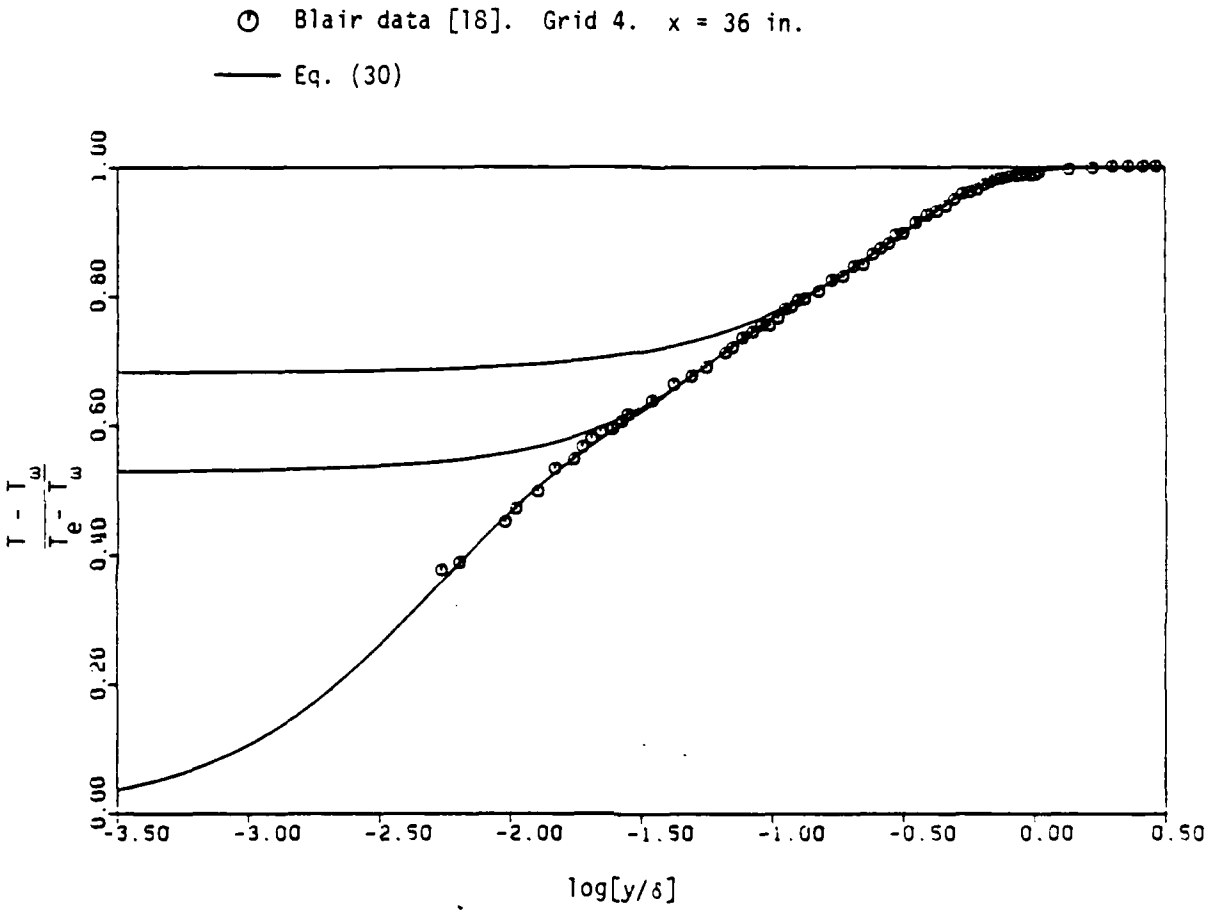



Figure 31: Temperature profile at x = 36 in. Grid 4.

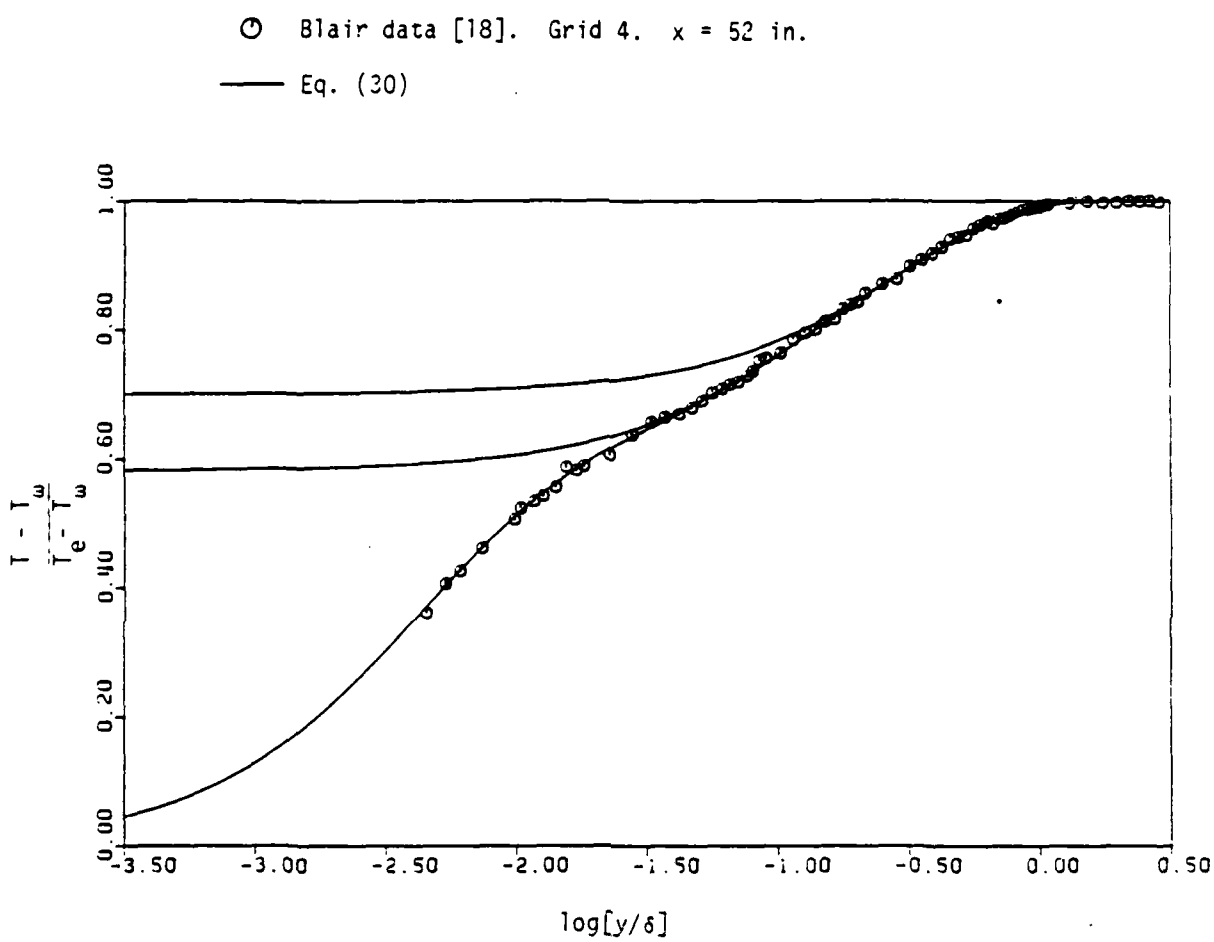



Figure 32: Temperature profile at x = 52 in. Grid 4.

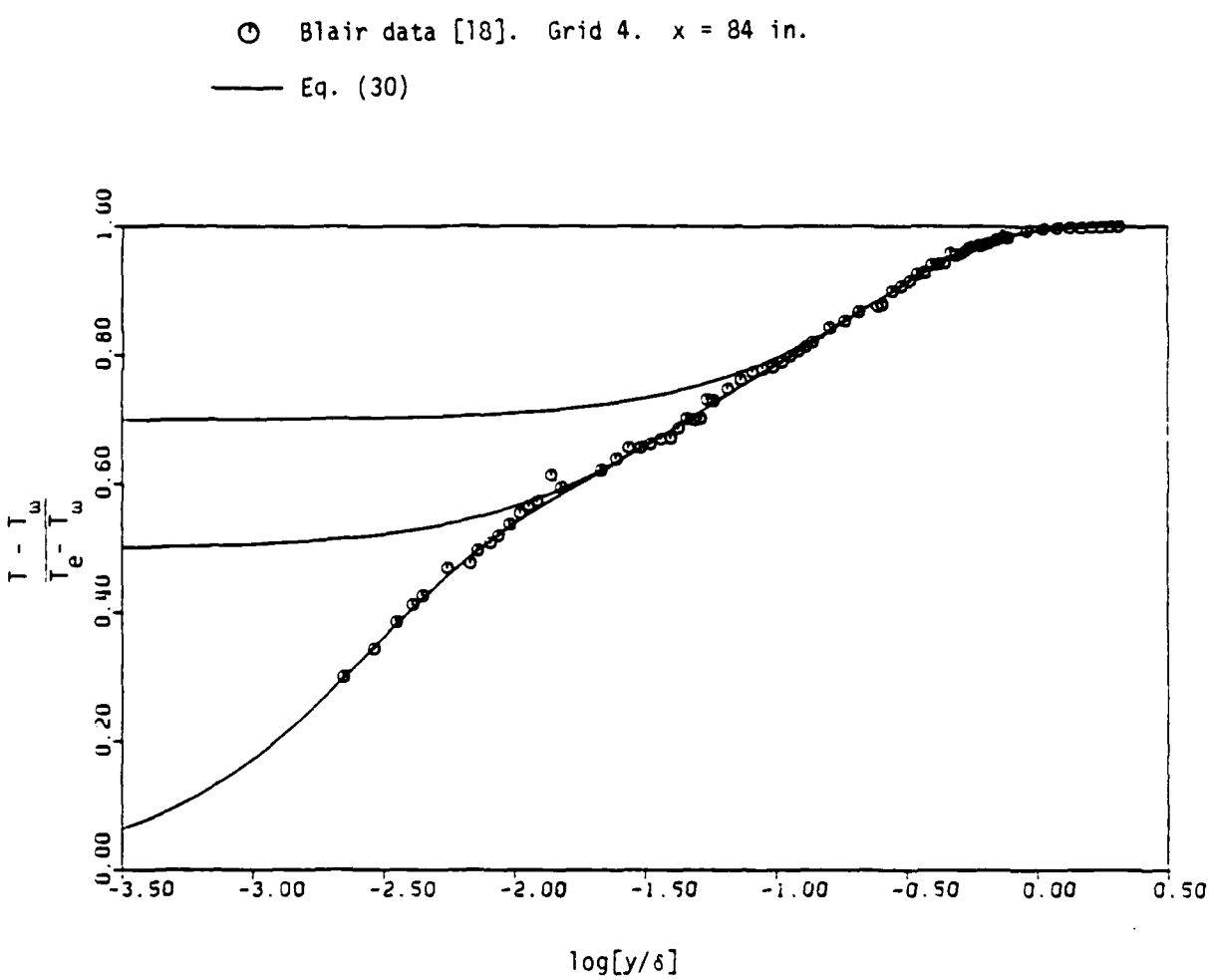



Figure 33: Temperature profile at x = 84 in. Grid 4.

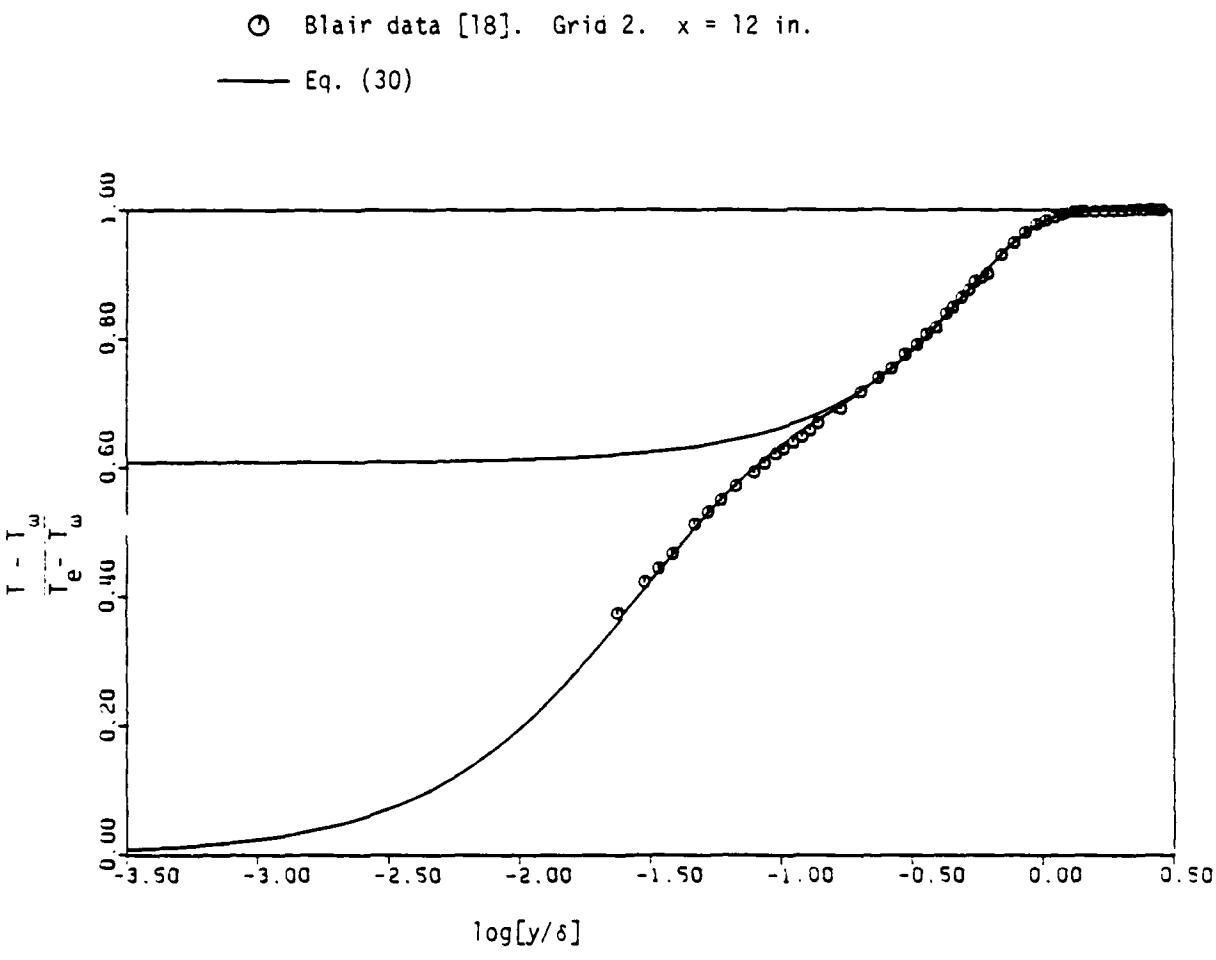



Figure 34: Temperature profile at x = 12 in. Grid 2.

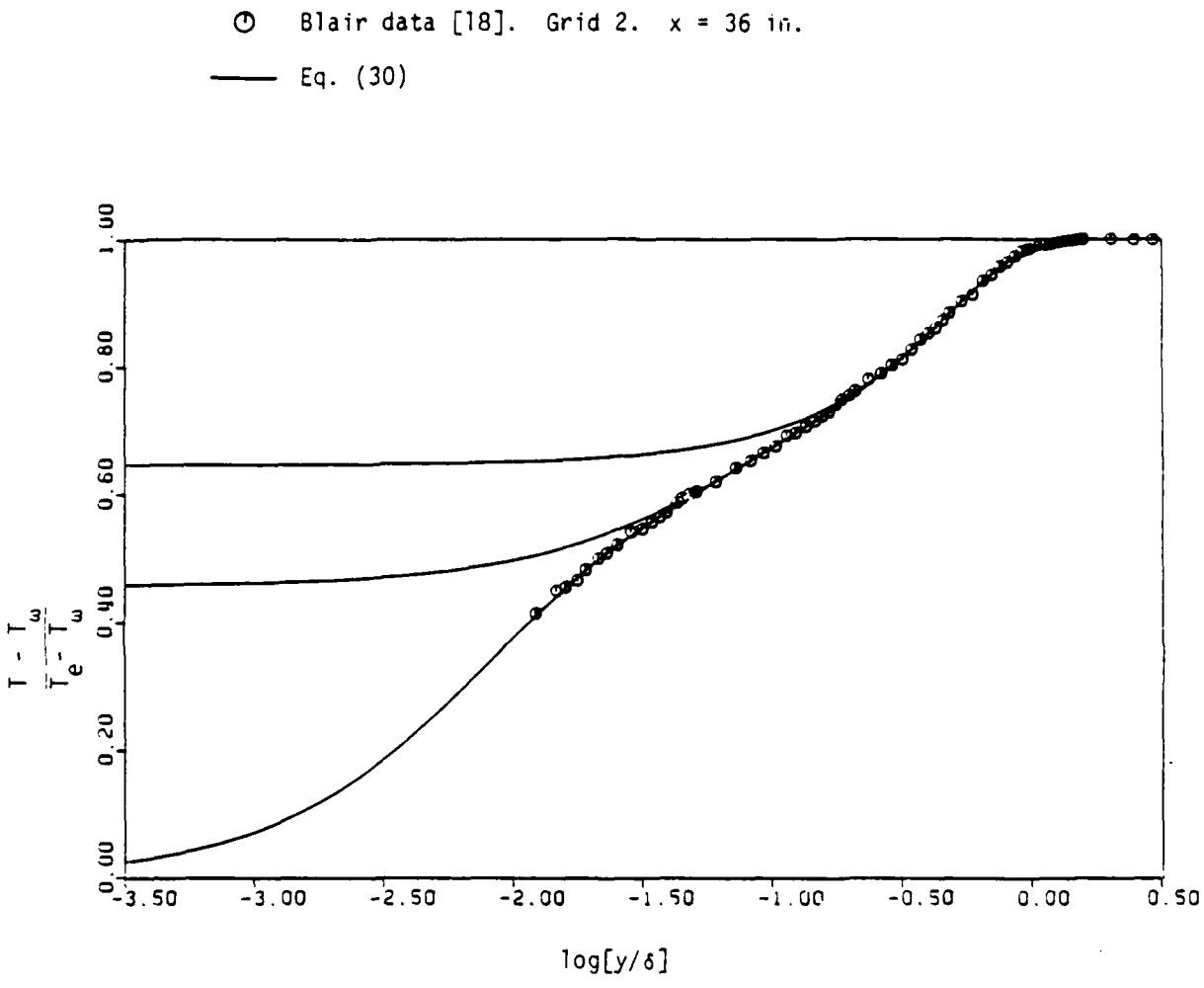



Figure 35: Temperature profile at x = 36 in. Grid 2.

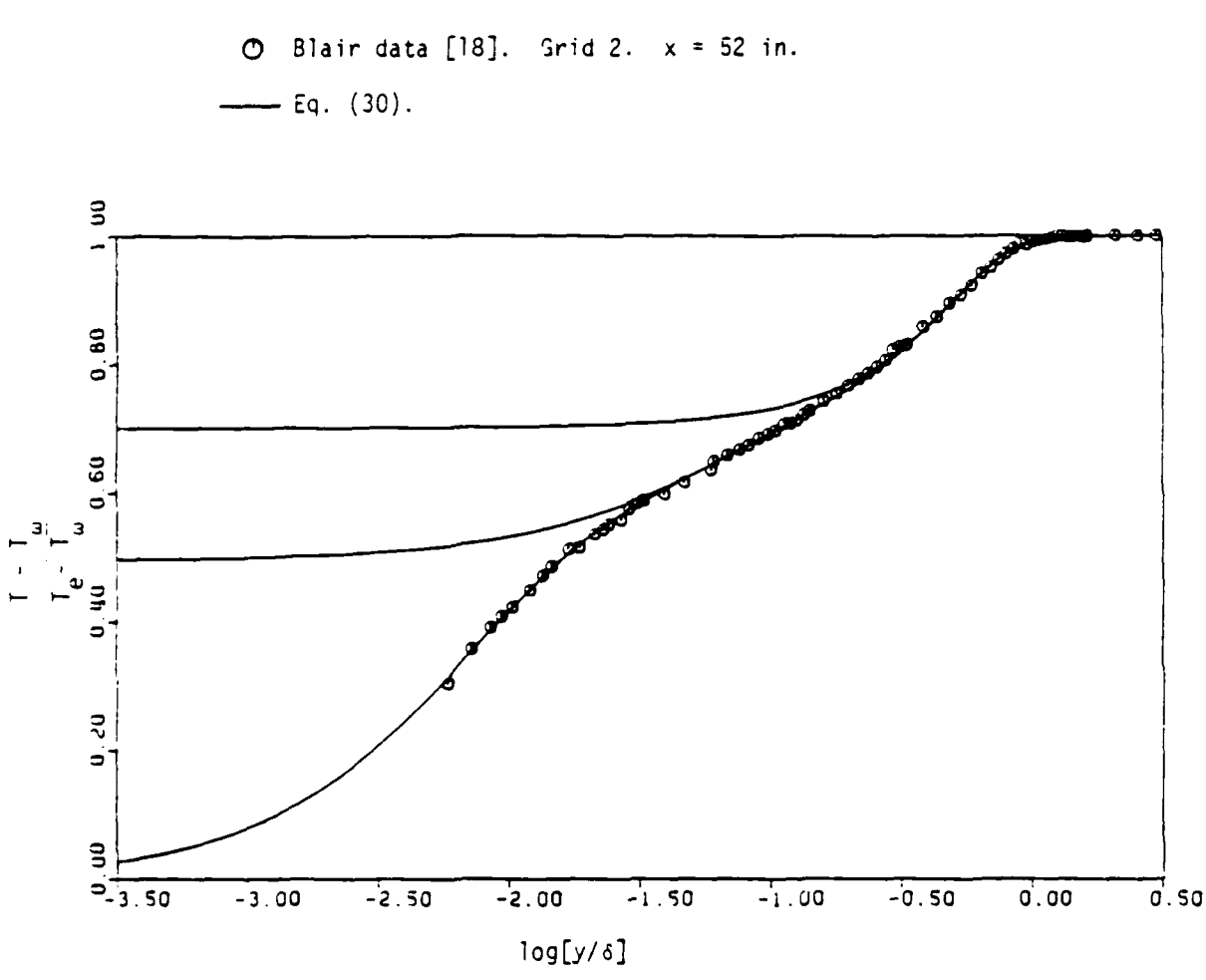



Figure 36: Temperature profile at x = 52 in. Grid 2.

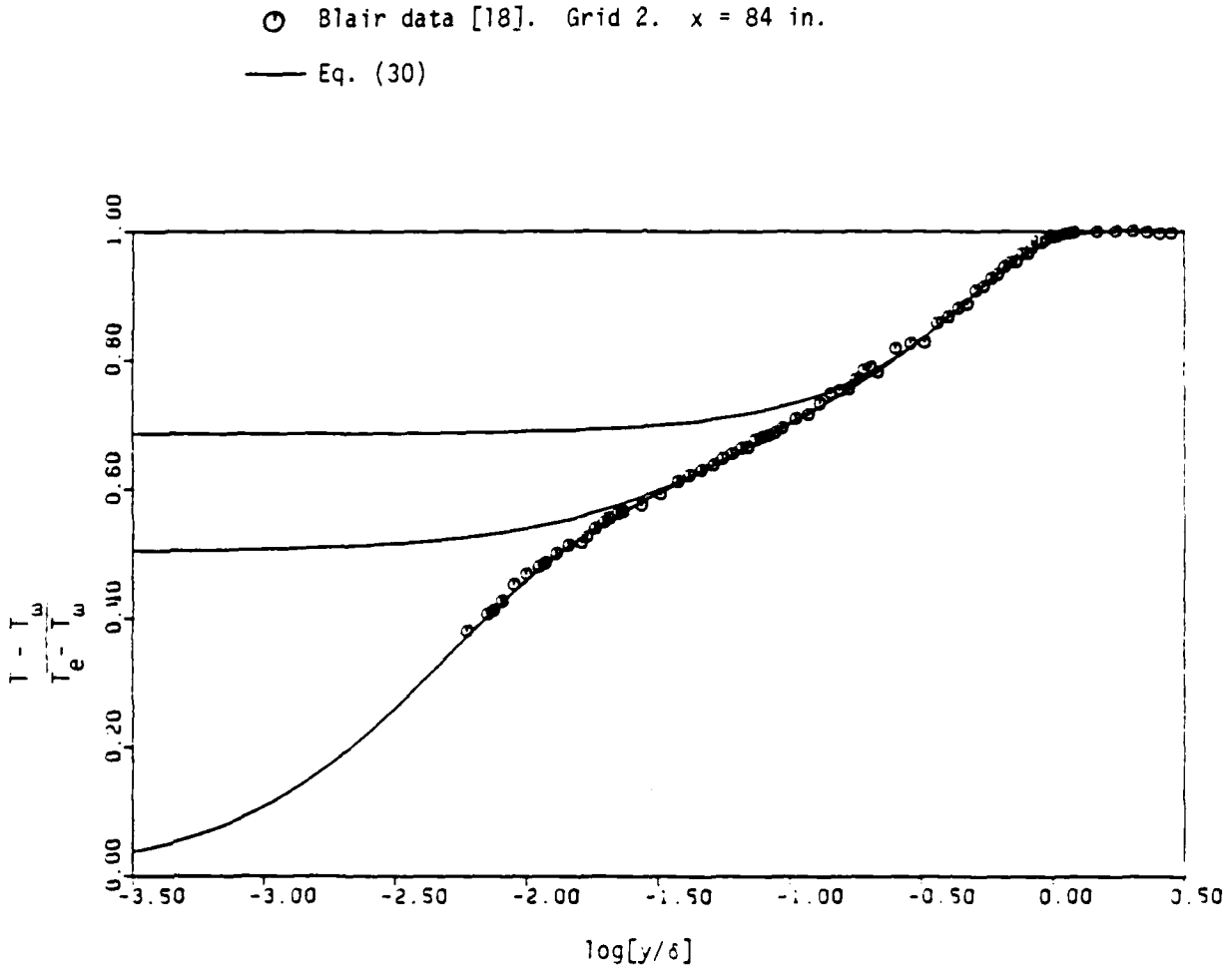



Figure 37: Temperature profile at x = 84 in. Grid 2.

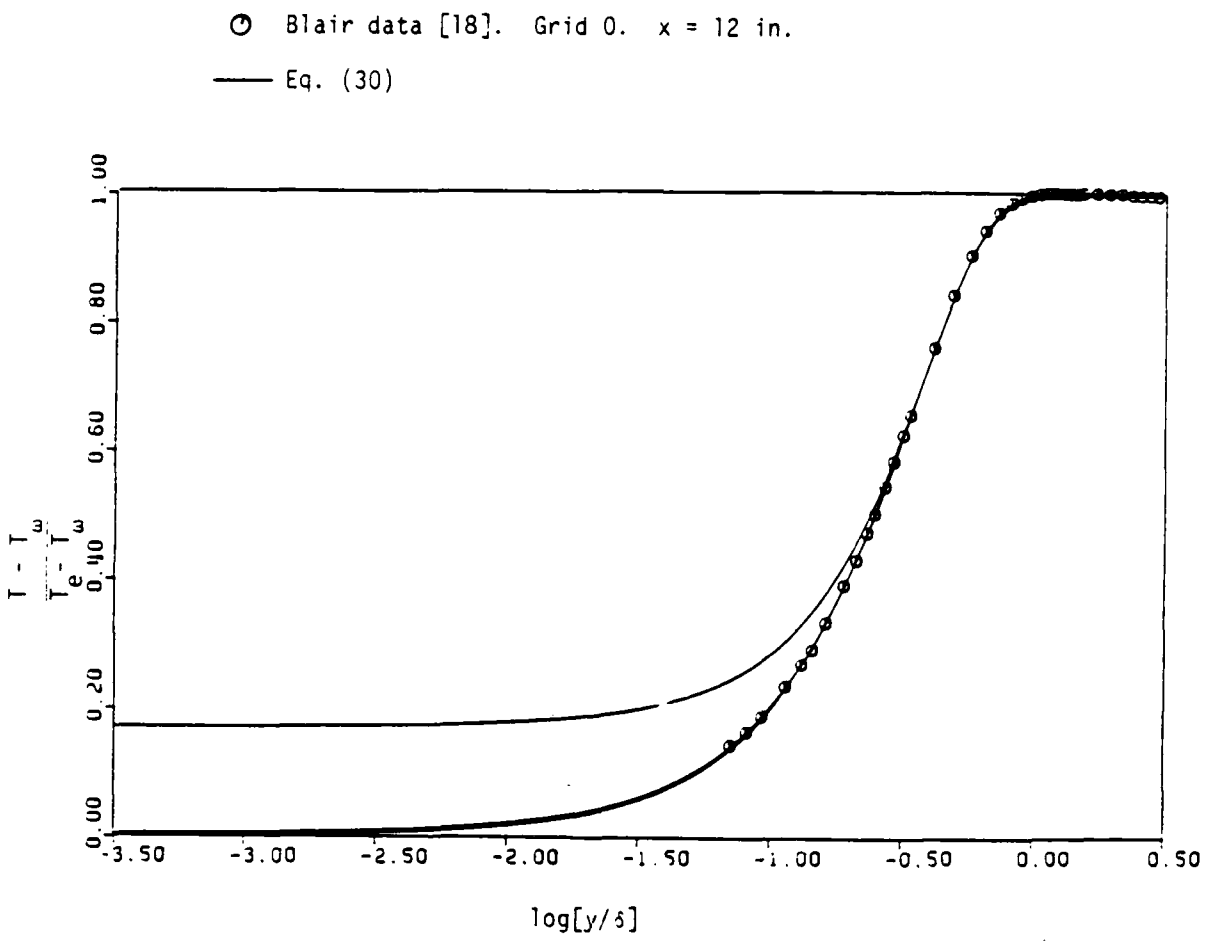



Figure 38: Temperature profile at x = 12 in. Grid 0.

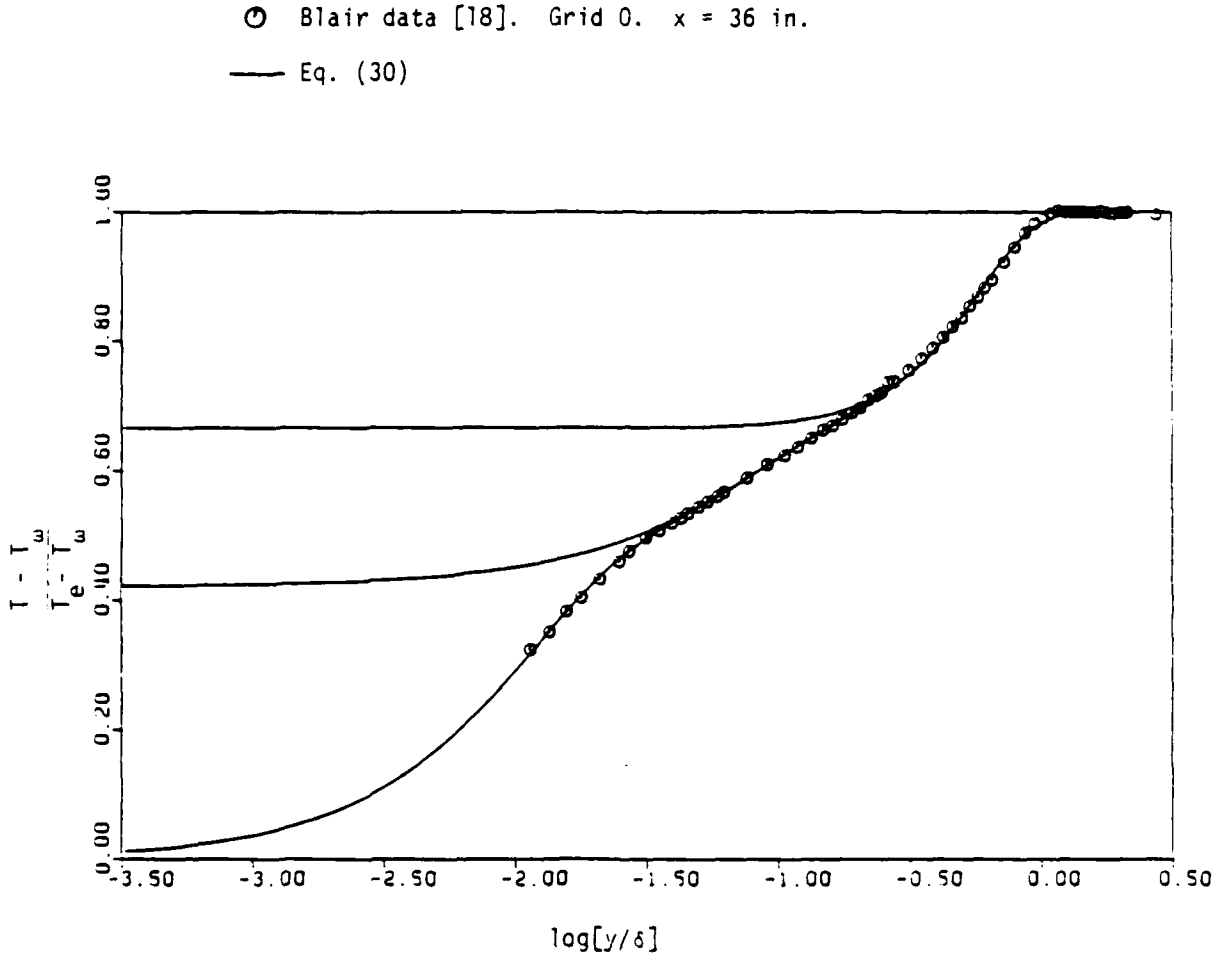



Figure 39: Temperature profile at x = 36 in. Grid 0.

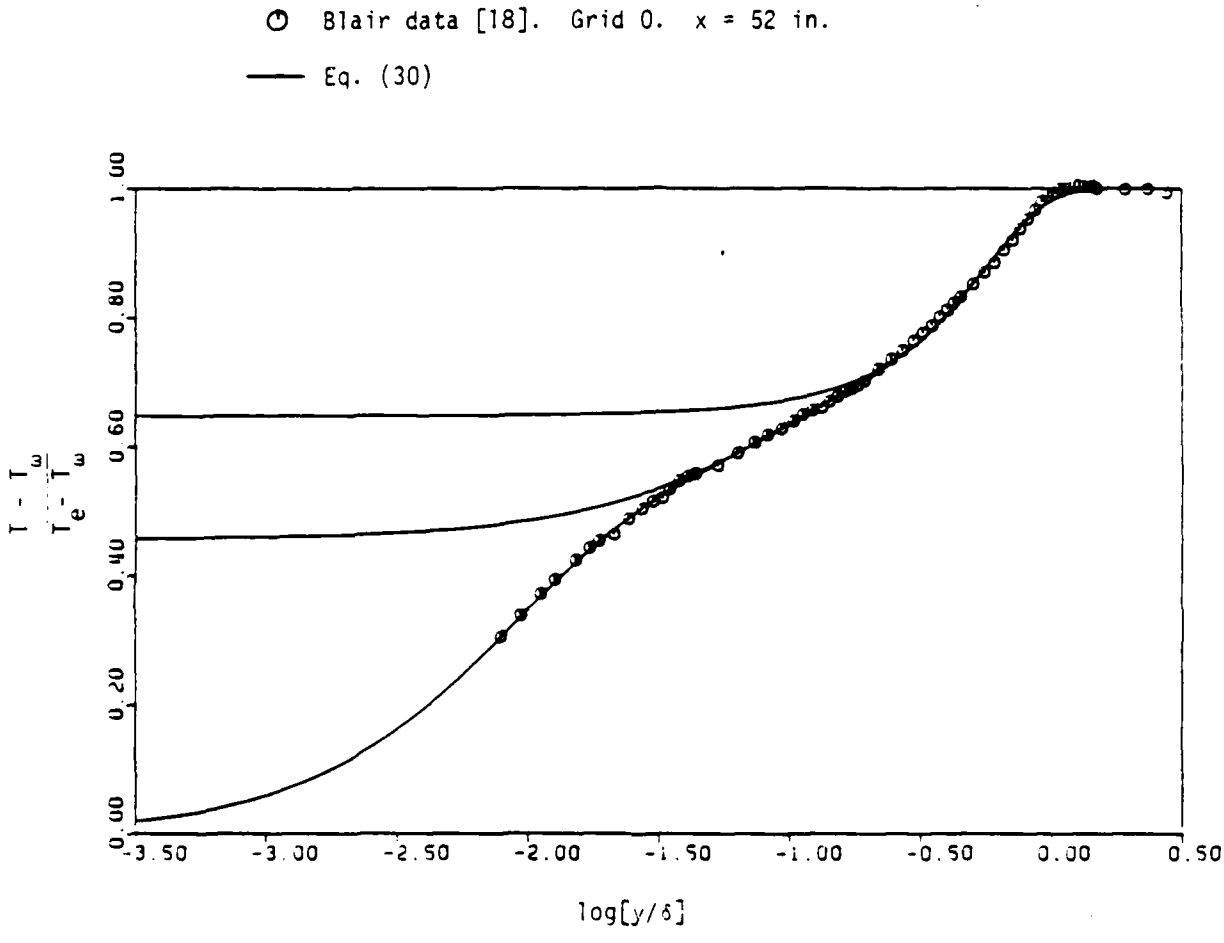



Figure 40: Temperature profile at x = 52 in. Grid 0.

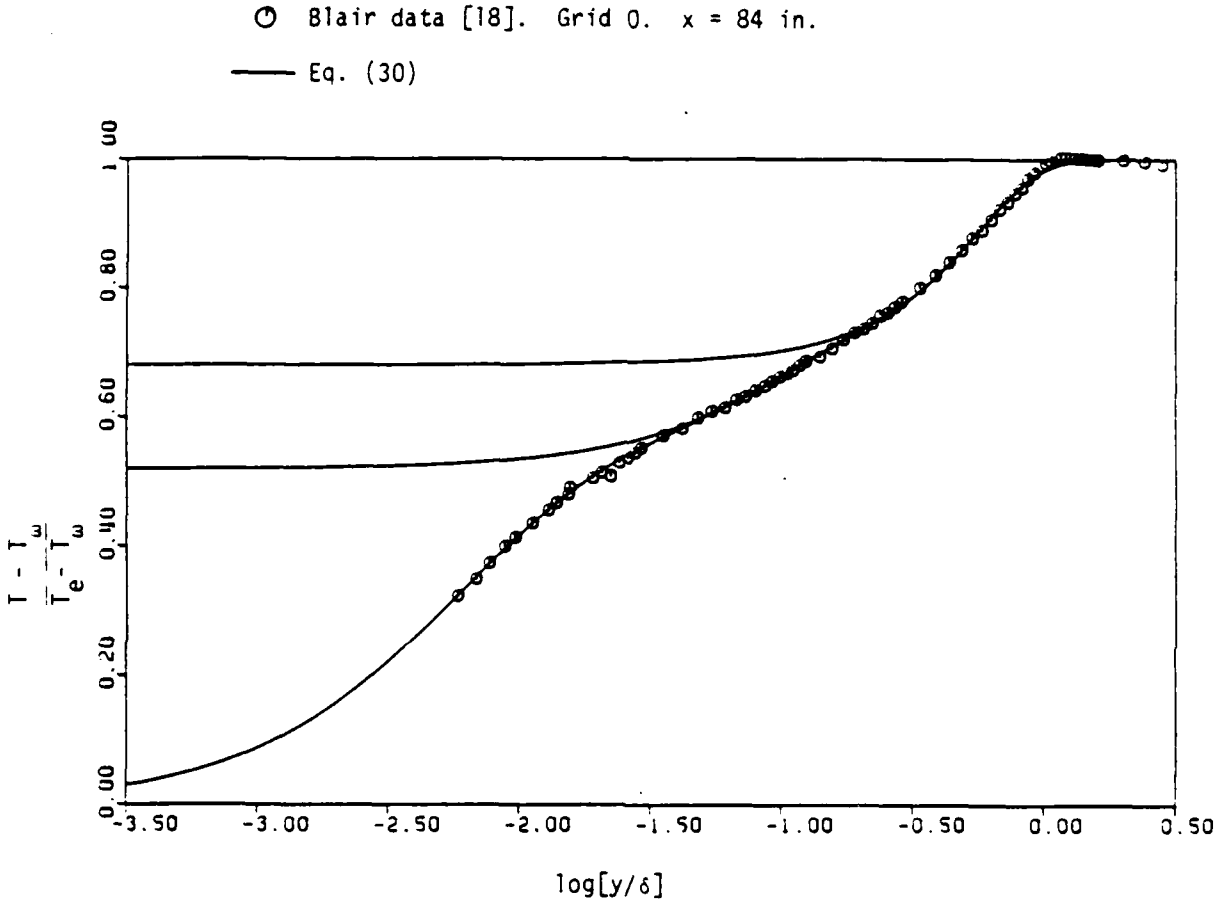



Figure 41: Temperature profile at x = 84 in. Grid 0.

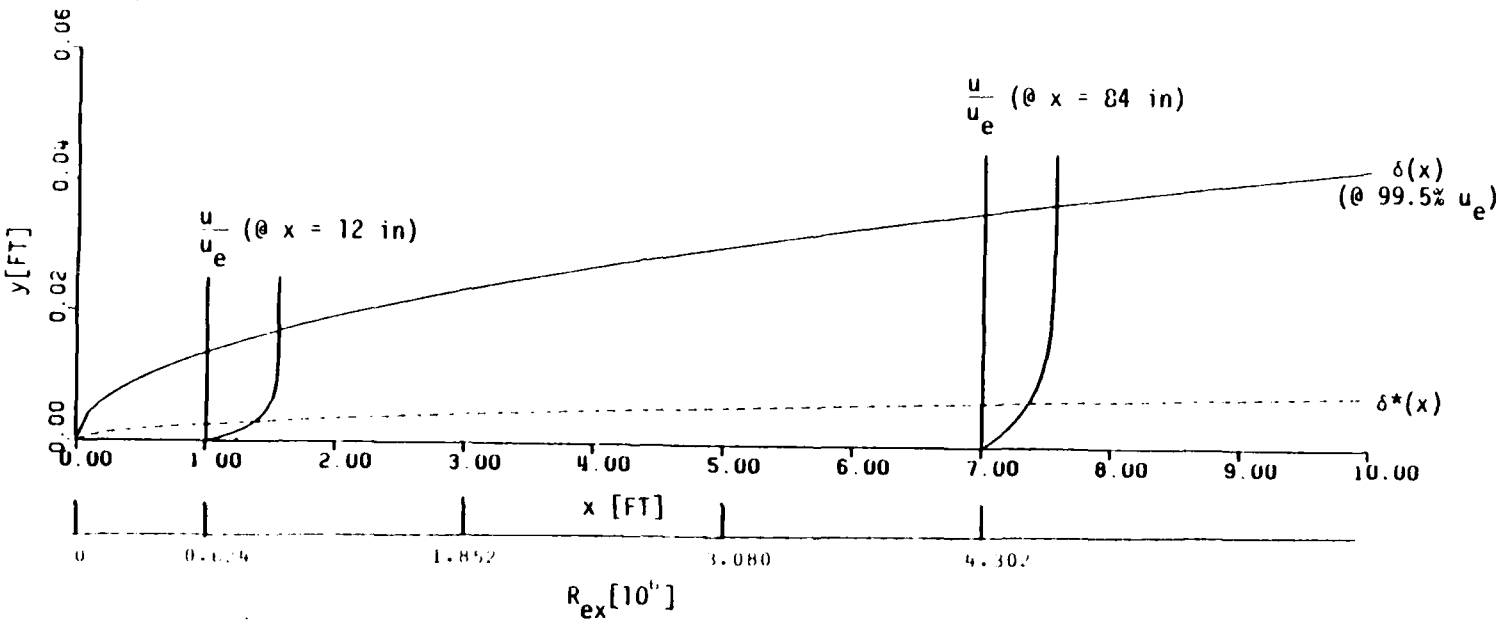



Figure 42: Analytical Test Case Corresponding to Blair's Experiment. See Eqs. (50)-(55).

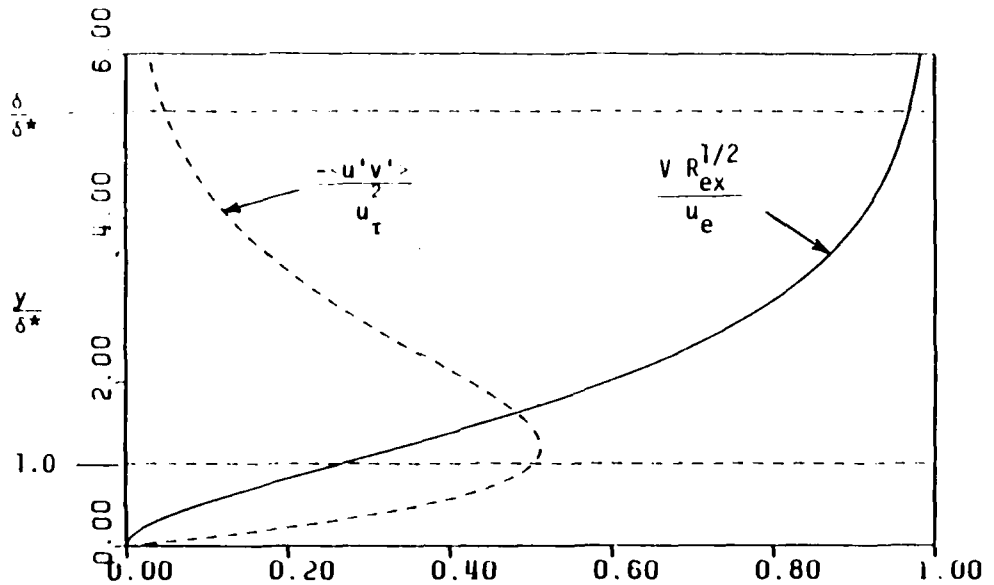



Figure 43: Analytical test case profiles for Reynolds stress and mean normal velocity component.

A = mean viscous dissipation [Eq. (56)]

B = turbulence production [Eq. (57)]

C = Reynolds stress [Eq. (53)]

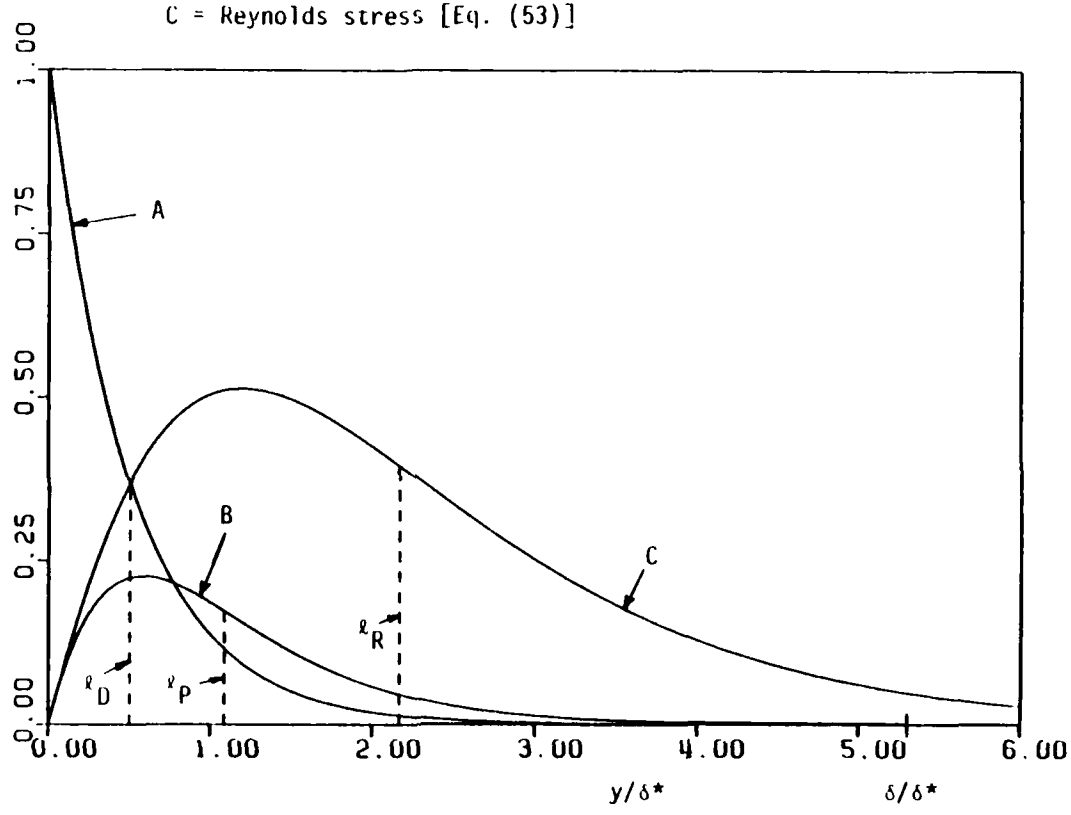



Figure 44: Turbulence related profiles of the analytical test case.

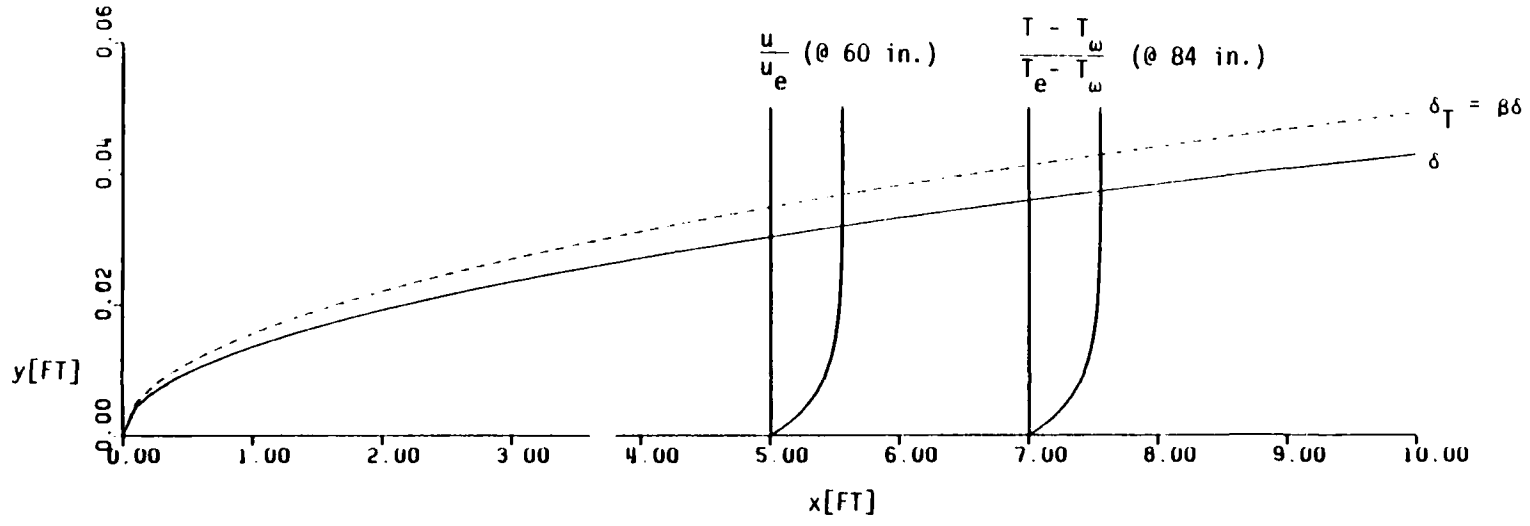



Figure 45: Comparison of thermal and velocity boundary layers for the analytical test case. (See Eqs. (50)-(65).)

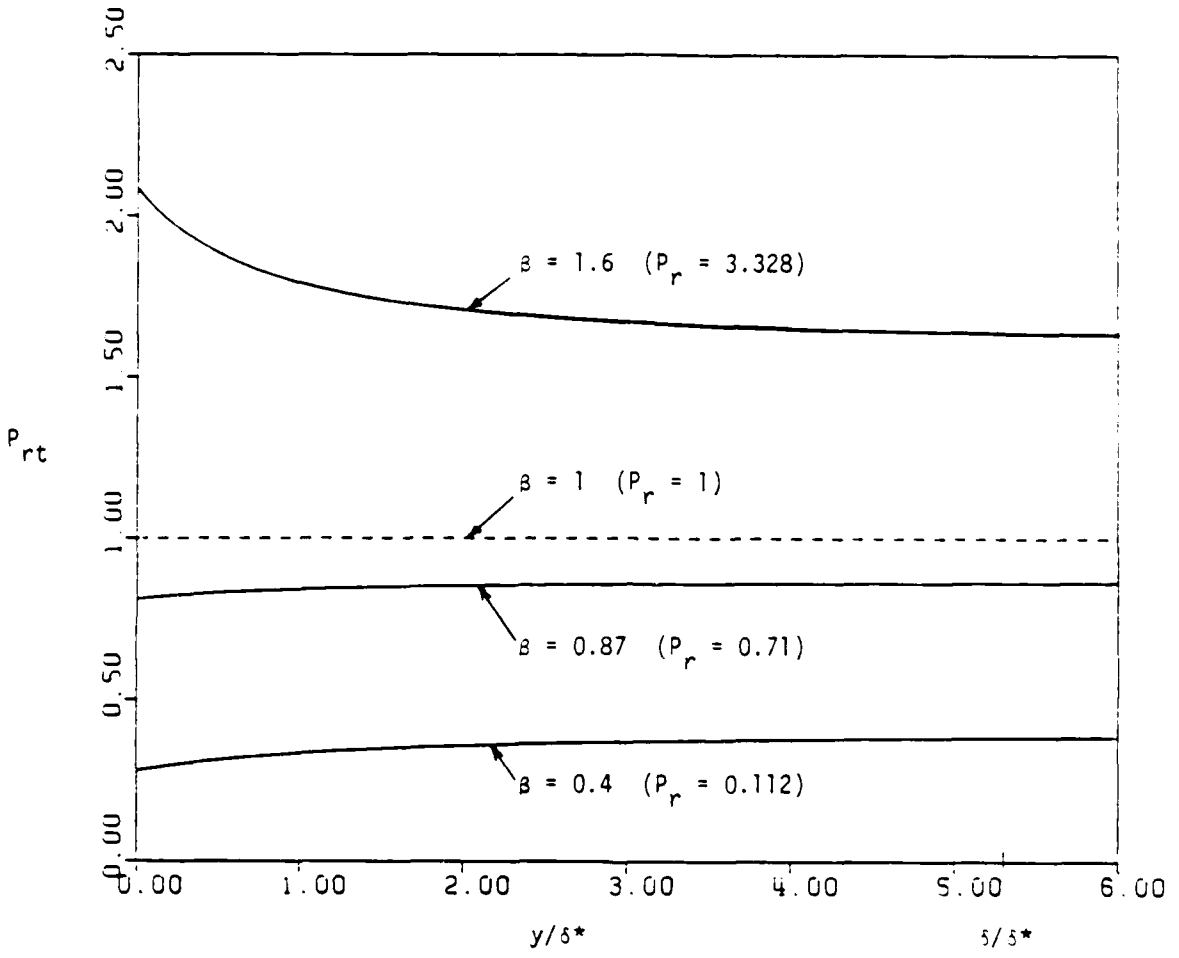



Figure 46: Turbulent Prandtl number for analytical test case. See Eq. (64).

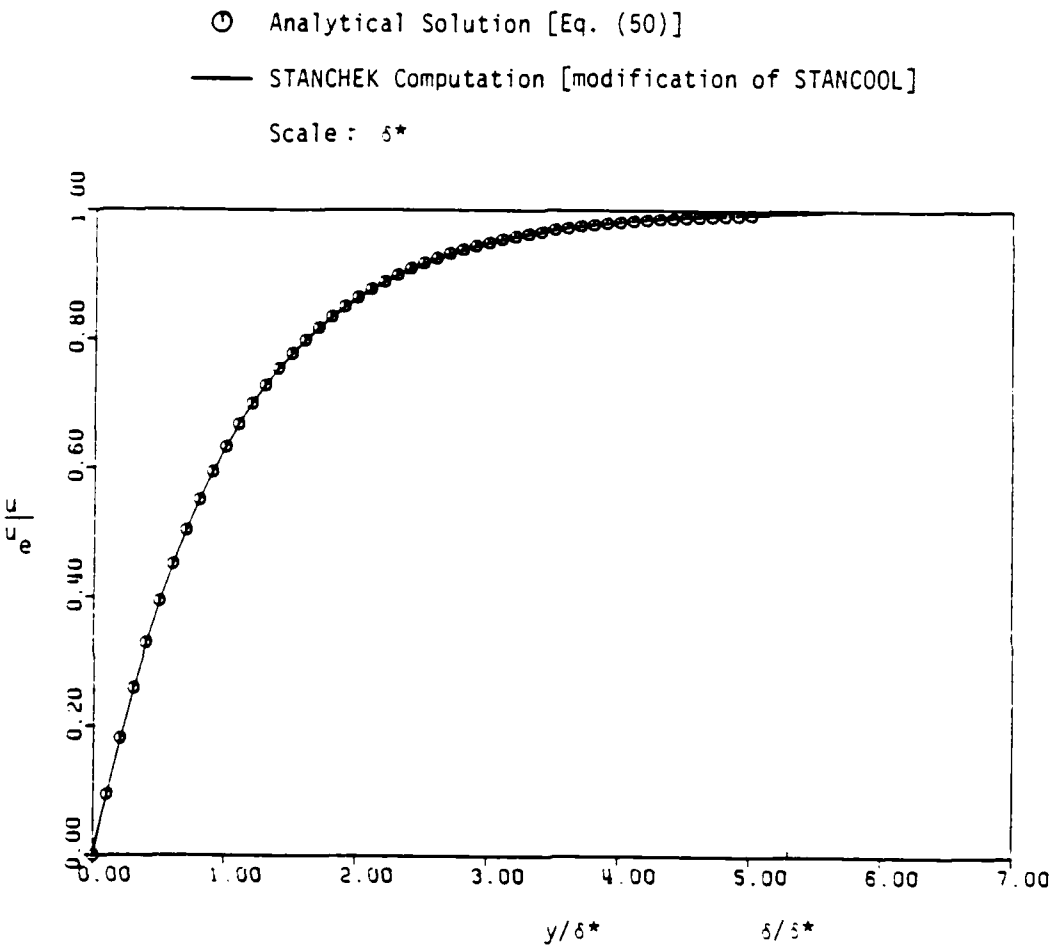



Figure 47: Comparison of STANCHEK with analytical test solution.
Both curves are scaled with respect to their own calculated δ*.

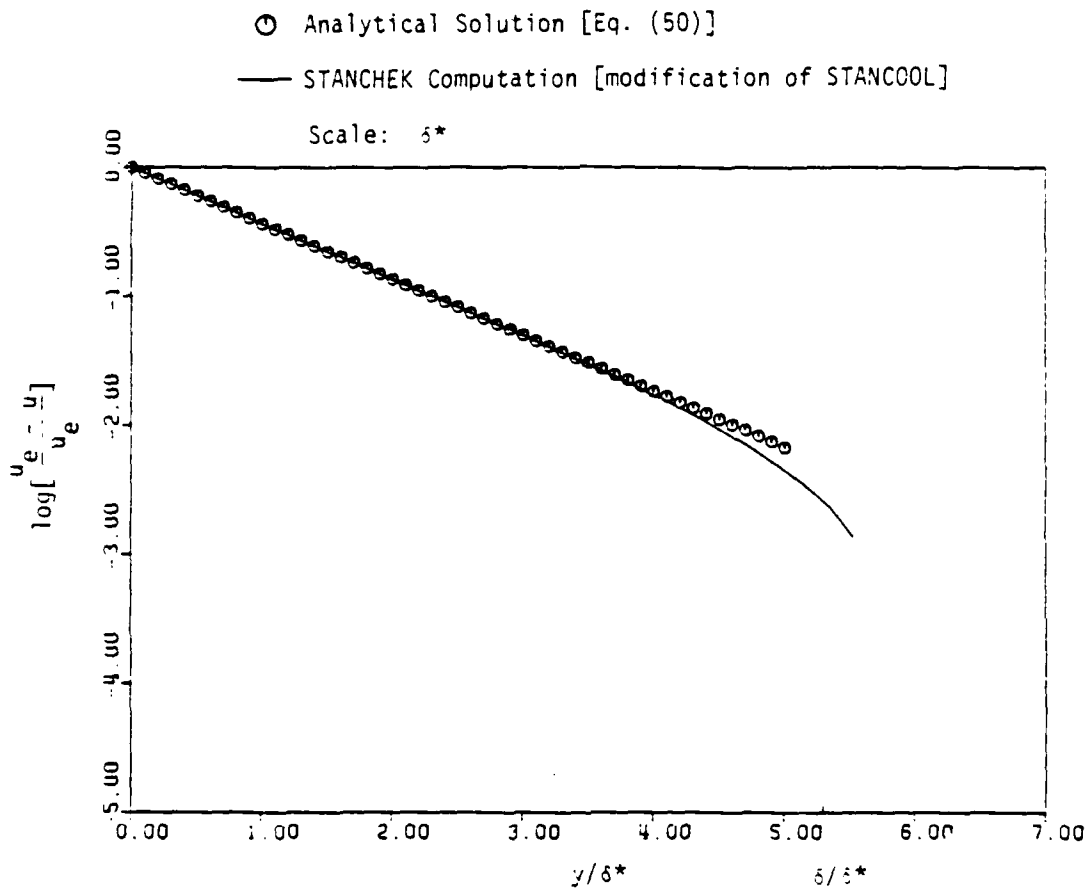



Figure 48: Wake region of analytical test case. Both curves are scaled with respect to their own calculated δ*.

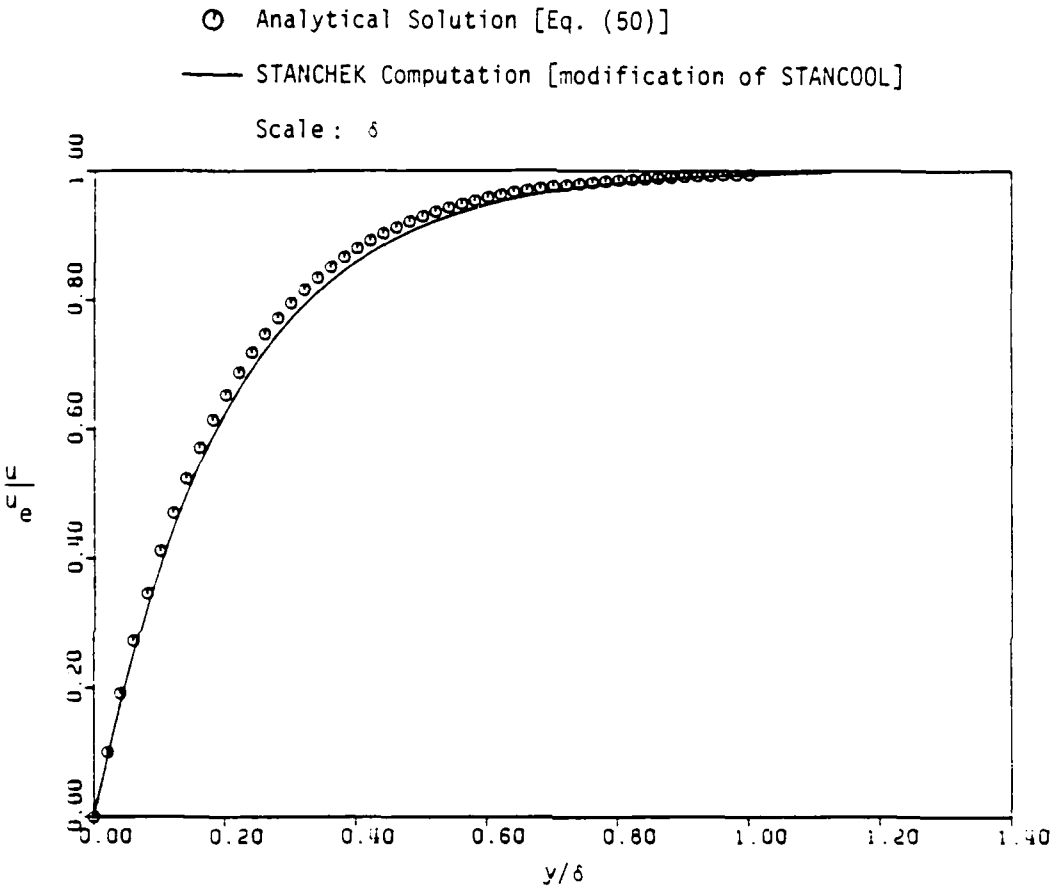



Figure 49: Comparison of STANCHEK with analytical test solution. Both curves are scaled with respect to their own calculated δ.

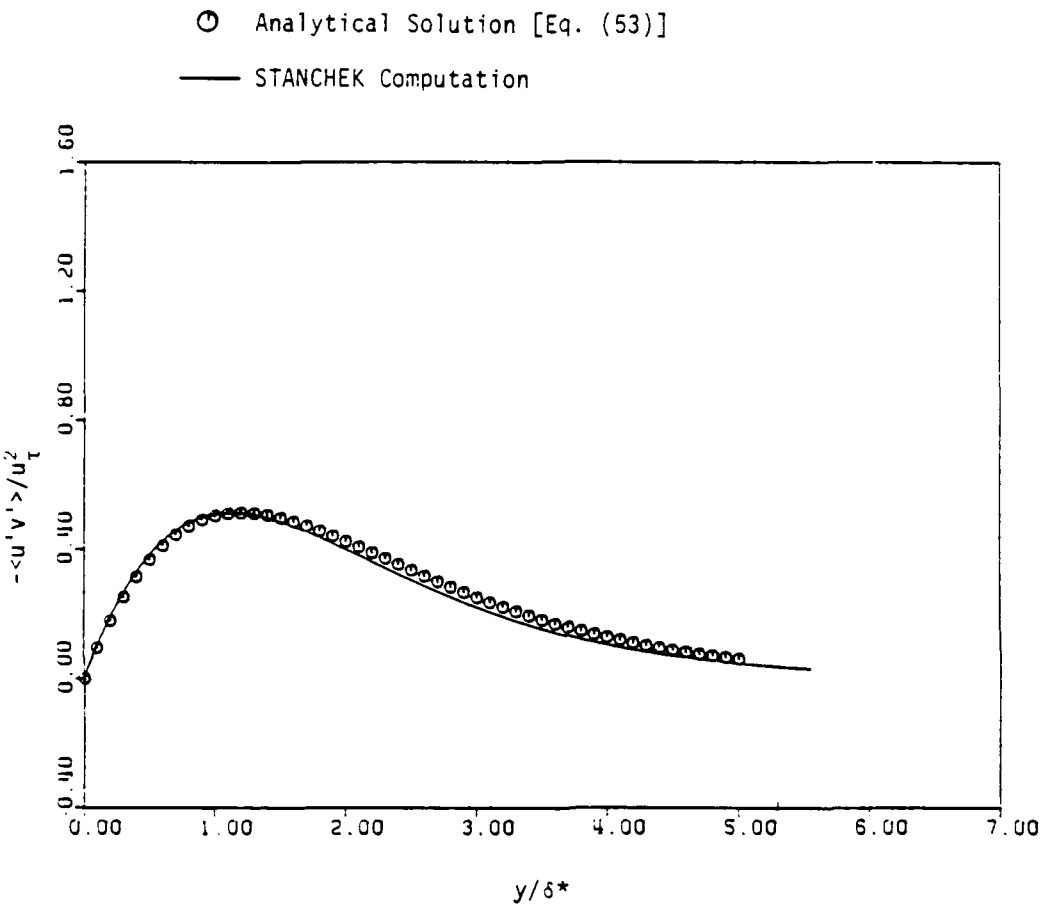



Figure 50: Comparison of STANCHEK with analytical test case Reynolds stress. [The profiles are forced to be identical in $y/\delta$.]

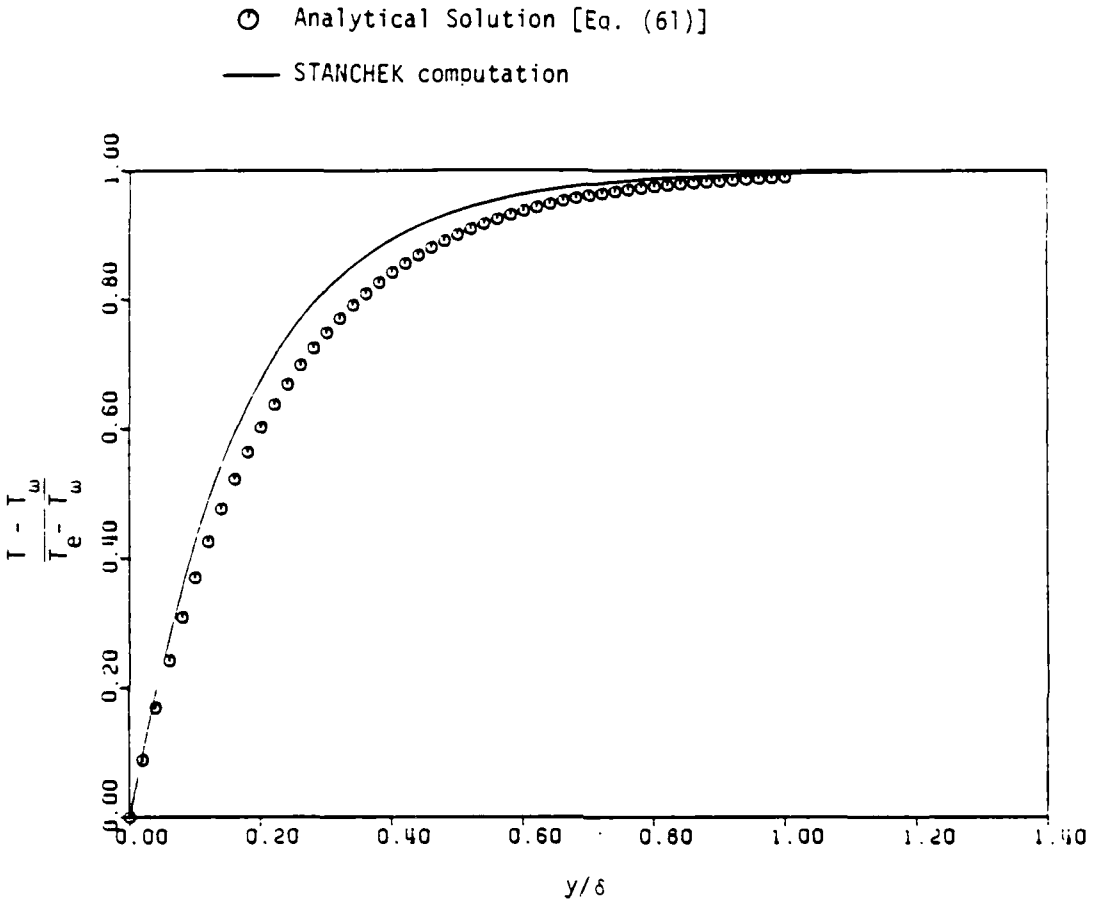



Figure 51: Comparison of STANCHEK with analytical test case temperature profile. $P_{rt}$ according to Eq. (64).

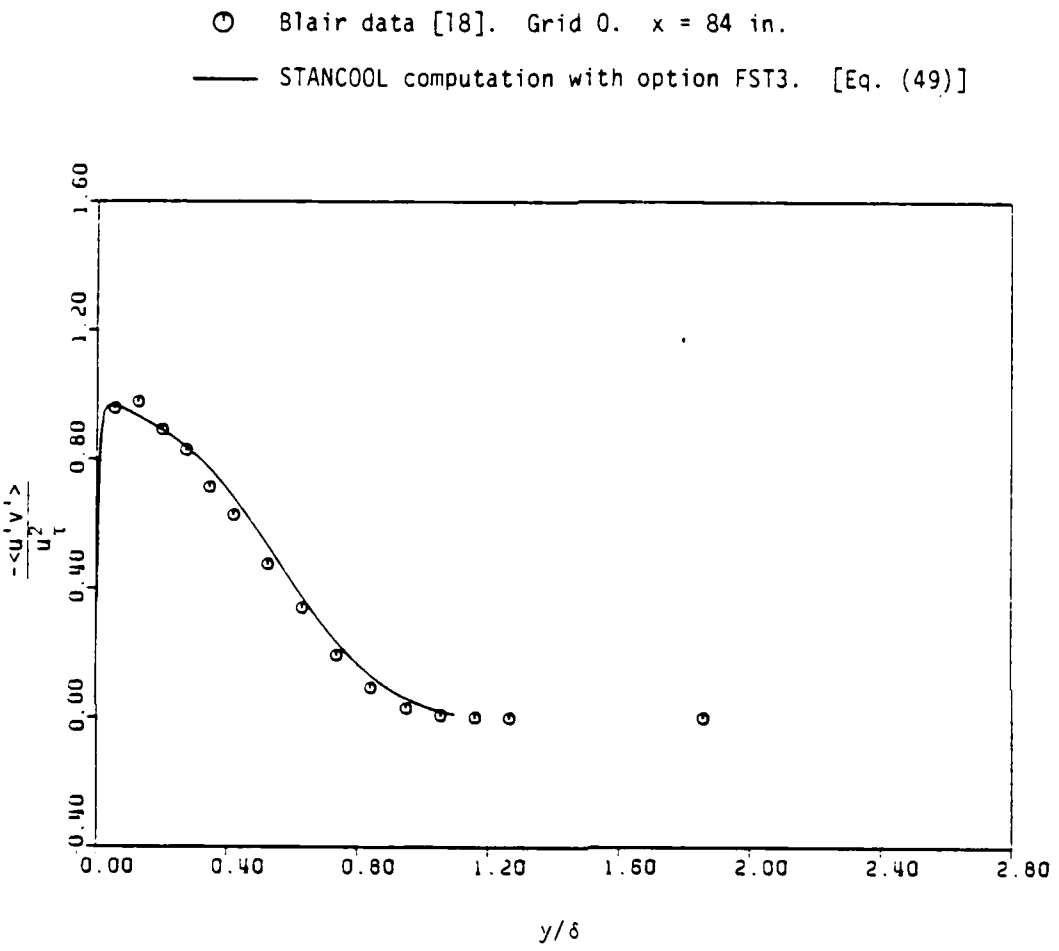



Figure 52: Calculated (FST3) and measured Reynolds stress profiles.

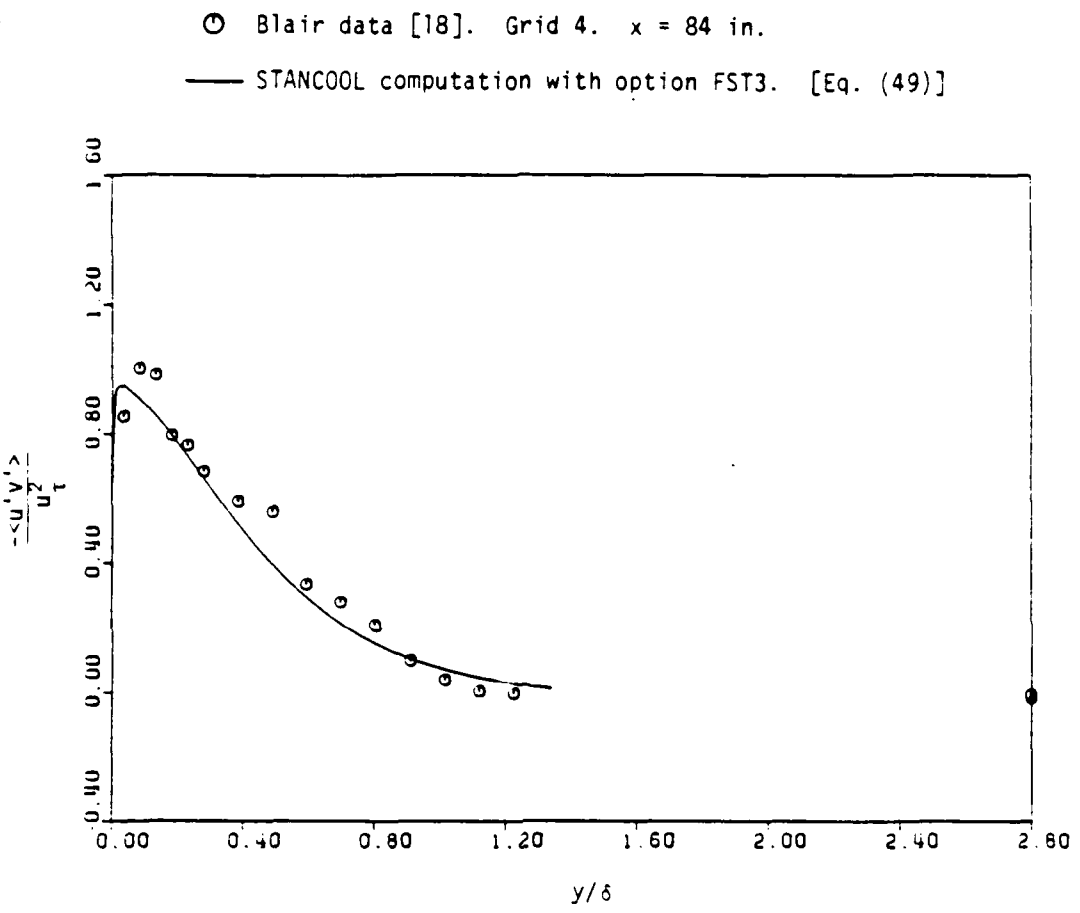



Figure 53: Calculated (FST3) and measured Reynolds stress profiles.

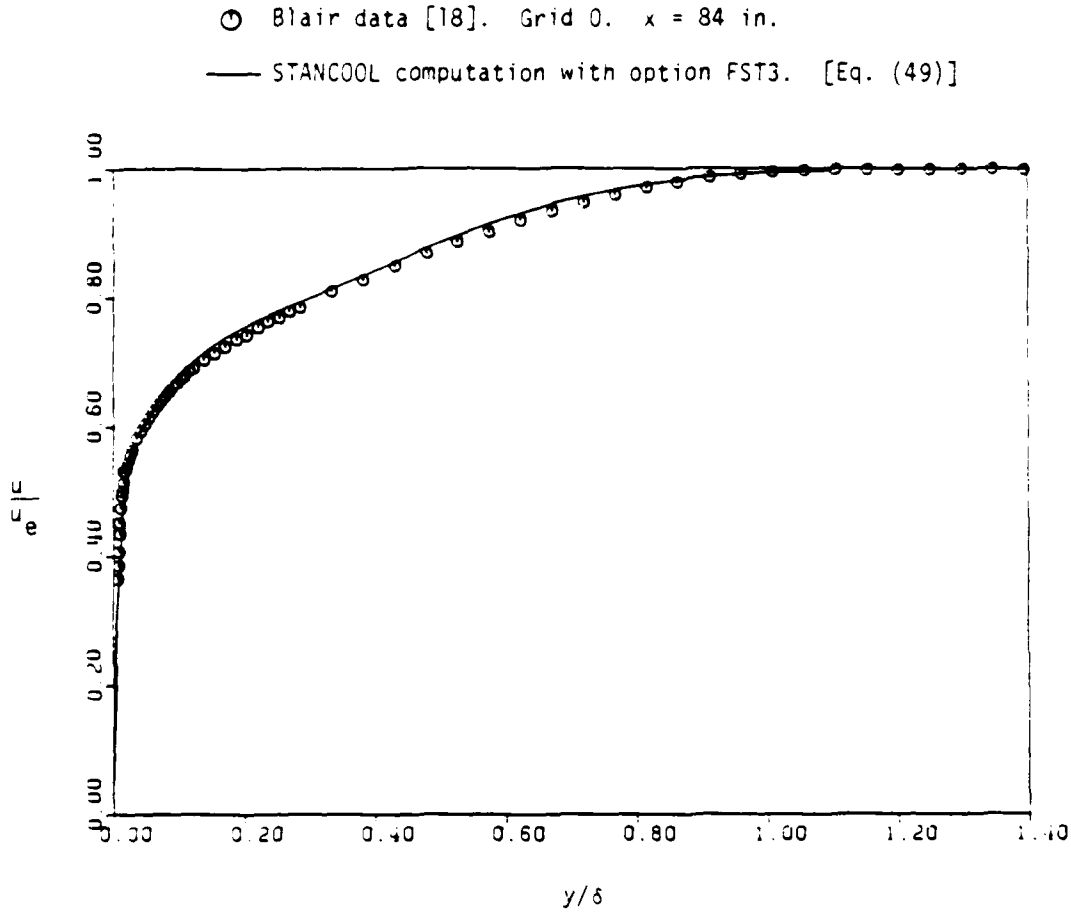



Figure 54: Calculated (FST3) and measured mean velocity profiles.

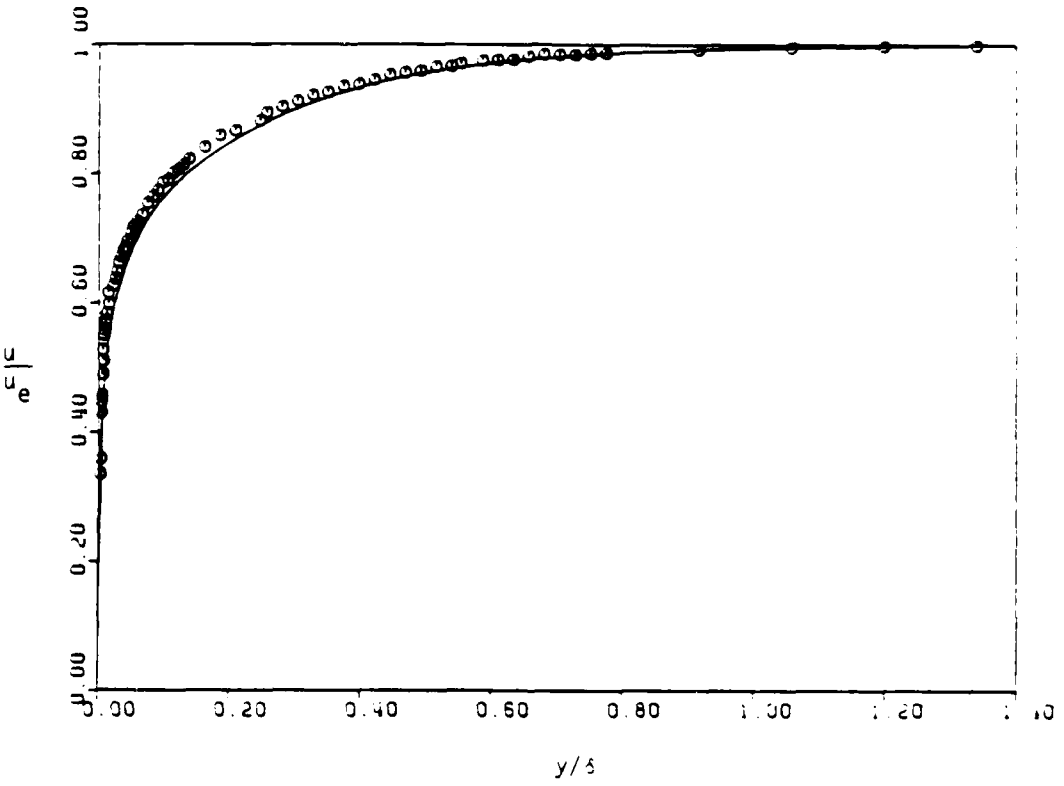



Figure 55: Calculated (FST3) and measured mean velocity profiles.

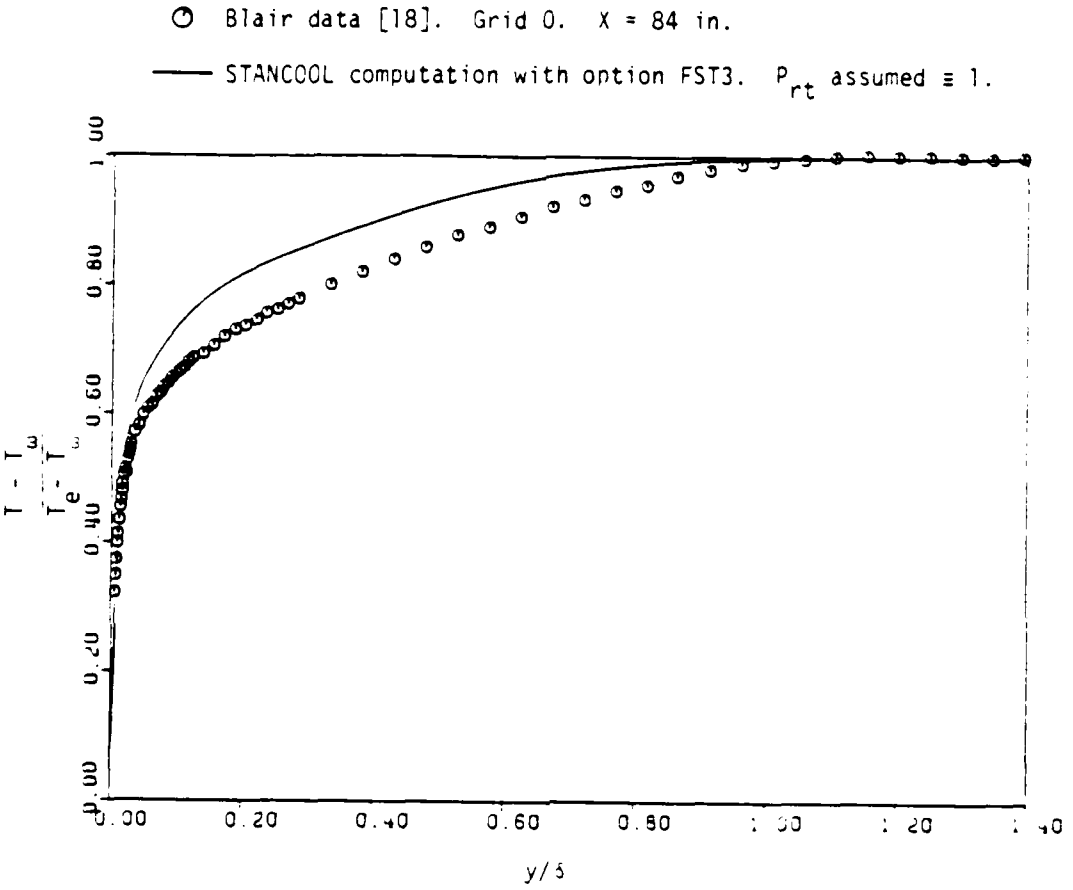



Figure 56: Calculated (FST3) and measured mean temperature profiles. Unity $P_{rt}$ assumed.

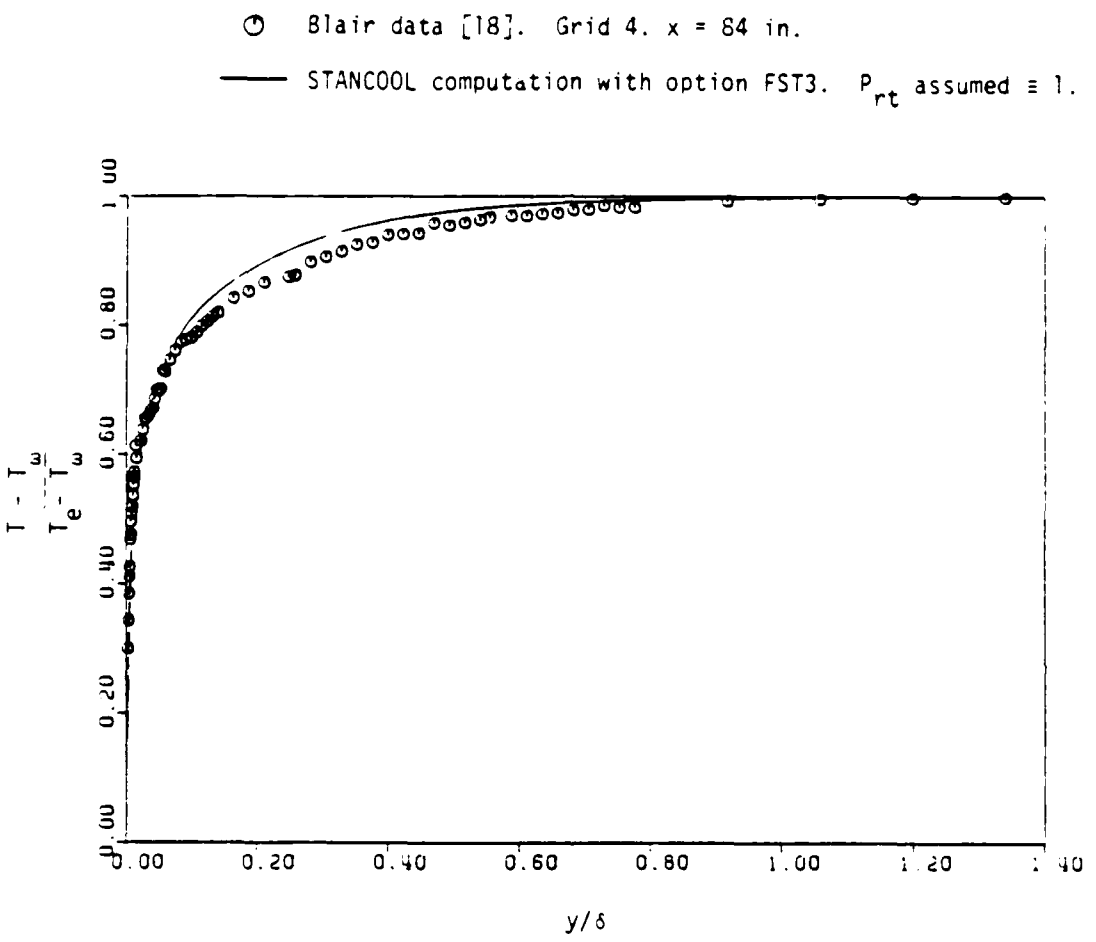



Figure 57: Calculated (FST3) and measured mean temperature profiles. Unity $P_{rt}$ assumed.

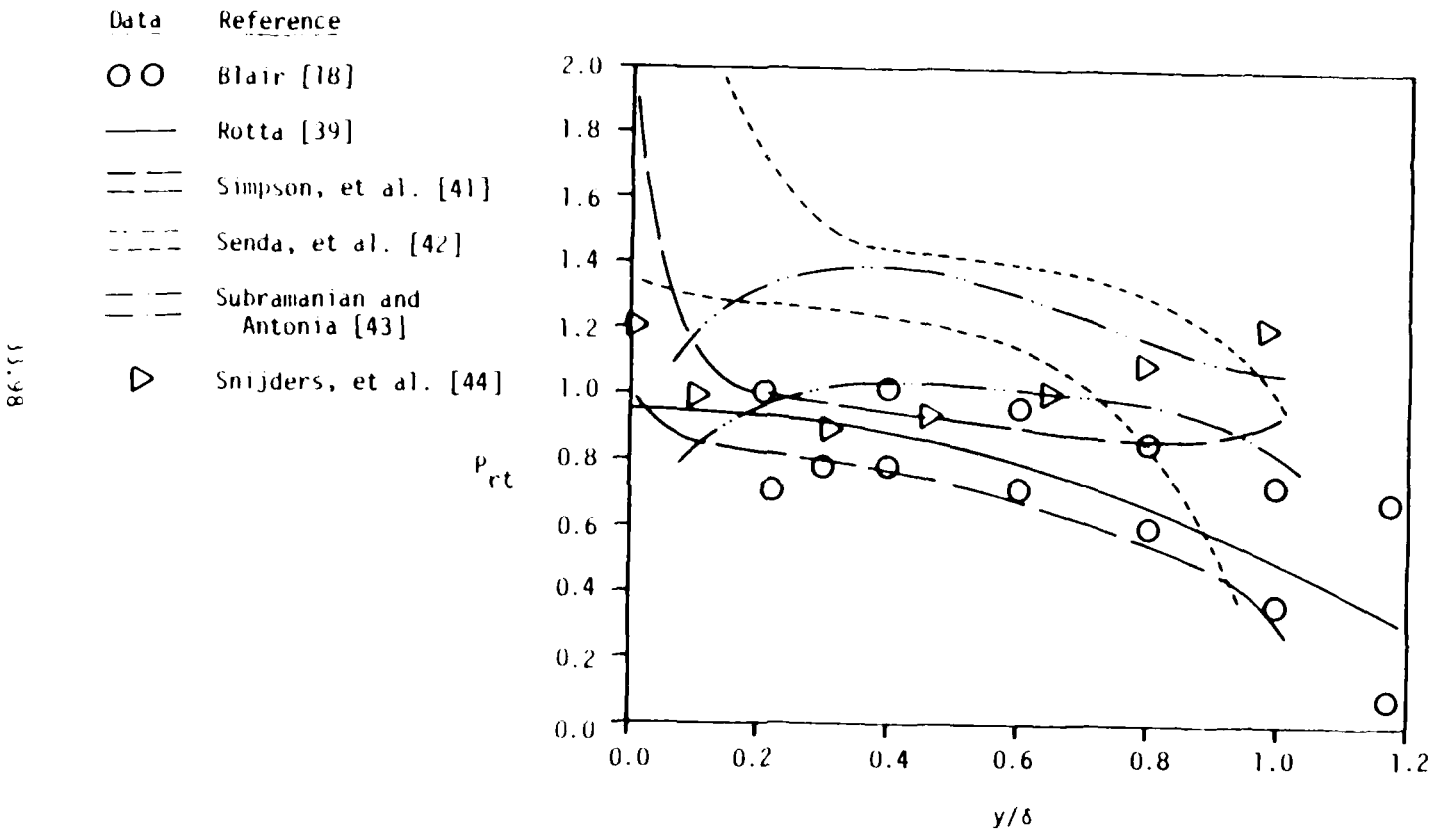



Figure 58: Summary of turbulent Prandtl number data from several references. Boundary layer flows.

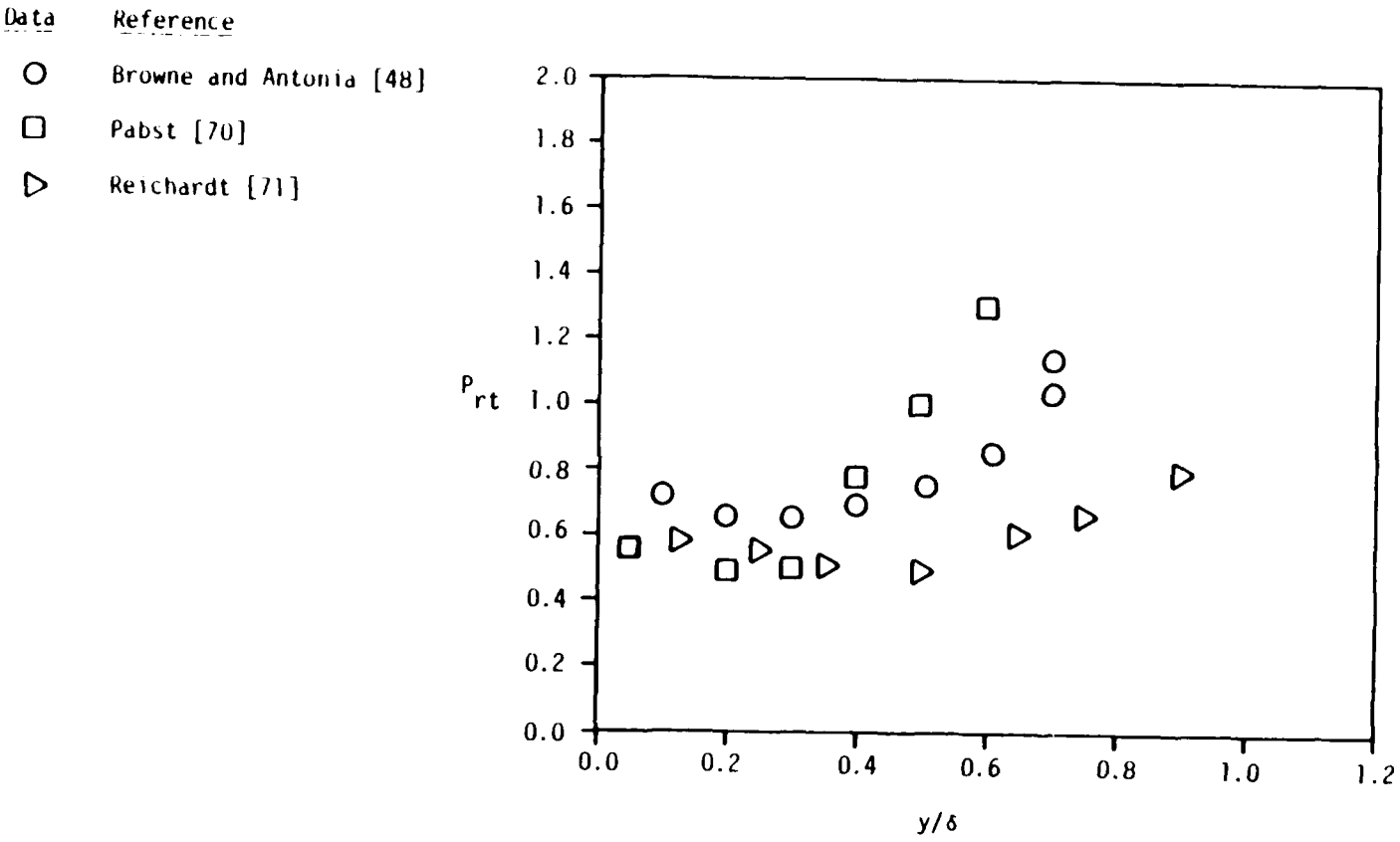



Figure 59: Turbulent Prandtl number data for turbulent jets and wakes from three references.

# Study of Cold Reacting and Combusting Flows Around Bluff-Body Combustors

by

Xianguo Li and Richard S. Tankin

Department of Mechanical and Nuclear Engineering
Northwestern University
Evanston, Illinois 60201

Prepared for

Southeastern Center for Electrical Engineering Education
Contract F49620-82-C-0035
January 1, 1986

Abstract

The results from visual observations and measurements of flows over axisymmetric, unducted, and vertically mounted bluff-body combustors are presented for low Reynolds number. The flow visualization is accomplished by adding $TiCl_4$ vapor into the central gaseous propane jet for cold reacting and combusting flows, or by injecting $TiCl_4$-$N_2$ mixture into the flow field behind bluff-body combustors through a 1.5 mm O.D. probe for pure annular air jet. Micron size particles of $TiO_2$ are formed from the reaction between $TiCl_4$ and $H_2O$ vapor either contained in the annular air or as a product of combustion. Vertical laser light sheets provide a remarkably detailed visualization of the dynamic structures in the recirculating zone behind the bluff-body combustors. For the pure annular air jet, the length of the recirculating zone has a maximum at approximately 700~800 annular Reynolds number (Ra) and approaches to a constant value for very large Ra. For the cold reacting flow, an empirical formula is found from thousands of the experimental data for the relation between the central jet height and the flow conditions at the nozzle exit as well as the nozzle diameters. The introduction of the central jet into the flow enlarges the recirculating zone. The vortices in the recirculating zone appear more organized, stationary and intense for attached flames compared to the cold reacting flows. However, the size of the recirculating zone and the height of the central jet are reduced by more than half. Also for the attached flames, the central jet penetrates more easily through the recirculating zone than for the cold reacting flow. For the detached flame, the height of the central jet is greatly reduced; whereas the length of the recirculating zone is increased slightly, when compared to the corresponding cold flow. It is noted that when the annular air velocity is less than 1.6 m/sec, the flame always remains attached; however, when the

annular air velocity is greater than 1.6 m/sec, the flame appears attached first for the very low central fuel velocity ($V_{co}$), becomes detached when $V_{co}$ exceeds a certain value, then when $V_{co}$ is increased further it becomes attached again. Photographs are presented to reveal the structures of the recirculating zones for the three different kinds of flows. Theoretical considerations based on Bejan's scaling method are also presented.

## 1. Introduction

Non-premixed flame stabilized by a bluff-body combustor, such as occurs when a central fuel jet issues into a surrounding annular air jet, are often used industrially. Examples of the use of such burners are in the combustion chambers of gas turbines, tubular cooler, metallurgical furnaces, aircraft jet engines, etc. Such bluff-body combustors provide good flame stabilization as well as easy control of combustion. Both the fuel and air jets leave their nozzles with considerable momenta. During the mixing process, there is transfer of mass, momentum and energy between the two jets and also between the jets and the ambient air surrounding the bluff-body combustor.

Bluff-body combustors are widely used for combustion processes requiring a fuel-rich mixture at the flame front but an overall stoichiometric or lean mixture further downstream. This type of combustor avoids pre-ignition or explosion dangers inherent in premixed combustion system and can improve the stability of overall lean flames.

From a practical point of view, it is necessary to better understand how the geometrical arrangements and opera ing conditions of the bluff-body combustor influence the flame processes - particularly the flame stability. It is well known that the recirculation region and large scale mixing behind the bluff-body combustor account for flame stabilization. In short, many of the characteristics of these combustors are determined by the aerodynamics of the flow. Therefore the details of the flow - particularly the recirculation zones, the location of the forward and aft stagnation points are needed to better understand the flame stabilization processes. In this study, cold reacting flow (isothermal) and combusting flow were investigated. Experiments were also conducted for pure annular air flow. These experiments give some insight into how the central fuel jet changes the recirculation zone,

especially the recirculating zone length.

Flows behind bluff-body combustors are very complicated due to separation and recirculation, exchange of mass and momentum between the two jets, the chemical reactions involving large amounts of heat release and vortex shedding. Thus these flows are very sensitive to probe interference. Therefore, laser sheet-lighting technique was used and non-intrusive measurements were made for cold reacting and combusting flows.

Though numerous experiments have been conducted on this type of combustor - either ducted (Ref. 4 and 5) or unducted (Ref. 3, 6 and 7), and numerical simulations (Ref. 8), there is still not enough understanding of the overall flow field. Therefore, flow visualization coupled with simultaneous pointwise measurements are essential for understanding the details of the flow consisting of large-scale structures.

The present experiments are visual in nature and are aimed at providing a better understanding of combustion for bluff-body combustors. The micron size $TiO_2$ particles act as scattering media for laser sheet-lighting, providing flow visualization of the entire reacting zone. Traditionally, schlieren, shadowgraph, interferometry, and direct photography have been used in combusting flows. Unfortunately, information obtained by these methods are integrated across the flame (Ref. 10). Thus their use has been limited to a great extent to two dimensional, steady flows. By sheet-lighting the flow, a plane (vertical or horizontal) in the flame is observed. The $TiO_2$ particles are formed as a product of the reaction between $TiCl_4$ vapor and water vapor. Thus the $TiO_2$ particles are formed in the reacting portion of the flame. Since the $TiCl_4$ vapor is added to the propane (central jet), the occurrence of $TiO_2$ will be on the rich zone of the diffusion flame. By adding the $TiCl_4$ to dry air in the annulus, the formation of $TiO_2$ particles would occur in the

lean zone of the flame. Records are made on either film or video tapes. To reduce the continuum radiation from the soot particles, a narrow-band pass filter centered at 5145 Å is used.

The $TiO_2$ particles have been reported to be fairly uniform and generally in the 0.2 to 1 micron range - only a small fraction in the 2 or 3 micron range (Ref. 9). Particles in this size range follow the flow and also act as good Mie scattering center (Ref. 28). The reaction of $TiCl_4$ with water vapor seems to be nearly instantaneous, i.e., mixing limited, thus it can be used effectively to study turbulent mixing processes (Ref. 3).

It is well known that separated recirculating flow established behind the bluff bodies stabilizes flames in high-velocity reacting systems. Zukoski and Marble (Ref. 26) in an early paper experimentally reported that the length of the recirculating zone plays an important role in flame stabilization. The dynamics of the near wake region is very important in the understanding of the mechanism of flame stabilization. For example, the size of the recirculating zone (and recirculating intensity) strongly affects the rate of production of hot products of combustion; i.e., the rate of heat release from the combustion process and thermal efficiency.

Many investigations on separated, recirculating flow for the isothermal case have been carried out over the past few decades, and a few on combusting flows (see, for example, Ref. 1, 11, 12, and 13). For most of these investigations, the bluff body was either a disk or cone of various cone angles. An exception was the study by Davis and Beer (Ref. 13) who used a cylinder as one of these bluff bodies. The annular flow in these studies was at very high Reynolds numbers. In the present experiment, cylinders were chosen as the bluff bodies and the Reynolds numbers for the annular flow varied from low to moderately high. We were limited in the annular Reynolds

number by pressure available in house air supply.

This study is an extension of the work reported by Roquemore, et al. (Ref. 3) and a result of research proposed by Tankin (Ref. 19). The main objectives are:

(1) To visually determine the behavior of the mean flow pattern for free annular air jet and central fuel jet with and without combustion under the influence of various bluff-body blockage ratios;

(2) To determine the difference between cold reacting flow and combusting flow;

(3) To measure the penetration lengths of the central jet under various flow conditions and blockage ratios;

(4) Compare the results of this study with previous measurements by other investigators.

## 2. Experimental Set-Up

The bluff-body combustor consisted of a fuel nozzle located concentric to an annular region where air flowed. The fuel nozzle was located in the center of a bluff body. The outer shell of the combustion tunnel could be translated, thus insuring the annular region and the central nozzle were concentric. This was important because small eccentricities would lead to an asymmetric flow. The design of the combustion tunnel was such that the outer rim of the combustion tunnel (outer annulus diameter) could be changed by merely changing the threaded insert. Likewise, the fuel nozzle diameter could be changed by changing threaded fuel nozzle insert. These nozzles were tapered, so that the fuel jet had a flat velocity profile at the nozzle exit and low turbulence intensity. The annular region was also tapered for the same reason.

To insure the flow would be uniform, screens and fiber glass were placed in the annular region as well as the central pipe almost 6 inches upstream of the nozzle exits. A schematic diagram of the combustion tunnel is shown in Figure 1.

The annular flow of air was controlled by a needle valve and measured with a rotameter which was calibrated with a precision wet-test meter. The calibration curve for the rotameter could be found in Appendix A. The air used in these experiments was pressurized room air. The fuel flow was measured with either of the two Gilmont rotameters that were connected in parallel. Along with the rotameters, a pressure gauge and thermocouple were installed. The fuel velocity at the nozzle exit was calculated using a computer subroutine, from equations provided by Gilmont, Co., with fuel temperature, pressure, rotameter scale reading and nozzle diameters as input parameters. The computer subroutine was titled CENFV and listed in either the Appendix B or C.

For the experiments of the cold reacting flow and combusting flow, building air flowed in the annular region and propane with small amounts of $TiCl_4$ vapor issued from the central nozzle. For the combusting flow, the mixture was ignited. The propane flow was controlled by three valves. The propane might pass over the surface of liquid $TiCl_4$, which was in a stainless steel container, picking up some $TiCl_4$ vapor. Also it was possible to have the propane by-pass the $TiCl_4$ container.

For the case of the pure annular flow, the central fuel jet was closed and air was supplied to the annular nozzle. A small diameter probe (1.5 mm O.D.) was used to inject a mixture of dry nitrogen gas and $TiCl_4$ vapor. The $TiCl_4$ vapor was entrained by the nitrogen gas in the same manner as for the propane. This injected mixture, which flowed from the nozzle of the probe,

was rapidly entrained into the recirculation zone where the $TiO_2$ particles acted as scattering centers. The recirculation zone length, which is defined as the axial distance from the bluff-body surface where the velocity is zero (stagnation point), was visually determined where approximately half of the $TiO_2$ particles moved downwards and half moved upwards.

All the gas lines from $TiCl_4$ container downstream consisted of stainless steel piping and stainless steel valves. Even so, there was occasional clogging of the lines. Provision was made so that $TiCl_4$ system could easily be disconnected and cleaned. If partial blockage occurred, the fuel flow developed oscillations that were detected on the fuel rotameter. The partially plugged line or valves were cleaned by passing water through the line, followed with acetone and then air.

The optical set-up used to visualize the flow field consisted of a 4 watt argon-ion laser. The 5145 Å line was used in these experiments. When the laser light struck a glass rod, which behaved like a cylindrical lens, the light beam spread in a plane normal to the axis of the glass rod. The angle of spreading depended on the diameter of the glass rod - large diameter gave smaller angle of spread. The width of the sheet of laser could be reduced by forming a slit on the surface of the glass rod. For the cold reacting flow, where the aft stagnation point was relatively far from the nozzle, a small rod of 8 mm diameter was used. On the other hand, for the combusting flow (attached flame only), the aft stagnation point was much closer to the nozzle and a rod of 25 mm was used. The intensity of illumination in the sheet, of course, was much larger. This was fortunate because we needed more intensity to overcome the illumination of the flame. To virtually eliminate the luminous radiation from the hot carbon particles in the flame a narrow band-pass optical filter centered at 5145 Å was used. This filter had a half width

of 90 Å and reduced the light intensity at 5145 Å by 40%.

To measure lengths of the stagnation points above the nozzle, a neon helium laser (6328 Å) was mounted on a vertical traversing platform. This laser light formed a red spot due to scattering of the $TiO_2$ particles. Attached to the traversing platform was a 3" dial gauge, thus allowing one to read the vertical position of the platform. The dial gauge was "zeroed" when the neon-helium laser was at the nozzle elevation. Also a narrow band pass filter centered at 6328 Å was considered, but was not found to be necessary.

## 3. Experimental Conditions

For the pure annular air flow, the central nozzle was blocked with a silicone type caulking compound. This was carefully done so that the surface was smooth; resulting in a configuration similar to that used by Durão and Whitelaw (Ref. 11). The ratio of the diameter of the inner annulus to the diameter of the outer annulus was either 0.57, 0.72 or 0.85; with blockage ratio 32%, 52% and 72% respectively. The Reynolds number, Ra, ranged from 120 to $4.3 \times 10^3$ - based on the exit velocity of the annular air flow and hydraulic diameter (the Reynolds number based on the diameter of the bluff-body combustor, $R_{D_1}$, varied from 320 to $1.3 \times 10^4$). Schematic diagrams for nozzles are shown in Figure 2.

Where flow occurred in the fuel nozzle, the Reynolds number in the annulus, Ra, varied from 500 to 1900 (or $R_{D_1}$ from 1100 to 4500). The Reynolds number in the central fuel jet, $R_c$, based on the exit velocity and the diameter of the central fuel nozzle, ranged from several tens to 1600. The flows in this study were mostly laminar, with the higher Reynolds number flow near transition to turbulence. In the case of the combusting flow, the tests were all in the laminar region (laminarization of combusting flow is quite

obvious) except for the case of detached flames.

All experiments were performed with a vertically mounted, unducted combustor. The combustor was located directly under a ventilation hood which removed $TiO_2$, HCl and combustion products from the room - discharging them outside the building. Occasionally there were some air disturbances in the room which affected the flow pattern, but this was only noted at low annular air flow and even then were not significant.

For the experiments conducted on the cold reacting and combusting flows, no intrusive measurements were made. Only lasers were used and the laser light was scattered by the small particles ($TiO_2$ and soot). For the case of the pure annular flow, an intrusive, small diameter probe was used to inject $TiCl_4$ vapor and dry nitrogen, and thus enable one to observe the recirculation zone. This intrusive probe had some effect on the flow field, particularly at low air velocities.

As Durão and Whitelaw observed (Ref. 11) the instantaneous aft stagnation point fluctuated in spite of the low air and fuel Reynolds numbers. Thus, the aft stagnation point was obtained by taking the average of several measurements.

Measurements were made of the length of the recirculating zone for the pure annular air flow, and the axial location of the forward and aft stagnation points for the cold reacting flow and combusting flow. An attempt was made to correlate those measured quantities with exit velocities and nozzle diameters.

## 4. Coordinate System

The origin is at the center of the combustor surface (the same elevation or plane as the nozzle exit). The z-axis is in the axial direction, positive

downstream (i.e., vertical upwards). The r-axis is radially out along the combustor surface.

## 5. Observations, Experimental Results and Discussions

This section is organized into three parts: pure annular free jet, cold reacting flow and combusting flow. In the first part, the results of measurements on the length of the recirculation zone, comparisons with the previous investigations and description of the flow field are presented. In the second part, the description of the flow for different central fuel velocities and the empirical formula about the location of the forward stagnation point with respect to flow conditions and geometries, drawn from thousands of experimental data, are given for the under-penetration of the central jet. For flow fields with combustion, the same measurements were made as for the cold reacting flow. Some phenomena observed for the combusting flow are presented in the last part. For the cold reacting and combusting flows, $TiCl_4$ vapor was added to the central jet, which produced $TiO_2$ particles for flow visualization.

### 5.1 Pure Annular Air Jet

The flow system for a pure, free annular air jet is shown in Figure 3 which exhibits three distinct flow regions behind the bluff body: a region of recirculation where the mean velocity along the centerline is negative and the pressure at the center of the vortices is minimum; a transition region where the velocity along the centerline accelerates to a maximum velocity and a downstream region where the velocity decays (Ref. 11, 13 and 20).

The recirculation zone is a region of subatmospheric pressure caused by the annular jet with an associated closed ring vortex in the central region

(See plate 1-b). This picture was taken with the annular air velocity of 0.4821 m/sec, and the central propane velocity of 0.0076 m/sec. A small amount of $TiCl_4$ vapor was added into the central jet. Although this is not strictly pure annular flow, the ratio of central jet velocity to annular jet velocity is only 1.5%. This technique was used in this instance because it clearly showed the symmetry of the recirculating region. If one examines the central streamlines near the central jet exit (Plate 1-b), they are similar to those obtained for flow impinging on a flat surface. This is further evidence that the flow approaches the pure annular flow in this test. When actual data were taken for the pure annular flow, the central nozzle was plugged and a probe was used to inject the $TiCl_4$ vapor. The small asymmetry of the vortex may be attributed to the non-eccentricity of the combustor arrangement. The bounding surface of the recirculating zone is clearly shown in Plate 1-b. To obtain this surface from pointwise measurements, it would be necessary to measure axial velocity profiles and integrate these values radially. That is,

$$M_r = \int_0^{r_1} \rho u(r,z) \cdot 2\pi r dr = 0 \qquad (1)$$

where $M_r$ is the rate of the mass flow circulating in the recirculation zone; and $u(r,z)$ is the z-component of the velocity at location r in the plane z. By setting $M_r = 0$ and solving for $r_1$, one could determine the bounding surface of the recirculating zone.

It is obvious that it is much simpler to use flow visualization technique as described in this study to determine the bounding surface than to do it from Equation (1). However, as seen in Plate 1-b, there is some question concerning the exact location of the bounding surface at the stagnation point. Using the probe technique for supplying $TiCl_4$ vapor, we believe, can

better define the location of the bounding surface at the stagnation point. Plate 1-c shows the sheet-lighted recirculation zone when central jet is turned off and the mixture of $TiCl_4$ vapor and dry nitrogen gas is injected near the end of the recirculation zone ($L_{rz}$) through a probe.

For the downstream region (established flow region) shown in Figure 3, the flow is fully developed, and the flow patterns as described in Ref. 24 are similar to those of single round jet with a displacement of the origin. The single round jet problem has been thoroughly studied in the past (see Ref. 25).

The measured length of the recirculating zone, $L_{rz}$, normalized by the bluff-body diameter, $D_1$, is plotted against the Reynolds number, Ra (see Figure 4). The curves show that the recirculation zone length has a maximum where the Ra is approximately 700~800 for the geometries tested. One would expect such a maximum because as Ra → 0, the recirculation zone length goes to zero. When the flow changes from laminar to turbulent flow, one would expect the length of the recirculating zone to decrease because of increase in transfer of momentum. It was noticed in the experiments that flows appeared very steady when Ra was less than 700~800 and fluctuations appeared in flows at Ra greater than 700~800. It is believed that the data in this study at Ra > 800 represent transition to turbulent flow. The data points of Durão and Whitelaw (Ref. 11) are also plotted on Figure 4. Their bluff body is a disk rather than cylinder as used in this study. However, their results are in general agreement with those of the present study. It should be noted that Durão and Whitelaw's results were obtained at much higher Ra and that their values of the length of the recirculating zone decreased slightly with increase in Ra. It appears from Figure 4 that $L_{rz}/D_1$ approaches an asymptotic value. In the section of the study entitled "Analytical Approach", these

tendencies will be discussed in greater detail.

In Test I and Test II, the outer diameter of the annulus was kept constant and the inner diameter of the annulus was 38.5 mm and 45.2 mm respectively. This corresponds to blockage ratios of 52% and 72%. A possible explanation for the difference between the results of Test I and Test II is as follows: in Test I, the annular gap is 7.37 mm whereas in Test II it is 3.99 mm. One would expect the velocity profile at the exit to be different for Test I and II. Pope and Whitelaw (Ref. 14) in their numerical simulation mentioned that the shape of the velocity profile at the exit affects significantly the downstream flow characteristics. The results of Test III which has a blockage ratio of 32% would be expected to lie above the results of Test I (blockage of 52%). However it lies between Test I and Test II. A possible explanation for this discrepancy is that the nozzle used in Test III has a modified geometry. The inner and outer walls of the annulus are tapered $10.8^{\circ}$ (see Figure 2-c). This results in a radially inward component of the velocity at the nozzle exit. Thus it is expected that the length of the recirculation zone for such a configuration will be reduced. This is in accordance with the effect of the forebody shape on the length of the recirculating zone discussed by Davies and Beer (Ref. 13). The arguments presented concerning the variation between Test I, Test II and Test III are based on conjecture.

The results of this study are compared with those of previous investigations in Table 1. The recirculation length for confined flows is significantly larger than that for unconfined flows (approximately twice as large as for unconfined flows). The agreement is reasonably good for all the investigations of unconfined annular jets as seen in Table 1. Davis and Beer (Ref. 13) obtained $L_{rz}/D_i = 0.72$ for unconfined annular jet over a cylinder as

compared with our values of 1.00, 0.83. However their Ra was much larger than the values in this study. It should be noted that the flow near the stagnation point is more unsteady than elsewhere behind the bluff body in the experiments presented. Thus, the measured recirculation length is determined on a visual averaging of its value. As many as seven such data were taken and then numerically averaged.

Table 1. Length of recirculation zone for various flows over bluff bodies

| Authors | Flow type | B.R.* | Ra | $L_{rz}/D_1$ |
|---|---|---|---|---|
| Taylor & Whitelaw (1984) | confined disk | 25% | 34,000 | 1.75 |
| | confined 45° cone | 25% | 38,100 | 1.55 |
| | confined disk | 50% | 23,800 | 2.20 |
| Winterfeld (1965) | confined disk | 25% | | 2.0 |
| | confined 90° cone | 25% | | 1.9 |
| | confined 45° cone | 25% | | 1.7 |
| | confined disk | 4% | | 2.0 |
| | confined 90° cone | 4% | | 1.9 |
| | confined 45° cone | 4% | | 1.7 |
| Fujii (1978) | confined 60° wedge | 50% | | 1.88 |
| Bradbury (1976) | confined flat plate | 10% | | 1.98 |
| Calvert (1966) | confined disk | 0.56% | 50,000 | 3.04 |
| | confined 90° cone | 0.56% | 50,000 | 2.18 |
| | confined 60° cone | 0.56% | 50,000 | 1.88 |
| | confined 40° cone | 0.56% | 50,000 | 1.58 |
| | confined 20° cone | 0.56% | 50,000 | 1.30 |
| | confined cylinder | 0.56% | 50,000 | 1.14 |
| Davies & Beer (1971) | unconfined annular jet, disk | 25% | fully turbulent | 1.52 |
| | unconfined annular jet, 45° cone | 25% | | 1.24 |
| | unconfined annular jet, cylinder | 25% | | 0.72 |
| | unconfined annular jet, disk | 54% | | 1.16 |
| Durão & Whitelaw (1978) | unconfined annular jet, disk | 20% | 28,300 | 1.45 |
| | unconfined annular jet, disk | 39% | 19,100 | 1.15 |
| | unconfined annular jet, disk | 50% | 14,800 | 1.00 |
| | unconfined annular jet, disk | 50% | 6,300 | 1.01 |
| | unconfined annular jet, disk | 50% | 3,500 | 1.04 |
| Chigier & Beer (1964) | unconfined annular jet | 44% | 100,000 | 1.10 |
| Carmody (1964) | unconfined disk | 2% | 70,000 | 2.5 |
| present results | unconfined annular jet, cylinder | 52% | 2,500 | 1.00 |
| | unconfined annular jet, cylinder | 72% | 2,300 | 0.83 |
| | unconfined annular jet, tapered cylinder (21.6°) | 32% | 4,300 | 0.91 |

*B.R. means blockage ratio.

5.2 Cold Reacting Flow

The flow field behind bluff-body combustors could be thought of as two widely spaced jets: an annular jet and a central fuel jet (Ref. 3 and 19). A schematic diagram for the jets is shown in Figure 5. At the nozzle exit, the two jets are separated from each other, and flow independently. They behave as though no surrounding fluid exists. However the two jets soon interact due to vortices that form between the two jets (see Plate 2 and 3). As seen in the pure annular flow these vortices are set up by the annular jet and the central fuel jet. In the cold reacting flow these vortices are not stationary. There are several such vortices at any time within the recirculating region, which move usually downward and radially outward. At the edge of the recirculating zone there are vortices that are clearly observed on the shear layer (see Plate 2-a). They rapidly grow in magnitude and roll up into a spiral. In the vicinity of the aft stagnation point, some of the spiral vortices on the shear layer escape and move downstream, whereas others are recaptured by the recirculating zone. These spirals consist of air packets which are brought into the recirculating zone by the recaptured spirals. These are seen as dark regions near the aft stagnation point in the photograph. The dark region near the nozzle is the mixture of fuel and $TiCl_4$ vapor devoid of water vapor (i.e., $TiO_2$ particles). Then due to the vortices existing within the recirculating zone, the packets of air and fuel mix together (also see Ref. 3).

When the central jet velocity is very small compared to the reverse flow in the recirculating zone, the central jet is turned outward. Plate 2-b shows the streak lines of the central jet as well as the recirculating zone. To achieve this, some particles of $TiO_2$ are induced into the central propane jet. As can be seen the streamlines are similar to those of two impinging

streams. Where the central jet is turned defines the forward stagnation point.

Downstream of the aft stagnation point where the axis of the annular jet has converged at the central axis, the two jets have completely merged. The behavior of the combined jets is very similar to an equivalent single round jet. Chigier and Beer (Ref. 20) have determined the effective origin and the outside boundary of the equivalent jet as a function of the velocity ratio as well as the geometry of the nozzles for the case of air flow in the annular and central nozzles.

Two very important parameters characterizing the flow field behind a bluff-body combustor are the location of the forward and aft stagnation points. These occur where the velocity along the centerline vanishes. Since these points are usually oscillatory they are not easy to determine precisely. With probe measurements, which disturb the flow field, or laser doppler measurements, one has to interpolate the mean velocities in front of and behind the stagnation points. This introduces some uncertainty into the measurement results. We found that the forward stagnation point is stationary when it is less than half of the recirculation zone length. When the forward stagnation point reaches the half of the recirculation zone length it becomes non-stationary. The aft stagnation point has the recaptured spiral vortices in its immediate vicinity and hence is unsteady. For non-stationary fuel jet, its bounding surface is not as distinct as that of stationary fuel jet since the fuel jet is on the verge of breaking up into smaller packets.

From video tapes recorded, the flow field behind bluff-body combustors may be divided into three categories, although the numerical values of w, ratio of momentum of the central jet to the annular jet, i.e., $w = \rho_c V_{co}^2 A_{co} / \rho_a V_{ao}^2 A_{ao}$, where $A_{co}$ and $A_{ao}$ are the central and annular nozzle exit

areas, respectively, are not exactly defined for the categorizing. The three categories are, respectively, that the annular jet is dominant; neither jet dominates and the central jet dominates.

If the central jet is weak, i.e., the momentum of the reverse flow set up by the annular jet is larger than that of the central jet. This reverse flow will force the central jet outward radially. If the momentum of the central jet is so low that it can not penetrate into the recirculation zone, the forward stagnation point is zero. In this case, the central jet is completely absorbed by the annular jet. In this regime the central jet motion is not stationary - it is pushed randomly from one side to another by the reverse flow.

If the momentum of the central jet is comparable with that of the reverse flow, neither jet dominates the flow field. The tip of the central jet which has mushroom shape is unsteady; however, the stem is very steady. When the central jet flow is increased, the forward penetration length increases and the main vortices in the recirculation region move laterally and become smaller.

If the central jet is very strong, the annular jet no longer plays an important role; the central jet dominates the flow field. The annular air is entrained into the central jet. Along the centerline no stagnation point could be found (overpenetration). As the central jet velocity is increased further, the central jet extracts more fluid from the annular jet to satisfy its entrainment requirement, and the size of the recirculating zone is reduced. At last, when the central jet velocity is so large that the central jet is completely dominant, it absorbs the annular jet totally. Then the central jet behaves as though no annular jet was present except for small vortices near the combustor surface. These small vortices are very organized

and stable.

The S-R saddle points which were computer simulation by Scott and Hankey for the flow field behind a ducted, pure annular flow (Ref. 8) are also observed in this study and presented in Plate 3-a and schematically shown in Figure 6. These saddle points occur on the centerline, the combustor surface and also the boundary of the central jet. On the centerline, such saddle points occur where flows approach either from opposite directions along the centerline and depart in a direction normal to the centerline, referred to as S-saddle point (i.e., the forward stagnation point, see point $S_2$ in Figure 6), or from a direction normal to the centerline and departs in opposite directions along the centerline, referred to as R-saddle point (i.e., aft stagnation point, see point $R_2$ in Figure 6). These saddle points are somewhat analogous to separation and reattachment points which occur at solid boundaries. More important is that on the boundary of the central fuel jet, S-saddle points occur as a result of the central jet entrained by the annular jet, the fuel is pulled into vortices formed at the tip and stem of the central jet, labelled as vortex A and B in Figure 6. Almost simultaneously vortex A moves towards the combustor surface while vortex C convects downstream and grows. During this time the vortex B grows and releases its fluid periodically into the region vortex C occupied previously. This probably aids the growth and convection of the vortex C. As vortex A is shed, the point $S_2$ (forward stagnation point) oscillates along the centerline. Likewise, the saddle points $S_2'$, $S_2''$ and $R_1$ are unsteady. On the right hand side of the central jet in Plate 3-a, vortex A is halfway to the combustor surface, Vortex C lost its identity, and vortex B was just releasing its fluid into the region close to the boundary of the recirculating zone. Thus it was not clearly shown there. On the combustor suface which is a solid boundary,

the S- and R-saddle points (separation (s) and reattachment (R)) are observed. It is noted, and also can be inferred that a stationary separation point $S_1$ (see Figure 6) always exists at the outside edge of the combustor surface, while the reattachment point $R_1$ moves in the radial direction along the combustor surface. A streamline originated near the point $S_1$ will evolve into a vortex D (Figure 6) above the forward stagnation point. The separation streamline starting at the point $S_1$ will form the boundary of the recirculating zone, and attach to the centerline. The reattaching point $R_2$ oscillates along the centerline as vortex D is shed. The interactions between adjacent vortices as they form and move up- or downstream are very important to the understanding of mixing process hence combustion process in the recirculating zone.

It should be emphasized that all the above discussion is for annular air velocity greater than 0.5 m/sec. If less than 0.5 m/sec, the annular air is not sufficiently strong to form the usual recirculating zone presented. Plate 4-a shows the flow with fuel velocity of 0.2 m/sec, and air velocity of 0.4 m/sec. The flow field is irregular and large amounts of air intrude deep into the recirculating zone, which is not confined by an annular jet. Eddies have torn away the boundaries of the recirculating zone except the region very close to the separation point. It is interesting to note that this phenomenon never occurs for the combusting flow.

## Experimental Results and Discussions

Using dimensional analysis, the following expression is obtained:

$$\frac{L}{D_j} = f\left(R_a, R_c, \frac{D_j}{D_i}, \frac{D_o - D_i}{D_i}, \frac{L_{rz}}{D_i}, \frac{V_{co}}{V_{ao}}\right) \qquad (2)$$

where L = location of the forward stagnation point along the centerline;

$D_j$ = diameter of the central nozzle;

$D_i$ = diameter of the inner annulus;

$D_o$ = diameter of the outer annulus;

$V_{ao}$ = velocity of the annular jet at the nozzle exit;

$V_{co}$ = velocity of the central jet at the nozzle exit;

$L_{rz}$ = length of the recirculating zone;

$R_a = \frac{V_{ao}(D_o-D_i)}{\nu_a}$, Reynolds number of the annular jet;

$R_c = \frac{V_{co}D_j}{\nu_c}$, Reynolds number of the central jet;

By comparing Equation (2) with the experimental results shown in Figure 7 and Equation (3) below, it appears that $L_{rz}/D_i$ and $V_{ao}/V_{co}$ have no effect on $\frac{L}{D_j}$. This could be explained as follows: the effects of $V_{ao}$ and $V_{co}$ have been taken into account in the parameter $R_c$ and $R_a$, and that $\frac{L_{rz}}{D_i}$ is nearly constant (see Figure 8). The forward stagnation point is strongly dependent on the geometry and the Reynolds numbers of the central jet and the annular jet.

The empirical formula shown in Figure 7, which is the result of thousands of experimental data, can be expressed in the following form:

$$\frac{L}{D_j} = A \frac{R_c}{R_a} \left(\frac{D_i}{D_j}\right)^{1.5} \left(\frac{D_o-D_i}{D_i}\right) \qquad (3)$$

where A is constant, given in Table 2.

From Table 2, it seems that A depends largely on fluids used in the central and annular jets. Later on, in an analytical approach it will be shown that A is really the function of the physical properties of fluids in

the two jets. The power of $R_a$ is always negative, i.e., as $R_a$ increases while keeping other parameters unchanged, the central jet will be shortened. Thus, when $R_a$ is increased, $R_c$ should be also increased in order to maintain the central jet at the same height. Equation (3) shows that for larger $R_c$, i.e., larger momentum of the central jet, the height of the central jet increases, and that for smaller central nozzle diameter $D_j$, the forward stagnation point moves downstream if keeping fuel volume flow rate fixed, which was also noted during the experiments. The latter can be easily shown as follows:

$$V_{co} = \frac{Q_c}{\frac{\pi}{4} D_j^2}$$

where $Q_c$ is the fuel volume flow rate. Thus the exit momentum of the central jet, $G_c$, is

$$G_c = \rho_c \frac{\pi}{4} D_j^2 V_{co}^2 = \rho_c \frac{Q_c^2}{\frac{\pi}{4} D_j^2}$$

Therefore if the central jet nozzle diameter is reduced, the momentum of the central jet is increased. Hence it can penetrate further into the recirculating zone.

The reason that L is normalized by $D_j$, not by $L_{rz}$ or $L_p$ as Tankin did (Ref. 3) is that for Tankin's case, the annular air velocity was very large, the aft stagnation point as reported remained almost constant, and coincided with the penetration point. However, for the present case, the annular velocity was small, the central jet had some effects on $L_{rz}$ and $L_p$, whose changes will be presented in the next section. Considering the unsteady nature of the points, which results in inaccurate measurements, ratios $L/L_{rz}$ or $L/L_p$ will amplify measurement errors. In addition curves $L/L_{rz}$ or $L/L_p$

vs. $V_{co}/V_{po}$ has been forced to pass through the point (1,1). Thus in the present case, although all the curves are similar to each other, they never coalesce into one curve. Figures 10 and 11 show curves $L/L_{rz}$ vs. $V_{co}/V_{po}$ and $V_{co}/V_{ao}$ respectively. The solid curves are the results of the least square fit to the experimental data. This is obtained by rearranging the data on Cyber 730 and plotting on the Tektronic plotter. The computer program for this can be found in Appendix B.

From Eq. (3) one could understand why Roquemore & Tankin (Ref. 3) and Namazian (Ref. 7) found out that the axial location of the forward stagnation point was the function of the velocity ratio $\frac{V_{co}}{V_{ao}}$ only because the nozzle diameters were fixed in their cases.

Table 2. Constant A and Experimental Ranges for Eq. (3)

| Authors | A | $R_a$ | fluid in central jet |
|---|---|---|---|
| present | 1.700 | 500-1,900 | propane |
| Namazian (Ref. 7) | 3.083 | 20,000-70,000 | methane |
| Tankin (Ref. 27) | 3.125 | 1,250-22,500 | air |

Note: the fluid used in the annular jet is air.

5.3 Combusting Flows

The effect of combustion is far more than just a density change. The large amount of heat released by chemical reaction during the combustion process has significant influence on the flow field, flow properties and physical properties of the fluids. A thorough understanding of combustion

process involves the mechanism of chemical reactions and the mixing of reactants and products as well as interactions between them. The distributions of velocity, temperature and species concentrations are required for a complete description of a combustion system. Before such detailed knowledge is obtained, the global features of the system is required, which can be gained by flow visualization technique. For a bluff-body combustor, the region close to the combustor is very important to flame ignition and stabilization. In such a system, combustion processes are conventionally taken for granted to be controlled by mixing and diffusion of various components in the system (Ref. 33), i.e., chemical reactions are almost always assumed to be fast compared with the rate of mixing and the overall rate of reaction is controlled by the rate of mixing. Hence, aerodynamic aspects are emphasized here rather than chemical kinetics and the reaction mechanisms.

Observations

It was noticed in the experiments and video tapes that when the annular air velocity at the exit is less than 1.6 m/sec, the flame always remains attached to the combustor surface. However, when the fuel velocity is reduced below a certain value, the flame appears only in the vortex region and opens at the top, i.e., no flame exists along the centerline. The vortices within the recirculating zone entrains the fuel from the central jet. The direction of the rotation of the vortices is such that the combustion products are directed downward along the centerline. In essence, the combustion products extinguish the flame. Thus, no combustion occurs along the centerline - resulting in top-open flame. This was noticed to occur when the forward stagnation point is almost located in the plane of the combustor surface. Plate 5 shows the top-open flame. This kind of top-open flame is different

from that treated first by Lewis and von Elbe (Ref. 29), and later by many others like Law (Ref. 23).

For this top-open flame soot particles are deposited quickly on the combustor surface covering almost 80% of the surface area - the outer 20% being free of soot. After several minutes of burning, this layer may be as high as a few millimeters, having its greatest thickness at the outer edge of the layer. The formation of this soot layer could be explained as follows: since the penetration of the fuel jet is so small (nearly zero), all the soot particles that are formed are trapped in the vortices. Under steady state condition, soot particles which are continuously being formed settle on the combustor surface. The fuel is drawn outward along the combustor surface by the vortices. This fuel flow brings the soot particles outwards to form the greatest thickness of the soot layer at the outer edge of the layer. The formation of soot is discussed in Ref. 2 and 21.

The flame is predominantly yellow in color; however a blue region exists. For the case of an attached flame, this region - short in length - appears in the inner shear layer of the annular jet close to the combustor surface (see Plate 6). For a detached flame no burning appears in the vicinity of the combustor for a distance of between (0.5~1.0) $D_1$. The blue region appears between the upstream non-burning zone and downstream yellow flame (see Plate 7). Vortices are observed near the tip of the fuel penetration - which are highly unstable. The shedding of the vortices is noted to occur simultaneously with large oscillation of the whole flow field - including the flame.

It is interesting to note that the flame in our study always attaches to the combustor surface when the annular air velocity, $V_{ao}$, is less than 1.6 m/sec, no matter how the central fuel velocity, $V_{co}$, is changed, either

increased or decreased. However when $V_{ao}$ exceeds 1.6 m/sec, the flame is attached to the combustor surface for only very small $V_{co}$ (see Plate 6). It becomes unstable if $V_{co}$ is larger than a certain value, any external disturbances could lead to the flame detachment from the surface. Sirignano has presented the effect of external disturbances on axisymmetric diffusion flame (Ref. 34). In our experiments, when the flame has just detached from the surface, it is easily extinguished. In fact, blow-off was observed several times at this condition during the experiments. Plate 7 shows such detached flames. However if $V_{co}$ is increased further, the flame reattaches to the combustor (see Plate 8). The sizes of the recirculation zone and vortices diminish as $V_{co}$ continues to be increased. The yellow flame appearing near the stem of the central jet is anchored by the vortices and is reduced with a reduction of the vortex size. These vortices, rotating on their upper boundaries from the annular jet to the central jet, are well organized and have large-scale structure as seen in Plate 8-b and c. At the instant of reattachment, above this yellow flame near the combustor is a blue zone which followed by another yellow flame. The blue flame decreases with the increase of $V_{co}$, and disappears at last. When the annular air jet is fully absorbed by the central jet, the vortices near the combustor surface are no longer observed. Usually the downstream yellow flame dominates the flow, occupying the whole flow region when the blue flame region is absent. Plate 8 shows this. In the photographs, the blue zone is less noticeable than it is in the laboratory perhaps due to dominance of the radiation from the yellow portion of the flame. The downstream yellow flame is severely distorted. The dark region in the flame is the intruded air.

The appearance of the blue flame reported in Reference 7 is similar to the present observation. However, Ramohalli observed (Ref. 32) that the lift-

off (detached) non-premixed flame appeared blue practically devoid of yellow flame (carbon glow). As far as the present observation is concerned, the blue flame seems to surround the yellow flame. This difference may be due to different experimental conditions between those in this study and those of Ramohalli.

The characteristics of the vortices depends on the geometry, the velocities of the central and annular jets. For $D_j$ = 6.35 mm, $V_{ao}$ < 1.6 m/sec, and small $V_{co}$, the size of the vortices is comparable with the recirculating zone. However, vortex size is reduced when either the annular jet velocity or the central jet velocity is increased. Plate 9-a shows such a flame (attached).

For $D_j$ = 12.7 mm and $V_{ao}$ < 1.6 m/sec (the flame is attached, see Plate 9-c); the annular vortices are believed to be always located above the forward stagnation point. When $V_{co}$ values are low, the vortices are large and occupy the region between the forward and aft stagnation points. As $V_{co}$ is increased, the forward stagnation point pushes the vortices ahead of it. When the forward stagnation point reaches about as high as the central nozzle diameter $D_j$ (12.7 mm), small vortices form near the tip and stem of the central jet, and vortices due to the annular jet appear at the outside edge of the combustor surface. These annular vortices are designated as lower vortices. Initially the annular vortices which are being pushed forward by the central jet are called the upper vortices. The upper vortices are reduced in size and intensity as the forward stagnation point pushes them towards the aft stagnation point, and lose their identity as penetration of the central jet through the recirculating zone occurs. During this process the lower vortices behave very similarly to those of $D_j$ = 6.35 mm (Plate 9-a).

The development of the vortices for $D_j$ = 9.45 mm and $V_{ao}$ < 1.6 m/sec is

between the above two cases. Since the space between two jets is large enough to allow the vortices due to the annular jet (annular jet vortices) to remain more or less fixed in location. However, there is distortion of such vortices due to the vortices caused by the central jet (central jet vortices). These central jet vortices alternately shed and thus distort the annular jet vortices. The rotations of the annular jet vortices are opposite to those of the central jet vortices. Plate 9-b shows the annular jet vortices and the central jet vortices. The annular jet vortices are the outer ones and the central jet vortices are the inner pairing ones. When the central jet velocity increases, the inner vortices (central jet vortices) grow and the height of their centers increases; the outer vortices (annular jet vortices) are distorted. In this photograph, the inner vortices are asymmetrically shed (the right one is about to move downward and out along the combustor surface; the left one will grow and move upwards until it reaches an elevation of the right one), distorting the annular vortices asymmetrically. Thus, the flow field is dynamically changing, and an axisymmetrical model is inadequate for this flame. The dark region near the central nozzle exit and between the inner and outer vortices is fuel, which is turned at the forward stagnation point and moves downward to the combustor surface, then outward to the boundary of the recirculating zone, where the blue flame appears. The inner and outer vortices are green indicating they contain $TiO_2$ particles. An important question that is not answered is why the $TiO_2$ particles occurs in the central jet region (the inner vortices) - since $TiO_2$ particles are formed from the reaction of $TiCl_4$ with water vapor which is one of the combustion products. A possible explanation is that these $TiO_2$ particles may have come from the fuel line before the nozzle exit.

For $V_{ao} > 1.6$ m/sec, the vortices appear as the flame attaches to the

surface for low $V_{co}$ (the order of magnitude is centimeters per second), and no stationary vortices could be observed for detached flames. However, the flow field and flame are disturbed violently as vortices are shed near the tip of the central jet for detached flames. The shed vortices first move downward, outward and then upward along the recirculation zone boundary. The overall flame structure also moves with these shed vortices. The flame becomes attached again from the detachment if $V_{co}$ is increased above a certain value. Vortices due to the annular jet form near the combustor surface again. Thus, it may be regarded that the large-scale annular jet vortices in the recirculating zone are very important for the flame attachment. These vortices are not observed in the detached flame. For Test III, reattachment was not observed - blow-off usually occurs when the central jet velocity is slightly increased after the flame is detached. Probably, the spaces between the two jets, and of the entire recirculating zone are so small that only very small amount of the fluid circulates in the recirculating zone. Therefore, large bluff bodies and small central nozzles, that is, large values of $D_1$ and $D_1-D_j$, have beneficial effects on the flame stabilization.

In Plate 4-b, where the blockage ratio is only 32%, $TiO_2$ particles are added to the fuel jet, thus resulting in visualization of the streamlines. In this case, the flame boundary is smooth and extends to the combustor surface. The flame in this photograph starts at the outer edge of the combustor, contracts downstream first, then diverges as it spreads further downstream, and the flame thickness also increases downstream. The streamlines in the recirculating zone diverge before the forward stagnation point (bright horizontal zone). No streamlines in the central fuel jet reach the flame front, which is the case for the Bunsen flame as shown by Lewis and von Elbe (Ref. 29).

The flow field becomes turbulent when the flame lifts from the surface at a distance less than one diameter of the inner annulus, $D_1$, which was also reported in Ref. 7, and measured by Ramohalli (Ref. 32). The large fluctuations of the flow field occurs due to the vortices being shed. The small unsteady vortices in the recirculating zone have replaced the large-scale, orderly annular air jet vortices. The central jet becomes a mushroom shape (see Plate 7). The flame surface is violently distorted. The blue flame in the photographs is less noticeable than it is in the laboratory. It is clear from the photographs that the flame initiates around the aft stagnation point, where the mean velocity is very small, and the large fluctuations there are instrumental to the mixing of air and fuel. The flame is confined to a region downstream of the aft stagnation point. This differs from Namazian's finding (Ref. 7) in that he reported that the flame initiation was around the forward stagnation point, where the central jet terminated on the central axis. In his experiments, both the central and annular velocities were much larger than in the present study, and the fuel was methane. Although his geometry is similar to that of the present study, our present experimental set-up is not capable of obtaining such high velocities.

The criterion for characterizing the flow field as was done in the cold reacting flow is extremely difficult owing to the onset of combustion. For example, the flame may be attached, detached, or blown off for the same annular velocity. Beer and Chigier stated (Ref 24): "Although geometrical similarity can be maintained for studies of non-compressible fluid dynamics in isothermal system, it has to be abandoned when the system is non-isothermal or when chemical reaction plays an important role in the process investigated." The distribution of the velocity, temperature and species concentrations in the flow field affects the chemical reaction, which, in turn, influences the

flow field by releasing large amount of heat. Thus, the fluid mechanics, the heat transfer, and chemical reactions are coupled. The flow field is extremely complicated, no relationship between $\frac{L}{D_j}$ and flow conditions as well as geometries could be found (experimental data for the combusting flow can be found in Appendix D). Such a relation requires considering the details of the flow field and chemical kinetics. According to Damköhler model (Ref. 24), five dimensionless parameters have to be considered. They are:

1. chemical reaction/bulk flow;
2. chemical reaction/molecular diffusion;
3. heat released/heat transported by bulk flow;
4. heat released/heat transported by conduction;
5. momentum transported by bulk flow/momentum transferred by viscosity (Reynolds number).

Normally it is extremely difficult to obtain empirical formula using the above five ratios due to limitations of measurement. Detailed chemical composition, temperature and velocity measurements are needed to understand the combustion process.

## 6. Some Comparisons

This section is divided into two subsections: the first subsection presents comparisions between the pure annular free jet and the cold reacting flow. The comparisons between the cold reacting flow and combusting flow are given in the second subsection.

6.1 Comparision Between the Pure Annular Jet and the Cold Reacting Flow

The introduction of the central jet into the vortex region established by the annular jet changes the flow pattern in the recirculating zone substantially. It may push away the vortices, distort them, or even make the irregular small vortices take the place of the large-scale vortices present in the case of the pure annular jet. The results of this interaction between the vortices and the central jet depend on the relative magnitude of the momenta of the central and annular jets, and the space between two jets (or $D_i$-$D_j$). these are shown in Plate 1-b, Plate 2, 3 and 4-a as well as in Figures 3, 5 and 7.

Figure 8 shows that when the central jet velocity is increased from zero (pure annular jet) to penetration velocity (when the central jet penetrates through the recirculating zone, i.e., when $L = L_{rz} = L_p$), the length of the recirculating zone, $L_{rz}$, increases from its value for the pure annular jet to the penetration length, $L_p$. At penetration, $L = L_{rz} = L_p$. The presence of the central jet causes the aft stagnation point to move further downstream. Thus, the central jet effectively changes the shape and extent of the recirculating zone. However, Fujii et al. (Ref. 16) found that the introduction of the central jet into the flow field behind a bluff body placed in a ducted stream shifted the recirculating zone upstream, this is contrary to our finding. Figure 8 also shows that the effect of the central nozzle diameter on the length of the recirculating zone. At the same central jet velocity, $L_{rz}$ is larger for the larger central nozzle diameter. This is probably due to the larger momentum of the central jet, which is proportional to the nozzle exit area. When the velocity of the annular jet is increased, the influence of the central jet on the length of the recirculation zone is reduced. For large annular velocity, as reported in Ref. 3, the length of the

recirculation zone $L_{rz}$ is almost constant, and independent of the central jet velocity. Thus, $L_{rz} = L_p$ in this case.

## 6.2 Comparison Between Cold Reacting and Combusting Flows

The spreading of the detached and attached flames leads to two different phenomena from that of the cold reacting flow. For the attached flame, as described before, the flow is laminar, thus along the boundary of the recirculating zone, only species diffusion could occur as the means of the mass exchange across the boundary except the region very close to the combustor surface. Probably a stoichiometric fuel-air mixture occurs in the immediate vicinity of the combustor where the flame is blue. Then the flame spreads downstream along the boundary surface, converging at the central axis around the forward stagnation point developing further downstream (see Plate 9). In this case, the fluid viscosity is increased very much (approximately 10 times, see Ref. 3). Thus, compared with the cold reacting flow, this results in the faster growth of the boundary layer, which starts at the separation point (outer edge of the combustor) where its thickness is zero. Therefore, the onset of combustion reduces the recirculating zone. As observed from the experiments, the forward and aft stagnation points are moved closer to the combustor surface for the combusting flow than for the corresponding cold reacting flow (e.g., compare Plate 4-b to Plate 2-b). Figure 9 shows $\frac{L_p}{D_i}$ vs. $R_a$ for the cold reacting flow and the combusting flow (attached flame only). It is clear that the combustion causes the penetration length or the recirculating zone length to be reduced by more than half. Thus, it is much easier for the central fuel jet to penetrate through the recirculating zone in the combusting case. The penetration velocity increases with the annular air velocity for both cold and combusting flow cases.

However, the measured value $V_{co}$ at penetration (i.e., $V_{po}$) and its incremental change corresponding to an incremental change in $V_{ao}$ is much smaller in the presence of the flame (0.5 ~ 1.0 times smaller) than those for the corresponding cold reacting flow. This may be due to the corresponding reduction of the recirculating zone length in the attached flame. The shortening effect of the laminar flame on the length of the recirculating zone was also observed by Lewis and von Elbe for the flow behind the end of a small cylinder inserted into a low-velocity stream (Ref. 29). However, their results were for a premixed flame.

For the detached flame, the flow field is violently disturbed, perhaps due to the sudden expansion of combusting mixture, turbulence, and the shedding of vortices. The flame first appears in the region between the forward and aft stagnation points (closer to the aft one). It was observed that the forward stagnation point in the detached flame is shifted significantly closer to the combustor surface compared to the cold reacting flow; and the aft stagnation point moves slightly downstream. Quantitative values were not obtained due to limitations of the present experimental set-up. This finding is contrary to Namazian's result (Ref. 7), which showed that the fuel jet had greater height for the combusting flow than for the cold reacting flow. But it should be noted that Namazian used methane as fuel and the exit velocities of the fuel and air were about 10 times greater than in this study. The prolonging of the recirculating zone was also reported in the literature for bluff-body flame stabilizers inserted in premixed streams in a duct (e.g., see Ref. 15 and 30).

Due to the reduction of the recirculating zone with attached flames, the vortices sizes are also limited. However, the vortices seem more orderly, stationary, and intense. These have been presented in the previous sections.

## 7. Analytical Approach

The flow field behind a combustor is so complex that no analytical solution nor numerical solution for unducted flow are available. The present analytical approach is made possible by employing the scaling method proposed by Bejan (Ref. 31) even without knowing the details of the flow field. Due to the extreme complexities in the combusting flow case, the analyses here are only given to the pure annular air jet and the cold reacting flow cases.

The governing equations are continuity and momentum equations expressed in cylindrical coordinate as follows:

$$\frac{\partial u_r}{\partial r} + \frac{u_r}{r} + \frac{\partial u_z}{\partial z} = 0 \tag{4}$$

$$u_r \frac{\partial u_r}{\partial r} + u_z \frac{\partial u_r}{\partial z} = -\frac{1}{\rho}\frac{\partial p}{\partial r} + \nu\left(\frac{\partial^2 u_r}{\partial r^2} + \frac{1}{r}\frac{\partial u_r}{\partial r} - \frac{u_r}{r^2} + \frac{\partial^2 u_r}{\partial z^2}\right) \tag{5}$$

$$u_r \frac{\partial u_z}{\partial r} + u_z \frac{\partial u_z}{\partial z} = -\frac{1}{\rho}\frac{\partial p}{\partial z} + \nu\left(\frac{\partial^2 u_z}{\partial r^2} + \frac{1}{r}\frac{\partial u_z}{\partial r} + \frac{\partial^2 u_z}{\partial z^2}\right) \tag{6}$$

By these equations, we have assumed that the flow field is steady and axisymmetrical, and the gravitational effect is negligible.

### 7.1 Pure Annular Air Jet

By scaling method, the Equations (4)-(6) can be expressed for the flow around the recirculating zone as

$$\frac{u_r}{r} \sim \frac{u_z}{z} \tag{7}$$

$$\frac{u_r^2}{r} + u_z \frac{u_r}{z} \sim -\frac{1}{\rho_a}\frac{p}{r} + \nu_a\left(\frac{u_r}{r^2} + \frac{u_r}{z^2}\right) \tag{8}$$

$$u_r \frac{u_z}{r} + \frac{u_z^2}{z} \sim -\frac{1}{\rho_a}\frac{p}{z} + \nu_a\left(\frac{u_z}{r^2} + \frac{u_z}{z^2}\right) \tag{9}$$

where $u_r$ and $u_z$ should be regarded as characteristic velocity of the flow field around the recirculation zone. Similarly, r and z are characteristic length.

Substituting Equation (7) into (8) and (9), then eliminating pressure term gives

$$\left[\left(\frac{r}{z}\right)^2 - 1\right]u_z^2 \sim \nu_a\left(\frac{1}{r^2} + \frac{1}{z^2}\right)\left[\left(\frac{r}{z}\right)^2 - 1\right]u_z z \tag{10}$$

The solutions are

$$\frac{r}{z} \sim 1 \tag{11}$$

$$u_z \sim \nu_a\left(\frac{1}{r^2} + \frac{1}{z^2}\right)z \tag{12}$$

Now for the flow around the recirculating zone, from the mean velocity distribution along the centerline reported in the literature (e.g., Ref. 11, 13 and 22), it may be assumed that

$$u_z \sim V_{ao};$$

$$r \sim \frac{D_j}{2} \sim D_j;$$

and $$z \sim L_{rz} .$$

Thus, Equation (11) becomes

$$\frac{L_{rz}}{D_j} \sim 1 \tag{13}$$

and Equation (12) leads to

$$V_{ao} \sim \nu_a \left(\frac{1}{D_i^2} + \frac{1}{L_{rz}^2}\right) L_{rz}$$

or
$$\frac{D_o - D_i}{D_i}\left(\frac{L_{rz}}{D_i}\right)^2 - R_a \frac{L_{rz}}{D_i} + \frac{D_o - D_i}{D_i} \sim 0 \qquad (14)$$

where $R_a = \frac{V_{ao}(D_o - D_i)}{\nu_a}$. Therefore, the solutions of Equation (14) are obtained if it is assumed that $R_a \gg \frac{D_o - D_i}{D_i}$, which is always true in this study:

$$\frac{L_{rz}}{D_i} \sim \frac{D_i}{D_o - D_i} R_a$$

and
$$\frac{L_{rz}}{D_i} \sim \frac{D_o - D_i}{D_i} \frac{1}{R_a}$$

or
$$\frac{L_{rz}}{D_i} = C_1 R_a \qquad (15)$$

and
$$\frac{L_{rz}}{D_i} = \frac{C_1^{-1}}{R_a} \qquad (16)$$

Thus, the three solutions are: $\frac{L_{rz}}{D_i} = C_1 R_a$, $\frac{C_1^{-1}}{R_a}$, $C_2$ ($C_2 = O(1)$), where $C_1$ is a function of the geometries, $C_2$ is a function of the blockage ratio and forebody shape. When compared with Figure 4, it seems that Equation (15) is suitable for the laminar flow in which case the length of the recirculating zone increases with $R_a$. Equation (15) shows that if $R_a = 0$, i.e., $V_{ao} = 0$, no recirculating zone could exist. Equation (16) appears to be valid for the transition flow region, and Equation (13) appears to be valid when the flow is fully turbulent ($R_a \to \infty$). For example, some authors like Durão and Whitelaw (Ref. 11) reported that for very large $R_a$ (about $10^5$), $\frac{L_{rz}}{D_i}$ was constant. The transition region and fully turbulent flow region (Equations (13) and (16))

will be combined as

$$\frac{L_{rz}}{D_j} = \left(C_2 + \frac{C_1^{-1}}{R_a}\right)$$

Thus, there are two adjustable constants ($C_1$ and $C_2$). Fig. 4 shows the results when $C_1$ is set equal to 0.006 and $C_2$ to 0.934. These results are in general agreement with the experiments.

## 7.2 Cold Reacting Flow

Because of the fact that the region of subatmospheric pressure behind a bluff body, formed by bending streamlines, is set up by the annular air jet, it may be valid to assume that for both jets, the pressure gradients in the r-direction which cause the annular streamlines to converge radially inward and the central jet streamlines to diverge outward are at the same order of magnitude (they are comparable), i.e.,

$$\left(\frac{\partial p}{\partial r}\right)_a \sim \left(\frac{\partial p}{\partial r}\right)_c \tag{17}$$

Again using scaling arguments, the following assumptions for the central flow are made:

$$u_{cz} \sim V_{co};$$

$$z \sim L;$$

and $$r \sim D_j.$$

Thus, Equations (4) and (5) become

$$\frac{u_{cr}}{D_j} \sim \frac{V_{co}}{L} \tag{18}$$

$$u_{cr}\frac{u_{cr}}{D_j} + V_{co}\frac{u_{cr}}{L} \sim -\frac{1}{\rho_c}\left(\frac{\partial p}{\partial r}\right)_c + \nu_c\left(\frac{u_{cr}}{D_j^2} + \frac{u_{cr}}{L^2}\right) \tag{19}$$

where L is the location of the forward stagnation point along the z axis.

Likewise, for the annular air jet, it is assumed that

$$u_{az} \sim V_{ao} \quad ;$$

$$r \sim D_i \quad ;$$

and $$z \sim L_{rz} \quad .$$

Thus, applying Eqs. (4) and (5) to the annular jet leads to

$$\frac{u_{ar}}{D_i} \sim \frac{V_{ao}}{L_{rz}} \tag{20}$$

$$u_{ar}\frac{u_{ar}}{D_i} + V_{ao}\frac{u_{ar}}{L_{rz}} \sim -\frac{1}{\rho_a}\left(\frac{\partial p}{\partial r}\right)_a + \nu_a\left(\frac{u_{ar}}{D_i^2} + \frac{u_{ar}}{L_{rz}^2}\right) \tag{21}$$

Combining Equations (18) with (19), and (20) with (21), then using relation (17) gives the following equation:

$$R_c^2\frac{L}{D_j} - R_c\left(\frac{L}{D_j}\right)^2 + 1 \sim \frac{1}{E^2}\left(\frac{L}{D_j}\right)^3 + R_a^2\left(\frac{D_i}{D_o - D_i}\right)^2\left(\frac{D_i}{D_j}\right)^3 - R_a\left(\frac{D_i}{D_o - D_i}\right)\left(\frac{D_i}{D_j}\right)^3 \tag{22}$$

where $R_c = \frac{V_{co}D_j}{\nu_c}$ , $R_a = \frac{V_{ao}(D_o - D_i)}{\nu_a}$ , $E = \frac{\nu_c}{\nu_a}\left(\frac{\rho_c}{\rho_a}\right)^{1/2}$

and $L_{rz}$ has been replaced by $D_i$ since from the measurements $\frac{L_{rz}}{D_i}$ is order of unity and changes only slightly (e.g., see Figure 8).

Now if $R_c \gg \frac{L}{D_j} + \frac{D_j}{L}$ (which it is), the second term is negligible compared with the first term on the left hand side of the Equation (22). Likewise, if $R_a \gg \frac{D_o - D_i}{D_i}$ (which it is), the second term on the right hand side of the same equation can be neglected compared with the first term. Thus, Equation (22) reduces to

$$R_c^2 \sim \frac{1}{E^2}\left(\frac{L}{D_j}\right)^2 R_a^2 \frac{D_j}{D_o - D_i}\left(\frac{D_j}{D_i}\right)^3$$

or

$$\frac{L}{D_j} \sim E\, R_c R_a^{-1}\left(\frac{D_o - D_i}{D_i}\right)\left(\frac{D_i}{D_j}\right)^{1.5} \qquad (23)$$

It is remarkable to note that Eq. (23), our very simplified analytical result, appears to be exactly the same as that obtained from the experimental data, Eq. (3). From the definition of E

$$E = \frac{\mu_c}{\mu_a}\left(\frac{\rho_c}{\rho_a}\right)^{0.5}$$

$$= \frac{\mu_c}{\mu_a}\left(\frac{\rho_a}{\rho_c}\right)^{0.5}$$

where $\mu_c$ and $\mu_a$ are the dynamic viscosities of the fluids in the annular and central jets, respectively. It has been shown here that the constant A in Eq. (3) is a function of the physical properties of the fluids in the two jets as presented before, i.e.,

$$A = BE$$

where B is a constant. Using the equation of state for the perfect gas, we have

$$\frac{\rho_a}{\rho_c} = \frac{M_a}{M_c}$$

where $M_a$ and $M_c$ are the molecular weights of the fluids flowing in the annular and central jets. Table 3 gives the values of $\mu$ (from Ref. 35) and M (from Ref. 36) for propane, air and methane corresponding to the fluids used in the experiments of this study, Tankin (Ref. 27) and Namazian (Ref. 3). The values of A, B, and E corresponding to these studies are given in Table 4 where the

value of A is taken from Table 2. The value of B as shown in Table 4 is almost constant if one considers the uncertainty of the experiments. Thus, Eq. (23) could be expressed in a more general form:

$$\frac{L}{D_j} = B\left(\frac{\mu_c}{\mu_a}\frac{\rho_a}{\rho_c}\right)^{0.5}\frac{R_c}{R_a}\left(\frac{D_i}{D_j}\right)^{1.5}\left(\frac{D_o-D_i}{D_i}\right) \qquad (24)$$

Table 3. Values of $\mu$ and M for Propane, Air and Methane

| Fluid | $\mu^*$ (at 30°C) | M |
|---|---|---|
| Propane | 84 | 44.097 |
| Air | 186 | 28.96 |
| Methane | 113 | 16.04 |

*The unit of $\mu$ is $10^{-5}$ gm cm sec.

Table 4. Values of A, B and E

| Authors | Fluid in Central Jet | A | E | B |
|---|---|---|---|---|
| Present | Propane | 1.700 | 0.3660 | 4.644 |
| Rankin Ref. [ ] | Air | 3.125 | 1.0000 | 3.125 |
| Namazian Ref. [ ] | Methane | 3.183 | 0.4163 | 3.[illegible] |

## 5. Conclusions

The following conclusions may be extracted from this study:

The [illegible] mixing zone length has a maximum around [illegible]=800 annular

Reynolds number and tends to approach a constant value of the order of unity for large annular Reynolds number in the case of the pure annular air flow.

(2) For the cold reacting flow, an empirical formula for the axial location of the forward stagnation point in terms of the exit flow conditions and nozzle diameters is found:

$$\frac{L}{D_j} = A \frac{R_c}{R_a} \left(\frac{D_i}{D_j}\right)^{1.5} \left(\frac{D_o - D_i}{D_i}\right)$$

The introduction of the central jet into the recirculating zone causes the aft stagnation point to move downstream and increases the size of the recirculating zone. However, if the annular air velocity is less than 0.5 m/sec, no regular, orderly recirculating zone could be formed.

(3) If the annular air velocity is less than 1.6 m/sec, the flame is always attached to the combustor surface, if the annular air velocity is greater than 1.6 m/sec, the flame is attached for the low central fuel velocity, detached if the central fuel velocity is increased over a certain value, and then reattached to the combustor for further increase in the central fuel velocity. This was an unexpected and unexplained result. The structures of the central jet and the recirculating zone are greatly different for these attached, detached and reattached flames.

(4) In the presence of the attached flame, the forward and aft stagnation points are much closer to the combustor than in the corresponding cold flow. For the detached flame, the forward stagnation point moves upstream considerably whereas the aft stagnation point moves downstream slightly when compared to the corresponding cold reacting flow.

(5) For the attached flame, the vortices due to the annular jet are more orderly, stationary and intense than those in the cold reacting flow. These

are also true for the vortices due to the central jet. For the detached flame, usually no orderly vortices could be observed, occasionally the unsteady vortices shed at the tip of the central jet disturb the whole flow field significantly. Only the well-organized vortices due to the annular jet could be observed near the combustor for the reattached flame. Thus, it seems that the large-scale well-organized annular jet vortices are crucial to the flame reattachment.

More work is needed to understand the flame stabilization processes and flow field dynamics. In the future, it would be very fruitful to correlate the visualization of vortex dynamics with the results of simultaneous pointwise measurements made with advanced diagnostic techniques such as Laser Doppler anemometer and coherent anti-Stokes Raman spectroscopy as being undertaken at the Aero Propulsion Lab nat by at Wright-Patterson AFB.

## Nomenclature

$L$ - the height of the central jet, or the distance between the forward stagnation point and the combustor surface

$L_p$ - length of the recirculation zone when the central jet penetrates through it

$L_{rz}$ - length of the recirculation zone

$M$ - molecular weight

$r$ - radial coordinate

$R_a$ - $= V_{ao}(D_o - D_i)\rho_a$

$R_{D_i}$ - $= V_{ao} D_i \rho_a$

$R_c$ - $= V_{co} D_i \rho_c$

$v$ - velocity

$V_{ao}$ - velocity of the annular jet at the outer nozzle exit

$V_{co}$ - velocity of the central jet at the inner nozzle exit

$V_{cp}$ - velocity of the central jet when it penetrates through the recirculation zone, i.e., when $L = L_{rz} = L_p$

$J$ - $= \frac{\rho_c V_{co}^2 D_i^2}{\rho_a V_{ao}^2 (D_o^2 - D_i^2)}$ momentum ratio of the central jet to the annular jet

$x$ - vertical coordinate

$\rho$ - density of fluid

$\nu$ - kinematic viscosity

$\mu$ - dynamic viscosity

Subscripts

$a$ - annular jet

$c$ - central jet

$i$ - diameter at the nozzle exit

$o$ - diameter of recirculation

$p$ - diameter of recirculation

## References


1. Beer, J. M., Chigier, N. A. and Lee, K. B. (1963), Modeling of the Double Concentric Burning Jets, Ninth Symposium (International) on Combustion, The Combustion Institute, Academic Press, New York, p. 892.

2. Glassman, I. (1977), Combustion, Academic Press.

3. Roquemore, W. M. and Tankin, R. S., et al., The Role of Vortex Shedddding in a Bluff Body Combustor, Symposium on Experiments and Techniques in Turbulent Reactive and Non-Reactive Flows, ASME 105th Winter Annual Meeting.

4. Roquemore, W. M., et al. (1983), Influence of the Vortex Shedding Process on a Bluff-Body Diffusion Flame, AIAA-83-0335.

5. Switzer, G. L., et al. (1983), Simultaneous Cars and Luminosity Measurements in a Bluff-Body Combustor, AIAA-83-1481.

6. Kyoji, Kimoto, et al. (1981), Structure of Turbulent Jet Flame Stabilized in Annular Air Jet, Combustion Science and Technology, Vol. 25, pp. 31-41.

7. Namazian, M., et al. (1985), Flow and Combustion in Bluff-Body stabilized Flames, presented at the Combustion Institute, San Antonio, Texas, Paper No. 2-1B.

8. Scott, J. M. and Hankey, W. K. (1983), Numerical Simulation of Cold Flow in an Axisymmetric Centerbody Combustor.

9. Craig, R. R., et al. (1984), A General Approach for Obtaining Unbiased LDV Data in Highly Turbulent Non-Reacting and Reacting Flows, AIAA-84-0366.

10. Lysaght, A. J. R., Bilger, R. W. and Kent, J. H. (1982), Visualization of Mixing in Turbulent Diffusion Flames, Combustion and Flame 46, pp. 105-108.

11. Durão, D. F. G. and Whitelaw, J. H. (1978), Velocity Characteristics of the Flow in the Near Wake of a Disk, J. Fluid Mech., Vol. 85, Part 2, pp. 369-385.

12. Taylor, A. M. P. K. and Whitelaw, J. H. (1984), Velocity Characteristics in the Turbulent Near Wakes of Confined Axisymmetric Bluff Bodies, J. Fluid Mech., Vol. 139, pp. 391-416.

13. Davies, T. W. and Beer, J. M. (1971), Flow in the Wake of Bluff-Body Flame Stabilizers, Proc. 13th Int. Symp. Combustion, p. 361.

14. Pope, S. B. and Whitelaw, J. H. (1976), The Calculation of Near-Wake Flows, J. Fluid Mech., Vol. 73, Part 1, pp. 9-32.

15. Winterfeld, G. (1965), On Processes of Turbulent Exchange Behind Flame Holders, Proc. 10th Int. Symp. Combustion, pp. 1265-1275, Combustion Institute, Pittsburgh.

16. Fujii, S., Gomi, M. and Eguchi, K. (1978), Cold Flow Tests of a Bluff-Body Flame Stabilizer, Trans. ASME I: J. Fluids Engng. 100, pp. 323-333.

17. Bradbury, L. J. S. (1976), Measurements with a Pulsed-Wire and a Hot-Wire Anemometer in the Highly Turbulent Wake of a Normal Flat Plate, J. Fluid Mech. 77, pp. 473-497.

18. Carmody, T. (1964), Establishment of the Wake Behind a Disc, Trans. ASME D: J. Basic Engng. 86, pp. 869-882.

19. Tankin, R. S. (1984), Study of Forward and Aft Stagnation Points in Cold Reacting and Combusting Flows, Proposal to Southeastern Center of Electrical Engineering Education.

20. Chigier, N. A. and Beer, J. M. (1964), The Flow Region Near the Nozzle in Double Concentric Jets, J. Basic Engng. 86, pp. 797-804.

21. Strehlow, R. A. (1984), Combustion Fundamentals, McGraw-Hill Co.

22. Calvert, J. R. (1967), Experiments on the Low-Speed Flow Past Cones, J. Fluid Mech., Vol. 27, Part 2, pp. 273-289.

23. Law, C. K., et al. (1982), On the Opening of Premixed Bunsen Flame Tips, Combustion Science and Technology, Vol. 28, pp. 89-96.

24. Beer, J. M. and Chigier, N. A. (1972), Combustion Aerodynamics, Halsted Press Division, John Wiley & Sons, Inc., New York.

25. Abramovich, G. N. (1963), The Theory of Turbulent Jets, MIT Press, Cambridge, Massachusetts.

26. Zukoski, E. E. and Marble, F. E. (1956), Gasdynamics Symposium, p. 205, Northwestern University, Evanston, Illinois.

27. Tankin, R. S. (1984), unpublished notes.

28. Dyer, M. J. and Crosley, D. R. (1982), Optics Letters, Vol. 7, p. 382.

29. Lewis and von Elbe, Combustion, Flames and Explosions of Gases, 2nd Ed., (1961), Academic Press, Inc.

30. Fujii, S. and Eguchi, K. (1981), A Comparison of Cold and Reacting Flows Around a Bluff-Body Flame Stabilizer, J. Fluid Engng., Vol. 103, p. 328.

31. Bejan, A. (1984), Convection Heat Transfer, John Wiley & Sons.

32. Ramohalli, et al. (1981), Some Experimental Data on Liftoff Characteristics in Turbulent Jet Flames, Combustion Science and Technology, Vol. 36, pp. 199-203.

33. Libby, P. A. and Williams, F. A., Eds. (1980), Turbulent Reacting Flows, Springer-Verlag, Berlin, pp. 65-113.

34. Sirignano, W. A., et al. (1971), The Effect of High-Frequency Periodic Disturbances on Axisymmetric Wake Diffusion Flames, Combustion Science and Technology, Vol. 2, pp. 351-364.

35. Kanury, A. M. (1975), Introduction to Combustion Phenomena, Gordon Breach.

36. Rossini, F. D., et al. (1953), Selected Values of Physical and Thermodynamic Properties of Hydrocarbon and Related Compounds, API Research Project 44, Carnegie Institute of Technology, Pittsburgh, Pennsylvania.

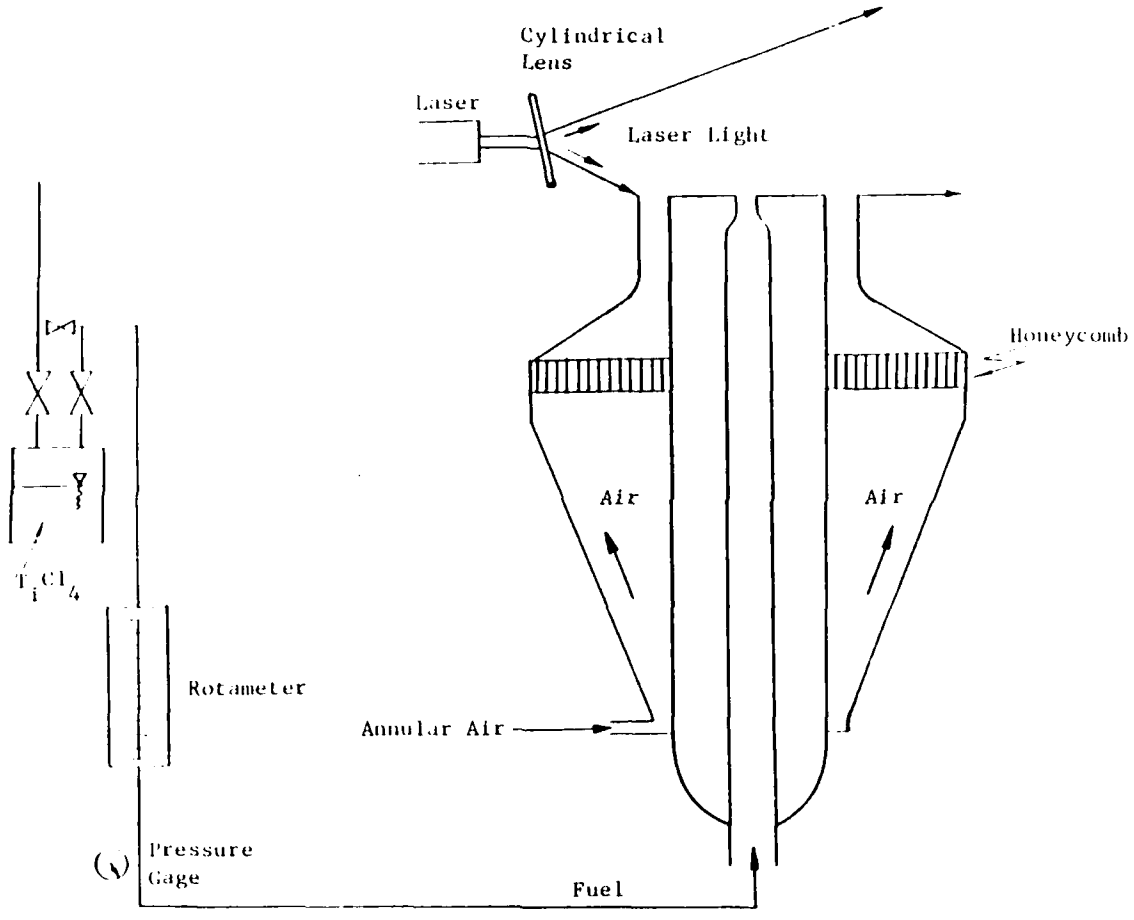



Fig. 1. Illustration of the experimental set-up.

$D_o$ = 53.2 mm

$D_i$ = 38.5 mm

$D_j$ = 6.35 mm; 9.45 mm; 12.7 mm

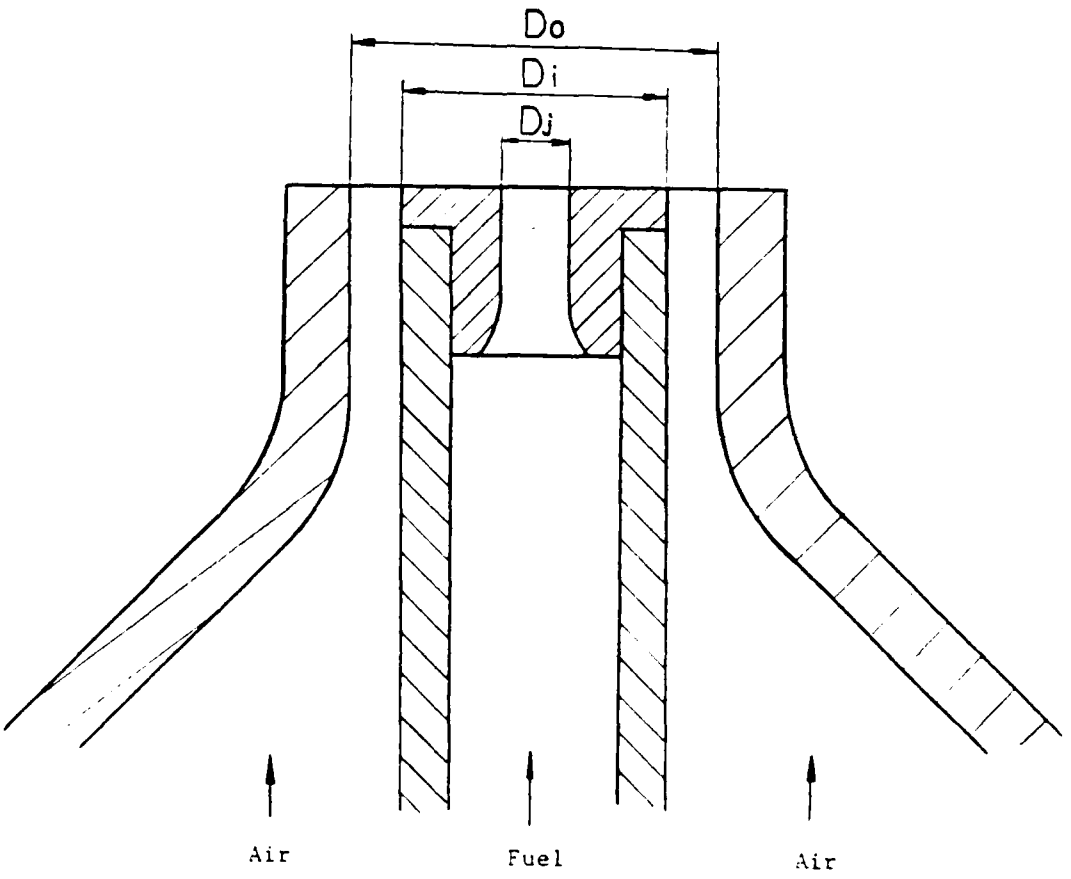



Fig. 2a. Schematic drawing of fuel and air nozzles used in Test I.

$D_o$ = 53.2 mm

$D_i$ = 45.2 mm

$D_j$ = 6.35 mm; 9.45 mm; 12.7 mm

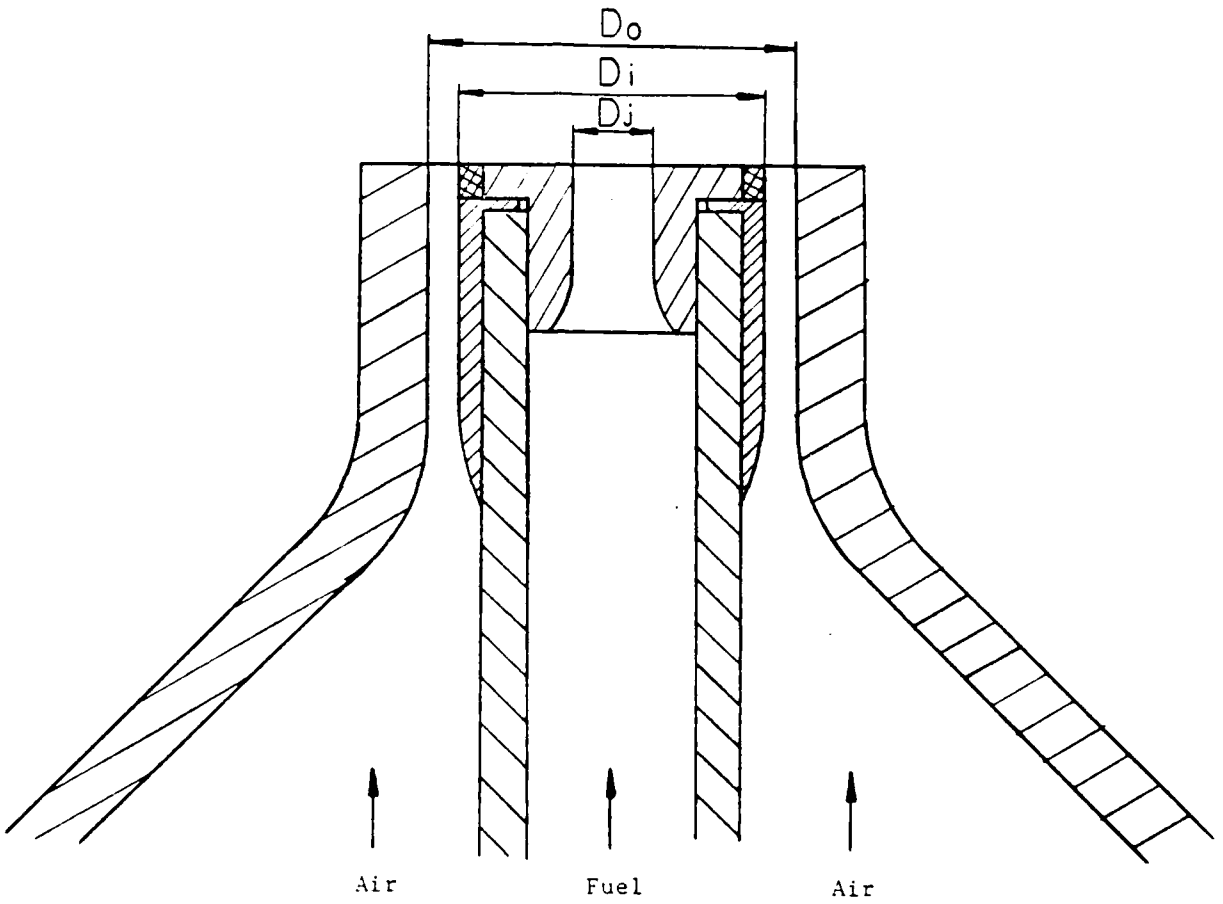



Fig. 2b. Schematic drawing of fuel and air nozzles used in Test II.

$D_o$ = 33.5 mm
$D_i$ = 19.1 mm
$D_j$ = 12.7 mm

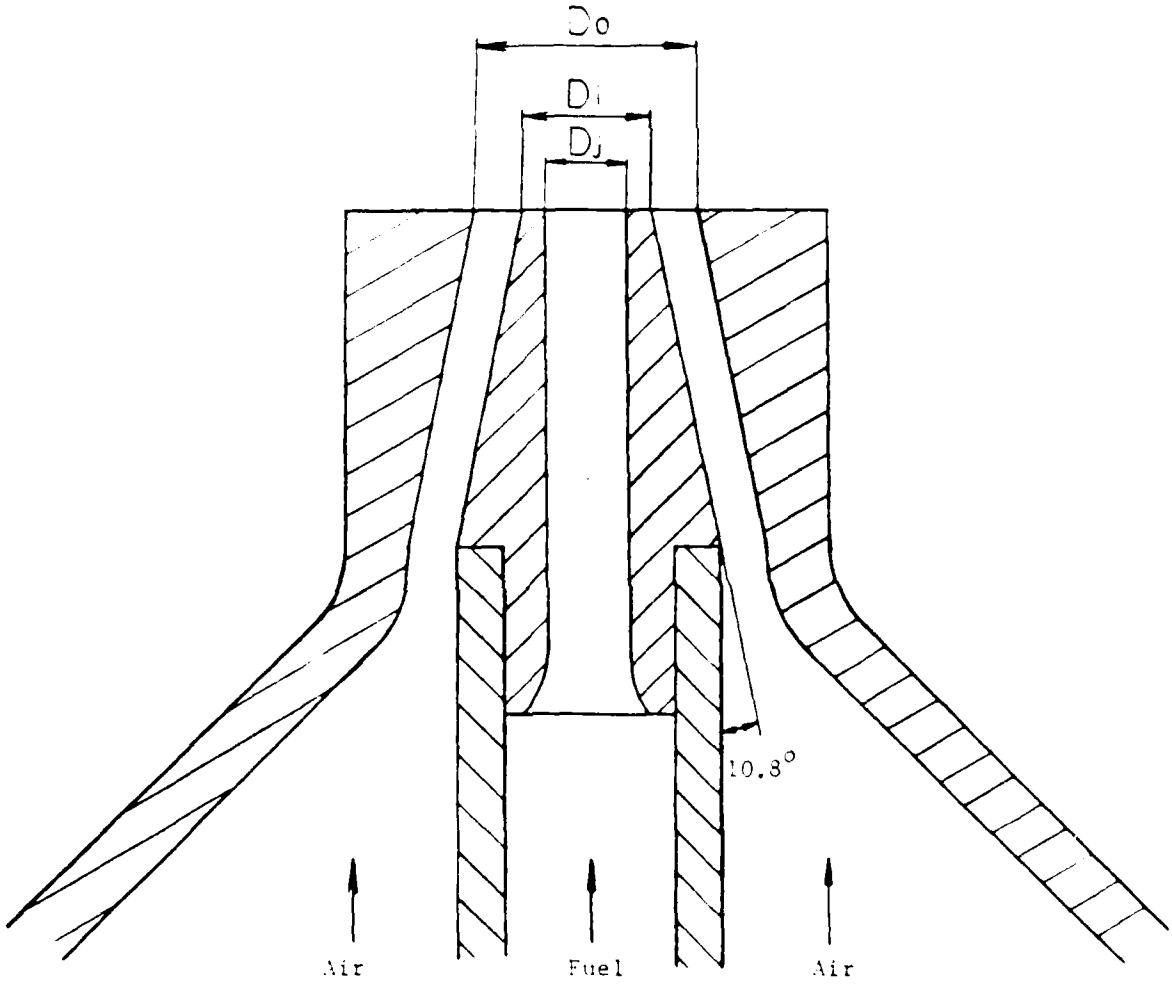
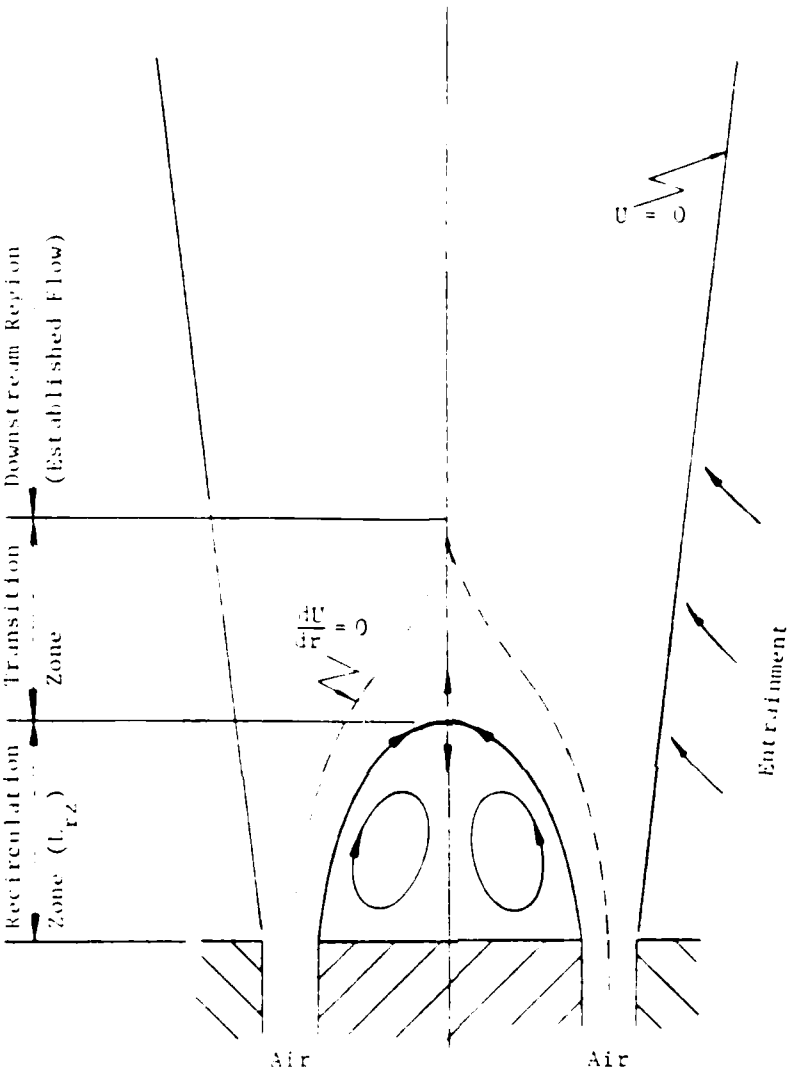


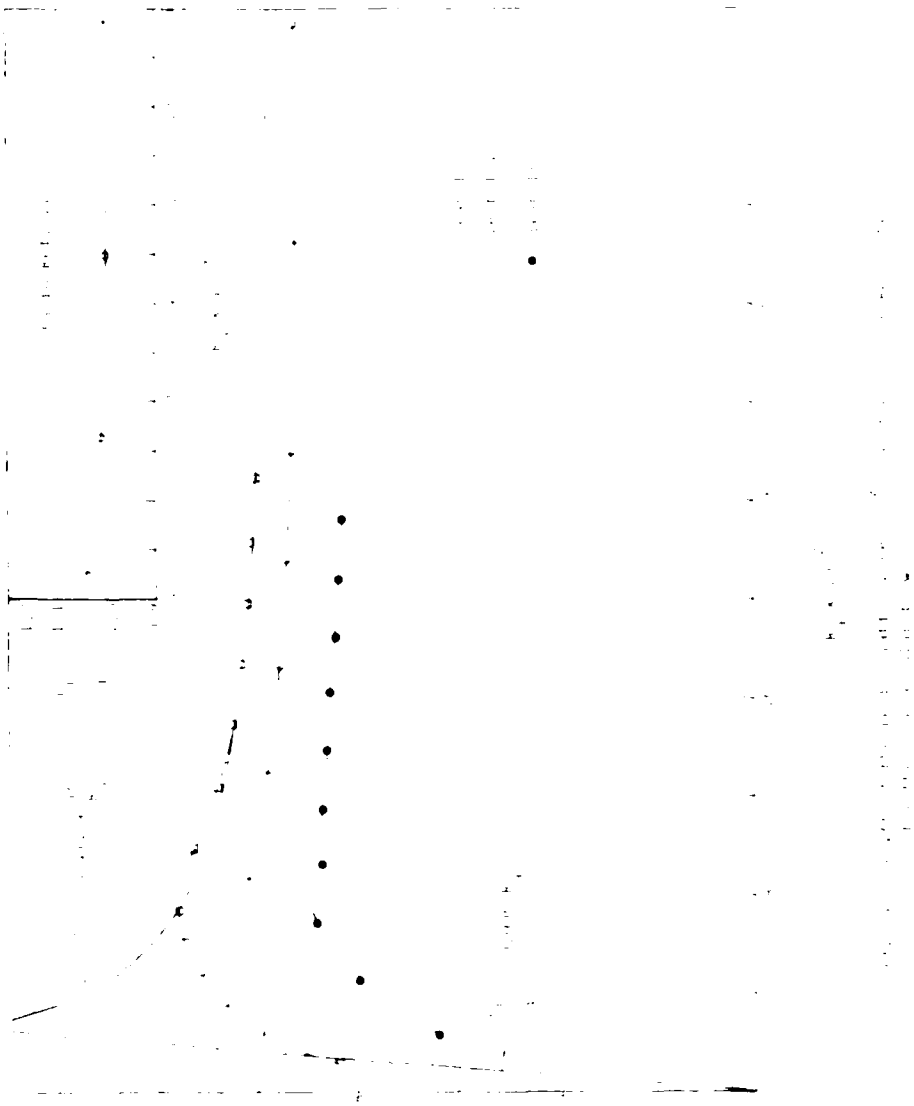

Fig. 2c. Schematic drawing of the fuel and air nozzles used in Test III.




U - Mean axial velocity

r - Radial distance

Fig. 3. Flow diagram for the pure annular air jet.



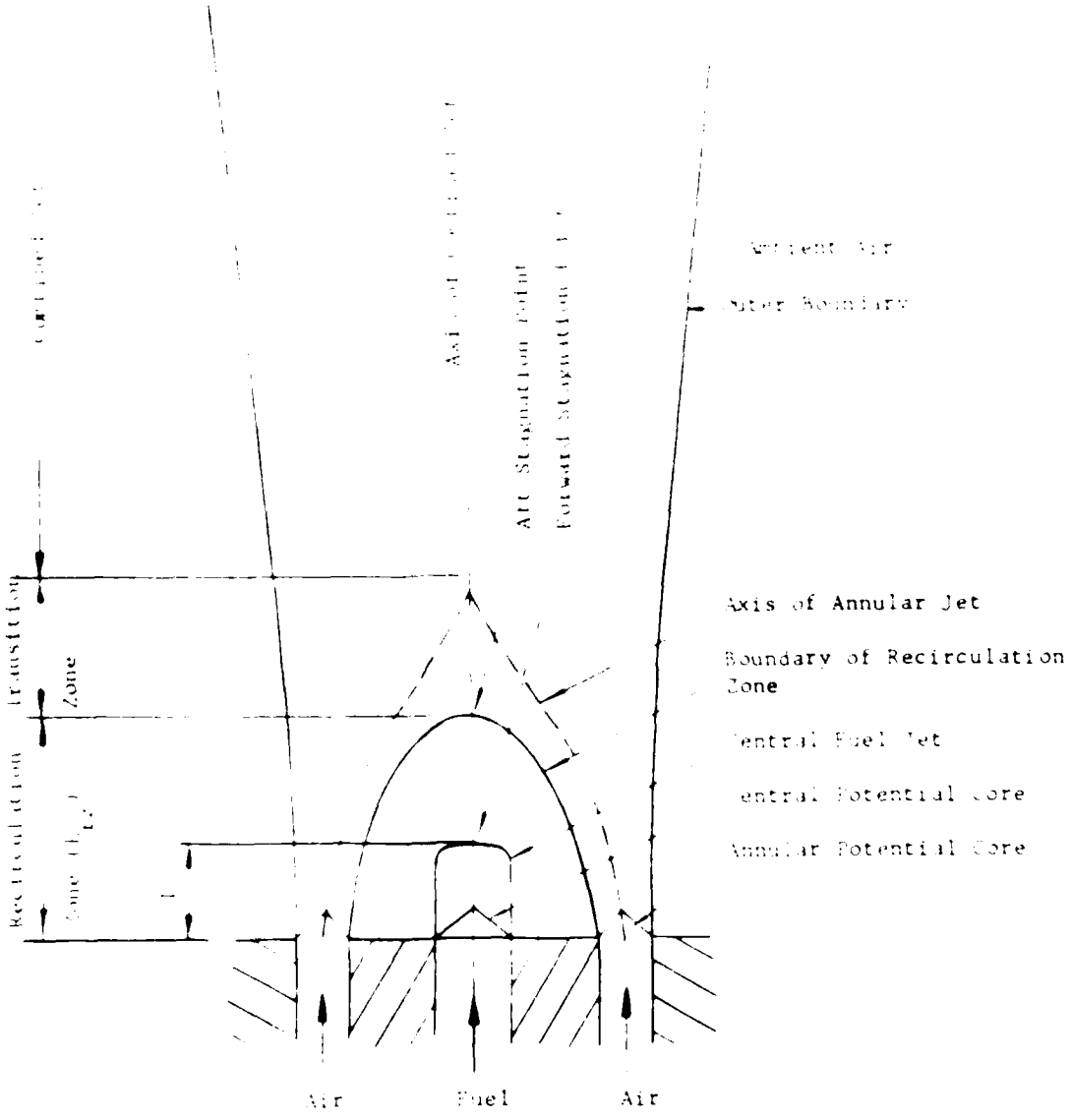



Fig. 5. Schematic diagram of the flow from annular and fuel jets from the combustion tunnel.

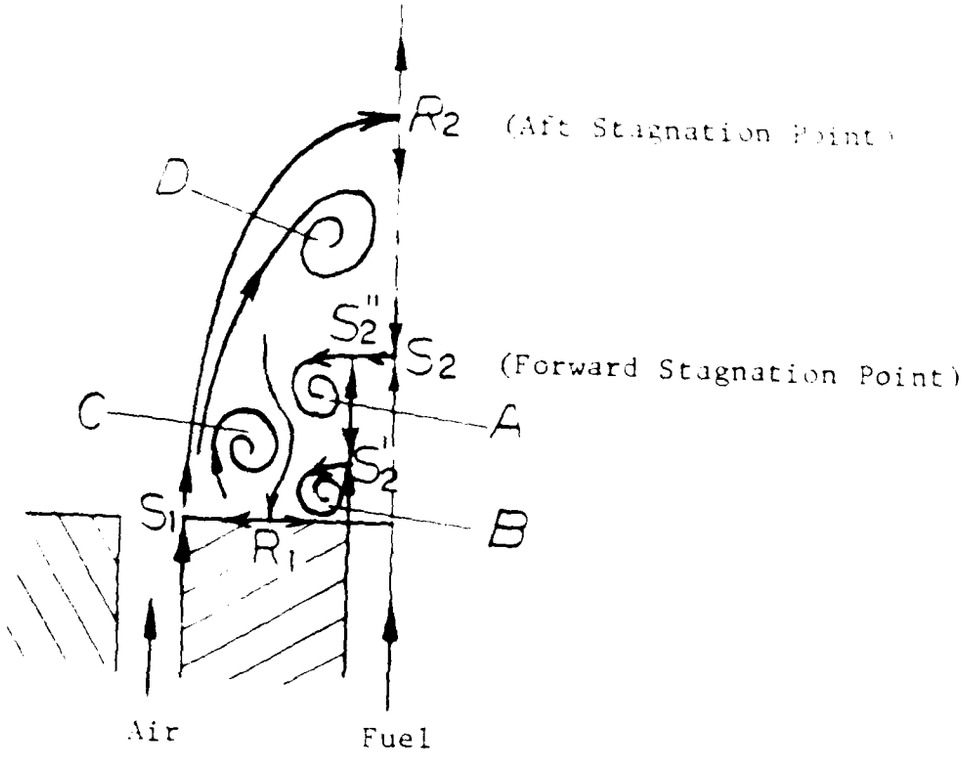



Fig. 9. Typical S and R saddle points (also see Plate 3a).

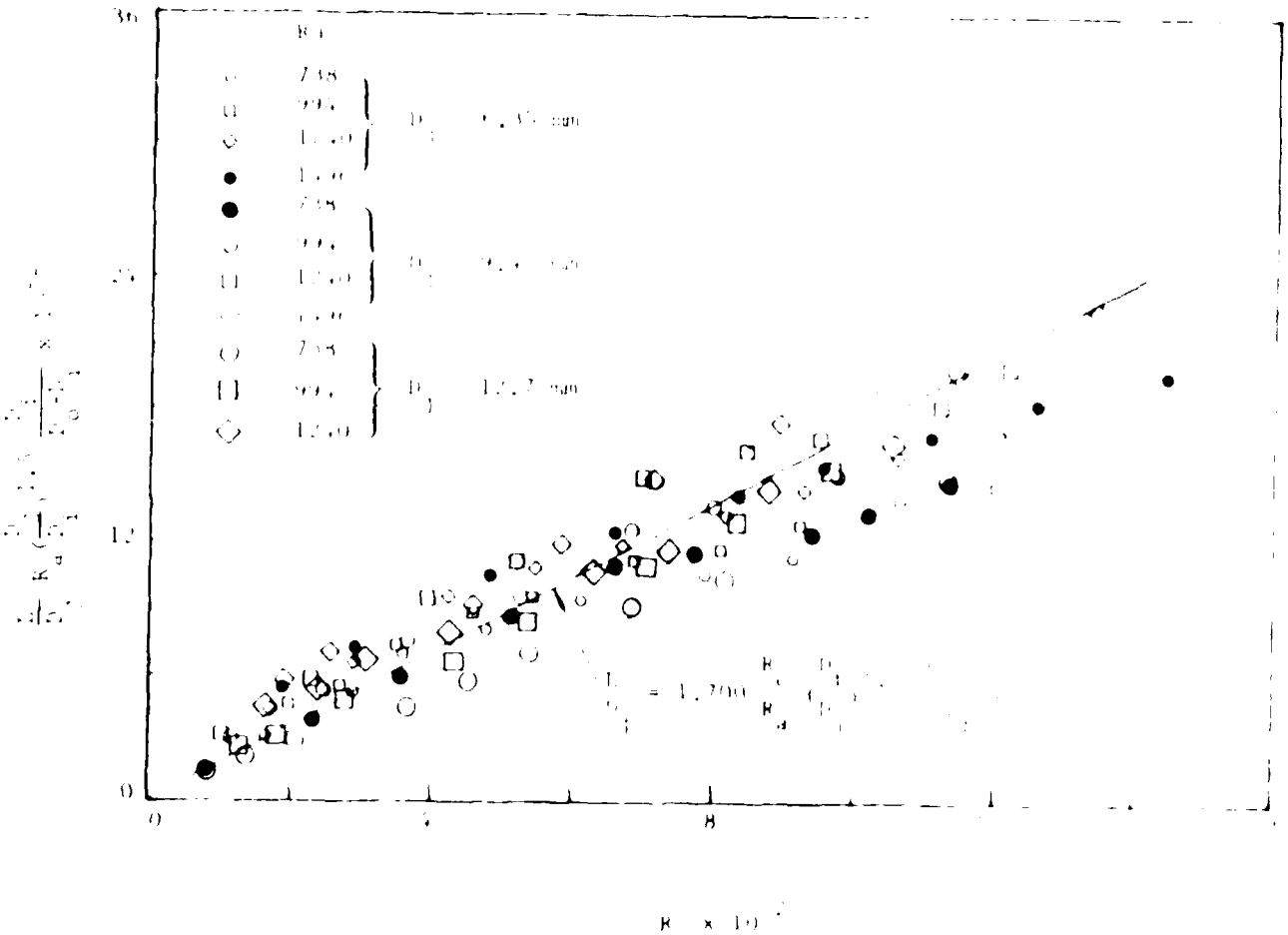


FIG. 7.1. Axial location of the forward [illegible]
for test [illegible] coil reaction [illegible]

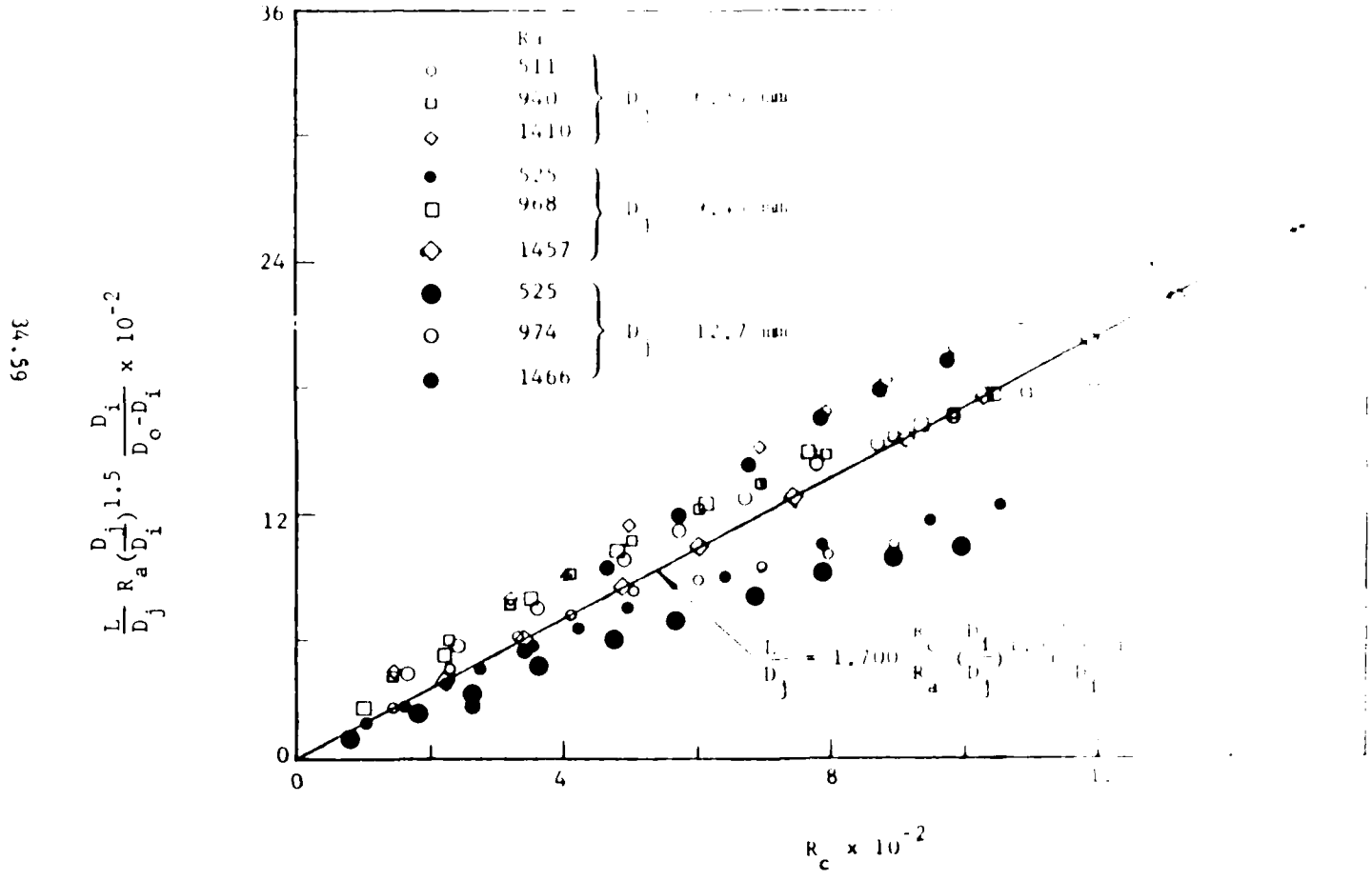
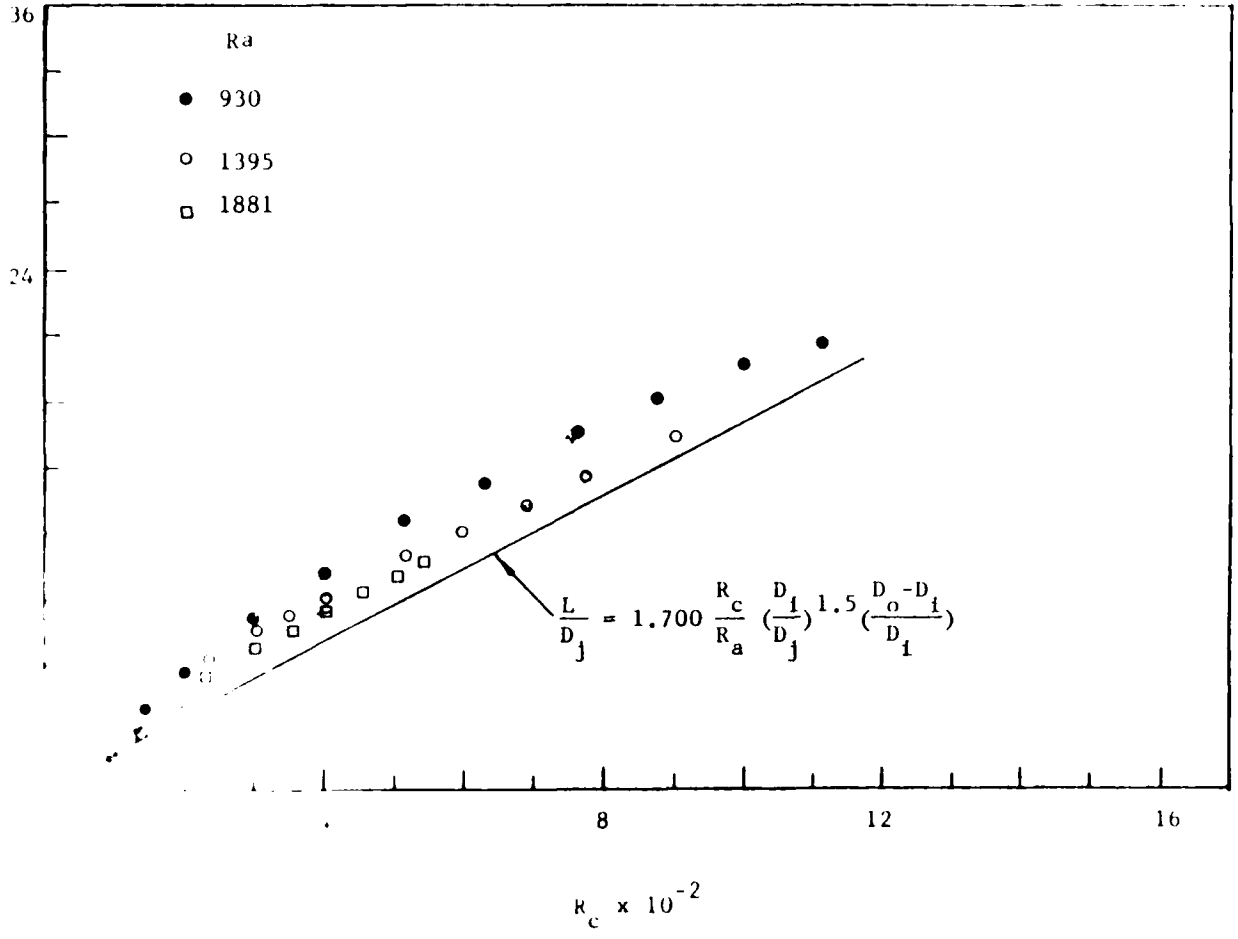
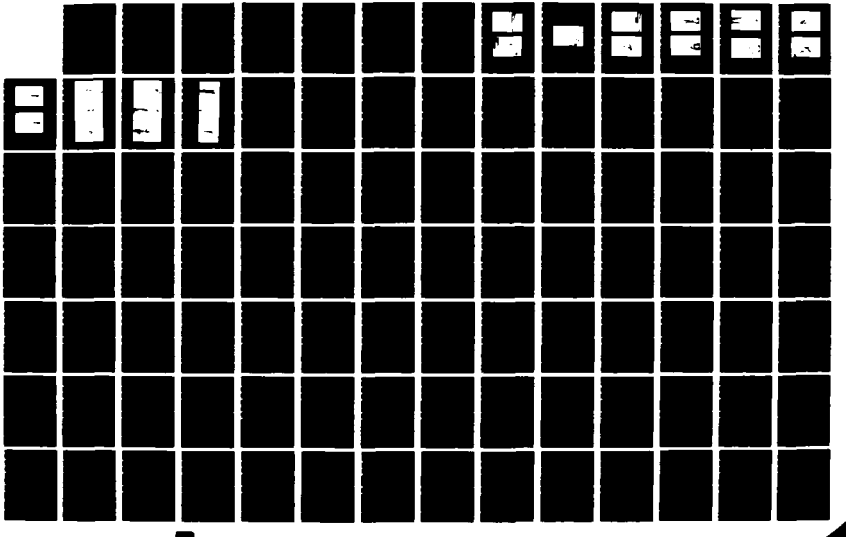


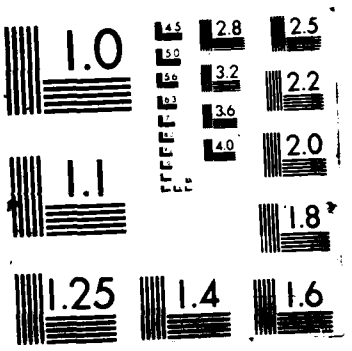

Fig. 7b. Axial location of the [illegible] for Test II - cold reacting flow.




...t the forward stagnation point, $\frac{L}{D_j}$,
...ld reacting flow.

AD-A186 490 UNITED STATES AIR FORCE RESEARCH INITIATION PROGRAM 08/11
1984 RESEARCH REPORTS (U) SOUTHEASTERN CENTER FOR
ELECTRICAL ENGINEERING EDUCATION INC S W D PEELE
UNCLASSIFIED MAY 86 AFOSR-TR-87-1721 F49620-82-C-0035 F/G 15/1 NL




1.0
1.1
1.25
1.4
1.6
1.8
2.0
2.2
2.5
2.8
3.2
3.6
4.0
4.5
5.0
5.6
6.3
7.1

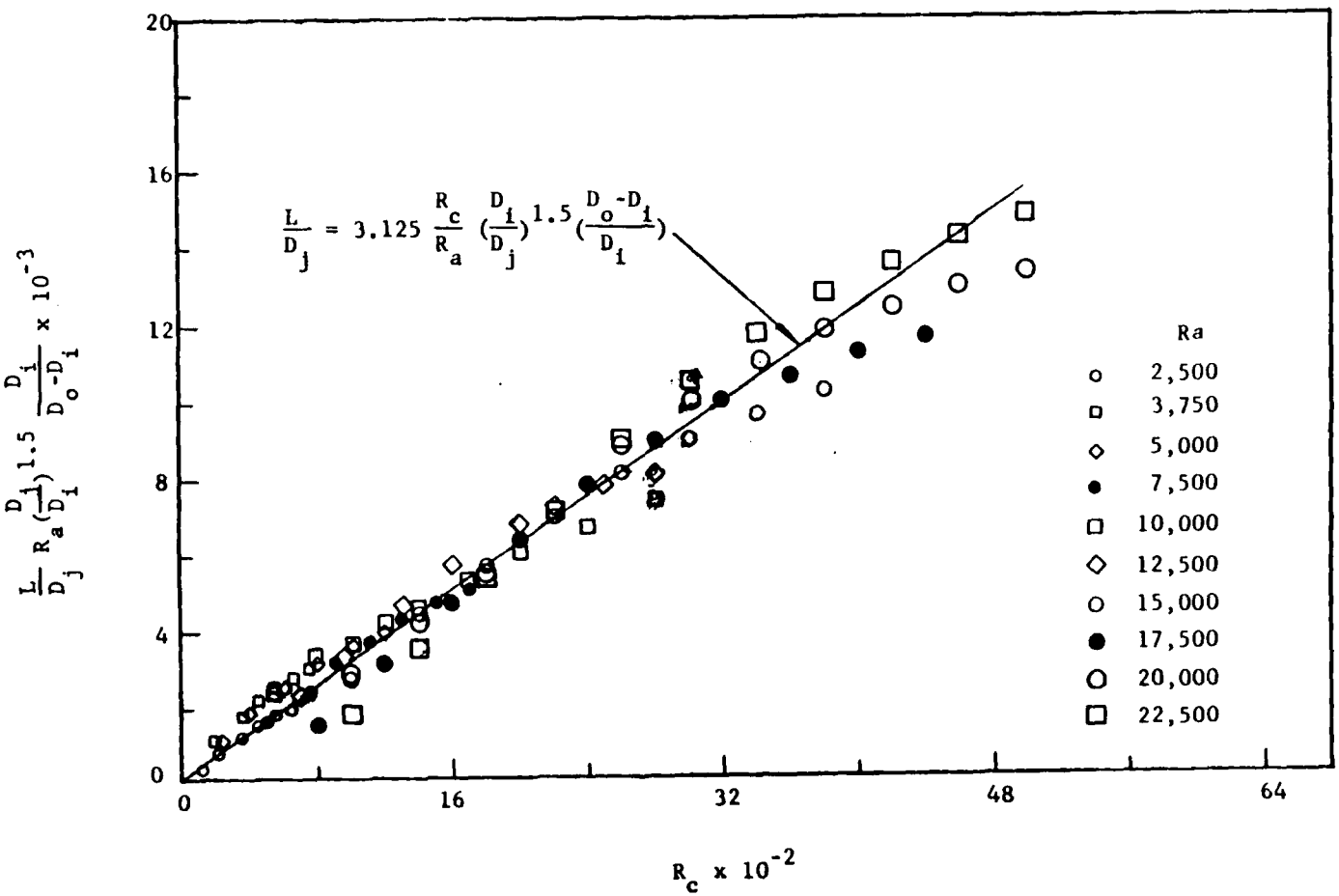



Fig. 7d. Axial location of the forward stagnation points, $\frac{L}{D_j}$, for data in reference 27.

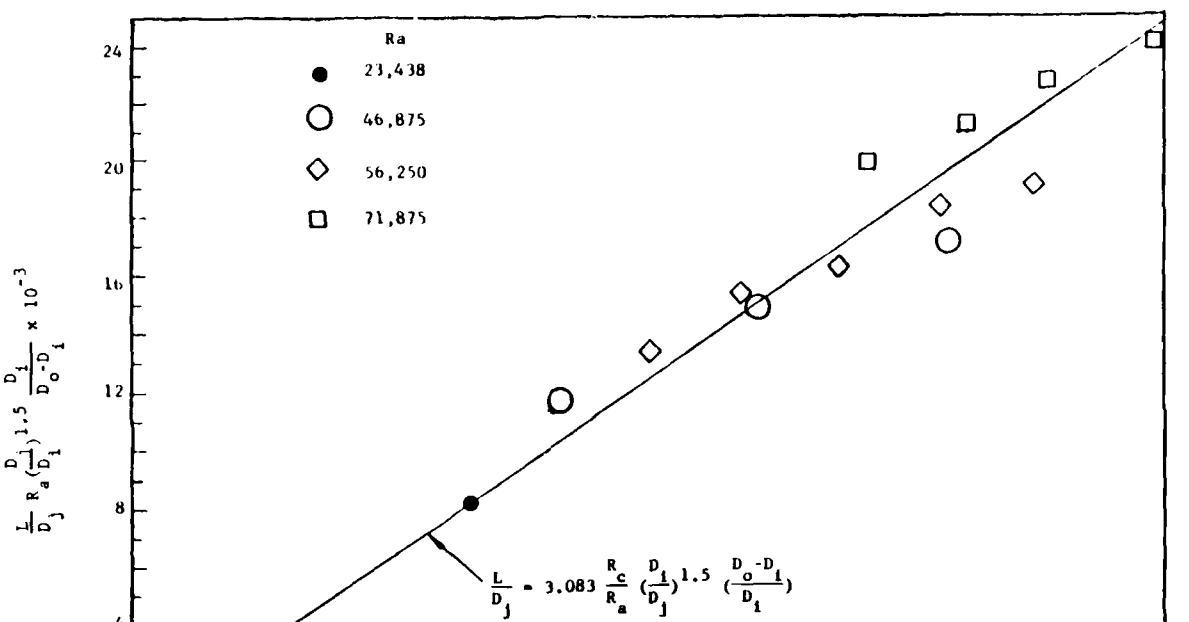



Fig. 7e. Axial location of the forward stagnation points, $\frac{L}{D_j}$, for Namazian's data (Ref. 7).

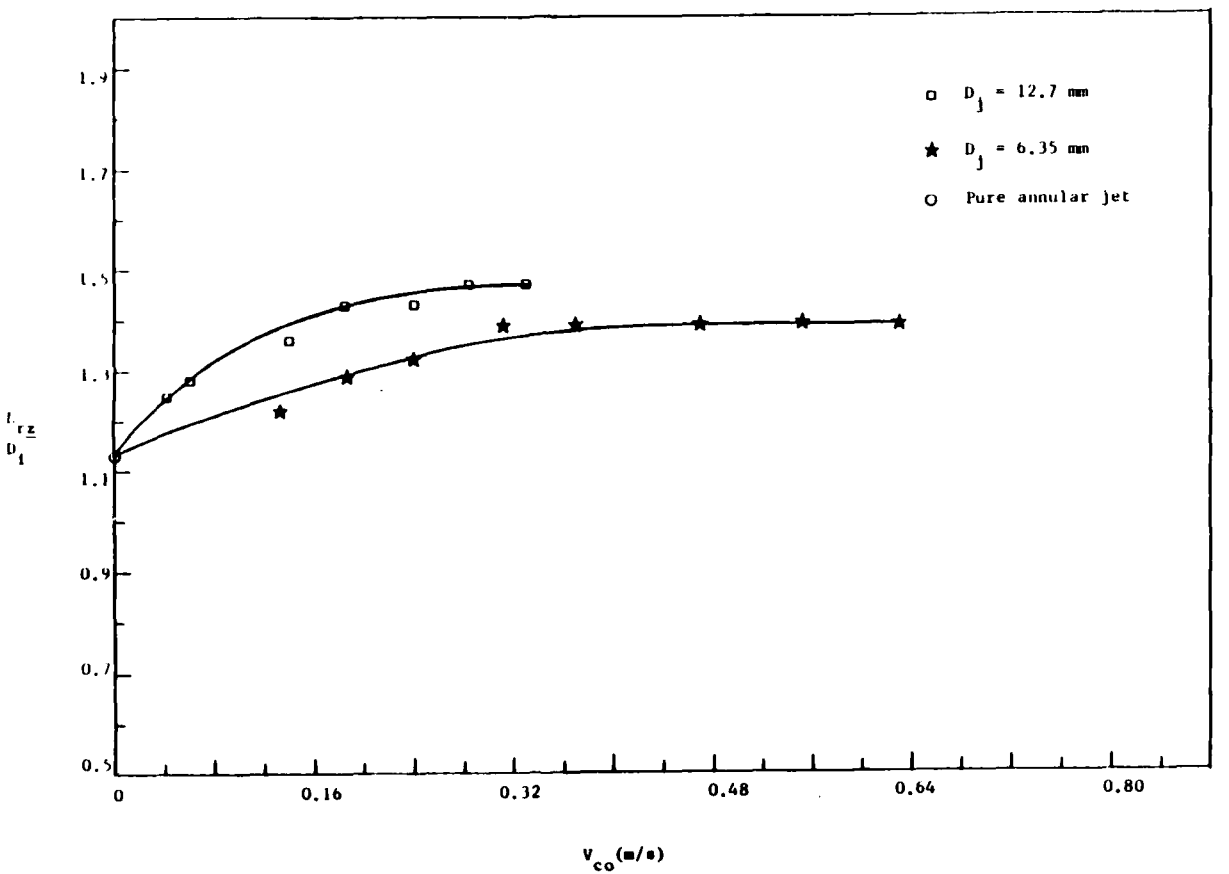



Fig. 8. The length of the recirculation zone, $\frac{L_{rz}}{D_j}$, vs. the exit velocity of the central jet, $V_{co}$, at the annular air velocity, $V_{ao}$, equal to 1.0793 m/s for Test I.

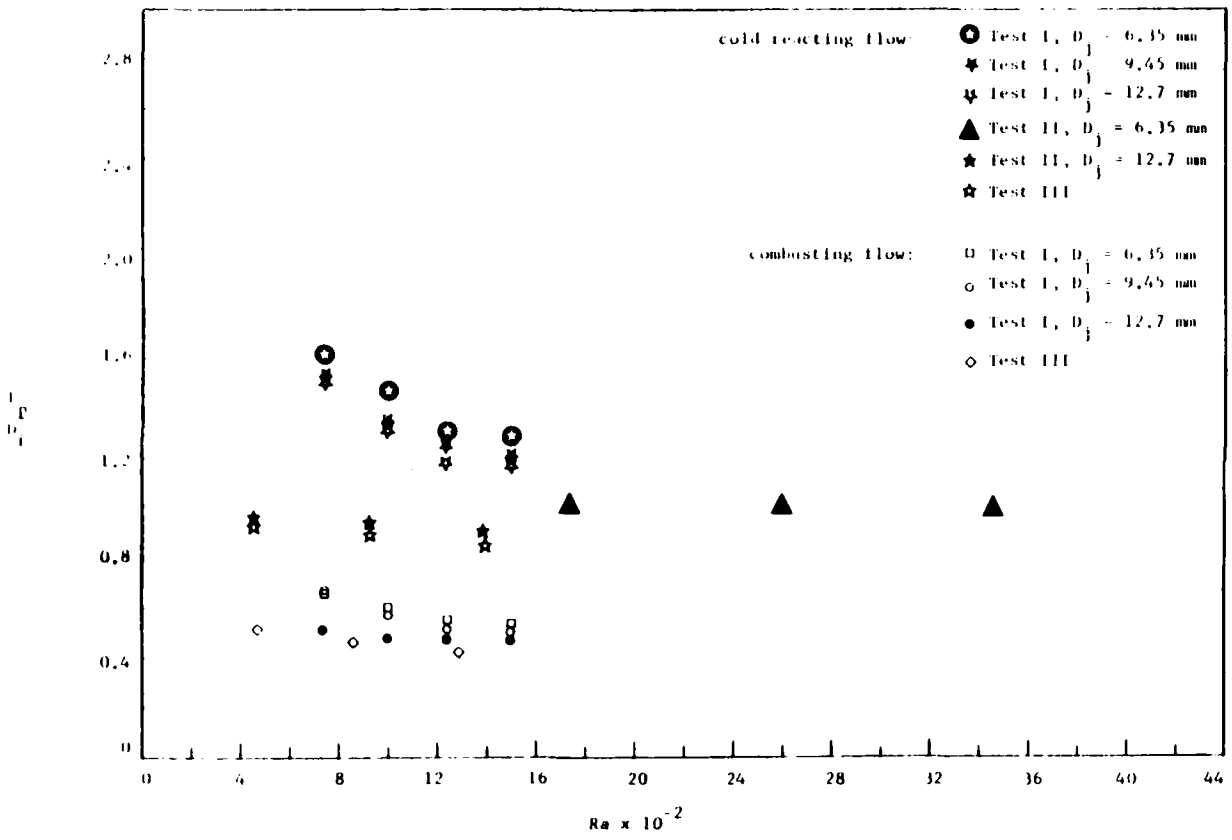



Fig. 9. Penetration length, $\frac{L_p}{D_1}$, vs. annular air Reynolds number, $R_a$, for the cold reacting flow and combusting flow (attached flame only).

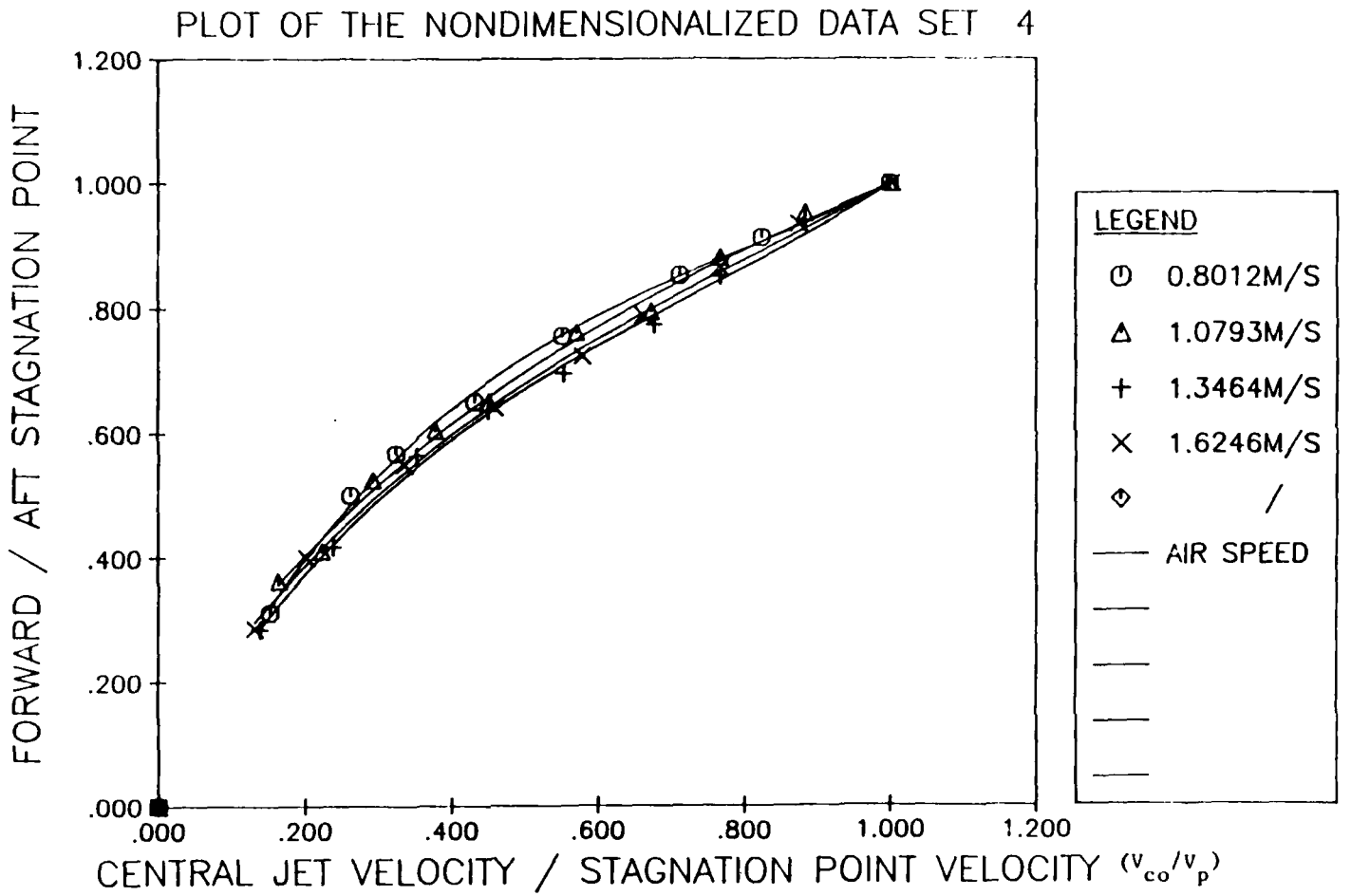



Fig. 10. Plot of $L/L_{rz}$ versus $V_{co}/V_p$ for Test I with $D_j$ = 6.35 mm - cold reacting flow.

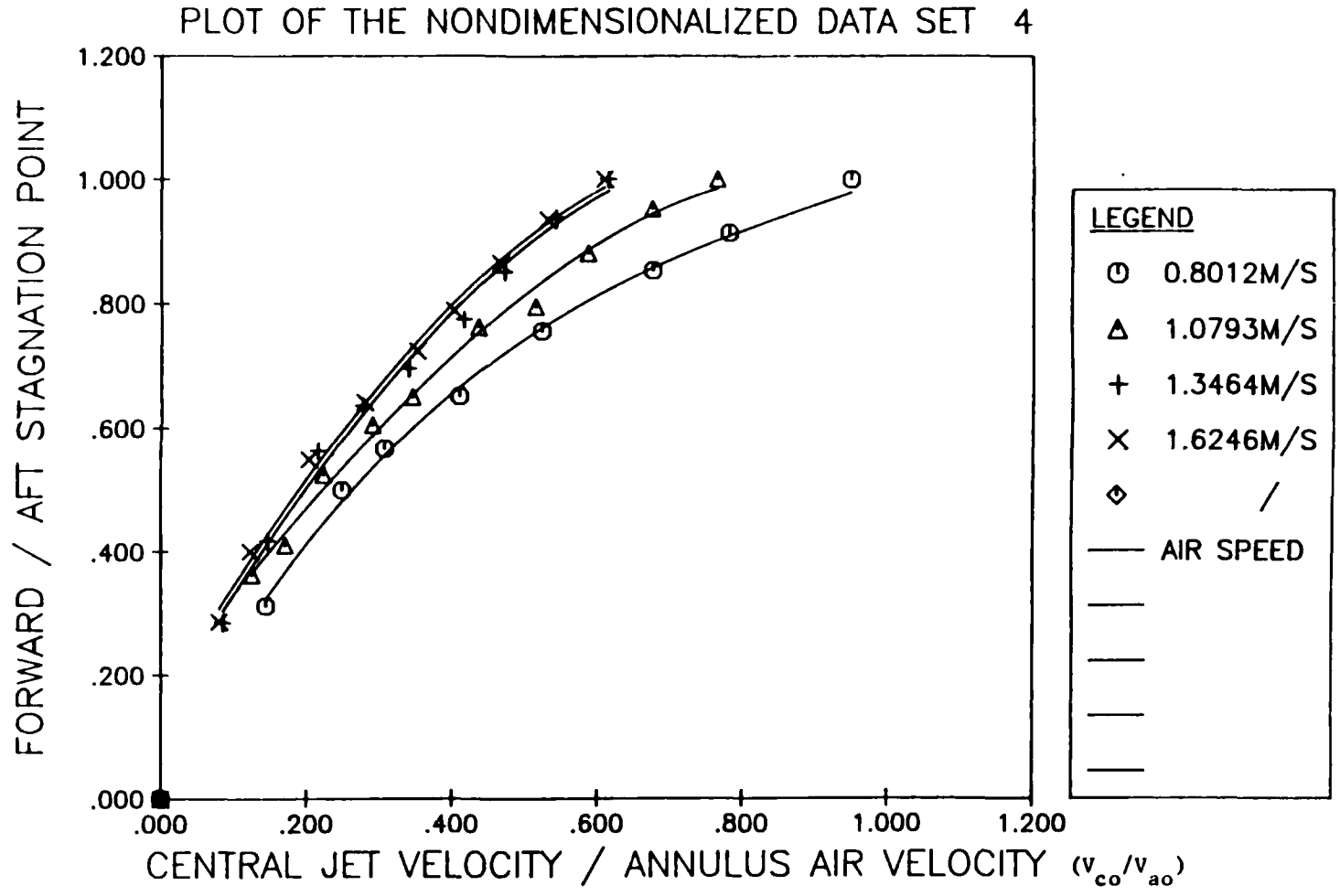



Fig. 11. Plot $L/L_{rz}$ versus $V_{co}/V_{ao}$ for Test I with $D_j$ = 6.35 mm - cold reacting flow.

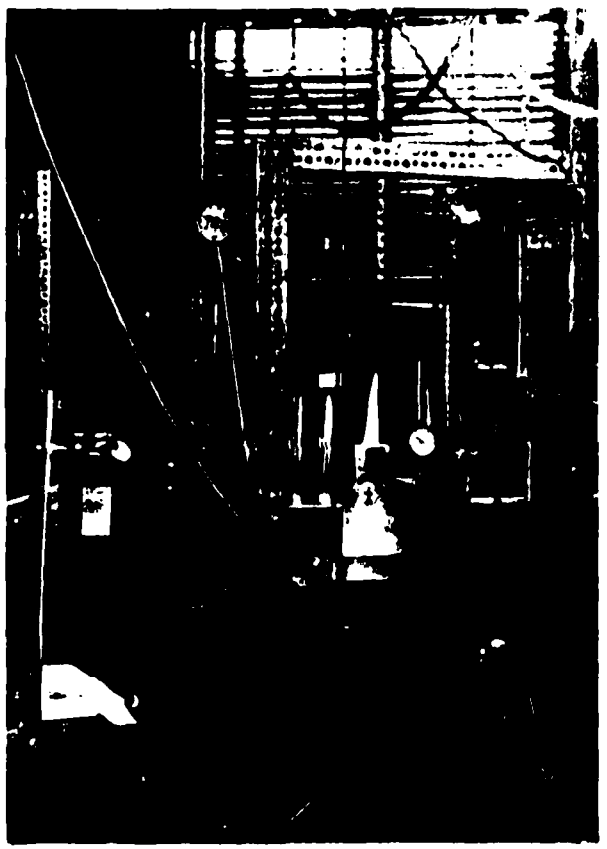


Plate 1a. Photograph showing experimental set-up.

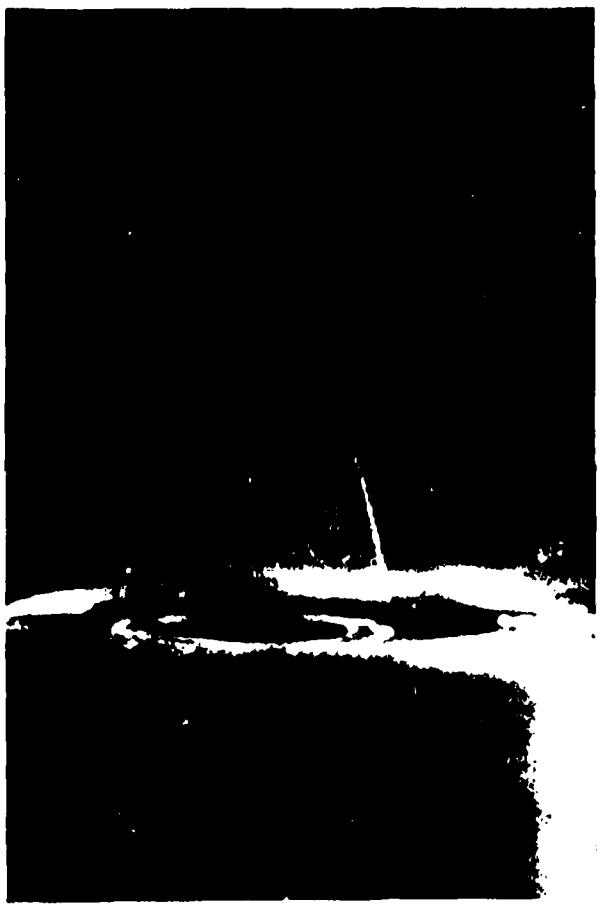


Plate 1b. Photograph of sheet-lighted cold flow for Test 111; air velocity 0.4821 m/sec, fuel velocity 0.0076 m/sec.



Plate 1c. Photograph showing the measurement of the length of the recirculation zone for pure annular air flow.



Plate 2a. Photograph of sheet-lighted cold flow for Test I; air velocity 0.534 m/sec, fuel velocity 0.111 m/sec, and $D_j$ = 12.7 mm

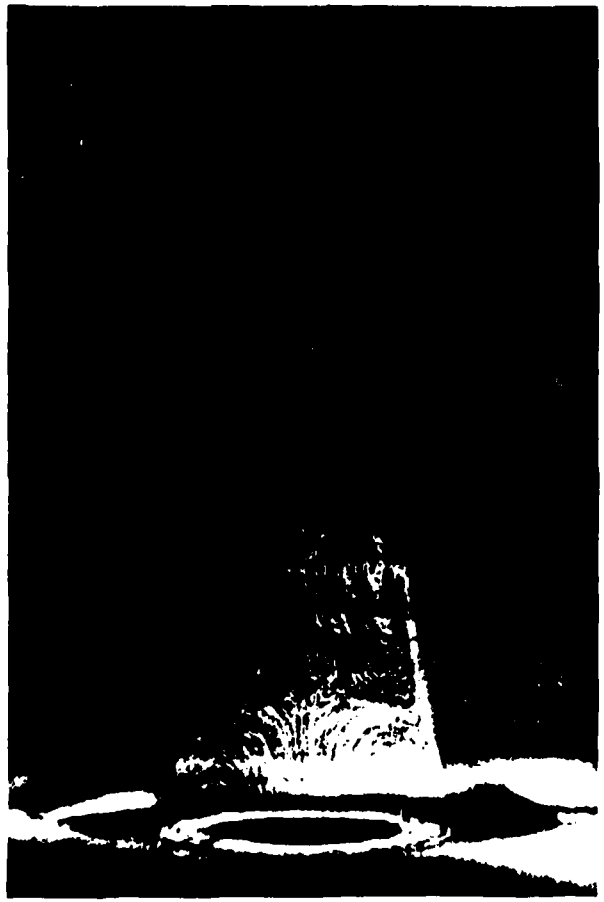


Plate 2b. Photograph of sheet-lighted cold flow for Test III; air velocity 0.964 m/sec and fuel velocity 0.050 m/sec.



Plate 3a. Photograph of sheet-lighted cold flow for Test I; air velocity 0.801 m/sec, fuel velocity 0.236 m/sec, and $D_j$ = 9.45 mm.



Plate 3b. Photograph of sheet-lighted cold flow for Test I; air velocity 1.892 m/sec, fuel velocity 0.279 m/sec and $D_j$ = 12.7 mm.



Plate 4a. Photograph of sheet-lighted cold flow for Test I; air velocity 0.401 m/sec, fuel velocity 0.201 m/sec, and $D_j$ = 12.7 mm

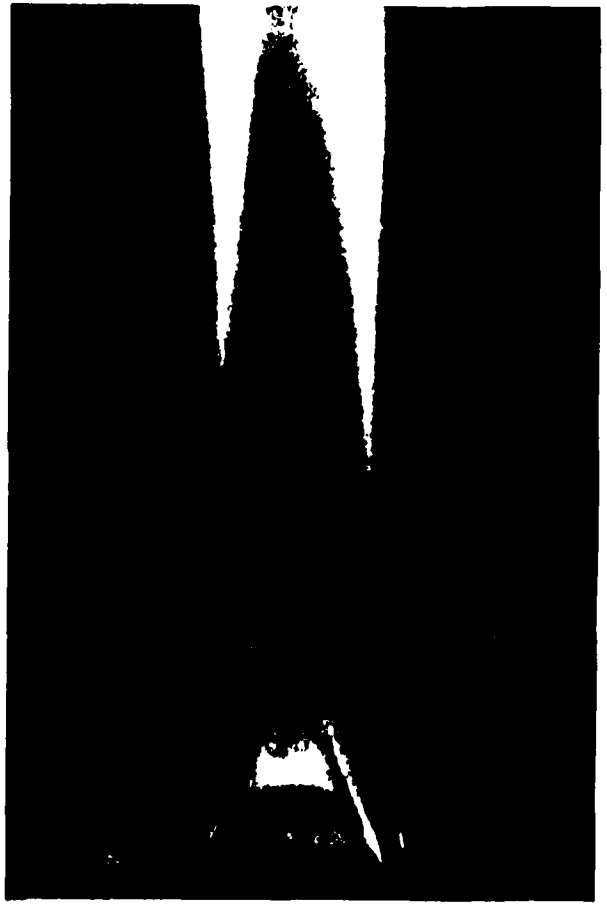


Plate 4b. Photograph of sheet-lighted combusting flow with filter for Test III; air velocity 0.964 m/sec, fuel velocity 0.050 m/sec.



Plate 5a. Photograph of combusting flow (no sheet-lighting) for Test I; air velocity 1.08 m/sec, fuel velocity 0.0258 m/sec.



Plate 5b. Photograph of sheet-lighted flow with filter for same conditions as in Plate 5a.



Plate 6a. Photograph of combusting flow (no sheet-lighting) for Test 1; air velocity 1.76 m/sec, fuel velocity 0.0527 m/sec, and $D_j$ = 9.55 mm.

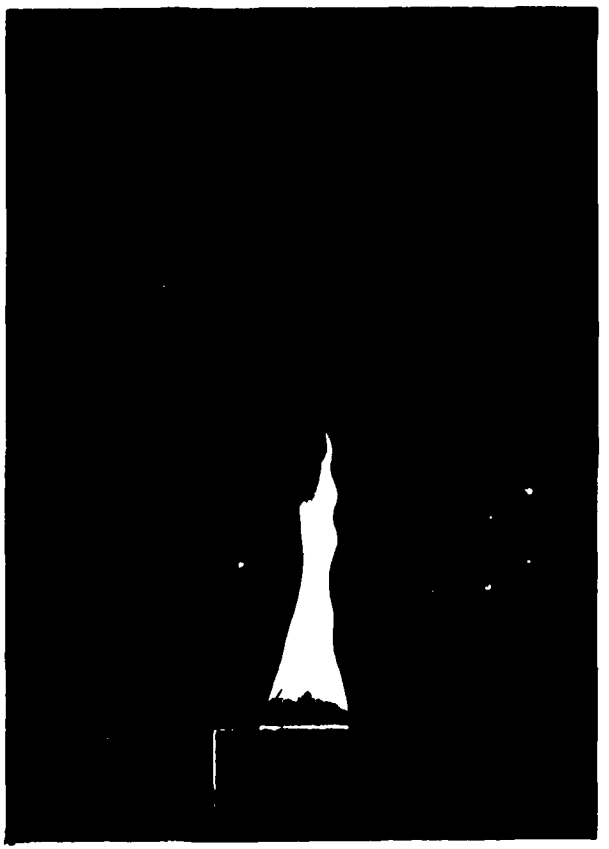


Plate 6b. Photograph of combusting flow with sheet-lighting for same conditions as in Plate 6a.

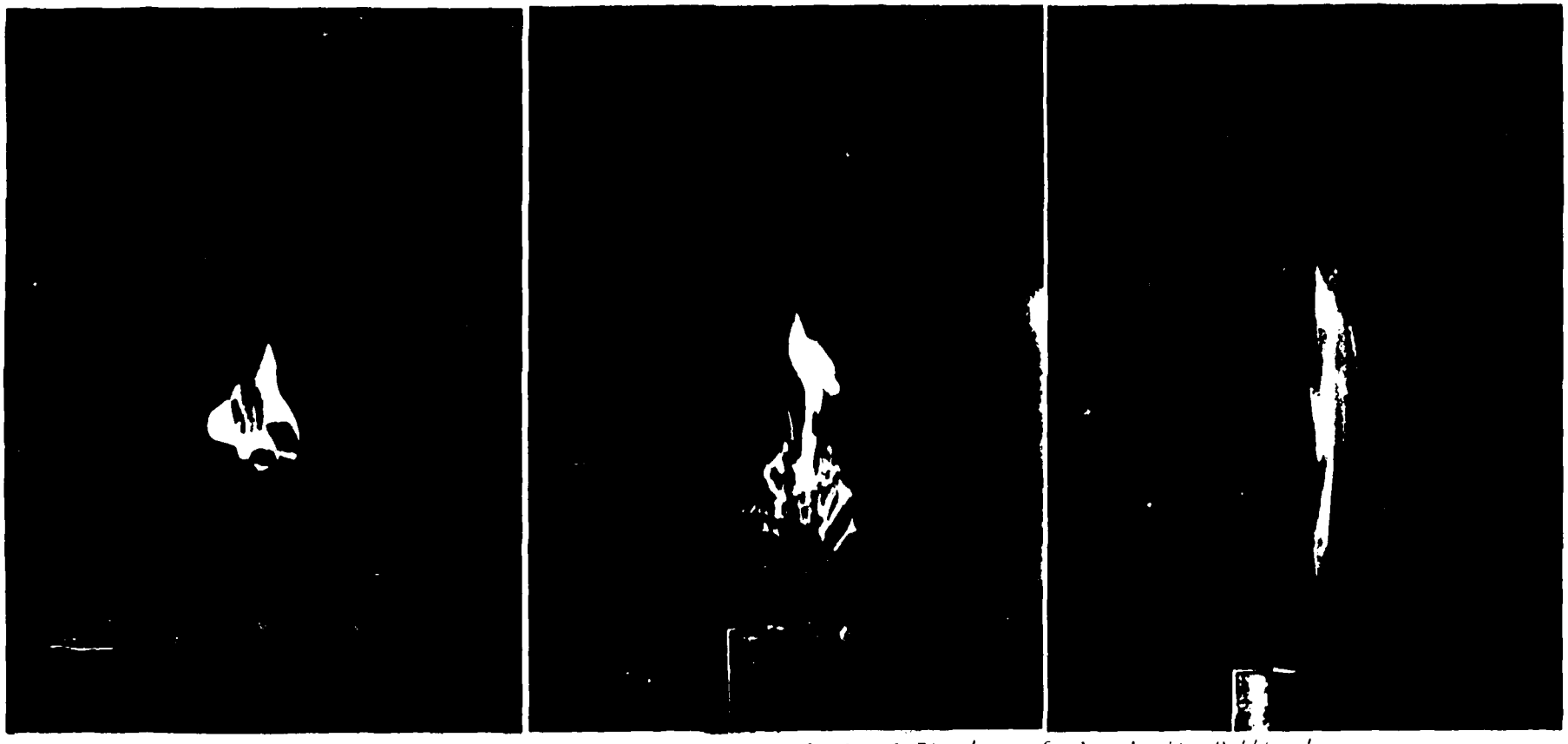


Plate 7. Photographs of detached flame for Test I; air velocity 1.76 m/sec, fuel velocity 0.446 m/sec, and $D_j$ = 9.45 mm. Plate 7a is without laser sheet-lighting; Plate 7b is with sheet-lighting; Plate 7c is with sheet-lighting and filter.

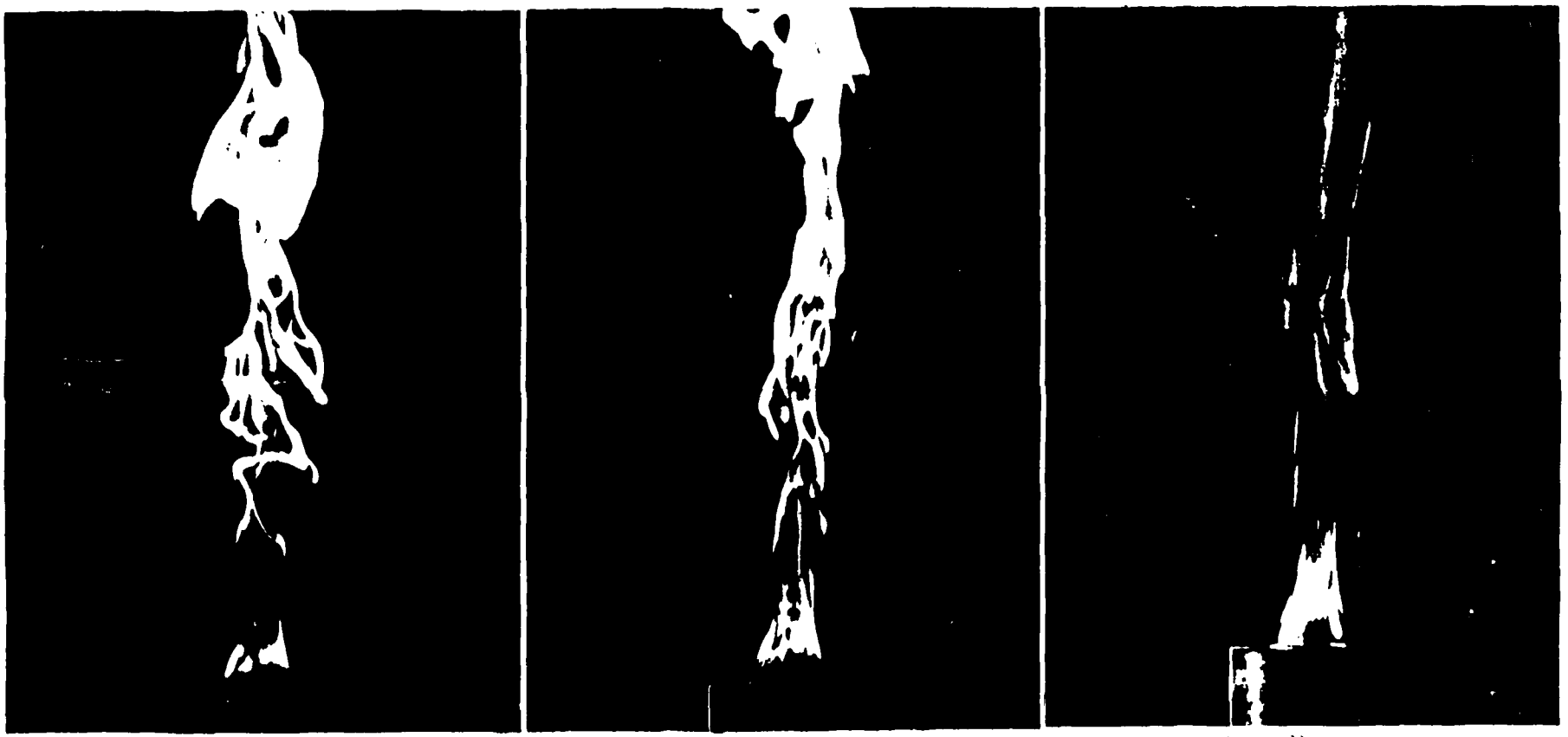
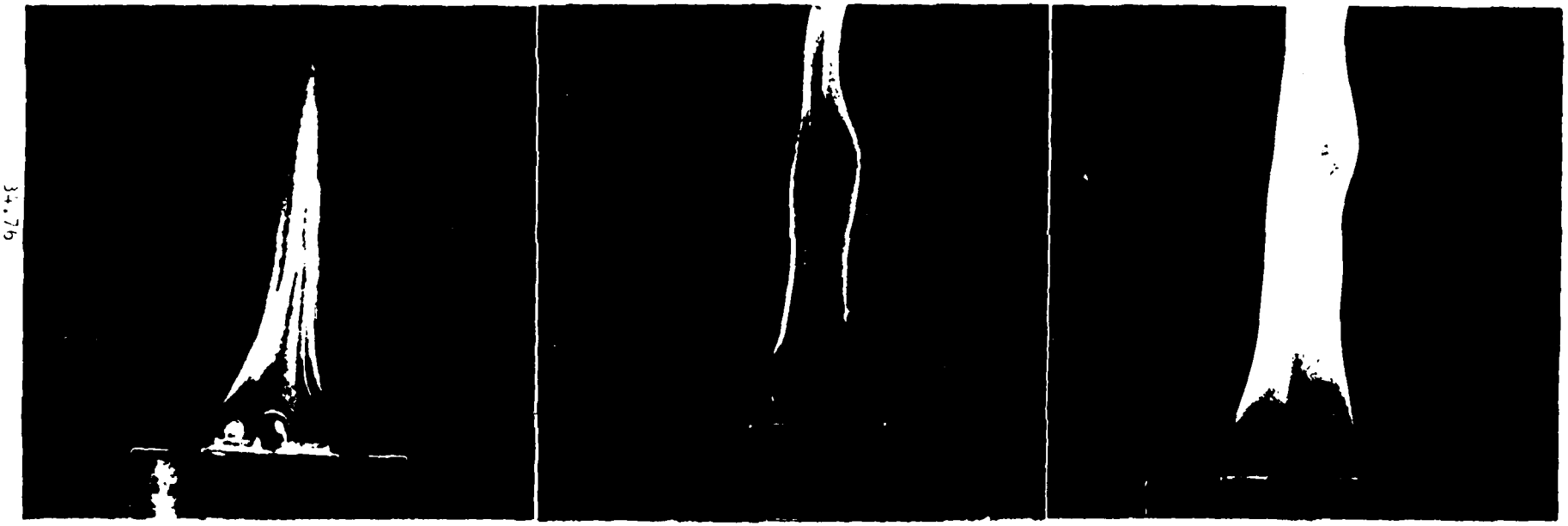


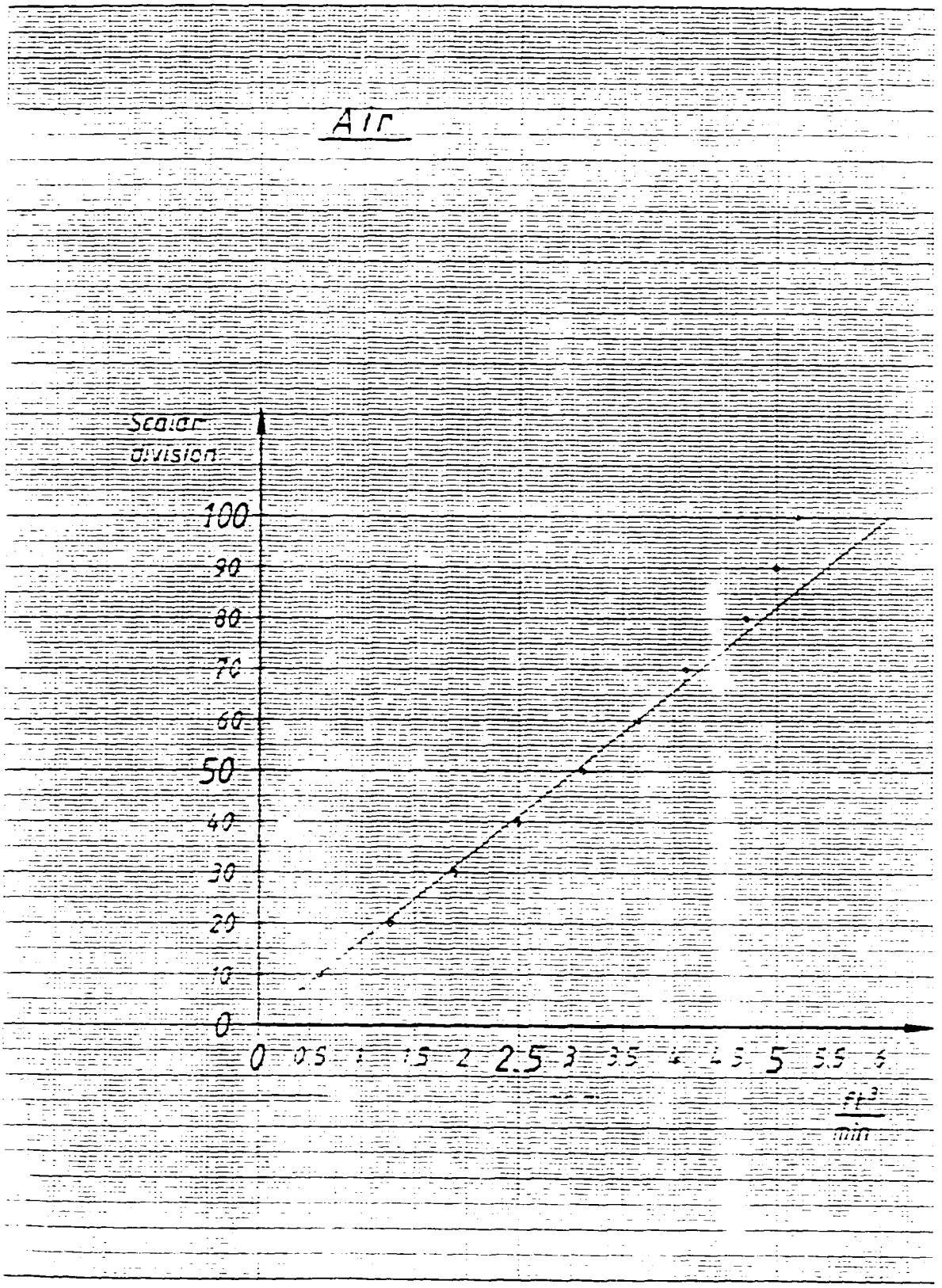
Plate 8. Photographs of reattached flame for Test I; air velocity 1.76 m/sec (same as in Plate 7), fuel velocity 0.700 m/sec, and $D_j$ = 9.45 mm. Plate 8a is without laser sheet-lighting; Plate 8b is with sheet-lighting; Plate 8c is with sheet-lighting and filter.



34.76

Plate 9. Photographs illustrating the effect of $D_j$ for similar flow conditions. Flame is sheet-lighted and nozzles are Test I. Plate 9a, the air velocity is 1.08 m/sec, the fuel velocity is 0.142 m/sec and $D_j$ = 6.35 mm. Plate 9b, the air velocity is 1.08 m/sec, the fuel velocity is 0.140 m/sec and $D_j$ = 9.45 mm. Plate 9c, the air velocity is 1.08 m/sec, the fuel velocity is 0.138 m/sec and $D_j$ = 12.7 mm.

Appendix A: Calibration Curve of the [illegible]meter
for the Annular Air Flow


Air
Scalar division
100
90
80
70
60
50
40
30
20
10
0
0 0.5 1 1.5 2 2.5 3 3.5 4 4.5 5 5.5 6
ft³/min

```
C            IF ITYP=3,PUTS OUT LEAST SQUARE FIT WITHOUT PLOTTING
C            IF ITYP=4,PUTS OUT LEAST SQUARE FIT WITH PLOTTING.
C
      DATA IM,ITYP/5,4/
      CALL DRIVE(IM,ITYP)
      STOP
      END
C
C     ******************************************************************
C
      SUBROUTINE DRIVE(IM,ITYP)
C
C     DRIVE
C     *****
C
C     CONTROL THE FLOW OF THE WHOLE PROGRAM
C
C     SUBROUTINE CALLED
C     *****************
C
C     VARIABLES
C     *********
C
C     IM  --NUMBER OF THE EXPERIMENTAL DATAA SETS
C     ITYP--VALUE OF ITYP CONTROLS THE PRINTOUT(SEE MAIN PROGRAM)
C     N   --NUMBER OF MEASUREMENT POINTS FOR EACH EXPERIMENTAL DATA SET
C     SCALEA--SCALE READING OF FLOWMETER FOR AIR
C     T    --TEMPERATURE OF THE LAB('C)
C     AREIN--AREA OF INNER NOZZLE(IN**2)
C     AREOT--AREA OF OUTER NOZZLE(IN**2)
C     WFUM --WEIGHT OF FUEL MOLECULE,FOR PROPANE,WFUM=44.097
C     HEIMAX,HEIF--MAXIMUM HEIGHT AND HEIGHT OF FUEL JET,
C                  RESPECTIVELY (IN)
C     SCALFM,SCALEF--MAXIMUM SCALE READING AND SCALE READING OF
C                  FLOWMETER FOR FUEL
C     P,PM--FUEL GAUGE PRESSURE AT FLOWMETER,OR FOR PENETRATION (KPA)
C     VORL,VORR--HEIGHTS OF LEFT,RIGHT VORTICES (IN)
C
      DIMENSION M(5),X(100,10),Y(100,10)
      COMMON /VALUE2/ X,Y
      DATA X,Y /1000*0.0,1000*0.0/
C
      DO 500 I1=1,IM
      READ(5,*) N,SCALEA,T,D1
      M(I1)=N
C
      PI=4.0*ATAN(1.0)
      D2=1.514
      D3=2.094
      AREOT=(D3*D3-D2*D2)*PI/4.0
      AREIN=PI*D1*D1/4.0
      WFUM=44.097
C
      CALL CONVT(AREIN,AREAIN,2)
      CALL CONVT(AREOT,AREAOT,2)
      CALL AIRVEL(SCALEA,AREAOT,VELAMS)
C
      READ(5,*) HEIMAX,SCALFM,PM
      CALL CENFV(SCALFM,PM,T,AREAIN,VELMAX,WFUM,2)
      DO 10 I=1,N
      READ(5,*) SCALEF,P,VORL,VORR,HEIF
      CALL NONDIM(HEIF,HEIMAX,HEINON)
      CALL CENFV(SCALEF,P,T,AREAIN,VELFMS,WFUM,2)
      CALL NONDIM(VELFMS,VELMAX,FULNON)
      CALL STORE2(FULNON,HEINON,I,I1)
      CALL CONVT(HEIF,HEIFMS,1)
```

```
      CALL CONVT(VORL,VORLFT,1)
      CALL CONVT(VORR,VORRIG,1)
      CALL STORE1(VELEMS,HEIEMS,VORLFT,VORRIG,HEINCN,I)
10 CONTINUE
      CALL RESTOR(N)
      CALL PRINT(N,AREAOT,AREAIN,VELAMS,I1)
      IF(ITYP.EQ.2) CALL DRAW(N,0,2,I1)
500 CONTINUE
      DO 600 I1=1,IM
      M=M(I1)
      IF(ITYP.GE.3) CALL FCTDET(N,I1,ITYP,IM)
600 CONTINUE
      RETURN
      END
C
C*****************************************************************
      SUBROUTINE AIRVEL(SCALE,AREAOT,VELAMS)
C
C     CALCULATION OF VELOCITY OF ANNULAR AIR FROM SCALE READING OF
C     FLOWMETER
C
C     VARIABLES
C     *********
C
C     SCALE --SCALE READING OF FLOWMETER FOR ANNULAR AIR
C     AREAOT--AREA OF OUTER(ANNULAR) NOZZLE (CM**2)
C     VELAMS--VELOCITY OF AIR (M/SEC)
C
      DIMENSION VOLFR(10)
      DATA VOLFR/0.6,1.2,1.8,2.425,3.025,3.65,4.25,4.85,5.45,6.075/
C
      DO 100 I=1,10
      IF(SCALE/10.EQ.I) THEN
      VOL=VOLFR(I)
      GO TO 200
      ENDIF
100 CONTINUE
200 AB=0.3048
      VELAMS=VOL*AB*AB*AB/60.0/AREAOT*10000.0
C     M/SEC  FT**3-->M**3 MIN-->SEC CM**2-->M**2
      RETURN
      END
C
C*****************************************************************
      SUBROUTINE CENFV(SCALE,P,T,AREAIN,VELEMS,WFUM,ISIZE)
C
C     CALCULATION OF VELOCITY OF CENTRAL FUEL JET FROM THE SCALE
C     READING OF GILMONT FLOWMETER , CATALOG NO. 1100,SIZE 1,IF
C     ISIZE=1;OR,CATALO NO. F1200,SIZE 2,IF ISIZE=2;OR,CATALOG NO.
C     F1300,SIZE 3,IF ISIZE=3.
C
C     VARIABLES
C     *********
C
C     SCALE --SCALE READING FROM FLOWMETER
C     P     --GAUGE PRESSURE AT FLOWMETER (KPA)
C     T     --TEMPERATURE INSIDE LAB (°C)
C     AREAIN--AREA OF INNER (CENTRAL)NOZZLE (CM**2)
C     VELEMS--VELOCITY OF FUEL (M/SEC)
C     WFUM  --WEIGHT OF FUEL MOLECULE,FOR PROPANE WFUM=44.097
C
C     FOR THE FORMULA USED HERE,PLEASE SEE GILMONT FLOWMETER
C     SPECIFICATION FOR SIZE 1 OR 2,OR 3.
C
      P1=101325.0+P*1000.0
      T1=T+273.15
```

Appendix B: Computer Program Run on Cyber 170

Plotting Curves $\frac{\dot{\varepsilon}}{\dot{\varepsilon}_{ref}}$ vs. $\frac{\sigma_D}{\sigma_D}$ or $\frac{\sigma_D}{\sigma_{eD}}$,

```
 (XXXX)  ACCOUNT 2314
08/05/85
10.47.34 $$$$
```

```
*** ALL JOBS AND FILES WERE LOST AT 11.45 ON 8/5/85 ***
.
** THIS COMPUTER IS LEAVING AUGUST 9, 1985.  CONVERT NOW!! **
.
$$601 07/25/85 NEWLY CONVERTED SOFTWARE FOR THE CYBER 845
$$660 07/13/85 SOFTWARE WHICH WILL BE CONVERTED LATE OR NEVER
$$650 07/13/85 NEW RELEASE OF NOS OPERATING SYSTEM
$$650 06/27/85 MODIFICATION TO READING IBM CROSS-X FILES ON THE 180
$$650 06/26/85 COPYS & USERLIB TAPES CAN BE CONVERTED ON CYBER 845
$$650 06/09/85 CARD EQUIPMENT WILL BE REMOVED BY AUGUST 9, 1985
$$650 06/21/85 CYBER 845 REMOTE JOB ENTRY SUPPORT AT CHICAGO AND TECH
$$650 06/21/85 READING CROSS-X SYSTEM FILES FROM THE 830 ON THE 845
$$651 06/20/85 CYBER 845 SRU RATES SUBSTANTIALLY REDUCED
$$650 06/17/85 PREFERRED BATCH SERVICE CLASS ON CY 8E 845
$$640 06/10/85 CPSS, CPSSX INTERACTIONS WITH RESTORE AND REPLN
$$640 06/07/85 FIRST VERSION OF CPSS-X NOW READS SYSTEM FILES
$$647 06/06/85 ATTENTION: SWITCH TO THE NEW CYBER 845 FOR COMPUTING
$$630 05/17/85 LAST DAY OF CYBER 170/730 SERVICE IS AUGUST 9, 1985
** USE "$CALL,$TTTELL" TO READ OR PRINT THE ABOVE NOTICES.
10 /XXXX,CM 03401-0010,T25.
20 FTN5,L=0.
30 LGO.
40 PROGRAM,TAPE99 (O=DAT).
50       PROGRAM DISTMG(INPUT,OUTPUT,TAPE5=INPUT,TAPE6=OUTPUT,TAPE99)
60 C
70 C      ******************************************************************
80 C
100 C     DISTMG
110 C     ******
120 C
130 C     THIS PROGRAM + DTD IN THE EXPERIMENTAL DATA OF A SLOPE-STORY
140 C     FLOOR DECK AND PRINTS OUT TABLES OF VALUES,DIFFERENCES AND ANY
150 C     PLOTTING FOR THE DATA.
160 C
170 C     CURRENT DIM
180 C     ***********
190 C
200 C     REAL
210 C
220 C
230 C     VARIABLES
240 C     *********
250 C
260 C     IM  NUMBER OF THE EXPERIMENTAL DATA SETS
270 C     DIMENSION DIM(10),D(40,10),A(10,10),B(10),C(10)
280 C               FOR (A) DISTANCE OF AXE AND FUEL,AND HEIGHTS OF FUEL JET
290 C               AND D, DISTANCE FROM AXE
300 C               TO DIMENSION A,B AND C FOR A TABLE OF VALUES AND DIFFERENCES
```

```
C            IF ITYP=3,PUTS OUT LEAST SQUARE FIT WITHOUT PLOTTING
C            IF ITYP=4,PUTS OUT LEAST SQUARE FIT WITH PLOTTING.
C
      DATA IM,ITYP/5,4/
      CALL DRIVE(IM,ITYP)
      STOP
      END
C
C     ******************************************************************
C
      SUBROUTINE DRIVE(IM,ITYP)
C
C     DRIVE
C     *****
C
C     CONTROL THE FLOW OF THE WHOLE PROGRAM
C
C     SUBROUTINE CALLED
C     *****************
C
C     VARIABLES
C     *********
C
C     IM  --NUMBER OF THE EXPERIMENTAL DATAA SETS
C     ITYP--VALUE OF ITYP CONTROLS THE PRINTOUT(SEE MAIN PROGRAM)
C     N   --NUMBER OF MEASUREMENT POINTS FOR EACH EXPERIMENTAL DATA SET
C     SCALEA--SCALE READING OF FLOWMETER FOR AIR
C     T    --TEMPERATURE OF THE LAB('C)
C     AREIN--AREA OF INNER NOZZLE(IN**2)
C     AREOT--AREA OF OUTER NOZZLE(IN**2)
C     WFUM --WEIGHT OF FUEL MOLECULE,FOR PROPANE,WFUM=44.097
C     HEIMAX,HEIF--MAXIMUM HEIGHT AND HEIGHT OF FUEL JET,
C                  RESPECTIVELY (IN)
C     SCALFM,SCALEF--MAXIMUM SCALE READING AND SCALE READING OF
C                  FLOWMETER FOR FUEL
C     P,PM--FUEL GAUGE PRESSURE AT FLOWMETER,OR FOR PENETRATION (KPA)
C     VORL,VORR--HEIGHTS OF LEFT,RIGHT VORTICES (IN)
C
      DIMENSION N(5),X(100,10),Y(100,10)
      COMMON /VALUE2/ X,Y
      DATA X,Y /1000*0.0,1000*0.0/
C
      DO 500 I1=1,IM
      READ(5,*) N,SCALEA,T,D1
      N(I1)=N
C
      PI=4.0*ATAN(1.0)
      D2=1.514
      D3=2.094
      AREOT=(D3*D3-D2*D2)*PI/4.0
      AREIN=PI*D1*D1/4.0
      WFUM=44.097
C
      CALL CONVT(AREIN,AREAIN,2)
      CALL CONVT(AREOT,AREAOT,2)
      CALL AIRVEL(SCALEA,AREAOT,VELAMS)
C
      READ(5,*) HEIMAX,SCALFM,PM
      CALL CENFV(SCALFM,PM,T,AREAIN,VELMAX,WFUM,2)
      DO 10 I=1,N
      READ(5,*) SCALEF,P,VORL,VORR,HEIF
      CALL NONDIM(HEIF,HEIMAX,HEINON)
      CALL CENFV(SCALEF,P,T,AREAIN,VELFMS,WFUM,2)
      CALL NONDIM(VELFMS,VELMAX,FULNON)
      CALL STORE2(FULNON,HEINON,I,I1)
      CALL CONVT(HEIF,HEIFMS,1)
```

```
      970         CALL CONVT(VORL,VORLFT,1)
      980         CALL CONVT(VORR,VORRIG,1)
      990         CALL STORE1(VELEMS,HEIEMS,VORLFT,VORRIG,HEINON,I)
     1000 10      CONTINUE
     1010         CALL RESTOR(N)
     1020         CALL PRINT(N,AREAOT,AREAIN,VELAMS,I1)
     1030         IF(ITYP.EQ.2) CALL DRAW(N,0,2,I1)
     1040 500     CONTINUE
     1050          DO 600 I1=1,IM
     1060          N=M(I1)
     1070          IF(ITYP.GE.3) CALL FCTDET(N,I1,ITYP,IM)
     1080 600      CONTINUE
     1090         RETURN
     1100         END
     1110 C
     1120 C       ********************************************************************
     1130         SUBROUTINE AIRVEL(SCALE,AREAOT,VELAMS)
     1140 C
     1150 C       CALCULATION OF VELOCITY OF ANNULAR AIR FROM SCALE READING OF
     1160 C       FLOWMETER
     1170 C
     1180 C       VARIABLES
     1190 C       *********
     1200 C
     1210 C       SCALE --SCALE READING OF FLOWMETER FOR ANNULAR AIR
     1220 C       AREAOT--AREA OF OUTER(ANNULAR) NOZZLE (CM**2)
     1230 C       VELAMS--VELOCITY OF AIR (M/SEC)
     1240 C
     1250         DIMENSION VOLFR(10)
     1260         DATA VOLFR/0.6,1.2,1.8,2.425,3.025,3.65,4.25,4.85,5.45,6.075/
     1270 C
     1280         DO 100 I=1,10
     1290         IF(SCALE/10.EQ.I) THEN
     1300         VOL=VOLFR(I)
     1310         GO TO 200
     1320         ENDIF
     1330 100     CONTINUE
     1340 200     AB=0.3048
     1350         VELAMS=VOL*AB*AB*AB/60.0/AREAOT*10000.0
     1360 C       M/SEC  FT**3-->M**3 MIN-->SEC CM**2-->M**2
     1370         RETURN
     1380         END
     1390 C
     1400 C       ********************************************************************
     1410         SUBROUTINE CENFV(SCALE,P,T,AREAIN,VELEMS,WFUM,ISIZE)
     1420 C
     1430 C       CALCULATION OF VELOCITY OF CENTRAL FUEL JET FROM THE SCALE
     1440 C       READING OF GILMONT FLOWMETER , CATALOG NO. 1100,SIZE 1,IF
     1450 C       ISIZE=1;OR,CATALOG NO. F1200,SIZE 2,IF ISIZE=2;OR,CATALOG NO.
     1460 C       F1300,SIZE 3,IF ISIZE=3.
     1470 C
     1480 C       VARIABLES
     1490 C       *********
     1500 C
     1510 C       SCALE --SCALE READING FROM FLOWMETER
     1520 C       P     --GAUGE PRESSURE AT FLOWMETER (KPA)
     1530 C       T     --TEMPERATURE INSIDE LAB (°C)
     1540 C       AREAIN--AREA OF INNER (CENTRAL)NOZZLE (CM**2)
     1550 C       VELEMS--VELOCITY OF FUEL (M/SEC)
     1560 C       WFUM  --WEIGHT OF FUEL MOLECULE,FOR PROPANE WFUM=44.097
     1570 C
     1580 C       FOR THE FORMULA USED HERE,PLEASE SEE GILMONT FLOWMETER
     1590 C       SPECIFICATION FOR SIZE 1 OR 2,OR 3.
     1600 C
     1610         P1=101325.0+P*1000.0
     1620         T1=T+273.15
```

```
2290 C      VALMES--THE VALUE TO BE NONDIMENSIONALIZED
2300 C      VALMAX--THE REFERENCE VALUE WITH RESPECT TO WHICH
2310 C              VALMES WILL BE NONDIMENSIONALIZED
2320 C      VALNON--NONDIMENSIONALIZED VARIABLE
2330 C
2340        VALNON=VALMES/VALMAX
2350        RETURN
2360        END
2370 C
2380 C      ************************************************************
2390        SUBROUTINE STORE2(FULNON,HEINON,I,I1)
2400 C
2410 C      STORE HERE ALL THE NONDIMENSIONALIZED VARIABLES WHICH
2420 C      WILL BE PLOTTED.
2430 C
2440 C      VARIABLES
2450 C      *********
2460 C
2470 C      FULNON--FUEL VELOCITY
2480 C      HEINON--HEIGHT OF CENTRAL JET
2490 C      VORNON--MEAN HEIGHT OF VORTICES
2500 C      I       --NUMBER OF ACTUAL DATA SET TO BE STORED
2510 C
2520 C      COMMON
2530 C      ******
2540 C      VALUE2--X(MAXDAT,10) : X-VALUE FOR THE SCATTERGRAMS AND
2550 C                             THE CURVE FITTINGS
2560 C              Y(MAXDAT,10) : Y-VALUE FOR THE SAME THING AS ABOVE
2570 C
2580        PARAMETER(MAXDAT=100)
2590        DIMENSION X(MAXDAT,10),Y(MAXDAT,10)
2600        COMMON / VALUE2 / X,Y
2610        X(I,I1)=FULNON
2620        Y(I,I1)=HEINON
2630        RETURN
2640        END
2650 C
2660 C      ************************************************************
2670        SUBROUTINE STORE1(VELFUL,HEIMS,VORLMS,VORRMS,PEN,I)
2680 C
2690 C      STORE ALL THE PHYSICAL VALUES IN THE COMMON 'SAVE1'
2700 C
2710 C      VARIABLES
2720 C      *********
2730 C
2740 C      VELFUL--VELOCITY OF THE FUEL
2750 C      HEIMS --HEIGHT OF THE CENTRAL JET
2760 C      VORLMS--HEIGHT OF THE LEFT VORTEX
2770 C      VORRMS--HEIGHT OF THE RIGHT VORTEX
2780 C      PEN   --PENETRATION
2790 C      I     --NUMBER OF ACTUAL DATA SET TO BE STORED
2800 C
2810 C      COMMON
2820 C      ******
2830 C
2840 C      SAVE1(5,MAXDAT)--CONTAIN ALL THE PHYSICAL DATA TO BE PRINTED
2850 C
2860        PARAMETER(MAXDAT=100)
2870        DIMENSION SAVE1(5,MAXDAT)
2880        COMMON / VALUE1 /SAVE1
2890        SAVE1(1,I)=VELFUL
2900        SAVE1(2,I)=HEIMS
2910        SAVE1(3,I)=VORLMS
2920        SAVE1(4,I)=VORRMS
2930        SAVE1(5,I)=PEN
2940        RETURN
```

```
2950        END
2960 C      ****************************************************************
2970        SUBROUTINE RESTOR(MAX)
2980 C
2990 C      REARRANGE THE EXPERIMENTAL DATA STORED IN COMMON 'VALUE1'
3000 C      SUCH THAT THE VELOCITY VALUES ARE IN AN INCREASING ORDER.
3010 C
3020 C      VARIABLES
3030 C      *********
3040 C
3050 C      MAX--NUMBER OF DATA SETS STORED IN VALUE1
3060 C
3070 C      COMMON
3080 C      ******
3090 C
3100 C      VALUE1--SAVE1(5,MAXDAT) : THE EXPERIMENTAL DATA TO BE PRINTED
3110 C
3120        PARAMETER(MAXDAT=100)
3130        DIMENSION SAVE1(5,MAXDAT) ,TEMP(5)
3140        LOGICAL LOG
3150        COMMON / VALUE1 /SAVE1
3160        DO 500 I=1,1000
3170         LOG=.TRUE.
3180         DO 100 J=2,MAX
3190          IF(SAVE1(1,J).LT.SAVE1(1,J-1)) THEN
3200            DO 10 K=1,5
3210             TEMP(K)=SAVE1(K,J)
3220             SAVE1(K,J)=SAVE1(K,J-1)
3230             SAVE1(K,J-1)=TEMP(K)
3240 10       CONTINUE
3250            LOG=.FALSE.
3260          ENDIF
3270 100     CONTINUE
3280          IF(LOG) GOTO 510
3290 500     CONTINUE
3300 510    CONTINUE
3310        RETURN
3320        END
3330 C      ****************************************************************
3340        SUBROUTINE PRINT(MAX,AREAOT,AREAIN,VELAIR,J)
3350 C
3360 C      CREATE A TABLE OF VALUES FOR EACH EXPERIMENTAL DATA SET
3370 C
3380 C      VARIABLES
3390 C      *********
3400 C
3410 C      MAX    --NUMBER OF DATA SETS STORED IN COMMON 'VALUE1'
3420 C      AREAOT-- AREA OF OUTER NOZZLE
3430 C      AREAIN--AREA OF INNER NOZZLE
3440 C      VELAIR--VELOCITY OF AIR
3450 C      I      --NUMBER OF THE ACTUAL EXPERIMENTAL SET
3460 C
3470 C      COMMON
3480 C      ******
3490 C
3500 C      VALUE1--SAVE1(5,MAXDAT) : PHYSICAL VALUES TO BE PRINTED
3510 C
3520        PARAMETER(MAXDAT=100)
3530        DIMENSION SAVE1(5,MAXDAT)
3540        CHARACTER*3 PEN
3550        COMMON / VALUE1 / SAVE1
3560        WRITE(6,'(''1'')')
3570        WRITE(6,901)
3580        WRITE(6,905) 'TABLE OF VALUES FOR EXPERIMENTAL DATA SET ',J
3590        WRITE(6,901) '*********************************************'
3600        WRITE(6,901)
```

```
      WRITE(6,901)
      WRITE(6,902) 'AREA OF OUTER NOZZLE',AREAOT, ' CM**2'
      WRITE(6,902) 'AREA OF INNER NOZZLE',AREAIN, ' CM**2'
      WRITE(6,902) 'VELOCITY OF AIR     ',VELAIR, ' M/SEC'
      WRITE(6,901)
      WRITE(6,901)
      WRITE(6,901)
      WRITE(6,903) 'VELOCITY    ','HEIGHT OF    ',
     Q             'HEIGHT OF   ','HEIGHT OF    '
      WRITE(6,903) 'OF FUEL     ','CENTRAL JET  ',
     Q             'LEFT VORTEX ','RIGHT VORTEX '
      WRITE(6,903) '[ M/SEC ]   ',' [ MM ]      ',
     Q             ' [ MM ]     ',' [ MM ]      '
      WRITE(6,901)
      DO 100 I=1,MAX
        PEN='   '
        IF(SAVE1(5,I).GT.0.9)  PEN='(*)'
        WRITE(6,904) (SAVE1(K,I),K=1,4),PEN
  100 CONTINUE
      WRITE(6,901)
      WRITE(6,901) 'THE PENTRATION POINT IS SIGHED BY (*)'
      RETURN
  901 FORMAT(2X,A)
  902 FORMAT(2X,A,F10.4,A)
  903 FORMAT(4X,4(A,5X))
  904 FORMAT(1X,4(F10.4,8X),A)
  905 FORMAT(2X,A, I2)
      END
C
C     ******************************************************
      SUBROUTINE DRAW(NMES,NPTS,I,N)
C
C     CREATE THE SCATTERGRAM OF THE NONDIMENSIONALIZED
C     DATA AND THE PLOTS OF THE CURVES
C
C     VARIABLES
C     *********
C
C     NMES--NUMBER OF MEASUREMENT POINT
C     NPTS--NUMBER OF POINTS FOR THE PLOT OF THE CURVE
C     I   --NUMBER OF PLOTS TO BE MADE
C     N   --NUMBER OF THE ACTUAL EXPERIMENT
C
C     COMMON
C     ******
C
C     VALUE2--X(MAXDAT,10) : X-VALUES OF THE POINTS TO BE PLOTTED
C             Y(MAXDAT,10) : Y-VALUES OF THE POINTS TO BE PLOTTED
C
      PARAMETER(MAXDAT=100)
      CHARACTER*20 LEGEND(10)
      CHARACTER*60 XAXIS,YAXIS
      CHARACTER*60 TITLE
      DIMENSION X(MAXDAT,10),Y(MAXDAT,10),NSYMB(10),KCHAR(10),L(10)
      COMMON / VALUE2 /X,Y
      LEGEND(1)= '0.5341M/S'
      LEGEND(2)= '0.8012M/S'
      LEGEND(3)= '1.0793M/S'
      LEGEND(4)= '1.3464M/S'
      LEGEND(5)= '1.6246M/S'
      LEGEND(6)= 'AIR SPEED'
      LEGEND(7)= '          '
      LEGEND(8)= '          '
      LEGEND(9)= '          '
      LEGEND(10)='          '
      XAXIS= 'CENTRAL JET VELOCITY / STAGNATION POINT VELOCITY'
```

```
      YAXIS= 'FORWARD / AFT STAGNATION POINT'
      WRITE(TITLE,901) N
      DATA NSYMB / 5*-1,5*0/
      DATA KCHAR / 1,2,3,4,5,5*1/
      L(1)=NMES
      L(2)=NMES
      L(3)=NMES
      L(4)=NMES
      L(5)=NMES
      L(6)=NPTS
      L(7)=NPTS
      L(8)=NPTS
      L(9)=NPTS
      L(10)=NPTS
      CALL NAMPLT
      CALL MRANGX(0.0,1.2)
      CALL MRANGY(0.0,1.2)
      CALL MDIV(6.0,6.0)
      CALL MSTARTA(X,L,MAXDAT,TITLE,XAXIS,1,I,1,8.0,6.0)
      CALL MLINEA (X,L,Y,MAXDAT,I,YAXIS,LEGEND,1,NSYMB,KCHAR)
      CALL ENDPLT
      RETURN
  901 FORMAT(1X, 'PLOT OF THE NONDIMENSIONALIZED DATA SET ',I2)
      END
C     ****************************************************************
      SUBROUTINE FCTDET(NMES,N,ITYP,IM)
C
C     CONTROL THE FLOW OF THE SUBROUTINES TO FIND THE CONSTANTS
C     OF A FUNCTION BY A LEAST SQUARE METHOD
C
C
C     VARIABLES
C     *********
C
C     NMES--NUMBER OF MEASUREMENT POINTS IN COMMON 'VALUE2'
C     N   --NUMBER OF ACTUAL EXPERIMENT
C
C     COMMON
C     ******
C
C     VALUE2--X(MAXDAT,10) : X-VALUES OF EXPERIMENTAL DATA AND
C                            THE CURVE FITTING
C             Y(MAXDAT,10) : Y-VALUES OF THE ABOVE
C
C     SUBROUTINES CALLED
C     ******************
C
C     FCTFIT--DETERMINE THE CONSTANTS
C     FCTPRT--PRINT THE FUNCTION AND THE CONSTANTS
C     FCTPLT--FIND THE X AND Y-VALUES OF THE CURVE FITTING
C
      PARAMETER(MAXDAT=100,MAXCON=10)
      DIMENSION X(MAXDAT,10),Y(MAXDAT,10),A(MAXCON)
      COMMON / VALUE2 /X,Y
      NPTS=50
      CALL FCTFIT(X(1,N),Y(1,N),MAXDAT,NMES, A,ERR,IERR,IT)
      IF(IERR.LT.0)  THEN
       WRITE(6,901) 'NO LEAST SQUARE FITTING POSSIBLE '
       WRITE(6,902) 'IERR= ',IERR
      RETURN
      ENDIF
      CALL FCTPRT(A,ERR,IT)
      CALL FCTPLT(X(1,N),Y(1,N),A,NPTS,NMES,X(1,N+5),Y(1,N+5))
      IF((ITYP.EQ.4).AND.(N.EQ.IM))  CALL DRAW(NMES,NPTS,10,N)
      RETURN
  901 FORMAT(2X,A)
```

```
4930 902   FORMAT(2X,A,I5)
4940       END
4950 C     ***************************************************************
4960       SUBROUTINE FCTFIT(X,Y,MAXDAT,NMES,A,ERR,IERR,IT)
4970 C
4980 C     DETERMINE THE CONSTANTS OF THE FUNCTION
4990 C
5000 C     VARIABLES
5010 C     *********
5020 C
5030 C     X(MAXDAT,*)--X-VALUES OF THE EXPERIMENTAL DATA
5040 C     Y(MAXDAT,*)--Y-VALUES OF THE EXPERIMENTAL DATA
5050 C     MAXDAT--MAXIMUM NUMBER OF EXPERIMENTAL DATA (ONLY USED
5060 C              FOR DIMENSION)
5070 C     NMES  --ACTUAL NUMBER OF EXPERIMENTAL DATA SETS
5080 C     A(MAX)--VECTOR CONTAINING THE CONSTANTS
5090 C     ERR   --LEAST SQUARE ERROR NORM
5100 C     IERR  --NUMBER SHOWING HOW FCTFIT WORKED
5110 C               IERR>0 : FCTFIT GOT RESULTS
5120 C               IERR<0 : SOME KIND OF ERROR WITHIN FCTFIT
5130 C
5140 C     SUBROUTINES CALLED
5150 C     ******************
5160 C
5170 C     FCT --CONTAIN THE FUNCTION AND ITS PARTIAL DERIVATIVES
5180 C     ELIM--SOLVE A SET OF EQUATIONS
5190 C
5200       PARAMETER(MAX=100,MAXP1=11)
5210       DIMENSION X(MAXDAT,*),Y(MAXDAT,*),A(MAX),F(MAX),W(MAX),
5220      C          XSAVE(MAX),FSAVE(MAX),ARR(MAX,MAXP1)
5230       CHARACTER *50 STRING
5240       LOGICAL FINISH
5250       CALL FCT(A,F,X,Y,W,1,NCONST,STRING,ERR,MAXIT,DELTA,
5260      C          XTOL, FTOL,0)
5270       IF(MAXIT.LT.0) MAXIT=50
5280       IF(DELTA.LT. 0.0) DELTA=.01
5290       IF(XTOL.LT.0.0) XTOL=.0001
5300       IF(FTOL.LT.0.0) FTOL=.0005
5310       NP1=NCONST+1
5320       DO 500 IT=1,MAXIT
5330         DO 10 I=1,NCONST
5340         XSAVE(I)=A(I)
5350 10      CONTINUE
5360         CALL FCT(A,F,X,Y,W,NMES,NCONST,STRING,ERR,F,F,F,F,
5370      C          2)
5380         FINISH=.TRUE.
5390         DO 20 I=1,NCONST
5400           IF(ABS(F(I)).GT.FTOL)  FINISH=.FALSE.
5410           FSAVE(I)=F(I)
5420 20      CONTINUE
5430         IF(FINISH) THEN
5440           IERR=2
5450           RETURN
5460         ENDIF
5470         DO 100 J=1,NCONST
5480           A(J)=XSAVE(J)+DELTA
5490           CALL FCT(A,F,X,Y,W,NMES,NCONST,STRING,ERR,F,F,F,F,
5500      C          2)
5510         DO 150 I=1,NCONST
5520           ARR(I,J)=(F(I)-FSAVE(I))/DELTA
5530 150     CONTINUE
5540         A(J)=XSAVE(J)
5550 100     CONTINUE
5560         DO 200 I=1,NCONST
5570           ARR(I,NP1)=-FSAVE(I)
5580 200     CONTINUE
```

```
      CALL ELIM(ARR,NCONST,NP1,MAX)
      DO 300 I=1,NCONST
        IF(ABS(ARR(I,I)).LE.0.0000001) THEN
          IERR=-2
          RETURN
        ENDIF
300   CONTINUE
      FINISH=.TRUE.
      DO 400 I=1,NCONST
        A(I)=XSAVE(I)+ARR(I,NP1)
        IF(ABS(ARR(I,NP1)).GT.XTOL) FINISH=.FALSE.
400   CONTINUE
      IF(FINISH) THEN
        IERR=1
        RETURN
      ENDIF
500   CONTINUE
      IERR=-1
      RETURN
      END
C     ****************************************************************
      SUBROUTINE FCT(A,F,X,Y,DYDA,MAX,NCONST,STRING,
     Q               ERRSQ,MAXIT,DELTA, XTOL, FTOL, ITYP)
C
C     CONTAIN THE FUNCTION AND ITS PARTIAL DERIVATIVES WITH RESPECT TO
C     CONSTANTS A(I)
C
C     VARIABLES
C     *********
C
C     A(NCONST)--VECTOR CONTAINING THE CONSTANTS A1...AN  OF THE
C                FUNCTION
C     F(NCONST)--VECTOR CONTAINING THE SUM FOR ALL GIVEN
C                EXPERIMENTAL DATA OF THE PARTIAL DERIVATIVES OF
C                THE FUNCTION WITH RESPECT TO THE CONSTANTS A(I)
C     X(MAX)    --VECTOR CONTAINING THE X-VALUES OF THE
C                EXPERIMENTAL DATA
C     Y(MAX)    --FOR ITYP=1 : FOR THE GIVEN X-VALUES ARE Y-VALUES
C                COMPUTED WITH THE FUNCTION AND STORED IN Y
C                FOR ITYP=2 : Y CONTAINING THE Y-VALUES OF THE
C                EXPERIMENTAL DATA CORRESPONDING TO X
C     DYDA(NCONST)--VECTOR CONTAINING THE PARTIAL DERIVATIVES
C                OF THE FUNCTION
C     MAX       --NUMBER OF EXPERIMENTL DATA (FOR ITYP=2) OR
C                NUMBER OF Y-VALUES TO BE COMPUTED (FOR ITYP=1)
C     NCONST    --NUMBER OF CONSTANTS
C     STRING    --CHARACTER VARIABLE CONTAINING THE FUNCTION
C     ERRSQ     --CONTAIN LEAST SQUARE ERROR NORM FOR THE GIVEN
C                FUNCTION,CONSTANTS AN EXPERIMENTAL DATA
C     MAXIT     --MAXIMUM NUMBER OF ITERATIONS FOR LEAST SQUARE
C                FIT
C                IF MAXIT=-1,A DEFAULT VALUE WILL BE USED
C     DELTA     --SMALL VALUE TO COMPUTE THE PARTIAL DERIVATIVES
C                FOR NEWTON METHOD OF SOLVING NONLINEAR EQUATIONS
C                IF DELTA=-1.0,A DEFAULT VALUE WILL BE USED
C     FTOL      --CONTAIN THE TOLERANCE IN THE COMPUTED VALUES OF
C                PARTIAL DERIVATIVES TO STOP THE ITERATION
C                IF FTOL=-1.0,A DEFAULT VALUE WILL BE USED
C     XTOL      --CONTAIN THE TOLERANC IN THE CONSTANTS OF THE
C                FUNCTION TO STOP THE ITERATION
C                IF XTOL =-1,0,A DEFAULT VALUE WILL BE USED
C
      CHARACTER *50 STRING
      DIMENSION A(*),F(*),X(*),Y(*),DYDA(*)
C
C     YOU SHOULD INSERT HERE THE VALUES FOR MAXIT,DELTA,FTOL AND XTOL
```

```
C
C     IF YOU DON'T HAVE ANY SPECIAL PURPOSES OR IF YOU ARE NOT SURE
C     ABOUT THEM,JUST SET THEM TO -1.0,A DEFAULT VALUE WILL BE USED
C
      MAXIT=-1
      DELTA=-1.0
      XTOL= -1.0
      FTOL =-1.0
C
C     YOU HAVE TO INSERT HERE HOW MANY CONSTANTS YOUR FUNCTION CONTAINS
C
      NCONST=3
C
C     YOU SHOULD INSERT HERE YOUR FUNCTION AS A CHARACTER STRING,
C     THIS WILL BE USED FOR THE OUTPUT ONLY,SO CHOOSE ANY FORM
C     CONVENIENT TO YOU
C
      STRING='Y = 1+A1*(1-X)+A2*(1-Y)**2+A3*(1-X)**3 '
C
      IF(ITYP .EQ. 0) THEN
C
C     YOU HAVE TO INSERT HERE THE STARTING VALUES FOR ALL YOUR
C     CONSTANTS A1...AN,JUST MAKE ANY GUESS FOR THEM
C
      A(1)=0.1
      A(2)=2.3
      A(3)=1.5
C
      ELSE IF (ITYP.EQ.1) THEN
       DO 100 I=1,MAX
C
C     YOU HAVE TO INSERT HERE THE FUNCTION WHICH IS THE BASIS FOR THE
C     LEAST SQUARE FIT
C
      Y(I)=1.0+(1.-X(I))*(A(1)+(1.-X(I))*(A(2)+A(3)*(1.-Y(I))))
C
  100 CONTINUE
      ELSE IF (ITYP.EQ.2)  THEN
        DO 150 I=1,NCONST
          F(I)=0.0
  150 CONTINUE
      ERRSQ=0.0
      DO 200 I=1,MAX
C
C     YOU HAVE TO PROGRAM HERE YOUR FUNCTION IN THE FORM
C     Y(I)=(FUNCTION)
C
      E=Y(I)-1.0-(1.-X(I))*(A(1)+(1.-X(I))*(A(2)+A(3)*(1.-X(I))))
C
C     YOU HAVE TO PROGRAM HERE ALL PARTIAL DERIVATIVES OF THE FUNCTION
C     WITH RESPECT TO CONSTANTS A1...AN.
C
      DYDA(1)=1.0-X(I)
      DYDA(2)=(1.0-Y(I))*(1.0-X(I))
      DYDA(3)=(1.0-Y(I))*(1.0-X(I))*(1.0-X(I))
C
      DO 210 II=1,NCONST
        F(II)=F(II)-2.0*E*DYDA(II)
  210 CONTINUE
      ERRSQ=ERRSQ+E*E
  200 CONTINUE
      ENCODE
      RETURN
      END
C     ******************************************************************
      SUBROUTINE PUTPRT(A,ERR,IT)
```

```
C      PRINT OUT THE FUNCTION OF THE LEAST SQUARE FIT AND ITS CONSTANTS
C
C      VARIABLES
C      *********
C
C      A  --VECTOR CONTAINING THE CONSTANTS
C      ERR--THE LEAST SQUARE ERROR NORM
C      IT --ITERATION INDEX
C
C      SUBROUTINES CALLED
C      ******************
C
C      FCT--CONTAIN THE FUNCTION AS A CHARACTER STRING
C
       PARAMETER(MAX=10)
       DIMENSION P(MAX),A(MAX),AO(MAX)
       CHARACTER *50 STRING
       CALL FCT (AO,P,P,P,P,1,NCONST,STRING,ERRSQ,P,P,P,P,0)
       WRITE(6,'(''1'')')
       WRITE(6,901)
       WRITE(6,901)
       WRITE(6,901) 'FUNCTION FOR THIS DATA SET'
       WRITE(6,901) '**************************'
       WRITE(6,901)
       WRITE(6,901)
       WRITE(6,901) 'THE VALUES ARE NONDIMENSIONALIZED BY THE RULES'
       WRITE(6,901)
       WRITE(6,901) '        VELOCITY OF FUEL'
       WRITE(6,901) ' X = ---------------------'
       WRITE(6,902) '     PENETRATION  VELOCITY  '
       WRITE(6,901)
       WRITE(6,901) '     FORWARD STAGNATION POINT'
       WRITE(6,901) ' Y = ------------------------'
       WRITE(6,901) '       AFT STAGNATION POINT'
       WRITE(6,901)
       WRITE(6,902) 'CONSTANTS ARE DETERMINED BY A LEAST SQUARE METHOD'
       WRITE(6,901)
       WRITE(6,901)
       WRITE(6,902) 'FUNCTION:         ',STRING
       WRITE(6,901) '*********'
       WRITE(6,901)
       WRITE(6,901)
       WRITE(6,906) 'INITIAL VALUES:  ','A1 = ',AO(1)
       WRITE(6,906) '***************  ','A2 = ',AO(2)
       DO 50 I=3,NCONST
         WRITE(6,907) ' A',I,' = ',AO(I)
   50  CONTINUE
       WRITE(6,901)
       WRITE(6,901)
       WRITE(6,906) 'CONSTANTS:        ','A1 = ',A(1)
       WRITE(6,906) '*********         ','A2 = ',A(2)
       DO 100 I = 3,NCONST
         WRITE(6,907) ' A',I,' = ', A(I)
  100  CONTINUE
       WRITE(6,901)
       WRITE(6,901)
       WRITE(6,908) 'LEAST SQUARE ERROR NORM:  E = ',ERR
       WRITE(6,901)
       WRITE(6,909) 'THE SOLUTION WAS FOUND AFTER',IT,'ITERATIONS'
       RETURN
  901  FORMAT(2X,A)
  902  FORMAT(2X,A,A)
  906  FORMAT(2X,A,A,G10.3)
  907  FORMAT(2X,17X,A,I1,A,G10.3)
  908  FORMAT(2X,A,G15.5)
  909  FORMAT(2X,A,I4,1X,A)
```

```
      END
C     ****************************************************************
      SUBROUTINE FCTPLT (X,Y,A,NPTS,NMES,XX,YY)

C     COMPUTE THE X- AND Y-VALUES OF THE CURVE DETERMINED BY
C     THE LEAST SQUARE METHOD AND PLOT THEM

C     VARIABLES
C     *********

C     X(*)    --CONTAIN THE X-VALUES OF THE EXPERIMENTAL DATA
C     Y(*)    --CONTAIN THE Y-VALUES OF THE EXPERIMENTAL DATA
C     A(*)    --CONTAIN THE CONSTANTS OF THE FUNCTION
C     NPTS    --NUMBER OF THE POINTS FOR THE CURVE
C     NMES    --NUMBER OF MEASUREMENT POINTS OF EXPERIMENTAL DATA
C     XX(*)   --X-VALUES FOR THE CURVE
C     YY(*)   --Y-VALUES FOR THE CURVE

C     SUBROUTINE CALLED
C     *****************

C     FCT  --FUNCTION OF THE LEAST SQUARE CURVE

      PARAMETER(MAXDAT=100)
      CHARACTER *50 STRING
      DIMENSION X(MAXDAT),Y(MAXDAT),A(*),R(1),XX(MAXDAT),YY(MAXDAT)
      XMIN=X(1)
      XMAX=X(1)
      DO 100 I=2,NMES
        IF (XMIN.GT.X(I))  XMIN=X(I)
        IF (XMAX.LT.X(I))  XMAX=X(I)
100   CONTINUE
      STEP= (XMAX-XMIN)/(NPTS-1)
      DO 200 I=1,NPTS
        XX(I)=XMIN+(I-1)*STEP
200   CONTINUE
      CALL FCT (A,R,XX,YY,P,NPTS,NCONST,STRING,ERP,
     &          P,P,P,P,1)
      RETURN
      END
C     ****************************************************************
      SUBROUTINE ELIM (AB,N,NP,NDIM)

C     SOLVE A SET OF LINEAR EQUATIONS

C     VARIABLES
C     *********

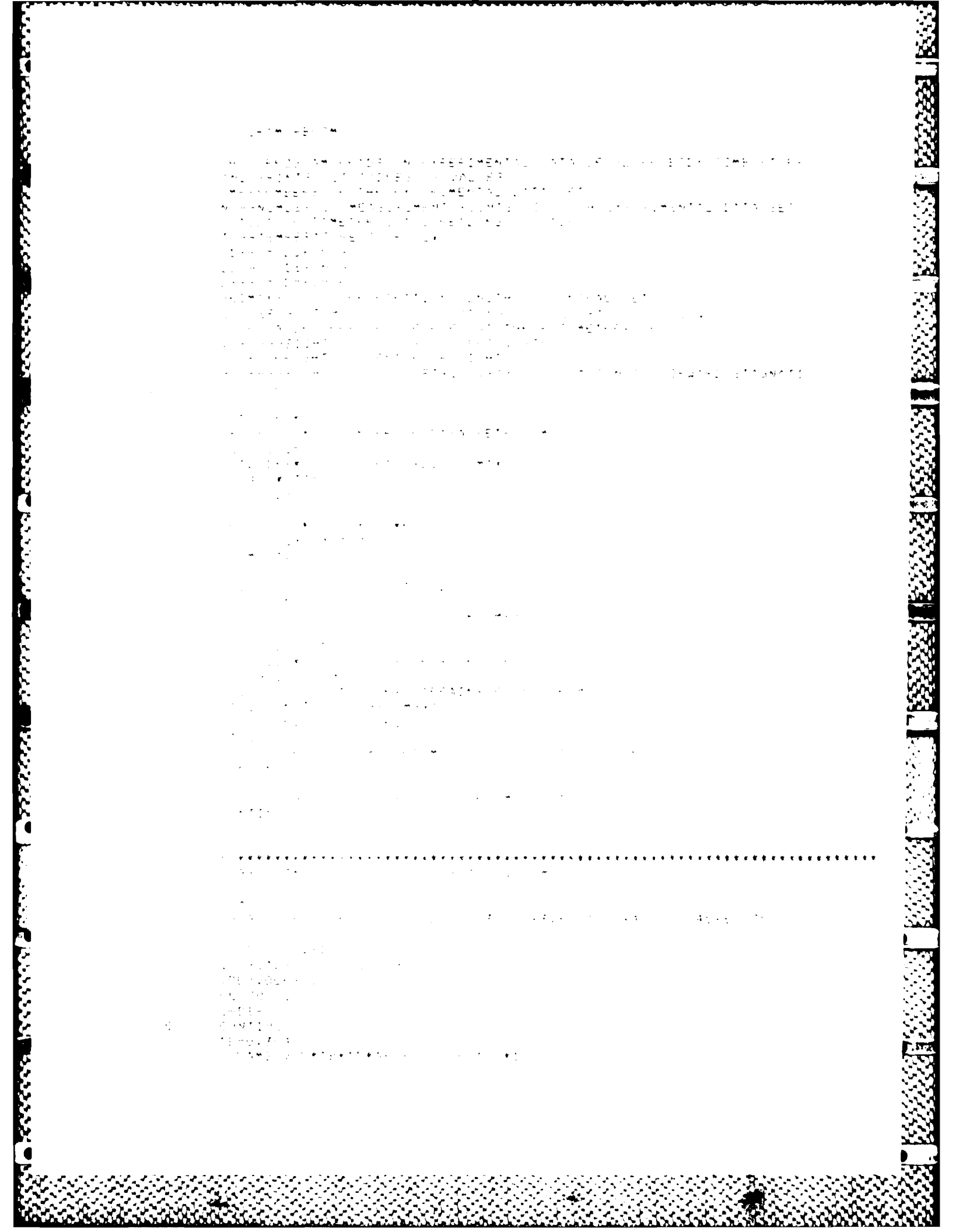
C     AB(NDIM,*)--ARRAY CONTAINING THE COEFFICIENT MATRIX AND THE
C                 RIGHT HAND SIDE OF THE MATRIX EQUATION
C     N       ---NUMBER OF EQUATIONS
C     NP      ---NUMBER OF EQUATIONS + NUMBER OF RIGHT HAND SIDE VECTORS
C     NDIM    ---MAXIMUM NUMBER OF EQUATIONS

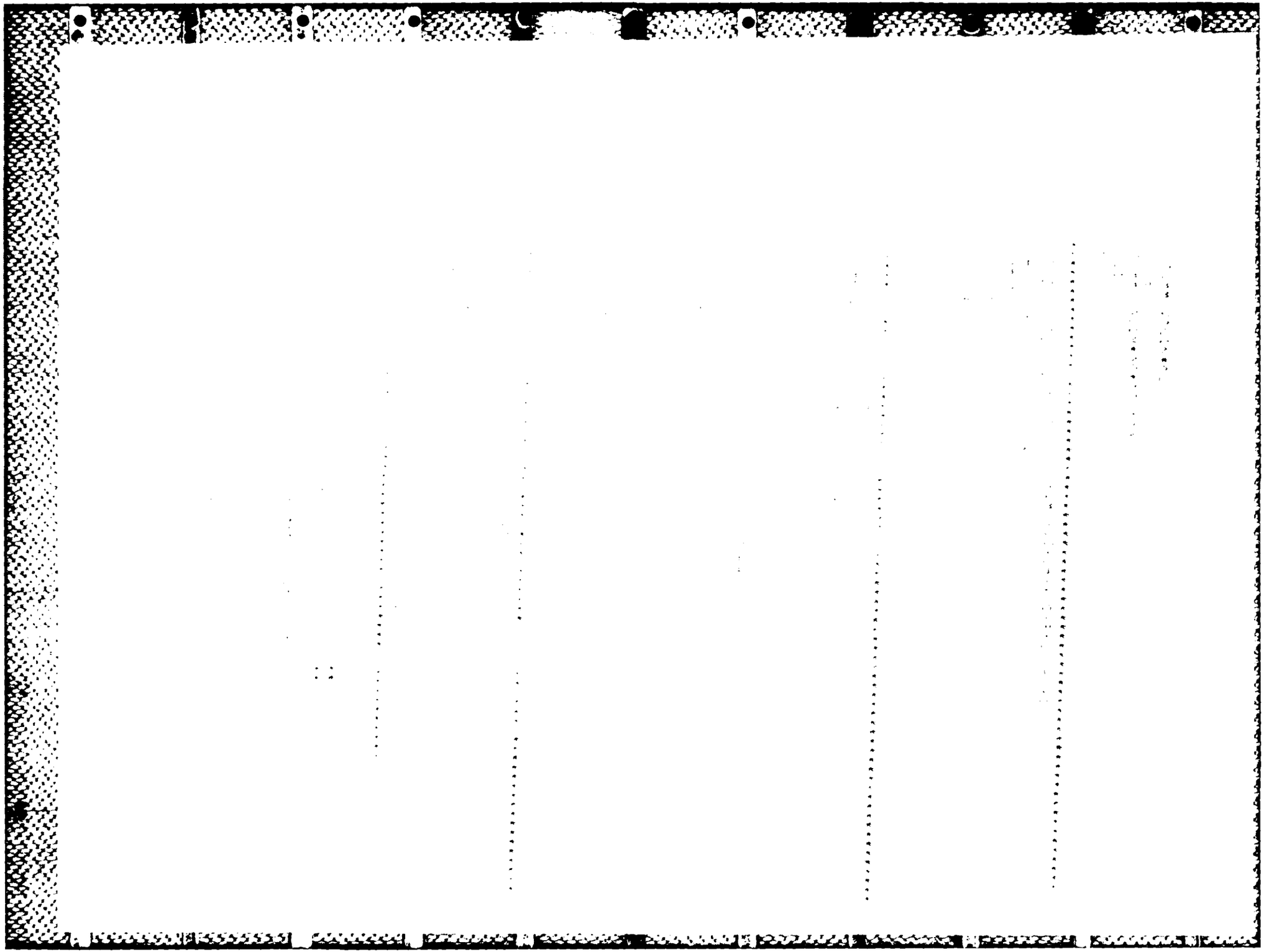
      REAL AB (NDIM,NP)
      NM1=N-1
      DO 35 I = 1,NM1
        IPVT=I
        IP1 = I+1
        DO 10 J = IP1,N
          IF ( ABS ( AB(IPVT,I)).LT. ABS(AB(J,I)) ) IPVT = J
10      CONTINUE
        IF (ABS(AB(IPVT,I)) .LT. 0.0000001 ) THEN
        WRITE(6,901) 'MATRIX NEAR SINGULAR - PIVOT SEARCH'
        RETURN
      ENDIF
```

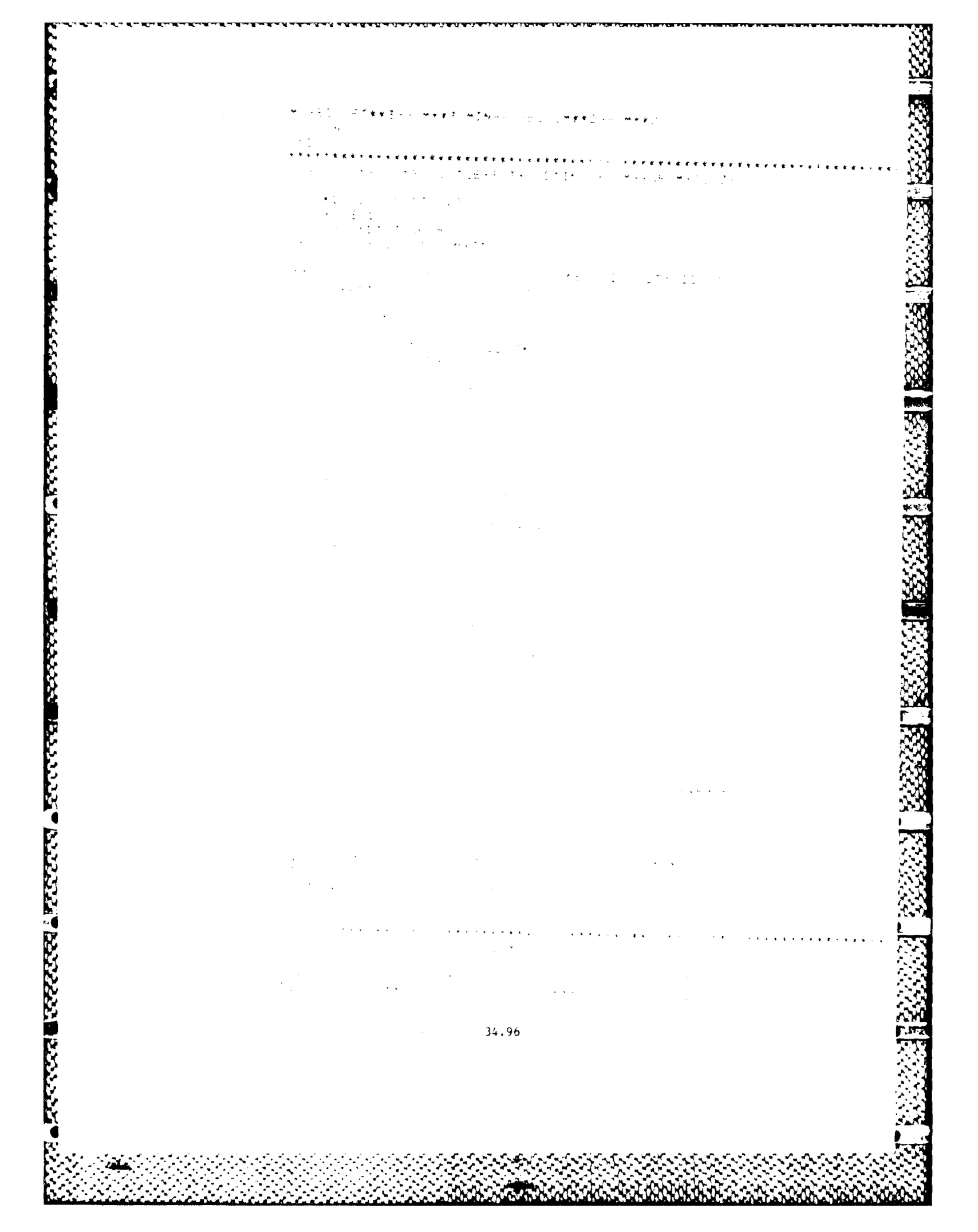
```
8330         IF ( IPVT.NE.I ) THEN
8340           DO 30 JCOL = 1,NP
8350             SAVE=AB(I,JCOL)
8360             AB(I,JCOL)=AB(IPVT,JCOL)
8370             AB(IPVT,JCOL)=SAVE
8380 30          CONTINUE
8390         ENDIF
8400         DO 32 JROW=IP1,N
8410           IF(AB(JROW,I).EQ.0.0) GOTO 32
8420           RATIO=AB(JROW,I)/AB(I,I)
8430           AB(JROW,I)=RATIO
8440           DO 30 KCOL = IP1,NP
8450             AB(JROW,KCOL)=AB(JROW,KCOL)-RATIO*AB(I,KCOL)
8460 30        CONTINUE
8470 32        CONTINUE
8480 35      CONTINUE
8490         IF ( ABS(AB(N,N)).LT. 0.0000001 ) THEN
8500           WRITE(6,901) 'MATRIX NEAR SINGULAR'
8510           RETURN
8520         ENDIF
8530         NP1=N+1
8540         DO 50 KCOL=NP1,NP
8550           AB(N,KCOL)=AB(N,KCOL)/AB(N,N)
8560           DO 45 J=2,N
8570             NVBL=NP1-J
8580             L=NVBL+1
8590             VALUE=AB(NVBL,KCOL)
8600             DO 40 K=L,N
8610               VALUE=VALUE-AB(NVBL,K)*AB(K,KCOL)
8620 40          CONTINUE
8630             AB(NVBL,KCOL)=VALUE/AB(NVBL,NVBL)
8640 45        CONTINUE
8650 50      CONTINUE
8660         RETURN
8670 901     FORMAT(2X,A)
8680         END
8690 8,20.0,30.5,0.372
8700 0.75,47.1,66.0
8710 33.5,67.1,0.208,0.208,0.511
8720 45.1,66.5,0.197,0.267,0.71
8730 47.1,66.0,0.196,0.262,0.75
8740 39.5,66.5,0.190,0.233,0.632
8750 24.4,67.1,0.210,0.224,0.40
8760 20.5,67.6,0.188,0.231,0.29
8770 14.0,67.3,0.175,0.257,0.146
8780 9.50,68.0,0.1267,0.215,0.089
8790 8,30.0,29.5,0.372
8800 1.058,53.0,63.1
8810 53.0,63.1,0.200,0.206,1.058
8820 47.0,64.0,0.200,0.2515,0.985
8830 41.0,64.9,0.225,0.246,0.855
8840 27.0,65.1,0.240,0.300,0.45
8850 32.5,65.0,0.231,0.278,0.6
8860 22.0,65.9,0.226,0.348,0.389
8870 12.0,66.9,0.220,0.317,0.158
8880 9.00,68.1,0.196,0.274,0.119
8890 6,40.0,29.5,0.372
8900 0.963,53.0,63.0
8910 53.0,63.0,0.231,0.250,0.363
8920 43.0,64.1,0.256,0.275,0.77
8930 32.0,64.8,0.257,0.298,0.598
8940 24.0,65.1,0.258,0.405,0.429
8950 15.5,66.0,0.2545,0.369,0.222
8960 9.0,67.8,0.2365,0.339,0.117
8970 7,50.0,29.5,0.372
8980 0.9,50.0,61.9
```

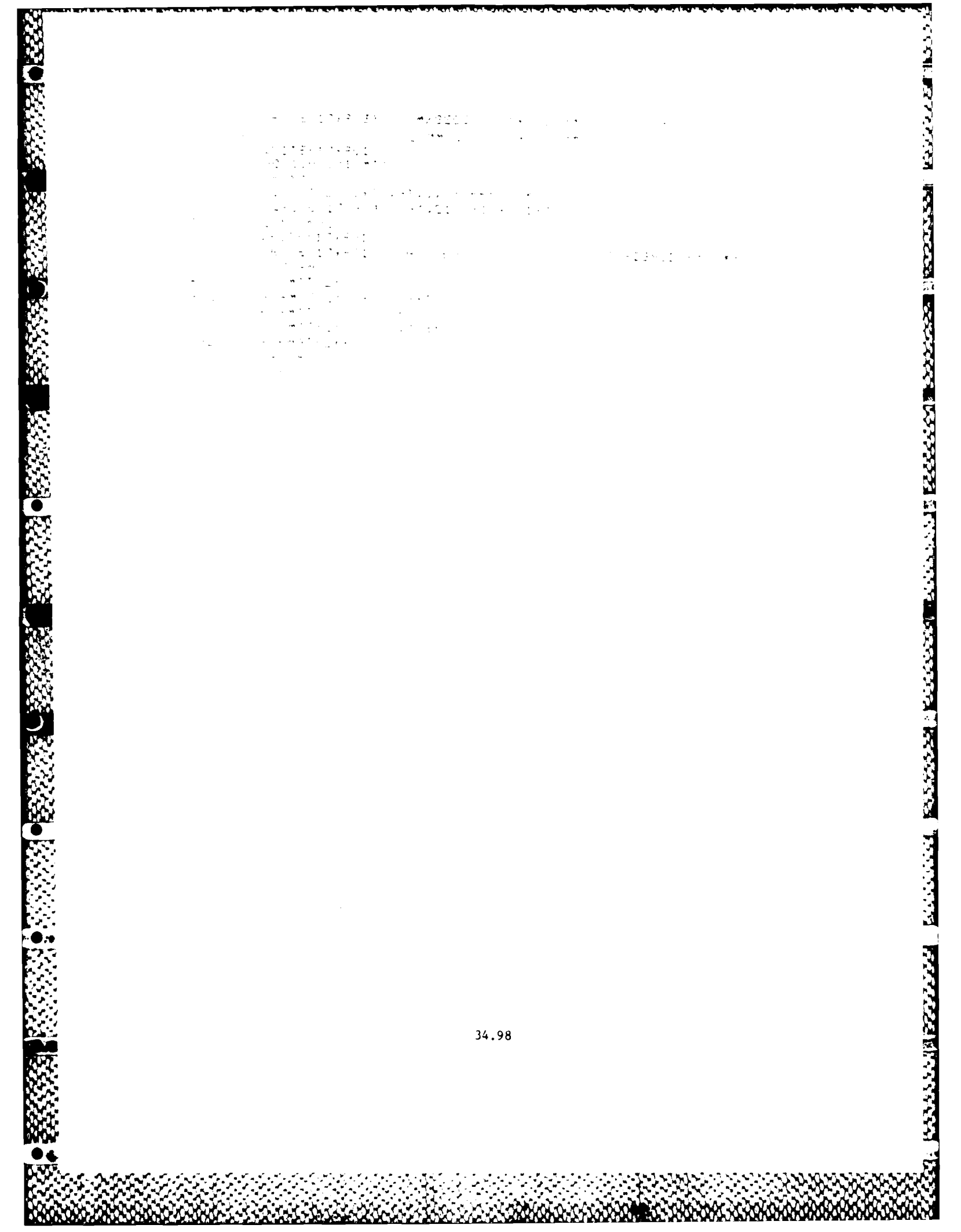
Appendix C: Computer Program Run on Harris 800

(Plotting Curves $\frac{L}{D_i}$ vs. Flow Conditions)





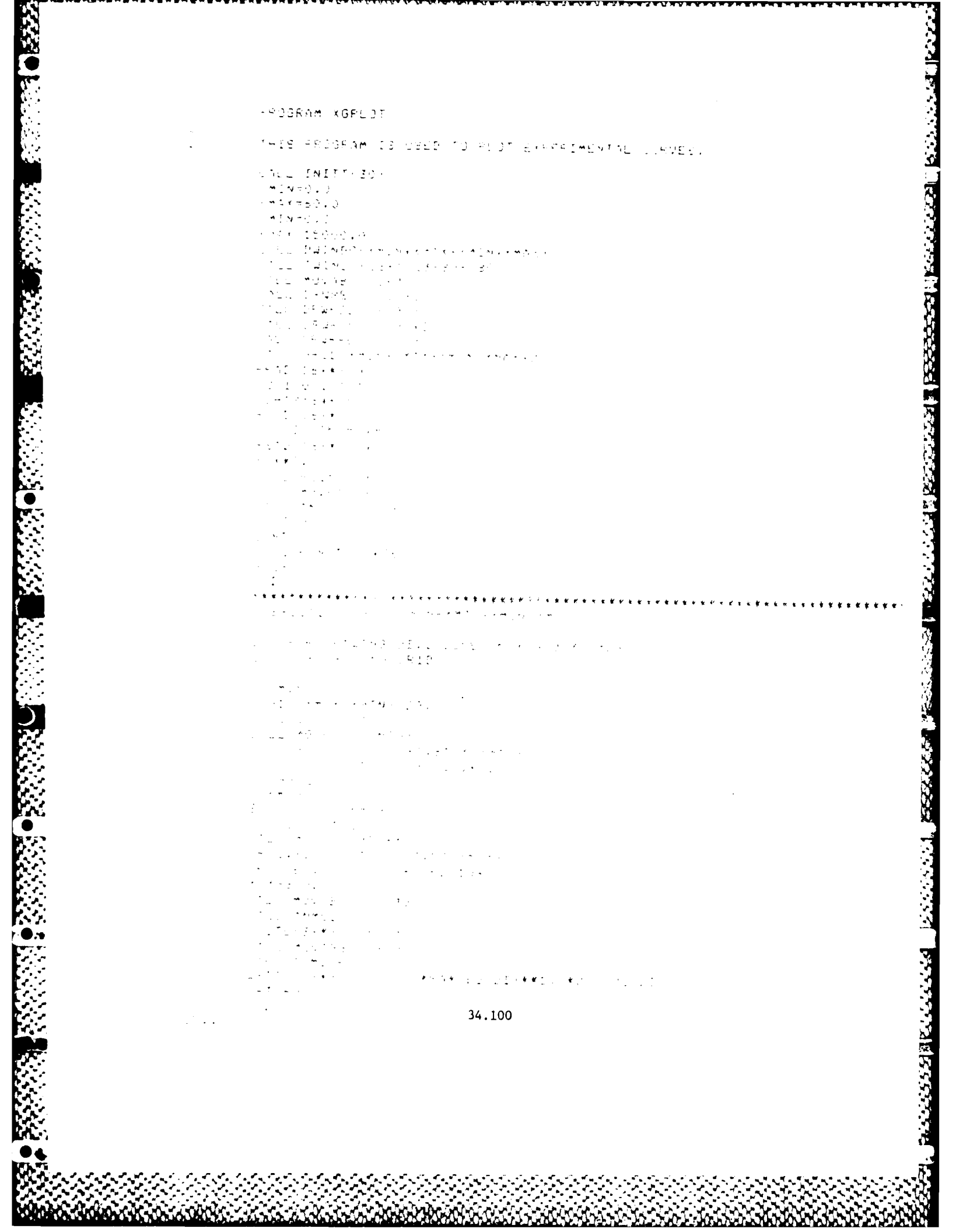




```
      PROGRAM COLL

C     REARRANGE EXPERIMENTAL DATA OF BLUFF BODY (OMEGUSUF EX
C     (NO HEIN_LOS NUMBER)
C     WITH ONE INPUT PARAMETER(D)--(NONDIMENSIONAL DIAMETER
C     (1.800*(10**14)*(D**6) SEC

      REAL L,LDU
      L=1.750*2.54/100.
      D=2.750*2.54/100.
      DU=0.043*9.000
      WRITE(12,*)
      WRITE(12,*)
      WRITE(12,*)
      WRITE(12,*)      NUMBER OF DATA SETS IS
      WRITE(12,*)
      WRITE(12,*)
      WRITE(12,*)
      WRITE(12,*)
```



Appendix D: List of All Measurements

I: Output from Cyber 730

1. Experimental Results of Test I for the Cold Reacting Flow

TABLE OF VALUES FOR EXPERIMENTAL DATA SET 1
**********

AREA OF OUTER NOZZLE 10.6036 CM**2
AREA OF INNER NOZZLE .3167 CM**2
VELOCITY OF AIR .3012 M/SEC

| VELOCITY OF FUEL [ M/SEC ] | HEIGHT OF CENTRAL JET [ MM ] | HEIGHT OF LEFT VORTEX [ MM ] | HEIGHT OF RIGHT VORTEX [ MM ] | |
|---|---|---|---|---|
| .1154 | 15.2400 | .0000 | .0000 | |
| .1995 | 25.4160 | .0000 | .0000 | |
| .2444 | 34.2900 | .0000 | .0000 | |
| .3291 | 39.3700 | .0000 | .0000 | |
| .4188 | 45.7200 | .0000 | .0000 | |
| .5415 | 51.5620 | .0000 | .0000 | |
| .6261 | 55.1942 | .0000 | .0000 | (*) |
| .7600 | 60.4520 | .0000 | .0000 | (*) |

THE PENTRATION POINT IS SIGHED BY (*)

FUNCTION FOR THIS DATA SET
**********

THE VALUES ARE NONDIMENSIONALIZED BY THE RULES

$$Y = \frac{\text{VELOCITY OF FUEL}}{\text{PENETRATION VELOCITY}}$$

$$Y = \frac{\text{FORWARD STAGNATION POINT}}{\text{AFT STAGNATION POINT}}$$

CONSTANTS ARE DETERMINED BY A LEAST SQUARE METHOD

FUNCTION: $Y = 1+A1*(1-X)+A2*(1-X)**2+A3*(1-X)**3$
********

INITIAL VALUES: A1 = .100
********** A2 = 2.30
A3 = 1.50

CONSTANTS: A1 = -.601
****** A2 = .569
A3 = -.952

LEAST SQUARE ERROR NORM: E = .68196E-03

THE SOLUTION WAS FOUND AFTER 2 ITERATIONS

FUNCTION FOR THIS DATA SET
**********

THE VALUES ARE NONDIMENSIONALIZED BY THE RULES

$$X = \frac{\text{VELOCITY OF FUEL}}{\text{ANNULUS AIR VELOCITY}}$$

$$Y = \frac{\text{FORWARD STAGNATION POINT}}{\text{AFT STAGNATION POINT}}$$

CONSTANTS ARE DETERMINED BY A LEAST SQUARE METHOD

FUNCTION: Y = 1+A1*(1-X)+A2*(1-X)**2+A3*(1-X)**3
********

INITIAL VALUES: A1 = .100
********** A2 = 2.30
A3 = 1.50

CONSTANTS: A1 = -.420
****** A2 = .172
A3 = -.707

LEAST SQUARE ERROR NORM: E = .13377E-02

THE SOLUTION WAS FOUND AFTER 2 ITERATIONS

TABLE OF VALUES FOR EXPERIMENTAL DATA SET 2
**********

AREA OF OUTER NOZZLE 10.6036 CM**2
AREA OF INNER NOZZLE .3167 CM**2
VELOCITY OF AIR 1.0793 M/SEC

| VELOCITY OF FUEL [ M/SEC ] | HEIGHT OF CENTRAL JET [ MM ] | HEIGHT OF LEFT VORTEX [ MM ] | HEIGHT OF RIGHT VORTEX [ MM ] | |
|---|---|---|---|---|
| .1351 | 17.0180 | .0000 | .0000 | |
| .1846 | 20.3200 | .0000 | .0000 | |
| .2415 | 26.6700 | .0000 | .0000 | |
| .3128 | 32.2580 | .0000 | .0000 | |
| .3721 | 34.6710 | .0000 | .0000 | |
| .4705 | 40.6400 | .0000 | .0000 | |
| .5553 | 42.4180 | .0000 | .0000 | |
| .6333 | 46.9900 | .0000 | .0000 | |
| .7290 | 50.8000 | .0000 | .0000 | (*) |
| .8249 | 53.3400 | .0000 | .0000 | (*) |

THE PENTRATION POINT IS SIGHED BY (*)

FUNCTION FOR THIS DATA SET
**********

THE VALUES ARE NONDIMENSIONALIZED BY THE RULES

$$X = \frac{\text{VELOCITY OF FUEL}}{\text{PENETRATION VELOCITY}}$$

$$Y = \frac{\text{FORWARD STAGNATION POINT}}{\text{AFT STAGNATION POINT}}$$

CONSTANTS ARE DETERMINED BY A LEAST SQUARE METHOD

FUNCTION: $Y = 1+A1*(1-X)+A2*(1-X)**2+A3*(1-X)**3$
********

INITIAL VALUES: A1 = .100
********** A2 = 2.30
A3 = 1.50

CONSTANTS: A1 = -.531
****** A2 = .721E-01
A3 = -.428

LEAST SQUARE ERROR NORM: E = .18074E-02

THE SOLUTION WAS FOUND AFTER 2 ITERATIONS

FUNCTION FOR THIS DATA SET
**********

THE VALUES ARE NONDIMENSIONALIZED BY THE RULES

$$Y = \frac{\text{VELOCITY OF FUEL}}{\text{ANNULUS AIR VELOCITY}}$$

$$Y = \frac{\text{FORWARD STAGNATION POINT}}{\text{AFT STAGNATION POINT}}$$

CONSTANTS ARE DETERMINED BY A LEAST SQUARE METHOD

FUNCTION: $Y = 1+A1*(1-X)+A2*(1-X)**2+A3*(1-X)**3$
********

INITIAL VALUES: A1 = .100
********** A2 = 2.30
A3 = 1.50

CONSTANTS: A1 = .249
****** A2 = -1.40
A3 = .324

LEAST SQUARE ERROR NORM: E = .27014E-02

THE SOLUTION WAS FOUND AFTER 2 ITERATIONS

TABLE OF VALUES FOR EXPERIMENTAL DATA SET 3
**********

AREA OF OUTER NOZZLE 10.6036 CM**2
AREA OF INNER NOZZLE .3167 CM**2
VELOCITY OF AIR 1.3464 M/SEC

| VELOCITY OF FUEL [ M/SEC ] | HEIGHT OF CENTRAL JET [ MM ] | HEIGHT OF LEFT VORTEX [ MM ] | HEIGHT OF RIGHT VORTEX [ MM ] | |
|---|---|---|---|---|
| .1151 | 12.7000 | .0000 | .0000 | |
| .1979 | 19.9120 | .0000 | .0000 | |
| .2916 | 27.9400 | .0000 | .0000 | |
| .3729 | 31.4960 | .0000 | .0000 | |
| .4576 | 34.4678 | .0000 | .0000 | |
| .5601 | 38.3540 | .0000 | .0000 | |
| .6359 | 42.1640 | .0000 | .0000 | |
| .7310 | 46.4820 | .0000 | .0000 | (*) |
| .8274 | 49.5300 | .0000 | .0000 | (*) |

THE PENTRATION POINT IS SIGHED BY (*)

FUNCTION FOR THIS DATA SET
**********

THE VALUES ARE NONDIMENSIONALIZED BY THE RULES

$$Y = \frac{\text{VELOCITY OF FUEL}}{\text{PENETRATION VELOCITY}}$$

$$Y = \frac{\text{FORWARD STAGNATION POINT}}{\text{AFT STAGNATION POINT}}$$

CONSTANTS ARE DETERMINED BY A LEAST SQUARE METHOD

FUNCTION: $Y = 1+A1*(1-X)+A2*(1-X)**2+A3*(1-X)**3$
********

INITIAL VALUES: A1 = .100
********** A2 = 2.30
A3 = 1.50

CONSTANTS: A1 = -.769
****** A2 = .632
A3 = -.814

LEAST SQUARE ERROR NORM: E = .12735E-02

THE SOLUTION WAS FOUND AFTER 2 ITERATIONS

FUNCTION FOR THIS DATA SET
**********

THE VALUES ARE NONDIMENSIONALIZED BY THE RULES

$$X = \frac{\text{VELOCITY OF FUEL}}{\text{ANNULUS AIR VELOCITY}}$$

$$Y = \frac{\text{FORWARD STAGNATION POINT}}{\text{AFT STAGNATION POINT}}$$

CONSTANTS ARE DETERMINED BY A LEAST SQUARE METHOD

FUNCTION: $Y = 1+A1*(1-X)+A2*(1-X)**2+A3*(1-X)**3$
********

INITIAL VALUES:
**********
A1 = .100
A2 = 2.30
A3 = 1.50

CONSTANTS:
******
A1 = .567
A2 = -1.70
A3 = .268

LEAST SQUARE ERROR NORM: E = .34427E-02

THE SOLUTION WAS FOUND AFTER 2 ITERATIONS

TABLE OF VALUES FOR EXPERIMENTAL DATA SET 4
**********

AREA OF OUTER NOZZLE 10.6036 CM**2
AREA OF INNER NOZZLE .3167 CM**2
VELOCITY OF AIR 1.6246 M/SEC

| VELOCITY OF FUEL [ M/SEC ] | HEIGHT OF CENTRAL JET [ MM ] | HEIGHT OF LEFT VORTEX [ MM ] | HEIGHT OF RIGHT VORTEX [ MM ] | |
|---|---|---|---|---|
| .1300 | 12.7000 | .0000 | .0000 | |
| .1999 | 17.7800 | .0000 | .0000 | |
| .3314 | 25.8319 | .0000 | .0000 | |
| .4536 | 30.1498 | .0000 | .0000 | |
| .5715 | 34.0360 | .0000 | .0000 | |
| .6534 | 37.0840 | .0000 | .0000 | |
| .7578 | 40.6400 | .0000 | .0000 | |
| .8632 | 43.9420 | .0000 | .0000 | (*) |
| .9897 | 46.9900 | .0000 | .0000 | (*) |

THE PENTRATION POINT IS SIGHED BY (*)

FUNCTION FOR THIS DATA SET
**********

THE VALUES ARE NONDIMENSIONALIZED BY THE RULES

$$Y = \frac{\text{VELOCITY OF FUEL}}{\text{PENETRATION VELOCITY}}$$

$$Y = \frac{\text{FORWARD STAGNATION POINT}}{\text{AFT STAGNATION POINT}}$$

CONSTANTS ARE DETERMINED BY A LEAST SQUARE METHOD

FUNCTION: Y = 1+A1*(1-X)+A2*(1-X)**2+A3*(1-X)**3
********

INITIAL VALUES: A1 = .100
********** A2 = 2.30
A3 = 1.50

CONSTANTS: A1 = -.651
****** A2 = .306
A3 = -.563

LEAST SQUARE ERROR NORM: E = .94812E-03

THE SOLUTION WAS FOUND AFTER 2 ITERATIONS

FUNCTION FOR THIS DATA SET
**********

THE VALUES ARE NONDIMENSIONALIZED BY THE RULES

$$X = \frac{\text{VELOCITY OF FUEL}}{\text{ANNULUS AIR VELOCITY}}$$

$$Y = \frac{\text{FORWARD STAGNATION POINT}}{\text{AFT STAGNATION POINT}}$$

CONSTANTS ARE DETERMINED BY A LEAST SQUARE METHOD

FUNCTION: $Y = 1+A1*(1-X)+A2*(1-X)**2+A3*(1-X)**3$
********

INITIAL VALUES: A1 = .100
********** A2 = 2.30
A3 = 1.50

CONSTANTS: A1 = .598
****** A2 = -1.71
A3 = .265

LEAST SQUARE ERROR NORM: E = .19057E-02

THE SOLUTION WAS FOUND AFTER 2 ITERATIONS

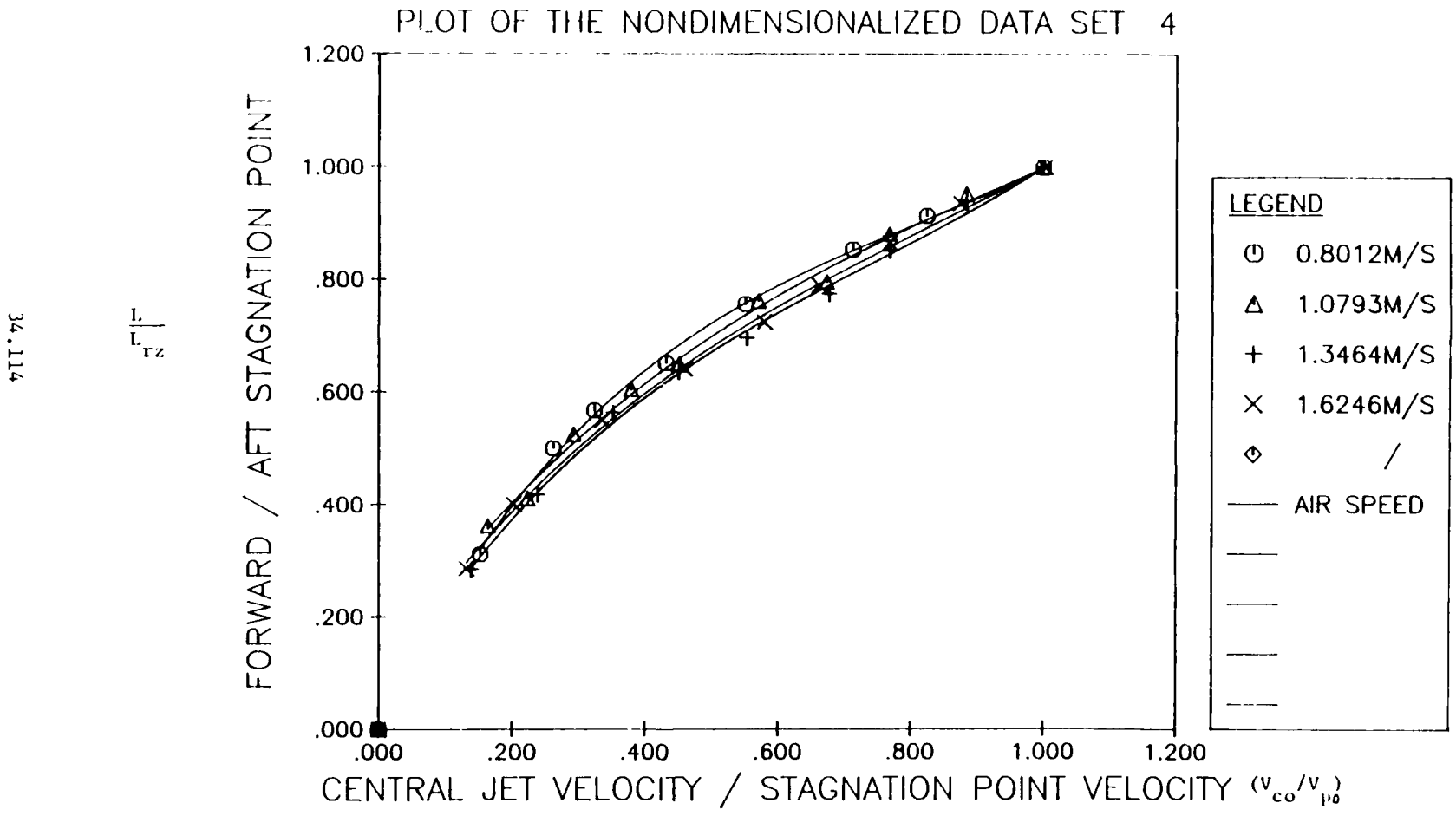



Fig. 10. Plot of $L/L_{rz}$ versus $V_{co}/V_p$ for Test I with $D_j$ = 6.35 mm - cold reacting flow.

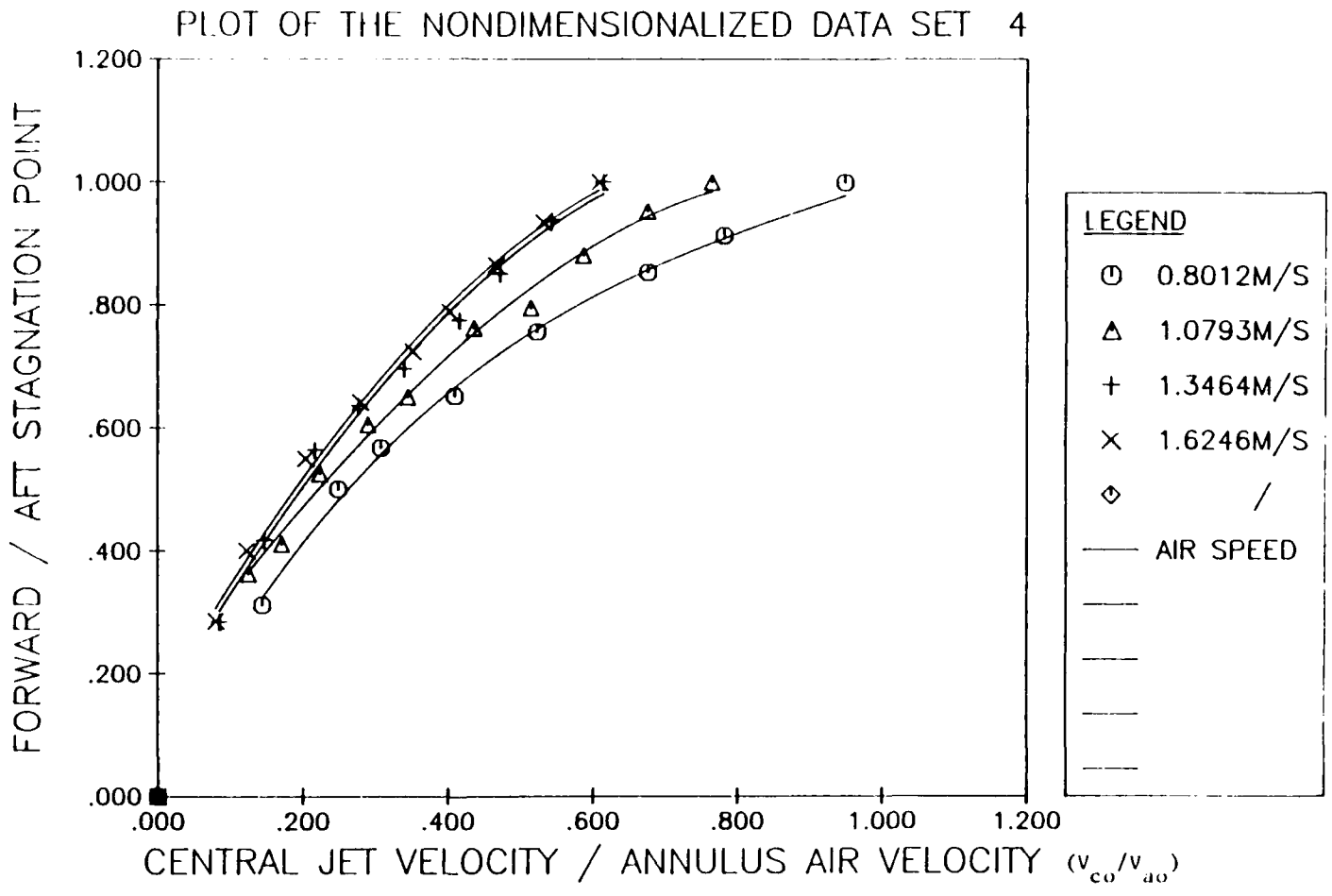



Fig. 11. Plot $L/L_{rz}$ versus $V_{co}/V_{ao}$ for Test I with $D_j$ = 6.35 mm - cold reacting flow.

TABLE OF VALUES FOR EXPERIMENTAL DATA SET 1
**********

AREA OF OUTER NOZZLE 10.6036 CM**2
AREA OF INNER NOZZLE .7012 CM**2
VELOCITY OF AIR .8012 M/SEC

| VELOCITY OF FUEL [ M/SEC ] | HEIGHT OF CENTRAL JET [ MM ] | HEIGHT OF LEFT VORTEX [ MM ] | HEIGHT OF RIGHT VORTEX [ MM ] | |
|---|---|---|---|---|
| .0405 | 5.5118 | .0000 | .0000 | |
| .1061 | 14.7955 | .0000 | .0000 | |
| .1638 | 22.9616 | .0000 | .0000 | |
| .2362 | 34.8488 | .0000 | .0000 | |
| .3044 | 43.1800 | .0000 | .0000 | |
| .3576 | 45.7200 | .0000 | .0000 | |
| .4331 | 49.1490 | .0000 | .0000 | |
| .4700 | 52.5780 | .0000 | .0000 | |
| .5264 | 58.4200 | .0000 | .0000 | (*) |

THE PENTRATION POINT IS SIGHED BY (*)

FUNCTION FOR THIS DATA SET
**********

THE VALUES ARE NONDIMENSIONALIZED BY THE RULES

$$X = \frac{\text{VELOCITY OF FUEL}}{\text{PENETRATION VELOCITY}}$$

$$Y = \frac{\text{FORWARD STAGNATION POINT}}{\text{AFT STAGNATION POINT}}$$

CONSTANTS ARE DETERMINED BY A LEAST SQUARE METHOD

FUNCTION: $Y = 1+A1*(1-X)+A2*(1-X)**2+A3*(1-X)**3$
********

INITIAL VALUES: A1 = .100
********** A2 = 2.30
A3 = 1.50

CONSTANTS: A1 = -.789
******* A2 = .542
A3 = -.827

LEAST SQUARE ERROR NORM: E = .43068E-02

THE SOLUTION WAS FOUND AFTER 2 ITERATIONS

FUNCTION FOR THIS DATA SET
**********

THE VALUES ARE NONDIMENSIONALIZED BY THE RULES

$$X = \frac{\text{VELOCITY OF FUEL}}{\text{ANNULUS AIR VELOCITY}}$$

$$Y = \frac{\text{FORWARD STAGNATION POINT}}{\text{AFT STAGNATION POINT}}$$

CONSTANTS ARE DETERMINED BY A LEAST SQUARE METHOD

FUNCTION: Y = 1+A1*(1-X)+A2*(1-X)**2+A3*(1-X)**3
********

INITIAL VALUES: A1 = .100
********** A2 = 2.30
A3 = 1.50

CONSTANTS: A1 = .248
****** A2 = -.940
A3 = -.341

LEAST SQUARE ERROR NORM: E = .49449E-02

THE SOLUTION WAS FOUND AFTER 2 ITERATIONS

TABLE OF VALUES FOR EXPERIMENTAL DATA SET 2
**********

AREA OF OUTER NOZZLE 10.6036 CM**2
AREA OF INNER NOZZLE .7012 CM**2
VELOCITY OF AIR 1.0793 M/SEC

| VELOCITY OF FUEL [ M/SEC ] | HEIGHT OF CENTRAL JET [ MM ] | HEIGHT OF LEFT VORTEX [ MM ] | HEIGHT OF RIGHT VORTEX [ MM ] | |
|---|---|---|---|---|
| .0547 | 8.8900 | .0000 | .0000 | |
| .1192 | 17.0180 | .0000 | .0000 | |
| .1486 | 22.7833 | .0000 | .0000 | |
| .2421 | 29.7020 | .0000 | .0000 | |
| .3144 | 38.1000 | .0000 | .0000 | |
| .3683 | 41.4020 | .0000 | .0000 | |
| .4504 | 44.9326 | .0000 | .0000 | |
| .5202 | 48.2600 | .0000 | .0000 | (*) |
| .5902 | 52.3240 | .0000 | .0000 | (*) |

THE PENTRATION POINT IS SIGHED BY (*)

FUNCTION FOR THIS DATA SET
**********

THE VALUES ARE NONDIMENSIONALIZED BY THE RULES

$$X = \frac{\text{VELOCITY OF FUEL}}{\text{PENETRATION VELOCITY}}$$

$$Y = \frac{\text{FORWARD STAGNATION POINT}}{\text{AFT STAGNATION POINT}}$$

CONSTANTS ARE DETERMINED BY A LEAST SQUARE METHOD

FUNCTION: $Y = 1+A1*(1-X)+A2*(1-X)**2+A3*(1-X)**3$
********

INITIAL VALUES: A1 = .100
********** A2 = 2.30
A3 = 1.50

CONSTANTS: A1 = -.458
****** A2 = -.293
A3 = -.238

LEAST SQUARE ERROR NORM: E = .27204E-02

THE SOLUTION AS FOUND AFTER 2 ITERATIONS

FUNCTION FOR THIS DATA SET
**********

THE VALUES ARE NONDIMENSIONALIZED BY THE RULES

$$Y = \frac{\text{VELOCITY OF FUEL}}{\text{ANNULUS AIR VELOCITY}}$$

$$Y = \frac{\text{FORWARD STAGNATION POINT}}{\text{AFT STAGNATION POINT}}$$

CONSTANTS ARE DETERMINED BY A LEAST SQUARE METHOD

FUNCTION: $Y = 1+A1*(1-X)+A2*(1-X)**2+A3*(1-X)**3$
********

INITIAL VALUES: A1 = .100
********** A2 = 2.30
A3 = 1.50

CONSTANTS: A1 = .479
****** A2 = -.823
A3 = -.638

LEAST SQUARE ERROR NORM: E = .26008E-02

THE SOLUTION WAS FOUND AFTER 2 ITERATIONS

TABLE OF VALUES FOR EXPERIMENTAL DATA SET 3
**********

AREA OF OUTER NOZZLE 10.6036 CM**2
AREA OF INNER NOZZLE .7012 CM**2
VELOCITY OF AIR 1.3464 M/SEC

| VELOCITY OF FUEL [ M/SEC ] | HEIGHT OF CENTRAL JET [ MM ] | HEIGHT OF LEFT VORTEX [ MM ] | HEIGHT OF RIGHT VORTEX [ MM ] | |
|---|---|---|---|---|
| .0467 | 7.5692 | .0000 | .0000 | |
| .1048 | 14.0462 | .0000 | .0000 | |
| .1819 | 22.5600 | .0000 | .0000 | |
| .2396 | 27.0510 | .0000 | .0000 | |
| .3224 | 35.9918 | .0000 | .0000 | |
| .3904 | 38.8112 | .0000 | .0000 | |
| .4380 | 40.1320 | .0000 | .0000 | |
| .5173 | 43.1800 | .0000 | .0000 | (*) |
| .5629 | 47.7520 | .0000 | .0000 | (*) |

THE PENTRATION POINT IS SIGHED BY (*)

FUNCTION FOR THIS DATA SET
**********

THE VALUES ARE NONDIMENSIONALIZED BY THE RULES

$$X = \frac{\text{VELOCITY OF FUEL}}{\text{PENETRATION VELOCITY}}$$

$$Y = \frac{\text{FORWARD STAGNATION POINT}}{\text{AFT STAGNATION POINT}}$$

CONSTANTS ARE DETERMINED BY A LEAST SQUARE METHOD

FUNCTION: $Y = 1+A1*(1-X)+A2*(1-X)**2+A3*(1-X)**3$
********

INITIAL VALUES:
**********
A1 = .100
A2 = 2.30
A3 = 1.50

CONSTANTS:
******
A1 = -.589
A2 = .303
A3 = -.618

LEAST SQUARE ERROR NORM: E = .45395E-02

THE SOLUTION WAS FOUND AFTER 2 ITERATIONS

FUNCTION FOR THIS DATA SET
**********

THE VALUES ARE NONDIMENSIONALIZED BY THE RULES

$$Y = \frac{\text{VELOCITY OF FUEL}}{\text{ANNULUS AIR VELOCITY}}$$

$$Y = \frac{\text{FORWARD STAGNATION POINT}}{\text{AFT STAGNATION POINT}}$$

CONSTANTS ARE DETERMINED BY A LEAST SQUARE METHOD

FUNCTION: $Y = 1+A1*(1-X)+A2*(1-X)**2+A3*(1-X)**3$
********

INITIAL VALUES: A1 = .100
********** A2 = 2.30
A3 = 1.50

CONSTANTS: A1 = .202
****** A2 = .594
A3 = -1.77

LEAST SQUARE ERROR NORM: E = .41146E-02

THE SOLUTION WAS FOUND AFTER 2 ITERATIONS

TABLE OF VALUES FOR EXPERIMENTAL DATA SET 4
**********

AREA OF OUTER NOZZLE 10.6036 CM**2
AREA OF INNER NOZZLE .7012 CM**2
VELOCITY OF AIR 1.6246 M/SEC

| VELOCITY OF FUEL [ M/SEC ] | HEIGHT OF CENTRAL JET [ MM ] | HEIGHT OF LEFT VORTEX [ MM ] | HEIGHT OF RIGHT VORTEX [ MM ] | |
|---|---|---|---|---|
| .0973 | 11.1506 | .0000 | .0000 | |
| .1170 | 14.0462 | .0000 | .0000 | |
| .2110 | 18.2118 | .0000 | .0000 | |
| .2695 | 23.9522 | .0000 | .0000 | |
| .3293 | 29.8196 | .0000 | .0000 | |
| .4116 | 34.8742 | .0000 | .0000 | |
| .4805 | 37.5412 | .0000 | .0000 | |
| .5277 | 39.3700 | .0000 | .0000 | |
| .6209 | 44.3564 | .0000 | .0000 | (*) |

THE PENTRATION POINT IS SIGHED BY (*)

FUNCTION FOR THIS DATA SET
**********

THE VALUES ARE NONDIMENSIONALIZED BY THE RULES

$$X = \frac{\text{VELOCITY OF FUEL}}{\text{PENETRATION VELOCITY}}$$

$$Y = \frac{\text{FORWARD STAGNATION POINT}}{\text{AFT STAGNATION POINT}}$$

CONSTANTS ARE DETERMINED BY A LEAST SQUARE METHOD

FUNCTION: $Y = 1+A1*(1-X)+A2*(1-X)**2+A3*(1-X)**3$
********

INITIAL VALUES: A1 = .100
********** A2 = 2.30
A3 = 1.50

CONSTANTS: A1 = -.529
****** A2 = -.711
A3 = .362

LEAST SQUARE ERROR NORM: E = .43444E-02

THE SOLUTION WAS FOUND AFTER 2 ITERATIONS

FUNCTION FOR THIS DATA SET
**********

THE VALUES ARE NONDIMENSIONALIZED BY THE RULES

$$Y = \frac{\text{VELOCITY OF FUEL}}{\text{ANNULUS AIR VELOCITY}}$$

$$Y = \frac{\text{FORWARD STAGNATION POINT}}{\text{AFT STAGNATION POINT}}$$

CONSTANTS ARE DETERMINED BY A LEAST SQUARE METHOD

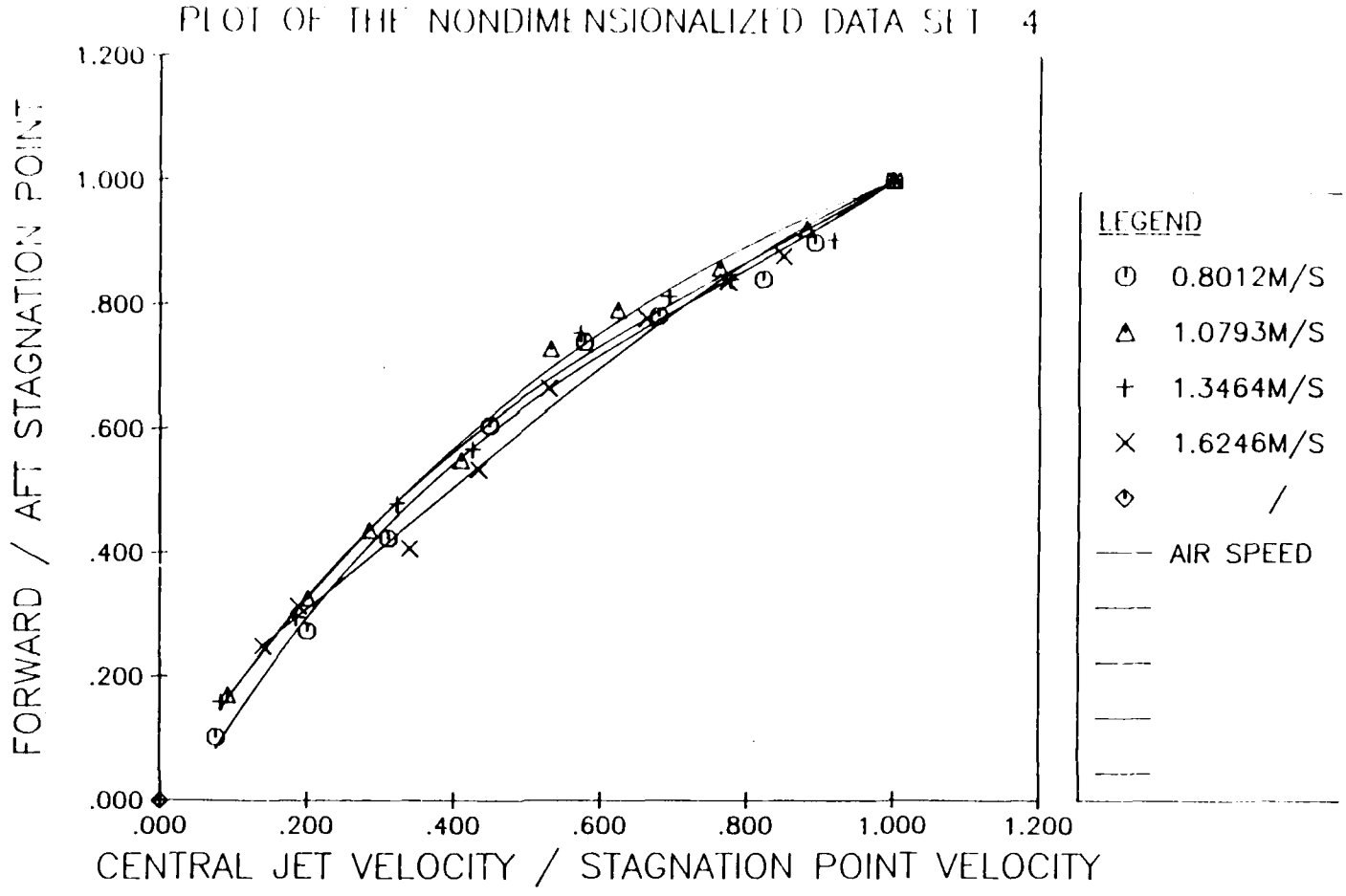
FUNCTION: $Y = 1+A1*(1-X)+A2*(1-X)**2+A3*(1-X)**3$
********

INITIAL VALUES: A1 = .100
********** A2 = 2.30
A3 = 1.50

CONSTANTS: A1 = 1.95
****** A2 = -3.64
A3 = .778

LEAST SQUARE ERROR NORM: E = .46371E-02

THE SOLUTION WAS FOUND AFTER 2 ITERATIONS


PLOT OF THE NONDIMENSIONALIZED DATA SET 4
FORWARD / AFT STAGNATION POINT
1.200
1.000
.800
.600
.400
.200
.000
.000
.200
.400
.600
.800
1.000
1.200
CENTRAL JET VELOCITY / STAGNATION POINT VELOCITY
LEGEND
0.8012M/S
1.0793M/S
1.3464M/S
1.6246M/S
/
AIR SPEED

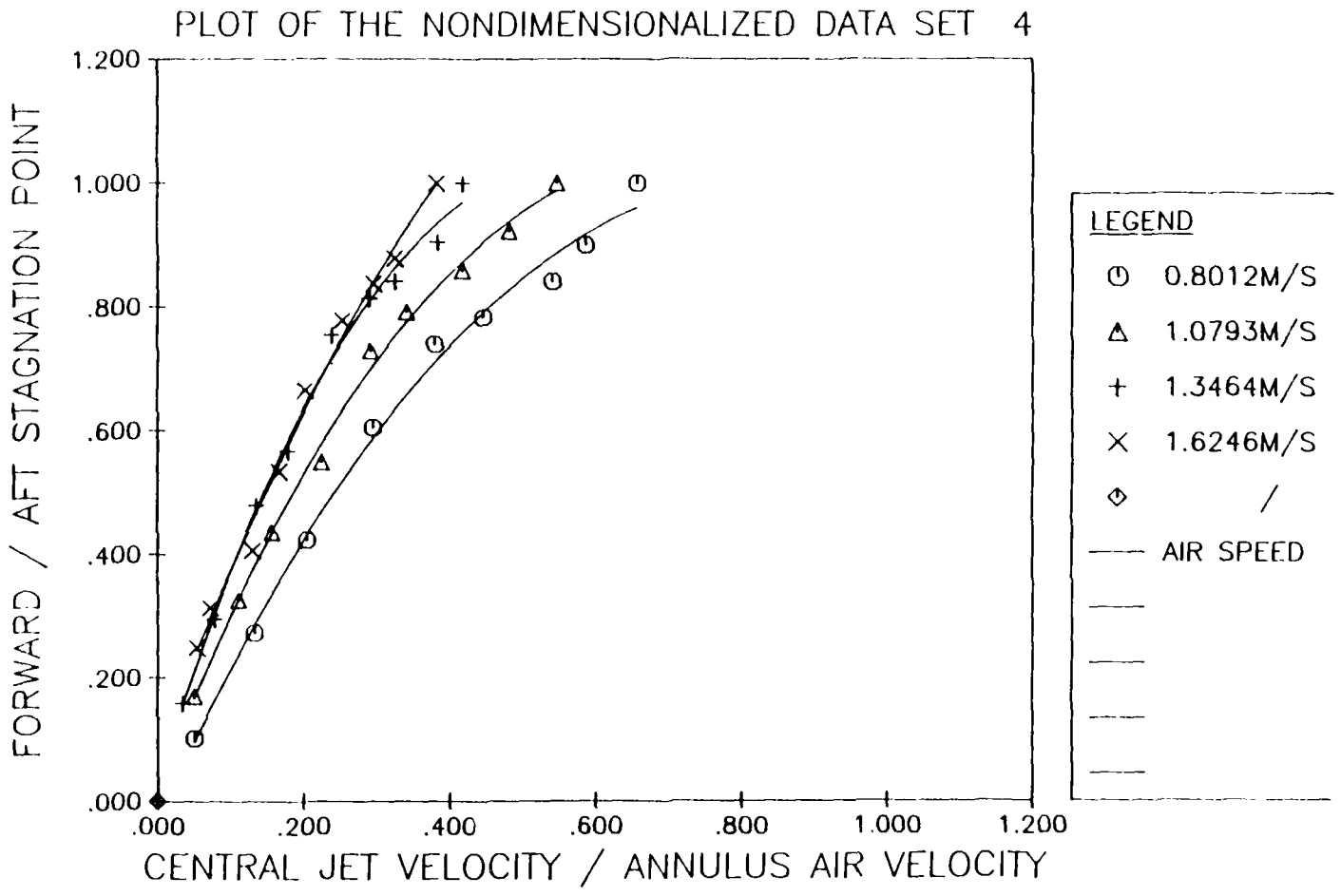

PLOT OF THE NONDIMENSIONALIZED DATA SET 4
FORWARD / AFT STAGNATION POINT
1.200
1.000
.800
.600
.400
.200
.000
.000
.200
.400
.600
.800
1.000
1.200
CENTRAL JET VELOCITY / ANNULUS AIR VELOCITY
LEGEND
0.8012M/S
1.0793M/S
1.3464M/S
1.6246M/S
/
AIR SPEED

TABLE OF VALUES FOR EXPERIMENTAL DATA SET 1
**********

AREA OF OUTER NOZZLE 10.6036 CM**2
AREA OF INNER NOZZLE 1.2668 CM**2
VELOCITY OF AIR .3012 M/SEC

| VELOCITY OF FUEL [ M/SEC ] | HEIGHT OF CENTRAL JET [ MM ] | HEIGHT OF LEFT VORTEX [ MM ] | HEIGHT OF RIGHT VORTEX [ MM ] |
|---|---|---|---|
| .0280 | 5.3086 | .0000 | .0000 |
| .0465 | 7.1628 | .0000 | .0000 |
| .0710 | 9.7790 | .0000 | .0000 |
| .1247 | 13.9700 | .0000 | .0000 |
| .1654 | 19.1770 | .0000 | .0000 |
| .1848 | 23.6982 | .0000 | .0000 |
| .2350 | 30.9118 | .0000 | .0000 |
| .2803 | 35.8140 | .0000 | .0000 |
| .3983 | 50.2031 | .0000 | .0000 |

THE PENETRATION POINT IS SIGNED BY (*)

FUNCTION FOR THIS DATA SET
**********

THE VALUES ARE NONDIMENSIONALIZED BY THE RULES

$$Y = \frac{\text{VELOCITY OF FUEL}}{\text{ANNULUS AIR VELOCITY}}$$

$$Y = \frac{\text{FORWARD STAGNATION POINT}}{\text{AFT STAGNATION POINT}}$$

CONSTANTS ARE DETERMINED BY A LEAST SQUARE METHOD

FUNCTION: $Y = 1+A1*(1-X)+A2*(1-X)**2+A3*(1-X)**3$
********

INITIAL VALUES: A1 = .100
********** A2 = 2.30
A3 = 1.50

CONSTANTS: A1 = 1.54
****** A2 = -5.02
A3 = 2.56

LEAST SQUARE ERROR NORM: E = .77811E-03

THE SOLUTION WAS FOUND AFTER 2 ITERATIONS

TABLE OF VALUES FOR EXPERIMENTAL DATA SET 2
**********

AREA OF OUTER NOZZLE 10.6036 CM**2
AREA OF INNER NOZZLE 1.2668 CM**2
VELOCITY OF AIR 1.0793 M/SEC

| VELOCITY OF FUEL [ M/SEC ] | HEIGHT OF CENTRAL JET [ MM ] | HEIGHT OF LEFT VORTEX [ MM ] | HEIGHT OF RIGHT VORTEX [ MM ] |
|---|---|---|---|
| .0426 | 6.6529 | .0000 | .0000 |
| .0456 | 7.9502 | .0000 | .0000 |
| .0604 | 8.1280 | .0000 | .0000 |
| .0936 | 13.4206 | .0000 | .0000 |
| .1480 | 16.5862 | .0000 | .0000 |
| .1840 | 21.5900 | .0000 | .0000 |
| .2414 | 27.9400 | .0000 | .0000 |
| .2836 | 33.0200 | .0000 | .0000 |
| .3298 | 39.1160 | .0000 | .0000 |

THE PENETRATION POINT IS SIGHED BY (*)

FUNCTION FOR THIS DATA SET
**********

THE VALUES ARE NONDIMENSIONALIZED BY THE RULES

$$X = \frac{\text{VELOCITY OF FUEL}}{\text{ANNULUS AIR VELOCITY}}$$

$$Y = \frac{\text{FORWARD STAGNATION POINT}}{\text{AFT STAGNATION POINT}}$$

CONSTANTS ARE DETERMINED BY A LEAST SQUARE METHOD

FUNCTION: $Y = 1+A1*(1-X)+A2*(1-X)**2+A3*(1-X)**3$
********

INITIAL VALUES: A1 = .100
********** A2 = 2.30
A3 = 1.50

CONSTANTS: A1 = 2.80
****** A2 = -6.84
A3 = 3.11

LEAST SQUARE ERROR NORM: E = .64470E-03

THE SOLUTION WAS FOUND AFTER 2 ITERATIONS

TABLE OF VALUES FOR EXPERIMENTAL DATA SET 3
**********

AREA OF OUTER NOZZLE 10.6036 CM**2
AREA OF INNER NOZZLE 1.2668 CM**2
VELOCITY OF AIR 1.3464 M/SEC

| VELOCITY OF FUEL [ M/SEC ] | HEIGHT OF CENTRAL JET [ MM ] | HEIGHT OF LEFT VORTEX [ MM ] | HEIGHT OF RIGHT VORTEX [ MM ] |
|---|---|---|---|
| .0577 | 9.1694 | .0000 | .0000 |
| .0842 | 10.8712 | .0000 | .0000 |
| .1049 | 13.9446 | .0000 | .0000 |
| .1458 | 16.3576 | .0000 | .0000 |
| .1798 | 19.7612 | .0000 | .0000 |
| .2161 | 22.0980 | .0000 | .0000 |
| .2527 | 23.8760 | .0000 | .0000 |
| .2790 | 26.1620 | .0000 | .0000 |
| .3017 | 29.6672 | .0000 | .0000 |
| .3625 | 33.7312 | .0000 | .0000 |

THE PENETRATION POINT IS SIGHED BY (*)

FUNCTION FOR THIS DATA SET
**********

THE VALUES ARE NONDIMENSIONALIZED BY THE RULES

$$X = \frac{\text{VELOCITY OF FUEL}}{\text{ANNULUS AIR VELOCITY}}$$

$$Y = \frac{\text{FORWARD STAGNATION POINT}}{\text{AFT STAGNATION POINT}}$$

CONSTANTS ARE DETERMINED BY A LEAST SQUARE METHOD

FUNCTION: $Y = 1+A1*(1-X)+A2*(1-X)**2+A3*(1-X)**3$
********

INITIAL VALUES: A1 = .100
********** A2 = 2.30
A3 = 1.50

CONSTANTS: A1 = 1.78
****** A2 = -4.40
A3 = 1.71

LEAST SQUARE ERROR NORM: E = .14186E-02

THE SOLUTION WAS FOUND AFTER 2 ITERATIONS

TABLE OF VALUES FOR EXPERIMENTAL DATA SET 4

AREA OF OUTER NOZZLE 10.6034 CM**2
AREA OF INNER NOZZLE 1.2668 CM**2
VELOCITY OF AIR 1.6246 M/SEC

| VELOCITY OF FUEL [ M/SEC ] | HEIGHT OF CENTRAL JET [ MM ] | HEIGHT OF LEFT VORTEX [ MM ] | HEIGHT OF RIGHT VORTEX [ MM ] |
|---|---|---|---|
| .0544 | 8.2550 | .0000 | .0000 |
| .0825 | 10.6299 | .0000 | .0000 |
| .1196 | 12.7762 | .0000 | .0000 |
| .1460 | 13.4620 | .0000 | .0000 |
| .1507 | 15.2908 | .0000 | .0000 |
| .1845 | 17.3736 | .0000 | .0000 |
| .2252 | 19.8629 | .0000 | .0000 |
| .2815 | 22.3266 | .0000 | .0000 |
| .3447 | 25.9080 | .0000 | .0000 |

THE PENETRATION POINT IS SIGHED BY (*)

FUNCTION FOR THIS DATA SET
**********

THE VALUES ARE NONDIMENSIONALIZED BY THE RULES

$$Y = \frac{\text{VELOCITY OF FUEL}}{\text{ANNULUS AIR VELOCITY}}$$

$$Y = \frac{\text{FORWARD STAGNATION POINT}}{\text{AFT STAGNATION POINT}}$$

CONSTANTS ARE DETERMINED BY A LEAST SQUARE METHOD

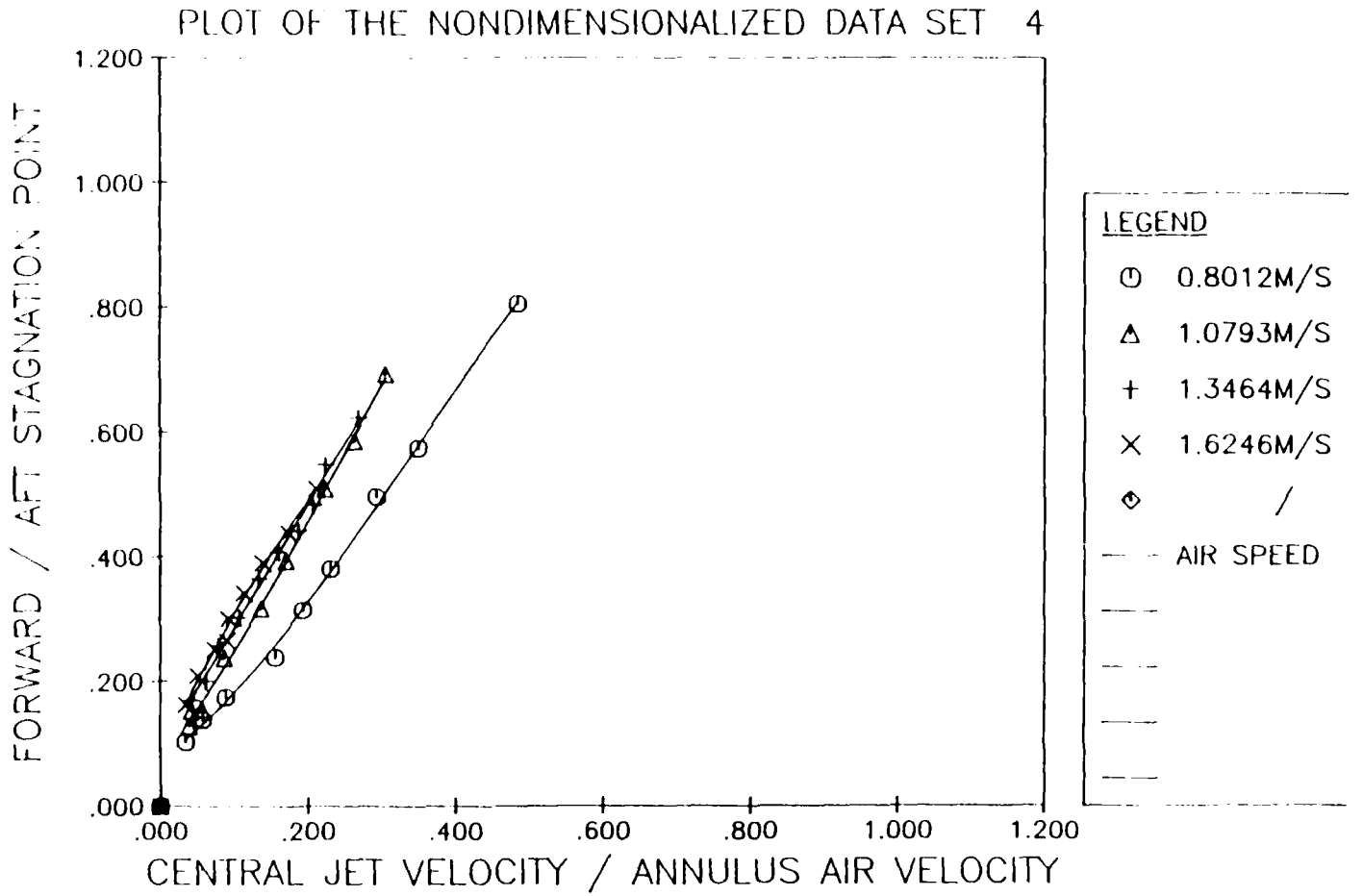
FUNCTION: Y = 1+A1*(1-X)+A2*(1-X)**2+A3*(1-X)**3
********

INITIAL VALUES: A1 = .100
********** A2 = 2.30
A3 = 1.50

CONSTANTS: A1 = -.311
****** A2 = .395
A3 = -1.00

LEAST SQUARE ERROR NORM: E = .75145E-03

THE SOLUTION WAS FOUND AFTER 2 ITERATIONS


PLOT OF THE NONDIMENSIONALIZED DATA SET 4
FORWARD / AFT STAGNATION POINT
1.200
1.000
.800
.600
.400
.200
.000
.000
.200
.400
.600
.800
1.000
1.200
CENTRAL JET VELOCITY / ANNULUS AIR VELOCITY
LEGEND
0.8012M/S
1.0793M/S
1.3464M/S
1.6246M/S
/
AIR SPEED

2. Experimental Results of Test I for the Combusting Flow

TABLE OF VALUES FOR EXPERIMENTAL DATA SET 1
**********

AREA OF OUTER NOZZLE 10.0 SQ CMS
AREA OF INNER NOZZLE .587 SQ CMS
VELOCITY OF JET .0241 M/SEC

| VELOCITY OF FUEL [ M/SEC ] | WIDTH OF CENTRAL JET [ MM ] | HEIGHT OF LEFT VORTEX [ MM ] | HEIGHT OF RIGHT VORTEX [ MM ] | |
|---|---|---|---|---|
| .0402 | 3.4134 | 4.2324 | 5.1562 | |
| .0402 | 3.1488 | 4.0640 | 5.1562 | |
| .0619 | 4.1067 | 4.2164 | 5.1054 | |
| .0736 | 3.8354 | 4.2418 | 5.3340 | |
| .0940 | 3.1750 | 4.3180 | 5.1562 | |
| .0973 | 3.8608 | 4.4432 | 5.1562 | |
| .1047 | 4.3688 | 4.4450 | 5.1562 | |
| .1131 | 11.7119 | 4.7750 | 5.1562 | |
| .1260 | 12.3540 | 4.9530 | 5.1308 | |
| .1447 | 14.3110 | 4.8530 | 5.1308 | |
| .1813 | 15.0180 | 4.7244 | 5.4610 | (*) |

THE PENETRATION DUE TO DIGGER BY (*)

[illegible]

[illegible]

[illegible]

$$Y = \frac{\text{VELOCITY AT POINT}}{\text{DENSITY VELOCITY}}$$

$$Y = \frac{\text{FREE-FLOW STAGNATION POINT}}{\text{ART STAGNATION POINT}}$$

[illegible]

EVALUATION: $Y = 1+A1*(1-X)+A2*(1-X)**2+A3*(1-X)**3$

INITIAL VALUES: A1 = .100
A2 = 1.31
A3 = 1.50

CONSTANTS: A1 = -.0961
A2 = -1.07
A3 = .92

[illegible] E = .999218E-02

THE [illegible]

FUNCTION FOR THIS DATA SET
**********

THE VALUES ARE NONDIMENSIONALIZED BY THE RULES

$$X = \frac{\text{VELOCITY AT FUEL}}{\text{ANNULUS AIR VELOCITY}}$$

$$Y = \frac{\text{FORWARD STAGNATION POINT}}{\text{AFT STAGNATION POINT}}$$

CONSTANTS ARE DETERMINED BY A LEAST SQUARES METHOD

FUNCTION: $Y = 1+A1*(1-X)+A2*(1-X)**2+A3*(1-X)**3$
********

INITIAL VALUES: A1 = .100
********** A2 = -.30
A3 = 1.50

CONSTANTS: A1 = .703
******** A2 = .760
A3 = -2.7

LEAST SQUARES ERROR NORM: E = .110755E-01

THE SOLUTION WAS FOUND AFTER 2 ITERATIONS

TABLE OF VALUES FOR EXPERIMENTAL DATA SET  2
**********

AREA OF OUTER NOZZLE  = 17.100 CM**2
AREA OF INNER NOZZLE  = .3167 CM**2
VELOCITY OF AIR  = .7011 M/SEC

| VELOCITY OF FUEL [ M/SEC ] | HEIGHT OF CENTRAL JET [ MM ] | HEIGHT OF LEFT VORTEX [ MM ] | HEIGHT OF RIGHT VORTEX [ MM ] | |
|---|---|---|---|---|
| .2681 | 3.2020 | 5.4510 | 7.2200 | |
| .2819 | 4.0346 | 5.0300 | 6.1976 | |
| .2959 | 4.1962 | 5.0385 | 6.0960 | |
| .3237 | 5.2146 | 4.9530 | 5.9690 | |
| .3937 | 7.0677 | 4.9276 | 5.6642 | |
| .1196 | 11.8870 | 4.7244 | 5.7404 | |
| .1391 | 13.0182 | 4.4450 | 5.8420 | |
| .1585 | 14.3670 | 4.3022 | 5.4102 | |
| .1757 | 14.3048 | 5.0546 | 5.9156 | |
| .2107 | 14.4120 | 4.6736 | 5.7785 | (*) |

THE PENETRATION POINT IS SIGNED BY (*)

FUNCTION FOR THIS DATA SET
**********

THE VALUES ARE NONDIMENSIONALIZED BY THE RULES

$$Y = \frac{\text{VELOCITY OF SHELL}}{\text{PENETRATION VELOCITY}}$$

$$Y = \frac{\text{FORWARD STAGNATION POINT}}{\text{AFT STAGNATION POINT}}$$

CONSTANTS ARE DETERMINED BY A LEAST SQUARE METHOD

FUNCTION: $Y = A1*(1-Y)+A2*(1-X)**2+A3*(1-X)**3$
********

INITIAL VALUES: A1 = .100
********** A2 = 2.30
A3 = 1.50

CONSTANTS: A1 = -.357
********** A2= -2.74
A3 = 1.64

LEAST SQUARE ERROR TERM: S = .5674*E-02

THE SOLUTION HAS BEEN FOUND AFTER 2 ITERATIONS

FUNCTION FOR THIS DATA SET
**********

THE VALUES ARE NORMALIZED BY THE FIXED

$$Y = \frac{\text{VELOCITY OF FUEL}}{\text{ANNULUS AIR VELOCITY}}$$

$$X = \frac{\text{FORWARD STAGNATION POINT}}{\text{AFT STAGNATION POINT}}$$

CONSTANTS ARE DETERMINED BY A LEAST SQUARE METHOD

FUNCTION: $Y = 1+A1*(1-X)+A2*(1-X)**2+A3*(1-X)**3$
********

INITIAL VALUES: A1 = .100
********** A2 = 2.30
A3 = 1.50

CONSTANTS: A1 = 2.04
********* A2 = -2.49
A3 = -1.00

LEAST SQUARE ERROR NORM: E = .1356E-01

THE SOLUTION WAS FOUND AFTER 2 ITERATIONS

TABLE OF VALUES FOR EXPERIMENTAL DATA SET 3
**********

AREA OF OUTER NOZZLE 11.6034 CM**2
AREA OF INNER NOZZLE .3167 CM**2
VELOCITY OF AIR .0703 M/SEC

| VELOCITY OF FUEL [ M/SEC ] | HEIGHT OF CENTRAL JET [ MM ] | HEIGHT OF LEFT VORTEX [ MM ] | HEIGHT OF RIGHT VORTEX [ MM ] | |
|---|---|---|---|---|
| .0649 | 4.4459 | 5.5536 | 6.3421 | |
| .0811 | 5.5033 | 6.1466 | 7.0994 | |
| .0974 | 7.4143 | 6.1974 | 7.5692 | |
| .1217 | 9.7127 | 6.1976 | 7.3406 | |
| .1298 | 11.1252 | 6.1976 | 7.0612 | |
| .1381 | 12.0410 | 6.1976 | 6.7310 | |
| .1503 | 12.8854 | 6.6240 | 7.3860 | |
| .1785 | 13.6409 | 6.4770 | 7.3440 | |
| .2147 | 13.6410 | 6.3700 | 7.3460 | (*) |

THE CENTRATION POINT IS USED BY (*)

FUNCTION FOR THIS DATA SET 2
**********

THE VALUES ARE NONDIMENSIONALIZED BY THE RULES

$$X = \frac{\text{VELOCITY OF FUEL}}{\text{PENETRATION VELOCITY}}$$

$$Y = \frac{\text{FORWARD STAGNATION POINT}}{\text{AFT STAGNATION POINT}}$$

CONSTANTS ARE DETERMINED BY A LEAST SQUARE METHOD

FUNCTION: $Y = 1+A1*(1-X)+A2*(1-X)**2+A3*(1-X)**3$
********

INITIAL VALUES: A1 = .100
********** A2 = 2.30
A3 = 1.50

CONSTANTS: A1 = -.939
********* A2= .476
A3 = -1.06

LEAST SQUARE ERROR NORM: E = .44479E-02

THE SOLUTION WAS FOUND AFTER 2 ITERATIONS

FUNCTION FOR THIS DATA SET :
**********

THE VALUES ARE NON-DIMENSIONALIZED BY THE PILES

$$X = \frac{\text{VELOCITY OF FUEL}}{\text{ANNULUS AIR VELOCITY}}$$

$$Y = \frac{\text{FORWARD STAGNATION POINT}}{\text{AFT STAGNATION POINT}}$$

CONSTANTS ARE DETERMINED BY A LEAST SQUARE METHOD

FUNCTION: $Y = 1+A1*(1-X)+A2*(1-X)**2+A3*(1-X)**3$
********

INITIAL VALUES: A1 = .100
********** A2 = 0.30
A3 = 1.50

CONSTANTS: A1 = -5.33
******** A2 = 17.2
A 3 = -13.2

LEAST SQUARE ERROR NORM: E = .50443E-02

THE SOLUTION WAS FOUND AFTER 2 ITERATIONS

TABLE OF VALUES FOR EXPERIMENTAL DATA SET 4
**********

AREA OF CENTRAL NOZZLE = 12.0036 CM**2
AREA OF INNER A NOZZLE = .3167 CM**2
VELOCITY OF AIR = 1.2484 M/SEC

| VELOCITY OF FUEL [ M/SEC ] | HEIGHT OF CENTRAL JET [ MM ] | HEIGHT OF LEFT VORTEX [ MM ] | HEIGHT OF RIGHT VORTEX [ MM ] | |
|---|---|---|---|---|
| .0777 | 5.3630 | 4.3334 | 10.0534 | |
| .0955 | 5.7664 | 7.0263 | -.7960 | |
| .1060 | 5.8725 | 7.0104 | 8.6360 | |
| .1191 | 11.3616 | 6.0590 | 8.4012 | |
| .1284 | 11.4300 | 6.4072 | 8.3566 | |
| .1410 | 12.7432 | 6.7310 | -.0772 | |
| .1434 | 12.8040 | 6.6348 | 8.0772 | |
| .1515 | 14.1022 | 6.5642 | 8.0772 | |
| .2230 | 13.1410 | 6.4262 | 8.2423 | (*) |

THE BIFURCATION POINT IS SIGNED BY (*)

FUNCTION FOR THIS DATA SET ...
**********

THE VALUES ARE NONDIMENSIONALIZED BY THE RULES

$$Y = \frac{\text{VELOCITY OF FUEL}}{\text{PENETRATION VELOCITY}}$$

$$Y = \frac{\text{FORWARD STAGNATION POINT}}{\text{AFT STAGNATION POINT}}$$

CONSTANTS ARE DETERMINED BY A LEAST SQUARE METHOD

FUNCTION: $Y = A+A1*(1-X)+A2*(1-X)**2+A3*(1-X)**3$
********

INITIAL VALUES: A1 = .100
********** A2 = 2.30
A3 = 1.50

CONSTANTS: A1 = -.759
******** A2= -.214E-01
A3 = -.656

LEAST SQUARE ERROR NORM: E = .521138E-02

THE SOLUTION WAS FOUND AFTER 2 ITERATIONS

FUNCTION FOR THIS DATA SET :
**********

THE VALUES ARE NONDIMENSIONALIZED BY THE RULES

$$Y = \frac{\text{VELOCITY OF FUEL}}{\text{ANNULUS AIR VELOCITY}}$$

$$Y = \frac{\text{FORWARD STAGNATION POINT}}{\text{AFT STAGNATION POINT}}$$

CONSTANTS ARE DETERMINED BY A LEAST SQUARE METHOD

FUNCTION: $Y = 1+A1*(1-X)+A2*(1-X)**2+A3*(1-X)**3$
********

INITIAL VALUES: A1 = .100
********** A2 = 2.30
A3 = 1.50

CONSTANTS: A1 = -10.3
********* A2 = 23.1
A 3 = -20.1

LEAST SQUARE ERROR NORM: E = .5293E-02

THE SOLUTION WAS FOUND AFTER 2 ITERATIONS

TABLE OF VALUES FOR TIME INCREMENT DATA SET 5
**********

AREA OF OUTER NOZZLE = 10.000 IN**2
AREA OF INNER NOZZLE = .2187 IN**2
VELOCITY OF AIR = 1.0000 M/SEC

| VELOCITY OF FUEL [ M/SEC ] | WEIGHT OF CENTRAL JET [ MM ] | WEIGHT OF LEFT VORTEX [ MM ] | WEIGHT OF RIGHT VORTEX [ MM ] | |
|---|---|---|---|---|
| .0740 | .0000 | .1230 | .0000 | |
| .0888 | .0000 | .6740 | 11.1760 | |
| .1139 | .0177 | .8740 | .7790 | |
| .1183 | .0754 | .6240 | .6600 | |
| .1305 | 11.4574 | .0772 | .3980 | |
| .1518 | 13.7185 | .0375 | .5758 | |
| .1744 | 14.9733 | .0264 | .3523 | |
| .2072 | 15.0730 | .2550 | .1440 | |
| .2464 | 11.1410 | .0010 | .0670 | (*) |

THE CONCENTRATION POINT IS GIVEN BY (*)

FUNCTION FOR THIS DATA SET
**********

THE VALUES ARE NORMALIZED BY THE RULES

$$Y = \frac{\text{VELOCITY OF FUEL}}{\text{PENETRATION VELOCITY}}$$

$$Y = \frac{\text{FORWARD STAGNATION POINT}}{\text{AFT STAGNATION POINT}}$$

CONSTANTS ARE DETERMINED BY A LEAST SQUARE METHOD

FUNCTION: $Y = 1+A1*(1-X)+A2*(1-X)**2+A3*(1-X)**3$
********

INITIAL VALUES: A1 = .100
********** A2 = 2.30
A3 = 1.50

CONSTANTS: A1 = -.495
******* A2= -.505
A3 = -.432

LEAST SQUARE ERROR NORM: E = .2040±E-02

THE SOLUTION HAS FOUND AFTER 2 ITERATIONS

FUNCTION FOR THIS DATA SET
**********

THE VALUES ARE NONDIMENSIONALIZED BY THE RULES

$$Y = \frac{\text{VELOCITY OF PIXEL}}{\text{MAXIMUS AIR VELOCITY}}$$

$$Y = \frac{\text{FORWARD STAGNATION POINT}}{\text{AFT STAGNATION POINT}}$$

CONSTANTS ARE DETERMINED BY A LEAST SQUARE METHOD

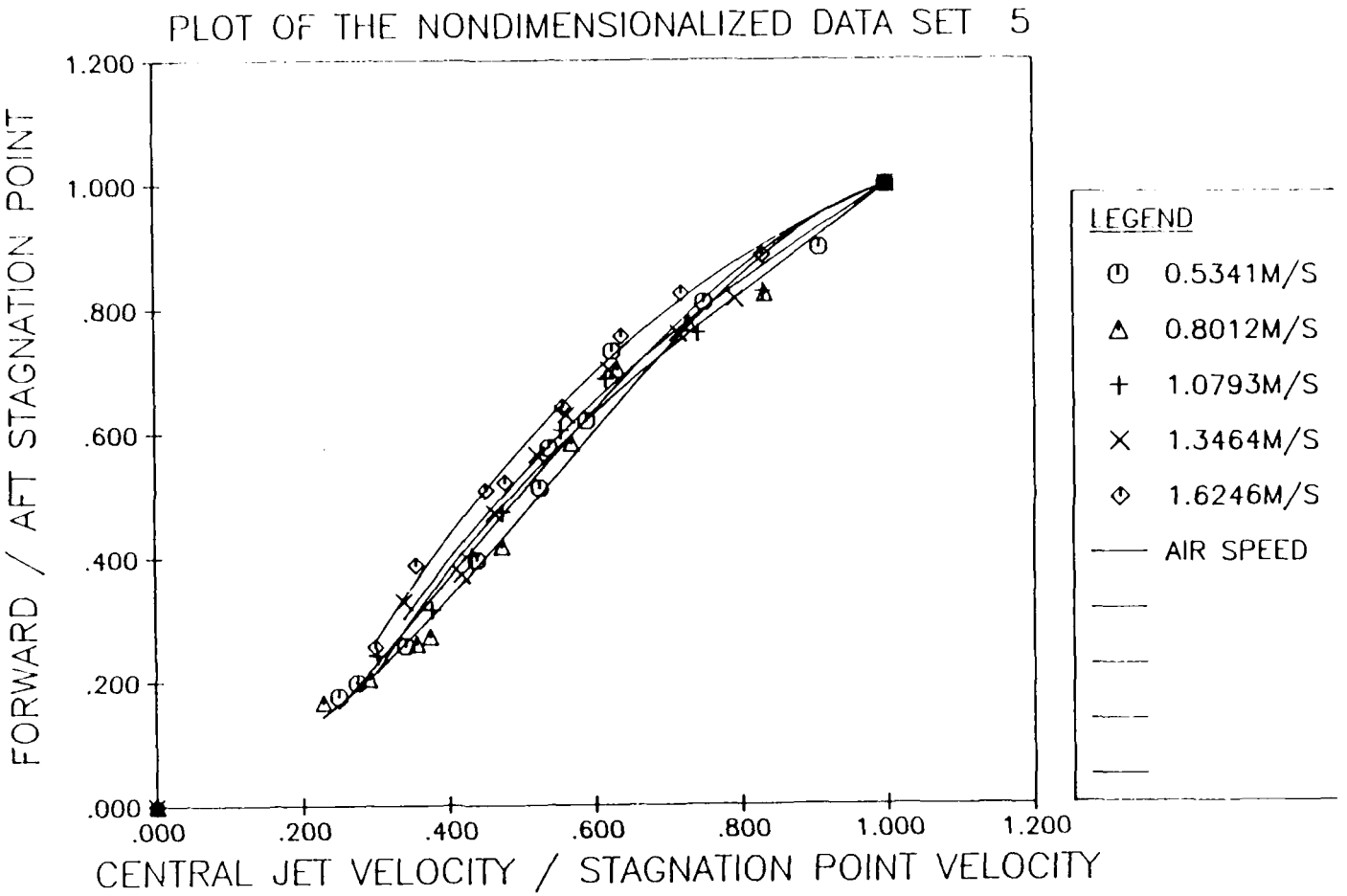
FUNCTION: $Y = 1+A1*(1-X)+A2*(1-X)**2+A3*(1-X)**3$
********

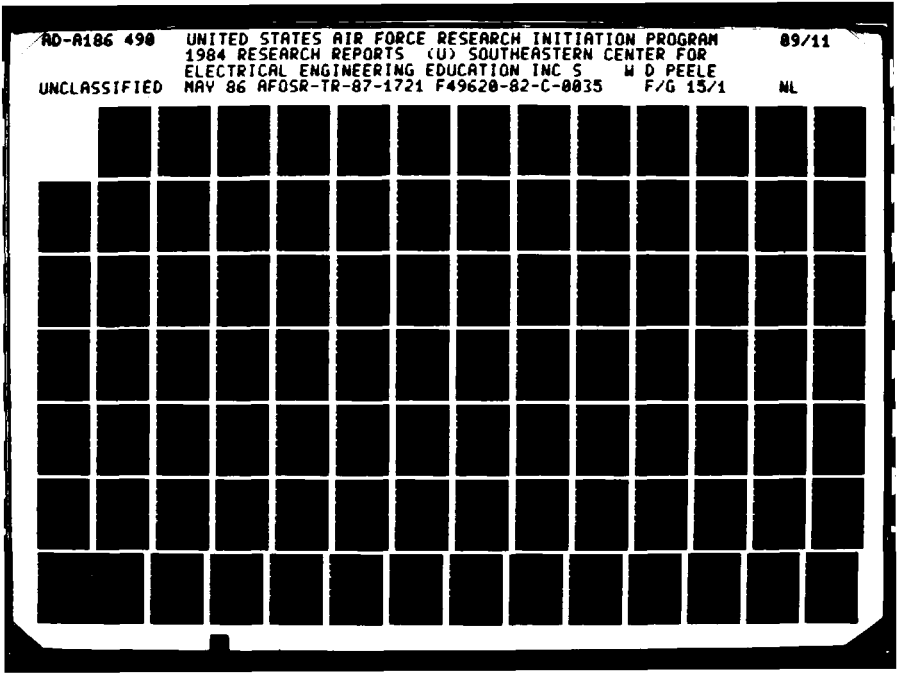
INITIAL VALUES: A1 = .100
********** A2 = 2.30
A3 = 1.50

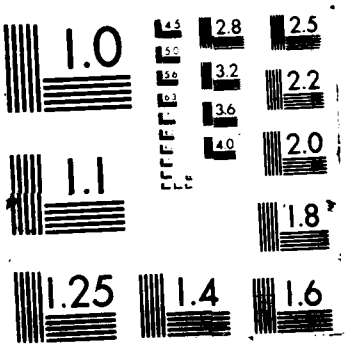
CONSTANTS: A1 = -24.9
******* A2 = 41.7
A 3 = -38.2

LEAST SQUARE ERROR NORM: E = .20e39E-02

THE SOLUTION WAS FOUND AFTER 2 ITERATIONS


PLOT OF THE NONDIMENSIONALIZED DATA SET 5
FORWARD / AFT STAGNATION POINT
1.200
1.000
.800
.600
.400
.200
.000
.000
.200
.400
.600
.800
1.000
1.200
CENTRAL JET VELOCITY / STAGNATION POINT VELOCITY
LEGEND
0.5341M/S
0.8012M/S
1.0793M/S
1.3464M/S
1.6246M/S
AIR SPEED


AD-A186 490 UNITED STATES AIR FORCE RESEARCH INITIATION PROGRAM 09/11
1984 RESEARCH REPORTS (U) SOUTHEASTERN CENTER FOR
ELECTRICAL ENGINEERING EDUCATION INC S W D PEELE
UNCLASSIFIED NAV 86 AFOSR-TR-87-1721 F49620-82-C-0035 F/G 15/1 NL


1.0
1.1
1.25
1.4
1.6
1.8
2.0
2.2
2.5
2.8
3.2
3.6
4.0
4.5
5.0
5.6
6.3
7.1
8.0
9.0
10.0

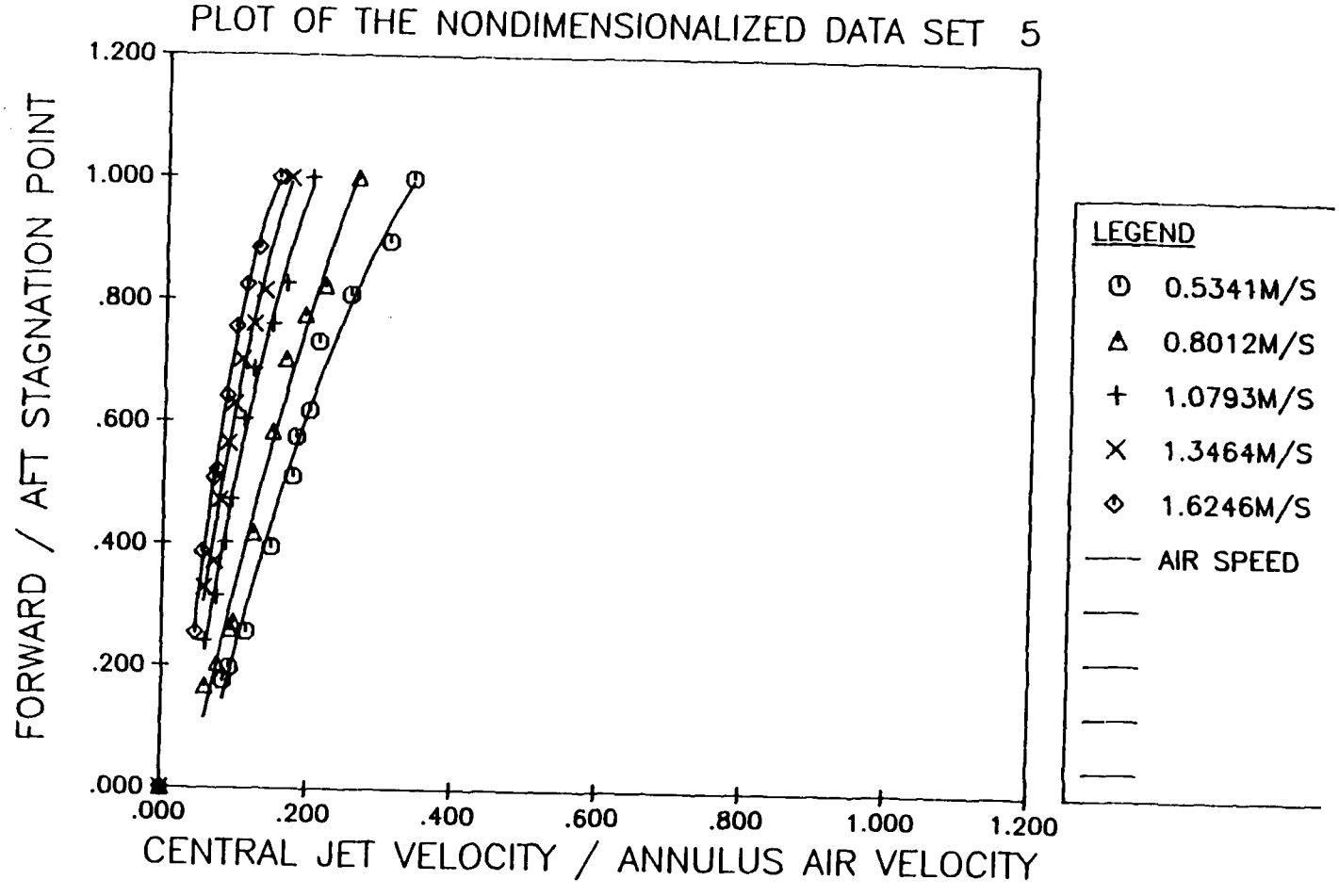

PLOT OF THE NONDIMENSIONALIZED DATA SET 5
FORWARD / AFT STAGNATION POINT
1.200
1.000
.800
.600
.400
.200
.000
.000
.200
.400
.600
.800
1.000
1.200
CENTRAL JET VELOCITY / ANNULUS AIR VELOCITY
LEGEND
0.5341M/S
0.8012M/S
1.0793M/S
1.3464M/S
1.6246M/S
AIR SPEED

TABLE OF VALUES FOR EXPERIMENTAL DATA SET 1
**********

AREA OF OUTER NOZZLE 1?.?03? CM**2
AREA OF INNER NOZZLE .7?1? CM**2
VELOCITY OF AIR .?341 M/SEC

| VELOCITY OF FUEL [ M/SEC ] | HEIGHT OF CENTRAL JET [ MM ] | HEIGHT OF LEFT VORTEX [ MM ] | HEIGHT OF RIGHT VORTEX [ MM ] | |
|---|---|---|---|---|
| .0?8? | ?.?3?2 | 3.?1?2 | 5.4610 | |
| .0404 | 3.7?94 | 4.4450 | 5.527? | |
| .1085 | 7.3660 | 4.2672 | 5.8674 | |
| .1443 | 10.1500 | 5.?340 | 5.6896 | |
| .1900 | 12.?794 | 5.2?32 | 5.2?32 | |
| .?2?4 | 1?.0??? | 4.?250 | 5.9182 | |
| .2659 | 14.0340 | 5.0038 | 6.7818 | (*) |
| .2?80 | 1?.0500 | 4.?794 | 6.6548 | (*) |

THE PENTRATION POINT IS SIGNED BY (*)

FUNCTION FOR THIS DATA SET
**********

THE VALUES ARE NONDIMENSIONALIZED BY THE RULES

$$X = \frac{\text{VELOCITY OF FUEL}}{\text{PENETRATION VELOCITY}}$$

$$Y = \frac{\text{FORWARD STAGNATION POINT}}{\text{AFT STAGNATION POINT}}$$

CONSTANTS ARE DETERMINED BY A LEAST SQUARE METHOD

FUNCTION: $Y = 1+A1*(1-X)+A2*(1-X)**2+A3*(1-X)**3$
********

INITIAL VALUES: A1 = .100
********** A2 = 2.30
A3 = 1.50

CONSTANTS: A1 = -.322
********* A2= -.521
A3 = .318

LEAST SQUARE ERROR NORM: E = .196588E-02

THE SOLUTION WAS FOUND AFTER 2 ITERATIONS

FUNCTION FOR THIS DATA SET /
**********

THE VALUES ARE NONDIMENSIONALIZED BY THE RULES

$$Y = \frac{\text{VELOCITY OF FUEL}}{\text{ANNULUS AIR VELOCITY}}$$

$$Y = \frac{\text{FORWARD STAGNATION POINT}}{\text{AFT STAGNATION POINT}}$$

CONSTANTS ARE DETERMINED BY A LEAST SQUARE METHOD

FUNCTION: $Y = 1+A1*(1-X)+A2*(1-X)**2+A3*(1-X)**3$
********

INITIAL VALUES: A1 = .100
********** A2 = 2.30
A3 = 1.50

CONSTANTS: A1 = 2.02
******** A2 = -5.35
A3 = 2.30

LEAST SQUARE ERROR NORM: E = .16001E-02

THE SOLUTION WAS FOUND AFTER 2 ITERATIONS

TABLE OF VALUES FOR EXPERIMENTAL DATA SET 2
**********

AREA OF OUTER NOZZLE 10.6036 CM**2
AREA OF INNER NOZZLE .7012 CM**2
VELOCITY OF AIR .4012 M/SEC

| VELOCITY OF FUEL [ M/SEC ] | HEIGHT OF CENTRAL JET [ MM ] | HEIGHT OF LEFT VORTEX [ MM ] | HEIGHT OF RIGHT VORTEX [ MM ] | |
|---|---|---|---|---|
| .0414 | 3.0226 | 4.9784 | 6.9596 | |
| .0580 | 4.0132 | 5.5380 | 8.0518 | |
| .1170 | 8.3806 | 5.7404 | 8.8392 | |
| .1474 | 11.4300 | 6.0960 | 7.6200 | |
| .1820 | 15.2400 | 5.8674 | 7.0612 | |
| .2371 | 21.7170 | 5.7404 | 6.2484 | |
| .2742 | 25.0190 | 5.0800 | 6.3881 | (*) |
| .3158 | 26.8732 | 5.0800 | 5.2324 | (*) |

THE PENETRATION POINT IS SIGNED BY (*)

FUNCTION FOR THIS DATA SET
**********

THE VALUES ARE NONDIMENSIONALIZED BY THE RULES

$$X = \frac{\text{VELOCITY OF FUEL}}{\text{PENETRATION VELOCITY}}$$

$$Y = \frac{\text{FORWARD STAGNATION POINT}}{\text{AFT STAGNATION POINT}}$$

CONSTANTS ARE DETERMINED BY A LEAST SQUARE METHOD

FUNCTION: $Y = 1+A1*(1-X)+A2*(1-X)**2+A3*(1-X)**3$
********

INITIAL VALUES: A1 = .100
********** A2 = 2.30
A3 = 1.50

CONSTANTS: A1 = -.434
******** A2= -1.85
A3 = 1.30

LEAST SQUARE ERROR NORM: E = .247426E-02

THE SOLUTION WAS FOUND AFTER 2 ITERATIONS

FUNCTION FOR THIS DATA SET
**********

THE VALUES ARE NONDIMENSIONALIZED BY THE RULES

$$X = \frac{\text{VELOCITY OF FUEL}}{\text{ANNULUS AIR VELOCITY}}$$

$$Y = \frac{\text{FORWARD STAGNATION POINT}}{\text{AFT STAGNATION POINT}}$$

CONSTANTS ARE DETERMINED BY A LEAST SQUARE METHOD

FUNCTION: $Y = 1+A1*(1-X)+A2*(1-X)**2+A3*(1-X)**3$
********

INITIAL VALUES: A1 = .100
********** A2 = 2.30
A3 = 1.60

CONSTANTS: A1 = 3.92
******** A2 = -3.61
A3 = 3.67

LEAST SQUARE ERROR NORM: E = .46121E-02

THE SOLUTION WAS FOUND AFTER 2 ITERATIONS

TABLE OF VALUES FOR EXPERIMENTAL DATA SET 3
**********

AREA OF OUTER NOZZLE 10.6036 CM**2
AREA OF INNER NOZZLE .7012 CM**2
VELOCITY OF AIR 1.0793 M/SEC

| VELOCITY OF FUEL [ M/SEC ] | HEIGHT OF CENTRAL JET [ MM ] | HEIGHT OF LEFT VORTEX [ MM ] | HEIGHT OF RIGHT VORTEX [ MM ] | |
|---|---|---|---|---|
| .0413 | 2.3718 | 6.0071 | 8.5852 | |
| .0741 | 5.6390 | 6.4543 | 9.3726 | |
| .1288 | 10.8966 | 6.5532 | 10.2870 | |
| .1787 | 15.1392 | 6.5278 | 7.5692 | |
| .2494 | 19.5580 | 6.5024 | 6.9850 | |
| .3157 | 21.2202 | 6.8674 | 6.3500 | (*) |

THE PENTRATION POINT IS SIGHED BY (*)

FUNCTION FOR THIS DATA SET
**********

THE VALUES ARE NONDIMENSIONALIZED BY THE RULES

$$X = \frac{\text{VELOCITY OF FUEL}}{\text{PENETRATION VELOCITY}}$$

$$Y = \frac{\text{FORWARD STAGNATION POINT}}{\text{AFT STAGNATION POINT}}$$

CONSTANTS ARE DETERMINED BY A LEAST SQUARE METHOD

FUNCTION: $Y = 1+A1*(1-X)+A2*(1-X)**2+A3*(1-X)**3$
********

INITIAL VALUES: A1 = .100
********** A2 = 2.30
A3 = 1.50

CONSTANTS: A1 = -.147
******** A2 = -1.69
A3 = .811

LEAST SQUARE ERROR NORM: E = .71551E-03

THE SOLUTION WAS FOUND AFTER 2 ITERATIONS

FUNCTION FOR THIS DATA SET =
**********

THE VALUES ARE NONDIMENSIONALIZED BY THE RULES

$$Y = \frac{\text{VELOCITY OR FUEL}}{\text{ANNULUS AIR VELOCITY}}$$

$$X = \frac{\text{FORWARD STAGNATION POINT}}{\text{AFT STAGNATION POINT}}$$

CONSTANTS ARE DETERMINED BY A LEAST SQUARE METHOD

FUNCTION: $Y = 1+A1*(1-X)+A2*(1-X)**2+A3*(1-X)**3$
********

INITIAL VALUES: A1 = .100
********** A2 = 2.30
A3 = 1.50

CONSTANTS: A1 = -.263
******** A2 = 3.42
A3 = -4.25

LEAST SQUARE ERROR NORM: E = .21925E-02

THE SOLUTION WAS FOUND AFTER 2 ITERATIONS

TABLE OF VALUES FOR EXPERIMENTAL DATA SET  4
**********

AREA OF OUTER NOZZLE    10.6036 CM**2
AREA OF INNER NOZZLE      .7012 CM**2
VELOCITY OF AIR          1.3464 M/SEC

| VELOCITY OF FUEL [ M/SEC ] | HEIGHT OF CENTRAL JET [ MM ] | HEIGHT OF LEFT VORTEX [ MM ] | HEIGHT OF RIGHT VORTEX [ MM ] | |
|---|---|---|---|---|
| .0443 | 3.6068 | 7.1374 | 10.2108 | |
| .0640 | 5.9420 | 7.4574 | 9.9642 | |
| .1229 | 8.3010 | 8.8900 | 13.1318 | |
| .1726 | 11.6840 | 7.9248 | 7.6200 | |
| .2299 | 15.7540 | 7.5200 | 7.9756 | |
| .3099 | 19.3040 | 7.6708 | 7.9248 | (*) |
| .3426 | 20.3200 | 5.7564 | 7.6200 | (*) |

THE PENETRATION POINT IS SIGNED BY (*)

FUNCTION FOR THIS DATA SET :
**********

THE VALUES ARE NONDIMENSIONALIZED BY THE RULES

$$Y = \frac{\text{VELOCITY OF FUEL}}{\text{PENETRATION VELOCITY}}$$

$$Y = \frac{\text{FORWARD STAGNATION POINT}}{\text{AFT STAGNATION POINT}}$$

CONSTANTS ARE DETERMINED BY A LEAST SQUARE METHOD

FUNCTION: $Y = 1+A1*(1-Y)+A2*(1-X)**2+A3*(1-X)**3$
********

INITIAL VALUES: A1 = .100
********** A2 = 2.30
A3 = 1.50

CONSTANTS: A1 = .234
******* A2= -2.33
A3 = 1.70

LEAST SQUARE ERROR NORM: E = .25552E-02

THE SOLUTION WAS FOUND AFTER 2 ITERATIONS

FUNCTION FOR THIS DATA SET 4
**********

THE VALUES ARE NONDIMENSIONALIZED BY THE PILES

$$Y = \frac{\text{VELOCITY OF FUEL}}{\text{ANNULUS AIR VELOCITY}}$$

$$Y = \frac{\text{FORWARD STAGNATION POINT}}{\text{AFT STAGNATION POINT}}$$

CONSTANTS ARE DETERMINED BY A LEAST SQUARE METHOD

FUNCTION: $Y = 1+A1*(1-X)+A2*(1-X)**2+A3*(1-X)**3$
********

INITIAL VALUES: A1 = .100
********** A2 = 2.30
A3 = 1.50

CONSTANTS: A1 = -.434
******** A2 = 4.10
A3 = -4.73

LEAST SQUARE ERROR NORM: E = .20361E-02

THE SOLUTION WAS FOUND AFTER 2 ITERATIONS

TABLE OF VALUES FOR EXPERIMENTAL DATA SET 6
**********

AREA OF OUTER NOZZLE 10.6036 CM**2
AREA OF INNER NOZZLE .7012 CM**2
VELOCITY OF AIR 1.5746 M/SEC

| VELOCITY OF FUEL [ M/SEC ] | HEIGHT OF CENTRAL JET [ MM ] | HEIGHT OF LEFT VORTEX [ MM ] | HEIGHT OF RIGHT VORTEX [ MM ] | |
|---|---|---|---|---|
| .0484 | 5.4102 | 7.2988 | 11.9390 | |
| .0605 | 7.7067 | 8.1280 | 12.1691 | |
| .0697 | 9.4491 | 8.3312 | 12.5730 | |
| .0823 | 11.2268 | 8.1534 | 12.3952 | |
| .1044 | 14.2282 | 7.9248 | 8.6360 | |
| .1045 | 14.4760 | 7.9736 | 8.9459 | |
| .1339 | 17.0434 | 7.7470 | 8.2296 | |
| .1741 | 14.3713 | 8.4074 | 9.3980 | (*) |
| .2119 | 10.8120 | 7.6200 | 10.7315 | (*) |

THE PENTRATION POINT IS SIGNED BY (*)

FUNCTION FOR THIS DATA SET 5
**********

THE VALUES ARE NONDIMENSIONALIZED BY THE FILES

$$Y = \frac{\text{VELOCITY OF FUEL}}{\text{PENETRATION VELOCITY}}$$

$$Y = \frac{\text{FORWARD STAGNATION POINT}}{\text{AFT STAGNATION POINT}}$$

CONSTANTS ARE DETERMINED BY A LEAST SQUARE METHOD

FUNCTION: $Y = 1+A1*(1-X)+A2*(1-X)**2+A3*(1-X)**3$
********

INITIAL VALUES: A1 = .100
********** A2 = 2.30
A3 = 1.50

CONSTANTS: A1 = -.117
******** A2 = -.362
A3 = -.900

LEAST SQUARE ERROR SUM: E = .31994E-03

THE SOLUTION WAS FOUND AFTER 2 ITERATIONS

FUNCTION FOR THIS DATA SET 5
**********

THE VALUES ARE NONDIMENSIONALIZED BY THE RULES

$$Y = \frac{\text{VELOCITY OF FUEL}}{\text{ANNULUS AIR VELOCITY}}$$

$$Y = \frac{\text{FORWARD STAGNATION POINT}}{\text{AFT STAGNATION POINT}}$$

CONSTANTS ARE DETERMINED BY A LEAST SQUARE METHOD

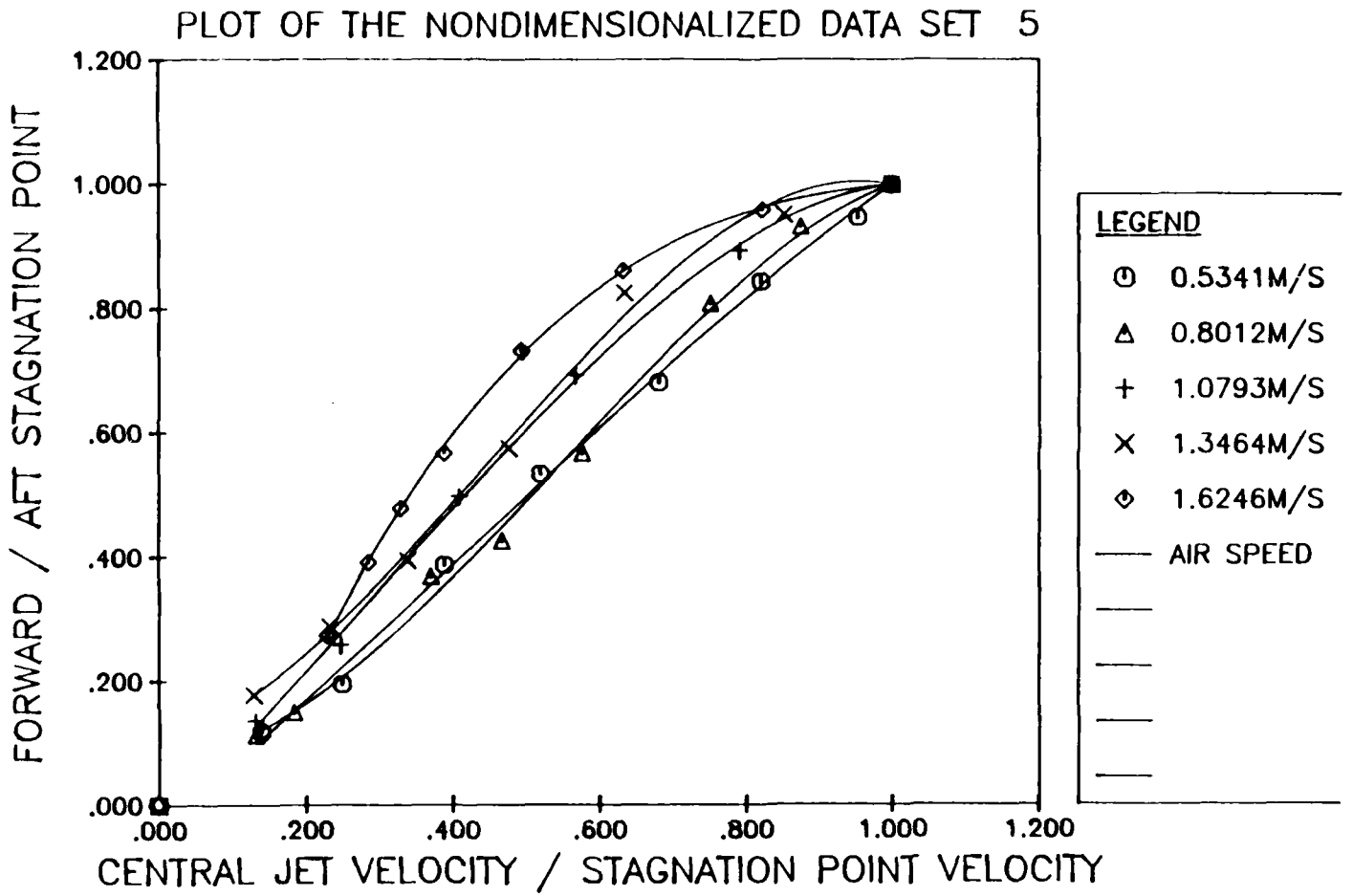
FUNCTION: $Y = 1+A1*(1-X)+A2*(1-X)**2+A3*(1-X)**3$
********

INITIAL VALUES: A1 = .100
********** A2 = 2.30
A3 = 1.50

CONSTANTS: A1 = -65.5
******** A2 = 149.
A3 = -85.1

LEAST SQUARE ERROR MEAN: E = .80838E-03

THE SOLUTION WAS FOUND AFTER 3 ITERATIONS


PLOT OF THE NONDIMENSIONALIZED DATA SET 5
FORWARD / AFT STAGNATION POINT
1.200
1.000
.800
.600
.400
.200
.000
.000
.200
.400
.600
.800
1.000
1.200
CENTRAL JET VELOCITY / STAGNATION POINT VELOCITY
LEGEND
0.5341M/S
0.8012M/S
1.0793M/S
1.3464M/S
1.6246M/S
AIR SPEED

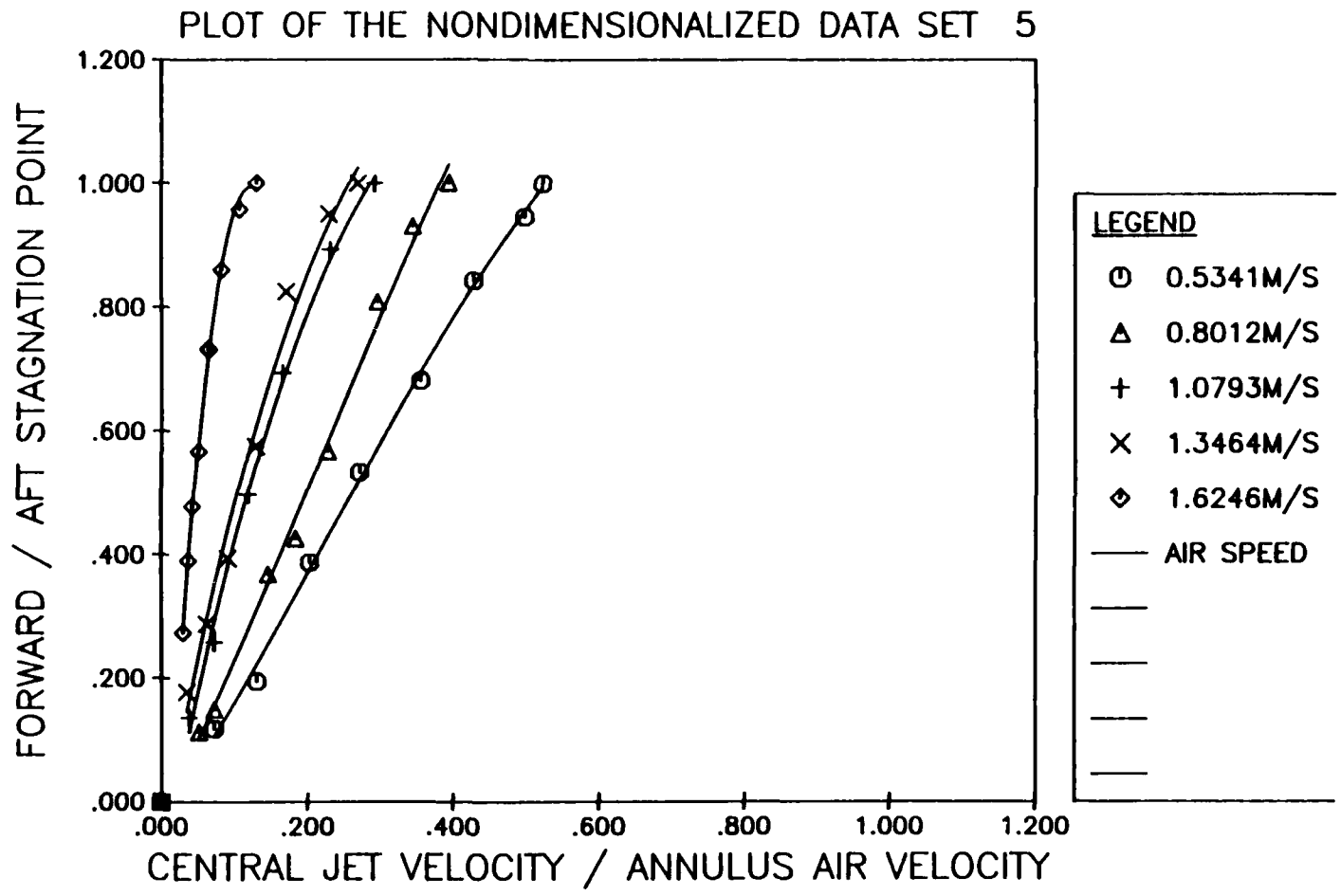

PLOT OF THE NONDIMENSIONALIZED DATA SET 5
FORWARD / AFT STAGNATION POINT
1.200
1.000
.800
.600
.400
.200
.000
.000
.200
.400
.600
.800
1.000
1.200
CENTRAL JET VELOCITY / ANNULUS AIR VELOCITY
LEGEND
0.5341M/S
0.8012M/S
1.0793M/S
1.3464M/S
1.6246M/S
AIR SPEED

TABLE OF VALUES FOR EXPERIMENTAL DATA SET 1
**********

AREA OF OUTER NOZZLE 10.6036 CM**2
AREA OF INNER NOZZLE 1.2668 CM**2
VELOCITY OF AIR .5341 M/SEC

| VELOCITY OF FUEL [ M/SEC ] | HEIGHT OF CENTRAL JET [ MM ] | HEIGHT OF LEFT VORTEX [ MM ] | HEIGHT OF RIGHT VORTEX [ MM ] | |
|---|---|---|---|---|
| .0239 | 1.9558 | 3.4468 | 4.6990 | |
| .0376 | 2.8194 | 4.7498 | 5.6007 | |
| .0643 | 4.2723 | 6.2230 | 7.1399 | |
| .0894 | 5.7023 | 7.0739 | 7.4346 | |
| .1096 | 7.5438 | 8.9562 | 10.0863 | |
| .1209 | 8.3591 | 10.9195 | 11.3030 | |
| .1403 | 9.6977 | 13.6093 | 13.6093 | |
| .1595 | 12.1158 | 16.1290 | 16.1290 | |
| .1834 | 13.5915 | 4.6736 | 5.2578 | |
| .2044 | 14.7904 | 5.4381 | 5.4381 | |
| .2205 | 16.2560 | 5.1562 | 5.7150 | |
| .2584 | 19.8120 | 4.4704 | 5.1054 | |
| .2841 | 21.5900 | 4.4704 | 5.1054 | |
| .3410 | 23.4950 | 4.4704 | 5.1054 | (*) |
| .3710 | 24.3840 | 5.0900 | 5.5143 | (*) |

THE PENTRATION POINT IS SIGHED BY (*)

FUNCTION FOR THIS DATA SET
**********

THE VALUES ARE NONDIMENSIONALIZED BY THE RULES

$$X = \frac{\text{VELOCITY OF FUEL}}{\text{PENETRATION VELOCITY}}$$

$$Y = \frac{\text{FORWARD STAGNATION POINT}}{\text{AFT STAGNATION POINT}}$$

CONSTANTS ARE DETERMINED BY A LEAST SQUARE METHOD

FUNCTION: $Y = 1+A1*(1-X)+A2*(1-X)**2+A3*(1-X)**3$
********

INITIAL VALUES: A1 = .100
********** A2 = 2.30
A3 = 1.50

CONSTANTS: A1 = -.126
****** A2 = -2.16
A3 = 1.34

LEAST SQUARE ERROR NORM: E = .20902E-02

THE SOLUTION WAS FOUND AFTER 2 ITERATIONS

FUNCTION FOR THIS DATA SET
**********

THE VALUES ARE NONDIMENSIONALIZED BY THE RULES

$$X = \frac{\text{VELOCITY OF FUEL}}{\text{ANNULUS AIR VELOCITY}}$$

$$Y = \frac{\text{FORWARD STAGNATION POINT}}{\text{AFT STAGNATION POINT}}$$

CONSTANTS ARE DETERMINED BY A LEAST SQUARE METHOD

FUNCTION: $Y = 1+A1*(1-X)+A2*(1-X)**2+A3*(1-X)**3$
********

INITIAL VALUES: A1 = .100
********** A2 = 2.30
A3 = 1.50

CONSTANTS: A1 = 1.15
****** A2 = -4.03
A3 = 1.89

LEAST SQUARE ERROR NORM: E = .50355E-02

THE SOLUTION WAS FOUND AFTER 2 ITERATIONS

TABLE OF VALUES FOR EXPERIMENTAL DATA SET 2
**********

AREA OF OUTER NOZZLE 10.5036 CM**2
AREA OF INNER NOZZLE 1.2668 CM**2
VELOCITY OF AIR .8012 M/SEC

| VELOCITY OF FUEL [ M/SEC ] | HEIGHT OF CENTRAL JET [ MM ] | HEIGHT OF LEFT VORTEX [ MM ] | HEIGHT OF RIGHT VORTEX [ MM ] | |
|---|---|---|---|---|
| .0190 | 2.0320 | 5.0800 | 7.1374 | |
| .0239 | 2.1590 | 4.8006 | 6.2484 | |
| .0419 | 2.2860 | 5.4102 | 7.8994 | |
| .0575 | 3.8100 | 5.6134 | 8.1280 | |
| .0891 | 5.0800 | 8.3058 | 9.9822 | |
| .1088 | 6.6040 | 9.7028 | 10.1092 | |
| .1242 | 7.8740 | 11.1760 | 11.7348 | |
| .1436 | 9.4996 | 13.9700 | 13.9700 | |
| .1594 | 10.4140 | 15.2400 | 15.2400 | |
| .1794 | 11.6586 | 5.3340 | 5.3340 | |
| .1999 | 13.4620 | 5.3340 | 5.3340 | |
| .2286 | 14.4780 | 5.3340 | 5.3340 | |
| .2706 | 17.2720 | 5.3340 | 5.3340 | |
| .2915 | 18.7960 | 5.5880 | 5.5880 | |
| .3035 | 19.8120 | 5.4864 | 5.5880 | |
| .3249 | 22.3520 | 5.0800 | 5.9690 | |
| .3874 | 25.4000 | 5.5880 | 6.0198 | (*) |

THE PENTRATION POINT IS SIGHED BY (*)

FUNCTION FOR THIS DATA SET
**********

THE VALUES ARE NONDIMENSIONALIZED BY THE RULES

$$X = \frac{\text{VELOCITY OF FUEL}}{\text{PENETRATION VELOCITY}}$$

$$Y = \frac{\text{FORWARD STAGNATION POINT}}{\text{AFT STAGNATION POINT}}$$

CONSTANTS ARE DETERMINED BY A LEAST SQUARE METHOD

FUNCTION: $Y = 1+A1*(1-X)+A2*(1-X)**2+A3*(1-X)**3$
********

INITIAL VALUES: A1 = .100
********** A2 = 2.30
A3 = 1.50

CONSTANTS: A1 = -.906
****** A2 = -.384
A3 = .321

LEAST SQUARE ERROR NORM: E = .45390E-02

THE SOLUTION WAS FOUND AFTER 2 ITERATIONS

FUNCTION FOR THIS DATA SET
**********

THE VALUES ARE NONDIMENSIONALIZED BY THE RULES

$$X = \frac{\text{VELOCITY OF FUEL}}{\text{ANNULUS AIR VELOCITY}}$$

$$Y = \frac{\text{FORWARD STAGNATION POINT}}{\text{AFT STAGNATION POINT}}$$

CONSTANTS ARE DETERMINED BY A LEAST SQUARE METHOD

FUNCTION: $Y = 1+A1*(1-X)+A2*(1-X)**2+A3*(1-X)**3$
********

INITIAL VALUES: A1 = .100
********** A2 = 2.30
A3 = 1.50

CONSTANTS: A1 = 2.69
****** A2 = -6.87
A3 = 3.21

LEAST SQUARE ERROR NORM: E = .45575E-02

THE SOLUTION WAS FOUND AFTER 2 ITERATIONS

TABLE OF VALUES FOR EXPERIMENTAL DATA SET 3
**********

AREA OF OUTER NOZZLE 10.6036 CM**2
AREA OF INNER NOZZLE 1.2666 CM**2
VELOCITY OF AIR 1.0793 M/SEC

| VELOCITY OF FUEL [ M/SEC ] | HEIGHT OF CENTRAL JET [ MM ] | HEIGHT OF LEFT VORTEX [ MM ] | HEIGHT OF RIGHT VORTEX [ MM ] | |
|---|---|---|---|---|
| .0221 | 1.7018 | 5.4364 | 7.7470 | |
| .0370 | 2.3876 | 6.6548 | 9.3980 | |
| .0479 | 3.0480 | 6.7564 | 9.4234 | |
| .0641 | 4.0386 | 7.7470 | 10.4953 | |
| .0825 | 5.2070 | 9.2354 | 11.4935 | |
| .0938 | 6.4262 | 9.4717 | 12.4638 | |
| .1305 | 8.4252 | 11.7602 | 13.7160 | |
| .1434 | 9.8552 | 13.1064 | 15.1130 | |
| .1641 | 11.8872 | 15.5575 | 15.5575 | |
| .1822 | 12.8524 | 17.1958 | 17.1958 | |
| .2039 | 14.6355 | 5.6388 | 6.2738 | |
| .2293 | 16.3754 | 5.8420 | 5.8420 | |
| .2629 | 18.3214 | 5.9690 | 6.1468 | |
| .3049 | 21.1074 | 6.0960 | 6.1722 | |
| .3325 | 22.5552 | 6.2230 | 6.1976 | (*) |
| .3918 | 23.8760 | 6.8580 | 6.8580 | (*) |

THE PENTRATION POINT IS SIGHED BY (*)

FUNCTION FOR THIS DATA SET
**********

THE VALUES ARE NONDIMENSIONALIZED BY THE RULES

$$X = \frac{\text{VELOCITY OF FUEL}}{\text{PENETRATION VELOCITY}}$$

$$Y = \frac{\text{FORWARD STAGNATION POINT}}{\text{AFT STAGNATION POINT}}$$

CONSTANTS ARE DETERMINED BY A LEAST SQUARE METHOD

FUNCTION: $Y = 1+A1*(1-X)+A2*(1-X)**2+A3*(1-X)**3$
********

INITIAL VALUES: A1 = .100
********** A2 = 2.30
A3 = 1.50

CONSTANTS: A1 = -.231
****** A2 = -1.78
A3 = 1.04

LEAST SQUARE ERROR NORM: E = .89464E-03

THE SOLUTION WAS FOUND AFTER 2 ITERATIONS

FUNCTION FOR THIS DATA SET
**********

THE VALUES ARE NONDIMENSIONALIZED BY THE RULES

$$X = \frac{\text{VELOCITY OF FUEL}}{\text{ANNULUS AIR VELOCITY}}$$

$$Y = \frac{\text{FORWARD STAGNATION POINT}}{\text{AFT STAGNATION POINT}}$$

CONSTANTS ARE DETERMINED BY A LEAST SQUARE METHOD

FUNCTION: $Y = 1+A1*(1-X)+A2*(1-X)**2+A3*(1-X)**3$
********

INITIAL VALUES: A1 = .100
********** A2 = 2.30
A3 = 1.50

CONSTANTS: A1 = 2.90
****** A2 = -5.25
A3 = 1.31

LEAST SQUARE ERROR NORM: E = .60688E-02

THE SOLUTION WAS FOUND AFTER 2 ITERATIONS

TABLE OF VALUES FOR EXPERIMENTAL DATA SET 4
**********

AREA OF OUTER NOZZLE 10.6036 CM**2
AREA OF INNER NOZZLE 1.2668 CM**2
VELOCITY OF AIR 1.3464 M/SEC

| VELOCITY OF FUEL [ M/SEC ] | HEIGHT OF CENTRAL JET [ MM ] | HEIGHT OF LEFT VORTEX [ MM ] | HEIGHT OF RIGHT VORTEX [ MM ] | |
|---|---|---|---|---|
| .0360 | 2.1336 | 6.1722 | 9.0678 | |
| .0554 | 2.4130 | 5.7818 | 10.1600 | |
| .0658 | 3.3020 | 8.0772 | 10.3378 | |
| .0807 | 3.8100 | 8.8900 | 11.1760 | |
| .0964 | 5.3340 | 9.6520 | 11.6840 | |
| .1235 | 7.0358 | 10.4648 | 14.6558 | |
| .1455 | 8.7630 | 12.4206 | 15.6718 | |
| .1637 | 10.4140 | 13.7160 | 16.0782 | |
| .1840 | 12.0904 | 16.8656 | 16.8656 | |
| .2008 | 13.1826 | 5.8420 | 5.8420 | |
| .2199 | 14.7320 | 6.3500 | 6.8580 | |
| .2457 | 16.1544 | 5.8420 | 6.7310 | |
| .2822 | 17.4650 | 6.0960 | 6.7310 | |
| .3120 | 18.9738 | 6.0960 | 6.0960 | |
| .3702 | 20.7264 | 5.3594 | 6.1722 | (*) |
| .3833 | 21.0820 | 6.1976 | 6.6294 | (*) |

THE PENTRATION POINT IS SIGHED BY (*)

FUNCTION FOR THIS DATA SET
**********

THE VALUES ARE NONDIMENSIONALIZED BY THE RULES

$$X = \frac{\text{VELOCITY OF FUEL}}{\text{PENETRATION VELOCITY}}$$

$$Y = \frac{\text{FORWARD STAGNATION POINT}}{\text{AFT STAGNATION POINT}}$$

CONSTANTS ARE DETERMINED BY A LEAST SQUARE METHOD

FUNCTION: $Y = 1+A1*(1-X)+A2*(1-X)**2+A3*(1-X)**3$
********

INITIAL VALUES: A1 = .100
********** A2 = 2.30
A3 = 1.50

CONSTANTS: A1 = -.380E-01
****** A2 = -2.06
A3 = 1.13

LEAST SQUARE ERROR NORM: E = .41026E-02

THE SOLUTION WAS FOUND AFTER 2 ITERATIONS

FUNCTION FOR THIS DATA SET
**********

THE VALUES ARE NONDIMENSIONALIZED BY THE RULES

$$X = \frac{\text{VELOCITY OF FUEL}}{\text{ANNULUS AIR VELOCITY}}$$

$$Y = \frac{\text{FORWARD STAGNATION POINT}}{\text{AFT STAGNATION POINT}}$$

CONSTANTS ARE DETERMINED BY A LEAST SQUARE METHOD

FUNCTION: $Y = 1+A1*(1-X)+A2*(1-X)**2+A3*(1-X)**3$
********

INITIAL VALUES: A1 = .100
********** A2 = 2.30
A3 = 1.50

CONSTANTS: A1 = .715
****** A2 = 1.22
A3 = -3.05

LEAST SQUARE ERROR NORM: E = .11030E-01

THE SOLUTION WAS FOUND AFTER 2 ITERATIONS

TABLE OF VALUES FOR EXPERIMENTAL DATA SET 5
**********

AREA OF OUTER NOZZLE 10.6036 CM**2
AREA OF INNER NOZZLE 1.2668 CM**2
VELOCITY OF AIR 1.6246 M/SEC

| VELOCITY OF FUEL [ M/SEC ] | HEIGHT OF CENTRAL JET [ MM ] | HEIGHT OF LEFT VORTEX [ MM ] | HEIGHT OF RIGHT VORTEX [ MM ] | |
|---|---|---|---|---|
| .0273 | 2.0320 | 6.9088 | 9.7536 | |
| .0393 | 2.4638 | 7.1120 | 9.7536 | |
| .0530 | 2.7940 | 6.8580 | 9.7536 | |
| .0911 | 4.3358 | 9.0678 | 10.2362 | |
| .1133 | 5.4356 | 9.0678 | 10.2362 | |
| .1211 | 6.1976 | .0000 | .0000 | |
| .1411 | 7.9248 | .0000 | .0000 | |
| .1625 | 10.1270 | .0000 | .0000 | |
| .1786 | 11.7140 | .0000 | .0000 | |
| .1978 | 12.8428 | .0000 | .0000 | |
| .2011 | 13.9243 | .0000 | .0000 | |
| .2113 | 14.9352 | .0000 | .0000 | |
| .2259 | 15.7988 | .0000 | .0000 | |
| .2427 | 17.0942 | .0000 | .0000 | |
| .2680 | 18.5674 | .0000 | .0000 | |
| .3021 | 20.3200 | .0000 | .0000 | (*) |
| .3967 | 21.0820 | .0000 | .0000 | (*) |

THE PENTRATION POINT IS SIGNED BY (*)

FUNCTION FOR THIS DATA SET
**********

THE VALUES ARE NONDIMENSIONALIZED BY THE RULES

$$X = \frac{\text{VELOCITY OF FUEL}}{\text{PENETRATION VELOCITY}}$$

$$Y = \frac{\text{FORWARD STAGNATION POINT}}{\text{AFT STAGNATION POINT}}$$

CONSTANTS ARE DETERMINED BY A LEAST SQUARE METHOD

FUNCTION: $Y = 1+A1*(1-X)+A2*(1-X)**2+A3*(1-X)**3$
********

INITIAL VALUES: A1 = .100
********** A2 = 2.30
A3 = 1.50

CONSTANTS: A1 = .987
****** A2 = -5.05
A3 = 3.17

LEAST SQUARE ERROR NORM: E = .36666E-02

THE SOLUTION WAS FOUND AFTER 2 ITERATIONS

FUNCTION FOR THIS DATA SET
**********

THE VALUES ARE NONDIMENSIONALIZED BY THE RULES

$$X = \frac{\text{VELOCITY OF FUEL}}{\text{ANNULUS AIR VELOCITY}}$$

$$Y = \frac{\text{FORWARD STAGNATION POINT}}{\text{AFT STAGNATION POINT}}$$

CONSTANTS ARE DETERMINED BY A LEAST SQUARE METHOD

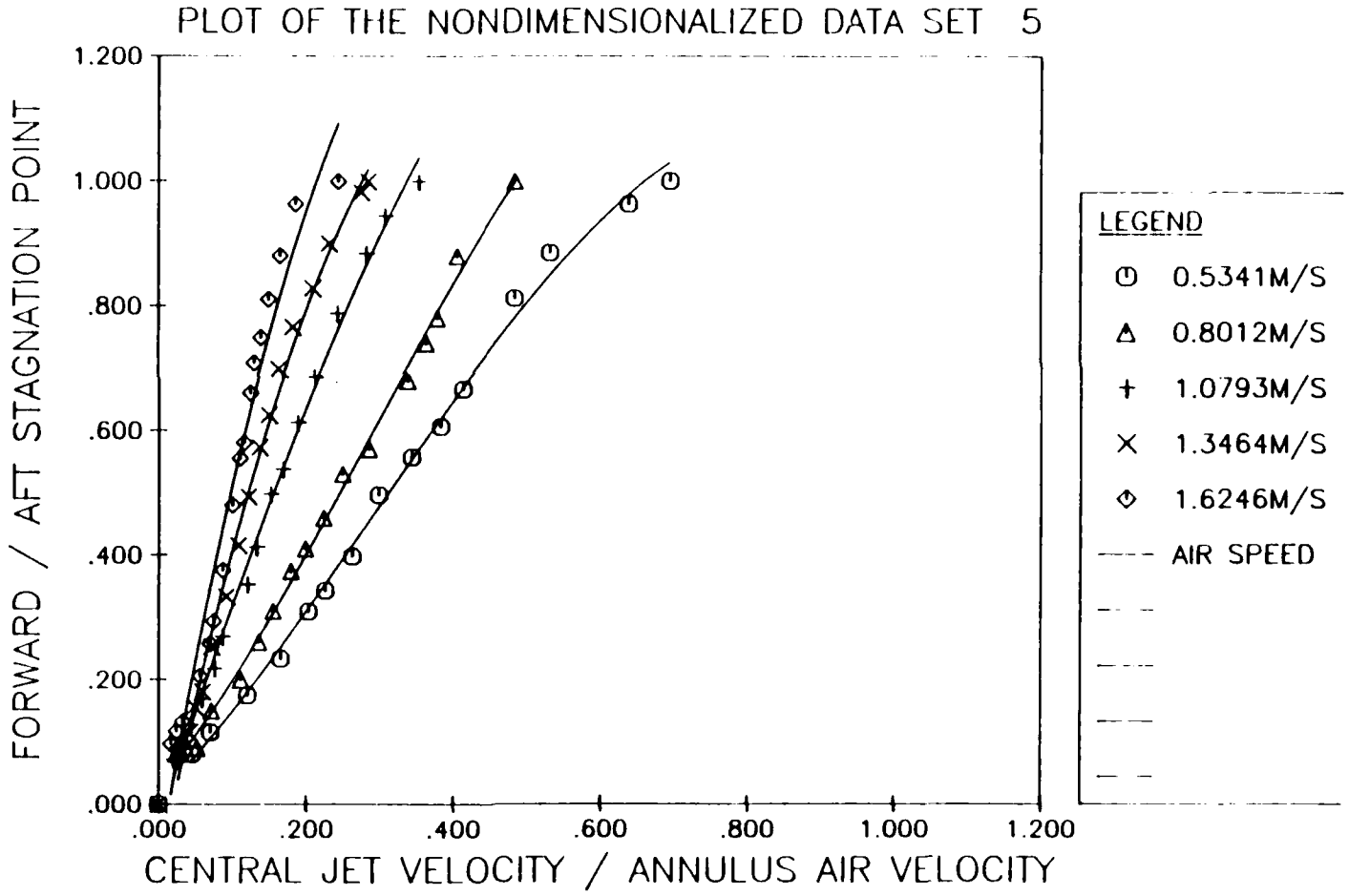
FUNCTION: $Y = 1+A1*(1-X)+A2*(1-X)**2+A3*(1-X)**3$
********

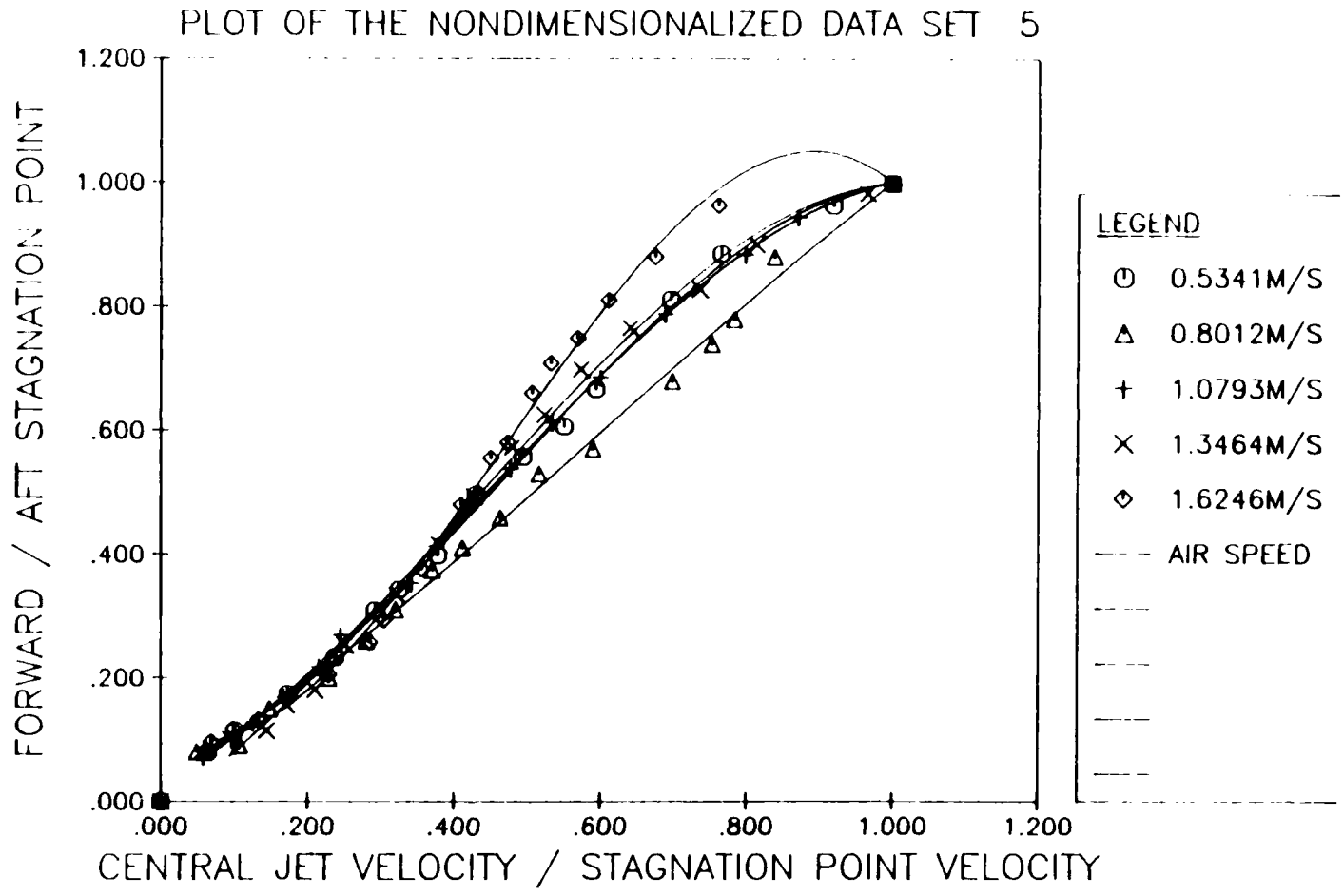
INITIAL VALUES: A1 = .100
********** A2 = 2.30
A3 = 1.50

CONSTANTS: A1 = .832
****** A2 = 2.15
A3 = -4.08

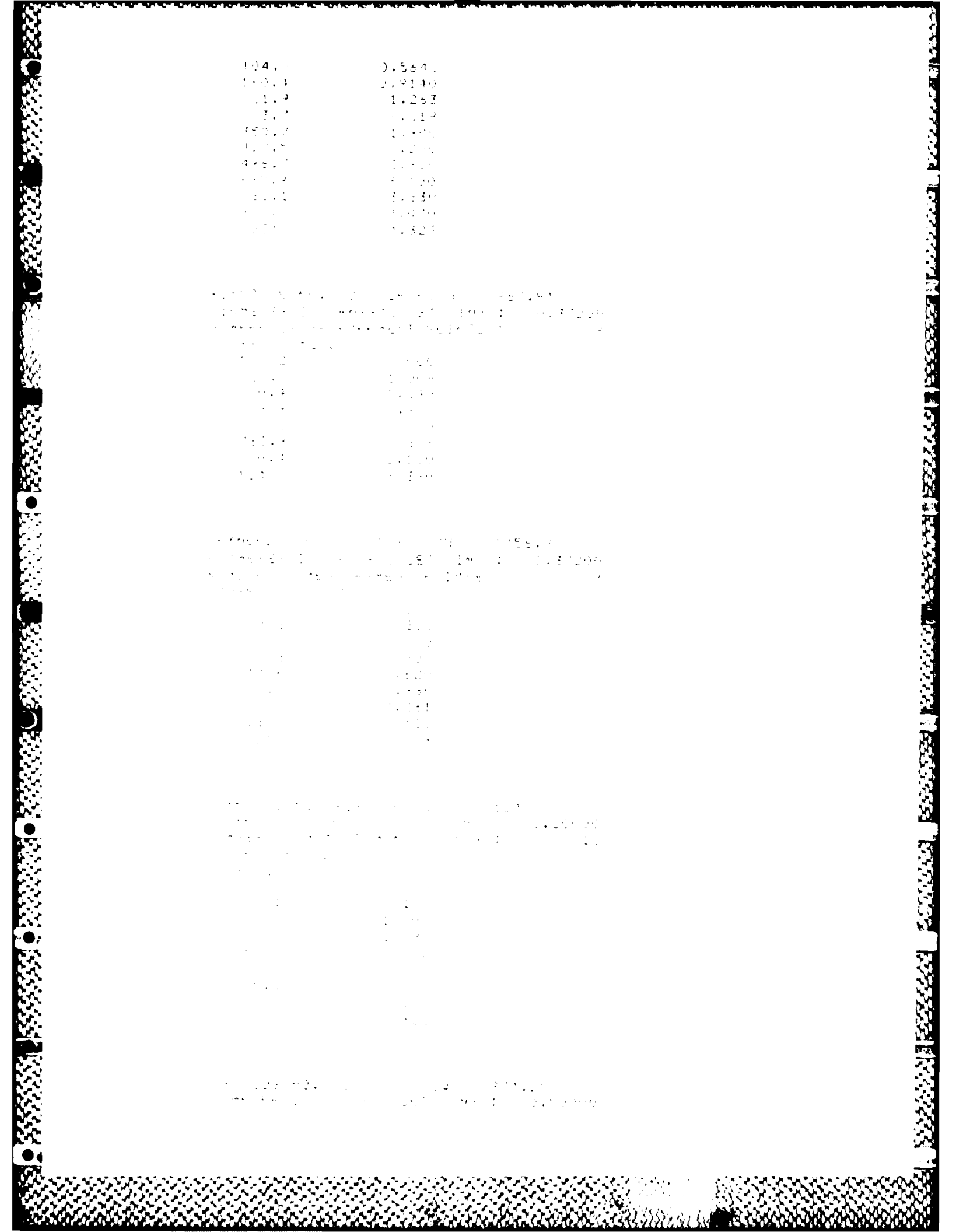
LEAST SQUARE ERROR NORM: E = .59244E-01

THE SOLUTION WAS FOUND AFTER 2 ITERATIONS


PLOT OF THE NONDIMENSIONALIZED DATA SET 5
FORWARD / AFT STAGNATION POINT
CENTRAL JET VELOCITY / ANNULUS AIR VELOCITY
1.200
1.000
.800
.600
.400
.200
.000
.000
.200
.400
.600
.800
1.000
1.200
LEGEND
0.5341M/S
0.8012M/S
1.0793M/S
1.3464M/S
1.6246M/S
AIR SPEED


PLOT OF THE NONDIMENSIONALIZED DATA SET 5
FORWARD / AFT STAGNATION POINT
1.200
1.000
.800
.600
.400
.200
.000
.000
.200
.400
.600
.800
1.000
1.200
CENTRAL JET VELOCITY / STAGNATION POINT VELOCITY
LEGEND
0.5341M/S
0.8012M/S
1.0793M/S
1.3464M/S
1.6246M/S
AIR SPEED

II: Output from Harris 800



NUMBER OF MEASUREMENT POINTS : 9

| RF | FLUID |
|---|---|
| 164.9 | 0.5200 |
| 339.2 | 0.6880 |
| 357.5 | 0.9150 |
| 451.1 | 1.200 |
| [illegible] | [illegible] |
| [illegible] | 1.460 |
| [illegible] | 1.744 |
| [illegible] | 1.960 |
| [illegible] | 2.000 |

[illegible] NOZZLE NO. FOR THIS RUN : 1455.4

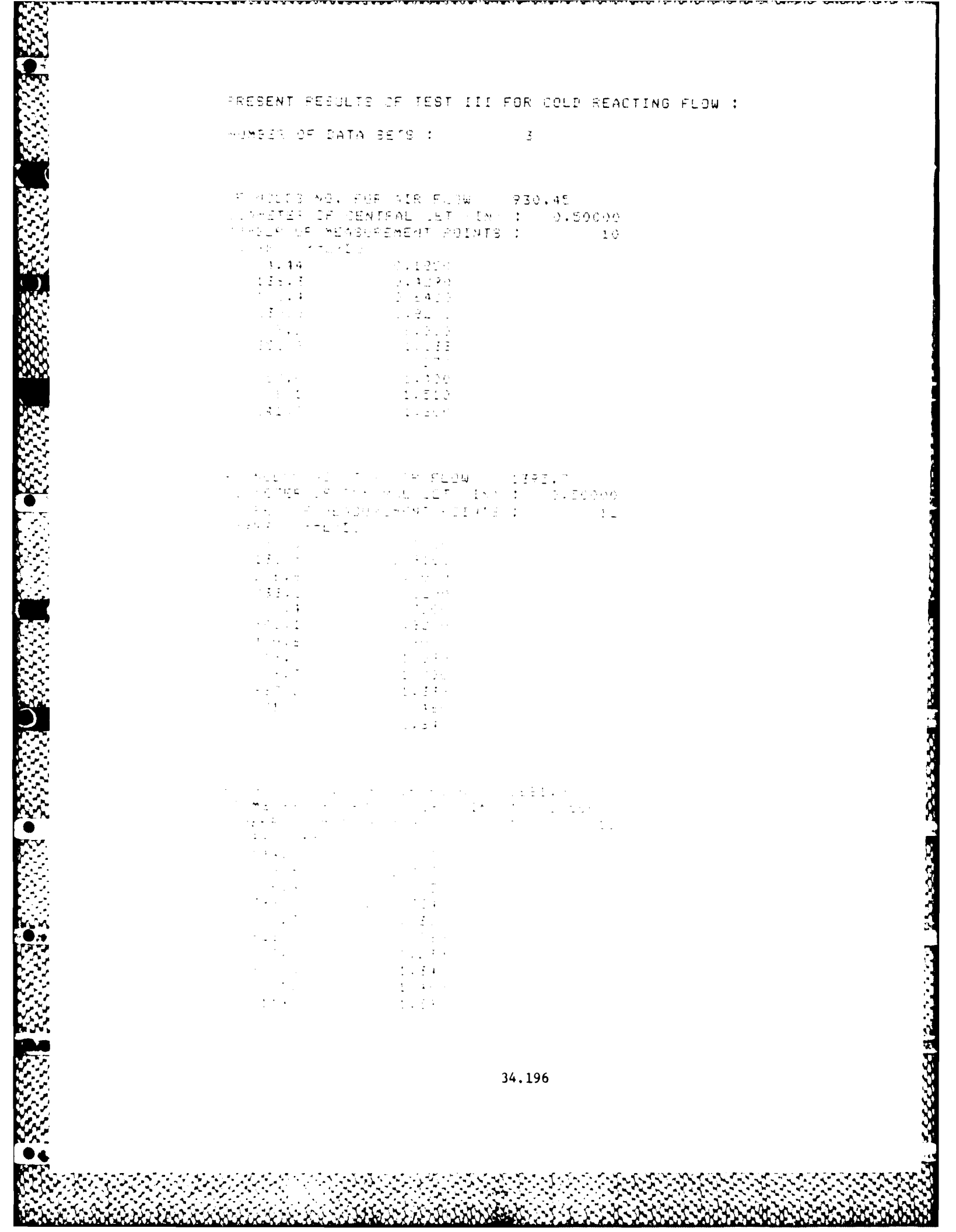
DIAMETER OF CENTRAL JET (IN) : 0.50000

NUMBER OF MEASUREMENT POINTS : 9

| [illegible] | [illegible] |
|---|---|
| [illegible] | .2130 |
| [illegible] | 0.4500 |
| [illegible] | [illegible] |
| [illegible] | [illegible] |
| [illegible] | .1440 |
| [illegible] | 1.320 |
| [illegible] | 1.620 |
| [illegible] | 1.540 |

PRESENT RESULTS OF TEST III FOR COLD REACTING FLOW :

NUMBER OF DATA SETS :  3



...EJECTING FLOW FOR TEST II

...MBER OF DATA SETS 19

...LUE OF ...UES FOR EXPERIMENTAL DATA SET 1
**********

...OF JET NOZZLE ...188 CM**2
...OF ... JET NOZZLE ... CM
...ITY OF AIR ...188 M/SEC
...GLE OF ...UVERING ...

| JET ... | ...IGHT OF ... JET (MM) | HEIGHT OF LEFT VORTEX (MM) | HEIGHT OF RIGHT VORTEX (MM) |
|---|---|---|---|
| ... | ... | 7.3380 | 7.4930 |
| ... | ... | 7.3660 | 7.1970 |
| ... | ... | 7.4160 | 8.0010 |
| ... | ... | 7.4930 | 8.0010 |
| ... | ... | 7.3770 | 7.8740 |
| ... | ... | 7.6200 | 7.7724 |

...

...

...

TABLE OF VALUES FOR EXPERIMENTAL DATA SET 3

**********

AREA OF OUTER MESH =  0.1038 CM**2
AREA OF INNER CYCLE =  0.0167 CM**2
VOLUME OF AIR =  1.5E-03 M**3
NUMBER OF MEASUREMENT POINTS =

| | | HEIGHT OF LEFT VORTEX [ MM ] | HEIGHT OF RIGHT VORTEX [ MM ] |
|---|---|---|---|
| | 0.1030 | 0.0000 | 0.0000 |
| | 0.1030 | 0.0000 | 0.0000 |
| | 0.1030 | 0.0000 | 0.0000 |
| | 0.1030 | 0.0000 | 0.0000 |
| | 0.1030 | 0.0000 | 0.0000 |
| | 0.1030 | 0.0000 | 0.0000 |
| | 0.1030 | 0.0000 | 0.0000 |

THE PRESSURE COEFFICIENT IS DEFINED BY **

TABLE OF VALUES FOR EXPERIMENTAL DATA SET 4

**********

VOLUME OF AIR =  1.5E-03 M**3
NUMBER OF MEASUREMENT POINTS =

| | | HEIGHT OF LEFT VORTEX [ MM ] | HEIGHT OF RIGHT VORTEX [ MM ] |
|---|---|---|---|
| | 0.1030 | 0.0000 | 0.0000 |
| | 0.1030 | 0.0000 | 0.0000 |
| | 19.1200 | 10.4140 | 9.8900 |
| | 19.1200 | 10.9200 | 8.7220 |
| | 19.1200 | 15.2400 | 16.2560 |
| | 19.1200 | 15.2400 | 20.9550 |
| | 19.1200 | 14.4122 | 14.6050 |
| | 19.1200 | 13.7140 | 15.2400 |

THE CONCENTRATION HEIGHT IS DEFINED BY **

TABLE OF VALUES FOR EXPERIMENTAL DATA SET 5

**********

| | | | |
|---|---|---|---|
| | | HEIGHT OF LEFT VERTEX ( MM ) | HEIGHT OF RIGHT VERTEX ( MM ) |
| | | 0.0000 | 0.0000 |
| | | 0.0000 | 0.0000 |
| | | 0.0000 | 0.0000 |
| | | 0.0000 | 0.0000 |
| | | 0.0000 | 0.0000 |
| | | 0.0000 | 0.0000 |
| | | 0.0000 | 0.0000 |
| | | 0.0000 | 0.0000 |
| | | 0.0000 | 0.0000 |

TABLE OF VALUES FOR EXPERIMENTAL DATA SET 6

**********

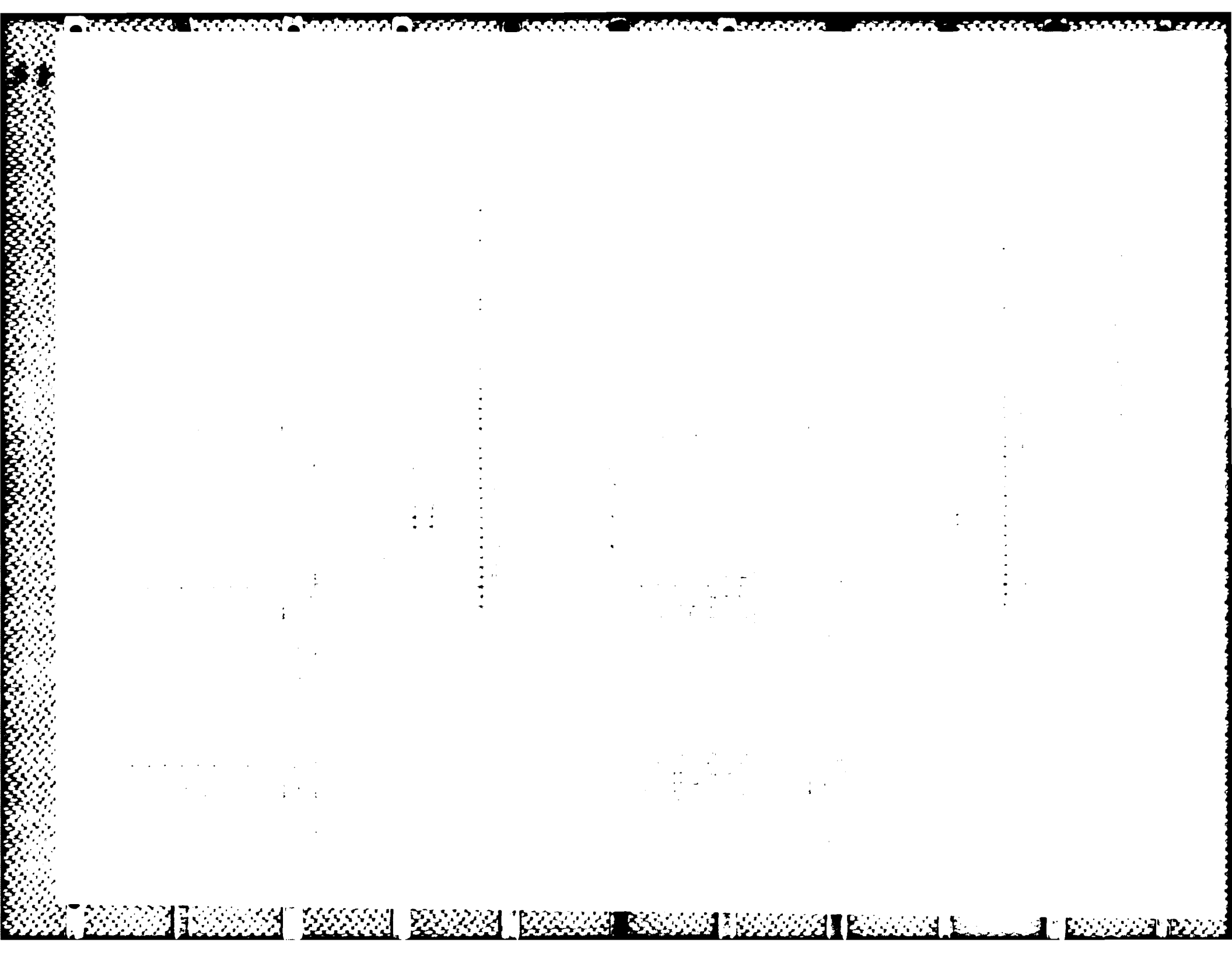
| | | | |
|---|---|---|---|
| | | HEIGHT OF LEFT VERTEX ( MM ) | HEIGHT OF RIGHT VERTEX ( MM ) |
| | | 0.0000 | 0.0000 |
| | | 0.0000 | 0.0000 |
| | | 0.0000 | 0.0000 |
| | | 0.0000 | 0.0000 |
| | | 0.0000 | 0.0000 |
| | | 0.0000 | 0.0000 |
| | | 0.0000 | 0.0000 |
| | | 0.0000 | 0.0000 |
| | | 0.0000 | 0.0000 |

TABLE OF VALUES FOR EXPERIMENTAL DATA SET 7

**********

| | | | |
|---|---|---|---|
| | | | |
| | | | |
| | | | |
| | | | |
| | | | |
| | | | |
| | | | |
| | | | |
| | | | |
| | | | |
| | | | |

| | | | |
|---|---|---|---|
| | | | |
| | | | |
| | | | |
| | | | |
| | | | |
| | | | |
| | | | |
| | | | |
| | | | |
| | | | |
| | | | |



Appendix E: All the Experimental Data for Figure 7
(Including the results of this study,
Tankin (Ref. 27) and Namazian (Ref. 7))



| | |
|---|---|
| 584.0 | 1206. |
| 713.6 | 1501. |
| 902.0 | 1 [illegible] |
| [illegible]041. | [illegible]. |
| 1144. | 1482. |
| 1345. | 1259. |

[illegible] NUMBER OF AIR FLOW [illegible]

DIAMETER OF [illegible] JET [IN] [illegible]

NUMBER OF [illegible]-EMENT POINTS : [illegible]

| [illegible] | [illegible] | [illegible] |
|---|---|---|
| [illegible]1.5E | [illegible] | [illegible] |
| [illegible]2[illegible].3 | [illegible] | [illegible] |
| [illegible]3.[illegible] | [illegible] | [illegible] |
| [illegible]4[illegible]. | [illegible] | [illegible] |
| [illegible]5. | [illegible] | [illegible] |
| [illegible]6. | [illegible] | [illegible] |
| [illegible]7. | [illegible] | [illegible] |
| [illegible]8[illegible]. | [illegible] | [illegible] |
| [illegible]9[illegible]. | [illegible]1.81. | [illegible] |
| [illegible]1[illegible]. | [illegible] | [illegible] |

[illegible] AIR FLOW [illegible]

[illegible] JET [IN] 0.50000

[illegible] POINTS : [illegible]

| [illegible] | [illegible] | [illegible] |
|---|---|---|
| [illegible]1[illegible].1 | [illegible] | [illegible] |
| [illegible]1[illegible].2 | [illegible] | [illegible] |
| [illegible]1[illegible]. | [illegible]1[illegible]. | [illegible] |
| [illegible]1[illegible]. | [illegible] | [illegible] |
| [illegible]1[illegible]. | [illegible] | [illegible] |
| [illegible]1[illegible].1 | [illegible]. | [illegible] |
| [illegible]1[illegible].1 | [illegible]. | [illegible] |
| [illegible]1[illegible]. | [illegible]1021. | [illegible] |
| [illegible]1[illegible]. | [illegible]1[illegible]. | [illegible] |
| [illegible]1[illegible]. | 1515. | [illegible] |

[illegible] AIR FLOW 1[illegible]

[illegible] JET [IN] [illegible]

[illegible] POINTS : [illegible]

| [illegible] | [illegible] | [illegible] |
|---|---|---|
| [illegible] | [illegible]1[illegible]. | [illegible] |
| [illegible]1[illegible]. | [illegible]. | [illegible] |
| [illegible]1[illegible]. | [illegible]1.3 | [illegible] |
| [illegible]1[illegible]. | [illegible]1[illegible]. | [illegible] |
| [illegible]1[illegible]. | [illegible]1[illegible]. | [illegible] |
| [illegible]1[illegible]. | [illegible]. | [illegible] |
| [illegible]1[illegible]. | 1[illegible]. | [illegible] |
| [illegible]1[illegible]. | 1[illegible]. | [illegible] |
| [illegible]1[illegible]. | 1[illegible]. | [illegible] |
| [illegible]1[illegible]. | 1[illegible]. | [illegible] |

[illegible] NUMBER OF AIR FLOW 1495.[illegible]

[illegible] OF [illegible] JET [IN] 0.50000

[illegible] OF [illegible] POINTS : [illegible]

| [illegible] | [illegible] | [illegible] |
|---|---|---|
| [illegible] 4.7 | [illegible]1.[illegible] | [illegible] |
| [illegible]40.3 | [illegible]20.[illegible] | 34.212 |

| | |
|---|---|
| 348.4 | 745.5 |
| 425.3 | 795.5 |
| 439.0 | 892.2 |
| 537.4 | 1014. |
| 596.3 | 1159. |
| 639.0 | 1303. |
| 1 [illegible]4. | 1512. |

PRESENT RESULTS OF TEST II :

NUMBER OF DATA SETS : 9

[illegible] NO. [illegible] AIR FLOW 511.26
[illegible]METER OF CENTRAL JET (IN) : 0.25000
NUMBER OF MEASUREMENT POINTS : 9
[illegible] VEL DU*DU*(DU-DU) **1.5*DU (DU-DU)
[illegible] 344.1
[illegible] 442.4
[illegible] [illegible]
[illegible] [illegible]
[illegible] [illegible]
[illegible] [illegible]
[illegible] [illegible]
[illegible] [illegible]
[illegible] [illegible]

[illegible] NO. [illegible] AIR FLOW 946.4
[illegible] 0.25000
NUMBER OF MEASUREMENT POINTS : 12
[illegible] [illegible] 1743.
[illegible]

[illegible] NO. [illegible] AIR FLOW [illegible]
[illegible] 0.25000
NUMBER OF MEASUREMENT POINTS : 11
[illegible]

[illegible] NO. [illegible] AIR FLOW [illegible]
[illegible] 0.25000
NUMBER OF MEASUREMENT POINTS : 11
[illegible]

| | |
|---|---|
| 104.0 | 160.4 |
| 160.4 | 259.7 |
| 1.9 | 358.9 |
| 7.7 | 431.7 |
| 0.7 | 530.9 |
| . | 625.2 |
| 1 . | 730.0 |
| . | 841.0 |
| . | 1032. |
| . | 1127. |
| . | 1230. |

| | |
|---|---|
| . | . |
| . | 139.4 |
| . | . |
| . | 1 . 2 . |
| . | 1294. |
| . | 1502. |
| . | 1625. |
| . | 1751. |

| | |
|---|---|
| 100.0 | 10.0 |
| . | . |
| . | . |
| . | 1025. |
| . | 1128. |
| . | 1250. |
| . | 1375. |
| . | 1500. |
| . | 1625. |
| . | 1750. |

| | |
|---|---|
| . | . |
| . | 125.0 |
| . | 314.1 |
| . | 41 . . |
| . | 5 . 6 . |
| . | 625. 1 |
| . | 7 . . |
| . | 8 0 . |
| . | 9 . 3 . |
| . | 1051 |

```
NUMBER OF MEASUREMENT POINTS :
 SF    VEL DU*RA*(DU/DI)**1.5*DI*(DO-DI)
 94.7              420.6
 [illegible]       [illegible]
 [illegible]       [illegible]
 [illegible]       [illegible]
 [illegible]       [illegible]
 [illegible]       [illegible]
 [illegible]       [illegible]
 [illegible]       [illegible]
 [illegible]       [illegible]

 [illegible]                    1155.1
 [illegible]
 [illegible]  POINTS :
 [illegible]  VEL DU*RA*[illegible] DI **1.5*DI*(DO-DI)
 [illegible]       [illegible]
 [illegible]       [illegible]
 [illegible]       [illegible]
 [illegible]       [illegible]
 [illegible]       [illegible]
 [illegible]       [illegible]
 [illegible]       [illegible]
 [illegible]       [illegible]
```

PRESENT RESULTS OF TEST [illegible] :

NUMBER OF DATA SETS : [illegible]

[illegible] FOR AIR FLOW [illegible]
[illegible] OF CENTRAL JET [illegible] :
[illegible] OF MEASUREMENT POINTS :
[illegible]

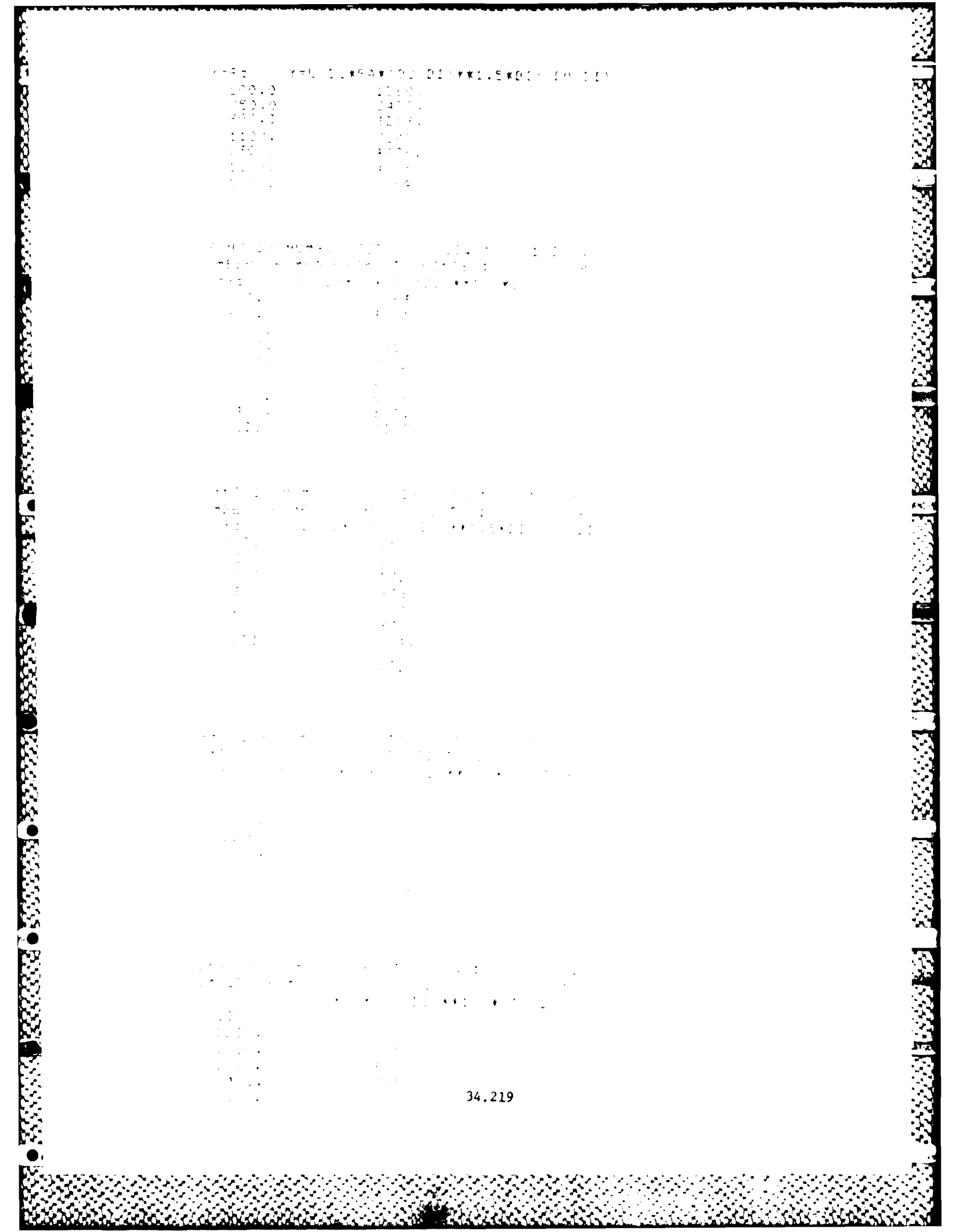
[illegible]

[illegible] OF [illegible] AIR FLOW [illegible]
[illegible] OF [illegible] JET [illegible] :
[illegible] OF MEASUREMENT POINTS :
[illegible]

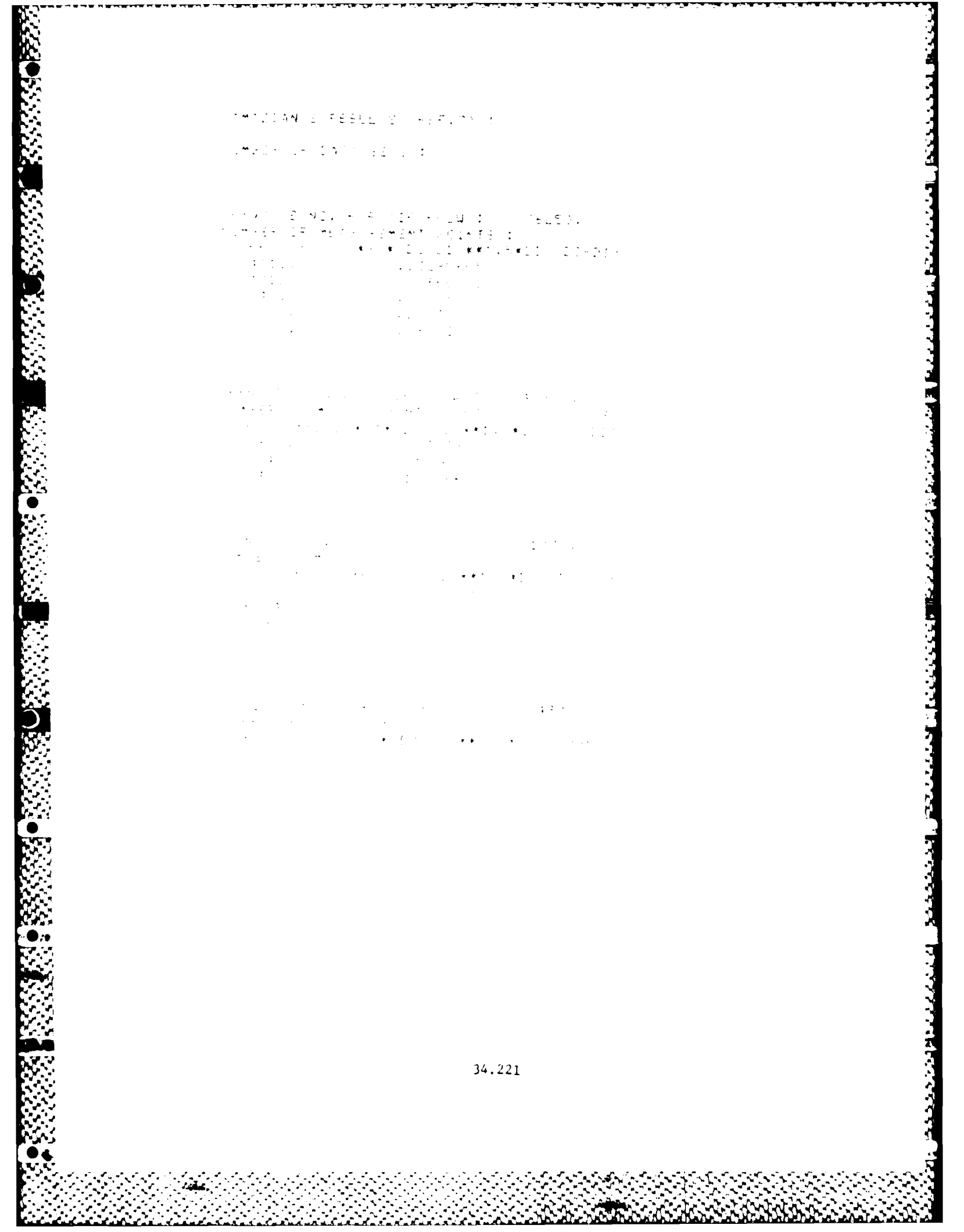
[illegible]

[illegible] FOR AIR FLOW [illegible]
[illegible] OF [illegible] JET [illegible] :
[illegible] OF MEASUREMENT POINTS :
[illegible]

[illegible]







1984 USAF-SCEEE RESEARCH INITIATION PROJECT

Sponsored by the

AIR FORCE OFFICE OF SCIENTIFIC RESEARCH

Conducted by the

SOUTHEASTERN CENTER FOR ELECTRICAL ENGINEERING EDUCATION

Final Report

# NUMERICAL MODELING OF MULTIPHASE TURBULENT RECIRCULATING FLOWS IN SUDDEN-EXPANSION RAMJET GEOMETRY


| | |
|---|---|
| Principal Investigator: | Dr. Albert Y. Tong |
| Academic Rank: | Assistant Professor |
| Department<br>University: | Department of Mechanical Engineering<br>University of Texas at Arlington |



| | |
|---|---|
| Contract No: | F49620-82-C-0035 (84 RIP 35) |
| Funding Duration: | January 1, 1986 to December 15, 1986 |

CONTENTS

I. Introduction

II. Fuel Spray Model Formulation and Overall Solution Scheme

III. Program Execution Procedure

IV. Plotting Programs

V. Summary

Acknowledgement

References

Figures

Appendices

A: Program Listing of Modified STARPIC

B: Program Listing of STRMSORT

C: Program Listing of STRMPLOT

D. Program Listing of PLOTGEN

E. Program Listing of PLOTR

## I. Introduction

The numerical modeling of multiphase flow in a sudden-expansion ramjet combustor geometry had been studied by the present author during his participation in the AFOSR/SCEEE Summer Faculty Research Program in the summer of 1984. It was part of several research efforts undertaken at the Aero Propulsion Laboratory. (Wright-Patterson AFB; Dayton, Ohio) to gain further insights into the characteristics of multiphase flow field in a ramjet dump combustor.

The basic configuration of the so-called sudden expansion dump combustor is shown in Figure 10. In this type of combustor, liquid fuel is sprayed into the ram air upstream of the dump station. It may also be injected directly into the chamber via side-wall inlets. Primary flame stabilization is provided by the flow recirculation regions, which may be supplemented with mechanical flame holding devices at the air inlet/combustor interface and/or the presence of inlet air swirl, obtained by the use of tangential injection or swirl vanes.

The goal of the summer research was to investigate via numerical modeling, the flow characteristics in a sudden-expansion ramjet combustor. The particular problem is concerned with liquid fuel spray in the combustor. The objective was to develop a computer code which can be used for the systematic study of the multiphase flow characteristics.

Liquid fuel spray plays an important role in combustion performance and emission of pollutants. Local values of air/fuel ratio are governed by trajectories of individual droplets, rates of vaporization and mixing of fuel vapor with air. Atomizers produce sprays with a wide range of droplet sizes, velocities and initial directions of flight. The droplets interact with gas streams, which can deflect the droplets from their trajectories. Vapor is released in the wakes of the droplets and these trails of vapor mix by

[illegible] and diffusion with the airstreams. The rates of vaporization are [illegible] to the temperature and species concentrations of the environment [illegible] which the droplets traverse. Since combustion efficiency and temperature distributions are directly dependent upon air/fuel ratio distributions, an accurate prediction of composition of the fuel vapor [illegible] at the droplet surface is important for spray combustion analysis.

The possibility of adapting and modifying developed computer codes to the present geometry and flow conditions had been considered. Several existing computer codes on fluid flow modeling available at the Aero Propulsion Laboratory had been examined. They were described briefly in [1]. It had been felt that it would be most efficient to develop a custom-made droplet spray code and incorporate it into the existing STARRC code for the multiphase flow calculation. Subsequently, a droplet spray model was formulated along with an overall solution scheme (see [1]).

The present research work is a continuation of the summer work conducted by the author at the Aero Propulsion Laboratory. The goal is to implement the two-spray model along with the overall solution scheme into the STARCC code which ultimately can be used for the systematic study of the flow characteristics.

In the present study, a liquid spray model has been inserted into the STARPIC code. The details of the formulation, overall solution scheme and procedure are given in this report. More details on the liquid spray model formulation is given in [1]. Due to some programming difficulties encountered in running STARRC, STARPIC was used instead. Since STARPIC considers only the fluid dynamics, only the droplet momentum source terms are considered in the liquid spray model. However, provision has been made in the liquid spray computer code to account for the thermal energy and species source terms.

The liquid phase is modelled as a steady droplet flow from a set of ports. The ports may be at any location inside the flow field as well as at the inlet perimeter and can have arbitrary input for mass flow rate, velocity, droplet diameter and temperature. A listing of the modified STARPIC program is given in this report.

STARPIC generates tables of property data including velocity, stream function, turbulence energy and turbulent dissipation. These data are given for an array of points mapped in a grid over the length of the combustor along a plane from the centerline to the edge of the combustor. A set of computer programs (STRMPLOT, STRMSORT) have been developed to plot the streamlines. Numerical data can be hard to interpret and use, while plots can help make the interpretation easier. The procedure used to plot the streamlines can be broken down into two separate steps. In the first step, a subroutine (STRMSORT) working in the STARPIC program generates plotting points and stores these points in a data file. The second step is to plot the data using a postprocessor program (STRMPLOT) running with a Calcomp pen plotter. This set of programs is a very specialized point generating subroutines that is designed specifically for stream function plotting and is unsuitable for plotting anything but stream function. In order to plot other properties as well as stream function a more universal point generating program (PLOTGEN) is developed.

The plotting software developed in the present work can also be used with minor modifications to produce pen plots of the output of other similar programs as well. The programs are written for the user who has a mild working knowledge of Fortran 77 or similar version. The details of the theory and operation of these plotting softwares are included in this report.

## II. Fuel Spray Model Formulation and Overall Solution Scheme

In the present work, a liquid spray model has been inserted into the STARPIC Code. The liquid phase is modelled as a steady flow from a set of ports. The ports may be at any location inside the flow field and can have arbitrary input mass flow rate, velocity and temperature. The liquid flows in the form of a stream of droplets in an annular section. The model is founded on the idea of regarding the liquid phase as a source of mass, momentum and energy to the gas phase continuum. The calculation scheme utilizes the cellular approach in which each computational cell is regarded as a control volume. Eulerian conservation equations are applied to the gas phase and Lagrangian equations of droplet motion and thermal energy are applied to a finite number of droplet size ranges representing the size distribution within the spray. Recording the mass, momentum and energy of the droplets on crossing cell boundaries provide the droplet source terms for the gas flow equations.

The calculation begins by solving the gas flow field assuming no droplets are present. Using this flow field, droplet trajectories together with the size and temperature histories can be calculated as a solution to a system of ordinary differential equations developed from the Lagrangian formulation. In this program the droplet trajectory is calculated by numerical integration using a fourth order Runge-Kutta method. The droplet trajectory is followed from the port inlet to the point where it either leaves the flow domain or hits the outer wall. No attempt has been made to account for the history of the droplet after splashing off the wall. Also excluded are the possibility of the drop crossing the center line or colliding with any other droplet as reliable models for these collisions have not yet been developed. The drag forces on the droplet are computed assuming a spherical drop shape. The equation of motion of a droplet is given by

$$\frac{d\vec{V}}{dt} = \frac{3}{8} \frac{\rho_g}{\rho_\ell} \frac{C_D}{R} (\vec{U}-\vec{V}) |\vec{U} - \vec{V}| + \vec{g}$$

$$\frac{d\vec{X}}{dt} = \vec{V}$$

where $\vec{U}$ and $\vec{V}$ are the gas and droplet velocities respectively. $C_D$ is the drag coefficient, R is the droplet radius, $\vec{g}$ is the gravity vector and $\vec{X}$ is the droplet location vector. The gas phase velocity components used in the numerical integration are assumed to be constant in a given time step. The value of the gas phase velocity component is chosen as the velocity corresponding to the U or V cell that the droplet is in.

It should be mentioned that STARPIC as well as STARRC and TEACH employ a special grid system known as the staggered grid system. A schematic of the staggered grid system is given in Figure 1 where the C, U and V cells are shown. The C cells are the control volume cells for quantities such as temperature and pressure which are referenced at the grid points. The U cells are the control volume cells for the horizontal velocity components U which are referenced at midway between two neighboring horizontal grid points. Similarly, the V cells are the control volume cells for the vertical velocity components V which are referenced at midway between two neighboring vertical grid points. As shown in Figure 2, the boomerang-shaped envelope encloses a triad of points with reference location P at (I,J).

In order to correctly identify when and which C, U and V cell boundaries the droplets traverse, finer grid cells called the B cells are introduced in the present work. Basically, they are the four unit cells of a C cell. As shown in Figure 2, there are four B cells attached to a grid point. They can be categorized into types 1,2,3 and 4 as indicated in the figure. The location of a B cell relative to a grid point can then be identified once the cell type

At each integration step, a check is made to see if the droplet crosses either a C, U or V cell boundary. For example, if a drop crosses a U cell boundary, the cell it has just departed from has lost some axial momentum and the cell it has entered has gained an equal amount of momentum. This is accounted for by adjusting the source term used in the gas phase calculation. The same is true when the droplet crosses a V cell boundary. Provision has been made to account for thermal energy adjustment as the droplet crosses the C cell boundary, but this source term adjustment has not been implemented yet because STARPIC does not handle energy equation calculations.

The source terms are adjusted at each integration step, and the process is repeated for the remaining ports. Subsequently, the gas phase calculations are repeated to generate a new gas phase solution subject to the adjusted droplet source terms. The gas phase velocity distribution is checked for convergence between two consecutive solutions. A mean squared difference convergence criterion is used. Flow charts for the overall solution algorithm and the droplet calculation procedure are presented in Figures 5 and 6.
is determined. The information is needed for determining the cell boundaries the droplets traverse in the source term calculations.

## III. Program Execution Procedure

In an attempt to keep as much of the original code undisturbed as possible, some of the variables that are also used in the subroutines for the liquid phase calculations are duplicated. A listing of the modified STARPIC program is given in Appendix A with the inserted sections clearly indicated. All the variables used in the liquid phase calculations are declared in two common blocks, namely DROPS and GGF. The common block GGF is used to declare the source term adjustment variables inserted in the gas phase subroutines CALCU and CALCV, and the remaining variables are declared in the common block DROPS.

The gas phase data is obtained first, and the corresponding initialization subroutines are executed. The liquid phase data is then read. The user must choose the mode to input data by assigning the value of the integer NDATA. If it is equal to 0 only the gas phase calculations are executed. If it is equal to 1 the data is read interactively from the terminal. If it is equal to 2, the data is read from a file. If it is equal to 3, the data is assigned in the program code. Thus, the program can be run both interactively or in a batch mode.

The variables to be supplied for the liquid phase are:

(i) MAXPOR, the total number of ports from which the liquid is sprayed. A maximum of 10 is allowed but this can be increased by modifying the variable declaration statements.

(ii) DRPDEN, the liquid density. The liquid from separate ports may have different densities. ($kg/m^3$)

(iii) DRPDIA, the drop diameter (m)

(iv) XDINIT and YDINIT, the axial and radial location of the port. The port may be located anywhere inside the flow domain. The location is with respect to the coordinates used in the gas phase (m).

(v) UDINIT and VDINIT, the axial and radial velocity of the drop at injection (m/s).

(vi) TDINIT, the initial temperature of the liquid (K).

(vii) DRMDOT, the liquid mass flow rate from the port (kg/s).

The location of the lower left hand corner of the B-cell, XB and YB, are assigned. All flags and counters are initialized. The input data is written into a file. The integration time step and scaling factors are initialized. The droplet injection frequency is calculated from the mass flow rate.

The gas phase solution is now executed, and the equivalent gas velocity variables used in the liquid phase calculations are updated. The source term adjustment variables, RMOMU and RMOMV, are reinitialized to zero. The subroutine DROP is now invoked to perform the entire liquid phase calculations. It also returns the global convergence flag IFLAGZ. If the value of IFLAGZ returned is 1, then global convergence has been achieved. Consequently, the gas phase results are printed and the execution is terminated. If IFLAGZ is 0, the system has not converged globally and the gas phase calculations are executed again, and this is done by transferring control to statement number 2000. This causes a re-execution of both the gas phase and liquid phase calculations until either convergence is achieved or until the maximum number of iterations allowed, MAXCT, is exceeded.

Subroutine DROP is invoked by the main program, and it executes all the calculations required for the liquid phase. A brief description of the subroutines created in the present work is given in the latter part of this section. To begin, the droplet location, velocity, temperature, radius and density are initialized for the first injection port. Then, the flags and counters are initialized to zero. Subroutine FINDB is now called to obtain the B, C, U and V cells where the injection port is located. The source term adjustment variables RMOMU and RMOMV at the injection port are initialized.

UGAS and VGAS are set to the gas velocities of the mid-point of the U and V cells where the droplet is located. The numerical integration subroutine RUNGA is now called to obtain the new location and velocity for the droplet. Subroutine DOMCHK is called to check if the droplet is inside the flow domain. If the droplet has departed from the flow domain the flag IHIT is set to 1, and the control is transferred to statement number 900 to start calculations for the next port. The B cell in which the droplet is located after integration is identified by calling subroutine FINDB. The subroutine HITWAL is then called. If the droplet has hit the outside wall, IHIT is set to 1 and the control is transferred to statement number 900 to start calculations for the next port. No attempt has been made to account for the history of the droplet after splashing off the wall. Also excluded are the possibility of the drop crossing the center line or colliding with any other droplet as reliable models for these collisions have not yet been developed. If the droplet is still in the flow domain, subroutine STPCHK is called to check if the droplet has migrated to one of the eight immediate neighboring B cells. If the droplet remains inside the same B cell, the time step DT is increased by a scaling factor DTINC and the integration step is redone again with the adjusted time step to ensure that the droplet leaves the B cell in one integration step. If, however, the droplet travels beyond one of the eight neighboring cells, the integration time step is reduced by a scaling factor DTRED. As before, the integration step is redone with the adjusted time step, so that finally the droplet does move into one of its neighboring cells. The reason for this restriction is for easier bookkeeping of the droplet source term.

The integer variable NCASE which specifies the type of B cell is determined by calling subroutine FINDN. For a given value of NCASE, there are eight neighboring cells that the droplet may enter. This is shown in Figure 4. An integer variable MCASE is used to signify the relative position of the

neighboring cells. This is indicated in the figure. The value of MCASE is determined by calling subroutine FINDM.

There are all together thirty-two different cases depending on the values of MCASE and NCASE. With this information it is possible to identify exactly which C, U and V cell boundaries the droplet has crossed. If a U cell boundary has been crossed, a linearly interpolated value of the droplet axial velocity at the boundary is obtained by calling subroutine INTERP and the source term modification variables RMOMU are updated by calling subroutine UMOD. Similarly, if a V cell subroutine is crossed, the variables RMOMV are updated by calling subroutine VMOD. If a C cell boundary has been crossed, subroutine CMOD is invoked. At present, subroutine CMOD has no executable statements, but it can be used to update the source terms corresponding to temperature and other variables when the thermal energy calculations for the liquid phase are implemented. Once the source term variables have been updated, the location of the droplet is stored into a file. The counter ISTEPS is incremented. If ISTEPS exceeds the maximum number of steps allowed, as would be the case if the droplet enters a recirculation zone, the calculations for the next port are initiated.

When the calculations for all the ports are completed, subroutine COMPAR is called to check for convergence by comparing the two consecutive gas phase solutions, and then control is returned to the main program.

Several spray calculations have been performed using the present modified STARPIC program. These include spray injection at the inlet perimeter as well as at the inlet center with various droplet diameters and initial velocities. In most cases, three (3) overall global iterations between gas phase and liquid phase calculations is needed.

A comprehensive documentation on STARPIC is given in [2]. Here a brief description of the various subroutines inserted in the present modified

STARPIC code is given below followed by a nomenclature list of the variables used in these subroutines.

[Subroutine DROP]

DROP is the master subroutine that when invoked by the main program, obtains the trajectories of all the droplets. A major function of this subroutine is to keep track of the droplet location with respect to the B,C,U and V cells. Whenever, the droplet crosses one of the control volume cells C,U, or V, the corresponding subroutines CMOD, VMOD and UMOD and are called to adjust the source terms for these cells. The gas phase solution convergence is checked by calling subroutine COMPAR after the liquid phase calculation is completed. The flow chart for this subroutine is shown in Fig. 6.

[Subroutine FINDB]

FINDB returns the index numbers IB and JB corresponding to the B cell that the droplet is in. FINDB also returns the index numbers IC, JC, IU, JU, IV and JV corresponding to the C,U and V cells that the droplet is in.

[Subroutine DOMCHK]

DOMCHK returns a nonzero value for the flag IHIT if the drop has left the flow domain.

[Subroutine INTERP]

Performs linear interpolation between two points.

Subroutine FINDM

The B cell to which the droplet travels can have one of four locations in the main grid cell. FINDM returns the value of MCASE corresponding to the cell location.

Subroutine FINDN

FINDN returns the value of NCASE corresponding to the one of eight neighboring cells that the droplet can travel to.

Subroutine STPCHK

STPCHK checks if the drop travels to one of the neighboring cells. The time step is increased if the drop did not cross any cell boundary, or reduced if the drop has travelled beyond a neighboring cell.

Subroutine COMPAR

COMPAR checks for the global convergence of the system, and is invoked by Subroutine DROP, after the liquid phase calculations are complete. The average squared gas velocity error is used as the criterion for convergence.

Subroutine RUNGA

RUNGA does the numerical integration of a system of first order ordinary differential equations by fourth order Runga Kutta numerical integration, and is called by Subroutine DROP for each integration step. The derivative values are obtained by calling Subroutine XPSYS.

Subroutine HITWAL

The flag IHIT is set to 1 if the droplet has hit the outer wall.

Subroutine UMOD

The source terms for axial momentum are adjusted to account for the droplet crossing a U boundary.

Subroutine VMOD

The source terms for radial momentum are adjusted to account for the droplet crossing a V cell boundary.

Nomenclature

INTERGER VARIABLES:

IB - AXIAL INDEX NUMBER FOR THE B CELL.

IBOLD - OLD AXIAL INDEX NUMBER FOR THE B CELL.

IC - AXIAL INDEX NUMBER FOR THE C CELL.

ICOUNT - COUNTER FOR NUMBER OF LIQUID PHASE ITERATIONS.

IFLAGZ - GLOBAL CONVERGENCE FLAG.

IHIT - FLAG: 0 IF DROP IS IN THE FLOW DOMAIN.

INTCTR - NUMBER OF RE-INTEGRATIONS.

INTFLG - INTEGRATION FLAG.

ISTEPS - NUMBER OF STEPS TRAVELLED BY THE DROP.

IU - AXIAL INDEX NUMBER FOR THE U CELL.

IV - AXIAL INDEX NUMBER FOR THE V CELL.

JB - RADIAL INDEX NUMBER FOR THE B CELL.

JBOLD - OLD RADIAL INDEX NUMBER FOR THE B CELL.

JC - RADIAL INDEX NUMBER FOR THE C CELL.

JDMAX() - VARIABLE EQUIVALENT TO JMAX() IN THE MAIN PROGRAM.

JU - RADIAL INDEX NUMBER FOR THE U CELL.

JV - RADIAL INDEX NUMBER FOR THE V CELL.

MAXCT - MAXIMUM NUMBER OF OVERALL GAS-PHASE LIQUID-PHASE ITERATIONS ALLOWED.

MAXPOR - MAXIMUM NUMBER OF PORTS.

MAXSTP - MAXIMUM NUMBER OF STEPS ALLOWED FOR DROP.

NPORT - PORT NUMBER.

NDI - VARIABLE EQUIVALENT TO NI IN THE MAIN PROGRAM.

NDJ - VARIABLE EQUIVALENT TO NJ IN THE MAIN PROGRAM.

REAL VARIABLES:

CDD - COEFFICIENT OF DRAG FOR THE DROPLET.

DRPDEN(N) - LIQUID DENSITY OF PORT NUMBER N.

DRPDIA(N) - DROP DIAMETER OF PORT NUMBER N.

DT - INTEGRATION TIME STEP.

DTINC - INCREMENT SCALE FACTOR FOR DT.

DTRED - REDUCTION SCALE FACTOR FOR DT.

GRAVX - AXIAL ACCELERATION FORCE COMPONENT.

GRAVY - RADIAL ACCELERATION FORCE COMPONENT.

PI - 3.14159265

RAD - DROPLET RADIUS.

RHOGAS - DENSITY OF THE GAS.

RMOMU() - CONTRIBUTION TO AXIAL MOMENTUM SOURCE TERM.

RMOMV() - CONTRIBUTION TO RADIAL MOMENTUM SOURCE TERM

TDINIT() - INITIAL TEMPERATURE OF DROPLET.

TDNEW - NEW TEMPERATURE OF DROPLET.

TDOLD - OLD TEMPERATURE OF DROPLET.

UDINIT() - INITIAL AXIAL VELOCITY OF DROPLET.

UDNEW - NEW AXIAL VELOCITY OF DROPLET.

UDOLD - OLD AXIAL VELOCITY OF DROPLET.

UG() - VARIABLE EQUIVALENT TO U( ) IN THE MAIN PROGRAM.

UGAS - AXIAL VELOCITY OF THE GAS.

UGOLD() - OLD AXIAL VELOCITY OF GAS.

VDINIT() - INITIAL RADIAL VELOCITY OF DROPLET.

VDNEW - NEW RADIAL VELOCITY OF DROPLET.

VDOLD - OLD RADIAL VELOCITY OF DROPLET.

VG() - VARIABLE EQUIVALENT TO V( ) IN THE MAIN PROGRAM.

VGAS - RADIAL VELOCITY OF THE GAS.

VGOLD() - OLD RADIAL VELOCITY OF GAS.

XB() - AXIAL COORDINATE OF LOWER LEFT CORNER OF B-CELL.

XDINIT() - INITIAL AXIAL-COORDINATE OF DROPLET.

XDNEW - NEW AXIAL LOCATION OF DROPLET.

XDOLD - OLD AXIAL LOCATION OF DROPLET.

YB() - RADIAL-COORDINATE OF LOWER LEFT CORNER OF B-CELL.

YDINIT() - INITIAL RADIAL-COORDINATE OF DROPLET.

YDNEW - NEW RADIAL LOCATION OF DROPLET.

YDOLD - OLD RADIAL LOCATION OF DROPLET.

## IV. Plotting Programs

### A. Streamline Plot

The first step of the process is to generate plotting data from the data generated in the STARPIC program. Just before the modified STARPIC program ends, the subroutine STRMSORT is called. To this subroutine, the following generated data is passed: array of stream function values for grid points, the number of i grid lines, the number of j grid lines for each i grid value, an array of the x values corresponding to each i grid line, and an array of the y values corresponding to each j grid line. The subroutine STRMSORT first generates the outer boundary line points for the combustor through the use of the IMAX and JMAX values. The maximum j value is found for each i value up to IMAX, the last i grid line within the combustor. As each outer j coordinate is found it is checked against the previous one. If it is different, then it is assumed that the expansion step has occurred between this i grid line and the last. In this case two extra points are included, defining the corners of the step, then the rest of the points. As each point is defined the boundary j value is corrected by averaging between the last active j line and the first one outside the boundary. The i and j values are converted to their corresponding x and y values respectively as each point is found. The boundary points are then written to a disk file and followed by an end of block marker, 999.9 for both x and y values to signify the end of a line definition. When the points are recorded on disk they are recorded x value first then y value for each point. This is true of all points, boundary or otherwise.

Now, the main loop of the STRMSORT is executed. A listing of the subroutine is given in Appendix B. First a stream function value is defined for the particular streamline, lines 2073 to 2079. Next the subroutine INTERP is called. As is explained later, INTERP finds the actual points with the previously defined stream-function value. Once execution has returned from the

INTERP subroutine, STRMSORT checks for the existence of two special cases. The first is no points found with the desired stream function value. If this occurs, the next value is defined and execution continues. The other special case is when the stream-function value is greater than 1.0. When this occurs, it is assumed that a loop exists and the loop sort section is executed. Once the special cases are handled, the points are converted from i,j coordinates to x,y coordinates for plotting.

The i,j to x,y conversion section, lines 2086 to 2106, first checks to see if the i coordinate is an integer. If so, then the i grid coordinate is converted directly to an x value with the appropriate number from the array 'X'. If not, then the x value is interpolated linearly between the x values of the two consecutive i grid lines surrounding the point. The y value of the point is interpolated from the j grid value in the same manner.

The sorting of the points of a loop is accomplished in lines 2114 through 2153. Since the interpolation routine selects points along set i grid lines, it is assumed that the points in a loop will occur in pairs, with the possible exception of the ends of the loop. Since the interpolation routine selects points by starting at the inlet and ending at the outlet, the points or point-pairs are in ascending order by i grid value. In these pairs of points the point with the higher j grid value occurs second because the interpolation routine checks the j grid intervals starting at the centerline and moving outward to the boundary. The first step in sorting for the loop is splitting up the pairs. In lines 2116 to 2133, a loop is executed in which the i grid value of each point is compared with the previous point. If if matches, this point is the upper point of the pair and is put at the bottom of the temporary storage array 'TEMPPTS'. The points are to be sorted so that the loop is plotted counter-clockwise starting with outer point with the highest i grid value. With this in mind, the upper points are placed in the temporary array

starting at the bottom of the array so that their order is reversed, and the lower points and any single points are placed in the temporary array in the order of occurrence starting at the top. In lines 2134 through 2143, the upper points are moved to the top of the array and the lower points are moved down with no change in order for either group. The points are now in the proper order for plotting as a loop. As a final step, the first point is added at the end to close the loop in plotting. If the first point occurs at the outlet boundary, it is not added because this would indicate that the loop continued out of the control region.

The interpolation subroutine INTERP functions as follows. Starting at the centerline and moving outward, each j grid interval is checked to see if the specified stream function value exists in it. This is carried out along each i grid line starting at the inlet and proceeding toward the outlet. If the desired stream function value is less than or equal to one, each j interval is checked until the outer value of the interval is lower than the inner value. When this occurs, the process restarts at the next i grid line. If the desired value does fall within the interval, the actual j grid value is found by linearly interpolating between the inner and outer boundary values for that interval, lines 2197 to 2201. Two special cases are handled by the interpolation routine. The first is when the desired streamline has the value one. When this occurs, the first i grid line checked is immediately following the expansion corner. Before the interpolation loop is executed, though, the lower corner point is added. If the last point is not at the outlet boundary, the last two points are used to linearly extrapolate the intersection with the outer boundary, with this point being added at the end. The second special case is when the desired stream function value is greater than one. When this occurs, the interpolation loop checks every interval out to the boundary. This is to capture the points in the recirculation region.

The plotting program STRMPLOT functions as follows. The program reads points until either the end of block marker '999.9' or the end of file marker '888.8' is read. When the end of file marker is read the points that have been read are processed and plotted. If it is the first group of points, it is considered to be the boundary points. From this group the scaling factor is determined to make the plot 10 inches long, lines 45 and 46. These scaling factors are applied to every group of points. This first group is then scaled, lines 47 to 56, and then plotted. Connecting lines to complete the boundary are then plotted using the first and last points, lines 59 to 71. An arrow is then plotted to indicate the flow direction. Each succeeding group of points is then read, scaled and plotted using smooth lines to connect the points. When the end of file marker is read the plot is ended.

Two streamline plots generated by these programs are shown in Figure 7.

B. Universal Plot

STRMSORT is a very specialized point generating subroutine that is designed specifically for stream function plotting and is therefore unsuitable for plotting anything but stream function. For this reason, a more universal point generating program, PLOTGEN, is developed along with a plotting post-processor, PLOTR, which is taken almost directly from its predecessor, STRMPLOT, with minor modifications allowing easier user selection of plotting options.

The assumptions and limitations in the theory behind PLOTGEN FOR are as follows. The first and most important assumption is that physical properties are continuous. It is also assumed that if two points are close enough together and the property values are known at these two points, that a point, whose property value is between the other two, can be located with sufficient accuracy by the linear proportional distance between the two previous points corresponding to the proportionality of the corresponding property values.

It is further assumed that if two points exist such that their property values are the same and the spacial intervals surrounding these two points immediately border each other, horizontally, vertically or diagonally, that these two points may be connected by a line or similar curve along which the property value is constant. PLOTGEN is limited to working with cases in which a property is a function of the physical point of interest in a two dimensional cartesian-coordinate plane.

The first step in generating the plotting data, is to find points whose property value equals the desired. To do this, the interval between each pair of grid points, that neighbor either vertically or horizontally, is checked to determine whether the desired property value occurs between these two grid points. If the value does occur between in this interval, the location of this new point is taken to correspond to the linear proportionality of the desired property value within the interval. Since both grid points have either the same x-value or the same y-value, one coordinate of the new point is known. To find the other point, the value is found through linear interpolation on the range between the two grid points. In this way, a set of points whose property value is given, can be physically located. The next step is to connect these points to produce a plot.

The method of detecting point links and of linking these points approximates the method a human would use if provided with only a group of points. The first step is to find a point in the set of points. In this case, find the lowest that is farthest to the left. With this point, there is an associated interval, between two grid points on some known grid line. Around this interval, there are eight other-bordering intervals; four diagonally, two vertically, and two horizontally. Beginning with the direction from which the current point was found, proceed in a counter-clockwise direction, checking each of these eight intervals until another point is

detected. If a point is detected, then the plot will be connected to this new point, and the intervals around this new point are checked for new points. This continues until a point is reached where no adjoining point is detected. If this occurs, the location of the first point of this plot line is checked. If this first point would have been detected here, it is repeated to close the curve. After this the process starts again with another first point until all of the points have been used. Only the intervals between active grid points are checked as outlying points could cause error.

The program PLOTGEN is written in a block style to make programming and modification easier. A listing of the program is given in Appendix D. In the setup section, the variables are defined in comment statements and declared. Here also, the point arrays and control variables are initialized. In the read section, the data table with the data to be plotted, is read into the program for processing. This section includes subsections to read from either the STARPIC or the TEACH output. Following this is the boundary definition section. Here, the physical boundaries are determined and output to the plot file. Here also, the grid boundaries for the rest of the program are set. The next sections work together in the master loop. The first section determines in which intervals the plot points are found and where within each of these intervals the point is located. Following this, the first point section searches the two interval arrays to find a first point for plotting. The succeeding points section then attempts to link up adjoining points. The last section checks for the case where the last point adjoins the location of the first point.

At the first of the setup section, there is a large group of comment statements defining the use or purpose of each variable. Following this, the arrays and variables are declared with the appropriate types. Certain variables and arrays are then loaded with the proper values. Next, the array

VALUE is initialized with the desired property values for plotting. Here the user sets NUMVALS to the number of values to be plotted. Finally, the interval arrays are set to -1 in every cell to indicate no point present.

In the read section, the data table for plotting is read according to the format type set by the variable READTYP. If READTYP equals one the data is read in the TEACH format, if two it is read in the STARPIC format.

At the beginning of the boundary definition section, the plot file is opened with the desired file name. Beginning at the left, each i grid line is checked from the bottom up until a zero value is found. This grid point is assumed to be the first beyond the wall, so the median value between this point and the previous grid point is converted to x,y coordinates and output to the plot file. This occurs at every i grid line until the first i grid line of zeroes is found. This is assumed to be the right end wall, so the value between this grid line and last is used to define the wall. The left wall was assumed to occur at an x value of zero. If a step is detected as the upper wall is being defined, the step is defined by two points whose x value equals the median of the two succeeding i grid lines and with the y values equal to that of the appropriate j grid line. After the boundary points have been output, the value 0.0 is output to close the boundary curve and the end of group marker, 999.9, and the symbol change marker, 777.7, are output.

The next four sections work together in the master loop. In the first, the point detection section, the interval to the right and the interval above each point is checked for the occurrence of each desired value. If this value is on a horizontal grid line, the proportional location of the plot point between the two end points of the interval, is stored in the interval array as type-one point and the counter of plot points found, PTNUM, is incremented. Points found in vertical intervals are stored as type-two points. Points are stored in the interval array location corresponding to either the left or

lower grid location of the interval, whichever is appropriate. If the grid location currently being checked for a plot point is at the maximum i grid line, the interval to the right of the grid point is not checked. Similarly, the intervals above grid points on the maximum j grid location of each i grid line are not checked. This is to avoid detecting phantom points at the wall.

The next block of statements checks through the interval array to find one with a point. In this case, the intervals that do not contain a point are represented by a value of -1 in the corresponding array cell. If the interval contains a point, its corresponding array cell will contain a value equal to or greater than zero and less than one. This value is the proportional location of the plot point between the two grid points at the ends of the interval. To find a point, the intervals are checked along each i grid line from left to right and from the inside j value out, with the type one cell checked first. When a point is found, its grid coordinates are converted to x,y coordinates and the point is written to the plot file. The i,j address of the interval of this point are saved along with the type of the first point and its x,y coordinates. This interval is then cleared, set to -1, and the point counter decremented, so this point will not be discovered again. Execution continues with the succeeding points section.

The succeeding points section is the heart of this plotting scheme. Here, the points are linked up to form lines, loops and other curves. Upon entering this section the i, j, and point-type values are those of the previous point, and the direction is assumed to be three. Here the eight cells adjoining the previous point are checked for a neighboring point. The addresses of these eight cells are a function of the location of the previous point, its type, and the direction from the previous point to the cell to be checked. The type of each cell to be checked is the same as the previous point if adjoins the previous point vertically or horizontally. If the new

cell neighbors the previous cell diagonally, the new cell is of the opposite type. The i,j address of the new cell is found by adding the appropriate delta values to the i,j coordinates of the previous point. The delta i value is found from the array DELI and is indexed by the type of the previous point and the direction from the previous cell to the new cell. The delta j value is found similarly from the array DELJ. These parameters are used to check the intervals in the eight directions proceeding counter-clockwise, with the direction one being to the right. The first direction checked is one past the direction from which the previous point was found. The neighboring intervals are checked until either a new point is found or all directions have been checked. If a new point is found, its grid coordinates, one of which is on a grid line and the other is between two lines, are converted to x,y coordinates and the point is written to the plot file. The interval is then cleared and the point counter decremented. The linking procedure is then repeated with this new point being the previous value. If no point were found execution would continue at the last point section.

In the last point section, the most recently found point is checked to see if it borders the first point in this plot line. If these two points do not border or they are the same point, the end of block marker, 999.9, is written to the plot file. If point counter is greater than zero then execution continues at the first point section. If all of the points have been used, the symbol change marker, 777.7, is written to the plot file and execution continues at the start of the master loop for a new property value. If the last point and the first point do border each other, then the first point is again written to the plot file to close the curve, and the end of block marker is also written to file. Execution continues as in above, according to whether or not all of the points have been used. If this is the last point and the last property value to be plotted, the end of file marker, 888.8, is written to

file, the file closed and the program ended. Otherwise, execution continues until whole list of desired property values is exhausted.

PLOTR is a simple plotting post-processor designed as a companion to PLOTGEN. It is composed of four major sections. The first is the set up and initialization section. Here the variables are defined and declared. The user defined parameters, with the exception of plot file name, are set. The appropriate value of LTYP is set to produce lines, symbols or a combination of the two. Following this is the master read loop. In this loop, points are read into two arrays, one each for the x and y coordinates of the plot points, until a control code is read. If the control code is 777.7, the symbol number is incremented. If the code is 999.9 and this is first group of points, control passes to the boundary plot section. If the code is 999.9 and this is not the first point group, the control passes the standard plot section. If the code 888.8 is read, the plot is ended, the plot file closed and the program ended.

In the boundary plot section, the boundary is plotted and the scaling factors are set. Since a counter of points read was kept in the read loop section, the number of points in this group is known. Since the last point of the boundary definition will be 0.0 the second to last point will have the maximum y value. With this in mind, the scaling factor for both x and y scales is set so that the maximum y value is plotted as some desired value, such as 1.5 inches. To produce a plot that is compressed or expanded in the x direction, the scaling factor for the x scale can be divided or multiplied by an appropriate factor. The boundary points are then each scaled and sent to the plotter in the order in which they occur in the plot file. A flow direction arrow is then plotted by calling the subroutine AROHD. Control then passes back to the read loop section.

In the standard plot section, the plot points representing the data table are scaled and plotted. Using the scale factors determined in the boundary plot section. Each point is scaled and then sent to plotter in the order in which it occurs in the plot file. If the value of the point counter, NUMPTS, is set to its negative in the subroutine call to FLINE, the points will be connected with a smooth curve fit to the plot points. Control is then passed back to the read loop section.

Included with this report are two sample plots. The first one shown in Figure 8 is the mixture ratio predicted by TEACH code. The inlet fuel temperature at the center is at 450 K and the air inlet temperature at the outer annular is at 300 K. The other one shown in Figure 9 is the temperature profile predicted by TEACH from the same calculation.

## V. Summary

A fuel-spray model has been successfully implemented into the STARPIC code which allows calculations of multiphase flow in a dump combustor. While STARRC and STARPIC both belong to the TEACH, there is no foreseeable difficulty in extending the fuel-spray model developed on the present study to STARRC or TEACH.

A set of computer programs to plot the streamlines as well as other properties such as isotherms have also been developed. The plots generated by these programs can help make the interpretations of data easier. These plotting software can also be used with minor modifications to produce pen plots of the output of other similar programs.

Acknowledgement

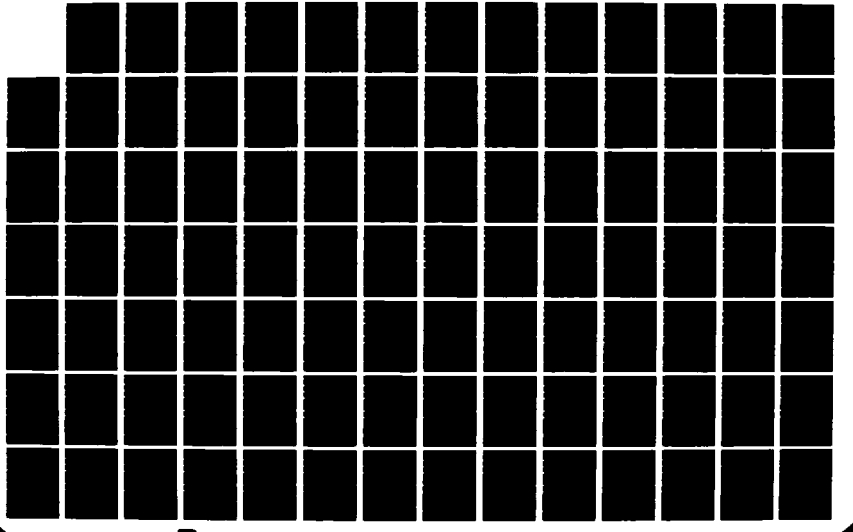
The support of the Air Force Office of Scientific Research for this research is gratefully acknowledged.

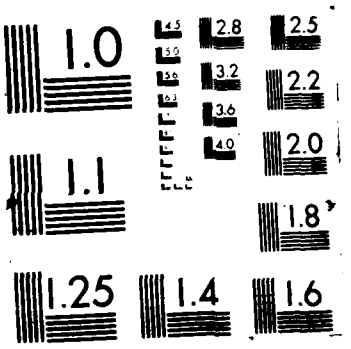
References

1. A. Y. Tong, "Numerical Modeling of Multiphase Turbulent Recirculating Flows in Sudden-Expansion Ramjet Geometry," USAF-SCEEE SFRP Final Report (AF-9620-82-C-0035; August 1984).

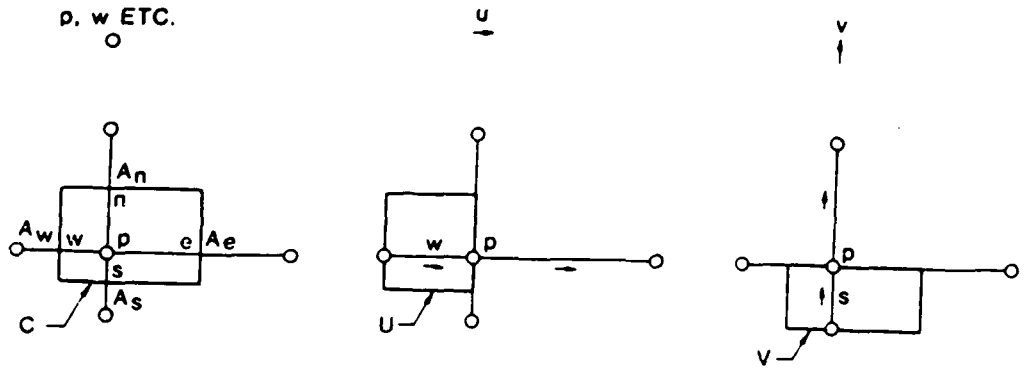
2. D. G. Lilley and D. L. Rhode, "A Computer Code for Swirling Turbulent Axisymmetric Recirculating Flows in Practical Isothermal Combustor Geometries," NASA Contractor Report 3442.

AD-A186 490 UNITED STATES AIR FORCE RESEARCH INITIATION PROGRAM 10/11
1984 RESEARCH REPORTS (U) SOUTHEASTERN CENTER FOR
ELECTRICAL ENGINEERING EDUCATION INC S W D PEELE
UNCLASSIFIED MAY 86 AFOSR-TR-87-1721 F49620-82-C-0035 F/G 15/1 NL




1.0
1.1
1.25
1.4
1.6
2.8
3.2
3.6
4.0
2.5
2.2
2.0
1.8

FIGURES




CONTROL VOLUMES C, U, V FACE

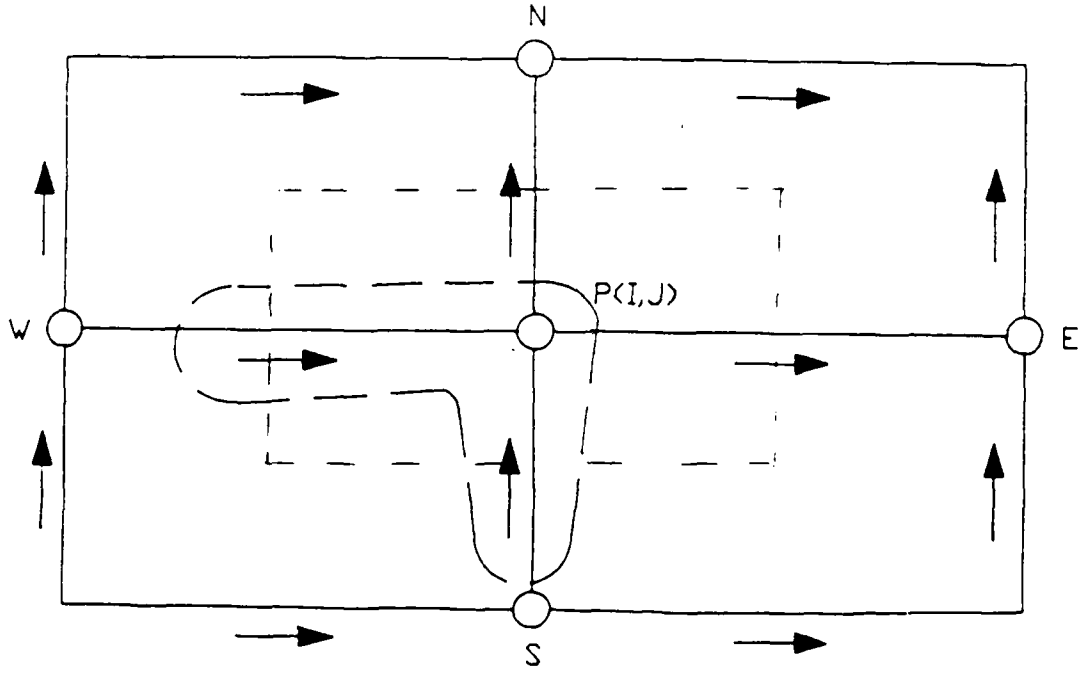



Fig. 1 Staggered grid for the computational mesh.

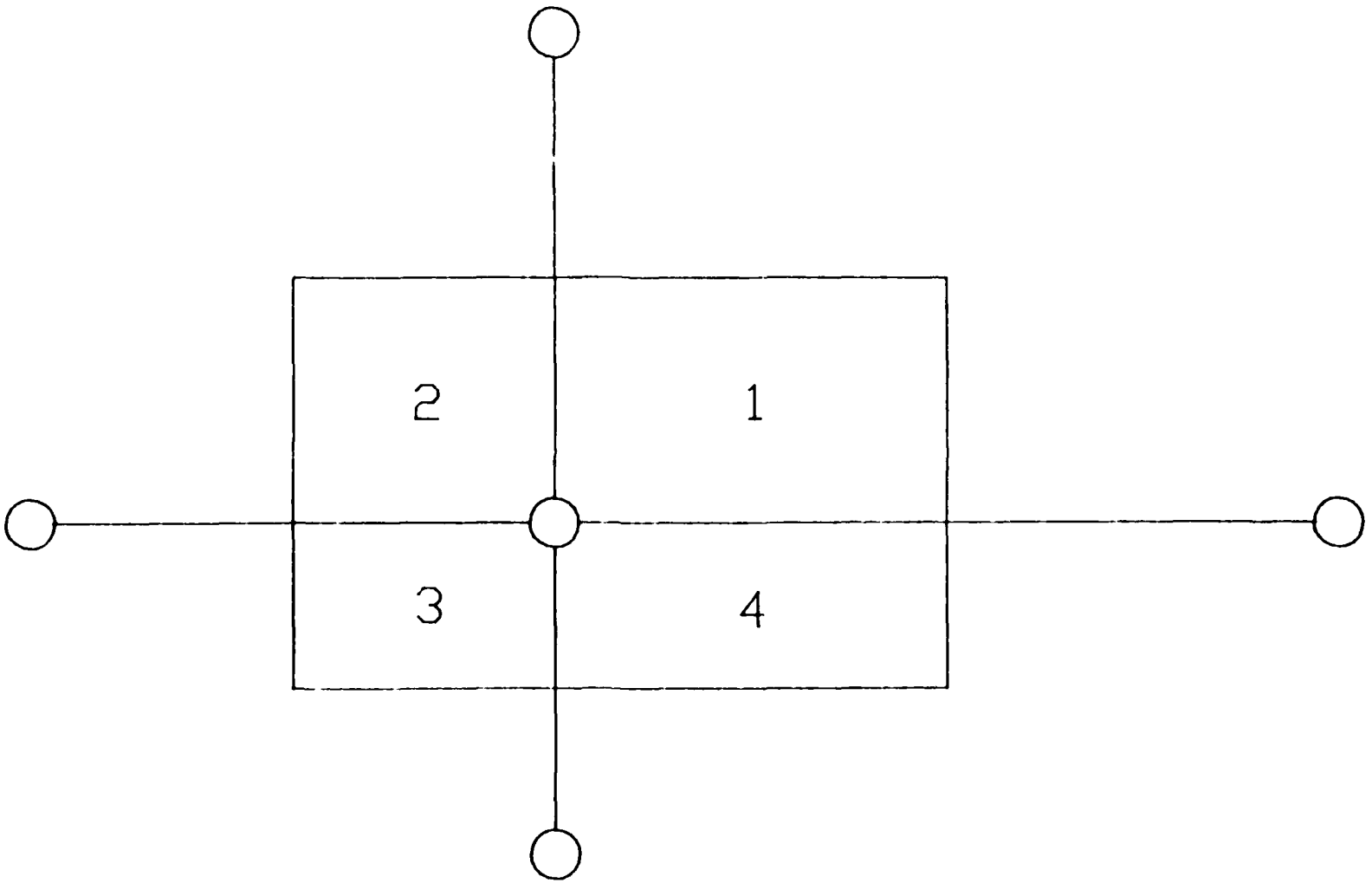



Fig. 2 The four types of B cells and their MCASE values

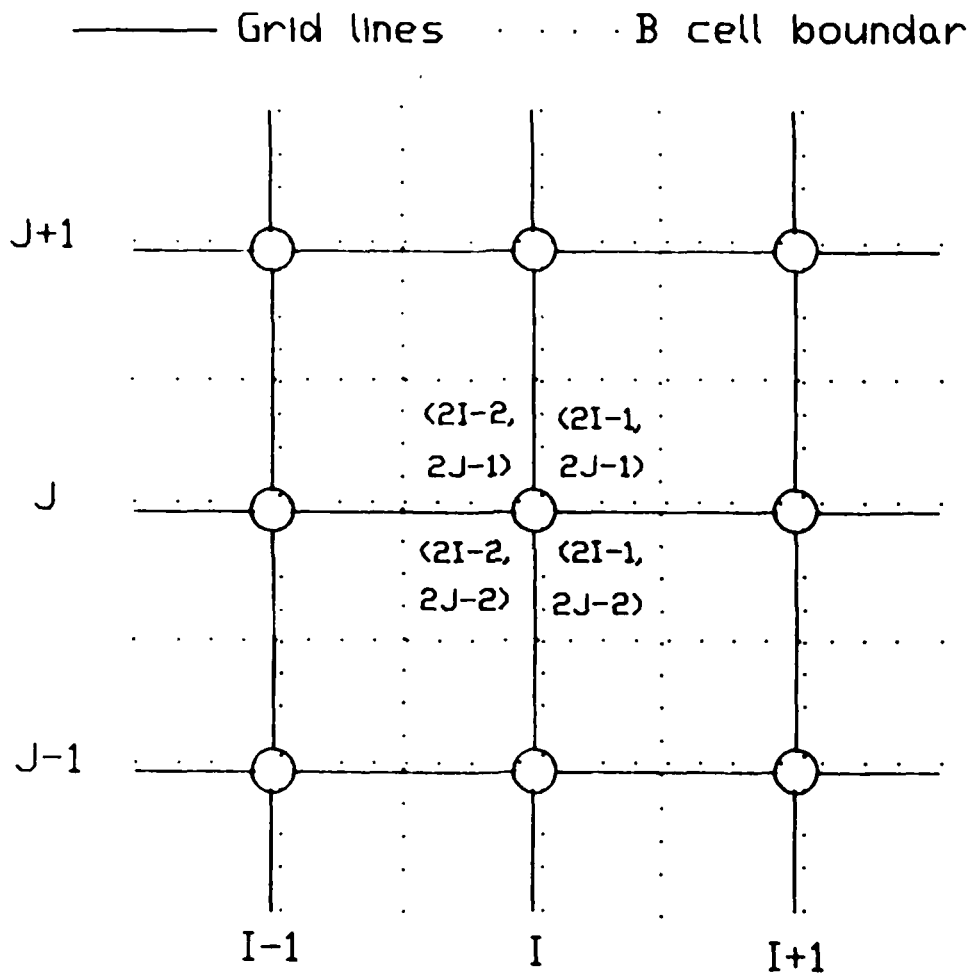



Fig. 3 B cells and their corresponding index numbers

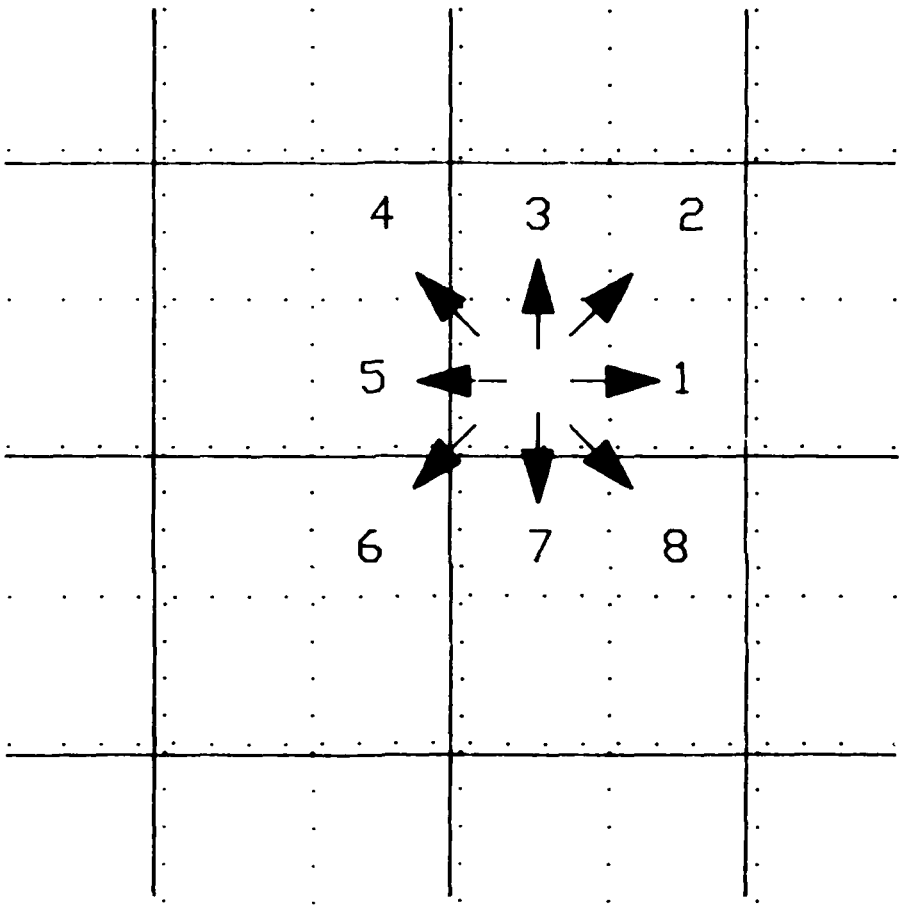



Fig. 4 The eight neighbouring B cells and their NCASE values

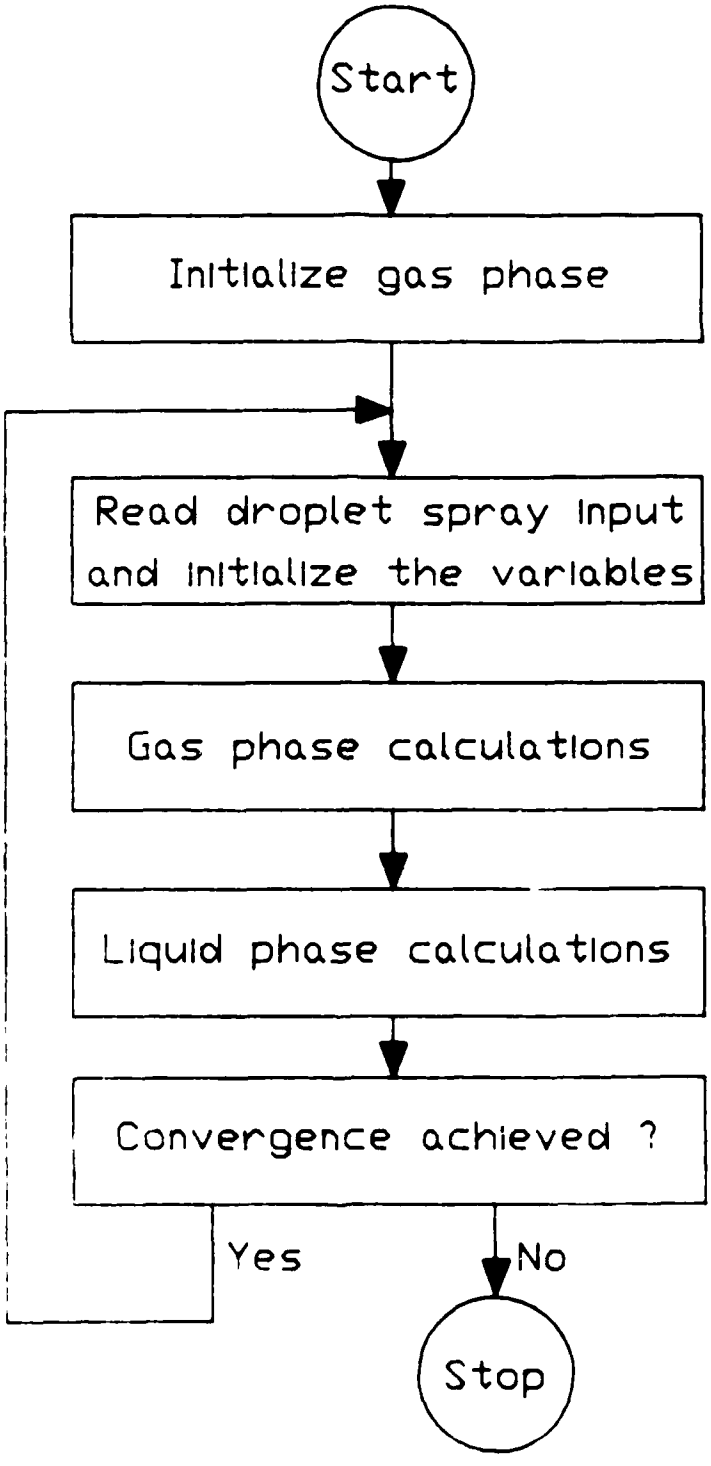



Fig. 5 Flow chart for the overall algorithm

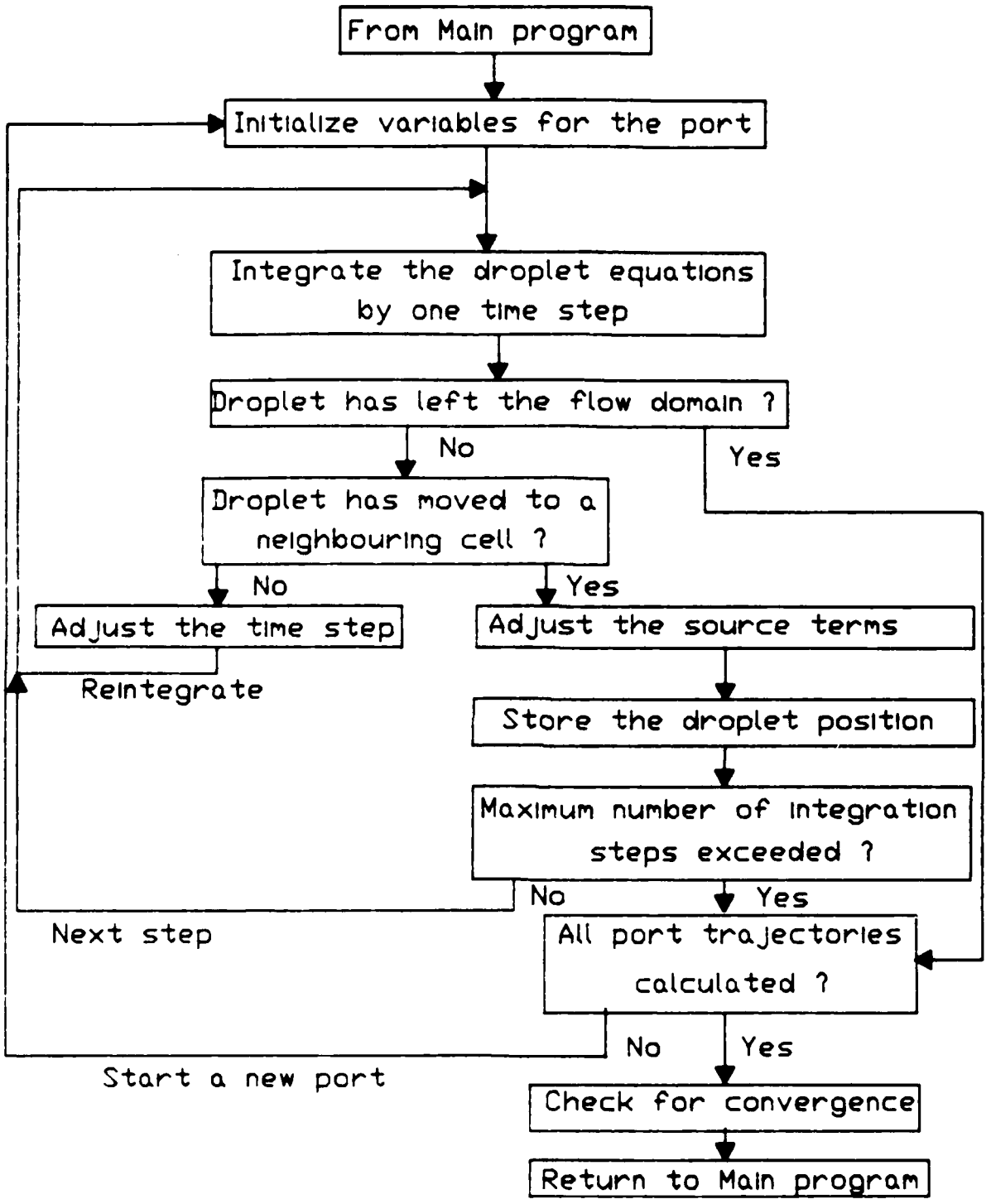



Fig. 6 Flow chart for subroutine DROP

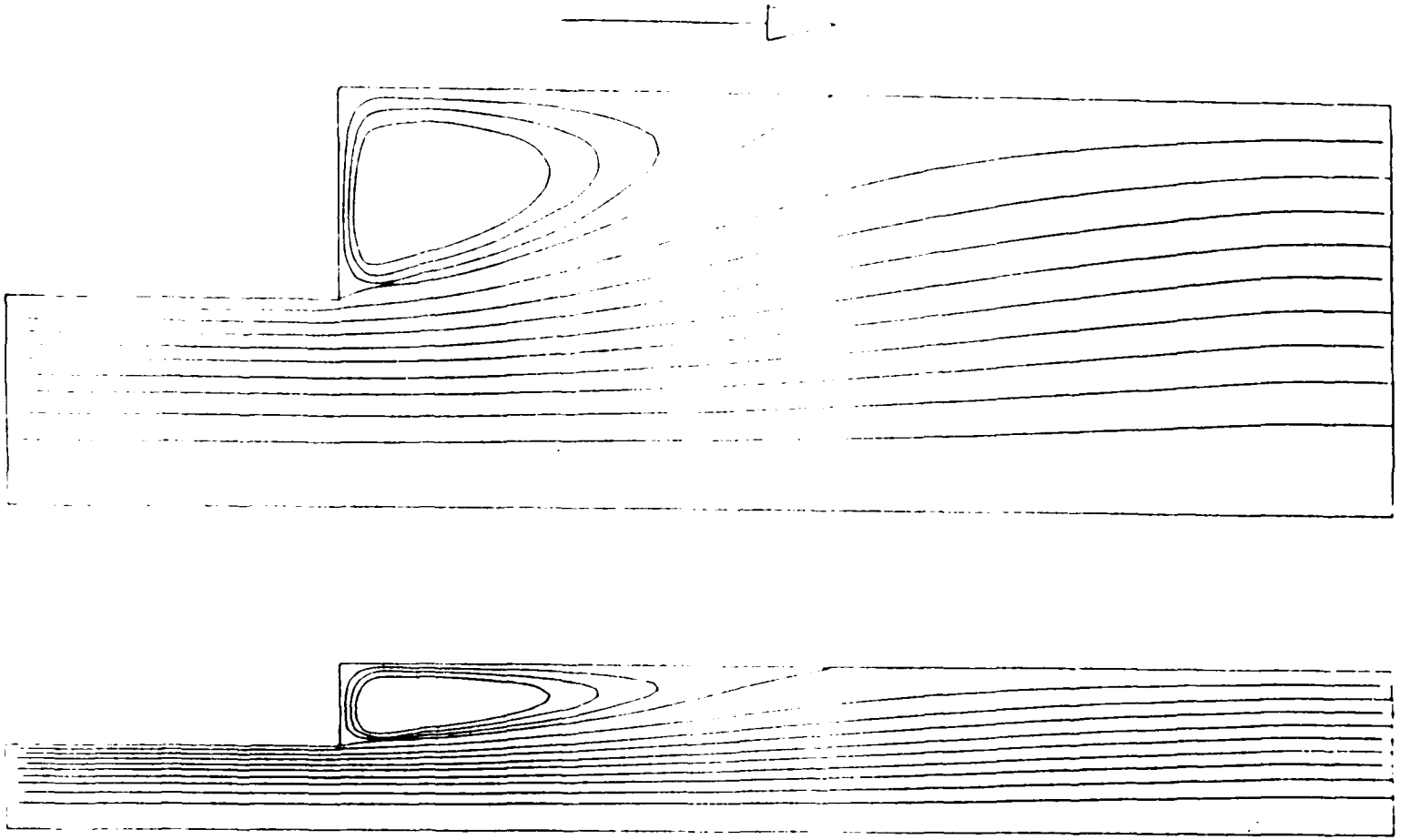


Figure 7 Streamline plots from program STRMSORT

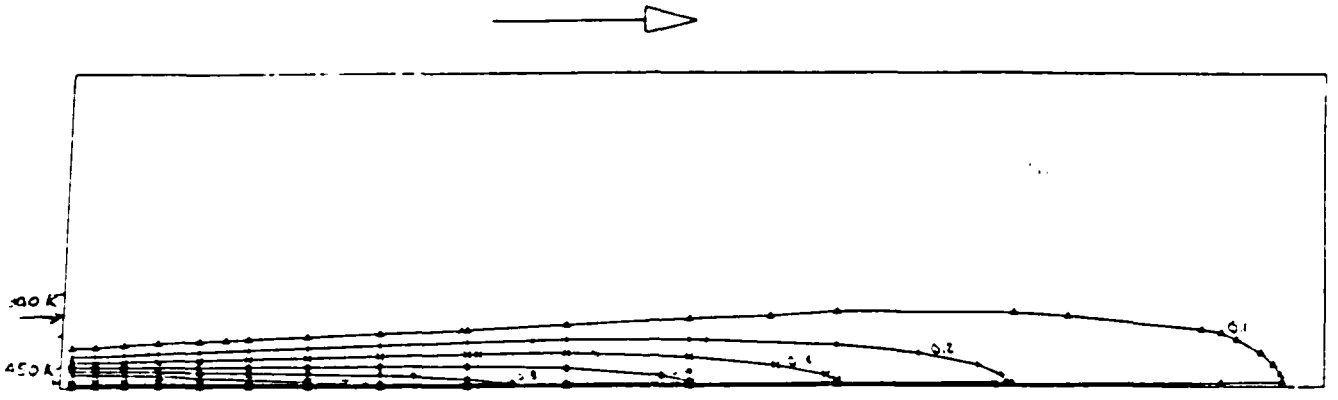



Figure 8 Mixture ratio profile from program PLOTGEN

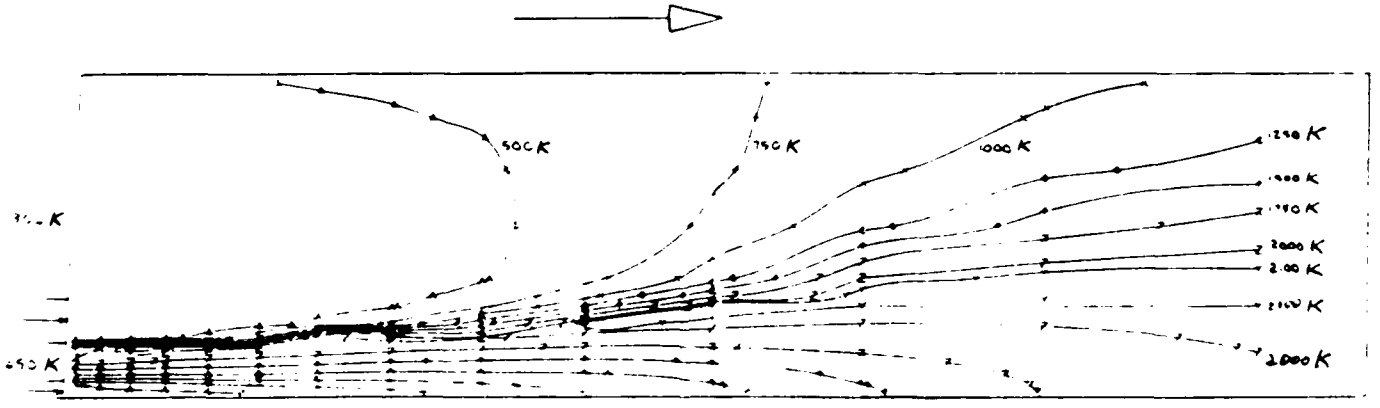



Figure 9 Temperature profile from program PLOTGEN

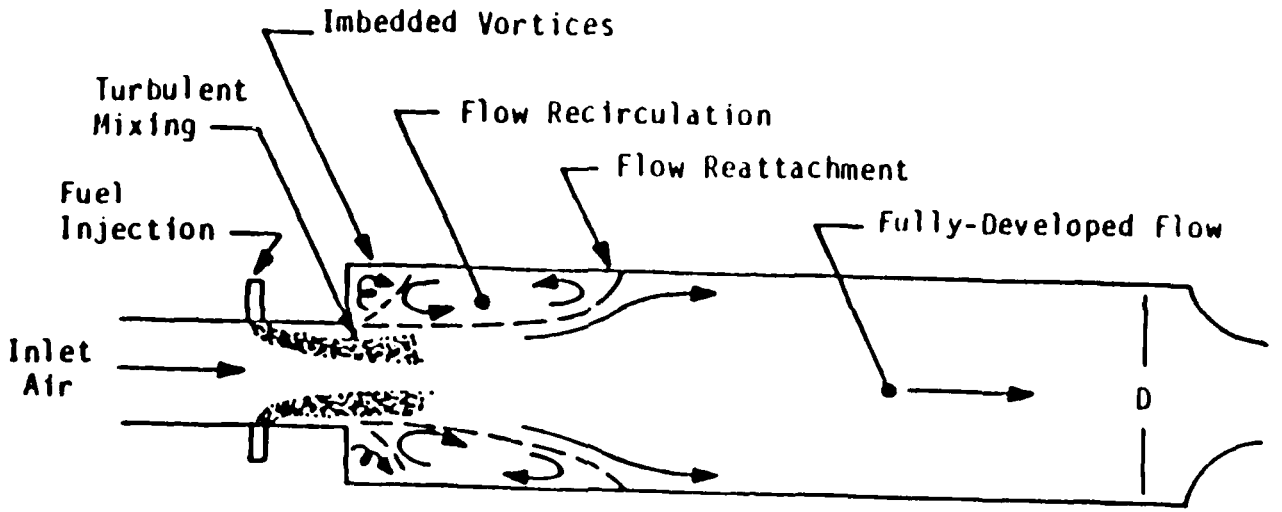



Figure 10 Ramjet Combustor Flowfield

# APPENDIX A

## PROGRAM LISTING OF MODIFIED STARPIC

```
00100      C       PROGRAM MAIN
00200      C
00300      C*************************************************************
00400      C
00500      C
00600      C      A COMPUTER PROGRAM FOR TURBULENT, SWIRLING,
00700      C      RECIRCULATING FLOW IN COMBUSTOR GEOMETRIES
00800      C      VERSION OF APRIL 1981 - NASA CR 3442
00900      C      S.L. RHODE AND DG LILLEY
01000      C      MECHANICAL AND AEROSPACE ENGINEERING, OKLAHOMA STATE
01100      C      UNIVERSITY, STILLWATER, OKLAHOMA 74078.
01200      C
01300      C*** BEGINNING OF INSERTED SECTION ** BEGINNING OF INSERTED SECTION ***
01400      C
01500      C       WITH LIQUID SPRAY MODEL INSERTED BY
01600      C       ALBERT Y. TONG  (FEBRUARY 1985)
01700      C       DEPARTMENT OF MECHANICAL ENGINEERING
01800      C       UNIVERSITY OF TEXAS AT ARLINGTON
01900      C       ARLINGTON, TEXAS 76019
02000      C
02100      C       INSERTED SECTIONS ARE INDICATED IN THE PROGRAM
02200      C
02300      C*** END OF INSERTED SECTION ** END OF INSERTED SECTION ***
02400      C
02500      C
02600      C*************************************************************
02700      CHARTER              PRELIMINARIES
02800      C
02900            DIMENSION HEDG(5), HELV(5),HEGW(5),HEGH(5),HEGT(5),
03000           *HEGP(5),HEDL(5),HEDY(5),HEGL(5),VAMP(7),SWIRL(7),
03100           $HEGIP(5),HEGIL(5),HEGD(5),HEGGV(5),HEGGW(5),
03200           $HELLP(5),HEGTM(5),HEGGGL(5),HEGGVS(5)
03300            DIMENSION YAXES(10),CYMBOL(10)
03400            COMMON
03500           $/GVEL/HEGGRG,NGMPG,GREG,GXPG(45),GXPWG(45),GRWG(45)
03600           $/VVEL/HEGGRV,NGMPV,GREV,GYMPV(24),GYPGV(24),GMGV(24)
03700           $/WVEL/HEGGRW,NGMPW,GREW
03800           $/PCOR/HEGGRM,NGMPP,GREP,GG(45,24),GV(45,24),IPREF,JPREF
03900           $/TEMP/HEGGRH,NGMPK,GREK
04000           $/TDIS/HEGGRE,NGMPD,GREE
04100           $/VAR/G(45,24),V(45,24),.(45 ,24),P(45,24),PP(45,24),
04200           $TE(45,24),ED(45,24),GTEN(45,24),YGTEN(45,24),GTVAL(24),
04300           $GGTAR(45,24),VGTAR(45,24),WGTAR(45,24),HGTAR(45,24),
04400           $TEGTAR(45,24),YGTEN0(45,24),VGTAR(45,24)
04500           ./ALL/IT,JT,NI,NJ,NIM1,NJM1,GREAT,JMAX(45),JMAX1(45)
04600           $/HEGM/X,GGRL,X(45),Y(24),DXEP(45),DXP(45),DYP(24), YEP(24),
04700           $    YGG(24),GEW(45),XG(45),YV(24),F(24),F1(24),
04800           $    FL(24),GFE(24),GFE(45),GFW(45),GFW(45),GC(24),GD(45),GL(45),
04900           DYG(24),YMID(24)
05000            COMMON
05100           $/FLOPA/GRFLIG,VISCOS,STRCNT,PRANDT,DEN(45,24),VIS(45,24)
05200           $/PACE TI/BIG,TEIG,EPIG,FLOWIN,ALAMDA,
05300           $GPHEL,HEAD,ALI,ALG,JGTEF,IGTEP,JGTEP,JGT 1,ICTP1,IJTP1
05400           $/TURB/VAR(45,24),CL,CMU,C1,C2,CAPPA,ELOG,ERFE,ERTE
05500           $/WALLF/YPLUS(45 ),XPLUSW(24),TAUW(45),TAUW(24)
05600           $/COEF/AP(45,24),AM(45,24),AG(45,24),AP(45,24),AW(45,24),SU(45,24),
05700           $SP(45,24)
05800           $/PLOTT/GTLE,GPLTL,XPTS,YSLPLT(10,45),XUSPLT(45),IPLOT
05900            LOGICAL INCALU,INCALV,INCALW,INCALP,IWRT,IPCALC,INCALC,ICALC,
06000           $INCALA,ICALM,ICALC,INPLOT,IWRITE,GDUM,IREAD,INLET,
06100           $INITAL,IPIPE
```

```
C
C*** BEGINNING OF INSERTED SECTION ** BEGINNING OF INSERTED SECTION ***
C
      COMMON /CRCPS/ MAXPUR, NPOST,
     $   CRPDEN(10), CRPDIA(10), CRMOUT(10), CRFRFC(10),
     $   XOINIT(10), YOINIT(10), TOINIT(10), UOINIT(10), VOINIT(10),
     $   XB(9B), YB(4B),
     $   UG(4B, 24), VG(4B, 24), UGOLD(4B, 24), VGOLD(4B, 24),
     $   UOO, GRAVX, GRAVY, RAD, RHOGAS, PI, UGAS, VGAS,
     $   XOOLD, YOOLD, TOOLD, UOOLD, VOOLD,
     $   XONEW, YONEW, TONEW, UONEW, VONEW,
     $   DT, DTINC, DTREF, RHOL,
     $   ISTEPC, INTCTR, IFLAG2, IFIT, MAXSTP, MAXCT, I.T-LG,
     $   IC, JC, IV, JV, IU, JU, IE, JE, IUOLD, JUOLD, ICONT,
     $   NCASE, NCASE, JDMAX(4B), NOI, NOJ
      COMMON/USF/RHOMV(50,50),RHOML(50,50)
C
C*** END OF INSERTED SECTION ** END OF INSERTED SECTION ***
C
      OPEN(UNIT=1,DEVICE='DSK:',FILE='FOR01.DAT',STATUS='OLD')
C
C*****     ALL PRELIMINARY USER INPUTS ARE LOCATED HERE.............
C
      DATA XA/.5,.4,.3,.2,.15,.1,.05,0./,
     $YA/0.,.5,1.0,1.25,1.5,1.75,2.0/
      DATA XAA/1*.1/
      DATA  YAA/3H 00,3H 10,3H 04,3H 06,3H 08,3H 10,
     $3H 12,3H 07,3H 08,3H 09/
      DATA SYMBOL /1H*,1H2,1H4,1H6,1H8,1H1,1H6,1H7,1H8,1H9/
C******DEFINE U,DEFLW FOR USE MESSAGES, CALL TRACE WHEN USING WATFIV
C      CALL TRACE(1,1,4000)
C------  SET INPLOT =.TRUE. ONLY FOR STREAMLINE LINE PRINTER PLOT
      INPLOT = .FALSE.
C------  SET INWRITE=.TRUE. ONLY FOR WRITING SOLUTION ON DATA FILES
      INWRITE=.FALSE.
C------  SET NONDIME=.TRUE. ONLY FOR PRINTING DIMENSIONLESS SOLUTION.
      NONDIME=.FALSE.
C------  SET INPAGE=.TRUE. ONLY FOR READING INITIAL GUESS OF SOLN.
C------                                          FROM DATA FILES.
      INPAGE=.FALSE.
C------  SET INITIAL =.TRUE. ONLY FOR PRINTING INITIAL GUESS OF SOLN.
      INITIAL=.FALSE.
C------  SET IFINE=.TRUE. ONLY FOR FINE GRID IN X DIRECTION
      IFINE=.FALSE.
      IF(.NOT. INPAG) GO TO 2
      READ(11,*) X
      READ(11,*) Y
    2 CONTINUE
      NOTL = 11
      NPLTL = 1
      NPRL = 1
      NITER = 1
      NPRINT = NITER+300
      NPRINT = NITER+1
      LFILE1 = 1
      LFILMAX=1
      NOPRES
      MAXITE=NITER+50
C------USE STATE VAR 304 FOR MAXIT SPEC. FOR PORTRAN SWAPL CASES
      RESIT = 1.0E11
      IT = 1
```

```
12300           JT =24
12400           GREAT=1.E30
12500           NS=PU=4
12600           NS=PV=3
12700           NS=PW=3
12800           NS=PP=5
12900           NS=PK=3
13000           NS=PD=3
13100           READ(1,10) MESU,MESV,MESW,MESP,MELT,MESK,MESD,MESM,MESL,
13200          1 MESF,MESSL,MESDU,MESDV,MESDW,MESDP,MESDK,MESDL,MESDF
13300       10 FORMAT(924)
13400      C------
13500      C---   CHAPTER   1    PARAMETERS AND PRELIMINARIES
13600      C
13700      C---   GRID
13800           ISTEP = 1
13900           JSTEP = 1
14000           IMSSSS= 2
14100           NJ=21
14200           NJM1=NJ-1
14300           ISTP1=ISTEP+1
14400           ISTM1=ISTEP-1
14500           JSTP1=JSTEP+1
14600           JSTM1=JSTEP-1
14700           RLARGE=1.0E25
14800           ALTJT=0.375
14900           IF(IFIME) 30 TO 120
15000      C---    SQUARE MESH GRID LINED IN X-DIRECTION
15100           NI = 33
15200           NIM1 = NI-1
15300           EPSX = 1.11
15400           IF(EPSX-1.) 15,12,13
15500        13    SUMX=0.5*EPSX**(NI-4)*(EPSX**(NI-3)-1.)/(EPSX-1.)**2
15600           GO TO 15
15700        14    CONTINUE
15800           SUMX=NI-1
15900        15    DX=ALTJT/SUMX
16000           X(1)=-.5*DX
16100           X(2)=-X(1)
16200           DO 100 I = 3,NIM1
16300           X(I)=X(I-1)+DX
16400       100    DX=EPSX*DX
16500           X(NI)=X(NIM1)+(X(NIM1)-X(NI-2))
16600           X(21)=X(20)+(X(20)-X(19))
16700           X(22)=X(21)+(X(20)-X(19))
16800           X(23)=X(22)+(X(20)-X(19))
16900           NI=23
17000           NIM1 = NI-1
17100           ALTJT=(X(1)+X(13))/2.
17200           ALI=0.0*(X(ISTEP)+X(ISTM1))
17300           ALI=ALTJT-ALI
17400      C-----    FINE MESH GRID LINED IN X-DIRECTION
17500           IF(.NOT. IFIME) GO TO 130
17600         120    NI=33
17700           NIM1=NI-1
17800           EPSX=1.122
17900           IF(EPSX-1.)17,16,17
18000        17    SUMX=1.5*EPSX**(NI-4)*(EPSX**(NI-3)-1.)/(EPSX-1.)+1.5
18100           GO TO 19
18200        18    CONTINUE
18300           SUMX=NIM1-1
```

```
      DX = ALTOT/COMX
      X(1)=-0.5*DX
      X(2)=-X(1)
      DO 170 I=3,NIM1
      X(I)=X(I-1)+DX
  170 DX=EPDX*DX
      X(NI)=X(NIM1)+(X(NIM1)-X(NI-2))
      DO 180 L=1,35
  180 X(L)=X(L-1)+(X(NI)-X(NIM1))
      NI = 36
      NIM1=NI-1
      ALTOT=(X(NIM1)+X(NI))/0.2
      AL1 = 0.5*(X(ICTEP)+X(ICTM1))
      AL2 = ALTOT-AL1
C-----   SPECIFY INITIAL CELL (# OF U-CELLS)OF COMPUCTOR
C-----   WALL FOR EACH I WAVE LINE
  190 CONTINUE
      DO 195 I=1,10
      UMAX(I)=UCTOP
      UMAXP1(I)=UMAX(I)+1
  195 CONTINUE
      DO 196 I=11,NI
      UMAX(I)=NUM1
      UMAXP1(I)=0
  196 CONTINUE
C-----   WHILE LINEAR IN Y  INCLUDING
      Y(1)=-4.[illegible]E-2
      Y(2)=1.[illegible]E-3
      Y(3)=0.[illegible]E-2
      Y(4)=1.[illegible]E-2
      Y(5)=1.[illegible]E-2
      Y(6)=2.1[illegible]E-2
      Y(7)=3.[illegible]E-2
      Y(8)=3.[illegible]E-2
      Y(9)=3.[illegible]E-2
      Y(10)=3.[illegible]E-2
      Y(11)=3.[illegible]E-2
      Y(12)=4.[illegible]E-2
      Y(13)=4.[illegible]E-2
      Y(14)=4.[illegible]E-2
      Y(15)=4.[illegible]E-2
      Y(16)=4.[illegible]E-2
      Y(17)=4.[illegible]E-2
      Y(18)=4.[illegible]E-2
      Y(19)=4.[illegible]E-2
      Y(20)=4.[illegible]E-2
      Y(21)=4.[illegible]E-2
      DO ALLE. .*(Y(ICTP1)+Y(ICTM1))
C-----   [illegible]
      [illegible]E.[illegible].
      [illegible]E.[illegible].
      [illegible]E.[illegible].
      [illegible]E.[illegible].
      [illegible]E.[illegible].
      [illegible]E.[illegible].
      [illegible]E.[illegible].
      [illegible]E.[illegible].
      [illegible]E.[illegible].
C-----   [illegible]
C-----   [illegible]
      [illegible]
      [illegible]
```

```
24500            C1=1.44
24600            C2=1.96
24700            CAPPA=1.4167
24800            ELOGE=2.718
24900            PRLOG=CAPPA*CAPPA/(C2-C1)/(CAPPA+1.)
25000            PRTE=1.0
25100  C------     COMPARE VALUES
25200            C1=30.0
25300            CLAMBDA=(PI*ALC/PLAM)**2
25400            TCHIME=0.0
25500            TSINET=SIN(PI/180.*ETA)
25600            ALAMDA=0.00
25700            SCIENT=(PI*1.0/(ALAMDA*PLAM))
25800            WICOND=1.E-5
25900  C------     RECOMPUTE CALCULATION
26000            IPREF=1
26100            JPREF=1
26200  C------     READ IN THE DATA
26300            IM=NIM1
26400            JM=NJM1
26500            COMMENT=0.0
26600  C
26700  C*****          ENTRY                    ************
26800  C
26900            CALL INIT
27000  C-----     WRITE OUTPUT HEADING
27100            DO 1 I=1,NI
27200            XNI(I)=X(I)/(1.+CLAMBDA)
27300          1 XNJ(I)=Y(I)/(1.+CLAMBDA)
27400            DO 2 J=1,NJ
27500            YNI(J)=Y(J)/(1.+CLAMBDA)
27600          2 YNJ(J)=Y(J)/(1.+CLAMBDA)
27700  C-----     INITIALIZE VARIABLE FIELDS
27800            PSI=1.0
27900            DPSI=0.0
28000            APSI=0.0
28100            XPSI=0.0
28200            YPSI=0.0
28300            APSIM=0.0
28400  C
28500  C----- INSERT GRID VELOCITY ROUTINE
28600  C
28700  C----- SET INITIAL VELOCITY FIELD
28800            WINIT=1.0+1.0/(1.0+EXP(-(J-1)))+...
28900            DO 3 J=1,NJ
29000          3 W(1,J)=WINIT*(1.0+0.0/(1.0+EXP(-(J-1))))
29100  C----- WRITE OUTPUT FILE
29200  C----- WRITE INITIAL VELOCITY FIELD
29300            IF(...
29400  C-----     WRITE INITIAL FILE
29500            WINIT=WINIT*(1.0/((PI)*2.0*PI  /1.  ))
29600            DO 37 J=1,NJ
29700          37 W(1,J)=WINIT
29800            CONTINUE
29900  C----- INITIALIZE ...
30000            DO 4 J=1,NJ
30100            U(1,J)=0.0
30200            V(1,J)=0.0
30300            ST(1,J)=0.0
30400            PSI(1,J)=PSI*(1.0/(1.0+EXP(-(J-1.0))))*(1.0/(1.0+EXP(-(J-1.0))))
30500            APSI(1,J)=APSI+(1.0/(1.0+EXP(-(J-1.0))))*(1.0/(1.0+EXP(-(J-1.0))))
```

```
```

```
      WRITE(1,*)XUNO
  237 CONTINUE
      IF(.NOT.IREAD) GO TO 238
      READ(12,*) U
      READ(12,*) V
      READ(12,*) W
      READ(12,*) P
      READ(12,*) TE
      READ(12,*) ED
      READ(12,*) VIS
      READ(12,*) CTEN
  238 CONTINUE
      IF(.NOT. INITAL) GO TO 239
      IF(INCALL) CALL PRINT(1,IL,IU,NU,IT,UT,AU,VU,WU,PU,TEU,EDU,
      IF(ANCALL) CALL PRINT(1,IL,IU,NU,IT,UT,AU,VU,WU,PU,TEU,EDU,
      IF(INCALW) CALL PRINT(1,IL,IU,NU,IT,UT,AU,VU,WU,PU,TEU,EDU
      IF(INCALN) CALL PRINT(1,IL,IU,NU,IT,UT,AU,VU,WU,PU,TEU,EDU
      IF(ANCALL) CALL PRINT(1,IL,IU,NU,IT,UT,AU,VU,WU,PU,TEU,EDU
  239 CONTINUE
C
C*** BEGINNING OF INSERTED SECTION ** BEGINNING OF INSERTED SECTION ***
C
C         Initialize EM, ML, and EMOM..
          DO 1000 I = 1, IU
            DO 1000 J = 1, JU
              EM(I, J) = 0.
              EML(I, J) = 0.0
 1000       CONTINUE
C
C         Input the liquid data.
          NDATA = 0
          IF (NDATA .EQ. 0) THEN
C           To only the gas phase calculations.
            GO TO 1000
          ELSE IF (NDATA .EQ. 1) THEN
C           Input the data from the terminal.
            WRITE (6, *) ' INPUT THE NUMBER OF POINTS '
            READ (6, *) NPOIN
            DO 1100 NPOINT = 1, NPOIN
              WRITE(6, *) ' POINT NUMBER ', NPOINT
              WRITE(6, *) ' INPUT THE LIQUID DENSITY '
              READ (6, *) RHOL
              WRITE(6, *) ' INPUT THE VISCOSITY '
              READ (6, *) VISL(NPOINT)
              WRITE (6, *) ' INPUT THE INITIAL AXIAL LIQUID VELOCITY '
              READ (6, *) ALIQ(NPOINT)
              WRITE (6, *) ' INPUT THE INITIAL RADIAL LIQUID VELOCITY '
              READ (6, *) RLIQ(NPOINT)
              WRITE (6, *) ' INPUT THE INITIAL TANGENTIAL VELOCITY '
              READ (6, *) TLIQ(NPOINT)
              WRITE (6, *) ' INPUT THE INITIAL DROPLET DIAMETER '
              READ (6, *) DIAM(NPOINT)
              WRITE (6, *) ' INPUT THE INITIAL DROPLET TEMPERATURE '
              READ (6, *) TEMP(NPOINT)
              WRITE (6, *) ' INPUT THE INITIAL MASS FLOW RATE '
              READ (6, *) FLOW(NPOINT)
              WRITE (6, *) ' INPUT THE INITIAL NUMBER OF DROPLETS '
              READ (6, *) NDROP(NPOINT)
 1100       CONTINUE
C
            ELSE IF (NDATA .EQ. 2) THEN
              Input data from a file.
              READ (12, *) NPOIN
```

```
*2800                DO 1200 NPORT = 1, MAXPOR
*2900                  READ (21, *) CHRGEN(NPORT), CHRGIA(NPORT), XOINIT(NPORT),
*3000         $         YOINIT(NPORT), TOINIT(NPORT),
*3100         $         UOINIT(NPORT), VOINIT(NPORT), CHROUT(NPORT)
*3200    1200         CONTINUE
*3300    C
*3400              ELSE IF (NDATA .EQ. 0) THEN
*3500    C           Input data in the program.
*3600                MAXPOR = 1
*3700                CHRGEN(1) = 700.0
*3800                CHRGIA(1) = 0.03002
*3900                XOINIT(1) = 0.0
*4000                YOINIT(1) = 0.0
*4100                TOINIT(1) = 0.0
*4200                UOINIT(1) = 10.0
*4300                VOINIT(1) = 0.0
*4400                CHROUT(1) = 0.0
*4500              ELSE
*4600    C
*4700    C
*4800    C           Initialize XM and YM.
*4900                XM1 = XI
*5000                XM0 = XO
*5100                DO 1300 I = 2, MXM
*5200                  XM(I - 1) = XM(I)
*5300                  AM(I - 1) = AM(I + 1)
*5400                  DXMAX(I) = DXMAX(I)
*5500    1300        CONTINUE
*5600                DO 1400 J = 2, MYM
*5700                  YM(J - 1) = YM(J)
*5800                  BM(J - 1) = BM(J + 1)
*5900    1400        CONTINUE
*6000    C
*6100    C           Initialize flags and counters.
*6200                MARCH = 0
*6300                MARCH = 1
*6400                ICOUNT = 0
*6500                IFLAG = 0
*6600                ITEST = 0
*6700                ATEST = 0.0
*6800    C
*6900    C           Store input data from a file.
*7000                WRITE (6, *) MAXPOR
*7100                DO 1500 NPORT = 1, MAXPOR
*7200                  WRITE (6, *) CHRGEN(NPORT), CHRGIA(NPORT),
*7300         $          XOINIT(NPORT), YOINIT(NPORT), TOINIT(NPORT),
*7400         $            UOINIT(NPORT), VOINIT(NPORT), CHROUT(NPORT)
*7500         $              FORMAT
*7600    1500        CONTINUE
*7700    C
*7800    C           Initialize
*7900                DO 1600 I = 1, MXM
*8000                  DO 1600 J = 1, MYM
*8100                    U(I, J) = UO(I, J)
*8200                    V(I, J) = VO(I, J)
*8300    1600        CONTINUE
*8400    C
*8500    C           Initialize time step and scale factors.
*8600                T = 0.0
*8700                DTOLD = 0.01
*8800                DTMIN = 0.01
```

```
C
C       Assign gravity and grav term values.
C
        GRAV = 0.0
        GRAVX = 0.0
        GRAVY = 0.0
        PI = 3.14159265
        RADIAN = 180./PI
C
C       Calculate the grid parameters
C
        DO 170 COUNT = 1, MAXJ
          XJ = -XJ1-(XJ-1.) / 2.
          YJ = YJ1+(COUNT-1)
          DO 160 I = 1, IMAX
            XI = XI1+(I-1) * DELXI * COS(YJ) / 2.
            IF (I .EQ. 1 .AND. COUNT .EQ. 1) GO TO 150
            IF (I .EQ. IMAX .AND. COUNT .EQ. 1) GO TO 150
            IF (I .EQ. 1 .AND. COUNT .EQ. MAXJ) GO TO 150
            IF (I .EQ. IMAX .AND. COUNT .EQ. MAXJ) GO TO 150
            GO TO 160
  150       CONTINUE
  160     CONTINUE
  170   CONTINUE
C
C       Returns here if total convergence is not achieved
C       to start a new iteration.
C
  180   CONTINUE
C
C*** PRINT FINAL CONVERGENCE RESULTS ***
C
        WRITE(6,
        WRITE(6,
        WRITE(6,
        WRITE(6,
        IF(I .EQ. IMAX) WRITE(6,
        WRITE(6,
        WRITE(6,
        IF(I .EQ. IMAX) WRITE(6,
        WRITE(6,
        WRITE(6,
        WRITE(6,
        WRITE(6,
        WRITE(6,
        WRITE(6,
        WRITE(6,
        IF(I .EQ. IMAX) WRITE(6,
        WRITE(6,
        WRITE(6,
        WRITE(6,
        WRITE(6,
        WRITE(6,
        WRITE(6,
        WRITE(6,
        
```

```
      IF(PRESSRE .LT. .1E+0) GREEC.5E
  430 CONTINUE
C-----   UPDATE MAIN DEPENDENT VARIABLES
      IF(INCALL) CALL CALCU
      IF(INCALV) CALL CALCV
      IF(INCALP) CALL CALCP
      IF(INCALW) CALL CALCW
      IF(INCALK) CALL CALCTE
      IF(INCALD) CALL CALCED
C-----   UPDATE FLUID PROPERTIES
      IF(INPROP) CALL PROPS
C------  INTERMEDIATE OUTPUT
      PRSUM = PRSUM/FLOAT(
      PRSUC = PRSUC/AMAX1(
      PRSUV = PRSUV/AMAX1(
      PRSUW = PRSUW/AMAX1(
      PRSUK = PRSUK/AMAX1(
      PRSUD = PRSUD/(FLOAT(
      IF(LITER.EQ.1.OR.MOD(LITER,
      ITER=ITER+1
      WRITE(*,611) LITER,PRSUM,PRSUC,PRSUV,PRSUW,PRSUK,
     1PRSUD,(IM,UM(I),W(IM,JM(I)),P(IM,JM(I)),
     2(IM,JM(I)),I=1,
      IF(LITER.GE.
      IF(INCALL) CALL PRINT(1,1,IL,NU,IT,UT,RU,V,,RESU)
      IF(INCALV) CALL PRINT(1,1,IL,NV,IT,UT,RV,V,,RESV)
      IF(INCALW) CALL PRINT(1,1,IL,NW,IT,UT,RW,V,W,RESW)
      IF(INCALP) CALL PRINT(1,1,IL,NP,IT,UT,RP,V,,RESP)
      IF(INCALK) CALL PRINT(1,1,IL,NK,IT,UT,RK,V,,RESK)
      IF(INCALD) CALL PRINT(1,1,IL,ND,IT,UT,RD,V,,RESD)
      WRITE(
      WRITE(
  610 FORMAT(
C-----
      IF(
      IF(
      IF(
```

```
      IF(INCALW) CALL PRINT(1,1,NI,NJ,IT,JT,X,Y,W,HEDW)
      IF(INCALP) CALL PRINT(1,1,NI,NJ,IT,JT,X,Y,P,HEDP)
      IF(INCALP) CALL PRINT(1,1,NI,NJ,IT,JT,X,Y,PF,HEDP)
      IF(INCALK) CALL PRINT(1,1,NI,NJ,IT,JT,X,Y,TE,HEDK)
      IF(INCALD) CALL PRINT(1,1,NI,NJ,IT,JT,X,Y,E,,HEDD)
      IF(INCALS) CALL PRINT(1,1,NI,NJ,IT,JT,XL,Y,STEN,HEDSF)
      IF(INCALD) CALL PRINT(1,1,NI,NSTLN,IT,JT,XL,STVAL,YSTLN,HEDSL)
      IF(.NOT. NONDIM) GO TO 750
      IF(INCALD) CALL PRINT(1,1,NI,NJ,IT,JT,XUND,YND,USTAR,HEDDU)
      IF(INCALV) CALL PRINT(1,1,NI,NJ,IT,JT,XND,YND,VSTAR,HEDDV)
      IF(INCALW) CALL PRINT(1,1,NI,NJ,IT,JT,XND,YND,WSTAR,HEDDW)
      IF(INCALS) CALL PRINT(1,1,NI,NSTLN,IT,JT,XUND,STVAL,YSTLND,HEDDSL)
      IF(INCALP) CALL PRINT(1,1,NI,NJ,IT,JT,XND,YND,PSTAR,HEDDP)
      IF(INCALK) CALL PRINT(1,1,NI,NJ,IT,JT,XND,YND,TESTAR,HEDDK)
      IF(INCALK) CALL PRINT(5,2,NI,NJ,IT,JT,X,Y,SF,HEDL)
      IF(INCALK) CALL PRINT(1,1,NI,NJ,IT,JT,XND,YND,WISTAR,HEDDVS)
  750 CONTINUE
      IF(.NOT. IWRITE) GO TO 760
      WRITE(11,*) U
      WRITE(11,*) V
      WRITE(11,*) W
      WRITE(11,*) P
      WRITE(11,*) TE
      WRITE(11,*) ED
      WRITE(11,*) VIS
      WRITE(11,*) DTE
      WRITE(11,*) YSTLN
  760 CONTINUE
C---- CALCULATION OF SMEAR STRESS COEFFICIENT ALONG LARGE DOT WALL
      WRITE(*,*)
      DO 801 IEL=1,IMI
      SMEAR=(TAUW(I))/(1.5*RHO*UIN*UIN)
      WRITE(9,*) I,YND(I),SMEAR
  801 CONTINUE
      WRITE(*,811)
C---- PLOT IMPINGING STREAMLINES
      CALL PLOTS
      IF(INCALP .AND. INCALS) CALL PLOT(XSPLT,IT,YPTS,XA,IP,YSLPLT,
     1XMAG,XPLTS,YSTLN,YAXES,SYMBOL,LARGE)
      CALL PLOT
      IF(INCALT .AND. INCALS) CALL PLOT(XSPLT,IT,YPTS,XA,IP,YSLPLT,
     1XMAG,XPLTS,YSTLN,YAXES,SYMBOL,LARGE)
C---- RESET INITIAL CONDITIONS FOR ANOTHER CASE
      IF(LPS .GE. LPSMAX) GO TO 904
      LPS=LPS+1
      IT=IBL
      JT=ITE(IT)+1
      IF(JT .GE. ITE(IT)+1
      IF(LPS .GT. 0) READ(5,*) ITE(2)
      IF(JT .GE. JE ) GO TO 904
      WRITE(*,*) JT,ITE(JT),(LPS)/(1.*SMAX-(LPS))*DIN
      GO TO 903
  904 WRITE(*,*) 'ALL CASES COMPLETED'
      GO TO 905
  903 WRITE(*,*) 'NEXT CASE'
      READ(5,*) IBL,IEL,IMI,JMI,IT,JT,IP,IPS,IPE,IPI,IPO,I
      WRITE(*,*) IBL,IEL,IMI,JMI,IT,JT,IP,IPS,IPE,IPI,IPO,I
      READ(5,*) (ITE(I),I=1,IMI)
      WRITE(*,*) (ITE(I),I=1,IMI)
      READ(5,*) DIN,DTE,DTEF,DTEFF,DTEFFF,DTEFFFF,DTEFFFFF,DTEFFFFFF
      WRITE(*,*) DIN,DTE,DTEF,DTEFF,DTEFFF,DTEFFFF,DTEFFFFF,DTEFFFFFF
      READ(5,*) (YND(I),I=1,JMI)
      WRITE(*,*) (YND(I),I=1,JMI)
      READ(5,*) (XND(I),I=1,IMI)
      WRITE(*,*) (XND(I),I=1,IMI)
      READ(5,*) (TAUW(I),I=1,IMI)
      WRITE(*,*) (TAUW(I),I=1,IMI)
      READ(5,*) (UND(I),I=1,IMI)
      WRITE(*,*) (UND(I),I=1,IMI)
      READ(5,*) (VND(I),I=1,IMI)
      WRITE(*,*) (VND(I),I=1,IMI)
      READ(5,*) (PND(I),I=1,IMI)
      WRITE(*,*) (PND(I),I=1,IMI)
      READ(5,*) (TEND(I),I=1,IMI)
      WRITE(*,*) (TEND(I),I=1,IMI)
      READ(5,*) (EDND(I),I=1,IMI)
      WRITE(*,*) (EDND(I),I=1,IMI)
      READ(5,*) (VISND(I),I=1,IMI)
      WRITE(*,*) (VISND(I),I=1,IMI)
      READ(5,*) (DTEND(I),I=1,IMI)
      WRITE(*,*) (DTEND(I),I=1,IMI)
      READ(5,*) (YSTLND(I),I=1,IMI)
      WRITE(*,*) (YSTLND(I),I=1,IMI)
      GO TO 902
  905 CONTINUE
      STOP
      END
```

```
      ANGMOM = 0.0
      xMOMIN = 0.0
C-----   READ INITIAL GUESS OF NEXT SPIRL PROBLEM FROM
C-----   PREVIOUS SOLN. OF SIMILAR PROBLEM
      IF(.NOT. IREAD) GO TO 445
      READ(12,*) U
      READ(12,*) V
      READ(12,*) W
      READ(12,*) P
      READ(12,*) TE
      READ(12,*) ED
      READ(12,*) STEN
  445 CONTINUE
      DO 490 J=2,JSTEP
      AREA=0.5*(DEN(1,J)+DEN(2,J))*RCV(J)*SNS(J)
      XMOMIN=XMOMIN+AREA*U(2,J)*U(2,J)
      xMOMIN=xMOMIN+AREA*U(2,J)*W(1,J)
      ANGMOM=ANGMOM+AREA*U(2,J)*W(1,J)*R(J)
      AREAT=AREAT+AREA
  490 FLOWIN=FLOWIN+AREA*U(2,J)
      UMEAN=FLOWIN/AREAT
      SWRLNO=ANGMOM/(XMOMIN*RDMAX)
      IF(W(1,JSTEP) .EQ. 0.0) xMOMIN = 1.0
      WRITE(6,510) IMON,UMON
      GO TO 500
  409 CONTINUE
C
C*** BEGINNING OF INSERTED SECTION ** BEGINNING OF INSERTED SECTION ***
C
        IF (NDATA .EQ. 0) THEN
C         Liquid phase solution not required.
          STOP
        ENDIF
C       Reassign gas velocities.
        DO 2510 I = 1, MI
          DO 2505 J = 1, MJ
            UGOLD(I, J) = UG(I, J)
            VGOLD(I, J) = VG(I, J)
            U(I, J) = UG(I, J)
            V(I, J) = VG(I, J)
2505      CONTINUE
2510    CONTINUE
C
C       Reset RMOMU and RMOMV.
        DO 2520 I = 1, MI
          DO 2515 J = 1, MJ
            RMOMU(I, J) = 0.0
            RMOMV(I, J) = 0.0
2515      CONTINUE
2520    CONTINUE
C       Get the liquid phase solution.
        CALL LIQUID
        IF (IFLAG2 .NE. 1) THEN
C         The system has not converged globally so iterate again.
          IF (ITERPC .GT. MAXOT) THEN
            WRITE(6, *) ' Global convergence not achieved ',
     $           'after 10 iterations for both phases.'
            STOP
          ENDIF
          NOTLN = 11
          NPTLN = 0
          MAXOT = 10
          NITER = 0
```

```
73300              JPRINT = NITER + 300
73400              IPRINT = NITER + 1
73500              LFS = 1
73600              LFSMAX = 1
73700              NSHR = 0
73800              MAXIT = NITER + 250
73900              GOTO 2000
74000            ELSE
74100     C        System global convergence achieved.
74200            WRITE(6,312)
74300            WRITE(6,410) LFS,NSHR,SWIRL(LFS),VANE(LFS),SWRLNO,CMEAN,FLOWIN
74400            IF(INCALU) CALL PRINT(1,1,NI,NJ,IT,JT,XL,Y,HEDU)
74500            IF(INCALV) CALL PRINT(1,1,NI,NJ,IT,JT,X,YW,V,HEDV)
74600            IF(INCALW) CALL PRINT(1,1,NI,NJ,IT,JT,X,Y,W,HEDW)
74700            IF(INCALP) CALL PRINT(1,1,NI,NJ,IT,JT,X,Y,P,HEDP)
74800            IF(INCALP) CALL PRINT(1,1,NI,NJ,IT,JT,X,Y,PP,HEDP)
74900            IF(INCALK) CALL PRINT(1,1,NI,NJ,IT,JT,X,Y,TE,HEDK)
75000            IF(INCALE) CALL PRINT(1,1,NI,NJ,IT,JT,X,Y,ED,HEDD)
75100            IF(INCALS) CALL PRINT(1,1,NI,NJ,IT,JT,XL,Y,STEN,HEDSF)
75200            IF(INCALS) CALL PRINT(1,1,NI,NSTLN,IT,JT,AU,STVAL,YSTLN,HEDSL)
75300            IF(.NOT. MONDIM) GO TO 2750
75400            IF(INCALU) CALL PRINT(1,1,NI,NJ,IT,JT,XLNO,YNO,USTAR,HEDDU)
75500            IF(INCALV) CALL PRINT(1,1,NI,NJ,IT,JT,XNO,YYNO,VSTAR,HEDDV)
75600            IF(INCALW) CALL PRINT(1,1,NI,NJ,IT,JT,XNO,YNO,WSTAR,HEDDW)
75700            IF(INCALS) CALL PRINT(1,1,NI,NSTLN,IT,JT,XLNO,STVAL,YSTLNO,HEDDSL)
75800            IF(INCALP) CALL PRINT(1,1,NI,NJ,IT,JT,XNO,YNO,PSTAR,HEDDP)
75900            IF(INCALK) CALL PRINT(1,1,NI,NJ,IT,JT,XNO,YNO,TESTAR,HEDDK)
76000            IF(.NOT.K) CALL PRINT(5,2,NI,NJ,IT,JT,X,Y,DP,HEDL)
76100            IF(INCALK) CALL PRINT(1,1,NI,NJ,IT,JT,XNO,YNO,WISTAR,HEDDWO)
76200     2750     CONTINUE
76300              STOP
76400            ENDIF
76500     C
76600     C*** END OF INSERTED SECTION ** END OF INSERTED SECTION ***
76700     C
76800              STOP
76900     C---     FORMAT STATEMENTS
77000       211 FORMAT(1H1,T37,'AXISYMMETRIC ISOTHERMAL GT COMBUSTION CHAMBER
77100          $FLOW FIELD SIMULATION',//T35,'USING THE STARSTEP APPROXIMATION
77200          $FOR THE SWIRLING EXPANSION WALL',//T53,'AND THE K-E TURBULENCE
77300          $MODEL')
77400       225 FORMAT(////,T40,'EXPANSION ANGLE (DEG) =',T77,1PE13.5)
77500       230 FORMAT(//,T40,'NUMBER OF STAIR STEPS = ',T71,I1)
77600       235 FORMAT(//,T40,'INLET RADIUS(M) =',T77,1PE13.3)
77700       240 FORMAT(//,T40,'COMBUSTOR RADIUS(M)=',T77,1PE13.5)
77800       245 FORMAT(//,T40,'COMBUSTOR LENGTH(M)=',T77,1PE13.3)
77900       250 FORMAT(//,T40,'INLET REYNOLDS NO.(USING DIAM.) =',T77,1PE13.3)
78000       255 FORMAT(//,T40,'LAMINAR VISCOSITY(KG/M/S) =',T77,1PE13.3)
78100       260 FORMAT(//,T40,'DENSITY(KG/CU. M) =',T77,1PE13.3,////)
78200       310 FORMAT(13HOITER     I---,  8X,23HMAX GLOBAL RESIDUAL SOURCE SUMS,9X,
78300          $11H---I    I---,37H FIELD VALUES AT MONITORING LOCATION(,I2,1H,
78400          $I2,6H) ---I/14H  NO       UMOM,7X,'VMOM',7X,'WMOM',7X,'MASS',7X,
78500          $'TKIN',7X,4HDISP,9X,1HU,9X,1HV,10X,1HW,10X,1HP,10X,1HD/)
78600       311 FORMAT (2X,I4,11E11.4)
78700       312 FORMAT (1HO,59(1H= ))
78800       402 FORMAT (///9X,1HI,8X,3HX/D,8X,10HU.D.OOEF. )
78900       403 FORMAT (/5X,I5,2(1PE11.3))
79000       410 FORMAT (//,23H SWIRL CASE WITH LFS = ,I3/
79100          $       23H                 AND NSHR = ,I3//
79200          $63H CORRESPONDS IF NSHR = 1 TO SWIRL GENERATOR WITH SWIRL NUMBER =
79300          $,F10.3///37H OR IF NSHR = 0 TO SWIRL VANE ANGLE =,F10.3//
```

```
79400          $1X,'COMPUTED INLET SWIRL NUMBER=',F10.4//
79500          $1X,'COMPUTED INLET MEAN AXIAL VELOCITY =',F10.4//
79600          $1X,'COMPUTED INLET MASS FLOW RATE =',F10.5////)
79700      950 FORMAT(10X,6F10.5,/,10X,6F10.5,/,10X,4F10.5)
79800      960 FORMAT(15X,'  THE SOLN. IS NOT CONVERGING')
79900      C       DEBUG UNIT(6),INIT(SUMX,EPSX,RLARGE,RSMALL,XMONIN,WMONIN,FLOWIN,
80000      C      $UMEAN,DENSIT,VISCOS,UIN), SUBCHK(ALL)
80100           END
80200      C
80300      C-----------------------------------------------------------------------
80400      C
80500           SUBROUTINE INIT
80600      CA*****************************************************************
80700      C
80800      CHAPTER              PRELIMINARIES
80900      C
81000           COMMON
81100          $/UVEL/RESORU,NSWPU,URFU,DXEPU(48),DXPWU(48),SEWU(48)
81200          $/VVEL/RESORV,NSWPV,URFV,DYNPV(24),DYPSV(24),CNSV(24)
81300          $/WVEL/RESORW,NSWPW,URFW
81400          $/PCOR/RESORM,NSWPP,URFP,DU(48,24),DV(48,24),IPREF,JPREF
81500          $/VAR/U(48,24),V(48,24),W(48,24),P(48,24),PP(48,24),
81600          $TE(48,24),ED(48,24),STEN(48,24),YSTLN(48,24),STVAL(24),
81700          $USTAR(48,24),VSTAR(48,24),WSTAR(48,24),PSTAR(48,24),
81800          $TESTAR(48,24),YSTLNP(48,24),VISTAR(48,24)
81900          $/ALL/IT,JT,NI,NJ,NIM1,NJM1,GREAT,JMAX(48),JMAX1(48)
82000          $/GEOM/INCOMP,X(48),Y(24),DXEP(48),DXPW(48),DYNP(24),DYPS(24),
82100          $    CNS(24),SEW(48),XU(48),YV(24),R(24),RV(24),
82200          $    WFN(24),WFS(24),WFF(48),WFW(48),RCV(24),XMP(48),XJAC(48),
82300          $YMP(24),YJAC(24)
82400           COMMON
82500          $/FLOPR/URF,VIS,VISCOS,DENSIT,PRANDT,DEN(48,24),VIS(48,24)
82600          $/BASE T1/CON,TEIN,EDIN,FLOWIN,ALAMDA,
82700          $RSMALL,RLARGE,AL1,AL2,JSTEP,ISTEP,JSTP1,JSTM1,ISTP1,ISTM1
82800          $/TURB/GEN(48,24),CD,CMU,C1,C2,CAPPA,ELOG,PRED,PRTE
82900          $/WALLF/YPLUS(48),XPLUSW(24),TAUW(48),TAUW(24)
83000          $/COEF/AP(48,24),AN(48,24),AS(48,24),AE(48,24),AW(48,24),SU(48,24),
83100          $SP(48,24)
83200          $/PLOTT/NSTLN,NPLTLN,NPTS,YSLPLT(10,48),XUPLT(48),INFLOT
83300      C
83400      C       CHAPTER   1          CALCULATE GEOMETRICAL QUANTITIES
83500      C
83600           DO 100 J=1,NJ
83700           R(J) = Y(J)
83800      100  IF(INCOMP .EQ. 1) R(J) = 1.0
83900           DXPW(1) = 0.0
84000           DXEP(NI) = 0.0
84100           DO 101 I = 1,NIM1
84200           DXEP(I) = X(I+1)-X(I)
84300      101  DXPW(I+1) = DXEP(I)
84400           DYPS(1) = 0.0
84500           DYNP(NJ) = 0.0
84600           DO 102 J = 1,NJM1
84700           DYNP(J) = Y(J+1)-Y(J)
84800      102  DYPS(J+1) = DYNP(J)
84900           SEW(1) = 0.0
85000           SEW(NI) = 0.0
85100           DO 103 I = 2,NIM1
85200      103  SEW(I) = 0.5*(DXEP(I)+DXPW(I))
85300           CNS(1) = 0.0
85400           CNS(NJ) = 0.0
```

```
      DO 104 J = 2,NJM1
  104 SNS(J) = 0.5*(DYNP(J)+DYPS(J))
      XU(1) = 0.0
      DO 105 I = 2,NI
  105 XU(I) = 0.5*(X(I)+X(I-1))
      DXPwU(1) = 0.0
      DXPwU(2) = 0.0
      DXEPU(1) = 0.0
      DXEPU(NI) = 0.0
      DO 106 I = 2,NIM1
      DXEPU(I) = XU(I+1)-XU(I)
  106 DXPwU(I+1) = DXEPU(I)
      SEwU(1) = 0.0
      DO 107 I = 2,NI
  107 SEwU(I) = X(I)-X(I-1)
C---- U-VELOCITITES WEIGHTING FACTORS
      DO 111 I = 2,NIM1
      wFE(I) = SEwU(I+1)/(SEwU(I+1)+SEwU(I))
      IF(I .LE. 2) GO TO 111
      wFw(I) = SEwU(I-1)/(SEwU(I-1)+SEwU(I))
  111 CONTINUE
      YV(1) = 0.0
      RV(1) = 0.0
      DO 108 J = 2,NJ
      RV(J) = 0.5*(R(J)+R(J-1))
  108 YV(J) = 0.5*(Y(J)+Y(J-1))
      RCV(1) = R(1)
      RCV(NJ) = R(NJ)
      DO 113 J=2,NJM1
  113 RCV(J) = 0.5*(RV(J+1)+RV(J))
      DYPSV(1) = 0.0
      DYPSV(2) = 0.0
      DYNPV(NJ) = 0.0
      DO 109 J = 2,NJM1
      DYNPV(J) = YV(J+1)-YV(J)
  109 DYPSV(J+1) = DYNPV(J)
      DNSV(1) = 0.0
      DO 110 J = 2,NJ
  110 DNSV(J) = Y(J)-Y(J-1)
C---- V-VELOCITIES WEIGHTING FCATORS
      DO 112 J=3,NJM1
      wFN(J) = DNSV(J+1)/(DNSV(J+1)+DNSV(J))
      wFS(J) = DNSV(J-1)/(DNSV(J-1)+DNSV(J))
  112 CONTINUE
C
C------CHAPTER     2 : 2 SET VARIABLES TO ZERO
C
      DO 200 I = 1,NI
      TAUX(I) = 1.0
      DO 200 J = 1,NJ
      TAUW(J) = 1.0
      U(I,J) = 0.0
      V(I,J) = 0.0
      W(I,J) = 0.0
      P(I,J) = 0.0
      PP(I,J) = 0.0
      TE(I,J) = 0.0
      ED(I,J) = 0.0
      DEN(I,J) = DENSIT
      VIS(I,J) = VISCOS
      DU(I,J) = 0.0
```

```
      DV(I,J) = 0.0
      SU(I,J) = 0.0
      SP(I,J) = 0.0
      STEN(I,J) = 0.0
  200 CONTINUE
      DO 300 I = 1,NI
      DO 300 J = 1,NSTLN
      YSTLN(I,J)=0.0
      YSTLND(I,J) = 0.0
      STVAL(J) = 0.0
  300 CONTINUE
      DO 400 N = 1,NPLTLN
      DO 400 I = 1,NI
      YSLPLT(N,I) = 0.0
  400 CONTINUE
      RETURN
      END
C
C-----------------------------------------------------------------------
C
      SUBROUTINE PROPS
C***********************************************************************
C
CHAPTER         PRELIMINARIES
C
      COMMON
     $/FLOPR/UREVIS,VISCOS,DENCIT,PRANDT,DEN(48,24),VIS(48,24)
     $/VAR/U(48,24),V(48,24),W(48,24),P(48,24),PP(48,24),
     $TE(48,24),ED(48,24),STEN(48,24),YSTLN(48,24),STVAL(24),
     $USTAR(48,24),VSTAR(48,24),WSTAR(48,24),PP STAR(48,24),
     $TESTAR(48,24),YSTLND(48,24),VISTAR(48,24)
     $/ALL/IT,JT,NI,NJ,NIM1,NJM1,GREAT,JMAX(48),JMAXP1(48)
     $/TURB/GEN(48,24),CD,CMU,C1,C2,CAPPA,ELOG,PREC,PRTE
C
C       CHAPTER   1   VISCOSITY
C
      DO 100 I = 2,NIM1
      DO 100 J = 2,NJM1
      VISOLD = VIS(I,J)
      IF(ED(I,J) .EQ. 0.0) GO TO 102
      VIS(I,J) = DEN(I,J)*TE(I,J)**2*CMU/ED(I,J)+VISCOS
      GO TO 101
  102 VIS(I,J) = VISCOS
C     UNDERRELAX VISCOSITY
  101 VIS(I,J) = UREVIS*VIS(I,J)+(1.0-UREVIS)*VIS OLD
  100 CONTINUE
      RETURN
      END
C
C-----------------------------------------------------------------------
C
      SUBROUTINE CALCU
C***********************************************************************
C
CHAPTER         PRELIMINARIES
      COMMON
     $/UVEL/RESORU,NSWPU,URFU,DXEPU(48),DXPWU(48),SEWU(48)
     $/VVEL/RESORV,NSWPV,URFV,DYNPV(24),DYPSV(24),SNSV(24)
     $/PCOR/RESORM,NSWPP,URFP,DU(48,24),DV(48,24),IPREF,JPREF
     $/VAR/U(48,24),V(48,24),W(48,24),P(48,24),PP(48,24),TE(48,24),
     $ED(48,24),STEN(48,24),YSTLN(48,24),STVAL(24),USTAR(48,24),
```

```
97700          $VSTAR(46,24),WSTAR(48,24),PSTAR(48,24),TESTAR(48,24),YSTLND(48,24)
97800          $,VISTAR(48,24)
97900          $/ALL/IT,JT,NI,NJ,NIM1,NJM1,GREAT,JMAX(48),JMAXP1(48)
98000          $/GEOM/INDCOS,X(48),Y(24),DXEP(48),DXPW(48),DYNP(24),DYPS(24),
98100          $SNS(24),SEW(46),XU(46),YV(24),R(24),RV(24),
98200          $WFN(24),WFS(24),WFE(48),WFW(46),RCV(24),XND(48),XUND(48),
98300          $YND(24),YVND(24)
98400           COMMON
98500          $/FLOPR/UREVIS,VISCOS,DENSIT,PRANDT,GEN(48,24),VIS(46,24)
98600          $/COEF/AP(46,24),AN(46,24),AS(48,24),AE(48,24),AW(48,24),SU(48,24),
98700          $SP(48,24)
98800          $/BASE T1/UIN,TEIN,EDIN,FLOWIN,ALAMDA,
98900          $       RSMALL,RLARGE,AL1,AL2,JSTEP,ISTEP,JSTP1,JSTM1,ISTP1,ISTM1
99000            COMMON/GGF/RMOMV(50,50),RMOMU(50,50)
99100    C
99200    C        CHAPTER   11111      ASSEMBLY OF COEFFICIENTS
99300           DO 100 I = 3,NIM1
99400           DO 101 J = 2,NJM1
99500    C------COMPUTE AREAS AND VOLUME
99600           AREAN = RV(J+1)*SEWU(I)
99700           AREAS = RV(J)*SEWU(I)
99800           AREAEW = RCV(J)*SNS(J)
99900           VOL = RCV(J)*SEWU(I)*SNS(J)
```

```
00100   C----- CALCULATE CONVECTION COEFFICIENTS
00200         GN = 0.5*(DEN(I,J+1)+DEN(I,J))*V(I,J+1)
00300         GNW = 0.5*(DEN(I-1,J)+DEN(I-1,J+1))*V(I-1,J+1)
00400         GS = 0.5*(DEN(I,J-1)+DEN(I,J))*V(I,J)
00500         GSW = 0.5*(DEN(I-1,J)+DEN(I-1,J-1))*V(I-1,J)
00600         GE = DEN(I,J)*(U(I+1,J)*(1.0-WFE(I))+U(I,J)*WFE(I))
00700         GW = DEN(I-1,J)*(U(I-1,J)*(1.0-WFW(I))+U(I,J)*WFW(I))
00800         CN = 0.5*(GN+GNW)*AREAN
00900         CS = 0.5*(GS+GSW)*AREAS
01000         CE = GE*AREAEW
01100         CW = GW*AREAEW
01200   C-----  CALCULATE DIFFUSION COEFFICIENTS
01300         VISN = 0.25*(VIS(I,J)+VIS(I,J+1)+VIS(I-1,J)+VIS(I-1,J+1))
01400         VISS = 0.25*(VIS(I,J)+VIS(I,J-1)+VIS(I-1,J)+VIS(I-1,J-1))
01500         DN = VISN*AREAN/DYNP(J)
01600         DS = VISS*AREAS/DYPS(J)
01700         DE = VIS(I,J)*AREAEW/DXEPU(I)
01800         DW = VIS(I-1,J)*AREAEW/DXPWU(I)
01900   C-----CALCULATE COEFFICIENT OF SOURCE TERMS
02000         SMP = DN-DS+DE-DW
02100         SP = AMAX1(0.0,SMP)
02200         SP0 = SP
02300   C----- ASSEMBLE MAIN COEFFICIENTS
02400         AN(I,J) = AMAX1(ABS(0.5*DN),DN)-0.5*DN
02500         AS(I,J) = AMAX1(ABS(0.5*DS),DS)+0.5*DS
02600         DE = AMAX1(DE,-WFE(I)*DF,(1.0-WFE(I))*DE)
02700         DW = AMAX1(DW,WFW(I)*DW,-(1.0-WFW(I))*DW)
02800         AE(I,J) = DE-(1.0-WFE(I))*DE
02900         AW(I,J) = DW+(1.0-WFW(I))*DW
03000         SU(I,J) = AREAEW
03100         DUDXE = (U(I+1,J)-U(I,J))/DXEPU(I)
03200         DUDXW = (U(I,J)-U(I-1,J))/DXPWU(I)
03300         SORCE1 = (DUDXE*VIS(I,J)-DUDXW*VIS(I-1,J))/DEWU(I)
03400         DVDXN = (V(I,J+1)-V(I-1,J+1))/SCWU(I)
03500         DVDXS = (V(I,J)-V(I-1,J))/DEWU(I)
03600         SORCE2 = (RV(J+1)*VISN*DVDXN-RV(J)*VISS*DVDXS)/(RCV(J)*DYNP(J))
03700         SU(I,J) = SP0*U(I,J)+SU(I,J)+(P(I-1,J)-P(I,J))
03800   C*****************************************************************
03900   C     RMOMU(I,J) IS THE MOMENTUM CONTRIBUTION BY THE DROPLET SPRAY TO
04000   C     MAIN GAS FLOW FIELD AS A RESULT OF THE AXIAL VELOCITY.
04100         SU(I,J)=SU(I,J)-RMOMU(I,J)
04200   C*****************************************************************
04300         SU(I,J) = SU(I,J)+(SORCE1+SORCE2)*VOL
04400         SP(I,J) = -SP
04500     101 CONTINUE
04600     100 CONTINUE
04700   C
04800   C----CHAPTER  2.2.2   PROBLEM MODIFICATIONS
04900   C
05000         CALL PROMOD (2)
05100   C
05200   CHAPTER  3  FINAL COEF. ASSEMBLY AND RESIDUAL SOURCE CALCULATION
05300   C
05400         RESORU = 0.0
05500         DO 300  I = 3,NIM1
05600         DO 301  J = 2,NJM1
05700         AP(I,J) = AN(I,J)+AS(I,J)+AE(I,J)+AW(I,J)-SP(I,J)
05800         DU(I,J) = SU(I,J)/AP(I,J)
05900         RESOR = AN(I,J)*U(I,J+1)+AS(I,J)*U(I,J-1)+AE(I,J)*U(I+1,J)
06000        $    +AW(I,J)*U(I-1,J)-AP(I,J)*U(I,J)+SU(I,J)
06100         VOL = RCV(J)*DEWU(I)*DNS(J)
```

```
06200           CORVOL = GREAT*VOL
06300           IF(-CP(I,J) .GT. 0.8*CORF/VOL) RELOR = RELOR/2.+VOL
06400           RELORL = RELORL*ABS(1-RELOR)
06500     C------OVERRELAXATION
06600           AP(I,J) = AP(I,J)/OMEGA
06700           SU(I,J) = SU(I,J)*(1.0-OMEGA)*AP(I,J)*U(I,J)
06800           SV(I,J) = SV(I,J)*OMEGA
06900     301 CONTINUE
07000     300 CONTINUE
07100     C
07200     CHAPTER    4     SOLUTION OF DIFFERENCE EQUATION  +  +  +  +  +
07300     C
07400           DO 400 I = 1,NUMPS
07500     400 CALL LISOLV(I,2,NI,JMAX,IT,UT,U,D)
07600           RETURN
07700     C     DEBUG UNIT(6), DISPLAY(PMAP,PMPS,PMPSL,PMAX,PMAXL,PMAXR,
07800     C    $AP,SU,VOL,OMEGA)
07900           END
08000     C
08100     C-----------------------------------------------------------------
08200     C
08300           SUBROUTINE CALC1
08400     C*****************************************************************
08500     C
08600     CHAPTER 3  PRELIMINARIES
08700     C
08800           COMMON
08900          $/ VEL/PSORU,VSORV,UREF,DXPS(50),DYPS(50),DXPU(50),DYPV(50)
09000          $/VOLL/RESORU,RESORV,URF,DYPU(50),DXPV(50),DXSU(50),DYSV(50)
09100          $/MISC/RESORP,RESORM,VREF,IT(50,24),JT(50,24),IPR(50),
09200          $/JAP/U(50,24),V(50,24),P(50,24),PP(50,24),
09300          $TE(50,24),EL(50,24),DTEN(50,24),YCTLN(50,24),CTAU(50),
09400          $UDTAP(50,24),VDTAP(50,24),WDTAP(50,24),DTAP(50,24),
09500          $TUDTAP(50,24),YCTLN(50,24),VDTAP(50,24)
09600          $/ALL/IT,JT,NI,NJ,NIM1,NJM1,NPRT,JMAX(50),JMAXP1(50)
09700          $/SEQ/IPSOL,A(50),Y(24),DAEP(50),DAPW(50),DYP(24),DYP(24),
09800          $    DXU(24),DXW(50),X(50),Y(24),DY(24),DYV(24),
09900          $    DPU(24),DPV(24),APP(24),APW(50),APU(50),DU(24),DV(24),
10000          $YNU(24),YNV(24)
10100           COMMON
10200          $/PCORR/UPVIC,VPICO,DENSIT,PRANDT,TEN(50,24),VIC(50,24)
10300          $/MADE II/UIN,TEIN,EDIN,FLOWIN,ALAMDA,
10400          $FLOWALL,WALPOS,ALI,ALG,JUTER,ICTER,JUTP1,JUT1,ICTP1,ICTM1
10500          $/COEF/AP(50,24),AN(50,24),AS(50,24),AE(50,24),AW(50,24),SU(50,24),
10600          $SP(50,24)
10700             COMMON/ REF/WORK(50),ARRAY(50,50)
10800     C
10900     CHAPTER 1  1  1  1  1  1 MODIFY OF COEFFICIENTS 1  1  1  1  1  1
11000     C
11100           DO 100 I = 2,NIM1
11200           DO 101 J = 2,NJM1
11300     C------COMPUTE AREAS AND VOLUME
11400           AREAN = R(J)*DX(I)
11500           AREAS = R(J-1)*DX(I)
11600           AREAEW = RV(J)*DYV(J)
11700           VOL = RV(J)*DX(I)*DYV(J)
11800     C------CALCULATE CONVECTION COEFFICIENTS
11900           SN = DENS(I,J)*(V(I,J+1)*(1.0-WPV(J)))*AREAN
12000           SS = DENS(I,J-1)*(V(I,J-1)*(1.0-WPV(J)))*AREAS
12100           SE = 0.5*(DENS(I+1,J)+DENS(I,J))*U(I+1,J)
12200           SSE = 0.5*(DENS(I+1,J-1)+DENS(I,J-1))*U(I+1,J-1)
```

```
12300           GW = 0.5*(DEN(I,J)+DEN(I-1,J))*U(I,J)
12400           GGW = 0.5*(DEN(I,J-1)+DEN(I-1,J-1))*U(I,J-1)
12500           GN = GN*AREAN
12600           GS = GS*AREAS
12700           GE = 0.5*(GE+GSE)*AREAE
12800           GW = 0.5*(GW+GGW)*AREAE
12900   C----------CALCULATE DIFFUSION COEFFICIENTS
13000           VISE = 0.25*(VIS(I,J)+VIS(I+1,J)+VIS(I,J-1)+VIS(I+1,J-1))
13100           VISW = 0.25*(VIS(I,J)+VIS(I-1,J)+VIS(I,J-1)+VIS(I-1,J-1))
13200           VN = VIS(I,J)*AREAN/DYNPV(J)
13300           VS = VIS(I,J-1)*AREAS/DYPSV(J)
13400           VE = VISE*AREAE/DXEP(I)
13500           VW = VISW*AREAE/DXPW(I)
13600   C----------CALCULATE COEFFICIENTS OF SOURCE TERMS
13700           SMP = VN+VS+VE+VW
13800           SP = AMAX1(0.0, SMP)
13900           SPO = SP
14000   C----------ASSEMBLE MAIN COEFFICIENTS
14100           AN(I,J) = AMAX1(VN,-GN*FN(J)+VN,(1.0-GN*FN(J)))*DN
14200           AS(I,J) = AMAX1(VS,GS*FS(J)+VS,(1.0-GS*FS(J)))*DS
14300           AN(I,J) = (VN-(1.0-GN*FN(J)))*GN
14400           AS(I,J) = (VS+(1.0-GS*FS(J)))*GS
14500           AE(I,J) = AMAX1(0.0,-0.5*GE),DE)-0.5*GE
14600           AW(I,J) = AMAX1(0.0,0.5*GW),DW)+0.5*GW
14700           DV(I,J) = 0.5*(AREAN+AREAS)
14800           DUDXE = (U(I+1,J)-U(I+1,J-1))/DYDV(J)
14900           DUDXW = (U(I,J)-U(I,J-1))/DYDV(J)
15000           SOURCE1 = (DUDXE*VISE-DUDXW*VISW)/DXEP(I)
15100           DVDYN = (V(I,J+1)-V(I,J))/DYNPV(J)
15200           DVDYS = (V(I,J)-V(I,J-1))/DYPSV(J)
15300           SOURCE = (VIS(I,J)*(DVDYN-VIS(I,J-1)*(U(J-1)*DYDY)
15400          $ /(DXV(J)*DYDV(J))
15500           SU(I,J) = SOURCE*V(I,J)*DV(I,J)*(FI,J-1)-FI,J))
15600   C**********************************************************************
15700   C     AMOMV(I,J) IS THE MOMENTUM CONTRIBUTION, BY THE CROSSFLOW TERM TO
15800   C     MAIN GAS FLOW FIELD AS A RESULT OF THE RADIAL VELOCITY.
15900           SU(I,J)=SU(I,J)+AMOMV(I,J)
16000   C**********************************************************************
16100           S (I,J) = SU(I,J)+(SOURCE1+SOURCE2)*VOL
16200           SP(I,J) = -SP
16300           IF(INSOLVE .EQ. 1) GO TO 101
16400           SU(I,J) = SU(I,J)+VOL*((DEN(I,J)+DEN(I,J-1))*(W(I,J)+W(I,J-1)
16500          $)**2)/(8.0*DY(J))
16600           SP(I,J) = SP(I,J)-(VIS(I,J)+VIS(I,J-1))*VOL/RV(J)**2
16700     101 CONTINUE
16800     100 CONTINUE
16900
17000   C-----------------------PRESSURE MULTIPLICATION
17100   C
17200           CALL PRESU(1)
17300   C
17400   C-----------------------FINAL COEF. ASSEMBLY AND RESIDUAL SOURCE CALC.
17500           RESORV = 0.0
17600           DO 200 I = 2,IM1
17700           DO 201 J = 2,JM1
17800           AP(I,J) = AN(I,J)+AS(I,J)+AE(I,J)+AW(I,J)-SP(I,J)
17900           DV(I,J) = DV(I,J)/AP(I,J)
18000           RESOR = AN(I,J)*V(I,J+1)+AS(I,J)*V(I,J-1)+AE(I,J)*V(I+1,J)
18100          $      +AW(I,J)*V(I-1,J)-AP(I,J)*V(I,J)+SU(I,J)
18200           VOL = DV(J)*DZW(I)*RSV(J)
18300           RESORV = RESORV+VOL
```

```
      IF(-SP(I,J) .GT. 0.5*SORVOL) RESOR = RESOR/SORVOL
      RESORV = RESORV+ABS(RESOR)
C---------- UNDER-RELAXATION
      AP(I,J) = AP(I,J)/OMEV
      SU(I,J) = SU(I,J)+(1.0-OMEV)*AP(I,J)*V(I,J)
      SV(I,J) = SV(I,J)*OMEV
  301 CONTINUE
  300 CONTINUE
C
CHAPTER   4   *   *   SOLUTION OF DIFFERENCE EQUATION
C
      DO 400 N = 1,NSWPV
  400 CALL LISOLV(2,J,NI,JMAX,IT,JT,W,3)
      RETURN
      END
C
C-----------------------------------------------------------------
C
      SUBROUTINE CALC
C*****************************************************************
CHAPTER  0 0 0 0 0 0 0 0    PRELIM.ENABLED      0 0 0   0 0 0 0 0
C
      COMMON
     $/CVELL/RESOR,NSWPU,OMEU,SORU(48),SNPU(48),SEMU(48)
     $/VVELL/RESORV,NSWPV,OMEV,SORV(24),SYPV(24),SNSV(24)
     $/PPELL/RESORM,NSWPM,OMEM
     $/TEMP/RESORH,NSWPH,OMEH
     $/TURB/RESORE,NSWPE,OMEE
     $/VAR/U(48,24),V(48,24),W(48,24),P(48,24),PP(48,24),
     $TE(48,24),ED(48,24),STEN(48,24),YDTLN(48,24),DTVAL(24),
     $UDTAR(48,24),VDTAR(48,24),WDTAR(48,24),EDTAR(48,24),
     $TEDTAR(48,24),YDTLN(48,24),VISTAR(48,24)
     $/ALL/IT,JT,NI,NU,NIM1,NJM1,GREAT,JMAX(48),JMAXP1(48)
     $/GEOM/IFTYP,X(48),Y(24),DXEP(48),DXPW(48),DYNP(24),DYPS(24),
     $    SNS(24),SEW(48),AU(48),YV(24),R(24),RV(24),
     $    RMN(24),RMS(24),RMU(48),RMV(24),RMC(48),XCND(48),
     $YND(24),YVD(24)
      COMMON
     $/FLOPR/RHO,VISCOS,DENSIT,PRANDT,CEN(48,24),VIS(48,24)
     $/RADE TH/SIN,TEIN,EDIN,FLOMIN,ALAMDA,
     $SMALL,FLARGE,AL1,AL2,JSTEP,ISTEP,JSTP1,JSTM1,ISTP1,ISTM1
     $/TURB/CMU,(48,24),C0,CMU,C1,C2,CAPPA,ELOG,RFQ,PRTE
     $/WALL/YPLUS(48),YPLUSM(24),TAUW(48),TAUW(24)
     $/COEF/AP(48,24),AN(48,24),AS(48,24),AE(48,24),AW(48,24),SU(48,24),
     $SP(48,24)
C-------IF NO SWIRL RETURN TO MAIN
      IF (W(1,1) .LE. 0.0) GO TO 400
C
CHAPTER  1  1  1  1  ASSEMBLY OF COEFFICIENTS  1  1  1  1  1
C
      DO 100 I = 2,NIM1
      DO 101 J = 2,NJM1
C
C-------COMPUTE AREAS AND VOLUME
C
      AREAN = RU(J+1)*SEW(I)
      AREAS = RU(J)*SEW(I)
      AREAEW = RV(J)*SNS(J)
      VOL = RU(J)*SNS(J)*SEW(I)
C
```

```
C----------CALCULATE CONVECTION COEFFICIENTS
C
        CN = 0.5*(CEN(I,J)+CEN(I,J+1))*V(I,J+1)
        CS = 0.5*(CEN(I,J)+CEN(I,J-1))*V(I,J)
        CE = 0.5*(CEN(I,J)+CEN(I+1,J))*U(I+1,J)
        CW = 0.5*(CEN(I,J)+CEN(I-1,J))*U(I,J)
        CN = CN*AREAN
        CS = CS*AREAS
        CE = CE*AREAE
        CW = CW*AREAW
C
C----------CALCULATE DIFFUSION COEFFICIENTS
C
        DIFN = 0.5*(DIF(I,J)+DIF(I,J+1))
        DIFS = 0.5*(DIF(I,J)+DIF(I,J-1))
        DIFE = 0.5*(DIF(I+1,J)+DIF(I,J))
        DIFW = 0.5*(DIF(I-1,J)+DIF(I,J))
        DN = DIFN*AREAN/DYN(J)
        DS = DIFS*AREAS/DYS(J)
        DE = DIFE*AREAE/DXE(I)
        DW = DIFW*AREAW/DXW(I)
C
C----------UPWIND FLOW
C
        WP = CW-CE+CS-CN
        DP = AMAX1(0.0, WP)
        DPO = DP
C
C       ADJUSTMENT FOR UPWIND DIFFERENCING
C
        AN(I,J) = AMAX1(ABS(0.5*CN),DN)+DN-0.5*CN
        AS(I,J) = AMAX1(ABS(0.5*CS),DS)+DS+0.5*CS
        AE(I,J) = AMAX1(ABS(0.5*CE),DE)-DE+0.5*CE
        AW(I,J) = AMAX1(ABS(0.5*CW),DW)+0.5*CW
        DP = DP+(DP-ABS(WP))*ARFAC
        VAU = 0.5*(V(I,J+1)+V(I,J))
        UE(I,J) = U(I,J)
        IF(J.EQ.1) GO TO 101
        DP = DP1-RO(I,J)*VEL*U(I,J)/DXV(J)
        DP=DP1-(VAU-V(J+1)-VIS*V(J))*U(I,J)/(DYAV(J)*0.5*(DXV(J)+DXV(J-1)))
        UE(I,J) = UE(I,J)+(DPO-DP)*VOL
        DP(I,J) = DP
  101 CONTINUE
  100 CONTINUE
C
C----------CALCULATE THE FINAL COEFFICIENT AND RHS FOR EACH CELL
C
        CALL RHSUV (U)
C
C       ADJUST THE FINAL COEFFICIENT AND RHS FOR EACH CELL
C
        RESOR = 0.0
        DO 200 I = 2,IMM1
        DO 200 J = 2,JMM1
        AP(I,J) = DP(I,J)+AN(I,J)+AS(I,J)+AE(I,J)+AW(I,J)-SP(I,J)
        RESOR = AN(I,J)*U(I,J+1)+AS(I,J)*U(I,J-1)+AE(I,J)*U(I+1,J)
     1  +AW(I,J)*U(I-1,J)-AP(I,J)*U(I,J)+SU(I,J)
        VOL = DX(I)*DYN(J)*DZ(I)
        SORVOL = SORMAT*VOL
        IF(-SP(I,J) .GT. SORVOL) RESOR = RESOR/VOL
        IF(J .EQ. 2) RESOR = 0.0
```

```
      RESORM = RESORM*ABS(RES(M))
C
C--------UNDER-RELAXATION
C
      AP(I,J) = AP(I,J)/OMEGA
      SU(I,J) =    (I,J)*(1.0- OMEGA)*AP(I,J)*U(I,J)
  301 CONTINUE
  302 CONTINUE
C
CHAPTER      SOLUTION OF DIFFERENCE EQUATION
C
      DO 400 I = 1, NM
  400 CALL TDS(2,2,NI,JMAX,IT,JT,AA,M)
  401 CONTINUE
      RETURN
      END
C
C-----------------------------------------------------------------------
C
C--------SUBROUTINE TAUX
C
C**********************************************************************
C
CHAPTER          SUBROUTINE LIMITATION OF CORRECTIONS
C
      COMMON
     $/PRES/P(NI,NJ),DPEF,DPEFI,DU(NI,NJ),TV(NI,NJ),IREFP,JREFP
     $/AMAT/AA(NI,NJ),AS(NI,NJ),AW(NI,NJ),AP(NI,NJ),
     $TE(NI,NJ),TT(NI,NJ),STEP(NI,NJ),VISTL(NI,NJ),ST,AL(NJ),
     $STSTAR(NI,NJ),VISTAR(NI,NJ),WISTAR(NI,NJ),STAR(NI,NJ),
     $TESTAR(NI,NJ),VISTL*(NI,NJ),VISTAR(NI,NJ)
     $/ALL/IT,JT,NI,NJ,NIM1,NJM1,GREAT,UMAX(NI),UMAB,P1(NI)
     $/GEOM/I,DX(NI),X(NI),DY(NJ),Y(NJ),DXP(NI),DXPM(NI),YNP(NJ),DYPT(NJ),
     $    DS(NJ),DEW(NI),RU(NI),YV(NJ),RV(NJ),
     $    RN(NI),RP(NJ),RPP(NI),RPM(NI),RCV(NJ),RVT(NI),RST(NI),
     $YNS(NJ),YST(NJ)
      COMMON
     $/FLOW/UBF,VISCOS,DENSIT,PRANDT,DEN(NI,NJ),VIS(NI,NJ)
     $/COEF/AP(NI,NJ),AN(NI,NJ),AS(NI,NJ),AE(NI,NJ),AW(NI,NJ),SU(NI,NJ),
     $SP(NI,NJ)
     $/MAGE TI/DTM,TIM,ECIM,FLOWIN,ALAMDA,
     $NCMAGE,NLAMDE,ALI,AL2,JSTEP,ISTEP,JSTP1,JSTM1,ISTP1,ISTM1
      RESORM = 0.0
C
CHAPTER   1   1   1   1   1   1 ASSEMBLY OF COEFFICIENTS 1   1   1   1
C
      DO 100 J = 2,JM1
      DO 101 I = 2,IM1
C--------CALCULATE AREAS AND VOLUME
      AREAN = RV(J+1)*DEW(I)
      AREAS = RV(J)*DEW(I)
      AREAE = RU(I)*DSU(J)
      VOL = RU(I)*DSU(J)*DEW(I)
C-------CALCULATE COEFFICIENTS
      DENN = 0.5*(DEN(I,J)+DEN(I,J+1))
      DENS = 0.5*(DEN(I,J)+DEN(I,J-1))
      DENE = 0.5*(DEN(I,J)+DEN(I+1,J))
      DENW = 0.5*(DEN(I,J)+DEN(I-1,J))
      AN(I,J) = DENN*AREAN*DV(I,J+1)
      AS(I,J) = DENS*AREAS*DV(I,J)
      AE(I,J) = DENE*AREAE*DU(I+1,J)
      AW(I,J) = DENW*AREAE*DU(I,J)
```

```
C--------CALCULATE
      AN = AEN*.(I,J-1)*A
      AS = AES*.(I,J)*A
      AE = AEE*.(I,J)*A*A
      AW = AEW*.(I-1,J)*A*A
      AP = AEP*.(I,J)*A*A
      SP(I,J) = 0.0
      SC(I,J) = -AP
C-------- MODIFY SP AT BOUNDARY CELLS
      IF (AP.EQ.0.0) SP(I,J)=-1.0
  111 CONTINUE
  222 CONTINUE
C
C-----CHAPTER 4 ------ SOLUTION OF DIFFERENCE EQUATIONS
C
      CALL SOR(AP,AN,AS,AE,AW,SP,SC,PP,IM1,JM1,1.5,RESORM)
C
C-----CHAPTER 5 ------ CORRECT VELOCITIES AND PRESSURE
C
C---------- VELOCITIES
      DO 501 I = 2,IM1
      JJ = JMAX(I)
      DO 501 J = 3,JJ
      V(I,J) = V(I,J)+DV(I,J)*(PP(I,J-1)-PP(I,J))
  501 CONTINUE
      DO 502 I = 2,IM1
      JJ = JMAX(I-1)
      DO 502 J = 2,JJ
      IF(I.NE.2) U(I,J) = U(I,J)+DU(I,J)*(PP(I-1,J)-PP(I,J))
  502 CONTINUE
  503 CONTINUE
C----------PRESSURES WITH PROVISION FOR UNDER-RELAXATION
      PPREF = PP(IPREF,JPREF)
      DO 506 I = 2,IM1
      JJ = JMAX(I)
      DO 506 J = 2,JJ
      P(I,J) = P(I,J)+ORF*(PP(I,J)-PPREF)
C-------- PP IS SENDED AT TOP OF CHAPTER 4, MAIN
  504 CONTINUE
  506 CONTINUE
      RETURN
      END
C
C-----------------------------------------------------------------------
C
      SUBROUTINE CALCTE
C**********************************************************************
C
CHAPTER 3 ------ PRELIMINARIES
C
```

```
      COMMON
     $/TEN/REC(4**,2**),NUM(4**,2**),
     $/AA/C(4**,2*),V(4**,2*),W(4**,2*),P(4**,2*),PP(4**,2*),
     $TE(4**,2*),FT(4**,2*),CTEN(4**,2*),VSTLN(4**,2*),CT,AL(2*),
     $_STAR(4**,2*),VSTAR(4**,2*),WSTAR(4**,2*),PSTAR(4**,2*),
     $TESTAR(4**,2*),VSTEN(4**,2*),VISTAR(4**,2*)
     $/ALL/IT,NTEN,NUM,NIM1,NUM1,SELAT,NMAX(4**),NMAX1(4**)
     $/GEOM/IN(4**),X(4**),Y(2*),XSF(4**),XPM(4**),YMP(2*),YSF(2*),
     $     XS(2*),XM(4**),RS(4**),YS(2*),R(2*),RW(2*),
     $   RFW(2*),WF(2*),WFF(4**),WFW(4**),RCW(2*),AW(4**),VOF(4**),
     $YW(2*),YOC(2*)
      COMMON
     $/FLOW/ZERO,IT,WIDTH,LEN,NIT,FRANGT,TEN(4**,2*),VIS(4**,2*)
     $/WALL/MAXIT,ITSTOP,ITEP,ITSTP1,ITSTP2,ITSTM1,ITSTP1,ITSTM1
     $/TURB/CL,CLP,CLPP,ALL,ALL0,ITSTP,ITSTP1,ITSTM1,ITSTP1,ITSTM1
     $/TURB/CL(4**,2*),CL0(4**,2*),CLPP(4**,2*),CL00,PHIC,PHIE
     $/WALL/XW(4**),XWW(2*),TAU(4**),TAUW(2*)
     $/TURB/ZK(4**,2*),ZE(4**,2*),ZKP(4**,2*),ZL(4**,2*),AW(4**,2*),
     $ZP(4**,2*)
     $/ZZZ/A(4**,2*),B(4**,2*)

C***** I  I  I  I  I  COMPUTE THE COEFFICIENTS  I  I  I  I

      DO 1 I=1,IT
      IF(I.EQ.1) GO TO 2
      IF(I.EQ.NIM1) GO TO 3
      GO TO 4
2     DO 5 J=1,NUM
      AA(I,J)=0.
      BB(I,J)=1.
      CC(I,J)=0.
      DD(I,J)=V(I,J)
5     CONTINUE
      GO TO 1
3     DO 6 J=1,NUM
      AA(I,J)=0.
      BB(I,J)=1.
      CC(I,J)=0.
      DD(I,J)=V(I,J)
6     CONTINUE
      GO TO 1
4     DO 7 J=1,NUM
      AA(I,J)=-(V(I,J)+V(I-1,J))/4.-TE
      BB(I,J)=(V(I,J)-V(I-1,J))/4.+TE
      CC(I,J)=-(V(I,J)+V(I+1,J))/4.-TE
      DD(I,J)=(V(I,J)-V(I+1,J))/4.+TE
7     CONTINUE
      DO 8 J=1,NUM
      IF(J.EQ.1) GO TO 9
      IF(J.EQ.NUM) GO TO 10
      GO TO 11
9     AA(I,J)=0.
      BB(I,J)=1.
      CC(I,J)=0.
      DD(I,J)=W(I,J)
      GO TO 8
10    AA(I,J)=-(W(I,J)+W(I,J-1))/4.-TE
      BB(I,J)=(W(I,J)-W(I,J-1))/4.+TE
      CC(I,J)=0.
      DD(I,J)=W(I,J)
      GO TO 8
11    AA(I,J)=-(W(I,J)+W(I,J-1))/4.-TE
      BB(I,J)=(W(I,J)-W(I,J-1))/4.+TE
      CC(I,J)=-(W(I,J)+W(I,J+1))/4.-TE
      DD(I,J)=(W(I,J)-W(I,J+1))/4.+TE
8     CONTINUE
1     CONTINUE
      DO 12 I=1,IT
      IF(I.EQ.1) GO TO 13
      IF(I.EQ.NIM1) GO TO 14
      GO TO 15
13    DO 16 J=1,NUM
      AA(I,J)=0.
      BB(I,J)=1.
      CC(I,J)=-1.
      DD(I,J)=0.
16    CONTINUE
      GO TO 12
14    DO 17 J=1,NUM
      AA(I,J)=-1.
      BB(I,J)=1.
      CC(I,J)=0.
      DD(I,J)=0.
17    CONTINUE
      GO TO 12
15    DO 18 J=1,NUM
      IF(J.EQ.1) GO TO 19
      IF(J.EQ.NUM) GO TO 20
      GO TO 21
19    AA(I,J)=0.
      BB(I,J)=1.
      CC(I,J)=-1.
      DD(I,J)=0.
      GO TO 18
20    AA(I,J)=-1.
      BB(I,J)=1.
      CC(I,J)=0.
      DD(I,J)=0.
      GO TO 18
21    AA(I,J)=-(W(I,J)+W(I-1,J))/4.-TE
      BB(I,J)=(W(I,J)-W(I-1,J))/4.+TE
      CC(I,J)=-(W(I,J)+W(I+1,J))/4.-TE
      DD(I,J)=(W(I,J)-W(I+1,J))/4.+TE
18    CONTINUE
12    CONTINUE
      DO 22 I=1,IT
      IF(I.EQ.1) GO TO 23
      IF(I.EQ.NIM1) GO TO 24
      GO TO 25
23    DO 26 J=1,NUM
      AA(I,J)=0.
      BB(I,J)=1.
      CC(I,J)=0.
      DD(I,J)=P(I,J)
26    CONTINUE
      GO TO 22
24    DO 27 J=1,NUM
      AA(I,J)=0.
      BB(I,J)=1.
      CC(I,J)=0.
      DD(I,J)=P(I,J)
27    CONTINUE
      GO TO 22
25    DO 28 J=1,NUM
      IF(J.EQ.1) GO TO 29
      IF(J.EQ.NUM) GO TO 30
      GO TO 31
29    AA(I,J)=0.
      BB(I,J)=1.
      CC(I,J)=-1.
      DD(I,J)=0.
      GO TO 28
30    AA(I,J)=-1.
      BB(I,J)=1.
      CC(I,J)=0.
      DD(I,J)=0.
      GO TO 28
31    AA(I,J)=-(W(I,J)+W(I-1,J))/4.-TE
      BB(I,J)=(W(I,J)-W(I-1,J))/4.+TE
      CC(I,J)=-(W(I,J)+W(I+1,J))/4.-TE
      DD(I,J)=(W(I,J)-W(I+1,J))/4.+TE
28    CONTINUE
22    CONTINUE
```

```
      GEN(I,J) = (2.0*(DUDX**2+DVDY**2)+(DUDY+DVDX)**2)*VIS(I,J)
      IF(INDCOS .EQ. 2) GEN(I,J) = GEN(I,J)*VIS(I,J)*(DWDY**2+DWDY**2)
      IF(RV(J) .EQ. 0.0) GO TO 110
      VOR = V(I,J)/RV(J)
      IF(INDCOS .EQ. 2) GEN(I,J)=GEN(I,J)*VIS(I,J)*0.5*(VOR+V(I,J+1)/
     $RV(J+1))**2
      GO TO 120
  110 IF(INDCOS .EQ. 2) GEN(I,J)=GEN(I,J)*VIS(I,J)*0.5*(V(I,J+1)/
     $RV(J+1))**2
  120 CONTINUE
C---------ASSEMBLE MAIN COEFFICIENTS
      AN(I,J) = AMAX1(ABS(0.5*CN),CN)-0.5*CN
      AS(I,J) = AMAX1(ABS(0.5*CS),CS)+0.5*CS
      AE(I,J) = AMAX1(ABS(0.5*CE),CE)-0.5*CE
      AW(I,J) = AMAX1(ABS(0.5*CW),CW)+0.5*CW
      SC(I,J) = CPO*TE(I,J)
      SCRC(I,J) = SC(I,J)
      SC(I,J) = SC(I,J)+GEN(I,J)*VOL
      SP(I,J) = -SP
      SPRC(I,J) = SP(I,J)
      SP(I,J) = SP(I,J)-SO*CMU*GEN(I,J)**2*TE(I,J)*VOL/VIS(I,J)
  101 CONTINUE
  100 CONTINUE
C
CHAPTER  2  2  2  PROBLEM MODIFICATION  2  2  2
C
      CALL PROMOD(6)
C
CHAPTER  3  FINAL COEFFICIENT ASSEMBLY AND RESIDUAL SOURCE CALCULATION
C
      RESORK = 0.0
      DO 300 I = 2,NIM1
      DO 301 J = 2,NJM1
      AP(I,J) = AN(I,J)+AS(I,J)+AE(I,J)+AW(I,J)-SP(I,J)
      RESOR = AN(I,J)*TE(I,J+1)+AS(I,J)*TE(I,J-1)+AE(I,J)*TE(I+1,J)
     $     +AW(I,J)*TE(I-1,J)-AP(I,J)*TE(I,J)+SC(I,J)
      VOL = RDV(J)*DNS(J)*DEW(I)
      SORVOL = SMEAT*VOL
      IF(-SP(I,J) .GT. 0.5*SORVOL) RESOR = RESOR/SORVOL
      RESORK = RESORK+ABS(RESOR)
C---------VOLUME RELAXATION
      AP(I,J) = AP(I,J)/URFK
      SC(I,J) = SC(I,J)+(1.0-URFK)*AP(I,J)*TE(I,J)
  301 CONTINUE
  300 CONTINUE
C
CHAPTER  4  4  4  4  SOLUTION OF DIFFERENCE EQUATION  4  4  4
C
      DO 400 N = 1,NSWPK
  400 CALL LISOLV(2,2,NI,JMAX,IT,OT,TE,6)
      RETURN
      END
C
C-----------------------------------------------------------------------
C
      SUBROUTINE CALCFS
C*************************************************************************
C
CHAPTER  5  5  5  PRELIMINARIES  5  5  5  5  5
C
      COMMON
```

```
55000         $/TOIS/RESORE,NSWPO,URFE
55100         $/VAR/U(48,24),V(48,24),W(48,24),P(48,24),PP(48,24),
55200         $TE(48,24),ED(48,24),STEN(48,24),YSTLN(48,24),STVAL(24),
55300         $USTAR(48,24),VSTAR(48,24),WSTAR(48,24),PSTAR(48,24),
55400         $TESTAR(48,24),YSTLNO(48,24),VISTAR(48,24)
55500         $/ALL/IT,JT,NI,NJ,NIM1,NJM1,GREAT,JMAX(48),JMAXP1(48)
55600         $/GEOM/IMODE,X(48),Y(24),DXEP(48),DXPW(48),DYNP(24),DYPS(24),
55700         $   DNS(24),SEW(48),XU(48),YV(24),R(24),RV(24),
55800         $   WFN(24),WFS(24),WFE(48),WFW(48),RCV(24),XND(48),XUND(48),
55900         $YND(24),YVND(24)
56000          COMMON
56100         $/FLUPR/URFVIS,VISCOS,DENSIT,PRANDT,DEN(48,24),VIS(48,24)
56200         $/BASE T1/UIN,TEIN,EDIN,FLOWIN,ALAMDA,
56300         $RSMALL,RLARGE,AL1,AL2,JSTEP,ISTEP,JSTP1,JSTM1,ISTP1,ISTM1
56400         $/TURB/GEN(48,24),CO,CMU,C1,C2,CAPPA,ELOG,PRED,PRTE
56500         $/WALLF/YPLUSN(48),YPLUSW(24),TAUN(48),TAUW(24)
56600         $/COEF/AP(48,24),AN(48,24),AS(48,24),AE(48,24),AW(48,24),SU(48,24),
56700         $SP(48,24)
56800         $/SUSP/SUSO(48,24),SPSO(48,24)
56900    C
57000    CHAPTER  1  1  1  1  ASSEMBLY OF COEFFICIENTS  1  1  1
57100    C
57200          DO 100 I = 2,NIM1
57300          JJ = JMAX(I)
57400          DO 101 J = 2,JJ
57500    C-------COMPUTE AREAS AND VOLUME
57600          AREAN = RV(J+1)*SEW(I)
57700          AREAS = RV(J)*SEW(I)
57800          AREAEW = RCV(J)*DNS(J)
57900          VOL = RCV(J)*DNS(J)*SEW(I)
58000    C---------CALCULATE CONVECTION COEFFICIENTS
58100          GN = 0.5*(DEN(I,J)+DEN(I,J+1))*V(I,J+1)
58200          GS = 0.5*(DEN(I,J)+DEN(I,J-1))*V(I,J)
58300          GE = 0.5*(DEN(I,J)+DEN(I+1,J))*U(I+1,J)
58400          GW = 0.5*(DEN(I,J)+DEN(I-1,J))*U(I,J)
58500          CN = GN*AREAN
58600          CS = GS*AREAS
58700          CE = GE*AREAEW
58800          CW = GW*AREAEW
58900    C---------CALCULATE DIFFUSION COEFFICIENTS
59000          GAMN = 0.5*(VIS(I,J)+VIS(I,J+1))/PRED
59100          GAMS = 0.5*(VIS(I,J)+VIS(I,J-1))/PRED
59200          GAME = 0.5*(VIS(I,J)+VIS(I+1,J))/PRED
59300          GAMW = 0.5*(VIS(I,J)+VIS(I-1,J))/PRED
59400          DN = GAMN*AREAN/DYNP(J)
59500          DS = GAMS*AREAS/DYPS(J)
59600          DE = GAME*AREAEW/DXEP(I)
59700          DW = GAMW*AREAEW/DXPW(I)
59800    C--------SOURCE TERMS
59900          CMP = CN-CS+CE-CW
60000          SP = AMAX1(0.0,CMP)
60100          SPO = SP
60200    C------- ASSEMBLE MAIN COEFFICIENTS
60300          AN(I,J) = AMAX1(ABS(0.5*CN),DN)-0.5*CN
60400          AS(I,J) = AMAX1(ABS(0.5*CS),DS)+0.5*CS
60500          AE(I,J) = AMAX1(ABS(0.5*CE),DE)-0.5*CE
60600          AW(I,J) = AMAX1(ABS(0.5*CW),DW)+0.5*CW
60700          SU(I,J) = SPO*ED(I,J)
60800          SUSO(I,J) = SU(I,J)
60900          SU(I,J) = SU(I,J)+C1*CMU*GEN(I,J)*VOL*DEN(I,J)*TE(I,J)/VIS(I,J)
61000          SP(I,J) = -SP
```

```
      SPKO(I,J) = SP(I,J)
      SP(I,J) = SP(I,J)-C2*DEN(I,J)*EO(I,J)*VOL/TE(I,J)
  101 CONTINUE
  100 CONTINUE
C
CHAPTER  2  2  2  2  PROBLEM MODIFICATION  2  2  2  2
C
      CALL PROMOD(7)
C
CHAPTER  3  3  3  COEFFICIENT ASSEMBLY AND RESIDUAL SOURCE CALCULATION
C
      RESORE = 0.0
      DO 300 I = 2,NIM1
      DO 301 J = 2,NJM1
      AP(I,J) = AN(I,J)+AS(I,J)+AE(I,J)+AW(I,J)-SP(I,J)
      RESOR = AN(I,J)*EO(I,J+1)+AS(I,J)*EO(I,J-1)+AE(I,J)*EO(I+1,J)
     $       +AW(I,J)*EO(I-1,J)-AP(I,J)*EO(I,J)+SU(I,J)
      VOL = RCV(J)*DXC(J)*DEW(I)
      SORVOL = SREAT*VOL
      IF(-SP(I,J) .GT. 0.5*SORVOL) RESOR = RESOR/SORVOL
      RESORE = RESORE+ABS(RESOR)
C--------OVER-RELAXATION
      AP(I,J) = AP(I,J)/ORFE
      SU(I,J) = SU(I,J)*(1.0-ORFE)*AP(I,J)*EO(I,J)
  301 CONTINUE
  300 CONTINUE
C
CHAPTER  4  4  4  4  4 SOLUTION OF DIFFERENCE EQUATION  4  4  4  4
C
      DO 400 K = 1,NSWPO
  400 CALL LISOLV(2,2,NI,JMAX,IT,JT,EO,7)
      RETURN
      END
C
C-----------------------------------------------------------------------
C
      SUBROUTINE LISOLV(ISTART,JSTART,NI,JMAX,IT,JT,PHI,NCHAP)
C***********************************************************************
C
CHAPTER    0  1  PRELIMINARIES  0  0  0  0  1  0  0
C
      DIMENSION PHI(IT,JT),A(4P),B(4P),C(4P),D(4P),JMAX(IT)
      COMMON
     $/PACE TI/DTN,TEIN,EOIN,FLOWIN,ALAMDA,
     $SMALL,RLAMDA,ALI,ALJ,JSTEP,ISTEP,JSTP1,JSTM1,ISTP1,ISTM1
     $/COEF/AP(4P,24),AN(4P,24),AS(4P,24),AE(4P,24),AW(4P,24),SU(4P,24),
     $SP(4P,24)
      JSM1 = JSTART-1
      NIM1 = NI-1
      A(JSM1) = 0.0
C---------COMMENCE SWEEP OVER I
      DO 100 I=ISTART,NIM1
      C(JSM1) = PHI(I,JSM1)
C---------COMMENCE J-LINE TRAVERSE
      JI = JMAX(I)
      IF(NCHAP .EQ. 2) JI=JMAX(I-1)
      DO 101 J = JSTART,JI
C--------- ASSEMBLE TDMA COEFFICIENTS
      A(J) = AN(I,J)
      B(J) = AS(I,J)
      C(J) = AE(I,J)*PHI(I+1,J)+AW(I,J)*PHI(I-1,J)+SU(I,J)
```

```
67200           C(J) = AP(I,J)
67300     C-------- CALCULATE COEFFICIENTS OF RECURRENCE FORMULA
67400           TERM = 1.0/(C(J)-B(J)*A(J-1))
67500           A(J) = A(J)*TERM
67600           C(J) = (C(J)+B(J)*C(J-1))*TERM
67700       101 CONTINUE
67800     C-------- OBTAIN NEW PHIS
67900           DO 102 JJ = JSTART,JI
68000           J = JI+1+JSM1-JJ
68100       102 PHI(I,J) = A(J)*PHI(I,J+1)+C(J)
68200       100 CONTINUE
68300           RETURN
68400           END
68500     C
68600     C-----------------------------------------------------------------------
68700     C
68800           SUBROUTINE PRINT(ISTART,JSTART,NI,NJ,IT,JT,X,Y,PHI,HEAD)
68900     C***********************************************************************
69000     C
69100           DIMENSION PHI(IT,JT),X(IT),Y(JT),HEAD(9),STORE(49)
69200           ISKIP = 1
69300           JSKIP = 1
69400           WRITE(6,110) HEAD
69500           ISTA = ISTART - 12
69600       100 CONTINUE
69700           ISTA = ISTA+12
69800           IEND = ISTA+11
69900           IF(NI .LT. IEND) IEND = NI
70000           WRITE(6,111) (I,I=ISTA,IEND,ISKIP)
70100           WRITE(6,114) (X(I),I=ISTA,IEND,ISKIP)
70200           WRITE(6,112)
70300           DO 101 JJ=JSTART,NJ,JSKIP
70400           J = JSTART+NJ-JJ
70500           DO 120 I = ISTA,IEND
70600           A = PHI(I,J)
70700           IF(ABS(A) .LT. 1.E-20) A=0.0
70800       120 STORE(I) = A
70900       101 WRITE(6,113) J,Y(J),(STORE(I),I=ISTA,IEND,ISKIP)
71000           IF(IEND .LT. NI) GO TO 100
71100           RETURN
71200       110 FORMAT(1H0,17(2H+-),7X,9A4,7X,17(2H-+))
71300       111 FORMAT(1HO,13H      I=       ,I2,11I9)
71400       112 FORMAT(1HO J     Y)
71500       113 FORMAT(I3,0PF8.5,1X,1P,12E9.2)
71600       114 FORMAT(11H       X =  ,F8.5,11F9.5)
71700           END
71800     C
71900     C-----------------------------------------------------------------------
72000     C
72100           SUBROUTINE PROMOD (NCHAP)
72200     C***********************************************************************
72300     C
72400     CHAPTER  C  O  D  O PRELIMINARIES  O  O  C  O
72500     C
72600           COMMON
72700          $/UVEL/RESORU,NSWPU,URFU,CMEPU(48),CXPWU(48),SRWU(48)
72800          $/VVEL/RESORV,NSWPV,URFV,CYNPV(24),CYPSV(24),SNSV(24)
72900          $/WVEL/RESORW,NSWPW,URFW
73000          $/PCOR/RESORM,NSWPP,URFP,DU(48,24),DV(48,24),IPREF,JPREF
73100          $/VAR/U(48,24),V(48,24),W(48,24),P(48,24),PP(48,24),
73200          $TE(48,24),ED(48,24),STEN(48,24),YCTLN(48,24),STVAL(24),
```

```
      $USTAR(48,24),VSTAR(48,24),WSTAR(48,24),PSTAR(48,24),
      $TESTAR(48,24),YSTLND(48,24),VISTAR(48,24)
      $/ALL/IT,JT,NI,NJ,NIM1,NJM1,GREAT,JMAX(48),JMAXP1(48)
      $/GEOM/INDCOS,X(48),Y(24),DXEP(48),DXPW(48),DYNP(24),DYPS(24),
      $   SNG(24),SEW(48),XU(48),YV(24),R(24),RV(24),
      $   WFN(24),WFS(24),WFE(48),WFW(48),RCV(24),XND(48),XCND(48),
      $YND(24),YVND(24)
       COMMON
      $/FLOPR/UREVIS,VISCOS,DENSIT,PRANDT,DEN(48,24),VIS(48,24)
      $/KASE T1/UIN,TEIN,EDIN,FLOWIN,ALAMDA,
      $RSMALL,RLARGE,AL1,AL2,JSTEP,ISTEP,JSTP1,JSTM1,ISTP1,ISTM1
      $/SUSP/SUKE(48,24),SPKE(48,24)
      $/TURB/GEN(48,24),CD,CMU,C1,C2,CAPPA,ELOG,PRED,PRTE
      $/WALLF/YPLUSN(48),XPLUSW(24),TAUN(48),TAUW(24)
      $/COEF/AP(48,24),AN(48,24),AS(48,24),AE(48,24),AW(48,24),SU(48,24),
      $SP(48,24)
       IF(NCHAP .EQ. 2) GO TO 1150
       IF(JSTEP .EQ. NJM1) GO TO 1150
C--------OUT OF RANGE VALUES
      DO 1100 I = 2,NI
      IF(JMAX(I) .EQ. NJM1) GO TO 1150
      JJ = JMAXP1(I)
      DO 1100 J = JJ,NJM1
 1100 SP(I,J) = -GREAT
 1150 CONTINUE
      GO TO (1,2,3,4,5,6,7,8),NCHAP
C
C
C
CHAPTER  1  1  1   PROPERTIES  1   1   1   1   1
C
C
      1 CONTINUE
C----------NO MODIFICATIONS FOR THIS PROBLEM
      RETURN
C
CHAPTER  2   2   2   2  2   U-MOMENTUM  2   2   2   2
C
      2 CONTINUE
C--------OUT OF RANGE VALUES
      IF(JSTEP .EQ. NJM1) GO TO 202
      DO 200 I =3,NI
      IF(JMAX(I-1) .EQ. NJM1) GO TO 202
      JJ = JMAXP1(I-1)
      DO 200 J = JJ,NJM1
      SP(I,J) = -GREAT
  200 CONTINUE
  202 CONTINUE
C-----------------TOP WALL
      CDTERM = CMU**0.25
      DO 210 I = 3,NIM1
      J = JMAX(I-1)
      YP = YV(J+1)-Y(J)
      SQRTK = SQRT(0.5*(TE(I,J)+TE(I-1,J)))
      DENW = 0.5*(DEN(I,J)+DEN(I-1,J))
      YPLUSA = 0.5*(YPLUSN(I)+YPLUSN(I-1))
      IF(YPLUSA .LE. 11.63) GO TO 211
      TMULT = DENW*CDTERM*SQRTK*CAPPA/ALOG(ELOG*YPLUSA)
      GO TO 212
  211 TMULT = VISCOS/YP
  212 CONTINUE
```

```
79400      205 SP(I,J) = SP(I,J)-TMULT*SEWU(I)*RV(J+1)
79500          IF(JMAX(I-1) .NE. JMAX(I)) SP(I,J) = SP(I,J)/2.0
79600      210 AN(I,J) = 0.0
79700    C-------- SIDE WALL
79800          IF(JSTEP. EQ. NJM1) GO TO 214
79900          DO 225 I = 3,NIM1
80000          IF(JMAX(I-2) .GE. JMAX(I-1)) GO TO 225
80100          JJ = JMAXP1(I-2)
80200          JI = JMAX(I-1)
80300          DO 220 J = JJ,JI
80400          AW(I,J) = 0.0
80500      220 CONTINUE
80600      225 CONTINUE
80700    C--------- SYMMETRY AXIS
80800      214 CONTINUE
80900          DO 203 I = 1,NI
81000      203 AS(I,2) = 0.0
81100    C----------OUTLET
81200          ARDENT = 0.0
81300          FLOW = 0.0
81400          DO 209 J = 2,NJM1
81500          ARDEN = 0.5*(DEN(NIM1,J)+DEN(NIM1-1,J))*RCV(J)*SNS(J)
81600          ARDENT = ARDENT+ARDEN
81700      209 FLOW = FLOW+ARDEN*U(NIM1,J)
81800          DINC = (FLOWIN-FLOW)/ARDENT
81900          DO 215 J = 2,NJM1
82000      215 U(NI,J) = U(NIM1,J)+DINC
82100          RETURN
82200    C
82300    CHAPTER   3   3   3  V-MOMENTUM   3   3   3
82400    C
82500        3 CONTINUE
82600    C-----------SIDE WALL
82700          IF(JSTEP .EQ. NJM1) GO TO 314
82800          CUTERM = CMU**0.25
82900          DO 325 I = 2,NIM1
83000          IF(JMAX(I-1) .GE. JMAX(I)) GO TO 325
83100          JJ = JMAXP1(I-1)
83200          JI = JMAX(I)
83300          DO 320 J = JJ,JI
83400          XP = X(I)-XU(I)
83500          SQRTK = SQRT(0.5*(TE(I,J)+TE(I,J-1)))
83600          DENV = 0.5*(DEN(I,J)+DEN(I,J-1))
83700          XPLUSA = 0.5*(XPLUSW(J)+XPLUSW(J-1))
83800          IF(XPLUSA .LE. 11.63) GO TO 311
83900          TMULT = DENV*CUTERM*SQRTK*CAPPA/ALOG(ELOG*XPLUSA)
84000          GO TO 312
84100      311 TMULT = VISCOS/XP
84200      312 CONTINUE
84300      305 SP(I,J)=SP(I,J)-TMULT*SNSV(J)*RV(J)
84400          IF(J .EQ. JMAXP1(I-1)) SP(I,J)= SP(I,J)/2.0
84500      310 AW(I,J) = 0.0
84600      320 CONTINUE
84700      325 CONTINUE
84800    C--------- TOP WALL
84900      314 CONTINUE
85000          DO 313 I=2,NIM1
85100          J = JMAX(I)
85200      313 AN(I,J) = 0.0
85300          RETURN
85400    C
```

```
      CHAPTER  4   4   4   PRESSURE CORRECTION   4   4   4
C
    4 CONTINUE
C------- SIDE WALL
      IF(JSTEP .EQ. NJM1) GO TO 414
      DO 412 I = 2,NIM1
      IF(JMAX(I-1) .GE. JMAX(I)) GO TO 412
      JJ = JMAXP1(I-1)
      JI = JMAX(I)
      DO 410 J = JJ,JI
      AW(I,J) = 0.0
  410 CONTINUE
  412 CONTINUE
C---------TOP WALL
  414 CONTINUE
      DO 402 I=2,NIM1
      J = JMAX(I)
  402 AN(I,J) = 0.0
C---------- SYMMETRY AXIS
      DO 420 I = 2,NIM1
      AS(I,2) = 0.0
  420 CONTINUE
C--------- OUTLET
      DO 440 J = 2,NJM1
      AE(NIM1,J) = 0.0
  440 CONTINUE
      RETURN
C
      CHAPTER  5   5   5   THERMAL ENERGY  5   5   5   5
C
    5 CONTINUE
C-------NO MODIFICATIONS FOR THIS PROBLEM
      RETURN
C
      CHAPTER   6   6   6   TURBULENT KINETIC ENERGY   6   6   6
C
C
    6 CONTINUE
C------- TOP WALL
      CDTERM = CMU**0.25
      DO 610 I = 2,NIM1
      J = JMAX(I)
      DWDY = (W(I,J+1)-W(I,J-1))/(DYP(J)+DYP(J))
      UAVG = U(I,J)*FE(I)+(1.0-FE(I))*U(I+1,J)
      UEFF = SQRT(UAVG*UAVG+W(I,J)*W(I,J))
      YP = Y(J+1)-Y(J)
      DENO = DEN(I,J)
      SQRTK = SQRT(TE(I,J))
      VOL = RNV(J)*SNS(J)*SEW(I)
      YPLUSN(I) = DENO*SQRTK*CDTERM*YP/VISCOS
      IF(YPLUSN(I) .LE. 11.63) GO TO 608
      TMULT = DENO*CDTERM*SQRTK*CAPPA/ALOG(ELOG*YPLUSN(I))
      TAUN(I) = -TMULT*UEFF
      DITERM=DEN(I,J)*(CMU**0.75)*SQRTK*ALOG(ELOG*YPLUSN(I))/(CAPPA*YP)
      GO TO 609
  608 TAURX = -VISCOS*UAVG/YP
      TAURW = VISCOS*(-W(I,J)/YP-W(I,J)/Y(J))
      TAUN(I) = SQRT(TAURX**2+TAURW**2)
      DITERM = DEN(I,J)*(CMU**0.75)*SQRTK*YPLUSN(I)/YP
  609 DUDY = ((U(I,J)+U(I+1,J)+U(I,J+1)+U(I+1,J+1))/4.0-
     $   (U(I,J)+U(I+1,J)+U(I,J-1)+U(I+1,J-1))/4.0)/SNS(J)
```

```
      GENCOU = TAUN(I)**2/VIS(I,J)
      GENRES = GEN(I,J)-VIS(I,J)*(DUDY**2+(DWDY-W(I,J)/Y(J))**2)
      GEN(I,J) = GENRES+GENCOU
      SU(I,J) = GEN(I,J)*VOL+SUKD(I,J)
      SP(I,J) = -DITERM*VOL+SPKD(I,J)
      AN(I,J) = 0.0
  610 CONTINUE
      TAUN(NI) = TAUN(NIM1)
C---------SIDE WALL
      IF(JSTEP .EQ. NJM1) GO TO 614
      DO 625 I=2,NIM1
      IF(JMAX(I-1) .GE. JMAX(I)) GO TO 625
      JJ = JMAXP1(I-1)
      JI = JMAX(I)
      DO 620 J = JJ,JI
      DWDX = (W(I+1,J)-W(I-1,J))/(DXPW(I)+DXEP(I))
      VAVG = V(I,J)*FEN(J)+(1.0-FEN(J))*V(I,J+1)
      VEFF = SQRT(VAVG*VAVG + W(I,J)*W(I,J))
      XP = X(I) - XU(I)
      DENV = DEN(I,J)
      SQRTK = SQRT(TE(I,J))
      VOL = RCV(J)*SNS(J)*DFW(I)
      XPLUSW(J) = DENV*SQRTK*CDTERM*XP/VISCOS
      IF(XPLUSW(J) .LE. 11.63) GO TO 621
      TMULT = DENV*CDTERM*SQRTK*CAPPA/ALOG(ELOG*XPLUSW(J))
      TAUW(J) = -TMULT*VEFF
      DITERM=DEN(I,J)*(CMU**0.75)*SQRTK*ALOG(ELOG*XPLUSW(J))/(CAPPA*XP)
      GO TO 622
  621 TAUXP = VISCOS*VAVG/XP
      TAUXW = VISCOS*W(I,J)/XP
      TAUW(J)=SQRT(TAUXP**2+TAUXW**2)
      DITERM = DEN(I,J)*(CMU**0.75)*SQRTK*XPLUSW(J)/XP
  622 DVDX = ((V(I,J)+V(I,J+1)+V(I+1,J)+V(I+1,J+1))/4.0-
     $        (V(I,J)+V(I,J+1)+V(I-1,J)+V(I-1,J+1))/4.0)/DFW(I)
      GENCOU = TAUW(J)**2/VIS(I,J)
      GENRES = GEN(I,J)-VIS(I,J)*(DVDX**2+DWDX**2)
      GEN(I,J) = GENRES+GENCOU
      SU(I,J) = SU(I,J)+SUKD(I,J)+GEN(I,J)*VOL
      SP(I,J) = SP(I,J)+SPKD(I,J)-DITERM*VOL
      AW(I,J) = 0.0
  620 CONTINUE
  625 CONTINUE
      TAUW(NJ) = TAUW(NJM1)
C--------- SYMMETRY AXIS
  614 CONTINUE
      J = 2
      DO 630 I = 2,NIM1
      DUDY = ((U(I,J)+U(I+1,J)+U(I,J+1)+U(I+1,J+1))/4.0-
     $        (U(I,J)+U(I+1,J)+U(I,J-1)+U(I+1,J-1))/4.0)/DNS(J)
      VOL = RCV(J)*SNS(J)*SEW(I)
      GEN(I,J) = GEN(I,J)-VIS(I,J)*DUDY**2
      SU(I,J) = SUKD(I,J)+GEN(I,J)*VOL
  630 AS(I,2) = 0.0
C--------------OUTLET
      DO 640 J = 2,NJM1
      AE(NIM1,J) = 0.0
  640 CONTINUE
      RETURN
C
CHAPTER  7  7  7  7  DISSIPATION  7  7  7  7  7
C
```

```
      7 CONTINUE
C---------TOP @ALL
        DO 710 I = 2,NIM1
        J = JMAX(I)
        YP=Y(J+1)-Y(J)
        TERM = (CMU**0.75)/(CAPPA*YP)
        QQ(I,J) = GREAT*TERM*TE(I,J)**1.5
  710 SP(I,J) = -GREAT
C---------SIDE @ALL
        IF(JSTEP .EQ. NJM1) GO TO 714
        DO 725 I = 2,NIM1
        IF(JMAX(I-1) .GE. JMAX(I)) GO TO 725
        JJ = JMAXP1(I-1)
        JI = JMAX(I)
        DO 720 J = JJ,JI
        IF (J .EQ. JMAX(I)) GO TO 720
        XP = X(I)-XC(I)
        TERM = (CMU**0.75)/(CAPPA*XP)
        QQ(I,J) = GREAT*TERM*TE(I,J)**1.5
        SP(I,J) = -GREAT
  720 CONTINUE
  725 CONTINUE
C--------------SYMMETRY AXIS
```

```
00100      714 CONTINUE
00200          DO 730 I = 2,NIM1
00300      730 AE(I,2) = 0.0
00400    C-----------------OUTLET
00500          DO 740 J = 2,NJM1
00600          AE(NIM1,J) = 0.0
00700      740 CONTINUE
00800          RETURN
00900    C
01000    CHAPTER    B     J     M  SUPER VELOCITY R  R   F   R
01100    C
01200        + CONTINUE
01300    C------------ TOP WALL
01400          SUTERM = SMU**0.25
01500          DO 810 I = 2,NIM1
01600          J = JMAX(I)
01700          YP = Y(J+1)-Y(J)
01800          SQRTK = SQRT(TE(I,J))
01900          DENW = DEN(I,J)
02000          YPLUSA = YPLUSM(I)
02100          IF(YPLUSA .LE. 11.63) GO TO 811
02200          TMULT = DENW*CMTERM*SQRTK*CAPPA/ALOG(ELOG*YPLUSA)-VIS(I,J)/YP(J)
02300          GO TO 812
02400      811 TMULT = VISCOS/YP
02500      812 SP(I,J) = SP(I,J)-TMULT*DENW(I)*RV(J+1)
02600          AN(I,J) = 0.0
02700      810 CONTINUE
02800    C-----------DIE WALL
02900          IF(JSTEP .EQ. NJM1) GO TO 814
03000          DO 855 I = 2,NIM1
03100          IF(JMAX(I-1) .GE. JMAX(I)) GO TO 855
03200          JJ = JMAXP1(I-1)
03300          JI = JMAX(I)
03400          DO 850 J = JJ,JI
03500          XP = X(I) - XC(I)
03600          SQRTK = SQRT(TE(I,J))
03700          DENW = DEN(I,J)
03800          XPLUSA = XPLUSM(J)
03900          IF(XPLUSA .LE. 11.63) GO TO 851
04000          TMULT = DENW*CMTERM*SQRTK*CAPPA/ALOG(ELOG*XPLUSA)
04100          GO TO 852
04200      851 TMULT = VISCOS/XP
04300      852 SP(I,J) = SP(I,J)-TMULT*DNC(J)*RCJ(J)
04400          AW(I,J) = 0.0
04500      850 CONTINUE
04600      855 CONTINUE
04700    C-----------SYMMETRY AXIS
04800      814 CONTINUE
04900    C------FIX W FOR SOLID BODY ROTATION AT J=2 USING W AT J=3
05000          DO 860 I = 2,NIM1
05100          TERM = W(I,3)*R(2)/R(3)
05200          SU(I,2) = SWBAT*TERM
05300      860 SP(I,2) = -SWBAT
05400    C-------- OUTLET
05500          DO 870 J = 2,NJM1
05600      870 AE(NIM1,J) = 0.0
05700          RETURN
05800          END
05900    C
06000    C-------------------------------------------------------------------------
06100    C
```

```
      SUBROUTINE STRMFN
C*****************************************************************
C
CHAPTER  0  0  0  0 PRELIMINARIES  0  0  0  0
C
      COMMON
     $/VVEL/RESERV,NSWPV,CREV,DYNPV(24),DYPSV(24),SNSV(24)
     $/VAR/U(48,24),V(48,24),W(48,24),P(48,24),PP(48,24),
     $TE(48,24),ED(48,24),STFN(48,24),YSTLN(48,24),STVAL(24),
     $USTAR(48,24),VSTAR(48,24),WSTAR(48,24),PSTAR(48,24),
     $TESTAR(48,24),YSTLNO(48,24),VISTAR(48,24)
     $/ALL/IT,JT,NI,NJ,NIM1,NJM1,GREAT,JMAX(48),JMAXP1(48)
     $/GEOM/INCOOR,X(48),Y(24),DXEP(48),DXPW(48),DYNP(24),DYPS(24),
     $   SNS(24),DEW(48),XU(48),YV(24),R(24),RV(24),
     $   WFN(24),WFS(24),WFE(48),WFW(48),RCV(24),XNO(48),XUO(48),
     $YYNO(24),YYSO(24)
     $/BASE T1/DIN,TEIN,EDIN,FLOWIN,ALAMDA,
     $SMALL,FLARGE,AL1,AL2,JSTEP,ISTEP,JSTP1,JSTM1,ISTP1,ISTM1
     $/PLOTT/YSTLN,NPLTLN,NPTS,YSLPLT(10,48),XUSPLT(48),INPLOT
      LOGICAL INPLOT
C
CHAPTER  1  1  1
CALCULATE STREAM FUNCTION BASED ON VOLUMETRIC FLOW
C
      C = DIN*(HSMALL**2)/2.0
      DO 400 I = 2,NI
      IF(JMAX(I-1) .LT. 3) GO TO 400
      STFN(I,2) = (Y(2)*R(2)*U(I,2)*0.5)/C
      JJ = JMAX(I-1)
      DO 200 J = 3,JJ
      STFN(I,J)=STFN(I,J-1)+SNSV(J)*(R(J-1)*U(I,J-1)+R(J)*U(I,J))*0.5/C
  200 CONTINUE
  400 CONTINUE
C
      DO 600 I = 2,NI
      IJ = JMAXP1(I-1)
      DO 700 K = 1,STLN
      KK = K-1
      STVAL(K) = KK*0.1
      JJ = JMAX(I-1)
      DO 650 J = 2,JJ
      IF(STFN(I,J) .GE. STVAL(K)) GO TO 650
  600 CONTINUE
      YSTLN(I,K) = RV(IJ)
      GO TO 670
  650 IF(J .EQ. 2) YSTLN(I,K) = 0.0
      IF(J .EQ. 2) GO TO 670
      SLOPE = (STVAL(K)-STFN(I,J-1))/(STFN(I,J)-STFN(I,J-1))
      YSTLN(I,K) = Y(J-1)+SLOPE*(Y(J)-Y(J-1))
  670 CONTINUE
      YSTLNO(I,K) = YSTLN(I,K)/(2.0*FLARGE)
  700 CONTINUE
  800 CONTINUE
C       IF( .NOT. INPLOT) GO TO 740
      N = 0
      DO 730 K= 1,11,2
      N = N+1
      DO 730 I = 1,NIM1
      YSLPLT(N,I) = YSTLNO(I+1,K)
  730 CONTINUE
      DO 740 I = 1,NIM1
```

```
12300          XCOPLT(I) = XCNT(I+1)
12400      740 CONTINUE
12500 C          WRITE(14,*) '       COORDINATES   FOR   STREAMLINE'
12600 C          DO 1411 K=1,11
12700 C          WRITE(14,*) 'STREAMLINE # ',K,'   VALUE =  ',CVAL(K)
12800 C          DO 1411 I=1,NIM1
12900 C        WRITE(14,*) '  X-COORD   ',XCNT(I),'  Y-COORD    ',YCNT(I,K)
13000 C 1411     CONTINUE
13100        740 NPTS = NIM1
13200          RETURN
13300          END
13400 C
13500 C
13600          SUBROUTINE PLOT (X,IDIM,IMAX,XAXIS,Y,JDIM,JMAX,YAXES,SYMBOL,LA)
13700 C*****************************************************************
13800 C
13900 C      X AND Y ARE ASSUMED TO BE IN ANY RANGE EXCEPT THAT NEGATIVE
14000 C      VALUES ARE PLOTTED AS ZERO
14100 C      X AND Y ARE SCALED TO THE RANGE 0 TO 1 BY DIVISION BY THE
14200 C      MAXIMA, WHICH ARE ALSO PRINTED.
14300 C      IDIM IS THE DIMENSION FOR X
14400 C      IMAX IS THE NUMBER OF X VALUES
14500 C      XAXIS STORES THE NAME OF THE XAXIS
14600 C      JDIM IS THE VARIABLE DIMENSION FOR Y
14700 C      JMAX IS THE NUMBER OF CURVES TO BE PLOTTED ( UP TO 10)
14800 C      THE ARRAY YAXES(J) STORES THE NAMES OF THE CURVES
14900 C      THE ARRAY SYMBOL(J) STORES THE SINGLE CHARACTERS USED FOR PLOTTING
15000 C
15100 C*****************************************************************
15200          DIMENSION X(IDIM),Y(JDIM,IDIM),YAXES(JDIM),SYMBOL(JDIM),A(1,1),
15300         1YMAX(10),AA(20)
15400          CHARACTER A,DOT,CROSS,BLANK
15500          DATA DOT,CROSS,BLANK/'.','+',' '/
15600 C---------SCALING X-ARRAY TO THE RANGE 0 TO 10
15700          XMAX = 1.0E-30
15800          DO 1 I = 1,IMAX
15900          IF(X(I) .GT. XMAX) XMAX=X(I)
16000        1 CONTINUE
16100          DO 2 I = 1,IMAX
16200          X(I) = X(I)/XMAX*10.0
16300          IF(X(I) .LT. 0.0) X(I) = 0.0
16400        2 CONTINUE
16500 C--------SCALING Y ARRAY TO THE RANGE 0 TO 100
16600          DO 3 J = 1,JMAX
16700          YMAX(J) = 1.0E-30
16800          DO 4 I = 1,IMAX
16900          IF(Y(J,I) .LT. YMAX(J)) YMAX(J) = Y(J,I)
17000        4 CONTINUE
17100          DO 5 I = 1,IMAX
17200 C--------  5 Y-SCALING
17300          Y(J,I) = Y(J,I)*100.0
17400          IF(YMAX .GT. 1) Y(J,I) = 1.0E2*Y(J,I)
17500          IF(Y(J,I) .LT. 0.0) Y(J,I) = 0.0
17600        5 CONTINUE
17700 C------- IDENTIFYING THE VARIOUS CURVES TO BE PLOTTED
17800          WRITE(6,103) XAXIS
17900          WRITE(6,100) (YAXES(I),I = 1,JMAX)
18000          WRITE(6,104) (SYMBOL(I),I = 1,JMAX)
18100          WRITE(6,102) (YMAX(I),I = 1,JMAX)
18200          DO 6 I = 1,11
18300        6 A(I)=I*.1*(I-1)
```

```
C
C
C
C     CAUTION ))))))))))))))))))))))))))))))))))))))))))))
C          BLANK IN SYMBOL AND IN THE PREVIOUS STATEMENT
C
C
      IF(LA .EQ. 1) WRITE(3,120)
      IF(LA .EQ. 0) WRITE(3,115)
      WRITE(3,101) (AA(I),I = 1,11)
C-------- MAIN LOOP, EACH PASS PRODUCES AN X-CONSTANT LINE.
      DO 40 II = 1,81
      I = II
      IF(I .EQ. 1 .OR. I .EQ. 11) GO TO 35
      GO TO 38
C-------- ALLOCATE . OR + AS MARKS ON THE Y-AXIS
   35 DO 30 K = 1,101
      IF A(K) = BLT
      DO 31 K = 11,101,10
   31 A(K) = PLUS
C------ ALLOCATE . OR + MARK ON THE X-AXIS
C---------------------SET THE APPROPRIATE X-VALUE
      DO A(1) = BLT
      A(1,1) = PLT
      K = I - 1
      WRITE(3,K) K
      IF(K) 47,47,46
   47 A(1) = PLUS
      WRITE(3,1) A(1)
   46 XLOC=1.+(I-1)
C*****CAUTION*****CAUTION*****CAUTION*****CAUTION*****CAUTION*****CAUTION*****
C*****CAUTION*****CAUTION*****CAUTION*****CAUTION*****CAUTION*****CAUTION*****
C----------WHICH IF ANY Y( A(I) ) VALUES LIES ON THIS X-CONSTANT LINE
C----------IF YES GO TO 41, OTHERWISE GO TO 42
      DO 45 K = 1,MAX
      IFIX = A(K)+1.5
      IF(AFIX-1) 43,41,43
C-------- LOCATE Y( A(I) )
   41 DO 44 J = 1,JMAX
      AY = Y(J,K)+1.5
      WRITE(3,4) AY
      DO 5 J = 1,
      WRITE(3,4)
C-------- PRINT X-CONSTANT LINE
   42 WRITE(3,4)
      IF(LA .EQ. 1)    TO 51
      WRITE(3,100) XL,(A(K),K=1,101),XL
      GO TO 52
   51 WRITE(3,107) XL,(A(K),K=1,101),XL
   52 WRITE(3,4)
C-------- SETTING  (ARRAY INIT) X-CONSTANT LINE
      DO 49 K = 1,101
   49 A(K) = BLANK
      WRITE(3,4)
      DO 9 XL=1,11
    9    AA(XL)= 1+(XL-1)
C*****CAUTION*****CAUTION*****CAUTION*****CAUTION*****CAUTION*****CAUTION*****
C*****CAUTION*****CAUTION*****CAUTION*****CAUTION*****CAUTION*****CAUTION*****
      WRITE(3,104) (AA(I),I=1,11)
      WRITE(3,110)
      RETURN
```

```
      1)  FORMAT(11H Y-AXIS 1HE,5X,10(1X,A10))
     1    FORMAT(1H0,2A,11F10.1)
     1    FORMAT(15H MAXIMUM VELOCI,  10F11.3)
     1    FORMAT(11H1X-AXIS IS ,A5)
     1    FORMAT(14,11F10.1)
     1    FORMAT( H ,F6.2,5X,10(1A1,F6.2)
     1    FORMAT(/H  Y-H-CL,11(4,1U(1X,A10))
     1    FORMAT(/H ,F6.2,5X,10(1A1,F6.2)
     1    FORMAT(//,T5,'RADIAL POSITION R/D',/)
          FORMAT(//,T5,'RADIAL POSITION R/D',/)
          FORMAT(///,T45,'DIMENSIONLESS STREAMLINE PLOT')
          END

*** BEGINNING OF INCLUDE SECTION ** BEGINNING OF INCLUDE SECTION ***

      List of variables:
        Integers:
C               - Axial index number for the E cell.
C               - Old axial index number for the M cell.
C               - Axial index number for the C cell.
C               - Counter for number of liquid phase iterations.
C               - Global convergence flag.
C               - Flag = 0 if drop is in the flow domain.
C               - Number of re-integrations.
C               - Integration flag.
C               - Number of steps travelled by the drop.
C               - Axial index number for the I cell.
C               - Axial index number for the J cell.
C               - Axial index number for the M cell.
C               - Old radial index number for the M cell.
C               - Radial index number for the I cell.
C               - Variable equivalent to JMAX() in the main program.
C               - Radial index number for the J cell.
C               - Radial index number for the M cell.
C               - Maximum number of liquid phase iterations allowed.
C               - Maximum number of ports.
C               - Maximum number of steps allowed for drop.
C               - Port number.
C               - Variable equivalent to II in the main program.
C               - Variable equivalent to JJ in the main program.
        Reals:
C               - Coefficient of drag for the droplet.
C               - Liquid density.
C               - Drop diameter.
C               - Integration time step.
C               - Increment scale factor for T.
C               - Reduction scale factor for T.
C               - Axial gravitational component.
C               - Radial gravitational component.
C               - 3.1415926
C               - Droplet radius.
C               - Density of the gas.
C               - Contribution to axial momentum source term.
C               - Contribution to radial momentum source term.
C               - Initial temperature of droplet.
C               - New temperature of droplet.
C               - Old temperature of droplet.
C               - Initial axial speed of droplet.
C               - New axial velocity of droplet.
C               - Old axial velocity of droplet.
C               - Axial velocity of gas.
```

```
C         UGAS     - Axial speed of the gas.
C         UGOLD()  - Old axial velocity of gas.
C         UINIT()  - Initial radial speed of droplet.
C         UNEW     - New radial velocity of droplet.
C         UOLD     - Old radial velocity of droplet.
C         VG()     - Radial velocity of gas.
C         VGAS     - Radial speed of the gas.
C         VGOLD()  - Old radial velocity of gas.
C         XH()     - Coordinates of lower left corner of
C         XINIT()  - Initial axial-coordinate of droplet.
C         XNEW     - New axial location of droplet.
C         XOLD     - Old axial location of droplet.
C         YH()     - the H-cells.
C         YINIT()  - Initial radial-coordinate of droplet.
C         YNEW     - New radial location of droplet.
C         YOLD     - Old radial location of droplet.
C
C*****************************************************************************
C
      SUBROUTINE PRTP
      COMMON /PROPC/ MAXPOR, NPORT,
     &  DRPDEN(10), DRPDIA(10), DRMDOT(10), DRFREQ(10),
     &  XOINIT(10), YOINIT(10), TOINIT(10), UOINIT(10), VOINIT(10),
     &  XH(40), YH(40),
     &  UG(40, 24), VG(40, 24), UGOLD(40, 24), VGOLD(40, 24),
     &  DRG, GRAVX, GRAVY, PAD, PMOLWT, PI, UGAS, VGAS,
     &  XGOLD, YGOLD, TGOLD, WGOLD, WDOLD,
     &  XNEW, YNEW, TNEW, UNEW, VNEW,
     &  DT, DTING, DTHED, PMOL,
     &  ICTER, IMTCTR, IFLAG2, IHIT, MAXCTR, MAXCT, INTFLG,
     &  IC, JC, IV, JV, IG, JG, IP, JP, IPOLD, JPOLD, ICOUNT,
     &  XCELL, YCELL, JCMAX(40), XDI, YDI
      COMMON/BOF/RMOMV(50,50),RMOMU(50,50)
      INTEGER LOWER
      OPEN (UNIT = 20)
      DO 1000 NPORT = 1, MAXPOR
C     Integrate for each port.
C
C       Initialize parameters for drop.
        XGOLD = XOINIT(NPORT)
        YGOLD = YOINIT(NPORT)
        TGOLD = TOINIT(NPORT)
        UGOLD = UOINIT(NPORT)
        VGOLD = VOINIT(NPORT)
        XNEW = XOINIT(NPORT)
        YNEW = YOINIT(NPORT)
        TNEW = TOINIT(NPORT)
        UNEW = UOINIT(NPORT)
        VNEW = VOINIT(NPORT)
        PAD = DRPDI(NPORT)/2.0
        PMOL = DRPDEN(NPORT)
C
C       Initialize counters and flags.
        ICOUNT = 0
        WDOLD = 0
        INTCTR = 0
        ICTER = 0
        IHIT = 0
        INTFLG = 0
C
C       Initialize IP, JP, IC, JC, IG, JG, IV and JV.
```

```
              CALL FINDB
      C       Initialize drop momentum source term at injection point.
      C
              IIMPORT
              DELTA=4.0*PI*RHOL*RAD**3/3.0*DRFREQ(II)
              RMOMU(IU,JU)=DELTA*UDINIT(II)
              RMOMV(IV,JV)=DELTA*VDINIT(II)
      C
                IBOLD = IB
                JBOLD = JB
      100     CONTINUE
      C         New integration step starts here.
                UGAS = UG(IU, JU)
                VGAS = VG(IV, JV)
      200     CONTINUE
      C         Returns here for reintegration if the time step
      C         was incorrect.
      C
                CALL RUNGA
                CALL DOMCHK
                IF (IHIT .NE. 0) THEN
                  WRITE (6, *) ' DOMCHK: IHIT = ', IHIT, 'NPORT = ', NPORT
                  GOTO 900
                ENDIF
                CALL FINDB
                CALL HITWAL
                IF (IHIT .NE. 0) THEN
                  WRITE (6, *) ' HITWAL: IHIT = ', IHIT, 'NPORT = ', NPORT
                  GOTO 900
                ENDIF
                CALL DTPCHK
                IF (INTFLG .NE. 0) THEN
      C           Reintegration is required.
                  INTCTR = INTCTR + 1
                  IF (INTCTR .GT. 20) THEN
                    WRITE(6, *) ' TOO MANY REINTEGRATIONS'
                    WRITE(6, *) ' NPORT = ', NPORT, 'X = ', XOLD,
     &              'Y = ', YOLD, ' ICOUNT = ', ICOUNT
                    IF (INTFLG .EQ. 1) THEN
                      WRITE (6, *) ' TIME STEP TOO LARGE, DT =', DT
                      WRITE (6, *) ' INPUT NEW TIME STEP'
                    ELSE IF (INTFLG .EQ. 2) THEN
                      WRITE (6, *) ' TIME STEP TOO SMALL, DT =', DT
                      WRITE (6, *) ' INPUT NEW TIME STEP'
                    ENDIF
                    READ(5, *) DT
                    INTCTR = 0
                  ENDIF
                  GOTO 200
                ENDIF
                INTCTR = 0
                CALL FINDN
                CALL FINDM
              WRITE(24, *) ' DROP: ',XOLD, YOLD, TOOLD, UOOLD, VOOLD,
     &    XONEW, YONEW, TONEW, UONEW, VONEW,
     &    DT, DTING, DTREQ,
     &    ISTEPS, INTCTR, IFLAGZ, IHIT, MAXSTP, MAXCT, INTFLG,
     &    IU, JU, IV, JV, IB, JB, IBOLD, JBOLD, ICOUNT,
     &    NCASE, MCASE
      C
                IF (NCASE .EQ. 0) THEN
```

```
42900                 WRITE(5, *) 'ERROR: NCASE = 0'
43000                 STOP
43100               ENDIF
43200     C
43300               IF (NCASE .EQ. 1) THEN
43400                 IF (NCASE .EQ. 1) THEN
43500     C           C-cell vertical boundary.
43600                   X1 = XC(LC)
43700                   X2 = XC(LE)
43800                   X3 = XB(IB)
43900                   Y1 = YC(LC)
44000                   Y2 = YC(LE)
44100                   IM1 = IC - 1
44200                   IM2 = IC
44300                   JM1 = JC
44400                   JM2 = JC
44500                   CALL INTERP(X1, Y1, X2, Y2, X3, Y3)
44600                   CALL SWAP(IM1, IM2, JM1, JM2, Y3)
44700     C           V-cell vertical boundary.
44800                   X1 = XV(LC)
44900                   Y2 = YV(LE)
45000                   IM1 = IV - 1
45100                   IM2 = IV
45200                   JM1 = JV
45300                   JM2 = JV
45400                   CALL INTERP(X1, Y1, X2, Y2, X3, Y3)
45500                   CALL SWAP(IM1, IM2, JM1, JM2, Y3)
45600     C
45700                 ELSE IF (NCASE .EQ. 2) THEN
45800     C           Check for path.
45900                   X1 = XC(LC)
46000                   X2 = XC(LE)
46100                   X3 = XB(IB)
46200                   Y1 = YC(LC)
46300                   Y2 = YC(LE)
46400                   CALL INTERP(X1, Y1, X2, Y2, X3, Y3)
46500                   IF (Y3 .LT. YB(JB)) THEN
46600                     LOWER = 1
46700                   ELSE
46800                     LOWER = 2
46900                   ENDIF
47000     C             C-cell vertical boundary.
47100                   Y1 = YC(LC)
47200                   Y2 = YC(LE)
47300                   IM1 = IC - 1
47400                   IM2 = IC
47500                   IF (LOWER .EQ. 1) THEN
47600                     JM1 = JC - 1
47700                     JM2 = JC - 1
47800                   ELSE
47900                     JM1 = JC
48000                     JM2 = JC
48100                   ENDIF
48200                   CALL INTERP(X1, Y1, X2, Y2, X3, Y3)
48300                   CALL SWAP(IM1, IM2, JM1, JM2, Y3)
48400     C             V-cell vertical boundary.
48500                   Y1 = YC(LC)
48600                   Y2 = YC(LE)
48700                   IM1 = IV - 1
48800                   IM2 = IV
48900                   JM1 = JV
```

```
                    JM2 = JV
                    CALL INTERP(X1, Y1, X2, Y2, X3, Y3)
                    CALL VMOD(IM1, IM2, JM1, JM2, Y3)
C                 C-cell horizontal boundary.
                    X1 = YDOLD
                    X2 = YDNEW
                    X3 = YB(JB)
                    Y1 = TDOLD
                    Y2 = TDNEW
                    IF (LOWER .EQ. 1) THEN
                      IM1 = IC
                      IM2 = IC
                    ELSE
                      IM1 = IC - 1
                      IM2 = IC - 1
                    ENDIF
                    JM1 = JC - 1
                    JM2 = JC
                    CALL INTERP(X1, Y1, X2, Y2, X3, Y3)
                    CALL CMOD(IM1, IM2, JM1, JM2, Y3)
C                 U-cell horizontal boundary.
                    Y1 = UDOLD
                    Y2 = UDNEW
                    IM1 = IC
                    IM2 = IC
                    JM1 = JC - 1
                    JM2 = JJ
                    CALL INTERP(X1, Y1, X2, Y2, X3, Y3)
                    CALL UMOD(IM1, IM2, JM1, JM2, Y3)
C
                  ELSE IF (NCASE .EQ. 3) THEN
C                 C-cell horizontal boundary.
                    X1 = YDOLD
                    X2 = YDNEW
                    X3 = YB(JB)
                    Y1 = TDOLD
                    Y2 = TDNEW
                    IM1 = IC
                    IM2 = IC
                    JM1 = JC - 1
                    JM2 = JC
                    CALL INTERP(X1, Y1, X2, Y2, X3, Y3)
                    CALL CMOD(IM1, IM2, JM1, JM2, Y3)
C                 U-cell horizontal boundary.
                    Y1 = UDOLD
                    Y2 = UDNEW
                    IM1 = IC
                    IM2 = IC
                    JM1 = JC - 1
                    JM2 = JC
                    CALL INTERP(X1, Y1, X2, Y2, X3, Y3)
                    CALL UMOD(IM1, IM2, JM1, JM2, Y3)
C
                  ELSE IF (NCASE .EQ. 4) THEN
C                 Check for path.
                    X1 = XDOLD
                    X2 = XDNEW
                    X3 = XB(IB + 1)
                    Y1 = YDOLD
                    Y2 = YDNEW
                    CALL INTERP(X1, Y1, X2, Y2, X3, Y3)
```

```
55100                   IF (Y3 .LT. YB(JB)) THEN
55200                     LOWER = 1
55300                   ELSE
55400                     LOWER = 0
55500                   ENDIF
55600     C           U-cell vertical boundary.
55700                   Y1 = UOOLD
55800                   Y2 = UONEW
55900                   IM1 = IU + 1
56000                   IM2 = IU
56100                   IF (LOWER .EQ. 1) THEN
56200                     JM1 = JU - 1
56300                     JM2 = JU - 1
56400                   ELSE
56500                     JM1 = JU
56600                     JM2 = JU
56700                   ENDIF
56800                   CALL INTERP(X1, Y1, X2, Y2, X3, Y3)
56900                   CALL UMOD(IM1, IM2, JM1, JM2, Y3)
57000     C           C-cell horizontal boundary.
57100                   X1 = YOOLD
57200                   X2 = YONEW
57300                   X3 = YB(JB)
57400                   Y1 = TOOLD
57500                   Y2 = TONEW
57600                   IM1 = IC
57700                   IM2 = IC
57800                   JM1 = JC - 1
57900                   JM2 = JC
58000                   CALL INTERP(X1, Y1, X2, Y2, X3, Y3)
58100                   CALL CMOD(IM1, IM2, JM1, JM2, Y3)
58200     C           U-cell horizontal boundary.
58300                   Y1 = UOOLD
58400                   Y2 = UONEW
58500                   IF (LOWER .EQ. 1) THEN
58600                     IM1 = IU
58700                     IM2 = IU
58800                   ELSE
58900                     IM1 = IU + 1
59000                     IM2 = IU + 1
59100                   ENDIF
59200                   JM1 = JU - 1
59300                   JM2 = JU
59400                   CALL INTERP(X1, Y1, X2, Y2, X3, Y3)
59500                   CALL UMOD(IM1, IM2, JM1, JM2, Y3)
59600     C
59700                 ELSE IF (NCASE .EQ. 5) THEN
59800     C           U-cell vertical boundary.
59900                   X1 = XOOLD
60000                   X2 = XONEW
60100                   X3 = XB(IB + 1)
60200                   Y1 = UOOLD
60300                   Y2 = UONEW
60400                   IM1 = IU + 1
60500                   IM2 = IU
60600                   JM1 = JU
60700                   JM2 = JU
60800                   CALL INTERP(X1, Y1, X2, Y2, X3, Y3)
60900                   CALL UMOD(IM1, IM2, JM1, JM2, Y3)
61000     C
61100                 ELSE IF (NCASE .EQ. 6) THEN
```

```
61200    C          U-cell vertical boundary.
61300                   X1 = XOOLD
61400                   X2 = XONEW
61500                   X3 = XB(IB + 1)
61600                   Y1 = UOOLD
61700                   Y2 = UONEW
61800                   IM1 = IU + 1
61900                   IM2 = IU
62000                   JM1 = JU
62100                   JM2 = JU
62200                   CALL INTERP(X1, Y1, X2, Y2, X3, Y3)
62300                   CALL UMOD(IM1, IM2, JM1, JM2, Y3)
62400    C          V-cell horizontal boundary.
62500                   X1 = YOOLD
62600                   X2 = YONEW
62700                   X3 = YB(JB + 1)
62800                   Y1 = VOOLD
62900                   Y2 = VONEW
63000                   IM1 = IV
63100                   IM2 = IV
63200                   JM1 = JV + 1
63300                   JM2 = JV
63400                   CALL INTERP(X1, Y1, X2, Y2, X3, Y3)
63500                   CALL VMOD(IM1, IM2, JM1, JM2, Y3)
63600    C
63700    C
63800                 ELSE IF (NCASE .EQ. 7) THEN
63900    C          V-cell horizontal boundary.
64000                   X1 = YOOLD
64100                   X2 = YONEW
64200                   X3 = YB(JB + 1)
64300                   Y1 = VOOLD
64400                   Y2 = VONEW
64500                   IM1 = IV
64600                   IM2 = IV
64700                   JM1 = JV + 1
64800                   JM2 = JV
64900                   CALL INTERP(X1, Y1, X2, Y2, X3, Y3)
65000                   CALL VMOD(IM1, IM2, JM1, JM2, Y3)
65100    C
65200                 ELSE IF (NCASE .EQ. 8) THEN
65300    C          Check for path.
65400                   X1 = XOOLD
65500                   X2 = XONEW
65600                   X3 = XB(IB)
65700                   Y1 = YOOLD
65800                   Y2 = YONEW
65900                   CALL INTERP(X1, Y1, X2, Y2, X3, Y3)
66000                   IF (Y3 .LT. YB(JB + 1)) THEN
66100                     LOWER = 1
66200                   ELSE
66300                     LOWER = 0
66400                   ENDIF
66500    C          C-cell vertical boundary.
66600                   Y1 = TOOLD
66700                   Y2 = TONEW
66800                   IM1 = IC - 1
66900                   IM2 = IC
67000                   JM1 = JC
67100                   JM2 = JC
67200                   CALL INTERP(X1, Y1, X2, Y2, X3, Y3)
```

```
67300                   CALL CMOD(IM1, IM2, JM1, JM2, Y3)
67400     C           V-cell vertical boundary.
67500                   Y1 = VDOLD
67600                   Y2 = VDNEW
67700                   IM1 = IV - 1
67800                   IM2 = IV
67900                   IF (LOWER .EQ. 1) THEN
68000                     JM1 = JV
68100                     JM2 = JV
68200                   ELSE
68300                     JM1 = JV + 1
68400                     JM2 = JV + 1
68500                   ENDIF
68600                   CALL INTERP(X1, Y1, X2, Y2, X3, Y3)
68700                   CALL VMOD(IM1, IM2, JM1, JM2, Y3)
68800     C           V-cell horizontal boundary.
68900                   X1 = YDOLD
69000                   X2 = YDNEW
69100                   X3 = YB(JB + 1)
69200                   IF (LOWER .EQ. 1) THEN
69300                     IM1 = IV - 1
69400                     IM2 = IV - 1
69500                   ELSE
69600                     IM1 = IV
69700                     IM2 = IV
69800                   ENDIF
69900                   JM1 = JV + 1
70000                   JM2 = JV
70100                   CALL INTERP(X1, Y1, X2, Y2, X3, Y3)
70200                   CALL VMOD(IM1, IM2, JM1, JM2, Y3)
70300                 ENDIF
70400     C
70500               ELSE IF (MCASE .EQ. 2) THEN
70600                 IF (NCASE .EQ. 1) THEN
70700     C           U-cell vertical boundary.
70800                   X1 = XDOLD
70900                   X2 = XDNEW
71000                   X3 = XB(IB)
71100                   Y1 = UDOLD
71200                   Y2 = UDNEW
71300                   IM1 = IU - 1
71400                   IM2 = IU
71500                   JM1 = JU
71600                   JM2 = JU
71700                   CALL INTERP(X1, Y1, X2, Y2, X3, Y3)
71800                   CALL UMOD(IM1, IM2, JM1, JM2, Y3)
71900     C
72000                 ELSE IF (NCASE .EQ. 2) THEN
72100     C           Check for path.
72200                   X1 = XDOLD
72300                   X2 = XDNEW
72400                   X3 = XB(IB)
72500                   Y1 = YDOLD
72600                   Y2 = YDNEW
72700                   CALL INTERP(X1, Y1, X2, Y2, X3, Y3)
72800                   IF (Y3 .LT. YB(JB)) THEN
72900                     LOWER = 1
73000                   ELSE
73100                     LOWER = 0
73200                   ENDIF
73300     C           U-cell vertical boundary.
```

```
73400                     Y1 = UDOLD
73500                     Y2 = UDNEW
73600                     IM1 = IU - 1
73700                     IM2 = IU
73800                     IF (LOWER .EQ. 1) THEN
73900                       JM1 = JU - 1
74000                       JM2 = JU - 1
74100                     ELSE
74200                       JM1 = JU
74300                       JM2 = JU
74400                     ENDIF
74500                     CALL INTERP(X1, Y1, X2, Y2, X3, Y3)
74600                     CALL UMOD(IM1, IM2, JM1, JM2, Y3)
74700     C             C-cell horizontal boundary.
74800                     X1 = YDOLD
74900                     X2 = YDNEW
75000                     X3 = Y6(JB)
75100                     Y1 = TDOLD
75200                     Y2 = TDNEW
75300                     IM1 = IC
75400                     IM2 = IC
75500                     JM1 = JC - 1
75600                     JM2 = JC
75700                     CALL INTERP(X1, Y1, X2, Y2, X3, Y3)
75800                     CALL CMOD(IM1, IM2, JM1, JM2, Y3)
75900     C             U-cell horizontal boundary.
76000                     Y1 = UDOLD
76100                     Y2 = UDNEW
76200                     IF (LOWER .EQ. 1) THEN
76300                       IM1 = IU
76400                       IM2 = IU
76500                     ELSE
76600                       IM1 = IU - 1
76700                       IM2 = IU - 1
76800                     ENDIF
76900                     JM1 = JC - 1
77000                     JM2 = JC
77100                     CALL INTERP(X1, Y1, X2, Y2, X3, Y3)
77200                     CALL UMOD(IM1, IM2, JM1, JM2, Y3)
77300     C
77400                   ELSE IF (NCASE .EQ. 3) THEN
77500     C             C-cell horizontal boundary.
77600                     X1 = YDOLD
77700                     X2 = YDNEW
77800                     X3 = Y6(JB)
77900                     Y1 = TDOLD
78000                     Y2 = TDNEW
78100                     IM1 = IC
78200                     IM2 = IC
78300                     JM1 = JC - 1
78400                     JM2 = JC
78500                     CALL INTERP(X1, Y1, X2, Y2, X3, Y3)
78600                     CALL CMOD(IM1, IM2, JM1, JM2, Y3)
78700     C             U-cell horizontal boundary.
78800                     Y1 = UDOLD
78900                     Y2 = UDNEW
79000                     IM1 = IC
79100                     IM2 = IC
79200                     JM1 = JC - 1
79300                     JM2 = JC
79400                     CALL INTERP(X1, Y1, X2, Y2, X3, Y3)
```

```
795 00                    CALL UMOD(IM1, IM2, JM1, JM2, Y3)
796 00    C
797 00                  ELSE IF (NCASE .EQ. 4) THEN
798 00    C           Check for path.
799 00                    X1 = XOOLD
800 00                    X2 = XONEW
801 00                    X3 = XB(IB + 1)
802 00                    Y1 = YOOLD
803 00                    Y2 = YONEW
804 00                    CALL INTERP(X1, Y1, X2, Y2, X3, Y3)
805 00                    IF (Y3 .LT. YB(JB)) THEN
806 00                      LOWER = 1
807 00                    ELSE
808 00                      LOWER = 0
809 00                    ENDIF
810 00    C           C-cell vertical boundary.
811 00                    Y1 = TOOLD
812 00                    Y2 = TONEW
813 00                    IM1 = IC + 1
814 00                    IM2 = IC
815 00                    IF (LOWER .EQ. 1) THEN
816 00                      JM1 = JC - 1
817 00                      JM2 = JC - 1
818 00                    ELSE
819 00                      JM1 = JC
820 00                      JM2 = JC
821 00                    ENDIF
822 00                    CALL INTERP(X1, Y1, X2, Y2, X3, Y3)
823 00                    CALL CMOD(IM1, IM2, JM1, JM2, Y3)
824 00    C           V-cell vertical boundary.
825 00                    Y1 = VOOLD
826 00                    Y2 = VONEW
827 00                    IM1 = IV + 1
828 00                    IM2 = IV
829 00                    JM1 = JV
830 00                    JM2 = JV
831 00                    CALL INTERP(X1, Y1, X2, Y2, X3, Y3)
832 00                    CALL VMOD(IM1, IM2, JM1, JM2, Y3)
833 00    C           C-cell horizontal boundary.
834 00                    X1 = YOOLD
835 00                    X2 = YONEW
836 00                    X3 = YB(JB)
837 00                    Y1 = TOOLD
838 00                    Y2 = TONEW
839 00                    IF (LOWER .EQ. 1) THEN
840 00                      IM1 = IC
841 00                      IM2 = IC
842 00                    ELSE
843 00                      IM1 = IC + 1
844 00                      IM2 = IC + 1
845 00                    ENDIF
846 00                    JM1 = JC - 1
847 00                    JM2 = JC
848 00                    CALL INTERP(X1, Y1, X2, Y2, X3, Y3)
849 00                    CALL CMOD(IM1, IM2, JM1, JM2, Y3)
850 00    C           U-cell horizontal boundary.
851 00                    Y1 = UOOLD
852 00                    Y2 = UONEW
853 00                    IM1 = IU
854 00                    IM2 = IU
855 00                    JM1 = JU - 1
```

```
                    JM2 = JU
                    CALL INTERP(X1, Y1, X2, Y2, X3, Y3)
                    CALL UMOD(IM1, IM2, JM1, JM2, Y3)
C
                  ELSE IF (NCASE .EQ. 5) THEN
C           C-cell vertical boundary.
                    X1 = XDOLD
                    X2 = XDNEW
                    X3 = XB(IB + 1)
                    Y1 = TDOLD
                    Y2 = TDNEW
                    IM1 = IC + 1
                    IM2 = IC
                    JM1 = JC
                    JM2 = JC
                    CALL INTERP(X1, Y1, X2, Y2, X3, Y3)
                    CALL CMOD(IM1, IM2, JM1, JM2, Y3)
C           V-cell vertical boundary.
                    Y1 = VDOLD
                    Y2 = VDNEW
                    IM1 = IV + 1
                    IM2 = IV
                    JM1 = JV
                    JM2 = JV
                    CALL INTERP(X1, Y1, X2, Y2, X3, Y3)
                    CALL VMOD(IM1, IM2, JM1, JM2, Y3)
C
                  ELSE IF (NCASE .EQ. 6) THEN
C           Check for path.
                    X1 = XDOLD
                    X2 = XDNEW
                    X3 = XB(IB + 1)
                    Y1 = YDOLD
                    Y2 = YDNEW
                    CALL INTERP(X1, Y1, X2, Y2, X3, Y3)
                    IF (Y3 .LT. YB(JB + 1)) THEN
                      LOWER = 1
                    ELSE
                      LOWER = 0
                    ENDIF
C           C-cell vertical boundary.
                    Y1 = TDOLD
                    Y2 = TDNEW
                    IM1 = IC + 1
                    IM2 = IC
                    JM1 = JC
                    JM2 = JC
                    CALL INTERP(X1, Y1, X2, Y2, X3, Y3)
                    CALL CMOD(IM1, IM2, JM1, JM2, Y3)
C           V-cell vertical boundary.
                    Y1 = VDOLD
                    Y2 = VDNEW
                    IM1 = IV + 1
                    IM2 = IV
                    IF (LOWER .EQ. 1) THEN
                      JM1 = JV
                      JM2 = JV
                    ELSE
                      JM1 = JV + 1
                      JM2 = JV + 1
                    ENDIF
```

```
91700                   CALL INTERP(X1, Y1, X2, Y2, X3, Y3)
91800                   CALL VMOD(IM1, IM2, JM1, JM2, Y3)
91900     C           V-cell horizontal boundary.
92000                   X1 = YOOLD
92100                   X2 = YONEW
92200                   X3 = YB(JB + 1)
92300                   IF (LOWER .EQ. 1) THEN
92400                     IM1 = IV + 1
92500                     IM2 = IV + 1
92600                   ELSE
92700                     IM1 = IV
92800                     IM2 = IV
92900                   ENDIF
93000                   JM1 = JV + 1
93100                   JM2 = JV
93200                   CALL INTERP(X1, Y1, X2, Y2, X3, Y3)
93300                   CALL VMOD(IM1, IM2, JM1, JM2, Y3)
93400     C
93500                 ELSE IF (NCASE .EQ. 7) THEN
93600     C           V-cell horizontal boundary.
93700                   X1 = YOOLD
93800                   X2 = YONEW
93900                   X3 = YB(JB + 1)
94000                   Y1 = VOOLD
94100                   Y2 = VONEW
94200                   IM1 = IV
94300                   IM2 = IV
94400                   JM1 = JV + 1
94500                   JM2 = JV
94600                   CALL INTERP(X1, Y1, X2, Y2, X3, Y3)
94700                   CALL VMOD(IM1, IM2, JM1, JM2, Y3)
94800     C
94900                 ELSE IF (NCASE .EQ. 6) THEN
95000     C           U-cell vertical boundary.
95100                   X1 = XOOLD
95200                   X2 = XONEW
95300                   X3 = XB(IB)
95400                   Y1 = UOOLD
95500                   Y2 = UONEW
95600                   IM1 = IU - 1
95700                   IM2 = IU
95800                   JM1 = JU
95900                   JM2 = JU
96000                   CALL INTERP(X1, Y1, X2, Y2, X3, Y3)
96100                   CALL VMOD(IM1, IM2, JM1, JM2, Y3)
96200     C           V-cell horizontal boundary.
96300                   X1 = YOOLD
96400                   X2 = YONEW
96500                   X3 = YB(JB + 1)
96600                   Y1 = VOOLD
96700                   Y2 = VONEW
96800                   IM1 = IV
96900                   IM2 = IV
97000                   JM1 = JV + 1
97100                   JM2 = JV
97200                   CALL INTERP(X1, Y1, X2, Y2, X3, Y3)
97300                   CALL VMOD(IM1, IM2, JM1, JM2, Y3)
97400                 ENDIF
97500     C
97600               ELSE IF (MCASE .EQ. 3) THEN
97700                 IF (NCASE .EQ. 1) THEN
```

```
97800    C          U-cell vertical boundary.
97900                   X1 = XOOLD
98000                   X2 = XONEW
98100                   X3 = XB(IB)
98200                   Y1 = UOOLD
98300                   Y2 = UONEW
98400                   IM1 = IU - 1
98500                   IM2 = IU
98600                   JM1 = JU
98700                   JM2 = JU
98800                   CALL INTERP(X1, Y1, X2, Y2, X3, Y3)
98900                   CALL UMOD(IM1, IM2, JM1, JM2, Y3)
99000    C
99100                 ELSE IF (NCASE .EQ. 2) THEN
99200    C          V-cell vertical boundary.
99300                   X1 = XOOLD
99400                   X2 = XONEW
99500                   X3 = XB(IB)
99600                   Y1 = UOOLD
99700                   Y2 = UONEW
99800                   IM1 = IU - 1
99900                   IM2 = IU
```

```
00100                     JM1 = JC
00200                     JM2 = JD
00300                     CALL INTERP(X1, Y1, X2, Y2, X3, Y3)
00400                     CALL CMOD(IM1, IM2, JM1, JM2, Y3)
00500     C           V-cell horizontal boundary.
00600                     X1 = XOOLD
00700                     X2 = XONEW
00800                     X3 = XB(IB)
00900                     Y1 = VOOLD
01000                     Y2 = VONEW
01100                     IM1 = IV
01200                     IM2 = IV
01300                     JM1 = JV - 1
01400                     JM2 = JV
01500                     CALL INTERP(X1, Y1, X2, Y2, X3, Y3)
01600                     CALL VMOD(IM1, IM2, JM1, JM2, Y3)
01700     C
01800                   ELSE IF (NCASE .EQ. 3) THEN
01900     C           V-cell horizontal boundary.
02000                     X1 = XOOLD
02100                     X2 = XONEW
02200                     X3 = XB(IB)
02300                     Y1 = VOOLD
02400                     Y2 = VONEW
02500                     IM1 = IV
02600                     IM2 = IV
02700                     JM1 = JV - 1
02800                     JM2 = JV
02900                     CALL INTERP(X1, Y1, X2, Y2, X3, Y3)
03000                     CALL VMOD(IM1, IM2, JM1, JM2, Y3)
03100     C
03200                   ELSE IF (NCASE .EQ. 4) THEN
03300     C           Check for path.
03400                     X1 = XOOLD
03500                     X2 = XONEW
03600                     X3 = XB(IB + 1)
03700                     Y1 = YOOLD
03800                     Y2 = YONEW
03900                     CALL INTERP(X1, Y1, X2, Y2, X3, Y3)
04000                     IF (Y3 .LT. YB(JB)) THEN
04100                       LOWER = 1
04200                     ELSE
04300                       LOWER = 0
04400                     ENDIF
04500     C           C-cell vertical boundary.
04600                     Y1 = TOOLD
04700                     Y2 = TONEW
04800                     IM1 = IC + 1
04900                     IM2 = IC
05000                     JM1 = JC
05100                     JM2 = JC
05200                     CALL INTERP(X1, Y1, X2, Y2, X3, Y3)
05300                     CALL CMOD(IM1, IM2, JM1, JM2, Y3)
05400     C           V-cell vertical boundary.
05500                     Y1 = VOOLD
05600                     Y2 = VONEW
05700                     IM1 = IV + 1
05800                     IM2 = IV
05900                     IF (LOWER .EQ. 1) THEN
06000                       JM1 = JV - 1
06100                       JM2 = JV - 1
```

```
062 00                    ELSE
063 00                      JM1 = JV
064 00                      JM2 = JV
065 00                    ENDIF
066 00                    CALL INTERP(X1, Y1, X2, Y2, X3, Y3)
067 00                    CALL VMOD(IM1, IM2, JM1, JM2, Y3)
068 00    C           V-cell horizontal boundary.
069 00                    X1 = YOOLD
070 00                    X2 = YONEW
071 00                    X3 = YB(JB)
072 00                    IF (LOWER .EQ. 1) THEN
073 00                      IM1 = IV
074 00                      IM2 = IV
075 00                    ELSE
076 00                      IM1 = IV + 1
077 00                      IM2 = IV + 1
078 00                    ENDIF
079 00                    JM1 = JV - 1
080 00                    JM2 = JV
081 00                    CALL INTERP(X1, Y1, X2, Y2, X3, Y3)
082 00                    CALL VMOD(IM1, IM2, JM1, JM2, Y3)
083 00    C
084 00                  ELSE IF (NCASE .EQ. 5) THEN
085 00    C           C-cell vertical boundary.
086 00                    X1 = XOOLD
087 00                    X2 = XONEW
088 00                    X3 = XB(IB + 1)
089 00                    Y1 = TOOLD
090 00                    Y2 = TONEW
091 00                    IM1 = IC + 1
092 00                    IM2 = IC
093 00                    JM1 = JC
094 00                    JM2 = JC
095 00                    CALL INTERP(X1, Y1, X2, Y2, X3, Y3)
096 00                    CALL CMOD(IM1, IM2, JM1, JM2, Y3)
097 00    C           V-cell vertical boundary.
098 00                    Y1 = VOOLD
099 00                    Y2 = VONEW
100 00                    IM1 = IV + 1
101 00                    IM2 = IV
102 00                    JM1 = JV
103 00                    JM2 = JV
104 00                    CALL INTERP(X1, Y1, X2, Y2, X3, Y3)
105 00                    CALL VMOD(IM1, IM2, JM1, JM2, Y3)
106 00    C
107 00                  ELSE IF (NCASE .EQ. 6) THEN
108 00    C           Check for path.
109 00                    X1 = XOOLD
110 00                    X2 = XONEW
111 00                    X3 = XB(IB + 1)
112 00                    Y1 = YOOLD
113 00                    Y2 = YONEW
114 00                    CALL INTERP(X1, Y1, X2, Y2, X3, Y3)
115 00                    IF (Y3 .LT. YB(JB + 1)) THEN
116 00                      LOWER = 1
117 00                    ELSE
118 00                      LOWER = 0
119 00                    ENDIF
120 00    C           C-cell vertical boundary.
121 00                    Y1 = TOOLD
122 00                    Y2 = TONEW
```

```
12300                   IM1 = IC + 1
12400                   IM2 = IC
12500                   IF (LOWER .EQ. 1) THEN
12600                     JM1 = JC
12700                     JM2 = JC
12800                   ELSE
12900                     JM1 = JC + 1
13000                     JM2 = JC + 1
13100                   ENDIF
13200                   CALL INTERP(X1, Y1, X2, Y2, X3, Y3)
13300                   CALL CMOD(IM1, IM2, JM1, JM2, Y3)
13400     C           V-cell vertical boundary.
13500                   Y1 = VOOLD
13600                   Y2 = VONEW
13700                   IM1 = IV + 1
13800                   IM2 = IV
13900                   JM1 = JV
14000                   JM2 = JV
14100                   CALL INTERP(X1, Y1, X2, Y2, X3, Y3)
14200                   CALL VMOD(IM1, IM2, JM1, JM2, Y3)
14300     C           U-cell horizontal boundary.
14400                   X1 = XOOLD
14500                   X2 = XONEW
14600                   X3 = XB(JB + 1)
14700                   Y1 = TOOLD
14800                   Y2 = TONEW
14900                   IF (LOWER .EQ. 1) THEN
15000                     IM1 = IC + 1
15100                     IM2 = IC + 1
15200                   ELSE
15300                     IM1 = IC
15400                     IM2 = IC
15500                   ENDIF
15600                   JM1 = JC + 1
15700                   JM2 = JC
15800                   CALL INTERP(X1, Y1, X2, Y2, X3, Y3)
15900                   CALL CMOD(IM1, IM2, JM1, JM2, Y3)
16000     C           U-cell horizontal boundary.
16100                   Y1 = UOOLD
16200                   Y2 = UONEW
16300                   IM1 = IU
16400                   IM2 = IU
16500                   JM1 = JU + 1
16600                   JM2 = JU
16700                   CALL INTERP(X1, Y1, X2, Y2, X3, Y3)
16800                   CALL CMOD(IM1, IM2, JM1, JM2, Y3)
16900     C
17000                 ELSE IF (NCASE .EQ. 7) THEN
17100     C           U-cell horizontal boundary.
17200                   X1 = XOOLD
17300                   X2 = XONEW
17400                   X3 = XB(JB + 1)
17500                   Y1 = TOOLD
17600                   Y2 = TONEW
17700                   IM1 = IC
17800                   IM2 = IC
17900                   JM1 = JC + 1
18000                   JM2 = JC
18100                   CALL INTERP(X1, Y1, X2, Y2, X3, Y3)
18200                   CALL CMOD(IM1, IM2, JM1, JM2, Y3)
18300     C           U-cell horizontal boundary.
```

```
18400                   Y1 = UDOLD
18500                   Y2 = UDNEW
18600                   IM1 = IU
18700                   IM2 = IU
18800                   JM1 = JU + 1
18900                   JM2 = JU
19000                   CALL INTERP(X1, Y1, X2, Y2, X3, Y3)
19100                   CALL UMOD(IM1, IM2, JM1, JM2, Y3)
19200     C
19300                 ELSE IF (NCASE .EQ. 8) THEN
19400     C           Check for path.
19500                   X1 = XDOLD
19600                   X2 = XDNEW
19700                   X3 = XB(IB)
19800                   Y1 = YDOLD
19900                   Y2 = YDNEW
20000                   CALL INTERP(X1, Y1, X2, Y2, X3, Y3)
20100                   IF (Y3 .LT. YB(JB + 1)) THEN
20200                     LOWER = 1
20300                   ELSE
20400                     LOWER = 0
20500                   ENDIF
20600     C           U-cell vertical boundary.
20700                   Y1 = UDOLD
20800                   Y2 = UDNEW
20900                   IM1 = IU - 1
21000                   IM2 = IU
21100                   IF (LOWER .EQ. 1) THEN
21200                     JM1 = JU
21300                     JM2 = JU
21400                   ELSE
21500                     JM1 = JU + 1
21600                     JM2 = JU + 1
21700                   ENDIF
21800                   CALL INTERP(X1, Y1, X2, Y2, X3, Y3)
21900                   CALL UMOD(IM1, IM2, JM1, JM2, Y3)
22000     C           D-cell horizontal boundary.
22100                   X1 = YDOLD
22200                   X2 = YDNEW
22300                   X3 = YB(JB + 1)
22400                   Y1 = TDOLD
22500                   Y2 = TDNEW
22600                   IM1 = IC
22700                   IM2 = IC
22800                   JM1 = JC + 1
22900                   JM2 = JC
23000                   CALL INTERP(X1, Y1, X2, Y2, X3, Y3)
23100                   CALL DMOD(IM1, IM2, JM1, JM2, Y3)
23200     C           U-cell horizontal boundary.
23300                   Y1 = UDOLD
23400                   Y2 = UDNEW
23500                   IF (LOWER .EQ. 1) THEN
23600                     IM1 = IU - 1
23700                     IM2 = IU - 1
23800                   ELSE
23900                     IM1 = IU
24000                     IM2 = IU
24100                   ENDIF
24200                   JM1 = JU + 1
24300                   JM2 = JU
24400                   CALL INTERP(X1, Y1, X2, Y2, X3, Y3)
```

```
24500                     CALL UMOD(IM1, IM2, JM1, JM2, Y3)
24600                   ENDIF
24700     C
24800                 ELSE IF (MCASE .EQ. 4) THEN
24900                   IF (MCASE .EQ. 1) THEN
25000     C             C-cell vertical boundary.
25100                     X1 = XOOLD
25200                     X2 = XONEW
25300                     X3 = XP(IP)
25400                     Y1 = YOOLD
25500                     Y2 = YONEW
25600                     IM1 = IC - 1
25700                     IM2 = IC
25800                     JM1 = JC
25900                     JM2 = JC
26000                     CALL INTERP(X1, Y1, X2, Y2, X3, Y3)
26100                     CALL CMOD(IM1, IM2, JM1, JM2, Y3)
26200     C             V-cell vertical boundary.
26300                     Y1 = VOOLD
26400                     Y2 = VONEW
26500                     IM1 = IV - 1
26600                     IM2 = IV
26700                     JM1 = JV
26800                     JM2 = JV
26900                     CALL INTERP(X1, Y1, X2, Y2, X3, Y3)
27000                     CALL VMOD(IM1, IM2, JM1, JM2, Y3)
27100     C
27200                   ELSE IF (MCASE .EQ. 2) THEN
27300     C             Check for path.
27400                     X1 = XOOLD
27500                     X2 = XONEW
27600                     X3 = XP(IP)
27700                     Y1 = YOOLD
27800                     Y2 = YONEW
27900                     CALL INTERP(X1, Y1, X2, Y2, X3, Y3)
28000                     IF (Y3 .LT. YB(JF)) THEN
28100                       LOWER = 1
28200                     ELSE
28300                       LOWER = 0
28400                     ENDIF
28500     C             C-cell vertical boundary.
28600                     Y1 = YOOLD
28700                     Y2 = YONEW
28800                     IM1 = IC - 1
28900                     IM2 = IC
29000                     JM1 = JC
29100                     JM2 = JC
29200                     CALL INTERP(X1, Y1, X2, Y2, X3, Y3)
29300                     CALL CMOD(IM1, IM2, JM1, JM2, Y3)
29400     C             V-cell vertical boundary.
29500                     Y1 = VOOLD
29600                     Y2 = VONEW
29700                     IM1 = IV - 1
29800                     IM2 = IV
29900                     IF (LOWER .EQ. 1) THEN
30000                       JM1 = JV - 1
30100                       JM2 = JV - 1
30200                     ELSE
30300                       JM1 = JV
30400                       JM2 = JV
30500                     ENDIF
```

```
30600                 CALL INTERP(X1, Y1, X2, Y2, X3, Y3)
30700                 CALL VMOD(IM1, IM2, JM1, JM2, Y3)
30800     C         V-cell horizontal boundary.
30900                 X1 = YOOLD
31000                 X2 = YONEW
31100                 X3 = YB(JB)
31200                 IF (LOWER .EQ. 1) THEN
31300                   IM1 = IV
31400                   IM2 = IV
31500                 ELSE
31600                   IM1 = IV - 1
31700                   IM2 = IV - 1
31800                 ENDIF
31900                 JM1 = JV - 1
32000                 JM2 = JV
32100                 CALL INTERP(X1, Y1, X2, Y2, X3, Y3)
32200                 CALL VMOD(IM1, IM2, JM1, JM2, Y3)
32300     C
32400               ELSE IF (NCASE .EQ. 3) THEN
32500     C         U-cell horizontal boundary.
32600                 X1 = YOOLD
32700                 X2 = YONEW
32800                 X3 = YB(JB)
32900                 Y1 = VOOLD
33000                 Y2 = VONEW
33100                 IM1 = IV
33200                 IM2 = IV
33300                 JM1 = JV - 1
33400                 JM2 = JV
33500                 CALL INTERP(X1, Y1, X2, Y2, X3, Y3)
33600                 CALL VMOD(IM1, IM2, JM1, JM2, Y3)
33700     C
33800               ELSE IF (NCASE .EQ. 4) THEN
33900     C         U-cell vertical boundary.
34000                 X1 = XOOLD
34100                 X2 = XONEW
34200                 X3 = XB(IB + 1)
34300                 Y1 = UOOLD
34400                 Y2 = UONEW
34500                 IM1 = IU + 1
34600                 IM2 = IU
34700                 JM1 = JU
34800                 JM2 = JU
34900                 CALL INTERP(X1, Y1, X2, Y2, X3, Y3)
35000                 CALL UMOD(IM1, IM2, JM1, JM2, Y3)
35100     C         V-cell horizontal boundary.
35200                 X1 = YOOLD
35300                 X2 = YONEW
35400                 X3 = YB(JB)
35500                 Y1 = VOOLD
35600                 Y2 = VONEW
35700                 IM1 = IV
35800                 IM2 = IV
35900                 JM1 = JV - 1
36000                 JM2 = JV
36100                 CALL INTERP(X1, Y1, X2, Y2, X3, Y3)
36200                 CALL VMOD(IM1, IM2, JM1, JM2, Y3)
36300     C
36400               ELSE IF (NCASE .EQ. 5) THEN
36500     C         U-cell vertical boundary.
36600                 X1 = XOOLD
```

```
36700                   X2 = XONEW
36800                   X3 = XB(IB + 1)
36900                   Y1 = UOOLD
37000                   Y2 = UONEW
37100                   IM1 = IC + 1
37200                   IM2 = IC
37300                   JM1 = JU
37400                   JM2 = JU
37500                   CALL INTERP(X1, Y1, X2, Y2, X3, Y3)
37600                   CALL UMOD(IM1, IM2, JM1, JM2, Y3)
37700                 ELSE IF (NCASE .EQ. 6) THEN
37800     C           Check for path.
37900                   X1 = XOOLD
38000                   X2 = XONEW
38100                   X3 = XB(IB + 1)
38200                   Y1 = YOOLD
38300                   Y2 = YONEW
38400                   CALL INTERP(X1, Y1, X2, Y2, X3, Y3)
38500                   IF (Y3 .LT. YB(JB + 1)) THEN
38600                     LOWER = 1
38700                   ELSE
38800                     LOWER = 0
38900                   ENDIF
39000     C           U-cell vertical boundary.
39100                   Y1 = UOOLD
39200                   Y2 = UONEW
39300                   IM1 = IC + 1
39400                   IM2 = IC
39500                   IF (LOWER .EQ. 1) THEN
39600                     JM1 = JC
39700                     JM2 = JC
39800                   ELSE
39900                     JM1 = JC + 1
40000                     JM2 = JC + 1
40100                   ENDIF
40200                   CALL INTERP(X1, Y1, X2, Y2, X3, Y3)
40300                   CALL UMOD(IM1, IM2, JM1, JM2, Y3)
40400     C           C-cell horizontal boundary.
40500                   X1 = YOOLD
40600                   X2 = YONEW
40700                   X3 = YB(JB + 1)
40800                   Y1 = TOOLD
40900                   Y2 = TONEW
41000                   IM1 = IC
41100                   IM2 = IC
41200                   JM1 = JC + 1
41300                   JM2 = JC
41400                   CALL INTERP(X1, Y1, X2, Y2, X3, Y3)
41500                   CALL CMOD(IM1, IM2, JM1, JM2, Y3)
41600     C           U-cell horizontal boundary.
41700                   Y1 = UOOLD
41800                   Y2 = UONEW
41900                   IF (LOWER .EQ. 1) THEN
42000                     IM1 = IU + 1
42100                     IM2 = IU + 1
42200                   ELSE
42300                     IM1 = IU
42400                     IM2 = IU
42500                   ENDIF
42600                   JM1 = JC + 1
42700                   JM2 = JC
```

```
42800                   CALL INTERP(X1, Y1, X2, Y2, X3, Y3)
42900                   CALL UMOD(IM1, IM2, JM1, JM2, Y3)
43000     C
43100                 ELSE IF (NCASE .EQ. 7) THEN
43200     C           C-cell horizontal boundary.
43300                   X1 = YOOLD
43400                   X2 = YONEW
43500                   X3 = YB(JB + 1)
43600                   Y1 = TOOLD
43700                   Y2 = TONEW
43800                   IM1 = IC
43900                   IM2 = IC
44000                   JM1 = JC + 1
44100                   JM2 = JC
44200                   CALL INTERP(X1, Y1, X2, Y2, X3, Y3)
44300                   CALL CMOD(IM1, IM2, JM1, JM2, Y3)
44400     C           U-cell horizontal boundary.
44500                   Y1 = UOOLD
44600                   Y2 = UONEW
44700                   IM1 = IU
44800                   IM2 = IU
44900                   JM1 = JU + 1
45000                   JM2 = JU
45100                   CALL INTERP(X1, Y1, X2, Y2, X3, Y3)
45200                   CALL UMOD(IM1, IM2, JM1, JM2, Y3)
45300     C
45400                 ELSE IF (NCASE .EQ. 8) THEN
45500     C           Check for path.
45600                   X1 = XOOLD
45700                   X2 = XONEW
45800                   X3 = XB(IB)
45900                   Y1 = YOOLD
46000                   Y2 = YONEW
46100                   CALL INTERP(X1, Y1, X2, Y2, X3, Y3)
46200                   IF (Y3 .LT. YB(JB + 1)) THEN
46300                     LOWER = 1
46400                   ELSE
46500                     LOWER = 0
46600                   ENDIF
46700     C           C-cell vertical boundary.
46800                   Y1 = TOOLD
46900                   Y2 = TONEW
47000                   IM1 = IC - 1
47100                   IM2 = IC
47200                   IF (LOWER .EQ. 1) THEN
47300                     JM1 = JC
47400                     JM2 = JC
47500                   ELSE
47600                     JM1 = JC + 1
47700                     JM2 = JC + 1
47800                   ENDIF
47900                   CALL INTERP(X1, Y1, X2, Y2, X3, Y3)
48000                   CALL CMOD(IM1, IM2, JM1, JM2, Y3)
48100     C           V-cell vertical boundary.
48200                   Y1 = VOOLD
48300                   Y2 = VONEW
48400                   IM1 = IV - 1
48500                   IM2 = IV
48600                   JM1 = JV
48700                   JM2 = JV
48800                   CALL INTERP(X1, Y1, X2, Y2, X3, Y3)
```

```
48900                     CALL VMOD(IM1, IM2, JM1, JM2, Y3)
49000     C           C-cell horizontal boundary.
49100                     X1 = XOOLD
49200                     X2 = XONEW
49300                     X3 = XB(JB + 1)
49400                     Y1 = TOOLD
49500                     Y2 = TONEW
49600                     IF (LOWER .EQ. 1) THEN
49700                       IM1 = IC - 1
49800                       IM2 = IC - 1
49900                     ELSE
50000                       IM1 = IC
50100                       IM2 = IC
50200                     ENDIF
50300                     JM1 = JC + 1
50400                     JM2 = JC
50500                     CALL INTERP(X1, Y1, X2, Y2, X3, Y3)
50600                     CALL CMOD(IM1, IM2, JM1, JM2, Y3)
50700     C           C-cell horizontal boundary.
50800                     Y1 = COOLD
50900                     Y2 = CONEW
51000                     IM1 = IC
51100                     IM2 = IC
51200                     JM1 = JC + 1
51300                     JM2 = JC
51400                     CALL INTERP(X1, Y1, X2, Y2, X3, Y3)
51500                     CALL CMOD(IM1, IM2, JM1, JM2, Y3)
51600     C
51700                   ENDIF
51800                 ENDIF
51900     C
52000                 IPOLD = IP
52100                 JPOLD = JP
52200                 XOOLD = XONEW
52300                 YOOLD = YONEW
52400                 TOOLD = TONEW
52500                 COOLD = CONEW
52600                 UOOLD = UONEW
52700                 VOOLD = VONEW
52800                 ISTEPS = ISTEPS + 1
52900                 IF (ISTEPS .GT. MAXSTP) THEN
53000                   WRITE(6, *) ' MAX. STEPS EXCEEDED FOR ', NPART
53100                   WRITE(6, *) ' X=', XOOLD, ' Y=', YOOLD, ' ICOUNT=', ICOUNT
53200                 ELSE
53300                   WRITE (22, *) XOOLD, YOOLD
53400                   GOTO 100
53500                 ENDIF
53600     C         Mark the end of path.
53700     900         CONTINUE
53800                 DUMMY = -1.0
53900                 WRITE (22, *) DUMMY
54000     C
54100     C         Re-initialize the source terms for the last cell as the
54200     C         droplet leaves the flow domain.
54300     C
54400                 DELTA = 4.0 * PI * RHOL * RAD ** 3 / 3.0 * DFREQ(NPART)
54500                 RHSMU(IU,JU) = RHSMU(IU,JU) - DELTA * UDIMIT(NPART)
54600                 RHSMV(IV,JV) = RHSMV(IV,JV) - DELTA * VDIMIT(NPART)
54700     C
54800     1000        CONTINUE
54900                 CALL COMPAR
55000     C           Mark the end of file.
```

```
55000            DUMMY = -11.0
55100            WRITE (22, *) DUMMY
55200            CLOSE (UNIT = 22)
55300            RETURN
55400            END
55500      C
55600      C*****************************************************************
55700      C
55800            SUBROUTINE DOMCHK
55900      C     Checks if the DROP is within the finite
56000      C     difference mesh rectangle.
56100      C
56200            COMMON /DROPS/ MAXDR, NDRT,
56300           $  DRDEN(10), DRDIA(10), DRMOST(10), DRFRQ(10),
56400           $  XDINIT(10), YDINIT(10), TDINIT(10), UDINIT(10), VDINIT(10),
56500           $  XB(50), YB(49),
56600           $  UG(49, 24), VG(49, 24), UGOLD(49, 24), VGOLD(49, 24),
56700           $  DDD, GRAVX, GRAVY, RAD, RHOGAS, PI, UGAS, VGAS,
56800           $  XDOLD, YDOLD, TDOLD, UDOLD, VDOLD,
56900           $  XDNEW, YDNEW, TDNEW, UDNEW, VDNEW,
57000           $  DT, DTINC, DTRED, RHOL,
57100           $  ISTEPS, INTCTR, IFLAG2, IHIT, MAXSTP, MAXCT, INTFLG,
57200           $  IC, JC, IV, JV, IU, JU, IR, JR, IROLD, JROLD, ICOUNT,
57300           $  NCASE, MCASE, UDMAX(49), NDI, NDJ
57400      C
57500            IF (XDNEW .GT. XB(2 * (NDI - 1))) THEN
57600              WRITE(6, *) ' DROP OVER-TRAVELLED RIGHT'
57700              IHIT = 1
57800            ELSE IF (XDNEW .LT. XB(2)) THEN
57900              WRITE(6, *) ' REVERSE FLOW AT ENTRANCE'
58000              IHIT = 2
58100            ELSE IF (YDNEW .LT. YB(2)) THEN
58200              WRITE(6, *) ' FLOW CROSSED AXIS'
58300              IHIT = 3
58400            ELSE IF (YDNEW .GT. YB(2 * (NDJ - 1))) THEN
58500              WRITE(6, *) ' DROP OVER-TRAVELLED UP'
58600              IHIT = 4
58700            ELSE
58800              IHIT = 0
58900            ENDIF
59000            RETURN
59100            END
59200      C
59300      C*****************************************************************
59400      C
59500            SUBROUTINE FINDR
59600      C     Finds IR, JR, IC, JC, IU, JU, IV and JV for the
59700      C     new D-cell.
59800      C
59900            COMMON /DROPS/ MAXDR, NDRT,
60000           $  DRDEN(10), DRDIA(10), DRMOST(10), DRFRQ(10),
60100           $  XDINIT(10), YDINIT(10), TDINIT(10), UDINIT(10), VDINIT(10),
60200           $  XB(50), YB(49),
60300           $  UG(49, 24), VG(49, 24), UGOLD(49, 24), VGOLD(49, 24),
60400           $  DDD, GRAVX, GRAVY, RAD, RHOGAS, PI, UGAS, VGAS,
60500           $  XDOLD, YDOLD, TDOLD, UDOLD, VDOLD,
60600           $  XDNEW, YDNEW, TDNEW, UDNEW, VDNEW,
60700           $  DT, DTINC, DTRED, RHOL,
60800           $  ISTEPS, INTCTR, IFLAG2, IHIT, MAXSTP, MAXCT, INTFLG,
60900           $  IC, JC, IV, JV, IU, JU, IR, JR, IROLD, JROLD, ICOUNT,
61000           $  NCASE, MCASE, UDMAX(49), NDI, NDJ
```

```
C
      IM = IMOLD
      JM = JMOLD
100   IF (IM .GE. (I + NOI)) THEN
        WRITE(5, *) 'ERROR: IM OUT OF RANGE', IM
        STOP
      ENDIF
      IF (IM .LE. 0) THEN
        WRITE(5, *) 'ERROR: IM BELOW RANGE', IM
        STOP
      ENDIF
      IF (XNEW .LT. XM(IM)) THEN
        IM = IM - 1
        GOTO 100
      ELSE IF (XNEW .GE. XM(IM + 1)) THEN
        IM = IM + 1
        GOTO 100
      ENDIF
200   IF (JM .GE. (J + NOJ)) THEN
        WRITE(5, *) 'ERROR: JM OUT OF RANGE', JM
        STOP
      ENDIF
      IF (JM .LE. 0) THEN
        WRITE(5, *) 'ERROR: JM BELOW RANGE', JM
        STOP
      ENDIF
      IF (YNEW .LT. YM(JM)) THEN
        JM = JM - 1
        GOTO 200
      ELSE IF (YNEW .GE. YM(JM + 1)) THEN
        JM = JM + 1
        GOTO 200
      ENDIF
      IC = (IM + 2) / 3
      JC = (JM + 2) / 3
      IV = (IM + 3) / 4
      JV = (JM + 3) / 4
      IU = (IM + 2) / 3
      JU = (JM + 3) / 4
      RETURN
      END
C
C*****************************************************************
C
      SUBROUTINE STACHK
C     Checks if the integration step size is in
C     the allowable range, and modifies the step size.
C
      COMMON / BLOCK1/ MAXBLK, NPORT,
     $   DRHOEN(10), DRHOIA(10), DRMOMT(10), DREFRG(10),
     $   XDINIT(10), YDINIT(10), TDINIT(10), UDINIT(10), VDINIT(10),
     $   XM(50), YM(45),
     $   UG(45, 24), VG(45, 24), UGOLD(45, 24), VGOLD(45, 24),
     $   GDD, GRAVX, GRAVY, RAD, RHOGAS, PI, UGAS, VGAS,
     $   XDOLD, YDOLD, TDOLD, UDOLD, VDOLD,
     $   XDNEW, YDNEW, TDNEW, UDNEW, VDNEW,
     $   DT, DTINC, DTREC, RHOL,
     $   ISTEPS, INTCTR, IFLAGZ, IMIT, MAXSTP, MAXCT, INTPLT,
     $   IC, JC, IV, JV, IU, JU, IB, JB, IBOLD, JMOLD, ICOUNT,
     $   NCASE, MCASE, JCMAX(45), NOI, NOJ
C
```

```
67200            IF (ABS(IB - IBOLD) .GT. 1) THEN
67300              DT = DTRED * DT
67400              IB = IBOLD
67500              JB = JBOLD
67600              INTFLG = 1
67700              RETURN
67800            ENDIF
67900      C
68000            IF (ABS(JB - JBOLD) .GT. 1) THEN
68100              DT = DTRED * DT
68200              IB = IBOLD
68300              JB = JBOLD
68400              INTFLG = 1
68500              RETURN
68600            ENDIF
68700      C
68800            IF (IB .EQ. IBOLD) THEN
68900              IF (JB .EQ. JBOLD) THEN
69000                DT = DTINC * DT
69100                IB = IBOLD
69200                JB = JBOLD
69300                INTFLG = 2
69400                RETURN
69500              ENDIF
69600            ENDIF
69700      C
69800            INTFLG = 0
69900            RETURN
70000            END
70100      C
70200      C*****************************************************************
70300      C
70400            SUBROUTINE FINDN
70500      C     Returns the value of NCASE corresponding
70600      C     to the identity of the neighbouring cell
70700      C     that the DROP travels to.
70800      C
70900            COMMON /CROPS/ MAXDRP, NDROP,
71000           &  XRPOSN(10), XRPOLA(10), XAMOUT(10), XWPRPS(10),
71100           &  XDINIT(10), YDINIT(10), TDINIT(10), UDINIT(10), VDINIT(10),
71200           &  XM(96), YM(49),
71300           &  UR(49,24), VR(49,24), UROLD(49,24), VROLD(49,24),
71400           &  UBR, VBRAVE, UBRAVV, XMUL, XMOBAR, PI, UGAS, VGAS,
71500           &  XDWALL, YDWALL, TDOLD, UDWALL, VDOLD,
71600           &  XDNEW, YDNEW, TDNEW, UDNEW, VDNEW,
71700           &  DT, DTINC, DTRED, XMOL,
71800           &  XDTRED, INTCTR, IFLAG2, IHIT, MAXDTR, MAXDT, INTFLG,
71900           &  IB, JB, IW, JW, IO, JO, IM, JM, IBOLD, JBOLD, ICOUNT,
72000           &  XPROP, MCASE, UDMAX(49), NDI, NDJ
72100      C
72200            IF (IM .LT. IBOLD) THEN
72300              IF (JM .GT. JBOLD) THEN
72400                NCASE = 8
72500              ELSE IF (JM .LT. JBOLD) THEN
72600                NCASE = 7
72700              ELSE
72800                NCASE = 0
72900              ENDIF
73000            ELSE IF (IM .LT. IBOLD) THEN
73100              IF (JM .GT. JBOLD) THEN
73200                NCASE = 4
```

```
73300               ELSE IF (JB .EQ. JBOLD) THEN
73400                 NCASE = 5
73500               ELSE
73600                 NCASE = 6
73700               ENDIF
73800             ELSE
73900               IF (JB .LT. JBOLD) THEN
74000                 NCASE = 3
74100               ELSE IF (JB .EQ. JBOLD) THEN
74200                 NCASE = 1
74300               ELSE
74400                 NCASE = 2
74500               ENDIF
74600             ENDIF
74700             RETURN
74800             END
74900     C
75000     C*****************************************************************
75100     C
75200             SUBROUTINE FINDM
75300     C       returns the value of NCASE corresponding to
75400     C       the four possible locations of the H-cell of
75500     C       of origin, in the mesh cell.
75600     C
75700             COMMON /CMCPC/ MAXPOR, NPORT,
75800            $  IAREA(10),  RPSIA(10), DRMDOT(10), DFREQ(10),
75900            $  XOINIT(10), YOINIT(10), TOINIT(10), UOINIT(10), VOINIT(10),
76000            $  XB(30), YH(48),
76100            $  UB(48, 24), JB(48, 24), JBOLD(48, 24), VBOLD(48, 24),
76200            $  ERR, SHEARX, SHEARY, RAD, RHOGAS, PI, UGAS, VGAS,
76300            $  XOLD, YOLD, TOLD, UOLD, VOLD,
76400            $  XNEW, YNEW, TNEW, UNEW, VNEW,
76500            $  T, DTIME, DTHEO, RHOL,
76600            $  ISTEPS, INJSTR, IFLAGS, IHIT, MAXSTP, MAXST, INJFLG,
76700            $  IC, JC, IV, JV, IH, JH, IHOLD, JHOLD, ICOUNT,
76800            $  NCASE, MCASE, JBMAX(48), NJI, NJO
76900     C
77000             IF ((IH - (IHOLD / 2) * 2) .EQ. 0) THEN
77100               IHOLD is even.
77200               IF ((JH - (JHOLD / 2) * 2) .EQ. 0) THEN
77300     C           JHOLD is even.
77400                 MCASE = 2
77500               ELSE
77600     C           JHOLD is odd.
77700                 MCASE = 4
77800               ENDIF
77900             ELSE
78000     C         IHOLD is odd.
78100               IF ((JH - (JH / 2) * 2) .EQ. 0) THEN
78200     C           JHOLD is even.
78300                 MCASE = 3
78400               ELSE
78500     C           JHOLD is odd.
78600                 MCASE = 1
78700               ENDIF
78800             ENDIF
78900             RETURN
79000             END
79100     C
79200     C*****************************************************************
79300     C
```

```
      SUBROUTINE INTERP(X1, Y1, X2, Y2, X3, Y3)
C     The inputs are (X1, Y1), (X2, Y2) and X3.
C     The value of Y3 is returned, such that the
C     three points lie on a straight line.
      IF ((X2 - X1) .EQ. 0) THEN
        WRITE(6, *) '*** ERROR IN INTERP ** : X1 = X2'
        STOP
      ENDIF
      Y3 = Y1 + (Y2 - Y1) * (X3 - X1) / (X2 - X1)
      RETURN
      END
C
C*****************************************************************
C
      SUBROUTINE CMOD(IM1, IM2, JM1, JM2, Y3)
      COMMON/GRF/RMOMV(50,50),RMOMO(50,50)
      COMMON /ERROR/ MAXPOR, NPORT,
     $  ERPOEN(10), ERPOIA(10), ERMSOT(10), ERFREQ(10),
     $  XDINIT(10), YDINIT(10), TDINIT(10), DDINIT(10), VDINIT(10),
     $  XM(96), YM(96),
     $  DG(96, 24), VG(96, 24), DGOLD(96, 24), VGOLD(96, 24),
     $  DDD, GRAVX, GRAVY, RMU, RMUGAS, PI, DGAS, VGAS,
     $  XDOLD, YDOLD, TDOLD, DDOLD, VDOLD,
     $  XDNEW, YDNEW, TDNEW, DDNEW, VDNEW,
     $  DT, DTINC, DTREF, RHOL,
     $  ISTEPS, INTCTR, IFLAG2, IHIT, MAXSTP, MAXCT, INTFLG,
     $  IC, JC, IV, JV, IC, JC, IM, JM, IBOLD, JMOLD, ICOUNT,
     $  XSCALE, YSCALE, DDMAX(96), NDI, NDJ
C
      RETURN
      END
C
C*****************************************************************
C
      SUBROUTINE DMOD(IM1, IM2, JM1, JM2, Y3)
      COMMON/GRF/RMOMV(50,50),RMOMO(50,50)
      COMMON /ERROR/ MAXPOR, NPORT,
     $  ERPOEN(10), ERPOIA(10), ERMSOT(10), ERFREQ(10),
     $  XDINIT(10), YDINIT(10), TDINIT(10), DDINIT(10), VDINIT(10),
     $  XM(96), YM(96),
     $  DG(96, 24), VG(96, 24), DGOLD(96, 24), VGOLD(96, 24),
     $  DDD, GRAVX, GRAVY, RMU, RMUGAS, PI, DGAS, VGAS,
     $  XDOLD, YDOLD, TDOLD, DDOLD, VDOLD,
     $  XDNEW, YDNEW, TDNEW, DDNEW, VDNEW,
     $  DT, DTINC, DTREF, RHOL,
     $  ISTEPS, INTCTR, IFLAG2, IHIT, MAXSTP, MAXCT, INTFLG,
     $  IC, JC, IV, JV, IC, JC, IM, JM, IBOLD, JMOLD, ICOUNT,
     $  XSCALE, YSCALE, DDMAX(96), NDI, NDJ
C
      DELTA = (4.0 * PI * RHOL * (RAD ** 3) / 3.0) * VF
     $  * RFRAC(INCNT)
      RMOMO(IM1, JM1) = RMOMO(IM1, JM1) - DELTA
      RMOMO(IM2, JM2) = RMOMO(IM2, JM2) + DELTA
      RETURN
      END
C
C*****************************************************************
C
      SUBROUTINE VMOD(IM1, IM2, JM1, JM2, Y3)
      COMMON/GRF/RMOMV(50,50),RMOMO(50,50)
      COMMON /ERROR/ MAXPOR, NPORT,
```

```
      $    DRPDEN(10), DRPDIA(10), DRMDOT(10), DRFRES(10),
      $    XOINIT(10), YOINIT(10), TOINIT(10), UOINIT(10), ..INIT(10),
      $    XB(96), YB(96),
      $    UG(48, 24), VG(48, 24), UGOLD(96, 24), VGOLD(48, 24),
      $    DDD, GRAVX, GRAVY, RAD, RHOGAS, PI, UGAS, VGAS,
      $    XOOLD, YOOLD, TOOLD, UOOLD, VOOLD,
      $    XONEW, YONEW, TONEW, UONEW, VONEW,
      $    DT, DTINC, DTREQ, RHOL,
      $    ICTEPS, INTCTR, IFLAGZ, IHIT, MAXSTP, MAXCT, INTFLG,
      $    IC, JC, IV, JV, IU, JU, IP, JP, IHOLD, JHOLD, ICOUNT,
      $    NCASE, MCASE, UJMAX(48), NCI, NCU
C
      DELTA = (4.0 * PI * RHOL * (RAD ** 3) / 3.0) * VS
      $    * DRFRES(NPORT)
      RMOMV(IM1, JM1) = RMOMV(IM1, JM1) - DELTA
      RMOMV(IM2, JM2) = RMOMV(IM2, JM2) + DELTA
      RETURN
      END
C
C*****************************************************************
C
      SUBROUTINE HITWAL
C     Flag IHIT is set to 1 if the DROP hits the wall.
C     else, it is set to 0.
      COMMON /DROPC/ MAXPOR, NPORT,
      $    DRPDEN(10), DRPDIA(10), DRMDOT(10), DRFRES(10),
      $    XOINIT(10), YOINIT(10), TOINIT(10), UOINIT(10), ..INIT(10),
      $    XB(96), YB(48),
      $    UG(48, 24), VG(48, 24), UGOLD(96, 24), VGOLD(48, 24),
      $    DDD, GRAVX, GRAVY, RAD, RHOGAS, PI, UGAS, VGAS,
      $    XOOLD, YOOLD, TOOLD, UOOLD, VOOLD,
      $    XONEW, YONEW, TONEW, UONEW, VONEW,
      $    DT, DTINC, DTREQ, RHOL,
      $    ICTEPS, INTCTR, IFLAGZ, IHIT, MAXSTP, MAXCT, INTFLG,
      $    IC, JC, IV, JV, IU, JU, IP, JP, IHOLD, JHOLD, ICOUNT,
      $    NCASE, MCASE, UJMAX(48), NCI, NCU
C
      IF (JP .GT. (2 * UJMAX(IP / 2 + 1))) THEN
        WRITE(*, *) 'DROP HITS THE WALL'
        IHIT = 1
      ELSE
        IHIT = 0
      ENDIF
      RETURN
      END
C
C*****************************************************************
C
      SUBROUTINE RK3A
C     This routine does a fourth order Runge-Kutta integration.
C     It calls the routine XPRIME which calculates the
C     Runge-Kutta coefficients K0, K1, K2 and K3.
C
      COMMON /DROPC/ MAXPOR, NPORT,
      $    DRPDEN(10), DRPDIA(10), DRMDOT(10), DRFRES(10),
      $    XOINIT(10), YOINIT(10), TOINIT(10), UOINIT(10), ..INIT(10),
      $    XB(96), YB(48),
      $    UG(48, 24), VG(48, 24), UGOLD(96, 24), VGOLD(48, 24),
      $    DDD, GRAVX, GRAVY, RAD, RHOGAS, PI, UGAS, VGAS,
      $    XOOLD, YOOLD, TOOLD, UOOLD, VOOLD,
      $    XONEW, YONEW, TONEW, UONEW, VONEW,
```

```
      $    DT, DTINC, DTREC, RHOL,
      $    ISTEPS, INTCTR, IFLAG2, IHIT, MAXSTP, MAXCT, INTFLG,
      $    IC, JC, IV, JV, IU, JU, IP, JP, IPOLD, JPOLD, ICNT,
      $    NCASE, MCASE, DUMAX(4), VDI, VDJ
      DIMENSION XXX(10), YYY(10),
      $    F1(10), F2(10), F3(10), F4(10)
      NEW
      XXX(1) = UOLD
      XXX(2) = VOLD
      XXX(3) = XOLD
      XXX(4) = YOLD
      IF (DT .EQ. 0.0) THEN
        WRITE(*, *) ' INPUT THE INTEGRATION TIME STEP'
        READ(5, *) DT
        WRITE(*, *) ' INTEGRATION TIME STEP = ', DT
      ENDIF
      DTH = 0.5 * DT
      CALL DYDX(N, XXX, F1)
      DO I = 1, N
        YYY(I) = XXX(I) + DTH * F1(I)
      ENDDO
      CALL DYDX (N, YYY, F2)
      DO I = 1, N
        YYY(I) = XXX(I) + DTH * F2(I)
      ENDDO
      CALL DYDX (N, YYY, F3)
      DO I = 1, N
        YYY(I) = XXX(I) + DT * F3(I)
      ENDDO
      CALL DYDX (N, YYY, F4)

      DO I = 1, N
        DELXI = (F1(I) + 2.0 * (F2(I) + F3(I)) + F4(I)) / 6.0
        XXX(I) = XXX(I) + DT * DELXI
      ENDDO

      UNEW = XXX(1)
      VNEW = XXX(2)
      XNEW = XXX(3)
      YNEW = XXX(4)
      RETURN
      END

C*****************************************************************

      SUBROUTINE DYDX(N, XXX, F)
C     THIS SUBROUTINE EVALUATES THE DERIVATIVE COEFFICIENTS
C     FOR INTEGRATION.

      IMPLICIT REAL*8 (A-H, O-Z)
      DIMENSION XXX(10), F(10),
     $    UOLD(10), VOLD(10), XOLD(10), YOLD(10), DUMAX(10),
     $    UINIT(10), VINIT(10), XINIT(10), YINIT(10),
     $    XX(10), YY(10),
     $    U(10), V(10), X(10), Y(10), UOLD(10), VOLD(10),
     $    UDOT, VDOT, UDOTA, VDOTA, RHOA, RHOBAR, PI, CBAR, MBAR,
     $    XOLD, YOLD, IOLD, JOLD, UNEW, VNEW,
     $    XINEW, YINEW, TIMEW, ICNEW, VDNEW,
     $    DT, DTINC, DTREC, RHOL,
     $    ISTEPS, INTCTR, IFLAG2, IHIT, MAXSTP, MAXCT, INTFLG,
     $    IC, JC, IV, JV, IU, JU, IP, JP, IPOLD, JPOLD, ICNT,
     $    NCASE, MCASE, DUMAX(10), VDI, VDJ
```

```
      DIMENSION X(N),F(N)
      COMMON/GGF/RMOMV(50,50),RMOMC(50,50)
      CONST = (RHOGAS * CDD * 3.0) / (4.0 * RHOL * RAD)
     $ * SQRT((UGAS - X(1)) ** 2 + (VGAS - X(2)) ** 2)
      F(1) = CONST * (UGAS - X(1)) + GRAVX
      F(2) = CONST * (VGAS - X(2)) + GRAVY
      F(3) = X(1)
      F(4) = X(2)
      RETURN
      END
C
C*****************************************************************
C
C     SUBROUTINE COLLIS
C     THIS SUBROUTINE IS USED FOR CHECKING FOR THE
C     OVERALL DISAPPEARANCE OF THE SYSTEM. A FLAG OF ISOAREA
C     IS SET
C
C
      SUBROUTINE COLLIS(MAXP,NP,
     $  XP(50),YP(50),UP(50),VP(50),
     $  XPOLD(50),YPOLD(50),UPOLD(50),VPOLD(50),
```

```
      $    XB(96), YB(4c),
      $    UG(4c, 24), VG(4B, 24), UGOLD(4B, 24), VGOLD(4B, 24),
      $    CCD, GRAVX, GRAVY, RAD, RHOGAS, PI, UGAS, VGAS,
      $    XCOLD, YCOLD, TCOLD, UCOLD, VCOLD,
      $    XONEw, YONEw, TONEw, UONEw, VONEw,
      $    DT, DTINV, DTHED, RHOL,
      $    ISTEPC, IMTCYS, IFLAG2, IHIT, MAXCTP, MAXCT, INTFLG,
      $    IC, JC, IV, JV, IU, JU, IR, JR, IHOLD, JHOLD, ICOUNT,
      $    MCASE, MCASE, UUMAX(4e), NCI, NJJ
C
C
      ICOUNT = ICOUNT + 1
      IF (ICOUNT .EQ. 1) THEN
        Ignore the first iteration.
        IFLAG2 =
        RETURN
      ENDIF
      SUMUE=0.0
      SUMVE=0.0
      DO 20 I = 1, NCI
        DO 20 J = 1, NJJ
          SUMUE = SUMUE + ((UGOLD(I,J) - UG(I,J)) ** 2)
20    CONTINUE
      ACCUM = NCI * NJJ * 0.025
      IF (ACCUM .GE. SUMUE) THEN
        IFLAG2 = 1
      ELSE
        IFLAG2 = 0
      ENDIF
      DO 30 I = 1, NCI
        DO 30 J = 1, NJJ
          SUMVE = SUMVE + ((VGOLD(I,J) - VG(I,J)) ** 2)
30    CONTINUE
      IF (ACCUM .GE. SUMVE) THEN
        IFLAG3 = 1
      ELSE
        IFLAG3 = 0
      ENDIF
      IF (IFLAG2 .EQ. 1) THEN
        IF (IFLAG3 .EQ. 1) THEN
          IFLAG2 = 1
        ENDIF
      ELSE
        IFLAG2 =
      ENDIF
      IF (I
      ENDIF
      ENDIF
      ENDIF
C
*** END OF INTERMEDIATE SECTION ***
```

# APPENDIX B

## PROGRAM LISTING OF STRSORT

```
      SUBROUTINE STRMPLOT(STRMFUNC,IMAX,JMAX,X,Y)
C***        Subroutine to find and record data for
C                   streamline plots.
C                   Jones Nichols     8 March 85
C
C  ** Variable Definitions **
C
C  STRMFUNC...Array of position values of grid points
C  PSIMIN...Minimum psi value
C  PSIMAX...Maximum psi value of largest streamline
C  DELPSI...Interval between streamlines  grid dx
C  NUMSTRM...Number of streamlines to be plotted
C  NUMPTS...Number of points in a grid lines
C  IBEGIN...Beginning point in grid line
C  IEND...Ending point in grid line
C  ISTART...Starting point for search for next point
C  JSTART...Starting point for search for next point
C  IMAX...Number of grid lines in I direction
C  JMAX...Number of grid lines in J direction
C  XPLOT...Array of x coordinates for plotting
C  YPLOT...Array of y coordinates for plotting
C  NPTS...Number of points for plotting
C
      DIMENSION STRMFUNC(IMAX,JMAX),X(IMAX,JMAX),Y(IMAX,JMAX)
      REAL XPLOT(2000),YPLOT(2000)
      INTEGER IMAX,JMAX,NUMSTRM,IBEGIN,IEND,ISTART,JSTART
      CHARACTER*1 ANS
      OPEN(UNIT=5,FILE='CON',STATUS='OLD')
C
C           Generate boundary points for plot...
C
      DO 10 I=1,IMAX
C
C
C
C           Add point for corner of a cell...
C
C
C
C
```

```
      IF (XMAX.EQ.0.0) GOTO 20
C                   Sort points for loop condition...
      IF (ETVAL.GT.1) GOTO 50
C           Convert points from grid coordinates to x,y values
   30 DO 34 J=1,FMAX
      IF (POINTS(J,1).GT.0.) GOTO 31
      POINTS(J,1)=1.0
   31 IF (POINTS(J,2).GT.0.) GOTO 32
      POINTS J,2)=0.0
C           Find y-value by linear interpolation
   32 DELL=POINTS(J,2)-INT(POINTS(J,2))
      IELY=Y(INT(POINTS(J,2)+1))-Y(INT(POINTS(J,2)))
      POINTS(J,2 =Y(INT(POINTS(J,2)))+DELY*DEL
C           Find x-value by linear interpolation...
      IF (INT POINTS J,1)+.EQ.POINTS J,1) GOTO 33
      DELL=POINTS(J,1)-INT(POINTS(J,1))
      IELY=X INT POINTS(J,1) +1)-X INT(POINTS(J,1))
      POINTS(J,1 =X(INT POINTS J,1)))+DELY*IELI
      GOTO 34
   33 POINTS J,1 =X INT POINTS J,1
   34 CONTINUE
      DO 100 J=1,FMAX
      WRITE 9,* POINTS J,1),POINTS(J,2)
  100 CONTINUE
C           Write end of block marker after each group of points...
      WRITE 9,* 999.,999.0
   50 CONTINUE
C           Write end of file marker after all points...
      WRITE 9,* 888.8,888.8
      CLOSE UNIT=9)
      RETURN
C**         Loop sort section       **
C                   Initialize pointers...
   60 INPTR=0
      OUTCOUNT=1
      ILOOP=1
      DO 71 I8=1,FMAX
C                   Split points with duplicate x-grid values.
C                   Put points with higher  value in end of
C                   array, starting at end and moving in...
      IF (POINTS(I8,1).EQ.OLDX) THEN
            TEMPPTS (FMAX-OUTCOUNT),1)=POINTS(I8,1)
            TEMPPTS(FMAX-OUTCOUNT),2 =POINTS(I8,2)
            OUTCOUNT=OUTCOUNT+1
      ELSE
            INPTR=INPTR+1
            TEMPPTS(INPTR,1 =POINTS I8,1)
            TEMPPTS(INPTR,2)=POINTS I8,2)
      ENDIF
      OLDX=POINTS I8,1
   71 CONTINUE
C           Move lower points to top of array...
      DO 72 I8=1,INPTR
      POINTS OUTCOUNT+I8,1 =TEMPPTS(I8,1)
      POINTS(OUTCOUNT-I8,2)=TEMPPTS(I8,2)
   72 CONTINUE
C           Add extra point to close loop...
C                   unless loop is open.
      IF (POINTS 1,1 .EQ.POINTS FMAX) GOTO 55
      FMAX=FMAX+1
      POINTS FMAX,1 =POINTS(1,1
```

```
      55  GOTO 30
          END

          SUBROUTINE INTERP (F,N,IMAX,JMAX,STVAL,POINTS,PMAX,IEXP)
C--   *       Sub to find grid points of streamline points
C             intermediate linearly between grid points along
C             lines of constant integrid value...
C
C     ** Variable Definitions **
C
C     F,N...stream function values for grid points
C     STVAL...streamfunction value for this stream line
C     POINTS...array of plotting points for stream line
C     PMAX...number of plotting points found
C     IMAX,...number of I grid lines
C     JMAX...number of J grid lines (I.E. each I grid line
C            grid line following a portion
C     REATTACH...flag for reattachment point if loop
C     IMIN...lower loop boundary for stvalue)
C
          REAL F(IMAX,JMAX),STVAL,POINTS(200,2),FRAC,DELTA,DELTB
          INTEGER PMAX,IMAX,JMAX,NB,IEXP,REATTACH,IMIN
          PMAX=1
          REATTACH=0
C             Set appropriate lower I grid value for loop
          IF (STVAL.EQ.0.0) THEN
C             Add beginning point for stvalue=0 case...
              IMIN=IEXP
              POINTS(1,1)=IEXP-1
              POINTS(1,2)=JMAX-IEXP+1.0
              PMAX=2
          ELSE
              IMIN=1
          ENDIF
C             Now enter loop for points...
          DO 100 I=IMIN,IMAX
          DO 100 J=1,JMAX-1
          IF (REATTACH.EQ.1) GOTO 100
          IF ((F(I,J).LT.STVAL).AND.(F(I,J+1).GT.STVAL)) GOTO 110
          IF ((F(I,J).GT.STVAL).AND.(F(I,J+1).LT.STVAL)) GOTO 110
          IF (F(I,J).EQ.STVAL) GOTO 120
          IF ((F(I,J).LT.STVAL).AND.(F(I,J+1).EQ.STVAL)) GOTO 100
C             Start here with division solution with divide by zero
C                                                 consideration...
C     Determine if (F-STVAL) for this and next point are equal...
          PMAX=PMAX+1
          POINTS(PMAX,1)=I
          POINTS(PMAX,2)=J+0.0
          IF (J.NE.JMAX-1) GOTO 110
C             Also reattachment condition...
          REATTACH=1
          GOTO 110
  120     CONTINUE
          IF ((F(I,J).NE.F(I-1,J)).OR.(POINTS(PMAX,1).NE.IMAX-1)) GOTO 130
C             Add reattachment point if necessary...
          PMAX=PMAX+1
          POINTS(PMAX,1)=IMAX-1
          POINTS(PMAX,2)=JMAX+0.0
          DELTA=POINTS(PMAX-1,1)-1.0
          DELTB=POINTS(PMAX-1,2)-POINTS(PMAX-2,2)
          IF (DELTB.EQ.0.0) GOTO 130
          POINTS(PMAX-1,2)=POINTS(PMAX-2,2)+DELTB/DELTA
  130     RETURN
          END
```

# APPENDIX C

## PROGRAM LISTING OF STRIPLOT

```
//PLOTTR JOB 8475-AFT,'NIXIRK'
//STEP1 EXEC FPLOTCLG
//FORT.SYSIN DD *
C - - -   STREAMLINE PLOTTING PROGRAM FOR DATA FROM STARPIC
C - - -       SUMMER 1986    JAMES L NIXIRK
C
C*****    VARIABLE DECLARATIONS
C       PTX...ARRAY OF PLOTTING POINT X VALUES
C       PTY...ARRAY OF PLOTTING POINT Y VALUES
C       SCX...X AXIS SCALING FACTOR
C       SCY...Y AXIS SCALING FACTOR
C       NUMPTS...NUMBER OF POINTS
C
      REAL PTX(200),PTY(200),SCX,SCY
      INTEGER NUMPTS
C       SWITCH USE PLOTTER TO STANDARD PEN
      CALL SYMPLT (1)
      OPEN (UNIT=5,STATUS='OLD',
C       ** CONTROL LOOP **
C
   10 READ(
C
   20 READ(
      READ(5,*  PTX(I),PTY(I)
C       ** IF X VALUE=999.9 END PLOT
      IF (PTX(I).EQ.999.9) GOTO 100
C       ** ZERO NEGATIVE Y VALUES
      IF (PTY(I).LE.0) GOTO 30
      PTY(I)=0
   30 IF (PTX(I).LT.999.) GOTO 20
C       ** IF = 9999 THEN PLOT POINTS READ
      NUMPTS=I
C       ** IF FIRST LINE GO TO BOUNDARY SECTION
C       IF(I.EQ.1) GOTO 40
C       ** IF NOT FIRST LINE GO TO MAIN PLOT SECTION
      IF (I.GT.1) GOTO 200
   40 CALL ENDPLT
      CLOSE(UNIT=5)
      STOP
C
C       ** BOUNDARY PLOT SECTION **
C       * FIND BEST SCALING FACTORS FOR ALL POINTS *
C
C       ** GET SCALING FACTORS FOR DESIRED MAXIMUM PLOT SIZE
      SCX=10./PTX(1)
      SCY=10./PTY(1)
C       ** SCALE BOUNDARY POINTS
      DO 50 I=1,NUMPTS
      PTX(I)=PTX(I)*SCX
      PTY(I)=PTY(I)*SCY
   50 CONTINUE
C       ** CALCULATE SCALING FACTORS IN ARRAYS FOR SUBROUTINES
      PTX(NUMPTS+1)=0
      PTY(NUMPTS+1)=0
      PTX(NUMPTS+2)=10
      PTY(NUMPTS+2)=10
C       ** PLOT LOWER BOUNDARY LINES
      CALL LINE(PTX,PTY,NUMPTS,1,0,0)
C       ** SET UP POINTS FOR LOWER BOUNDARY LINE
      PTX(1)=0
      PTY(1)=0
      PTX(2)=100.0
      PTY(2)=0
      DO 60 I=3,
```

```
C                 PTX(3)=PTX(2)
C                 PTX(4)=0
C                 PTX(5)=10
C                 PTY(4)=0
C                 PTY(5)=10
C       C         ** PLOT LOWER BOUNDARY LINE
C                 CALL LINE(PTX,PTY,2,1,0,0)
C       C         ** PLOT FLOW DIRECTION ARROW
C                 CALL ARROW(4.0,3.5,6.0,3.5,0.5,0.25,1)
C                 GOTO 10
C       C
C       C         ** STANDARD PLOT SECTION
C       C
C       C         ** INCLUDE SCALING FACTORS IN ARRAYS FOR 3.5"LINES
C       C000      PTX(NUMPTS+1)=0
C                 PTX(NUMPTS+2)=10
C                 PTY(NUMPTS+1)=0
C                 PTY(NUMPTS+2)=0
C       C         ** SCALE POINTS
C                 DO 5 I=1,NUMPTS
C                 PTX(I)=PTX(I)*SCLX
C                 PTY(I)=PTY(I)*SCLY
C               5 CONTINUE
C       C         ** PLOT POINTS WITH SPECIAL SYMBOL
C                 CALL LINE(PTX,PTY,NUMPTS,1,0,0)
C                 GOTO 10
C               END
C     SUBROUTINE TO SIZE SATELLITE ANTENNA BEAM
C
```

# APPENDIX D

## PROGRAM LISTING OF PLOTGEN

```
C*****************************************************************
C*                                                               *
C*      PLOTGEN FOR          DATA PLOTTING PROGRAM               *
C*                                                               *
C*       GENERATES PLOT FILE FOR USE WITH PLOT84 OR              *
C*            OR OTHER SUITABLE PLOTTING ROUTINE                 *
C*                                                               *
C*      ML4286       ALL  85          JAMES L  NIFFRK           *
C*                                                               *
C*****************************************************************


C>> VARIABLE DEFINITIONS <<

C     TRASH      FOUR CHARACTER TEST STRING TO LOCATE DATA
C     JUNK       80 CHARACTER READ STRING FOR LOCATING DATA
C     TT         ARRAY OF DATA POINTS FROM PRINT FILE
C     X          ARRAY OF X VALUES FOR I GRID LINES
C     Y          ARRAY OF Y VALUES FOR J GRID LINES
C     YB         OLD Y VALUE FOR STAIRSTEP IN BOUNDARY PLOT
C     PVAL       VALUE OF DATA CURRENTLY BEING PLOTTED
C     PTPVAL     PROP. POSITION VALUE FOR FIRST POINT
C     PGD        ARRAY OF PROP. POSITION VALUES FOR PLOT POINTS
C     XX         X VALUE OF CURRENT POINT FOR WRITE TO FILE
C     YY         Y VALUE OF CURRENT POINT FOR WRITE TO FILE
C     J          LOOP VARIABLE = J GRID VALUE
C     JJ         LOOP VARIABLE = J VALUE IN READ SECTION
C     PTII       I GRID VALUE OF FIRST POINT
C     PTIJ       J GRID VALUE OF FIRST POINT
C     IMAX       NUMBER OF I GRID LINES
C     OLDJMAX    NUMBER OF J GRID LINES AT PREVIOUS I LINE
C     PTNUM      NUMBER OF POINTS FOUND FOR THIS DATA VALUE
C     I          LOOP VARIABLE = I GRID VALUE
C     K          MASTER LOOP INDEX
C     JMAX       ARRAY OF NUMBER OF GRID LINES FOR EACH I LINE
C     DIR        DIRECTION NUMBER TO LOOK FOR NEXT POINT
C     NI         I VALUE OF POSSIBLE NEXT POINT
C     NJ         J VALUE OF POSSIBLE NEXT POINT
C     NTYP       POINT TYPE OF POSSIBLE NEXT POINT
C     TYP        POINT TYPE OF CURRENT POINT
C     PTITYP     POINT TYPE OF FIRST POINT
C     NUMI       NUMBER OF I GRID LINES TO READ FOR
C     NUMJ       NUMBER OF J GRID LINES TO READ FOR
C     FOLDI      NUMBER OF I GRID LINES ON 1ST ROW OF PRINT OUT
C     NZ         VERY SMALL NON-ZERO NUMBER
C     CHKCNTR    COUNTER FOR NUMBER OF CHECKS FOR NEXT POINT
C     DELI       DELTA I VALUE FOR CHECK FOR NEXT POINT
C     DELJ       DELTA J VALUE FOR CHECK FOR NEXT POINT
C     ********** USER DEFINED VALUES **********
C     DUMP       CONTROL FLAG FOR POINT DUMP RUN
C     VALUE      ARRAY OF VALUES TO BE PLOTTED
C     NUMVALS    NUMBER OF DATA VALUES TO BE PLOTTED
C     READTYP    TYPE OF FILE READ
C

      CHARACTER*4 TRASH
      CHARACTER*80 JUNK
      REAL*8 PVAL,VALUE(12),PGD(30,30,2),TT(30,30),NZ
      REAL XX,YY,XXI,YYI,YB,X(30),Y(30)
      INTEGER J,JJ,PTII,PTIJ,IMAX,OLDJMAX,NUMVALS,READTYP
      INTEGER PTNUM,I,K,JMAX(30),DIR,NI,NJ,NTYP,TYP,PTITYP
      INTEGER CHKCNTR,DELI(8,2),DELJ(8,2),NUMI,NUMJ,FOLDI
      LOGICAL DUMP                    35.120
      DATA NZ/0.000000001/
```

```
      DATA DE/ 1.0, 1.0, 1.0, 1.0, 1.0, 1.0, 1.0, 1.0, 1.0, 1.0,
     DATA DE/ 320*1.0/, FOLDED/ 320*0.0/, ITEST/0/
C
C     >>> VARIABLE PRESET SECTION <<<
C
      DATA VALUE/ 0.0, 1.0, 2.0, 3.0, 4.0, 5.0, 6.0, 7.0, 8.0, 9.0, 10.0, 11.0, 12.0,
     NUMVAL=13
C     ** IF READOUT=1 FOR TEKTRONIX FORMAT,2 FOR STARPLOT FORMAT
      READOUT=2
      TEMP=0.5
      DO 1 I=1,80
      DO 1 J=1,65
      PLOT(I,J)=' '
      PLOT(I,J,2)=' '
    1 CONTINUE
C
C     >>> SECTION TO READ DATA FROM PRINT FILE <<<
C
      OPEN(UNIT=9,FILE='PRINT.DAT',STATUS='OLD')
   10 READ(9,1000,END=20)
      IF(ERASE.EQ.'ERASE') GOTO 10
      IF(READOUT.EQ.2) GOTO 25
C     >>> TEKTRONIX FORMAT READ SECTION <<<
      NUM=0
      NUM2=0
      DO 21 I=1,320
      READ(9,1001,END=20)
      IF(DE(I).LT.TEMP) GOTO 21
      NUM=NUM+1
      READ(9,1002,END=20) (X(J,NUM),Y(J,NUM),J=1,2),FOLDED(NUM),Y(3,NUM)
   21 CONTINUE
      READ(9,1003,END=20) (X(J,NUM),J=1,2),FOLDED(NUM)
      READ(9,1001,END=20)
      DO 30 J=1,NUM-1
      IF(NUM.EQ.1) GOTO 30
      READ(9,1003,END=20) (X(I,J),I=1,2),FOLDED(J),NUM(J)
   30 CONTINUE
      READ(9,1004,END=20) (X(I,NUM),I=1,2),FOLDED(NUM),NUM(NUM)
      GOTO 35
C     >>> STARPLOT FORMAT READ SECTION <<<
   25 NUM=0
      NUM2=1
      FOLDED=0.0
      READ(9,1005,END=20)
      READ(9,1006,END=20) X(1,1),Y(1,1),FOLDED(1)
      READ(9,1005,END=20)
      DO 26 I=1,NUM2
      IF(NUM.EQ.1) GOTO 26
      READ(9,1007,END=20) X(1,I),Y(1,I),X(2,I),Y(2,I),FOLDED(I)
   26 CONTINUE
      READ(9,1008,END=20) X(1,NUM2),Y(1,NUM2),FOLDED(NUM2)
      READ(9,1009,END=20)
      DO 34 I=1,NUM2-1
      IF(NUM.EQ.1) GOTO 34
      READ(9,1010,END=20) X(2,I),Y(2,I),X(1,I+1),Y(1,I+1),FOLDED(I),NUM(I)
   34 CONTINUE
   35 CLOSE(UNIT=9)
C
C     >>> BOUNDARY DETINITION SECTION <<<
C     >> ALSO SETS UP PLOT FILE <<
C
  200 OPEN(UNIT=2,FILE='PLOT.DAT',STATUS='NEW')
      WRITE(2,*) 0.0,0.0
```

```
```

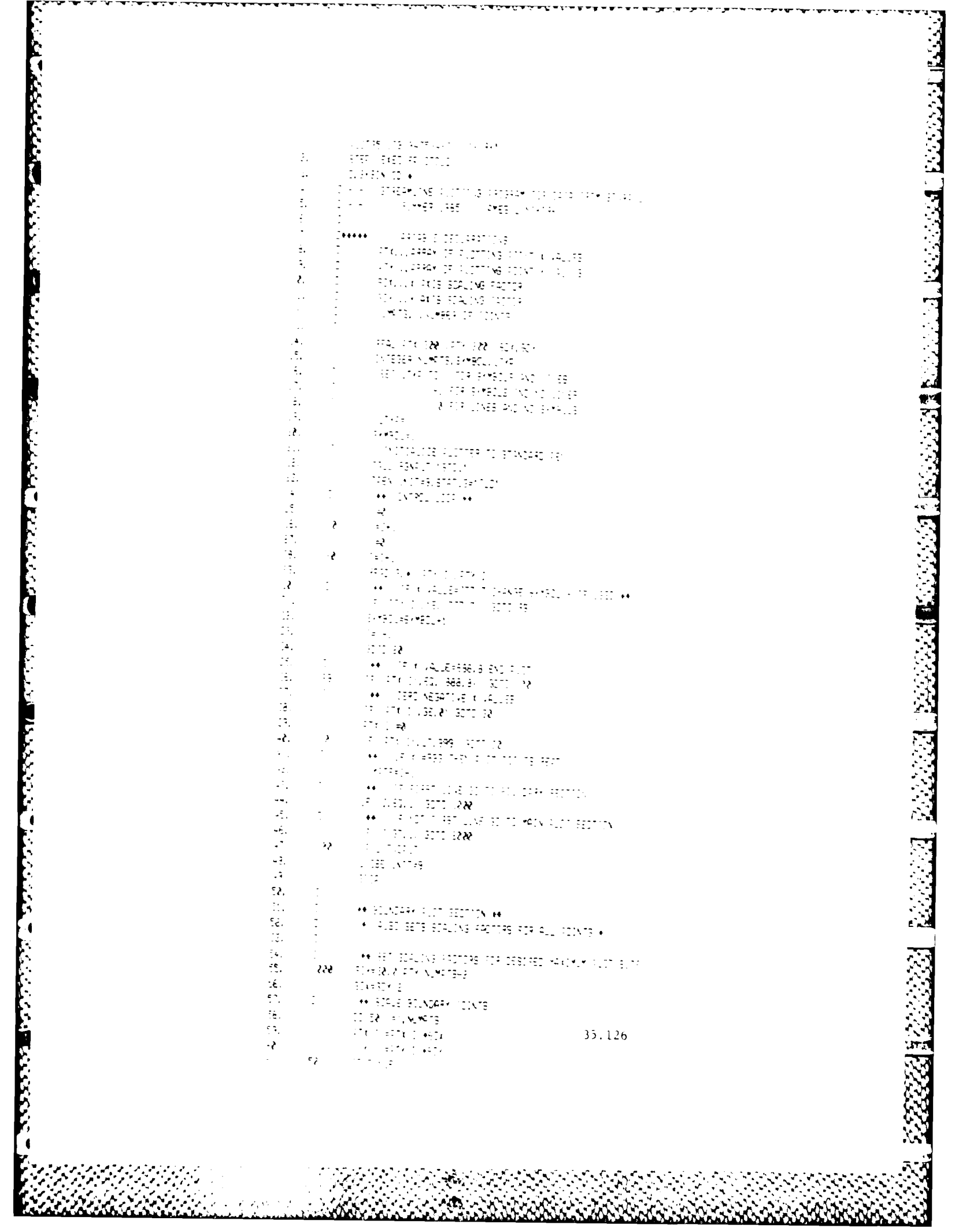
35.122

```
            J=0
802         J=J+1
            IF(J.GT.JMAX(I)) GOTO 801
            IF(PGD(I+1,J+1).LT.(0.0)) GOTO 804
            XX1=X(I)
            YY1=Y(I)+Y(I+1)-Y(I))*PGD(I+1,J+1)
            TYP=1
            GOTO 803
804         IF(PGD(I+1,J+1).LT.(0.0)) GOTO 802
            XX1=X(I)+(X(I+1)-X(I))*PGD(I+1,J+1)
            YY1=Y(I)
            TYP=2
803         PTTYP=TYP
            PTI=I
            PTJ=J
            PGD(I+1,J+1)=TYP+1.0
            WRITE(7,*) XX1,YY1
            PTNUM=PTNUM+1
            IF(PTNUM.EQ.0) GOTO 400
C
C           *** END SOCKET BEND POINTS ***
C
600         IF(PTNUM.LT.3) GOTO 803
            DIR=DIR+5
            DIRCNTR=0
601         DIR=MOD(DIR,8)+1
            NTYP=1+MOD(DIR+TYP,2)
            NI=I+IDEL(DIR,1)
            NJ=J+JDEL(DIR,1)
            IF(PVG.NE.1.0) GOTO 608
608         IF(PGD(NI+1,NJ+1,NTYP).GE.0.0) GOTO 602
            DIRCNTR=DIRCNTR+1
            IF(DIRCNTR.GE.8) GOTO 603
            DIR=DIR+1
            GOTO 601
602         IF(NTYP.EQ.2) GOTO 606
                  YY=Y(NI)+(Y(NI+1)-Y(NI))*PGD(NI+1,NJ+1,NTYP)
                  XX=X(NI)
            GOTO 604
606               XX=X(NI)+(X(NI+1)-X(NI))*PGD(NI+1,NJ+1,NTYP)
                  YY=Y(NJ)
604         TYP=NTYP
            PGD(NI+1,NJ+1,NTYP)=TYP+1.0
              NI
              NJ
            WRITE(7,*) XX,YY
            PTNUM=PTNUM+1
            GOTO 600
C
C              *** END SOCKET BEND ***
C
603         DIR=DIR+4
            NTYP=1+MOD(DIR/2+TYP,2)
            NI=I+IDEL(DIR,1)
            NJ=J+JDEL(DIR,1)
            IF(NI.NE.PTI+1.OR.NJ.NE.PTJ+1.OR.NTYP.NE.PTTYP) GOTO 605
            WRITE(7,*) XX1,YY1
605         CONTINUE
            WRITE(7,*) 999.9,999.9
            IF(PTNUM.EQ.0) GOTO 402
            GOTO 800
402         WRITE(7,*) 777.7,777.7
401         CONTINUE
C                 WRITE END OF FILE MARK
            WRITE(7,*) 888.8,888.8
            CLOSE(UNIT=7)
```

```
      STOP
C
C     >> READ FORMATS FOR DATA READ SECTION <<
C
  299 FORMAT(1X,A80)
  300 FORMAT(1X,A80)
  301 FORMAT(4X,'OPERATION ',
      1 'NUMBER',/)
  302 FORMAT(8X,I2,
      1 4X,I2,/)
  303 FORMAT(8X,I2,/)
  304 FORMAT(8X,I2,/)
  305 FORMAT(1X,'ERROR IN ',A6,' NUMBER',I2,
      1 ' - ',A80,/)
  306 FORMAT(1X,A80)
      END
```

# APPENDIX E

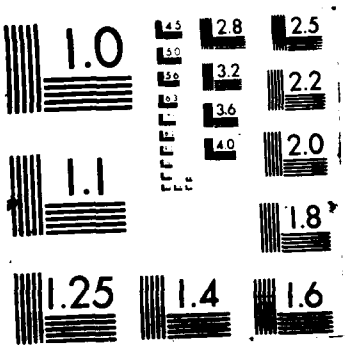
## PROGRAM LISTING OF PLOTR



```
```

AD-A186 498 UNITED STATES AIR FORCE RESEARCH INITIATION PROGRAM 11/11
1984 RESEARCH REPORTS (U) SOUTHEASTERN CENTER FOR
ELECTRICAL ENGINEERING EDUCATION INC S W D PEELE
UNCLASSIFIED MAY 86 AFOSR-TR-87-1721 F49620-82-C-0035 F/G 15/1 NL




1.0
1.1
1.25
1.4
1.6
2.8
3.2
3.6
4.0
2.5
2.2
2.0
1.8

# SiC FIBER REINFORCED GLASS-CERAMIC COMPOSITES IN THE ZIRCONIA/MAGNESIUM ALUMINOSILICATE SYSTEM

Charles H. Drummond III
Department of Ceramic Engineering

For the Period
November 1, 1984 - December 15, 1985

SOUTHEASTERN CENTER FOR ELECTRICAL ENGINEERING EDUCATION
Management Office, Central Florida Facility
11th & Massachusetts Avenue
St. Cloud, FL 32769

SubContract No. 84 RIP 36

April 1986

# SiC Fiber Reinforced Glass-Ceramic Composites in the Zirconia/Magnesium Aluminosilicate System

Charles H. Drummond III
Dept. of Ceramic Engineering, The Ohio State University
Columbus, Ohio 43210

ABSTRACT

Glass-ceramic matrix compositions derived from metal alkoxides were vacuum hot-pressed. The compositions were nominally cordierite with variations in silica content and additions of up to 30% zirconia. Composites fabricated by vacuum hot-pressing the matrix compositions with SiC Nicalon® fibers were also studied. Variations in pressing conditions and subsequent heat treatments were examined. Crystalline phase development, bend strength and fracture toughness were evaluated as a function of hot-pressing parameters.

## EXPERIMENTAL PROCEDURES

The matrix compositions investigated were primarily from the magnesia, alumina, zirconia and silica system. Each composition also contained a 5 weight percent $Nb_2O_5$ addition which has been purported to provide barrier protection to the SiC fibers. The compositions were studied for phase development with and without the SiC fibers.

The matrix compositions were synthesized from the base metal or metal chloride from the following reactions:

$$Mg + 2C_2H_5OH \xrightarrow{HgI_2} Mg(OC_2H_5)_2 + H_2$$

$$Al + 3C_3H_7OH \xrightarrow{HgCl_2} Al(OC_3H_7)_3 + 3/2H_2$$

$$ZrCl_4 + 4C_3H_7OH + 4NH_3 \xrightarrow{C_6H_{14}} Zr(OC_3H_7)_4 + 4NH_4Cl$$

$$NbCl_5 + 5C_3H_7OH + 5NH_3 \xrightarrow{C_6H_{14}} Nb(OC_3H_7)_5 + 5NH_4Cl$$

The silica was added to the composition in the form of commercially available $Si(OC_2H_5)_4$ (TEOS). The organic solutions were dropwise acid hydrolyzed in water. In order to study the matrix material only, part of the slurry was vacuum dried. The dried material was then calcined in air at 600°C to remove the bulk of the organics from the material. The calcined material was vacuum hot-pressed into inch round discs which were evaluated by XRD. The samples were then cut and polished for 4 point bend testing and indentation toughness using the Marshall, Noma and Evans indentation toughness method.[1]

The materials not processed into discs for the matrix material studies were slurry coated onto fibers which were then dried and calcined to 450°C prior to vacuum hot-pressing. These composite samples were evaluated for XRD. The study at this point is incomplete in the areas of composite mechanical properties. TEM studies are also planned for the composite and matrix only samples.

COMPOSITION SELECTION

Composition ZSPIN lies nearly midway between cordierite [$2MgO \cdot 2Al_2O_3 \cdot 5SiO_2$] and spinel [$MgAl_2O_4$] for its magnesia, alumina and silica content. The second composition studied was ZCOR which had a magnesia, alumina, and silica content corresponding to stoichiometric cordierite. ZMAS and MAS compositions contained excess silica beyond stoichiometric cordierite. These compositions are plotted on the magnesia, alumina, and silica ternay phase diagram in Figure 1.[2]

The MAS (magnesia, alumina, and silica) system has been

detailed by McMillan [3] to yield particularly high strengths when formed into glass-ceramics . The microstructure of glass-ceramics generally produces a very fine grained and dense material with superior strength to ceramics formed by traditional powder processing methods. The MAS system contains minerals that form platey and elongated grains that further enhance the strength due to the microstructure of the resulting glass-ceramic.

It has been shown by Faber and Evans [4] that the interweaving structure of elongated grains produces enhanced strength and toughness over the same mineral phases developed with lower resulting aspect ratios. Cordierite [$2MgO \cdot 2Al_2O_3 \cdot 5SiO_2$] is an example of a mineral capable of forming platey and elongated grains consistent with the Faber and Evans model.

The thermal expansion of cordierite is less than the SiC fibers used in the composite. The choice of cordierite in the matrix was to enhance the formation of residual compressive forces in the matrix material while distributing the tensile load to the fibers. Spinel was chosen as a possible second phase in the Z3PIN composition due to its higher tensile strength than cordierite.

Each of the compositions in this study contained additions of $ZrO_2$. These additions were intended to act as a nucleation catalyst and as a means of transformation toughening to the matrix. It was understood in this study that critical conditions for successful transformation toughening were not optimized. The grain size and amount of the tetragonal zirconia phase are examples of two critical parameters regarding the toughening mechanism that were not optimized in this study.

## PHASE DEVELOPMENT IN THE MATRIX MATERIAL

Experiments determined that the first phases formed from the starting ZSPIN composition (without SiC) glass were spinel, sapphirine (a spinel type structure with formula $Mg_7Al_{18}Si_3O_{40}$) and the tetragonal form of zirconia. These phases formed at temperatures of about 600°C. Zircon and cordierite formation were observed at 1300°C or greater. This temperature for zircon formation is consistent with the study of Conrad[5] regarding a glass-ceramic with a 10% $ZrO_2$ content and a magnesium aluminosilicate composition between ZSPIN and ZCOR. The amount of zircon formed was found to increase with prolonged heating. After over an hour at 1300°, only about half the zirconia had been transformed to zircon. The amount of cordierite appeared to decrease as zircon was formed. Both cordierite and zircon form at the expense of sapphirine.

Kinetics appear to favor the formation of spinel, sapphirine and tetragonal zirconia for the ZSPIN composition. Sapphirine is similar in composition to cordierite and, therefore, likely enhances the kinetics of cordierite formation in the ZSPIN composition. Zircon, though favored in a free energy analysis, is slow to form.[6,7,8] From additional heatings at 1300°, it appeared that zircon and spinel would be the predominant final equilibrium phases. The kinetics of the zircon formation appear to be the rate limiting process in the reactions occurring at temperatures above 1250°C.

The objective of the composition ZSPIN was to develop spinel, cordierite and zirconia in the tetragonal structure. Equilibrium conditions would likely not allow the coexistance of these phases for the ZSPIN composition. The difference between the more rapid cordierite formation kinetics and the zircon kinetics was not sufficient to form cordierite without a significant amount of zircon for the ZSPIN composition utilized in this study.

The ZSPIN matrix material strength (no SiC fibers added) in a 4 point bend test showed the strength decreased rapidly as the cordierite and zircon phases formed. The samples with spinel, sapphirine and tetragonal zirconia phases exhibited 22 to 24 KSI strength with up to 2.2 $MPam^{1/2}$ toughness. Bend bars with spinel, cordierite, zircon and the remaining tetragonal zirconia had only 7.5 to 13 KSI strength with the toughness values averaging approximately 1.6. This strength degredation can be readily explained when viewing a polished matrix material sample magnified at 100X. With the formation of zircon, a large number of significant flaws were readily apparent within the samples. Zircon represents roughly a 20% density increase over spinel (or sapphirine) and a 30% density increase over cordierite. No appreciable shrinkage occurred during hot-pressing in the temperature range of the zircon formation. It is apparent that the formation of the higher density zircon phase caused the resultant flaws observed on the low strength samples.

Experimentally, ZCOR and ZMAS compositions were found to contain primarily cordierite with tetragonal zirconia.

At 1300° and above, zircon began to form. This pattern of zircon formation parallels the situation found in ZSPIN and the Conrad study.[5] It appears that the zircon formation mechanism is not sensitive to modest variations in zirconia or silica concentration.

The transition from 1250°C to 1300°C not only introduced zircon but cordierite was observed to transform from the $\mu$ to the $\alpha$ form. This transformation also accompanied the disappearance of sapphirine. Tetragonal zirconia remained, since the reaction to form zircon was sluggish. The tetragonal zirconia content was not only being diminished by the zircon formation, but a portion of the tetragonal phase appeared to become destabilized and monoclinic zirconia was then observed. The monoclinic zirconia formation at 1300°C corresponded to the disappearance of sapphirine and the formation of spinel only as the ternary component. Since spinel contains a higher magnesia content than sapphirine, it is likely that a portion of the magnesia which had been a stabilizer for the tetragonal zirconia had reacted with the sapphirine to form spinel which in turn freed silica for the zircon formation.

From the compositions studied in these experiments, a simplified nonequilibrium isothermal ternary section can be approximated. With $MgAl_2O_4$ being considered as a single component and the aid of the $ZrO_2$-$SiO_2$ phase diagram [9], these compositions and their resulting phases can be illustrated semiquantitatively. Figures 2 and 3 illustrate the spinel-zirconia-silica nonequilibrium ternary isothermal section at 1250°C and 1300°C.

Sapphirine cannot be properly depicted on the 1250° metastable ternary as shown with spinel, zirconia, and silica components. However, a combination of spinel and sapphirine appeared to be present at 1250°. Since structurally and compositionally spinel and sapphirine are very similar and the ternary provides a useful tool in visualizing the phase development of these materials, sapphirine is included on the isothermal section with spinel.

The metastable ternary section shown in Figure 2 indicates that even though the composition ZSPIN was unable to form cordierite and spinel with tetragonal zirconia without the formation of zircon, a slightly higher silica content composition than ZSPIN may cross out of the two phase region between spinel and zirconia that was observed at 1250°C. From examining the diagram, it is inferred that a metastable coexistence between spinel, cordierite and zirconia could be achieved with a composition of slightly higher silica content than ZSPIN.

## DENSIFICATION

The matrix materials (without SiC fibers) densified most rapidly at 1200°C through 1250°C. The final density was dependent upon the applied pressure and the rate of temperature increase or hold time in this temperature range. Compositions ZSPIN and ZCOR were the most extensively studied for densification characteristics. ZSPIN densified up to 95% of theoretical when hot-pressed at 10°C/minute heating rate and 15 minutes at 1250°C under 1100 psi applied pressure. Crystalline phase development appeared to be unaffected by the applied pressure when varied from 0 to 1100 psi. Composition ZCOR was

extremely difficult to densify. At 1700 psi applied pressure, a 10°C/ minute heating rate and 15 minutes at top temperatures of 1250°C and 1300°C, the density appeared to be near 90% of theoretical.

Densification appeared to be one of the major difficulties encountered with the not only the matrix material without the SiC fibers but also in the composite materials as well. The composite materials required a densification temperature of approximately 1300°C. This relatively high densification temperature requirement also corresponds to a temperature range that has been reported by Mah et al [11,12] to seriously degrade the integrity of the SiC fibers.

In short, densification of the matrix material with and without the SiC fibers is a major reason for the poor mechanical properties exhibited in the compositions studied and would be a significant barrier for their use in any practical application. A fluxing additive to the matrix composition appears to be necessary in order to overcome the densification barrier of these materials.

ZIRCONIA TRANSFORMATION TOUGHENING

Comparing the strength and toughness of the samples prepared in this study with data from a Claussen[13] study (shown in table 1), it appears the transformation toughening was not realized in these experiments. The low density of the samples distorts the evaluation of the effectiveness of the zirconia toughening Since the toughness measurement was conducted using an indentor method, the indentor location could be chosen to minimize the

crack interaction with the porosity. The toughness of the samples as well as the strength appears to be more consistent with non-toughened ceramics. A planned microscopy study of these materials should provide insight regarding the apparently unsuccessful toughening.

TABLE 1: Strength and Toughness

| Primary Phases | Data Source | (MPa) | $K_{IC}$(MPam$^{1/2}$ |
|---|---|---|---|
| Spinel,$ZrO_2$t | Powers,Drummond | 110-165 | 2.0-2.4 |
| Spinel | Claussen[13] | 180 | 2.0 |
| Spinel,$ZrO_2$t (toughened) | Claussen[13] | 350-500 | 4-5 |
| Cordierite,$ZrO_2$t | Powers,Drummond | 60-85 | 1.4-1.6 |
| Cordierite | Claussen[13] | 120 | 1.4 |
| Cordierite,$ZrO_2$t (toughened) | Claussen[13] | 300 | 3 |

PHASE DEVELOPMENT IN THE SiC FIBER COMPOSITE

The final composite was comprised of between 30% to 50% fibers. The fibers were the ceramic grade Nicalon®. The fibers were continuous and approximately 13 microns in diameter. The as received fibers were coated with a sizing. The sizing was removed by a rapid heat treatment at under 600°C before slurry coating the matrix material onto the fibers. The heat treatment time was less than a minute in an air atmosphere.

The major phases developed in the composites are illustrated in Figure 4. The matrix compositions appeared to contain a higher silica content than the matrix material alone. Since the fibers used contained a significant $SiO_2$ fraction, the higher silica matrix was not surprising.

The phase development in the composites appeared to be sluggish compared to the matrix material without the fibers. Comparing the composite metastable ternary at 1300°C with that of

the matrix only material (figures 4 and 3 respectively), it is apparent that the $\mu$ to $\alpha$ transformation is retarded and the zircon formation region is reduced in the composite materials. The mechanical properties evaluation of these composites is not yet complete to correlate with phase development.

It has been shown by Brennan[14] that $Nb_2O_5$ precipitates as NbC near the fiber surface with a high carbon content material surrounding the fiber. Analytical microscopy is planned for the composites fabricated in this study. Results are not yet available to add to the observations made by Brennan. However, to understand the driving forces behind the role of the $Nb_2O_5$ in the formation of NbC or carbon in the SiC fiber composites, a Nb-Si-C-O stability diagram was constructed. By examining a large number of potential reactions between Nb, Si, C and O, a diagram for the condensed phases stable at a given oxygen partial pressure and temperature was constructed. This diagram can be seen in Figure 5.

This stability diagram was constructed from data available in the JANAF thermochemical tables.[7] The data available in these tables do not consider the nonstoichiometric character of $Nb_2O_5$ at high temperatures [15] nor of NbC. [16] Intermetallic compounds of Nb and Si as shown by Kocherzhinskiy et al [18] also do not have available the required thermochemical data, therefore, the lowest oxygen partial pressure region of the stability diagram is left unlabled and is therefore incomplete.

The stability diagram shows some general trends:

1. Carbon can be stable in the presence of niobia and silica.
2. Niobia is not stable in the presence of its own carbide.

If both species are present, this would indicate localized variations in oxygen partial pressure within the composite exist. Such localized regions would suggest a diffusion barrier layer exists.

3. The oxides of niobium are not stable in the presence of SiC. The large free energy release for the formation of silica from SiC will drive the niobia-SiC reaction.

4. Silica is stable in the presence of carbon and niobium oxides at higher oxygen pressures and stable with NbC at lower oxygen pressures. The coexistance of carbon or niobia with NbC is separated by $SiO_2$ if the $SiO_2$ is acting as an oxygen or carbon diffusion barrier.

The stability diagram agrees with experimental evidence by supporting the potential existence of carbon between the SiC fiber surface and the matrix material. NbC would not be expected to coexist with carbon except at the oxygen partial pressure boundary which separates the NbC and C containing regions. Since the stability diagram does not illustrate the nonstoichiometric character of NbC, the boundary between NbC and C may actually be a region of nonstoichiometry rather than a distinct line.

## CONCLUSIONS

The compositions investigated in general showed a substantial change in the crystalline phases formed between 1250°C and 1300°C. Accompanying this change was the development of zircon at the expense of the zirconia and the transformation of cordierite from the $\mu$ to the $\alpha$ form. The formation of

zircon coincided with the formation of large flaws in the matrix material which greatly degraded the material strength.

Metastable ternary isothermal diagrams at 1250°C and 1300°C were constructed for the compositions used in this study. The resulting diagram should be extremely useful in selecting future compositions for study.

Crystalline phase development of the composite samples seemed to lag behind that of the matrix material without the SiC fibers. The $\mu$ to $\alpha$ transformation of cordierite and the formation of zircon were two examples of lagging reactions. An isothermal section for the composite materials was estimated based on the experimental XRD diffraction data and is shown in Figure 4.

By utilizing available thermochemical data, a Nb-Si-O-C stability diagram was calculated. This stability diagram is offered as an aid in understanding the role of $Nb_2O_5$ in SiC fiber composites.

References


1. Marshall, D.B., Noma,T., Evans,A.G. "A Simple Method for Determining Elastic Modulous-to-Hardness Ratios using Knoop Indentation Measurements". Communications of the American Ceramic Society, Oct. 1982,C175-176.

2. Osborn,E.F., Muan,A. "$MgO-Al_2O_3-SiO_2$",Fig.712,Phase Diagrams for Ceramists, The American Ceramic Society.

3. McMillan, P.W., Glass-Ceramics, Academic Press London, 1979.

4. Faber, K.T. and Evans, A.G. "Crack Deflection Processes", Acta Metall. Vol.31 [4], 565-584.

5. Conrad, M.A. "Phase Transitions in a Zirconia Nucleated $MgO\ Al_2O_3\ 3SiO_2$ Glass-Ceramic", Journ. Material Science 7, 1972,527-530.

6. Besmann,T.M., "SOLGASMIX-PV, A Computer Program to Calculate Equilibrium Relationships in Complex Chemical Systems", Oak Ridge National Laboratory Report No. ORNL/TM-5775, Oak Ridge, Tenn. 37830, 1977.

7. JANAF Thermochemical Tables, NSRDS-NBS37 1971 edition and 1975 Supplement. Stull,D.R. and Prophet, H. Eds.

8. Geological Survey Bulletin #1452, "Thermodynamic Properties of Minerals and Related Substances", 1979, Robie, R., Hemingway,B. and Fisher,J. Eds., U.S. Government Printing Office , Washington, D.C. 1978.

9. Geller, R.F. and Lang,S.M. "$SiO_2-ZrO_2$ Phase Diagram", Levin, E.M., Robbins, C.R., McMurdie,H.F. and Reser,M.K. Eds., NBS, American Ceramic Society, Columbus 1974.

10. Claussen,N., Ruhle,M. Heuer,A.H. Advances in Ceramics,Vol. 12, Science and Technology of Zirconia II.

11. Mah,T., Mendiratta,M.G., Katz,A.P., Ruh,R. and Mazdiyasni,K.S. "Room-Temperature Mechanical Behavior of Fiber-Reinforced Ceramic-Matrix Composites", Communications of the American Ceramic Society, Journ. Am. Cer. Soc., 68 [1] C-27-30 (1985).

12. Mah,T., Hecht,N.L., McCullum,D.E.,Hoenigman,J.R., Kim,H.M., Katz, A.P. and Lipsitt,H.A. "Thermal Stability of SiC Fibres", Journ. Material Science 1984 [19], 1191-1201.

13. Claussen, N. "Strengthening Strategies for $ZrO_2$-Toughened Ceramics at High Temperatures" Materials Science and Engineering, 71 (1985) 23-38.

14. Brennan, J.J. "Additional Studies of SiC Fiber Reinforcement Glass-Ceramic Composites", Annual Report R83-916018-2 on ONR Contract N00014-82-C-0096, 14 Feb. 1983.

15. Balachandran, U., Eror,N.G. "Nonstoichiometric Disorder in Alpha $Nb_2O_5$ at Elevated Temperatures", Journ. Mater. Sci. 1982 17 [5] 1286-96.

16. Samsonov,G.V., Upadkhaya, G.Sh. "Physical Properties of the Monocarbides of the Transition Metals in their Homogeneity Regions I. $TiC_{1-x}$ and $NbC_{1-x}$" Sov. Pow. Met. and Met.Cer. 1969, 5, 394-398.

17. Kruger, J. Vacuum Metallurgy, Winkler, O. and Bakish,R. Eds., Elsevier Publishing Company, Amsterdam 1971, 165-167.

18. Kocherzhinskiy, Yu.A., Yupko,L.M. and Shishkin,E.A. "The Nb-Si Phase Diagram", Russian Metallurgy 1980 [1], 184-188.

Figure 1: $MgO-Al_2O_3-SiO_2$ Diagram taken from that of E.F. Osborn and A. Muan. Figure 712, Phase Diagrams for Ceramists, The American Ceramic Society.

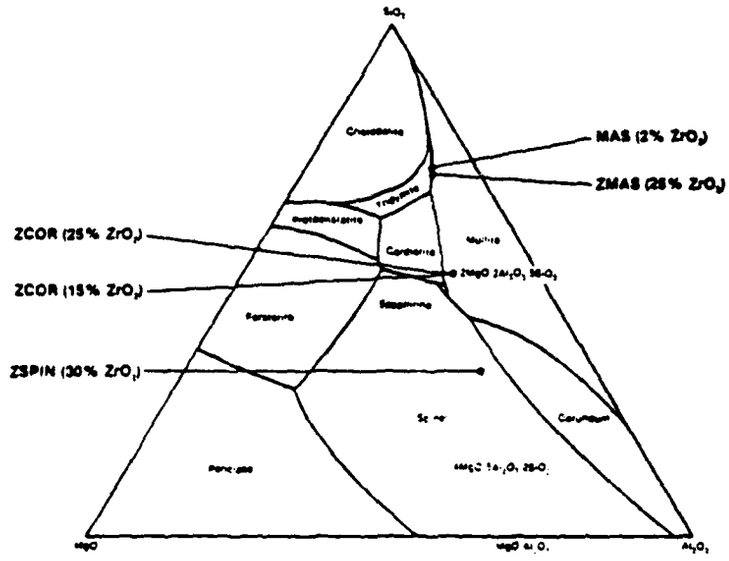


Figure 2: **Predominant Crystalline Phases at 1250°C, 15 min.**

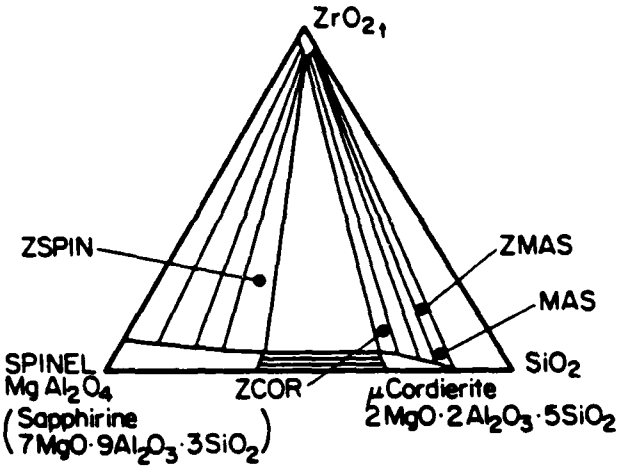



Figure 3: **Predominant Crystalline Phases at 1300°C**

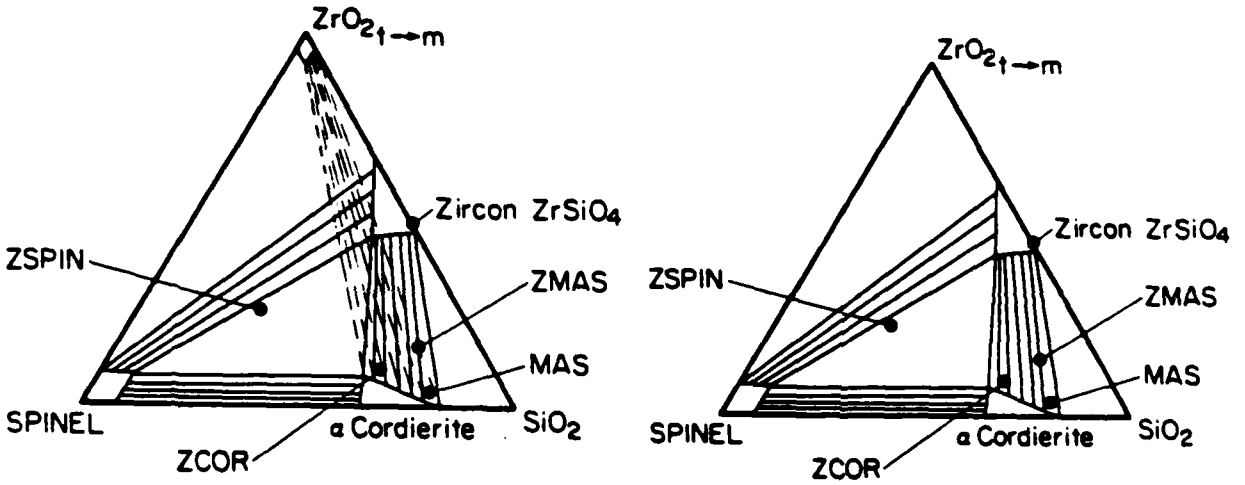



Figure 3 Left shows the major phases formed after 15 min. at 1300°. The dotted lines indicate that $ZrO_2$ remains. Figure 3 Right indicates the expected final phases after extended heat treatment times.

Figure 4: **Matrix & SiC fibers at 1300°C. 15 min.**

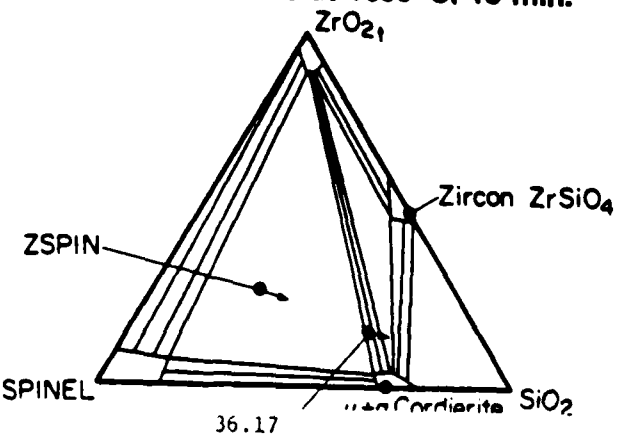
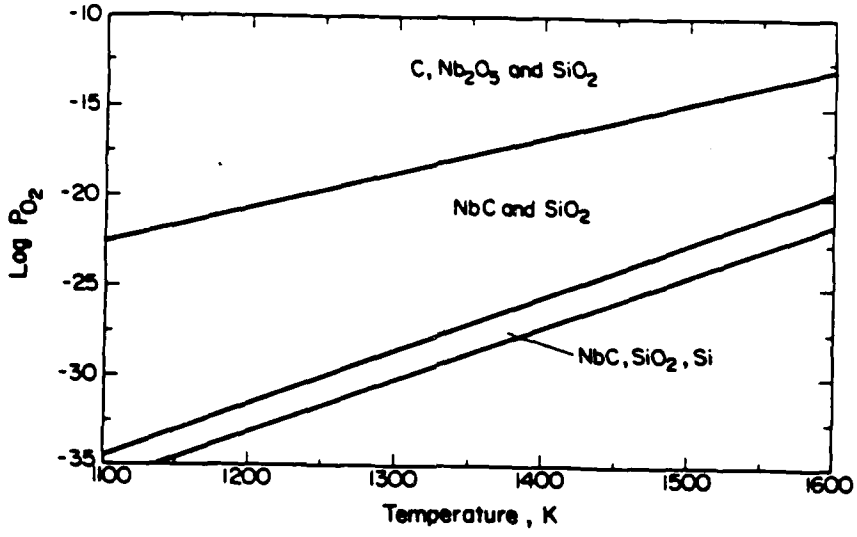


Figure 5: **Nb-Si-O-C System Stability Diagram**



END

DATE

FILM

JAN

1988